IN-22070

NASA Technical Memorandum 87263

Bibliography of Lewis Research Center Technical Publications Announced in 1985

(NASA-TM-87263) BIBLIOGRAPHY OF LEWIS RESEARCH CENTER TECHNICAL PUBLICATIONS ANNOUNCED IN 1985 (NASA) 307 p CSCL 05B

N86-32336

Unclas
G3/82 43097

May 1986

NASA

PREFACE

In 1985, Lewis Research Center's 1127 research authors published 422 technical publications which were announced to and reached the worldwide scientific community. The 422 papers included 197 symposium/seminar presentations and 74 articles sent directly to journals for publication. In 1985, Lewis authors published approximately 65 percent of their research contributions in outside publications and the remainder as NASA research reports. Sixty percent of Lewis-authored society presentations and journal articles were addressed to members of the following technical societies: AIAA, 65 papers; ASME, 62 papers; SAE, 24 papers; IEEE, 18 papers; ACS (American Ceramic Society), 17 papers; ASM, 17 papers: ASLE, 13 papers; AVS (American Vacuum Society), 12 papers.

In 1985, 220 contractor-authored research reports were produced. In addition, 6 patent applications were filed and 25 patents were issued.

Many Lewis authors have received awards for their contributions; among them are the following:

The 1985 Lewis Distinguished Paper Award was presented to Robert A. Miller for his paper entitled "An Oxidation-Based Model for Thermal Barrier Coating Life" which was published in the Journal of the American Ceramic Society. James A. DiCarlo's paper "Fibers for Structurally Reliable Metal and Ceramic Composites" was the most popular technical article in 1985 according to the Journal of Metals.

A few Lewis-authored publications are not included in this compilation due to FEDD (For Early Domestic Dissemination) and ITAR (International Traffic in Arms Regulations) considerations which limit their announcement and distribution.

All the publications in this collection were announced in the 1985 issues of STAR (Scientific and Technical Aerospace Reports) and IAA (International Aerospace Abstracts).

The arrangement of the material is by NASA subject category, as noted in the Contents. The various indexes will help locate specific publications by subject, author, contractor organization, contract number, and report number.

George Mandel
Chief, Technical Information Services Division

TABLE OF CONTENTS

PREFACE i

Includes aeronautics (general); aerodynamics; air transportation and safety; aircraft communications and navigation; aircraft design, testing and performance; aircraft instrumentation; aircraft propulsion and power; aircraft stability and control; and research and support facilities (air).

For related information see also *Astronautics.*

01 AERONAUTICS (GENERAL) 1

02 AERODYNAMICS 1

Includes aerodynamics of bodies, combinations, wings, rotors, and control surfaces; and internal flow in ducts and turbomachinery.

For related information see also *34 Fluid Mechanics and Heat Transfer*

03 AIR TRANSPORTATION AND SAFETY 10

Includes passenger and cargo air transport operations; and aircraft accidents.

For related information see also *16 Space Transportation* and *85 Urban Technology and Transportation.*

04 AIRCRAFT COMMUNICATIONS AND NAVIGATION N.A.

Includes digital and voice communication with aircraft; air navigation systems (satellite and ground based); and air traffic control.

For related information see also *17 Spacecraft Communications, Command and Tracking* and *32 Communications.*

05 AIRCRAFT DESIGN, TESTING AND PERFORMANCE 12

Includes aircraft simulation technology.

For related information see also *18 Spacecraft Design, Testing and Performance* and *39 Structural Mechanics.*

06 AIRCRAFT INSTRUMENTATION 13

Includes cockpit and cabin display devices; and flight instruments.

For related information see also *19 Spacecraft Instrumentation* and *35 Instrumentation and Photography.*

07 AIRCRAFT PROPULSION AND POWER 13

Includes prime propulsion systems and systems components, e.g., gas turbine engines and compressors; and on-board auxiliary power plants for aircraft.

For related information see also *20 Spacecraft Propulsion and Power, 28 Propellants and Fuels,* and *44 Energy Production and Conversion.*

08 AIRCRAFT STABILITY AND CONTROL 34

Includes aircraft handling qualities; piloting; flight controls; and autopilots.

09 RESEARCH AND SUPPORT FACILITIES (AIR) 34

Includes airports, hangars and runways; aircraft repair and overhaul facilities; wind tunnels; shock tube facilities; and engine test blocks.

For related information see also *14 Ground Support Systems and Facilities (Space).*

ASTRONAUTICS

Includes astronautics (general); astrodynamics; ground support systems and facilities (space); launch vehicles and space vehicles; space transportation; spacecraft communications, command and tracking; spacecraft design, testing and performance; spacecraft instrumentation; and spacecraft propulsion and power.

For related information see also *Aeronautics*

12 ASTRONAUTICS (GENERAL) 35

For extraterrestrial exploration see *91 Lunar and Planetary Exploration.*

13 ASTRODYNAMICS 36

Includes powered and free-flight trajectories; and orbit and launching dynamics.

14 GROUND SUPPORT SYSTEMS AND FACILITIES (SPACE) N.A.

Includes launch complexes, research and production facilities; ground support equipment, e.g., mobile transporters; and simulators.

For related information see also *09 Research and Support Facilities (Air).*

15 LAUNCH VEHICLES AND SPACE VEHICLES 36

Includes boosters; manned orbital laboratories; reusable vehicles; and space stations.

16 SPACE TRANSPORTATION 38

Includes passenger and cargo space transportation, e.g., shuttle operations; and rescue techniques.

For related information see also *03 Air Transportation and Safety* and *85 Urban Technology and Transportation.*

17 SPACECRAFT COMMUNICATION, COMMAND AND TRACKING 38

Includes telemetry; space communications networks; astronavigation; and radio blackout.

For related information see also *04 Aircraft Communications and Navigation* and *32 Communications.*

18 SPACECRAFT DESIGN, TESTING AND PERFORMANCE 38

Includes spacecraft thermal and environmental control; and attitude control.

For life support systems see *54 Man/System Technology and Life Support.* For related information see also *05 Aircraft Design, Testing and Performance* and *39 Structural Mechanics.*

19 SPACECRAFT INSTRUMENTATION 41

For related information see also *06 Aircraft Instrumentation* and *35 Instrumentation and Photography.*

20 SPACECRAFT PROPULSION AND POWER 41

Includes main propulsion systems and components, e.g., rocket engines; and spacecraft auxiliary power sources.

For related information see also *07 Aircraft Propulsion and Power, 28 Propellants and Fuels,* and *44 Energy Production and Conversion.*

PRECEDING PAGE BLANK NOT FILMED

CHEMISTRY AND MATERIALS

Includes chemistry and materials (general); composite materials; inorganic and physical chemistry; metallic materials; nonmetallic materials; and propellants and fuels.

23 CHEMISTRY AND MATERIALS (GENERAL) 53
Includes biochemistry and organic chemistry.

24 COMPOSITE MATERIALS 54
Includes laminates.

25 INORGANIC AND PHYSICAL CHEMISTRY 59
Includes chemical analysis, e.g., chromatography; combustion theory; electrochemistry; and photochemistry.
For related information see also *77 Thermodynamics and Statistical Physics.*

26 METALLIC MATERIALS 64
Includes physical, chemical, and mechanical properties of metals, e.g., corrosion; and metallurgy.

27 NONMETALLIC MATERIALS 78
Includes physical, chemical, and mechanical properties of plastics, elastomers, lubricants, polymers, textiles, adhesives, and ceramic materials.

28 PROPELLANTS AND FUELS 92
Includes rocket propellants, igniters, and oxidizers; storage and handling; and aircraft fuels.
For related information see also *07 Aircraft Propulsion and Power, 20 Spacecraft Propulsion and Power,* and *44 Energy Production and Conversion.*

ENGINEERING

Includes engineering (general); communications; electronics and electrical engineering; fluid mechanics and heat transfer; instrumentation and photography; lasers and masers; mechanical engineering; quality assurance and reliability; and structural mechanics.
For related information see also *Physics.*

31 ENGINEERING (GENERAL) 94
Includes vacuum technology; control engineering; display engineering; and cryogenics.

32 COMMUNICATIONS 95
Includes land and global communications; communications theory; and optical communications.
For related information see also *04 Aircraft Communications and Navigation* and *17 Spacecraft Communications, Command and Tracking.*

33 ELECTRONICS AND ELECTRICAL ENGINEERING 100
Includes test equipment and maintainability; components, e.g., tunnel diodes and transistors; microminiaturization; and integrated circuity.
For related information see also *60 Computer Operations and Hardware* and *76 Solid-State Physics.*

34 FLUID MECHANICS AND HEAT TRANSFER 106
Includes boundary layers; hydrodynamics; fluidics; mass transfer; and ablation cooling.
For related information see also *02 Aerodynamics* and *77 Thermodynamics and Statistical Physics.*

35 INSTRUMENTATION AND PHOTOGRAPHY 120
Includes remote sensors; measuring instruments and gages; detectors; cameras and photographic supplies; and holography.
For aerial photography see *43 Earth Resources.* For related information see also *06 Aircraft Instrumentation* and *19 Spacecraft Instrumentation.*

36 LASERS AND MASERS 126
Includes parametric amplifiers.

37 MECHANICAL ENGINEERING 126
Includes auxiliary systems (non-power); machine elements and processes; and mechanical equipment.

38 QUALITY ASSURANCE AND RELIABILITY 137
Includes product sampling procedures and techniques; and quality control.

39 STRUCTURAL MECHANICS 139
Includes structural element design and weight analysis; fatigue; and thermal stress.
For applications see *05 Aircraft Design, Testing and Performance* and *18 Spacecraft Design, Testing and Performance.*

GEOSCIENCES

Includes geosciences (general); earth resources; energy production and conversion; environment pollution; geophysics; meteorology and climatology; and oceanography.
For related information see also *Space Sciences.*

42 GEOSCIENCES (GENERAL) N.A.

43 EARTH RESOURCES 153
Includes remote sensing of earth resources by aircraft and spacecraft; photogrammetry; and aerial photography.
For instrumentation see *35 Instrumentation and Photography.*

44 ENERGY PRODUCTION AND CONVERSION 153
Includes specific energy conversion systems, e.g., fuel cells and batteries; global sources of energy; fossil fuels; geophysical conversion; hydroelectric power; and wind power.
For related information see also *07 Aircraft Propulsion and Power, 20 Spacecraft Propulsion and Power, 28 Propellants and Fuels,* and *85 Urban Technology and Transportation.*

45 ENVIRONMENT POLLUTION 165
Includes air, noise, thermal and water pollution; environment monitoring; and contamination control.

46 GEOPHYSICS 166
Includes aeronomy; upper and lower atmosphere studies; ionospheric and magnetospheric physics; and geomagnetism.
For space radiation see *93 Space Radiation.*

47 METEOROLOGY AND CLIMATOLOGY 166
Includes weather forecasting and modification.

48 OCEANOGRAPHY N.A.
Includes biological, dynamic and physical oceanography; and marine resources.

LIFE SCIENCES

Includes sciences (general); aerospace medicine; behavioral sciences; man/system technology and life support; and planetary biology.

51 LIFE SCIENCES (GENERAL) 168
Includes genetics.

52 AEROSPACE MEDICINE N.A.
Includes physiological factors; biological effects of radiation; and weightlessness.

53 BEHAVIORAL SCIENCES N.A.
Includes psychological factors; individual and group behavior; crew training and evaluation; and psychiatric research.

54 MAN/SYSTEM TECHNOLOGY AND LIFE SUPPORT 168
Includes human engineering; biotechnology; and space suits and protective clothing.

55 PLANETARY BIOLOGY N.A.
Includes exobiology; and extraterrestrial life.

MATHEMATICAL AND COMPUTER SCIENCES

Includes mathematical and computer sciences (general); computer operations and hardware; computer programming and software; computer systems; cybernetics; numerical analysis; statistics and probability; systems analysis; and theoretical mathematics.

59 MATHEMATICAL AND COMPUTER SCIENCES (GENERAL) 168

60 COMPUTER OPERATIONS AND HARDWARE 168
Includes computer graphics and data processing.
For components see *33 Electronics and Electrical Engineering.*

61 COMPUTER PROGRAMMING AND SOFTWARE 169
Includes computer programs, routines, and algorithms.

62 COMPUTER SYSTEMS 170
Includes computer networks.

63 CYBERNETICS 171
Includes feedback and control theory.
For related information see also *54 Man/System Technology and Life Support.*

64 NUMERICAL ANALYSIS 171
Includes iteration, difference equations, and numerical approximation.

65 STATISTICS AND PROBABILITY N.A.
Includes data sampling and smoothing; Monte Carlo method; and stochastic processes.

66 SYSTEMS ANALYSIS N.A.
Includes mathematical modeling; network analysis; and operations research.

67 THEORETICAL MATHEMATICS N.A.
Includes topology and number theory.

PHYSICS

Includes physics (general); acoustics; atomic and molecular physics; nuclear and high-energy physics; optics; plasma physics; solid-state physics; and thermodynamics and statistical physics.
For related information see also *Engineering.*

70 PHYSICS (GENERAL) N.A.
For geophysics see *46 Geophysics.* For astrophysics see *90 Astrophysics.* For solar physics see *92 Solar Physics.*

71 ACOUSTICS 172
Includes sound generation, transmission, and attenuation.
For noise pollution see *45 Environment Pollution.*

72 ATOMIC AND MOLECULAR PHYSICS 177
Includes atomic structure and molecular spectra.

73 NUCLEAR AND HIGH-ENERGY PHYSICS 177
Includes elementary and nuclear particles; and reactor theory.
For space radiation see *93 Space Radiation.*

74 OPTICS 178
Includes light phenomena.

75 PLASMA PHYSICS 178
Includes magnetohydrodynamics and plasma fusion.
For ionospheric plasmas see *46 Geophysics.* For space plasmas see *90 Astrophysics.*

76 SOLID-STATE PHYSICS 180
Includes superconductivity.
For related information see also *33 Electronics and Electrical Engineering* and *36 Lasers and Masers.*

77 THERMODYNAMICS AND STATISTICAL PHYSICS 184
Includes quantum mechanics; and Bose and Fermi statistics.
For related information see also *25 Inorganic and Physical Chemistry* and *34 Fluid Mechanics and Heat Transfer.*

SOCIAL SCIENCES

Includes social sciences (general); administration and management; documentation and information science; economics and cost analysis; law and political science; and urban technology and transportation.

80 SOCIAL SCIENCES (GENERAL) **N.A.**
Includes educational matters.

81 ADMINISTRATION AND MANAGEMENT **N.A.**
Includes management planning and research.

82 DOCUMENTATION AND INFORMATION SCIENCE **184**
Includes information storage and retrieval technology; micrography; and library science.
For computer documentation see *61 Computer Programming and Software.*

83 ECONOMICS AND COST ANALYSIS **N.A.**
Includes cost effectiveness studies.

84 LAW AND POLITICAL SCIENCE **N.A.**
Includes space law; international law; international cooperation; and patent policy.

85 URBAN TECHNOLOGY AND TRANSPORTATION **184**
Includes applications of space technology to urban problems; technology transfer; technology assessment; and surface and mass transportation.
For related information see *03 Air Transportation and Safety, 16 Space Transportation,* and *44 Energy Production and Conversion.*

SPACE SCIENCES

Includes space sciences (general); astronomy; astrophysics; lunar and planetary exploration; solar physics; and space radiation.
For related information see also *Geosciences.*

88 SPACE SCIENCES (GENERAL) **N.A.**

89 ASTRONOMY **N.A.**
Includes radio and gamma-ray astronomy; celestial mechanics; and astrometry.

90 ASTROPHYSICS **N.A.**
Includes cosmology; and interstellar and interplanetary gases and dust.

91 LUNAR AND PLANETARY EXPLORATION **N.A.**
Includes planetology; and manned and unmanned flights.
For spacecraft design see *18 Spacecraft Design, Testing and Performance.* For space stations see *15 Launch Vehicles and Space Vehicles.*

92 SOLAR PHYSICS **N.A.**
Includes solar activity, solar flares, solar radiation and sunspots.

93 SPACE RADIATION **N.A.**
Includes cosmic radiation; and inner and outer earth's radiation belts.
For biological effects of radiation see *52 Aerospace Medicine.* For theory see *73 Nuclear and High-Energy Physics.*

GENERAL

99 GENERAL **186**

Note: N.A. means that no abstracts were assigned to this category for this issue.

SUBJECT INDEX **A-1**
PERSONAL AUTHOR INDEX **B-1**
CORPORATE SOURCE INDEX **C-1**
CONTRACT NUMBER INDEX **D-1**
REPORT/ACCESSION NUMBER INDEX **E-1**

Bibliography of Lewis Research Center Technical Publications Announced in 1985

01

AERONAUTICS (GENERAL)

N85-15658*# National Aeronautics and Space Administration. Lewis Research Center, Cleveland, Ohio.
TEMPERATURE DISTORTION GENERATOR FOR TURBOSHAFT ENGINE TESTING
G. A. KLANN, R. L. BARTH, and T. J. BIESIADNY Dec. 1984 34 p refs Presented at the SAE Aerospace Congr. and Exposition, Long Beach, Calif., 15-18 Oct. 1984
(NASA-TM-83748; USAAVSCOM-TR-84-C-12; E-2197; NAS 1.15:83748) Avail: NTIS HC A03/MF A01 CSCL 01B

The procedures and unique hardware used to conduct an experimental investigation into the response of a small-turboshaft-engine compression system to various hot gas ingestion patterns are presented. The temperature distortion generator described herein uses gaseous hydrogen to create both steady-state and time-variant, or transient, temperature distortion at the engine inlet. The range of transient temperature ramps produced by the distortion generator during the engine tests was from less than 111 deg K/sec (200 deg R/sec) to above 611 deg K/sec (1100 deg R/sec); instantaneous temperatures to 422 deg K (760 deg R) above ambient were generated. The distortion generator was used to document the maximum inlet temperatures and temperature rise rates that the compression system could tolerate before the onset of stall for various circumferential distortions as well as the compressor system response during stall. Author

N85-17935*# National Aeronautics and Space Administration. Lewis Research Center, Cleveland, Ohio.
DESIGN DESCRIPTION OF A MICROPROCESSOR BASED ENGINE MONITORING AND CONTROL UNIT (EMAC) FOR SMALL TURBOSHAFT
A. N. BAEZ Jan. 1985 30 p refs
(NASA-TM-86860; E-2324; NAS 1.15:86860) Avail: NTIS HC A03/MF A01 CSCL 01B

Research programs have demonstrated that digital electronic controls are more suitable for advanced aircraft/rotorcraft turbine engine systems than hydromechanical controls. Commercially available microprocessors are believed to have the speed and computational capability required for implementing advanced digital control algorithms. Thus, it is desirable to demonstrate that off-the-shelf microprocessors are indeed capable of performing real time control of advanced gas turbine engines. The engine monitoring and control (EMAC) unit was designed and fabricated specifically to meet the requirements of an advanced gas turbine engine control system. The EMAC unit is fully operational in the Army/NASA small turboshaft engine digital research program. Author

N85-23685*# National Aeronautics and Space Administration. Lewis Research Center, Cleveland, Ohio.
FUTURE DIRECTIONS IN AEROPROPULSION TECHNOLOGY
N. T. SAUNDERS and A. J. GLASSMAN 6 Sep. 1985 39 p refs Proposed for presentation at 7th Intern. Symp. on Air Breathing Eng., Beijing, China, 2-6 Sep. 1985
(NASA-TM-87010; E-2553; NAS 1.15:87010) Avail: NTIS HC A03/MF A01 CSCL 01B

Future directions in aeropropulsion technology that have been identified in a series of studies recently sponsored by the U.S. Government are discussed. Advanced vehicle concepts that could become possible by the turn of the century are presented along with some of their projected capabilities. Key building-block propulsion technologies that will contribute to making these vehicle concepts a reality are discussed along with projections of their status by the year 2000. Some pertinent highlights of the NASA aeropropulsion program are included in the discussion. Author

02

AERODYNAMICS

Includes aerodynamics of bodies, combinations, wings, rotors, and control surfaces; and internal flow in ducts and turbomachinery.

A85-10352* National Aeronautics and Space Administration. Lewis Research Center, Cleveland, Ohio.
GENERATION OF INSTABILITY WAVES IN FLOWS SEPARATING FROM SMOOTH SURFACES
M. E. GOLDSTEIN (NASA, Lewis Research Center, Cleveland, OH) Journal of Fluid Mechanics (ISSN 0022-1120), vol. 145, Aug. 1984, p. 71-94. refs

This paper analyses the coupling between an imposed disturbance and an instability wave that propagates downstream on a shear layer which emanates from a separation point on a smooth surface. Since the wavelengths of the most-amplified instability waves will generally be small compared with the streamwise body dimensions, the analysis is restricted to this 'high-frequency' limit and the solution is obtained by using matched asymptotic expansions. An 'inner' solution, valid near the separation point, is matched onto an outer solution, which represents an instability wave on a slowly diverging mean flow. The analysis relates the amplitude of this instability to that of the imposed disturbance. Author

A85-10357* National Aeronautics and Space Administration. Lewis Research Center, Cleveland, Ohio.
RESONANCE IN FLOWS WITH VORTEX SHEETS AND EDGES
P. A. DURBIN (NASA, Lewis Research Center, Cleveland, OH) Journal of Fluid Mechanics (ISSN 0022-1120), vol. 145, Aug. 1984, p. 275-285. refs

It is shown that the vortex sheet in a slot between two semi-infinite plates does not admit incompressible resonant perturbations. The semi-infinite vortex sheet entering a duct does admit incompressible resonance. These results indicate that the vortex-sheet approximation is less useful for impinging shear flows than for non-impinging flows. They also suggest an important role

of downstream vortical disturbances in resonant flows. The general solution for perturbations to flow with a vortex sheet and edges is written in terms of a Cauchy integral. Requirements on the behavior of this solution at edges and at downstream infinity fix the criteria for resonance. Author

A85-10870*# National Aeronautics and Space Administration. Lewis Research Center, Cleveland, Ohio.
ACOUSTIC PRESSURES EMANATING FROM A TURBOMACHINE STAGE
S. M. RAMACHANDRA (NASA, Lewis Research Center, Cleveland, OH) American Institute of Aeronautics and Astronautics and NASA, Aeroacoustics Conference, 9th, Williamsburg, VA, Oct. 15-17, 1984. 13 p. Previously announced in STAR as N84-30224. refs
(AIAA PAPER 84-2325)

A knowledge of the acoustic energy emission of each blade row of a turbomachine is useful for estimating the overall noise level of the machine and for determining its discrete frequency noise content. Because of the close spacing between the rotor and stator of a compressor stage, the strong aerodynamic interactions between them have to be included in obtaining the resultant flow field. This paper outlines a three-dimensional theory for determining the discrete frequency noise content of an axial compressor consisting of a rotor and a stator each with a finite number of blades. The lifting surface theory and the linearized equation of an ideal, nonsteady compressible fluid motion are used for thin blades of arbitrary cross section. The combined pressure field at a point of the fluid is constructed by linear addition of the rotor and stator solutions together with an interference factor obtained by matching them for net zero vorticity behind the stage. Author

A85-11646*# National Aeronautics and Space Administration. Lewis Research Center, Cleveland, Ohio.
ANALYTICAL STUDY OF BLOWING BOUNDARY LAYER CONTROL FOR SUBSONIC V/STOL INLETS
D. P. HWANG (NASA, Lewis Research Center, Cleveland, OH) IN: Computation of internal flows; Methods and applications; Proceedings of the Energy Sources Technology Conference, New Orleans, LA, February 12-16, 1984 . New York, American Society of Mechanical Engineers, 1983, p. 151-157. refs

The analytical methods used to study blowing boundary-layer control (BLC) for subsonic V/STOL inlets at the NASA Lewis Research Center are briefly described. The methods are then shown to give good agreement with experimental results, both with and without blowing BLC. Finally, because of this good agreement, the methods have been used to determine analytically the optimum (minimum blowing power required) location and height for a blowing slot within a subsonic V/STOL inlet. Results of this analytical study are presented. Author

A85-18679*# National Aeronautics and Space Administration. Lewis Research Center, Cleveland, Ohio.
EFFICIENT SOLUTION OF THE EULER AND NAVIER-STOKES EQUATIONS WITH A VECTORIZED MULTIPLE-GRID ALGORITHM
R. C. CHIMA (NASA, Lewis Research Center, Cleveland, OH) and G. M. JOHNSON (Colorado State University, Fort Collins, CO) (Computational Fluid Dynamics Conference, 6th, Danvers, MA, July 13-15, 1983, Collection of Technical Papers, p. 72-89) AIAA Journal (ISSN 0001-1452), vol. 23, Jan. 1985, p. 23-32. Previously cited in issue 18, p. 2634, Accession no. A83-39359. refs

A85-19489*# National Aeronautics and Space Administration. Lewis Research Center, Cleveland, Ohio.
ACCELERATED CONVERGENCE FOR INCOMPRESSIBLE FLOW CALCULATIONS
G. M. NEELY and R. W. CLAUS (NASA, Lewis Research Center, Cleveland, OH) American Institute of Aeronautics and Astronautics, Aerospace Sciences Meeting, 23rd, Reno, NV, Jan. 14-17, 1985. 8 p. Previously announced in STAR as N85-10949. refs
(AIAA PAPER 85-0058)

Two improved algorithms which solve the steady-state Navier-Stokes equations, PISO and SIMPLER, are studied. Computations were carried out on progressively finer grids for the driven cavity and flow over a backward-facing step. The effects of relaxation factor, number of grid nodes and number of sweeps through the pressure equations are studied to evaluate the performance of the PISO and SIMPLER schemes. Results show that these improved schemes accelerate the convergence rate of the solution generally by a factor of two as compared to the SIMPLE method. Author

A85-19490*# Texas Technological Univ., Lubbock.
FLOW VISUALIZATION OF LATERAL JET INJECTION INTO SWIRLING CROSSFLOW
G. B. FERRELL (Texas Tech University, Lubbock, TX; Oklahoma State University, Stillwater, OK), K. AOKI (Oklahoma State University, Stillwater, OK; Tokai University, Hiratsuka, Japan), and D. G. LILLEY (Oklahoma State University, Stillwater, OK) American Institute of Aeronautics and Astronautics, Aerospace Sciences Meeting, 23rd, Reno, NV, Jan. 14-17, 1985. 12 p. refs
(Contract NAG3-159)
(AIAA PAPER 85-0059)

Flow visualization experiments have been conducted to characterize the time-mean flowfield of a deflected turbulent jet in a confining cylindrical crossflow. Jet-to-crossflow velocity ratios of 2, 4, and 6 were investigated, under crossflow inlet swirler vane angles of 0 (swirler removed), 45 and 70 degrees. Smoke, neutrally-buoyant helium-filled soap bubbles, and multi-spark flow visualization were employed to highlight interesting features of the deflected jet, as well as the trajectory and spread pattern of the jet. Gross flowfield characterization was obtained for a range of lateral jet-to-crossflow velocity ratios and a range of inlet swirl strengths in the main flow. The flow visualization results agree well with the measurements obtained elsewhere with the six-orientation single hot-wire method. Author

A85-19510*# United Technologies Research Center, East Hartford, Conn.
THREE-DIMENSIONAL INVISCID FLOW ANALYSIS OF TURBOFAN FORCED MIXERS
T. J. BARBER, G. L. MULLER, S. M. RAMSAY (United Technologies Research Center, East Hartford, CT), and E. M. MURMAN (MIT, Cambridge, MA) American Institute of Aeronautics and Astronautics, Aerospace Sciences Meeting, 23rd, Reno, NV, Jan. 14-17, 1985. 14 p. refs
(Contract NAS3-23039)
(AIAA PAPER 85-0086)

A three-dimensional potential analysis has been formulated and applied to the inviscid flow over a turbofan forced mixer. The method uses a unique small disturbance formulation to analytically uncouple the circumferential flow from the radial and axial flow problem, thereby reducing the analysis to the solution of a series of axisymmetric problems. These equations are discretized using a flux volume formulation along a Cartesian grid. The method extends earlier applications of the Cartesian method to complex cambered geometries. The effects of power addition are also included within the potential formulation. Good agreement is obtained with an alternate small disturbance analysis for a symmetric mixer in a planar duct. In addition calculations showing pressure distributions and induced secondary vorticity fields are presented for practical turbofan mixer configurations, and where possible, comparison has been made with available experimental data. Author

A85-19731*# Akron Univ., Ohio.
PROGRESS IN DEVELOPMENT OF A NAVIER-STOKES SOLVER FOR EVALUATION OF ICED AIRFOIL PERFORMANCE
M. G. POTAPCZUK (Akron, University, Akron, OH) and P. M. GERHART (Evansville, University, Evansville, IN; Akron, University, Akron, OH) American Institute of Aeronautics and Astronautics, Aerospace Sciences Meeting, 23rd, Reno, NV, Jan. 14-17, 1985. 19 p. refs
(Contract NAG3-416)
(AIAA PAPER 85-0410)

A method is being developed for evaluation of the flow field behavior about an airfoil with significant ice accretion on the leading edge. The computer code, being evaluated for this purpose, solves the Navier-Stokes equations in a body-fitted curvilinear coordinate system. This requires the use of a grid generation code to transform the x-y coordinates of the physical space into xi-eta coordinates of the computational space. Evaluation of the suitability of these two codes for predicting iced airfoil performance is presently being carried out in anticipation of use in an overall icing analysis effort. Results of this evaluation to date indicate good correlation with known information on clean airfoils. Preliminary results for rime and glaze, iced airfoil shapes are also presented. Author

A85-20744* United Technologies Corp., East Hartford, Conn.
A LINEARIZED UNSTEADY AERODYNAMIC ANALYSIS FOR TRANSONIC CASCADES
J. M. VERDON and J. R. CASPAR (United Technologies Research Center, East Hartford, CT) Journal of Fluid Mechanics (ISSN 0022-1120), vol. 149, Dec. 1984, p. 403-429. refs
(Contract NAS3-23696)

The unsteady airloads generated by the vibrations of turbomachine blades operating at transonic Mach numbers are predicted by a linearized potential flow analysis whose unsteady aerodynamics model encompasses the effects of blade geometry, nonzero mean pressure variation across the blade row, high frequency blade motion, and shock motion, all within the framework of a linearized frequency-domain formulation. A numerical solution for the entire unsteady flow field is determined by matching a solution covering an extended blade passage region to another covering, and extending beyond, the supersonic region(s) adjacent to a blade surface. Results are given for cascades of double circular arc and flat plate blades, in order to demonstrate the unsteady analysis and to partially illustrate the effects of blade geometry, inlet Mach number, vibration frequency and shock motion on unsteady response. O.C.

A85-25135*# Ohio State Univ., Columbus.
PREDICTING RIME ICE ACCRETION ON AIRFOILS
M. B. BRAGG (Ohio State University, Columbus, OH) AIAA Journal (ISSN 0001-1452), vol. 23, March 1985, p. 381-387. refs
(Contract NAG3-28)

A method for predicting the droplet impingement and resulting rime ice accretion on airfoils in an incompressible, inviscid flowfield is presented. The governing equations for the water droplet trajectories are described briefly and the appropriate similarity parameters presented. Droplet impingement parameters are described for both monodisperse and arbitrary droplet size distributions. A time-stepping ice accretion process is presented where the flowfield and droplet impingement characteristics are updated periodically to model the time-dependent nature of the process. The method compares well to experimental results of both droplet impingement and rime ice shapes. The time stepping improves the accuracy of the ice shape predictions. Recommendations are given for further research. Author

A85-25928*# Tennessee Univ. Space Inst., Tullahoma.
FLOW CONTROL IN A DIFFUSING S-DUCT
A. D. VAKILI, J. M. WU, P. LIVER, and M. K. BHAT (Tennessee, University, Space Institute, Tullahoma, TN) American Institute of Aeronautics and Astronautics, Shear Flow Control Conference, Boulder, CO, Mar. 12-14, 1985. 8 p. refs
(Contract NAG3-364)
(AIAA PAPER 85-0524)

Accurate measurements have been made of secondary flow in a 1.51 area ratio diffusing 30 deg - 30 deg S-Duct with circulair cross section. Turbulent flow was entering the duct at Mach number of 0.6, the boundary layer thickness at the duct entrance was ten percent of the duct inlet diameter. Through measurements made, local flow velocity vector as well as static and total pressures mapping of the flow at several stations were obtained. Strong secondary flow was measured in the first bend which continued into the second bend with new vorticity produced in there in the opposite direction. Surface oil flow visualization and wall pressures indicated a region of separated flow starting at theta approximately equal to 22 deg on the inside of the first bend up to theta approximately equal to 44 deg on the outside of the second bend. The flow separated in 'cyclone' form and never reattached in the duct. As a result of the secondary flow and the flow separation, significant total pressure distortion was observed at the exit of the duct. Using flow control devices the separation was eliminated while the exit distortion was improved. Author

A85-26389*# National Aeronautics and Space Administration. Lewis Research Center, Cleveland, Ohio.
ANALYTICAL MODELING OF CIRCUIT AERODYNAMICS IN THE NEW NASA LEWIS ALTITUDE WIND TUNNEL
C. E. TOWNE, L. A. POVINELLI, W. G. KUNIK, K. K. MURAMOTI, C. E. HUGHES (NASA, Lewis Research Center, Cleveland, OH), and R. LEVY (Scientific Research Associates, Inc., Glastonbury, CT) American Institute of Aeronautics and Astronautics, Aerospace Sciences Meeting, 23rd, Reno, NV, Jan. 14-17, 1985. 21 p. Previously announced in STAR as N85-15688. refs
(AIAA PAPER 85-0380)

Rehabilitation and extention of the capability of the altitude wind tunnel (AWT) was analyzed. The analytical modelling program involves the use of advanced axisymmetric and three dimensional viscous analyses to compute the flow through the various AWT components. Results for the analytical modelling of the high speed leg aerodynamics are presented; these include: an evaluation of the flow quality at the entrance to the test section, an investigation of the effects of test section bleed for different model blockages, and an examination of three dimensional effects in the diffuser due to reentry flow and due to the change in cross sectional shape of the exhaust scoop. E.A.K.

A85-28899*# National Aeronautics and Space Administration. Lewis Research Center, Cleveland, Ohio.
FEEDBACK IN SEPARATED FLOWS OVER SYMMETRIC AIRFOILS
H. M. ATASSI (NASA, Lewis Research Center, Cleveland, OH; Notre Dame, University, Notre Dame, IN) American Institute of Aeronautics and Astronautics and NASA, Aeroacoustics Conference, 9th, Williamsburg, VA, Oct. 15-17, 1984. 14 p. NASA-USAF-supported research. Previously announced in STAR as N84-31091. refs
(AIAA PAPER 84-2297)

For a flow over an airfoil with laminar separation, a feedback cycle may exist whereby a Kelvin-Helmholtz instability wave emanating from the separation point on the airfoil surface grows along the shear layer and is diffracted as it interacts with the sharp trailing edge of the airfoil, causing acoustic radiation which , in turn, propagates upstream and regenerates the initial instability wave. The analysis is restricted to the high frequency limit. Solutions to the boundary-value problem are obtained using the slowly varying approximation and the method of matched asymptotic expansions. Resonant solutions exist for certain discrete values of the Reynolds and Strouhal numbers. The results are discussed and compared with available data. Author

A85-29126*# National Aeronautics and Space Administration. Lewis Research Center, Cleveland, Ohio.
REVIEW - COMPUTATIONAL METHODS FOR INTERNAL FLOWS WITH EMPHASIS ON TURBOMACHINERY
W. D. MCNALLY and P. M. SOCKOL (NASA, Lewis Research Center, Cleveland, OH) ASME, Transactions, Journal of Fluids Engineering (ISSN 0098-2202), vol. 107, March 1985, p. 6-22. Previously announced in STAR as N82-13113. refs

Current computational methods for analyzing flows in turbomachinery and other related internal propulsion components are presented. The methods are divided into two classes. The inviscid methods deal specifically with turbomachinery applications. Viscous methods, deal with generalized duct flows as well as flows in turbomachinery passages. Inviscid methods are categorized into the potential, stream function, and Euler approaches. Viscous methods are treated in terms of parabolic, partially parabolic, and elliptic procedures. Various grids used in association with these procedures are also discussed. Author

A85-29259*# Pennsylvania State Univ., University Park.
COMPUTATION OF THREE-DIMENSIONAL VISCOUS FLOWS USING A SPACE-MARCHING METHOD
K. N. S. MURTHY and B. LAKSHMINARAYANA (Pennsylvania State University, University Park, PA) Journal of Aircraft (ISSN 0021-8669), vol. 22, April 1985, p. 311-317. Previously cited in issue 17, p. 2418, Accession no. A84-36971. refs
(Contract NSG-3266)

A85-30175* Virginia Polytechnic Inst. and State Univ., Blacksburg.
VORTEX INDUCED LIFT ON A FLAT PLATE WITH A CURVED FORWARD-FACING FLAP
S. TANVEER (Virginia Polytechnic Institute and State University, Blacksburg, VA; California Institute of Technology, Pasadena, CA) Studies in Applied Mathematics (ISSN 0022-2526), vol. 72, April 1985, p. 173-187. Navy-supported research. refs
(Contract NAG3-179)

Free streamline solutions are obtained for two-dimensional inviscid incompressible flow past a flat plate with a forward-facing curved flap. It is shown that it is possible to shape the curved flap to make the adverse pressure gradient on top of the flap less severe than for a straight flap and thus increase the prospects of making the flow experimentally realizable. Author

A85-32961*# National Aeronautics and Space Administration. Lewis Research Center, Cleveland, Ohio.
ASSESSMENT OF THREE-DIMENSIONAL INVISCID CODES AND LOSS CALCULATIONS FOR TURBINE AERODYNAMIC COMPUTATIONS
L. A. POVINELLI (NASA, Lewis Research Center, Cleveland, OH) ASME, Transactions, Journal of Engineering for Gas Turbines and Power (ISSN 0022-0825), vol. 107, April 1985, p. 265-275; Discussion, p. 275, 276; Author's Closure, p. 276. Previously announced in STAR as N84-16142. refs
(ASME PAPER 84-GT-187)

An assessment of several three dimensional inviscid turbine aerodynamic computer codes and loss models used at the NASA Lewis Research Center is presented. Five flow situations are examined, for which both experimental data and computational results are available. The five flows form a basis for the evaluation of the computational procedures. It was concluded that stator flows may be calculated with a high degree of accuracy, whereas, rotor flow fields are less accurately determined. Exploitation of contouring, leaning, bowing, and sweeping will require a three dimensional viscous analysis technique. Author

A85-32963*# National Aeronautics and Space Administration. Lewis Research Center, Cleveland, Ohio.
INVESTIGATION OF FLOW PHENOMENA IN A TRANSONIC FAN ROTOR USING LASER ANEMOMETRY
A. J. STRAZISAR (NASA, Lewis Research Center, Cleveland, OH) ASME, Transactions, Journal of Engineering for Gas Turbines and Power (ISSN 0022-0825), vol. 107, April 1985, p. 427-435. Previously announced in STAR as N84-17143. refs
(ASME PAPER 84-GT-199)

Several flow phenomena including flowfield periodicity, rotor shock oscillation, and rotor shock system geometry were investigated in a transonic low aspect ratio fan rotor using laser anemometry. Flow periodicity is found to increase with increasing rotor pressure rise, and to correlate with blade geometry variations. Analysis of time-accurate laser anemometer data indicates that the rotor shock oscillates about its mean location with an amplitude of 3 to 4 percent of rotor chord. The shock surface is nearly two-dimensional for levels of rotor pressure rise at and above the peak efficiency level but becomes more complex for lower levels of pressure rise. Spanwise shock lean generates radial flows due to streamline deflection in the hub-to-shroud streamsurface. Author

A85-32964*# National Aeronautics and Space Administration. Lewis Research Center, Cleveland, Ohio.
DESIGN AND PERFORMANCE OF A FIXED, NONACCELERATING GUIDE VANE CASCADE THAT OPERATES OVER AN INLET FLOW ANGLE RANGE OF 60 DEG
J. M. SANZ (NASA, Lewis Research Center, Cleveland, OH; *Universities Space Research Association, Columbia, MD*), E. R. MCFARLAND, N. L. SANGER, T. F. GELDER, and R. H. CAVICCHI (NASA, Lewis Research Center, Cleveland, OH) ASME, Transactions, Journal of Engineering for Gas Turbines and Power (ISSN 0022-0825), vol. 107, April 1985, p. 477-484. Previously announced in STAR as N84-14120. refs
(ASME PAPER 84-GT-75)

A unique set of wind tunnel guide vanes are designed with an inverse design code and analyzed with a panel method and an integral boundary layer code developed at the NASA Lewis Research Center. The fixed guide vanes, 80 feet long with 6-foot chord length, were designed for the NASA Ames 40 x 80/80 x 120 ft Wind Tunnel. Low subsonic flow is accepted over a 60 deg range of inlet angle from either the 40 x 80 leg or the 80 x 120 leg of the wind tunnel, and directed axially into the main leg of the tunnel where drive fans are located. Experimental tests of 1/10-scale models were conducted to verify design calculations. Author

A85-32965*# Iowa State Univ. of Science and Technology, Ames.
A NOTE ON BLADE WAKE INTERACTION INFLUENCE ON COMPRESSOR STATOR ROW AERODYNAMIC PERFORMANCE
T. H. OKIISHI, J. L. HANSEN (Iowa State University of Science and Technology, Ames, IA), and M. D. HATHAWAY (U.S. Army, Propulsion Laboratory, Cleveland, OH) ASME, Transactions, Journal of Engineering for Gas Turbines and Power (ISSN 0022-0825), vol. 107, April 1985, p. 549-551. refs
(Contract F49620-83-K-0023; NAG3-356)

Attention is given to the effect of blade wake interactions on the performance of an axial flow compressor's stator row, for the case of compressor and fan stator flows without shocks. The measured midspan loss of total pressure can be related to stator surface boundary layers, the chopped rotor wakes passing through the stator row, and the interaction between these flows. The interaction between rotor blade wake segments and stator blade surface boundary layers generates much higher losses than expected in both the stator wake and in the region of flow between stator boundary layers/wakes, if interaction effects are ignored. O.C.

A85-39728*# National Aeronautics and Space Administration. Lewis Research Center, Cleveland, Ohio.
APPLICATION OF RUNGE KUTTA TIME MARCHING SCHEME FOR THE COMPUTATION OF TRANSONIC FLOWS IN TURBOMACHINES
S. V. SUBRAMANIAN (NASA, Lewis Research Center, Cleveland, OH; Avco Corp., Avco Lycoming Div., Stratford, CT) and R. BOZZOLA (Avco Corp., Avco Lycoming Div., Stratford, CT) AIAA, SAE, ASME, and ASEE, Joint Propulsion Conference, 21st, Monterey, CA, July 8-10, 1985. 8 p. refs
(AIAA PAPER 85-1332)

Numerical solutions of the unsteady Euler equations are obtained using the classical fourth order Runge Kutta time marching scheme. This method is fully explicit and is applied to the governing equations in the finite volume, conservation law form. In order to determine the efficiency of this scheme for solving turbomachinery flows, steady blade-to-blade solutions are obtained for compressor and turbine cascades under subsonic and transonic flow conditions. Computed results are compared with other numerical methods and wind tunnel measurements. The present study also focuses on other important numerical aspects influencing the performance of the algorithm and the solution accuracy such as grid types, boundary conditions, and artificial viscosity. For this purpose, H, O, and C type computational grids as well as characteristic and extrapolation type boundary conditions are included in the solution procedure. Author

A85-39767*# National Aeronautics and Space Administration. Lewis Research Center, Cleveland, Ohio.
CALCULATION OF THREE-DIMENSIONAL, VISCOUS FLOW THROUGH TURBOMACHINERY BLADE PASSAGES BY PARABOLIC MARCHING
T. KATSANIS (NASA, Lewis Research Center, Cleveland, OH) AIAA, SAE, ASME, and ASEE, Joint Propulsion Conference, 21st, Monterey, CA, July 8-10, 1985. 14 p. Previously announced in STAR as N85-23711. refs
(AIAA PAPER 85-1408)

The three-dimensional compressible Navier-Stokes equations are formulated in a rotating coordinate system, so as to include centrifugal and Coriolis forces. The equations are parabolized by using a previously calculated inviscid static pressure field. The thin layer Navier-Stokes approximation, which neglects streamwise diffusion, is used. A body-fitted coordinate system is used. The streamwise momentum equation is uncoupled from the cross-stream momentum equation by using contravariant momentum components, and then using the contravariant velocity components as primary unknowns. To reduce problems with small separating regions, the Reyhner and Flugge-Lotz approximation is used. The energy equation is included to allow for calculation of heat transfer. The flow may be laminar, or a simple eddy-viscosity turbulence may be used. A number of curved ducts and an axial stator were analyzed, including cases for which experimental data are available. Author

A85-40691*# Washington Univ., Seattle.
AN EXPERIMENTAL STUDY OF THREE-DIMENSIONAL SHOCK WAVE/TURBULENT BOUNDARY LAYER INTERACTIONS IN A SUPERSONIC FLOW
J. H. CHOU, M. E. CHILDS (Washington, University, Seattle), and R. S. WONG (TRW, Inc., Redondo Beach, CA) American Institute of Aeronautics and Astronautics, Fluid Dynamics and Plasmadynamics and Lasers Conference, 18th, Cincinnati, OH, July 16-18, 1985. 9 p. refs
(Contract NAG3-256)
(AIAA PAPER 85-1566)

Wall static pressure distributions, surface flow patterns, pitot pressures, and yaw angle profiles were measured in a skewed three-dimensional shock wave/turbulent boundary layer interaction region. The test section was axisymmetric with a constant diameter. The nominal freestream Mach number was 4. Upstream of the interaction, the boundary layer thickness was 0.31 in. (0.787 cm). The three-dimensional flow was produced by azimuthal pressure gradients which were generated by an 8-degree cone aligned with the primary flow direction, but with the cone axis displaced 0.3 in. (0.76 cm) from the channel centerline. The yaw angle was found to be a function of both the azimuthal angle and the distance from the beginning of the interaction. It was observed that yaw angle increased substantially near the wall. The maximum yaw angle for the whole flow field was obtained in the 90 degree azimuthal plane. Author

A85-40817*# Douglas Aircraft Co., Inc., Long Beach, Calif.
CALCULATION OF COMPRESSIBLE FLOW ABOUT THREE-DIMENSIONAL INLETS WITH AUXILIARY INLETS, SLATS AND VANES BY MEANS OF A PANEL METHOD
J. L. HESS, D. M. FRIEDMAN, and R. W. CLARK (Douglas Aircraft Co., Long Beach, CA) AIAA, SAE, ASME, and ASEE, Joint Propulsion Conference, 21st, Monterey, CA, July 8-10, 1985. 9 p. refs
(Contract NAS3-22250)
(AIAA PAPER 85-1196)

An efficient and user-oriented method has been constructed for calculating flow in and about complex inlet configurations. Efficiency is attained by: the use of a panel method, a technique of superposition for obtaining solutions at any inlet operating condition, and employment of an advanced matrix-iteration technique for solving large full systems of equations, including the nonlinear equations for the Kutta condition. User concerns are addressed by the provision of several novel graphical output options that, taken together, yield a more complete comprehension of the flowfield than had been possible previously. Examples of these features are presented for some complicated configurations, and where possible, comparisons are made between calculation and experiment. Author

A85-40819*# Douglas Aircraft Co., Inc., Long Beach, Calif.
LOW-SPEED AERODYNAMIC TEST OF AN AXISYMMETRIC SUPERSONIC INLET WITH VARIABLE COWL SLOT
A. G. POWELL, H. R. WELGE (Douglas Aircraft Co., Long Beach, CA), and C. J. TREFNY (NASA, Lewis Research Center, Cleveland, OH) AIAA, SAE, ASME, and ASEE, Joint Propulsion Conference, 21st, Monterey, CA, July 8-10, 1985. 5 p. Previously announced in STAR as N85-26710.
(AIAA PAPER 85-1210)

The experimental low-speed aerodynamic characteristics of an axisymmetric mixed-compression supersonic inlet with variable cowl slot are described. The model consisted of the NASA P-inlet centerbody and redesigned cowl with variable cowl slot powered by the JT8D single-stage fan simulator and driven by an air turbine. The model was tested in the NASA Lewis Research Center 9- by 15-foot low-speed tunnel at Mach numbers of 0, 0.1, and 0.2 over a range of flows, cowl slot openings, centerbody positions, and angles of attack. The variable cowl slot was effective in minimizing lip separation at high velocity ratios, showed good steady-state and dynamic distortion characteristics, and had good angle-of-attack tolerance. Author

A85-41814* Politecnico di Torino (Italy).
TIME DEPENDENT COMPUTATION OF THE EULER EQUATIONS FOR DESIGNING 2-D CASCADES, INCLUDING THE CASE OF TRANSONIC SHOCK FREE DESIGN
L. ZANNETTI (Torino, Politecnico, Turin, Italy) IN: 1983 Tokyo International Gas Turbine Congress, Tokyo, Japan, October 23-29, 1983, Proceedings. Volume 2 . Tokyo, Gas Turbine Society of Japan, 1984, p. 423-429. refs
(Contract NAS3-22772)

A numerical method to solve the inverse problem for airfoil cascades is described. The case of compressible, inviscid flow is considered. The proposed method is based on the finite difference approximation of the time-dependent Euler equations. Numerical examples show the capability of the method to design subsonic or transonic shockless blades. Author

A85-41826* Cincinnati Univ., Ohio.
THE THREE-DIMENSIONAL COMPRESSIBLE FLOW IN A RADIAL INFLOW TURBINE SCROLL
A. HAMED, W. TABAKOFF, and M. MALAK (Cincinnati, University, OH) IN: 1983 Tokyo International Gas Turbine Congress, Tokyo, Japan, October 23-29, 1983, Proceedings. Volume 2 . Tokyo, Gas Turbine Society of Japan, 1984, p. 515-521. refs
(Contract NAG3-52; NAG3-26)

This work presents the results of an analytical study and an experimental investigation of the three-dimensional flow in a turbine scroll. The finite element method is used in the iterative numerical solution of the locally linearized governing equations for the three-dimensional velocity potential field. The results of the numerical computations are compared with the experimental measurements in the scroll cross sections, which were obtained using laser Doppler velocimetry and hot wire techniques. The results of the computations show a variation in the flow conditions around the rotor periphery which was found to depend on the scroll geometry. Author

A85-42954*# Grumman Aerospace Corp., Bethpage, N.Y.
THE COMPUTATION OF VISCID/INVISCID INTERACTION ON AIRFOILS WITH SEPARATED FLOW
R. E. MELNIK and J. W. BROOK (Grumman Research and Development Center, Bethpage, NY) IN: Symposium on Numerical and Physical Aspects of Aerodynamic Flows, 3rd, Long Beach, CA, January 21-24, 1985, Proceedings . Long Beach, CA, California State University, 1985, p. 1-21 to 1-37. Research supported by the Grumman Aerospace Independent Research and Development Program. refs
(Contract NAS3-24082)

Attention is given to the computation of viscous subsonic and transonic flow over two-dimensional airfoils at high Reynolds numbers, where the boundary layers are thin and turbulent over most of the airfoil and its wake. An attempt is made to develop a fast viscid/inviscid interaction method for the computation of viscous flows over airfoils with extensive low separation regions, which can be used as the basis of predictions of the stalling characteristics of airfoils with reasonable accuracy. These insights are applied in the form of changes to the GRUMFOIL computer code, in order to improve separated flow prediction capabilities. O.C.

A85-42988*# National Aeronautics and Space Administration. Langley Research Center, Hampton, Va.
A THREE-DIMENSIONAL BOUNDARY-LAYER ANALYSIS INCLUDING HEAT-TRANSFER AND BLADE-ROTATION EFFECTS
V. N. VATSA (NASA, Langley Research Center, Hampton, VA) IN: Symposium on Numerical and Physical Aspects of Aerodynamic Flows, 3rd, Long Beach, CA, January 21-24, 1985, Proceedings . Long Beach, CA, California State University, 1985, p. 10-45 to 10-59. refs
(Contract NAS3-23716)

An analysis has been developed for calculating three-dimensional viscous flows over arbitrary bodies through the solution of complete three-dimensional boundary-layer equations. The governing equations include the effect of blade rotation and are written in nonorthogonal surface-fitted coordinates to allow maximum flexibility. A coupled finite-difference numerical scheme is used for solving the governing equations. The accuracy of this scheme has been assessed through comparisons with known analytical/experimental results for several test cases. The present analysis has then been applied to compute viscous flows over a turbine endwall and airfoil suction surface, and fairly good correlation has been obtained with available experimental data for surface heat transfer and viscous streamline skewing. Author

A85-43974*# Army Propulsion Lab., Cleveland, Ohio.
ROTOR WAKE CHARACTERISTICS OF A TRANSONIC AXIAL FLOW FAN
M. D. HATHAWAY (U.S. Army, Propulsion Laboratory, Cleveland, OH), J. GERTZ, A. EPSTEIN (MIT, Cambridge, MA), and A. J. STRAZISAR (NASA, Lewis Research Center, Cleveland, OH) AIAA, SAE, ASME, and ASEE, Joint Propulsion Conference, 21st, Monterey, CA, July 8-10, 1985. 12 p. refs
(AIAA PAPER 85-1133)

State of the art turbomachinery flow analysis codes are not capable of predicting the viscous flow features within turbomachinery blade wakes. Until efficient 3D viscous flow analysis codes become a reality there is therefore a need for models which can describe the generation and transport of blade wakes and the mixing process within the wake. To address the need for experimental data to support the development of such models, high response pressure measurements and laser anemometer velocity measurements have been obtained in the wake of a transonic axial flow fan rotor. Author

A85-43977*# National Aeronautics and Space Administration. Lewis Research Center, Cleveland, Ohio.
INVISCID ANALYSIS OF ADVANCED TURBOPROP PROPELLER FLOW FIELDS
J. M. BARTON, O. YAMAMOTO (Sverdrup Technology, Inc., Middleburg Heights, OH), and L. J. BOBER (NASA, Lewis Research Center, Cleveland, OH) AIAA, SAE, ASME, and ASEE, Joint Propulsion Conference, 21st, Monterey, CA, July 8-10, 1985. 12 p. refs
(Contract NAS3-24105)
(AIAA PAPER 85-1263)

A three-dimensional Euler code, previously developed for high speed propellers, was rewritten and vectorized for the Cray computer. Calculations were compared with previous results and measurements. The new code requires less memory and is more than two times faster than its predecessor. The new boundary conditions produced more accurate results and improved stability. The accuracy and stability characteristics also resulted in reduced manual intervention required to obtain solutions. The code is a useful tool for examining the fluid dynamics and performance of propellers. Author

A85-47023*# National Aeronautics and Space Administration. Lewis Research Center, Cleveland, Ohio.
APPLICATION OF COMPUTATIONAL FLUID DYNAMICS TO COMPLEX INLET DUCTS
C. E. TOWNE (NASA, Lewis Research Center, Cleveland, OH) and E. F. SCHUM (Rockwell International Corp., Columbus, OH) AIAA, SAE, ASME, and ASEE, Joint Propulsion Conference, 21st, Monterey, CA, July 8-10, 1985. 14 p. Previously announced in STAR as N85-30247. refs
(AIAA PAPER 85-1213)

A three-dimensional parabolic Navier-Stokes code, PEPSIG, was used to analyze the flow in the subsonic diffuser section of a typical modern inlet design. The effect of curvature of the diffuser centerline and transitioning cross sections was studied to determine the primary cause of flow distortion in the duct. Total pressure values at the engine compressor face are reported. M. G.

A85-47025*# National Aeronautics and Space Administration. Lewis Research Center, Cleveland, Ohio.
WIND TUNNEL RESULTS OF ADVANCED HIGH SPEED PROPELLERS IN THE TAKEOFF, CLIMB, AND LANDING OPERATING REGIMES
G. L. STEFKO and R. J. JERACKI (NASA, Lewis Research Center, Cleveland, OH) AIAA, SAE, ASME, and ASEE, Joint Propulsion Conference, 21st, Monterey, CA, July 8-10, 1985. 22 p. Previously announced in STAR as N85-29925. refs
(AIAA PAPER 85-1259)

Low speed wind tunnel performance tests of two advanced propellers were completed. The 62.2 cm diameter adjustable pitch models were tested at Mach numbers typical of takeoff, initial climbout, and landing speeds in the 10 by 10 ft Supersonic Wind

Tunnel. Both models had eight blades and a cruise design point operating condition of 0.80 Mach number, 10.668 km S.A. altitude, 243.8 m/s tip speed and a high power loading of 301 kW sq m. No adverse or unusual low speed operating conditions were found during the test with either the straight blade SR-2 or the 45 deg swept SR-3 propellers. The 45 deg swept propeller efficiency exceeded the straight blade efficiency by 4 to 5 percent. Typical net efficiencies of the straight and 45 deg swept propeller at a Mach 0.20 takeoff condition were 50.2 and 54.9 percent respectively. At a Mach 0.34 climb condition, the efficiencies were 53.7 and 59.1 percent. Reverse thrust data indicates that these propellers are capable of producing more reverse thrust at Mach 0.20 than a high bypass turbofan engine at Mach 0.20. E.A.K.

A85-48539*# National Aeronautics and Space Administration. Lewis Research Center, Cleveland, Ohio.
INVISCID AND VISCOUS FLOWS IN CASCADES WITH AN EXPLICIT MULTIPLE-GRID ALGORITHM
R. V. CHIMA (NASA, Lewis Research Center, Cleveland, OH) AIAA Journal (ISSN 0001-1452), vol. 23, Oct. 1985, p. 1556-1563. Previously cited in issue 17, p. 2427, Accession no. A84-38043. refs

A85-50106* National Aeronautics and Space Administration. Lewis Research Center, Cleveland, Ohio.
NOISE CONSTRAINTS EFFECTING OPTIMAL PROPELLER DESIGNS
C. J. MILLER (NASA, Lewis Research Center, Cleveland, OH) and J. P. SULLIVAN (Purdue University, West Lafayette, IN) SAE, General Aviation Aircraft Meeting and Exposition, Wichita, KS, Apr. 16-19, 1985. 11 p. Previously announced in STAR as N85-19923. refs
(SAE PAPER 850871)

A preliminary design tool for advanced propellers was developed combining a fast vortex lattice aerodynamic analysis, a fast subsonic point source noise analysis, and an optimization scheme using a conjugate directions method. Twist, chord and sweep distributions are optimized to simultaneously improve both the aerodynamic performance and the noise observed at a fixed relative position. The optimal noise/performance tradeoffs for straight and advanced concept blades are presented. The techniques used include increasing the blade number, blade sweep, reducing the rotational speed, shifting the spanwise loading and diameter changes. E.A.K.

N85-10919*# Ohio State Univ., Columbus.
DESIGN AND WIND TUNNEL EVALUATION OF A SYMMETRIC AIRFOIL SERIES FOR LARGE WIND TURBINE APPLICATIONS Final Report
G. M. GREGOREK May 1984 27 p refs
(Contract NAG3-330; DE-AI01-76ET-20320)
(NASA-CR-174764; DOE/NASA/0330-1; NAS 1.26:174764)
Avail: NTIS HC A03/MF A01 CSCL 01A

A family of symmetric airfoils with thickness to chord ratios of 0.21, 0.25, and 0.29 was designed for applications to large wind turbines using the Eppler analytic design methodology. The airfoil series, designed for Reynolds numbers above 4x1,000,000, has a contour that maintains its thickness to the 0.7 chord position, allowing use of a deep aft spar for structural integrity. Wind tunnel tests of the 21 percent thick airfoil conducted in the Ohio State University Airfoil Test Facilities at $M = 0.25$ and $Re = 2, 4$ and 8x1,000,000 showed good agreement with predicted surface pressures and lift and drag coefficients when the angle of attack was low and the Reynolds number was 8x1,000,000. At the lowest Reynolds number, both the measured lift curve slope and the maximum lift coefficient differ significantly from theory. In the post stall region, agreement with theory and experiment is poor, at all Reynolds numbers, verifying the need for improved analytic methods in this important flow regime. Author

N85-12008*# GMAF, Inc., Freeport, N.Y.
INVERSE DESIGN TECHNIQUE FOR CASCADES Final Report
L. ZANNETTI and M. PANDOLFI Washington NASA Nov. 1984 33 p refs
(Contract NAS3-22772)
(NASA-CR-3836; E-2275; NAS 1.26:3836) Avail: NTIS HC A03/MF A01 CSCL 01A

A numerical technique to generate cascades is presented. The basic prescribed parameters are: inlet angle, exit pressure, and distribution of blade thickness and lift along a blade. Other sets of parameters are also discussed. The technique is based on the lambda scheme. The problem of stability of the computation as a function of the prescribed set of parameters and the treatment of boundary conditions is discussed. A one dimensional analysis to indicate a possible way for assuring stability for any two dimensional calculation is provided. E.A.K.

N85-12036*# National Aeronautics and Space Administration. Lewis Research Center, Cleveland, Ohio.
MODEL EQUATION FOR SIMULATING FLOWS IN MULTISTAGE TURBOMACHINERY
J. J. ADAMCZYK Nov. 1984 37 p refs
(NASA-TM-86869; E-2291; NAS 1.15:86869) Avail: NTIS HC A03/MF A01 CSCL 01A

A steady, three-dimensional average-passage equation system is derived for use in simulating multistage turbomachinery flows. These equations describe a steady, viscous flow that is periodic from blade passage to blade passage. From this system of equations, various reduced forms can be derived for use in simulating the three-dimensional flow field within multistage machinery. It is suggested that a properly scaled form of the average-passage equation system would provide an improved mathematical model for simulating the flow in multistage machines at design and, in particular, at off-design conditions. Author

N85-12039*# National Aeronautics and Space Administration. Lewis Research Center, Cleveland, Ohio.
INCOMPRESSIBLE LIFTING-SURFACE AERODYNAMICS FOR A ROTOR-STATOR COMBINATION
S. M. RAMACHANDRA Oct. 1984 32 p refs
(NASA-TM-83767; E-2258; NAS 1.15:83767) Avail: NTIS HC A03/MF A01 CSCL 01A

Current literature on the three dimensional flow through compressor cascades deals with a row of rotor blades in isolation. Since the distance between the rotor and stator is usually 10 to 20 percent of the blade chord, the aerodynamic interference between them has to be considered for a proper evaluation of the aerothermodynamic performance of the stage. A unified approach to the aerodynamics of the incompressible flow through a stage is presented that uses the lifting surface theory for a compressor cascade of arbitrary camber and thickness distribution. The effects of rotor stator interference are represented as a linear function of the rotor and stator flows separately. The loading distribution on the rotor and stator flows separately. The loading distribution on the rotor and stator blades and the interference factor are determined concurrently through a matrix iteration process. Author

N85-14798*# National Aeronautics and Space Administration. Lewis Research Center, Cleveland, Ohio.
A THREE-DIMENSIONAL AXISYMMETRIC CALCULATION PROCEDURE FOR TURBULENT FLOWS IN A RADIAL VANELESS DIFFUSER
L. F. SCHUMANN 1984 17 p refs Proposed for presentation at the 30th Intern. Gas Turbine Conf. and Exhibit, Houston, Tex., 17-21 Mar. 1985; sponsored by the American Society of Mechanical Engineers
(NASA-TM-86903; E-2387; NAS 1.15:86903; USAAVSCOM-TR-84-C-21; AD-A157113) Avail: NTIS HC A02/MF A01 CSCL 01A

An analytical model is proposed to calculate the three-dimensional axisymmetric turbulent flowfield in a radial vaneless diffuser. The model assumes that the radial and tangential

boundary layer profiles are approximated by power law profiles. Then, using the integrated radial and tangential momentum and continuity equations for the boundary layer and corresponding inviscid equations for the core flow, there results six ordinary differential equation in six unknowns which are easily solved using a Runge-Kutta technique. A model is also proposed for fully developed flow. The results using this technique were compared with the results from a three-dimensional viscous, axisymmetric duct code and with experimental data and good quantitative agreement was obtained. Author

N85-15688*# National Aeronautics and Space Administration. Lewis Research Center, Cleveland, Ohio.
ANALYTICAL MODELING OF CIRCUIT AERODYNAMICS IN THE NEW NASA LEWIS WIND TUNNEL
C. E. TOWNE, L. A. POVINELLI, W. G. KUNIK, K. K. MURAMOTO, C. E. HUGHES, and R. LEVY (Scientific Research Associates) 1985 22 p refs Presented at the 23rd Aerospace Sci. Meeting, Reno, Nev., 14-17 Jan. 1985; sponsored by AIAA
(NASA-TM-86912; E-2405; NAS 1.15:86912; AIAA-85-0380) Avail: NTIS HC A02/MF A01 CSCL 01A

Rehabilitation and extention of the capability of the altitude wind tunnel (AWT) was analyzed. The analytical modeling program involves the use of advanced axisymmetric and three dimensional viscous analyses to compute the flow through the various AWT components. Results for the analytical modeling of the high speed leg aerodynamics are presented; these include: an evaluation of the flow quality at the entrance to the test section, an investigation of the effects of test section bleed for different model blockages, and an examination of three dimensional effects in the diffuser due to reentry flow and due to the change in cross sectional shape of the exhaust scoop. E.A.K.

N85-15689*# *National Aeronautics and Space Administration.* Lewis Research Center, Cleveland, Ohio.
UNSTEADY PRESSURE MEASUREMENTS ON A BICONVEX AIRFOIL IN A TRANSONIC OSCILLATING CASCADE
L. M. SHAW, D. R. BOLDMAN, A. E. BUGGELE, and D. H. BUFFUM (Purdue Univ.) 1985 18 p refs Proposed for presentation at the 30th Intern. Gas Turbine Conf. and Exhibit, Houston, Tex., 17-21 Mar. 1985; sponsored by the American Society of Mechanical Engineering
(NASA-TM-86914; E-2408; NAS 1.15:86914) Avail: NTIS HC A02/MF A01 CSCL 01A

Flush-mounted dynamic pressure transducers were installed on the center airfoil of a transonic oscillating cascade to measure the unsteady aerodynamic response as nine airfoils were simultaneously driven to provide 1.2 deg of pitching motion about the midchord. Initial tests were performed at an incidence and angle of 0 deg and A Mach number of 0.65 in order to obtain results in a shock-free compressible flowfield. Subsequent tests were performed at an incidence angle of 7 deg and Mach number of 0.8 in order to observe the surface pressures with an oscillating shock near the leading edge of the airfoil. Results are presented for interblade phase angles of 90 and -90 deg and at blade oscillatory frequencies of 200 and 500 Hz (semi-chord reduced frequencies up to about 0.5 at a Mach number of 0.8). Results from the zero-incidence cascade are compared with a classical unsteady flat-plate analysis. Flow visualization results depicting the shock motion on the airfoils in the high-incidence cascade are discussed. The airfoil pressure data are tabulated. Author

N85-19923*# National Aeronautics and Space Administration. Lewis Research Center, Cleveland, Ohio.
NOISE CONSTRAINTS EFFECTING OPTIMAL PROPELLER DESIGNS
C. J. MILLER and J. P. SULLIVAN 1985 15 p refs To be presented at the Soc. of Automotive Engr. Gen. Aviation Aircraft Meeting and Exposition, Wichita, Kan., 16-19 Apr. 1985
(NASA-TM-86967; E-2449; NAS 1.15:86967) Avail: NTIS HC A02/MF A01 CSCL 01A

A preliminary design tool for advanced propellers was developed combining a fast vortex lattice aerodynamic analysis, a fast subsonic point source noise analysis, and an optimization scheme using a conjugate directions method. Twist, chord and sweep distributions are optimized to simultaneously improve both the aerodynamic performance and the noise observed at a fixed relative position. The optimal noise/performance tradeoffs for straight and advanced concept blades are presented. The techniques used include increasing the blade number, blade sweep, reducing the rotational speed, shifting the spanwise loading and diameter changes. E.A.K.

N85-21114*# National Aeronautics and Space Administration. Lewis Research Center, Cleveland, Ohio.
PRELIMINARY ANALYSIS OF TONE-EXCITED TWO-STREAM JET VELOCITY DECAY
U. H. VONGLAHN 1985 22 p refs Presented at the 109th Meeting of the Acoustical Society of America, Austin, Tex., 8-12 Apr. 1985
(NASA-TM-86951; E-2473; NAS 1.15:86951) Avail: NTIS HC A02/MF A01 CSCL 01A

Acoustic research related to jet flows has established that sound, by amplifying the naturally occuring large-scale structures in turbulent shear layers, can cause a more rapidly decay of the jet plume velocity and temperature and an increase in jet spreading rate. One possible application of this sound-flow interaction phenomenon is to future STOL aircraft that may require modified jet plume characteristics in order to reduce the loads and temperatures on the deflected flaps during take-off and landing operations. The tone-excitation effect on the velocity decay of model-scale, two-stream jet plumes is analyzed. Measured data are correlated in terms of parameters that include excitation sound level and outer-to-inner stream velocity ratio. The effect of plume tone-excitation on far-field jet noise is examined and its implication for large-scale two-stream jets is discussed. A.R.H.

N85-21115*# National Aeronautics and Space Administration. Lewis Research Center, Cleveland, Ohio.
ADVANCED LINER-COOLING TECHNIQUES FOR GAS TURBINE COMBUSTORS
C. T. NORGREN and S. M. RIDDLEBAUGH 1985 21 p refs Proposed for presentation at the 21st Joint Propulsion Conf., Monterey, Calif., 8-10 Jul. 1985; sponsored by AIAA, SAE and ASME
(NASA-TM-86952; E-2475; NAS 1.15:86952) Avail: NTIS HC A02/MF A01 CSCL 21E

Component research for advanced small gas turbine engines is currently underway at the NASA Lewis Research Center. As part of this program, a basic reverse-flow combustor geometry was being maintained while different advanced liner wall cooling techniques were investigated. Performance and liner cooling effectiveness of the experimental combustor configuration featuring counter-flow film-cooled panels is presented and compared with two previously reported combustors featuring: splash film-cooled liner walls; and transpiration cooled liner walls (Lamilloy). Author

N85-21117*# Cornell Univ., Ithaca, N.Y. School of Mechanics and Aerospace Engineering.
A THEORY OF POST-STALL TRANSIENTS IN MULTISTAGE AXIAL COMPRESSION SYSTEMS Final Report
F. K. MOORE and E. M. GREITZER Washington NASA Mar. 1985 115 p refs Prepared in cooperation with M.I.T., Cambridge)
(Contract NAG3-34; NSG-3208)
(NASA-CR-3878; NAS 1.26:3878) Avail: NTIS HC A06/MF A01 CSCL 01A

A theory is presented for post stall transients in multistage axial compressors. The theory leads to a set of coupled first-order ordinary differential equations capable of describing the growth and possible decay of a rotating-stall cell during a compressor mass-flow transient. These changing flow features are shown to have a significant effect on the instantaneous compressor pumping characteristic during unsteady operation, and henace on the overall system behavior. It is also found from the theory that the ultimate mode of system response, stable rotating stall or surge, depends

not only on the B parameter but also on other parameters, such as the compressor length-to-diameter ratio. Small values of this latter quantity tend to favor the occurrence of surge, as do large values of B. A limited parametric study is carried out to show the impact of the different system features on transient behavior. Based on analytical and numerical results, several specific topics are suggested for future research on post-stall transients. M.G.

N85-22368*# Hamilton Standard, Windsor Locks, Conn.
LARGE-SCALE ADVANCED PROPFAN (LAP) PERFORMANCE, ACOUSTIC AND WEIGHT ESTIMATION, JANUARY, 1984
D. PARZYCH, A. SHENKMAN, and S. COHEN Feb. 1985 61 p (Contract NAS3-23051)
(NASA-CR-174782; NAS 1.26:174782; SP-06A83) Avail: NTIS HC A04/MF A01 CSCL 01A

In comparison to turbo-prop applications, the Prop-Fan is designed to operate in a significantly higher range of aircraft flight speeds. Two concerns arise regarding operation at very high speeds: aerodynamic performance and noise generation. This data package covers both topics over a broad range of operating conditions for the eight (8) bladed SR-7L Prop-Fan. Operating conditions covered are: Flight Mach Number 0 - 0.85; blade tip speed 600-800 ft/sec; and cruise power loading 20-40 SHP/D2. *Prop-Fan weight and weight scaling estimates are also included.* Author

N85-23711*# National Aeronautics and Space Administration. Lewis Research Center, Cleveland, Ohio.
CALCULATION OF THREE-DIMENSIONAL, VISCOUS FLOW THROUGH TURBOMACHINERY BLADE PASSAGES BY PARABOLIC MARCHING
T. KATSANIS 11 Jul. 1985 29 p refs Proposed for presentation at 21st Joint Propulsion Conf., Monterey, Calif., 8-11 Jul. 1985; sponsored by AIAA, SAE and ASME
(NASA-TM-86984; E-2527; NAS 1.15:86984) Avail: NTIS HC A03/MF A01 CSCL 01A

The three-dimensional compressible Navier-Stokes equations are formulated in a rotating coordinate system, so as to include centrifugal and Coriolis forces. The equations are parabolized by using a previously calculated inviscid static pressure field. The thin layer Navier-Stokes approximation, which neglects streamwise diffusion, is used. A body-fitted coordinate system is used. The streamwise momentum equation is uncoupled from the cross-stream momentum equation by using contravariant momentum components, and then using the contravariant velocity components as primary unknowns. To reduce problems with small separated regions, the Reyhner and Flugge-Lotz approximation is used. The energy equation is included to allow for calculation of heat transfer. The flow may be laminar, or a simple eddy-viscosity turbulence may be used. A number of curved ducts and an axial stator were analyzed, including cases for which experimental data are available. Author

N85-26668*# General Electric Co., Cincinnati, Ohio. Aircraft Engine Business Group.
DEVELOPMENT OF A ROTOR WAKE-VORTEX MODEL, VOLUME 1 *Final Technical Report*
R. K. MAJJIGI and P. R. GLIEBE Jun. 1984 171 p refs (Contract NAS3-23681)
(NASA-CR-174849; NAS 1.26:174849) Avail: NTIS HC A08/MF A01 CSCL 01A

Certain empirical rotor wake and turbulence relationships were developed using existing low speed rotor wave data. A tip vortex model was developed by replacing the annulus wall with a row of image vortices. An axisymmetric turbulence spectrum model, developed in the context of rotor inflow turbulence, was adapted to predicting the turbulence spectrum of the stator gust upwash. G.L.C.

N85-26670*# National Aeronautics and Space Administration. Lewis Research Center, Cleveland, Ohio.
AERODYNAMIC DETUNING ANALYSIS OF AN UNSTALLED SUPERSONIC TURBOFAN CASCADE
D. HOYNIAK and S. FLEETER 21 Mar. 1985 25 p refs Presented at the 30th Intern. Gas Turbine Conf. and Exhibit, Houston, Tex., 17-21 Mar. 1985; sponsored by ASME
(NASA-TM-87001; E-2546; NAS 1.15:87001) Avail: NTIS HC A02/MF A01 CSCL 01A

An approach to passive flutter control is aerodynamic detuning, defined as designed passage-to-passage differences in the unsteady aerodynamic flow field of a rotor blade row. Thus, aerodynamic detuning directly affects the fundamental driving mechanism for flutter. A model to demonstrate the enhanced supersonic aeroelastic stability associated with aerodynamic detuning is developed. The stability of an aerodynamically detuned cascade operating in a supersonic inlet flow field with a subsonic leading edge locus is analyzed, with the aerodynamic detuning accomplished by means of nonuniform circumferential spacing of adjacent rotor blades. The unsteady aerodynamic forces and moments on the blading are defined in terms of influence coefficients in a manner that permits the stability of both a conventional uniformally spaced rotor configuration as well as the detuned nonuniform circumferentially spaced rotor to be determined. With Verdon's uniformly spaced Cascade B as a baseline, this analysis is then utilized to demonstrate the potential enhanced aeroelastic stability associated with this particular type of aerodynamic detuning. Author

N85-29916*# Toledo Univ., Ohio. Dept. of Mechanical Engineering.
AERODYNAMIC ANALYSIS OF A HORIZONTAL AXIS WIND TURBINE BY USE OF HELICAL VORTEX THEORY. VOLUME 1: THEORY Final Report
D. R. JENG, T. G. KEITH, JR., and A. ALIAKBARKHANAFJEH Dec. 1982 88 p refs
(Contract NCC3-5; DE-AI01-76ET-20320)
(NASA-CR-168054; DOE/NASA/0005-1; NAS 1.26:168054)
Avail: NTIS HC A05/MF A01 CSCL 01A

The theoretical development of a method of analysis for prediction of the aerodynamic performance of horizontal axis wind turbines is presented. The method is based on the assumption that a helical vortex emanates from each blade element. Collectively these vortices form a vortex system that extends infinitely far downstream of the blade. Velocities induced by this vortex system are found by applying the Biot-Savart law. Accordingly, this method avoids the use of any interference factors which are used in many of the momentum theories. The method can be used to predict the performance of wind turbines with a small number of blades. The wind turbine performance of a two-bladed rotor is determined and compared to existing experimental data and to corresponding values computed from the widely used PROP code. It was found that the present method compared favorably with experimental data, especially for low wind velocities. The wind turbine performance of a single-bladed rotor is determined subject to the condition that there was no lift on the counterweight or support span. Output power for a one-bladed wind turbine was compared to that of a two-bladed machine. R.J.F.

N85-29925*# National Aeronautics and Space Administration. *Lewis Research Center, Cleveland, Ohio.*
WIND TUNNEL RESULTS OF ADVANCED HIGH SPEED PROPELLERS IN THE TAKEOFF, CLIMB AND LANDING OPERATING REGIMES
G. L. STEFKO and R. J. JERACKI 1985 23 p refs Prepared for the 21st Joint Propulsion Conf., Monterey, Calif., 8-10 Jul. 1985; sponsored in part by AIAA, SAE, ASME and ASEE Previously announced in IAA as A85-47025
(NASA-TM-87054; E-2621; NAS 1.15:87054; AIAA-85-1259)
Avail: NTIS HC A02/MF A01 CSCL 01A

Low speed wind tunnel performance tests of two advanced propellers were completed. The 62.2 cm diameter adjustable pitch

models were tested at Mach numbers typical of takeoff, initial climbout, and landing speeds in the 10 by 10 ft Supersonic Wind Tunnel. Both models had eight blades and a cruise design point operating condition of 0.80 Mach number, 10.668 km S.A. altitude, 243.8 m/s tip speed and a high power loading of 301 kW sq m. No adverse or unusual low speed operating conditions were found during the test with either the straight blade SR-2 or the 45 deg swept SR-3 propellers. The 45 deg swept propeller efficiency exceeded the straight blade efficiency by 4 to 5%. Typical net efficiencies of the straight and 45 deg swept propeller at a Mach 0.20 takeoff condition were 50.2 and 54.9% respectively. At a Mach 0.34 climb condition, the efficiencies were 53.7 and 59.1%. Reverse thrust data indicates that these propellers are capable of producing more reverse thrust at Mach 0.20 than a high bypass turbofan engine at Mach 0.20. E.A.K.

N85-35158*# Braun (Willis H.), Berea, Ohio.
UNSTEADY FLOW IN A SUPERSONIC CASCADE WITH TWO IN-PASSAGE SHOCKS Final Report
W. H. BRAUN Sep. 1985 90 p refs
(Contract NAS3-24100)
(NASA-CR-3925; E-2129; NAS 1.26:3925) Avail: NTIS HC A05/MF A01 CSCL 01A

A model for a supersonic blade row with two in-passage shock waves is developed. It accounts for three-dimensional effects in real flows by using an altered blade shape in a two-dimensional cascade. There is enough flexibility in the choice of blade shape to accommodate a desired entrance angle, exit angle, boundary-layer thickness and stage pressure ratio at a given entrance Mach number. The model divides the mean flow into regions of uniform or one-dimensional flow in which the solutions for the unsteady flow may be formed successively. The analysis makes use of previous solutions for unsteady flow in cascades and over an oscillation wedge. Six flow conditions are chosen in the range of parameters for which the two-shock model is valid for studies of flutter in torsion and bending. It is found, in keeping with previous results from a single-shock model, that in each case there is increasing instability with decreasing frequency. Author

N85-35159*# Stanitz (John D.), University Heights, Ohio.
GENERAL DESIGN METHOD FOR 3-DIMENSIONAL, POTENTIAL FLOW FIELDS. PART 2: COMPUTER PROGRAM DIN3D1 FOR SIMPLE, UNBRANCHED DUCTS Final Report
J. D. STANITZ Washington NASA Sep. 1985 88 p refs
(Contract NAS3-21991)
(NASA-CR-3926; E-2388; NAS 1.26:3926) Avail: NTIS HC A05/MF A01 CSCL 01A

The general design method for three-dimensional, potential, incompressible or subsonic-compressible flow developed in part 1 of this report is applied to the design of simple, unbranched ducts. A computer program, DIN3D1, is developed and five numerical examples are presented: a nozzle, two elbows, an S-duct, and the preliminary design of a side inlet for turbomachines. The two major inputs to the program are the upstream boundary shape and the lateral velocity distribution on the duct wall. As a result of these inputs, boundary conditions are overprescribed and the problem is ill posed. However, it appears that there are degrees of compatibility between these two major inputs and that, for reasonably compatible inputs, satisfactory solutions can be obtained. By not prescribing the shape of the upstream boundary, the problem presumably becomes well posed, but it is not clear how to formulate a practical design method under this circumstance. Nor does it appear desirable, because the designer usually needs to retain control over the upstream (or downstream) boundary shape. The problem is further complicated by the fact that, unlike the two-dimensional case, and irrespective of the upstream boundary shape, some prescribed lateral velocity distributions do not have proper solutions. Author

N85-35162*# Douglas Aircraft Co., Inc., Long Beach, Calif.
CALCULATION OF COMPRESSIBLE FLOW ABOUT THREE-DIMENSIONAL INLETS WITH AUXILIARY INLETS, SLATS AND VANES BY MEANS OF A PANEL METHOD Final Contractor Report, 17 Feb. 1983 - 15 Aug. 1985
J. L. HESS, D. M. FRIEDMAN, and R. W. CLARK Jun. 1985 197 p refs
(Contract NAS3-22250)
(NASA-CR-174975; NAS 1.26:174975; MDC-J3789) Avail: NTIS HC A09/MF A01 CSCL 01A

An efficient and user oriented method was constructed for calculating flow in and about complex inlet configurations. Efficiency is attained by: (1) the use of a panel method; (2) a technique of superposition for obtaining solutions at any inlet operating condition; and (3) employment of an advanced matrix iteration technique for solving large full systems of equations, including the nonlinear equations for the Kutta condition. User concerns are addressed by the provision of several novel graphical output options that yield a more complete comprehension of the flowfield than was possible previously. E.A.K.

03

AIR TRANSPORTATION AND SAFETY

Includes passenger and cargo air transport operations; and aircraft accidents.

A85-10653*# National Aeronautics and Space Administration. Lewis Research Center, Cleveland, Ohio.
PROGRESS TOWARD THE DEVELOPMENT OF AN AIRCRAFT ICING ANALYSIS CAPABILITY
R. J. SHAW (NASA, Lewis Research Center, Cleveland, OH) American Institute of Aeronautics and Astronautics, Aerospace Sciences Meeting, 22nd, Reno, NV, Jan. 9-12, 1984. 36 p. Previously announced in STAR as N84-20490. refs
(AIAA PAPER 84-0105)

An overview of the NASA efforts to develop an aircraft icing analysis capability is presented. Discussions are included of the overall and long term objectives of the program as well as current capabilities and limitations of the various computer codes being developed. Descriptions are given of codes being developed to analyze two and three dimensional trajectories of water droplets, airfoil ice accretion, aerodynamic performance degradation of components and complete aircraft configurations, electrothermal deicer, and fluid freezing point depressant deicer. The need for bench mark and verification data to support the code development is also discussed. Author

A85-20872*# Wichita State Univ., Kans.
ICING TUNNEL TESTS OF ELECTRO-IMPULSE DE-ICING OF AN ENGINE INLET AND HIGH-SPEED WINGS
G. W. ZUMWALT (Wichita State University, Wichita, KS) American Institute of Aeronautics and Astronautics, Aerospace Sciences Meeting, 23rd, Reno, NV, Jan. 14-17, 1985. 8 p. refs
(Contract NAG3-284)
(AIAA PAPER 85-0466)

A brief review is given of four earlier tests in the NASA Lewis Icing Research Tunnel and of flight tests in NASA's Icing Research Aircraft and in a Cessna 206 airplane. Details are given of recent icing tunnel tests of thicker-skinned wings, a Gates Learjet, a composite leading edge, and a Boeing 767, and of a Falcon Fanjet engine inlet. These were tested at speeds from 87 to 220 knots, air temperatures from -2 to -15 C, LWC values of 0.6 to 2.4 grams/cu meter, and median droplet diameters from 12 to 20 microns. Energy requirements are reported, as well as conclusions from comparisons of several Electro-Impulse De-Icing coil system designs. Fundamental studies of the structural dynamics and ice shedding of a 12.7 cm (5 inch) diameter semicylinder are described. Some potential problem areas are discussed: fatigue of skin and

coil mountings, system weight and cost, electro-magnetic interference and noise. Author

A85-28898*# National Aeronautics and Space Administration. Lewis Research Center, Cleveland, Ohio.
THE UH-1H HELICOPTER ICING FLIGHT TEST PROGRAM - AN OVERVIEW
R. J. SHAW and G. P. RICHTER (NASA, Lewis Research Center, Cleveland, OH) American Institute of Aeronautics and Astronautics, Aerospace Sciences Meeting, 23rd, Reno, NV, Jan. 14-17, 1985. 25 p. Previously announced in STAR as N85-15702. refs
(AIAA PAPER 85-0338)

An ongoing joint NASA/Army program to study the effects of ice accretion on unprotected helicopter rotor aerodynamic performance is discussed. This program integrates flight testing, wind tunnel testing, and analytical modeling. Results are discussed for helicopter flight testing in the Canadian NRC hover spray rig facility to measure rotor aero performance degradation and document rotor ice accretion characteristics. The results of dry wind tunnel testing of airfoil sections with artificial ice accretions and predictions of rotor performance degradation using available rotor performance codes and the wind tunnel data are presented. An alternative approach to conducting future helicopter icing flight programs is discussed. Author

A85-30192*# National Aeronautics and Space Administration. Lewis Research Center, Cleveland, Ohio.
ICING FLIGHT RESEARCH - AERODYNAMIC EFFECTS OF ICE AND ICE SHAPE DOCUMENTATION WITH STEREO PHOTOGRAPHY
K. L. MIKKELSEN, R. C. MCKNIGHT, R. J. RANAUDO (NASA, Lewis Research Center, Cleveland, OH), and P. J. PERKINS, JR. (Sverdrup Technology, Inc., Middleburg Heights, OH) American Institute of Aeronautics and Astronautics, Aerospace Sciences Meeting, 23rd, Reno, NV, Jan. 14-17, 1985. 31 p. Previously announced in STAR as N85-18049. refs
(AIAA PAPER 85-0468)

Aircraft icing flight research was performed in natural icing conditions. A data base consisting of icing cloud measurements, ice shapes, and aerodynamic measurements is being developed. During research icing encounters the icing cloud was continuously measured. After the encounter, the ice accretion shapes on the wing were documented with a stereo camera system. The increase in wing section drag was measured with a wake survey probe. The overall aircraft performance loss in terms of lift and drag coefficient changes were obtained by steady level speed/power measurements. Selective deicing of the airframe components was performed to determine their contributions to the total drag increase. Engine out capability in terms of power available was analyzed for the iced aircraft. It was shown that the stereo photography system can be used to document ice shapes in flight and that the wake survey probe can measure increases in wing section drag caused by ice. On one flight, the wing section drag coefficient (c sub d) increased approximately 120 percent over the uniced baseline at an aircraft angle of attack of 6 deg. On another flight, the aircraft drag coefficient (c sub d) increased by 75 percent over the uniced baseline at an aircraft lift coefficient (c sub d) of 0.5. Author

A85-42937*# Texas A&M Univ., College Station.
PERFORMANCE DEGRADATION OF HELICOPTER ROTOR IN FORWARD FLIGHT DUE TO ICE
K. D. KORKAN (Texas A & M University, College Station), L. DADONE (Boeing Vertol Co., Philadelphia, PA), and R. J. SHAW (NASA, Lewis Research Center, Cleveland, OH) Journal of Aircraft (ISSN 0021-8669), vol. 22, Aug. 1985, p. 713-718. refs
(Contract NAG3-242)

This study addresses the analytical assessment of the degradation in the forward flight performance of the front rotor Boeing Vertol CH47D helicopter in a rime ice natural icing encounter. The front rotor disk was divided into 24 15-deg sections and the local Mach number and angle of attack were evaluated as a function of azimuthal and radial location for a specified flight condition. Profile drag increments were then calculated as a function of azimuthal and radial position for different times of exposure to icing, and the rotor performance was re-evaluated including these drag increments. The results of the analytical prediction method, such as horsepower required to maintain a specific flight condition, as a function of icing time have been generated. The method to illustrate the value of such an approach in assessing performance changes experienced by a helicopter rotor as a result of rime ice accretion is described. Author

N85-15702*# National Aeronautics and Space Administration. Lewis Research Center, Cleveland, Ohio.
THE UH-1H HELICOPTER ICING FLIGHT TEST PROGRAM: AN OVERVIEW
R. J. SHAW and G. P. RICHTER 1985 26 p refs Presented at the 23rd Aerospace Sci. Meeting, Reno, Nevada, 14-17 Jan. 1985; sponsored by AIAA, 14-17 Jan. 1985
(NASA-TM-86925; E-2421; NAS 1.15:86925; AIAA-85-0338)
Avail: NTIS HC A03/MF A01 CSCL 01C

An ongoing joint NASA/Army program to study the effects of ice accretion on unprotected helicopter rotor aerodynamic performance is discussed. This program integrates flight testing, wind tunnel testing, and analytical modeling. Results are discussed for helicopter flight testing in the Canadian NRC hover spray rig facility to measure rotor aero performance degradation and document rotor ice accretion characteristics. The results of dry wind tunnel testing of airfoil sections with artificial ice accretions and predictions of rotor performance degradation using available rotor performance codes and the wind tunnel data are presented. An alternative approach to conducting future helicopter icing flight programs is discussed. B.W.

N85-27839*# National Aeronautics and Space Administration. Lewis Research Center, Cleveland, Ohio.
ICE SHAPES AND THE RESULTING DRAG INCREASE FOR A NACA 0012 AIRFOIL
W. OLSEN, R. J. SHAW, and J. NEWTON 12 Jan. 1984 31 p refs Presented at the 22nd Aerospace Sci. Meeting, Reno, Nev., 9-12 Jan. 1984; sponsored by AIAA
(NASA-TM-83556; E-1935; NAS 1.15:83556) Avail: NTIS HC A03/MF A01 CSCL 01C

Experimental measurements of the ice shapes and resulting drag increases were measured in the NASA-Lewis Icing Research Tunnel. The measurements were made over a large range of conditions (e.g., airspeed and temperature, drop size and liquid water content of the cloud, and the angle of attack of the airfoil). The measured drag increase did not agree with the existing correlation. Additional results were given which are helpful in understanding the ice structure and the way it forms, and in improving the ice accretion modeling theories. There are data on the ice surface roughness, on the effect of the ice shape on the local droplet catch, and on the relative importance of various parts of the ice shape on the drag increase. Experimental repeatability is also discussed. Author

05

AIRCRAFT DESIGN, TESTING AND PERFORMANCE

Includes aircraft simulation technology.

A85-21844*# Texas A&M Univ., College Station.
EXPERIMENTAL AERODYNAMIC CHARACTERISTICS OF AN NACA 0012 AIRFOIL WITH SIMULATED ICE
K. D. KORKAN, E. J. CROSS, JR., and C. C. CORNELL (Texas A&M University, College Station, TX) Journal of Aircraft (ISSN 0021-8669), vol. 22, Feb. 1985, p. 130-134. Previously cited in issue 06, p. 719, Accession no. A84-17937. refs
(Contract NAG3-242)

A85-40811*# Wichita State Univ., Kans.
ELECTRO-IMPULSE DE-ICING OF A TURBOFAN ENGINE INLET
G. W. ZUMWALT (Wichita State University, KS) AIAA, SAE, ASME, and ASEE, Joint Propulsion Conference, 21st, Monterey, CA, July 8-10, 1985. 8 p. refs
(Contract NAG3-284)
(AIAA PAPER 85-1118)

The application of electromagnetic impulse deicing (EIDI) systems to turbofan engine inlets on business aircraft has been investigated experimentally. The tests were performed in the Icing Research Tunnel at NASA's Lewis Research Center. The deicing system testbed was a Falcon Fanjet 20 engine nacelle. The effectiveness of various deicing coil configurations and mount designs were compared, and design parameters were developed specifically for EIDI systems in turbofan engines. Flight tests were also carried out at altitudes in the range 3000-6000 ft corresponding to a temperature range of -3 to -8 C. It is shown that the ice particles removed from the engine inlet by the deicing system were small enough for the engine to ingest. Tentative design specifications are given with respect to the optimum coil configuration, and operating power of a EIDI production candidate. I.H.

N85-12887*# National Aeronautics and Space Administration. Lewis Research Center, Cleveland, Ohio.
INITIAL FEASIBILITY GROUND TEST OF A PROPOSED PHOTOGRAMMETRIC SYSTEM FOR MEASURING THE SHAPES OF ICE ACCRETIONS ON HELICOPTER ROTOR BLADES DURING FORWARD FLIGHT Final Report, 1 Oct. - 31 Dec. 1983
R. L. PALKO (Calspan Field Services, Inc., Arnold Air Force Station, Tenn.), P. L. CASSADY (Calspan Field Services, Inc., Arnold Air Force Station, Tenn.), R. C. MCKNIGHT, and R. J. FREEDMAN Aug. 1984 45 p
(NASA-TM-87391; NAS 1.15:87391; AD-A146051; AEDC-TR-84-10) Avail: NTIS HC A03/MF A01 CSCL 01C

A ground test was accomplished to determine if a combination of standard photographic system parameters could be chosen that would allow stereophotographs to be made of the main rotor of a UH-1H helicopter in forward flight. The photographs would be used to measure the shape of ice accretions on the rotor in forward flight. During the ground test, 83 photographic pairs were obtained at three camera shutter speeds for a range of ambient light conditions from dark to complete daylight. Twenty-seven of these photographic pairs were evaluated on the AEDC analytical stereocompiler for readability. The test showed that quality photographs could be taken using standard equipment with shutter speeds of 1/30 and 1/60 sec for up to three hours per day. The test also showed that the addition of a specifically designed control circuit for synchronization at 1/500-sec shutter speed would allow testing for the complete day for most winter days. GRA

N85-18049*# National Aeronautics and Space Administration. Lewis Research Center, Cleveland, Ohio.
ICING FLIGHT RESEARCH: AERODYNAMIC EFFECTS OF ICE AND ICE SHAPE DOCUMENTATION WITH STEREO PHOTOGRAPHY
K. L. MIKKELSEN, R. C. MCKNIGHT, R. J. RANAUDO, and P. J. PERKINS, JR. (Sverdrup Technology, Inc., Middleburg Heights, Ohio) 1985 32 p refs Presented at the 23rd Aerospace Sci. Meeting, Reno, Nevada, 14-17 Jan. 1985; sponsored by AIAA
(NASA-TM-86906; E-2395; NAS 1.15:86906; AIAA-85-0468)
Avail: NTIS HC A03/MF A01 CSCL 01C

Aircraft icing flight research was performed in natural icing conditions. A data base consisting of icing cloud measurements, ice shapes, and aerodynamic measurements is being developed. During research icing encounters the icing cloud was continuously measured. After the encounter, the ice accretion shapes on the wing were documented with a stereo camera system. The increase in wing section drag was measured with a wake survey probe. The overall aircraft performance loss in terms of lift and drag coefficient changes was obtained by steady level speed/power measurements. Selective deicing of the airframe components was performed to determine their contributions to the total drag increase. Engine out capability in terms of power available was analyzed for the iced aircraft. It was shown that the stereo photography system can be used to document ice shapes in flight and that the wake survey probe can measure increases in wing section drag caused by ice. On one flight, the wing section drag coefficient (c sub d) increased approximately 120 percent over the uniced baseline at an aircraft angle of attack of 6 deg. On another flight, the aircraft darg coefficient (c sub d) increased by 75 percent over the uniced baseline at an aircraft lift coefficient (C sub d) of 0.5. Author

N85-19978*# General Electric Co., Cincinnati, Ohio. Aircraft Engine Business Group.
STUDY OF ADVANCED FUEL SYSTEM CONCEPTS FOR COMMERCIAL AIRCRAFT
G. A. COFFINBERRY Jan. 1985 256 p refs
(Contract NAS3-23267)
(NASA-CR-174751; NAS 1.26:174751; R85AEB166) Avail: NTIS HC A12/MF A01 CSCL 01C

An analytical study was performed in order to assess relative performance and economic factors involved with alternative advanced fuel systems for future commercial aircraft operating with broadened property fuels. The DC-10-30 wide-body tri-jet aircraft and the CF6-8OX engine were used as a baseline design for the study. Three advanced systems were considered and were specifically aimed at addressing freezing point, thermal stability and lubricity fuel properties. Actual DC-10-30 routes and flight profiles were simulated by computer modeling and resulted in prediction of aircraft and engine fuel system temperatures during a nominal flight and during statistical one-day-per-year cold and hot flights. Emergency conditions were also evaluated. Fuel consumption and weight and power extraction results were obtained. An economic analysis was performed for new aircraft and systems. Advanced system means for fuel tank heating included fuel recirculation loops using engine lube heat and generator heat. Environmental control system bleed air heat was used for tank heating in a water recirculation loop. The results showed that fundamentally all of the three advanced systems are feasible but vary in their degree of compatibility with broadened-property fuel. B.W.

N85-35185*# SKF Industries, Inc., King of Prussia, Pa.
PLANETARY-GEAR-SUPPORT BEARING TEST RIG DESIGN Contractor Report, 8 Feb. 1983 - 8 Jan. 1985
J. W. ROSENLIEB Mar. 1985 81 p
(Contract NAS3-23702)
(NASA-CR-174927; NAS 1.26:174927; AT85T004) Avail: NTIS HC A05/MF A01 CSCL 01C

A test rig was designed to evaluate the performance of a spherical roller bearing with a geared outer ring operating under conditions similar to those of a planet bearing in a helicopter

transmission. The configuration is an extension of the widely accepted four-square gearbox arrangement. It provides for testing of two bearings simultaneously with outer ring rotation, misalignment, diametrically opposed loading through the gear teeth, and under race lubrication. Instrumentation permits the measurement of inner and outer ring temperature, bearing drag torque, degree of misalignment, outer ring speed, cage speed, and applied load. Author

06

AIRCRAFT INSTRUMENTATION

Includes cockpit and cabin display devices; and flight instruments.

A85-16098*# Army Propulsion Lab., Cleveland, Ohio.
COMPARISON OF ICING CLOUD INSTRUMENTS FOR 1982-1983 ICING SEASON FLIGHT PROGRAM
R. F. IDE (U.S. Army, Propulsion Laboratory, Cleveland, OH) and G. P. RICHTER (NASA, Lewis Research Center, Cleveland, OH) American Institute of Aeronautics and Astronautics, Aerospace Sciences Meeting, 22nd, Reno, NV, Jan. 9-12, 1984. 24 p. Previously announced in STAR as N84-29870. refs
(AIAA PAPER 84-0020)

A number of modern and old style liquid water content (LWC) and droplet sizing instruments were mounted on a DeHavilland DHC-6 Twin Otter and operated in natural icing clouds in order to determine their comparative operating characteristics and their limitations over a broad range of conditions. The evaluation period occurred during the 1982-1983 icing season from January to March 1983. Time histories of all instrument outputs were plotted and analyzed to assess instrument repeatability and reliability. Scatter plots were also generated for comparison of instruments. The measured LWC from four instruments differed by as much as 20 percent. The measured droplet size from two instruments differed by an average of three microns. The overall effort demonstrated the need for additional data, and for some means of calibrating these instruments to known standards. Author

07

AIRCRAFT PROPULSION AND POWER

Includes prime propulsion systems and systems components, e.g., gas turbine engines and compressors; and on-board auxiliary power plants for aircraft.

A85-13627*# National Aeronautics and Space Administration. Lewis Research Center, Cleveland, Ohio.
THE ROLE OF MODERN CONTROL THEORY IN THE DESIGN OF CONTROLS FOR AIRCRAFT TURBINE ENGINES
W. MERRILL, B. LEHTINEN, and J. ZELLER (NASA, Lewis Research Center, Cleveland, OH) Journal of Guidance, Control, and Dynamics (ISSN 0731-5090), vol. 7, Nov.-Dec. 1984, p. 652-661. Previously cited in issue 11, p. 1707, Accession no. A82-26526. refs

A85-13630*# National Aeronautics and Space Administration. Lewis Research Center, Cleveland, Ohio.
IDENTIFICATION OF MULTIVARIABLE HIGH-PERFORMANCE TURBOFAN ENGINE DYNAMICS FROM CLOSED-LOOP DATA
W. MERRILL (NASA, Lewis Research Center, Aerodynamics and Engine Systems Div., Cleveland, OH) (Identification and system parameter estimation 1982; Proceedings of the Sixth Symposium, Washington, DC, June 7-11, 1982. Volume 1, p. 427-434) Journal of Guidance, Control, and Dynamics (ISSN 0731-5090), vol. 7, Nov.-Dec. 1984, p. 677-683. Previously cited in issue 06, p. 723, Accession no. A84-18582. refs

A85-13953*# General Electric Co., Cincinnati, Ohio.
COMPARISON OF SCALED MODEL DATA TO FULL SIZE ENERGY EFFICIENT ENGINE TEST RESULTS
S. P. LAVIN, P. Y. HO (General Electric Co., Aircraft Engine Business Group, Cincinnati, OH), and R. CHAMBERLIN (NASA, Lewis Research Center, Cleveland, OH) American Institute of Aeronautics and Astronautics and NASA, Aeroacoustics Conference, 9th, Williamsburg, VA, Oct. 15-17, 1984. 15 p. refs
(Contract NAS3-20643)
(AIAA PAPER 84-2281)

Acoustic tests of a subscale fan and a subscale mixer nozzle were conducted in anechoic chambers over a variety of operating conditions. The subscale fan test was an investigation into the effects of vane/blade ratio and spacing on fan generated noise. A turbulence control structure (TCS) was used to simulate the 'turbulence-free' condition in flight. The subscale mixer nozzle test investigated the acoustic properties of several different forced mixer designs. A tertiary flow was utilized on the mixer model to simulate the forward velocity effects on the jet. The results were scaled up to full size conditions and compared with measured engine data. The comparisons showed good agreement between the component scaled model results and the full scale engine data. Author

A85-13954*# General Electric Co., Cincinnati, Ohio.
MEASUREMENT AND PREDICTION OF ENERGY EFFICIENT ENGINE NOISE
S. P. LAVIN, P. Y. HO (General Electric Co., Aircraft Engine Business Group, Cincinnati, OH), and R. CHAMBERLIN (NASA, Lewis Research Center, Cleveland, OH) American Institute of Aeronautics and Astronautics and NASA, Aeroacoustics Conference, 9th, Williamsburg, VA, Oct. 15-17, 1984. 11 p. refs
(AIAA PAPER 84-2284)

The NASA/GE Energy Efficient Engine (E3) static noise levels were measured in an acoustic arena on the Integrated Core and Low Spool Test System. These measured levels were scaled to the appropriate size to power four study aircraft and were projected to flight for evaluation of noise levels relative to FAR36, Stage III limits. As a result of these evaluations, it is predicted that the NASA/GE E3 engine with a wide spacing cut-on blade/vane ratio fan and a forced mixer nozzle can meet FAR36 Stage III limits with sufficient design margin. Author

A85-16097*# National Aeronautics and Space Administration. Lewis Research Center, Cleveland, Ohio.
SENSOR FAILURE DETECTION FOR JET ENGINES USING ANALYTICAL REDUNDANCY
W. C. MERRILL (NASA, Lewis Research Center, Cleveland, OH) AIAA, SAE, and ASME, Joint Propulsion Conference, 20th, Cincinnati, OH, June 11-13, 1984. 23 p. Previously announced in STAR as N84-24585. refs
(AIAA PAPER 84-1452)

Analytical redundant sensor failure detection, isolation and accommodation techniques for gas turbine engines are surveyed. Both the theoretical technonlogy base and demonstrated concepts are discussed. Also included is a discussion of current technology needs and angoing Government sponsored programs to meet those needs. Author

A85-18792*# General Electric Co., Cincinnati, Ohio.
CONSIDERATIONS FOR DAMAGE ANALYSIS OF GAS TURBINE HOT SECTION COMPONENTS
T. S. COOK and J. H. LAFLEN (General Electric Co., Cincinnati, OH) American Society of Mechanical Engineers, Pressure Vessels and Piping Conference and Exhibition, San Antonio, TX, June 17-21, 1984. 7 p. refs
(Contract NAS3-22534)
(ASME PAPER 84-PVP-77)

The hot flowpath of a gas turbine engine contains static and rotating components operating in a very hostile environment. Since the reliable operation of these components is critical to the safe and efficient performance of the engine, structural life analysis of these members is carried out with great care. However, the complex nature of the strain-temperature-time cycle affecting the engine makes a general analysis procedure difficult and usually leads to separating the damage into regimes where one damage mode dominates. In particular, cycle dependent, time dependent, and thermomechanical fatigue regimes have been identified and some general considerations of each region are discussed. This discussion includes both the damage models themselves and the application of the models. Specific examples of several models are given and important factors affecting each are presented. Author

A85-19509*# National Aeronautics and Space Administration. Lewis Research Center, Cleveland, Ohio.
COMPUTATIONAL THERMO-FLUID DYNAMICS CONTRIBUTIONS TO ADVANCED GAS TURBINE ENGINE DESIGN
R. W. GRAHAM, J. J. ADAMCZYK, and H. E. ROHLIK (NASA, Lewis Research Center, Cleveland, OH) American Institute of Aeronautics and Astronautics, Aerospace Sciences Meeting, 23rd, Reno, NV, Jan. 14-17, 1985. 10 p. Previously announced in STAR as N85-10069. refs
(AIAA PAPER 85-0083)

The design practices for the gas turbine are traced throughout history with particular emphasis on the calculational or analytical methods. Three principal components of the gas turbine engine will be considered: namely, the compressor, the combustor and the turbine. B.W.

A85-20867*# Texas A&M Univ., College Station.
ANALYTICAL DETERMINATION OF PROPELLER PERFORMANCE DEGRADATION DUE TO ICE ACCRETION
T. L. MILLER (Sverdrup Technology, Inc., Middleburg Heights, OH), K. D. KORKAN (Texas A&M University, College Station, TX), and R. J. SHAW (NASA, Lewis Research Center, Cleveland, OH) American Institute of Aeronautics and Astronautics, Aerospace Sciences Meeting, 23rd, Reno, NV, Jan. 14-17, 1985. 42 p. refs
(Contract NAG3-242)
(AIAA PAPER 85-0339)

It is pointed out that ice accretion on aircraft produces an adverse effect on aircraft performance in terms of decreased lift and increased drag of the lifting surface. Ice on the surface of a propeller may also cause a decrease in thrust, increase in the required power, and a resultant decrease in propeller efficiency. During the past years, a number of attempts have been made to analyze the effects of ice accretion on both fixed wings and propellers. The present investigation is concerned with the development of a single user-oriented computer code which makes it possible to calculate propeller performance degradation due to ice accretion for specified flight conditions, atmospheric conditions, and propeller geometry. This development is based on a combination of several of the codes and correlations considered in earlier studies. G.R.

A85-21866*# Pennsylvania State Univ., University Park.
EFFECTS OF FRICTION DAMPERS ON AERODYNAMICALLY UNSTABLE ROTOR STAGES
A. SINHA (Pennsylvania State University, University Park, PA) and J. H. GRIFFIN (Carnegie-Mellon University, Pittsburgh, PA) AIAA Journal (ISSN 0001-1452), vol. 23, Feb. 1985, p. 262-270. Previously cited in issue 14, p. 1976, Accession no. A83-32791. refs
(Contract NAG3-231)

A85-25442* Washington Univ., Seattle.
AN EXPERIMENTAL INVESTIGATION AND NUMERICAL PREDICTION OF THERMOMECHANICAL PHENOMENA IN HIGH SPEED ROTOR TIP RUBBING
A. F. EMERY, S. ETEMAD, J. WOLAK, and S. R. CHOI (Washington, University, Seattle, WA) IN: Numerical methods in thermal problems. Volume 3 Proceedings of the Third International Conference, Seattle, WA, August 2-5, 1983 . Swansea, Wales, Pineridge Press, 1983, p. 1040-1049. refs
(Contract NAG3-7)

A thermomechanical study of the intermittent rubbing of a rotor blade tip and a casing seal is carried out taking into account the existence of thermal contact resistance. The effect of the thermal properties of a plasma sprayed coating on the blade tip is studied. The influence of a variable heat generation and variable thermal contact resistance at the blade tip as it passes along the path of rubbing is also discussed. Author

A85-25984* General Electric Co., Cincinnati, Ohio.
ALTITUDE TESTING OF A FLIGHT WEIGHT, SELF-COOLED, 2D THRUST VECTORING EXHAUST NOZZLE
W. H. WOOTEN, J. T. BLOZY, D. W. SPEIR (General Electric Co., Cincinnati, OH), and R. A. LOTTIG (NASA, Lewis Research Center, Cleveland, OH) Society of Automotive Engineers, Aerospace Congress and Exposition, Long Beach, CA, Oct. 15-18, 1984. 11 p.
(SAE PAPER 841557)

The Augmented Deflector Exhaust Nozzle (ADEN) was tested in PSL-3 at NASA-Lewis Research Center using an F404 engine. The ADEN is a flight weight Single Expansion Ramp Nozzle with thrust vectoring, an internal cooling system utilizing the available engine fan flow, and a variable area throat controlled by the engine control system. Test conditions included dry and max A/B operation at nozzle pressure ratios from 2.0 to 15.0. High nozzle pressure loading was simulated to verify structural integrity at near maximum design pressure. Nozzle settings covered the full range in throat area and + or - 15 deg deflection angle. Test results demonstrated expected aerodynamic performance, cooling system effectiveness, control system stability, and mechanical integrity. Author

A85-30378*# National Aeronautics and Space Administration. Lewis Research Center, Cleveland, Ohio.
THE EFFECT OF AERODYNAMIC AND STRUCTURAL DETUNING ON TURBOMACHINE SUPERSONIC UNSTALLED TORSIONAL FLUTTER
D. HOYNIAK (NASA, Lewis Research Center, Cleveland, OH) and S. FLEETER (Purdue University, West Lafayette, IN) IN: Structures, Structural Dynamics, and Materials Conference, 26th, Orlando, FL, April 15-17, 1985, Technical Papers. Part 2 . New York, American Institute of Aeronautics and Astronautics, 1985, p. 500-514. refs
(AIAA PAPER 85-0761)

The effects of alternate-blade structural detuning and adjacent-blade alternate-circumferential-spacing aerodynamic detuning on the supersonic unstalled torsional flutter stability of a turbomachine rotor are investigated analytically. An unsteady aerodynamic model employing influence coefficients is constructed for the case of a flat-plate-airfoil cascade in torsion-mode harmonic oscillation in a supersonic inviscid isentropic adiabatic irrotational perfect-gas inlet flow with a subsonic leading-edge locus. The influence coefficients and equations of motion are derived; the model is verified by applying it to the 12-blade cascade-B flow geometry studied by Verdon and McCune (1975); and the results are presented graphically. It is found that the rotor can be stabilized

over the entire reduced frequency range by applying a combination of structural and aerodynamic detuning as the passive flutter-control mechanism. T.K.

A85-32005*# General Electric Co., Lynn, Mass.
CONTINGENCY POWER CONCEPTS FOR HELICOPTER TURBOSHAFT ENGINE
R. HIRSCHKRON, R. H. DAVIS, D. N. GOLDSTEIN, J. F. HAYNES (General Electric Co., Lynn, MA), and J. W. GAUNTNER (NASA, Lewis Research Center, Cleveland, OH) IN: American Helicopter Society, Annual Forum, 40th, Arlington, VA, May 16-18, 1984, Proceedings . Alexandria, VA, American Helicopter Society, 1984, p. 597-608. Previously announced in STAR as N84-23648.
(Contract NAS3-23705)

Twin helicopter engines are often sized by power requirement of safe mission completion after the failure of one of the two engines. This study was undertaken for NASA Lewis by General Electric Co. to evaluate the merits of special design features to provide a 2-1/2 minute Contingency Power rating, permitting an engine size reduction. The merits of water injection, cooling flow modulation, throttle push and an auxiliary power plant were evaluated using military life cycle cost (LCC) and commercial helicopter direct operating cost (DOC) merit factors in a rubber engine/rubber aircraft scenario. Author

A85-32006*# General Electric Co., Lynn, Mass.
TF34 CONVERTIBLE ENGINE CONTROL SYSTEM DESIGN
D. R. GILMORE, JR. (General Electric Co., Aircraft Engine Business Group, Lynn, MA) IN: American Helicopter Society, Annual Forum, 40th, Arlington, VA, May 16-18, 1984, Proceedings . Alexandria, VA, American Helicopter Society, 1984, p. 609-620. refs
(Contract NAS3-22752)

The characteristics of the TF34 convertible engine, capable of producing shaft power, thrust, or a combination of both, is investigated with respect to the control system design, development, bench testing, and the anticipated transient response during engine testing at NASA. The modifications to the prototype standard TF34-GE-400 turbofan, made primarily in the fan section, consist of the variable inlet guide vanes and variable exit guide vanes. The control system was designed using classical frequency domain techniques and was based on the anticipated convertible/VTOL airframe requirements. The engine has been run in the fan mode and in the shaft mode, exhibiting a response of 0.14 second to a 5-percent thrust change. L.T.

A85-34013*# National Aeronautics and Space Administration. Lewis Research Center, Cleveland, Ohio.
PREDICTED TURBINE STAGE PERFORMANCE USING QUASI-THREE-DIMENSIONAL AND BOUNDARY-LAYER ANALYSES
R. J. BOYLE, J. E. HAAS (NASA, Lewis Research Center, Cleveland, OH), and T. KATSANIS (NASA, Lewis Research Center; U.S. Army, Research and Technology Laboratories, Cleveland, OH) Journal of Propulsion and Power (ISSN 0748-4658), vol. 1, May-June 1985, p. 242-251. Previously cited in issue 17, p. 2432, Accession no. A84-36972. refs

A85-39065* Army Propulsion Lab., Cleveland, Ohio.
TEMPERATURE DISTORTION GENERATOR FOR TURBOSHAFT ENGINE TESTING
G. A. KLANN (U.S. Army, Propulsion Laboratory, Cleveland, OH), R. L. BARTH, and T. J. BIESIADNY (NASA, Lewis Research Center, Cleveland, OH) IN: *Advances in aerospace propulsion*; Proceedings of the Aerospace Congress and Exposition, Long Beach, CA, October 15-18, 1984 . Warrendale, PA, Society of Automotive Engineers, Inc., 1984, p. 89-99. Previously announced in STAR as N85-15659. refs
(SAE PAPER 841541)

The procedures and unique hardware used to conduct an experimental investigation into the response of a small-turboshaft-engine compression system to various hot gas ingestion patterns are presented. The temperature distortion generator described herein uses gaseous hydrogen to create both steady-state and time-variant, or transient, temperature distortion at the engine inlet. The range of transient temperature ramps produced by the distortion generator during the engine tests was from less than 111 deg K/sec (200 deg R/sec) to above 611 deg K/sec (1100 deg R/sec); instantaneous temperatures to 422 deg K (760 deg R) above ambient were generated. The distortion generator was used to document the maximum inlet temperatures and temperature rise rates that the compression system could tolerate before the onset of stall for various circumferential distortions as well as the compressor system response during stall. Author

A85-39580*# National Aeronautics and Space Administration. Lewis Research Center, Cleveland, Ohio.
FLAME RADIATION AND LINEAR HEAT TRANSFER IN A TUBULAR-CAN COMBUSTOR
R. W. CLAUS, G. M. NEELY, and F. M. HUMENIK (NASA, Lewis Research Center, Cleveland, OH) Journal of Propulsion and Power (ISSN 0748-4658), vol. 1, July-Aug. 1985, p. 270-278. Previously cited in issue 07, p. 872, Accession no. A84-21300. refs

A85-39606*# National Aeronautics and Space Administration. Lewis Research Center, Cleveland, Ohio.
EXPERIMENTS IN DILUTION JET MIXING - EFFECTS OF MULTIPLE ROWS AND NON-CIRCULAR ORIFICES
J. D. HOLDEMAN (NASA, Lewis Research Center, Modeling and Verification Branch, Cleveland, OH), R. SRINIVASAN, E. B. COLEMAN, G. D. MEYERS, and C. D. WHITE (Garrett Turbine Engine Co., Phoenix, AZ) AIAA, SAE, ASME, and ASEE, Joint Propulsion Conference, 21st, Monterey, CA, July 8-10, 1985. 12 p. Previously announced in STAR as N85-25266. refs
(AIAA PAPER 85-1104)

Experimental and empirical model results are presented that extend previous studies of the mixing of single-sided and opposed rows of jets in a confined duct flow to include effects of non-circular orifices and double rows of jets. Analysis of the mean temperature data obtained in this investigation showed that the effects of orifice shape and double rows are significant only in the region close to the injection plane, provided that the orifices are symmetric with respect to the main flow direction. The penetration and mixing of jets from 45-degree slanted slots is slightly less than that from equivalent-area symmetric orifices. The penetration from two-dimensional slots is similar to that from equivalent-area closely-spaced rows of holes, but the mixing is slower for the 2-D slots. Calculated mean temperature profiles downstream of jets from non-circular and double rows of orifices, made using an extension developed for a previous empirical model, are shown to be in good agreement with the measured distributions. Author

A85-39703*# National Aeronautics and Space Administration. Lewis Research Center, Cleveland, Ohio.
ADVANCED LINER-COOLING TECHNIQUES FOR GAS TURBINE COMBUSTORS
C. T. NORGREN and S. M. RIDDLEBAUGH (NASA, Lewis Research Center, Cleveland, OH) AIAA, SAE, ASME, and ASEE, Joint Propulsion Conference, 21st, Monterey, CA, July 8-10, 1985. 13 p. Previously announced in STAR as N85-21115. refs
(AIAA PAPER 85-1290)

Component research for advanced small gas turbine engines is currently underway at the NASA Lewis Research Center. As part of this program, a basic reverse-flow combustor geometry was being maintained while different advanced liner wall cooling techniques were investigated. Performance and liner cooling effectiveness of the experimental combustor configuration featuring counter-flow film-cooled panels is presented and compared with two previously reported combustors featuring: splash film-cooled liner walls; and transpiration cooled liner walls (Lamilloy). Author

A85-39717*# National Aeronautics and Space Administration. Lewis Research Center, Cleveland, Ohio.
SMALL GAS TURBINE COMBUSTOR STUDY - FUEL INJECTOR PERFORMANCE IN A TRANSPIRATION-COOLED LINER
S. M. RIDDLEBAUGH and C. T. NORGREN (NASA, Lewis Research Center, Cleveland, OH) AIAA, SAE, ASME, and ASEE, Joint Propulsion Conference, 21st, Monterey, CA, July 8-10, 1985. 12 p. refs
(AIAA PAPER 85-1312)

The effect of fuel injection technique on the performance of an advanced reverse flow combustor liner constructed of Lamilloy (a multilaminate transpiration type material) was determined. Performance and emission levels are documented over a range of simulated flight conditions using simplex pressure atomizing, spill return, and splash cone airblast injectors. A parametric evaluation of the effect of increased combustor loading with each of the fuel injector types is obtained. E.A.K.

A85-40841*# General Electric Co., Cincinnati, Ohio.
STALL RECOVERY CONTROL STRATEGY METHODOLOGY AND RESULTS
W. R. HOPF and W. G. STEENKEN (General Electric Co., Cincinnati, OH) AIAA, SAE, ASME, and ASEE, Joint Propulsion Conference, 21st, Monterey, CA, July 8-10, 1985. 14 p. refs
(Contract NAS3-23540)
(AIAA PAPER 85-1433)

The nonrecoverable stall condition in high performance turbofan engines is characterized by thrust loss, rising turbine temperatures, high pressure compressor rotating stall, and loss of engine control. Stall recovery control is presently investigated by means of an engine system computer model capable of either surge or rotating stall postinstability operation. Several techniques are examined which can yield rapid recovery from stall; a composite strategy which involves reduction of engine speed to idle while simultaneously opening the 10th- and 14th-stage compressor bleed ports allowed recovery to speeds slightly higher than idle while combustor fuel flow continued. O.C.

A85-41778* National Aeronautics and Space Administration. Lewis Research Center, Cleveland, Ohio.
THE TREND OF FUTURE GAS TURBINE TECHNOLOGY
M. J. HARTMANN (NASA, Lewis Research Center, Cleveland, OH) IN: 1983 Tokyo International Gas Turbine Congress, Tokyo, Japan, October 23-29, 1983, Proceedings. Volume 1 . Tokyo, Gas Turbine Society of Japan, 1984, p. S-19 to S-25.

Future gas turbine technology will be based on contributions to the technology base being made today. At the NASA Lewis Research Center in Cleveland, OH, research is being conducted on turbomachinery system components and in a number of associated disciplines to advance the technology of aviation turbofan and torbojet engines. Areas of research include compressors, turbines, internal flow analysis, combustion, fuels, materials, structures, bearings, seals, lubrication, dynamics and controls, and instrumentation. A review of the research directions being taken in these areas and the steady advances being made provides a reasonable glimpse at gas turbine technology of the future. Author

A85-42365*# Virginia Polytechnic Inst. and State Univ., Blacksburg.
OPTIMIZATION OF CASCADE BLADE MISTUNING. I - EQUATIONS OF MOTION AND BASIC INHERENT PROPERTIES
E. NISSIM (Virginia Polytechnic Institute and State University, Blacksburg) AIAA Journal (ISSN 0001-1452), vol. 23, Aug. 1985, p. 1213-1222. refs
(Contract NAG3-347)

Attention is given to the derivation of the equations of motion of mistuned compressor blades, interpolating aerodynamic coefficients by means of quadratic expressions in the reduced frequency. If the coefficients of the quadratic expressions are permitted to assume complex values, excellent accuracy is obtained and Pade rational expressions are obviated. On the basis of the resulting equations, it is shown analytically that the sum of all the real parts of the eigenvalues is independent of the mistuning introduced into the system. Blade mistuning is further treated through the aerodynamic energy approach, and the limiting vibration modes associated with alternative mistunings are identified. O.C.

A85-42671*# National Aeronautics and Space Administration. Lewis Research Center, Cleveland, Ohio.
FUTURE FUNDAMENTAL COMBUSTION RESEARCH FOR AEROPROPULSION SYSTEMS
E. J. MULARZ (NASA, Lewis Research Center; U.S. Army, Propulsion Laboratory, Cleveland, OH) AIAA, SAE, ASME, and ASEE, Joint Propulsion Conference, 21st, Monterey, CA, July 8-10, 1985. 7 p. Army-supported research. Previously announced in STAR as N85-27870. refs
(AIAA PAPER 85-1398)

Physical fluid mechanics, heat transfer, and chemical kinetic processes which occur in the combustion chamber of aeropropulsion systems were investigated. With the component requirements becoming more severe for future engines, the current design methodology needs the new tools to obtain the optimum configuration in a reasonable design and development cycle. Research efforts in the last few years were encouraging but to achieve these benefits research is required into the fundamental aerothermodynamic processes of combustion. It is recommended that research continues in the areas of flame stabilization, combustor aerodynamics, heat transfer, multiphase flow and atomization, turbulent reacting flows, and chemical kinetics. Associated with each of these engineering sciences is the need for research into computational methods to accurately describe and predict these complex physical processes. Research needs in each of these areas are highlighted. E.A.K.

A85-45715*# Virginia Polytechnic Inst. and State Univ., Blacksburg.
OPTIMIZATION OF CASCADE BLADE MISTUNING. II - GLOBAL OPTIMUM AND NUMERICAL OPTIMIZATION
E. NISSIM and R. T. HAFTKA (Virginia Polytechnic Institute and State University, Blacksburg) AIAA Journal (ISSN 0001-1452), vol. 23, Sept. 1985, p. 1402-1410.
(Contract NAG3-347)

The values of the mistuning which yield the most stable eigenvectors are analytically determined, using the simplified equations of motion which were developed in Part I of this work. It is shown that random mistunings, if large enough, may lead to the maximal stability, whereas the alternate mistunings cannot. The problem of obtaining maximum stability for minimal mistuning is formulated, based on numerical optimization techniques. Several local minima are obtained using different starting mistuning vectors. The starting vectors which lead to the global minimum are identified. It is analytically shown that all minima appear in multiplicities which are equal to the number of compressor blades. The effect of mistuning on the flutter speed is studied using both an optimum mistuning vector and an alternate mistuning vector. Effects of mistunings in elastic axis locations are shown to have a negligible effect on the eigenvalues. Finally, it is shown that any general two-dimensional bending-torsion system can be reduced to an equivalent uncoupled torsional system. Author

A85-45854*# National Aeronautics and Space Administration. Lewis Research Center, Cleveland, Ohio.
VIBRATION AND FLUTTER OF MISTUNED BLADED-DISK ASSEMBLIES
K. R. V. KAZA and R. E. KIELB (NASA, Lewis Research Center, Cleveland, OH) Journal of Propulsion and Power (ISSN 0748-4658), vol. 1, Sept.-Oct. 1985, p. 336-344. Previously cited in issue 05, p. 602, Accession no. A85-16095. refs

A85-47021*# National Aeronautics and Space Administration. Lewis Research Center, Cleveland, Ohio.
LARGE-SCALE ADVANCED PROPFAN (LAP) PROGRAM PROGRESS REPORT
D. A. SAGERSER (NASA, Lewis Research Center, Cleveland, OH) and S. G. LUDEMANN (United Technologies Corp., Hamilton Standard Div., Windsor Locks, CT) AIAA, SAE, ASME, and ASEE, Joint Propulsion Conference, 21st, Monterey, CA, July 8-10, 1985. 26 p. Previously announced in STAR as N85-29964. refs
(AIAA PAPER 85-1187)

The propfan is an advanced propeller concept which maintains the high efficiencies traditionally associated with conventional propellers at the higher aircraft cruise speeds associated with jet transports. The large-scale advanced propfan (LAP) program extends the research done on 2 ft diameter propfan models to a 9 ft diameter article. The program includes design, fabrication, and testing of both an eight bladed, 9 ft diameter propfan, designated SR-7L, and a 2 ft diameter aeroelastically scaled model, SR-7A. The LAP program is complemented by the propfan test assessment (PTA) program, which takes the large-scale propfan and mates it with a gas generator and gearbox to form a propfan propulsion system and then flight tests this system on the wing of a Gulfstream 2 testbed aircraft. Author

A85-49021* National Aeronautics and Space Administration. Lewis Research Center, Cleveland, Ohio.
A GENERALIZED COMPUTER CODE FOR DEVELOPING DYNAMIC GAS TURBINE ENGINE MODELS (DIGTEM)
C. J. DANIELE (NASA, Lewis Research Center, Cleveland, OH) IN: Aerospace simulation; Proceedings of the Conference, San Diego, CA, February 2-4, 1984 . La Jolla, CA, Society for Computer Simulation, 1984, p. 212-221. Previously announced in STAR as N84-12166. refs

This paper describes DIGTEM (digital turbofan engine model), a computer program that simulates two spool, two stream (turbofan) engines. DIGTEM was developed to support the development of a real time multiprocessor based engine simulator being designed at the Lewis Research Center. The turbofan engine model in DIGTEM contains steady state performance maps for all the components and has control volumes where continuity and energy balances are maintained. Rotor dynamics and duct momentum dynamics are also included. DIGTEM features an implicit integration scheme for integrating stiff systems and trims the model equations to match a prescribed design point by calculating correction coefficients that balance out the dynamic equations. It uses the same coefficients at off design points and iterates to a balanced engine condition. Transients are generated by defining the engine inputs as functions of time in a user written subroutine (TMRSP). Closed loop controls can also be simulated. DIGTEM is generalized in the aerothermodynamic treatment of components. This feature, along with DIGTEM's trimming at a design point, make it a very useful tool for developing a model of a specific turbofan engine. B.W.

N85-10064*# National Aeronautics and Space Administration. Lewis Research Center, Cleveland, Ohio.
COMBUSTION GAS PROPERTIES I-ASTM JET A FUEL AND DRY AIR
R. E. JONES, A. M. TROUT, J. D. WEAR, and B. J. MCBRIDE Oct. 1984 12 p refs Document incl. microfiche supplement
(NASA-TP-2359; NAS 1.60:2359) Avail: NTIS HC E03/MF A01 CSCL 21E

A series of computations was made to produce the equilibrium temperature and gas composition for ASTM jet A fuel and dry air. The computed tables and figures provide combustion gas property data for pressures from 0.5 to 50 atmospheres and equivalence ratios from 0 to 2.0. S.B.

N85-10065*# National Aeronautics and Space Administration. Lewis Research Center, Cleveland, Ohio.
COMPARISON OF NUMERICAL TECHNIQUES FOR INTEGRATION OF STIFF ORDINARY DIFFERENTIAL EQUATIONS ARISING IN COMBUSTION CHEMISTRY
K. RADHAKRISHNAN Oct. 1984 41 p refs Sponsored in part by Michigan Univ. and NRC
(Contract NAG3-147; NAG3-294)
(NASA-TP-2372; E-2149; NAS 1.60:2372) Avail: NTIS HC A03/MF A01 CSCL 21E

The efficiency and accuracy of several algorithms recently developed for the efficient numerical integration of stiff ordinary differential equations are compared. The methods examined include two general-purpose codes, EPISODE and LSODE, and three codes (CHEMEQ, CREK1D, and GCKP84) developed specifically to integrate chemical kinetic rate equations. The codes are applied to two test problems drawn from combustion kinetics. The comparisons show that LSODE is the fastest code currently available for the integration of combustion kinetic rate equations. An important finding is that an interactive solution of the algebraic energy conservation equation to compute the temperature does not result in significant errors. In addition, this method is more efficient than evaluating the temperature by integrating its time derivative. Significant reductions in computational work are realized by updating the rate constants (k = at(supra N) N exp(-E/RT) only when the temperature change exceeds an amount delta T that is problem dependent. An approximate expression for the automatic evaluation of delta T is derived and is shown to result in increased efficiency. Author

N85-10067*# National Aeronautics and Space Administration. Lewis Research Center, Cleveland, Ohio.
EFFECT OF COMBINED PRESSURE AND TEMPERATURE DISTORTION ORIENTATION ON HIGH-BYPASS-RATIO TURBOFAN ENGINE STABILITY
R. H. SOEDER and C. M. MEHALIC Washington Oct. 1984 37 p refs
(NASA-TM-83771; E-2262; NAS 1.15:83771) Avail: NTIS HC A03/MF A01 CSCL 21E

Total-temperature, static-pressure and total-pressure distributions were measured in the inlet duct upstream of the engine inlet and within the fan and compressor of a YTF34 turbofan engine. Free-stream and boundary layer yaw angle variations were measured between a rotable screen assembly and the engine inlet. Total pressure distortions were generated using three 180 deg extent screens and total temperature distortions were generated using a rotatable hydrogen burner. Reynolds number index upstream of the rotatable screen assembly was maintained at 0.5 (based on the undistorted sectors at station 1, the inlet flow measuring station). The engine mechanical fan speed at sea level condition was rated at 7005 rpm. The engine was tested at a corrected fan speed of 90 percent of rated condition. Yaw angle increased between the rotatable screen assembly and the engine inlet. The largest variation in free-stream and boundary layer yaw angle occurs when the combined distortions are 180 deg out-of-phase. Static-pressure distortion increased exponentially as flow approached the engine. Total-pressure distortions were attenuated between the engine inlet and the compressor exit. Total-temperature distortion persisted through the compressor for all four combined distortions investigated. Author

N85-10068*# National Aeronautics and Space Administration. Lewis Research Center, Cleveland, Ohio.
CREKID: A COMPUTER CODE FOR TRANSIENT, GAS-PHASE COMBUSTION OF KINETICS
D. T. PRATT (Washington Univ., Seattle) and K. RADHAKRISHNAN Washington Oct. 1984 38 p refs
(Contract NAG3-147)
(NASA-TM-83806; E-2176; NAS 1.15:83806) Avail: NTIS HC A03/MF A01 CSCL 21B

A new algorithm was developed for fast, automatic integration of chemical kinetic rate equations describing homogeneous, gas-phase combustion at constant pressure. Particular attention is

paid to the distinguishing physical and computational characteristics of the induction, heat-release and equilibration regimes. The two-part predictor-corrector algorithm, based on an exponentially-fitted trapezoidal rule, includes filtering of ill-posed initial conditions, automatic selection of Newton-Jacobi or Newton iteration for convergence to achieve maximum computational efficiency while observing a prescribed error tolerance. The new algorithm was found to compare favorably with LSODE on two representative test problems drawn from combustion kinetics.
B.W.

N85-10069*# National Aeronautics and Space Administration. Lewis Research Center, Cleveland, Ohio.
COMPUTATIONAL THERMO-FLUID DYNAMICS CONTRIBUTIONS TO ADVANCED GAS TURBINE ENGINE DESIGN
R. W. GRAHAM, J. J. ADAMCZYK, and H. E. ROHLIK Washington 1984 13 p refs Proposed for presentation at the 23d Aerospace Sciences Meeting, Reno, Nev., 14-17 Jan. 1985; sponsored by AIAA Previously announced in IAA as A85-19509
(NASA-TM-86865; E-2194; NAS 1.15:86865) Avail: NTIS HC A02/MF A01 CSCL 21E

The design practices for the gas turbine are traced throughout history with particular emphasis on the calculational or analytical methods. Three principal components of the gas turbine engine will be considered: namely, the compressor, the combustor and the turbine.
B.W.

N85-10947*# United Technologies Corp., East Hartford, Conn. Engineering Div.
ENERGY EFFICIENT ENGINE FLIGHT PROPULSION SYSTEM PRELIMINARY ANALYSIS AND DESIGN REPORT Final Update Report
J. W. BISSET and D. C. HOWE Sep. 1983 166 p refs
(Contract NAS3-20646)
(NASA-CR-174701; NAS 1.26:174701; PWA-5594-248) Avail: NTIS HC A08/MF A01 CSCL 21E

The final design and analysis of the flight propulsion system is presented. This system is the conceptual study engine defined to meet the performance, economic and environmental goals established for the Energy Efficient Engine Program. The design effort included a final definition of the engine, major components, internal subsystems, and nacelle. Various analytical representations and results from component technology programs are used to verify aerodynamic and structural design concepts and to predict performance. Specific design goals and specifications, reflecting future commercial aircraft propulsion system requirements for the mid-1980's, are detailed by NASA and used as guidelines during engine definition. Information is also included which details salient results from a separate study to define a turbofan propulsion system, known as the maximum efficiency engine, which reoptimized the advanced fuel saving technologies for improved fuel economy and direct operating costs relative to the flight propulsion system.
M.A.C.

N85-10948*# Washington Univ., Seattle.
AN INTERACTIVE COMPUTER CODE FOR CALCULATION OF GAS-PHASE CHEMICAL EQUILIBRIUM (EQLBRM) Final Report
B. S. PRATT and D. T. PRATT Oct. 1984 22 p refs
(Contract NAG3-277)
(NASA-CR-168337; NAS 1.26:168337) Avail: NTIS HC A02/MF A01 CSCL 21E

A user friendly, menu driven, interactive computer program known as EQLBRM which calculates the adiabatic equilibrium temperature and product composition resulting from the combustion of hydrocarbon fuels with air, at specified constant pressure and enthalpy is discussed. The program is developed primarily as an instructional tool to be run on small computers to allow the user to economically and efficiency explore the effects of varying fuel type, air/fuel ratio, inlet air and/or fuel temperature, and operating pressure on the performance of continuous combustion devices such as gas turbine combustors, Stirling engine burners, and power generation furnaces.
M.A.C.

N85-10949*# National Aeronautics and Space Administration. Lewis Research Center, Cleveland, Ohio.
ACCELERATED CONVERGENCE FOR INCOMPRESSIBLE FLOW CALCULATIONS
G. M. NEELY and R. W. CLAUS 1984 13 p refs Proposed for presentation at the 23rd Aerospace Sci. Meeting, Reno, Nev., 14-17 Jan. 1985; sponsored by the American Inst. of Aeronautics and Astronautics
(NASA-TM-86863; E-2327; NAS 1.15:86863) Avail: NTIS HC A02/MF A01 CSCL 21E

Two improved algorithms which solve the steady-state Navier-Stokes equations, PISO and SIMPLER, are studied. Computations were carried out on progressively finer grids for the driven cavity and flow over a backward-facing step. The effects of relaxation factor, number of grid nodes and number of sweeps through the pressure equations are studied to evaluate the performance of the PISO and SIMPLER schemes. Results show that these improved schemes accelerate the convergence rate of the solution generally by a factor of two as compared to the SIMPLE method.
Author

N85-10950*# United Technologies Corp., East Hartford, Conn.
ENERGY EFFICIENT ENGINE COMBUSTOR TEST HARDWARE DETAILED DESIGN REPORT
M. H. ZEISSER, W. GREENE, and D. J. DUBIEL Mar. 1982 105 p refs
(Contract NAS3-20646)
(NASA-CR-167945; NAS 1.26:167945; PWA-5594-197) Avail: NTIS HC A06/MF A01 CSCL 21E

The combustor for the Energy Efficient Engine is an annular, two-zone component. As designed, it either meets or exceeds all program goals for performance, safety, durability, and emissions, with the exception of oxides of nitrogen. When compared to the configuration investigated under the NASA-sponsored Experimental Clean Combustor Program, which was used as a basis for design, the Energy Efficient Engine combustor component has several technology advancements. The prediffuser section is designed with short, strutless, curved-walls to provide a uniform inlet airflow profile. Emissions control is achieved by a two-zone combustor that utilizes two types of fuel injectors to improve fuel atomization for more complete combustion. The combustor liners are a segmented configuration to meet the durability requirements at the high combustor operating pressures and temperatures. Liner cooling is accomplished with a counter-parallel FINWALL technique, which provides more effective heat transfer with less coolant.
Author

N85-10951*# National Aeronautics and Space Administration. Lewis Research Center, Cleveland, Ohio.
TURBINE ENGINE HOT SECTION TECHNOLOGY (HOST)
Washington Oct. 1982 356 p refs Workshop held in Cleveland, 19-20 Oct. 1982
(NASA-TM-83022; E-1458; NAS 1.15:83022) Avail: NTIS HC A16/MF A01 CSCL 21E

Research and plans concerning aircraft gas turbine engine hot section durability problems were discussed. Under the topics of structural analysis, fatigue and fracture, surface protective coatings, combustion, turbine heat transfer, and instrumentation specific points addressed were the thermal and fluid environment around liners, blades, and vanes, material coatings, constitutive behavior, stress-strain response, and life prediction methods for the three components.

N85-10954*# National Aeronautics and Space Administration. Lewis Research Center, Cleveland, Ohio.
NONLINEAR STRUCTURAL AND LIFE ANALYSES OF A TURBINE BLADE
A. KAUFMAN *In its* Turbine Eng. Hot Sect. Technol. (HOST) p 39-44 Oct. 1982
Avail: NTIS HC A16/MF A01 CSCL 21E

The most critical structural requirements that aircraft gas turbine engines must meet result from the diversity of extreme environmental conditions in the turbine section components. Accurate life assessment of the components under these conditions requires sound analytical tools and techniques. The utility of advanced structural analysis techniques and advanced life prediction techniques in the life assessment of hot-section components was evaluated. The extend to which a three-dimensional cyclic isoparametric finite element analysis of a hot-section component would improve the accuracy of component life predictions was assessed. At the same time, high temperature life prediction theories such as strainrange partitioning and the frequency modified approaches were applied and their efficiency judged. A stress analysis was performed on a commercial air-cooled turbine blade. The evaluation of the life prediction methods indicated that none of those studied were satisfactory. R.S.F.

N85-10955*# National Aeronautics and Space Administration. Lewis Research Center, Cleveland, Ohio.
NONLINEAR STRUCTURAL AND LIFE ANALYSES OF A COMBUSTOR LINER
A. KAUFMAN *In its* Turbine Eng. Hot Sect. Technol. (HOST) p 45-53 Oct. 1982
Avail: NTIS HC A16/MF A01 CSCL 21E

Three-dimensional, nonlinear, finite element structural analyses were performed for a simulated aircraft combustor liner specimen in order to assess the capability of nonlinear analyses using classical inelastic material models to represent the thermoplastic-creep response of the component. In addition, the computed stress-strain history at the critical location was input into life prediction methods in order to evaluate the ability of these procedures to predict crack initiation life. It is concluded that: (1) elastic analysis is adequate for obtaining strain range and critical location; (2) inelastic analyses did not accurately represent cyclic behavior of materials; and (3) none of the crack initiation life prediction methods were satisfactory. R.S.F.

N85-10956*# National Aeronautics and Space Administration. Lewis Research Center, Cleveland, Ohio.
PRE-HOST HIGH TEMPERATURE CRACK PROPAGATION
T. W. ORANGE *In its* Turbine Eng. Hot Sect. Technol. (HOST) p 55-63 Oct. 1982
Avail: NTIS HC A16/MF A01 CSCL 21E

The highlights of NASA contract CR-167896, Fracture Mechanics Criteria for Turbine Engine Hot Section Components, are presented. The five technical tasks of the program are reviewed. Results of several tasks are presented. R.S.F.

N85-10957*# National Aeronautics and Space Administration. Lewis Research Center, Cleveland, Ohio.
HOST INSTRUMENTATION R AND D PROGRAM OVERVIEW
N. C. WENGER *In its* Turbine Eng. Hot Sect. Technol. (HOST) p 65-68 Oct. 1982
Avail: NTIS HC A16/MF A01 CSCL 21E

The turbine hot-section technology (HOST) Instrumentation R&D program focuses on two main classes of instrumentation: (1) those that characterizes the environment around the turbine engine components, which include gas flows measurement, gas temperatures, and heat fluxes; (2) to characterize the effect of the environment on the turbine engine components, which include strain measurements and an optical system to structural responses such as cracking, buckling, spalling, carbon buildup. The HOST Instrumentation R&D program concentrates on the critical measurements that can not be made by commercially available instruments or with instruments that are already in development. The measurements of strain and gas flow are emphasized, these measurements are extremely critical to the success of the HOST program and the HOST requirements differ from the current state of the art by a considerable margin. E.A.K.

N85-10959*# United Technologies Research Center, East Hartford, Conn.
HIGH TEMPERATURE STATIC STRAIN SENSOR DEVELOPMENT PROGRAM
C. HULSE, F. LEMKEY, R. BAILEY, and H. GRANT *In* NASA. Lewis Research Center Turbine Eng. Hot Sect. Technol. (HOST) p 83-91 Oct. 1982
(Contract NAS3-23169)
Avail: NTIS HC A16/MF A01 CSCL 21E

The development of resistance strain gages which are useful for static strain measurements on nickel or cobalt superalloy parts inside a gas turbine engine on a test stand were examined. These measurements of a strain gage alloy development program which to be followed by an optional investigation of complete strain gage systems which will use the best of the alloys developed together with other system improvements is reviewed. The specific goal for the complete system is to make measurements to 2,000 micro epsilon with error of only + or - 10% over a 50 hour period. In addition to simple survival and stability, attaining a low thermal coefficient to resistivity, of order 100 ppm/K or less, is also a major goal. The first task was to select candidate alloys or alloy systems using a search of the literature and the available metallurgical theory. Alloy candidates were evaluated and compared by a grading system. Equipment and techniques were developed which are suitable for iterative studies of a variety of compositions. Many compositions were examined and significantly improved alloys were identified. E.A.K.

N85-10962*# National Aeronautics and Space Administration. Lewis Research Center, Cleveland, Ohio.
HOT SECTION LASER ANEMOMETRY
W. C. NIEBERDING *In its* Turbine Eng. Hot Sect. Technol. (HOST) p 109-112 Oct. 1982 refs
Avail: NTIS HC A16/MF A01 CSCL 21E

The objectives and problems faced in the development of a laser anemometry system for hot section applications was discussed. The goal was to map the flow profiles through and between the vanes and between the rotating blades of a turbine. A laser anemometer system was developed which measures the Doppler shift directly along the optical axis. Some testing is being conducted in a small bench top combustor facility. The cost involved in this testing was also discussed. E.R.

N85-10964*# National Aeronautics and Space Administration. Lewis Research Center, Cleveland, Ohio.
TURBINE HEAT TRANSFER
J. E. ROHDE *In its* Turbine Eng. Hot Sect. Technol. (HOST) p 119-136 Oct. 1982
Avail: NTIS HC A16/MF A01 CSCL 21E

Objectives and approaches to research in turbine heat transfer are discussed. Generally, improvements in the method of determining the hot gas flow through the turbine passage is one area of concern, as is the cooling air flow inside the airfoil, and the methods of predicting the heat transfer rates on the hot gas side and on the coolant side of the airfoil. More specific areas of research are: (1) local hot gas recovery temperatures along the airfoil surfaces; (2) local airfoil wall temperature; (3) local hot gas side heat transfer coefficients on the airfoil surfaces; (4) local coolant side heat transfer coefficients inside the airfoils; (5) local hot gas flow velocities and secondary flows at real engine conditions; and (6) local delta strain range of the airfoil walls. E.R.

N85-10968*# National Aeronautics and Space Administration. Lewis Research Center, Cleveland, Ohio.
COOLANT PASSAGE HEAT TRANSFER WITH ROTATION
J. E. ROHDE *In its* Turbine Eng. Hot Sect. Technol. (HOST) p 175-179 Oct. 1982
Avail: NTIS HC A16/MF A01 CSCL 21E

Although the effects of the coriolis and buoyancy forces due to rotation on coolant-side heat transfer are generally not included in the design methods for blades, the influence of these forces could be large. Comparisons of nonrotating heat transfer data and extrapolations of available correlation for the average heat transfer coefficients with radial outflow of cooling air showed that neglecting rotation at gas turbine engine conditions result in variations in the heat transfer coefficient by as much as 45 percent. This, in effect, results in blade metal temperatures running as much as 100 F different from predicted values. This also may explain why rotating blade metal temperatures in engine tests are often higher than expected from results obtained in nonrotating cascade tests. B.G.

N85-10969*# National Aeronautics and Space Administration. Lewis Research Center, Cleveland, Ohio.
STRUCTURAL ANALYSIS
R. H. JOHNS *In its* Turbine Eng. Hot Sect. Technol. (HOST) p 181-184 Oct. 1982
Avail: NTIS HC A16/MF A01 CSCL 21E

Hot section components of aircraft gas turbine engines are subjected to severe thermal-structural loading conditions, especially during the start-up and take-off portions of the engine cycle. The most severe and damaging stresses and strains are those induced by the steep thermal gradients induced during the start-up transient. These transient stresses and strains are also the most difficult to predict, in part because the temperature gradients and distributions are not well known or predictable, and also because the cyclic elasto-viscoplastic behavior of the materials at these extremes of temperature and strain are not well known or predictable. One element of the structures program will develop improved time-varying thermal-mechanical load models for the entire engine mission cycle from start-up to shutdown. The thermal model refinements will be consistent with those required by the structural code including considerations of mesh-point density, strain concentrations, and thermal gradients. Models will be developed for the burner liner, turbine vane and turbine blade. B.G.

N85-10971*# National Aeronautics and Space Administration. Lewis Research Center, Cleveland, Ohio.
COMPONENT-SPECIFIC MODELING
M. S. HIRSCHBEIN *In its* Turbine Eng. Hot Sect. Technol. (HOST) p 197-202 Oct. 1982
Avail: NTIS HC A16/MF A01 CSCL 21E

The ability to accurately structurally analyze engine components to assure that they can survive for their designed lifetime in an increasingly harsh environment is discussed. Under the HOST (HOt Section Technology) program, advanced component-specific modeling methods, with built-in analysis capability, will be developed separately for burner liners, turbine blades and vanes. These modeling methods will make maximum use of, but will not rely solely on, existing analysis methods and techniques, to analyze the three identified components. Nor will the complete structural analysis of a component necessarily be performed as a single analysis. The approach to be taken will develop complete software analysis packages with internal, component-specific, self-adaptive solution strategies. Each package will contain a set of modeling and analysis tools. The selection and order of specific methods and techniques within the set to be applied will depend on the specific-component, the current thermo-mechanical loading, and the current state of the component. All modeling and analysis decisions will be made internally based on developed decision criteria within the solution strategies; minimal user intervention will be required. B.W.

N85-10972*# National Aeronautics and Space Administration. Lewis Research Center, Cleveland, Ohio.
THE 3-D INELASTIC ANALYSIS METHODS FOR HOT SECTION COMPONENTS: BRIEF DESCRIPTION
C. C. CHAMIS *In its* Turbine Eng. Hot Sect. Technol. (HOST) p 203-208 Oct. 1982
Avail: NTIS HC A16/MF A01

Advanced 3-D inelastic structural/stress analysis methods and solution strategies for more accurate yet more cost-effective analysis of components subjected to severe thermal gradients and loads in the presence of mechanical loads, with steep stress and strain gradients are being developed. Anisotropy, time and temperature dependent plasticity and creep effects are also addressed. The approach is to develop four different theories, one linear and three higher order theories (polynomial function, special function, general function). The theories are progressively more complex from linear to general function in order to provide streamlined analysis capability with increasing accuracy for each hot section component and for different parts of the same component according to the severity of the local stress, strain and temperature gradients associated with hot spots, cooling holes and surface coating cracks. To further enhance the computational effectiveness, the higher order theories will have embedded singularities (cooling passages, for example) in the generic modeling region. Each of the four theories consists of three formulation models derivable from independent theoretical formulations. These formulation models are based on: (1) mechanics of materials; (2) special finite elements; and (3) an advanced formulation to be recommended by the contractor. B.W.

N85-10973*# National Aeronautics and Space Administration. Lewis Research Center, Cleveland, Ohio.
LIFE PREDICTION AND CONSTITUTIVE BEHAVIOR: OVERVIEW
G. R. HALFORD *In its* Turbine Eng. Hot Sect. Technol. (HOST) p 209-212 Oct. 1982
Avail: NTIS HC A16/MF A01 CSCL 21E

The evolution of programs to investigate high temperature consititutive behavior and develop cyclic life prediction methods is reviewed. Contracts granted for developing and verifying workable engineering methods for the calculation, in advance of service, of the local stress-strain response at the critical life governing location in typical hot section components as well as the resultant cyclic crack initiation and crack growth lifetimes are listed. The Langley fatigue facility is being upgraded to include: (1) a servocontrolled testing machine for high temperature crack growth; (2) three servocontrolled tension/torsion machines for biaxial studies; (3) a HOST/satellite computer for data acquisition, processing, storage, and retrieval; and (4) HCV/LCF machines for cumulative damage studies. A.R.H.

N85-10975*# National Aeronautics and Space Administration. Lewis Research Center, Cleveland, Ohio.
CONSTITUTIVE MODEL DEVELOPMENT FOR ISOTROPIC MATERIALS
A. KAUFMAN *In its* Turbine Eng. Hot Sect. Technol. (HOST) p 215-221 Oct. 1982
Avail: NTIS HC A16/MF A01 CSCL 21E

The objective is to develop a unified constitutive model for finite-element structural analysis of turbine engine hot section components. This effort constitutes a different approach for nonlinear finite-element computer codes which were heretofore based on classical inelastic methods. A unified constitutive theory will avoid the simplifying assumptions of classical theory and should more accurately represent the behavior of superalloy materials under cyclic loading conditions and high temperature environments. Model development will be directed toward isotropic, cast nickel-base alloys used for aircooled turbine blades and vanes. The contractor will select a base material for model development and an alternate material for verification purposes from a list of three alloys specified by NASA. The candidate alloys represent a cross-section of turbine blade and vane materials of interest to

both large and small size engine manufacturers. Material stock for the base and alternate materials will be supplied to the Contractor by the government. R.J.F.

N85-10977*# National Aeronautics and Space Administration. Lewis Research Center, Cleveland, Ohio.
HOST HIGH TEMPERATURE CRACK PROPAGATION
T. W. ORANGE *In its* Turbine Eng. Hot Sect. Technol. (HOST) p 227-229 Oct. 1982
Avail: NTIS HC A16/MF A01 CSCL 21E

Methods for characterizing and predicting crack growth at elevated temperatures are discussed. Nonlinear behavior, thermal gradients, and thermomechanical cycling are discussed. R.J.F.

N85-10978*# National Aeronautics and Space Administration. Lewis Research Center, Cleveland, Ohio.
SURFACE PROTECTION OVERVIEW
S. R. LEVINE *In its* Turbine Eng. Hot Sect. Technol. (HOST) p 231-239 Oct. 1982
Avail: NTIS HC A16/MF A01 CSCL 21E

A first-cut integrated environmental attack life prediction methodology for hot section components is addressed. The HOST program is concerned with oxidation and hot corrosion attack of metallic coatings as well as their degradation by interdiffusion with the substrate. The effects of the environment and coatings on creep/fatigue behavior are being addressed through a joint effort with the Fatigue sub-project. An initial effort will attempt to scope the problem of thermal barrier coating life prediction. Verification of models will be carried out through benchmark rig tests including a 4 atm. replaceable blade turbine and a 50 atm. pressurized burner rig. B.W.

N85-10979*# National Aeronautics and Space Administration. Lewis Research Center, Cleveland, Ohio.
AIRFOIL DEPOSITION MODEL
F. J. KOHL *In its* Turbine Eng. Hot Sect. Technol. (HOST) p 241-257 Oct. 1982 refs
Avail: NTIS HC A16/MF A01 CSCL 21E

The methodology to predict deposit evolution (deposition rate and subsequent flow of liquid deposits) as a function of fuel and air impurity content and relevant aerodynamic parameters for turbine airfoils is developed in this research. The spectrum of deposition conditions encountered in gas turbine operations includes the mechanisms of vapor deposition, small particle deposition with thermophoresis, and larger particle deposition with inertial effects. The focus is on using a simplified version of the comprehensive multicomponent vapor diffusion formalism to make deposition predictions for: (1) simple geometry collectors; and (2) gas turbine blade shapes, including both developing laminar and turbulent boundary layers. For the gas turbine blade the insights developed in previous programs are being combined with heat and mass transfer coefficient calculations using the STAN 5 boundary layer code to predict vapor deposition rates and corresponding liquid layer thicknesses on turbine blades. A computer program is being written which utilizes the local values of the calculated deposition rate and skin friction to calculate the increment in liquid condensate layer growth along a collector surface. B.W.

N85-10980*# National Aeronautics and Space Administration. Lewis Research Center, Cleveland, Ohio.
EFFECTS OF SURFACE CHEMISTRY ON HOT CORROSION LIFE: OVERVIEW
J. MERUTKA *In its* Turbine Eng. Hot Sect. Technol. (HOST) p 263-267 Oct. 1982
Avail: NTIS HC A16/MF A01 CSCL 21E

This program concentrates on analyzing a limited number of hot corroded components from the field and the carrying out of a series of controlled laboratory experiments to establish the effects of oxide scale and coating chemistry on hot corrosion life. This is to be determined principally from the length of the incubation period, the investigation of the mechanisms of hot corrosion attack, and the fitting of the data generated from the test exposure experiments to an empirical life prediction model. Author

N85-10984*# National Aeronautics and Space Administration. Lewis Research Center, Cleveland, Ohio.
DILUTION ZONE MIXING STUDIES
J. D. HOLDEMAN *In its* Turbine Eng. Hot Sect. Technol. (HOST) p 307-314 Oct. 1982 refs
Avail: NTIS HC A16/MF A01 CSCL 21E

The objectives and status of a project to investigate various aspects of the jet in a confined cross flow problem are outlined. The experiments performed thus far dealt primarily with a single row of jets mixing into an isothermal flow in a constant cross section duct. Variations in the mixing were observed as a function of jet to mainstream momentum ratio, orifice size, and spacing. The current experiments examine perturbations of this problem characteristic to gas turbine combustion chambers, namely: flow area convergence, nonisothermal mainstream flow, and opposed in line and staggered injection. An empirical model was developed to describe the observed temperature distributions. The current interactive code provides a 3-D pictorial representation of the temperature, as given by these correlations, for any user specified downstream location, flow, and orifice parameters. M.G.

N85-10986*# National Aeronautics and Space Administration. Lewis Research Center, Cleveland, Ohio.
COMBUSTION SYSTEM FOR RADIATION INVESTIGATIONS
J. D. WEAR *In its* Turbine Eng. Hot Sect. Technol. (HOST) p 331-334 Oct. 1982
Avail: NTIS HC A16/MF A01 CSCL 21E

An inlet interface flange, inlet diffuser, fuel struts and nozzles, combustor liner, liner housing and exhaust flange comprise a system to be installed in an existing test facility. The system was designed for operation at 40 atmospheres inlet pressure, 900 K inlet temperature, and air flow to 80 kg/sec. Six penetrations are provided in the outer pressure housing. Adapters at the penetrations, permit use of various types of radiation instrumentation. Five total radiation radiometers and two heat flux gases were installed. Rotating exhaust instrumentation can also be used to determine combustor performance. Data are presented showing total radiation at three axial positions of the combustor, and comparison of total radiation with data from a heat flux gage. A.R.H.

N85-10987*# National Aeronautics and Space Administration. Lewis Research Center, Cleveland, Ohio.
VALIDATION OF STRUCTURAL ANALYSIS METHODS USING THE IN-HOUSE LINER CYCLIC RIGS
R. L. THOMPSON *In its* Turbine Eng. Hot Sect. Technol. (HOST) p 335-344 Oct. 1982
Avail: NTIS HC A16/MF A01 CSCL 21E

Test conditions and variables to be considered in each of the test rigs and test configurations, and also used in the validation of the structural predictive theories and tools, include: thermal and mechanical load histories (simulating an engine mission cycle; different boundary conditions; specimens and components of different dimensions and geometries; different materials; various cooling schemes and cooling hole configurations; several advanced burner liner structural design concepts; and the simulation of hot streaks. Based on these test conditions and test variables, the test matrices for each rig and configurations can be established to verify the predictive tools over as wide a range of test conditions as possible using the simplest possible tests. A flow chart for the thermal/structural analysis of a burner liner and how the analysis relates to the tests is shown schematically. The chart shows that several nonlinear constitutive theories are to be evaluated. A.R.H.

N85-10988*# National Aeronautics and Space Administration. Lewis Research Center, Cleveland, Ohio.
HOST LINER CYCLIC FACILITIES: FACILITY DESCRIPTION
D. SCHULTZ *In its* Turbine Eng. Hot Sect. Technol. (HOST) p 345-360 Oct. 1982
Avail: NTIS HC A16/MF A01 CSCL 21E

A quartz lamp box, a quartz lamp annular rig, and a low pressure liner cyclic can rig planned for liner cyclic tests are described. Special test instrumentation includes an IR-TV camera system for measuring liner cold side temperatures, thin film thermocouples for measuring liner hot side temperatures, and laser and high temperature strain gages for obtaining local strain measurements. A plate temperature of 2,000 F was obtained in an initial test of an apparatus with three quartz lamps. Lamp life, however, appeared to be limited for the standard commercial quartz lamps available. The design of vitiated and nonvitiated preheaters required for the quartz lamp annular rig and the cyclic can test rigs is underway. A.R.H.

N85-10989*# General Electric Co., Cincinnati, Ohio. Aircraft Engine Business Group.
ENERGY EFFICIENT ENGINE COMPONENT DEVELOPMENT AND INTEGRATION PROGRAM Semiannual Report, 1 Oct. 1981 - 31 Mar. 1982
Apr. 1982 346 p
(Contract NAS3-20643)
(NASA-CR-169496; NAS 1.26:169496; R82AEB285; SAR-8)
Avail: NTIS HC A15/MF A01 CSCL 21E

The development of the technology to improve energy efficiency of propulsion systems for subsonic commercial aircrafts was examined. Goals established include: (1) fuel consumption, reduction in flight propulsion system; (2) direct operation cost; (3) noise, with provision for engine growth corresponding to future engine application; and (4) emissions, EPA new engine standards. E.A.K.

N85-10990*# General Electric Co., Cincinnati, Ohio. Aircraft Engine Business Group.
ENERGY EFFICIENT ENGINE COMPONENT DEVELOPMENT AND INTEGRATION PROGRAM Semiannual Report, 1 Apr. - 30 Sep. 1981
30 Oct. 1981 338 p
(Contract NAS3-20643)
(NASA-CR-170034; NAS 1.26:170034; R81AEG709; SAR-7)
Avail: NTIS HC A15/MF A01 CSCL 21E

Accomplishments in the Energy Efficient Engine Component Development and Integration program during the period of April 1, 1981 through September 30, 1981 are discussed. The major topics considered are: (1) propulsion system analysis, design, and integration; (2) engine component analysis, design, and development; (3) core engine tests; and (4) integrated core/low spool testing. R.S.F.

N85-10991*# TRW, Inc., Cleveland, Ohio. Materials Technology.
ENERGY EFFICIENT ENGINE. VOLUME 2. APPENDIX A: COMPONENT DEVELOPMENT AND INTEGRATION PROGRAM Final Semiannual Status Report, 1 Apr. - 30 Sep. 1981
D. J. MORACZ and C. R. COOK East Hartford, Conn. Pratt and Whitney Aircraft 30 Oct. 1981 200 p refs Prepared for Pratt and Whitney Aircraft, East Hartford, Conn. 2 Vol.
(Contract NAS3-20646)
(NASA-CR-173085; NAS 1.26:173085; PWA-5594-179-VOL-2-APP-A; ER-8050-F-VOL-2-APP-A; SASR-7-VOL-2-APP-A) Avail: NTIS HC A09/MF A01 CSCL 21E

The large size and the requirement for precise lightening cavities in a considerable portion of the titanium fan blades necessitated the development of a new manufacturing method. The approach which was selected for development incorporated several technologies including HIP diffusion bonding of titanium sheet laminates containing removable cores and isothermal forging of the blade form. The technology bases established in HIP/DB for composite blades and in isothermal forging for fan blades were applicable for development of the manufacturing process. The process techniques and parameters for producing and inspecting the cored diffusion bonded titanium laminate blade preform were established. The method was demonstrated with the production of twelve hollow simulated blade shapes for evaluation. Evaluations of the critical experiments conducted to establish procedures to produce hollow structures by a laminate/core/diffusion bonding approach are included. In addition the transfer of this technology to produce a hollow fan blade is discussed. B.G.

N85-10992*# Pratt and Whitney Aircraft, East Hartford, Conn. Commercial Products Div.
ENERGY EFFICIENT ENGINE. VOLUME 1: COMPONENT DEVELOPMENT AND INTEGRATION PROGRAM Semiannual Status Report, 1 Apr. - 30 Sep. 1981
30 Oct. 1981 228 p 2 Vol.
(Contract NAS3-20646)
(NASA-CR-173084; NAS 1.26:173084; PWA-5594-179-VOL-1; SASR-7-VOL-1) Avail: NTIS HC A11/MF A01 CSCL 21E

Technology for achieving lower installed fuel consumption and lower operating costs in future commercial turbofan engines are developed, evaluated, and demonstrated. The four program objectives are: (1) propulsion system analysis; (2) component analysis, design, and development; (3) core design, fabrication, and test; and (4) integrated core/low spoon design, fabrication, and test. B.G.

N85-10993*# General Electric Co., Cincinnati, Ohio. Aircraft Engine Business Group.
ENERGY EFFICIENT ENGINE ICLS NACELLE DETAIL DESIGN REPORT
R. R. ESKRIDGE, A. P. KUCHAR, and C. L. STOTLER Jul. 1982 125 p refs
(Contract NAS3-20643)
(NASA-CR-167870; NAS 1.26:167870; R81AEG700) Avail: NTIS HC A06/MF A01 CSCL 21E

The results of the detail design of the Nacelle for the General Electric Energy Efficient Engine (E3) Integrated Core Low Spool (ICLS) test vehicles are presented. A slave nacelle is designed for the ICLS test. Cost and reliability are the important factors considered. The slave nacelle simulates the internal flow lines of the actual Flight Propulsion System (FPS) but has no external fairing. The aerodynamic differences between the ICLS and FPS nacelles are presented, followed by the structural description and analysis of the various nacelle components. M.A.C.

N85-10994*# General Electric Co., Cincinnati, Ohio. Aircraft Engine Business Group.
ENERGY EFFICIENT ENGINE. LOW PRESSURE TURBINE TEST HARDWARE DETAILED DESIGN REPORT
D. G. CHERRY, C. H. GAY, and D. T. LENAHAN Aug. 1982 186 p
(Contract NAS3-20643)
(NASA-CR-167956; NAS 1.26:167956; R81AEG597) Avail: NTIS HC A09/MF A01 CSCL 21E

The low pressure turbine for the energy efficient engine is a five-stage configuration with moderate aerodynamic loading incorporating advanced features of decambered airfoils and extended blade overlaps at platforms and shrouds. Mechanical integrity of 18,000 hours on flowpath components and 36,000 hours on all other components is achieved along with no aeromechanical instabilities within the steady-state operating range. Selection of a large number (156) of stage 4 blades, together with an increased stage 4 vane-to-blade gap, assists in achieving FAR 36 acoustic goals. Active clearance control (ACC) of gaps at blade tips and interstage seals is achieved by fan air cooling judiciously applied at responsive locations on the casing. This ACC system is a major improvement in preventing deterioration of the 0.0381 cm (0.015 in.) clearances required to meet the integrated-core/low-spool turbine efficiency goal of 91.1% and the light propulsion system efficiency goal of 91.7%. Author

N85-10995*# General Electric Co., Cincinnati, Ohio. Aircraft Engine Business Group.
ENERGY EFFICIENT ENGINE HIGH PRESSURE TURBINE TEST HARDWARE DETAILED DESIGN REPORT
E. E. HALILA, D. T. LENAHAN, and T. T. THOMAS Jun. 1982 194 p refs
(Contract NAS3-20643)
(NASA-CR-167955; NAS 1.26:167955; R81AEG284) Avail: NTIS HC A09/MF A01 CSCL 21E

The high pressure turbine configuration for the Energy Efficient Engine is built around a two-stage design system. Moderate aerodynamic loading for both stages is used to achieve the high level of turbine efficiency. Flowpath components are designed for 18,000 hours of life, while the static and rotating structures are designed for 36,000 hours of engine operation. Both stages of turbine blades and vanes are air-cooled incorporating advanced state of the art in cooling technology. Direct solidification (DS) alloys are used for blades and one stage of vanes, and an oxide dispersion system (ODS) alloy is used for the Stage 1 nozzle airfoils. Ceramic shrouds are used as the material composition for the Stage 1 shroud. An active clearance control (ACC) system is used to control the blade tip to shroud clearances for both stages. Fan air is used to impinge on the shroud casing support rings, thereby controlling the growth rate of the shroud. This procedure allows close clearance control while minimizing blade tip to shroud rubs. Author

N85-10996*# General Electric Co., Cincinnati, Ohio. Aircraft Engine Business Group.
ENERGY EFFICIENT ENGINE HIGH PRESSURE TURBINE CERAMIC SHROUD SUPPORT TECHNOLOGY REPORT
W. A. NELSON and R. G. CARLSON Nov. 1982 56 p refs
(Contract NAS3-20643)
(NASA-CR-168036; NAS 1.26:168036; R82AEB399) Avail: NTIS HC A04/MF A01 CSCL 21E

This work represents the development and fabrication of ceramic HPT (high pressure turbine) shrouds for the Energy Efficient Engine (E3). Details are presented covering the work performed on the ceramic shroud development task of the NASA/GE Energy Efficient Engine (E3) component development program. The task consists of four phases which led to the selection of a ZrO2-BY2O3 ceramic shroud material system, the development of an automated plasma spray process to produce acceptable shroud structures, the fabrication of select shroud systems for evaluation in laboratory, component, and CF6-50 engine testing, and finally, the successful fabrication of ZrO2-8Y2O3/superpeg, engine quality shrouds for the E3 engine. Author

N85-10997*# General Electric Co., Cincinnati, Ohio. Aircraft Engine Business Group.
ENERGY EFFICIENT ENGINE ICLS ENGINE BEARINGS, DRIVES AND CONFIGURATION: DETAIL DESIGN REPORT
C. L. BROMAN Jun. 1982 76 p refs
(Contract NAS3-20643)
(NASA-CR-167871; NAS 1.26:167871; R81AEG821) Avail: NTIS HC A05/MF A01 CSCL 21E

The detailed design of the forward and aft sumps, the accessory drive system, the lubrication system, and the piping/manifold configuration to be employed in the ICLS engine test of the Energy Efficient Engine is addressed in the report. The design goals for the above components were established based on the requirements of the test cell engine. Author

N85-10998*# General Electric Co., Cincinnati, Ohio. Aircraft Engine Business Group.
ENERGY EFFICIENT ENGINE. HIGH PRESSURE COMPRESSOR DETAIL DESIGN REPORT
P. R. HOLLOWAY, C. C. KOCH, G. L. KNIGHT, and S. L. SHAFFER May 1982 168 p refs
(Contract NAS3-20643)
(NASA-CR-165558; NAS 1.26:165558; R81AEG710) Avail: NTIS HC A08/MF A01 CSCL 21E

A compressor optimization study defined a 10-stage configuration with a 22.6:1 pressure ratio, and adiabatic efficiency goal of 86.1%, and a polytropic efficiency of 90.6%; the corrected airflow is 53.5 kg/sec. Subsequent component testing included three full-scale tests: a six-stage rig test, and another 10-stage rig test completed in the second quarter of 1982. Information from these tests is being used to select the configuration for a core engine test scheduled for July 1982 and an integrated core/low spool test slated for early 1983. The test results will also provide data base for the flight propulsion system. Author

N85-10999*# General Electric Co., Cincinnati, Ohio. Aircraft Engine Business Group.
ADVANCED BLADE TIP SEAL SYSTEM, VOLUME 2 Final Report
J. W. ZELAHY and N. P. FAIRBANKS Feb. 1982 28 p
(Contract NAS3-20074)
(NASA-CR-167851; NAS 1.26:167851; TIS-R82AEB403-VOL-2)
Avail: NTIS HC A03/MF A01 CSCL 21E

The results of the endurance and performance engine tests conducted on monocrystal/abrasive-tipped CF6-50 Stage 1 HPT blades fabricated in Task VII of MATE Project 3 are presented. Two engine tests are conducted. The endurance engine test is conducted for 1000 C cycles. The performance engine test is conducted on a variable cycle core engine. Posttest evaluation and analyses of the blades and shrouds included visual, dimensional, and destructive evaluations. M.A.C.

N85-12059*# General Electric Co., Cincinnati, Ohio. Aircraft Engine Engineering Div.
MATERIALS FOR ADVANCED TURBINE ENGINES. PROJECT 2: RENE 150 DIRECTIONALLY SOLIDIFIED SUPERALLOY TURBINE BLADES, VOLUME 2 Final Report
G. J. DEBOER Feb. 1982 39 p 2 Vol.
(Contract NAS3-20074)
(NASA-CR-167993; NAS 1.26:167993; R82AEB540-VOL-2)
Avail: NTIS HC A03/MF A01 CSCL 21E

The results of the engine testing of Rene 150 Stage 1 high pressure turbine blades in CF6-50 core and fan engines are presented. The core engine test was conducted for 233 hours with a variety of test cycles, and the fan engine test was conducted for 1000 C cycles. Post-test analysis of the core engine test data confirmed the suitability of the Rene 150 HPT blade for fan engine testing. Post-test evaluation and analysis of the fan engine test blades included visual and dimensional inspection as well as metallographic examination of selected blades. The Rene 150 HPT blade met the target goal of this project by demonstrating increased metal temperature capability; however, the post-test analysis revealed several areas that would have to be addressed in designing a long-life Rene 150 CF6-50 HPT blade. R.S.F.

N85-13798*# National Aeronautics and Space Administration. Lewis Research Center, Cleveland, Ohio.
NEW INTEGRATION TECHNIQUES FOR CHEMICAL KINETIC RATE EQUATIONS. 2: ACCURACY COMPARISON
K. RADHAKRISHNAN (Michigan Univ., Ann Arbor) 1985 15 p refs Proposed for presentation at the 30th Intern. Gas Turbine Conf. and Exhibit, Houston, 17-21 Mar. 1985; sponsored by ASME
(NASA-TM-86893; E-2366; NAS 1.15:86893) Avail: NTIS HC A02/MF A01 CSCL 21E

A comparison of the accuracy of several techniques recently developed for solving stiff differential equations is presented. The techniques examined include two general purpose codes

EEPISODE and LSODE developed for an arbitrary system of ordinary differential equations, and three specialized codes CHEMEQ, CREKID, and GCKP84 developed specifically to solve chemical kinetic rate equations. The accuracy comparisons are made by applying these solution procedures to two practical combustion kinetics problems. Both problems describe adiabatic, homogeneous, gas phase chemical reactions at constant pressure, and include all three combustion regimes: induction, heat release, and equilibration. The comparisons show that LSODE is the most efficient code - in the sense that it requires the least computational work to attain a specified accuracy level. An important finding is that an iterative solution of the algebraic enthalpy conservation equation for the temperature can be more accurate and efficient than computing the temperature by integrating its time derivative. M.G.

N85-14840*# National Aeronautics and Space Administration. Lewis Research Center, Cleveland, Ohio.

REDUCING NUMERICAL DIFFUSION FOR INCOMPRESSIBLE FLOW CALCULATIONS

R. W. CLAUS, G. M. NEELY, and S. A. SYED (United Technologies, East Hartford, Conn.) 1984 20 p refs Presented at the Western States Meeting of the Combustion Inst., Boulder, Colo., 2-3 Apr. 1984

(NASA-TM-83621; E-2055; NAS 1.15:83621) Avail: NTIS HC A02/MF A01 CSCL 21E

A number of approaches for improving the accuracy of incompressible, steady-state flow calculations are examined. Two improved differencing schemes, Quadratic Upstream Interpolation for Convective Kinematics (QUICK) and Skew-Upwind Differencing (SUD), are applied to the convective terms in the Navier-Stokes equations and compared with results obtained using hybrid differencing. In a number of test calculations, it is illustrated that no single scheme exhibits superior performance for all flow situations. However, both SUD and QUICK are shown to be generally more accurate than hybrid differencing. Author

N85-15724*# Tuskegee Inst., Ala. School of Engineering and Architecture.

AN IMPROVED COMPUTER MODEL FOR PREDICTION OF AXIAL GAS TURBINE PERFORMANCE LOSSES Final Report

R. M. JENKINS Aug. 1984 119 p refs

(Contract NSG-3295)

(NASA-CR-174246; NAS 1.26:174246) Avail: NTIS HC A03/MF A01 CSCL 21E

The calculation model performs a rapid preliminary pitchline optimization of axial gas turbine annular flowpath geometry, as well as an initial estimate of blade profile shapes, given only a minimum of thermodynamic cycle requirements. No geometric parameters need be specified. The following preliminary design data are determined: (1) the optimum flowpath geometry, within mechanical stress limits; (2) initial estimates of cascade blade shapes; and (3) predictions of expected turbine performance. The model uses an inverse calculation technique whereby blade profiles are generated by designing channels to yield a specified velocity distribution on the two walls. Velocity distributions are then used to calculate the cascade loss parameters. Calculated blade shapes are used primarily to determine whether the assumed velocity loadings are physically realistic. Model verification is accomplished by comparison of predicted turbine geometry and performance with an array of seven NASA single-stage axial gas turbine configurations. B.W.

N85-15725*# National Aeronautics and Space Administration. Lewis Research Center, Cleveland, Ohio.

EFFECT OF STEADY-STATE TEMPERATURE DISTORTION ON INLET FLOW TO A HIGH-BYPASS-RATION TURBOFAN ENGINE

R. H. SOEDER, C. M. MEHALIC, and K. STANCIK (AFSC) Jan. 1985 32 p refs

(NASA-TM-86896; E-2369; NAS 1.15:86896) Avail: NTIS HC A03/MF A01 CSCL 21E

The effects of circumferential inlet temperature distortion on the flow characteristics between a distortion generator and a high bypass ratio turbofan engine and through its compression system were evaluated to support the effort to generate analytical models. The flow characteristics are defined by the inlet duct, the flow angles, and the total temperature, total pressure, and static pressure profiles in the inlet duct and through the fan and compressor. The effects of Reynolds number, rotor speed, and distortion extent are also considered. E.A.K.

N85-15726*# National Aeronautics and Space Administration. Lewis Research Center, Cleveland, Ohio.

INTEGRATING CHEMICAL KINETIC RATE EQUATIONS BY SELECTIVE USE OF STIFF AND NONSTIFF METHODS

K. RADHAKRISHNAN 1985 15 p refs Presented at the 23rd Aerospace Sci. Meeting, Reno, Nev., 14-17 Jan. 1985; sponsored by AIAA Previously announced in IAA as A85-19607

(NASA-TM-86923; E-2418; NAS 1.15:86923; AIAA-85-0237) Avail: NTIS HC A02/MF A01 CSCL 21E

The effect of switching between nonstiff and stiff methods on the efficiency of algorithms for integrating chemical kinetic rate equations was examined. Different integration methods were tested by application of the packaged code LSODE to four practical combustion kinetics problems. The problems describe adiabatic, and homogeneous gas phase combustion reactions. It is shown that selective use of nonstiff and stiff methods in different regimes of a typical batch combustion problem is faster than the use of either method for the entire problem. The implications which result in the development of fast integration techniques for combustion kinetic rate equations are discussed. E.A.K.

N85-15727*# National Aeronautics and Space Administration. Lewis Research Center, Cleveland, Ohio.

EXPERIMENTAL STUDY OF THE SPRAY CHARACTERISTICS OF A RESEARCH AIRBLAST ATOMIZER

W. A. ACOSTA 1985 16 p refs Proposed for presentation at the 30th Intern. Gas Turbine Conf. and Exhibit, Houston, Tex., 17-21 Mar. 1985; sponsored by ASME

(NASA-TM-86911; E-2404; NAS 1.15:86911; USAAVSCOM-TR-84-C-18) Avail: NTIS HC A02/MF A01 CSCL 21E

Airblast atomization was studied using a especially designed atomizer in which the liquid first impinges on a splash plate, then is directed radially outward and is atomized by the air passing through two concentric, vaned swirlers that swirl the air in opposite directions. The effect of flow conditions, air mass velocity (mass flow rate per unit area) and liquid to air ratio on the mean drop size was studied. Seven different ethanol solutions were used to simulate changes in fuel physical properties. The range of atomizing air velocities was from 30 to 80 m/s. The mean drop diameter was measured at ambient temperature (295 K) and atmospheric pressure. Author

N85-15728*# Pennsylvania State Univ., University Park.

THE STRUCTURE OF DILUTE COMBUSTING SPRAYS Final Report

J. S. SHUEN, A. S. P. SOLOMON, and F. M. FAETH Jan. 1985 124 p refs

(Contract NAG3-190)

(NASA-CR-174838; NAS 1.26:174838) Avail: NTIS HC A06/MF A01 CSCL 21E

An experimental and theoretical study of drop processes in a turbulent flame is described. The experiments involved a monodisperse (105 and 180 micro m initial diameter) stream of

methanol drops injected at the base of a turbulent methane-fueled diffusion flame burning in still air. The following measurements were made: mean and fluctuating phase velocities, mean drop number flux, drop-size distributions and mean gas-phase temperatures. Measurements were compared with predictions of two separated flow models: (1) deterministic separated flow, where drop-turbulence interactions are ignored; and (2) stochastic separated flow, where drop-turbulence interactions are considered using random-walk computations. The stochastic separated flow analysis yielded best agreement with measurements, since it provides for turbulent dispersion of drops which was important for present test conditions (and probably for most combusting sprays as well). Distinguishing the presence or absence of envelope flames around the drops, however, was relatively unimportant for present test conditions, since the drops spent most of their lifetime in fuel-rich regions of the flow where this distinction is irrelevant. Author

N85-15744*# National Aeronautics and Space Administration. Lewis Research Center, Cleveland, Ohio.
ENGINE CYCLIC DURABILITY BY ANALYSIS AND MATERIAL TESTING
A. KAUFMAN and G. R. HALFORD *In* AGARD Eng. Cyclic Durability by Analysis and Testing 12 p Sep. 1984 refs Previously announced as N84-18683
Avail: NTIS HC A12/MF A01 CSCL 21E

The problem of calculating turbine engine component durability is addressed. Nonlinear, finite-element structural analyses, cyclic constitutive behavior models, and an advanced creep-fatigue life prediction method called strainrange partitioning were assessed for their applicability to the solution of durability problems in hot-section components of gas turbine engines. Three different component or subcomponent geometries are examined: a stress concentration in a turbine disk; a louver lip of a half-scale combustor linear; and a squealer tip of a first-stage high-pressure turbine blade. Cyclic structural analyses were performed for all three problems. The computed strain-temperature histories at the critical locations of the combustor linear and turbine blade components were imposed on smooth specimens in uniaxial, strain-controlled, thermomechanical fatigue tests of evaluate the structural and life analysis methods. Author

N85-18057*# National Aeronautics and Space Administration. Lewis Research Center, Cleveland, Ohio.
EXPERIMENTAL AND ANALYTICAL STUDY OF CERAMIC-COATED TURBINE-TIP SHROUD SEALS FOR SMALL TURBINE ENGINES
T. J. BIESIADNY, G. E. MCDONALD, R. C. HENDRICKS, J. K. LITTLE, R. A. ROBINSON (AVSCOM Research and Technology Labs, Cleveland, Ohio), G. A. KLANN (AVSCOM Research and Technology Labs, Cleveland, Ohio), and E. S. LASSOW (Howmet Turbine Components Corp., Whitehall, Mich.) Jan. 1985 32 p refs
(NASA-TM-86881; E-2343; NAS 1.15:86881; USAAVSCOM-TR-84-C-19) Avail: NTIS HC A03/MF A01 CSCL 21E

The results of an experimental and analytical evaluation of ceramic turbine tip shrouds within a small turbine engine operating environment are presented. The ceramic shrouds were subjected to 1001 cycles between idle and high power and steady-state conditions for a total of 57.8 engine hr. Posttest engine inspection revealed mud-flat surface cracking, which was attributed to microcracking under tension with crack penetration to the ceramic and bond coat interface. Sections and micrographs tend to corroborate the thesis. The engine test data provided input to a thermomechanical analysis to predict temperature and stress profiles throughout the ceramic gas-path seal. The analysis predicts cyclic thermal stresses large enough to cause the seal to fail. These stresses are, however, mitigated by inelastic behavior of the shroud materials and by the microfracturing that tensile stresses produce. Microfracturing enhances shroud longevity during early life but provides the failure mechanism during life but provides the failure mechanism during extended life when coupled with the time dependent inelastic materials effects. Author

N85-18058*# Pratt and Whitney Aircraft Group, East Hartford, Conn. Commercial Engineering.
STUDY OF CONTROLLED DIFFUSION STATOR BLADING Final Report
R. F. BEHLKE, J. D. BROOKY, and E. CANAL Mar. 1983 134 p refs
(Contract NAS3-22008)
(NASA-CR-167995; NAS 1.26:167995; PWA-5698-77) Avail: NTIS HC A07/MF A01 CSCL 21E

Tests were conducted on a high tip speed, highly loaded front compressor stage having low aspect ratio rotor and stator airfoils. The stator airfoils were designed by the controlled diffusion procedure recently developed by P&WA for designing transonic cascade airfoils. The rotor blades consisted of multiple-circular-arc airfoil sections. The stage had a tip speed of 442 m/sec (1450 ft/sec), a hub/tip ratio of 0.597, a rotor aspect ratio of 1.3, and a stator aspect ratio of 1.45. At design speed the rotor-stator stage achieved an adiabatic efficiency of 89.1% at design flow and pressure ratio. Surge margin was 14%. The stage efficiency exceeded the design goal by 0.6 percentage points. The rotor efficiency was 92.4%, exceeding design by 0.3 percentage points. The controlled diffusion stator demonstrated a lower minimum loss over the multiple-circular-arc stator from the root to 70 percent span. A surge diffusion factor of 0.72 was reached at both the rotor tip and the stator root. The NAS3-22008 program demonstrated its intent: high efficiency and loading levels with low aspect ratio blades and the controlled diffusion stator in the unfavorable front stage environment. Author

N85-21162*# National Aeronautics and Space Administration. Lewis Research Center, Cleveland, Ohio.
A COMPARISON OF THE EFFICIENCY OF NUMERICAL METHODS FOR INTEGRATING CHEMICAL KINETIC RATE EQUATIONS
K. RADHAKRISHNAN 1984 18 p refs Presented at JANNAF Propulsion Meeting, New Orleans, 7-9 Feb. 1984 Previously announced as N84-31280
(Contract NAG3-147)
(NASA-TM-83590; E-1988; NAS 1.15:83590) Avail: NTIS HC A02/MF A01 CSCL 21E

A comparison of the efficiency of several algorithms recently developed for the efficient numerical integration of stiff ordinary differential equations is presented. The methods examined include two general-purpose codes EPISODE and LSODE and three codes (CHEMEQ, CREK1D, and GCKP84) developed specifically to integrate chemical kinetic rate equations. The codes are applied to two test problems drawn from combustion kinetics. The comparisons show that LSODE is the fastest code currently available for the integration of combustion kinetic rate equations. An important finding is that an iterative solution of the algebraic energy conservation equation to compute the temperature can be more efficient than evaluating the temperature by integrating its time-derivative. Author

N85-21163*# John Deere Technologies International, Inc., Wood-Ridge, N.J. Rotary Engine Div.
STRATIFIED CHARGE ROTARY AIRCRAFT ENGINE TECHNOLOGY ENABLEMENT PROGRAM Final Report
P. R. BADGLEY, C. E. IRION, and D. M. MYERS 31 Jan. 1985 110 p refs
(Contract NAS3-23056)
(NASA-CR-174812; NAS 1.26:174812; JDTI-RED-85-1) Avail: NTIS HC A06/MF A01 CSCL 21E

The multifuel stratified charge rotary engine is discussed. A single rotor, 0.7L/40 cu in displacement, research rig engine was tested. The research rig engine was designed for operation at high speeds and pressures, combustion chamber peak pressure providing margin for speed and load excursions above the design requirement for a high is advanced aircraft engine. It is indicated that the single rotor research rig engine is capable of meeting the

established design requirements of 120 kW, 8,000 RPM, 1,379 KPA BMEP. The research rig engine, when fully developed, will be a valuable tool for investigating, advanced and highly advanced technology components, and provide an understanding of the stratified charge rotary engine combustion process. E.A.K.

N85-21164*# National Aeronautics and Space Administration. Lewis Research Center, Cleveland, Ohio.
COMBUSTION RESEARCH FOR GAS TURBINE ENGINES
E. J. MULARZ and R. W. CLAUS 1985 19 p refs To be presented at the 7th Intern. Symp. on Air Breathing Engines, Peking, 2-6 Sep. 1985
(NASA-TM-86963; E-2490; NAS 1.15:86963; AD-A153977) Avail: NTIS HC A02/MF A01 CSCL 21E

Research on combustion is being conducted at Lewis Research Center to provide improved analytical models of the complex flow and chemical reaction processes which occur in the combustor of gas turbine engines and other aeropropulsion systems. The objective of the research is to obtain a better understanding of the various physical processes that occur in the gas turbine combustor in order to develop models and numerical codes which can accurately describe these processes. Activities include in-house research projects, university grants, and industry contracts and are classified under the subject areas of advanced numerics, fuel sprays, fluid mixing, and radiation-chemistry. Results are high-lighted from several projects. Author

N85-21165*# Massachusetts Inst. of Tech., Cambridge. Dept. of Aeronautics and Astronautics.
ADVANCED STRESS ANALYSIS METHODS APPLICABLE TO TURBINE ENGINE STRUCTURES Final Report
T. H. H. PIAN Mar. 1985 44 p refs
(Contract NAG3-33)
(NASA-CR-175573; NAS 1.26:175573) Avail: NTIS HC A03/MF A01 CSCL 21E

Advanced stress analysis methods applicable to turbine engine structures are investigated. Constructions of special elements which containing traction-free circular boundaries are investigated. New versions of mixed variational principle and version of hybrid stress elements are formulated. A method is established for suppression of kinematic deformation modes. semiLoof plate and shell elements are constructed by assumed stress hybrid method. An elastic-plastic analysis is conducted by viscoplasticity theory using the mechanical subelement model. B.W.

N85-21166*# Illinois Univ., Urbana-Champaign.
THE MECHANISMS OF FLAME HOLDING IN THE WAKE OF A BLUFF BODY Final Report
R. A. STREHLOW and S. MALIK Mar. 1985 196 p refs
(Contract NAG3-60)
(NASA-CR-3866; NAS 1.26:3866) Avail: NTIS HC A09/MF A01 CSCL 21E

The flame holding mechanism for lean methane- and lean propane-air flames is examined under conditions where the recirculation zone is absent. The main objective of this work is to study the holding process in detail in an attempt to determine the mechanism of flame holding and also the conditions where this mechanism is viable and when it fails and blow-off occurs. Inverted flames held in the wake of a flat strip were studied. Experiments with different sizes of flame holders were performed. The velocity flow field was determined using a laser Doppler velocimetry technique. Equation of continuity was used to calculate the flame temperature from the change in area of flow streamlines before and after the flame. Observations of the inverted flame itself were obtained using schlieren and direct photography. Results show that there are different mechanisms operative at the time of blow-off for lean propane and methane flames. Blow-off or extinction occurs for lean propane-air flame in spite of the reaction going to completion and the disparity between the heat loss and the gain in mass diffusion in the reaction zone i.e., Le 1.0 causes the flame to blow-off. For methane-air flame the controlling factor or blow-off is incomplete reaction due to higher blowing rate leading to reduced residence time in the reaction zone. M.G.

N85-21167*# Oklahoma State Univ., Stillwater. School of Mechanical and Aerospace Engineering.
INVESTIGATION OF FLOWFIELDS FOUND IN TYPICAL COMBUSTOR GEOMETRIES Final Report
D. G. LILLEY Washington NASA Feb. 1985 192 p refs Sponsored in part by AF
(Contract NAG3-74)
(NASA-CR-3869; NAS 1.26:3869) Avail: NTIS HC A09/MF A01 CSCL 21E

Activities undertaken during the entire course of research are summarized. Studies were concerned with experimental and theoretical research on 2-D axisymmetric geometries under low speed nonreacting, turbulent, swirling flow conditions typical of gas turbine and ramjet combustion chambers. They included recirculation zone characterization, time-mean and turbulence simulation in swirling recirculating flow, sudden and gradual expansion flowfields, and furher complexities and parameter influences. The study included the investigation of: a complete range of swirl strengths; swirler performance; downstream contraction nozzle sizes and locations; expansion ratios; and inlet side-wall angles. Their individual and combined effects on the test section flowfield were observed, measured and characterized. Experimental methods included flow visualization (with smoke and neutrally-buoyant helium-filled soap bubbles), five-hole pitot probe time-mean velocity field measurements, and single-, double-, and triple-wire hot-wire anemometry measurements of time-mean velocities, normal and shear Reynolds sresses. Computational methods included development of the STARPIC code from the primitive-variable TEACH computer code, and its use in flowfield prediction and turbulence model development. M.G.

N85-21168*# National Aeronautics and Space Administration. Lewis Research Center, Cleveland, Ohio.
COMBUSTION GAS PROPERTIES. 2: NATURAL GAS FUEL AND DRY AIR
J. D. WEAR, R. E. JONES, A. M. TROUT, and B. J. MCBRIDE Apr. 1985 12 p refs
(NASA-TP-2435; E-2435; NAS 1.60:2435) Avail: NTIS HC A02/MF A01 CSCL 21E

A series of computations has been made to produce the equilibrium temperature and gas composition for natural gas fuel and dry air. The computed tables and figures provide combustion gas property data for pressures from 0.5 to 50 atmospheres and equivalence ratios from 0 to 2.0. Only samples tables and figures are provided in this report. The complete set of tables and figures is provided on four microfiche films supplied with this report. Author

N85-22390*# Oklahoma State Univ., Stillwater. School of Mechanical and Aerospace Engineering.
DEFLECTED JET EXPERIMENTS IN A TURBULENT COMBUSTOR FLOWFIELD Ph.D. Thesis Final Report
G. B. FERRELL and D. G. LILLEY Feb. 1985 273 p refs
(Contract NAG3-549)
(NASA-CR-174863; NAS 1.26:174863) Avail: NTIS HC A12/MF A01 CSCL 21E

Experiments were conducted to characterize the time-mean and turbulent flow field of a deflected turbulent jet in a confining cylindrical crossflow. Jet-to-crossflow velocity ratios of 2, 4, and 6 were investigated, under crossflow inlet swirler vane angles of 0 (swirler removed), 45 and 70 degrees. Smoke, neutrally buoyant helium-filled soap bubbles, and multi-spark flow visualization were employed to highlight interesting features of the deflected jet, as well as the tracjectory and spread pattern of the jet. A six-position single hot-wire technique was used to measure the velocities and turbulent stresses in nonswirling crossflow cases. In these cases, measurements confirmed that the deflected jet is symmetrical about the vertical plan passing through the crossflow axis, and the jet penetration was found to be reduced from that of comparable velocity ratio infinite crossflow cases. In the swirling crossflow cases, the flow visualization techniques enabled gross flow field characterization to be obtained for a range of lateral jet-to-crossflow

velocity ratios and a range of inlet swirl strengths in the main flow. Author

N85-22391*# Massachusetts Inst. of Tech., Cambridge. Gas Turbine Lab.
STRUCTURAL RESPONSE OF A ROTATING BLADED DISK TO ROTOR WHIRL Final Report
E. F. CRAWLEY Apr. 1985 140 p refs
(Contract NAG3-200)
(NASA-CR-175605; NAS 1.26:175605) Avail: NTIS HC A07/MF A01 CSCL 21E

A set of high speed rotating whirl experiments were performed in the vacuum of the MIT Blowdown Compressor Facility on the MIT Aeroelastic Rotor, which is structurally typical of a modern high bypass ratio turbofan stage. These tests identified the natural frequencies of whirl of the rotor system by forcing its response using an electromagnetic shaker whirl excitation system. The excitation was slowly swept in frequency at constant amplitude for several constant rotor speeds in both a forward and backward whirl direction. The natural frequencies of whirl determined by these experiments were compared to those predicted by an analytical 6 DOF model of a flexible blade-rigid disk-flexible shaft rotor. The model is also presented in terms of nondimensional parameters in order to assess the importance of the interation between the bladed disk dynamics and the shaft-disk dynamics. The correlation between the experimental and predicted natural frequencies is reasonable, given the uncertainty involved in determining the stiffness parameters of the system. Author

N85-22392*# Case Western Reserve Univ., Cleveland, Ohio. Dept. of Mechanical and Aerospace Engineering.
DILUTION JET CONFIGURATIONS IN A REVERSE FLOW COMBUSTOR M.S. Thesis Final Report
J. ZIZELMAN Apr. 1985 214 p refs
(Contract NSG-3206)
(NASA-CR-174888; NAS 1.26:174888) Avail: NTIS HC A10/MF A01 CSCL 21E

Results of measurements of both temperature and velocity fields within a reverse flow combustor are presented. Flow within the combustor is acted upon by perpendicularly injected cooling jets introduced at three different locations along the inner and outer walls of the combustor. Each experiment is typified by a group of parameters: density ratio, momentum ratio, spacing ratio, and confinement parameter. Measurements of both temperature and velocity are presented in terms of normalized profiles at azimuthal positions through the turn section of the combustion chamber. Jet trajectories defined by minimum temperature and maximum velocity give a qualitative indication of the location of the jet within the cross flow. Results of a model from a previous temperature study are presented in some of the plots of data from this work.
Author

N85-25261*# National Aeronautics and Space Administration. Lewis Research Center, Cleveland, Ohio.
PERFORMANCE AND SURGE LIMITS OF A TF30-P-3 TURBOFAN ENGINE/AXISYMMETRIC MIXED-COMPRESSION INLET PROPULSION SYSTEM AT MACH 2.5
J. F. WASSERBAUER, H. E. NEUMANN, and R. J. SHAW May 1985 21 p refs
(NASA-TP-2461; E-2412; NAS 1.60:2461) Avail: NTIS HC A02/MF A01 CSCL 21E

Steady-state performance and inlet-engine compatibility were investigated with a low-bleed inlet. The inlet had minimum internal contraction, consistent with high total pressure recovery and low cowl drag. The inlet-engine combination displayed good performance with only about 2% of inlet performance bleed. The inlet-engine combination had 5.58 deg angle-of-attack capability with 6% bleed. Author

N85-25262*# Michigan State Univ., East Lansing. Coll. of Engineering.
DEVELOPMENT OF A TEMPERATURE MEASUREMENT SYSTEM WITH APPLICATION TO A JET IN A CROSS FLOW EXPERIMENT Final Report
C. WARK and J. F. FOSS Apr. 1985 123 p refs
(Contract NAG3-245)
(NASA-CR-174896; NAS 1.26:174896; FSFL-R-85-002) Avail: NTIS HC A06/MF A01 CSCL 21E

A temperature measurement system, which allows the simultaneous sampling of up to 80 separate thermocouples, was developed. The minimum resolution for the system corresponds to + or - 0.16 C per least significant bit of the A/D converter. The time constant values lambda, for each of the 64 thermocouples, were determined experimentally at 7 mps. Software routines were used to correct the measured temperatures for the effect of lambda for each thermocouple. The temperature measurement system was utilized to study the thermal field of a heated jet discharging perpendicularly into a low and a high disturbance level cross stream for a given momentum flux ratio and for three overheated values. The peak instantaneous temperatures reveal that strong molecular diffusion was operative. Various measures of the thermal field, for the disturbed case, suggest that the jet column remains relatively compact while being buffeted by the ambient turbulence field and that its penetration, into the cross wind, is inhibited by the presence of the strong disturbance field. E.A.K.

N85-25263*# National Aeronautics and Space Administration. Lewis Research Center, Cleveland, Ohio.
NUMERICAL CALCULATION OF SUBSONIC JETS IN CROSSFLOW WITH REDUCED NUMERICAL DIFFUSION
R. W. CLAUS 1985 19 p refs Presented at the 21st Joint Propulsion Conf., Monterey, Calif., 8-10 Jul. 1985; sponsored by AIAA, SAE and ASME
(NASA-TM-87003; E-2548; NAS 1.15:87003) Avail: NTIS HC A02/MF A01 CSCL 21E

A series of calculations are reported for two, subsonic jet in crossflow geometries. The parametric variation examined are the lateral spacing of a row of jets. The first series of calculations corresponds to a widely space jet geometry, S/D = 4, and the second series corresponds to closely spaced jets, S/D = 2. The calculations are done with alternate differencing schemes to illustrate the impact of numerical diffusion. The calculated jet trajectories agreed well with experimental data in the widely spaced jet geometry, but not in the closely spaced geometry. E.A.K.

N85-25264*# National Aeronautics and Space Administration. Lewis Research Center, Cleveland, Ohio.
SMALL GAS TURBINE COMBUSTOR STUDY: FUEL INJECTOR PERFORMANCE IN A TRANSPIRATION-COOLED LINER
S. M. RIDDLEBAUGH and C. T. NORGREN 1985 20 p refs Proposed for presentation at the 21st Joint Propulsion Conf., Monterey, Calif., 8-10 Jul. 1985; sponsoed by AIAA, SAE and ASME
(NASA-TM-86989; E-2533; NAS 1.15:86989) Avail: NTIS HC A02/MF A01 CSCL 21E

The effect of fuel injection technique on the performance of an advanced reverse flow combustor liner constructed of Lamilloy (a multilaminate transpiration type material) was determined. Performance and emission levels are documented over a range of simulated flight conditions using simplex pressure atomizing, spill return, and splash cone airblast injectors. A parametric evaluation of the effect of increased combustor loading with each of the fuel injector types is obtained. E.A.K.

N85-25265*# Arizona State Univ., Tempe. Dept. of Mechanical and Aerospace Engineering.
BEHAVIOR OF TURBULENT GAS JETS IN AN AXISYMMETRIC CONFINEMENT Final Report
R. M. C. SO and S. A. AHMED Jan. 1985 95 p refs
(Contract NAG3-260)
(NASA-CR-174829; NAS 1.26:174829; CR-R-84041) Avail: NTIS HC A05/MF A01 CSCL 20D

The understanding of the mixing of confined turbulent jets of different densities with air is of great importance to many industrial applications, such as gas turbine and Ramjet combustors. Although there have been numerous studies on the characteristics of free gas jets, little is known of the behavior of gas jets in a confinement. The jet, with a diameter of 8.73 mm, is aligned concentrically in a tube of 125 mm diameter, thus giving a confinement ratio of approximately 205. The arrangement forms part of the test section of an open-jet wind tunnel. Experiments are carried out with carbon dioxide, air and helium/air jets at different jet velocities. Mean velocity and turbulence measurements are made with a one-color, one-component laser Doppler velocimeter operating in the forward scatter mode. Measurements show that the jets are highly dissipative. Consequently, equilibrium jet characteristics similar to those found in free air jets are observed in the first two diameters downstream of the jet. These results are independent of the fluid densities and velocities. Decay of the jet, on the other hand, is a function of both the jet fluid density and momentum. In all the cases studied, the jet is found to be completely dissipated in approximately 30 jet diameters, thus giving rise to a uniform flow with a very high but constant turbulence field across the confinement. Author

N85-25266*# National Aeronautics and Space Administration. Lewis Research Center, Cleveland, Ohio.
EXPERIMENTS IN DILUTION JET MIXING EFFECTS OF MULTIPLE ROWS AND NON-CIRCULAR ORIFICES
J. D. HOLDEMAN, R. SRINIVASAN (Garrett Turbine Engine Co.), E. B. COLEMAN (Garrett Turbine Engine Co.), G. D. MEYERS (Garrett Turbine Engine Co.), and C. D. WHITE (Garrett Turbine Engine Co.) 1985 16 p refs Presented at the 21st Joint Propulsion Conf., Monterey, Calif., 8-10 Jul. 1985; sponsored by AIAA, SAE and ASME
(NASA-TM-86996; E-2542; NAS 1.15:86996) Avail: NTIS HC A02/MF A01 CSCL 21E

Experimental and empirical model results are presented that extend previous studies of the mixing of single-sided and opposed rows of jets in a confined duct flow to include effects of non-circular orifices and double rows of jets. Analysis of the mean temperature data obtained in this investigation showed that the effects of orifice shape and double rows are significant only in the region close to the injection plane, provided that the orifices are symmetric with respect to the main flow direction. The penetration and mixing of jets from 45-degree slanted slots is slightly less than that from equivalent-area symmetric orifices. The penetration from 2-dimensional slots is similar to that from equivalent-area closely-spaced rows of holes, but the mixing is slower for the 2-D slots. Calculated mean temperature profiles downstream of jets from non-circular and double rows of orifices, made using an extension developed for a previous empirical model, are shown to be in good agreement with the measured distributions. Author

N85-26709*# Detroit Diesel Allison, Indianapolis, Ind. Allison Gas Turbine Div.
ANALYTICAL FUEL PROPERTY EFFECTS--SMALL COMBUSTORS Final Report
R. D. SUTTON, D. L. TROTH, and G. A. MILES Oct. 1984 224 p refs
(Contract NAS3-23165)
(NASA-CR-174738; EDR-11683; NAS 1.26:174738; AVSCOM-TR-84-C-14) Avail: NTIS HC A10/MF A01 CSCL 21E

The consequences of using broad-property fuels in both conventional and advanced state-of-the-art small gas turbine combustors are assessed. Eight combustor concepts were selected for initial screening, of these, four final combustor concepts were chosen for further detailed analysis. These included the dual orifice injector baseline combustor (a current production 250-C30 engine combustor) two baseline airblast injected modifications, short and piloted prechamber combustors, and an advanced airblast injected, variable geometry air staged combustor. Final predictions employed the use of the STAC-I computer code. This quasi 2-D model includes real fuel properties, effects of injector type on atomization, detailed droplet dynamics, and multistep chemical kinetics. In general, fuel property effects on various combustor concepts can be classified as chemical or physical in nature. Predictions indicate that fuel chemistry has a significant effect on flame radiation, liner wall temperature, and smoke emission. Fuel physical properties that govern atomization quality and evaporation rates are predicted to affect ignition and lean-blowout limits, combustion efficiency, unburned hydrocarbon, and carbon monoxide emissions. Author

N85-26710*# National Aeronautics and Space Administration. Lewis Research Center, Cleveland, Ohio.
LOW-SPEED AERODYNAMIC TEST OF AN AXISYMMETRIC SUPERSONIC INLET WITH VARIABLE COWL SLOT
A. G. POWELL (Douglas Aircraft Co., Long Beach, Calif.), H. R. WELGE (Douglas Aircraft Co., Long Beach, Calif.), and C. J. TREFNY 1985 6 p refs Proposed for presentation at the 21st Joint Propulsion Conf., Monterey, Calif., 8-10 Jul. 1985; sponsored by AIAA, SAE and ASME
(Contract NAS1-16147)
(NASA-TM-87039; E-2595; NAS 1.15:87039; DOUGLAS-PAPER-7551) Avail: NTIS HC A02/MF A01 CSCL 21E

The experimental low-speed aerodynamic characteristics of an axisymmetric mixed-compression supersonic inlet with variable cowl slot are described. The model consisted of the NASA P-inlet centerbody and redesigned cowl with variable cowl slot powered by the JT8D single-stage fan simulator and driven by an air turbine. The model was tested in the NASA Lewis Research Center 9- by 15-foot low-speed tunnel at Mach numbers of 0, 0.1, and 0.2 over a range of flows, cowl slot openings, centerbody positions, and angles of attack. The variable cowl slot was effective in minimizing lip separation at high velocity ratios, showed good steady-state and dynamic distortion characteristics, and had good angle-of-attack tolerance. Author

N85-26711*# General Electric Co., Cincinnati, Ohio. Aircraft Engine Business Group.
EFFECTS OF SURFACE CHEMISTRY ON HOT CORROSION LIFE Annual Report, 2 May 1984 - 2 May 1985
R. E. FRYXELL Jun. 1985 47 p refs
(Contract NAS3-23926)
(NASA-CR-174915; NAS 1.26:174915; R85AEB307; AR-2) Avail: NTIS HC A03/MF A01 CSCL 21E

Burner rig tests were conducted under the following conditions: 900 C, hourly thermal cycling, 0.5 ppm sodium as MaCl in the gas stream, velocity 0.3 Mach. The alloys are Udiment 700, Rene 80, uncoated and with RT21, Codep, or NiCoCrAlY coatings. These tests were completed for specimens in the as-processed condition and after aging at 1100 C in oxidizing or inert evnivronments for time up to 600 hours. Coil inductance changes used for periodic nondestructive inspection of specimens were useful in following the course of corrosion. Typical sulfidation was observed in all cases, structurally similar to that observed for service-run turbine components. Aging at cuased a severe decrease in hot corrosion life of RT21 and Codep coatings and a significant but less decrease in the life of the NiCoCrAlY coating. The extent of these decreases was much greater for all three coatings on U700 substrates than on Rene 80 substrates. Coating/substrate interdiffusion rather than by surface oxidation. M.G.

N85-26712*# Virginia Polytechnic Inst. and State Univ., Blacksburg. Dept. of Mechanical Engineering.
THERMODYNAMIC EVALUATION OF TRANSONIC COMPRESSOR ROTORS USING THE FINITE VOLUME APPROACH Semiannual Status Report, 20 Dec. 1985 - 31 May 1985
S. NICHOLSON and J. MOORE 1985 42 p refs
(Contract NAG3-593)
(NASA-CR-175811; NAS 1.26:175811; JM/85-6) Avail: NTIS HC A03/MF A01 CSCL 21E

Progress made in extending the finite volume explicit time marching method to laminar and turbulent flow during the time period from January to May 1985 is documented. Previously, extensions were made to the finite volume method to improve the accuracy of the calculation of total pressure in compressible inviscid flow. The current work extends these ideas and develops new ideas which allow the calculation of laminar and turbulent boundary layers in internal flows. The method is verified using four test cases with free-stream Mach numbers ranging from .075 to 1.20. R.J.F.

N85-26713*# Notre Dame Univ., Ind. Dept. of Electrical Engineering.
ALTERNATIVES FOR JET ENGINE CONTROL Technical Progress Report, 1 Nov. 1983 - 31 Oct. 1984
M. K. SAIN 31 Oct. 1984 266 p refs
(Contract NSG-3048)
(NASA-CR-175831; NAS 1.26:175831) Avail: NTIS HC A12/MF A01 CSCL 21E

The technical progress of researches Alternatives for Jet Engine Control is reported. A numerical study employing feedback tensors for optimal control of nonlinear systems was completed. It is believed that these studies are the first of their kind. State regulation, with a decrease in control power is demonstrated. A detailed treatment follows. E.A.K.

N85-26714*# Notre Dame Univ., Ind. Dept. of Electrical Engineering.
ALTERNATIVES FOR JET ENGINE CONTROL Technical Progress Report, 1 Oct. 1982 - 31 Oct. 1983
M. K. SAIN 31 Oct. 1983 140 p refs
(Contract NSG-3048)
(NASA-CR-175832; NAS 1.26:175832) Avail: NTIS HC A07/MF A01 CSCL 21E

The technical progress of researches on alternatives for jet engine control, is reported. The principal new activities involved the initial testing of an input design method for choosing the inputs to a non-linear system to aid the approximation of its tensor parameters, and the beginning of order reduction studies designed to remove unnecessary monomials from tensor models. E.A.K.

N85-26715*# Notre Dame Univ., Ind. Dept. of Electrical Engineering.
ALTERNATIVES FOR JET ENGINE CONTROL Semiannual Status Report, 1 Nov. 1983 - 30 Apr. 1984
M. K. SAIN 30 Apr. 1984 271 p refs
(Contract NSG-3048)
(NASA-CR-175833; NAS 1.26:175833) Avail: NTIS HC A12/MF A01 CSCL 21E

The technical progress of researches on alternatives for jet engine control is reported. Extensive numerical testing is included. It is indicated that optimal inputs contribute significantly to the process of calculating tensor approximations for nonlinear systems, and that the resulting approximations may be order-reduced in a systematic way. E.A.K.

N85-26716*# Oklahoma State Univ., Stillwater. School of Mechanical and Aerospace Engineering.
CONFINED TURBULENT SWIRLING RECIRCULATING FLOW PREDICTIONS Ph.D. Thesis. Final Report
M. T. ABUJELALA and D. G. LILLEY May 1985 226 p refs
(Contract NAG3-74)
(NASA-CR-174917; NAS 1.26:174917) Avail: NTIS HC A11/MF A01 CSCL 21E

The capability and the accuracy of the STARPIC computer code in predicting confined turbulent swirling recirculating flows is presented. Inlet flow boundary conditions were demonstrated to be extremely important in simulating a flowfield via numerical calculations. The degree of swirl strength and expansion ratio have strong effects on the characteristics of swirling flow. In a nonswirling flow, a large corner recirculation zone exists in the flowfield with an expansion ratio greater than one. However, as the degree of inlet swirl increases, the size of this zone decreases and a central recirculation zone appears near the inlet. Generally, the size of the central zone increased with swirl strength and expansion ratio. Neither the standard k-epsilon turbulence mode nor its previous extensions show effective capability for predicting confined turbulent swirling recirculating flows. However, either reduced optimum values of three parameters in the mode or the empirical C sub mu formulation obtained via careful analysis of available turbulence measurements, can provide more acceptable accuracy in the prediction of these swirling flows. Author

N85-26717*# Oklahoma State Univ., Stillwater. School of Mechanical and Aerospace Engineering.
TURBULENCE CHARACTERISTICS OF SWIRLING *FLOWFIELDS* Ph.D. Thesis. Final Report
T. W. JACKSON and D. G. LILLEY May 1985 266 p refs
(Contract NAG3-74)
(NASA-CR-174918; NAS 1.26:174918) Avail: NTIS HC A13/MF A01 CSCL 21E

The time mean and turbulence properties of a confined swirling jet using the six orientation, single hot wire technique were obtained. The effect of swirl on a confined, expanding jet is to reduce the size of the corner recirculation zone and generate a central recirculation zone followed by a precessing vortex core. The effect of introducing a contraction nozzle of area ratio four, located two test section diameters downstream of the inlet, is to dramatically reduce the size and shape of the central recirculation zone for the swirling flows considered. The shear stresses are found to increase by an order of magnitude in the region of the contraction nozzle because of large radial gradients of axial velocity. Reduction of the expansion ratio to D/o = 1 causes the time mean flow field to be homogeneous throughout the entire test section with the tangential velocity dominating in the swirling cases. No recirculation zones were observed for these particular flows. Turbulence levels and dissipation rates were found to be low except in the entrance regions and in areas of acceleration in the swirling flow cases. Author

N85-27867*# Oklahoma State Univ., Stillwater. School of Mechanics and Aerospace Engineering.
PREDICTIONS AND MEASUREMENTS OF ISOTHERMAL FLOWFIELDS IN AXISYMMETRIC COMBUSTOR GEOMETRIES Ph.D. Thesis. Final Report
D. L. RHODES and D. G. LILLEY May 1985 169 p refs
(Contract NAG3-74)
(NASA-CR-174916; NAS 1.26:174916) Avail: NTIS HC A08/MF A01 CSCL 21E

Numerical predictions, flow visualization experiments and time-mean velocity measurements were obtained for six basic nonreacting flowfields (with inlet swirl vane angles of 0 (swirler removed), 45 and 70 degrees and sidewall expansion angles of 90 and 45 degrees) in an idealized axisymmetric combustor geometry. A flowfield prediction computer program was developed which solves appropriate finite difference equations including a conventional two equation k-epsilon eddy viscosity turbulence model. The wall functions employed were derived from previous swirling flow measurements, and the stairstep approximation was

employed to represent the sloping wall at the inlet to the test chamber. Recirculation region boundaries have been sketched from the entire flow visualization photograph collection. Tufts, smoke, and neutrally buoyant helium filled soap bubbles were employed as flow tracers. A five hole pitot probe was utilized to measure the axial, radial, and swirl time mean velocity components.
Author

N85-27868*# Ohio State Univ., Columbus. Dept. of Engineering Mechanics.
A STUDY OF INTERNAL AND DISTRIBUTED DAMPING FOR VIBRATING TURBOMACHINER BLADES Final Report, 15 Apr. 1983 - 15 Apr. 1985
A. W. LEISSA Jun. 1985 24 p refs
(Contract NAG3-424)
(NASA-CR-175901; NAS 1.26:175901) Avail: NTIS HC A02/MF A01 CSCL 21E

Internal and distributed damping as possible methods for reducing the vibration response of turbomachine blades and theoretical methods for analyzing damped vibration were studied. It is demonstrated how the Ritz-Galerkin methods may be used to straightforwardly to analyze forced vibrations with damping. This is done directly without requiring the free vibration eigenfunctions. The Galerkin method is an effective technique for these types of problems. The Ritz method has the further advantage of not needing to satisfy the force type boundary conditions, which is particularly important for plates and shells. But proper functionals representing the forcing and damping terms must be developed, and this is done. Two types of damping--viscous and material (hysteretic) are considered. Both distributed and concentrated exciting forces are treated. Numerical results are obtained for cantilevered beams and rectangular plates. Studies showing the rates of convergence of the solutions are made. In the case of the cantilever beam, approximate solutions from the present methods are compared with the exact solutions. R.J.F.

N85-27869*# Princeton Univ., N. J. Dept. of Mechanical and Aerospace Engineering.
THE ROLE OF SURFACE GENERATED RADICALS IN CATALYTIC COMBUSTION Final Report
D. A. SANTAVICCA, Y. STEIN, and B. S. H. ROYCE Jun. 1985 24 p refs
(Contract NAG3-353)
Avail: NTIS HC A02/MF A01 CSCL 21B

Experiments were conducted to better understand the role of catalytic surface reactions in determining the ignition characteristics of practical catalytic combustors. Hydrocarbon concentrations, carbon monoxide and carbon dioxide concentrations, hydroxyl radical concentrations, and gas temperature were measured at the exit of a platinum coated, stacked plate, catalytic combustor during the ignition of lean propane-air mixtures. The substrate temperature profile was also measured during the ignition transient. Ignition was initiated by suddenly turning on the fuel and the time to reach steady state was of the order of 10 minutes. The gas phase reaction, showed no pronounced effect due to the catalytic surface reactions, except the absence of a hydroxyl radical overshoot. It is found that the transient ignition measurements are valuable in understanding the steady state performance characteristics. E.A.K.

N85-27870*# National Aeronautics and Space Administration. Lewis Research Center, Cleveland, Ohio.
FUTURE FUNDAMENTAL COMBUSTION RESEARCH FOR AEROPROPULSION SYSTEMS
E. J. MULARZ 1985 8 p refs Presented at the 21st Joint Propulsion Conf., Monterey, Calif.; sponsored by AIAA, SAE, ASME and ASEE
(NASA-TM-87049; E-2612; NAS 1.15:87049; AIAA-85-1398; USAAVSCOM-TR-85-C-11) Avail: NTIS HC A02/MF A01 CSCL 21E

Physical fluid mechanics, heat transfer, and chemical kinetic processes which occur in the combustion chamber of aeropropulsion systems were investigated. With the component requirements becoming more severe for future engines, the current design methodology needs the new tools to obtain the optimum configuration in a reasonable design and development cycle. Research efforts in the last few years were encouraging but to achieve these benefits research is required into the fundamental aerothermodynamic processes of combustion. It is recommended that research continues in the areas of flame stabilization, combustor aerodynamics, heat transfer, multiphase flow and atomization, turbulent reacting flows, and chemical kinetics. Associated with each of these engineering sciences is the need for research into computational methods to accurately describe and predict these complex physical processes. Research needs in each of these areas are highlighted. E.A.K.

N85-28944*# National Aeronautics and Space Administration. Lewis Research Center, Cleveland, Ohio.
ADVANCED SECONDARY POWER SYSTEM FOR TRANSPORT AIRCRAFT
A. C. HOFFMAN, I. G. HANSEN, R. F. BEACH, R. M. PLENCNER, R. P. DENGLER, K. S. JEFFERIES, and R. J. FRYE May 1985 38 p refs
(NASA-TP-2463; E-2434; NAS 1.60:2463) Avail: NTIS HC A03/MF A01 CSCL 21E

A concept for an advanced aircraft power system was identified that uses 20-kHz, 440-V, sin-wave power distribution. This system was integrated with an electrically powered flight control system and with other aircraft systems requiring secondary power. The resulting all-electric secondary power configuration reduced the empty weight of a modern 200-passenger, twin-engine transport by 10 percent and the mission fuel by 9 percent. Author

N85-28945*# National Aeronautics and Space Administration. Lewis Research Center, Cleveland, Ohio.
DEAN: A PROGRAM FOR DYNAMIC ENGINE ANALYSIS
G. G. SADLER and K. J. MELCHER 1985 18 p refs Proposed for presentation at the 21st Joint Propulsion Conf., Monterey, Calif., 8-10 Jul. 1985; sponsored by AIAA, SAE and ASME Prepared in cooperation with Army Research and Technology Labs.
(NASA-TM-87033; E-2588; NAS 1.15:87033; USAAVSCOM-TR-85-C-10) Avail: NTIS HC A02/MF A01 CSCL 21E

The Dynamic Engine Analysis program, DEAN, is a FORTRAN code implemented on the IBM/370 mainframe at NASA Lewis Research Center for digital simulation of turbofan engine dynamics. DEAN is an interactive program which allows the user to simulate engine subsystems as well as a full engine systems with relative ease. The nonlinear first order ordinary differential equations which define the engine model may be solved by one of four integration schemes, a second order Runge-Kutta, a fourth order Runge-Kutta, an Adams Predictor-Corrector, or Gear's method for still systems. The numerical data generated by the model equations are displayed at specified intervals between which the user may choose to modify various parameters affecting the model equations and transient execution. Following the transient run, versatile graphics capabilities allow close examination of the data. DEAN's modeling procedure and capabilities are demonstrated by generating a model of simple compressor rig. Author

N85-29955*# Pratt and Whitney Aircraft Group, East Hartford, Conn. Engineering Div.
ENERGY EFFICIENT ENGINE HIGH-PRESSURE TURBINE COMPONENT RIG PERFORMANCE TEST REPORT
K. P. LEACH May 1983 249 p refs
(Contract NAS3-20646)
(NASA-CR-168189; NAS 1.26:168189; PWA-5594-243) Avail: NTIS HC A11/MF A01 CSCL 21E

A rig test of the cooled high-pressure turbine component for the Energy Efficient Engine was successfully completed. The principal objective of this test was to substantiate the turbine design point performance as well as determine off-design performance with the interaction of the secondary flow system. The measured efficiency of the cooled turbine component was 88.5 percent, which surpassed the rig design goal of 86.5 percent. The secondary

flow system in the turbine performed according to the design intent. Characterization studies showed that secondary flow system performance is insensitive to flow and pressure variations. Overall, this test has demonstrated that a highly-loaded, transonic, single-stage turbine can achieve a high level of operating efficiency. B.W.

N85-29956*# Pratt and Whitney Aircraft Group, East Hartford, Conn.
ENERGY EFFICIENT ENGINE INTEGRATED CORE/LOW SPOOL TEST HARDWARE DESIGN REPORT
J. W. BISSET and D. C. HOWE Mar. 1983 223 p refs
(Contract NAS3-20646)
(NASA-CR-168137; NAS 1.26:168137; PWA-5594-231) Avail: NTIS HC A10/MF A01 CSCL 21E

The National Aeronautics and Space Administration is sponsoring the Energy Efficient Engine Program to identify and verify the technology required to significantly lower fuel consumption and operating cost for commercial gas-turbine engines. A major task that has been completed under this program is the design and analysis of test hardware for the integrated core/low spool. The integrated core/low spool is a test simulation of the conceptual study engine defined to meet the performance, economic and environmental goals of the Energy Efficient Engine Program. It is intended to permit evaluation and verification of critical technologies in a full engine operating environment. This report describes the design and results of design-related analyses for the integrated core/low spool and its subsystems. The design effort included a definition of the engine, major components, internal and external subsystems, test ducting, and test instrumentation. Various analytical representations, in addition to results acquired from supporting component rig and subscale model tests, have been used to verify aerodynamic and structural design concepts as well as to predict performance. Author

N85-29957*# General Electric Co., Cincinnati, Ohio. Aircraft Engine Business Group.
ENERGY EFFICIENT ENGINE (E3) CONTROLS AND ACCESSORIES DETAIL DESIGN REPORT
R. S. BEITLER and J. P. LAVASH Dec. 1982 158 p refs
(Contract NAS3-20643)
(NASA-CR-168017; NAS 1.26:168017; R82AEB400) Avail: NTIS HC A08/MF A01 CSCL 21E

An Energy Efficient Engine program has been established by NASA to develop technology for improving the energy efficiency of future commercial transport aircraft engines. As part of this program, a new turbofan engine was designed. This report describes the fuel and control system for this engine. The system design is based on many of the proven concepts and component designs used on the General Electric CF6 family of engines. One significant difference is the incorporation of digital electronic computation in place of the hydromechanical computation currently used. Author

N85-29958*# Pratt and Whitney Aircraft, East Hartford, Conn. Commercial Products Div.
ENERGY EFFICIENT ENGINE COMPONENT DEVELOPMENT AND INTEGRATION PROGRAM Semiannual Status Report, 1 Oct. 1981 - 31 Mar. 1982
30 Apr. 1982 160 p refs
(Contract NAS3-20646)
(NASA-CR-172846; NAS 1.26:172846; PWA-5594-202; SASR-8) Avail: NTIS HC A08/MF A01 CSCL 21E

The objective of the Energy Efficient Engine Component Development and Integration program is to develop, evaluate, and demonstrate the technology for achieving lower installed fuel consumption and lower operating costs in future commercial turbofan engines. Minimum goals have been set for a 12 percent reduction in thrust specific fuel consumption (TSFC), 5 percent reduction in direct operating cost (DOC), and 50 percent reduction in performance degradation for the Energy Efficient Engine (flight propulsion system) relative to the JT9D-7A reference engine. The Energy Efficienct Engine features a twin spool, direct drive, mixed flow exhaust configuration, utilizing an integrated engine nacelle structure. A short, stiff, high rotor and a single stage high pressure turbine are among the major enhancements in providing for both performance retention and major reductions in maintenance and direct operating costs. Improved clearance control in the high pressure compressor and turbines, and advanced single crystal materials in turbine blades and vanes are among the major features providing performance improvement. Highlights of work accomplished and programs modifications and deletions are presented. B.W.

N85-29960*# Scientific Systems, Inc., Cambridge, Mass.
NONLINEAR GLOBAL STABILITY ANALYSIS OF COMPRESSOR STALL PHENOMENA
H. RAZAVI Jun. 1985 105 p refs
(Contract NAS3-24089)
(NASA-CR-174908; NAS 1.26:174908; SSI-24089) Avail: NTIS HC A06/MF A01 CSCL 21E

Compressor stall phenomena are analyzed from the point of view of nonlinear control theory, based on bifurcation-catastrophe techniques. This new approach appears promising and offers insight into such well-known compressor instability problems as surge and rotating stall and suggests strategies for recovery. Three interlocking dynamic nonlinear state space models are developed. It is shown that the problem of rotating stall can be viewed as an induced bifurcation of solution of the unstalled model. Hysteresis effects are shown to exist in the stall/recovery process. Surge cycles are observed for some critical parameter values. The oscillatory behavior is seen to be due to development of limit cycles, generated by Hopf bifurcation of solutions. More specifically, it is observed that at certain critical values of parameters, a family of stable limit cycles with growning and then diminishing amplitudes is generated, then giving rise to an unstable family of limit cycles. This unstable family in turn bifurcates into other unstable families. To further illustrate the utility of the methodology, some partial computation of domains is carried out, and parameter sensitivity analysis is performed. Author

N85-29961# Detroit Diesel Allison, Indianapolis, Ind. Engineering Dept.
ADVANCED GAS TURBINE (AGT) TECHNOLOGY PROJECT Semiannual Report
Mar. 1984 94 p
(Contract DEN3-168; DE-AE01-77CS-51040)
(NASA-CR-174798; DOE/NASA/0168-8; NAS 1.26:174798; EDR-11682) Avail: NTIS HC A05/MF A01 CSCL 21E

Significant development activity occurred during the July to December 1983 period in the Allison-Pontiac AGT 100 Advanced Gas Turbine Technology Project. Two engines were evaluated through dynamometer testing. Through 1983, total accumulated engine test time (burning) was 41 hr 19 min. Engine D-2 incorporated a modification to the interface system between the ceramic regenerator bulkhead and power turbine scroll assembly, solving the problem of cracked bulkheads experienced on the last builds of engine D-1. A design modification was defined to eliminate the tendency to leak hot gas from the engine flow path into the gearbox vent cavity. Compressor aerodynamic analyses that identified impeller modifications for improved performance were completed. These near-term improvements will be tested next period on a compressor rig. Two turbine aerodynamic improvements were designed for 1984 implementation: improved gasifier vane shape and a reduced capacity power turbine. Combustor development included rig changes to better simulate the engine flow path and to provide viewing stations for use of optical pyrometers. Rig testing was conducted to proof-test ceramic units, to examine starting and igniter relocations, and to map stability limits. Regenerator testing evaluated 23 disk/seal combinations in 145 hr of hot rig testing. Advanced concepts included a silicone leaf seal, polyimide integral wearface and seal platform, different crossarm cooling systems, low-leakage aluminum silicate risks, and an extruded magnesium-aluminum silicate disk. Ceramic turbine rotor development experienced improvement in molding, baking, and sintering engine configuration rotors. Nineteen sintered alpha

silicon carbide rotors were cold-spin tested to failure. Average burst speed was 94,930 rpm. R.J.F.

N85-29964*# National Aeronautics and Space Administration. Lewis Research Center, Cleveland, Ohio.
LARGE-SCALE ADVANCED PROPFAN (LAP) PROGRAM Progress Report
D. A. SAGERSER and S. G. LUDEMANN (Hamilton Standard, Windsor Locks, Conn.) 1985 28 p refs Presented at the 21st Joint Propulsion Conf., Monterey, Calif., 8-10 Jul. 1985; sponsored by AIAA, SAE, ASME, and ASEE
(NASA-TM-87067; E-2637; NAS 1.15:87067; AIAA-85-1187)
Avail: NTIS HC A03/MF A01 CSCL 21E

The propfan is an advanced propeller concept which maintains the high efficiencies traditionally associated with conventional propellers at the higher aircraft cruise speeds associated with jet transports. The large-scale advanced propfan (LAP) program extends the research done on 2 ft diameter propfan models to a 9 ft diameter article. The program includes design, fabrication, and testing of both an eight bladed, 9 ft diameter propfan, designated SR-7L, and a 2 ft diameter aeroelastically scaled model, SR-7A. The LAP program is complemented by the propfan test assessment (PTA) program, which takes the large-scale propfan and mates it with a gas generator and gearbox to form a propfan propulsion system and then flight tests this system on the wing of a Gulfstream 2 testbed aircraft. E.A.K.

N85-29965*# Pratt and Whitney Aircraft, West Palm Beach, Fla. Government Products Div.
CONVOLUTED NOZZLE DESIGN FOR THE RL10 DERIVATIVE 2B ENGINE Final Report
1 Jul. 1985 113 p refs Prepared in cooperation with Textron Bell Aerospace Co., Buffalo, N.Y.
(Contract NAS3-22902)
(NASA-CR-174953; NAS 1.26:174953; PWA-FR-18323-2; REPT-8881-933004) Avail: NTIS HC A06/MF A01 CSCL 21E

The convoluted nozzle is a conventional refractory metal nozzle extension that is formed with a portion of the nozzle convoluted to show the extendible nozzle within the length of the rocket engine. The convoluted nozzle (CN) was deployed by a system of four gas driven actuators. For spacecraft applications the optimum CN may be self-deployed by internal pressure retained, during deployment, by a jettisonable exit closure. The convoluted nozzle is included in a study of extendible nozzles for the RL10 Engine Derivative 2B for use in an early orbit transfer vehicle (OTV). Four extendible nozzle configurations for the RL10-2B engine were evaluated. Three configurations of the two position nozzle were studied including a hydrogen dump cooled metal nozzle and radiation cooled nozzles of refractory metal and carbon/carbon composite construction respectively. E.A.K.

N85-31057*# Pratt and Whitney Aircraft, East Hartford, Conn. Commercial Products Div.
CREEP FATIGUE LIFE PREDICTION FOR ENGINE HOT SECTION MATERIALS (ISOTROPIC) Annual Report
V. MORENO Aug. 1983 89 p refs
(Contract NAS3-23288)
(NASA-CR-168228; NAS 1.26:168228; PWA-5894-17; AR-1)
Avail: NTIS HC A05/MF A01 CSCL 21E

The Hot Section Technology (HOST) program, creep fatigue life prediction for engine hot section materials (isotropic), is reviewed. The program is aimed at improving the high temperature crack initiation life prediction technology for gas turbine hot section components. Significant results include: (1) cast B1900 and wrought IN 718 selected as the base and alternative materials respectively; (2) fatigue test specimens indicated that measurable surface cracks appear early in the specimen lives, i.e., 15% of total life at 871 C and 50% of life at 538 c; (3) observed crack initiation sites are all surface initiated and are associated with either grain boundary carbides or local porosity, transgrannular cracking is observed at the initiation site for all conditions tested; and (4) an initial evaluation of two life prediction models, representative of macroscopic (Coffin-Mason) and more microscopic (damage rate) approaches, was conducted using limited data generated at 871 C and 538 C. It is found that the microscopic approach provides a more accurate regression of the data used to determine crack initiation model constants, but overpredicts the effect of strain rate on crack initiation life for the conditions tested. E.A.K.

N85-31058*# National Aeronautics and Space Administration. Lewis Research Center, Cleveland, Ohio.
COMBUSTION GAS PROPERTIES. PART 3: HYDROGEN GAS FUEL AND DRY AIR
J. D. WEAR, R. E. JONES, B. J. MCBRIDE, and R. A. BEYERLE (Sverdrup Technology, Inc.) Jun. 1985 12 p refs Doc. includes microfiche supplement
(Contract NAS3-24105)
(NASA-TP-2477; E-2545; NAS 1.60:2477) Avail: NTIS HC A02/MF A01 CSCL 07D

A series of computations has been made to produce the equilibrium temperature and gas composition for hydrogen gas fuel and dry air. The computed tables and figures provide combustion gas property data for pressures from 0.5 to 50 atmospheres and equivalence ratios from 0 to 2.0. Only sample tables and figures are provided in this report. Author

N85-31060*# National Aeronautics and Space Administration. Lewis Research Center, Cleveland, Ohio.
SPIRAL BEVEL AND CIRCULAR ARC HELICAL GEARS: TOOTH CONTACT ANALYSIS AND THE EFFECT OF MISALIGNMENT ON CIRCULAR ARC HELICAL GEARS
F. L. LITVIN (Illinois Univ. at Chicago), W. T. TSUNG (Illinois Univ. at Chicago), C. B. TSAY (Illinois Univ. at Chicago), J. J. COY, and R. F. HANDSCHUH 1985 15 p refs Presented at the 21st Joint Propulsion Conf., Monterey, Calif. 8-10 Jul. 1985; sponsored in part by AIAA, SAE and ASME
(NASA-TM-87013; E-2557; NAS 1.15:87013; USAAVSCOM-TR-85-C-6) Avail: NTIS HC A02/MF A01 CSCL 21E

A computer aided method for tooth contact analysis was developed and applied. Optimal machine-tool settings for spiral bevel gears are proposed and when applied indicated that kinematic errors can be minimized while maintaining a desirable bearing contact. The effect of misalignment for circular arc helical gears was investigated and the results indicted that directed pinion refinishing can compensate the kinematic errors due to misalignment. Author

N85-32119*# General Electric Co., Cincinnati, Ohio. Aircraft Engine Business Group.
COMPONENT-SPECIFIC MODELING Annual Status Report, 1 Jan. - 31 Dec. 1984
R. L. MCKNIGHT 1985 131 p
(Contract NAS3-23687)
(NASA-CR-174925; NAS 1.26:174925; ASR-2) Avail: NTIS HC A07/MF A01 CSCL 21E

Accomplishments are described for the second year effort of a 3-year program to develop methodology for component specific modeling of aircraft engine hot section components (turbine blades, turbine vanes, and burner liners). These accomplishments include: (1) engine thermodynamic and mission models; (2) geometry model generators; (3) remeshing; (4) specialty 3-D inelastic stuctural analysis; (5) computationally efficient solvers, (6) adaptive solution strategies; (7) engine performance parameters/component response variables decomposition and synthesis; (8) integrated software architecture and development, and (9) validation cases for software developed. Author

N85-34138*# General Electric Co., Cincinnati, Ohio. Aircraft Engine Business Group.
HIGH PRESSURE COMPRESSOR COMPONENT PERFORMANCE REPORT
S. J. CLINE, W. FESLER, H. S. LIU, R. C. LOVELL, and S. J. SHAFFER Sep. 1983 170 p
(Contract NAS3-20643)
(NASA-CR-168245; NAS 1.26:168245; R82AEB437) Avail: NTIS HC A08/MF A01 CSCL 21E

A compressor optimization study defined a 10 stage configuration with a 22.6:1 pressure ratio, an adiabatic efficiency goal of 86.1%, and a polytropic efficiency of 90.6%; the corrected airflow is 53.5 kg/s. Subsequent component testing included three full scale tests: a six stage rig test, a 10 stage rig test, and another 10 stage rig test completed in the second quarter of 1982. Information from these tests is used to select the configuration for a core engine test and an integrated core/low spool test. The test results will also provide data base for the flight propulsion system. The results of the test series with both aerodynamic and mechanical performance of each compressor build are presented. The second 10 stage compressor adiabatic efficiency was 0.848 at a cruise operating point versus a test goal of 0.846. E.A.K.

N85-34140*# General Electric Co., Cincinnati, Ohio. Aircraft Engine Business Group.
COMPONENT-SPECIFIC MODELING Annual Status Report
R. L. MCKNIGHT May 1985 162 p refs
(Contract NAS3-23687)
(NASA-CR-174765; NAS 1.26:174765; ASR-1) Avail: NTIS HC A08/MF A01 CSCL 21E

A series of interdisciplinary modeling and analysis techniques that were specialized to address three specific hot section components are presented. These techniques will incorporate data as well as theoretical methods from many diverse areas including cycle and performance analysis, heat transfer analysis, linear and nonlinear stress analysis, and mission analysis. Building on the proven techniques already available in these fields, the new methods developed will be integrated into computer codes to provide an accurate, and unified approach to analyzing combustor burner liners, hollow air cooled turbine blades, and air cooled turbine vanes. For these components, the methods developed will predict temperature, deformation, stress and strain histories throughout a complete flight mission. Author

N85-34141*# General Electric Co., Cincinnati, Ohio. Aircraft Engine Business Group.
ENERGY EFFICIENT ENGINE. FAN AND QUARTER-STAGE COMPONENT PERFORMANCE REPORT
S. J. CLINE, P. H. HALTER, J. T. KUTNEY, JR., and T. J. SULLIVAN Jan. 1983 71 p refs
(Contract NAS3-20643)
(NASA-CR-168070; NAS 1.26:168070; R82AEB408) Avail: NTIS HC A04/MF A01 CSCL 21E

The fan configuration for the general Electric/NASA Energy Efficient Engine was selected following an extensive preliminary design study. The fan has an inlet radius ratio of 0.342 and a specific flowrate of 208.9 Kg/sec/sq. m (42.8 lbm/sec/sq. ft). The design corrected tip speed is 411.5 m/sec (1350 ft/sec) producing a bypass flow total-pressure ratio of 1.65 and a core flow total-pressure ratio of 1.6. The design bypass ratio is 6.8. The aerodynamic design point corresponds to the maximum climb power setting at Mach 0.8 and 10.67 Km (35,000 ft) altitude. The fully-instrumented fan component was tested in the Lynn Large Fan Test Facility in 1981. The overall performance results, reported herein, showed excellent fan performance with the fan meeting all of its component test goals of flow, efficiency and stall margin. Author

N85-35195* National Aeronautics and Space Administration. Lewis Research Center, Cleveland, Ohio.
FLOW MODIFYING DEVICE Patent
J. S. KELM (General Electric Co., Cincinnati), E. C. VICKERS (General Electric Co., Cincinnati), J. J. WILLIAMS (General Electric Co., Cincinnati), and J. R. TAYLOR, inventors (to NASA) (General Electric Co., Cincinnati) 13 Aug. 1985 10 p Continuation of abandoned US-Patent-Appl-SN-192677 filed 1 Oct. 1980
(NASA-CASE-LEW-13562-2; US-PATENT-4,534,166; US-PATENT-APPL-SN-500651; US-PATENT-CLASS-60-39.23; US-PATENT-CLASS-60-748; US-PATENT-CLASS-239-402.5)
Avail: US Patent and Trademark Office CSCL 21E

A swirler for a gas turbine engine combustor is disclosed for simultaneously controlling combustor flow rate, swirl angle, residence time and fuel-air ratio to provide three regimes of operation. A first regime is provided in which fuel-air ratio is less than stoichiometric, NOx is produced at one level, and combustor flow rate is high. In a second regime, fuel-air ratio is nearly stoichiometric, NOx production is less than that of the first regime, and combustor flow rate is low. In a third regime, used for example at highoff, fuel-air ratio is greater than stoichiometric and the combustor flow rate is less than in either of the other regimes. Author

N85-35197*# Pratt and Whitney Aircraft, East Hartford, Conn. Engineering Div.
ENERGY EFFICIENT ENGINE PROGRAM TECHNOLOGY BENEFIT/COST STUDY, VOLUME 1 Executive Summary
D. E. GRAY and W. B. GARDNER Oct. 1983 19 p 2 Vol.
(Contract NAS3-20646)
(NASA-CR-174766-VOL-1; NAS 1.26:174766-VOL-1; PWA-5594-258-VOL-1) Avail: NTIS HC A02/MF A01 CSCL 21E

Turbofan engine technologies required for the years 2000 to 2010 were studied, to assess the benefits of those technologies, and to formulate programs for developing the technologies required for that time period. Preliminary technology concepts that might be amenable to future development were ranked. Cycle studies, flowpath definition studies, and mechanical configuration studies were used to identify and establish the feasibility of the technologies that would be required in the 2000 to 2010 time frame. It is shown that a turbofan engine with advancements in aerodynamics, mechanical arrangements, and materials offer significant performance improvements over 1988 technology. The benefits of technologies are assessed using fuel burn and direct operating cost plus interest (DOC+I). The concepts could yield thrust specific fuel consumption benefits of almost 16%, fuel burn benefits of up to 24% and DOC+I benefits up to 14% in a long-range airplane relative to energy efficient engine technology levels. Technology development programs are formulated and recommended to realize those benefits E.A.K.

N85-35198*# Pratt and Whitney Aircraft, East Hartford, Conn. Engineering Div.
ENERGY EFFICIENT ENGINE PROGRAM TECHNOLOGY BENEFIT/COST STUDY, VOLUME 2
D. E. GRAY and W. B. GARDNER Oct. 1983 109 p refs 2 Vol.
(Contract NAS3-20646)
(NASA-CR-174766-VOL-2; NAS 1.26:174766-VOL-2; PWA-5594-251-VOL-2) Avail: NTIS HC A06/MF A01 CSCL 21E

The benefit/cost study to identify turbofan engine technologies required for the years 2000 to 2010, the benefits of those technologies were formulated, and programs for developing the technologies required for that time period were formulated. It is shown that there are still many potential benefits to be realized from the advancement of gas turbine engine technology. Preliminary technology concepts that might be amenable to future development were ranked. Cycle studies, flowpath definition studies, and mechancial configuration studies were used to identify and establish the feasibility of the technologies that would be required in the 2000 to 2010 time frame. It is shown that a turbofan engine with

advancements in aerodynamics, mechanical arrangements, and materials offers significant performance improvements over 1988 technology. The benefits of the technologies are assessed using fuel burn and direct operating cost plus interest (DOC+I). E.A.K.

N85-35199*# General Electric Co., Cincinnati, Ohio. Aircraft Engine Business Group.
ENERGY EFFICIENT ENGINE, HIGH PRESSURE TURBINE THERMAL BARRIER COATING. SUPPORT TECHNOLOGY REPORT
E. C. DUDERSTADT and P. AGARWAL May 1983 128 p refs
(Contract NAS3-20643)
(NASA-CR-168037; NAS 1.26:168037; R82AEB293) Avail: NTIS HC A07/MF A01 CSCL 21E

This report describes the work performed on a thermal barrier coating support technology task of the Energy Efficient Engine Component Development Program. A thermal barrier coating (TBC) system consisting of a Ni-Cr-Al-Y bond cost layer and ZrO2-Y2O3 ceramic layer was selected from eight candidate coating systems on the basis of laboratory tests. The selection was based on coating microstructure, crystallographic phase composition, tensile bond and bend test results, erosion and impact test results, furnace exposure, thermal cycle, and high velocity dynamic oxidation test results. Procedures were developed for applying the selected TBC to CF6-50, high pressure turbine blades and vanes. Coated HPT components were tested in three kinds of tests. Stage 1 blades were tested in a cascade cyclic test rig, Stage 2 blades were component high cycle fatigue tested to qualify thermal barrier coated blades for engine testing, and Stage 2 blades and Stage 1 and 2 vanes were run in factory engine tests. After completion of the 1000 cycle engine test, the TBC on the blades was in excellent condition over all of the platform and airfoil except at the leading edge above midspan on the suction side of the airfoil. The coating damage appeared to be caused by particle impingement; adjacent blades without TBC also showed evidence of particle impingement. B.W.

08

AIRCRAFT STABILITY AND CONTROL

Includes aircraft handling qualities; piloting; flight controls; and autopilots.

N85-12901*# United Technologies Research Center, East Hartford, Conn.
HIGH-TEMPERATURE OPTICALLY ACTIVATED GAAS POWER SWITCHING FOR AIRCRAFT DIGITAL ELECTRONIC CONTROL
J. M. BERAK, D. H. GRANTHAM, J. L. SWINDAL, J. F. BLACK, and L. B. ALLEN May 1983 201 p refs
(Contract NAS3-22535)
(NASA-CR-174711; NAS 1.26:174711; UTRC-R83-925312-25)
Avail: NTIS HC A10/MF A01 CSCL 01C

Gallium arsenide high-temperature devices were fabricated and assembled into an optically activated pulse-width-modulated power control for a torque motor typical of the kinds used in jet engine actuators. A bipolar heterojunction phototransistor with gallium aluminum arsenide emitter/window, a gallium arsenide junction field-effect power transistor and a gallium arsenide transient protection diode were designed and fabricated. A high-temperature fiber optic/phototransistor coupling scheme was implemented. The devices assembled into the demonstrator were successfully tested at 250 C, proving the feasibility of actuator-located switching of control power using optical signals transmitted by fibers. Assessments of the efficiency and technical merits were made for extension of this high-temperature technology to local conversion of optical power to electrical power and its control at levels useful for driving actuators. Optical power sources included in the comparisons were an infrared light-emitting diode, an injection laser diode, tungsten-halogen lamps and arc lamps. Optical-to-electrical power conversion was limited to photovoltaics located at the actuator. Impedance matching of the photovoltaic array to the load was considered over the full temperature range, -55 C to 260 C. Loss of photovoltaic efficiency at higher temperatures was taken into account. Serious losses in efficiency are: (1) in the optical source and the cooling which they may require in the assumed 125 C ambient, (2) in the decreased conversion efficiency of the gallium arsenide photovoltaic at 260 C, and (3) in impedance matching. Practical systems require improvements in these areas. Author

09

RESEARCH AND SUPPORT FACILITIES (AIR)

Includes airports, hangars and runways; aircraft repair and overhaul facilities; wind tunnels; shock tube facilities; and engine test blocks.

A85-19661*# National Aeronautics and Space Administration. Lewis Research Center, Cleveland, Ohio.
THE ALTITUDE WIND TUNNEL (AWT) - A UNIQUE FACILITY FOR PROPULSION SYSTEM AND ADVERSE WEATHER TESTING
R. CHAMBERLIN (NASA, Lewis Research Center, Cleveland, OH) American Institute of Aeronautics and Astronautics, Aerospace Sciences Meeting, 23rd, Reno, NV, Jan. 14-17, 1985. 12 p. refs
(AIAA PAPER 85-0314)

A need has arisen for a new wind tunnel facility with unique capabilities for testing propulsion systems and for conducting research in adverse weather conditions. New propulsion system concepts, new aircraft configurations with an unprecedented degree of propulsion system/aircraft integration, and requirements for aircraft operation in adverse weather dictate the need for a new test facility. Required capabilities include simulation of both altitude pressure and temperature, large size, full subsonic speed range, propulsion system operation, and weather simulation (i.e., icing, heavy rain). A cost effective rehabilitation of the NASA Lewis Research Center's Altitude Wind Tunnel (AWT) will provide a facility with all these capabilities. Author

A85-19709*# National Aeronautics and Space Administration. Lewis Research Center, Cleveland, Ohio.
ANALYTICAL AND PHYSICAL MODELING PROGRAM FOR THE NASA LEWIS RESEARCH CENTER'S ALTITUDE WIND TUNNEL (AWT)
J. M. ABBOTT, J. H. DIEDRICH, J. F. GROENEWEG, L. A. POVINELLI, L. REID, J. J. REINMANN, and J. R. SZUCH (NASA, Lewis Research Center, Cleveland, OH) American Institute of Aeronautics and Astronautics, Aerospace Sciences Meeting, 23rd, Reno, NV, Jan. 14-17, 1985. 13 p. refs
(AIAA PAPER 85-0379)

An effort is currently underway at the NASA Lewis Research Center to rehabilitate and extend the capabilities of the Altitude Wind Tunnel (AWT). This extended capability will include a maximum test section Mach number of about 0.9 at an altitude of 55,000 ft and a -20 F stagnation temperature (octagonal test section, 20 ft across the flats). In addition, the AWT will include an icing and acoustic research capability. In order to insure a technically sound design, an AWT modeling program (both analytical and physical) was initiated to provide essential input to the AWT final design process. This paper describes the modeling program, including the rationale and criteria used in program definition, and presents some early program results. Author

A85-26381*# National Aeronautics and Space Administration. Lewis Research Center, Cleveland, Ohio.
THE NASA ALTITUDE WIND TUNNEL - ITS ROLE IN ADVANCED ICING RESEARCH AND DEVELOPMENT
B. J. BLAHA and R. J. SHAW (NASA, Lewis Research Center, Cleveland, OH) American Institute of Aeronautics and Astronautics, Aerospace Sciences Meeting, 23rd, Reno, NV, Jan. 14-17, 1985. 20 p. Previously announced in STAR as A85-15758. refs
(AIAA PAPER 85-0090)

Currently experimental aircraft icing research is severly hampered by limitations of ground icing simulation facilities. Existing icing facilities do not have the size, speed, altitude, and icing environment simulation capabilities to allow accurate studies to be made of icing problems occurring for high speed fixed wing aircraft and rotorcraft. Use of the currently dormant NASA Lewis Altitude Wind Tunnel (AWT), as a proposed high speed propulsion and adverse weather facility, would allow many such problems to be studied. The characteristics of the AWT related to adverse weather simulation and in particular to icing simulation are discussed, and potential icing research programs using the AWT are also included. Author

N85-15757*# National Aeronautics and Space Administration. Lewis Research Center, Cleveland, Ohio.
ANALYTICAL AND PHYSICAL MODELING PROGRAM FOR THE NASA LEWIS RESEARCH CENTER'S ALTITUDE WIND TUNNEL (AWT)
J. M. ABBOTT, J. H. DEIDRICH, J. F. GROENEWEG, L.. A. POVINELLI, L. REID, J. J. REINMANN, and J. R. SZUCH 1985 21 p refs Presented at the 23rd Aerospace Sci. Meeting, Reno, Nevada, 14-17 Jan. 1985; sponsored by AIAA
(NASA-TM-86919; E-2413; NAS 1.15:86919; AIAA-85-0379)
Avail: NTIS HC A02/MF A01 CSCL 14B

An effort is currently underway at the NASA Lewis Research Center to rehabilitate and extend the capabilities of the Altitude Wind Tunnel (AWT). This extended capability will include a maximum test section Mach number of about 0.9 at an altitude of 55,000 ft and a -20 F stagnation temperature (octagonal test section, 20 ft across the flats). In addition, the AWT will include an icing and acoustic research capability. In order to insure a technically sound design, an AWT modeling program (both analytical and physical) was initiated to provide essential input to the AWT final design process. This paper describes the modeling program, including the rationale and criteria used in program definition, and presents some early program results. Author

N85-15758*# National Aeronautics and Space Administration. Lewis Research Center, Cleveland, Ohio.
THE NASA ALTITUDE WIND TUNNEL (AWT): ITS ROLE IN ADVANCED ICING RESEARCH AND DEVELOPMENT
B. J. BLAHA and R. J. SHAW 1985 21 p refs Presented at the 23rd Aerospace Sci. Meeting, Reno, Nevada, 14-17 Jan. 1985; sponsored by AIAA
(NASA-TM-86920; E-2414; NAS 1.15:86920; AIAA-85-0090)
Avail: NTIS HC A02/MF A01 CSCL 14B

Currently experimental aircraft icing research is severely hampered by limitations of ground icing simulation facilities. Existing icing facilities do not have the size, speed, altitude, and icing environment simulation capabilities to allow accurate studies to be made of icing problems occurring for high speed fixed wing aircraft and rotorcraft. Use of the currently dormant NASA Lewis Altitude Wind Tunnel (AWT), as a proposed high speed propulsion and adverse weather facility, would allow many such problems to be studied. The characteristics of the AWT related to adverse weather simulation and in particular to icing simulation are discussed, and potential icing research programs using the AWT are also included. Author

N85-18067*# National Aeronautics and Space Administration. Lewis Research Center, Cleveland, Ohio.
THE ALTITUDE WIND TUNNEL (AWT): A UNIQUE FACILITY FOR PROPULSION SYSTEM AND ADVERSE WEATHER TESTING
R. CHAMBERLIN 1985 21 p refs Presented at the 23rd Aerospace Sci. Meeting, Reno, Nevada, 14-17 Jan. 1985; sponsored by AIAA Previously announced in IAA as A85-19661
(NASA-TM-86921; E-2415; NAS 1.15:86921; AIAA-85-0314)
Avail: NTIS HC A02/MF A01 CSCL 14B

A need has arisen for a new wind tunnel facility with unique capabilities for testing propulsion systems and for conducting research in adverse weather conditions. New propulsion system concepts, new aircraft configurations with an unprecedented degree of propulsion system/aircraft integration, and requirements for aircraft operation in adverse weather dictate the need for a new test facility. Required capabilities include simulation of both altitude pressure and temperature, large size, full subsonic speed range, propulsion system operation, and weather simulation (i.e., icing, heavy rain). A cost effective rehabilitation of the NASA Lewis Research Center's Altitude Wind Tunnel (AWT) will provide a facility with all these capabilities. Author

N85-22400*# Mechanical Technology, Inc., Latham, N. Y.
DEVELOPMENT OF A MULTIPLANE MULTISPEED BALANCING SYSTEM FOR TURBINE SYSTEMS
M. R. MARTIN 19 Jul. 1984 114 p refs
(Contract NAS3-20609)
(NASA-CR-174750; NAS 1.26:174750; MTI-84TR39) Avail: NTIS HC A06/MF A01 CSCL 14B

A prototype high speed balancing system was developed for assembled gas turbine engine modules. The system permits fully assembled gas turbine modules to be operated and balanced at selected speeds up to full turbine speed. The balancing system is a complete stand-alone system providing all necesary lubrication and support hardware for full speed operation. A variable speed motor provides the drive power. A drive belt and gearbox provide rotational speeds up to 21,000 rpm inside a vacuum chamber. The heart of the system is a dedicated minicomputer with attendant data acquisition, storage and I/O devices. The computer is programmed to be completely interactive with the operator. The system was installed at CCAD and evaluated by testing 20 T55 power turbines and 20 T53 power turbines. Engine test results verified the performance of the high speed balanced turbines.
B.W.

12

ASTRONAUTICS (GENERAL)

N85-12071*# Battelle Columbus Labs., Ohio.
PRELIMINARY ANALYSIS OF SPACE MISSION APPLICATIONS FOR ELECTROMAGNETIC LAUNCHERS Final Technical Report
L. A. MILLER, E. E. RICE, R. W. EARHART, and R. J. CONLON 30 Aug. 1984 326 p refs
(Contract NAS3-23354)
(NASA-CR-174067; NAS 1.26:174067) Avail: NTIS HC A15/MF A01 CSCL 22A

The technical and economic feasibility of using electromagnetically launched EML payloads propelled from the Earth's surface to LEO, GEO, lunar orbit, or to interplanetary space was assessed. Analyses of the designs of rail accelerators and coaxial magnetic accelerators show that each is capable of launching to space payloads of 800 KG or more. A hybrid launcher in which EML is used for the first 2 KM/sec followed by chemical rocket stages was also tested. A cost estimates study shows that one to two EML launches per day are needed to break even,

compared to a four-stage rocket. Development models are discussed for: (1) Earth orbital missions; (2) lunar base supply mission; (3) solar system escape mission; (4) Earth escape missions; (5) suborbital missions; (6) electromagnetic boost missions; and (7) space-based missions. Safety factors, environmental impacts, and EML systems analysis are discussed. Alternate systems examined include electrothermal thrustors, an EML rocket gun; an EML theta gun, and Soviet electromagnetic accelerators. A.R.H.

N85-13886*# National Aeronautics and Space Administration. Lewis Research Center, Cleveland, Ohio.
MISSIONS/PLANNING PANEL
J. S. FORDYCE *In its* Space Power p 57 Apr. 1984
Avail: NTIS HC A14/MF A01 CSCL 22A

A panel discussion was held to develop a viewpoint of space power technology needs and state of readiness for future mission scenarios. Among the points made in the discussion, it was agreed that missions, particularly the far term ones, do serve to drive technology; however, as the missions become nearer term, issues of schedule and cost severely limit the willingness to accept risk. There are, in fact, no rewards to a mission manager for introducing new technology. Mission downscaling is the usual response to technology limitations. All panelists agreed that there exists a serious gap between when technologists feel their job is done and what mission managers need for decision. Typically a two to three year engineering development gap exists. It is essential to take technologies to the engineering model level and conduct a flight demonstration to close this gap. All agreed that increased effort should be made to achieve stronger interactions between planners and technologists and that workshops like the present one are a step in the right direction. Technologists need mission credibility and vice versa. R.J.F.

N85-27922*# Stanford Univ., Calif.
FREE-SURFACE PHENOMENA UNDER LOW- AND ZERO-GRAVITY CONDITIONS Final Technical Report
L. HESSELINK Jun. 1985 8 p
(Contract NAG3-557)
(NASA-CR-175885; NAS 1.26:175885) Avail: NTIS HC A02/MF A01 CSCL 22A

A free surface experiment using a liquid doped with a fluorescent dye under sheet illumination is summarized. The work includes the selection of a CCD camera for use during the design stages of the experiment as well as a preliminary demonstration of this technique in the production of a contour map of a liquid-liquid interface with better than 0.1 mm resolution. With a different data sampling and storage procedure, the image processing is reduced to a simple thresholding procedure which can be done in hardware. Author

13

ASTRODYNAMICS

Includes powered and free-flight trajectories; and orbit and launching dynamics.

N85-21228*# National Aeronautics and Space Administration. Lewis Research Center, Cleveland, Ohio.
RADIATION EXPOSURE AND PERFORMANCE OF MULTIPLE BURN LEO-GEO ORBIT TRANSFER TRAJECTORIES
S. H. GORLAND 1985 14 p refs Presented at the JANNAF Propulsion Meeting, San Diego, Calif., 9-12 Apr. 1985
(NASA-TM-86946; E-2465; NAS 1.15:86946) Avail: NTIS HC A02/MF A01 CSCL 22A

Many potential strategies exist for the transfer of spacecraft from low Earth orbit (LEO) to geosynchronous (GEO) orbit. One strategy has generally been utilized, that being a single impulsive burn at perigee and a GEO insertion burn at apogee. Multiple burn strategies were discussed for orbit transfer vehicles (OTVs) but the transfer times and radiation exposure, particularly for potentially manned missions, were used as arguments against those options. Quantitative results concerning the trip time and radiation encountered by multiple burn orbit transfer missions in order to establish the feasibility of manned missions, the vulnerability of electronics, and the shielding requirements are presented. The performance of these multiple burn missions is quantified in terms of the payload and propellant variances from the minimum energy mission transfer. The missions analyzed varied from one to eight perigee burns and ranged from a high thrust, 1 g acceleration, cryogenic hydrogen-oxygen chemical prpulsion system to a continuous burn, 0.001 g acceleration, hydrogen fueled resistojet propulsion system with a trip time of 60 days. Author

15

LAUNCH VEHICLES AND SPACE VEHICLES

Includes boosters; manned orbital laboratories; reusable vehicles; and space stations.

A85-23200*# National Aeronautics and Space Administration. Lewis Research Center, Cleveland, Ohio.
A HIGH ENERGY STAGE FOR THE NATIONAL SPACE TRANSPORTATION SYSTEM
A. J. STOFAN (NASA, Lewis Research Center, Cleveland, OH) International Astronautical Federation, International Astronautical Congress, 35th, Lausanne, Switzerland, Oct. 7-13, 1984. 12 p. Previously announced in STAR as N84-32411.
(IAF PAPER 84-15)

The Shuttle/Centaur is an expendable hydrogen/oxygen cryogenic upper stage for use with the National Space Transportation System. It is a modification of the existing Atlas/Centaur which was used by NASA since 1966 to launch interplanetary and earth orbital payloads for numerous organizations. Two configurations of the Shuttle/Centaur are being developed. Vehicle capability includes placing approximately 4500 kg (10,000 lb) in geostationary orbit, and initial applications will be for the interplanetary Galileo and Ulysses Missions in 1986. The Shuttle/Centaur development program is discussed, the configurations and performance are described, and the unique integration and operations requirements related to the Shuttle are indicated. Design changes to the current Atlas/Centaur required for Shuttle operation are described here, and include those related to Orbiter cargo bay dimensions, environment, and safety considerations. Author

A85-39730*# Martin Marietta Aerospace, Denver, Colo.
MAIN PROPULSION SYSTEM DESIGN RECOMMENDATIONS FOR AN ADVANCED ORBIT TRANSFER VEHICLE
L. REDD (Martin Marietta Aerospace, Denver, CO) AIAA, SAE, ASME, and ASEE, Joint Propulsion Conference, 21st, Monterey, CA, July 8-10, 1985. 9 p.
(Contract NAS3-23858)
(AIAA PAPER 85-1336)

Various main propulsion system configurations of an advanced OTV are evaluated with respect to the probability of nonindependent failures, i.e., engine failures that disable the entire main propulsion system. Analysis of the life-cycle cost (LCC) indicates that LCC is sensitive to the main propulsion system reliability, vehicle dry weight, and propellant cost; it is relatively insensitive to the number of missions/overhaul, failures per mission, and EVA and IVA cost. In conclusion, two or three engines are recommended in view of their highest reliability, minimum life-cycle cost, and fail operational/fail safe capability. L.T.

N85-16989*# National Aeronautics and Space Administration. Lewis Research Center, Cleveland, Ohio.
OTV PROPULSION ISSUES
Washington Apr. 1984 296 p refs Conf. held in Cleveland, 3-4 Apr. 1984
(NASA-CP-2347; E-2171; NAS 1.55:2347) Avail: NTIS HC A13/MF A01 CSCL 22B

The statistical technology needs of aero-assist maneuvering, propulsion, and usage of cryogenic fluids were presented. Industry panels discussed the servicing of reusable space based vehicles and propulsion-vehicle interation.

N85-16991*# National Aeronautics and Space Administration. Lewis Research Center, Cleveland, Ohio.
SHUTTLE/CENTAUR PROJECT PERSPECTIVE
E. T. MUCKLEY *In its* OTV Propulsion Issues p 15-27 Apr. 1984 refs
Avail: NTIS HC A13/MF A01 CSCL 22B

The shuttle/Centaur vehicle is being developed as an expendable, cryogenic high energy upper stage for use with the National Space Transportation System (NSTS). The stage is expected to meet the demands of a wide range of users. The shuttle/Centaur will be a modification of the highly successful Centaur stage, used extensively with the Atlas and Titan boosters since 1966 to launch planetary, geosynchronous and Earth orbital missions. The design changes required for use with the NSTS are described. These are primarily related to: (1) tank resizing to take advantage of the orbiter payload bay dimensions; (2) provisions for physically adopting Centaur to the orbiter; and, (3) accommodating safety requirements of the manned NSTS. The expected performance capabilities of two versions of the shuttle/Centaur are also described. The initial version, designated G-prime, is the larger of the two, with a length of about 9.1m (30 ft.). This vehicle will be used to launch the Galileo and International Solar Polar Mission to Jupiter in May 1986. B.G.

N85-16997*# *National Aeronautics and Space Administration.* Lewis Research Center, Cleveland, Ohio.
OTV PROPULSION TECHNOLOGY PROGRAMMATIC OVERVIEW
L. P. COOPER *In its* OTV Propulsion Issues p 97-102 Apr. 1984 refs
Avail: NTIS HC A13/MF A01 CSCL 22B

An advanced orbit transfer vehicles (OTV) which will be an integral part of the national space transportation system to carry men and cargo between low Earth orbit and geosynchronous orbit will perform planetary transfers and deliver large acceleration limited space structures to high Earth orbits is reviewed. The establishment of an advanced propulsion technology base for an OTV for the mid 1990's is outlined. The program supports technology for three unique engine concepts. Work is conducted to generic technologies which benefit all three concepts and specific technology which benefits only one of the concepts. Concept and technology definitions to identify propulsion innovations, and subcomponent research to explore and validate their potential benefits are included. E.A.K.

N85-17008*# National Aeronautics and Space Administration. Lewis Research Center, Cleveland, Ohio.
VEHICLE/ENGINE INTEGRATION
L. P. COOPER, T. J. VINOPAL (Boeing Aerospace Co., Seattle), D. E. FLORENCE (General Electric Corp., Fairfield, Conn.), R. W. MICHEL (Aerojet TechSystems Co.), J. R. BROWN (Pratt and Whitney Aircraft, East Hartford, Conn.), R. P. BERGERON (Rockwell International Corp., Pittsburg), and V. A. WELDON *In its* OTV Propulsion Issues p 229-245 Apr. 1984 refs
Avail: NTIS HC A13/MF A01 CSCL 22B

VEHICLE/ENGINE Integration Issues are explored for orbit transfer vehicles (OTV's). The impact of space basing and aeroassist on VEHICLE/ENGINE integration is discussed. The AOTV structure and thermal protection subsystem weights were scaled as the vehicle length and surface was changed. It is concluded that for increased allowable payload lengths in a ground-based system, lower length-to-diameter (L/D) is as important as higher mixture ration (MR) in the range of mid L/D ATOV's. Scenario validity, geometry constraints, throttle levels, reliability, and servicing are discussed in the context of engine design and engine/vehicle integration. R.S.F.

N85-21231*# National Aeronautics and Space Administration. Lewis Research Center, Cleveland, Ohio.
ADVANCED RESEARCH AND TECHNOLOGY PROGRAMS FOR ADVANCED HIGH-PRESSURE OXYGEN-HYDROGEN ROCKET PROPULSION
S. J. MARSIK and S. F. MOREA (NASA. Marshall Space Flight Center) 1985 14 p refs Proposed for presentation at the 1985 JANNAF Propulsion Meeting, San Diego, Calif., 9-12 Apr. 1985
(NASA-TM-86969; E-2495; NAS 1.15:86969) Avail: NTIS HC A02/MF A01 CSCL 20H

A research and technology program for advanced high pressure, oxygen-hydrogen rocket propulsion technology is presently being pursued by the National Aeronautics and Space Administration (NASA) to establish the basic discipline technologies, develop the analytical tools, and establish the data base necessary for an orderly evolution of the staged combustion reusable rocket engine. The need for the program is based on the premise that the USA will depend on the Shuttle and its derivative versions as its principal Earth-to-orbit transportation system for the next 20 to 30 yr. The program is focused in three principal areas of enhancement: (1) life extension, (2) performance, and (3) operations and diagnosis. Within the technological disciplines the efforts include: rotor-dynamics, structural dynamics, fluid and gas dynamics, materials fatigue/fracture/life, turbomachinery fluid mechanics, ignition/combustion processes, manufacturing/producibility/nondestructive evaluation methods and materials development/evaluation. An overview of the Advanced High Pressure Oxygen-Hydrogen Rocket Propulsion Technology Program Structure and Working Groups objectives are presented with highlights of several significant achievements. Author

N85-21233*# Ohio State Univ., Columbus. Dept. of Electrical Engineering.
ENGINEERING CALCULATIONS FOR COMMUNICATIONS SATELLITE SYSTEMS PLANNING Interim Report, 15 Jul. 1983 - 14 Jul. 1:984
C. A. LEVIS, C. H. MARTIN, C. H. REILLY, D. J. GONSALVEZ, and Y. YAMAURA Mar. 1985 59 p refs
(Contract NAG3-159)
(NASA-CR-175552; NAS 1.26:175552; ESL-713533-5) Avail: NTIS HC A04/MF A01 CSCL 22B

An extended gradient search code for broadcasting satellite service (BSS) spectrum/orbit assignment synthesis is discussed. Progress is also reported on both single-entry and full synthesis computational aids for fixed satellite service (FSS) spectrum/orbit assignment purposes. Author

N85-22520*# National Aeronautics and Space Administration. Lewis Research Center, Cleveland, Ohio.
PRELIMINARY ASSESSMENT OF POWER-GENERATING TETHERS IN SPACE AND OF PROPULSION FOR THEIR ORBIT MAINTENANCE
R. E. ENGLISH and P. M. FINNEGAN *In its* Spacecraft Environ. Interactions Technol., 1983 p 637-647 Mar. 1985 refs
Avail: NTIS HC A99/MF E03 CSCL 22B

The concept of generating power in space by means of a conducting tether deployed from a spacecraft was studied. Using hydrogen and oxygen as the rocket propellant to overcome the drag of such a power-generating tether would yield more benefit than if used in a fuel cell. The mass consumption would be 25 percent less than the reactant consumption of fuel cells. Residual hydrogen and oxygen in the external tank and in the orbiter could be used very effectively for this purpose. Many other materials (such as waste from life support) could be used as the propellant. Electrical propulsion using tether generated power can compensate for the drag of a power-generating tether, half the power going to

the useful load and the rest for electric propulsion. In addition, the spacecraft's orbital energy is a large energy reservoir that permits load leveling and a ratio of peak to average power equal to 2. Critical technologies to be explored before a power-generating tether can be used in space are delineated. Author

16

SPACE TRANSPORTATION

Includes passenger and cargo space transportation, e.g., shuttle operations; and rescue techniques.

N85-29987*# National Aeronautics and Space Administration. Lewis Research Center, Cleveland, Ohio.
TECHNOLOGY REQUIREMENTS TO BE ADDRESSED BY THE NASA LEWIS RESEARCH CENTER CRYOGENIC FLUID MANAGEMENT FACILITY PROGRAM
J. C. AYDELOTT and R. S. RUDLAND (Martin Marietta Aerospace, Denver) 1985 25 p refs Presented at the 21st Joint Propulsion Conf., Monterey, Calif., 8-10 Jul. 1985; sponsored in part by AIAA, SAE, ASME and ASEE Previously announced in IAA as A85-47024
(NASA-TM-87048; E-2610; NAS 1.15:87048; AIAA-85-1229)
Avail: NTIS HC A02/MF A01 CSCL 14B

The NASA Lewis Research Center is responsible for the planning and execution of a scientific program which will provide advance in space cryogenic fluid management technology. A number of future space missions were identified that require or could benefit from this technology. These fluid management technology needs were prioritized and a shuttle attached reuseable test bed, the cryogenic fluid management facility (CFMF), is being designed to provide the experimental data necessary for the technology development effort. Author

17

SPACECRAFT COMMUNICATION, COMMAND AND TRACKING

Includes telemetry; space communications networks; astronavigation; and radio blackout.

A85-36663* Toledo Univ., Ohio.
MODELING OF NASA'S 30/20 GHZ SATELLITE COMMUNICATIONS SYSTEM
S. C. KWATRA, B. W. MAPLES (Toledo, University, Toledo, OH), and G. A. STEVENS (NASA, Lewis Research Center, Cleveland, OH) IN: ICC '84 - Links for the future: Science, systems and services for communications; Proceedings of the International Conference on Communications, Amsterdam, Netherlands, May 14-17, 1984. Volume 3 . New York/Amsterdam, Institute of Electrical and Electronics Engineers, Inc./North-Holland, 1984, p. 1102-1106. refs
(Contract NAG3-157)

NASA is in the process of developing technology for a 30/20 GHz satellite communications link. Currently hardware is being assembled for a test transponder. A simulation package is being developed to study the link performance in the presence of interference and noise. This requires developing models for the components of the system. This paper describes techniques used to model the components for which data is available. Results of experiments performed using these models are described. A brief overview of NASA's 30/20 GHz communications satellite program is also included. Author

N85-15779*# National Aeronautics and Space Administration. Lewis Research Center, Cleveland, Ohio.
CHARACTERIZATION OF MMIC DEVICES FOR ACTIVE ARRAY ANTENNAS
J. SMETANA, E. FARR (Illinois Univ., Urbana), and R. MITTRA (Illinois Univ., Urbana) 1984 17 p refs Presented at the Antenna Appl. Symp., Monticello, Ill., 19-21 Sep. 1984; sponsored by Illinois Univ. and RADC
(NASA-TM-86907; E-2396; NAS 1.15:86907) Avail: NTIS HC A02/MF A01 CSCL 09F

Certain aspects of monolithic microwave integrated circuit (MMIC) interconnectivity were investigated. Considerations that lead to preserving the inherently reproducible characteristics of the MMIC are proposed. It is shown that at radio frequencies (RF) greater than 20 GHz, the transition from the MMIC device to other transmission media must be an accurate RF match. It is proposed that the RF match is sufficiently critical to include the transition as part of the delivered MMIC package. The model to analyze several transitions is presented. This model consists of a succession of abrupt discontinuities in printed circuit transmission lines. The analysis of these discontinuities is achieved by the Spectral Galerkin technique, to establish the modes and mode matching, to generate the generalized S parameters of the individual discontinuities. Preliminary results achieved with this method are presented. It is concluded that special effects should be coordinated by the active array antenna industry toward standardization of MMIC packaging and characterization. E.A.K.

N85-34150*# National Aeronautics and Space Administration. Lewis Research Center, Cleveland, Ohio.
TELECOMMUNICATIONS FORECAST FOR ITU REGION 2 TO THE YEAR 1995
J. E. HOLLANSWORTH, J. A. SALZMAN, and J. R. RAMLER Aug. 1985 131 p refs
(NASA-TM-87077; E-2653; NAS 1.15:87077) Avail: NTIS HC A07/MF A01 CSCL 17B

Telecommunications activity was studied. The primary objective was to forecast the need for fixed service satellites (FSS) by countries within ITU Region 2 excluding the United States and Greenland. Forecasts of telecommunications equipment needs were developed as a yardstick of the relative level of telecommunications activity among developing countries within the region. A likely scenario for the implementation of domestic and regional communications satellites is forecasted to provide services to and among countries in ITU Region 2. By 1995, it is forecast that 15 fixed service satellites will be implemented. A forecast of the countries requirements indicates that, with the possible exception of Canada, this constellation of satellites will meet these countries' needs to beyond the year 2000. E.A.K.

18

SPACECRAFT DESIGN, TESTING AND PERFORMANCE

Includes spacecraft thermal and environmental control; and attitude control.

A85-30303*# Analex Corp., Cleveland, Ohio.
INTERDISCIPLINARY DESIGN ANALYSIS OF A PRECISION SPACECRAFT ANTENNA
R. E. STEINBACH (Analex Corp., Cleveland, OH) and S. R. WINEGAR (NASA, Lewis Research Center, Cleveland, OH) IN: Structures, Structural Dynamics, and Materials Conference, 26th, Orlando, FL, April 15-17, 1985, Technical Papers. Part 1 . New York, American Institute of Aeronautics and Astronautics, 1985, p. 704-712.
(AIAA PAPER 85-0804)

The Advanced Communications Technology Satellite (ACTS) will operate in the 20/30 GHz range (Ka Band), and will include a

multi-beam antenna (MBA) capable of 0.3 degree scanning spot beams with very high beam-to-beam isolation. The antenna Radio Frequency (RF) performance requirements lead to stringent requirements on the antenna reflector surface shape. A prediction of RF performance of a potential flight model antenna reflector operating under space environmental conditions is made using a radiant heat input model (TRASYS), a thermal analyzer (SINDA), a structural model (NASTRAN), and RF far field pattern simulation. Interfacing software has been written to pass thermal model temperature results to the structural model, and structural model thermal deformation results to the RF far field pattern simulation. A complete analysis can be performed in a single computer run, and potential changes in design can be quickly and easily evaluated using this interdisciplinary design analysis tool. Author

A85-35379*# Alabama Univ., Huntsville.
EXPERIMENTS IN CHARGE CONTROL AT GEOSYNCHRONOUS ORBIT - ATS-5 AND ATS-6
R. C. OLSEN (Alabama, University, Huntsville, AL) Journal of Spacecraft and Rockets (ISSN 0022-4650), vol. 22, May-June 1985, p. 254-264. refs
(Contract NSG-3150; NAS5-23481; NAS8-33982)

In connection with existing theoretical concepts, it was difficult to explain the negative potentials found in sunlight, first on Applied Technology Satellite-5 (ATS-5) and then on ATS-6. The problem became important when an association between spacecraft charging and anomalies in spacecraft behavior was observed. A study of daylight charging phenomena on ATS-6 was conducted, and an investigation was performed with the objective to determine effective methods of charge control, taking into account the feasibility to utilize the ATS-5 and ATS-6 ion engines as current sources. In the present paper, data and analysis for the ion engine experiments on ATS-5 and ATS-6 are presented. It is shown that electron emission from a satellite with insulating surfaces is not an effective method of charge control because the increase in differential charging which results limits the effectiveness of electron emitters and increases the possibility of electrostatic discharges between surfaces at different potentials. G.R.

N85-14858*# National Aeronautics and Space Administration. Lewis Research Center, Cleveland, Ohio.
CIRCUIT TRANSIENTS DUE TO NEGATIVE BIAS ARCS ON A HIGH-VOLTAGE SOLAR ARRAY IN LOW EARTH ORBIT
R. N. METZ (Colby Coll., Waterville, Maine) Jan. 1985 12 p refs
(NASA-TP-2407; E-2239; NAS 1.60:2407) Avail: NTIS HC A02/MF A01 CSCL 22B

Arcing to negatively biased, exposed solar cell interconnects on solar arrays placed in plasma environments was established. Arcing, however, may cause damaging interference with the operation of electrical power systems in spacecraft planned to be driven with high-voltage solar arrays. An analytical model was developed to estimate the effects of netagive bias arcs on solar array power system performance. Solar cell characteristics, plasma interactions, and power system features are modeled by a linear, lumped element transient circuit, and the time domain equations are solved. Numerical results for solar array common mode and load voltage transients are calculated for typical conditions. Acceptable load transients are found for a range of arc current amplitudes and time constants. E.A.K.

N85-21250*# Pennsylvania State Univ., University Park. Dept. of Physics.
MASS ANALYSIS OF NEUTRAL PARTICLES AND IONS RELEASED DURING ELECTRICAL BREAKDOWNS ON SPACECRAFT SURFACES Final Report, 1 Sep. 1979 - 31 Dec. 1984
B. R. F. KENDALL 16 Mar. 1985 32 p refs
(Contract NSG-3301)
(NASA-CR-175585; NAS 1.26:175585) Avail: NTIS HC A03/MF A01 CSCL 22B

Charged-particle fluxes from breakdown events were studied. Methods to measure mass spectra and total emitted flux of neutral particles were developed. The design and construction of the specialized mass spectrometer was completed. Electrical breakdowns were initiated by a movable blunt contact touching the insulating surface. The contact discharge apparatus was used for final development of two different high-speed recording systems and for measurements of the composition of the materials given off by the discharge. It was shown that intense instantaneous fluxes of neutral particles were released from the sites of electrical breakdown events. A laser micropulse mass analyzer showed that visible discoloration at breakdown sites were correllated with the presence of iron on the polymer side of the film, presumably caused by punch-through to the Inconel backing. Kapton samples irradiated by an oxygen ion beam were tested. The irradiated samples were free of surface hydrocarbon contamination but otherwise behaved in the same way as the Kapton samples tested earlier. Only the two samples exposed to oxygen ion bombardment were relatively clean. This indicates an additional variable that should be considered when testing spacecraft materials in the laboratory. E.A.K.

N85-22470*# National Aeronautics and Space Administration. Lewis Research Center, Cleveland, Ohio.
SPACECRAFT ENVIRONMENTAL INTERACTIONS TECHNOLOGY, 1983
Washington Mar. 1985 673 p refs Conf. held in Colorado Springs, 4-6 Oct. 1983 Prepared in cooperation with AFGL, Hanscom AFB, Mass.
(NASA-CP-2359; E-2186; NAS 1.55:2359; AFGL-TR-85-0018)
Avail: NTIS HC A99/MF E03 CSCL 22B

State of the art of environment interactions dealing with low-Earth-orbit plasmas; high-voltage systems; spacecraft charging; materials effects; and direction of future programs are contained in over 50 papers.

N85-22474*# National Aeronautics and Space Administration, Washington, D.C.
ELECTRON AND ION DENSITY DEPLETIONS MEASURED IN THE STS-3 ORBITER WAKE
G. B. MURPHY (Iowa Univ., Iowa City), J. S. PICKETT (Iowa Univ., Iowa City), W. S. RAITT (Utah State Univ., Logan), and S. D. SHAWHAN *In* NASA. Lewis Research Center Spacecraft Environ. Interactions Technol., 1983 p 33-42 Mar. 1985 refs
(Contract NAG3-449)
Avail: NTIS HC A99/MF E03 CSCL 22B

The third Space Shuttle flight on Columbia carried instrumentation to measure thermal plasma density and temperature. Two separate investigations, the Plasma Diagnostics Package (PDP) and the Vehicle Charging and Potential Experiment (VCAP), carried a Langmuir Probe, and the VCAP also included a Spherical Retarding Potential Analyzer (SRPA). Only those measurements made while the PDP is in the payload bay are discussed here since the VCAP instrumentation remains in the payload bay at all times and the two measurements are compared. The wake behind a large structure (in this case the Space Shuttle Orbiter) flying through the ionospheric plasma is discussed. Much theoretical work was done regarding plasma wakes. The instrumentation on this mission gives the first data taken with a large vehicle in the ionospheric laboratory. First, the PDP Langmuir Probe and its data set will be presented, then the VCAP Langmuir Probe and SRPA with associated data. The agreement between the two data sets is discussed and then followed by some other PDP data which infers an even lower wake density. B.G.

N85-22478*# National Aeronautics and Space Administration. Lewis Research Center, Cleveland, Ohio.
ELECTRON BEAM CHARGING OF SPACE SHUTTLE THERMAL PROTECTION SYSTEM TILES
J. V. STASKUS *In its* Spacecraft Environ. Interactions Technol., 1983 p 91-102 Mar. 1985 refs
Avail: NTIS HC A99/MF E03 CSCL 22B

Six space shuttle reusable surface insulation tiles were tested in the NASA Lewis Research Center's electron bombardment test facility. The 30-cm-square specimens were assembled by using

the same materials and techniques used to apply the tiles to the space shuttle and were composed to 15-cm- and 20-cm-square tiles and pieces on 0.6-cm-thick aluminum substrates. There were two specimens of each of three thicknesses. One specimen of each thickness had gaps of less than 0.1 cm between tiles, and the other had gaps of approximately 0.15 cm. The specimens were exposed to monoenergetic electron beams (2 to 25 keV) with nominal fluxes of 0.1 and 1 nA/sq. cm. Tests were conducted with both grounded and floating substrates. The data presented include charging rates, equilibrium potentials, and substrate currents. There is evidence that discharging occurred. Author

N85-22486*# National Aeronautics and Space Administration. Lewis Research Center, Cleveland, Ohio.
THREE-DIMENSIONAL CALCULATION OF SHUTTLE CHARGING IN POLAR ORBIT
D. L. COOKE, I. KATZ, M. J. MANDELL, J. R. LILLEY, JR., and A. J. RUBIN (AFGL) *In* NASA. Lewis Research Center Spacecraft Environ. Interactions Technol., 1983 p 205-227 Mar. 1985 refs
(Contract F19628-82-C-0081)
Avail: NTIS HC A99/MF E03 CSCL 22B

The charged particles environment in polar orbit can be of sufficient intensity to cause spacecraft charging. In order to gain a quantitative understanding of such effects, the Air Force is developing POLAR, a computer code which simulates in three dimensions the electrical interaction of large space vehicles with the polar ionospheric plasma. It models the physical processes of wake generation, ambient ion collection, precipitating auroral electron fluxes, and surface interactions, including secondary electron generation and backscattering, which lead to vehicle charging. These processes may be followed dynamically on a subsecond timescale so that the rapid passage through intense auroral arcs can be simulated. POLAR models the ambient plasma as isotropic Maxwellian electrons and ions (0+, H+), and allows for simultaneous precipitation of power-law, energetic Maxwellian, and accelerated Gaussian distributions of electrons. Magnetic field effects will be modeled in POLAR but are currently ignored. G.L.C.

N85-22487*# National Aeronautics and Space Administration. Lewis Research Center, Cleveland, Ohio.
POLAR ORBIT ELECTROSTATIC CHARGING OF OBJECTS IN SHUTTLE WAKE
I. KATZ, D. E. PARKS, D. L. COOKE, M. J. MANDELL (AFGL), and A. J. RUBIN *In* NASA. Lewis Research Center Spacecraft Environ. Interactions Technol., 1983 p 229-234 Mar. 1985 refs
(Contract F19628-82-C-0081)
Avail: NTIS HC A99/MF E03 CSCL 22B

A survey of DMSP data has uncovered several cases where precipitating auroral electron fluxes are both sufficiently intense and energetic to charge spacecraft materials such as teflon to very large potentials in the absence of ambient ion currents. Analytical bounds are provided which show that these measured environments can cause surface potentials in excess of several hundred volts to develop on objects in the orbiter wake for particular vehicle orientations. G.L.C.

N85-22493*# Systems Science and Software, La Jolla, Calif.
SURFACE INTERACTIONS AND HIGH-VOLTAGE CURRENT COLLECTION
M. J. MANDELL and I. KATZ *In* NASA. Lewis Research Center Spacecraft Environ. Interactions Technol., 1983 p 305-320 Mar. 1985 refs
(Contract NAS3-23058)
Avail: NTIS HC A99/MF E03 CSCL 22B

Spacecraft of the future will be larger and have higher power requirements than any flown to date. For several reasons, it is desirable to operate a high power system at high voltage. While the optimal voltages for many future missions are in the range 500 to 5000 volts, the highest voltage yet flown is approximately 100 volts. The NASCAP/LEO code is being developed to embody the phenomenology needed to model the environmental interactions of high voltage spacecraft. Some plasma environment are discussed. The treatment of the surface conductivity associated with emitted electrons and some simulations by NASCAP/LEO of ground based high voltage interaction experiments are described. Author

N85-22500*# National Aeronautics and Space Administration. Lewis Research Center, Cleveland, Ohio.
DESIGN GUIDELINES FOR ASSESSING AND CONTROLLING SPACECRAFT CHARGING EFFECTS Abstract Only
C. K. PURVIS, H. B. GARRETT (JPL, California Inst. of Tech., Pasadena), A. WHITTLESEY (JPL, California Inst. of Tech., Pasadena), and N. J. STEVENS (Hughes Aircraft Co., El Segundo, Calif.) *In its* Spacecraft Environ. Interactions Technol. p 389 Mar. 1985 Previously announced as N84-33452
Avail: NTIS HC A99/MF E03 CSCL 22B

The need for uniform criteria, or guidelines, to be used in all phases of spacecraft design is discussed. Guidelines were developed for the control of absolute and differential charging of spacecraft surfaces by the lower energy space charged particle environment. Interior charging due to higher energy particles is not considered. A guide to good design practices for assessing and controlling charging effects is presented. Uniform design practices for all space vehicles are outlined. E.A.K.

N85-22512*# Case Western Reserve Univ., Cleveland, Ohio.
ELECTRON YIELDS FROM SPACECRAFT MATERIALS
K. YANG, W. L. GORDON, and R. W. HOFFMAN *In* NASA. Lewis Research Center Spacecraft Environ. Interactions Technol., 1983 p 537-545 Mar. 1985 refs
(Contract NSG-3197)
Avail: NTIS HC A99/MF E03 CSCL 22B

Photoyields and secondary electron emission (SEE) characteristics were determined under UHV conditions for a group of insulating materials used in spacecraft applications. The SEE studies were carried out with a pulsed primary beam while photoyields were obtained with a chopped photon beam from a Kr resonance source with major emission at 123.6 nm. This provides a photon flux close to that of the Lyman alpha in the space environment. Yields per incident photon are obtained relative to those from a freshly evaporated and air oxidized Al surface. Results are presented for Kapton, FEP Teflon, the borosilicate glass covering of a shuttle tile, and spacesuit outer fabric. E.A.K.

N85-22517*# National Aeronautics and Space Administration. Lewis Research Center, Cleveland, Ohio.
SPACECRAFT ENVIRONMENTAL INTERACTIONS: A JOINT AIR FORCE AND NASA RESEARCH AND TECHNOLOGY PROGRAM
C. P. PIKE (AFGL), C. K. PURVIS, and W. R. HUDSON (NASA, Washington) *In its* Spacecraft Environ. Interactions Technol., 1983 p 599-608 Mar. 1985
Avail: NTIS HC A99/MF E03 CSCL 22B

A joint Air Force/NASA comprehensive research and technology program on spacecraft environmental interactions to develop technology to control interactions between large spacecraft systems and the charged-particle environment of space is described. This technology will support NASA/Department of Defense operations of the shuttle/IUS, shuttle/Centaur, and the force application and surveillance and detection missions, planning for transatmospheric vehicles and the NASA space station, and the AFSC military space system technology model. The program consists of combined contractual and in-house efforts aimed at understanding spacecraft environmental interaction phenomena and relating results of ground-based tests to space conditions. A concerted effort is being made to identify project-related environmental interactions of concern. The basic properties of materials are being investigated to develop or modify the materials as needed. A group simulation investigation is evaluating basic plasma interaction phenomena to provide inputs to the analytical

modeling investigation. Systems performance is being evaluated by both groundbased tests and analysis. B.W.

N85-23904*# National Aeronautics and Space Administration. Lewis Research Center, Cleveland, Ohio.
LINEARIZATION OF DIGITAL DERIVED RATE ALGORITHM FOR USE IN LINEAR STABILITY ANALYSIS
R. E. GRAHAM and T. W. PORADA 21 Jun. 1985 13 p refs
Proposed for presentation at 4th Am. Control Conf., Boston, 19-21 Jun. 1985
(NASA-TM-87000; E-2522; NAS 1.15:87000) Avail: NTIS HC A02/MF A01 CSCL 22B

The digital derived rate (DDR) algorithm is used to calculate the rate of rotation of the Centaur upper-stage rocket. The DDR is highly nonlinear algorithm, and classical linear stability analysis of the spacecraft cannot be performed without linearization. The performance of this rate algorithm is characterized by a gain and phase curve that drop off at the same frequency. This characteristic is desirable for many applications. A linearization technique for the DDR algorithm is investigated. The linearization method is described. Examples of the results of the linearization technique are illustrated, and the effects of linearization are described. A linear digital filter may be used as a substitute for performing classical linear stability analyses, while the DDR itself may be used in time response analysis. Author

N85-29997*# Case Western Reserve Univ., Cleveland, Ohio. Dept. of Physics.
STUDY OF KAPTON UNDER SIMULATED SHUTTLE ENVIRONMENT Annual Report, 1 May 1984 - 30 Apr. 1985
T. G. ECK and R. W. HOFFMAN Jul. 1985 10 p
(Contract NAG3-426)
(NASA-CR-176003; NAS 1.26:176003) Avail: NTIS HC A02/MF A01 CSCL 22B

Weight loss and severe degradation of the surface of Kapton that occurs in low Earth orbit is studied. Atomic oxygen, the major ambient species at low Earth altitude and incident with approximately 5 eV energy in ram conditions, is the primary suspect, but a thorough study of oxygen-Kapton interactions has not yet been carried out. A low-energy ion source is used to simulate the shuttle low Earth orbit environment. This source, together with diagnostic tools including surface analysis and mass spectroscopic capability, is being used to carry out experiments from which quantum yields may be obtained. R.J.F.

19

SPACECRAFT INSTRUMENTATION

N85-27968*# National Aeronautics and Space Administration. Lewis Research Center, Cleveland, Ohio.
***THIN-FILM SENSORS FOR SPACE PROPULSION TECHNOLOGY* Abstract Only**
W. S. KIM and D. R. ENGLUND *In its* Struct. Integrity and Durability of Reusable Space Propulsion Systems p 183-188 May 1985 refs
Avail: NTIS HC A09/MF A01 CSCL 22B

SSME components such as the turbine blades of the high pressure fuel turbopump are subjected to rapid and extreme thermal transients that contribute to blade cracking and subsequent failure. The objective was to develop thin film sensors for SSME components. The technology established for aircraft gas turbine engines was adopted to the materials and environment encountered in the SSME. Specific goals are to expand the existing thin film sensor technology, to continue developing improved sensor processing techniques, and to test the durability of aircraft gas turbine engine technology in the SSME environment. A thin film sensor laboratory is being installed in a refurbished clean room, and new sputtering and photoresist exposure equipment is being acquired. Existing thin film thermocouple technology in an SSME environment are being tested. Various coatings and their insulating films are being investigated for use in sensor development. E.R.

N85-27970*# National Aeronautics and Space Administration. Lewis Research Center, Cleveland, Ohio.
HEAT FLUX SENSOR CALIBRATOR Abstract Only
C. H. LIEBERT *In its* Struct. Integrity and Durability of Reusable Space Propulsion Systems p 195-198 May 1985 refs
Avail: NTIS HC A09/MF A01 CSCL 22B

The heat flux to space shuttle main engine (SSME) turbopump turbine blades may be as high as 10 to the 7th power. The heat flux causes thermal transients that are of the order of 1 sec as temperature varies from perhaps 1500 K to 100 K. It is suspected that these transients cause durability problems in the turbine blades. To quantitatively evaluate the effect of these transients, heat flux sensors or gauges were developed to obtain data to verify analytical models. The objective is to design and fabricate a system for steady state and transient calibration and durability testing of heat flux sensors for use in SSME turbine blades. The calibrator consists of: (1) the arc lamp, (2) a high speed positioning table for placing standard and special heat flux sensors in the incident beam of radiant heat flux, (3) provision for cooling the blade and special sensors inserted in the blade, (4) a computer for controlling the positioning table, storing electrical output values from sensors, and calculating heat flux from these values, and (5) a pyrometer for measuring sensor surface temperatures. E.R.

N85-27971*# Rockwell International Corp., Canoga Park, Calif.
FEASIBILITY OF MAPPING VELOCITY FLOW FIELDS IN SSME POWERHEAD BY LASER ANEMOMETRY TECHNIQUES Abstract Only
D. G. PELACCIO, L. K. SHARMA, T. V. FERGUSON, J. M. MARAM, and S. PINKOWSKI *In* NASA. Lewis Research Center Struct. Integrity and Durability of Reusable Space Propulsion Systems p 199 May 1985
(Contract NAS3-24356)
Avail: NTIS HC A09/MF A01 CSCL 22B

Because of the flow environment associated with the SSME powerhead pressure (3000 psia), temperature (1800 R), and mechanical complexity and the high vibration test stand environment, detailed flow measurements are difficult to make. The feasibility of using laser anemometry techniques to map velocity flow fields in an SSME powerhead is studied. In the study three engine powerhead component flow environments: (1) the high pressure fuel turbopump preburner, (2) the fuel turbopump turbine rotor and stator region, and (3) the 180 deg turnaround duct - are being considered. Flow parameters measured by the anemometry techniques are time averaged values of the velocity magnitude and flow direction, turbulence intensity, velocity component correlation, integral time scale, and turbulence spectrum. E.R.

20

SPACECRAFT PROPULSION AND POWER

Includes main propulsion systems and components, e.g., rocket engines; and spacecraft auxiliary power sources.

A85-15512*# Colorado State Univ., Fort Collins.
THEORY OF ION ACCELERATION WITH CLOSED ELECTRON DRIFT
H. R. KAUFMAN (Colorado State University, Fort Collins, CO) *Journal of Spacecraft and Rockets* (ISSN 0022-4650), vol. 21, Nov.-Dec. 1984, p. 558-562. Previously cited in issue 2, p. 241, Accession no. A83-12490. refs
(Contract NSG-3011)

A85-16406*# Hughes Research Labs., Malibu, Calif.
IAPS (8-CM) ION THRUSTER CYCLIC ENDURANCE TEST
C. R. DULGEROFF, J. R. BEATTIE, R. L. POESCHEL, and J. HYMAN, JR. (Hughes Research Laboratories, Malibu, CA) IN: International Electric Propulsion Conference, 17th, Tokyo, Japan, May 28-31, 1984, *Proceedings . Tokyo, Japan Society for* Aeronautical and Space Sciences, 1984, p. 250-260. refs
(Contract NAS3-21741)

Attention is given to the cyclic endurance qualification test, performed in a vacuum facility with a liquid nitrogen-cooled cryosurface and a frozen mercury target, to which a mercury-ion thruster representative of Ion Auxiliary Propulsion System (IAPS) thrusters was subjected. At the time that the endurance test was successfully concluded, upon consumption of the IAPS propellant tank's mercury, 8,471 hours of 'beam-on time' and 599 cycles had been accumulated. The system's Power Electronics Unit accumulated 10,268 hours of test time with high voltage applied to the operating thruster or dummy load. O.C.

A85-16408*# National Aeronautics and Space Administration. Lewis Research Center, Cleveland, Ohio.
GROUND CORRELATION INVESTIGATION OF THRUSTER/SPACECRAFT INTERACTIONS TO BE MEASURED ON THE IAPS FLIGHT TEST
J. L. POWER (NASA, Lewis Research Center, Cleveland, OH) IN: International Electric Propulsion Conference, 17th, Tokyo, Japan, May 28-31, 1984, Proceedings . Tokyo, Japan Society for Aeronautical and Space Sciences, 1984, p. 266-285. Previously announced in STAR as N84-23691. refs

Preliminary ground correlation testing has been conducted with an 8 cm mercury ion thruster and diagnostic instrumentation replicating to a large extent the IAPS flight test hardware, configuration, and electrical grounding/isolation. Thruster efflux deposition retained at 25 C was measured and characterized. Thruster ion efflux was characterized with retarding potential analyzers. Thruster-generated plasma currents, the spacecraft common (SCC) potential, and ambient plasma properties were evaluated with a spacecraft potential probe (SPP). All the measured thruster/spacecraft interactions or their IAPS measurements depend critically on the SCC potential, which can be controlled by a neutralizer ground switch and by the SPP operation. Author

A85-16412*# Hughes Research Labs., Malibu, Calif.
ION PROPULSION FOR COMMUNICATIONS SATELLITES
R. L. POESCHEL (Hughes Research Laboratories, Malibu, CA) IN: International Electric Propulsion Conference, 17th, Tokyo, Japan, May 28-31, 1984, Proceedings . Tokyo, Japan Society for Aeronautical and Space Sciences, 1984, p. 306-313. refs
(Contract NAS3-23258)

In a recent study of potential applications for electric propulsion, it was determined that ion propulsion can provide North-South stationkeeping (NSSK) for communication satellites in geosynchronous orbit with appreciably less mass than chemical propulsion. While this finding is not new, the margin of benefit over advanced chemical propulsion technology depends strongly on the ion propulsion system specifications. Full advantage must be taken of the under-utilized stored energy available from the communication satellite's batteries. This paper describes a methodology for evaluating the benefits obtained in using ion propulsion for NSSK, both in terms of the mass reduction and its economic value. Author

A85-16438*# Hughes Research Labs., Malibu, Calif.
RING-CUSP ION THRUSTERS
J. R. BEATTIE and R. L. POESCHEL (Hughes Research Laboratories, Malibu, CA) IN: International Electric Propulsion Conference, 17th, Tokyo, Japan, May 28-31, 1984, Proceedings . Tokyo, Japan Society for Aeronautical and Space Sciences, 1984, p. 496-505. refs
(Contract NAS3-21943)

The high performance ion thruster technology presented is suitable for either geostationary satellite north-south stationkeeping or interplanetary spacecraft primary propulsion. The thruster employs a ring-cusp magnetic field arrangement for plasma confinement, incurring an ion production cost which at about 100 eV/ion, is approximately half the value for the state-of-the-art J-series mercury ion thruster. A comparison of the average plasma properties existing within the ion-production volumes indicates that the improved performance of the ring-cusp configuration is due to higher electron temperature, confirming the superiority of this design in confining the energetic electrons emitted by the cathode. O.C.

A85-16439*# National Aeronautics and Space Administration. Lewis Research Center, Cleveland, Ohio.
PERFORMANCE CAPABILITIES OF THE 12-CENTIMETER XENON ION THRUSTER
M. MANTENIEKS and M. SCHATZ (NASA, Lewis Research Center, Cleveland, OH) IN: International Electric Propulsion Conference, 17th, Tokyo, Japan, May 28-31, 1984, Proceedings . Tokyo, Japan Society for Aeronautical and Space Sciences, 1984, p. 506-523. Previously announced in STAR as N84-27825. refs

The 8- and 12-cm mercury ion thruster systems were developed primarily to provide N-S station keeping of satellites with masses up to about 1800 to 3600 kg respectively. The on-orbit propulsion requirements of recently proposed Large Space Systems (LSS) are beyond the thrust capabilities of the baseline 8- and 12-cm thruster systems. This paper presents a characterization of the performance capabilities of the 12-cm Xenon ion thruster to enable an evaluation of its application to LSS auxiliary propulsion requirements. With minor thruster modifications and simplifications the thrust was increased to 64 mN, a factor of six over the baseline 12-cm mercury thruster performance. The thruster was operated over a range of specific impulse of about 2000 to 4000 seconds and at total efficiencies up to 68.0 percent. The operating levels reached in this study were found to be close to the operating limits of the thruster design in terms of perveance, grid breakdown voltage and thruster component temperatures such as those of the magnets and cathode baffle. Author

A85-16440*# TRW, Inc., Redondo Beach, Calif.
ELECTROTHERMAL THRUSTER DIAGNOSTICS
S. ZAFRAN (TRW, Inc., TRW Space and Technology Group, Redondo Beach, CA) IN: International Electric Propulsion Conference, 17th, Tokyo, Japan, May 28-31, 1984, Proceedings . Tokyo, Japan Society for Aeronautical and Space Sciences, 1984, p. 524-528. refs
(Contract NAS3-23265)

A flight-qualified electrothermal thruster demonstrated its adaptability to a variety of propellants. Originally qualified for operation with hydrazine propellant, it was operated with nitrogen, hydrogen, and ammonia propellants, demonstrating 73, 61, and 52 percent overall efficiency with these propellants, respectively, when tested over a wide range of operating conditions. By introducing a preheater to admit hot, rather than cold, propellant inlet gases to the thruster's augmentation heat exchanger, delivered specific impulse closer to theoretical performance limits should be achieved. Author

A85-16441*# Michigan State Univ., East Lansing.
EXPERIMENTS WITH A MICROWAVE ELECTROTHERMAL THRUSTER CONCEPT
J. ASMUSSEN, S. WHITEHAIR (Michigan State University, East Lansing, MI), and S. NAKANISHI (NASA, Lewis Research Center, Cleveland, OH) IN: International Electric Propulsion Conference, 17th, Tokyo, Japan, May 28-31, 1984, Proceedings . Tokyo, Japan Society for Aeronautical and Space Sciences, 1984, p. 529-540. refs
(Contract NAG3-305)

The design and test of two microwave electrothermal thrusters is described. The coaxial and cylindrical cavity concepts are tested in nitrogen gas with 200-2,000 W of 2.45 GHz input power. Experimental measurements and calculations of thrust, specific impulse and energy efficiency are presented for different gas flow rates and discharge pressures. Measured energy efficiencies varied between 10-60 percent and the performance compared favorably

with other electrothermal thrusters operating in nitrogen gas. The experimental performance demonstrated the feasibility of the concept. Author

A85-16445*# National Aeronautics and Space Administration. Lewis Research Center, Cleveland, Ohio.
CATHODE DEGRADATION AND EROSION IN HIGH PRESSURE ARC DISCHARGES
T. L. HARDY and S. NAKANISHI (NASA, Lewis Research Center, Cleveland, OH) IN: International Electric Propulsion Conference, 17th, Tokyo, Japan, May 28-31, 1984, Proceedings . Tokyo, Japan Society for Aeronautical and Space Sciences, 1984, p. 560-573. Previously announced in STAR as N84-22631. refs

The various processes which control cathode erosion and degradation were identified and evaluated. A direct current arc discharge was established between electrodes in a pressure-controlled gas flow environment. The cathode holder was designed for easy testing of various cathode materials. The anode was a water cooled copper collector electrode. The arc was powered by a dc power supply with current and voltage regulated cross-over control. Nitrogen and argon were used as propellants and the materials used were two percent thoriated tungsten, barium oxide impregnated porous tungsten, pure tungsten and lanthanum hexaboride. The configurations used were cylindrical solid rods, wire bundles supported by hollow molybdenum tubes, cylindrical hollow tubes, and hollow cathodes of the type used in ion thrusters. The results of the mass loss tests in nitrogen indicated that pure tungsten eroded at a rate more than 10 times faster than the rates of the impregnated tungsten materials. It was found that oxygen impurities of less than 0.5 percent in the nitrogen increased the mass loss rate by a factor of 4 over high purity nitrogen. At power levels less than 1 kW, cathode size and current level did not significantly affect the mass loss rate. The hollow cathode was found to be operable in argon and in nitrogen only at pressures below 400 and 200 torr, respectively. M.A.C.

A85-18584* Hughes Aircraft Co., El Segundo, Calif.
ENVIRONMENTALLY-INDUCED VOLTAGE LIMITATIONS IN LARGE SPACE POWER SYSTEMS
N. J. STEVENS (Hughes Aircraft Co., El Segundo, CA) (IEEE, U.S. Defense Nuclear Agency, U.S. Department of Energy, and NASA, Annual Conference on Nuclear and Space Radiation Effects, 21st, Colorado Springs, CO, July 23-25, 1984) IEEE Transactions on Nuclear Science (ISSN 0018-9499), vol. NS-31, Dec. 1984, p. 1381-1386. refs
(Contract NAS3-23869)

Large power systems proposed for future space missions imply higher operating voltage requirements which, in turn, will interact with the space plasma environment. The effects of these interactions can only be inferred because of the limited data base of ground simulations, small test samples, and two space flight experiments. This report evaluates floating potentials for a 100 kW power system operating at 300, 500, 750, and 1000 volts in relation to this data base. Of primary concern is the possibility of discharging to space. The implications of such discharges were studied at the 500 volt operational setting. It was found that discharging can shut down the power system if the discharge current exceeds the array short circuit current. Otherwise, a power oscillation can result that ranges from 2 to 20 percent, depending upon the solar array area involved in the discharge. Means of reducing the effect are discussed. Author

A85-19713*# National Aeronautics and Space Administration. Lewis Research Center, Cleveland, Ohio.
THE EFFECT OF PLASMA ON SOLAR CELL ARRAY ARC CHARACTERISTICS
D. B. SNYDER (NASA, Lewis Research Center, Cleveland, OH) and E. TYREE (NASA, Lewis Research Center; Case Western Reserve University, Cleveland, OH) American Institute of Aeronautics and Astronautics, Aerospace Sciences Meeting, 23rd, Reno, NV, Jan. 14-17, 1985. 10 p. Previously announced in STAR as N85-11133. refs
(AIAA PAPER 85-0384)

The influence from the ambient plasma on the arc characteristics of a negatively biased solar cell array was investigated. The arc characteristics examined were the peak current during an arc, the decay time as the arc terminates, and the charge lost during the arc. These arc characteristics were examined in a nitrogen plasma with charge densities ranging from 15,000 to 45,000 cu cm. Background gas pressures ranged from 8x1,000,000 to 6x100,000 torr. Over these ranges of parameters no significant effect on the arc characteristics were seen. Arc characteristics were also examined for three gas species: helium, nitrogen and argon. The helium arcs have higher peak currents and shorter decay times than nitrogen and argon arcs. There are slight differences in the arc characteristics between nitrogen and argon. These differences may be caused by the differences in mass of the respective species. Also, evidence is presented for an electron emission mechanism appearing as a precursor to solar array arcs. Occasionally the plasma generator could be turned off, and currents could still be detected in the vacuum system. When these currents are presented, arcs may occur. Author

A85-19715*# System Science and Software, San Diego, Calif.
COMPUTER SIMULATION OF PLASMA ELECTRON COLLECTION BY PIX-II
M. J. MANDELL, I. KATZ, G. A. JONGEWARD (System Science and Software, La Jolla, CA), and J. C. ROCHE (NASA, Lewis Research Center, Cleveland, OH) American Institute of Aeronautics and Astronautics, Aerospace Sciences Meeting, 23rd, Reno, NV, Jan. 14-17, 1985. 9 p. refs
(Contract NAS3-23881)
(AIAA PAPER 85-0386)

A wake model was defined for the NASCAP/LEO finite element model for the plasma interaction experiment (PIX-II) launched to study the interaction between high-voltage large solar arrays with the space plasma environment. The cell surface model considers the individual cells, distances between interconnects, and the fraction of surface covered by interconnects. Account is taken of the electrostatic potential around the spacecraft, which travels at 7500 mps, over five times the speed of thermal ions. Ram ions are produced ahead of the array and the wake ion density is described with a geometric shadowing model. The model correctly predicted the currents in high and low bias voltages when compared to orbital data. The panel snapover, however, was projected to occur at 100 V and instead occurred at 300 V, which indicates that the snapover state is bistable. Finally, a low potential was both predicted and measured in the wake. M.S.K.

A85-29310*# Loral Electro-Optical Systems, Inc., Pasadena, Calif.
INERT GAS TEST OF TWO 12-CM MAGNETOSTATIC THRUSTERS
W. D. RAMSEY (Loral Corp., Pasadena, CA) Journal of Spacecraft and Rockets (ISSN 0022-4650), vol. 22, Mar.-Apr. 1985, p. 162-165. Previously cited in issue 02, p. 145, Accession no. A83-12494. refs
(Contract NAS3-22876)

A85-29314*# O'Donnell and Associates, Inc., Pittsburgh, Pa.
SIMPLIFIED DESIGN AND LIFE PREDICTION OF ROCKET THRUST CHAMBERS
J. S. POROWSKI, W. J. ODONNELL, M. L. BADLANI, B. KASRAIE, and H. J. KASPER Journal of Spacecraft and Rockets (ISSN 0022-4650), vol. 22, Mar.-Apr. 1985, p. 181-187. Previously cited in issue 17, p. 2708, Accession no. A82-35087. refs

A85-33144* Wisconsin Univ., Madison.
A ROTATING SUPERCONDUCTING SOLENOID FOR 100 KWH ENERGY STORAGE
J. WAYNERT, Y. M. EYSSA, G. E. MCINTOSH, and Z. FENG (Wisconsin, University, Madison, WI) IEEE Transactions on Magnetics (ISSN 0018-9464), vol. MAG-21, March 1985, p. 664-667. refs
(Contract NAG3-359)

Two concentric superconducting solenoids, one rotating, the other stationary are analyzed for energy storage in space. Energy is transferred from the rotating mass through a shaft coupled to a motor-generator. The inner windings interact with the magnetic field of the outer solenoid to cancel the centrifugal and self-field forces of the flywheel rim. Current is induced in the inner solenoid thus requiring no separate power supply, while the current in the outer solenoid must vary with the angular velocity of the flywheel. The effect of the gap and scaling laws are developed. The efficiency in energy per unit mass is marginally attractive. Author

A85-39267* Rockwell International Corp., Canoga Park, Calif.
REUSABLE ROCKET ENGINE TURBOPUMP CONDITION MONITORING
M. E. HAMPSON (Rockwell International Corp., Rocketdyne Div., Canoga Park, CA) IN: Space systems technology; Proceedings of the Aerospace Congress and Exposition, Long Beach, CA, October 15-18, 1984 . Warrendale, PA, Society of Automotive Engineers, Inc. (SAE SP-593), 1984, p. 157-165.
(Contract NAS3-23349)
(SAE PAPER 841619)

Significant improvements in engine readiness with reductions in maintenance costs and turn-around times can be achieved with an engine condition monitoring systems (CMS). The CMS provides health status of critical engine components, without disassembly, through monitoring with advanced sensors. Engine failure reports over 35 years were categorized into 20 different modes of failure. Rotor bearings and turbine blades were determined to be the most critical in limiting turbopump life. Measurement technologies were matched to each of the failure modes identified. Three were selected to monitor the rotor bearings and turbine blades: the isotope wear detector and fiberoptic deflectometer (bearings), and the fiberoptic pyrometer (blades). Signal processing algorithms were evaluated for their ability to provide useful health data to maintenance personnel. Design modifications to the Space Shuttle Main Engine (SSME) high pressure turbopumps were developed to incorporate the sensors. Laboratory test fixtures have been designed for monitoring the rotor bearings and turbine blades in simulated turbopump operating conditions. Author

A85-39626*# National Aeronautics and Space Administration. Lewis Research Center, Cleveland, Ohio.
SPACE STATION PROPULSION - THE ADVANCED DEVELOPMENT PROGRAM AT LEWIS
R. E. JONES (NASA, Lewis Research Center, Cleveland, OH) AIAA, SAE, ASME, and ASEE, Joint Propulsion Conference, 21st, Monterey, CA, July 8-10, 1985. 9 p. Previously announced in STAR as N85-25386.
(AIAA PAPER 85-1154)

A reference configuration was established for the initial operating capability (IOC) station. The reference configuration has assumed hydrazine fueled thrusters as the propulsion system. This was to establish costing and as a reference for comparison when other propulsion systems are considered. An integral part of the plan to develop the Space Station is the advanced development program. The objective of this program is to provide advanced technology alternatives for the initial and evolutionary Space Station which optimize the system's functional characteristics in terms of performance, cost, and utilization. The portion of the Advanced Development Program that is concerned with auxiliary propulsion and the research and programmatic activities conducted are discussed. E.A.K.

A85-39628*# Rocket Research Corp., Redmond, Wash.
PERFORMANCE CHARACTERIZATION TESTS OF A 1-KW RESISTOJET USING HYDROGEN, NITROGEN AND AMMONIA AS PROPELLANTS
C. I. MIYAKE and F. X. MCKEVITT (Rocket Research Co., Redmond, WA) AIAA, SAE, ASME, and ASEE, Joint Propulsion Conference, 21st, Monterey, CA, July 8-10, 1985. 8 p. refs
(Contract NAS3-23868)
(AIAA PAPER 85-1159)

A performance mapping test of a 1 kW radiatively heated resistojet demonstrated high specific impulse and efficiency with hydrogen, nitrogen and ammonia as propellants. The resistojet was based on an unmodified augmentation section of the flight-qualified Rocket Research Company Augmented Catalytic Thruster. Peak specific impulse values of 686.9 sec for hydrogen, 191.6 sec for nitrogen, and 342 sec for ammonia were demonstrated. A maximum specific impulse efficiency of 94.3 percent was demonstrated with hydrogen. Testing covered a thrust range of 27 to 112 mlbf with augmentation powers ranging from 300 to 1000 watts. A total of 83 runs accumulating 25 hours of operation were conducted with the three propellants. Comparison of specific impulse efficiency to other published resistojet performance data showed the radiatively heated resistojet compares favorably to other design concepts. Author

A85-39733*# Rockwell International Corp., Canoga Park, Calif.
CRYOGENIC UPPER STAGE TEST BED ENGINE
R. PAUCKERT, A. ZACHARY, E. DEGAETANO, and R. SUTTON (Rockwell International Corp., Rocketdyne Div., Canoga Park, CA) AIAA, SAE, ASME, and ASEE, Joint Propulsion Conference, 21st, Monterey, CA, July 8-10, 1985. 11 p.
(Contract NAS3-23773)
(AIAA PAPER 85-1339)

A vehicle system with unique characteristics will be needed in connection with the extension of the Space Transportation System (STS) from Low Earth Orbit (LEO) to Geosynchronous Equatorial Orbit (GEO) and beyond. These characteristics are determined by NASA missions related to the deployment of large space structures, satellite servicing, and manned sorties to geosynchronous orbit. Advances in vehicle design and operation will be required along with significant advances in engine technologies. A versatile, well-instrumented test bed engine will be needed for the evaluation of the required technologies. Developments leading to the fabrication and assembly of the first high chamber pressure expander cycle test bed engine are discussed. The test bed engine, which is called Integrated Component Evaluator (ICE), is required for the development of an advanced, cryogenic, upperstage engine. G.R.

A85-39735*# Aerojet Techsystems Co., Sacramento, Calif.
PROGRESS REPORT - ADVANCED CRYOGENIC OTV ENGINE TECHNOLOGY
L. SCHOENMAN (Aerojet TechSystems Co., Sacramento, CA) AIAA, SAE, ASME, and ASEE, Joint Propulsion Conference, 21st, Monterey, CA, July 8-10, 1985. 11 p. refs
(Contract NAS3-23772)
(AIAA PAPER 85-1341)

New technologies for space-based, reusable, throttleable, cryogenic orbit transfer propulsion are being evaluated. A variable-thrust (200 to 3000 lbF), 2000 psi chamber pressure, LO2/LH2 engine has been selected to demonstrate the 20-hour, 500-restart life goal, and a specific impulse in excess of 480 lbF-sec/lbM. The results of recent vehicle-engine integration analyses and the progress in design, fabrication, and testing are provided. Emphasis is placed on the following technology areas being investigated in support of the advanced engine design: LOX hydrostatic bearings; burn-resistant materials for high-pressure GOX

turbines and valves; high surface-low flux annular combustion chambers for the dual propellant expander cycle; improved cooling approaches for high-pressure combustion chambers, new concepts in integrated controls; and engine health diagnostics. Author

A85-42922*# Xerox Electro-Optical Systems, Pasadena, Calif.
DEVELOPMENT OF A LARGE INSERT GAS ION THRUSTER
G. STEINER (Xerox Electro-Optical Systems, Pasadena, CA) Journal of Spacecraft and Rockets (ISSN 0022-4650), vol. 22, July-Aug. 1985, p. 465-468. Previously cited in issue 02, p. 146, Accession no. A83-12496. refs
(Contract NAS3-22444)

A85-43975*# Boeing Aerospace Co., Seattle, Wash.
SPACE STATION PROPULSION OPTIONS
C. L. WILKINSON, S. M. BRENNAN (Boeing Aerospace Co., Seattle, WA), and M. E. VALGORA (NASA, Lewis Research Center, Cleveland, OH) AIAA, SAE, ASME, and ASEE, Joint Propulsion Conference, 21st, Monterey, CA, July 8-10, 1985. 9 p. refs
(Contract NAS3-23353)
(AIAA PAPER 85-1155)

The selection of the propulsion system for the Space Station represents a complex issue. The present paper provides a summary of the Station design factors which dictate the propulsion requirements, taking into account approaches for meeting these requirements. Factors which affect propulsion system selection are related to thrusting strategy, volume and mass limitations, safety and contamination, electrical power, time phasing, synergistic opportunities, propellant scavenging, water electrolysis, and free-flyers. In a discussion of propulsion systems, attention is given to monopropellant options, bipropellant options, and resistojets. G.R.

A85-43976*# Jet Propulsion Lab., California Inst. of Tech., Pasadena.
AN EVALUATION OF OXYGEN/HYDROGEN PROPULSION SYSTEMS FOR THE SPACE STATION
R. W. KLEMETSON, P. W. GARRISON (California Institute of Technology, Jet Propulsion Laboratory, Pasadena), and N. P. HANNUM (NASA, Lewis Research Center, Cleveland, OH) AIAA, SAE, ASME, and ASEE, Joint Propulsion Conference, 21st, Monterey, CA, July 8-10, 1985. 27 p. NASA-supported research. Previously announced in STAR as N85-28971. refs
(AIAA PAPER 85-1156)

Conceptual designs for O2/H2 chemical and resistojet propulsion systems for the Space Station was developed and evaluated. The evolution of propulsion requirements was considered as the Space Station configuration and its utilization as a space transportation node change over the first decade of operation. The characteristics of candidate O2/H2 auxiliary propulsion systems are determined, and opportunities for integration with the OTV tank farm and the Space Station life support, power and thermal control subsystems are investigated. OTV tank farm boiloff can provide a major portion of the growth station impulse requirements and CO2 from the life support system can be a significant propellant resource, provided it is not denied by closure of that subsystem. Waste heat from the thermal control system is sufficient for many propellant conditioning requirements. It is concluded that the optimum level of subsystem integration must be based on higher level Space Station studies. Author

A85-43978*# Rockwell International Corp., Canoga Park, Calif.
SMALL CENTRIFUGAL PUMPS FOR LOW THRUST ROCKETS
N. C. GULBRANDSEN, R. B. FURST, R. M. BURGESS (Rockwell International Corp., Rocketdyne Div., Canoga Park, CA), and D. D. SCHEER (NASA, Lewis Research Center, Cleveland, OH) AIAA, SAE, ASME, and ASEE, Joint Propulsion Conference, 21st, Monterey, CA, July 8-10, 1985. 12 p.
(Contract NAS3-23164)
(AIAA PAPER 85-1302)

This paper presents the results of a combined analytical and experimental investigation of low specific speed pumps for potential use as components of propellant feed systems for low thrust rocket engines. Shrouded impellers and open face impellers were tested in volute type and vaned diffuser type pumps. Full- and partial-emission diffusers and full- and partial-admission impellers were tested. Axial and radial loads, head and efficiency versus flow, and cavitation tests were conducted. Predicted performance of two pumps are compared when pumping water and liquid hydrogen. Detailed pressure loss and parasitic power values are presented for two pump configurations. Partial-emission diffusers were found to permit use of larger impeller and diffuser passages with a minimal performance penalty. Normal manufacturing tolerances were found to result in substantial power requirement variation with only a small pressure rise change. Impeller wear ring leakage was found to reduce pump pressure rise to an increasing degree as the pump flowrate was decreased. Author

A85-45370* National Aeronautics and Space Administration. Lewis Research Center, Cleveland, Ohio.
HIGH VOLTAGE-HIGH POWER COMPONENTS FOR LARGE SPACE POWER DISTRIBUTION SYSTEMS
D. D. RENZ (NASA, Lewis Research Center, Cleveland, OH) IN: IECEC '84: Advanced energy systems - Their role in our future; Proceedings of the Nineteenth Intersociety Energy Conversion Engineering Conference, San Francisco, CA, August 19-24, 1984. Volume 1 . La Grange Park, IL, American Nuclear Society, 1984, p. 176-184. Previously announced in STAR as N84-22615. refs

Space power components including a family of bipolar power switching transistors, fast switching power diodes, heat pipe cooled high frequency transformers and inductors, high frequency conduction cooled transformers, high power-high frequency capacitors, remote power controllers and rotary power transfer devices were developed. Many of these components such as the power switching transistors, power diodes and the high frequency capacitor are commercially available. All the other components were developed to the prototype level. The dc/dc series resonant converters were built to the 25 kW level. S.L.

A85-45371* National Aeronautics and Space Administration. Lewis Research Center, Cleveland, Ohio.
PRELIMINARY DESIGN OF A 10 KW THERMOPHOTOVOLTAIC SYSTEM FOR SPACE APPLICATIONS
M. F. PISZCZOR, JR. (NASA, Lewis Research Center, Cleveland, OH) and M. GHALLA-GORADIA (Cleveland State University, OH) IN: IECEC '84: Advanced energy systems - Their role in our future; Proceedings of the Nineteenth Intersociety Energy Conversion Engineering Conference, San Francisco, CA, August 19-24, 1984. Volume 1 . La Grange Park, IL, American Nuclear Society, 1984, p. 185-190. Previously announced in STAR as N84-32427. refs

A very high degree of reflection of sub-bandgap energy photons from the cell back to the emitter was found to be crucial in achieving high efficiencies for a TPV system. Results show that small increases in reflectance above 0.85 lead to progressively larger increases in cell efficiency. In general, for a required power output, the radiator area, emitter temperature, emitter material and cell temperature may be chosen to satisfy various external constraints. The results can then be used to determine the optimum cell material and its operating temperature. Author

A85-45377* Chronos Research Labs., Inc., Olivehain, Calif.
PYROELECTRIC CONVERSION IN SPACE
R. B. OLSEN (Chronos Research Laboratories, Inc., Olivenhain, CA) IN: IECEC '84: Advanced energy systems - Their role in our future; Proceedings of the Nineteenth Intersociety Energy Conversion Engineering Conference, San Francisco, CA, August 19-24, 1984. Volume 1 . La Grange Park, IL, American Nuclear Society, 1984, p. 224-228. refs
(Contract NAS3-23052)

Pyroelectric conversion in space deserves a close look as preliminary calculations indicate that a system specific power of 350 to 850 watts per kilogram will be feasible. This power-to-weight ratio far exceeds state-of-the-art photovoltaic systems (40 to 66 watts/kg) and surpasses proposed thin blanket photovoltaics (about 300 watts/kg). In addition to its high specific power, the pyroelectric

approach promises to be far less expensive than photovoltaics. Author

A85-45387* National Aeronautics and Space Administration. Lewis Research Center, Cleveland, Ohio.
A 37.5-KW POINT DESIGN COMPARISON OF THE NICKEL-CADMIUM BATTERY, BIPOLAR NICKEL-HYDROGEN BATTERY, AND REGENERATIVE HYDROGEN-OXYGEN FUEL CELL ENERGY STORAGE SUBSYSTEMS FOR LOW EARTH ORBIT
M. A. MANZO and M. A. HOBERECHT (NASA, Lewis Research Center, Cleveland, OH) IN: IECEC '84: Advanced energy systems - Their role in our future; Proceedings of the Nineteenth Intersociety Energy Conversion Engineering Conference, San Francisco, CA, August 19-24, 1984. Volume 1 . La Grange Park, IL, American Nuclear Society, 1984, p. 287-294. Previously announced in STAR as N84-23022.

Nickel-cadmium batteries, bipolar nickel-hydrogen batteries, and regenerative fuel cell storage subsystems were evaluated for use as the storage subsystem in a 37.5 kW power system for Space Station. Design requirements were set in order to establish a common baseline for comparison purposes. The storage subsystems were compared on the basis of effective energy density, round trip electrical efficiency, total subsystem weight and volume, and life. Author

A85-45388* National Aeronautics and Space Administration. Lewis Research Center, Cleveland, Ohio.
DILUTE PLASMA COUPLING CURRENTS TO A HIGH VOLTAGE SOLAR ARRAY IN WEAK MAGNETIC FIELDS
N. T. GRIER (NASA, Lewis Research Center, Cleveland, OH) IN: IECEC '84: Advanced energy systems - Their role in our future; Proceedings of the Nineteenth Intersociety Energy Conversion Engineering Conference, San Francisco, CA, August 19-24, 1984. Volume 1 . La Grange Park, IL, American Nuclear Society, 1984, p. 295-302. Previously announced in STAR as N84-24708. refs

The plasma coupling current to an approximately 2000 sq cm array was measured for externally biased positive and negative voltages on the array to 1000 V in applied magnetic field strengths from 0 to 0.93 G. The plasma density varied from 2,000 to 1.3 million electrons/cu cm. It was found that the magnetic field primarily increased the plasma coupling current for negative biases. For positive bias, the current could increase or decrease depending on the voltage, field strength, and plasma density. It was also found that the plasma coupling current was not very sensitive to how the plane of the array was oriented relative to the magnetic field. Author

A85-45429* Boeing Aerospace Co., Seattle, Wash.
HIGH VOLTAGE REQUIREMENTS AND ISSUES FOR THE 1990'S
W. G. DUNBAR (Boeing Aerospace Co., Seattle, WA) and K. A. FAYMON (NASA, Lewis Research Center, Cleveland, OH) IN: IECEC '84: Advanced energy systems - Their role in our future; Proceedings of the Nineteenth Intersociety Energy Conversion Engineering Conference, San Francisco, CA, August 19-24, 1984. Volume 1 . La Grange Park, IL, American Nuclear Society, 1984, p. 570-575. refs

The development of high-power high-voltage space systems will require advances in power generation and processing. The systems must be reliable, adaptable, and durable for space mission success. The issues, which must be resolved in order to produce a high power system, are weight and volume reduction of components and modules and the creation of a reliable high repetition pulse power processor. Capacitor energy density must be increased by twice the present capacity and packaging must be reduced by a factor of 10 to 20 times. The packaging must also protect the system from interaction with the natural space environment and the induced environment, produced from spacecraft systems and environment interaction. I.F.

A85-47042*# National Aeronautics and Space Administration. Lewis Research Center, Cleveland, Ohio.
ELECTRIC POWER - PHOTOVOLTAIC OR SOLAR DYNAMIC?
R. L. THOMAS (NASA, Lewis Research Center, Cleveland, OH), G. J. HALLINAN (Rockwell International Corp., Rocketdyne Div., Canoga Park, CA), and J. L. HIEATT (TRW, Inc., TRW Space and Technology Group, Redondo Beach, CA) Aerospace America (ISSN 0740-722X), vol. 23, Sept. 1985, p. 60-62.

The design of the power system for supplying the Space Station with insolation-generated electricity is the main Phase B task at NASA-Lewis Center. The advantages and limitations of two types of power systems, the photovoltaic arrays (PV) and the solar dynamic system (SD), are discussed from the points of view of cost, overall systems integration, and growth. Subsystems of each of these options are described, and a sketch of a projected SD system is shown. The PV technology is well developed and proven, but its low efficiency calls for solar arrays of large areas, which affect station dynamics, control, and drag compensation. The SD systems would be less costly to operate than VP, and are more efficient, needing less deployed area. The major drawback of the SD is its infancy. The conservative and forgiving designs for some of its components must still be created and tested, and the development risks assessed. I.S.

N85-11131*# Hughes Research Labs., Malibu, Calif.
CHARACTERIZATION OF 8-CM ENGINEERING MODEL THRUSTER Final Report, 12 Apr. 1978 - 12 Sep. 1982
W. S. WILLIAMSON Mar. 1984 87 p
(Contract NAS3-21358; NAS3-21036)
(NASA-CR-174673; NAS 1.26:174673) Avail: NTIS HC A05/MF A01 CSCL 21C

Development of 8 cm ion thruster technology which was conducted in support of the Ion Auxiliary Propulsion System (IAPS) flight contract (Contract NAS3-21055) is discussed. The work included characterization of thruster performance, stability, and control; a study of the effects of cathode aging; environmental qualification testing; and cyclic lifetesting of especially critical thruster components. R.J.F.

N85-11132*# GT-Devices, Alexandria, Va.
INVESTIGATION OF A PULSED ELECTROTHERMAL THRUSTER SYSTEM
R. L. BURTON, S. A. GOLDSTEIN, B. K. HILKO, D. A. TIDMAN, and N. K. WINSOR 31 Oct. 1984 64 p refs
(Contract NAS3-23866)
(NASA-CR-174768; NAS 1.26:174768; GTD-84-4) Avail: NTIS HC A04/MF A01 CSCL 21C

The performance of an ablative wall Pulsed Electrothermal (PET) thruster is accurately characterized on a calibrated thrust stand, using polyethylene propellant. The thruster is tested for four configurations of capillary length and pulse length. The exhaust velocity is determined with twin time-of-flight photodiode stagnation probes, and the ablated mass is measured from the loss over ten shots. Based on the measured thrust impulse and the ablated mass, the specific impulse varies from 1000 to 1750 seconds. The thrust to power varies from .05 N/kW (quasi-steady mode) to .10 N/kW (unsteady mode). The thruster efficiency varies from .56 at 1000 seconds to .42 at 1750 seconds. A conceptual design is presented for a 40 kW PET propulsion system. The point design system performance is .62 system efficiency at 1000 seconds specific impulse. The system's reliability is enhanced by incorporating 20, 20 kW thruster modules which are fired in pairs. The thruster design is non-ablative, and uses water propellant, from a central storage tank, injected through the cathode. M.A.C.

N85-11133*# National Aeronautics and Space Administration. Lewis Research Center, Cleveland, Ohio.
THE EFFECT OF PLASMA ON SOLAR CELL ARRAY ARC CHARACTERISTICS
D. B. SNYDER and E. TYREE 1984 17 p refs Proposed for presentation at the 23rd Aerospace Sci. Meeting, Reno, Nev., 14-17 Jan. 1985; sponsored by the American Inst. of Aeronautics and Astronautics Previously announced in IAA as A85-19713
(NASA-TM-86887; E-2351; NAS 1.15:86887) Avail: NTIS HC A02/MF A01 CSCL 10A

The influence from the ambient plasma on the arc characteristics of a negatively biased solar cell array was investigated. The arc characteristics examined were the peak current during an arc, the decay time as the arc terminates, and the charge lost during the arc. These arc characteristics were examined in a nitrogen plasma with charge densities ranging from 15,000 to 45,000 cu cm. Background gas pressures ranged from 8x1,000,000 to 6x100,000 torr. Over these ranges of parameters no significant effect on the arc characteristics were seen. Arc characteristics were also examined for three gas species: helium, nitrogen and argon. The helium arcs have higher peak currents and shorter decay times than nitrogen and argon arcs. There are slight differences in the arc characteristics between nitrogen and argon. These differences may be caused by the differences in mass of the respective species. Also, evidence is presented for an electron emission mechanism appearing as a precursor to solar array arcs. Occassionally the plasma generator could be turned off, and currents could still be detected in the vacuum system. When these currents are presented, arcs may occur. Author

N85-12937*# Hughes Research Labs., Malibu, Calif.
ION THRUSTER SYSTEM (8-CM) CYCLIC ENDURANCE TEST Final Report, 20 Sep. 1978 - 31 Jan. 1984
C. R. DULGEROFF, J. R. BEATTIE, R. L. POESCHEL, and J. HYMAN, JR. Oct. 1984 138 p refs
(Contract NAS3-21741)
(NASA-CR-174745; NAS 1.26:174745) Avail: NTIS HC A07/MF A01 CSCL 21C

This report describes the qualification test of an Engineering-Model 5-mN-thrust 8-cm-diameter mercury ion thruster which is representative of the Ion Auxiliary Propulsion System (IAPS) thrusters. Two of these thrusters are scheduled for future flight test. The cyclic endurance test described herein was a ground-based test performed in a vacuum facility with a liquid-nitrogen-cooled cryo-surface and a frozen mercury target. The Power Electronics Unit, Beam Shield, Gimal, and Propellant Tank that were used with the thruster in the endurance test are also similar to those of the IAPS. The IAPS thruster that will undergo the longest beam-on-time during the actual space test will be subjected to 7,055 hours of beam-on-time and 2,557 cycles during the flight test. The endurance test was successfully concluded when the mercury in the IAPS Propellant Tank was consumed. At that time, 8,471 hours of beam-on-time and 599 cycles had been accumulated. Subsequent post-test-evaluation operations were performed (without breaking vacuum) which extended the test values to 652 cycles and 9,489 hours of beam-on-time. The Power Electronic Unit (PEU) and thruster were in the same vacuum chamber throughout the test. The PEU accumulated 10,268 hr of test time with high voltage applied to the operating thruster or dummy load. Author

N85-13877*# National Aeronautics and Space Administration. Lewis Research Center, Cleveland, Ohio.
DEVELOPMENTS IN SPACE POWER COMPONENTS FOR POWER MANAGEMENT AND DISTRIBUTION
D. D. RENZ *In* NASA. Langley Research Center An Assessment of Integrated Flywheel System Technol. p 369-387 Nov. 1984 refs
Avail: NTIS HC A18/MF A01 CSCL 10B

Advanced power electronic components development for space applications is discussed. The components described include transformers, inductors, semiconductor devices such as transistors and diodes, remote power controllers, and transmission lines. M.G.

N85-13880*# National Aeronautics and Space Administration. Lewis Research Center, Cleveland, Ohio.
SPACE POWER
Washington Apr. 1984 322 p refs Workshop held in Cleveland, 10-12 Apr. 1984
(NASA-CP-2352; E-2305; NAS 1.55:2352) Avail: NTIS HC A14/MF A01 CSCL 22B

Appropriate directions for the applied research and technology programs that will develop space power systems for U.S. future space missions beyond 1995 are explored. Spacecraft power supplies; space stations, space power reactors, solar arrays, thermoelectric generators, energy storage, and communication satellites are among the topics discussed.

N85-13910*# Cleveland State Univ., Ohio. Coll. of Engineering.
A HISTORICAL OVERVIEW OF THE ELECTRICAL POWER SYSTEMS IN THE US MANNED AND SOME US UNMANNED SPACECRAFT Final Report, Apr. 1984 - Jan. 1985
J. E. MAISEL Nov. 1984 158 p refs
(Contract NAG3-547)
(NASA-CR-174806; NAS 1.26:174806; MAI-R4) Avail: NTIS HC A08/MF A01 CSCL 22B

A historical overview of electrical power systems used in the U.S. manned spacecraft and some of the U.S. unmanned spacecraft is presented in this investigation. A time frame of approximately 25 years, the period for 1959 to 1984, is covered in this report. Results indicate that the nominal bus voltage was 28 volts dc in most spacecraft and all other voltage levels were derived from this voltage through such techniques as voltage inversion or rectification, or a combination. Most spacecraft used solar arrays for the main source of power except for those spacecraft that had a relatively short flight duration, or deep spaceprobes that were designed for very long flight duration. Fuel cells were used on Gemini, Apollo, and Space Shuttle (short duration flights) while radioisotope thermoelectric generators were employed on the Pioneer, Jupiter/Saturn, Viking Lander, and Voyager spacecraft (long duration flights). The main dc bus voltage was unregulated on the manned spacecraft with voltage regulation provided at the user loads. A combination of regulated, semiregulated, and unregulated buses were used on the unmanned spacecraft depending on the type of load. For example, scientific instruments were usually connected to regulated buses while fans, relays, etc. were energized from an unregulated bus. Different forms of voltage regulation, such as shunt, buck/boot, and pulse-width modulated regulators, were used. This report includes a comprehensive bibliography on spacecraft electrical power systems for the space programs investigated. Author

N85-15804*# Little (Arthur D.), Inc., Cambridge, Mass.
PRELIMINARY EVALUATION OF A LIQUID BELT RADIATOR FOR SPACE APPLICATIONS Final Report
W. P. TEAGAN and K. FITZGERALD Dec. 1984 180 p refs
(Contract NAS3-22253)
(NASA-CR-174807; NAS 1.26:174807) Avail: NTIS HC A09/MF A01 CSCL 10B

The liquid belt radiator (LBR) is discussed. The LBR system operates either in the sensible heat mode or in the latent heat mode. Parametric analysis shows that the LBR may reduce the mass of heat pipe radiators by 70 to 90% when the LBR surface has a total emissivity in excess of 0.3. It is indicated that the diffusion pump oils easily meet this criteria with emissivities greater than 0.8. Measurements on gallium indicate that its emissivity is probably in excess of 0.3 in the solid state when small amounts of impurities are on the surface. The point design exhibits a characteristic mass of 3.1 kg/kW of power dissipation, a mass per unit prime radiating area of approximately 0.9 kg/sq ms and a total package volume of approximately 2.50 cubic m. This compares favorably with conventional technologies which have weights on the order of 4 kg/sq m. E.A.K.

N85-15806*# Hughes Research Labs., Malibu, Calif.
EXTENDED PERFORMANCE TECHNOLOGY STUDY 30-CM THRUSTER Final Report, 26 Jun. 1979 - 26 Oct. 1982
J. R. BEATTIE Jun. 1983 201 p refs
(Contract NAS3-21943)
(NASA-CR-168259; NAS 1.26:168259) Avail: NTIS HC A10/MF A01 CSCL 21C

The extended performance technology study was an investigation of advanced discharge chambers and thruster components that were designed to operate under conditions which result in an increase in the thrust and thrust to power ratio of the state of the art J-series thruster. The high level of performance was achieved by a discharge chamber that employs a ring cusp magnetic confinement arrangement and a three grid ion extraction assembly. It is shown that the ring cusp magnetic field geometry confines the plasma to the volume immediately adjacent to the ion extraction assembly. A high emission current hollow cathode that demonstrated operation at an emission current as high as J sub E = 40 A, and measurements which show the breakdown voltage of individual sections of the J-series propellant flow electrical isolator is about 340 V per section are investigated.
E.A.K.

N85-17023*# TRW Space Technology Labs., Redondo Beach, Calif. Energy Technology Div.
HIGH FREQUENCY PLASMA GENERATOR FOR ION THRUSTERS Final Report, Sep. 1980 - Apr. 1983
H. GOEDE, W. F. DIVERGILIO, V. V. FOSNIGHT, and G. KOMATSU Jul. 1984 74 p refs
(Contract NAS3-22473)
(NASA-CR-174772; NAS 1.26:174772) Avail: NTIS HC A04/MF A01 CSCL 21C

The results of a program to experimentally develop two new types of plasma generators for 30 cm electrostatic argon ion thrusters are presented. The two plasma generating methods selected for this study were by radio frequency induction (RFI), operating at an input power frequency of 1 MHz, and by electron cyclotron heating (ECH) at an operating frequency of 5.0 GHz. Both of these generators utilize multiline cusp permanent magnet configurations for plasma confinement and beam profile optimization. The program goals were to develop a plasma generator possessing the characteristics of high electrical efficiency (low eV/ion) and simplicity of operation while maintaining the reliability and durability of the conventional hollow cathode plasma sources. The RFI plasma generator has achieved minimum discharge losses of 120 eV/ion while the ECH generator has obtained 145 eV/ion, assuming a 90% ion optical transparency of the electrostatic acceleration system. Details of experimental tests with a variety of magnet configurations are presented. Author

N85-18084*# Creare, Inc., Hanover, N.H.
ANALYTICAL AND EXPERIMENTAL INVESTIGATION OF RUBBING INTERACTION IN LABYRINTH SEALS FOR A LIQUID HYDROGEN FUEL PUMP Final Report
F. X. DOLAN, F. E. KENNEDY, and E. M. SCHULSON Aug. 1984 200 p
(Contract NAS3-23276)
(NASA-CR-174657; NAS 1.26:174657; CREARE-TN-371) Avail: NTIS HC A09/MF A01 CSCL 21H

Cracking of the titanium knife edges on the labyrinth seals of the liquid hydrogen fuel pump in the Space Shuttle main engine is considered. Finite element analysis of the thermal response of the knife edge in sliding contact with the wear ring surface shows that interfacial temperatures can be quite high and they are significantly influenced by the thermal conductivity of the surfaces in rubbing contact. Thermal shock experiments on a test specimen similar to the knife edge geometry demonstrate that cracking of the titanium alloy is possible in a situation involving repeated thermal cycles over a wide temperature range, as might be realized during a rub in the liquid hydrogen fuel pump. High-speed rub interaction tests were conducted using a representative knife edge and seal geometry over a broad range of interaction rates and alternate materials were experimentally evaluated. Plasma-sprayed aluminum-graphite was found to be significantly better than presently used aluminum alloy seals from the standpoint of rub performance. Ion nitriding the titanium alloy knife-edges also improved rub performance compared to the untreated baseline.
A.B.H.

N85-19020*# Pratt and Whitney Aircraft, West Palm Beach, Fla. Government Products Div.
DESIGN AND ANALYSIS REPORT FOR THE RL10-2B BREADBOARD LOW THRUST ENGINE Final Report
J. R. BROWN, R. R. FOUST, D. E. GALLER, P. G. KANIC, T. D. KMIEC, C. D. LIMERICK, R. J. PECKHAM, and T. SWARTWOUT 12 Dec. 1984 138 p
(Contract NAS3-24238)
(NASA-CR-174857; NAS 1.26:174857; FR-18046-3) Avail: NTIS HC A07/MF A01 CSCL 21H

The breadboard low thrust RL10-2B engine is described. A summary of the analysis and design effort to define the multimode thrust concept applicable to the requirements for the upper stage vehicles is provided. Baseline requirements were established for operation of the RL10-2B engine under the following conditions: (1) tank head idle at low propellant tank pressures without vehicle propellant conditioning or settling thrust; (2) pumped idle at a ten percent thrust level for low G deployment and/or vehicle tank pressurization; and (3) full thrust (15,000 lb.). Several variations of the engine configuration were investigated and results of the analyses are included. Author

N85-21256* National Aeronautics and Space Administration. Lewis Research Center, Cleveland, Ohio.
RING-CUSP ION THRUSTER WITH SHELL ANODE Patent
J. S. SOVEY, V. K. RAWLIN, and R. F. ROMAN, inventors (to NASA) 21 Aug. 1984 6 p Filed 9 Mar. 1983 Supersedes N83-21903 (21 - 11, p 1783)
(NASA-CASE-LEW-13881-1; NAS 1.71:LEW-13881-1; US-PATENT-4,466,242; US-PATENT-APPL-SN-473498; US-PATENT-CLASS-60-202) Avail: US Patent and Trademark Office CSCL 21C

An improved ion thruster for low specific impulse operation in the 1500 sec to 6000 sec range has a multicusp boundary field provided by high strength magnets on an iron anode shell which lengthens the paths of electrons from a hollow cathode assembly. A downstream anode pole piece in the form of an iron ring supports a ring of magnets to provide a more uniform beam profile. A cylindrical cathode magnet can be moved selectively in an axial direction along a feed tube to produce the desired magnetic field at the cathode tip. Author

N85-21258*# National Aeronautics and Space Administration. Lewis Research Center, Cleveland, Ohio.
RAIL ACCELERATOR TECHNOLOGY AND APPLICATIONS
L. M. ZANA and W. R. KERSLAKE 25 Mar. 1985 18 p refs Presented at the JANNAF Propulsion Meeting, San Diego, Calif., 9-12 Apr. 1985; sponsored by the JANNAF Interagency Propulsion Committee
(NASA-TM-86947; E-2466; NAS 1.15:86947) Avail: NTIS HC A02/MF A01 CSCL 21H

Rail accelerators offer a viable means of launching ton-size payloads from the Earth's surface to space. The results of two mission studies which indicate that an Earth-to-Space Rail Launcher (ESRL) system is not only technically feasible but also economically beneficial, particularly when large amounts of bulk cago are to be delivered to space are given. An in-house experimental program at the Lewis Research Center (LeRC) was conducted in parallel with the mission studies with the objective of examining technical feasibility issues. A 1 m long - 12.5 by 12.5 mm bore rail accelerator as designed with clear polycarbonate sidewalls to visually observe the plasma armature acceleration. The general character of plasma/projectile dynamics is described for a typical test firing.
R.J.F.

N85-21259*# National Aeronautics and Space Administration. Lewis Research Center, Cleveland, Ohio.
VACUUM CHAMBER PRESSURE EFFECTS ON THRUST MEASUREMENTS OF LOW REYNOLDS NUMBER NOZZLES
J. S. SOVEY, P. F. PENKO, S. P. GRISNIK, and M. V. WHALEN 1985 12 p refs Presented at the 1985 JANNAF Propulsion Meeting, San Diego, Calif., 9-12 Apr. 1985
(NASA-TM-86955; E-2440; NAS 1.15:86955) Avail: NTIS HC A02/MF A01 CSCL 21H

Tests were conducted to investigate the effect of vacuum facility pressure on the performance of small thruster nozzles. Thrust measurements of two converging-diverging nozzles with an area ratio of 140 and an orifice plate flowing unheated nitrogen and hydrogen were taken over a wide range of vacuum facility pressures and nozzle throat Reynolds numbers. In the Reynolds number range of 2200 to 12 000 there was no discernable viscous effect on thrust below an ambient to total pressure ratio of 1000. In nearly all cases, flow separation occurred at a pressure ratio of about 1000. This was the upper limit for obtaining an accurate thrust measurement for a conical nozzle with an area ratio of 140. Author

N85-21260*# National Aeronautics and Space Administration. Lewis Research Center, Cleveland, Ohio.
COMPATIBILITY EXPERIMENTS OF FACILITIES, MATERIALS, AND PROPELLANTS FOR ELECTROTHERMAL THRUSTERS
M. V. WHALEN, S. P. GRISNIK, and J. S. SOVEY 1985 16 p refs Presented at the 1985 JANNAF Propulsion Meeting, San Diego, Calif., 9-12 Apr. 1985
(NASA-TM-86956; E-2479; NAS 1.15:86956) Avail: NTIS HC A02/MF A01 CSCL 21H

Experiments were performed to determine the compatibility of materials and propellants for electro-thermal thrusters. Candidate propellants for resistojet propulsion include carbon dioxide, methane, hydrogen, ammonia, and hydrazine. The materials being examined are grain stabilized platinum for resistojets for Space station and rhenium for high performance resistojets for satellites. Heater mass loss and deterioration of materials were evaluated. A coiled tube of platinum, with yttria dispersed throughout the base material to inhibit grain growth, was tested in carbon dioxide at 1300 C for 2000 hr. Post-test examination indicated the platinum-yttria heater would last over 100 000 hr with less than 10 percent mass loss. Short-term compatibility tests were conducted to test the integrity of the platinum-yttria in hydrogen, methane, carbon dioxide/methane mixtures and ammonia environments. In each of these 100 hr tests, the platinum-yttria mass change indicated a minimum coil life of 100 000 hr. Facility related effects were investigated in materials tests using rhenium heated to high tempertures. Vacuum facility water reduction was monitored using a mass spectrometer. In vacuum environments obtained using only diffusion pumping and those obtained with the assistance of cryogenic equipment there were mass gains in the rhenium heaters. These mass gains were the result of the high amount of oxygen and water contained in the gas. Propellant purity and preferred test facility environments are discussed.
G.L.C.

N85-21261*# National Aeronautics and Space Administration. Lewis Research Center, Cleveland, Ohio.
GAAS AND 3-5 COMPOUND SOLAR CELLS STATUS AND PROSPECTS FOR USE IN SPACE
D. J. FLOOD and D. J. BRINKER 1984 13 p refs Presented at the 4th European Symp. on Photovoltaic Generators in Space, Cannes, France, 18-20 Sep. 1984
(NASA-TM-86960; E-2485; NAS 1.15:86960) Avail: NTIS HC A02/MF A01 CSCL 10B

Gallium arsenide solar cells equal or supass the best silicon solar cells in efficiency, radiation resistance, annealability, and in the capability to produce usable power output at elevated temperatures. NASA has been involved in a long range research and development program to capitalize on these manifold advantages, and to explore alternative III-V compounds for additional potential improvements. The current status and future prospects for research and development in this area are reviewed and the progress being made toward development of GaAs cells suitable for variety of space missions is discussed. Cell types under various stages of development include n(+)/p shallow homojunction thin film GaAs cells, x100 concentration ratio p/n and n/p GaAs small area concentrator cells, mechanically-stacked, two-junction tandem cells, and three-junction monolithic cascade cells, among various other cell types. Author

N85-21263*# National Aeronautics and Space Administration. Lewis Research Center, Cleveland, Ohio.
HIGH-VOLTAGE, HIGH-POWER, SOLID-STATE REMOTE POWER CONTROLLERS FOR AEROSPACE APPLICATIONS
J. C. STURMAN Mar. 1985 34 p refs
(NASA-TP-2437; E-2359; NAS 1.60:2437) Avail: NTIS HC A03/MF A01 CSCL 10B

Two general types of remote power controller (RPC) that combine the functions of a circuit breaker and a switch were developed for use in direct-current (dc) aerospace systems. Power-switching devices used in these designs are the relatively new gate-turnoff thyristor (GTO) and poweer metal-oxide-semiconductor field-effect transistors (MOSFET). The various RPC's can switch dc voltages to 1200 V and currents to 100 A. Seven different units were constructed and subjected to comprehensive laboratory and thermal vacuum testing. Two of these were dual units that switch both positive and negative voltages simultaneously. The RPC's using MOSFET's have slow turnon and turnoff times to limit voltage spiking from high di/dt. The GTO's have much faster transition times. All RPC's have programmable overload tripout and microsecond tripout for large overloads. The basic circuits developed can be used to build switchgear limited only by the ratings of the switching device used. Author

N85-22569*# National Aeronautics and Space Administration. Lewis Research Center, Cleveland, Ohio.
THE HIGH VOLTAGE SILICON CELL: A COMPARATIVE ANALYSIS
V. G. WEIZER, C. K. SWARTZ, R. E. HART, and M. P. GODLEWSKI *In* ESA Photovoltaic Generators in Space p 25-29 Nov. 1984 refs
Avail: NTIS HC A20/MF A01 CSCL 21H

An experimental technique capable of resolving the dark saturation current into its base and emitter components is used in an analysis in which the voltage limiting mechanisms for high voltage, low resistivity silicon solar cells were determined. Hi-low emitter cells, multistep diffused cells, ion-implanted emitter cell, MINMIS and MINP cells were studied. The results are at variance with prior expectations: the MINP and the MINMIS voltage improvements are due, to a considerable extent, to an optimization of the base component of the saturation current. This result is substantiated by an independent analysis of the material used to fabricate the devices. Author (ESA)

N85-22580*# National Aeronautics and Space Administration. Lewis Research Center, Cleveland, Ohio.
GAAS AND 3-5 COMPOUND SOLAR CELLS STATUS AND PROSPECTS FOR USE IN SPACE
D. J. FLOOD and D. J. BRINKER *In* ESA Photovoltaic Generators in Space p 89-94 Nov. 1984 refs
Avail: NTIS HC A20/MF A01 CSCL 21H

The status and prospects of GaAs and 3-5 compound thin film and heterojunction solar cells for space missions are reviewed. Cell types considered include n+/p shallow homojunction thin film GaAs cells, 100x concentration ratio p/n and n/p GaAs small area concentrator cells; mechanically-stacked, two-junction tandem cells; and three-junction monolithic cascade cells. Author (ESA)

N85-22586# National Aeronautics and Space Administration. Lewis Research Center, Cleveland, Ohio.
THE EFFECTS OF LITHIUM COUNTERDOPING ON RADIATION DAMAGE AND ANNEALING IN N(+)P SILICON SOLAR CELLS
I. WEINBERG, H. W. BRANDHORST, JR., S. MEHTA, and C. K. SWARTZ *In* ESA Photovoltaic Generators in Space p 131-136 Nov. 1984 refs
Avail: NTIS HC A20/MF A01 CSCL 21H

Boron-doped silicon solar cells were counterdoped with lithium and the resultant n+p cells irradiated by 1 MeV electrons. Lithium counterdoped cells exhibit significantly increased radiation resistance with considerable annealing occurring at 100 C; DLTS studies indicate that the annealing behavior is controlled by a single defect at Ev + 0.43 eV. It is concluded that the increased radiation resistance of the counterdoped cells is due primarily to the interaction of lithium with oxygen, single vacancies and divacancies. It is speculated that the lithium-oxygen interaction is the most effective in contributing to the increased radiation resistance. Author (ESA)

N85-23926*# National Aeronautics and Space Administration. Lewis Research Center, Cleveland, Ohio.
FABRICATION OF CERAMIC SUBSTRATE-REINFORCED AND FREE FORMS
R. J. QUENTMEYER, G. MCDONALD, and R. C. HENDRICKS 19 Apr. 1985 26 p refs Presented at 12th Intern. Conf. on Met. Coatings, Los Angeles, 15-19 Apr. 1985; sponsored by American Vacuum Society
(NASA-TM-86994; E-2540; NAS 1.15:86994) Avail: NTIS HC A03/MF A01 CSCL 21H

Components fabricated of, or coated with, ceramics have lower parasitic cooling requirements. Techniques are discussed for fabricating thin-shell ceramic components and ceramic coatings for applications in rocket or jet engine environments. Thin ceramic shells with complex geometric forms involving convolutions and reentrant surfaces were fabricated by mandrel removal. Mandrel removal was combined with electroplating or plasma spraying and isostatic pressing to form a metal support for the ceramic. Rocket engine thrust chambers coated with 0.08 mm (3 mil) of ZrO2-8Y2O3 had no failures and a tenfold increase in engine life. Some measured mechanical properties of the plasma-sprayed ceramic are presented. B.G.

N85-25384*# United Technologies Corp., South Windsor, Conn. Power Systems Div.
LONG-LIFE HIGH PERFORMANCE FUEL CELL PROGRAM Interim Report, 28 May 1981 - 31 Oct. 1984
R. E. MARTIN Feb. 1985 187 p refs
(Contract NAS3-22234)
(NASA-CR-174874; NAS 1.26:174874; FCR-6853) Avail: NTIS HC A09/MF A01 CSCL 10B

A multihundred kilowatt Regenerative Fuel Cell for use in a space station is envisioned. Three 0.508 sq ft (471.9 cm) active area multicell stacks were assembled and endurance tested. The long term performance stability of the platinum on carbon catalyst configuration suitability of the lightweight graphite electrolyte reservoir plate, the stability of the free standing butyl bonded potassium titanate matrix structure, and the long life potential of a hybrid polysulfone cell edge frame construction were demonstrated. A 18,000 hour demonstration test of multicell stack to a continuous cyclical load profile was conducted. A total of 12,000 cycles was completed, confirming the ability of the alkaline fuel cell to operate to a load profile simulating Regenerative Fuel Cell operation. An orbiter production hydrogen recirculation pump employed in support of the cyclical load profile test completed 13,000 hours of maintenance free operation. Laboratory endurance tests demonstrated the suitability of the butyl bonded potassium matrix, perforated nickel foil electrode substrates, and carbon ribbed substrate anode for use in the alkaline fuel cell. Corrosion testing of materials at 250 F (121.1 C) in 42% wgt. potassium identified ceria, zirconia, strontium titanate, strontium zirconate and lithium cobaltate as candidate matrix materials. A.R.H.

N85-25385*# National Aeronautics and Space Administration. Lewis Research Center, Cleveland, Ohio.
MANRATING ORBITAL TRANSFER VEHICLE PROPULSION
L. P. COOPER 1985 14 p refs Proposed for presentation at the 21st Joint Propulsion Conf., Monterey, Calif., 8-10 Jul. 1985; sponsored by AIAA, SAE and ASME
(NASA-TM-87019; E-2570; NAS 1.15:87019) Avail: NTIS HC A02/MF A01 CSCL 21H

The expended capabilities for Orbital Transfer Vehicles (OTV) which will be needed to meet increased payload requirements for transporting materials and men to geosynchronous orbit are discussed. The requirement to provide manrating offers challenges and opportunities to the propulsion system designers. The propulsion approaches utilized in previous manned space vehicles of the United States are reviewed. The principals of reliability analysis are applied to the Orbit Transfer Vehicle. Propulsion system options are characterized in terms of the test requirements to demonstrate reliability goals and are compared to earlier vehicle approaches. E.A.K.

N85-25386*# National Aeronautics and Space Administration. Lewis Research Center, Cleveland, Ohio.
SPACE STATION PROPULSION: THE ADVANCED DEVELOPMENT PROGRAM AT LEWIS
R. E. JONES 1985 14 p refs Proposed for presentation at the 21st Joint Propulsion Conf., Monterey, Calif., 8-10 Jul. 1985; sponsored by AIAA, SAE and ASME
(NASA-TM-86999; E-2544; NAS 1.15:86999) Avail: NTIS HC A02/MF A01 CSCL 21H

A reference configuration was established for the initial operating capability (IOC) station. The reference configuration has assumed hydrazine fueled thrusters as the propulsion system. This was to establish costing and as a reference for comparison when other propulsion systems are considered. An integral part of the plan to develop the Space Station is the advanced development program. The objective of this program is to provide advanced technology alternatives for the initial and evolutionary Space Station which optimize the system's functional characteristics in terms of performance, cost, and utilization. The portion of the Advanced Development Program that is concerned with auxiliary propulsion and the research and programmatic activities conducted are discussed. E.A.K.

N85-26900*# National Aeronautics and Space Administration. Lewis Research Center, Cleveland, Ohio.
FUEL AND OXIDIZER TURBINE LOSS ANALYSIS
J. E. HAAS *In* NASA. Marshall Space Flight Center Advan. High Pressure O2/H2 Technol. p 560-570 Apr. 1985
Avail: NTIS HC A99/MF E03; SOD HC CSCL 21H

The turbine losses for the fuel and oxidizer turbines at the FPL condition were assessed by a quasi-3D loss analysis method. This loss analysis method uses two flow codes - MERIDL and TSONIC - to calculate the flow velocities along the blade surfaces and endwalls. The velocities are then used as input to the boundary layer code - BLAYER - to calculate the friction losses due to incidence, secondary flow, and tip clearance. The loss analysis for the fuel turbine indicated an overall two-stage efficiency of about 90%. The largest loss was due to rotor tip clearance. The loss analysis for the oxidizer turbine is nearly completed. Results for the first stage of the two-stage design indicates an efficiency of about 80%, with high losses due to rotor incidence and blade and endwall friction. E.A.K.

N85-26901*# National Aeronautics and Space Administration. Lewis Research Center, Cleveland, Ohio.
REDISTRIBUTION OF THE INLET TEMPERATURE PROFILE THROUGH THE SSME FUEL TURBINE
J. R. SCHWAB *In* NASA. Marshall Space Flight Center Advan. High Pressure O2/H2 Technol. p 571-578 Apr. 1985 refs
Avail: NTIS HC A99/MF E03; SOD HC CSCL 21H

A three-dimensional Euler code was used to predict radial inlet temperature profile redistribution through the two-stage fuel turbopump turbine. The calculation was made at the FPL condition

using a turbine inlet radial temperature profile. This same calculation was made earlier on single-stage turbine. There was a redistribution of the temperature profile such that the hotter gas that originated at the midspan region at the turbine inlet was shifted to the hub and tip regions on the blade pressure surface at the rotor exit. For the SSME fuel turbine, however, there was no redistribution of the inlet temperature profile. No strong secondary flow patterns were identified. It is indicated that this trend is attributed to the high solidity SSME blading. E.A.K.

N85-26907*# Rockwell International Corp., Canoga Park, Calif. Rocketdyne Div.

REUSABLE ROCKET ENGINE TURBOPUMP CONDITION MONITORING

M. E. HAMPSON and S. BARKHOUDARIAN *In* NASA. Marshall Space Flight Center Advan. High Pressure O2/H2 Technol. p 654-673 Apr. 1985 refs

(Contract NAS3-23349)

Avail: NTIS HC A99/MF E03; SOD HC CSCL 21H

Significant improvements in engine readiness with attendant reductions in maintenance costs and turnaround times can be achieved with an engine condition monitoring system (CMS). The CMS provides real time health status of critical engine components, without disassembly, through component monitoring with advanced sensor technologies. Three technologies were selected to monitor the rotor bearings and turbine blades: the isotope wear detector and fiber optic deflectometer (bearings), and the fiber optic pyrometer (blades). Signal processing algorithms were evaluated and ranked for their utility in providing useful component health data to unskilled maintenance personnel. Design modifications to current configuration Space Shuttle Main Engine (SSME) high pressure turbopumps and the MK48-F turbopump were developed to incorporate the sensors. Author

N85-26912*# National Aeronautics and Space Administration. Lewis Research Center, Cleveland, Ohio.

TETHERED NUCLEAR POWER FOR THE SPACE STATION

D. J. BENTS 1985 27 p refs Proposed for presentation at the 20th Intersoc. Energy Conversion Eng. Conf. (IECEC), Miami Beach, Fla., 18-23 Aug. 1985; sponsored by SAE, ANS, ASME, IEEE, AIAA, ACS, and AIChE

(NASA-TM-87023; E-2572; NAS 1.15:87023) Avail: NTIS HC A03/MF A01 CSCL 18L

A nuclear space power system the SP-100 is being developed for future missions where large amounts of electrical power will be required. Although it is primarily intended for unmanned spacecraft, it can be adapted to a manned space platform by tethering it above the station through an electrical transmission line which isolates the reactor far away from the inhabited platform and conveys its power back to where it is needed. The transmission line, used in conjunction with an instrument rate shield, attenuates reactor radiation in the vicinity of the space station to less than one-one hundredth of the natural background which is already there. This combination of shielding and distance attenuation is less than one-tenth the mass of boom-mounted or onboard man-rated shields that are required when the reactor is mounted nearby. This paper describes how connection is made to the platform (configuration, operational requirements) and introduces a new element the coaxial transmission tube which enables efficient transmission of electrical power through long tethers in space. Design methodology for transmission tubes and tube arrays is discussed. An example conceptual design is presented that shows SP-100 at three power levels 100 kWe, 300 kWe, and 1000 kWe connected to space station via a 2 km HVDC transmission line/tether. Power system performance, mass, and radiation hazard are estimated with impacts on space station architecture and operation. B.W.

N85-27941*# National Aeronautics and Space Administration. Lewis Research Center, Cleveland, Ohio.

STRUCTURAL INTEGRITY AND DURABILITY OF REUSABLE SPACE PROPULSION SYSTEMS

Washington May 1985 191 p refs Conf. held in Cleveland, Ohio, 4-5 Jun. 1985; sponsored by NASA, Washington and NASA. Lewis Research Center

(NASA-CP-2381; E-2554; NAS 1.55:2381) Avail: NTIS HC A09/MF A01 CSCL 21H

The space shuttle main engine (SSME), a reusable space propulsion system, is discussed. The advances in high pressure oxygen hydrogen rocket technology are reported to establish the basic technology and to develop new analytical tools for the evaluation in reusable rocket systems.

N85-27942*# National Aeronautics and Space Administration. Lewis Research Center, Cleveland, Ohio.

OVERVIEW OF AEROTHERMODYNAMIC LOADS DEFINITION STUDY Abstract Only

L. A. POVINELLI *In its* Struct. Integrity and Durability of Reusable Space Propulsion Systems p 3-5 May 1985 refs

Avail: NTIS HC A09/MF A01 CSCL 21H

The Aerothermodynamic Loads Definition were studied to develop methods to more accurately predict the operating environment in the space shuttle main engine (SSME) components. Development of steady and time-dependent, three-dimensional viscous computer codes and experimental verification and engine diagnostic testing are considered. The steady, nonsteady, and transient operating loads are defined to accurately predict powerhead life. Improvements in the structural durability of the SSME turbine drive systems depends on the knowledge of the aerothermodynamic behavior of the flow through the preburner, turbine, turnaround duct, gas manifold, and injector post regions. E.A.K.

N85-27943*# National Aeronautics and Space Administration. Lewis Research Center, Cleveland, Ohio.

SSME FUEL PREBURNER TWO-DIMENSIONAL ANALYSIS

T. J. VANOVERBEKE *In its* Struct. Integrity and Durability of Reusable Space Propulsion Systems p 7-14 May 1985

Avail: NTIS HC A09/MF A01 CSCL 21H

The durability of the SSME turbine is strongly affected by the temperature profile leaving the preburner. A reacting flow computer model to predict the turbine inlet temperature profile was used. Calculations were made by using a reacting flow code, to assess the sensitivity of the turbine inlet temperature profile to variations in the flow entering the SSME preburner. E.A.K.

N85-27972*# National Aeronautics and Space Administration. Lewis Research Center, Cleveland, Ohio.

PRIMARY PROPULSION OF ELECTROTHERMAL, ION AND CHEMICAL SYSTEMS FOR SPACE-BASED RADAR ORBIT TRANSFER

S. Y. WANG and P. J. STAIGER 1985 16 p refs Presented at 21st Joint Propulsion Conf., Monterey, Calif., 8-10 Jul. 1985; sponsored by AIAA, SAE and ASME

(NASA-TM-87043; E-2603; NAS 1.15:87043) Avail: NTIS HC A02/MF A01 CSCL 21C

An orbit transfer mission concept has been studied for a Space-Based Radar (SBR) where 40 kW required for radar operation is assumed available for orbit transfer propulsion. Arcjet, pulsed electrothermal (PET), ion, and storable chemical systems are considered for the primary propulsion. Transferring two SBR per shuttle flight to 1112 km/60 deg using electrical propulsion systems offers an increased payload at the expense of increased trip time, up to 2000 kg each, which may be critical for survivability. Trade offs between payload mass, transfer time, launch site, inclination, and height of parking orbits are presented. Author

N85-28971*# National Aeronautics and Space Administration. Lewis Research Center, Cleveland, Ohio.
AN EVALUATION OF OXYGEN-HYDROGEN PROPULSION SYSTEMS FOR THE SPACE STATION
R. W. KLEMETSON, P. W. GARRISON, and N. P. HANNUM 1985 28 p refs Presented at the 21st Joint Propulsion Conf., Monterey, Calif., 8-10 Jul. 1985; sponsored in part by AIAA, SAE, ASME, and ASEE Previously announced in IAA as A85-43976 Prepared in cooperation with JPL, Pasadena, Calif.
(NASA-TM-87059; E-2628; NAS 1.15:87059) Avail: NTIS HC A03/MF A01 CSCL 21H

Conceptual designs for O2/H2 chemical and resistojet propulsion systems for the space station was developed and evaluated. The evolution of propulsion requirements was considered as the space station configuration and its utilization as a space transportation node change over the first decade of operation. The characteristics of candidate O2/H2 auxiliary propulsion systems are determined, and opportunities for integration with the OTV tank farm and the space station life support, power and thermal control subsystems are investigated. OTV tank farm boiloff can provide a major portion of the growth station impulse requirements and CO2 from the life support system can be a significant propellant resource, provided it is not denied by closure of that subsystem. Waste heat from the thermal control system is sufficient for many propellant conditioning requirements. It is concluded that the optimum level of subsystem integration must be based on higher level space station studies. Author

N85-34176*# National Aeronautics and Space Administration. Lewis Research Center, Cleveland, Ohio.
OPTICAL ANALYSIS OF PARABOLIC DISH CONCENTRATORS FOR SOLAR DYNAMIC POWER SYSTEMS IN SPACE
K. S. JEFFERIES Aug. 1985 27 p refs
(NASA-TM-87080; E-2659; NAS 1.15:87080) Avail: NTIS HC A03/MF A01 CSCL 10B

An optical analysis of a parabolic solar collection system operating in Earth orbit was performed using ray tracing techniques. The analysis included the effects of: (1) solar limb darkening, (2) parametric variation of mirror surface error, (3) parametric variation of mirror rim angle, and (4) parametric variation of alignment and pointing error. This ray tracing technique used numerical integration to combine the effects of rays emanating from different parts of the sun at different intensities with the effects of normally distributed mirror-surface errors to compute the angular intensity distribution of rays leaving the mirror surface. A second numerical integration was then performed over the surface of the parabolic mirror to compute the radial distribution of brightness at the mirror focus. Major results of the analysis included: (1) solar energy can be collected at high temperatures with high efficiency, (2) higher absorber temperatures can be achieved at lower efficiencies, or higher efficiencies can be achieved at lower temperatures, and (3) collection efficiency is near its maximum level across a broad plateau of rim angles from 40 deg to 70 deg. Author

N85-34177*# National Aeronautics and Space Administration. Lewis Research Center, Cleveland, Ohio.
HEATERLESS IGNITION OF INERT GAS ION THRUSTER HOLLOW CATHODES
M. F. SCHATZ 1985 23 p refs Presented at the 18th Intern. Elec. Propulsion Conf., Alexandria, Va., 30 Sep. - 2 Oct. 1985; sponsored by AIAA, JSASS and DGLR
(NASA-TM-87086; E-2672; NAS 1.15:87086) Avail: NTIS HC A02/MF A01 CSCL 21C

Heaterless inert gas ion thruster hollow cathodes were investigated with the aim of reducing ion thruster complexity and increasing ion thruster reliability. Cathodes heated by glow discharges are evaluated for power requirements, flowrate requirements, and life limiting mechanisms. An accelerated cyclic life test is presented. E.A.K.

N85-34178*# National Aeronautics and Space Administration. Lewis Research Center, Cleveland, Ohio.
ELECTRODE EROSION IN ARC DISCHARGES AT ATMOSPHERIC PRESSURE
T. L. HARDY 1985 21 p refs Presented at the 18th Intern. Elec. Propulsion Conf., Alexandria, Va., 30 Sep. - 2 Oct. 1985; sponsored by AIAA, JSASS and DGLR
(NASA-TM-87087; E-2673; NAS 1.15:87087) Avail: NTIS HC A02/MF A01 CSCL 21C

An experimental investigation was performed in an effort to measure and increase lifetime of electrodes in an arcjet thruster. The electrode erosion of various anode and cathode materials was measured after tests in an atmospheric pressure nitrogen arc discharge at powers less than 1 kW. A free-burning arc configuration and a constricted arc configuration were used to test the materials. Lanthanum hexaboride and thoriated tungsten had low cathode erosion rates while thoriated tungsten and pure tungsten had the lowest anode erosion rates of the materials tested. Anode cooling, reverse gas flow, and external magnetic fields were all found to reduce electrode mass loss. Author

N85-34179*# National Aeronautics and Space Administration. Lewis Research Center, Cleveland, Ohio.
HOLLOW CATHODES IN HIGH PRESSURE ARC DISCHARGES
T. L. HARDY and F. M. CURRAN 1985 9 p refs Presented at the 18th Intern. Elec. Propulsion Conf., Alexandria, Va., 30 Sep. - 2 Oct. 1985; sponsored by AIAA, JSASS and DGLR
(NASA-TM-87098; E-2689; NAS 1.15:87098) Avail: NTIS HC A02/MF A01 CSCL 21C

An orified hallow cathode was tested at high pressure to improve lifetime and efficiency in arcjet thrusters. It is indicated that the arc would not operate with emission from the insert above 200 torr in nitrogen regardless of insert material, orifice diameter, or gas flow direction. Emission occurred from the insert in argon and xenon although it could not be ascertained whether diffuse or spot emission existed within the cathode. Over the extended range of configurations and operating parameters explored the desired diffuse emission mode could not be obtained at high enough pressures for orified hollow cathodes to operate in the range which is considered for arcjet applications. E.A.K.

N85-35225*# National Aeronautics and Space Administration. Lewis Research Center, Cleveland, Ohio.
STATUS OF ADVANCED ORBITAL TRANSFER PROPULSION
L. P. COOPER 1985 26 p refs Proposed for presentation at the 36th Intern. Astronautics Federation Congr., Stockholm, 7-12 Oct. 1985
(NASA-TM-87069; E-2638; NAS 1.15:87069; IAF-85-164) Avail: NTIS HC A03/MF A01 CSCL 21H

A new Orbital Transfer Vehicle (OTV) propulsion system that will be used in conjunction with the Space Shuttle, Space Station and Orbit Maneuvering Vehicle is discussed. The OTV will transfer men, large space structures and conventional payloads between low Earth and higher energy orbits. Space probes carried by the OTV will continue the exploration of the solar system. When lunar bases are established, the OTV will be their transportation link to Earth. Critical engine design considerations based upon the need for low cost payload delivery, space basing, reusability, aeroassist maneuvering, low g transfers of large space structures and man rating are described. The importance of each of these to propulsion design is addressed. Specific propulsion requirements discussed are: (1) high performance H2/O2 engine; (2) multiple engine configurations totalling no more than 15,000 lbf thrust 15 to 20 hr life; (3) space maintainable modular design; (4) health monitoring capability; and (5) safety and mission success with backup auxiliary propulsion. E.A.K.

23

CHEMISTRY AND MATERIALS (GENERAL)

Includes biochemistry and organic chemistry.

A85-36694* Sandia National Labs., Albuquerque, N. Mex.
PROPERTIES OF COATED AND MODIFIED SURFACES
D. M. MATTOX (Sandia National Laboratory, Albuquerque, NM), J. E. GREENE (Illinois, University, Urbana, IL), D. H. BUCKLEY (NASA, Lewis Research Center, Cleveland, OH), and G. A. SOMORJAI (California, University, Berkeley, CA) Materials Science and Engineering (ISSN 0025-5416), vol. 70, April 1985, p. 79-89. refs

The ability to create surface and near-surface properties distinct from the bulk properties of a material by means of coating or surface modification techniques is an important new field of development for engineering materials, encompassing ion implantation, plasma processing, reactive deposition methods, ion beam deposition and modification, molecular beam epitaxy, and fast quench thermal processing. Attention is given to specific areas of process control which illustrate (1) the use of process development to control material properties, (2) the importance of surface modification and coating to the tribology and ion-surface interactions of semiconductor film growth, and (3) recent findings in surface science which exemplify potential applications of ion-surface interactions that generate novel material qualities. O.C.

N85-10105*# National Aeronautics and Space Administration. Lewis Research Center, Cleveland, Ohio.
DYNAMICS OF GRAPHITE FIBER INTERCALATION: IN SITU RESISTIVITY MEASUREMENTS WITH A FOUR POINT PROBE
D. A. JAWORSKE 1984 14 p refs Presented at the Mater. Res. Soc. Symp. on Intercalated Graphite, Boston, 28-30 Nov. 1984; sponsored by American Physical Society
(NASA-TM-86858; E-2321; NAS 1.15:86858) Avail: NTIS HC A02/MF A01 CSCL 11D

The dynamics of ferric chloride intercalation of single graphite fibers were studied, in situ, using a four point dc bridge. Measurements before, during and after the intercalation showed that the intercalation occurred within minutes at 200 C. Changes in fiber resistivity after exposure to air suggested hydration of the graphite intercalation compound. Deintercalation of the ferric chloride was initiated at temperatures in excess of 400 C. cycling the intercalant into and out of the graphite fiber gave no improvements in fiber resistivity. The activation energy of the ferric chloride intercalation reaction was found to be 17 + or - 4 kcal/mol 1 consistent with the concept of a preliminary nucleation step in the intercalation reaction. Author

N85-14864*# National Aeronautics and Space Administration. Lewis Research Center, Cleveland, Ohio.
EFFECT OF WATER ON HYDROGEN PERMEABILITY
D. D. HULLIGAN (Sverdrup Technology, Middleburg Heights, Ohio) and W. A. TOMAZIC 1984 14 p refs Presented at the 22nd Automotive Technol. Develop. Contractors' Coordination meeting, Dearborn, Mich., 26 Oct. - 2 Nov. 1984; sponsored by DOE
(Contract DE-AI01-77CS-51040)
(NASA-TM-86904; E-2389; DOE/NASA/51040-59; NAS 1.15:86904) Avail: NTIS HC A02/MF A01 CSCL 07D

Doping of hydrogen with CO or CO2 was developed to reduce hydrogen permeation in Stirling engines by forming low permeability oxide coatings in the heater tubes. An end product of this process is water - which can condense in the cold parts of the engine system. If the water vapor is reduced to a low enough level, the hydrogen can reduce the oxide coating resulting in increased permeability. The equilibrium level of water (oxygen bearing gas) required to avoid reduction of the oxide coating was investigated. Results at 720 C and 13.8 MPa have shown that: (1) pure hydrogen will reduce the coating; (2) 500 ppm CO (500 ppm water equivalent) does not prevent the reduction; and (3) 500 ppm CO2 (1000 ppm water) appears to be close to the equilibrium level. Further tests are planned to define the equilibrium level more precisely and to extend the data to 820 C and 3.4, 6.9, and 13.8 MPa. R.S.F.

N85-21264*# National Aeronautics and Space Administration. Lewis Research Center, Cleveland, Ohio.
A COMPUTER SIMULATION OF THIN FILM NUCLEATION AND GROWTH: THE VOLMER-WEBER CASE
J. SALIK and H. M. GHOSE (Cuyahoga Community Coll.) 1985 12 p refs Proposed for presentation at the 12th Intern. Conf. on Met. Coatings, Los Angeles, 15-19 Apr. 1985; sponsored by the American Vacuum Society
(NASA-TM-86968; E-2493; NAS 1.15:86968) Avail: NTIS HC A02/MF A01 CSCL 07A

The computer simulation of thin film nucleation and growth, which was previously performed for the case of single monolayer, was modified to include multilayer growth via the Volmer-Weber mechanism. The simulation results show that: (1) the kinetics of multilayer film growth is nearly identical to that of monolayer growth; (2) when no reevaporation takes place, the cluster density resulting from multilayer growth is higher at high coverage than that resulting from monolayer growth; (3) when reevaporation does take place, the cluster density resulting from multilayer growth is nearly identical to that resulting from monolayer growth. This is not due, however, to similarity in microstructure. E.A.K.

N85-26921*# National Aeronautics and Space Administration. Lewis Research Center, Cleveland, Ohio.
GRAPHITE FIBER INTERCALATION: DYNAMICS OF THE BROMINE INTERCALATION PROCESS
D. A. JAWORSKE and R. ZINOLABEDINI (Cleveland State Univ.) 21 Jun. 1985 10 p refs Presented at 17th Biennial Conf. Carbon, Lexington, Ky., 16-21 Jun. 1985; sponsored by American Carbon Society
(NASA-TM-87015; E-2441; NAS 1.15:87015) Avail: NTIS HC A02/MF A01 CSCL 11D

The resistance of pitch-based graphite fibers was monitored, in situ, during a series of bromine intercalation experiments. The threshold pressure for the bromine intercalation of pitch-based fibers was estimated to be 102 torr. When the bromine atmosphere was removed from the reaction chamber, the resistivity of the intercalated graphite fibers increased consistently. This increase was attributed to loss of bromine from the perimeter of the fiber. The loss was confirmed by mapping the bromine concentration across the diameter of single intercalated fibers with either energy dispersive spectroscopy or scanning Auger microscopy. A statistical study comparing fibers intercalated in bromine vapor with fibers intercalated in bromine liquid showed that similar products were obtained with both methods of intercalation. Author

N85-30011*# National Aeronautics and Space Administration. Lewis Research Center, Cleveland, Ohio.
BURNER RIG CORROSION OF SIC AT 1000 DEG C
N. S. JACOBSON, C. A. STEARNS, and J. L. SMIALEK 1985 27 p refs Presented at the 87th Ann. Meeting of the Am. Ceram. Soc., Cincinnati, 5-9 May 1985
(NASA-TM-87061; E-2512; NAS 1.15:87061) Avail: NTIS HC A03/MF A01 CSCL 11B

Sintered alpha-SiC was examined in both oxidation and hot corrosion with a burner rig at 400 kPa (4 atm) and 1000 C with a flow velocity of 310 ft/sec. Oxidation tests for times to 46 hr produced virtually no attack, whereas tests with 4 ppm Na produced extensive corrosion in 13-1/2 hr. Thick glassy layers composed primarily of sodium silicate formed in the salt corrosion tests. This corrosion attack caused severe pitting of the silicon carbide substrate which led to a 32 percent strength decrease below the as-received material. Parallel furnace tests of Na2SO4/air induced attacked yielded basically similar results with some slight product composition differences. The differences are explained in terms of the continuous sulfate deposition which occurs in a burner rig. Author

24

COMPOSITE MATERIALS

Includes laminates.

A85-11926* Ohio State Univ., Columbus.
ULTRASONIC WAVE PROPAGATION IN TWO-PHASE MEDIA - SPHERICAL INCLUSIONS
L. S. FU and Y. C. SHEU (Ohio State University, Columbus, OH) Composite Structures (ISSN 0263-8223), vol. 2, no. 4, 1984, p. 289-303. Previously announced in STAR as N83-36500. refs
(Contract NAG3-340)

The scattering theory, recently developed via the extended method of equivalent inclusion, is used to study the propagation of time-harmonic waves in two-phase media of elastic matrix with randomly distributed elastic spherical inclusion materials. The elastic moduli and mass density of the composite medium are determined as functions of frequencies when given properties and concentration of the spheres and the matrix. Velocity and attenuation of ultrasonic waves in two-phase media are determined for cases of distributed spheres and localized damage. An averaging theorem that requires the equivalence of the strain energy and the kinetic energy between the effective medium and the original matrix with spherical inhomogeneities is employed to derive the effective moduli and mass density. The functional dependency of these quantities upon frequencies and concentration provides a method of data analysis in ultrasonic evaluation of material properties. Numerical results or moduli, velocity and/or attenuation as functions of concentration of inclusion material, or porosity, are graphically displayed. Author

A85-15632*# National Aeronautics and Space Administration. Lewis Research Center, Cleveland, Ohio.
HYGROTHERMOMECHANICAL EVALUATION OF TRANSVERSE FILAMENT TAPE EPOXY/POLYESTER FIBERGLASS COMPOSITES
R. F. LARK and C. C. CHAMIS (NASA, Lewis Research Center, Cleveland, OH) IN: Reinforced Plastics/Composites Institute, Annual Conference, 38th, Houston, TX, February 7-11, 1983, Preprints . New York, Society of the Plastics Industry, Inc., 1984, p. 12-C-1 to 12-C-15. refs

Transverse filament tape (TFT) fiberglass/epoxy and TFT polyester composites intended for low cost wind turbine blade fabrication have been subjected to static and cyclic load behavior tests whose results are presently evaluated on the basis of an integrated hygrothermomechanical response theory. Laminate testing employed simulated filament winding procedures. The results obtained show that the predicted hygrothermomechanical environmental effects on TFT composites are in good agreement with measured data for various properties, including fatigue at different R-ratio values. O.C.

A85-15636*# National Aeronautics and Space Administration. Lewis Research Center, Cleveland, Ohio.
DESIGN PROCEDURES FOR FIBER COMPOSITE STRUCTURAL COMPONENTS - RODS, BEAMS, AND BEAM COLUMNS
C. C. CHAMIS (NASA, Lewis Research Center, Cleveland, OH) IN: Reinforced Plastics/Composites Institute, Annual Conference, 38th, Houston, TX, February 7-11, 1983, Preprints . New York, Society of the Plastics Industry, Inc., 1984, p. 16-C-1 to 16-C-9. Previously announced in STAR as N83-24559. refs

Step by step procedures are described which are used to design structural components (rods, columns, and beam columns) subjected to steady state mechanical loads and hydrothermal environments. Illustrative examples are presented for structural components designed for static tensile and compressive loads, and fatigue as well as for moisture and temperature effects. Each example is set up as a sample design illustrating the detailed steps that are used to design similar components. Author

A85-16040* National Aeronautics and Space Administration. Lewis Research Center, Cleveland, Ohio.
SELECT FIBER COMPOSITES FOR SPACE APPLICATIONS - A MECHANISTIC ASSESSMENT
C. A. GINTY and C. C. CHAMIS (NASA, Lewis Research Center, Cleveland, OH) IN: Technology vectors; Proceedings of the Twenty-ninth National SAMPE Symposium and Exhibition, Reno, NV, April 3-5, 1984 . Covina, CA, Society for the Advancement of Material and Process Engineering, 1984, p. 979-993. Previously announced in STAR as N84-22702. refs

Three fiber composites (graphite-fiber epoxy, graphite-fiber aluminum, and graphite-fiber magnesium) are evaluated for their possible use in space applications. Using the composite mechanics theories for thermomechanical behavior embodied in the ICAN (Integrated Composites Analyzer) computer code, select composite thermal and mechanical properties are predicted and also their response to cryogenic temperatures, resembling those which occur in space applications. The predicted results are presented in graphical form as a function of the composite's laminate configuration, fiber volume ratio and the selected use temperature. These results are suitable for preliminary design purposes only and should serve as an aid in selecting controlled experiments for obtaining corresponding measured data. Author

A85-16094*# National Aeronautics and Space Administration. Lewis Research Center, Cleveland, Ohio.
ICAN - INTEGRATED COMPOSITES ANALYZER
P. L. N. MURTHY and C. C. CHAMIS (NASA, Lewis Research Center, Cleveland, OH) AIAA, ASME, ASCE, and AHS, Structures, Structural Dynamics and Materials Conference, 25th, Palm Springs, CA, May 14-16, 1984. 24 p. Previously announced in STAR as N84-26755. refs
(AIAA PAPER 84-0974)

The ICAN computer program performs all the essential aspects of mechanics/analysis/design of multilayered fiber composites. Modular, open-ended and user friendly, the program can handle a variety of composite systems having one type of fiber and one matrix as constituents as well as intraply and interply hybrid composite systems. It can also simulate isotropic layers by considering a primary composite system with negligible fiber volume content. This feature is specifically useful in modeling thin interply matrix layers. Hygrothermal conditions and various combinations of in-plane and bending loads can also be considered. Usage of this code is illustrated with a sample input and the generated output. Some key features of output are stress concentration factors around a circular hole, locations of probable delamination, a summary of the laminate failure stress analysis, free edge stresses, microstresses and ply stress/strain influence coefficients. These features make ICAN a powerful, cost-effective tool to analyze/design fiber composite structures and components.
A.R.H.

A85-16096*# National Aeronautics and Space Administration. Lewis Research Center, Cleveland, Ohio.
INTERPLY LAYER DEGRADATION EFFECTS ON COMPOSITE STRUCTURAL RESPONSE
C. C. CHAMIS (NASA, Lewis Research Center, Cleveland, OH) and G. C. WILLIAMS (Arizona, University, Tucson, AZ) AIAA, ASME, ASCE, and AHS, Structures, Structural Dynamics and Materials Conference, 25th, Palm Springs, CA, May 14-16, 1984. 29 p. Previously announced in STAR as N84-26756.
(AIAA PAPER 84-0849)

Recent research activities at NASA Lewis Research Center to computationally evaluate the effects of interply layer progressive weakening (degradation) on the structural response of a composite beam are summarized. The structural responses of interest include: (1) bending, (2) buckling, (3) free vibrations, (4) periodic excitation, and (5) impact. Finite element analysis was used for the computational evaluations. The interply layer degradation effects on the various structural responses were determined and assessed as a function of the interply layer modulus varying from 1 million psi down to 1000 psi and even lower for some limiting cases. The results obtained show that the interply layer degradation has

generally negligible effectss on composite structural response and, therefore, structural integrity, unless the interply layer modulus degrades to about 10,000 psi or less. Author

A85-21520* National Aeronautics and Space Administration. Lewis Research Center, Cleveland, Ohio.
PMR POLYIMIDE COMPOSITES FOR AEROSPACE APPLICATIONS
T. T. SERAFINI (NASA, Lewis Research Center, Cleveland, OH) IN: Polyimides: Synthesis, characterization, and applications. Volume 2 . New York, Plenum Press, 1984, p. 957-975. refs

A novel class of addition-type polyimides has been developed in response to the need for high temperature polymers with improved processability. The new plastic materials are known as PMR (for in situ polymerization of monomer reactants) polyimides. The highly processable PMR polyimides have made it possible to realize much of the potential of high temperature resistant polymers. Monomer reactant combinations for several PMR polyimides have been identified. The present investigation is concerned with a review of the current status of PMR polyimides. Attention is given to details of PMR polyimide chemistry, the processing of composites and their properties, and aerospace applications of PMR-15 polyimide composites. G.R.

A85-29133*# Drexel Univ., Philadelphia, Pa.
USE OF STATICAL INDENTATION LAWS IN THE IMPACT ANALYSIS OF LAMINATED COMPOSITE PLATES
T. M. TAN (Drexel University, Philadelphia, PA; Purdue University, West Lafayette, IN) and C. T. SUN (Purdue University, West Lafayette, IN) ASME, Transactions, Journal of Applied Mechanics (ISSN 0021-8936), vol. 52, March 1985, p. 6-12.
(Contract NSG-3185)

The low-velocity impact response of graphite/epoxy laminates was investigated theoretically and experimentally. A nine-node isoparametric plate finite element in conjunction with an empirical contact law was used for the theoretical investigation. Theoretical results are in good agreement with strain-gage experimental data. The results of the investigation indicate that the present theoretical procedure describes the impact response of laminate for low-impact velocities. Author

A85-37421*# National Aeronautics and Space Administration. Lewis Research Center, Cleveland, Ohio.
ANALYSIS OF STRESS-STRAIN, FRACTURE, AND DUCTILITY BEHAVIOR OF ALUMINUM MAXTRIX COMPOSITES CONTAINING DISCONTINUOUS SILICON CARBIDE REINFORCEMENT
D. L. MCDANELS (NASA, Lewis Research Center, Cleveland, OH) Metallurgical Transactions A - Physical Metallurgy and Materials Science (ISSN 0360-2133), vol. 16A, June 1985, p. 1105-1115. refs

Mechanical properties and stress-strain behavior were evaluated for several types of commercially fabricated aluminum matrix composites, containing up to 40 vol pct discontinuous SiC whisker, nodule, or particulate reinforcement. The elastic modulus of the composites was found to be isotropic, to be independent of type of reinforcement, and to be controlled solely by the volume percentage of SiC reinforcement present. The yield/tensile strengths and ductility were controlled primarily by the matrix alloy and temper condition. Type and orientation of reinforcement had some effect on the strengths of composites, but only for those in which the whisker reinforcement was highly oriented. Ductility decreased with increasing reinforcement content; however, the fracture strains observed were higher than those reported in the literature for this type of composite. This increase in fracture strain was probably attributable to cleaner matrix powder, better mixing, and increased mechanical working during fabrication. Comparison of properties with conventional aluminum and titanium structural alloys showed that the properties of the low-cost, lightweight composites demonstrated very good potential for application to aerospace structures. Author

A85-37483* National Aeronautics and Space Administration. Lewis Research Center, Cleveland, Ohio.
HIGH TEMPERATURE METAL AND CERAMIC COMPOSITES
R. A. SIGNORELLI and J. A. DICARLO (NASA, Lewis Research Center, Cleveland, OH) Journal of Metals (ISSN 0148-6608), vol. 37, June 1985, p. 41, 42.

The Materials Division at NASA Lewis is engaged in research and development efforts on behalf of fiber-reinforced composite materials that are lighter, stiffer, and more structurally reliable than conventional monolithic alloys and ceramics in applications that range from the cryogenic to the refractory. Attention is presently given to metal matrix composites, in which high performance depends on stiff, strong and thermally stable large diameter fibers, with chemically stable interfacial bonding and good coefficient of thermal expansion matching between fibers and matrices, and to ceramic matrix composites, in which intermediate strength interfacial bonds must allow cracks to propagate through the matrix only, while retaining good load transfer characteristics between fiber and matrix. O.C.

A85-37484* National Aeronautics and Space Administration. Lewis Research Center, Cleveland, Ohio.
FIBERS FOR STRUCTURALLY RELIABLE METAL AND CERAMIC COMPOSITES
J. A. DICARLO (NASA, Lewis Research Center, Ceramics Systems Branch, Cleveland, OH) Journal of Metals (ISSN 0148-6608), vol. 37, June 1985, p. 44-49. refs

In their current state of development, commercially available reinforcing fibers fail to meet the requirements formulated for metal or ceramic matrix composites of sufficient strength and toughness. Attention is presently given to criteria for high strength and toughness in metal and ceramic matrix composites, as well as the approach adopted in fiber evaluation as a result of studies at the NASA Lewis Research Center. Two areas of special interest have been strength improvement in large diameter boron fibers for tough, impact-resistant boron/aluminum composites, and the evaluation of SiC fibers as reinforcement in tough ceramic-matrix composites with service temperatures of the order of 1400 C. O.C.

A85-39215*# National Aeronautics and Space Administration. Lewis Research Center, Cleveland, Ohio.
INTERPLY LAYER DEGRADATION EFFECTS ON COMPOSITE STRUCTURAL RESPONSE
C. C. CHAMIS (NASA, Lewis Research Center, Cleveland, OH) and G. C. WILLIAMS Journal of Aircraft (ISSN 0021-8669), vol. 22, July 1985, p. 573-580. Previously cited in issue 05, p. 571, Accession no. A85-16096.

A85-41127* National Aeronautics and Space Administration. Lewis Research Center, Cleveland, Ohio.
A STUDY OF INTERPLY LAYER EFFECTS ON THE FREE EDGE STRESS FIELD OF ANGLEPLIED LAMINATES
P. L. N. MURTHY and C. C. CHAMIS (NASA, Lewis Research Center, Cleveland, OH) (George Washington University and NASA, Symposium on Advances and Trends in Structures and Dynamics, Washington, DC, Oct. 22-25, 1984) Computers and Structures (ISSN 0045-7949), vol. 20, no. 1-3, 1985, p. 431-441. Previously announced in STAR as N85-15822. refs

The general-purpose finite-element program MSC/NASTRAN is used to study the interply layer effects on the free-edge stress field of symmetric angleplied laminates subjected to uniform tensile stress. The free-edge region is modeled as a separate substructure (superelement) which enables easy mesh refinement and provides the flexibility to move the superelement along the edge. The results indicate that the interply layer reduces the stress intensity significantly at the free edge. Another important observation of the study is that the failures observed near free edges of these types of laminates could have been caused by the interlaminar shear stresses. Author

A85-46543* National Aeronautics and Space Administration. Lewis Research Center, Cleveland, Ohio.
IMPACT RESISTANCE OF FIBER COMPOSITES - ENERGY-ABSORBING MECHANISMS AND ENVIRONMENTAL EFFECTS
C. C. CHAMIS and J. H. SINCLAIR (NASA, Lewis Research Center, Cleveland, OH) IN: Recent advances in composites in the United States and Japan; Proceedings of the Symposium, Hampton, VA, June 6-8, 1983 . Philadelphia, PA, ASTM, 1985, p. 326-345. Previously announced in STAR as N84-24712. refs

Energy absorbing mechanisms were identified by several approaches. The energy absorbing mechanisms considered are those in unidirectional composite beams subjected to impact. The approaches used include: mechanic models, statistical models, transient finite element analysis, and simple beam theory. Predicted results are correlated with experimental data from Charpy impact tests. The environmental effects on impact resistance are evaluated. Working definitions for energy absorbing and energy releasing mechanisms are proposed and a dynamic fracture progression is outlined. Possible generalizations to angle-plied laminates are described. E.A.K.

A85-47022*# National Aeronautics and Space Administration. Lewis Research Center, Cleveland, Ohio.
TEN YEAR ENVIRONMENTAL TEST OF GLASS FIBER/EPOXY PRESSURE VESSELS
J. R. FADDOUL (NASA, Lewis Research Center, Cleveland, OH) AIAA, SAE, ASME, and ASEE, Joint Propulsion Conference, 21st, Monterey, CA, July 8-10, 1985. 10 p. Previously announced in STAR as N85-30034. refs
(AIAA PAPER 85-1198)

By the beginning of the 1970's composite pressure vessels had received a significant amount of development effort, and applications were beginning to be investigated. One of the first applications grew out of NASA Johnson Space Center efforts to develop a superior emergency breathing system for firemen. While the new breathing system provided improved wearer comfort and an improved mask and regulator, the primary feature was low weight which was achieved by using a glass fiber reinforced aluminum pressure vessel. Part of the development effort was to evaluate the long term performance of the pressure vessel and as a consequence, some 30 bottles for a test program were procured. These bottles were then provided to NASA Lewis Research Center where they were maintained in an outdoor environment in a pressurized condition for a period of up to 10 yr. During this period, bottles were periodically subjected to cyclic and burst testing. There was no protective coating applied to the fiberglass/epoxy composite, and significant loss in strength did occur as a result of the environment. Similar bottles stored indoors showed little, if any, degradation. This report contains a description of the pressure vessels, a discussion of the test program, data for each bottle, and appropriate plots, comparisons, and conclusions. Author

A85-47970* Martin Marietta Aerospace, Denver, Colo.
FIBERGLASS EPOXY LAMINATE FATIGUE PROPERTIES AT 300 AND 20 K
J. M. TOTH, JR., W. J. BAILEY, and D. A. BOYCE (Martin Marietta Aerospace, Denver, CO) IN: Fatigue at low temperatures; Proceedings of the Symposium, Louisville, KY, May 10, 1983 . Philadelphia, PA, ASTM, 1985, p. 163-172.
(Contract NAS3-23245)

A subcritical liquid hydrogen orbital storage and supply experiment is being designed for flight in the Space Shuttle cargo bay. The Cryogenic Fluid Management Experiment (CFME) includes a liquid hydrogen tank supported in a vacuum jacket by two fiberglass epoxy composite trunnion mounts. The ability of the CFME to last for the required seven missions depends primarily on the fatigue life of the composite trunnions at cryogenic temperatures. To verify the trunnion design and test the performance of the composite material, fatigue property data at 300 and 20 K were obtained for the specific E-glass fabric/S-glass unidirectional laminate that will be used for the CFME trunnions. The fatigue life of this laminate was greater at 20 K than at 300 K, and was satisfactory for the intended application. Author

N85-12095*# National Aeronautics and Space Administration. Lewis Research Center, Cleveland, Ohio.
HIGH PERFORMANCE FIBERS FOR STRUCTURALLY RELIABLE METAL AND CERAMIC COMPOSITES
J. A. DICARLO 1984 16 p refs Presented at a Conf. on High Performance Textiles Structures, Philadelphia, 6-8 Jun. 1984; sponsored by The Fiber Soc. and SAMPE
(NASA-TM-86878; E-2339; NAS 1.15:86878) Avail: NTIS HC A02/MF A01 CSCL 11D

Very few of the commercially available high performance fibers with low densities, high Young's moduli, and high tensile strengths possess all the necessary property requirements for providing either metal matrix composites (MMC) or ceramic matrix composites (CMC) with high structural reliability. These requirements are discussed in general and examples are presented of how these property guidelines are influencing fiber evaluation and improvement studies at NASA aimed at developing structurally reliable MMC and CMC for advanced gas turbine engines. A.R.H.

N85-12948*# National Aeronautics and Space Administration. Lewis Research Center, Cleveland, Ohio.
FUNDAMENTAL STUDIES OF COMPOSITE TOUGHNESS
K. J. BOWLES *In* NASA. Langley Research Center Tough Composite Mater. p 125-136 Dec. 1984
Avail: NTIS HC A17/MF A01 CSCL 11D

Evaluation of drop weight impact testing of neat resin and crossplied graphite fiber reinforced composites resulted in three conclusions: (1) during impact of cross-ply laminates, resin properties appear to influence the extent and mechanism of damage propagation; (2) by itself, neat resin strain to fracture is not a controlling influence on resin or composite fracture toughness; and (3) impact failure energy of neat resin plates can give a misleading indication of the resin contribution to composite impact behavior because of differences in the magnitude of diaphragm action in the two systems. Both geometric and composite constituent materials properties influence the drop weight impact resistance of crossplied composite plates. The matrix influence appears to be reflected in the incipient damage mechanism and the propagation of damage. M.G.

N85-14878*# National Aeronautics and Space Administration. Lewis Research Center, Cleveland, Ohio.
CREEP OF CHEMICALLY VAPOR DEPOSITED SIC FIBERS
J. A. DICARLO 1984 21 p refs Presented at the 8th Ann. Conf. on Composites and Advan. Ceram. Mater., Cocoa Beach, Fla., 15-18 Jan. 1984; sponsored by American Ceramic Society
(NASA-TM-86897; E-2372; NAS 1.15:86897) Avail: NTIS HC A02/MF A01 CSCL 11D

The creep, thermal expansion, and elastic modulus properties for chemically vapor deposited SiC fibers were measured between 1000 and 1500 C. Creep strain was observed to increase logarithmically with time, monotonically with temperature, and linearly with tensile stress up to 600 MPa. The controlling activation energy was 480 + or - 20 kJ/mole. Thermal pretreatments near 1200 and 1450 C were found to significantly reduce fiber creep. These results coupled with creep recovery observations indicate that below 1400 C fiber creep is anelastic with neglible plastic component. This allowed a simple predictive method to be developed for describing fiber total deformation as a function of time, temperature, and stress. Mechanistic analysis of the property data suggests that fiber creep is the result of beta-SiC grain boundary sliding controlled by a small percent of free silicon in the grain boundaries. Author

N85-14882*# National Aeronautics and Space Administration. Lewis Research Center, Cleveland, Ohio.
FABRICATION AND QUALITY ASSURANCE PROCESSES FOR SUPERHYBRID COMPOSITE FAN BLADES
R. F. LARK and C. C. CHAMIS 1983 15 p refs Presented at the 15th Ann. SAMPE Tech. Conf., Cincinnati, 4-5 Oct. 1983
(NASA-TM-83354; E-1611; NAS 1.15:83354) Avail: NTIS HC A02/MF A01 CSCL 11D

The feasibility of fabricating full-scale fan blades from superhybrid composites (SHC) for use large, commercial gas turbine engines was evaluated. The type of blade construction selected was a metal-spar/SHC-shell configuration, in which the outer shell was adhesively bonded to a short, internal, titanium spar. Various aspects of blade fabrication, inspection, and quality assurance procedures developed in the investigation are described. It is concluded that the SHC concept is feasible for the fabrication of prototype, full-scale, metal-spar/SHC-shell fan blades that have good structural properties and meet dimensional requirements.
R.S.F.

N85-15822*# National Aeronautics and Space Administration. Lewis Research Center, Cleveland, Ohio.
A STUDY OF INTERPLY LAYER EFFECTS ON THE FREE-EDGE STRESS FIELD OF ANGLEPLIED LAMINATES
P. L. N. MURTHY and C. C. CHAMIS 1984 31 p refs Presented at the Symp. on Adv. and Trends in Struct. Dyn., Washington, D.C., 22-25 Oct. 1984; sponsored by NASA and George Washington Univ.
(NASA-TM-86924; E-2201; NAS 1.15:86924) Avail: NTIS HC A03/MF A01 CSCL 11D

The general-purpose finite-element program MSC/NASTRAN is used to study the interply layer effects on the free-edge stress field of symmetric angleplied laminates subjected to uniform tensile stress. The free-edge region is modeled as a separate substructure (superelement) which enables easy mesh refinement and provides the flexibility to move the superelement along the edge. The results indicate that the interply layer reduces the stress intensity significantly at the free edge. Another important observation of the study is that the failures observed near free edges of these types of laminates could have been caused by the interlaminar shear stresses.
Author

N85-15823*# National Aeronautics and Space Administration. Lewis Research Center, Cleveland, Ohio.
DESIGN PROCEDURES FOR FIBER COMPOSITE STRUCTURAL COMPONENTS: PANELS SUBJECTED TO COMBINED IN-PLANE LOADS
C. C. CHAMIS 1985 29 p refs Presented at the 40th Ann. Conf. of the Society of the Plastics Industry (SPI) Reinforced Plastics/Composites Inst., Atlanta, 28 Jan. - 1 Feb. 1985
(NASA-TM-86909; E-2319; NAS 1.15:86909) Avail: NTIS HC A03/MF A01 CSCL 11D

Step by step procedures are described which can be used to design panels made from fiber composite angleplied laminates and subjected to combined in plane loads. The procedures are set up as a multistep sample design. Steps in the sample design procedure range from selection of the laminate configuration to the subsequent analyses required to check design requirements for: (1) displacement, (2) ply stresses, and (3) buckling. The sample design steps are supplemented with appropriate tabular and graphical data which can be used to expedite the design process.
Author

N85-21266* National Aeronautics and Space Administration. Lewis Research Center, Cleveland, Ohio.
THERMAL BARRIER COATING SYSTEM Patent
S. STECURA, inventor (to NASA) 27 Nov. 1984 7 p Filed 16 Aug. 1983 Supersedes N83-34014 (21 - 22, p 3601) Continuation-in-part of abandonded US Patent Appl. SN-375784, filed 6 May 1982
(NASA-CASE-LEW-13324-2; NAS 1.71:LEW-13324-2; US-PATENT-4,485,151; US-PATENT-APPL-SN-523297; US-PATENT-CLASS-428-633; US-PATENT-CLASS-428-656; US-PATENT-CLASS-428-678; US-PATENT-CLASS-428-679; US-PATENT-CLASS-428-680; US-PATENT-CLASS-428-681; US-PATENT-CLASS-428-682; US-PATENT-CLASS-428-683; US-PATENT-CLASS-428-684; US-PATENT-APPL-SN-375784) Avail: US Patent and Trademark Office CSCL 11D

A high temperature oxidation resistant, thermal barrier coating system is disclosed for a nickel cobalt, or iron base alloy substrate. An inner metal bond coating contacts the substrate, and a thermal barrier coating covers the bond coating. NiCrAlR, FeCrAlR, and CoCrAlR alloys are satisfactory as bond coating compositions where R=Y or Yb. These alloys contain, by weight, 24.9-36.7% chromium, 5.4-18.5% aluminum, and 0.05 to 1.55% yttrium or 0.05 to 0.53% ytterbium. The coatings containing ytterbium are preferred over those containing yttrium. An outer thermal barrier coating of partial stabilized zirconium oxide (zirconia) which is between 6% and 8%, by weight, of yttrium oxide (yttria) covers the bond coating. Partial stabilization provides a material with superior durability. Partially stabilized zirconia consists of mixtures of cubic, tetragonal, and monoclinic phases.
Official Gazette of the U.S. Patent and Trademark Office

N85-21267* National Aeronautics and Space Administration. Lewis Research Center, Cleveland, Ohio.
DIAMONDLIKE FLAKES Patent
B. A. BANKS, inventor (to NASA) 22 Jan. 1985 6 p Filed 19 Mar. 1984 Supersedes N84-22696 (22 - 13, p 1953) Continuation-in-part of US Patent-4,437,962, US Patent Appl. SN-495381, filed 17 May 1983
(NASA-CASE-LEW-13837-2; NAS 1.71:LEW-13837-2; US-PATENT-4,495,044; US-PATENT-APPL-SN-591089; US-PATENT-CLASS-204-192C; US-PATENT-CLASS-204-192R; US-PATENT-CLASS-204-192N; US-PATENT-CLASS-423-445; US-PATENT-CLASS-423-446; US-PATENT-CLASS-423-449; US-PATENT-CLASS-427-39; US-PATENT-4,437,962; US-PATENT-APPL-SN-495381) Avail: US Patent and Trademark Office CSCL 11D

A carbon coating was vacuum arc deposited on a smooth surface of a target which was simultaneously ion beam sputtered. The bombarding ions have sufficient energy to create diamond bonds. Spalling occurs as the carbon deposit thickens. The resulting diamond like carbon flakes improve thermal, electrical, mechanical, and tribological properties when used in aerospace structures and components.
Official Gazette of the U.S. Patent and Trademark Office

N85-21273*# National Aeronautics and Space Administration. Lewis Research Center, Cleveland, Ohio.
NONLINEAR ANALYSIS FOR HIGH-TEMPERATURE MULTILAYERED FIBER COMPOSITE STRUCTURES M.S. Thesis
D. A. HOPKINS Aug. 1984 120 p refs
(NASA-TM-83754; E-2242; NAS 1.15:83754) Avail: NTIS HC A06/MF A01 CSCL 11D

A unique upward-integrated top-down-structured approach is presented for nonlinear analysis of high-temperature multilayered fiber composite structures. Based on this approach, a special purpose computer code was developed (nonlinear COBSTRAN) which is specifically tailored for the nonlinear analysis of tungsten-fiber-reinforced superalloy (TFRS) composite turbine blade/vane components of gas turbine engines. Special features of this computational capability include accounting of; micro- and macro-heterogeneity, nonlinear (stess-temperature-time dependent) and anisotropic material behavior, and fiber degradation. A

demonstration problem is presented to mainfest the utility of the upward-integrated top-down-structured approach, in general, and to illustrate the present capability represented by the nonlinear COBSTRAN code. Preliminary results indicate that nonlinear COBSTRAN provides the means for relating the local nonlinear and anisotropic material behavior of the composite constituents to the global response of the turbine blade/vane structure.

Author

N85-27978*# National Aeronautics and Space Administration. Lewis Research Center, Cleveland, Ohio.

DESIGNING FOR FIBER COMPOSITE STRUCTURAL DURABILITY IN HYGROTHERMOMECHANICAL ENVIRONMENT

C. C. CHAMIS 1985 23 p refs Proposed for presentation at the 5th Intern. Conf. on Composite Mater., San Diego, Calif., 30 Jul. - 1 Aug. 1985; sponsored by American Society of Mining Engineers

(NASA-TM-87045; E-2606; NAS 1.15:87045) Avail: NTIS HC A02/MF A01 CSCL 11D

A methodology is described which can be used to design/analyze fiber composite structures subjected to complex hygrothermomechanical environments. This methodology includes composite mechanics and advanced structural analysis methods (finite element). Select examples are described to illustrate the application of the available methodology. The examples include: (1) composite progressive fracture; (2) composite design for high cycle fatigue combined with hot-wet conditions; and (3) general laminate design. E.A.K.

N85-30027* National Aeronautics and Space Administration. Lewis Research Center, Cleveland, Ohio.

ARC SPRAY FABRICATION OF METAL MATRIX COMPOSITE MONOTAPE Patent

L. J. WESTFALL, inventor (to NASA) 21 May 1985 7 p Filed 9 Dec. 1983

(NASA-CASE-LEW-13828-1; US-PATENT-4,518,625; US-PATENT-APPL-SN-560035; US-PATENT-CLASS-427-37; US-PATENT-CLASS-219-76.14; US-PATENT-CLASS-427-178; US-PATENT-CLASS-427-422) Avail: US Patent and Trademark Office CSCL 11D

Arc metal spraying is used to spray liquid metal onto an array of high strength fibers that were previously wound onto a large drum contained inside a controlled atmosphere chamber. This chamber is first evacuated to remove gaseous contaminants and then backfilled with a neutral gas up to atmospheric pressure. This process is used to produce a large size metal matrix composite monotape.

Official Gazette of the U.S. Patent and Trademark Office

N85-30034*# National Aeronautics and Space Administration. Lewis Research Center, Cleveland, Ohio.

TEN YEAR ENVIRONMENTAL TEST OF GLASS FIBER/EPOXY PRESSURE VESSELS

J. R. FADDOUL 1985 18 p refs Presented at the 21st Joint Propulsion Conf., Monterey, Calif., 8-10 Jul. 1985; sponsored by AIAA, SAE, ASME, and ASEE

(NASA-TM-87058; E-2625; NAS 1.15:87058) Avail: NTIS HC A02/MF A01 CSCL 11D

By the beginning of the 1970's composite pressure vessels had received a significant amount of development effort, and applications were beginning to be investigated. One of the first applications grew out of NASA Johnson Space Center efforts to develop a superior emergency breathing system for firemen. While the new breathing system provided improved wearer comfort and an improved mask and regulator, the primary feature was low weight which was achieved by using a glass fiber reinforced aluminum pressure vessel. Part of the development effort was to evaluate the long term performance of the pressure vessel and as a consequence, some 30 bottles for a test program were procured. These bottles were then provided to NASA Lewis Research Center where they were maintained in an outdoor environment in a pressurized condition for a period of up to 10 yr. During this period, bottles were periodically subjected to cyclic and burst testing. There was no protective coating applied to the fiberglass/epoxy composite, and significant loss in strength did occur as a result of the environment. Similar bottles stored indoors showed little, if any, degradation. This report contains a description of the pressure vessels, a discussion of the test program, data for each bottle, and appropriate plots, comparisons, and conclusions. R.J.F.

N85-30035*# Virginia Polytechnic Inst. and State Univ., Blacksburg.

A STUDY OF THE STRESS WAVE FACTOR TECHNIQUE FOR THE CHARACTERIZATION OF COMPOSITE MATERIALS Final Report

A. K. GOVADA, J. C. DUKE, JR., E. G. HENNEKE, II, and W. W. STINCHCOMB Feb. 1985 103 p refs

(Contract NAG3-172)

(NASA-CR-174870; NAS 1.26:174870; CCMS-84-13) Avail: NTIS HC A06/MF A01 CSCL 11D

This study has investigated the potential of the Stress Wave Factor as an NDT technique for thin composite laminates. The conventional SWF and an alternate method for quantifying the SWF were investigated. Agreement between the initial SWF number, ultrasonic C-scan, inplane displacements as obtained by full field moire interferometry, and the failure location have been observed. The SWF number was observed to be the highest when measured along the fiber direction and the lowest when measured across the fibers. The alternate method for quantifying the SWF used square root of the zeroth moment (square root of M sub o) of the frequency spectrum of the received signal as a quantitative parameter. From this study it therefore appears that the stress wave factor has an excellent potential to monitor damage development in thin composite laminates. B.W.

N85-30037*# Massachusetts Inst. of Tech., Cambridge. Dept. of Materials Science and Engineering.

STRUCTURAL CHARACTERISTICS OF HIGH TEMPERATURE COMPOSITES Progress Report, Mar. 1984 - Feb. 1985

J. F. MANDELL 1985 23 p refs

(Contract NAG3-377)

(NASA-CR-175998; NAS 1.26:175998) Avail: NTIS HC A02/MF A01 CSCL 11D

A progress report is presented for research carried from March 1984 through February 1985. A tensile test method has been developed which should give tensile and simulated shear (+ or - 45 deg) data for fiber composites up to 1000 C. Longitudinal and some transverse stress-strain data have been obtained for a glass matrix/Nicalon fiber system up to the matrix limiting temperature of 600 C. This demonstrates the functioning of the test method and the high temperature test facility which has been established on this grant. Transverse and longitudinal compression tests have been run, mostly in an end loaded configuration. A more satisfactory compression test is still required, and is under development.

B.W.

N85-32148*# National Aeronautics and Space Administration. Lewis Research Center, Cleveland, Ohio.

GRAPHITE/PMR POLYIMIDE COMPOSITES WITH IMPROVED TOUGHNESS

R. D. VANNUCCI and K. J. BOWLES 1985 15 p refs Proposed for presentation at the 17th Natl. SAMPE Tech. Conf., Kiamesha Lake, N.Y., 22-24 Oct. 1985

(NASA-TM-87081; E-2661; NAS 1.15:87081) Avail: NTIS HC A02/MF A01 CSCL 11D

The toughness of composites made with modified PMR (polymerization of monomer reactants) polyimides and Celion 6000 graphite fibers was studied. Various types/levels of monomer reactants containing flexible links were incorporated into PMR resin compositions used to prepare composites. The composites were evaluated for toughness using instrumented drop weight and 10 deg off axis tensile tests at room temperature, and for strength using flexure and short beam shear tests at room temperature and at elevated temperature. The effect of resin composition on

composite processability, thermo-oxidative stability, toughness and mechanical properties are discussed. Author

N85-34223*# National Aeronautics and Space Administration. Lewis Research Center, Cleveland, Ohio.
MECHANICAL PROPERTIES OF SIC FIBER-REINFORCED REACTION-BONDED SI3N4 COMPOSITES
R. T. BHATT 1985 14 p refs Presented at the 21st Univ. Conf. on Ceram. Sci., University Park, Pa., 17-19 Jul. 1985; sponsored by Pennsylvania State Univ. Prepared in cooperation with Army Aviation Research and Development Command, Cleveland
(NASA-TM-87085; E-2671; NAS 1.15:87085; USAAVSCOM-TR-85-C-14) Avail: NTIS HC A02/MF A01 CSCL 11D

The room temperature mechanical and physical properties of silicon carbide fiber reinforced reaction-bonded silicon nitride composites (SiC/RBSN) have been evaluated. The composites contained 23 and 40 volume fraction of aligned 140 micro m diameter chemically vapor deposited SiC fibers. Preliminary results for composite tensile and bend strengths and fracture strain indicate that the composites displayed excellent properties when compared with unreinforced RBSN of comparable porosity. Fiber volume fraction showed little influence on matrix first cracking strain but did influence the stressed required for matrix first cracking and for ultimate composite fracture strength. It is suggested that by reducing matrix porosity and by increasing the volume fraction of the large diameter SiC fiber, it should be possible to further improve the composite stress at which the matrix first cracks. Author

N85-35233* National Aeronautics and Space Administration. Lewis Research Center, Cleveland, Ohio.
THERMAL BARRIER COATING SYSTEM Patent
S. STECURA, inventor (to NASA) 13 Aug. 1985 5 p Filed 14 Aug. 1984 Supersedes N84-33595 (22 - 23, p 3724) Continuation-in-part of US Patent-4,485,151, US Patent-Appl-SN-523297, filed 16 Aug. 1983, and continuation-in-part of abandoned US Patent-Appl-SN-375784, filed 6 May 1982
(NASA-CASE-LEW-14057-1; US-PATENT-4,535,033; US-PATENT-4,485,151; US-PATENT-APPL-SN-640712; US-PATENT-APPL-SN-523297; US-PATENT-APPL-SN-375784; US-PATENT-CLASS-428-633; US-PATENT-CLASS-428-656; US-PATENT-CLASS-428-678; US-PATENT-CLASS-428-679; US-PATENT-CLASS-428-680; US-PATENT-CLASS-428-681; US-PATENT-CLASS-428-682) Avail: US Patent and Trademark Office CSCL 11D

An oxide thermal barrier coating comprises ZrO3-Yb2O3 that is plasma sprayed onto a previously applied bond coating. The zirconia is partially stabilized with about 124 w/c ytterbia to insure cubic, monoclinic, and terragonal phases.
Official Gazette of the U.S. Patent and Trademark Office

25

INORGANIC AND PHYSICAL CHEMISTRY

Includes chemical analysis, e.g., chromatography; combustion theory; electrochemistry; and photochemistry.

A85-11892* EIC, Inc., Norwood, Mass.
MODERATE TEMPERATURE SODIUM CELLS. V - DISCHARGE REACTIONS AND RECHARGEABILITY OF NIS AND NIS2 POSITIVE ELECTRODES IN MOLTEN NAALCL4
K. M. ABRAHAM and J. E. ELLIOT (EIC Laboratories, Inc., Norwood, MA) Electrochemical Society, Journal (ISSN 0013-4651), vol. 131, Oct. 1984, p. 2211-2217. refs
(Contract NAS3-21726)

NiS2 and NiS have been characterized as high energy density rechargeable positive electrodes for moderate-temperature Na batteries of the configuration, Na(1)/beta double prime-Al2O3/NaAlCl4(1), NiSx. The batteries operate in the temperature range 170 - 190 C. Positive electrode reactions during discharge/charge cycles have been characterized. Excellent rechargeability of the batteries has been demonstrated by extended cell cycling. A Na/NiS2 cell, operating at 190 C, exceeded 600 deep discharge/charge cycles with practically no capacity deterioration. The feasibility of secondary Na/NiSx batteries with specific energies equal to or greater than 50 Wh/lb and cycle lifes exceeding 1000 deep discharge/charge cycles has been demonstrated. Author

A85-11897* National Aeronautics and Space Administration. Lewis Research Center, Cleveland, Ohio.
REACTIONS OF NACL WITH GASEOUS SO3, SO2, AND O2
W. L. FIELDER, C. A. STEARNS, and F. J. KOHL (NASA, Lewis Research Center, Cleveland, OH) Electrochemical Society, Journal (ISSN 0013-4651), vol. 131, Oct. 1984, p. 2414-2417. Previously announced in STAR as N83-29358. refs

Hot corrosion of gas turbine engine components involves deposits of Na2SO4 which are produced by reactions between NaCl and oxides of sulfur. For the present investigation, NaCl single crystals were exposed at 100 to 850 C to gaseous mixtures of SO3, SO2, and O2. The products formed during this exposure depend, primarily, on the temperatures. The four product films were: NaCl-SO3; Na2S2O7; Na2SO4; and NaCl-Na2SO4. The kinetics of the reactions were measured. Author

A85-12713*# General Electric Co., Schenectady, N. Y.
PREDICTION OF AN AXISYMMETRIC COMBUSTING FLOW
S. M. CORREA (General Electric Co., Schenectady, NY) AIAA Journal (ISSN 0001-1452), vol. 22, Nov. 1984, p. 1602-1608. Previously cited in issue 16, p. 2326, Accession no. A83-36315. refs
(Contract NAS3-23525)

A85-12890* Louisiana State Univ., Baton Rouge.
SYSTEMATIC OPTIMIZATION OF A DETAILED KINETIC MODEL USING A METHANE IGNITION EXAMPLE
M. FRENKLACH (Louisiana State University, Baton Rouge, LA) Combustion and Flame (ISSN 0010-2180), vol. 58, Oct. 1984, p. 69-72. refs
(Contract NAG3-477)

An approach to the systematic optimization of a large-scale dynamic model is proposed which consists in parameterization of simulation results as response surfaces. The optimization procedure is carried out using a second-order orthogonal design. The approach proposed here is demonstrated by an example involving the shock-initiated ignition of methane. V.L.

A85-13092*# Kentucky Univ., Lexington.
GRAVITATIONAL EFFECTS ON FLAMES SPREADING OVER THICK SOLID SURFACES
M. VEDHA-NAYAGAM and R. A. ALTENKIRCH (Kentucky, University, Lexington, KY) International Astronautical Federation, International Astronautical Congress, 35th, Lausanne, Switzerland, Oct. 7-13, 1984. 8 p. refs
(Contract NAG3-258)
(IAF PAPER 84-154)

A theoretical model for the downward spread of a flame in the gas over a semi-infinitely thick fuel bed is presented. Gas-phase chemistry is assumed to proceed at an infinite rate while the fuel bed is taken to pyrolyze at the surface in an Arrhenius fashion. Spread rates and flame shapes are computed for two different ambient oxygen concentrations for gravitational accelerations both below and above that of the earth. Predicted spread rates decrease and actual flame size increases with decreasing gravity. Results agree favorably with available, experimental results and expected results from reduced gravity experimentation. Author

A85-15614* Stonehart Associates, Inc., Madison, Conn.
ELECTROCATALYST ADVANCES FOR HYDROGEN OXIDATION IN PHOSPHORIC ACID FUEL CELLS
P. STONEHART (Stonehart Associates, Inc., Madison, CT) International Journal of Hydrogen Energy (ISSN 0360-3199), vol. 9, no. 11, 1984, p. 921-928.
(Contract DE-AC03-78ET-15365; DEN3-176)

The important considerations that presently exist for achieving commercial acceptance of fuel cells are centered on cost (which translates to efficiency) and lifetime. This paper addresses the questions of electrocatalyst utilization within porous electrode structures and the preparation of low-cost noble metal electrocatalyst combinations with extreme dispersions of the metal. Now that electrocatalyst particles can be prepared with dimensions of 10 A, either singly or in alloy combinations, a very large percentage of the noble metal atoms in a crystallite are available for reaction. The cost savings for such electrocatalysts in the present commercially driven environment are considerable. Author

A85-19548*# Washington Univ., Seattle.
DIRECT NUMERICAL SIMULATIONS OF A REACTING MIXING LAYER WITH CHEMICAL HEAT RELEASE
P. A. MCMURTRY, W.-H. JOU, R. W. METCALFE (Flow Industries, Inc., Kent, WA), and J. J. RILEY (Flow Industries, Inc., Kent; Washington, University, Seattle, WA) American Institute of Aeronautics and Astronautics, Aerospace Sciences Meeting, 23rd, Reno, NV, Jan. 14-17, 1985. 9 p. refs
(Contract NAS3-24229)
(AIAA PAPER 85-0143)

In order to study the coupling between chemical heat release and fluid dynamics, direct numerical simulations of a chemically reacting mixing layer with heat release are performed. The fully compressible equations as well as an approximate set of equations that is asymptotically valid for low-Mach-number flows are treated. These latter equations have the computational advantage that high-frequency acoustic waves have been filtered out, allowing much larger time steps to be taken in the numerical solution procedure. A detailed derivation of these equations along with an outline of the numerical solution technique is given. Simulation results indicate that the rate of chemical product formed, the thickness of the mixing layer, and the amount of mass entrained into the layer all decrease with increasing rates of heat release. Author

A85-19550*# National Aeronautics and Space Administration. Lewis Research Center, Cleveland, Ohio.
FLAME FLASHBACK IN A PREMIXED DUMP COMBUSTOR
M. P. PROCTOR (Sverdrup Technology, Inc., Cleveland, OH), D. N. ANDERSON (NASA, Lewis Research Center, Cleveland, OH), and J. S. TIEN (Case Western Reserve University, Cleveland, OH) American Institute of Aeronautics and Astronautics, Aerospace Sciences Meeting, 23rd, Reno, NV, Jan. 14-17, 1985. 11 p. refs
(Contract NAG3-290)
(AIAA PAPER 85-0145)

A stainless steel, rectangular center-dump, premixed-prevaporized combustor was used at the NASA Lewis Research Center to study flashback in controlled conditions simulating gas turbine combustor operations under steady-state and transient conditions. The combustor allowed visual access to the combustion area, and was operated at inlet air temperatures from 600 to 850 K, premixer wall temperatures from 450 to 900 K, and average premixer velocity from 40 to 80 ft/s. A parametric study revealed a slight decrease in the flashback equivalence ratio as the inlet air temperatures increased. It also indicated that the premixer wall temperature and premixer velocity are not governing parameters of flashback. It is suggested that flashback occurs through the premixer wall boundary layer flow reversal caused by combustion instability. L.T.

A85-19607*# National Aeronautics and Space Administration. Lewis Research Center, Cleveland, Ohio.
INTEGRATING CHEMICAL KINETIC RATE EQUATIONS BY SELECTIVE USE OF STIFF AND NONSTIFF METHODS
K. RADHAKRISHNAN (NASA, Lewis Research Center, Cleveland, OH; Michigan, University, Ann Arbor, MI) American Institute of Aeronautics and Astronautics, Aerospace Sciences Meeting, 23rd, Reno, NV, Jan. 14-17, 1985. 11 p. refs
(AIAA PAPER 85-0237)

The effect of switching between nonstiff and stiff methods on the efficiency of algorithms for integrating chemical kinetic rate equations is presented. Different integration methods are tested by application of the packaged code LSODE to four practical combustion kinetics problems. The problems describe adiabatic, homogeneous gas-phase combustion reactions. It is shown that selective use of nonstiff and stiff methods in different regimes of a typical batch combustion problem is faster than the use of either method for the entire problem. The implications of this result to the development of fast integration techniques for combustion kinetic rate equations are discussed. Author

A85-19665*# Pennsylvania State Univ., University Park.
DROP-TURBULENCE INTERACTIONS IN A DIFFUSION FLAME
J.-S. SHUEN (Sverdrup Technology, Inc., Cleveland, OH; Pennsylvania State University, University Park, PA), A. S. P. SOLOMON (GM Research Laboratories, Warren, MI; Pennsylvania State University, University Park, PA), and G. M. FAETH (Pennsylvania State University, University Park, PA) American Institute of Aeronautics and Astronautics, Aerospace Sciences Meeting, 23rd, Reno, NV, Jan. 14-17, 1985. 12 p. refs
(Contract NAG3-190)
(AIAA PAPER 85-0319)

A monodisperse stream of methanol drops injected along the axis of a turbulent, methane-fueled diffusion flame burning in still air is studied experimentally and theoretically, in order to determine mean and fluctuating phase velocities, mean drop number flux, drop size distributions, and mean gas phase temperature. Measured values were compared with the predictions of two separated flow analyses, namely deterministic separated flow and stochastic separated flow. The stochastic analysis yielded the best agreement with measurements, due to its providing for the turbulent dispersion of drops. O.C.

A85-19666*# Flow Research, Inc., Kent, Wash.
DIRECT SIMULATIONS OF CHEMICALLY REACTING TURBULENT MIXING LAYERS
J. J. RILEY (Flow Research Co., Kent; Washington, University, Seattle, WA) and R. W. METCALFE (Flow Research Co., Kent, WA) American Institute of Aeronautics and Astronautics, Aerospace Sciences Meeting, 23rd, Reno, NV, Jan. 14-17, 1985. 16 p. refs
(Contract NAS3-23531)
(AIAA PAPER 85-0321)

The results of direct numerical simulations of chemically reacting mixing layers are presented. The reaction considered is a binary, irreversible reaction with no heat release, so that only the effect of the turbulence on the chemical reaction is investigated. The simulation results are shown to be consistent with similarity theory, and are found to be in approximate agreement with laboratory data, even though there are no adjustable constants in the method. Author

A85-23192*# Massachusetts Inst. of Tech., Cambridge.
METHANOL AS A SOOT REDUCER IN A TURBULENT SWIRLING BURNER
A. J. IZQUIERDO (Intevep, S. A., Venezuela) and D. P. HOULT (MIT, Cambridge, MA) American Society of Mechanical Engineers and Institute of Electrical and Electronics Engineers, Joint Power Generation Conference, Toronto, Canada, Oct. 1-4, 1984. 6 p. Research supported by Intevep, S.A. refs
(Contract NCC3-15)
(ASME PAPER 84-JPGC-GT-2)

The combined effect of using methanol as a fuel additive together with a prototype multifuel injector has been evaluated with regard to soot formation in a tubular laboratory burner with a turbulent swirl stabilized diffusion flame. Kerosene, ERBS fuel and Blending Stock with approximately 14,12.8 and 10.3 wt pct of hydrogen respectively were characterized in terms of soot loading at the axial positions Z/D = 2.5 and 4.0 and normalized radius r/R = + or 0.67. Mixtures of ERBS fuel and Blending Stock with 15 and 7.5 wt pct of methanol were also characterized in the same way. Measurements with the plain fuels showed a drastic reduction in soot formation, in the order of one hundred and fifty fold decrease, due to the new injector design. Further reductions by a factor of 2 and 1.5 were accomplished with the mixtures of 15 and 7.5 wt pct of methanol respectively. Author

A85-23199*# National Aeronautics and Space Administration. Lewis Research Center, Cleveland, Ohio.
EFFECT OF GRAVITY ON HALOGENATED HYDROCARBON FLAME RETARDANT EFFECTIVENESS
P. D. RONNEY (NASA, Lewis Research Center, Cleveland, OH) International Astronautical Federation, International Astronautical Congress, 35th, Lausanne, Switzerland, Oct. 7-13, 1984. 13 p. Previously announced in STAR as N84-33536. refs
(IAF PAPER 84-156)

Flammability limits, burning velocities, and minimum ignition energies under initially quiescent conditions were measured for stoichiometric and fuel-lean methane-, ethane-, and propane-air mixtures containing varying concentrations of Halon 1301. The characteristics of near-limit flames were strongly affected by fuel type but not Halon concentration. The conclusions were that the mechanism of the flammability limits was affected by fuel type but not Halon concentration, that the zero-g flammability limit is probably related to a stability criterion which is affected mostly by the molecular diffusion characteristics of the reactant gases and is mostly independent of chemical kinetics, and that the one-g upward flammability and ignition limits provide adequate criteria for safety at one-g and zero-g for both uninhibited and inhibited mixtures. Author

A85-33570* National Aeronautics and Space Administration. Lewis Research Center, Cleveland, Ohio.
HIGH TEMPERATURE OXIDATION OF PROPENE
A. BURCAT (NASA, Lewis Research Center, Cleveland, OH; Technion Israel Institute of Technology, Haifa, Israel) and K. RADHAKRISHNAN (NASA, Lewis Research Center, Cleveland, OH; Michigan, University, Ann Arbor, MI) Combustion and Flame (ISSN 0010-2180), vol. 60, May 1985, p. 157-169. refs
(Contract NAG3-147; NAG3-294)

An ignition delay correlation is established for propene-oxygen-argon mixtures on the basis of over 100 experiments with component concentrations being in the ranges of 0.6-1.6 percent for propene and 2.7-14.4 percent for oxygen diluted in argon. Temperatures in the range of 1274-1840 K were achieved, with average initial pressures ranging from 50 to 133 torr. Furthermore, standard numerical solutions were obtained using LSODE and CHEMEQ integration techniques, covering 59 reactions and 29 species. The partial agreement between the results indicates that the scheme used is adequate but incomplete. Two possible oxidative path-determining loops were identified, though neither was found conclusively superior to the other. L.T.

A85-33785* Spring Arbor Coll., Mich.
CHEMICAL AND ELECTROCHEMICAL BEHAVIOR OF THE CR(III)/CR(II) HALF-CELL IN THE IRON-CHROMIUM REDOX ENERGY STORAGE SYSTEM
D. A. JOHNSON (Spring Arbor College, Spring Arbor, MI) and M. A. REID (NASA, Lewis Research Center, Cleveland, OH) Electrochemical Society, Journal (ISSN 0013-4651), vol. 132, May 1985, p. 1058-1062. refs
(Contract DE-AI04-80AL-12726)

The Cr(III) complexes present in the acidified chromium solutions used in the iron-chromium redox energy storage system have been isolated and identified as Cr(H2O)6(3+) and Cr(H2O)5Cl(2+) by ion-exchange chromatography and visible spectrophotometry. The cell reactions during charge-discharge cycles have been followed by means of visible spectrophotometry. The spectral bands were resolved into component peaks and concentrations of the Cr(III) species calculated using Beer's law. During the charge mode, Cr(H2O)5Cl(2+) is reduced to Cr(H2O)5Cl(+), and during the discharge mode Cr(H2O)5Cl(+) is oxidized back to Cr(H2O)5Cl(2+). Electrode potential measurements also support this interpretation. Hysteresis effects in the charge-discharge curves can be explained by the slow attainment of equilibrium between Cr(H2O)6(3+) and Cr(H2O)5Cl(2+). Author

A85-41633* National Aeronautics and Space Administration. Lewis Research Center, Cleveland, Ohio.
AES AND LEED STUDY OF THE ZINC BLENDE SIC(100) SURFACE
M. DAYAN (NASA, Lewis Research Center, Cleveland, OH) Journal of Vacuum Science and Technology A (ISSN 0734-2101), vol. 3, Mar.-Apr. 1985, p. 361-366. refs

Auger and LEED measurements have been carried out on the (100) surface of zinc blende SiC. Two different phases of the clean surface, in addition to two kinds of oxygen-covered surfaces, have been obtained, identified, and discussed. In the oxygen-covered surface, the oxygen is bonded to the Si. The carbon-rich phase is reconstructed (2 x 1), similar to the (100) clean surfaces of Si, Ge, and diamond. The Si-topped surface is reconstructed. A model of alternating Si dimers is suggested for this surface. Author

A85-42571*# Cornell Univ., Ithaca, N.Y.
COMBUSTION EFFICIENCY OF A PREMIXED CONTINUOUS FLOW COMBUSTOR
M. S. ANAND and F. C. GOULDIN (Cornell University, Ithaca, NY) ASME, Transactions, Journal of Engineering for Gas Turbines and Power (ISSN 0022-0825), vol. 107, July 1985, p. 695-705. refs
(Contract NSG-3019)

Exhaust gas temperature, velocity, and composition measurements at various radial locations at the combustor exit are presented for a swirling-flow continuous combustor of a confined concentric jet configuration operating on premixed propane or methane and air. The main objective of the study is to determine the effect of fuel substitution and of changes in outer flow swirl conditions on the combustor performance. It is found that there is no difference in observed properties for propane and methane firing; the use of either of the fuels results in nearly the same exit temperature and velocity profiles and the same efficiency for a given operating condition. A mechanism for combustion is proposed which explains qualitatively the changes in efficiency and pollutant emissions observed with changing swirl. V.L.

A85-47320* California Inst. of Tech., Pasadena.
GROWTH OF A DIFFUSION FLAME IN THE FIELD OF A VORTEX
F. E. MARBLE (California Institute of Technology, Pasadena) IN: Recent advances in the aerospace sciences . New York, Plenum Press, 1985, p. 395-413. refs
(Contract AF-AFOSR-80-0265; NAG3-70)

In the present study of the growth of a diffusion flame in the field of a vortex, the motion in the core is converted into a solid

body rotation. The flame extension and distortion kinematics are presented, and the effect of the local flow field on local flame structure is analyzed in detail. The combustion field is found to consist of a totally reacted core region whose radius is time-dependent, and an external flame region which consists of a pair of spiral arms that extend at large radii toward their original positions on the horizontal axis. Two similarity rules are formulated which are independent of kinematic viscosity. O.C.

A85-48493* Case Western Reserve Univ., Cleveland, Ohio.
MECHANISM FOR CHELATED SULFATE FORMATION FROM SO2 AND BIS (TRIPHENYLPHOSPHINE) PLATINUM
S. P. MEHANDRU and A. B. ANDERSON (Case Western Reserve University, Cleveland, OH) Inorganic Chemistry (ISSN 0020-1669), vol. 24, no. 16, 1985, p. 2570-2573. refs
(Contract NAG3-341)

Structure and energy surface calculations using the atom superposition and electron delocalization molecular orbital theory show that the first step in the reaction between SO2 and the dioxygen complex (PPh3)2PtO2 is the coordination of SO2 with one oxygen atom of the complex, followed by metal-oxygen bond breaking and reorientation, leading to a five-membered cyclic structure. This then rearranges to form the bidentate coordinated sulfate. Alternative pathways are considered and are found to be less favorable. Author

A85-48513* Case Western Reserve Univ., Cleveland, Ohio.
MECHANISM FOR FORMING HYDROGEN CHLORIDE AND SODIUM SULFATE FROM SULFUR TRIOXIDE, WATER, AND SODIUM CHLORIDE
A. B. ANDERSON (Case Western Reserve University, Cleveland, OH) American Chemical Society, Journal (ISSN 0002-7863), vol. 106, no. 21, 1984, p. 6262-6265. refs
(Contract NAG3-341)

A molecular orbital study of sodium sulfate and hydrogen chloride formation from sulfur trioxide, water, and sodium chloride shows no activation barrier, in agreement with recent experimental work of Kohl, Fielder, and Stearns. Two overall steps are found for the process. First, gas-phase water reacts with sulfur trioxide along a pathway involving a linear O-H-O transition state yielding closely associated hydroxyl and bisulfite which rearrange to become a hydrogen sulfate molecule. Then the hydrogen sulfate molecule transfers a hydrogen atom to a surface chloride in solid sodium chloride while an electron and a sodium cation simultaneously transfer to yield sodium bisulfate and gas-phase hydrogen chloride. This process repeats. Both of these steps represent well-known reactions for which mechanisms have not been previously determined. Author

N85-10138*# National Aeronautics and Space Administration. Lewis Research Center, Cleveland, Ohio.
ANALYSIS OF GLOW DISCHARGES FOR UNDERSTANDING THE PROCESS OF FILM FORMATION
M. VENUGOPALAN (Univ. of Western Illinois, Macomb) and R. AVNI Washington Oct. 1984 127 p refs Submitted for publication
(NASA-TM-83750; E-2231; NAS 1.15:83750) Avail: NTIS HC A07/MF A01 CSCL 07D

The physical and chemical processes which occur during the formation of different types of films in a variety of glow discharge plasmas are discussed. Emphasis is placed on plasma diagnostic experiments using spectroscopic methods, probe analysis, mass spectrometric sampling and magnetic resonance techniques which are well suited to investigate the neutral and ionized gas phase species as well as some aspects of plasma surface interactions. The results on metallic, semi-conducting and insulating films are reviewed in conjunction with proposed models and the problem encountered under film deposition conditions. It is concluded that the understanding of film deposition process requires additional experimental information on plasma surface interactions of free radicals and the synergetic effects where photon, electron and ion bombardment change the reactivity of the incident radical with the surface. Author

N85-11149*# Illinois Univ., Urbana-Champaign. Dept. of Aeronautical and Astronautical Engineering.
THE MECHANISMS OF FLAME HOLDING IN THE WAKE OF A BLUFF BODY Final Report
R. A. STREHLOW and S. MALIK 30 Oct. 1984 194 p refs
(Contract NAG3-60)
(NASA-CR-174058; NAS 1.26:174058) Avail: NTIS HC A09/MF A01 CSCL 21B

The flame holding mechanism for lean methane and lean propane air flames is examined under conditions where the recirculation zone is absent. The holding process is studied in detail in an attempt to determine the mechanism of flame holding and also the conditions where this mechanism is viable and when it fails and blow off occurs. Inverted flames held in the wake of a flat strip are studied. The velocity flow field is determined using a Laser Doppler Velocimetry technique. Equation of continuity is used to calculate the flame temperature from the change in area of flow streamlines before and after the flame. For methane air flame the controlling factor for blow off is incomplete reaction due to higher blowing rate leading to reduced residence time in the reaction zone. M.A.C.

N85-13889*# National Aeronautics and Space Administration. Lewis Research Center, Cleveland, Ohio.
ELECTROCHEMISTRY AND STORAGE
L. H. THALLER *In its* Space Power p 95-99 Apr. 1984
Avail: NTIS HC A14/MF A01 CSCL 07D

The term electrochemistry implies the use of devices that convert chemical energy into electrical energy and sometimes vice versa. These devices are usually composed of some number of individual cells that are connected together to form a battery. In the cases where these devices cannot be electrically recharged they are usually referred to as primary batteries, whereas if these batteries can be charged and recharged repeatedly, they are called secondary batteries. The past and present uses of primary and secondary batteries in aerospace applications are discussed. R.J.F.

N85-21283*# Illinois Univ., Urbana. Dept. of Aeronautical and Astronautical Engineering.
BEHAVIOR OF THE LEAN METHANE-AIR FLAME AT ZERO-GRAVITY Final Report, Nov. 1983 - Dec. 1984
K. A. NOE and R. A. STREHLOW Feb. 1985 48 p refs
(Contract NCC3-35)
(NASA-CR-175586; NAS 1.26:175586; AAE-85-2; UILU-ENG-85-0502) Avail: NTIS HC A03/MF A01 CSCL 21B

A special rig was designed and constructed to be compatible with the NASA Lewis Research Center Airborne Research Laboratory to allow the study of the effect of gravity on the behavior of lean limit in a standard 50.4 mm (2 in.) internal diameter tube when the mixtures are ignited at the open end and propagate towards the closed end of the tube. The lean limit at zero gravity was found to be 5.10% methane and the flame was found to extenguish in a manner previously observed for downward propagating flames at one g. It was observed that g-jitter could be maintained at less than + or 0.04 g on most zero g trajectories. All of propagating lean limit flames were found to be sporadically cellularly unstable at zero g. There was no observable correlation between the occurrence of g-jitter and the lean limit, average propagation speed of the flame through the tube or the occurrence of cellular instability. B.W.

N85-22644*# National Aeronautics and Space Administration. Lewis Research Center, Cleveland, Ohio.
FORMATION OF HIGH MOLECULAR WEIGHT PRODUCTS FROM BENZENE DURING BOUNDARY LUBRICATION
W. MORALES Apr. 1985 18 p refs
(NASA-TM-86966; E-2433; NAS 1.15:86966) Avail: NTIS HC A02/MF A01 CSCL 07D

High molecular weight products were detected on the wear track of an iron disk at the end of a sliding friction and wear test using benzene as a lubricant. Size exclusion chromagography in conjunction with UV analysis gave evidence that the high molecular

weight products are polyphenyl ether type substances. Organic electrochemistry was used to elucidate the possible surface reaction mechanisms. Author

N85-23941*# National Aeronautics and Space Administration. Lewis Research Center, Cleveland, Ohio.
APPLICATIONS OF HIGH PRESSURE DIFFERENTIAL SCANNING CALORIMETRY TO AVIATION FUEL THERMAL STABILITY RESEARCH Final Report
M. C. NEVEU (State Univ. of New York, Fredonia) and D. P. STOCKER Apr. 1985 25 p refs
(NASA-TM-87002; E-2547; NAS 1.15:87002) Avail: NTIS HC A02/MF A01 CSCL 21D

High pressure differential scanning calorimetry (DSC) was studied as an alternate method for performing high temperature fuel thermal stability research. The DSC was used to measure the heat of reaction versus temperature of a fuel sample heated at a programmed rate in an oxygen pressurized cell. Pure hydrocarbons and model fuels were studied using typical DSC operating conditions of 600 psig of oxygen and a temperature range from ambient to 500 C. The DSC oxidation onset temperature was determined and was used to rate the fuels on thermal stability. Kinetic rate constants were determined for the global initial oxidation reaction. Fuel deposit formation is measured, and the high temperature volatility of some tetralin deposits is studied by thermogravimetric analysis. Gas chromatography and mass spectrometry are used to study the chemical composition of some DSC stressed fuels. E.A.K.

N85-25444*# Louisiana State Univ., Baton Rouge. Dept. of Chemical Engineering.
SHOCK TUBE STUDY OF THE FUEL STRUCTURE EFFECTS ON THE CHEMICAL KINETIC MECHANISMS RESPONSIBLE FOR SOOT FORMATION, PART 2 Final Report
M. FRENKLACH, D. W. CLARY, and M. K. RAMACHANDRA May 1985 171 p refs
(Contract NAG3-477)
(NASA-CR-174880; NAS 1.26:174880) Avail: NTIS HC A08/MF A01 CSCL 21B

Soot formation in oxidation of allene, 1,3-butadiene, vinylacetylene and chlorobenzene and in pyrolysis of ethylene, vinylacetylene, 1-butene, chlorobenzene, acetylen-hydrogen, benzene-acetylene, benzene-butadiene and chlorobenzene-acetylene argon-diluted mixtures was studied behind reflected shock waves. The results are rationalized within the framework of the conceptual models. It is shown that vinylacetylene is much less sooty than allene, which indicates that conjugation by itself is not a sufficient factor for determining the sooting tendency of a molecule. Structural reactivity in the context of the chemical kinetics is the dominant factor in soot formation. Detailed chemical kinetic modeling of soot formation in pyrolysis of acetylene is reported. The main mass growth was found to proceed through a single dominant route composed of conventional radical reactions. The practically irreversible formation reactions of the fused polycyclic aromatics and the overshoot by hydrogen atom over its equilibrium concentration are the g-driving kinetic forces for soot formation. E.A.K.

N85-28982* National Aeronautics and Space Administration. Lewis Research Center, Cleveland, Ohio.
CHEMICAL CONTROL OF NADIMIDE CURE TEMPERATURE AND RATE Patent
R. W. LAUVER, inventor (to NASA) 30 Apr. 1985 9 p Filed 22 Jul. 1983 Division of US Patent Appl-SN-404809, filed 3 Aug. 1982, US Patent-4,455,418
(NASA-CASE-LEW-13770-2; US-PATENT-4,514,557; US-PATENT-4,455,418; US-PATENT-APPL-SN-516217; US-PATENT-APPL-SN-404809; US-PATENT-CLASS-528-342; US-PATENT-CLASS-526-262; US-PATENT-CLASS-528-322)
Avail: US Patent and Trademark Office CSCL 07D

Polyimide resins suitable for use as composite matrix materials are formed by copolymerization of maleic and norbornenyl endcapped monomers and oligomers. The copolymers can be cured at temperatures under about 300 C by controlling the available concentration of the maleic end-capped reactant. This control can be achieved by adding sufficient amounts of said maleic reactant, or by chemical modification of either copolymer, so as to either increase Diels-Alder retrogression of the norbornenyl capped reactant and/or holding initiation and polymerization to a rate compatible with the availability of the maleic-capped reactant.
Official Gazette of the U.S. Patent and Trademark Office

N85-28983*# National Aeronautics and Space Administration. Lewis Research Center, Cleveland, Ohio.
FUEL RICH CATALYTIC COMUSTION: THE FIRST STAGE OF A TWO-STAGE COMBUSTOR
T. A. BRABBS and S. L. OLSON 1984 12 p refs Presented at Fall Meeting of the Eastern Sect. of the Combust. Inst., Clearwater Beach, Fla., 3-5 Dec. 1984
(NASA-TM-87042; E-2601; NAS 1.15:87042) Avail: NTIS HC A02/MF A01 CSCL 21B

An experimental program demonstrated that fuel-rich catalytic combustion can be accomplished soot free as long as the combustion temperature is less than the temperature at the rich limit of combustion. Although soot was not measured directly, three pieces of data strongly suggest that it was not present: (1) the product gases were completely transparent and produced no radiation characteristic of soot, (2) measured reaction temperatures followed closely those calculated for equilibrium with no soot present, and (3) over 99 percent of the carbon was accounted for in the measured reaction products. Data for two catalyst configurations were taken along with gas samples at two locations downstream of the catalyst bed. Author

N85-30039* National Aeronautics and Space Administration. Lewis Research Center, Cleveland, Ohio.
CHEMICAL APPROACH FOR CONTROLLING NADIMIDE CURE TEMPERATURE AND RATE Patent
R. W. LAUVER, inventor (to NASA) 22 Jun. 1985 8 p Filed 14 Dec. 1983 Division of abandoned US Patent Appl-SN-516217, filed 22 Jul. 1983
(NASA-CASE-LEW-13770-6; US-PATENT-4,495,339; US-PATENT-APPL-SN-561434; US-PATENT-APPL-SN-516217; US-PATENT-CLASS-526-262; US-PATENT-CLASS-526-204; US-PATENT-CLASS-526-217; US-PATENT-CLASS-528-314; US-PATENT-CLASS-528-322) Avail: US Patent and Trademark Office CSCL 07D

Polyimide resins suitable for use as composite matrix materials are formed by copolymerization of maleic and norbornenyl end-capped monomers and oligomers. The copolymers can be cured at temperatures under about 300 C. by controlling the available concentration of the maleic end-capped reactant. This control can be achieved by adding sufficient amounts of said maleic reactant, or by chemical modification of either copolymer, to increase Diels-Alder retrogression of the norbornenyl-capped reactant and/or holding initiation and polymerization to a rate compatible with the availability of the maleic-capped reactant.
Official Gazette of the U.S. Patent and Trademark Office

N85-31244*# National Aeronautics and Space Administration. Lewis Research Center, Cleveland, Ohio.
FUEL-RICH CATALYTIC COMBUSTION: A SOOT-FREE TECHNIQUE FOR IN SITU HYDROGEN-LIKE ENRICHMENT
T. A. BRABBS and S. L. OLSON Jul. 1985 12 p refs Presented at the Fall Meeting of the Eastern Sect. of the Combust. Inst., Clearwater Beach, Fla., 3-5 Dec. 1984
(NASA-TP-2498; E-2604; NAS 1.60:2498) Avail: NTIS HC A02/MF A01 CSCL 21B

An experimental program on the catalytic oxidation of iso-octane demonstrated the feasibility of the two-stage combustion system for reducing particulate emissions. With a fuel-rich (phi = 4.8 to 7.8) catalytic combustion preburner as the first stage the combustion process was soot free at reactor outlet temperatures of 1200 K or less. Although soot was not measured directly, its absence was indicated. Reaction products collected at two

positions downstream of the catalyst bed were analyzed on a gas chromatograph. Comparison of these products indicated that pyrolysis of the larger molecules continued along the drift tube and that benzene formation was a gas-phase reaction. The effective hydrogen-carbon ratio calculated from the reaction products increased by 20 to 68 percent over the range of equivalence ratios tested. The catalytic partial oxidation process also yielded a large number of smaller-containing molecules. The fraction of fuel carbon in compounds having two or fewer carbon atoms ranged from 30 percent at 1100 K to 80 percent at 1200 K. F.M.R.

N85-32156*# National Aeronautics and Space Administration. Lewis Research Center, Cleveland, Ohio.
SHOCK TUBE MEASUREMENTS OF GROWTH CONSTANTS IN THE BRANCHED-CHAIN ETHANE-CARBON MONOXIDE-OXYGEN SYSTEM
R. S. BROKAW, T. A. BRABBS, and C. A. SNYDER Jul. 1985 15 p refs
(NASA-TM-87068; E-2574; NAS 1.15:87068) Avail: NTIS HC A02/MF A01 CSCL 07D

Exponential free radical growth constants have been measured for ethane carbon monoxide oxygen mixtures by monitoring the growth of oxygen atom concentration as manifested by CO flame band emission. Data were obtained over the temperature range of 1200 to 1700 K. The data were analyzed using an ethane oxidation mechanism involving seven elementary reaction steps. Calculated growth constants were close to experimental values at lower temperatures, up to about 1400 K, but at higher temperatures computed growth constants were considerably smaller than experiment. In attempts to explain these results additional branching reactions were added to the mechanism. However, these additional reactions did not appreciably change calculated growth constants. Author

26

METALLIC MATERIALS

Includes physical, chemical, and mechanical properties of metals, e.g., corrosion; and metallurgy.

A85-11058* National Aeronautics and Space Administration. Lewis Research Center, Cleveland, Ohio.
DEFORMATION AND FRACTURE BEHAVIOR OF NI-MO-AL(GAMMA/GAMMA PRIME-ALPHA) IN SITU COMPOSITE
A. M. SRIRAMAMURTHY (Defence Metallurgical Research Laboratory, Hyderabad, India) and S. N. TEWARI (NASA, Lewis Research Center, Materials Processing Science Section, Cleveland, OH; Defence Metallurgical Research Laboratory, Hyderabad, India) Metallurgical Transactions A - Physical Metallurgy and Materials Science (ISSN 0360-2133), vol. 15A, Oct. 1984, p. 1905-1919. Research supported by the Ministry of Defence of India. refs

Tensile properties of a directionally solidified (DS) eutectic alloy of the nominal composition Ni-33 Mo-5.7 Al (weight percent) have been investigated both at room temperature and elevated temperatures. The microstructure-mechanical property relationship has been studied for the alloy both in the as-DS and heat-treated conditions. Changes in the yield strength, the work hardening behavior, and the fracture morphology have been explained in terms of the microstructural changes due to the heat treatment. The yield drops observed have been attributed to the microdebonding due to the possible segregation of impurities at the fiber-matrix interface, and partly to the strain aging. The deformation mechanism has been identified to be the cutting of gamma prime particles. Author

A85-11070* Rensselaer Polytechnic Inst., Troy, N.Y.
TOPOLOGICAL REACTION RATE MEASUREMENTS RELATED TO SCUFFING
J. L. LAUER, S. S. FUNG (Rensselaer Polytechnic Institute, Troy, NY), and W. R. JONES, JR. (NASA, Lewis Research Center, Cleveland, OH) ASLE Transactions, vol. 27, Oct. 1984, p. 288-293; Discussion, p. 293, 294; Authors' Closure, p. 294. Previously announced in STAR as N84-14288. refs
(Contract AF-AFOSR-81-0005; NSG-3180)

A ball-on-plate (both consisting of hardened M-50 steel) sliding elastohydrodynamic contact was run with trimethylolpropane triheptanoate (TMPTH) with and without tricresyl phosphate (TCP). The contact area of the plate was optically profiled with a phase-locked interference microscope (PLIM) both before and after exposure to alcoholic hydrochloric acid. As scuffing was approached, the profile within the contact region changed more rapidly after the acid treatment; after scuffing, it assumed a constant high value. A metallurgical phase found in the scuff mark was apparently responsible for the high reactivity. The microscopic profile changes (sensitivity, + or - 3 nm (+ or - A) in depth) involved primarily the small asperities (radius, 3 microns); the larger ones were unaffected. Soaking the steel in TCP smoothed the fine structure of the surface profile but increased its reactivity toward alcoholic hydrochloric acid before sliding was started. Thus it would appear that PLIM examination could be used for screening potentially scuff-resistant materials. Author

A85-11071* National Aeronautics and Space Administration. Lewis Research Center, Cleveland, Ohio.
FRICTION AND WEAR OF SOME FERROUS-BASE METALLIC GLASSES
K. MIYOSHI and D. H. BUCKLEY (NASA, Lewis Research Center, Cleveland, OH) ASLE Transactions, vol. 27, Oct. 1984, p. 295-303; Discussion, p. 303; Authors' Closure, p. 303, 304. Previously announced in STAR as N83-19886. refs

Sliding friction experiments, X-ray photoelectron spectroscopy (XPS) analysis, and electron microscopy and diffraction studies were conducted with ferrous base metallic glasses (amorphous alloys) in contact with aluminium oxide at temperatures to 750 C in a vacuum. Sliding friction experiments were also conducted in argon and air atmospheres. The results of the investigation indicate that the coefficient of friction increases with increasing temperature to 350 C in vacuum. The increase in friction is due to an increase in adhesion resulting from surface segregation of boric oxide and/or silicon oxide to the surface of the foil. Above 500 C the coefficient of friction decreased rapidly. The decrease correlates with the segregation of boron nitride to the surface. Contaminants can come from the bulk of the material to the surface upon heating and impart boric oxide and/or silicon oxide at 350 C and boron nitride above 500 C. The segregation of contaminants is responsible for the friction behavior. The amorphous alloys have superior wear resistance to crystalline 304 stainless steel. The relative concentrations of the various constituents at the surfaces of the amorphous alloys are very different from the nominal bulk compositions. Author

A85-11603*# National Aeronautics and Space Administration. Lewis Research Center, Cleveland, Ohio.
STRAINRANGE PARTITIONING - A TOTAL STRAIN RANGE VERSION
G. R. HALFORD and J. F. SALTSMAN (NASA, Lewis Research Center, Cleveland, OH) IN: International Conference on Advances in Life Prediction Methods, Albany, NY, April 18-20, 1983, Proceedings . New York, American Society of Mechanical Engineers, 1983, p. 17-26. Previously announced in STAR as N83-14246. refs

Procedures are presented for expressing the Strainrange Partitioning (SRP) method for creep fatigue life prediction in terms of total strain range. Inelastic and elastic strain-range - life relations are summed to give total strain-range - life relations. The life components due to inelastic strains are dealt with using conventional SRP procedures while the life components due to elastic strains are expressed as families of time-dependent terms

for each type of SRP cycle. Cyclic constitutive material behavior plays an important role in establishing the elastic strain-range life relations as well as the partitioning of the inelastic strains. To apply the approach, however, it is not necessary to have to determine the magnitude of the inelastic strain range. The total strain SRP approach is evaluated and verified using two nickel base superalloys, AF2-1DA and Rene 95. Excellent agreement is demonstrated between observed and predicted cyclic lifetimes with 70 to 80 percent of the predicted lives falling within factors of two of the observed lives. The total strain-range SRP approach should be of considerable practical value to designers who are faced with creep-fatigue problems for which the inelastic strains cannot be calculated with sufficient accuracy to make reliable life predictions by the conventional inelastic strain range SRP approach. Author

A85-11935* National Aeronautics and Space Administration. Lewis Research Center, Cleveland, Ohio.
CAVITATION EROSION SIZE SCALE EFFECTS
P. V. RAO and D. H. BUCKLEY (NASA, Lewis Research Center, Cleveland, OH) Wear (ISSN 0043-1648), vol. 96, July 9, 1984, p. 239-253. refs
(Contract NCC3-21)

Size scaling in cavitation erosion is a major problem confronting the design engineers of modern high speed machinery. An overview and erosion data analysis presented in this paper indicate that the size scale exponent n in the erosion rate relationship as a function of the size or diameter can vary from 1.7 to 4.9 depending on the type of device used. There is, however, a general agreement as to the values of n if the correlations are made with constant cavitation number. Author

A85-12098* Max-Planck-Inst. fuer Metallforschung, Stuttgart (West Germany).
A STUDY OF FATIGUE DAMAGE MECHANISMS IN WASPALOY FROM 25 TO 800 C
B. A. LERCH (Max-Planck-Institut fuer Metallforschung, Stuttgart, West Germany; Cincinnati, University, Cincinnati, OH), N. JAYARAMAN (Cincinnati, University, Cincinnati, OH), and S. D. ANTOLOVICH (Georgia Institute of Technology, Atlanta, GA) Materials Science and Engineering (ISSN 0025-5416), vol. 66, Sept. 15, 1984, p. 151-166. refs
(Contract NSG-3263)

The objective of the study was to examine the effect of various microstructures on the fatigue and damage accumulation behavior of Waspaloy, a nickel-base alloy commonly used in aircraft engines. Shearing was the dominant deformation mode in specimens with coarse grains and small (50-80 A) gamma prime particles, whereas Orowan looping was dominant in fine-grained specimens with large (about 900 A) gamma prime particles. At temperatures up to 500 C, cracks initiated transgranularly, while at 800 C the failure process was intergranular for both coarse-grained and fine-grained specimens. At temperatures above 500 C, a significant decrease in the fatigue life was observed for both coarse-grained and fine-grained material. V.L.

A85-12789* National Aeronautics and Space Administration. Lewis Research Center, Cleveland, Ohio.
DEFORMATION AND EROSION OF F.C.C. METALS AND ALLOYS UNDER CAVITATION ATTACK
B. C. S. RAO and D. H. BUCKLEY (NASA, Lewis Research Center, Cleveland, OH) Materials Science and Engineering (ISSN 0025-5416), vol. 67, Oct. 1984, p. 55-67. refs

Experimental investigations have been conducted to determine the early stages of cavitation attack on 6061-T6 aluminum alloy, electrolytic tough pitch copper, brass, and bronze, all having polycrystalline fcc matrices. The surface profiles and scanning electron micrographs show that the pits are initially formed at the grain boundaries, while the grain surfaces are progressively roughened by multiple slip and twinning. The initial erosion is noted to have occurred from the material in the grain boundaries, as well as by fragmentation of part of the grains. Further erosion occurred by shearing and necking of the surface undulations caused by plastic deformation. The mean penetration depth, computed on the basis of mass loss, was lowest on the bronze and greatest on the copper. Attention is given to the relation of cavitation attack to grain size, glide stress and stacking fault energy. O.C.

A85-14959* Columbia Univ., New York.
MODELING OF GAMMA/GAMMA-PRIME PHASE EQUILIBRIUM IN THE NICKEL-ALUMINUM SYSTEM
J. M. SANCHEZ, J. R. BAREFOOT, R. N. JARRETT, and J. K. TIEN (Columbia University, New York, NY) Acta Metallurgica (ISSN 0001-6160), vol. 32, Sept. 1984, p. 1519-1525. refs
(Contract NSF DMR-82-06195; NAG3-57)

A theoretical model is proposed for the determination of phase equilibrium in alloys, taking into consideration dissimilar lattice parameters. Volume-dependent pair interactions are introduced by means of phenomenological Lennard-Jones potentials and the configurational entropy of the system is treated in the tetrahedron approximation of the cluster variation method. The model is applied to the superalloy-relevant, nickel-rich, gamma/gamma-prime phase region of the Ni-Al phase diagram. The model predicts reasonable values for the lattice parameters and the enthalpy of formation as a function of composition, and the calculated phase diagram closely approximates the experimental diagram. Author

A85-15603* National Aeronautics and Space Administration. Lewis Research Center, Cleveland, Ohio.
EFFECTS OF SO2 AND SO3 ON THE NA2SO4 INDUCED CORROSION OF NICKEL
A. K. MISRA (NASA, Lewis Research Center, Materials Div., Cleveland, OH; California, University, Berkeley, CA) and D. P. WHITTLE Oxidation of Metals (ISSN 0030-770X), vol. 22, Aug. 1984, p. 1-33. refs
(Contract DE-AC03-76SF-00098)

The effects of SO2 and SO3 in the environment on the hot-corrosion behavior of Ni in the temperature range 750-950 C has been studied. Below the melting point of Na2SO4 (884 C), rapid corrosion takes place by formation of a Na2SO4-NiSO4 melt which can penetrate the porous oxide scale and give rise to sulfide information by coming in contact with the metal. The distribution of the sulfides depends on the SO2 level in the ambient gas. Continued corrosion occurs by a sulfidation-oxidation mechanism. At temperatures above the melting point of Na2SO4, accelerated degradation occurs via dissolution of the surface scale, followed by reprecipitation of the oxide in a nonprotective form. Author

A85-19084* National Aeronautics and Space Administration. Lewis Research Center, Cleveland, Ohio.
MECHANICAL-CONTACT-INDUCED TRANSFORMATION FROM THE AMORPHOUS TO THE PARTIALLY CRYSTALLINE STATE IN METALLIC GLASS
K. MIYOSHI and D. H. BUCKLEY (NASA, Lewis Research Center, Cleveland, OH) Thin Solid Films (ISSN 0040-6090), vol. 118, 1984, p. 363-373. Previously announced in STAR as N84-20673. refs

Friction and wear tests were conducted with 3.2- and 6.4-millimeter-diameter aluminum oxide spheres sliding, in reciprocating motion, on a Fe67Co18B14Si1 metallic foil. Crystallites with a size range of 10 to 150 nanometers were produced on the wear surface of the amorphous alloy. A strong interaction between transition metals and metalloids such as silicon and boron results in strong segregation during repeated sliding, provides preferential transition metal-metalloid clustering in the amorphous alloy, and subsequently produces the diffused honeycomb structure formed by dark grey bands and primary crystals, that is, alpha-Fe in the matrix. Large plastic flow occurs on an amorphous alloy surface with sliding and the flow film of the alloy transfers to the aluminum oxide pin surface. Multiple slip bands due to shear deformation are observed on the side of the wear track. Two distinct types of wear debris were observed as a result of sliding: an alloy wear debris, and/or powdery-whiskery oxide debris. A.R.H.

A85-24667* National Aeronautics and Space Administration. Lewis Research Center, Cleveland, Ohio.
ION-BEAM NITRIDING OF STEELS
J. SALIK (NASA, Lewis Research Center, Cleveland, OH) Journal of Applied Physics (ISSN 0021-8979), vol. 57, Feb. 15, 1985, p. 1328-1331. Previously announced in STAR as N84-21719. refs

The application of the ion beam technique to the nitriding of steels is described. It is indicated that the technique can be successfully applied to nitriding. Some of the structural changes obtained by this technique are similar to those obtained by ion nitriding. The main difference is the absence of the iron nitride diffraction lines. It is found that the dependence of the resultant microhardness on beam voltage for super nitralloy is different from that of 304 stainless steel. E.A.K.

A85-25835* Ball Aerospace Systems Div., Boulder, Colo.
FRACTURE TOUGHNESS OF HOT-PRESSED BERYLLIUM
D. D. LEMON (Ball Corp., Ball Aerospace Systems Div., Boulder, CO) and W. F. BROWN, JR. (NASA, Lewis Research Center, Cleveland, OH) Journal of Testing and Evaluation (ISSN 0090-3973), vol. 13, March 1985, p. 152-161. refs

This paper presents the results of an investigation into the fracture toughness, sustained-load flaw growth, and fatigue-crack propagation resistance of S200E hot-pressed beryllium at room temperature. It also reviews the literature pertaining to the influence of various factors on the fracture toughness of hot-pressed beryllium determined using fatigue-cracked specimens. Author

A85-26158* National Aeronautics and Space Administration. Lewis Research Center, Cleveland, Ohio.
DUCTILITY IN RAPIDLY SOLIDIFIED NIAL
D. J. GAYDOSH, R. W. JECH, and R. H. TITRAN (NASA, Lewis Research Center, Cleveland, OH) Journal of Materials Science Letters (ISSN 0261-8028), vol. 4, Feb. 1985, p. 138-140. refs

An attempt is made to refine the grain structure of equiatomic NiAl by means of rapid solidification processing, and to examine the effect of small grain size on room temperature ductility. Free melt spinning was used to produce the rapidly solidified material. Room temperature bend testing of both as-spun and heat-treated NiAl ribbon was conducted by free bending the ribbon around a mandrel of successively smaller diameter until failure occurred. Room-temperature plastic deformation was exhibited both before and after a 1-h heat treatment at 1000 C. Heat treatment increased the observed ductility. O.C.

A85-27808* Virginia Polytechnic Inst. and State Univ., Blacksburg.
NEW EUTECTIC ALLOYS AND THEIR HEATS OF TRANSFORMATION
D. FARKAS (Virginia Polytechnic Institute and State University, Blacksburg, VA) and C. E. BIRCHENALL (Delaware, University, Newark, DE) Metallurgical Transactions A - Physical Metallurgy and Materials Science (ISSN 0360-2133), vol. 16A, March 1985, p. 323-328. refs
(Contract NSG-3184)

Eutectic compositions and congruently melting intermetallic compounds in binary and multicomponent systems among common elements such as Al, Ca, Cu, Mg, P, Si, and Zn may be useful for high temperature heat storage. In this work, heats of fusion of new multicomponent eutectics and intermetallic phases are reported, some of which are competitive with molten salts in heat storage density at high temperatures. The method used to determine unknown eutectic compositions combined results of differential thermal analysis, metallography, and microprobe analysis. The method allows determination of eutectic compositions in no more than three steps. The heats of fusion of the alloys were measured using commercial calorimeters, a differential thermal analyzer, and a differential scanning calorimeter. Author

A85-27812*# National Aeronautics and Space Administration. Lewis Research Center, Cleveland, Ohio.
ELEVATED TEMPERATURE CREEP-RUPTURE BEHAVIOR OF THE SINGLE CRYSTAL NICKEL-BASE SUPERALLOY NASAIR 100
M. V. NATHAL (NASA, Lewis Research Center, Cleveland, OH) and L. J. EBERT (Case Western Reserve University, Cleveland, OH) Metallurgical Transactions A - Physical Metallurgy and Materials Science (ISSN 0360-2133), vol. 16A, March 1985, p. 427-439. refs

The creep and rupture behavior of 001-line-oriented single crystals of the nickel-base superalloy NASAIR 100 was investigated at temperatures of 925 and 1000 C. In the stress and temperature ranges studied, the steady state creep rate, time to failure, time to the onset of secondary creep, and the time to the onset of tertiary creep all exhibited power law dependencies on the applied stress. The creep rate exponents for this alloy were between seven and eight, and the modulus-corrected activation energy for creep was approximately 350 kjoule/mole, which was comparable to the measured activation energy for Ostwald ripening of the gamma-prime precipitates. Oriented gamma-prime coarsening to form lamellae perpendicular to the applied stress was very prominent during creep. At 1000 C, the formation of a continuous gamma-gamma-prime lamellar structure was completed during the primary creep stage. Shear through the gamma-gamma-prime interface is considerd to be the rate limiting step in the deformation process. Gradual thickening of the lamellae appeared to be the cause of the onset of tertiary creep. At 925 C, the fully developed lamellar structure was not achieved until the secondary or tertiary creep stages. At this temperature, the gamma-gamma-prime lamellar structure did not appear to be as beneficial for creep resistance as at the higher temperature. Author

A85-31688* National Aeronautics and Space Administration. Lewis Research Center, Cleveland, Ohio.
CHEMICAL REACTIONS INVOLVED IN THE INITIATION OF HOT CORROSION OF IN-738
G. C. FRYBURG, F. J. KOHL, and C. A. STEARNS (NASA, Lewis Research Center, Cleveland, OH) Electrochemical Society, Journal (ISSN 0013-4651), vol. 131, Dec. 1984, p. 2985-2997. Previously announced in STAR as N84-28958. refs

Sodium-sulfate-induced hot corrosion of preoxidized IN-738 was studied at 975 C with special emphasis placed on the processes occurring during the long induction period. Thermogravimetric tests were run for predetermined periods of time, and then one set of specimens was washed with water. Chemical analysis of the wash solutions yielded information about water soluble metal salts and residual sulfate. A second set of samples was cross sectioned dry and polished in a nonaqueous medium. Element distributions within the oxide scale were obtained from electron microprobe X-ray micrographs. Evolution of SO was monitored throughout the thermogravimetric tests. Kinetic rate studies were performed for several pertinent processes; appropriate rate constants were obtained from the following chemical reactions; Cr203 + 2 Na2S04(1) + 3/2 02 yields 2 Na2Cr04(1) + 2 S03(g)n TiO2 + Na2S04(1) yields Na20(T102)n + 503(g)n T102 + Na2Cro4(1) yields Na2(T102)n + Cr03(g). Author

A85-32387* National Aeronautics and Space Administration. Lewis Research Center, Cleveland, Ohio.
INFLUENCE OF COMPOSITION ON THE MICROSTRUCTURE AND MECHANICAL PROPERTIES OF A NICKEL-BASE SUPERALLOY SINGLE CRYSTAL
M. V. NATHAL (NASA, Lewis Research Center, Cleveland, OH) and L. J. EBERT (Case Western Reserve University, Cleveland, OH) IN: Superalloys 1984; Proceedings of the Fifth International Symposium, Champion, PA, October 7-11, 1984 . Warrendale, PA, Metallurgical Society of AIME, 1984, p. 125-133. Previously announced in STAR as N84-17354. refs
(Contract NSG-330)

The effects of cobalt, tantaium, and tungsten contents on the microstructure and mechanical properties of single crystal Mar-M247 were investigated. Elevated temperature tensile and

creep-rupture properties of 001 oriented single crystals were related to microstructural features of the alloys. Substitution of Ni for Co in the high refractory metal alloys increased the lattice mismatch, which was considered to be the cause of the increases in tensile and creep strength. Substitution of Ni for Ta caused large decreases in tensile strength and creep life, consistent with decreases in gamma prime volume fraction, lattice mismatch, and solid solution hardening. Substitution of W for Ta resulted in decreased life at high stresses, which was related to small decreases in mismatch and volume fraction. However, the W substitution resulted in improved life at low stresses, which was related to solid solution strengthening by W. Author

A85-32388* National Aeronautics and Space Administration. Lewis Research Center, Cleveland, Ohio.
FACTORS WHICH INFLUENCE DIRECTIONAL COARSENING OF GAMMA-PRIME DURING CREEP IN NICKEL-BASE SUPERALLOY SINGLE CRYSTALS
R. A. MACKAY (NASA, Lewis Research Center, Cleveland, OH) and L. J. EBERT (Case Western Reserve University, Cleveland, OH) IN: Superalloys 1984; Proceedings of the Fifth International Symposium, Champion, PA, October 7-11, 1984 . Warrendale, PA, Metallurgical Society of AIME, 1984, p. 135-144. Previously announced in STAR as N84-17355. refs
(Contract NSG-3246)

Changes in the morphology of the gamma prime precipitate were examined as a function of the time during creep at 982 C in 001 oriented single crystals of a Ni-Al-Mo-Ta superalloy. In this alloy, which has a large negative misfit of -0.80 pct., the gamma prime particles link together during creep to form platelets, or rafts, which are aligned with their broad faces perpendicular to the applied tensile axis. The effects of initial microstructure and alloy composition of raft development and creep properties were investigated. Directional coarsening of gamma prime begins during primary creep and continues well after the onset of second state creep. The thickness of the rafts remains constant up through the onset of tertiary creep, a clear indication of the stability of the finely-spaced gamma/gamma prime lamellar structure. The thickness of the rafts which formed was equal to the initial gamma prime size which was present prior to testing. The single crystals with the finest gamma prime size exhibited the longest creep lives, because the resultant rafted structure had a larger number of gamma/gamma prime interfaces per unit volume of material. Reducing the Mo content by only 0.73 wt. pct. increased the creep life by a factor of three, because the precipitation of a third phase was eliminated. Author

A85-32399* Rockwell International Corp., Canoga Park, Calif.
THE EFFECT OF MICROSTRUCTURE, TEMPERATURE, AND HOLD-TIME ON LOW-CYCLE FATIGUE OF AS HIP P/M RENE 95
S. BASHIR (Rockwell International Corp., Rocketdyne Div., Canoga Park, CA) and S. D. ANTOLOVICH (Georgia Institute of Technology, Atlanta, GA) IN: Superalloys 1984; Proceedings of the Fifth International Symposium, Champion, PA, October 7-11, 1984 . Warrendale, PA, Metallurgical Society of AIME, 1984, p. 295-307. refs
(Contract NSG-3147)

The effects of microstructure, temperature, plastic strain range, and hold time on the low-cycle fatigue (LCF) life were studied for Rene 95, an important Ni base superalloy used in jet engine disks. It was shown that the life could be varied by approximately an order of magnitude at elevated temperatures by simple heat treatments. The life was largest for the microstructure that promoted the most homogeneous deformation mode. The results are explained using the concept of a synergistic interaction between the deformation mode and boundary oxidation. Author

A85-32400* Rensselaer Polytechnic Inst., Troy, N.Y.
THE INFLUENCE OF HOLD TIMES ON LCF AND FCG BEHAVIOR IN A P/M NI-BASE SUPERALLOY
S. J. CHOE, S. V. GOLWALKER, D. J. DUQUETTE, and N. S. STOLOFF (Rensselaer Polytechnic Institute, Troy, NY) IN: Superalloys 1984; Proceedings of the Fifth International Symposium, Champion, PA, October 7-11, 1984 . Warrendale, PA, Metallurgical Society of AIME, 1984, p. 309-318. refs
(Contract NAG3-22)

The relative importance of creep and environmental interactions in high temperature fatigue behavior has been investigated for as-HIP Rene 95. Strain-controlled low cycle fatigue and load-controlled fatigue crack growth tests were performed at elevated temperatures in argon, followed by fractographic analyses of the fracture surfaces by scanning electron microscopy. Fatigue lives were drastically reduced and crack growth rates increased one hundred fold as a result of superposition of hold times on continuous cycling. A change in fracture mode with hold time also was noted. Chromium oxide was detected on the fracture surface by Auger electron spectroscopy. The drastic changes in fatigue resistance due to hold times were attributed primarily to environmental interactions with fatigue processes. Author

A85-32412* Columbia Univ., New York.
EFFECTS OF COBALT ON THE HOT WORKABILITY OF NICKEL-BASE SUPERALLOYS
R. N. JARRETT, J. P. COLLIER, and J. K. TIEN (Columbia University, New York, NY) IN: Superalloys 1984; Proceedings of the Fifth International Symposium, Champion, PA, October 7-11, 1984 . Warrendale, PA, Metallurgical Society of AIME, 1984, p. 455-466. refs
(Contract NAG3-57)

The effect of cobalt on the workability of nickel-base superalloys is examined with reference to experimental results for four heats of alloys based on the Nimonic 115 composition with varying amounts of nickel substituted for the nominal 14 percent cobalt. It is shown that Co lowers the gamma-prime solvus, which in turn lowers the Cr23C6 carbide solvus. It is further shown that these solvus temperatures bracket the hot working range for the alloys. However, thermomechanical processing modifications reflecting the effect of Co on the gamma-prime and carbide solvi are shown to restore the workability and the properties of alloys with little or no cobalt. V.L.

A85-32414* Illinois Univ., Urbana.
RAPID SOLIDIFICATION AND DYNAMIC COMPACTION OF NI-BASE SUPERALLOY POWDERS
R. D. FIELD, S. J. HALES, W. O. POWERS, and H. L. FRASER (Illinois, University, Urbana, IL) IN: Superalloys 1984; Proceedings of the Fifth International Symposium, Champion, PA, October 7-11, 1984 . Warrendale, PA, Metallurgical Society of AIME, 1984, p. 487-496. Research supported by the United Technologies Corp. and DARPA. refs
(Contract NAG3-325)

A Ni-base superalloy containing 13Al-9Mo-2Ta (in at. percent) has been characterized in both the rapidly solidified condition and after dynamic compaction. Dynamically compacted specimens were examined in the as-compacted condition and observations related to current theories of interparticle bonding. In addition, the recrystallization behavior of the compacted material at relatively low temperature (about 0.5-0.75 Tm) was investigated. Author

A85-32431* National Aeronautics and Space Administration. Lewis Research Center, Cleveland, Ohio.
CYCLIC OXIDATION BEHAVIOR OF BETA+GAMMA OVERLAY COATINGS ON GAMMA AND GAMMA+GAMMA-PRIME ALLOYS
J. A. NESBITT (NASA, Lewis Research Center, Cleveland, OH; Michigan Technological University, Houghton, MI), B. H. PILSNER, L. A. CAROL, and R. W. HECKEL (Michigan Technological University, Houston, MI) IN: Superalloys 1984; Proceedings of the Fifth International Symposium, Champion, PA, October 7-11, 1984 . Warrendale, PA, Metallurgical Society of AIME, 1984, p. 699-710. refs
(Contract NAG3-244; NAG3-216)

Detailed experimental studies of the cyclic oxidation behavior of low-pressure plasma sprayed beta+gamma coasting on gamma-phase Ni-Cr-Al alloys have shown the correlation of weight change, oxide type, and Cr and Al concentration-distance profiles as a function of oxidation time. Of special interest was the transition to breakway oxidation due to the loss of the Al flux to the oxide and the failure of the coated alloy to form an Al2O3-rich oxide scale. The experimental results on beta+gamma/gamma coating systems were used as the basis of a numerical model (ternary, semi-infinite, finite-difference analysis) which accurately predicted changes in Cr and Al concentration-distance profiles. The model was used to study parameters critical to enhancing the life of coatings which fail by a combination of Al loss in forming the oxide scale and Al loss via interdiffusion with the substrate alloy. Comparisons of beta+gamma/gamma coating behavior are made to the oxidation of coated gamma+gamma-prime substrates, both ternary Ni-Cr-Al alloys and Mar-M 247-type alloys. Author

A85-32434* National Aeronautics and Space Administration. Lewis Research Center, Cleveland, Ohio.
ON THE FATIGUE CRACK PROPAGATION BEHAVIOR OF SUPERALLOYS AT INTERMEDIATE TEMPERATURES
J. GAYDA, R. V. MINER, and T. P. GABB (NASA, Lewis Research Center, Cleveland, OH) IN: Superalloys 1984; Proceedings of the Fifth International Symposium, Champion, PA, October 7-11, 1984 . Warrendale, PA, Metallurgical Society of AIME, 1984, p. 731-740. refs

Two superalloys used in gas-turbine disks, Rene 95 and IN-100 were tested in several forms at 0.33 Hz in air, and the results were compared with earlier data on Astroloy to gain a better understanding of the effects of grain size, strength, and alloy composition on the fatigue crack propagation behavior. In addition, selected forms of Rene 95 were tested at 0.33 Hz in vacuum and in air using a cycle with a 120-sec tensile dwell to evaluate the effects of environment and creep. Results of the study emphasize the beneficial effect of large grain size on the fatigue and crep-fatigue crack growth resistance of the superalloys in the temperature range corresponding to the operating temperatures of aircraft gas-turbine engine disk rims. V.L.

A85-32440* Garrett Turbine Engine Co., Phoenix, Ariz.
DEVELOPMENT OF COATED SINGLE-CRYSTAL SUPERALLOY SYSTEMS FOR GAS TURBINE APPLICATIONS
T. E. STRANGMAN, M. FUJII, and X. NGUYEN-DINH (Garrett Turbine Engine Co., Phoenix, AZ) IN: Superalloys 1984; Proceedings of the Fifth International Symposium, Champion, PA, October 7-11, 1984 . Warrendale, PA, Metallurgical Society of AIME, 1984, p. 795-804. refs
(Contract NAS3-20073)

A85-37415*# National Aeronautics and Space Administration. Lewis Research Center, Cleveland, Ohio.
THE SUBSTITUTION OF NICKEL FOR COBALT IN HOT ISOSTATICALLY PRESSED POWDER METALLURGY UDIMET 700 ALLOYS
F. H. HARF (NASA, Lewis Research Center, Cleveland, OH) Metallurgical Transactions A - Physical Metallurgy and Materials Science (ISSN 0360-2133), vol. 16A, June 1985, p. 993-1003. refs

Nickel was substituted in various proportions for cobalt in a series of five hot-isostatically-pressed powder metallurgy alloys based on the UDIMET 700 composition. These alloys were given 5-step heat treatments appropriate for use in turbine engine disks. The resultant microstructures displayed three distinct sizes of gamma-prime particles in a gamma matrix. The higher cobalt-content alloys contained larger amounts of the finest gamma-prime particles, and had the lowest gamma-gamma-prime lattice mismatch. While all alloys had approximately the same tensile properties at 25 and 650 gamma C, the rupture lives at 650 and 760 C peaked in the alloys with cobalt contents between 12.7 and 4.3 pct. Minimum creep rates increased as cobalt contents were lowered, suggesting their correlation with the gamma-prime particle size distribution and the gamma-gamma-prime mismatch. It was also found that, on overaging at temperatures higher than suitable for turbine disk use, the high cobalt-content alloys were prone to sigma phase formation. Author

A85-39284* Garrett Turbine Engine Co., Phoenix, Ariz.
PROGRESS IN THE UTILIZATION OF AN OXIDE-DISPERSION-STRENGTHENED ALLOY FOR SMALL ENGINE TURBINE BLADES
T. G. BEATTY and P. P. MILLAN (Garrett Turbine Engine Co., Phoenix, AZ) IN: Advanced aerospace materials technology; Proceedings of the Aerospace Congress and Exposition, Long Beach, CA, October 15-18, 1984 . Warrendale, PA, Society of Automotive Engineers, Inc., 1984, p. 1-9. refs
(Contract NAS3-20073)
(SAE PAPER 841512)

The conventional means of improving gas turbine engine performance typically involves increasing the turbine inlet temperature; however, at these higher operational temperatures the high pressure turbine blades require air-cooling to maintain durability. Air-cooling imposes design, material, and economic constraints not only on the turbine blades but also on engine performance. The use of uncooled turbine blades at increased operating temperatures can offer significantly improved performance in small gas turbine engines. A program to demonstrate uncooled MA6000 high pressure turbine blades in a GTEC TFE731 turbofan engine is being conducted. The project goals include demonstration of the advantages of using uncooled MA6000 turbine blades as compared with cast directionally solidified MAR-M 247 blades. Author

A85-40275* Negev Univ., Beersheva (Israel).
SURFACE HARDENING OF STEEL BY BORIDING IN A COLD RF PLASMA
I. FINBERG, R. AVNI, A. GRILL (Negev, University, Beersheba, Israel), T. SPALVINS, and D. H. BUCKLEY (NASA, Lewis Research Center, Surface Science Branch, Cleveland, OH) Materials Letters (ISSN 0167-577X), vol. 3, April 1985, p. 187-190. Sponsorship: U.S. - Israel Binational Science Foundation. refs
(Contract USIBSF-2813/82)

Scanning electron spectroscopy, X-ray diffractometry, Auger electron spectroscopy, and microhardness measurements, are used to study the surfaces of 4340-steel samples that have been borided in a cold RF plasma which had been initiated in a gas mixture of 2.7 percent diborane in Ar. As a result of the dislocation of the diborane in the plasma, boron is deposited on the surface of the steel substrate and two crystalline phases, tetragonal Fe2B and orthorhombic FeB, are formed. The formation of boride phases then increases the surface microhardness from 2650 MPa to a maximum value of 7740 MPa. O.C.

A85-42568*# National Aeronautics and Space Administration. Lewis Research Center, Cleveland, Ohio.
EFFECT OF SURFACE CONFIGURATION DURING SOLID PARTICLE IMPINGEMENT EROSION
P. V. RAO and D. H. BUCKLEY (NASA, Lewis Research Center, Cleveland, OH) ASME, Transactions, Journal of Engineering for Gas Turbines and Power (ISSN 0022-0825), vol. 107, July 1985, p. 661-668. refs

A study of the progression of erosion and its detrimental effects due to solid particle impingement requires a detailed understanding of the erosion process and morphology of real surfaces of ductile metals. A series of experiments was conducted to investigate the erosion characteristics of aluminum alloy surfaces during spherical glass bead and angular crushed glass particle impingement. The effects of particle shape on cylindrical surfaces and surfaces with pre-existing holes and slits were determined. An attempt was made to understand the relationship between erosion rate and pit morphology. Based on the experimental observations, an empirical relationship between erosion rate and volume loss is presented. This technique provides an improved prediction method for a wide spectrum of ductile materials. Author

A85-42569*# National Aeronautics and Space Administration. Lewis Research Center, Cleveland, Ohio.
CHARACTERIZATION OF SOLID PARTICLE EROSION RESISTANCE OF DUCTILE METALS BASED ON THEIR PROPERTIES
P. V. RAO and D. H. BUCKLEY (NASA, Lewis Research Center, Cleveland, OH) ASME, Transactions, Journal of Engineering for Gas Turbines and Power (ISSN 0022-0825), vol. 107, July 1985, p. 669-678. refs

This paper presents experimental results pertaining to spherical glass bead and angular crushed glass particle impingement. A concept of energy absorption to explain the failure of material is proposed and is correlated with the erosion characteristics of several pure metals. Analyses of extensive erosion data indicate that the properties - surface energy, specific melting energy, strain energy, melting point, bulk modulus, hardness, atomic volume - and the product of the parameters - linear coefficient of thermal expansion x bulk modulus x temperature rise required for melting, and ultimate resilience x hardness - exhibit the best correlations. The properties of surface energy and atomic volume are suggested for the first time for correlation purposes and are found to correlate well with erosion rates at different angles of impingement. It further appears that both energy and thermal properties contribute to the total erosion. Author

A85-43551* National Aeronautics and Space Administration. Lewis Research Center, Cleveland, Ohio.
DIFFUSION WELDING OF MA 6000 AND A CONVENTIONAL NICKEL-BASE SUPERALLOY
T. J. MOORE and T. K. GLASGOW (NASA, Lewis Research Center, Cleveland, OH) Welding Journal, Research Supplement (ISSN 0043-2296), vol. 64, Aug. 1985, p. 219-s to 226-s. refs

A feasibility study of diffusion welding the oxide dispersion strengthened (ODS) alloy MA 6000 to itself and to conventional Ni-base superalloy Udimet 700 was conducted. Butt joints between MA 6000 pieces and lap joints between Udimet 700 and the ODS alloy were produced by hot pressing for 1.25 hr at temperatures ranging from 1000 to 1200 C (1832-2192 F) in vacuum. Following pressing, all weldments were heat treated and machined into mechanical property test specimens. While three different combinations of recrystallized and unrecrystallized MA 6000 butt joints were produced, the unrecrystallized to unrecrystallized joint was most successful as determined by mechanical properties and microstructural examination. Failure to weld the recrystallized material probably related to a lack of adequate deformation at the weld interface. While recrystallized MA 6000 could be diffusion welded to Udimet 700 in places, complete welding over the entire lap joint was not achieved, again due to the lack of sufficient deformation at the faying surfaces. Several methods are proposed to promote the intimate contact necessary for diffusion welding MA 6000 to itself and to superalloys. Author

A85-43979*# Pratt and Whitney Aircraft Group, East Hartford, Conn.
APPLICATION OF TWO CREEP FATIGUE LIFE MODELS FOR THE PREDICTION OF ELEVATED TEMPERATURE CRACK INITIATION OF A NICKEL BASE ALLOY
V. MORENO, D. M. NISSLEY (United Technologies Corp., Pratt and Whitney Group, East Hartford, CT), G. R. HALFORD, and J. F. SALTSMAN (NASA, Lewis Research Center, Cleveland, OH) AIAA, SAE, ASME, and ASEE, Joint Propulsion Conference, 21st, Monterey, CA, July 8-10, 1985. 15 p. refs
(Contract NAS3-23288)
(AIAA PAPER 85-1420)

Cyclic Damage Accumulation (CDA) and Total Strain-Strain Range Partitioning (TS-SRP) models for predicting the creep-fatigue crack initiation life of high temperature alloys are presented. The models differ in their fundamental assumptions regarding the controlling parameters for fatigue crack initiation and in the amount of data required to determine model constants. The CDA model represents a ductility exhaustion approach and uses stress quantities to calculate the cyclic fatigue damage. The TS-SRP model is based on the use of total mechanical strain and earlier concepts of the Strain Range Partitioning Method. Both models were applied to a well controlled fatigue data set at a high temperature nickel base alloy, B1900 + Hf, tested at 1600 F and 1800 F. The tests were divided into a baseline data set required to determine model constants and a verification data set for evaluation of the predictive capability of the models. Both models correlated the baseline data set to within factors of two in life, and predicted the verification data set to within a factor of three or better. In addition, sample calculations to demonstrate the application of each model and discusions of the predictive capabilities and areas requiring further development are presented. Author

A85-44703* National Aeronautics and Space Administration. Lewis Research Center, Cleveland, Ohio.
DENDRITIC SOLIDIFICATION. III - SOME FURTHER REFINEMENTS TO THE MODEL FOR DENDRITIC GROWTH UNDER AN IMPOSED THERMAL GRADIENT
V. LAXMANAN (NASA, Lewis Research Center, Cleveland, OH) Acta Metallurgica (ISSN 0001-6160), vol. 33, Aug. 1985, p. 1475-1480. refs
(Contract NAG3-417)

Some further refinements to a simple model for dendritic solidification in a binary alloy melt under an imposed positive thermal gradient are presented. Two new expressions for the dendrite tip undercooling have been obtained and shown to yield a limiting value of Delta T sub 0 and very small growth rates. Here Delta T sub 0 is the equilibrium solidification range of the alloy. At very large growth rates, all three tip undercooling expressions reach the same limiting value depending on the value of a dimensionless parameter lambda which is related to the effective diffusion distance ahead of the dendrite tip. The predicted tip undercoolings are, however, somewhat lower at intermediate growth rates. An improved calculation for the solute buildup at the dendrite tip due to curvature effects is also included. Author

A85-44772* National Aeronautics and Space Administration. Lewis Research Center, Cleveland, Ohio.
PM SUPERALLOYS - A TROUBLED ADOLESCENT?
R. L. DRESHFIELD and H. R. GRAY (NASA, Lewis Research Center, Cleveland, OH) Metal Powder Report (ISSN 0026-0657), vol. 40, March 1985, 6 p. Previously announced in STAR as N84-26785. refs

The history of powder metallurgy P/M superalloy technology is reviewed with a comment on the state of the art, and speculates on the technology's future potential growth and maturity. M.A.C.

A85-47972* Lockheed-California Co., Burbank.
EFFECT OF LOW TEMPERATURE ON FATIGUE AND FRACTURE PROPERTIES OF TI-5AL-2.5SN(ELI) FOR USE IN ENGINE COMPONENTS
J. T. RYDER (Lockheed-California Co., Burbank) and W. E. WITZELL (General Dynamics Corp., Convair Div., San Diego, CA) IN: Fatigue at low temperatures; Proceedings of the Symposium, Louisville, KY, May 10, 1983 . Philadelphia, PA, ASTM, 1985, p. 210-237. refs
(Contract NAS3-18896)

Experiments were conducted to evaluate the characteristics of the Ti-5Al-2.5Sn (ELI) alloy used in a fuel pump impeller at cryogenic temperatures. Tension, fracture toughness, and fatigue crack propagation data were collected determining the effect of frequency and load ratio on crack propagation. The results revealed that tensile strength increased significantly at 20 K compared to room temperature and fracture toughness was reduced at cryogenic temperatures. The fatigue crack growth rate was not sensitive to experimental conditions and there were only minimal crack orientation effects. Different frequencies produced no effect. At various temperatures and frequencies a load ratio increase resulted in higher crack growth rates. At low stress intensity levels the fatigue rate for both temperatures was the same; however, at high stress intensity levels the crack growth rate at 20 K increased because of the decrease in fracture toughness. The results correlated well with previous data. I.F.

N85-10165*# National Aeronautics and Space Administration. Lewis Research Center, Cleveland, Ohio.
MORPHOLOGICAL CHANGES OF GAMMA PRIME PRECIPITATES IN NICKEL-BASE SUPERALLOY SINGLE CRYSTALS Ph.D. Thesis - Case Western Reserve Univ., May 1984
R. A. MACKAY Jul. 1984 232 p refs
(Contract NSG-3246)
(NASA-TM-83698; E-2156; NAS 1.15:83698) Avail: NTIS HC A11/MF A01 CSCL 11F

Changes in the morphology of the gamma prime precipitate were examined during tensile creep at temperatures between 927 and 1038 C in 001-oriented single crystals of a Ni-Al-Mo-Ta superalloy. In this alloy, which has a large negative misfit of -0.80%, the gamma prime particles link together during creep to form platelets, or rafts, which are aligned with their broad faces perpendicular to the applied tensile axis. The dimensions of the gamma and gamma prime phases were measured as directional coarsening developed in an attempt to trace the changing morphology under various stress levels. In addition, the effects of initial microstructure, as well as slight compositional variations, were related to raft development and creep properties. The results showed that directional coarsening of gamma prime began during primary creep, and under certain conditions, continued to develop after the onset of steady-state creep. The length of the rafts increased linearly with time up to a plateau region. The thickness of the rafts, however, remained equal to the initial gamma prime size at least up through the onset of tertiary creep; this is a clear indication of the stability of the finely-spaced gamma-gamma prime lamellar structure. It was found that the single crystals with the finest gamma prime size exhibited the longest creep lives, because the resultant rafted structure had a larger number of gamma-gamma prime interfaces per unit volume of material. R.J.F.

N85-10166*# Purdue Univ., West Lafayette, Ind.
EFFECTS OF COBALT, BORON, AND ZIRCONIUM ON THE MICROSTRUCTURE OF UDIMET 738 M.S. Thesis. Final Report
T. G. NAKANISHI Sep. 1984 76 p refs
(Contract NAG3-59)
(NASA-CR-174762; NAS 1.26:174762) Avail: NTIS HC A05/MF A01 CSCL 11F

A structural study was carried out on Co modified Udimet 738 alloys containing 0.04, 0.10, and 0.20 wt % Zr at 0.01 and 0.03 wt % B levels. Samples in the as-cast and solution-treated conditions were exposed at 843 C to study structural stability. The structures produced by the interactions of Co, Zr, and B were studied by SEM, X-ray diffraction, and dispersive analysis techniques. The additions of large amounts of Zr and B were found to increase the solidification range of the U-738. Structural changes involved eutectic gamma prime islands, formation of low melting point compounds, and precipitation of borides and Zr rich phases. Boron and zirconium additions did not show substantial changes in mechanical properties. Removal of Co from the alloys resulted in reduction of the matrix solubility for carbon and increase in the gamma prime solvus. Structural instabilities found were continuous grain boundary M23C6 films, MC breakdown, and plate-like phases. Removal of cobalt resulted in a slight decrease in tensile and stress rupture properties. Detailed structural results presented. R.S.F.

N85-10168*# National Aeronautics and Space Administration. Lewis Research Center, Cleveland, Ohio.
THE EFFECTS OF SEVEN ALLOYING ELEMENTS ON THE MICROSTRUCTURE AND STRESS-RUPTURE BEHAVIOR OF NICKLE-BASE SUPERALLOYS
D. R. HULL, R. V. MINER, and C. A. BARRETT Oct. 1984 28 p refs
(NASA-TM-83791; E-2287; NAS 1.15:83791) Avail: NTIS HC A03/MF A01 CSCL 11F

Seven alloying elements: Al, Cr, Ti, Nb, Ta, Mo, and W were added at two levels of concentration to produce a series of experimental nickel-base superalloys. Fifty alloys, representing a fraction of a 2 to the 7th power factorial design, were cast, tested, and analyzed. Each alloy's microstructure was characterized by phase extractions, X-ray diffraction, metallography and energy dispersive X-ray spectroscopy. Regression analysis was used to determine the effect of alloying element content on microstructure and stress-rupture life. Author

N85-11217*# National Aeronautics and Space Administration. Lewis Research Center, Cleveland, Ohio.
THE REACTIONS OF COBALT, IRON AND NICKEL IN SO-2 ATMOSPHERES: SIMILARITIES AND DIFFERENCES
N. S. JACOBSON and W. L. WORRELL (Pennsylvania Univ., Philadelphia) Jun. 1984 13 p refs Presented at the 3rd Intern. Conf. on Transport in Non-Stoichiometric Compounds, University Park, Pa., 11-15 Jun. 1984
(Contract NSF DMR-79-23647)
(NASA-TM-86868; E-2331; NAS 1.15:86868) Avail: NTIS HC A02/MF A01 CSCL 11F

The reactions of cobalt, iron and nickel in SO2 atmospheres are reviewed and compared. A mixed oxide-sulfide product layer is observed in all cases. Cobalt and nickel exhibits similar behavior. The observed rates are near the sulfidation rates, and the reaction rate is strongly influenced by the outward diffusion of metal through an interconnected sulfide network. A continuous interconnected sulfide is not observed in the oxide-sulfide scales formed on iron, and the reaction rates are more difficult to summarize. The differences and similarities among the three metals are explained in terms of the absence of scale-gas equilibrium and the ratio of the metal diffusivity in the corresponding oxide and sulfide.
Author

N85-11221*# Case Western Reserve Univ., Cleveland, Ohio. Dept. of Metallurgy and Materials Science.
THE TRANSIENT OXIDATION OF SINGLE CRYSTAL NIAL+ZR M.S. Thesis. Final Report
J. K. DOYCHAK Sep. 1983 243 p refs
(Contract NAG3-58)
(NASA-CR-174756; NAS 1.26:174756) Avail: NTIS HC A11/MF A01 CSCL 11F

The 800 C oxidation of oriented single crystals of Zr doped beta-NiAl was studied using transmission electron microscopy. The oxide phases and metal-oxide orientation relationships were determined to characterize the transient stages of oxidation prior to the transformation to or formation of alpha-Al2O3. On (001) and (012) metal orientations, NiAl2O4 was the first oxide to form followed by delta-Al2O3 which becomes the predominant oxide

phase. All oxides were highly epitaxially related to the metal; the orientation relationships being function of parallel cation close-packed directions in the meta and oxide. On (011) and (111) metal orientations, gamma-Al2O3 became the predominant oxide phase rather than delta-Al2O3, indicating a structural stability from the highly epitaxial oxides. The relative concentration of aluminum in the oxide scales increased with time indicating preferential gamma-or delta-Al2O3 growth. The striking feature common to the orientation relationships is the alignment of 100 m and 110 ox directions, believed to result from the minimal 3 percent mismatch between the corresponding (100)m and (110)ox planes. M.G.

N85-11223*# Michigan Technological Univ., Houghton.
THE EFFECT OF TANTALUM AND CARBON ON THE STRUCTURE/PROPERTIES OF A SINGLE CRYSTAL NICKEL-BASE SUPERALLOY M.S. Thesis. Final Report
H. C. NGUYEN Oct. 1984 100 p refs
(Contract NAG3-216)
(NASA-CR-174779; NAS 1.26:174779) Avail: NTIS HC A05/MF A01 CSCL 11F

The microstructure, phase chemistry, and creep and hot tensile properties were studied as a function of tantalum and carbon levels in Mar-M247 type single crystal alloys. Microstructural studies showed that several types of carbides (MC, M23C6 and M5C) are present in the normal carbon (0.10 wt % C) alloys after heat treatment. In general, the composition of the MC carbides changes from titanium rich to tantalum rich as the tantalum level in the alloy increases. Small M23C6 carbides are present in all alloys. Tungsten rich M6C carbides are also observed in the alloy containing no tantalum. No carbides are present in the low carbon (0.01 wt % C) alloy series. The morphology of gamma prime is observed to be sensitive to heat treatment and tantalum level in the alloy. Cuboidal gamma prime is present in all the as cast structures. After heat treatment, the gamma prime precipitates tend to have a more spheroidal like morphology, and this tendency increases as the tantalum level decreases. On prolonged aging, the gamma prime reverts back to a cuboidal morphology or under stress at high temperatures, forms a rafted structure. The weight fraction and lattice parameter of the spheroidal gamma prime increases with increasing tantalum content. Changes in the phase chemistry of the gamma prime matrix and gamma prime have also been analyzed using phase extraction techniques. The partitioning ratio decreases for tungsten and aluminum and increases for tantalum as the tantalum content increases for both alloy series; no significant changes occur in the partitioning ratios of the other alloying elements. A reduction in secondary creep rate and an increase in rupture time result from increasing the tantalum content and decreasing the carbon level. R.J.F.

N85-11224*# National Aeronautics and Space Administration. Lewis Research Center, Cleveland, Ohio.
STUDIES ON THE HOT CORROSION OF A NICKEL-BASE SUPERALLOY, UDIMET 700
A. K. MISRA Nov. 1984 47 p refs
(Contract NCC3-43)
(NASA-TM-86882; E-2314; NAS 1.15:86882) Avail: NTIS HC A03/MF A01 CSCL 11F

The hot corrosion of a nickel-base superalloy, Udimet 700, was studied in the temperature range of 884 to 965 C and with different amounts of Na2SO4. Two different modes of degradation were identified: (1) formation of Na2MoO4 - MoO3 melt and fluxing by this melt, and (2) formation of large interconnected sulfides. The dissolution of Cr2O3, TiO2 in the Na2SO4 melt does not play a significant role in the overall corrosion process. The conditions for the formation of massive interconnected sulfides were identified and a mechanism of degradation due to sulfide formation is described. The formation of Ns2MoO4 - MoO3 melt requires an induction period and various physiochemical processes during the induction period were identified. The factors affecting the length of the induction period were also examined. The melt penetration through the oxide appears to be the prime mode of degradation whether the degradation is due to the formation of sulfides or the formation of the Na2MoO4 - MoO3 melt. Author

N85-11225*# Pratt and Whitney Aircraft, East Hartford, Conn.
HOT ISOSTATICALLY PRESSED MANUFACTURE OF HIGH STRENGTH MERL 76 DISK AND SEAL SHAPES Final Report
D. J. EVANS Jul. 1982 12 p 2 Vol.
(Contract NAS3-20072)
(NASA-CR-165550; NAS 1.26:165550; PWA-5574-149) Avail: NTIS HC A02/MF A01 CSCL 11F

The performance of a HIP MERL 76 disk installed in an experimental engine and exposed to realistic operating conditions in a 150 hour, 1500 cycle endurance test is examined. Post test analysis, based on visual, fluorescence penetrant and dimensional inspection, indicates that the disk performs satisfactorily. M.A.C.

N85-12129*# National Aeronautics and Space Administration. Lewis Research Center, Cleveland, Ohio.
EFFECTS OF TIN ON MICROSTRUCTURE AND MECHANICAL BEHAVIOR OF INCONEL 718
R. L. DRESHFIELD, W. A. JOHNSON, and G. A. MAURER 1984 13 p refs Presented at the TMS-AIME Fall Meeting, Detroit, 17-20 Sep. 1984
(NASA-TM-86866; E-2329; NAS 1.15:86866) Avail: NTIS HC A02/MF A01 CSCL 11F

Columbium, for which the United States is 100 percent import reliant, is of strategic importance to the U.S. aerospace industry. A major amount of the Cb is used in Inconel 718. Should Cb sources be disrupted, it may be desired to use a grade of Cb melting stock having greater Sn content then the preferred vacuum rade. Additions of Sn to Inconel 718 were varied from none added to 1 wt %. The Sn additions below 800 ppm had no detrimental effects on 650 C stress rupture behavior; however, 1-wt % Sn severely degraded both life and ductility. Additions of Sn in excess of 200 ppm were slightly detrimental to the 425 C tensile yield strength and ductility. The Sn additions had no effect on the microstructure of Inconel 718 even after stress rupture testing for over 6000 hr at 650 C. R.S.F.

N85-12131*# National Aeronautics and Space Administration. Lewis Research Center, Cleveland, Ohio.
THE EFFECTS OF CR, CO, AL, MO AND TA ON THE CYCLIC OXIDATION BEHAVIOR OF A PROTOTYPE CAST NI-BASE SUPERALLOY BASED ON A 2(5) COMPOSITE STATISTICALLY DESIGNED EXPERIMENT
C. A. BARRETT 1984 20 p refs Presented at the High Temp. Corrosion in Energy Systems 7, Detroit, 17 Sep. 1984; sponsored by AIME and ASM
(NASA-TM-83784; E-2280; NAS 1.15:83784) Avail: NTIS HC A02/MF A01 CSCL 11F

A series of cast Ni-base superalloys were systematically varied at selected levels of Co, Cr, Mo, Ta, and Al. The elemental levels varied were Mo, 0 to 4 percent; Cr, 6 to 18 percent; Co, 0 to 20 percent, Ta, 0 to 8 percent; and Al, 3.25 to 6.25 percent. The cyclic oxidation resistance was determined from specific weight change data as a function of time for 1 hr cycles in static air at 1100 C. The significant terms in decreasing order of their importance were Al, Ta, Cr2, Al-Cr, Cr-Co, Co2, Al-Mo, Cr-Mo, Al-Al, and Mo-Ta. The Al term alone accounted for close to 82 percent of the explained variability. The estimating equation showed that the Al level was the most important and should be at its 6.25 wt % maximum value. The Mo and Ta levels should also be at their maximum 4 and 8 wt % respectively. The cobalt composition should be as low as possible, i.e., 0 wt%. The Cr level optimum varies depending on the other 4 levels. The X-ray diffaction results indicate the most protective scales are alumina/aluminate spinel stabilizized with a tri-rutile oxide high in Ta and Mo. R.S.F.

N85-12132*# National Aeronautics and Space Administration. Lewis Research Center, Cleveland, Ohio.
UNIVERSAL BINDING ENERGY RELATIONS IN METALLIC ADHESION
J. FERRANTE, J. R. SMITH (General Motors Research Labs.), and J. J. ROSE (Iowa State Univ., Ames) 1984 14 p refs Presented at the Materials Research Society Ann. Meeting, Boston, 27-29 Nov. 1984
(NASA-TM-86889; E-2354; NAS 1.15:86889) Avail: NTIS HC A02/MF A01 CSCL 11F

Rose, Smith, and Ferrante have discovered scaling relations which map the adhesive binding energy calculated by Ferrante and Smith onto a single universal binding energy curve. These binding energies are calculated for all combinations of Al(111), Zn(0001), Mg(0001), and Na(110) in contact. The scaling involves normalizing the energy by the maximum binding energy and normalizing distances by a suitable combination of Thomas-Fermi screening lengths. Rose et al. have also found that the calculated cohesive energies of K, Ba, Cu, Mo, and Sm scale by similar simple relations, suggesting the universal relation may be more general than for the simple free electron metals for which it was derived. In addition, the scaling length was defined more generally in order to relate it to measurable physical properties. Further this universality can be extended to chemisorption. A simple and yet quite accurate prediction of a zero temperature equation of state (volume as a function of pressure for metals and alloys) is presented. Thermal expansion coefficients and melting temperatures are predicted by simple, analytic expressions, and results compare favorably with experiment for a broad range of metals. B.W.

N85-13006*# National Aeronautics and Space Administration. Lewis Research Center, Cleveland, Ohio.
EFFECT OF HUMIDITY ON FRETTING WEAR OF SEVERAL PURE METALS
H. GOTO (Cleveland State Univ., Ohio) and D. H. BUCKLEY Dec. 1984 12 p refs
(NASA-TP-2403; E-2184; NAS 1.60:2403) Avail: NTIS HC A02/MF A01 CSCL 11F

Fretting wear experiments with several pure metals were conducted in air at various relative humidity levels. The materials used were iron, aluminum, copper, silver, chromium, titanium, and nickel. Each pure metal had a maximum fretting wear volume at a specific humidity level RH sub max that was not dependent on mechanical factors such as contact load, fretting amplitude, and frequency in the ranges studied. The weight loss due to fretting wear at RH sub max for each pure metal decreased with increasing heat of oxygen adsorption on the metal, indicating that adhesive wear dominated at RH sub max. R.J.F.

N85-13007*# National Aeronautics and Space Administration. Lewis Research Center, Cleveland, Ohio.
STIRLING MATERIAL TECHNOLOGY
R. H. TITRAN, J. R. STEPHENS, and C. M. SCHEUERMANN 1984 22 p refs Presented at the 22nd Automotive Technol. Develop. Contractors' Conf. Coord. Meeting, Dearborn, Mich., 29 Oct. - 2 Nov. 1984; sponsored by the Society of Automotive Engineers
(Contract DE-AI01-77CS-51040)
(NASA-TM-86888; DOE/NASA/51040-57; E-2352; NAS 1.15:86888) Avail: NTIS HC A02/MF A01 CSCL 11F

The Stirling engine is an external combustion engine that offers the advantage of high fuel economy, low emissions, low noise, and low vibrations compared to current internal combustion automotive engines. The most critical component from a materials viewpoint is the heater head consisting of the cylinders, heating tubes, and regenerator housing. Materials requirements for the heater head include compatibility with hydrogen, resistance to hydrogen permeation, high temperature oxidation/corrosion resistance, and high temperature creep-rupture and fatigue properties. A materials research and technology program identified the wrought alloys CG-27 and 12RN72 and the cast alloys XF-818, NASAUT 4G-A1, and NASACC-1 as candidate replacements for the cobalt containing alloys used in current prototype engines. It is concluded that manufacture of the engine is feasible from low cost iron-base alloys rather than the cobalt alloys used in prototype engines. Results of research that lead to this conclusion are presented. R.S.F.

N85-15877*# Massachusetts Inst. of Tech., Cambridge. Dept. of Materials Science and Engineering.
THERMAL-MECHANICAL FATIGUE CRACK GROWTH IN INCONEL X-750 Final Report
N. MARCHAND and R. M. PELLOUX Oct. 1984 17 p refs (Contract NAG3-280)
(NASA-CR-174740; NAS 1.26:174740) Avail: NTIS HC A02/MF A01 CSCL 11F

Thermal-mechanical fatigue crack growth (TMFCG) was studied in a gamma-gamma' nickel base superalloy Inconel X-750 under controlled load amplitude in the temperature range from 300 to 650 C. In-phase (T sub max at sigma sub max), out-of-phase (T sub min at sigma sub max), and isothermal tests at 650 C were performed on single-edge notch bars under fully reversed cyclic conditions. A dc electrical potential method was used to measure crack length. The electrical potential response obtained for each cycle of a given wave form and R value yields information on crack closure and crack extension per cycle. The macroscopic crack growth rates are reported as a function of delta k and the relative magnitude of the TMFCG are discussed in the light of the potential drop information and of the fractographic observations. R.S.F.

N85-15878*# National Aeronautics and Space Administration. Lewis Research Center, Cleveland, Ohio.
OPTIMIZATION OF THE NICRAL-Y/ZRO-Y2O3 THERMAL BARRIER SYSTEM
S. STECURA 1985 24 p refs Presented at the 87th Ann. Meeting of the American Ceramic Society, Cincinnati, 5-9 May 1985
(NASA-TM-86905; E-2394; NAS 1.15:86905) Avail: NTIS HC A02/MF A01 CSCL 11F

The effects of bond and thermal barrier coating compositions, thicknesses, and densities on air plasma spray deposited Ni-Cr-Al-Y/ZrO2-Y2O3 life were evaluated in cyclic furnace oxidation tests at temperatures from 1110 to 1220 C. An empirical relation was developed to give life as a function of the above parameters. The thermal barrier system tested which had the longest life consisted of Ni-35.0 wt% Cr-5.9 wt% Al-0.95 wt% Y bond coating and ZrO2-6.1 wt% Y2O3 thermal barrier coating. Author

N85-18124*# National Aeronautics and Space Administration. Lewis Research Center, Cleveland, Ohio.
A STUDY OF SPECTRUM FATIGUE CRACK PROPAGATION IN TWO ALUMINUM ALLOYS. 1: SPECTRUM SIMPLIFICATION
J. TELESMAN and S. D. ANTOLOVICH (Georgia Inst. of Technology) Jan. 1985 16 p refs 2 Vol.
(NASA-TM-86929; E-2348; NAS 1.15:86929) Avail: NTIS HC A02/MF A01 CSCL 11F

The fatigue crack propagation behavior of two commercial Al alloys was studied using spectrum loading conditions characteristics of those encountered at critical locations in high performance fighter aircraft. A tension dominated (TD) and tension compression (TC) spectrum were employed for each alloy. Using a mechanics-based analysis, it was suggested that negative loads could be eliminated for the TC spectrum for low to intermediate maximum stress intensities. The suggestion was verified by subsequent testing. Using fractographic evidence, it was suggested that a further similification in the spectra could be accomplished by eliminating low and intermediate peak load points resulting in near or below threshold maximum peak stress intensity values. It is concluded that load interactions become more important at higher stress intensities and more plasticity at the crack tip. These results suggest that a combined mechanics/fractographic mechanisms approach can be used to simplify other complex spectra. M.G.

N85-18125*# National Aeronautics and Space Administration. Lewis Research Center, Cleveland, Ohio.
A STUDY OF SPECTRUM FATIGUE CRACK PROPAGATION IN TWO ALUMINUM ALLOYS. 2: INFLUENCE OF MICROSTRUCTURES
J. TELESMAN and S. D. ANTOLOVICH (Georgia Inst. of Technology) Jan. 1985 19 p refs 2 Vol.
(NASA-TM-86930; E-2439; NAS 1.15:86930) Avail: NTIS HC A02/MF A01 CSCL 11F

The important metallurgical factors that influence both constant amplitude and spectrum crack growth behavior in aluminum alloys were investigated. The effect of microstructural features such as grain size, inclusions, and dispersoids was evaluated. It was shown that a lower stress intensities, the I/M 7050 alloy showed better fatigue crack propagation (FCP) resistance than P/M 7091 alloy for both constant amplitude and spectrum testing. It was suggested that the most important microstructural variable accounting for superior FCP resistance of 7050 alloy is its large grain size. It was further postulated that the inhomogenous planar slip and large grain size of 7050 limit dislocation interactions and thus increase slip reversibility which improves FCP performance. The hypothesis was supported by establishing that the cyclic strain hardening exponent for the 7091 alloy is higher than that of 7050. M.G.

N85-18126*# National Aeronautics and Space Administration. Lewis Research Center, Cleveland, Ohio.
REPLACEABLE BLADE TURBINE AND STATIONARY SPECIMEN CORROSION TESTING FACILITY
G. J. SANTORO and F. D. CALFO Jan. 1985 21 p refs
(NASA-TM-86931; E-2371; NAS 1.15:86931) Avail: NTIS HC A02/MF A01 CSCL 11F

A facility was constructed to provide relatively low cost testing of hot section turbine blade and vane materials under hot corrosion conditions more akin to service environments. The facility consists of a small combustor whose pressurized gas flow can be directed to either a test section consisting of three small cascaded specimens or to a partial admittance single-stage axial flow turbine. The turbine rotor contains 28 replaceable turbine blades. The combustion gases resulting from the burning of Jet A-I fuel can be seeded with measured amounts of alkali salts. This facility is described here along with preliminary corrosion test results obtained during the final checkout of the facility. Author

N85-18127*# Michigan Technological Univ., Houghton.
THE EFFECT OF TANTALUM ON THE STRUCTURE/PROPERTIES OF TWO POLYCRYSTALLINE NICKEL-BASE SUPERALLOYS: B-1900 + HF MAR-M247 M.S. Thesis, Final Report
G. M. JANOWSKI Washington Feb. 1985 109 p refs
(Contract NAG3-216)
(NASA-CR-174847; NAS 1.26:174847) Avail: NTIS HC A06/MF A01 CSCL 11F

The microstructure, phase compositions, and phase fractions were studied in conventionally cast B-1900 + Hf and both conventionally cast and directionally solidified MAR-M247 as a function of tantalum concentration. The hot tensile and creep rupture properties of the solutionized and aged MAR-M247-type alloys were also determined as a function of tantalum level. The effects of tantalum on the microstructure and phase compositions of B-1900 + Hf and MAR-M247 (conventionally cast and directionally solidified) were found to be very similar. The addition of tantalum to the as cast and heat treated alloys was shown to cause the partial replacement of the Hf in the MC carbides by Ta, although the degree of replacement was decreased by the solutionizing and aging heat treatment. The gamma prime and minor phase fractions (primarily MC type carbides) both increased approximately linearly with tantalum concentration. The gamma prime phase compositions were relatively insensitive to tantalum variations with the exception of the tantalum and/or hafnium levels. Bulk tantalum additions increased the tantalum, chromium, and cobalt levels of the gamma phase in both alloy series. The increase in the concentrations of the latter two elements in the gamma phase was a result of the decrease in the gamma phase fraction with increasing bulk tantalum concentration and constant gamma/gamma prime partitioning ratio. Tantalum additions increased the yield stress and ultimate tensile strength of the directionally solidified MAR-M247 type alloys and had no significant effect on ductility. B.W.

N85-19072*# National Aeronautics and Space Administration. Lewis Research Center, Cleveland, Ohio.
HIGH TEMPERATURE PROPERTIES OF EQUIATOMIC FEAL WITH TERNARY ADDITIONS
R. H. TITRAN, K. M. VEDULA (Case Western Reserve Univ.), and G. G. ANDERSON (Case Western Reserve Univ.) 1984 14 p refs Presented at the Fall Meeting of the Mater. Res. Soc., Boston, 26-30 Nov. 1984
(NASA-TM-86938; E-2452; NAS 1.15:86938) Avail: NTIS HC A02/MF A01 CSCL 11F

The aluminide intermetallic compounds are considered potential structural materials for aerospace applications. The B2 binary aluminide FeAl has a melting point in excess of 1500 K, is of simple cubic structure, exits over a wide range of composition with solubility for third elements and is potentially self-protecting in extreme environments. The B2 FeAl compound has been alloyed with 1 to 5 at % ternary additions of Si, Ti, Zr, Hf, Cr, Ni, Co, Nb, Ta, Mo, W, and Re. The alloys were prepared by blending a third elemental powder with prealloyed binary FeAl powder. Consolidation was by hot extrusion at 1250 K. Annealing studies on the extruded rods showed that the third element addition can be classified into three categories based upon the amount of homogenization and the extent of solid solutioning. Constant strain rate compression tests were performed to determine the flow stress as a function of temperature and composition. The mechanical strength behavior was dependent upon the third element homogenization classification. Author

N85-19073*# Michigan Technological Univ., Houghton.
EFFECTS OF MAR-M247 SUBSTRATE (MODIFIED) COMPOSITION ON COATING OXIDATION COATING/SUBSTRATE INTERDIFFUSION M.S. Thesis. Final Report
B. H. PILSNER Feb. 1985 126 p refs
(Contract NAG3-216)
(NASA-CR-174851; NAS 1.26:174851) Avail: NTIS HC A07/MF A01 CSCL 11F

The effects of gamma+gamma' Mar-M247 substrate composition on gamma+beta Ni-Cr-Al-Zr coating oxidation and coating/substrate interdiffusion were evaluated. These results were also compared to a prior study for a Ni-Cr-Al-Zr coated gamma Ni-Cr-Al substrate with equivalent Al and Cr atomic percentages. Cyclic oxidation behavior at 1130 C was investigated using change in weight curves. Concentration/distance profiles were measured for Al, Cr, Co, W, and Ta. The surface oxides were examined by X-ray diffraction and scanning electron microscopy. The results indicate that variations of Ta and C concentrations in the substrate do not affect oxidation resistance, while additions of grain boundary strengthening elements (Zr, Hf, B) increase oxidation resistance. In addition, the results indicate that oxidation phenomena in gamma+beta/gamma+gamma' Mar-M247 systems have similar characteristics to the I gamma+beta/gamma Ni-Cr-Al system.
Author

N85-19074*# National Aeronautics and Space Administration. Lewis Research Center, Cleveland, Ohio.
LOW CYCLE FATIGUE OF MAR-M 200 SINGLE CRYSTALS AT 760 AND 870 DEG C
W. W. MILLIGAN (Georgia Inst. of Tech., Atlanta), N. JAYARAMAN (Cincinnati Univ.), and R. C. BILL 1984 31 p refs Presented at the TMS-AIME Fall Meeting, Detroit, 17-19 Sep. 1984 Prepared in cooperation with Army Research and Technology Labs., Cleveland
(Contract DA PROJ. 1L1-61101-AH-45)
(NASA-TM-86933; E-2444; NAS 1.15:86933; USAAVSCOM-TR-85-C-1) Avail: NTIS HC A03/MF A01 CSCL 11F

Fully reversed low cycle fatigue tests were conducted on single crystals of the nickel-base superalloys Mar-M 200 at 760 C and 870 C. At 760 C, planar slip (octahedral) lead to orientation-dependent strain hardening and cyclic lives. Multiple slip crystals strain hardened the most, resulting in relatively high stress ranges and low lives. Single slip crystals strain hardened the least, resulting in relatively low stress ranges and higher lives. A preferential crack initiation site which was related to slip plane geometry was observed in single slip orientated crystals. At 870 C, the trends were quite different, and the slip character was much more homogeneous. As the tensile axis orientation deviated from 001 , the stress ranges increased and the cyclic lives decreased. Two possible mechanisms were proposed to explain the behavior: one is based on Takeuchi and Kuramoto's cube cross-slip model, and the other is based on orientation-dependent creep rates. E.A.K.

N85-19075*# National Aeronautics and Space Administration. Lewis Research Center, Cleveland, Ohio.
CHARACTERIZATION OF EROSION OF METALLIC MATERIALS UNDER CAVITATION ATTACK IN A MINERAL OIL
B. C. S. RAO (Case Western Reserve Univ.) and D. H. BUCKLEY 1985 24 p refs Proposed for presentation at the Tribology Conf., Atlanta, 8-10 Oct. 1985; sponsored by the American Society of Lubrication Engineers and the American Society of Mechanical Engineers
(NASA-TM-86934; E-2049-1; NAS 1.15:86934) Avail: NTIS HC A02/MF A01 CSCL 11F

Cavitation erosion and erosion rates of eight metallic materials representing three crystal structures were studied. The erosion experiments were conducted with a 20-kHz ultrasonic magnetostrictive oscillator in a viscous mineral oil. The erosion rates of the metals with an fcc matrix were 10 to 100 times higher than that of an hop-matrix titanium alloy. The erosion rates of iron and molybdenum, with bcc matrices, were higher than that of the titanium alloy but lower than those of those of the fcc materials. Studies with scanning electron microscopy indicated that the cavitation pits were initially formed at the grain boundaries and precipitates and that the pits formed at the junction of grain boundaries grew faster than the others. Transcrystalline craters formed by cavitation attack over the surface of grains and roughened the surfaces by multiple slip and twinning. Surface roughness measurements showed that the pits that formed over the grain boundaries deepened faster than pits. Computer analysis revealed that a geometric expression describes the nondimensional erosion curves during the time period 0.5 t (sub 0) t 2.5 t (sub 0), where t (sub 0) is the incubation period. The fcc metals had very short incubation periods; the titanium alloy had the longest incubation period. Author

N85-19076*# National Aeronautics and Space Administration. Lewis Research Center, Cleveland, Ohio.
THE B2 ALUMINIDES AS ALTERNATIVE MATERIALS
J. R. STEPHENS 1984 26 p refs Presented at the Fall Meeting of the Mater. Res. Soc., Boston, 26-30 Nov. 1984
(NASA-TM-86937; E-2451; NAS 1.15:86937) Avail: NTIS HC A03/MF A01 CSCL 11F

The potential of the B2 aluminides as structural material alternatives for the strategic element containing superalloys currently used in gas turbine engines is being explored with emphasis on the equiatomic Fe and Ni aluminides. Although Co is a strategic material, the equiatomic Co aluminide is also being studied to gain a more complete understanding of these fourth period intermetallics. Research focuses on initial processing techniques such as ingot melting, power metallurgy, and rapid solidification with and without additional thermomechanical processing; high temperature deformation - primarily compressive creep; compositional effects within the binary B2 aluminides; third-element alloying addition effects on high temperature strength and oxidation resistance, and near room temperature ductility as influenced by processing, alloying, and grain size. Various programs now underway are reviewed and some highlights of research results are presented. A.R.H.

N85-19078*# IIT Research Inst., Chicago, Ill.
CREEP-RUPTURE BEHAVIOR OF IRON SUPERALLOYS IN HIGH-PRESSURE HYDROGEN Quarterly Narrative Report, 7 Dec. 1982 - 28 Feb. 1983
S. BHATTACHARYYA and W. PETERMAN Jun. 1984 44 p
(Contract DEN3-303)
(NASA-CR-174411; NAS 1.26:174411; IITRI-M06116-3; QNR-1)
Avail: NTIS HC A03/MF A01 CSCL 11F

The creep-rupture properties of five iron-base and one cobalt-base high temperature alloys were investigated to assess the feasibility of using the alloys as construction materials in a Stirling engine. The alloys were heat treated and hardness measurements were taken. Typical microstructures of the alloys are shown. The creep-rupture properties of the alloys were determined at 760 and 815 C in 15.0 MPa H2 for 200 to 1000 hours. Plots of rupture life versus stress for the six superalloys are presented along with creep strain-time plots. R.S.F.

N85-20041*# Michigan Technological Univ., Houghton.
A STUDY OF INTERDIFFUSION IN BETA + GAMMA/GAMMA + GAMMA PRIME NI-CR-AL M.S. Thesis. Final Report
L. A. CAROL Feb. 1985 191 p refs
(Contract NAG3-244)
(NASA-CR-174852; NAS 1.26:174852) Avail: NTIS HC A09/MF A01 CSCL 11F

Ternary diffusion in the NiCrAl system at 1200 C was studied with beta + gamma/gamma + gamma prime infinite diffusion couples. Interdiffusion resulted in the formation of complex, multiphase diffusion zones. Concentration/distance profiles for Cr and Al in the phases present in the diffusion zone were measured after 200 hr. The Ni-rich portion of the NiCrAl phase diagram (1200 C) was also determined. From these data, bulk Cr and Al profiles were calculated and translated to diffusion paths on the ternary isotherm. Growth layer kinetics of the layers present in the diffusion zone were also measured. B.G.

N85-20042*# National Aeronautics and Space Administration. Lewis Research Center, Cleveland, Ohio.
RAPIDLY SOLIDIFIED NIAL AND FEAL
D. J. GAYDOSH and M. A. CRIMP 1984 10 p refs
(NASA-TM-86941; E-2289; NAS 1.15:86941) Avail: NTIS HC A02/MF A01 CSCL 11F

Melt spinning was used to produce rapidly solidified ribbons of the B2 intermetallics NiAl and FeAl. Both Fe-40Al and Fe-45Al possessed some bend ductility in the as spun condition. The bend ductility of Fe-40Al, Fe-45Al, and equiatomic NiAl increased with subsequent heat treatment. Heat treatment at approximately 0.85 T (sub m) resulted in significant grain growth in equiatomic FeAl and in all the NiAl compositions. Low bend ductility in both FeAl and NiAl generally coincided with intergranular failure, while increased bend ductility was characterized by increasing amounts of transgranular cleavage fracture. Author

N85-20043*# National Aeronautics and Space Administration. Lewis Research Center, Cleveland, Ohio.
THE RESPONSE OF COBALT-FREE UDIMET 700 TYPE ALLOY TO MODIFIED HEAT TREATMENTS
F. H. HARF 28 Feb. 1985 27 p refs Presented at the 114th Ann. Meeting of the Am. Inst. of Mining, Met. and Petrol. Engr., New York, 24-28 Feb. 1985
(NASA-TM-86942; E-2335; NAS 1.15:86942) Avail: NTIS HC A03/MF A01 CSCL 11F

A superalloy based on Udimet 700, in which all of the cobalt was replaced by nickel, was prepared from hot isostatically pressed prealloyed powders. This material was given various heat treatments consisting of partial solutioning and aging in a sequence of four different temperatures. Comparisons were made of microstructures and mechanical properties. Best results were obtained by partially solutioning at 1145 deg C and aging through a sequence of 870, 1030, 650 and 760 deg C. This heat treatment also provided significantly improved properties for wrought material of the same composition. The results suggest that cobalt free Udimet 700 should be considered as a substitute for Udimet 700 with the standard 17 percent cobalt content. R.J.F.

N85-21320*# Case Western Reserve Univ., Cleveland, Ohio.
EFFECT OF REDUCTION OF STRATEGIC COLUMBIUM ADDITION IN 718 ALLOY ON THE STRUCTURE AND PROPERTIES Final Report
K. R. ZIEGLER and J. F. WALLACE Jan. 1985 179 p refs (Contract NAG3-268)
(NASA-CR-174841; NAS 1.26:174841) Avail: NTIS HC A09/MF A01 CSCL 11F

A series of alloys was developed having a base composition similar to Inconel 718, with reduced Cb levels of 3.00 and 1.10 wt% Cb. Substitutions of 3.0% W, 3.0W + 0.9V or Mo increased from 3.0% to 5.8% were made for the Cb in these alloys. Two additional alloys, one containing 3.49% Cb and 1.10% Ti and another containing 3.89% Cb and 1.29% Ti were also studied. Tensile properties at rooom and elevated temperatures, stress-rupture tests, and an analysis of extracted phases were carried out for each of the alloys. Additions of solid solution elements to a reduced Cb alloy had no significant effect on the properties of the alloys under either process condition. The solution and age alloys with substitutions of 1.27% i at 3.89% Cb had tensile properties similar top hose of the original alloy and stress-rupture properties superior to the original alloy. The improved stress-rupture properties were the result of significant precipitation of Ni3Ti-gamma prime in the alloy, which is more stable than gamma' at the elevated temperatures. At lower temperatures, the new alloy benefits from gamma' strengthening. With more precise control and proper processing, the reduced Cb direct-age alloy could substitute for Alloy 718 in high strength applications. A.R.H.

N85-21321*# National Aeronautics and Space Administration. Lewis Research Center, Cleveland, Ohio.
DIGITAL TEMPERATURE AND VELOCITY CONTROL OF MACH 0.3 ATMOSPHERIC PRESSURE DURABILITY TESTING BURNER RIGS IN LONG TIME, UNATTENDED CYCLIC TESTING
D. L. DEADMORE Mar. 1985 37 p refs
(NASA-TM-86959; E-2484; NAS 1.15:86959) Avail: NTIS HC A03/MF A01 CSCL 11F

Hardware and software were developed to implement the hybrid digital control of two Jet A-1 fueled Mach 0.3 burners from startup to completion of a preset number of hot corrosion flame durability cycle tests of materials at 1652 F. This was accomplished by use of a basic language programmable microcomputer and data aquisition and control unit connected together by the IEEE-488 Bus. The absolute specimen temperature was controlled to + or - 3 F by use of digital adjustment of the fuel flow using a P-I-D (Proportional-Integral-Derivative) control algorithm. The specimen temperature was within + or - 2 F of the set point more than 90 percent of the time. Pressure control was achieved by digital adjustment of the combustion air flow using a proportional control algorithm. The burner pressure was controlled at 1.0 + or - 0.02 psig. Logic schemes were incorporated into the system to protect the test specimen from abnormal test conditions in the event of a hardware of software malfunction. Author

N85-21322*# National Aeronautics and Space Administration. Lewis Research Center, Cleveland, Ohio.
ALLOYS BASED ON NIAL FOR HIGH TEMPERATURE APPLICATIONS
K. M. VEDULA (Case Western Reserve Univ.), V. PATHARE, I. ASLANIDIS (Case Western Reserve Univ.), and R. H. TITRAN 1984 13 p refs Presented at the 1984 Fall Meeting of Materials Research Society, Boston, 26-30 Nov. 1984
(NASA-TM-86976; E-2513; NAS 1.15:86976) Avail: NTIS HC A02/MF A01 CSCL 11F

The NiAl alloys for potential high temperature applications were studied. Alloys were prepared by powder metallurgy techniques. Flow stress values at slow strain rates and high temperatures were measured. Some ternary alloying additions (Hf, Ta and Nb) were identified. The mechanism of strengthening in alloys containing these additions appears to be a form of particle dislocation interaction. The effects of grain size and stoichiometry in binary alloys are also presented. E.A.K.

N85-21323*# National Aeronautics and Space Administration. Lewis Research Center, Cleveland, Ohio.
EFFECTS OF CHROMIUM AND ALUMINUM ON MECHANICAL AND OXIDATION PROPERTIES OF IRON-NICKEL-BASE SUPERALLOYS BASED ON CG-27
S. R. SCHUON Mar. 1985 26 p refs Presented at the TMS-AIME Fall Meeting, Detroit, 17-20 Sep. 1984
(NASA-TP-2443; E-2320; NAS 1.60:2443) Avail: NTIS HC A03/MF A01 CSCL 11F

The effects of chromium and aluminum on the mechanical and oxidation properties of a series of gamma-prime-strengthened alloys based on CG-27 were studied. Gamma-prime dispersion and solid-solution strengthening were the principal modes of alloy strengthening. The oxidation attack parameter K sub a decreased with increasing Cr and Al contents for each alloy group based on Al content. As a group, alloys with 3 wt % Al had the lowest attack parameters. Therefore, 3 wt % is the optimum level of Al for parabolic oxidation behavior. Spalling, due to diffusion-induced grain growth, was controlled by the overall Cr and Al levels. The alloy with 4 wt % Cr and 3 wt % Al had stress-rupture properties superior to those of the base alloy, CG-27, and maintained parabolic oxidation behavior while the Cr content was reduced by two-thirds of its value in cast CG-27. E.A.K.

N85-21324*# National Aeronautics and Space Administration. Lewis Research Center, Cleveland, Ohio.
ION-BEAM NITRIDING OF STEELS Patent Application
J. SALIK and T. E. HUBBELL, JR., inventors (to NASA) 16 Oct. 1984 12 p
(NASA-CASE-LEW-14104-1; NAS 1.71:LEW-14104-1; US-PATENT-APPL-SN-661481) Avail: NTIS HC A02/MF A01 CSCL 11F

A surface of a steel substrate is nitrided by exposing it to a beam of nitrogen ions under a low pressure. The pressure is much lower than that employed for ion-nitriding, and an ion source is used instead of a glow discharge. Both of these feathers reduce the introduction of impurities into the substrate surface. NASA

N85-22660*# National Aeronautics and Space Administration. Lewis Research Center, Cleveland, Ohio.
ORIENTATION AND TEMPERATURE DEPENDENCE OF SOME MECHANICAL PROPERTIES OF THE SINGLE-CRYSTAL NICKEL-BASE SUPERALLOY RENE N4. 3: TENSION-COMPRESSION ANISOTROPY
R. V. MINER, T. P. GAAB, J. GAYDA, and K. J. HEMKER (Cincinnati Univ.) 1985 21 p refs Presented at the 114th Ann. meeting of the American Inst. of Mining, Metallurgical and Petroleum Engineers, New York, 24-28 Feb. 1985
(NASA-TM-86982; E-2525; NAS 1.15:86982) Avail: NTIS HC A02/MF A01 CSCL 11F

Single crystal superalloy specimens with various crystallographic directions along their axes were tested in compression at room temperature, 650, 760, 870, and 980 deg C. These results are compared with the tensile behavior studied previously. The alloy, Rene N4, was developed for gas turbine engine blades and has the nominal composition 3.7 Al, 4.2 Ti, 4 Ta, 0.5 Nb, 6 W, 1.5 Mo 9 Cr. 7.5 Co, balance Ni, in weight percent. Slip trace analysis showed that primary cube slip occurred even at room temperature for the 111 specimens. With increasing test temperature more orientations exhibited primary cube slip, until at 870 deg C only the 100 and 011 specimens exhibited normal octahedral slip. The yield strength for octahedral slip was numerically analysed using a model proposed by Lall, Chin, and Pope to explain deviations from Schmid's Law in the yielding behavior of a single phase Gamma prime alloy, Ni3(Al, Nb). The Schmid's Law deviations in Rene N4 were found to be largely due to a tension-compression anisotropy. A second effect, which increases trength for orientations away from 001, was found to be small in Rene N4. Analysis of recently published data on the single crystal superalloy PWA 1480 yielded the same result. R.J.F.

N85-22661*# Georgia Inst. of Tech., Atlanta. School of Physics.
STUDY OF THE EFFECTS OF IMPLANTATION ON THE HIGH FE-NI-CR AND NI-CR-AL ALLOYS Final Report
M. W. RIBARSKY 12 Apr. 1985 36 p refs
(Contract NAG3-255)
(NASA-CR-175625; NAS 1.26:175625) Avail: NTIS HC A03/MF A01 CSCL 11F

A theoretical study of the effects of implantation on the corrosion resistance of Fe-Ni-Cr and Ni-Cr-Al alloys was undertaken. The purpose was to elucidate the process by which corrosion scales form on alloy surfaces. The experiments dealt with Ni implanted with Al, exposed to S at high temperatures, and then analyzed using scanning electron microscopy, scanning Auger spectroscopy and X-ray fluorescence spectroscopy. Pair bonding and tight-binding models were developed to study the compositions of the alloys and as a result, a new surface ordering effect was found which may exist in certain real alloys. With these models, the behavior of alloy constituents in the presence of surface concentrations of O or S was also studied. Improvements of the models to take into account the important effects of long- and short-range ordering were considered. The diffusion kinetics of implant profiles at various temperatures were investigated, and it was found that significant non-equilibrium changes in the profiles can take place which may affect the implants' performance in the presence of surface contaminants. R.J.F.

N85-26962*# Connecticut Univ., Storrs.
IRON RICH LOW COST SUPERALLOYS Ph.D. Thesis. Final Report
S. F. WAYNE Cleveland May 1985 169 p refs
(Contract NAG3-271)
(NASA-CR-174900; NAS 1.26:174900) Avail: NTIS HC A08/MF A01 CSCL 11F

An iron-rich low-cost superalloy was developed. The alloy, when processed by conventional chill casting, has physical and mechanical properties that compare favorably with existing nickel and cobalt based superalloys while containing significantly lower amounts of strategic elements. Studies were also made on the properties of Cr(20)-Mn(10)-C(3.4)-Fe(bal.), a eutectic alloy processed by chill casting and directional solidification which produced an aligned microstructure consisting of M7C3 fibers in a gamma-Fe matrix. Thermal expansion of the M7C3 (M = Fe, Cr, Mn) carbide lattice was measured up to 800 C and found to be highly anisotropic, with the a-axis being the predominant mode of expansion. Repetitive impact sliding wear experiments performed with the Fe rich eutectic alloy showed that the directionally solidified microstructure greatly improved the alloy's wear resistance as compared to the chill cast microstructure and conventional nickel base superalloys. Studies on the molybdenum cementite phase prove that the crystal structure of the xi phase is not orthorhombic. The crystal structure of the xi phase is made up of octahedra building elements consisting of four Mo and two Fe atoms and trigonal prisms consisting of four Fe and two Mo atoms. The voids are occupied by carbon atoms. The previous chemical formula for the molybdenum cementite MoFe2C is now clearly seen to be Mo12Fe22C10. Author

N85-26963*# National Aeronautics and Space Administration. Lewis Research Center, Cleveland, Ohio.
PROPERTIES AND MICROSTRUCTURES FOR DUAL ALLOY COMBINATIONS OF THREE SUPERALLOYS WITH ALLOY 901
F. H. HARF 1985 43 p refs Presented at the 114th Ann. Meeting of the Am. Inst. of Mining, Met. and Petroleum Engr., New York, 24-28 Feb. 1985
(NASA-TM-86987; E-2397; NAS 1.15:86987) Avail: NTIS HC A03/MF A01 CSCL 11F

Dual alloy combinations have potential for use in aircraft engine components such as turbine disks where a wide range of stress and temperature regimes exists during operation. Such alloy combinations may directly result in the conservation of elements which are costly or not available domestically. Preferably, a uniform heat treatment yielding good properties for both alloys should be used. Dual alloy combinations of iron rich Alloy 901 with nickel base superalloys Rene 95, Astroloy, or MERL 76 were not isostatically pressed from prealloyed powders. Individual alloys, alloy mixtures, and layered alloy combinations were given the heat treatments specified for their use in turbine disks or appropriate for Alloy 901. Selected specimens were overaged for 1500 hr at 650 C. Metallographic examinations revealed the absence of phases not originally present in either alloy of a combination. Mechanical tests showed adequate properties in combinations of Rene 95 or Astroloy with Alloy 901 when given the Alloy 901 heat treatment. Combinations with MERL 76 had better properties when given the MERL 76 heat treatment. The results indicate that these combinations are promising candidates for use in turbine disks. Author

N85-26964*# National Aeronautics and Space Administration. Lewis Research Center, Cleveland, Ohio.
MULTIAXIAL AND THERMOMECHANICAL FATIGUE CONSIDERATIONS IN DAMAGE TOLERANT DESIGN
G. E. LEESE (TRW, Inc., Cleveland) and R. C. BILL 1985 21 p refs Presented at the 60th Meeting of the Struct. and Mater. Panel, San Antonio, 21-26 Apr. 1985; sponsored by AGARD Prepared in cooperation with Army Research and Technology Labs., Cleveland
(NASA-TM-87022; E-2514; NAS 1.15:87022; USAAVSCOM-TR-85-C-5; AD-A157112) Avail: NTIS HC A02/MF A01 CSCL 11F

In considering damage tolerant design concepts for gas turbine hot section components, several challenging concerns arise: Complex multiaxial loading situations are encountered; Thermomechanical fatigue loading involving very wide temperature ranges is imposed on components; Some hot section materials are extremely anisotropic; and coatings and environmental interactions play an important role in crack propagation. The effects of multiaxiality and thermomechanical fatigue are considered from the standpoint of their impact on damage tolerant design concepts. Recently obtained research results as well as results from the open literature are examined and their implications for damage tolerant design are discussed. Three important needs required to advance analytical capabilities in support of damage tolerant design

become readily apparent: (1) a theoretical basis to account for the effect of nonproportional loading (mechanical and mechanical/thermal); (2) the development of practical crack growth parameters that are applicable to thermomechanical fatigue situations; and (3) the development of crack growth models that address multiple crack failures. Author

N85-31283*# National Aeronautics and Space Administration. Lewis Research Center, Cleveland, Ohio.
ADVANCED THERMAL BARRIER SYSTEM BOND COATINGS FOR USE ON NI, CO-, AND FE-BASE ALLOY SUBSTRATES
S. STECURA Jul. 1985 22 p refs
(NASA-TM-87062; E-2437; NAS 1.15:87062) Avail: NTIS HC A02/MF A01 CSCL 11F

New and improved Ni-, Co-, and Fe-base bond coatings have been identified for the ZrO2-Y2O3 thermal barrier coatings to be used on NI-, Co-, and Fe-base alloy substrates. These bond coatings were evaluated in a cyclic furnace between 1120 and 1175 C. It was found that MCrAlYb (where M = Ni, Co, or Fe) bond coating thermal barrier systems. The longest life was obtained with the FeCrAlYb thermal barrier system followed by NiCrAlYb and CoCrAlYb thermal barrier systems in that order. Author

N85-31284*# National Aeronautics and Space Administration. Lewis Research Center, Cleveland, Ohio.
A MULTIPLE LINEAR REGRESSION ANALYSIS OF HOT CORROSION ATTACK ON A SERIES OF NICKEL BASE TURBINE ALLOYS
C. A. BARRETT Jul. 1985 21 p refs
(NASA-TM-87020; E-2491; NAS 1.15:87020) Avail: NTIS HC A02/MF A01 CSCL 11F

Multiple linear regression analysis was used to determine an equation for estimating hot corrosion attack for a series of Ni base cast turbine alloys. The U transform (i.e., 1/sin (% A/100) to the 1/2) was shown to give the best estimate of the dependent variable, y. A complete second degree equation is described for the centered' weight chemistries for the elements Cr, Al, Ti, Mo, W, Cb, Ta, and Co. In addition linear terms for the minor elements C, B, and Zr were added for a basic 47 term equation. The best reduced equation was determined by the stepwise selection method with essentially 13 terms. The Cr term was found to be the most important accounting for 60 percent of the explained variability hot corrosion attack. Author

N85-32173*# Case Western Reserve Univ., Cleveland, Ohio. Dept. of Chemistry.
WHY CO BONDS SIDE-ON AT LOW COVERAGE AND BOTH SIDE-ON AND UPRIGHT AT HIGH COVERAGE ON THE CR(110) SURFACE
S. P. MEHANDRU and A. B. ANDERSON 1985 16 p refs
(Contract NAG3-341)
(NASA-CR-176071; NAS 1.26:176071) Avail: NTIS HC A02/MF A01 CSCL 11F

An atom superposition and electron delocalization molecular orbital study of CO adsorption on the Cr(110) surface shows a high coordinate lying down orientation is favored. This is a result of the large number of empty d-band energy levels in chromium, which allows the antibonding counterparts to sigma and pi donation bonds to the surface to be empty. When lying down, backbonding to CO pi sup * orbitals is enhanced. Repulsive interactions cause additional CO to stand upright at 1/4 monolyer coverage. The results confirm the recent experimental study of Shinn and Madey. Author

N85-32174*# Case Western Reserve Univ., Cleveland, Ohio. Dept. of Chemistry.
MOLECULAR ORBITAL STUDIES IN OXIDATION: SULFATE FORMATION AND METAL-METAL OXIDE ADHESION Final Report, 30 Oct. 1982 - 31 Jul. 1985
A. B. ANDERSON 31 Jul. 1985 5 p refs
(Contract NAG3-341)
(NASA-CR-176070; NAS 1.26:176070) Avail: NTIS HC A02/MF A01 CSCL 11F

The chemical mechanisms for sulfate formation from sodium chloride and sulfur trioxide, which is a product of jet fuel combustion was determined. Molten sodium sulfate leads to hot corrosion of the protective oxide layers on turbine blades. How yttrium dopants in nidkel-aluminum alloys used in turbine blades reduce the spalling rate of protective alumina films and enhance their adhesion was also determined. Two other fulfate mechanisms were deduced and structure of carbon monoxide on a clean chronium and clean platinum-titanium alloys surfaces was determined. All studies were by use of the atom superposition and electron delocalization molecular orbital (ASED-MO) theory. Seven studies were completed. Their titles and abstracts are given. Author

N85-32175*# Case Western Reserve Univ., Cleveland, Ohio. Dept. of Chemistry.
ADSORPTION OF O2, SO2, AND SO3 ON NICKEL OXIDE. MECHANISM FOR SULFATE FORMATION
S. P. MEHANDRU (Delhi Univ., India) and A. B. ANDERSON 1985 28 p refs
(Contract NAG3-341)
(NASA-CR-176072; NAS 1.26:176072) Avail: NTIS HC A03/MF A01 CSCL 11F

Calculations based on the atom superposition and electron delocalization molecular orbital (ASED-MO) technique suggest that O2 will adsorb perferentially end-on at an angle 45 deg from normal on a nickel cation site on the (100) surface of NiO. SO2 adsorption is also stronger on the nickel site; SO2 bonds through the sulfur atom is a plane perpendicular to the surface. Adsorption energies for SO3 on the nickel and oxygen sites are comparable in the perferred orientation in which the SO3 plane is parallel to the surface. On activation, SO3 adsorbed to an O2(-) site forms a trigonal pyramidal SO4 species which yields, with a low barrier, a tetrahedral sulfate anion. Subsequently the anion reorients on the surface. Possibilities for alternative mechanisms which require the formation of Ni3(+) or O2(-) are discussed. NiSO4 thus formed leads to the corrosion of Ni at high temperatures in the SO2+O2/SO3 The SO2+O2/SO3 atmosphere, as discussed in the experimental literature. Author

N85-32176*# Case Western Reserve Univ., Cleveland, Ohio. Dept. of Chemistry.
CO ADSORPTION ON (111) AND (100) SURFACES OF THE PT SUB 3 TI ALLOY. EVIDENCE FOR PARALLEL BINDING AND STRONG ACTIVATION OF CO
S. P. MEHANDRU, A. B. ANDERSON, and P. N. ROSS (California Univ., Lawrence Berkeley Lab.) 1985 25 p refs
(Contract NAG3-341; DE-AC03-76SF-00098)
(NASA-CR-176077; NAS 1.26:176077) Avail: NTIS HC A02/MF A01 CSCL 11F

The CO adsorption on a 40 atom cluster model of the (111) surface and a 36 atom cluster model of the (100) surface of the Pt3Ti alloy was studied. Parallel binding to high coordinate sites associated with Ti and low CO bond scission barriers are predicted for both surfaces. The binding of CO to Pt sites occurs in an upright orientation. These orientations are a consequence of the nature of the CO pi donation interactions with the surface. On the Ti sites the orbitals donate to the nearly empty Ti 3d band and the antibonding counterpart orbitals are empty. On the Pt sites, however, they are in the filled Pt 5d region of the alloy band, which causes CO to bond in a vertical orientation by 5 delta donation from the carbon end. E.A.K.

N85-34265*# National Aeronautics and Space Administration. Lewis Research Center, Cleveland, Ohio.
ALUMINUM WORK FUNCTION: EFFECT OF OXIDATION, MECHANICAL SCRAPING AND ION BOMBARDMENT
P. VINET, T. LEMOGNE (Ecole Centrale de Lyon), and H. MONTES (Ecole Centrale de Lyon) 1985 17 p refs Presented at Eurotrib 85, 4th Intern. Tribology Symp., Lyon, 9-12 Sep. 1985; sponsored by La Societe Francaise de Tribologie and the International Tribology Council
(NASA-TM-87079; E-2657; NAS 1.15:87079) Avail: NTIS HC A02/MF A01 CSCL 11F

Surface studies have been performed on aluminum polycrystalline surfaces which have been mechanically scraped. Such studies were initiated in order to understand surface effects occurring in tribological processes which involve rubbing surfaces and the effects of adsorption of oxygen. To characterize the surfaces, the following three different experimental approaches have been used: (1) X.P.S. (X-ray photoelectron spectroscopy), in order to check the cleanliness of the surfaces and follow the adsorption and oxidation kinetics; (2) Analysis of the work function changes by following the energy spectra of secondary electrons emitted under low energy electron bombardment; and (3) Analysis of photoemission intensities under U.V. excitation. The reference state being chosen to be the surface cleaned by ion bombardment and exposures to oxygen atmospheres have been shown to lower the work function of clean polycrystalline aluminum by 1.2 eV. The oxygen pressure is found to affect only the kinetics of these experiments. Mechanical scraping has been shown to induce a decrease (0.3 eV) in the work function, which could sharply modify the kinetics of adsorption on the surface. Author

N85-34266*# National Aeronautics and Space Administration. Lewis Research Center, Cleveland, Ohio.
MICROSTRUCTURES IN RAPIDLY SOLIDIFIED NI-MO ALLOYS
N. JAYARAMAN (Cincinnati Univ.), S. N. TEWARI, K. J. HEMKER, and T. K. GLASGOW 1985 8 p refs Presented at the Intern. Conf. on Rapidly Solidified Mater., San Diego, Calif., 3-5 Feb. 1985; sponsored by the American Society for Metals
(NASA-TM-87100; E-2694; NAS 1.15:87100) Avail: NTIS HC A02/MF A01 CSCL 11F

Ni-Mo alloys of compositions ranging from pure Ni to Ni-40 at % Mo were rapidly solidified by Chill Block Melt Spinning in vacuum and were examined by optical metallography, X-ray diffraction and transmission electron microscopy. Rapid solidification resulted in an extension of molybdenum solubility in nickel from 28 to 37.5 at %. A number of different phases and microstructures were seen at different depths (solidification conditions) from the quenched surface of the melt spun ribbons. Author

N85-34267# Department of Energy, Washington, D. C.
MANUFACTURING PROCESS TO REDUCE LARGE GRAIN GROWTH IN ZIRCONIUM ALLOYS Patent Application
P. M. ROSECRANS, inventor (to NASA) (GE, Schenectady, N.Y.) 1 Aug. 1984 11 p
(Contract DE-AC12-76SN-00052)
(DE85-011649; US-PATENT-APPL-SN-636659) Avail: NTIS HC A02/MF A01

A procedure for desensitizing zirconium based alloys to large grain growth (LGG) during thermal treatment above the recrystallization temperature of the alloy is presented. A method for treating zirconium based alloys which have been cold worked in the range of 2 to 8% strain to reduce large grain growth is devised. A method for fabricating a zirconium alloy clad nuclear fuel element wherein the zirconium clad is resistant to large grain growth is given. DOE

27

NONMETALLIC MATERIALS

Includes physical, chemical, and mechanical properties of plastics, elastomers, lubricants, polymers, textiles, adhesives, and ceramic materials.

A85-10310* National Aeronautics and Space Administration. Lewis Research Center, Cleveland, Ohio.
OXIDATION-BASED MODEL FOR THERMAL BARRIER COATING LIFE
R. A. MILLER (NASA, Lewis Research Center, Cleveland, OH) American Ceramic Society, Journal (ISSN 0002-7820), vol. 67, Aug. 1984, p. 517-521. refs

A procedure is described for modeling the lives of thermal barrier coatings subjected to high-temperatrue environments. The models is used to calculate cycles-to-failure as a function of heating cycle duration. It is based on the presumption that oxidation is the single important time-dependent factor which limits the life of these coatings, and that oxidation-induced strains combine with cyclic strains to promote slow crack growth in the ceramic layer. Good agreement is obtained between calculated and experimental lives for specimens tested in a furnace. This shows that an oxidation-based approach is promising. The importance of reproducible specimen preparation is also discussed. Author

A85-10675*# National Aeronautics and Space Administration. Lewis Research Center, Cleveland, Ohio.
LABORATORY DEGRADATION OF KAPTON IN A LOW ENERGY OXYGEN ION BEAM
D. C. FERGUSON (NASA, Lewis Research Center, Cleveland, OH) American Institute of Aeronautics and Astronautics, Shuttle Environment and Operations Meeting, Washington, DC, Oct. 31-Nov. 2, 1983. 14 p. Previously announced in STAR as N84-18310. refs
(AIAA PAPER 83-2658)

An atomic oxygen ion beam, accelerated from a tunable microwave resonant cavity, was used at Lewis Research Center to bombard samples of the widely used polyimide Kapton. The Kapton experienced degradation and mass loss at high rates, which may be comparable to those found in Space Shuttle operations if the activation energy supplied by the beam enabled surface reactions with the ambient oxygen. The simulation reproduced the directionality (ram-wake dependence) of the degradiation, the change in optical properties of the degraded materials, and the structure seen in scanning electron micrographs of samples returned on the Shuttle Trails with a substituted argon ion beam produced no rapid degradation. Energy Dispersive X-ray Analysis (EDAX) showed significant surface composition changes in all bombarded samples. Mass loss rates and surface composition changes are discussed in terms of the possible oxidation chemistry of the interaction. Finally, the question of how the harmful degradation of materials in low earth orbit can be minimized is addressed. Author

A85-10825* National Aeronautics and Space Administration. Lewis Research Center, Cleveland, Ohio.
DEMONSTRATION OF A SILICON NITRIDE ATTRITION MILL FOR PRODUCTION OF FINE PURE SI AND SI3N4 POWDERS
T. P. HERBELL, T. K. GLASGOW, and N. W. ORTH (NASA, Lewis Research Center, Cleveland, OH) American Ceramic Society Bulletin (ISSN 0002-7812), vol. 63, Sept. 1984, p. 1176-1178. refs

To avoid metallic impurities normally introduced by milling ceramic powders in conventional steel hardware, an attrition mill (high-energy stirred ball mill) was constructed with the wearing parts (mill body, stirring arms, and media) made from silicon nitride. Commercial silicon and Si3N4 powders were milled to fine uniform particles with only minimal contamination - primarily from wear of the sintered Si3N4 media. Author

A85-11072* National Aeronautics and Space Administration. Lewis Research Center, Cleveland, Ohio.
SPHERICAL MICROGLASS PARTICLE IMPINGEMENT STUDIES OF THERMOPLASTIC MATERIALS AT NORMAL INCIDENCE
P. VEERABHADRA RAO and D. H. BUCKLEY (NASA, Lewis Research Center, Cleveland, OH) ASLE Transactions, vol. 27, Oct. 1984, p. 373-379. Previously announced in STAR as N83-25883. refs

Light optical and scanning electron microscope studies were conducted to characterize the erosion resistance of polymethyl methacrylate (PMMA), polycarbonate (PC), polytetrafluoroethylene (PTFE) and ultra-high-molecular-weight-polyethylene (UHMWPE). Erosion was caused by a jet of spherical micro-glass beads at normal impact. During the initial stages of damage, the surfaces of these materials were studied using a profilometer. Material buildup above the original surface was observed on PC and PMMA. As erosion progressed, this buildup disappeared as the pit became deeper. Little or no buildup was observed on PTFE and on UHMWPE. UHMWPE and PTFE are the most resistant materials and PMMA the least. Favorable properties for high erosion resistance seem to be high values of ultimate elongation, and strain energy and a low value of the modulus of elasticity. Erosion-rate-versus-time curves of PC and PTFE exhibit incubation, acceleration and steady state periods. A continuously increasing erosion rate period was observed however for PMMA instead of a steady state period. At early stages of damage and at low impact pressure material removal mechanisms appear to be similar to those for metallic materials. Author

A85-15195* National Aeronautics and Space Administration. Lewis Research Center, Cleveland, Ohio.
EFFECT OF HOT ISOSTATIC PRESSING ON REACTION-BONDED SILICON NITRIDE
G. K. WATSON, T. J. MOORE, and M. L. MILLARD (NASA, Lewis Research Center, Cleveland, OH) American Ceramic Society, Communications (ISSN 0002-7820), vol. 67, Oct. 1984, p. C-208 to C-210. refs
(Contract DE-AI01-77CS-1040)

Specimens of nearly theoretical density have been obtained through the isostatic hot pressing of reaction-bonded silicon nitride under 138 MPa of pressure for two hours at 1850, 1950, and 2050 C. An amorphous phase that is introduced by the hot isostatic pressing partly accounts for the fact that while room temperature flexural strength more than doubles, the 1200 C flexural strength increases significantly only after pressing at 2050 C. O.C.

A85-19086* National Aeronautics and Space Administration. Lewis Research Center, Cleveland, Ohio.
DEPOSITION STRESS EFFECTS ON THE LIFE OF THERMAL BARRIER COATINGS ON BURNER RIGS
J. W. WATSON (NASA, Lewis Research Center, Cleveland, OH; Northwestern University, Evanston, IL) and S. R. LEVINE (NASA, Lewis Research Center, Cleveland, OH) Thin Solid Films (ISSN 0040-6090), vol. 119, 1984, p. 185-193. Previously announced in STAR as N84-25830. refs

A study of the effect of plasma spray processing parameters on the life of a two layer thermal barrier coating was conducted. The ceramic layer was plasma sprayed at plasma arc currents of 900 and 600 amps onto uncooled tubes, cooled tubes, and solid bars of Waspalloy in a lathe with 1 or 8 passes of the plasma gun. These processing changes affected the residual stress state of the coating. When the specimens were tested in a Mach 0.3 cyclic burner rig at 1130 deg C, a wide range of coating lives resulted. Processing factors which reduced the residual stress state in the coating, such as reduced plasma temperature and increased heat dissipation, significantly increased coating life. Author

A85-19087* National Aeronautics and Space Administration. Lewis Research Center, Cleveland, Ohio.
PERFORMANCE OF THERMAL BARRIER COATINGS IN HIGH HEAT FLUX ENVIRONMENTS
R. A. MILLER and C. C. BERNDT (NASA, Lewis Research Center, Cleveland, OH) Thin Solid Films (ISSN 0040-6090), vol. 119, 1984, p. 195-202. Previously announced in STAR as N84-24772. refs

Thermal barrier coatings were exposed to the high temperature and high heat flux produced by a 30 kW plasma torch. Analysis of the specimen heating rates indicates that the temperature drop across the thickness of the 0.038 cm ceramic layer was about 1100 C after 0.5 sec in the flame. An as-sprayed ZrO2-8 percent Y2O3 specimens survived 3000 of the 0.5 sec cycles with falling. Surface spalling was observed when 2.5 sec cycles were employed but this was attributed to uneven heating caused by surface roughness. This surface spalling was prevented by smoothing the surface with silicon carbide paper or by laser glazing. A coated specimen with no surface modification but which was heat treated in argon also did not surface spall. Heat treatment in air led to spalling in as early as 1 cycle from heating stresses. Failures at edges were investigated and shown to be a minor source of concern. Ceramic coatings formed from ZrO2-12 percent Y2O3 or ZrO2-20 percent Y2O3 were shown to be unsuited for use under the high heat flux conditions of this study. Author

A85-20938* Pennsylvania State Univ., University Park.
A MORPHOLOGICAL STUDY OF SILICON CARBIDE PREPARED BY CHEMICAL VAPOR DEPOSITION
P. TSUI and K. E. SPEAR (Pennsylvania State University, University Park, PA) IN: Emergent process methods for high-technology ceramics . New York, Plenum Press, 1984, p. 371-380. refs
(Contract NAG3-177)

Surface morphologies of SiC deposits obtained via chemical vapor deposition (CVD) were studied as functions of substrate surface temperature and the concentration of the silicon and carbon source material, methyltrichlorosilane. Substrates of graphite and alpha-SiC crystals were used. Explanations of the observed morphologies on graphite substrates and their marked changes with temperature are given in terms of chemical kinetics and mass transport arguments. The results of thermodynamic calculations were used to help explain the observed morphologies of the deposits on alpha-SiC substrates. Author

A85-21524* National Aeronautics and Space Administration. Lewis Research Center, Cleveland, Ohio.
POLYIMIDES - TRIBOLOGICAL PROPERTIES AND THEIR USE AS LUBRICANTS
R. L. FUSARO (NASA, Lewis Research Center, Cleveland, OH) IN: Polyimides: Synthesis, characterization, and applications. Volume 2 . New York, Plenum Press, 1984, p. 1053-1080. Previously announced in STAR as N83-13257. refs

Friction, wear, and wear mechanisms of several different polyimide films, solid bodies, composites, and bonded solid lubricant films are compared and discussed. In addition, the effect of such parameters as temperatures, type of atmosphere, contact stress, and specimen configuration are investigated. A friction and wear transition occurs in some polyimides at elevated temperatures and this transition is related to molecular relaxations that occur in polyimides. Friction and wear data from an accelerated test (pin-on-disk) are compared to similar data from an end use test device (plain spherical bearing), and to other polymers investigated in a similar geometry. Author

A85-21650* National Aeronautics and Space Administration. Lewis Research Center, Cleveland, Ohio.
MICROSTRUCTURAL DEVELOPMENT OF PROTECTIVE AL2O3 SCALES
J. L. SMIALEK (NASA, Lewis Research Center, Cleveland, OH) IN: Electron Microscopy Society of America, Annual Meeting, 42nd, Detroit, MI, August 13-17, 1984. San Francisco, San Francisco Press, Inc., 1984, p. 594-597. refs

Microstructural characteristics of Al2O3 scales grown as protective coatings on NiCrAl alloys used in jet engines are described. The alloys were pure or doped with 0.3 percent Zr or Y and oxidized in 1 atm air at 1100 C for 0.1, 1 or 20.0 hr. The scales were then examined under a microscope. Transient epitaxial scales, formed during the 0.1 hr treatment and containing Ni, Cr and Al, consisted of a mosaic of subgrains and precipitates of different phases. The Y and Zr dopants had no effect on the nucleation site locations. The appearance of intergranular porosity at 0.1 hr was exacerbated after the 1 hr treatment. A bimodal void distribution appeared after 20 hr, when no porosity was evident. The detection of local areas of preferred orientation is taken as a spur to further studies of scale growth to gain control of the grain size or even to produce single crystal scales. M.S.K.

A85-22276* National Aeronautics and Space Administration. Lewis Research Center, Cleveland, Ohio.
FRICTION, WEAR, TRANSFER, AND WEAR SURFACE MORPHOLOGY OF ULTRAHIGH-MOLECULAR-WEIGHT POLYETHYLENE
R. L. FUSARO (NASA, Lewis Research Center, Cleveland, OH) ASLE Transactions, vol. 28, Jan. 1985, p. 1-9; Discussion, p. 9; Author's Closure, p. 9, 10. Previously announced in STAR as N83-25882. refs

Tribological studies at 25 C in a 50-percent-relative-humidity air atmosphere were conducted using hemispherically tipped 440 C HT (high temperature) stainless steel pins sliding against ultra-high-molecular-weight polyethylene (UHMWPE) disks. The results indicate that sliding speed, sliding distance, contact stress and specimen geometry can markedly affect friction, UHMWPE wear, UHMWPE transfer and the type of wear mechanisms that occur. Adhesion appears to be the predominant wear mechanism; but after long sliding distances at slow speeds, heavy ridges of transfer result which can induce fatigue-like wear on the UHMWPE disk wear track. In one instance, abrasive wear to the metallic pin was observed. This was caused by a hard particle embedded in the UHMWPE disk wear track. Author

A85-23833* National Aeronautics and Space Administration. Lewis Research Center, Cleveland, Ohio.
FRICTION AND WEAR OF CERAMICS
D. H. BUCKLEY and K. MIYOSHI (NASA, Lewis Research Center, Cleveland, OH) Wear (ISSN 0043-1648), vol. 100, Dec. 1984, p. 333-353. refs

The adhesion, friction, wear and lubricated behaviors of both oxide and non-oxide ceramics are reviewed. Ceramics are examined in contact with themselves, other harder materials and metals. Elastic, plastic and fracture behavior of ceramics in solid state contact is discussed. The contact load necessary to initiate fracture in ceramics is shown to be appreciably reduced with tangential motion. Both friction and wear of ceramics are anisotropic and relate to crystal structure as with metals. Grit size effects in two- and three-body abrasive wear are observed for ceramics. Both free energy of oxide formation and the d valence bond character of metals are related to the friction and wear characteristics for metals in contact with ceramics. Surface contaminants affect friction and adhesive wear. For example, carbon on silicon carbide and chlorine on aluminum oxide reduce friction while oxygen on metal surfaces in contact with ceramics increases friction. Lubrication increases the critical load necessary to initiate fracture of ceramics both in indentation and with sliding or rubbing. Author

A85-24161* Akron Univ., Ohio.
PLASTIC FLOW OF PLASMA SPRAYED CERAMICS
J. PADOVAN, B. T. F. CHUNG, M. J. BRAUN (Akron, University, Akron, OH), G. MCDONALD, R. C. HENDRICKS (NASA, Lewis Research Center, Cleveland, OH), and R. L. MULLEN (Case Western Reserve University, Cleveland, OH) IN: Deformation of ceramic materials II; Proceedings of the International Symposium on Plastic Deformation of Ceramic Materials, University Park, PA, July 20-22, 1983 . New York, Plenum Press, 1984, p. 473-485. refs

The plastic flow of plasma-sprayed ZrO2-8Y2O3 ceramic has been measured at temperatures up to 1250 C and compared to the plastic flow of pressed and sintered ZrO2-8Y2O3. Plasma spraying of binary oxide ceramics is found to result in a metastable state which is inelastic at high temperature but can also be stabilized or devitrified through heat treating so as to decrease plastic properties. The mechanical properties of the as-plasma sprayed and devitrified ceramic sheet material was measured. An improved algorithm that incorporates the inherently nonlinear thermomechanical field equations was used to determine the influence of inelastic material behavior on the thermomechanical response of ceramic coated seal components. Significant creep was found during the thermal shock and steady heating periods with insufficient time during thermal quench to reverse the process, thereby inducing significant residual stresses into the components. C.D.

A85-25271* National Aeronautics and Space Administration. Lewis Research Center, Cleveland, Ohio.
STRENGTH AND MICROSTRUCTURE OF SINTERED SI3N4 WITH RARE-EARTH-OXIDE ADDITIONS
W. A. SANDERS and D. M. MIESKOWSKI (NASA, Lewis Research Center, Cleveland, OH) American Ceramic Society Bulletin (ISSN 0002-7812), vol. 64, Feb. 1985, p. 304-309. refs
(ACS PAPER 130-13-84)

Room temperature, 700-, 1000-, 1200-, and 1370-C examinations of the effect of 1.7-2.6 mol pct rare earth oxide additions to sintered Si3N4 are conducted. While the room temperature-1000 C bend strengths were higher for this material with Y2O3 additions than with CeO2, La2O3, or Sm2O3, the reverse was true at 1200-1370 C. This phenomenon is explained on the basis of microstructural differences, since quantitative microscopy of SEM replicas showed the Si3N4-Y2O3 composition to contain both a higher percentage of elongated grains and a coarser microstructure than the other three alternatives. The elongated grains appear to increase this composition's low temperature strength irrespective of microstructural coarseness; this coarseness, however, decreases strength relative to the other compositions at higher temperatures. O.C.

A85-25963* Illinois Univ., Urbana.
THE INFLUENCE OF TEMPERATURE ON THE LUBRICATING EFFECTIVENESS OF MOS2 DISPERSED IN MINERAL OILS
R. J. ROLEK, C. CUSANO (Illinois, University, Urbana, IL), and H. E. SLINEY (NASA, Lewis Research Center, Cleveland, OH) American Society of Lubrication Engineers and American Society of Mechanical Engineers, Lubrication Conference, San Diego, CA, Oct. 22-24, 1984. 10 p. refs
(Contract NAG3-153)
(ASLE PREPRINT 84-LC-2A-2)

The effects of oil viscosity, base oil temperature, and surface-active agents naturally present in mineral oils on the lubricating effectiveness of MoS2 dispersions under boundary lubrication conditions are investigated. Friction and wear data are obtained from tests conducted under a wide range of oil viscosities and operating temperatures. The dispersion temperature at which the friction dropped below that obtained with the base oils, depended upon the base oil viscosity and the concentration of surface-active agents present in the oil. White oils showed reductions in friction before mineral oils of like viscosity, and lower viscosity oils showed reductions in friction before heavier viscosity oils. The results show that for a given base oil, wear increases as temperature increases, while the wear obtained from a MoS2

dispersion made from the base oil remains approximately constant as temperature is increased. Author

A85-29728* National Aeronautics and Space Administration. Lewis Research Center, Cleveland, Ohio.
LIFE MODELING OF ATMOSPHERIC AND LOW PRESSURE PLASMA-SPRAYED THERMAL-BARRIER COATING
R. A. MILLER (NASA, Lewis Research Center, Cleveland, OH), P. ARGARWAL (Garrett Turbine Engines, Phoenix, AZ; General Electric Co., Aircraft Engine Group, Cincinnati, OH), and E. C. DUDERSTADT (General Electric Co., Aircraft Engine Group, Cincinnati, OH) Ceramic Engineering and Science Proceedings (ISSN 0196-6219), vol. 5, July-Aug. 1984, p. 470-478. refs

The cycles-to-failure vs cycle duration data for three different thermal barrier coating systems, which consist of atmospheric pressure plasma-sprayed ZrO2-8 percent Y2O3 over similarly deposited or low pressure plasma sprayed Ni-base alloys, are presently analyzed by means of the Miller (1980) oxidation-based life model. Specimens were tested at 1100 C for heating cycle lengths of 1, 6, and 20 h, yielding results supporting the model's value. O.C.

A85-29729* National Aeronautics and Space Administration. Lewis Research Center, Cleveland, Ohio.
MECHANICAL PROPERTY MEASUREMENTS OF PLASMA-SPRAYED THERMAL-BARRIER COATINGS SUBJECTED TO OXIDATION
C. C. BERNDT and R. A. MILLER (NASA, Lewis Research Center, Surface Protection Section, Cleveland, OH) Ceramic Engineering and Science Proceedings (ISSN 0196-6219), vol. 5, July-Aug. 1984, p. 479-490. refs

Techniques have been developed for measuring the tensile properties of plasma-sprayed coatings which are used in thermal barrier applications. The measurements have included the average Young's modulus, bond strength and elongation at failure. The oxidation behavior of the bond coat plays an important role in the integrity and adhesion of plasma-sprayed thermal barrier coatings. This work studies the nature of the high temperature degradation on the mechanical properties of the coating. Furnace tests have been carried out on U-700 alloy with bond coats of NiCrAlY or NiCrAlZr and an overlay of ZrO2-8 percent Y2O3. Weight gain measurements on the coatings have been examined with relation to the adhesion strength and failure observations. The results from an initial study are reported in this work. Author

A85-35139*# National Aeronautics and Space Administration. Lewis Research Center, Cleveland, Ohio.
RESIN SELECTION CRITERIA FOR 'TOUGH' COMPOSITE STRUCTURES
C. C. CHAMIS (NASA, Lewis Research Center, Cleveland, OH) and G. T. SMITH (Structures, Structural Dynamics and Materials Conference, 24th, Lake Tahoe, NV, May 2-4, 1983, Collection of Technical Papers. Part 1, p. 45-60) AIAA Journal (ISSN 0001-1452), vol. 23, June 1985, p. 902-911. Previously cited in issue 12, p. 1717, Accession no. A83-29734. refs

A85-36229* National Aeronautics and Space Administration. Lewis Research Center, Cleveland, Ohio.
DEPOSITION OF SILICON NITRIDE FROM SICL4 AND NH3 IN A LOW PRESSURE RF PLASMA
Y. RON, A. RAVEH, U. CARMI, A. INSPEKTOR (Atomic Energy Commission, Negev Nuclear Research Centre, Beersheba, Israel), and R. AVNI (NASA, Lewis Research Center, Cleveland, OH; Atomic Energy Commission, Negev Nuclear Research Centre, Beersheba, Israel) IN: Metallurgical coatings 1983; Proceedings of the Tenth International Conference, San Diego, CA, April 18-22, 1983. Volume 1 . Lausanne, Switzerland, Elsevier Sequoia, S.A., 1983, p. 181-189. refs

Silicon nitride coatings were deposited in a low-pressure (1-10 Torr) RF plasma from SiCl4 and NH3 in the presence of argon onto stainless martensitic steel grounded and floating substrates at 300 C and 440 C respectively. The heating of the substrates depends mainly on the position and the induced RF power. The coatings were identified as silicon nitride by X-ray investigation and were found to contain chlorine by energy-dispersive analysis of X-rays. The growth rate, the microhardness and the chlorine concentration of the coatings were determined as a function of the total gas pressure, the RF power input and the NH3-to-SiCl4 ratio. It was observed that the coatings on the floating substrates have higher deposition rates and are of superior quality. Author

A85-36240* Negev Univ., Beersheva (Israel).
RF-SPUTTERED SILICON AND HAFNIUM NITRIDES - PROPERTIES AND ADHESION TO 440C STAINLESS STEEL
A. GRILL (Negev, University, Beersheba, Israel) and P. R. ARON (NASA, Lewis Research Center, Cleveland, OH) IN: Metallurgical coatings 1983; Proceedings of the Tenth International Conference, San Diego, CA, April 18-22, 1983. Volume 2 . Lausanne, Switzerland, Elsevier Sequoia, S.A., 1983, p. 173-180. Previously announced in STAR as N83-27020. refs

Silicon nitride and hafnium nitride coatings were deposited by reactive RF sputtering on oxidized and unoxidized 440C stainless steel substrates. Sputtering was done in mixtures of argon and nitrogen gases from pressed powder silicon nitride and from hafnium metal targets. Depositions were at two background pressures, 8 and 20 mtorr, and at two different fractions (f) of nitrogen in argon, 0.25 and 0.60, for hafnium nitride and at f = 0.25 for silicon nitride. The coatings and the interface between the coating and substrates were investigated by X-ray diffractometry, scanning electron microscopy, energy dispersive X-ray analysis and Auger electron spectroscopy. A Knoop microhardness of 1650 + or 100 kg/sq mm was measured for hafnium nitride and 3900 + or 500 kg/sq mm for silicon nitride. The friction coefficients between a 440C rider and the coatings were measured under lubricated conditions. Scratch test results demonstrate that the adhesion of hafnium nitride to both oxidized and unoxidized 440C is superior to that of silicon nitride. Oxidized 440C is found to have increased adhesion, to both nitrides, over that of unoxidized 440C. Author

A85-36246* National Aeronautics and Space Administration. Lewis Research Center, Cleveland, Ohio.
FAILURE DURING THERMAL CYCLING OF PLASMA-SPRAYED THERMAL BARRIER COATINGS
C. C. BERNDT (NASA, Lewis Research Center, Surface Protection Section, Cleveland, OH; New York, State University, Stony Brook, NY) and H. HERMAN (New York, State University, Stony Brook, NY) IN: Metallurgical coatings 1983; Proceedings of the Tenth International Conference, San Diego, CA, April 18-22, 1983. Volume 2 . Lausanne, Switzerland, Elsevier Sequoia, S.A., 1983, p. 427-437. refs
(Contract NAG3-164)

The thermal cycling behavior of plasma-sprayed ZrO2-12 wt pct Y2O3 coatings was studied. Coatings were produced with and without bond coats of Ni-Cr-Al-Zr and in some cases the substrates were heated to above the optimum temperature prior to spraying. The coatings (attached to the substrate) were thermal cycled to 1200 C and their cracking behavior was followed by acoustic emission (AE) techniques. It was possible to examine the failure mechanisms by statistical analysis of the AE data and to evaluate the influence of preheating and bond coating. It is shown that the AE spectrum changes when a bond coat is used because of the presence of microcracks which, in turn, dissipate energy and improve the coating integrity. The preheating effect is reflected by a decrease in the peak count rate and an increase in the temperature at which AE activity is initiated. Author

A85-39339* National Aeronautics and Space Administration. Lewis Research Center, Cleveland, Ohio.
FEASIBILITY STUDY OF THE WELDING OF SIC
T. J. MOORE (NASA, Lewis Research Center, Cleveland, OH) American Ceramic Society, Communications (ISSN 0002-7820), vol. 68, June 1985, p. C-151 to C-153. refs

In a brief study of the feasibility of welding sintered alpha-SiC, solid-state welding and brazing were investigated. Joint quality was determined solely by microstructural examination. Hot-pressure

welding was shown to be feasible at 1950 C. Diffusion welding and brazing were also successful under hot isostatic pressure at 1950 C when boride, carbide, and silicide interlayers were used. Furnace brazing was accomplished at 1750 C when a TiSi2 interlayer was introduced. Author

A85-39549* National Aeronautics and Space Administration. Lewis Research Center, Cleveland, Ohio.
CERAMIC WEAR IN INDENTATION AND SLIDING CONTACT
K. MIYOSHI and D. H. BUCKLEY (NASA, Lewis Research Center, Cleveland, OH) ASLE Transactions, vol. 28, July 1985, p. 296-302. Previously announced in STAR as N84-19566. refs

The various wear mechanisms involved with single-crystal ceramic materials in indentation and in sliding contacts. Experiments simulating interfacial events have been conducted with hemispherical, conical and pyramidal indenters (riders). With spherical riders, under either abrasive or adhesive conditions, two types of fracture pits have been observed. First, spherical-shaped fracture pits and wear particles are found as a result of either indenting or sliding. These are shown to be due to a spherical-shaped fracture along the circular or spherical stress trajectories. Second, polyhedral fracture pits and debris, produced by anisotropic fracture, and also found both during indenting and sliding. These are primarily controlled by surface and subsurface cracking along cleavage planes. Several quantitative results have also been obtained from this work. For example, using a pyramidal diamond, crack length of Mn-Zn ferrite in the indentation process grows linearly with increasing normal load. Moreover, the critical load to fracture both in indentation and sliding is essentially isotropic and is found to be directly proportional to the indenter radius. Author

A85-39662*# National Aeronautics and Space Administration. Lewis Research Center, Cleveland, Ohio.
HIGH-TEMPERATURE EROSION OF PLASMA-SPRAYED, YTTRIA-STABILIZED ZIRCONIA IN A SIMULATED TURBINE ENVIRONMENT
R. F. HANDSCHUH (NASA, Lewis Research Center; U.S. Army Propulsion Laboratory, Cleveland, OH) AIAA, SAE, ASME, and ASEE, Joint Propulsion Conference, 21st, Monterey, CA, July 8-10, 1985. 13 p. Previously announced in STAR as N85-13045. refs
(AIAA PAPER 85-1219)

A series of rig calibration and high temperature tests simulating gas path seal erosion in turbine engines were performed at three impingement angles and at three downstream locations. Plasma sprayed, yttria stabilized zirconia specimens were tested. Steady state erosion curves presented for 19 test specimens indicate a brittle type of material erosion despite scanning electron microscopy evidence of plastic deformation. Steady state erosion results were not sensitive to downstream location but were sensitive to impingement angle. At different downstream locations specimen surface temperature varied from 1250 to 1600 C (2280 to 2900 F) and particle velocity varied from 260 to 320 m/s (850 to 1050 ft/s). The mass ratio of combustion products to erosive grit material was typically 240. Author

A85-40383* Nebraska Univ., Lincoln.
'DIAMONDLIKE' CARBON FILMS - OPTICAL ABSORPTION, DIELECTRIC PROPERTIES, AND HARDNESS DEPENDENCE ON *DEPOSITION PARAMETERS*
V. NATARAJAN, J. D. LAMB, J. A. WOOLLAM (Nebraska, University, Lincoln), D. C. LIU, and D. A. GULINO (NASA, Lewis Research Center, Cleveland, OH) Journal of Vacuum Science and Technology A (ISSN 0734-2101), vol. 3, May-June 1985, pt. 1, p. 681-685. Research supported by the University of Nebraska, U.S. Army, and NSF. refs
(Contract NAG3-95; NAG3-154)

An RF plasma deposition system was used to prepare amorphous 'diamondlike' carbon films. The source gases for the RF system include methane, ethylene, propane, and propylene, and the parameters varied were power, dc substrate bias, and postdeposition anneal temperature. Films were deposited on various substrates. The main diagnostics were optical absorption in the visible and in the infrared, admittance as a function of frequency, hardness, and Auger and ESCA spectroscopy. Band gap is found to depend strongly on RF power level and band gaps up to 2.7 eV and hardness up to 7 Mohs were found. There appears to be an inverse relationship between hardness and optical band gap. Author

A85-40384* National Aeronautics and Space Administration. Lewis Research Center, Cleveland, Ohio.
CERAMIC MICROSTRUCTURE AND ADHESION
D. H. BUCKLEY (NASA, Lewis Research Center, Cleveland, OH) Journal of Vacuum Science and Technology A (ISSN 0734-2101), vol. 3, May-June 1985, pt. 1, p. 762-771. Previously announced in STAR as N85-10186. refs

When a ceramic is brought into contact with a ceramic, a polymer, or a metal, strong bond forces can develop between the materials. The bonding forces will depend upon the state of the surfaces, cleanliness and the fundamental properties of the two solids, both surface and bulk. Adhesion between a ceramic and another solid are discussed from a theoretical consideration of the nature of the surfaces and experimentally by relating bond forces to interface resulting from solid state contact. Surface properties of ceramics correlated with adhesion include, orientation, reconstruction and diffusion as well as the chemistry of the surface specie. Where a ceramic is in contact with a metal their interactive chemistry and bond strength is considered. Bulk properties examined include elastic and plastic behavior in the surficial regions, cohesive binding energies, crystal structures and crystallographic orientation. Materials examined with respect to interfacial adhesive interactions include silicon carbide, nickel zinc ferrite, manganese zinc ferrite, and aluminum oxide. The surfaces of the contacting solids are studied both in the atomic or molecularly clean state and in the presence of selected surface contaminants. Author

A85-40973* Case Western Reserve Univ., Cleveland, Ohio.
DOPANT EFFECT OF YTTRIUM AND THE GROWTH AND ADHERENCE OF ALUMINA ON NICKEL-ALUMINUM ALLOYS
A. B. ANDERSON, S. P. MEHANDRU (Case Western Reserve University, Cleveland, OH), and J. L. SMIALEK (NASA, Lewis Research Center, Cleveland, OH) Electrochemical Society, Journal (ISSN 0013-4651), vol. 132, July 1985, p. 1695-1701. refs
(Contract NAG3-341)

The atom superposition and electron delocalization molecular orbital theory and large cluster models have been employed to study cation vacancy diffusion in alpha-Al2O3 and the bonding of alpha-Al2O3 to nickel, aluminum, and yttrium surfaces. Al(3+) diffusion barriers in alpha-Al2O3 by the vacancy mechanism are in reasonable agreement with experiment. The barrier to Y(3+) diffusion is predicted to be much higher. Since addition of yttrium to transition metal alloys is known to reduce the growth rate and stress convolutions in protective alumina scales, this result suggests the rate-limiting step in scale growth is cation vacancy diffusion. This may partially explain the beneficial effect of yttrium dopants on scale adhesion. The theory also predicts a very strong bonding between alumina and yttrium at the surface of the alloy. This may also be important to the adhesion phenomenon. It is also found that aluminum and yttrium atoms bond very strongly to nickel because of charge transfer from their higher lying valence orbitals to the lower lying nickel s-d band. Author

A85-42797* Ford Motor Co., Dearborn, Mich.
FRACTURE OF YTTRIA-DOPED, SINTERED REACTION-BONDED SILICON NITRIDE
R. K. GOVILA, J. A. MANGELS, and J. R. BAER (Ford Motor Co., Ceramic Material Dept., Dearborn, MI) American Ceramic Society, Journal (ISSN 0002-7820), vol. 68, July 1985, p. 413-418. DOE-supported research. refs
(Contract DEN3-167)
(ACS PAPER 7-J3-84)

Flexural strength of an yttria-doped, slip-cast, sintered reaction-bonded silicon nitride was evaluated as a function of temperature (20 to 1400 C in air), applied stress, and time. Static oxidation at 700 to 1400 C was investigated in detail; in tests at

1000 C in air, the material showed anomalous weight gain. Flexural stress-rupture testing at 800 to 1200 C in air indicated that the material is susceptible to stress-enhanced oxidation and early failure. Fractographic evidence for time-dependent and -independent failures is presented. Author

A85-42798* National Aeronautics and Space Administration. Lewis Research Center, Cleveland, Ohio.
OXIDATION OF SILICON NITRIDE SINTERED WITH RARE-EARTH OXIDE ADDITIONS
D. M. MIESKOWSKI and W. A. SANDERS (NASA, Lewis Research Center, Cleveland, OH) American Ceramic Society, Communications (ISSN 0002-7820), vol. 68, July 1985, p. C-160 to C-163. refs

The effects of rare-earth oxide additions on the oxidation of sintered Si3N4 were examined. Insignificant oxidation occurred at 700 and 1000 C, with no evidence of phase instability. At 1370 C, the oxidation rate was lowest for Y2O3 and increased for additions of La2O3, Sm2O3, and CeO2, in that order. Data obtained from X-ray diffraction, electron microprobe analysis, and scanning electron microscopy indicate that oxidation occurs via diffusion of cationic species from Si3N4 grain boundaries. Author

A85-42800* National Aeronautics and Space Administration. Lewis Research Center, Cleveland, Ohio.
EVALUATION OF ALPHA-SIC SINTERING USING STATISTICAL METHODS
J. B. HURST and M. L. MILLARD (NASA, Lewis Research Center, Cleveland, OH) American Ceramic Society, Communications (ISSN 0002-7820), vol. 68, July 1985, p. C-178 to C-181. refs

The effect of time and temperature on the density and strength of alpha-SiC was studied and mathematically modeled using a central composite experimental design. A sintering temperature of 2150 C for 1.7 h maximized the flexural strength and densification values. However, temperatures above 2200 C promoted abnormal grain growth, with resulting appreciable decreases in strength. Flexural strength increased exponentially with increasing density for specimens with densities less than or equal to 92 percent of theoretical. Author

A85-43930* General Motors Corp., Indianapolis, Ind.
PHOTOACOUSTIC MICROSCOPY OF CERAMIC TURBINE BLADES
P. K. KHANDELWAL, R. R. KINNICK, and P. W. HEITMAN (General Motors Corp., Indianapolis, IN) American Ceramic Society Bulletin (ISSN 0002-7812), vol. 64, Aug. 1985, p. 1112-1115. DOE-supported research.
(Contract DEN3-17)

Scanning photoacoustic microscopy (SPAM) is evaluated as a nondestructive technique for the detection of both surface and subsurface flaws in polycrystalline ceramics, such as those currently under consideration for the high temperature components of small vehicular and industrial gas turbine engines; the fracture strength of these brittle materials is controlled by small, 25-200 micron flaws. Attention is given to the correlation of SPAM-detected flaws with actual, fracture-controlling flaws in ceramic turbine blades. O.C.

A85-45302* National Aeronautics and Space Administration. Lewis Research Center, Cleveland, Ohio.
HOT CORROSION OF SINTERED ALPHA-SIC AT 1000 C
N. S. JACOBSON and J. L. SMIALEK (NASA, Lewis Research Center, Cleveland, OH) American Ceramic Society, Journal (ISSN 0002-7820), vol. 68, Aug. 1985, p. 432-439. refs
(ACS PAPER 19-B-84P)

The hot corrosion of sintered alpha-SiC by thin films of Na2SO4 and Na2CO3 was studied at 1000 C in controlled gas atmospheres. Under all conditions, corrosion led to 10 to 20 times the amount of SiO2 formed in pure oxidation after a 48-h exposure. In addition, small amounts of sodium silicate formed. Melts of Na2SO4/SO3 caused uniform pitting of the SiC substrate; Na2CO3/CO2 melts caused localized pitting and grain-boundary attack. In all cases, the protective SiO2 layer dissolved to form silicate, leading to corrosion. In the sulfate case, free carbon in the SiC promotes this process. In all cases the presence of liquid films is responsible for rapid transport rates and the subsequent rapid reaction. Author

A85-45304* National Aeronautics and Space Administration. Lewis Research Center, Cleveland, Ohio.
MICROSTRUCTURE OF REACTION-BONDED SILICON NITRIDE CONSOLIDATED BY ISOSTATIC HOT-PRESSING
D. M. MIESKOWSKI and W. A. SANDERS (NASA, Lewis Research Center, Cleveland, OH) American Ceramic Society, Communications (ISSN 0002-7820), vol. 68, Aug. 1985, p. C-217, C-218.

A microstructural examination and chemical analysis are conducted for reaction-bonded Si3N4 specimens that were isostatically hot pressed at 1850, 1950, and 2050 C. The present observations indicate that the previously reported increase in the 1200 C bend strength of reaction-bonded Si3N4, after pressing at 2050 C exclusively, is due to the relative oxygen levels of the isostatically hot pressed specimens; calculations show that an SiO2 content of less than about 2.2 vol pct is needed to yield the 1200 C strength increase. O.C.

A85-48757* National Aeronautics and Space Administration. Lewis Research Center, Cleveland, Ohio.
EFFECT OF HOT ISOSTATIC PRESSING ON THE PROPERTIES OF SINTERED ALPHA SILICON CARBIDE
G. K. WATSON, T. J. MOORE, and M. L. MILLARD (NASA, Lewis Research Center, Cleveland, OH) American Ceramic Society Bulletin (ISSN 0002-7812), vol. 64, Sept. 1985, p. 1253-1256. refs
(Contract DE-AI01-77CS-51040)

Two lots of alpha silicon carbide were isostatically hot-pressed under 138 MPa for 2 h in Ar at temperatures up to 2200 C. Nearly theoretically dense specimens resulted. Hot isostatic pressing increased both room-temperature strength and 1200 C strength, and resulted in improved reliability. One lot of material which was pressed at 2200 C showed increases of about 20 percent in room-temperature strength and about 50 percent in 1200 C flexural strength; the Weibull modulus improved about 100 percent. Author

N85-10186*# National Aeronautics and Space Administration. Lewis Research Center, Cleveland, Ohio.
CERAMIC MICROSTRUCTURE AND ADHESION
D. H. BUCKLEY 1984 33 p refs To be presented at the 31st Natl. Am. Vacuum Soc. Symp., Reno, Nevada, 4-7 Dec. 1984
(NASA-TM-83804; E-2311; NAS 1.15:83804) Avail: NTIS HC A03/MF A01 CSCL 11B

When a ceramic is brought into contact with a ceramic, a polymer, or a metal, strong bond forces can develop between the materials. The bonding forces will depend upon the state of the surfaces, cleanliness and the fundamental properties of the two solids, both surface and bulk. Adhesion between a ceramic and another solid are discussed from a theoretical consideration of the nature of the surfaces and experimentally by relating bond forces to interface resulting from solid state contact. Surface properties of ceramics correlated with adhesion include, orientation, reconstruction and diffusion as well as the chemistry of the surface specie. Where a ceramic is in contact with a metal their interactive chemistry and bond strength is considered. Bulk properties examined include elastic and plastic behavior in the surficial regions, cohesive binding energies, crystal structures and crystallographic orientation. Materials examined with respect to interfacial adhesive interactions include silicon carbide, nickel zinc ferrite, manganese zinc ferrite, and aluminum oxide. The surfaces of the contacting solids are studied both in the atomic or molecularly clean state and in the presence of selected surface contaminants. Author

N85-10187*# National Aeronautics and Space Administration. Lewis Research Center, Cleveland, Ohio.
STABILITY OF BROMINE INTERCALATED GRAPHITE FIBERS
J. R. GAIER 28 Nov. 1984 11 p refs To be presented at the Mater. Res. Soc. Symp., Boston, 28-30 Nov. 1984; sponsored by the Am. Phys. Soc.
(NASA-TM-86859; E-2322; NAS 1.15:86859) Avail: NTIS HC A02/MF A01 CSCL 11D

Previous evidence suggested that bromine intercalation compounds of crystalline graphite spontaneously deintercalate when the bromine atmosphere is removed. However, results show that bromine intercalated P-100 graphite fibers are stable for long periods of time. They are stable under vacuum conditions, high humidity, and current densities up to 24,000 A/sq cm. They are thermally stable to 200 C, and at temperatures as high as 400 C still retain 80 percent of the conductivity gained by intercalation. At temperatures greater than 300 C, there is significant oxidative degradation of the fibers. The environmental stability shown by the bromine compound makes it a promising candidate for practical applications in aerospace technology. R.S.F.

N85-10191*# National Aeronautics and Space Administration. Lewis Research Center, Cleveland, Ohio.
MILLING OF SI3N4 WITH SI3N4 HARDWARE
T. P. HERBELL, M. R. FREEDMAN, and J. D. KISER Washington 1984 20 p refs Presented at the 13th Intern. Gas Turbine Conf., Houston, Tex., 17-21 Mar. 1984; sponsored by American Society of Mechanical Engineers
(NASA-TM-86864; E-2328; NAS 1.15:86864) Avail: NTIS HC A02/MF A01 CSCL 11G

The grinding of Si3N4 powder using reaction bonded Si3N4 attrition, vibratory, and ball mills with Si3N4 media was examined. The rate of particle size reduction and the change in the chemical composition of the powder were determined in order to compare the grinding efficiency of each technique and the increase in impurity content resulting from mill and media wear. Attrition and vibratory milling exhibited rates of specific surface area increase that were approximately eight times that observed in ball milling. Ball milling and attrition milling provided the least contamination while vibratory milling introduced the greatest amount of impurity pickup. Author

N85-12162*# Case Western Reserve Univ., Cleveland, Ohio. Dept. of Metallurgy and Materials Science.
ANALYSIS TECHNIQUES FOR TRACER STUDIES OF OXIDATION M. S. Thesis Final Report
S. N. BASU Nov. 1984 127 p refs
(Contract NAG3-324)
(NASA-CR-174796; NAS 1.26:174796) Avail: NTIS HC A07/MF A01 CSCL 11G

Analysis techniques to obtain quantitative diffusion data from tracer concentration profiles were developed. Mass balance ideas were applied to determine the mechanism of oxide growth and to separate the fraction of inward and outward growth of oxide scales. The process of inward oxygen diffusion with exchange was theoretically modelled and the effect of lattice diffusivity, grain boundary diffusivity and grain size on the tracer concentration profile was studied. The development of the tracer concentration profile in a growing oxide scale was simulated. The double oxidation technique was applied to a FeCrAl-Zr alloy using 0-18 as a tracer. SIMS was used to obtain the tracer concentration profile. The formation of lacey oxide on the alloy was discussed. Careful consideration was given to the quality of data required to obtain quantitative information. Author

N85-13044*# National Aeronautics and Space Administration. Lewis Research Center, Cleveland, Ohio.
EFFECT OF BARRIER HEIGHT ON FRICTION BEHAVIOR OF THE SEMICONDUCTORS SILICON AND GALLIUM ARSENIDE IN CONTACT WITH PURE METALS
H. MISHINA (Inst. of Physical and Chemical Research, Saitama, Japan) and D. H. BUCKLEY Dec. 1984 12 p refs
(NASA-TP-2405; E-2219; NAS 1.60:2405) Avail: NTIS HC A02/MF A01 CSCL 11B

Friction experiments were conducted for the semiconductors silicon and gallium arsenide in contact with pure metals. Polycrystalline titanium, tantalum, nickel, palladium, and platinum were made to contact a single crystal silicon (111) surface. Indium, nickel, copper, and silver were made to contact a single crystal gallium arsenide (100) surface. Sliding was conducted both in room air and in a vacuum of 10 to the minus 9th power torr. The friction of semiconductors in contact with metals depended on a Schottky barrier height formed at the metal semiconductor interface. Metals with a higher barrier height on semiconductors gave lower friction. The effect of the barrier height on friction behavior for argon sputtered cleaned surfaces in vacuum was more specific than that for the surfaces containing films in room air. With a silicon surface sliding on titanium, many silicon particles back transferred. In contrast, a large quantity of indium transferred to the gallium arsenide surface. R.J.F.

N85-13045*# National Aeronautics and Space Administration. Lewis Research Center, Cleveland, Ohio.
HIGH-TEMPERATURE EROSION OF PLASMA-SPRAYED, YTTRIA-STABILIZED ZIRCONIA IN A SIMULATED TURBINE ENVIRONMENT
R. F. HANSCHUH Dec. 1984 19 p refs Prepared in cooperation with Army Research and Technology Labs., Cleveland
(NASA-TP-2406; E-2271; NAS 1.60:2406; AVSCOM-TR-84-C-17) Avail: NTIS HC A02/MF A01 CSCL 11B

A series of rig calibration and high temperature tests simulating gas path seal erosion in turbine engines were performed at three impingement angles and at three downstream locations. Plasma sprayed, yttria stablized zirconia specimens were tested. Steady state erosion curves presented for 19 test specimens indicate a brittle type of material erosion despite scanning electron microscopy evidence of plastic deformation. Steady state erosion results were not sensitive to downstream location but were sensitive to impingement angle. At difference downstream locations specimen surface temperature varied from 1250 to 1600 C (2280 to 2900 F) and particle velocity varied from 260 to 320 m/s (850 to 1050 ft/s). The mass ratio of combustion products to erosive grit material was typically 240. Author

N85-14928*# National Aeronautics and Space Administration. Lewis Research Center, Cleveland, Ohio.
EFFECTS OF SILVER AND GROUP 2 FLUORIDES ADDITION TO PLASMA SPRAYED CHROMIUM CARBIDE HIGH TEMPERATURE SOLID LUBRICANT FOR FOIL GAS BEARING TO 650 DEG C
R. C. WAGNER (Case Western Reserve Univ.) and H. E. SLINEY 1984 26 p refs Presented at the Ann. Meeting of the American Society of Lubrication Engineers, Las Vegas, Nev., 6-9 May 1985
(Contract DE-AI01-80CS-50194)
(NASA-TM-86895; E-2317; DOE/NASA/50194-40; NAS 1.15:86895) Avail: NTIS HC A03/MF A01 CSCL 11H

A new self-lubricating coating composition of nickel aluminide-bonded chromium carbide formulated with silver and Group II fluorides was developed in a research program on high temperature solid lubricants. One of the proposed applications for this new coating composition is as a wide temperature spectrum solid lubricant for complaint foil gas bearings. Friction and wear properties were obtained using a foil gas bearing start/stop apparatus at temperatures from 25 to 650 C. The journals were Inconel 718. Some were coated with the plasma sprayed experimental coating, others with unmodified nickel

aluminide/chromium carbide as a baseline for comparison. The addtitional components were provided to assist in achieving low friction over the temperature range of interest. Uncoated, preoxidized Inconel X-750 foil bearings were operated against these surfaces. The foils were subjected to repeated start/stop cycles under a 14-kPa (2-psi) bearing unit loading. Sliding contact occurred during lift-off and coastdown at surface velocities less than 6 m/s (3000 rpm). Testing continued until 9000 start/stop cycles were accumulated or until a rise in starting torque indicated the journal/bearing had failed. Comparison in coating performance as well as discussions of their properties and methods of application are given. Author

N85-14929*# National Aeronautics and Space Administration. Lewis Research Center, Cleveland, Ohio.
EFFECT OF SUBSTITUTED PHENYLNADIMIDES ON PROCESSING AND PROPERTIES OF PMR POLYIMIDE COMPOSITES
W. B. ALSTON and R. W. LAUVER 1985 19 p refs Presented at the 30th Natl. SAMPE Symp. and Exhibition, Anaheim, Calif., 19-21 Mar. 1985
(NASA-TM-86902; E-2380; USAAVSCOM-TR-84-C-20; NAS 1.15:86902) Avail: NTIS HC A02/MF A01 CSCL 11B

Three nitrophenylnadimide cure initiators and two phenylnadimides (without nitros) were evaluated as additives to PMR-15 resins and Celion 6000 graphite fiber composites. The results of a resin screening study eliminated all of the additives except 3-nitrophenylnadimide (NO2PN) for use as a low temperature curing additive for PMR-15. Thus, NO2PN and the two control additives were investigated in PMR-15 formulations from which Celion 6000 graphite fiber/PMR-15 composites were processed both with low temperature (274 C) and normal (316 C) cure cycles. Comparisons of the two processing cycles, the resultant glass transition temperatures (Tg), the ambient, 274 and 316 C composite mechanical properties determined before and after 316 C postcure, the 316 C thermo-oxidative weight losses and the retention of 316 C composite mechanical properties are presented. Empirical correlations of the type and amount of nadimide additives with processing parameters, Tg, composite mechanical properties, composite thermo-oxidative stability and long term retention of 316 C composite mechanical properties are also presented. Author

N85-15892*# United Technologies Research Center, East Hartford, Conn.
IMIDE MODIFIED EPOXY MATRIX RESINS Final Report
D. A. SCOLA Mar. 1984 74 p refs
(Contract NAS3-23528)
(NASA-CR-174695; NAS 1.26:174695; R84-916161-14) Avail: NTIS HC A04/MF A01 CSCL 11G

The results of a program designed to develop tough imide modified epoxy resins cured by bisimide amine (BIA) hardeners are described. State-of-the-art epoxides MY720 and DER383 were used, and four bismide amines were evaluated. These were the BIA's derived from the 6F anhydride (4,4'-(hexafluoroisopropylidene) bis(phthalic anhydride) and the diamines 3,3'-diaminodiphynyl sulfone, 4,4'-oxygianiline, 4,4'-methylene dianiline, and 1,12-dodecane diamine. A key intermediate, designated 6F anhydride, is required for the synthesis of the bisimide amines. Reaction parameters to synthesize a precursor to the 6F anhydride (6FHC) in high yields were investigated. The catalyst trifluoromethane sulfonic acid was studied. Although small scale runs yielded the 6FHC in 50 percent yield, efforts to ranslate these results to a larger scale synthesis gave the 6FHC in only 9 percent yield. Results show that the concept of using bisimide amine as curing agents to improve the toughness properties of epoxies is valid. R.S.F.

N85-15893*# National Aeronautics and Space Administration. Lewis Research Center, Cleveland, Ohio.
FUNDAMENTAL TRIBOLOGICAL PROPERTIES OF CERAMICS
D. H. BUCKLEY and K. MIYOSHI 1985 25 p refs Presented at the 9th Ann. Conf. on Composites and Advan. Ceram. Mater., Cocoa Beach, Fla., 20-24 Jan. 1985; sponsored by the American Ceramic Society
(NASA-TM-86915; E-2386; NAS 1.15:86915) Avail: NTIS HC A02/MF A01 CSCL 11B

When a ceramic is brought into contact with itself, another ceramic, or a metal, strong bond forces can develop between the materials. Adhesion between a ceramic and itself or another solid are discussed from a theoretical consideration of the nature of the surfaces and experimentally by relating bond forces to the interface resulting from solid state contact. Elastic, plastic, and fracture behavior of ceramics in solid-state contact are discussed as they relate to friction and wear. The contact load necessary to initiate fracture in ceramics is shown to be appreciably reduced with tangential motion. Both friction and wear of ceramics are anisotropic and relate to crystal structure as with metals. Both free energy of oxide formation and the d valence bond character of metals are related to the friction and wear characteristics for metals in contact with ceramics. Lubrication is found to increase the critical load necessary to initiate fracture of ceramics with sliding or rubbing contact. R.S.F.

N85-15895*# Case Western Reserve Univ., Cleveland, Ohio.
EXPERIMENTAL TEST PROGRAM FOR EVALUATION OF SOLID LUBRICANT COATING AS APPLIED TO COMPLIANT FOIL GAS BEARINGS TO 315 DEG C Final Report
R. C. WAGNER Jan. 1985 54 p refs
(Contract NCC3-30; DE-AI01-80CS-50194)
(NASA-CR-174837; DOE/NASA/0030-1; E-2416; NAS 1.26:174837) Avail: NTIS HC A04/MF A01 CSCL 11H

An experimental apparatus and test procedure was developed to compare the performance of two solid lubricant coatings for air lubricated compliant foil gas bearings in the temperature range of 25 to 315 C. Polyimide bonded additive (SBGC) were tested extensively for durability and frictional characteristics. A partial arc bearing constructed of Inconel X-750 was coated on the bore with one of these coatings. The foil was subjected to repeated start/stop cycles. Performance comparisons reveal that although both coatings survive thousands of start/stop cycles, only the PBGF coated bearing achieves the specified 9000 start/stops. There is enough wear on the SBGC coated bearing to warrant termination of the test prior to 9000 start/stop cycles due to coating failure. The frictional characteristics of the PBGF are better at the elevated temperatures than at lower temperatures; a marked increase in sliding friction occurs as the temperature decreases. The SBGC maintains relatively constant frictional characteristics independent of operating temperature. R.S.F.

N85-15896*# National Aeronautics and Space Administration. Lewis Research Center, Cleveland, Ohio.
SURFACE EFFECTS OF CORROSIVE MEDIA ON HARDNESS, FRICTION, AND WEAR OF MATERIALS
K. MIYOSHI, D. H. BUCKLEY, G. W. P. RENGSTORFF, and H. ISHIGAKI 1985 20 p refs Presented at the Intern. Conf. on Wear of Mater., Vancouver, British Columbia, 14-18 Apr. 1985; sponsored by ASME
(NASA-TM-83711; E-2088; NAS 1.15:83711) Avail: NTIS HC A02/MF A01 CSCL 11G

Hardness, friction, and wear experiments were conducted with magnesium oxide exposed to various corrosive media and also with elemental iron and nickel exposed to water and NaOH. Chlorides such as MgCl2 and sodium containing films were formed on cleaved magnesium oxide surfaces. The MgCl2 films softened the magnesium oxide surfaces and caused high friction and great deformation. Hardness was strongly influenced by the pH value of the HCl-containing solution. The lower the pH, the lower the microhardness. Neither the pH value of nor the immersion time in NaOH containing, NaCl containing, and HNO3 containing solutions influenced the microhardness of magnesium oxide. NaOH formed

a protective and low friction film on iron surfaces. The coefficient of friction and the wear for iron were low at concentrations of NaOH higher than 0.01 N. An increase in NaOH concentration resulted in a decrease in the concentration of ferric oxide on the iron surface. It took less NaOH to form a protective, low friction film on nickel than on iron. R.S.F.

N85-15897*# *National Aeronautics and Space Administration.* Lewis Research Center, Cleveland, Ohio.
CONTACT ANGLE AND SURFACE TENSION MEASUREMENTS OF A FIVE-RING POLYPHENYL ETHER
W. R. JONES, JR. 1985 25 p refs Proposed for presentation at the Ann. Meeting of the American Society of Lubrication Engineers, Las Vegas, Nev., 6-9 May 1985
(NASA-TM-86927; E-2313; NAS 1.15:86927) Avail: NTIS HC A02/MF A01 CSCL 11G

Contact angle measurements were performed for a five-ring polyphenyl ether isomeric mixture on M-50 steel in a dry nitrogen atmosphere. Two different techniques were used: (1) a tilting plate apparatus, and (2) a sessile drop apparatus. Measurements were made for the temperature range 25 to 190 C. Surface tension was measured by a differential maximum bubble pressure technique over the range 23 to 220C in room air. The critical surface energy of spreading (gamma (sub c)) was determined for the polyphenyl ether by plotting the cosine of the contact angle (theta) versus the surface tension (gamma (sub LV)). The straight line intercept at cosine theta = 1 is defined as gamma (sub c). Gamma (sub c) was found to be 30.1 dyn/cm for the tilting plate technique and 31.3 dyn/cm for the sessile drop technique. These results indicate that the polyphenyl ether is inherently autophobic (i.e., it will not spread on its own surface film until its surface tension is less than gamma (sub c). This phenomenon is discussed in light of the wettability and wear problems encountered with this fluid.
Author

N85-15916*# Oak Ridge National Lab., Tenn.
DISPERSED METAL-TOUGHENED CERAMICS AND CERAMIC BRAZING
A. J. MOORHEAD, T. N. TIEGS, and R. J. LAUF 1983 8 p refs Presented at the Automotive Technol. Develop. Contractor Coord. Meeting, Dearborn, Mich., 13 Nov. 1983
(Contract NASA ORDER C-74148-D; NASA ORDER C-72801-D; DE-AC05-84OR-21400; W-7405-ENG-26)
(NASA-CR-174284; NAS 1.26:174284; DE85-001552; CONF-831142-3) Avail: NTIS HC A02/MF A01 CSCL 11G

An alumina (Al2O3) based material that contains approximately 1 vol% finely dispersed platinum or chromium was developed for use in high temperature thermal shock resistant electrical insulators. The work at ORNL is divided into two areas: (1) development of DMT ceramics; and (2) development of brazing filler metals suitable for making ceramic to ceramic and ceramic to metal brazements. The DMT ceramics and brazements are intended for service at elevated temperatures and at high stress levels in the dirty environments of advanced heat engines. The development and characterization of DMT ceramics includes processing (powder preparation, densification and heat treatment) and detailed measurement of mechanical and physical properties (strength, fracture toughness, and thermal conductivity). The brazing work includes: (1) the formulation and melting of small quantities of experimental brazing filler metals; (2) evaluation of the wetting and bonding behavior of these filler metals on Al2O3, partially stabilized zirconia and (ALPHA)-SiC in a sessile drop apparatus; and (3) determine the short term strength and fracture toughness of brazements. DOE

N85-18153*# National Aeronautics and Space Administration. Lewis Research Center, Cleveland, Ohio.
TRIBOLOGICAL PROPERTIES OF GRAPHITE-FIBER-REINFORCED, PARTIALLY FLUORINATED POLYIMIDE COMPOSITES
R. L. FUSARO and W. F. HADY 1985 28 p refs Proposed for presentation at the Ann. Meeting of the American Society of Lubrication Engineers, Las Vegas, Nev., 6-9 May 1985
(NASA-TM-86926; E-2422; NAS 1.15:86926) Avail: NTIS HC A03/MF A01 CSCL 11G

Graphite-fiber-reinforced polyimide (GFRPI) composites were formulated from three new partially fluorinated polyimides and three types of graphite fiber. Nine composites were molded into pins and evaluated in a pin-on-disk tribometer. Friction coefficients, wear rates, pin wear surface morphology, and transfer film formation were assessed at 25 and 300 C. Also assessed was the effect of sliding speed on friction. Wear was up to two orders of magnitude lower at 25 C and up to one order of magnitude lower at 300 C than with previously formulated NASA GFRPI composites.
Author

N85-18154*# General Motors Corp., Indianapolis, Ind.
AN INVESTIGATION OF ENHANCED CAPABILITY THERMAL BARRIER COATING SYSTEMS FOR DIESEL ENGINE COMPONENTS Final Report
R. L. HOLTZMAN, J. L. LAYNE, and B. SCHECHTER Aug. 1984 140 p refs
(Contract DEN3-326; DE-AI01-80CS-50194)
(NASA-CR-174820; DOE/NASA/0326-1; NAS 1.26:174820; EDR-11869) Avail: NTIS HC A07/MF A01 CSCL 11B

Material systems and processes for the development of effective and durable thermal barriers for heavy duty diesel engines were investigated. Seven coating systems were evaluated for thermal conductivity, erosion resistance, corrosion/oxidation resistance, and thermal shock resistance. An advanced coating system based on plasma sprayed particle yttria stabilized zirconia (PS/HYSZ) was judged superior in these tests. The measured thermal conductivity of the selected coating was 0.893 W/m C at 371 C. The PS/HYSZ coating system was applied to the piston crown, fire deck and valves of a single cylinder low heat rejection diesel engine. The coated engine components were tested for 24 hr at power levels from 0.83 MPa to 1.17 MPa brake mean effective pressure. The component coatings survived the engine tests with a minimum of distress. The measured fire deck temperatures decreased 86 C (155 F) on the intake side and 42 C (75 F) on the exhaust side with the coating applied. M.G.

N85-19136*# National Aeronautics and Space Administration. Lewis Research Center, Cleveland, Ohio.
FACTORS INFLUENCING THE BALL MILLING OF SI3N4 IN WATER
M. R. FREEDMAN, J. D. KISER, and T. P. HERBELL 1985 14 p refs Presented at the 9th Ann. Conf. on Composites and Advanced Ceram. Mater., Cocoa Beach, Fla., 20-23 Jan. 1985; sponsored by American Ceramic Society.
(NASA-TM-86932; E-2420; NAS 1.15:86932) Avail: NTIS HC A02/MF A01 CSCL 11G

A statistical study of the ball milling of Si3N4 powder in Si3N4 hardware was undertaken to understand how the resulting increase in specific surface area is related to solids loading and mill speed. An attempt was made to optimize milling conditions. The degree of comminution was more dependent upon solids loading than mill speed. A practical grinding limit between 0.5 and 0.75 microns was achieved in 144 hr independent of solids loading. Ball mill wear and media wear were independent of both solids loading and mill speed. E.A.K.

N85-20127*# National Aeronautics and Space Administration. Lewis Research Center, Cleveland, Ohio.
THE ROLE OF SILVER IN SELF-LUBRICATING COATINGS FOR USE AT EXTREME TEMPERATURES
H. E. SLINEY 1985 20 p refs To be presented at the Ann. Meeting of the Am. Soc. of Lubrication Engr., Las Vegas, Nev., 6-9 May 1985
(NASA-TM-86943; E-2428; NAS 1.15:86943) Avail: NTIS HC A02/MF A01 CSCL 11H

The advantages and disadvantages of elemental silver as a tribological material are discussed. It is demonstrated that the relatively high melting point of 961 deg C, softness, marked plasticity, and thermochemical stability of silver combine to make this metal useful in thin film solid lubricant coatings over a wide temperature range. Disadvantages of silver during sliding, except when used as a thin film, are shown to be gross ploughing due to plastic deformation under load with associated high friction and excessive transfer to counterface surfaces. This transfer generates an irregular surface topography with consequent undesirable changes in bearing clearance distribution. Research to overcome these disadvantages of element silver is described. A comparison is made of the tribological behavior of pure silver with that of silver formulated with other metals and high-temperature solid lubricants. The composite materials are prepared by co-depositing the powdered components with an airbrush followed by furnace heat treatment or by plasma-spraying. Composite coatings were formulated which are shown to be self-lubricating over repeated, temperature cycles from low temperature to about 900 deg C.
R.J.F.

N85-21350* National Aeronautics and Space Administration. Lewis Research Center, Cleveland, Ohio.
CHEMICAL APPROACH FOR CONTROLLING NADIMIDE CURE TEMPERATURE AND RATE WITH MALEIMIDE Patent
R. W. LAUVER, inventor (to NASA) 5 Feb. 1985 9 p Filed 14 Dec. 1983 Supersedes N84-22698 (22 - 13, p 1953) Division of US Patent Appl. SN-516217, filed 22 Jul. 1983
(NASA-CASE-LEW-13770-3; NAS 1.71:LEW-13770-3; US-PATENT-4,497,948; US-PATENT-APPL-SN-561431; US-PATENT-CLASS-528-342; US-PATENT-CLASS-526-217; US-PATENT-CLASS-526-262; US-PATENT-CLASS-528-229; US-PATENT-CLASS-528-315; US-PATENT-CLASS-528-322; US-PATENT-CLASS-528-336; US-PATENT-APPL-SN-516217) Avail: US Patent and Trademark Office CSCL 07D

Polyimide resins suitable for use as composite matrix materials are formed by copolymerization of maleic and norbornenyl endcapped monomers and oligomers. The copolymers can be cured at temperatures under about 300 C by controlling the available concentration of the maleic end-capped reactant. Control can be achieved by adding sufficient amounts of said maleic reactant, or by chemical modification of either copolymers, so as to either increase Diels-Alder retrogression of the norbornenyl capped reactant and/or holding initiation and polymerization to a rate compatible with the availability of the maleic-capped reactant.
Author

N85-21351* National Aeronautics and Space Administration. Lewis Research Center, Cleveland, Ohio.
CHEMICAL APPROACH FOR CONTROLLING NADIMIDE CURE TEMPERATURE AND RATE WITH MALEIMIDE Patent
R. W. LAUVER, inventor (to NASA) 5 Feb. 1985 9 p Filed 14 Dec. 1983 Supersedes N84-22699 (22 - 13, p 1953) Division of US Patent Appl. SN-516217, filed 22 Jul. 1983
(NASA-CASE-LEW-13770-4; NAS 1.71:LEW-13770-4; US-PATENT-4,497,939; US-PATENT-APPL-SN-561429; US-PATENT-CLASS-526-262; US-PATENT-CLASS-528-229; US-PATENT-CLASS-528-322; US-PATENT-CLASS-528-342; US-PATENT-APPL-SN-516217) Avail: US Patent and Trademark Office CSCL 07D

Polyimide resins suitable for use as composite matrix materials are formed by copolymerization of maleic and norbornenyl endcapped monomers and oligomers. The copolymers can be cured at temperatures under about 300 C by controlling the available concentration of the maleic end-capped reactant. This control can be achieved by adding sufficient amounts of said maleic reactant, or by chemical modification of either copolymer, so as to either increase Diels-Alder retrogression of the norbornenyl capped reactant and/or holding initiation and polymerization to a rate compatible with the available of the maleic-capped reactant.
Author

N85-21352* National Aeronautics and Space Administration. Lewis Research Center, Cleveland, Ohio.
CHEMICAL APPROACH FOR CONTROLLING NADIMIDE CURE TEMPERATURE AND RATE Patent
R. W. LAUVER, inventor (to NASA) 5 Feb. 1985 8 p Filed 14 Dec. 1983 Supersedes N84-22700 (22 - 13, p 1953) Division of US Patent Appl. SN-516217, filed 22 Jul. 1983
(NASA-CASE-LEW-13770-5; NAS 1.71:LEW-13770-5; US-PATENT-4,497,940; US-PATENT-APPL-SN-561435; US-PATENT-CLASS-526-262; US-PATENT-CLASS-528-229; US-PATENT-CLASS-528-322; US-PATENT-CLASS-528-342; US-PATENT-APPL-SN-516217) Avail: US Patent and Trademark Office CSCL 07D

Polyimide resins suitable for use as composite matrix materials are formed by copolymerization of maleic and norbornenyl endcapped monomers and oligomers. The copolymers can be cured at temperatures under about 300 C by controlling the available concentration of the maleic endcapped reactant. This control is achieved by adding sufficient amounts of said maleic reactant or by chemical modification of either copolymer, to either increase Diels-Alder retrogression of the norbornenyl capped reactant and/or hold initiation and polymerization to a rate compatible with the availability of the maleic capped reactant.
Official Gazette of the U.S. Patent and Trademark Office

N85-21355*# National Aeronautics and Space Administration. Lewis Research Center, Cleveland, Ohio.
TRIBOLOGICAL PROPERTIES OF BORON NITRIDE SYNTHESIZED BY ION BEAM DEPOSITION
K. MIYOSHI, D. H. BUCKLEY, and T. SPALVINS' 1985 . 15 p refs Proposed for presentation at the 12th Intern. Conf. on Met. Coatings, Los Angeles, 15-19 Apr. 1985; sponsored by the American Vacuum Society
(NASA-TM-86962; E-2459; NAS 1.15:86962) Avail: NTIS HC A02/MF A01 CSCL 11G

The adhesion and friction behavior of boron nitride films on 440 C bearing stainless steel substrates was examined. The thin films containing the boron nitride were synthesized using an ion beam extracted from a borazine plasma. Sliding friction experiments were conducted with BN in sliding contact with itself and various transition metals. It is indicated that the surfaces of atomically cleaned BN coating film contain a small amount of oxides and carbides, in addition to boron nitride. The coefficients of friction for the BN in contact with metals are related to the relative chemical activity of the metals. The more active the metal, the higher is the coefficient of friction. The adsorption of oxygen on clean metal and BN increases the shear strength of the metal - BN contact and increases the friction. The friction for BN-BN contact is a function of the shear strength of the elastic contacts. Clean BN surfaces exhibit relatively strong interfacial adhesion and high friction. The presence of adsorbates such as adventitious carbon contaminants on the BN surfaces reduces the shear strength of the contact area. In contrast, chemically adsorbed oxygen enhances the shear strength of the BN-BN contact and increases the friction.
E.A.K.

N85-21356*# National Aeronautics and Space Administration. Lewis Research Center, Cleveland, Ohio.
PARAMETRIC EVALUATION OF BALL MILLING OF SIC IN WATER
J. D. KISER, T. P. HERBELL, and M. R. FREEDMAN 1985 17 p refs Presented at the 9th Ann. Conf. on Composites and Advanced Ceramic Mater., Cocoa Beach, Fla., 20-23 Jan. 1985
(NASA-TM-86974; E-2399; NAS 1.15:86974) Avail: NTIS HC A02/MF A01 CSCL 11G

A statistically designed experiment was conducted to determine optimum conditions for ball milling alpha-SiC in water. The influence of pH adjustment, volume percent solids loading, and mill rotational speed on grinding effectiveness was examined. An equation defining the effect of those milling variables on specific surface area was obtained. The volume percent solids loading of the slurry had the greatest influence on the grinding effectiveness in terms of increase in specific surface area. As grinding effectiveness improved, mill and media wear also increased. Contamination was minimized by use of sintered alpha-SiC milling hardware. Author

N85-21357*# National Aeronautics and Space Administration. Lewis Research Center, Cleveland, Ohio.
CHARACTERIZATION OF LUBRICATED BEARING SURFACES OPERATED UNDER HIGH LOADS
J. L. LAUER (Rensselaer Polytechnic Inst.), N. MARXER (Rensselaer Polytechnic Inst.), and W. R. JONES, JR. 1985 16 p refs Proposed for presentation at the Intern. Tribology Conf., Tokyo, 8-10 Jul. 1985; sponsored by the Japan Society of Lubrication Engineers
(Contract AF-AFOSR-0005-81; DAAG24-83-K-0058)
(NASA-TM-86964; E-2462; NAS 1.15:86964) Avail: NTIS HC A02/MF A01 CSCL 11H

The composition and surface profiles of M-50 steel surfaces were measured after operation at high loads in a bearing contact simulator. An ester lubricant (trimethyolpropane triheptanoate) was used with and without various additives. Optical profiles were obtained + or - to 30 depth resolution with a phase-locked interference microscope in 10 micron diameter areas within and outside the wear tracks. Optical constants and surface film thickness were measured in the same areas with an electronic scanning ellipsometer. Film composition was measured with a scanning Auger electron spectrometer. It is concluded that metal oxide formation is accelerated within the wear tracks. E.A.K.

N85-21358*# National Aeronautics and Space Administration. Lewis Research Center, Cleveland, Ohio.
OXIDATION AND HOT CORROSION OF HOT-PRESSED SI3N4 AT 1000 DEG C
W. L. FIELDER Apr. 1985 25 p refs
(NASA-TM-86977; E-2419; NAS 1.15:86977) Avail: NTIS HC A02/MF A01 CSCL 11G

The oxidation and hot corrosion of a commercial, hot-pressed Si3N4 were investigated at 1000 C under an atmosphere of flowing O2. For the hot corrosion studies, thin films of Na2SO4 were airbrushed on the Si3N4 surface. The hot corrosion attack was monitored by the following techniques: continuous weight measurements, SO2 evolution, film morphology, and chemical analyses. Even though the hot corrosion weight changes after 25 hr were relatively small, the formation of SiO2 from oxidation of Si3N4 was an order of magnitude greater in the presence of molten Na2SO4. The formation of a protective SiO2 phase at the Si3N4 surface is minimized by the fluxing action of the molten Na2SO4 thereby allowing the oxidation of the Si3N4 to proceed more rapidly. A simple process is proposed to account for the hot corrosion process. E.A.K.

N85-21359*# National Aeronautics and Space Administration. Lewis Research Center, Cleveland, Ohio.
HUMIDITY EFFECTS ON ADHESION OF NICKEL-ZINC FERRITE IN ELASTIC CONTACT WITH MAGNETIC TAPE AND ITSELF
K. MIYOSHI, D. H. BUCKLEY, T. KUSAKA (Osaka Inst. of Technology), and C. MAEDA (Osaka Inst. of Technology) Mar. 1985 10 p refs
(NASA-TP-2449; E-2361; NAS 1.60:2449) Avail: NTIS HC A02/MF A01 CSCL 11G

The effects of humidity on the adhesion of Ni-Zn ferrite and magnetic tape in elastic contact with a Ni-Zn ferrite hemispherical pin in moist nitrogen were studied. Adhesion was independent of normal load in dry, humid, and saturated nitrogen. Ferrites adhere to ferrites in a saturated atmosphere primarily from the surface tension effects of a thin film of water adsorbed on the ferrite surfaces. The surface tension of the water film calculated from the adhesion results was 48 times 0.00001 to 56 times 0.00001 N/cm; the accepted value for water is 72.7 x 0.00001 N/cm. The adhesion of ferrite-ferrite contacts increased gradually with increases in relative humidity to 80 percent, but rose rapidly above 80 percent. The adhesion at saturation was 30 times or more greater than that below 80 percent relative humidity. Although the adhesion of magnetic tape - ferrite contacts remained low below 40 percent relative humidity and the effect of humidity was small, the adhesion increased considerably with increasing relative humidity above 40 percent. The changes in adhesion of elastic contacts were reversible on humidifying and dehumidifying.
Author

N85-22511*# Pennsylvania State Univ., University Park.
MASS SPECTRA OF NEUTRAL PARTICLES RELEASED DURING ELECTRICAL BREAKDOWN OF THIN POLYMER FILMS
B. R. F. KENDALL *In* NASA. Lewis Research Center Spacecraft Environ. Interactions Technol., 1983 p 525-535 Mar. 1985 refs
(Contract NSG-3301)
Avail: NTIS HC A99/MF E03 CSCL 11G

A special type of time-of-flight mass spectrometer triggered from the breakdown event was developed to study the composition of the neutral particle flux released during the electrical breakdown of polymer films problem. Charge is fed onto a metal-backed polymer surface by a movable smooth platinum contact. A slowly increasing potential from a high-impedance source is applied to the contact until breakdown occurs. The breakdown characteristics is made similar to those produced by an electron beam charging system operating at similar potentials. The apparatus showed that intense instantaneous fluxes of neutral particles are released from the sites of breakdown events. For Teflon FEP films of 50 and 75 microns thickness the material released consists almost entirely of fluorocarbon fragments, some of them having masses greater than 350 atomic mass units amu, while the material released from a 50 micron Kapton film consists mainly of light hydrocarbons with masses at or below 44 amu, with additional carbon monoxide and carbon dioxide. The apparatus is modified to allow electron beam charging of the samples. E.A.K.

N85-22755*# National Aeronautics and Space Administration. Lewis Research Center, Cleveland, Ohio.
METALLIC AND METALLOCERAMIC COATING BY THERMAL DECOMPOSITION
R. C. HENDRICKS and G. MCDONALD 1985 7 p refs Presented at the 12th Intern. Conf. on Met. Coatings, Los Angeles, 15-19 Apr. 1985; sponsored by the American Vacuum Society
(NASA-TM-86992; E-2538; NAS 1.15:86992) Avail: NTIS HC A02/MF A01 CSCL 11G

Metallic and metalloceramic coatings were prepared by thermal decomposition of a number of inorganic and metallo-organic compounds. The compounds were applied by spraying and by immersion, especially on ceramic fibers and fiber forms, which are easily coated by this procedure. Penetration of low-density ceramics is examined, and procedures are described that were used for converting the deposited materials to metals, oxides, or

metal oxide films. Multiple-component films were also prepared. Photomicrographs illustrate the structure of these films. R.J.F.

N85-22756*# National Aeronautics and Space Administration. Lewis Research Center, Cleveland, Ohio.
FILM AND INTERSTITIAL FORMATION OF METALS IN PLASMA-SPRAYED CERAMICS
R. C. HENDRICKS, G. MCDONALD, and R. L. MULLEN (Case Western Reserve Univ., Cleveland) 1985 12 p refs Presented at the 12th Intern. Conf. on Metallurgical Coatings, Los Angeles, 15-19 Apr. 1985
(NASA-TM-86993; NAS 1.15:86993; E-2539) Avail: NTIS HC A02/MF A01 CSCL 11B

A method is described to electrodeposit noble metals such as platinum and ordinary metals such as copper on and within plasma-sprayed ceramic materials and ceramic fiber materials. Low-density ceramic fiber bodies were vacuum impregnated with plating solution and attached to an electrode. Light micrographs illustrating the density and location of deposited materials are presented and discussed. Voids in the plasma-sprayed ceramic were filled with deposits that vary from spherical to lens-shaped circular and have particle size corresponding to the full range of void size. Multiple coatings of ceramic and metal can be sequenced. Author

N85-22757*# Southwest Research Inst., San Antonio, Tex.
SLIDING SEAL MATERIALS FOR ADIABATIC ENGINES *Interim* Report, Feb. 1984 - Feb. 1985
J. LANKFORD Apr. 1985 70 p refs
(Contract DEN3-352; DE-AI01-80CS-50194)
(NASA-CR-174893; NAS 1.26:174893; SRI-06-7963; DOE/NASA/0352-1) Avail: NTIS HC A04/MF A01 CSCL 11B

The sliding friction coefficients and wear rates of promising carbide, oxide, and nitride materials were measured under temperature, environmental, velocity, loading conditions that are representative of the adiabatic engine environment. In order to provide guidance needed to improve materials for this application, the program stressed fundamental understanding of the mechanisms involved in friction and wear. Microhardness tests were performed on the candidate materials at elevated temperatures, and in atmospheres relevant to the piston seal application, and optical and electron microscopy were used to elucidate the micromechanisms of wear following wear testing. X-ray spectroscopy was used to evaluate interface/environment interactions which seemed to be important in the friction and wear process. Electrical effects in the friction and wear processes were explored in order to evaluate the potential usefulness of such effects in modifying the friction and wear rates in service. However, this factor was found to be of negligible significance in controlling friction and wear. R.J.F.

N85-22758*# Oak Ridge National Lab., Tenn. Metal and Ceramics Div.
DISPERSED-METAL-TOUGHENED ALUMINA
T. N. TIEGS and A. J. MOORHEAD Feb. 1984 31 p refs
(Contract NASA ORDER C-72801-D; DE-AC05-84OR-21400)
(NASA-CR-174687; DOE/NASA/2801-1; NAS 1.26:174687; ORNL/TM-9518) Avail: NTIS HC A03/MF A01 CSCL 11B

Hot-pressed alumina with a fine dispersion of Cr metal particles showed good fracture toughness (K sub I sub c MPa. m 1/2) and thermal shock resistance. However, the fracture strengths of these materials were relatively low (190 to 240 MPa vs 350 to 580 MPa for pure alumina). The good fracture toughness and thermal shock resistance were found to be related to the relatively large-grain duplex microstructure of the hot-pressed materials. The fracture toughness of alumina with dispersions of Ni and Pt was found to be inferior to that of the Al2O3-Cr materials. Hot-pressed solid solutions of Al2O3-Cr2O3 also showed good fracture toughness (K sub I sub c = 7.3 to 7.7 MPa.m 1/2), which was again due to the development of a relatively large-grain duplex microstructure. Author

N85-23781*# National Aeronautics and Space Administration. Lewis Research Center, Cleveland, Ohio.
TRANSMISSION EFFICIENCY MEASUREMENTS AND CORRELATIONS WITH PHYSICAL CHARACTERISTICS OF THE LUBRICANT
J. J. COY, A. M. MITCHELL, and B. J. HAMROCK *In* AGARD Gears and Power Transmission Systems for Helicopters and Turboprops 15 p Jan. 1985 refs Previously announced as N84-30293 Prepared in cooperation with Army Research and Technology Labs.
Avail: NTIS HC A17/MF A01 CSCL 11G

Data from helicopter transmission efficiency tests were compared to physical properties of the eleven lubricants used in those tests. The tests were conducted with the OH-58 helicopter main rotor transmission. Efficiencies ranged from 98.3 to 98.8 percent. The data was examined for correlation of physical properties with efficiency. There was a reasonable correlation of efficiency with absolute viscosity if the viscosity was first corrected for temperature and pressure in the lubricated contact. Between lubricants, efficiency did not correlate well with viscosity at atmospheric pressure. Between lubricants, efficiency did not correlate well with calculated lubricant film forming capacity. Bench type sliding friction and wear measurements could not be correlated to transmission efficiency and component wear. Author

N85-24000*# National Aeronautics and Space Administration. Lewis Research Center, Cleveland, Ohio.
ENVIRONMENTAL EFFECTS ON THE TENSILE STRENGTH OF CHEMICALLY VAPOR DEPOSITED SILICON CARBIDE FIBERS
R. T. BHATT and M. D. KRAITCHMAN Apr. 1985 33 p refs Presented at 8th Ann. Conf. on Composited and Adv. Ceramic Mater., Cocoa Beach, Fla.; sponsored by American Ceramic Soc. Prepared in cooperation with Army Research and Technology Labs.
(NASA-TM-86981; E-2519; NAS 1.15:86981; USAAVSCOM-TR-85-C-4; AD-A157111) Avail: NTIS HC A03/MF A01 CSCL 11G

The room temperature and elevated temperature tensile strengths of commercially available chemically vapor-deposited (CVD) silicon carbide fibers were measured after 15 min heat treatment to 1600 C in various environments. These environments included oxygen, air, argon and nitrogen at one atmosphere and vacuum at 10/9 atmosphere. Two types of fibers were examined which differed in the SiC content of their carbon-rich coatings. Threshold temperature for fiber strength degradation was observed to be dependent on the as-received fiber-flaw structure, on the environment and on the coating. Fractographic analyses and flexural strength measurements indicate that tensile strength losses were caused by surface degradation. Oxidation of the surface coating is suggested as one possible degradation mechanism. The SiC fibers containing the higher percentage of SiC near the surface of the carbon-rich coating show better strength retention and higher elevated temperature strength. E.A.K.

N85-25521*# National Aeronautics and Space Administration. Lewis Research Center, Cleveland, Ohio.
HOMOGENEITY OF PRISTINE AND BROMINE INTERCALATED GRAPHITE FIBERS
J. R. GAIER and D. MARINO 1985 16 p refs Presented at the 17th Bien. Conf. on Carbon, Lexington, Ky.; sponsored by the American Carbon Society
(NASA-TM-87016; E-2560; NAS 1.15:87016) Avail: NTIS HC A02/MF A01 CSCL 11G

Wide variations in the resistivity of intercalated graphite fibers and to use these materials for electrical applications, their bulk properties must be established. The homogeneity of the diameter, the resistivity, and the mass density of 50 graphite fibers, before and after bromine intercalation was measured. Upon intercalation the diameter was found to expand by about 5%, the resistivity to decrease by a factor of five, and the density to increase by about 6%. Each individual fiber was found to have uniform diameter and resistivity over macroscopic regions for lengths as long as 7 cm. The ratio of pristine to intercalated resistivity increases as the

pristine fiber diameter increases at a rate of 0.16 micron, but decreases with the increasing ratio of intercalated diameter to pristine diameter at a rate of 0.08. E.A.K.

N85-26867*# National Aeronautics and Space Administration. Lewis Research Center, Cleveland, Ohio.
ROCKET THRUST CHAMBER THERMAL BARRIER COATINGS
R. J. QUENTMEYER *In* NASA. Marshall Space Flight Center. Advan. High Pressure O2/H2 p 49-58 Apr. 1985
Avail: NTIS HC A99/MF E03; SOD HC CSCL 11B

Subscale rocket thrust chamber tests were conducted to evaluate the effectiveness and durability of thin yttria stabilized zirconium oxide coatings applied to the thrust chamber hot-gas side wall. The fabrication consisted of arc plasma spraying the ceramic coating and bond coat onto a mandrell and then electrodepositing the copper thrust chamber wall around the coating. Chambers were fabricated with coatings .008, and .005 and .003 inches thick. The chambers were thermally cycled at a chamber pressure of 600 psia using oxygen-hydrogen as propellants and liquid hydrogen as the coolant. The thicker coatings tended to delaminate, early in the cyclic testing, down to a uniform sublayer which remained well adhered during the remaining cycles. Two chambers with .003 inch coatings were subjected to 1500 thermal cycles with no coating loss in the throat region, which represents a tenfold increase in life over identical chambers having no coatings. An analysis is presented which shows that the heat lost to the coolant due to the coating, in a rocket thrust chamber design having a coating only in the throat region, can be recovered by adding only one inch to the combustion chamber length. M.G.

N85-26991*# National Aeronautics and Space Administration. Lewis Research Center, Cleveland, Ohio.
EFFECTS OF WEAR ON STRUCTURE-SENSITIVE MAGNETIC PROPERTIES OF CERAMIC FERRITE IN CONTACT WITH MAGNETIC TAPE
K. MIYOSHI, D. H. BUCKLEY, and K. TANAKA (Kanazawa Univ., Japan) 1985 26 p refs Proposed for presentation at the Tribology Conf., Atlanta, 8-10 Oct. 1985; sponsored in part by Am. Soc. of Lubrication Engr. and ASME
(NASA-TM-87007; E-2483; NAS 1.15:87007) Avail: NTIS HC A03/MF A01 CSCL 11G

Wear experiments and electron microscopy and diffraction studies were conducted to examine the wear and deformed layers in single-crystal Mn-Zn (ceramic) ferrite magnetic head material in contact with magnetic tape and the effects of that contact on magnetic properties. The crystalline state of the single-crystal magnetic head was changed drastically during the sliding process. A nearly amorphous structure was produced on its wear surface. Deformation in the surficial layer of the magnetic head was a critical factor in readback signal loss above 2.5 dB. The signal output level was reduced as applied normal load was increased. Considerable plastic flow occurred on the magnetic tape surface with sliding, and the signal loss due to the tape wear was approximately 1 dB. Author

N85-26992*# National Aeronautics and Space Administration. Lewis Research Center, Cleveland, Ohio.
ENVIRONMENTAL STABILITY OF INTERCALATED GRAPHITE FIBERS
J. R. GAIER and D. A. JAWORSKE May 1985 16 p refs Presented at the Intern. Symp. in Graphite Intercalation Compounds, Tsukuba, Japan, 27-30 May 1985; sponsored by Physical Society of Japan and the Carbon Society of Japan
(NASA-TM-87025; E-2580; NAS 1.15:87025) Avail: NTIS HC A02/MF A01 CSCL 11G

Graphite fibers intercalated with bromine, iodine monochloride, ferric chloride, and cupric chloride were subjected to stability tests under four environments which are encountered by engineering materials in the aerospace industry: ambient laboratory conditions, as would be experienced during handling operations and terrestrial applications; high vacuum, as would be experienced in space applications; high humidity, as would be experienced in marine applications; and high temperature, as would be experienced in some processing steps and applications. Monitoring the resistance of the fibers at ambient laboratory conditions revealed that only the ferric chloride intercalated fibers were unstable, due to absorption of water from the air. All four types of intercalated fibers were unstable, due to absorption of water from the air. All four types of intercalated fibers were stable for long periods under high vacuum. Ferric chloride, cupric chloride, and iodine monochloride intercalated fibers were sensitive to high humidity conditions. All intercalated fibers began to degrade above 250 C. The order of their thermal stability, from lowest to highest, was cupric chloride, iodine monochloride, bromine, and ferric chloride. Of the four types of intercalated fibers tested, the bromine intercalated fibers appear to have the most potential for application, based on environmental stability. Author

N85-26993*# National Aeronautics and Space Administration. Lewis Research Center, Cleveland, Ohio.
EFFECT OF COUNTERFACE MATERIAL TYPE AND ITS TOPOGRAPHY ON THE TRIBOLOGICAL PROPERTIES OF POLYIMIDE COMPOSITES
R. L. FUSARO 1985 33 p refs Proposed for presentation at the Tribology Conf., Atlanta, 8-10 Oct. 1985; sponsored by American Society of Lubrication Engineers and ASME
(NASA-TM-87036; E-2592; NAS 1.15:87036) Avail: NTIS HC A03/MF A01 CSCL 11B

Graphite fiber reinforced polyimide composite pins were slid against seven different counterfaces to determine the effect of material type on the tribological properties of polymer composites. In addition, the effect of sliding a new pin on a pre-established transfer film was investigated. The results indicated that almost a five order of magnitude difference in composite wear rate can occur just by varying the counterface material. An attempt to make all surfaces as smooth as possible was made, but due to differences in material composition this was not possible and a range of surface roughnesses were obtained. The results indicate that the smoother the surface, the lower the composite wear rate; but that small protrusions (not discernible with arithmetic surface roughness measurements) can markedly increase wear rates. A pre-established transfer film improved both run in and steady state wear rates. M.G.

N85-26994*# Westinghouse Research Labs., Pittsburgh, Pa.
BREAKWAY FRICTION AND DYNAMIC FRICTION/WEAR MEASUREMENTS OF VARIOUS CERAMIC MATERIALS FROM 25 C (75 F) TO 650 C (1200 F) Final Report
D. J. BOES Sep. 1984 82 p refs
(Contract DEN3-346; DE-AI01-80CS-50194)
(NASA-CR-174803; DOE/NASA/0346-1; NAS 1.26:174803; REPT-85-9JDIESL-R1) Avail: NTIS HC A05/MF A01 CSCL 11B

This report describes the results of a program designed to evaluate the breakaway friction and dynamic friction/wear characteristics of materials having potential for use as load bearing components in a high-performance high-temperature heavy duty diesel engine. Ten candidate materials were selected, six of which were evaluated under all possible material combinations as both stationary as well as moving breakaway specimens. The remaining materials were evaluated either in the static mode against themselves and all other materials, or against themselves only. Experiments were performed at five temperatures up to 650 C (1200 F) and unit pressures of 700 kPa (100 lb/sq in.), 3500 kPa (500 lb/sq in.), and 7000 kPa (1000 lb/sq in.). Experimental results indicate that under dynamic conditions, four of the ten materials exhibited good to excellent friction/wear characteristics in various material combinations. These materials were: titanium carbide, silicon nitride, silicon carbide (reaction sintered), and Refel (SiC). B.W.

N85-28107*# National Aeronautics and Space Administration. Lewis Research Center, Cleveland, Ohio.
PREPARATION OF SILICON CARBIDE-SILICON NITRIDE FIBERS BY THE PYROLYSIS OF POLYCARBOSILAZANE PRECURSORS Final Report
B. G. PENN, J. G. DANIELS, F. E. LEDBETTER, III, and J. M. CLEMONS Mar. 1985 12 p refs
(NASA-TM-86505; NAS 1.15:86505) Avail: NTIS HC A02/MF A01 CSCL 11G

The development of silicon carbide-silicon nitride fibers (SiC-Si3N4) by the pyrolysis of polycarbosilazane precursors is reviewed. Precursor resin, which was prepared by heating tris(N-methylamino)methylsilane or tris(N-methylamino)phenylsilane to about 520 C, was drawn into fibers from the melt and then made unmeltable by humidity conditioning at 100 C and 95 percent relative humidity. The humidity treated precursor fibers were pyrolyzed to ceramic fibers with good mechanical properties and electrical resistivity. For example, SiC-Si3N4 fibers derived from tris(N-methylamino)methylsilane had a tensile rupture modulus of 29 million psi and electrical resistivity of 6.9 x ten to the 8th power omega-cm, which is ten to the twelfth power times greater than that obtained for graphite fibers. R.J.F.

N85-28109*# General Motors Corp., Indianapolis, Ind. Gas Turbine Div.
CERAMIC APPLICATIONS IN TURBINE ENGINES Final Report
H. E. HELMS, P. W. HEITMAN, L. C. LINDGREN, and S. R. THRASHER Oct. 1984 268 p refs
(Contract DEN3-17; DE-AI01-77CS-51040)
(NASA-CR-174715; DOE/NASA/0017-6; NAS 1.26:174715; EDR-11442) Avail: NTIS HC A12/MF A01 CSCL 11B

The application of ceramic components to demonstrate improved cycle efficiency by raising the operating temperature of the existing Allison IGI 404 vehicular gas turbine engine is discussed. This effort was called the Ceramic Applications in Turbine Engines (CATE) program and has successfully demonstrated ceramic components. Among these components are two design configurations featuring stationary and rotating caramic components in the IGT 404 engine. A complete discussion of all phases of the program, design, materials development, fabrication of ceramic components, and testing-including rig, engine, and vehicle demonstation test are presented. During the CATE program, a ceramic technology base was established that is now being applied to automotive and other gas turbine engine programs. This technology base is outlined and also provides a description of the CATE program accomplishments. Author

N85-28110*# National Aeronautics and Space Administration. Lewis Research Center, Cleveland, Ohio.
A MICROGRAPHIC AND GRAVIMETRIC STUDY OF INTERCALATION AND DEINTERCALATION OF GRAPHITE FIBERS
C. C. HUNG 1985 13 p refs Presented at 17th Biennial Conf. on Carbon, Lexington, Ky., 16-21 Jun. 1985; sponsored by American Carbon Society
(NASA-TM-87026; E-2582; NAS 1.15:87026) Avail: NTIS HC A02/MF A01 CSCL 11D

Intercalation and deintercalation of Union Carbide P-100 graphite fibers with liquid and vaporous bromine was studied gravimetrically and microscopically. The mass of the bromine intercalated fibers was found to be 17 to 20 percent greater than their pristine counterpart. This variation decreased to 17 to 18 percent after heating in air for 3 days at 200 C and to 14.5 to 18 percent after 6 days of 260 C heating. The fiber length did not change throughout the experiment. The fiber diameter increased during intercalation and decreased slightly upon deintercalation but was not affected by heating to 260 C for 3 days in air. Comparing the mass and volume data to those with highly oriented pyrolitic graphite or natural single crystal graphite suggested the possibility that the intercalated P-100 fibers could be mostly stage 4. Author

N85-30135*# National Aeronautics and Space Administration. Lewis Research Center, Cleveland, Ohio.
MECHANISM OF STRENGTH DEGRADATION FOR HOT CORROSION OF ALPHA-SIC
J. L. SMIALEK and N. S. JACOBSON 1984 40 p refs Presented at the Reg. Meeting of the Am. Ceram. Soc., San Francisco, 28-31 Oct. 1984
(NASA-TM-87052; E-2507; NAS 1.15:87052) Avail: NTIS HC A03/MF A01 CSCL 11G

Sintered alpha SiC was corroded by thin films of Na2SO4 and Na2CO3 molten salts at 1000%. This hot corrosion attack reduced room temperature strengths by as much as 50%. Strength degradation was porportional to the degree and uniformity of corrosion pitting attack as controlled by the chemistry of the molten salt. Extensive fractography identified corrosion pits as the most prevalent source of failure. A fracture mechanics treatment of the strength/pit depth relationship produced an average K sub IC equal to 2.6 MPa sub m 1/2, which is consistent with published values. E.A.K.

N85-30137*# National Aeronautics and Space Administration. Lewis Research Center, Cleveland, Ohio.
ION BEAM SPUTTER-DEPOSITED THIN FILM COATINGS FOR PROTECTION OF SPACECRAFT POLYMERS IN LOW EARTH ORBIT
B. A. BANKS, M. J. MIRTICH, S. K. RUTLEDGE, D. M. SWEC, and H. K. NAHRA (Cleveland State Univ.) 1985 24 p refs Presented at the 23rd Aerospace Sci. Meeting, Reno, Nev., 14-17 Jan. 1985; sponsored by AIAA
(NASA-TM-87051; E-2454; NAS 1.15:87051) Avail: NTIS HC A02/MF A01 CSCL 11B

Ion beam sputter-deposited thin films of Al2O3, SiO2, and a codeposited mixture of predominantly SiO2 with small amounts of a fluoropolymer were evaluated both in laboratory plasma ashing tests and in space on board shuttle flight STS-8 for effectiveness in preventing oxidation of polyimide Kapton. Measurements of mass loss and optical performance of coated and uncoated polyimide samples exposed to the low Earth orbital environment are presented. Optical techniques were used to measure loss rates of protective films exposed to atomic oxygen. Results of the analysis of the space flight exposed samples indicate that thin film metal oxide coatings are very effective in protecting the polyimide. Metal oxide coatings with a small amount of fluoropolymer codeposited have the additional benefit of great flexibility. Author

N85-30138*# National Aeronautics and Space Administration. Lewis Research Center, Cleveland, Ohio.
MECHANICAL PROTECTION OF DLC FILMS ON FUSED SILICA SLIDES
D. NIR 1985 27 p refs Presented at the 12th Intern. Conf. on Met. Coatings, Los Angeles, 15-19 Apr. 1985; sponsored by American Vacuum Society
(NASA-TM-87056; E-2423; NAS 1.15:87056) Avail: NTIS HC A03/MF A01 CSCL 11G

Measurements were made with a new test for improved quantitative estimation of the mechanical protection of thin films on optical materials. The mechanical damage was induced by a sand blasting system using spherical glass beads. Development of the surface damage was measured by the changes in the specular transmission and reflection, and by inspection using a surface profilometer and a scanning electron microscope. The changes in the transmittance versus the duration of sand blasting was measured for uncoated fused silica slides and coated ones. It was determined that the diamond like carbon films double the useful optical lifetime of the fused silica. Theoretical expressions were developed to describe the stages in surface deterioration. Conclusions were obtained for the SiO2 surface mechanism and for the film removal mechanism. Author

N85-34284*# National Aeronautics and Space Administration. Lewis Research Center, Cleveland, Ohio.
RELIABILITY OF TWO SINTERED SILICON NITRIDE MATERIALS
D. M. MIESKOWSKI, W. A. SANDERS, and L. A. PIERCE Aug. 1985 15 p refs
(NASA-TM-87092; E-2325-1; NAS 1.15:87092) Avail: NTIS HC A02/MF A01 CSCL 11B

Two types of sintered silicon nitride were evaluated in terms of reliability: an experimental high pressure nitrogen sintered material and a commercial material. The results show wide variations in strength for both materials. The Weibull moduli were 5.5, 8.9, and 11 for the experimental material at room temperature, 1200, and 1370 C, respectively. The commercial material showed Weibull moduli of 9.0, 8.6, and 8.9 at these respective temperatures. No correlation between strength and flaw size was noted for the experimental material. The applicability of the Weibull and Griffith theories to processing defects on the order of 100 microns or less in size are discussed. E.A.K.

28

PROPELLANTS AND FUELS

Includes rocket propellants, igniters, and oxidizers; storage and handling; and aircraft fuels.

N85-10209*# SRI International Corp., Menlo Park, Calif.
CHEMISTRY OF FUEL DEPOSITS AND SEDIMENTS AND THEIR PREDURSORS Final Report
F. R. MAYO, B. Y. LAN, S. E. BUTTRILL, JR., and G. A. ST.JOHN Oct. 1984 50 p refs
(Contract NAS3-22510)
(NASA-CR-174778; NAS 1.26:174778; YU-2115) Avail: NTIS HC A03/MF A01 CSCL 21D

The mechanism of solid deposit formation on hot engine parts from turbine fuels is investigated. Deposit formation is associated with oxidation of the hydrocarbon fuel. Therefore, oxidation rates and soluble gum formation were measured for several jet turbine fuels and pure hydrocarbon mixtures. Experiments were performed at 130 C using thermal initiation and at 100 C using ditertiary butyl peroxide as a chemical initiator. Correlation of the data shows that the ratio of rate of oxidation to rate of gum formation for a single fuel is not much affected by experimental conditions, even though there are differences in the abilities of different hydrocarbons to initiate and continue the oxidation. This indicates a close association of gum formation with the oxidation process. Oxidations of n-dodecane, tetralin and the more unstable jet fuels are autocatalytic, while those of 2-ethylnaphthalene and a stable jet fuel are self-retarding. However, the ratio of oxidation rate to gum formation rate appear to be nearly constant for each substrate. The effect of oxygen pressure on gum and oxidation formation was also studied. Dependence of gum formation on the concentration of initiator at 100 C is discussed and problems for future study are suggested. Author

N85-11252*# United Technologies Research Center, East Hartford, Conn.
EXTERNAL FUEL VAPORIZATION STUDY, PHASE 2 Interim Report
E. J. SZETELA and L. CHIAPPETTA Jan. 1981 27 p refs
(Contract NAS3-21971)
(NASA-CR-174079; NAS 1.26:174079; R81-915326-5) Avail: NTIS HC A03/MF A01 CSCL 21D

An analytical study was conducted to evaluate the effect of variations in fuel properties on the design of an external fuel vaporizaton system. The fuel properties that were considered included thermal stability, critical temperature, enthalpy a critical conditions, volatility, and viscosity. The design parameters that were evaluated included vaporizer weight and the impact on engine requirement such as maintenance, transient response, performance, and altitude relight. The baseline fuel properties were those of Jet A. The variation in thermal stability was taken as the thermal stability variation for Experimental Referee Broad Specification (ERBS) fuel. The results of the analysis indicate that a change in thermal stability equivalent to that of ERBS would increase the vaporization system weight by 20 percent, decrease oprating time between cleaning by 40 percent and make altitude relight more difficult. An increase in fuel critical temperature of 39 K would require a 40 percent increase in vaporization system weight. The assumed increase in enthalpy and volatility would also increase vaporizer weight by 40 percent and make altitude relight extremely difficult. The variation in fuel viscosity would have a negligible effect on the design parameters. R.S.F.

N85-12183*# National Aeronautics and Space Administration. Lewis Research Center, Cleveland, Ohio.
LUBRICITY OF WELL-CHARACTERIZED JET AND BROAD-CUT FUELS BY BALL-ON-CYLINDER MACHINE
G. M. PROK and W. S. KIM Nov. 1984 15 p refs
(NASA-TM-83807; E-2308; NAS 1.15:83807) Avail: NTIS HC A02/MF A01 CSCL 21D

A ball-on-cylinder machine (BOCM) was used to measure the lubricity of fuels. The fuels tested were well-characterized fuels available from other programs at the NASA Lewis Research Center plus some in-house mildly hydroprocessed shale fuels from other programs included Jet-A, ERBS fuel, ERBS blends, and blend stock. The BOCM tests were made before and after clay treatment of some of these fuels with both humidified air and dry nitrogen as the preconditioning and cover gas. As expected, clay treatment always reduced fuel lubricity. Using nitrogen preconditioning and cover gas always resulted in a smaller wear scar diameter than when humidified air was used. Also observed was an indication of lower lubricity with lower boiling range fuels and lower aromatic fuels. Gas chromatographic analysis indicted changes in BOCM-stressed fuels. Author

N85-13066*# National Aeronautics and Space Administration. Lewis Research Center, Cleveland, Ohio.
LIQUID PHASE PRODUCTS AND SOLID DEPOSIT FORMATION FROM THERMALLY STRESSED MODEL JET FUELS
W. S. KIM and D. A. BITTKER Nov. 1984 30 p refs
(NASA-TM-86874; E-2334; NAS 1.15:86874) Avail: NTIS HC A03/MF A01 CSCL 21D

The relationship between solid deposit formation and liquid degradation product concentration was studied for the high temperature (400 C) stressing of three hydrocarbon model fuels. A Jet Fuel Thermal Oxidation Tester was used to simulate actual engine fuel system conditions. The effects of fuel type, dissolved oxygen concentration, and hot surface contact time (reaction time) were studied. Effects of reaction time and removal of dissolved oxygen on deposit formation were found to be different for n-dodecane and for 2-ethylnaphthalene. When ten percent tetralin is added to n-dodecane to give a simpler model of an actual jet fuel, the tetralin inhibits both the deposit formation and the degradation of n-dodecane. For 2-ethylnaphthalene primary product analyses indicate a possible self-inhibition at long reaction times of the secondary reactions which form the deposit precursors. The mechanism of the primary breakdown of these fuels is suggested and the primary products which participate in these precursor-forming reactions are identified. Some implications of the results to the thermal degradation of real jet fuels are given. R.S.F.

C-2

N85-19175*# General Electric Co., Lynn, Mass. Aircraft Engine Business Group.
ANALYTICAL FUEL PROPERTY EFFECTS: SMALL COMBUSTORS, PHASE 2 Final Report
T. G. HILL, J. D. MONTY, and H. L. MORTON Mar. 1985 45 p
(Contract NAS3-22829)
(NASA-CR-174848; NAS 1.26:174848; R85AEB014) Avail: NTIS HC A03/MF A01 CSCL 21D

The effects of non-standard aviation fuels on a typical small gas turbine combustor were studied and the effectiveness of design changes intended to counter the effects of these fuels was evaluated. The T700/CT7 turboprop engine family was chosen as being representative of the class of aircraft power plants desired for this study. Fuel properties, as specified by NASA, are characterized by low hydrogen content and high aromatics levels. No. 2 diesel fuel was also evaluated in this program. Results demonstrated the anticipated higher than normal smoke output and flame radiation intensity with resulting increased metal temperatures on the baseline T700 combustor. Three new designs were evaluated using the non standard fuels. The three designs incorporated enhanced cooling features and smoke reduction features. All three designs, when burning the broad specification fuels, exhibited metal temperatures at or below the baseline combustor temperatures on JP-5. Smoke levels were acceptable but higher than predicted. R.S.F.

N85-19176*# Lockheed-California Co., Burbank. Commercial Advanced Design Div.
STUDY OF ADVANCED FUEL SYSTEM CONCEPTS FOR COMMERCIAL AIRCRAFT AND ENGINES Final Report
E. F. VERSAW, G. D. BREWER, W. D. BYERS, H. W. FOGG, D. E. HANKS, and J. CHIRIVELLA (Ergo-Tech, Inc.) Jan. 1983 142 p refs
(Contract NAS3-23271)
(NASA-CR-174752; NAS 1.26:174752) Avail: NTIS HC A07/MF A01 CSCL 21D

The impact on a commercial transport aircraft of using fuels which have relaxed property limits relative to current commercial jet fuel was assessed. The methodology of the study is outlined, fuel properties are discussed, and the effect of the relaxation of fuel properties analyzed. Advanced fuel system component designs that permit the satisfactory use of fuel with the candidate relaxed properties in the subject aircraft are described. The two fuel properties considered in detail are freezing point and thermal stability. Three candidate fuel system concepts were selected and evaluated in terms of performance, cost, weight, safety, and maintainability. A fuel system that incorporates insulation and electrical heating elements on fuel tank lower surfaces was found to be most cost effective for the long term. R.S.F.

N85-19185*# California Univ., Berkeley. Lawrence Berkeley Lab. Dept. of Mechanical Engineering.
KNOCK SYNDROME: ITS CURES AND ITS VICTIMS
A. K. OPPENHEIM Jul. 1984 11 p refs Presented at the SAE Fuels and Lubricants Meeting, Baltimore, 8 Oct. 1984
(Contract NAG3-133; NAG3-137; DE-AC03-76SF-00098; NSF CPF-81-15163)
(NASA-CR-174395; DE84-016884; LBL-18163; CONF-8410138-1; NAS 1.26:174395) Avail: NTIS HC A02/MF A01 CSCL 21D

The knock phenomenon imposes a major technological constraint upon the automotive and oil industries; its various cures are reviewed. Essential features of combustion instability leading to its onset are exposed, and the methodology is outlined for a rational attack upon the problem it poses. Three different cures for solving the problem are proposed: (1) development of mechanical design for the combustion chamber; (2) alteration of chemical composition of fuel; and (3) mechanical-kinetic development of direct control of the combustion process. DOE

N85-27012*# Exxon Research and Engineering Co., Linden, N.J. Products Research Div.
JET FUEL PROPERTY CHANGES AND THEIR EFFECT ON PRODUCIBILITY AND COST IN THE U.S., CANADA, AND EUROPE Final Report
G. M. VARGA, JR., A. J. AVELLA, JR., A. R. CUNNINGHAM, C. D. FEATHERSTON, J. F. GORGOL, A. J. GRAF, M. LIEBERMAN, and G. A. OLIVER Feb. 1985 205 p refs
(Contract NAS3-22769)
(NASA-CR-174840; NAS 1.26:174840; RL-1PD-85) Avail: NTIS HC A10/MF A01 CSCL 21D

The effects of changes in properties and blending stocks on the refinery output and cost of jet fuel in the U.S., Canada, and Europe were determined. Computerized refinery models that minimize production costs and incorporated a 1981 cost structure and supply/demand projections to the year 2010 were used. Except in the West U.S., no changes in jet fuel properties were required to meet all projected demands, even allowing for deteriorating crude qualities and changes in competing product demand. In the West U.S., property changes or the use of cracked blendstocks were projected to be required after 1990 to meet expected demand. Generally, relaxation of aromatics and freezing point, or the use of cracked stocks produced similar results, i.e., jet fuel output could be increased by up to a factor of three or its production cost lowered by up to $10/cu m. High quality hydrocracked stocks are now used on a limited basis to produce jet fuel. The conversion of U.S. and NATO military forces from wide-cut to kerosene-based jet fuel is addressed. This conversion resulted in increased costs of several hundred million dollars annually. These costs can be reduced by relaxing kerosene jet fuel properties, using cracked stocks and/or considering the greater volumetric energy content of kerosene jet fuel. E.A.K.

N85-28127*# Colorado School of Mines, Golden. Dept. of Chemistry and Geochemistry.
JET FUEL INSTABILITY MECHANISMS Final Technical Report, 1 Aug. 1981 - 31 Mar. 1985
S. R. DANIEL 31 Mar. 1985 104 p refs
(Contract NAG3-197)
(NASA-CR-175856; NAS 1.26:175856) Avail: NTIS HC A06/MF A01 CSCL 21D

The mechanisms of the formation of fuel-insoluble deposits were studied in several real fuels and in a model fuel consisting of tetralin in dodecane solution. The influence of addition to the fuels of small concentrations of various compounds on the quantities of deposits formed and on the formation and disappearance of oxygenated species in solution was assessed. The effect of temperature on deposit formation was also investigated over the range of 308-453 K. G.L.C.

N85-31307*# National Aeronautics and Space Administration. Lewis Research Center, Cleveland, Ohio.
RAPID ESTIMATION OF CONCENTRATION OF AROMATIC CLASSES IN MIDDISTILLATE FUELS BY HIGH-PERFORMANCE LIQUID CHROMATOGRAPHY
D. A. OTTERSON and G. T. SENG Washington Jul. 1985 16 p refs
(NASA-TP-2495; E-2376; NAS 1.60:2495) Avail: NTIS HC A02/MF A01 CSCL 21D

An high performance liquid chromatography (HPLC) method to estimate four aromatic classes in middistillate fuels is presented. Average refractive indices are used in a correlation to obtain the concentrations of each of the aromatic classes from HPLC data. The aromatic class concentrations can be obtained in about 15 min when the concentration of the aromatic group is known. Seven fuels with a wide range of compositions were used to test the method. Relative errors in the concentration of the two major aromatic classes were not over 10 percent. Absolute errors of the minor classes were all less than 0.3 percent. The data show that errors in group-type analyses using sulfuric acid derived standards are greater for fuels containing high concentrations of polycyclic aromatics. Corrections are based on the change in refractive index of the aromatic fraction which can occur when

sulfuric acid and the fuel react. These corrections improved both the precision and the accuracy of the group-type results. Author

N85-31308*# Boeing Commercial Airplane Co., Seattle, Wash.
DETAILED STUDIES OF AVIATION FUEL FLOWABILITY Final Report
H. K. MEHTA and R. S. ARMSTRONG Jun. 1985 95 p refs
(Contract NAS3-24081)
(NASA-CR-174938; NAS 1.26:174938; D6-52996) Avail: NTIS HC A05/MF A01 CSCL 21D

Six Jet A fuels, with varying compositions, were tested for low temperature flowability in a 190-liter simulator tank that modeled a section of a wing tank of a wide-body commercial airplane. The insulated tank was chilled by circulating coolant through the upper and lower surfaces. Flow-ability was determined as a function of fuel temperature by holdup, the fraction of unflowable fuel remaining in the tank after otherwise complete withdrawal. In static tests with subfreezing tank conditions, hold up varied with temperature and fuel composition. However, a general correlation of two or three classes of fuel type was obtained by plotting holdup as a function of the difference between freezing point and boundary-layer temperature, measured 0.6 cm above the bottom tank surface. Dynamic conditions of vibrations and slosh or rate of fuel withdrawal had very minor effects on holdup. Tests with cooling schedules to represent extreme, cold-day flights showed, at most, slight holdup for any combination of fuel type or dynamic conditions. Tests that superimposed external fuel heating and recirculation during the cooldown period indicates reduced hold up by modification of the low-temperature boundary layer. Fuel heating was just as effective when initiated during the later times of the tests as when applied continuously. Author

N85-34295*# Akron Univ., Ohio. Dept. of Chemical Engineering.
MEASUREMENT AND CORRELATION OF JET FUEL VISCOSITIES AT LOW TEMPERATURES Final Report
D. L. SCHRUBEN Aug. 1985 31 p refs
(Contract NAG3-488)
(NASA-CR-174911; NAS 1.26:174911) Avail: NTIS HC A03/MF A01 CSCL 21D

Apparatus and procedures were developed to measure jet fuel viscosity for eight current and future jet fuels at temperatures from ambient to near -60 C by shear viscometry. Viscosity data showed good reproducibility even at temperatures a few degrees below the measured freezing point. The viscosity-temperature relationship could be correlated by two linear segments when plotted as a standard log-log type representation (ASTM D 341). At high temperatures, the viscosity-temperature slope is low. At low temperatures, where wax precipitation is significant, the slope is higher. The breakpoint between temperature regions is the filter flow temperature, a fuel characteristic approximated by the freezing point. A generalization of the representation for the eight experimental fuels provided a predictive correlation for low-temperature viscosity, considered sufficiently accurate for many design or performance calculations. E.A.K.

31

ENGINEERING (GENERAL)

Includes vacuum technology; control engineering; display engineering; and cryogenics.

A85-29556* National Aeronautics and Space Administration. Lewis Research Center, Cleveland, Ohio.
A HIGH-SPEED IMPLEMENTATION OF THE RANDOM DECREMENT ALGORITHM
L. J. KIRALY (NASA, Lewis Research Center, Cleveland, OH) IN: International Instrumentation Symposium, 29th, Albuquerque, NM, May 2-6, 1983, Proceedings . Research Triangle Park, NC, Instrument Society of America, 1983, p. 153-168. Previously announced in STAR as N82-22388.

The algorithm is useful for measuring net system damping levels in stochastic processes and for the development of equivalent linearized system response models. The algorithm works by summing together all subrecords which occur after predefined threshold level is crossed. The random decrement signature is normally developed by scanning stored data and adding subrecords together. The high speed implementation of the random decrement algorithm exploits the digital character of sampled data and uses fixed record lengths of 2(n) samples to greatly speed up the process. The contributions to the random decrement signature of each data point was calculated only once and in the same sequence as the data were taken. A hardware implementation of the algorithm using random logic is diagrammed and the process is shown to be limited only by the record size and the threshold crossing frequency of the sampled data. With a hardware cycle time of 200 ns and 1024 point signature, a threshold crossing frequency of 5000 Hertz can be processed and a stably averaged signature presented in real time. T.M.

A85-47024*# National Aeronautics and Space Administration. Lewis Research Center, Cleveland, Ohio.
TECHNOLOGY REQUIREMENTS TO BE ADDRESSED BY THE NASA LEWIS RESEARCH CENTER CRYOGENIC FLUID MANAGEMENT FACILITY PROGRAM
J. C. AYDELOTT (NASA, Lewis Research Center, Cleveland, OH) and R. S. RUDLAND (Martin Marietta Aerospace, Denver, CO) AIAA, SAE, ASME, and ASEE, Joint Propulsion Conference, 21st, Monterey, CA, July 8-10, 1985. 24 p. Previously announced in STAR as N85-29987. refs
(AIAA PAPER 85-1229)

The NASA Lewis Research Center is responsible for the planning and execution of a scientific program which will provide advance in space cryogenic fluid management technology. A number of future space missions were identified that require or could benefit from this technology. These fluid management technology needs were prioritized and a shuttle attached reuseable test bed, the cryogenic fluid management facility (CFMF), is being designed to provide the experimental data necessary for the technology development effort. Author

N85-11261*# National Aeronautics and Space Administration. Lewis Research Center, Cleveland, Ohio.
PLASMA VARIABLES AND TRIBOLOGICAL PROPERTIES OF COATINGS IN LOW PRESSURE (0.1 - 10.0 TORR) PLASMA SYSTEMS
R. AVNI (Ben Gurion Univ. of the Negev) and T. SPALVINS 1984 30 p refs Presented at the 11th Intern. Conf. on Met. Coatings, San Diego, Calif., 9-13 Apr. 1984; sponsored by the American Vacuum Society
(NASA-TM-83798; E-2238; NAS 1.15:83798) Avail: NTIS HC A03/MF A01 CSCL 11G

A detailed treatment is presented of the dialog known as plasma surface interactions (PSI) with respect to the coating process and its tribological behavior. Adsorption, morphological changes, defect formation, sputtering, chemical etching, and secondary electron

emission are all discussed as promoting and enhancing the surface chemistry, thus influencing the tribological properties of the deposited flux. Phenomenological correlations of rate of deposition, flux composition, microhardness, and wear with the plasma layer variables give an insight to the formation of chemical bonding between the deposited flux and the substrate surface. B.W.

N85-20153* National Aeronautics and Space Administration. Lewis Research Center, Cleveland, Ohio.
DEPOSITION OF DIAMONDLIKE CARBON FILMS Patent
M. J. MIRTICH, J. S. SOVEY, and B. A. BANKS, inventors (to NASA) 25 Dec. 1984 6 p Filed 9 Jul. 1984 Supersedes N84-28986 (22 - 19, p 2996)
(NASA-CASE-LEW-14080-1; NAS 1.71:LEW-14080-1; US-PATENT-4,490,229; US-PATENT-APPL-SN-628866; US-PATENT-CLASS-204-192C; US-PATENT-CLASS-204-192R; US-PATENT-CLASS-204-192SP; US-PATENT-CLASS-423-414; US-PATENT-CLASS-423-445; US-PATENT-CLASS-423-446; US-PATENT-CLASS-423-449; US-PATENT-CLASS-423-DIG.10) Avail: US Patent and Trademark Office CSCL 13H

A diamondlike carbon film is deposited in the surface of a substrate by exposing the surface to an argon ion beam containing a hydrocarbon. The current density in the ion beam is low during initial deposition of the film. Subsequent to this initial low current condition, the ion beam is increased to full power. At the same time, a second argon ion beam is directed toward the surface of the substrate. The second ion beam has an energy level much greater than that of the ion beam containing the hydrocarbon. This addition of energy to the system increases mobility of the condensing atoms and serves to remove lesser bound atoms.
Official Gazette of the U.S. Patent and Trademark Office

N85-20155*# National Aeronautics and Space Administration. Lewis Research Center, Cleveland, Ohio.
APPARATUS FOR PRODUCING DIAMOND-LIKE CARBON FLAKES Patent Application
B. A. BANKS, inventor (to NASA) 5 Nov. 1984 12 p
(NASA-CASE-LEW-13837-3; NAS 1.71:LEW-13837-3; US-PATENT-APPL-SN-668433) Avail: NTIS HC A02/MF A01 CSCL 13H

A vacuum are from a spot at the face of a graphite cathode to a graphite anode produces a beam of carbon ions and atoms. A carbon coating from this beam is deposited on an ion beam sputtered target to produce diamondlike carbon flakes. A graphite tube encloses the cathode, and electrical isolation is provided by an insulating sleeve. The tube forces the vacuum arc spot to be confined to the surface on the outermost end of the cathode. Without the tube the arc spot will wander to the side of the cathode. This spot movement results in low rates of carbon deposition, and the properties of the deposited flakes are more graphite-like than diamond-like. NASA

N85-20156*# National Aeronautics and Space Administration. Lewis Research Center, Cleveland, Ohio.
TEXTURED CARBON SURFACES ON COPPER Patent Application
A. N. CURREN, K. A. JENSEN, and R. F. ROMAN, inventors (to NASA) 10 Oct. 1984 12 p
(NASA-CASE-LEW-14130-1; NAS 1.71:LEW-14130-1; US-PATENT-APPL-SN-659475) Avail: NTIS HC A02/MF A01 CSCL 13H

A very thin layer of highly textured carbon is applied to a copper surface by a triode sputtering process. A carbon target and a copper substrate are simultaneously exposed to an argon plasma in a vacuum chamber. The resulting carbon surface is characterized by a dense, random array of needle like spries or peaks which extend perpendicularly from the copper surface. The coated copper is especially useful for electrode plates in multistage depressed collectors. NASA

N85-29085*# National Aeronautics and Space Administration. Lewis Research Center, Cleveland, Ohio.
THE STRUCTURE OF ION PLATED FILMS IN RELATION TO COATING PROPERTIES
T. SPALVINS 1985 17 p refs Presented at the Appl. of Ion Plating and Ion Implantation to Mater. Conf., Atlanta, 3-5 Jun. 1985; sponsored in part by American Society for Metals and Georgia Inst. of Technology
(NASA-TM-87055; E-2599; NAS 1.15:87055) Avail: NTIS HC A02/MF A01 CSCL 13H

Ion plating is an ion assisted or glow discharge deposition technique, where ions or energetic atoms transfer energy, momentum and charge to the substrate and the growing film in a manner which can be controlled to favorably modify surface, subsurface chemistry, and microstructure. The glow discharge energizing effects from the initial nucleation stages to the final film growth are discussed. As a result, adherence, coherence, internal stresses, density and morphology of the coatings are significantly improved, over the conventional (nonion-assisted) techniques which in turn favorably affect the surface initiated failures caused by friction, wear, erosion, corrosion and fatigue. Ion plated films because of their graded coating/substrate interface, fine, uniform, densely packed film structure also induce a surface strengthening effect which improved the mechanical properties such as yield, tensile strength and fatigue life. Since a uniform, continuous film can be obtained at lower nominal film thickness, this effect is of great importance in solid film lubrication and in corrosion protection. B.W.

32

COMMUNICATIONS

Includes land and global communications; communications theory; and optical communications.

A85-14434* Motorola, Inc., Scottsdale, Ariz.
SATELLITE BASEBAND PROCESSOR TEST PERFORMANCE SUMMARY
J. T. SHANEYFELT, S. W. ATTWOOD, and D. R. CARROLL (Motorola, Inc., Communications Div., Scottsdale, AZ) IN: EASCON '83; Proceedings of the Sixteenth Annual Electronics and Aerospace Conference and Exposition, Washington, DC, September 19-21, 1983 . New York, Institute of Electrical and Electronics Engineers, 1983, p. 75-83. refs
(Contract NAS3-22502)

A satellite baseband processor (BBP) has been developed for the NASA Lewis 30/20 GHz Satellite Communications Program. The BBP design, reported elsewhere, has been implemented in a proof-of-concept (POC) model. The results of the laboratory system tests of the POC are summarized. Bit error rate test results are presented for the FDM/TDMA communication system operating at 27.5, 110, and 550 Mbps over a variety of operating conditions. The results clearly demonstrate the applicability of baseband processing to future high capacity satellite communication system concepts. A brief description of the system concept, its function, and the role of the baseband processor are presented. The test conditions and means of simulation are also described. The methods of test evaluation and their significance in a system context are given. Author

A85-14436* TRW, Inc., Redondo Beach, Calif.
ADVANCED 30/20 GHZ MULTIPLE BEAM ANTENNA FOR FUTURE COMMUNICATIONS SATELLITES
C. C. CHEN and W. A. MINNIN (TRW, Inc., Space Communications Div., Redondo Beach, CA) IN: EASCON '83; Proceedings of the Sixteenth Annual Electronics and Aerospace Conference and Exposition, Washington, DC, September 19-21, 1983 . New York, Institute of Electrical and Electronics Engineers, 1983, p. 95-102. (Contract NAS3-22499)

The technologies which will be implemented in advanced satellite communications systems being studied by NASA and the intended coverage scenarios are described. The systems will function at 30/20 GHz with 2.5 GHz bandwidth for the uplink and downlink. Subfrequencies will have 500 MHz bandwidth and operations will include TDMA modes. Sample scan patterns are presented for the centerminous U.S. The signals will be broadcast from a multibeam offset Cassegrain reflector antenna to obtain a low sidelobe, wide angle scan. Three contiguous low sidelobe beams will be generated with a diplex feed cluster and a 19 element scanning beam-forming network. The same technology will be used to double the capacity of current 14/12 GHz satellites. M.S.K.

A85-28233*# National Aeronautics and Space Administration. Lewis Research Center, Cleveland, Ohio.
TECHNICAL CHARACTERISTICS OF THE BROADCASTING SATELLITE PLAN AT 12 GHZ FOR THE WESTERN HEMISPHERE
E. F. MILLER (NASA, Lewis Research Center, Cleveland, OH) IN: Globecom '83 - Global Telecommunications Conference, San Diego, CA, November 28-December 1, 1983, Conference Record. Volume 1 . New York, Institute of Electrical and Electronics Engineers, Inc., 1983, p. 225-231. Previously announced in STAR as N84-19640.

Technical parameters such as satellite antenna characteristics, earth station requirements, bandwidths, channelization, and allowable carrier-to-interference ratios are discussed. An overview of the downlink plan is given, including a histogram of the transmitter power requirements. The plan includes satellite orbit positions, spacecraft transmitted powers, antennas beam sizes, channel assignments, and polarizations. Author

A85-28234* National Aeronautics and Space Administration. Lewis Research Center, Cleveland, Ohio.
THE SUBJECTIVE EFFECT OF MULTIPLE CO-CHANNEL FREQUENCY MODULATED TELEVISION INTERFERENCE
W. A. WHYTE, M. A. CAULEY (NASA, Lewis Research Center, Cleveland, OH), and P. P. GROUMPOS (Cleveland State University, Cleveland, OH) IN: Globecom '83 - Global Telecommunications Conference, San Diego, CA, November 28-December 1, 1983, Conference Record. Volume 1 . New York, Institute of Electrical and Electronics Engineers, Inc., 1983, p. 232-236. Previously announced in STAR as N84-11360. refs
(Contract NAG3-156)

As the geostationary orbit/spectrum becomes saturated, there is a need for the ability to reuse frequency assignments. Protection ratios (the ratio of wanted signal power to interfering signal power at the receiver) play a key role in determining efficient frequency reuse plans. A knowledge of the manner in which multiple sources of co-channel interference combine is vital in determining protection ratio requirements such that suitable margin may be allocated for multiple interfering signals. Results of tests examining the subjective assessment of multiple co-channel frequency modulated television signals interfering with another frequency modulated TV system are presented. Author

A85-28241* Cleveland State Univ., Ohio.
ON THE SUBJECTIVE EVALUATION OF THE INTERFERENCE PROTECTION RATIOS' MEASUREMENTS FOR CO-CHANNEL FM-TV SIGNALS
P. P. GROUMPOS (Cleveland State University, Cleveland, OH) and W. WHYTE (NASA, Lewis Research Center, Space Communications Div., Cleveland, OH) IN: Globecom '83 - Global Telecommunications Conference, San Diego, CA, November 28-December 1, 1983, Conference Record. Volume 1 . New York, Institute of Electrical and Electronics Engineers, Inc., 1983, p. 513-518. refs
(Contract NAG3-156)

Results of subjective measurements made to determine the relationship between the image impairment grade and the wanted-signal to interference power ratios (C/I) for co-channel FM television signals are presented. The variation of C/I ratio with picture impairment grade is investigated for three different noise levels. The assessment of impairment grade due to thermal noise only and to picture content is also investigated. A statistical analysis for performed experiments is presented. The results presented here may be used by communication system designers to determine the required system characteristics. Author

A85-29605* Department of Communications, Ottawa (Ontario).
DEVELOPMENT AND USE OF THE COMPUTER SOFTWARE PACKAGE FOR PLANNING THE 12 GHZ BROADCASTING-SATELLITE SERVICE AT RARC '83
R. R. BOWEN, K. E. BROWN, H. S. HOTHI (Department of Communications, Ottawa, Canada), and E. F. MILLER (NASA, Lewis Research Center, Cleveland, OH) IEEE Journal on Selected Areas in Communications (ISSN 0733-8716), vol. SAC-3, Jan. 1985, p. 36-43. refs

The 1983 Regional Administrative Radio Conference (RARC '83) had mainly the objective to draw up a plan of detailed frequency assignments and orbital positions for the 12 GHz broadcasting-satellite service (BSS) in ITU Region 2 (the Western Hemisphere) and associated feeder links (earth-to-space) in the 17 GHz band. It was found that for RARC '83 new planning methods and procedures would be needed. The new requirements made it necessary to develop a new generation of planning software. Attention is given to the development of the computer programs to be used at the conference, the package of computer programs, and the use of the computer programs. G.R.

A85-29611* Department of Communications, Ottawa (Ontario).
EXPERIMENTAL RESULTS SUPPORTING THE DETERMINATION OF SERVICE QUALITY OBJECTIVES FOR DBS SYSTEMS
G. CHOUINARD (Department of Communications, Communications Research Centre, Ottawa, Canada), W. A. WHYTE, JR. (NASA, Lewis Research Center, Cleveland, OH), A. A. GOLDBERG, and B. L. JONES (CBS Technology Center, Stamford, CT) IEEE Journal on Selected Areas in Communications (ISSN 0733-8716), vol. SAC-3, Jan. 1985, p. 87-99. refs

A summary of the results of a joint United States and Canadian program on subjective measurements of the picture degradation caused by noise and interference on an NTSC encoded color television signal is given in this paper. The effects of system noise, cochannel and adjacent channel interference, and both single entry and aggregate as well as a combination of these types of interference were subjectively evaluated by expert and nonexpert viewers under reference conditions. These results were used to develop the rationale used at RARC '83 to establish the service quality objective for planning the DBS service for the American continents. Author

A85-32249* Illinois Univ., Urbana.
ON THE CALCULATION OF THE DIRECTIVITY OF PLANAR ARRAY FEEDS FOR SATELLITE REFLECTOR APPLICATIONS
P. T. LAM (Illinois, University, Urbana, IL) IEEE Transactions on Antennas and Propagation (ISSN 0018-926X), vol. AP-33, May 1985, p. 570, 571.
(Contract NAG3-419)

The calculation of the directivity of a reflector antenna excited by a planar array feed which is generally polarized, involves a coefficient C(mn). A series representation of C(mn), which allows efficient numerical evalulation is derived. Numerical results and comments on the behavior of C(mn) are discussed. M.D.

A85-34470* Mitre Corp., Bedford, Mass.
A FREQUENCY-ROUTED SATELLITE SYSTEM CONCEPT USING MULTIPLE ORTHOGONALLY-POLARIZED BEAMS FOR FREQUENCY REUSE
E. ROTHOLZ (Mitre Corp., Bedford, MA) and B. E. WHITE (Signatron, Inc., Lexington, MA) IN: Milcom '83; Proceedings of the Military Communications Conference, Washington, DC, October 31-November 2, 1983. Volume 1 . New York, Institute of Electrical and Electronics Engineers, Inc., 1983, p. 140-154.
(Contract NASA ORDER C-49029-D)

The design concepts of a multibeam frequency-division multiplexed satellite system accessed by many moderately sized earth stations are outlined. In the system proposed here, traffic is routed from beam to beam through appropriate apportionment and filtering. Within a beam, the routing to particular users is achieved by conventional FDM. The optimum beam size, beam isolation, orthogonal polarization assignment to beams, the concept of beam groups yielding a simple transponder design, and the establishment of a frequency plan providing interference-free band assignments are discussed. V.L.

A85-36653* Virginia Univ., Charlottesville.
FOUR-DIMENSIONAL MODULATION AND CODING - AN ALTERNATE TO FREQUENCY-REUSE
S. G. WILSON, H. A. SLEEPER, and N. K. SRINATH (Virginia, University, Charlottesville, VA) IN: ICC '84 - Links for the future: Science, systems and services for communications; Proceedings of the International Conference on Communications, Amsterdam, Netherlands, May 14-17, 1984. Volume 2 . New York/Amsterdam, Institute of Electrical and Electronics Engineers, Inc./North-Holland, 1984, p. 919-923. Previously announced in STAR as N83-36300. refs
(Contract NAG3-141)

Four dimensional modulation as a means of improving communication efficiency on the band-limited Gaussian channel, with the four dimensions of signal space constituted by phase orthogonal carriers (cos omega sub c t and sin omega sub c t) simultaneously on space orthogonal electromagnetic waves are discussed. 'Frequency reuse' techniques use such polarization orthogonality to reuse the same frequency slot, but the modulation is not treated as four dimensional, rather a product of two-D modulations, e.g., QPSK. It is well known that, higher dimensionality signalling affords possible improvements in the power bandwidth sense. Four-D modulations based upon subsets of lattice-packings in four-D, which afford simplification of encoding and decoding are described. Sets of up to 1024 signals are constructed in four-D, providing a (Nyquist) spectral efficiency of up to 10 bps/Hz. Energy gains over the reuse technique are in the one to three dB range t equal bandwidth. S.L.

A85-39356* Illinois Univ., Urbana.
FOCAL SHIFTS IN PARABOLIC REFLECTORS
H. LING, S.-W. LEE, P. T. C. LAM (Illinois, University, Urbana, IL), and W. V. T. RUSCH (Southern California, University, Los Angeles, CA) IEEE Transactions on Antennas and Propagation (ISSN 0018-926X), vol. AP-33, July 1985, p. 744-748. refs
(Contract NAG3-419; NSF ECS-81-20305)

The case of a parabolic reflector and a point feed is considered, taking into account the question regarding the location in which the feed should be placed for an achievement of maximum directivity. Based on the tracing of geometrical rays, the obvious answer is obtained that the feed should be placed at the focal point. In the present paper, it is shown that this answer is not always correct. There are situations in which the maximum directivity is achieved when the feed is axially displaced toward the reflector or away from it. This 'focal shift' phenomenon is a result of three competing factors which affect the directivity of a reflector. The factors are related to phase synchronism over the reflector aperture, aperture illumination efficiency, and spillover loss. For achieving the maximum directivity, it is necessary to find the best compromise among the three factors. G.R.

N85-10234*# National Aeronautics and Space Administration. Lewis Research Center, Cleveland, Ohio.
CASE STUDY OF SAMPLE SPACING IN PLANAR NEAR-FIELD MEASUREMENT OF HIGH GAIN ANTENNAS
R. J. ACOSTA and R. Q. LEE Washington 1984 10 p refs Presented at the Antenna Appl. Symp., Montecello, Ill., 18-21 Sep. 1984; sponsored by Illinois Univ.
(NASA-TM-86872; E-2301; NAS 1.15:86872) Avail: NTIS HC A02/MF A01 CSCL 20N

Far field antenna patterns can be reconstructed from planar near field measurements acquired at a sample spacing of lambda/2 or less. For electrically large antennas, sampling at the Nyquist rate may result in errors due to system electronic drift over long acquisition times. The computer capacity may limit the largest size of the near field data set. The requirement to sample at the Nyquist rate is relaxed for high gain antennas which concentrate most of the radiated energy into a small angular region of the far field. The criteria for sample spacing at greater than lambda/e through the use of a priori information of the antenna radiation characteristics are presented. Far field patterns of a 30 GHz dual offset reflector system with a 2.7 m parabolic main reflector are computed from near field data obtained at sample spacings ranging from 0.1 lambda to 10 lambda. The effects of sampling interval and spectrum cutoff on the far field patterns are discussed. E.A.K.

N85-11265*# Illinois Univ., Urbana-Champaign. Electromagnetics Lab.
THE STUDY OF MICROSTRIP ANTENNA ARRAYS AND RELATED PROBLEMS Semiannual Report, 22 May - 21 Nov. 1984
Y. T. LO 19 Nov. 1984 42 p refs Sponsored in part by AF (Contract NAG3-418)
(NASA-CR-174054; NAS 1.26:174054) Avail: NTIS HC A03/MF A01 CSCL 20N

The physical layout of the array elements and the proximity of the microstrip feed network makes the input impedance and radiation pattern values dependent upon the effects of mutual coupling, feedline discontinuities and feed point location. The extent of these dependences was assessed and a number of single patch and module structures were constructed and measured at an operating frequency of approximately 4.0 GHz. The empirical results were compared with the ones which were theoretically predicted by the cavity model of thin microstrip antennas. Each element was modelled as an independent radiating patch and each microstrip feedline as an independent, quasi-TEM transmission line. The effects of the feedline discontinuities are approximated by lumped L-C circuit models. E.A.K.

N85-15099*# National Aeronautics and Space Administration. Lewis Research Center, Cleveland, Ohio.
DEMAND FOR SATELLITE-PROVIDED DOMESTIC COMMUNICATIONS SERVICES UP TO THE YEAR 2000
S. STEVENSON, W. POLEY, J. LEKAN, and J. A. SALZMAN Nov. 1984 43 p refs
(NASA-TM-86894; E-2367; NAS 1.15:86894) Avail: NTIS HC A03/MF A01 CSCL 17B

Three fixed service telecommunications demand assessment studies were completed for NASA by The Western Union Telegraph Company and the U.S. Telephone and Telegraph Corporation. They provided forecasts of the total U.S. domestic demand, from 1980

to the year 2000, for voice, data, and video services. That portion that is technically and economically suitable for transmission by satellite systems, both large trunking systems and customer premises services (CPS) systems was also estimated. In order to provide a single set of forecasts a NASA synthesis of the above studies was conducted. The services, associated forecast techniques, and data bases employed by both contractors were examined, those elements of each judged to be the most appropriate were selected, and new forecasts were made. The demand for voice, data, and video services was first forecast in fundamental units of call-seconds, bits/year, and channels, respectively. Transmission technology characteristics and capabilities were then forecast, and the fundamental demand converted to an equivalent transmission capacity. The potential demand for satellite-provided services was found to grow by a factor of 6, from 400 to 2400 equivalent 36 MHz satellite transponders over the 20-year period. About 80 percent of this was found to be more appropriate for trunking systems and 20 percent CPS. M.G.

N85-15943*# Illinois Univ., Urbana. Electromagnetic Communication Lab.

MMIC DEVICES FOR ACTIVE PHASED ARRAY ANTENNAS Semiannual Report, 21 May - 20 Dec. 1984

R. MITTRA Dec. 1984 17 p refs

(Contract NCC3-38)

(NASA-CR-174281; NAS 1.26:174281) Avail: NTIS HC A02/MF A01 CSCL 20N

The study of printed circuit discontinuities is necessary in order to design, for example, transitions between rectangular waveguides and printed circuits. New developments with respect to the analytical approaches to this problem are discussed. A summary of the progress in the experimental approach is presented. The accurate solution for the modes in various millimeter-wave waveguides is essential in the analysis of many integrated circuit components, such as filters and impedance transformers. Problems associated with the numerical computation of these modes in two frequently used waveguide forms, namely, the finline and microstrip, are presented. The spectral domain method of formulation, with a moment method solution, is considered. This approach can be readily extended to analyze an arbitrary configuration of dielectric and metallized regions in a shielded enclosure. Galerkin's method is used, where the testing and basic functions are the same. It is shown that the mode functions, or eigenfunctions, are more sensitive to errors than the phase constants, or eigenvalues. The approximate mode functions do not satisfy the orthogonality relationship well, resulting in difficulties when these modal solutions are used to form an approximate Green's function or are used in a mode matching analysis. B.W.

N85-15944*# Ford Aerospace and Communications Corp., Palo Alto, Calif.

THE 20 GHZ PROOF-OF-CONCEPT TEST MODEL RESULTS FOR A MULTIPLE SCAN BEAM DUAL REFLECTOR ANTENNA

T. ROBERTS, A. SMOLL, H. LUH, E. W. MATTHEWS, and W. G. SCOTT 1984 15 p Presented at the IEEE Antenna Propagation Symp., Houston, Tex., 23-27 May 1983

(Contract NAS3-22498)

(NASA-CR-174268; NAS 1.26:174268) Avail: NTIS HC A02/MF A01 CSCL 17B

A full scale 20 GHz antenna model was designed, fabricated and tested. The model is intended to test the low sidelobe beam scanning capability of a new class of an offset dual reflector and feed array configuration. The offset main reflector and subreflector surfaces are custom shaped by a computer synthesis procedure. The derived optics result in beam scan loss under 1 db over the + or - 12.3 beamwidths by + or - 5.8 beamwidths scan volume while maintaining low sidelobes. It is found that the measured and computed patterns are in good agreement. E.A.K.

N85-17258*# Ohio State Univ., Columbus. ElectroScience Lab.

ADAPTIVE ANTENNA ARRAYS FOR WEAK INTERFERING SIGNALS

I. J. GUPTA Jan. 1985 71 p refs

(Contract NAG3-536)

(NASA-CR-174336; NAS 1.26:174336; ESL-716111-2) Avail: NTIS HC A04/MF A01 CSCL 09E

The interference protection provided by adaptive antenna arrays to an Earth station or satellite receive antenna system is studied. The case where the interference is caused by the transmission from adjacent satellites or Earth stations whose signals inadverently enter the receiving system and interfere with the communication link is considered. Thus, the interfering signals are very weak. To increase the interference suppression, one can either decrease the thermal noise in the feedback loops or increase the gain of the auxiliary antennas in the interfering signal direction. Both methods are examined. It is shown that one may have to reduce the noise correlation to impractically low values and if directive auxiliary antennas are used, the auxiliary antenna size may have to be too large. One can, however, combine the two methods to achieve the specified interference suppression with reasonable requirements of noise decorrelation and auxiliary antenna size. Effects of the errors in the steering vector on the adaptive array performance are studied. R.S.F.

N85-18238*# General Electric Co., Syracuse, N.Y. Electronics Lab.

CONFIGURATION STUDY FOR A 30 GHZ MONOLITHIC RECEIVE ARRAY: TECHNICAL ASSESSMENT

W. H. NESTER, B. CLEAVELAND, B. EDWARD, S. GOTKIS, G. HESSERBACKER, J. LOH, and B. MITCHELL 1 Nov. 1984 47 p refs 3 Vol.

(Contract NAS3-23780)

(NASA-CR-174697; NAS 1.26:174697) Avail: NTIS HC A03/MF A01 CSCL 17B

The current status of monolithic microwave integrated circuits (MMICs) in phased array feeds is discussed from the point of view of cost performance, reliability, and design considerations. Transitions to MMICs, compatible antenna radiating elements and reliability considerations are addressed. Hybrid antennas, feed array antenna technology, and offset reflectors versus phased arrays are examined. A.R.H.

N85-18239*# General Electric Co., Syracuse, N.Y. Electronics Lab.

CONFIGURATION STUDY FOR A 30 GHZ MONOLITHIC RECEIVE ARRAY, VOLUME 1

W. H. NESTER, B. CLEAVELAND, B. EDWARD, S. GOTKIS, G. HESSERBACKER, J. LOH, and B. MITCHELL 1 Nov. 1984 181 p refs 3 Vol.

(Contract NAS3-23780)

(NASA-CR-174697-VOL-1; NAS 1.26:174697-VOL-1) Avail: NTIS HC A09/MF A01 CSCL 17B

Gregorian, Cassegrain, and single reflector systems were analyzed in configuration studies for communications satellite receive antennas. Parametric design and performance curves were generated. A preliminary design of each reflector/feed system was derived including radiating elements, beam-former network, beamsteering system, and MMIC module architecture. Performance estimates and component requirements were developed for each design. A recommended design was selected for both the scanning beam and the fixed beam case. Detailed design and performance analysis results are presented for the selected Cassegrain configurations. The final design point is characterized in detail and performance measures evaluated in terms of gain, sidelobe level, noise figure, carrier-to-interference ratio, prime power, and beamsteering. The effects of mutual coupling and excitation errors (including phase and amplitude quantization errors) are evaluated. Mechanical assembly drawings are given for the final design point. Thermal design requirements are addressed in the mechanical design. A.R.H.

N85-18240*# General Electric Co., Syracuse, N.Y. Electronics Lab.
CONFIGURATION STUDY FOR A 30 GHZ MONOLITHIC RECEIVE ARRAY, VOLUME 2
W. H. NESTER, B. CLEAVELAND, B. EDWARD, S. GOTKIS, G. HESSERBACKER, J. LOH, and B. MITCHELL 1 Nov. 1984 375 p 3 Vol.
(Contract NAS3-23780)
(NASA-CR-174697-VOL-2; NAS 1.26:174697-VOL-2) Avail: NTIS HC A16/MF A01 CSCL 17B

The formalism of the sidelobe suppression algorithm and the method used to calculate the system noise figure for a 30 GHz monolithic receive array are presented. Results of array element weight determination and performance studies of a Gregorian aperture image system are also given. A.R.H.

N85-20223*# National Aeronautics and Space Administration. Lewis Research Center, Cleveland, Ohio.
EFFECT OF INTERFACIAL CHARACTERISTICS OF METAL CLAD POLYMERIC SUBSTRATES ON ELECTRICAL HIGH FREQUENCY INTERCONNECTION PERFORMANCE
K. B. BHASIN, R. R. ROMANOFSKY, G. E. PONCHAK, and D. C. LIU 29 Nov. 1984 10 p refs Presented at the Fall Meeting of the Mater. Res. Soc., Boston, 27-29 Nov. 1984
(NASA-TM-86948; E-2469; NAS 1.15:86948) Avail: NTIS HC A02/MF A01 CSCL 20N

Etched metallic conductor lines on metal clad polymeric substrates are used for electronic component interconnections. Significant signal losses are observed for microstrip conductor lines used for interconnecting high frequency devices. At these frequencies, the electronic signal travels closer to the metal-polymer interface due to the skin effect. Copper-teflon interfaces were characterized by scanning electron microscopy (SEM) and Auger electron spectroscopy (AES) to determine the interfacial properties. Data relating roughness of the copper film to signal losses was compared to theory. Films used to enhance adhesion are found, to contribute to these losses. E.A.K.

N85-20224*# National Aeronautics and Space Administration. Lewis Research Center, Cleveland, Ohio.
AN EXPERIMENTAL INVESTIGATION OF MICROSTRIP PROPERTIES ON SOFT SUBSTRATES FROM 2 TO 40 GHZ
R. R. ROMANOFSKY, K. B. BHASIN, G. E. PONCHAK, A. N. DOWNEY, and D. J. CONNOLLY 1985 10 p refs To be presented at the Intern. Microwave Symp., St. Louis, 4-6 Jun. 1985; sponsored by the IEEE
(NASA-TM-86961; E-2489; NAS 1.15:86961) Avail: NTIS HC A02/MF A01 CSCL 17B

Dispersion and loss characteristics of microstrip lines on 10 mil and 31 mil electrodeposited and electroless copper clad-Teflon substrates were experimentally obtained from 2 to 40 GHz. The roles of surface roughness and radiation in total loss were examined. Author

N85-21438*# Illinois Univ., Urbana. Electromagnetics Lab.
NUMERICAL METHODS FOR ANALYZING ELECTROMAGNETIC SCATTERING Semiannual Report, 25 Sep. 1984 - 24 Mar. 1985
S. W. LEE, Y. T. LO, S. L. CHUANG, and C. S. LEE 24 Mar. 1985 66 p refs
(Contract NAG3-475)
(NASA-CR-175507; NAS 1.26:175507) Avail: NTIS HC A04/MF A01 CSCL 20N

Numerical methods to analyze electromagnetic scattering are presented. The dispersions and attenuations of the normal modes in a circular waveguide coated with lossy material were completely analyzed. The radar cross section (RCS) from a circular waveguide coated with lossy material was calculated. The following is observed: (1) the interior irradiation contributes to the RCS much more than does the rim diffraction; (2) at low frequency, the RCS from the circular waveguide terminated by a perfect electric conductor (PEC) can be reduced more than 13 dB down with a coating thickness less than 1% of the radius using the best lossy material available in a 6 radius-long cylinder; (3) at high frequency, a modal separation between the highly attenuated and the lowly attenuated modes is evident if the coating material is too lossy, however, a large RCS reduction can be achieved for a small incident angle with a thin layer of coating. It is found that the waveguide coated with a lossy magnetic material can be used as a substitute for a corrugated waveguide to produce a circularly polarized radiation yield. E.A.K.

N85-23815*# National Aeronautics and Space Administration. Lewis Research Center, Cleveland, Ohio.
ALTERNATIVES FOR SATELLITE SOUND BROADCAST SYSTEMS AT HF AND VHF
B. E. LEROY *In* NASA. Langley Research Center Large Space Antenna Systems Technol., 1984 p 27-37 Apr. 1985
Avail: NTIS HC A20/MF A01 CSCL 20N

The National Aeronautics and Space Administration and the United States Information Agency (USIA) are currently engaged in a joint program to assess the technical and economic feasibility of direct sound broadcast satellite systems to meet USIA mission needs. The cooperative effort calls for a series of interrelated studies to provide the respective Agency managements with information on the potential role of direct broadcast satellites. Initial studies focused on HF propagation phenomena and broadcast coverage requirements. These studies served as the basis for parallel systems studies currently in progress. The systems studies are to provide a data base on various satellite configurations and systems concepts capable of supporting potential broadcast requirements ranging from a small fraction to a substantial addition to USIA requirements. Antenna concepts for LEO and GEO orbits are briefly described. M.G.

N85-25686*# Ohio State Univ., Columbus. ElectroScience Lab.
ANALYSIS OF THE ELECTROMAGNETIC SCATTERING FROM AN INLET GEOMETRY WITH LOSSY WALLS Progress Report
N. H. MYUNG, P. H. PATHAK, and C. D. CHUNANG Apr. 1985 91 p refs
(Contract NAG3-476)
(NASA-CR-175743; NAS 1.26:175743; PR-715723) Avail: NTIS HC A05/MF A01 CSCL 20N

One of the primary goals is to develop an approximate but sufficiently accurate analysis for the problem of electromagnetic (EM) plane wave scattering by an open ended, perfectly-conducting, semi-infinite hollow circular waveguide (or duct) with a thin, uniform layer of lossy or absorbing material on its inner wall, and with a simple termination inside. The less difficult but useful problem of the EM scattering by a two-dimensional (2-D), semi-infinite parallel plate waveguide with an impedance boundary condition on the inner walls was chosen initially for analysis. The impedance boundary condition in this problem serves to model a thin layer of lossy dielectric/ferrite coating on the otherwise perfectly-conducting interior waveguide walls. An approximate but efficient and accurate ray solution was obtained recently. That solution is presently being extended to the case of a moderately thick dielectric/ferrite coating on the walls so as to be valid for situations where the impedance boundary condition may not remain sufficiently accurate. R.J.F.

N85-27092*# Western Union Telegraph Co., McLean, Va. Government Systems Div.
SATELLITE PROVIDED CUSTOMER PROMISES SERVICES, A FORECAST OF POTENTIAL DOMESTIC DEMAND THROUGH THE YEAR 2000. VOLUME 4: SENSITIVITY ANALYSIS
D. KRATOCHVIL, J. BOWYER, C. BHUSHAN, K. STEINNAGEL, D. KAUSHAL, and G. AL-KINANI Mar. 1984 261 p 4 Vol.
(Contract NAS3-23255)
(NASA-CR-174662; NAS 1.26:174662) Avail: NTIS HC A12/MF A01 CSCL 17B

The overall purpose was to forecast the potential United States domestic telecommunications demand for satellite provided customer promises voice, data and video services through the year 2000, so that this information on service demand would be available to aid in NASA program planning. To accomplish this overall purpose the following objectives were achieved: (1)

development of a forecast of the total domestic telecommunications demand; (2) identification of that portion of the telecommunications demand suitable for transmission by satellite systems; (3) identification of that portion of the satellite market addressable by consumer promises service (CPS) systems; (4) identification of that portion of the satellite market addressable by Ka-band CPS system; and (5) postulation of a Ka-band CPS network on a nationwide and local level. The approach employed included the use of a variety of forecasting models, a parametric cost model, a market distribution model and a network optimization model. Forecasts were developed for: 1980, 1990, and 2000; voice, data and video services; terrestrial and satellite delivery modes; and C, Ku and Ka-bands. R.J.F.

N85-31348*# National Aeronautics and Space Administration. Lewis Research Center, Cleveland, Ohio.
AUTOMATED TESTING OF DEVELOPMENTAL SATELLITE COMMUNICATIONS SYSTEMS AND SUBSYSTEMS
K. A. SHALKHAUSER and R. J. KERCZEWSKI 1985 20 p refs Presented at the 25th Conf. of the Automated RF Tech. Group, St. Louis, 6-7 Jun. 1985
(NASA-TM-87070; E-2642; NAS 1.15:87070) Avail: NTIS HC A02/MF A01 CSCL 17B

Lower frequency bands allocated for satellite communications use are becoming saturated due to steadily increasing demand. An ongoing program to develop the new technologies required to meet the demands of future systems is described. Higher frequency components and more efficient system techniques are developed. In order to accurately evaluate the performance of these technologies, an automated test system was designed and built. The automated system's design an capabilities are discussed. E.A.K.

N85-34329*# Ohio State Univ., Columbus. Dept. of Electrical Engineering.
ADAPTIVE ANTENNA ARRAYS FOR SATELLITE COMMUNICATIONS: DESIGN AND TESTING
I. J. GUPTA, W. G. SWARNER, and E. K. WALTON Sep. 1985 116 p refs
(Contract NAG3-536)
(NASA-CR-176162; NAS 1.26:176162; ESL-716111-3) Avail: NTIS HC A06/MF A01 CSCL 20N

When two separate antennas are used with each feedback loop to decorrelate noise, the antennas should be located such that the phase of the interfering signal in the two antennas is the same while the noise in them is uncorrelated. Thus, the antenna patterns and spatial distribution of the auxiliary antennas are quite important and should be carefully selected. The selection and spatial distribution of auxiliary elements is discussed when the main antenna is a center fed reflector antenna. It is shown that offset feeds of the reflector antenna can be used as auxiliary elements of an adaptive array to suppress weak interfering signals. An experimental system is designed to verify the theoretical analysis. The details of the experimental systems are presented. Author

N85-35320*# Illinois Univ., Urbana. Electromagnetics Lab.
NORMAL MODES IN AN OVERMODED CIRCULAR WAVEGUIDE COATED WITH LOSSY MATERIAL
C. S. LEE, S. W. LEE, and S. L. CHUANG Sep. 1985 55 p refs
(Contract NAG3-475)
(NASA-CR-176186; NAS 1.26:176186; TR-85-8) Avail: NTIS HC A04/MF A01 CSCL 20N

The normal modes in an overmoded waveguide coated with a lossy material are analyzed, particularly for their attenuation properties as a function of coating material, layer thickness, and frequency. When the coating material is not too lossy, the low-order modes are highly attenuated even with a thin layer of coating. This coated guide serves as a mode suppressor of the low-order modes, which can be particularly useful for reducing the radar cross section (RCS) of a cavity structure such as a jet inlet. When the coating material is very lossy, low-order modes fall into two distinct groups: highly and lowly attenuated modes. However, as a/lambda (a = radius of the cylinder; lambda = the free-space wavelength) increases, the separation between these two groups becomes less distinctive. The attenuation constants of most of the low-order modes become small, and decrease as a function of lambda sup 2/a sup 3. Author

N85-35321*# Case Western Reserve Univ., Cleveland, Ohio. Dept. of Electrical Engineering and Applied Physics.
PERTURBATION-ITERATION THEORY FOR ANALYZING MICROWAVE STRIPLINES
B. E. KRETCH Sep. 1985 137 p refs
(Contract NCC3-29)
(NASA-CR-176189; NAS 1.26:176189; WGR-85-5) Avail: NTIS HC A07/MF A01 CSCL 20N

A perturbation-iteration technique is presented for determining the propagation constant and characteristic impedance of an unshielded microstrip transmission line. The method converges to the correct solution with a few iterations at each frequency and is equivalent to a full wave analysis. The perturbation-iteration method gives a direct solution for the propagation constant without having to find the roots of a transcendental dispersion equation. The theory is presented in detail along with numerical results for the effective dielectric constant and characteristic impedance for a wide range of substrate dielectric constants, stripline dimensions, and frequencies. Author

33

ELECTRONICS AND ELECTRICAL ENGINEERING

Includes test equipment and maintainability; components, e.g., tunnel diodes and transistors; microminiaturization; and integrated circuity.

A85-12669* Virginia Polytechnic Inst. and State Univ., Blacksburg.
BIPOLAR-FET COMBINATIONAL POWER TRANSISTORS FOR POWER CONVERSION APPLICATIONS
D. Y. CHEN and S. A. CHIN (Virginia Polytechnic Institute and State University, Blacksburg, VA) (International Telecommunication Energy Conference, 5th, Tokyo, Japan, Oct. 1983) IEEE Transactions on Aerospace and Electronic Systems (ISSN 0018-9251), vol. AES-20, Sept. 1984, p. 659-664. refs
(Contract NAG3-40)

Four bipolar-FET (field-effect transistor) combinational transistor configurations are compared from the application point of view. The configurations included are FET-Darlington (cascade), emitter-open switch (cascode), parallel configuration, and FET-gated bipolar transistors (FGT). Author

A85-14432*# National Aeronautics and Space Administration, Washington, D.C.
STATUS OF NASA'S MULTIBEAM COMMUNICATIONS TECHNOLOGY PROGRAM
D. E. SANTARPIA (NASA Washington, DC) and J. W. BAGWELL (NASA, Lewis Research Center, Cleveland, OH) IN: EASCON '83; Proceedings of the Sixteenth Annual Electronics and Aerospace Conference and Exposition, Washington, DC, September 19-21, 1983 . New York, Institute of Electrical and Electronics Engineers, 1983, p. 53-68.

Progress with prototype components for demonstrating an acceptable performance level for multibeam 30/20 GHz satellite communications scheduled for service in 1988 is summarized. Numerous companies were contracted by NASA for the various components and subsystems, which include 20 GHz transmitters, a traveling wave tube transmitter, an IMPATT amplifier, a GaAs FET amplifier, a 30 GHz low noise receiver, a trunking matrix switch, and a baseband processor. The key system is a 20 GHz offset dual reflector antenna with shaped surfaces for multibeam

transmission. Tests to date have indicated success at meeting the performance objectives. M.S.K.

A85-14433* *Hughes Aircraft Co., Torrance, Calif.*
A 20 GHZ, 75 WATT, HELIX TWT FOR SPACE COMMUNICATIONS
J. F. HENEY and R. N. TAMASHIRO (Hughes Aircraft Co., Electron Dynamics Div., Torrance, CA) IN: EASCON '83; Proceedings of the Sixteenth Annual Electronics and Aerospace Conference and Exposition, Washington, DC, September 19-21, 1983 . New York, Institute of Electrical and Electronics Engineers, 1983, p. 69-74.
(Contract NAS3-23351)

A space-qualified, helix-type traveling wave tube is being developed for satellite communication systems in the frequency band of 17.7 to 21.2 GHz. The design approach stresses very high efficiency operation, but with very low distortion. The tube provides multi-mode operation, permitting CW saturated power output levels of 75, 40, and 7.5 W. Operation is also anticipated at 5 dB below these saturation levels to achieve the required low distortion levels. Advanced construction features include a five-stage depressed collector, a diamond supported helix slow-wave circuit, and a type M dispenser cathode. High reliability and long life (10 yr) are objectives of the tube design. Preliminary test results on early developmental models of this tube are very encouraging. An output power of 75 to 90 W has been achieved over the full bandwidth with about 40 dB of saturated gain. More importantly, the basic electronic efficiency of the interaction process has been increased from about 7.5-11 percent by the use of the diamond helix support compared to earlier tubes using BeO support rods. This effort is supported by NASA Lewis Research Center and is aimed toward application in the NASA Advanced Communications Satellite Technology Program. Author

A85-14435*# National Aeronautics and Space Administration. Lewis Research Center, Cleveland, Ohio.
THE NASA SATELLITE COMMUNICATION 20 X 20 MATRIX SWITCHES
A. L. SAUNDERS (NASA, Lewis Research Center, Cleveland, OH) IN: EASCON '83; Proceedings of the Sixteenth Annual Electronics and Aerospace Conference and Exposition, Washington, DC, September 19-21, 1983 . New York, Institute of Electrical and Electronics Engineers, 1983, p. 85-94.

The characteristics of two matrix switches designed for high capacity satellite communications systems are described. The switches provide routing between 20 input and 20 output ports at an IF frequency during TDMA operations. Switching speeds of 10 nsec are projected for dual gate GaAs FETs. The two designs differed in the coupling configurations, bandwidth (2.69-1.2 GHz), off-state isolation (-54 to -40 dB), switching speeds (16-37 nsec), and gain ripple (5.3-2.2 dB). Both designs achieved a 2 nsec reconfiguration rate. Further development is required to reduce the ripple effects and attain the potential 2 nsec switching speed offered by the GaAs FETs. M.S.K.

A85-16424*# Tuskegee Inst., Ala.
FRICTION IN RAIL GUNS
P. K. KAY (Tuskegee Institute, Tuskegee, AL) IN: International Electric Propulsion Conference, 17th, Tokyo, Japan, May 28-31, 1984, Proceedings . Tokyo, Japan Society for Aeronautical and Space Sciences, 1984, p. 384-389. refs
(Contract NAG3-76)

The influence of friction is included in the present equations describing the performance of an inductively driven rail gun. These equations, which have their basis in an empirical formulation, are applied to results from two different experiments. Only an approximate physical description of the problem is attempted, in view of the complexity of details in the interaction among forces of this magnitude over time periods of the order of milisecs. O.C.

A85-20170* Case Western Reserve Univ., Cleveland, Ohio.
CIRCULAR WAVEGUIDE BIFURCATION FOR ASYMMETRIC MODES
H. W. SCHILLING (LTV Steel Research Center, Independence, OH) and R. E. COLLIN (Case Western Reserve University, Cleveland, OH) IEE Proceedings, Part H - Microwaves, Optics and Antennas (ISSN 0143-7097), vol. 131, pt. H, no. 6, Dec. 1984, p. 397-404. refs
(Contract NSF ECS-79-10269; NAS3-22342)

An analytical solution for a circular waveguide bifurcation with incident TE(11)- and TM(11)-modes is presented using the residue calculus method. It is shown how the coupling between the TE(1n)- and TM(1n)-modes can be taken into account by expressing the coupling factor as a contour integral, which is the key step enabling the residue calculus method to be applied. Graphical results for the scattering matrix parameters of the junction are given for a range of waveguide radii of interest in the design of dual-mode coaxial prime focus feeds for paraboloidal antennas. Author

A85-20171* Case Western Reserve Univ., Cleveland, Ohio.
DUAL-MODE COAXIAL FEED WITH LOW CROSSPOLARISATION
R. E. COLLIN (Case Western Reserve University, Cleveland, OH) and H. W. SCHILLING (LTV Steel Research Center, Independence, OH) IEE Proceedings, Part H - Microwaves, Optics and Antennas (ISSN 0143-7097), vol. 131, pt. H, no. 6, Dec. 1984, p. 405-410. refs
(Contract NAS3-22342; NSF ECS-79-10269)

Design data for optimized TE(11)-TM(11) dual-mode coaxial prime focus feeds is presented. The optimized feeds have a crosspolarization below -30 dB, an input reflection coefficient below 0.1 and very little phase error in their radiation patterns, over a 5 percent bandwidth. Experimental patterns are also given that show that the theoretically derived design data can be relied upon. The optimized feeds are useful for paraboloidal reflectors with focal-length/diameter ratios in the range 0.3 to 0.5, and will give overall efficiencies as high as 70 percent or more with sidelobes below -30 dB. Author

A85-20900*# Bell Telephone Labs., Inc., Whippany, N. J.
A FAST TIME DOMAIN DIGITAL SIMULATION TECHNIQUE FOR POWER CONVERTERS - APPLICATION TO A BUCK CONVERTER WITH FEEDFORWARD COMPENSATION
S. S. KELKAR (AT & T Electronic Power Systems Laboratory, Whippany, NJ) and F. C. LEE (Virginia Polytechnic Institute and State University, Blacksburg, VA) Institute of Electrical and Electronics Engineers, Power Electronics Specialists Conference, Gaithersburg, MD, June 18-21, 1984, Paper. 12 p. refs
(Contract NAG3-220)

Small signal analysis was performed earlier to demonstrate the marked improvement of dynamic properties and stability margins of a switching regulator employing a novel feedforward input filter compensation scheme. A large signal nonlinear recurrent time domain model is presented for the converter to analyse the transient response due to a step input change with and without the presence of the proposed feedforward loop. The results are verified with experimental data. Author

A85-25170* Illinois Univ., Urbana.
PLOT OF MODAL FIELD DISTRIBUTION IN RECTANGULAR AND CIRCULAR WAVEGUIDES
C. S. LEE, S. W. LEE, and S. L. CHUANG (Illinois, University, Urbana, IL) IEEE Transactions on Microwave Theory and Techniques (ISSN 0018-9480), vol. MTT-33, March 1985, p. 271-274.
(Contract NAG3-475)

A85-28230* Toledo Univ., Ohio.
AN ALLPASS FILTER DESIGN FOR LUMINANCE AND CHROMINANCE SEPARATION OF NTSC SIGNALS
D. A. BORDER and S. C. KWATRA (Toledo, University, Toledo, OH) IN: Globecom '83 - Global Telecommunications Conference, San Diego, CA, November 28-December 1, 1983, Conference Record. Volume 1 . New York, Institute of Electrical and Electronics Engineers, Inc., 1983, p. 174-178. refs
(Contract NAG3-42)

Abstract- Digital techniques for separation of luminance and chrominance components from composite NTSC broadcast television signals are explored. First, comb filters are introduced. Secondly, filters based on linear regression are developed. Finally, a third filtering form, the allpass filter is considered. Techniques are compared based on mean squared error criteria and subjective testing. It is demonstrated that the allpass filtering technique is superior to both the comb filtering as well as the regression filtering. Author

A85-35306* Kansas Univ., Lawrence.
NUMERICAL SIMULATION OF POSITIVE-POTENTIAL CONDUCTORS IN THE PRESENCE OF A PLASMA AND A SECONDARY-EMITTING DIELECTRIC
R. L. KESSEL, R. A. MURRAY, R. HETZEL, and T. P. ARMSTRONG (Kansas, University, Lawrence, KS) Journal of Applied Physics (ISSN 0021-8979), vol. 57, June 1, 1985, p. 4991-4995. refs
(Contract NSG-3290)

A 2 1/2-dimensional, cylindrically symmetric particle in cell program is used to simulate the interaction of a plasma with a positively biased disk covered by a dielectric material (Kapton). Several runs using different combinations of bias voltages and secondary electron yields are discussed. Special attention is paid to the role of the secondaries as the dielectric surface changes from a negative potential to become increasingly positive. This is termed the 'snapover' process. The contribution due to secondaries is examined by plotting the distribution (number versus position) of the particles emitted by the impacting on the dielectric. These plots show that secondaries are drawn back into the dielectric as well as the conductor in the case of snapover. Mechanisms and experimental implications for these particular distributions are discussed. Author

A85-39453* Toledo Univ., Ohio.
SMALL-SIGNAL MODEL FOR THE SERIES RESONANT CONVERTER
R. J. KING and T. A. STUART (Toledo, University, Toledo, OH) IEEE Transactions on Aerospace and Electronic Systems (ISSN 0018-9251), vol. AES-21, May 1985, p. 301-319. refs
(Contract NSG-3281)

The results of a previous discrete-time model of the series resonant dc-dc converter are reviewed and from these a small signal dynamic model is derived. This model is valid for low frequencies and is based on the modulation of the diode conduction angle for control. The basic converter is modeled separately from its output filter to facilitate the use of these results for design purposes. Experimental results are presented. Author

A85-42156* Naval Research Lab., Washington, D. C.
THE J3 SCR MODEL APPLIED TO RESONANT CONVERTER SIMULATION
R. L. AVANT (U.S. Navy, Naval Research Laboratory, Washington, DC) and F. C. Y. LEE (Virginia Polytechnic Institute and State University, Blacksburg) IEEE Transactions on Industrial Electronics (ISSN 0278-0046), vol. IE-32, Feb. 1985, p. 1-12. Research supported by the Industry-University Partnership Program in Power Electronics. refs
(Contract NAG3-425)

The J3 SCR model is a continuous topology computer model for the SCR. Its circuit analog and parameter estimation procedure are uniformly applicable to popular computer-aided design and analysis programs such as SPICE2 and SCEPTRE. The circuit analog is based on the intrinsic three pn junction structure of the SCR. The parameter estimation procedure requires only manufacturer's specification sheet quantities as a data base. Author

A85-45362* National Aeronautics and Space Administration. Lewis Research Center, Cleveland, Ohio.
ADVANCED IN SOLID STATE SWITCHGEAR TECHNOLOGY FOR LARGE SPACE POWER SYSTEMS
G. R. SUNDBERG (NASA, Lewis Research Center, Cleveland, OH) IN: IECEC '84: Advanced energy systems - Their role in our future; Proceedings of the Nineteenth Intersociety Energy Conversion Engineering Conference, San Francisco, CA, August 19-24, 1984. Volume 1 . La Grange Park, IL, American Nuclear Society, 1984, p. 123-132. Previously announced in STAR as N84-22891. refs

High voltage solid state remote power controllers (RPC's) and the required semiconductor power switches to provide baseline technology for large, high power distribution systems in the Space Station, all electric airplane and other advanced aerospace applications were developed. The RPC's were developed for dc voltages from 28 to 1200 V and ac voltages of 115, 230, and 440 V at frequencies of 400 Hz to 20 kHz. The benefits and operation of solid state RPC's and highlights of several developments to bring the RPC to technology readiness for future aerospace needs are examined. The 28 V dc Space Shuttle units, three RPC types at 120 V dc, two at 270/300 V dc, two at 230 V ac and several high power RPC models at voltages up to 1200 V dc with current ratings up to 100 A are reviewed. New technology programs to develop a new family of (DI)2 semiconductor switches and 20 kHz, 440 V ac RPC's are described. E.A.K.

A85-45373* National Aeronautics and Space Administration. Lewis Research Center, Cleveland, Ohio.
DEVELOPMENT OF HIGH FREQUENCY LOW WEIGHT POWER MAGNETICS FOR AEROSPACE POWER SYSTEMS
G. E. SCHWARZE (NASA, Lewis Research Center, Cleveland, OH) IN: IECEC '84: Advanced energy systems - Their role in our future; Proceedings of the Nineteenth Intersociety Energy Conversion Engineering Conference, San Francisco, CA, August 19-24, 1984. Volume 1 . La Grange Park, IL, American Nuclear Society, 1984, p. 196-204. Previously announced in STAR as N84-22892. refs

A dominant design consideration in the development of space type power magnetic devices is the application of reliable thermal control methods to prevent device failure which is due to excessive temperature rises and hot temperatures in critical areas. The resultant design must also yield low weight, high efficiency, high reliability and maintainability, and long life. The weight savings and high efficiency that results by going to high frequency and unique thermal control techniques is demonstrated by the development of a 25 kVA, 20 kHz space type transformer under the power magnetics technology program. Work in the area of power rotary transformer is also discussed. E.A.K.

N85-12300*# TRW Electronic Systems Group, Redondo Beach, Calif.
THE 30 GHZ SOLID STATE AMPLIFIER FOR LOW COST LOW DATA RATE GROUND TERMINALS Final Report, Jun. 1982 - Jun. 1984
Y. C. NGAN and M. A. QUIJIJE Sep. 1984 189 p
(Contract NAS3-23266)
(NASA-CR-174795; NAS 1.26:174795; REPT-4-9-T-10-F) Avail: NTIS HC A09/MF A01 CSCL 09C

This report details the development of a 20-W solid state amplifier operating near 30 GHz. The IMPATT amplifier not only met or exceeded all the program objectives, but also possesses the ability to operate in the pulse mode, which was not called for in the original contract requirements. The ability to operate in the pulse mode is essential for TDMA (Time Domain Multiple Access) operation. An output power of 20 W was achieved with a 1-dB instantaneous bandwidth of 260 MHz. The amplifier has also been tested in pulse mode with 50% duty for pulse lengths ranging from 200 ns to 2 micro s with 10 ns rise and fall times and no degradation in output power. This pulse mode operation was made

possible by the development of a stable 12-diode power combiner/amplifier and a single-diode pulsed driver whose RF output power was switched on and off by having its bias current modulated via a fast-switching current pulse modulator. Essential to the overall amplifier development was the successful development of state-of-the-art silicon double-drift IMPATT diodes capable of reproducible 2.5 W CW output power with 12% dc-to-RF conversion efficiency. Output powers of as high as 2.75 W has been observed. Both the device and circuit design are amenable to low cost production. B.W.

N85-13157*# National Aeronautics and Space Administration. Lewis Research Center, Cleveland, Ohio.
CONTROL ASPECTS OF THE SCHUCHULI VILLAGE STAND-ALONE PHOTOVOLTAIC POWER SYSTEM Final Report
P. P. GROUMPOS (Cleveland State Univ., Ohio), J. E. CULLER (Cleveland State Univ., Ohio), and R. DELOMBARD Nov. 1984 31 p refs
(Contract DE-AI01-79ET-20485)
(NASA-TM-83790; DOE/NASA/20485-17; E-2286; NAS 1.15:83790) Avail: NTIS HC A03/MF A01 CSCL 09B

A photovoltaic power system in an Arizona Indian village was installed. The control subsystem of this photovoltaic power system was analyzed. The four major functions of the control subsystem are: (1) voltage regulation; (2) load management; (3) water pump control; and (4) system protection. The control subsystem functions flowcharts for the control subsystem operation, and a computer program that models the control subsystem are presented. E.A.K.

N85-18259*# Massachusetts Inst. of Tech., Cambridge. Office of Sponsored Programs.
METAL VAPOR ARC SWITCH ELECTROMAGNETIC ACCELERATOR TECHNOLOGY Report, 3 Sep. 1983 - 2 Sep. 1984
P. P. MONGEAU Dec. 1984 60 p refs
(Contract NAG3-283)
(NASA-CR-174380; NAS 1.26:174380) Avail: NTIS HC A04/MF A01 CSCL 09A

A multielectrode device housed in an insulator vacuum vessel, the metal vapor vacuum switch has high power capability and can hold off voltages up to the 100 kilovolt level. Such switches can be electronically triggered and can interrupt or commutate at a zero current crossing. The physics of arc initiation, arc conduction, and interruption are examined, including material considerations; inefficiencies; arc modes; magnetic field effects; passive and forced extinction; and voltage recovery. Heating, electrode lifetime, device configuration, and external circuit configuration are discussed. The metal vapor vacuum switch is compared with SCRs, GTOs, spark gaps, ignitrons, and mechanical breakers. A.R.H.

N85-19328*# Varian Associates, Palo Alto, Calif. Microwave Tube Div.
DESIGN OF LOW LOSS HELIX CIRCUITS FOR INTERFERENCE FITTED AND BRAZED CIRCUITS Final Report
A. JACQUEZ Jan. 1983 113 p refs
(Contract NAS3-21509; NAS3-22441)
(NASA-CR-168313; NAS 1.26:168313) Avail: NTIS HC A06/MF A01 CSCL 09C

The RF loss properties and thermal capability of brazed helix circuits and interference fitted circuits were evaluated. The objective was to produce design circuits with minimum RF loss and maximum heat transfer. These circuits were to be designed to operate at 10 kV and at 20 GHz using a gamma a approximately equal to 1.0. This represents a circuit diameter of only 0.75 millimeters. The fabrication of this size circuit and the 0.48 millimeter high support rods required considerable refinements in the assembly techniques and fixtures used on lower frequency circuits. The transition from the helices to the waveguide was designed and the circuits were matched from 20 to 40 GHz since the helix design is a broad band circuit and at a gamma a of 1.0 will operate over this band. The loss measurement was a transmission measurement and therefore had two such transitions. This resulting double-ended match required tuning elements to achieve the broad band match and external E-H tuners at each end to optimize the match for each frequency where the loss measurement was made. The test method used was a substitution method where the test fixture was replaced by a calibrated attenuator. B.W.

N85-20246*# National Aeronautics and Space Administration. Lewis Research Center, Cleveland, Ohio.
A NEW VERY HIGH VOLTAGE SEMICONDUCTOR SWITCH
G. R. SUNDBERG 1985 17 p refs To be presented at the 16th Ann. Power Electron. Spec. Conf. (PESC), Toulouse, 24-28 Jun. 1985; sponsored by Inst. of Electrical and Electronics Engineers
(NASA-TM-86957; E-2480; NAS 1.15:86957) Avail: NTIS HC A02/MF A01 CSCL 09A

A new family of semiconductor switches using double injection techniques and compensated deep impurities is described. They have the potential to raise switching voltages a factor of 10 higher (up to 100 kV) than p-n junction devices while exhibiting extremely low (or zero) forward voltage. Several potential power switching applications are indicated. E.A.K.

N85-20248*# National Aeronautics and Space Administration. Lewis Research Center, Cleveland, Ohio.
PRECISION TUNABLE RESONANT MICROWAVE CAVITY Patent Application
S. NAKANISHI, F. S. CALCO, and A. R. SCARPELLI, inventors (to NASA) 11 Feb. 1985 9 p
(NASA-CASE-LEW-13935-1; NAS 1.71:LEW-13935-1; US-PATENT-APPL-SN-700255) Avail: NTIS HC A02/MF A01 CSCL 09A

A tunable microwave cavity containing ionizable metallic vapor or gases and an apparatus for precisely positioning a microwave coupling tip in the cavity and for precisely adjusting at least one dimension of the cavity are disclosed. With this combined structure, resonance may be achieved with various types of ionizable gases. A coaxial probe extends into a microwave cavity through a tube. One end of the tube is retained in a spherical joint attached in the cavity wall. This allows the coaxial probe to be pivotally rotated. The coaxial probe is slideable within the tube thus allowing the probe to be extended toward or retracted from the center of the cavity. A tunable wall in the cavity is precisely positioned by a plurality of threated rods extending through threaded bushings which are geared together. Thus, rotation of one of the bushings caused rotation of the other bushings simultaneously whereby the tuning wall is accurately positioned. Means are provided for moving the tube through which the coaxial probe extends in both a side to side and back and forth motion. NASA

N85-21492* National Aeronautics and Space Administration. Lewis Research Center, Cleveland, Ohio.
INELASTIC TUNNEL DIODES Patent
L. M. ANDERSON, inventor (to NASA) 13 Nov. 1984 7 p Filed 19 Apr. 1983 Supersedes N83-25983 (21 - 15, p 2390)
(NASA-CASE-LEW-13833-1; NAS 1.71:LEW-13833-1; US-PATENT-4,482,779; US-PATENT-APPL-SN-486471; US-PATENT-CLASS-136-255; US-PATENT-CLASS-357-12; US-PATENT-CLASS-357-30) Avail: US Patent and Trademark Office CSCL 09A

Power is extracted from plasmons, photons, or other guided electromagnetic waves at infrared to midultraviolet frequencies by inelastic tunneling in metal-insulator-semiconductor-metal diodes. Inelastic tunneling produces power by absorbing plasmons to pump electrons to higher potential. Specifically, an electron from a semiconductor layer absorbs a plasmon and simultaneously tunnels across an insulator into metal layer which is at higher potential. The diode voltage determines the fraction of energy extracted from the plasmons; any excess is lost to heat.
Official Gazette of the U.S. Patent and Trademark Office

N85-28222*# National Aeronautics and Space Administration. Lewis Research Center, Cleveland, Ohio.
PERFORMANCE ANALYSIS OF RADIATION COOLED DC TRANSMISSION LINES FOR HIGH POWER SPACE SYSTEMS
G. E. SCHWARZE 1985 32 p refs Prepared for presentation at the 20th Intersoc. Energy Conversion Eng. Conf., Miami Beach, Fla., 18-23 Aug. 1985; sponsored in part by SAE, ANS, ASME, IEEE, AIAA, ACS and AIChE
(NASA-TM-87040; E-2596; NAS 1.15:87040) Avail: NTIS HC A03/MF A01 CSCL 09C

As space power levels increase to meet mission objectives and also as the transmission distance between power source and load increases, the mass, volume, power loss, and operating voltage and temperature become important system design considerations. This analysis develops the dependence of the specific mass and percent power loss on hte power and voltage levels, transmission distance, operating temperature and conductor material properties. Only radiation cooling is considered since the transmission line is assumed to operate in a space environment. The results show that the limiting conditions for achieving low specific mass, percent power loss, and volume for a space-type dc transmission line are the permissible transmission voltage and operating temperature. Other means to achieve low specific mass include the judicious choice of conductor materials. The results of this analysis should be immediately applicable to power system trade-off studies including comparisons with ac transmission systems. Author

N85-29144* National Aeronautics and Space Administration. Lewis Research Center, Cleveland, Ohio.
ALKALINE BATTERY CONTAINING A SEPARATOR OF A CROSS-LINKED COPOLYMER OF VINYL ALCOHOL AND UNSATURATED CARBOXYLIC ACID Patent
L. C. HSU, W. H. PHILIPP, D. W. SHEIBLEY, and O. D. GONZALEZ-SANABRIA, inventors (to NASA) 19 Mar. 1985 6 p Filed 10 Jul. 1981
(NASA-CASE-LEW-13102-1; US-PATENT-4,505,998; US-PATENT-APPL-SN-282298; US-PATENT-CLASS-429-206; US-PATENT-CLASS-429-249) Avail: US Patent and Trademark Office CSCL 10C

A battery separator for an alkaline battery is described. The separator comprises a cross linked copolymer of vinyl alcohol units and unsaturated carboxylic acid units. The cross linked copolymer is insoluble in water, has excellent zincate diffusion and oxygen gas barrier properties and a low electrical resistivity. Cross linking with a polyaldehyde cross linking agent is preferred.
Official Gazette of the U.S. Patent and Trademark Office

N85-29149*# National Aeronautics and Space Administration. Lewis Research Center, Cleveland, Ohio.
APPARATUS FOR MOUNTING A FIELD EMISSION CATHODE Patent Application
B. T. EBIHARA and R. FORMAN, inventors (to NASA) 9 May 1985 9 p
(NASA-CASE-LEW-14108-1; NAS 1.71:LEW-14108-1; US-PATENT-APPL-SN-732321) Avail: NTIS HC A02/MF A01 CSCL 09A

A field emission cathode is positioned in a pair of intersecting cross grooves, in the end of a ceramic tube by a metal end cap. A spring in electrical contact with the base of the cathode provides the necessary pressure to maintain continuous circumferential electrical contact between the gate film and a raised edge on the end cap. With this structure the cathode chip is self centering and easily replaceable. Also the gate film of the cathode is not abraded or rubbed during installation, and the holder is readily degassed. Author

N85-31372*# National Aeronautics and Space Administration. Lewis Research Center, Cleveland, Ohio.
REGENERATIVE FUEL CELL SYSTEMS FOR SPACE STATION
M. A. HOBERECHT and D. W. SHEIBLEY *In* NASA. Goddard Space Flight Center The 1984 Goddard Space Flight Center Battery Workshop p 21-29 Jul. 1985
Avail: NTIS HC A25/MF A01 CSCL 10A

Regenerative fuel cell (RFC) systems are the leading energy storage candidates for Space Station. Key design features are the advanced state of technology readiness and high degree of system level design flexibility. Technology readiness was demonstrated through testing at the single cell, cell stack, mechanical ancillary component, subsystem, and breadboard levels. Design flexibility characteristics include independent sizing of power and energy storage portions of the system, integration of common reactants with other space station systems, and a wide range of various maintenance approaches. The design features led to selection of a RFC system as the sole electrochemical energy storage technology option for the space station advanced development program. E.A.K.

N85-31375*# National Aeronautics and Space Administration. Lewis Research Center, Cleveland, Ohio.
SYSTEM LEVEL ELECTROCHEMICAL PRINCIPLES
L. H. THALLER *In* NASA. Goddard Space Flight Center The 1984 Goddard Space Flight Center Battery Workshop p 69-76 Jul. 1985 refs
Avail: NTIS HC A25/MF A01 CSCL 10C

The traditional electrochemical storage concepts are difficult to translate into high power, high voltage multikilowatt storage systems. The increased use of electronics, and the use of electrochemical couples that minimize the difficulties associated with the corrective measures to reduce the cell to cell capacity dispersion were adopted by battery technology. Actively cooled bipolar concepts are described which represent some attractive alternative system concepts. They are projected to have higher energy densities lower volumes than current concepts. They should be easier to scale from one capacity to another and have a closer cell to cell capacity balance. These newer storage system concepts are easier to manage since they are designed to be a fully integrated battery. These ideas are referred to as system level electrochemistry. The hydrogen-oxygen regenerative fuel cells (RFC) is probably the best example of the integrated use of these principles. E.A.K.

N85-31378*# Rensselaer Polytechnic Inst., Troy, N.Y.
DEVELOPMENT OF A LITHIUM SECONDARY BATTERY SEPARATOR
J. A. MOORE and R. WILLIE *In* NASA. Goddard Space Flight Center The 1984 Goddard Space Flight Center Battery Workshop p 105-114 Jul. 1985 refs
(Contract NAG3-199)
Avail: NTIS HC A25/MF A01 CSCL 10C

A nonporous membrane based on the polymerization of 2,3-dihydrofuran followed by crosslinking in situ was prepared. The material is compatible with rechargeable Li battery components and, when swollen with an appropriate solvent such as tetrahydrofuran, exhibits separator resistance and Li transport equivalent to Celgard. Author

N85-31398*# National Aeronautics and Space Administration. Lewis Research Center, Cleveland, Ohio.
DESIGN PRINCIPLES FOR NICKEL HYDROGEN CELLS AND BATTERIES
L. H. THALLER *In* NASA. Goddard Space Flight Center The 1984 Goddard Space Flight Center Battery Workshop p 427-436 Jul. 1985 refs
Avail: NTIS HC A25/MF A01 CSCL 10C

Nickel hydrogen cells, and more recently, bipolar batteries have been built by a variety of organizations. The design principles that have been used by the technology group at the Lewis Research Center draw upon their extensive background in separator technology, alkaline fuel cell technology, and several alkaline cell

technology areas. These design principles have been incorporated into both the more contemporary individual pressure vessel (IPV) designs that were pioneered by other groups, as well as the more recent bipolar battery designs using active cooling that are being developed at LeRC and their contractors. These principles are rather straightforward applications of capillary force formalisms, coupled with the slowly developing data base resulting from careful post test analyses. The objective of this overall effort is directed towards the low Earth orbit (LEO) application where the cycle life requirements are much more severe than the geosynchronous orbit (GEO) application. Nickel hydrogen cells have already been successfully flown in an increasing number of GEO missions.
Author

N85-31404*# National Aeronautics and Space Administration. Lewis Research Center, Cleveland, Ohio.
INITIAL PERFORMANCE OF ADVANCED DESIGNS FOR IPV NICKEL-HYDROGEN CELLS
J. J. SMITHRICK, M. A. MANZO, and O. D. GONZALEZ-SANABRIA *In* NASA. Goddard Space Flight Center The 1984 Goddard Space Flight Center Battery Workshop p 513-524 Jul. 1985 refs Previously announced as N85-28444
Avail: NTIS HC A25/MF A01 CSCL 10C

Advanced designs for individual pressure vessel nickel hydrogen cells were conceived which should improve the life cycle at deep depths of discharge and improve thermal management. Features of the designs which are new and not incorporated in either of the contemporary cells (Air Force/Hughes, Comsat) are: (1) the use of alternate methods of oxygen recombination, (2) use of serrated edge separators to facilitate movement of gas within the cell while still maintaining required physical contact with the wall wick, and (3) use of an expandable stack to accommodate some of the nickel electrode expansion. The designs also consider electrolyte volume requirements over the life of the cells, and are fully compatible with the Air Force/Hughes design. R.J.F.

N85-31406*# National Aeronautics and Space Administration. Lewis Research Center, Cleveland, Ohio.
LIFE CYCLE TEST RESULTS OF A BIPOLAR NICKEL HYDROGEN BATTERY
R. L. CATALDO *In* NASA. Goddard Space Flight Center The 1984 Goddard Space Flight Center Battery Workshop p 537-548 Jul. 1985 refs
Avail: NTIS HC A25/MF A01 CSCL 09C

A history is given of low Earth orbit (LEO) laboratory test data on a 6.5 ampere-hour bipolar nickel hydrogen battery designed and built at the NASA Lewis Research Center. The bipolar concept is a means of achieving the goal of producing an acceptable battery, of higher energy density, able to withstand the demands of low-Earth-orbit regimes. Over 4100 LEO cycles were established on a ten cell battery. It seems that any perturbation on normal cycling effects the cells performance. Explanations and theories of the battery's behavior are varied and widespread among those closely associated with it. Deep discharging does provide a reconditioning effect and further experimentation is planned in this area. The battery watt-hour efficiency is about 75 percent and the time averaged, discharge voltage is about 1.26 volts for all cells at both the C/4 and LEO rate. Since a significant portion of the electrode capacity has degraded, the LEO cycle discharges are approaching depths of 90 to 100 percent of the high rate capacity. Therefore, the low end-of-discharge voltages occur precipitously after the knee of the discharge curve and is more an indication of electrode capacity and is a lesser indicator of overall cell performance. R.J.F.

N85-31408*# Hughes Research Labs., Malibu, Calif.
THE FAILURE MECHANISM OF A NICKEL ELECTRODE IN A NICKEL-HYDROGEN CELL
H. S. LIM and S. A. VERZWYVELT *In* NASA. Goddard Space Flight Center The 1984 Goddard Space Flight Center Battery Workshop p 565-582 Jul. 1985 refs
(Contract NAS3-22238)
Avail: NTIS HC A25/MF A01 CSCL 10C

Studies on a number of types of nickel electrodes after cycle failure in a Ni/H2 cell showed that the failure is due to the loss of high rate discharge capability rather than an absolute capacity loss. The failure mechanism is speculated to be a combination of migration of the active material away from the current collecting nickel sinter, increased porosity of the active material caused by cycling, and an electrical isolation process of the active material during discharge. Author

N85-32251*# Electrotek Concepts, Inc., Knoxville, Tenn.
EXPERIMENTAL INVESTIGATION OF A VARIABLE SPEED CONSTANT FREQUENCY ELECTRIC GENERATING SYSTEM FROM A UTILITY PERSPECTIVE
J. I. HERRERA, T. W. REDDOCH, and J. S. LAWLER May 1985 52 p refs
(Contract NAS3-24105; DE-AI01-76ET-20320)
(NASA-CR-174950; NAS 1.26:174950; DOE/NASA/4105-1)
Avail: NTIS HC A03/MF A01 CSCL 09C

As efforts are accelerated to improve the overall capability and performance of wind electric systems, increased attention to variable speed configurations has developed. A number of potentially viable configurations have emerged. Various attributes of variable speed systems need to be carefully tested to evaluate their performance from the utility points of view. With this purpose, the NASA experimental variable speed constant frequency (VSCF) system has been tested. In order to determine the usefulness of these systems in utility applications, tests are required to resolve issues fundamental to electric utility systems. Legitimate questions exist regarding how variable speed generators will influence the performance of electric utility systems; therefore, tests from a utility perspective, have been performed on the VSCF system and an induction generator at an operating power level of 30 kW on a system rated at 200 kVA and 0.8 power factor. Author

N85-33293*# Hughes Aircraft Co., Torrance, Calif. Microwave Products Div.
SIXTY GHZ IMPATT DIODE DEVELOPMENT Final Report, Nov. 1981 - Feb. 1985
Y. E. MA, J. CHEN, E. BENKO, M. J. BARGER, H. NGHIEM, T. Q. TRINH, and J. KUNG May 1985 180 p refs
(Contract NAS3-23253)
(NASA-CR-174969; NAS 1.26:174969; W-45797) Avail: NTIS HC A09/MF A01 CSCL 09C

The objective of this program is to develop 60 GHz GaAs IMPATT Diodes suitable for communications applications. The performance goal of the 60 GHz IMPATT is 1W CW output power with a conversion efficiency of 15 percent and 10 year life time. During the course of the program, double drift (DD) GaAs IMPATT Diodes have been developed resulting in the state of the art performance at V band frequencies. A CW output power of 1.12 W was demonstrated at 51.9 GHz with 9.7 percent efficiency. The best conversion efficiency achieved was 15.3 percent. V band DD GaAs IMPATTs were developed using both small signal and large signal analyses. GaAs wafers of DD flat, DD hybrid, and DD Read profiles using molecular beam epitaxy (MBE) were developed with excellent doping profile control. Wafer evaluation was routinely made by the capacitance versus voltage (C-V) measurement. Ion mass spectrometry (SIMS) analysis was also used for more detailed profile evaluation. B.W.

N85-35342*# Illinois Univ., Urbana. Electromagnetic Communication Lab.
CHARACTERIZATION OF MICROSTRIP DISCONTINUITIES IN THE TIME AND FREQUENCY DOMAINS
U. FELDMAN and R. MITTRA Sep. 1985 49 p refs
(Contract NCC3-38)
(NASA-CR-176190; NAS 1.26:176190; UILU-ENG-85-2565; REPT-85-6) Avail: NTIS HC A03/MF A01 CSCL 09C

A number of impedance transitions and interconnections to a microstrip were designed and investigated. The double-step discontinuity on a microstrip was studied in detail, and a procedure was developed to design these structures. Their response was determined by making measurements in both the frequency and time domains in a consistent and repeatable manner. The time-domain presentation of the data was the most useful feature of the measuring system. All undesirable signal components were filtered out through the use of gating functions. Theoretically computed results were verified experimentally. Author

34

FLUID MECHANICS AND HEAT TRANSFER

Includes boundary layers; hydrodynamics; fluidics; mass transfer; and ablation cooling.

A85-11630* National Aeronautics and Space Administration. Lewis Research Center, Cleveland, Ohio.
COMPUTATION OF INTERNAL FLOWS: METHODS AND APPLICATIONS; PROCEEDINGS OF THE ENERGY SOURCES TECHNOLOGY CONFERENCE, NEW ORLEANS, LA, FEBRUARY 12-16, 1984
P. M. SOCKOL, ED. (NASA, Lewis Research Center, Cleveland, OH) and K. N. GHIA, ED. (Cincinnati, University, Cincinnati, OH) Conference sponsored by the American Society of Mechanical Engineers. New York, American Society of Mechanical Engineers (Fluids Engineering Symposia Series. FED Volume 14), 1983, 182 p. For individual items see A85-11631 to A85-11648.

The present conference covers computational method applications, viscous-inviscid interaction techniques, viscous flow computational methods, and design-related methods. Attention is given to viscous flows in turbomachinery cascades, forbidden signals and apparent Mach numbers in supersonic cascades, the flow field in an engine particle separator, two-dimensional separated channel flows, turbulent separating flows over a rearward-facing step, the semielliptic analysis of two-dimensional internal and compressible viscous flows, spline solutions of the incompressible Navier-Stokes equations in a mildly nonorthogonal coordinate system, the design of highly loaded blades with blockage in cascade, and a finite analytic method for unsteady, three-dimensional Navier-Stokes equations. O.C.

A85-11631*# Pennsylvania State Univ., University Park.
COMPUTATION OF VISCOUS FLOWS IN TURBOMACHINERY CASCADES
M. POUAGARE, B. LAKSHMINARAYANA, and T. R. GOVINDAN (Pennsylvania State University, University Park, PA) IN: Computation of internal flows: Methods and applications; Proceedings of the Energy Sources Technology Conference, New Orleans, LA, February 12-16, 1984 . New York, American Society of Mechanical Engineers, 1983, p. 1-10. refs
(Contract NSG-3266)

Analytic and numerical experiments involving the use of the space-marching method for the prediction of the viscous flow field in turbomachinery cascades indicate that the grid lines in the physical domain must be nearly orthogonal in order to arrive at accurate predictions. For staggered cascades, a nonperiodic grid system was used and appropriate approximations were applied in place of the periodicity boundary conditions upstream and downstream of the cascade. Predicted drag coefficient, turning angle, boundary layer momentum thicknesses, and velocity profiles are compared with experimental data. Good agreement is obtained in most cases. O.C.

A85-11634*# National Aeronautics and Space Administration. Lewis Research Center, Cleveland, Ohio.
COMPARISON OF SECONDARY FLOWS PREDICTED BY A VISCOUS CODE AND AN INVISCID CODE WITH EXPERIMENTAL DATA FOR A TURNING DUCT
J. R. SCHWAB and L. A. POVINELLI (NASA, Lewis Research Center, Cleveland, OH) IN: Computation of internal flows: Methods and applications; Proceedings of the Energy Sources Technology Conference, New Orleans, LA, February 12-16, 1984 . New York, American Society of Mechanical Engineers, 1983, p. 29-36. Previously announced in STAR as N84-17142. refs

A comparison of the secondary flows computed by the viscous Kreskovsky-Briley-McDonald code and the inviscid Denton code with benchmark experimental data for turning duct is presented. The viscous code is a fully parabolized space-marching Navier-Stokes solver while the inviscid code is a time-marching Euler solver. The experimental data were collected by Taylor, Whitelaw, and Yianneskis with a laser Doppler velocimeter system in a 90 deg turning duct of square cross-section. The agreement between the viscous and inviscid computations was generally very good for the streamwise primary velocity and the radial secondary velocity, except at the walls, where slip conditions were specified for the inviscid code. The agreement between both the computations and the experimental data was not as close, especially at the 60.0 deg and 77.5 deg angular positions within the duct. This disagreement was attributed to incomplete modeling of the vortex development near the suction surface. Author

A85-11640*# Cincinnati Univ., Ohio.
TWO-DIMENSIONAL INTERNAL COMPRESSIBLE VISCOUS FLOWS USING SEMI-ELLIPTIC ANALYSIS
K. N. GHIA, U. GHIA, and R. RAMAMURTI (Cincinnati, University, Cincinnati, OH) IN: Computation of internal flows: Methods and applications; Proceedings of the Energy Sources Technology Conference, New Orleans, LA, February 12-16, 1984 . New York, American Society of Mechanical Engineers, 1983, p. 99, 100. refs
(Contract NAG3-194)

Subsonic viscous flows through planar cascades are examined by means of a semielliptic form of the Navier-Stokes equations, which is obtained by neglecting the streamwise diffusion of momentum and energy in their respective equations and providing upstream interaction through the pressure field. The influence of downstream conditions is propagated upstream in the subsonic flow, via a streamwise implicit determination of the pressure field, in order to permit departure-free solutions for the overall flow problem. The continuity equation is thereby satisfied directly. Governing equations are written in strong conservation law form, in terms of general, nonorthogonal transformed coordinates and Cartesian velocity components. O.C.

A85-11647*# Iowa Univ., Iowa City.
DEVELOPMENT OF FINITE ANALYTIC METHOD FOR UNSTEADY THREE-DIMENSIONAL NAVIER-STOKES EQUATION
H.-C. CHEN and C.-J. CHEN (Iowa, University, Iowa City, IA) IN: Computation of internal flows; Methods and applications; Proceedings of the Energy Sources Technology Conference, New Orleans, LA, February 12-16, 1984 . New York, American Society of Mechanical Engineers, 1983, p. 159-165. refs
(Contract NSG-3305)

A finite analytic (FA) numerical method is described for the numerical study of three-dimensional fluid flow problems. The FA method incorporates a local linearization scheme and a classical analytic solution technique to formulate the algebraic representation of unsteady three-dimensional Navier Stokes Equations. The twenty-eight point FA formula thus obtained gives all positive coefficients and desired upwind shift. Cubic cavity flows are then solved by the FA method for Reynolds numbers of 100 and 400.

A simple variant of SIMPLER algorithm is used to resolve the pressure-velocity coupling problem. The numerical solutions show that the presence of side walls reduce the strength of the primary vortex when compared with the two-dimensional square cavity flows. Author

A85-11648*# Purdue Univ. School of Science at Indianapolis, Ind.
A FINITE ELEMENT SOLUTION OF THREE-DIMENSIONAL INVISCID ROTATIONAL FLOWS THROUGH CURVED DUCTS
A. ECER, H. U. AKAY, and B. SENER (Purdue University, Indianapolis, IN) IN: Computation of internal flows: Methods and applications; Proceedings of the Energy Sources Technology Conference, New Orleans, LA, February 12-16, 1984 . New York, American Society of Mechanical Engineers, 1983, p. 167-176. refs
(Contract NSG-3294)

A previously developed two-dimensional finite element algorithm for the solution of steady Euler equations is extended to three-dimensional problems. Starting with the general three-dimensional problem, the formulation of steady, rotational flows is presented. The boundary conditions for steady flows where the rotationality is introduced through entropy or total enthalpy gradients are introduced. A three-dimensional flow through a curved duct is analyzed as a sample problem, demonstrating the efficiency of the relaxation scheme. The accuracy of the numerical results is investigated by calculating the velocity and vorticity distributions at different sections of the channel, including the exit. C.D.

A85-14241* Arizona Univ., Tucson.
THE LINEAR TWO-DIMENSIONAL STABILITY OF INVISCID VORTEX STREETS OF FINITE-CORED VORTICES
D. I. MEIRON (Arizona, University, Tucson, AZ; California Institute of Technology, Pasadena, CA), P. G. SAFFMAN (California Institute of Technology, Pasadena, CA), and J. C. SCHATZMAN (Chevron Oil Field Research Co., La Habra; California Institute of Technology, Pasadena, CA) Journal of Fluid Mechanics (ISSN 0022-1120), vol. 147, Oct. 1984, p. 187-212. Research supported by the U.S. Department of Energy and U.S. Navy. refs
(Contract NAG3-179)
(AD-A153032)

The stability of two-dimensional infinitesimal disturbances of the steady inviscid incompressible flow produced by infinite rows of finite-cored particles is studied. Numerical results are obtained for the growth rate and oscillation frequencies of disturbances of arbitrary subharmonic wavenumber, and the stability boundaries are calculated. The stabilization of the pairing instability by finite area demonstrated by Saffman and Schatzman (1982) is confirmed, as is Kida's (1982) result that this is not the most unstable disturbance when the area is finite. However, the finite area does not stabilize the inviscid Karman vortex street of finite-area vortices to infinitesimal two-dimensional disturbances of arbitrary wavelength. The finite area is always unstable except for one isolated value of the aspect ratio which depends upon the size of the vortices. C.D.

A85-14349*# Pennsylvania State Univ., University Park.
COMPUTATION AND TURBULENCE CLOSURE MODELS FOR SHEAR FLOWS IN ROTATING CURVED BODIES
M. POUAGARE and B. LAKSHMINARAYANA (Pennsylvania State University, University Park, PA) IN: Symposium on Turbulent Shear Flows, 4th, Karlsruhe, West Germany, September 12-14, 1983, Proceedings . University Park, PA, Pennsylvania State University, 1984, p. 6.6-6.13. refs
(Contract NSG-3266)

This paper is concerned with the effects of rotation and curvature on the turbulence closure model. The k-epsilon model that includes the effects of curvature has been modified to include the anisotropy in turbulence. A space-marching algorithm which solves the parabolized Navier-Stokes equations is coupled with the turbulence closure model to predict the turbulent shear flow over a rotating cylinder and inside a rotating channel. The agreement between the predictions and available data is good. The rotation and curvature effects are predicted well. Author

A85-14376*# California Univ., Irvine.
A TWO-EQUATION TURBULENCE MODEL FOR TWO-PHASE JETS
S. ELGHOBASHI, T. ABOU-ARAB, M. RIZK, and A. MOSTAFA (California, University, Irvine, CA) IN: Symposium on Turbulent Shear Flows, 4th, Karlsruhe, West Germany, September 12-14, 1983, Proceedings . University Park, PA, Pennsylvania State University, 1984, p. 12.9-12.14. refs
(Contract DE-FG22-80PC-30303; NAG3-176)

A recently-developed two-equation turbulence model for two-phase flows (Elghobashi and Abou-Arab, 1983) is tested for the flow of a turbulent axisymmetric gaseous jet laden with spherical solid particles of uniform size. The agreement between the predictions of experimental data is good. Author

A85-14399*# United Technologies Research Center, East Hartford, Conn.
MASS AND MOMENTUM TURBULENT TRANSPORT EXPERIMENTS WITH CONFINED COAXIAL JETS
B. V. JOHNSON (United Technologies Research Center, East Hartford, CT) and J. C. BENNETT (Connecticut, University, Storrs, CT) IN: Symposium on Turbulent Shear Flows, 4th, Karlsruhe, West Germany, September 12-14, 1983, Proceedings . University Park, PA, Pennsylvania State University, 1984, p. 18.14-18.19. refs
(Contract NAS3-22771)

An experimental study of mixing downstream of coaxial jets discharging into an expanded circular duct was conducted to obtain data for the evaluation and improvement of turbulent transport models. A combination of turbulent momentum transport rate and two components of velocity data were obtained from simultaneous measurements with a two-color LV system. A combination of turbulent mass transport rate, concentration and velocity data were obtained from simultaneous measurements with laser velocimeter (LV) and laser induced fluorescence (LIF) systems. Author

A85-16533* Massachusetts Inst. of Tech., Cambridge.
A NUMERICAL STUDY OF THE STEADY SCALAR CONVECTIVE DIFFUSION EQUATION FOR SMALL VISCOSITY
M. B. GILES (MIT, Cambridge, MA) and M. E. ROSE (NASA, Langley Research Center, Institute for Computer Applications in Science and Engineering, Hampton, VA) Journal of Computational Physics (ISSN 0021-9991), vol. 56, Dec. 1984, p. 513-529. Previously announced in STAR as N83-35999. refs
(Contract NAG3-9; NAS1-17070; NAS1-17130)

A time-independent convection diffusin equation is studied by means of a compact finite difference scheme and numerical solutions are compared to the analytic inviscid solutions. The correct internal and external boundary layer behavior is observed, due to an inherent feature of the scheme which automatically produces upwind differencing in inviscid regions and the correct viscous behavior in viscous regions. Author

A85-19377* National Aeronautics and Space Administration. Lewis Research Center, Cleveland, Ohio.
APPROXIMATE ANALYSIS FOR RESONANCE OF AN INCOMPRESSIBLE SHEAR LAYER PLUS EDGES
P. A. DURBIN (NASA, Lewis Research Center, Cleveland, OH) Physics of Fluids (ISSN 0031-9171), vol. 27, Dec. 1984, p. 2814-2818. refs

A method for approximately analyzing the feedback between downstream and upstream edges in incompressible shear flow is described. The shear flow is modeled by a vortex sheet. Equations for resonance eigenvalues are derived. After the reduction of growth rate by finite shear layer thickness is allowed for, agreement is found between calculated resonances and those that have been observed experimentally. Author

A85-19488*# United Technologies Corp., East Hartford, Conn.
FINITE DIFFERENCE METHODS FOR REDUCING NUMERICAL DIFFUSION IN TEACH-TYPE CALCULATIONS
S. A. SYED (United Technologies Corp., Engineering Div., East Hartford, CT) and L. M. CHIAPPETTA (United Technologies Research Center, East Hartford, CT) American Institute of Aeronautics and Astronautics, Aerospace Sciences Meeting, 23rd, Reno, NV, Jan. 14-17, 1985. 17 p. refs
(Contract NAS3-2368)
(AIAA PAPER 85-0057)

A methodological evaluation for two-finite differencing schemes for computer-aided gas turbine design is presented. The two computational schemes include; a Bounded Skewed Finite Differencing Scheme (BSUDS); and a Quadratic Upwind Differencing Scheme (QSDS). In the evaluation, the derivations of the schemes were incorporated into two-dimensional and three-dimensional versions of the Teaching Axisymmetric Characteristics Heuristically (TEACH) computer code. Assessments were made according to performance criteria for the solution of problems of turbulent, laminar, and coannular turbulent flow. The specific performance criteria used in the evaluation were simplicity, accuracy, and computational economy. It is found that the BSUDS scheme performed better with respect to the criteria than the QUDS. Some of the reasons for the more successful performance BSUDS are discussed. I.H.

A85-19491*# United Technologies Corp., East Hartford, Conn.
CALCULATION OF CONFINED SWIRLING FLOWS
G. J. STURGESS and S. A. SYED (United Technologies Corp., Engineering Div., East Hartford, CT) American Institute of Aeronautics and Astronautics, Aerospace Sciences Meeting, 23rd, Reno, NV, Jan. 14-17, 1985. 16 p. refs
(Contract NAS3-235924; NAS3-23686)
(AIAA PAPER 85-0060)

Swirling jets are an important constituent flow of many types of combustion equipment. Flame size, shape, stability and combustion intensity are all favorably influenced by swirling some portion of the incoming air with the fuel. Fluid dynamics computer codes are being developed for the mathematical simulation of flows in practical combustors. It is important that these codes have the ability to accurately and reliably calculate swirling flows. Turbulent flow calculations with swirl can be inaccurate due to at least three major reasons: limitations of the turbulence modeling used, incorrect or inadequate specifications of inlet boundary conditions, and, error introduced through the numerics. These sources of error are described, and examples provided of each. The state-of-the-art in such calculations is reviewed. The controlling character of current numerics is demonstrated, and it is concluded that as a first priority, better numerics must be arrived at, and that an improved understanding of the discharge flow from swirl generators is essential as a second priority. When these priorities are satisfied an improved turbulence model is desirable. It is also concluded that an improved understanding of swirl-induced recirculation would be an asset. Author

A85-19564*# Duke Univ., Durham, N. C.
A SPACE-MARCHING METHOD FOR INCOMPRESSIBLE NAVIER-STOKES EQUATIONS
M. POUAGARE (Duke University, Durham, NC; Pennsylvania State University, University Park, PA) and B. LAKSHMINARAYANA (Pennsylvania State University, University Park, PA) American Institute of Aeronautics and Astronautics, Aerospace Sciences Meeting, 23rd, Reno, NV, Jan. 14-17, 1985. 14 p. refs
(Contract NSG-3266)
(AIAA PAPER 85-0170)

This paper deals with the development of a space-marching method for incompressible flows. The method solves the continuity and momentum equations as a coupled system at each streamwise station. The character of the system of equations has been changed from elliptic to hyperbolic/parabolic in order to enable the equations to be marched in space. The present method has many advantages compared to the existing parabolic or space-marching methods for incompressible flow: (1) it avoids the solution of Poisson equations, (2) it conserves the mass flow with no additional computation, (3) it does not require the specification of an assumed pressure field when used in the prediction of duct flows. The present method can capture strong secondary velocities and strong transverse pressure gradients. Predictions of the flow through straight and curved ducts are in good agreement with analytical and experimental results. Author

A85-19574*# Oklahoma State Univ., Stillwater.
SWIRLING FLOWS IN TYPICAL COMBUSTOR GEOMETRIES
D. G. LILLEY (Oklahoma State University, Stillwater, OK) American Institute of Aeronautics and Astronautics, Aerospace Sciences Meeting, 23rd, Reno, NV, Jan. 14-17, 1985. 26 p. refs
(Contract NAG3-74)
(AIAA PAPER 85-0184)

The results of experimental attempts and subsequent computational efforts targeted at improving numerical models for swirling recirculating confined turbulent combustion flows are reported. Attention was focused on the mean flow patterns, scales and shapes of the recirculation zones, mapping the flowfield time-mean velocity, normal and Re shear stresses, and producing a predictive computer code based on the TEACH-T program. The work was performed mainly by graduate students. The studies covered swirl strengths, swirler performance, the effects of downstream contraction nozzle size and placement, expansion ratios, and inlet side-wall angles. The STARPIC program was developed in FORTRAN 4 for computing air flow through expansions and over a wide range of inlet swirl vane angles. M.S.K.

A85-19672*# Purdue Univ., West Lafayette, Ind.
A STAGNATION PRESSURE PROBE FOR DROPLET-LADEN AIR FLOW
S. N. B. MURTHY, M. LEONARDO, and C. M. EHRESMAN (Purdue University, West Lafayette, IN) American Institute of Aeronautics and Astronautics, Aerospace Sciences Meeting, 23rd, Reno, NV, Jan. 14-17, 1985. 12 p. refs
(Contract F33615-78-C-2401; NAG3-62)
(AIAA PAPER 85-0330)

It is often of interest in a droplet-laden gas flow to obtain the stagnation pressure of both the gas phase and the mixture. A flow-decelerating probe (TPF), with separate, purged ports for the gas phase and the mixture and with a bleed for accumulating liquid at the closed end, has been developed. Measurements obtained utilizing the TPF in a nearly isothermal air-water droplet mixture flow in a smooth circular pipe under various conditions of flow velocity, pressure, liquid concentration and droplet size are presented and compared with data obtained under identical conditions with a conventional, gas phase stagnation pressure probe (CSP). The data obtained with the CSP and TPF probes are analyzed to determine the applicability of the two probes in relation to the multi-phase characteristics of the flow and the geometry of the probe. Author

A85-19751*# Pratt and Whitney Aircraft Group, East Hartford, Conn.
ASSESSMENT OF DISCRETIZATION SCHEMES TO REDUCE NUMERICAL DIFFUSION IN THE CALCULATION OF COMPLEX FLOWS
S. A. SYED (United Technologies Corp., Pratt and Whitney Group, East Hartford, CT), A. D. GOSMAN, and M. PERIC (Imperial College of Science and Technology, London, England) American Institute of Aeronautics and Astronautics, Aerospace Sciences Meeting, 23rd, Reno, NV, Jan. 14-17, 1985. 14 p. refs
(Contract NAS3-2368)
(AIAA PAPER 85-0441)

Comprehensive criteria for evaluating finite-difference schemes to reduce numerical diffusion in the solution of the Reynolds averaged Navier-Stokes equations have been established in this study. Several candidate schemes have been examined, based on these criteria. Taylor series analyses, model problem studies and examination of the difference equations have been used to assess the schemes. Two schemes, which showed the most

promise, and satisfied a majority of the criteria, are recommended for incorporation into two dimensional and three dimensional computer codes for further evaluation. Author

A85-24445* National Aeronautics and Space Administration. *Lewis Research Center, Cleveland, Ohio.*
A UNIFIED RELATION FOR CAVITATION EROSION
P. VEERABHADRA RAO (NASA, Lewis Research Center; Cleveland State University, Cleveland, OH), D. H. BUCKLEY (NASA, Lewis Research Center, Cleveland, OH), and M. MATSUMURA (Hiroshima University, Hiroshima, Japan) International Journal of Mechanical Sciences (ISSN 0020-7403), vol. 26, no. 5, 1984, p. 325-335. refs

A power-law relationship between the average erosion rate and cumulative erosion is presented. Data analyses from Venturi, magnetostriction, and liquid-impingement devices conform to this unified relation. A normalization technique is also suggested for prediction purposes. Author

A85-25137*# Pennsylvania State Univ., University Park.
STRUCTURE OF PARTICLE-LADEN JETS - MEASUREMENTS AND PREDICTIONS
J.-S. SHUEN, A. S. P. SOLOMON, G. M. FAETH (Pennsylvania State University, University Park, PA), and Q.-F. ZHANG (Nanjing Aeronautical Institute, Nanjing, People's Republic of China; Pennsylvania State University, University Park, PA) AIAA Journal (ISSN 0001-1452), vol. 23, March 1985, p. 396-404. Previously cited in issue 06, p. 762, Accession no. A84-17842. refs
(Contract NAG3-190)

A85-25951*# Lockheed-Georgia Co., Marietta.
ACOUSTIC CONTROL OF FREE JET MIXING
J. LEPICOVSKY, K. K. AHUJA, W. H. BROWN (Lockheed-Georgia Co., Marietta, GA), and P. J. MORRIS (Pennsylvania State University, University Park, PA; Lockheed-Georgia Co., Marietta, GA) American Institute of Aeronautics and Astronautics, Shear Flow Control Conference, Boulder, CO, Mar. 12-14, 1985. 10 p. refs
(Contract NAS3-23708)
(AIAA PAPER 85-0569)

The paper reports a detailed study on the acoustic control of free jet mixing at realistic Reynolds numbers. The experimental results were obtained at Mach numbers of 0.3 and 0.8 and flow total temperatures up to 800 K. The Reynolds numbers ranged from 350,000 to 1,300,000. Excitation Strouhal numbers were in the range of 0.2 to 0.6. The experimental results are compared with predictions, based on an extension of the analysis by Tam and Morris. The results showed that proper upstream tone excitation enhances mixing of unheated jets for both high-speed, high Reynolds number conditions and for low-speed conditions. The heated jet, however, shows a response to upstream excitation that depends on jet Mach number. The agreement between the predictions and the experiments is very good for unheated jet conditions. However, for jets heated to temperatures above 600 K, the theoretical predictions differ from the experimental results. Author

A85-26077*# Nevada Univ., Reno.
OSCILLATORY CONDUCTIVE HEAT TRANSFER FOR A FIBER IN AN IDEAL GAS
H. L. KUNTZ (Hoover Keith and Bruce, Inc., Houston, TX) and N. D. PERREIRA (Nevada, University, Reno, NV) ASME, Transactions, Journal of Heat Transfer (ISSN 0022-1481), vol. 107, Feb. 1985, p. 52-56. Navy-supported research. refs
(Contract NSG-3198)

A description of the thermal effects created by placing a cylindrical fiber in an inviscid, ideal gas, through which an acoustic wave propagates, is presented. The fibers and the gas have finite heat capacities and thermal conductivities. Expressions for the temperature distribution in the gas and in the material are determined. The temperature distribution is caused by pressure oscillations in the gas which, in turn, are caused by the passage of an acoustic wave. The relative value of a dimensionless parameter is found to be indicative of whether the exact or approximate equations should be used in the solution. This parameter is a function of the thermal conductivities and heat capacities of the fiber and gas, the acoustic frequency, and the fiber diameter. Author

A85-26526* National Aeronautics and Space Administration. Lewis Research Center, Cleveland, Ohio.
A COMPARISON OF FLOW RATES AND PRESSURE PROFILES FOR N-SEQUENTIAL INLETS AND THREE RELATED SEAL CONFIGURATIONS
R. C. HENDRICKS (NASA, Lewis Research Center, Cleveland, OH) IN: Advances in cryogenic engineering. Volume 29 - Proceedings of the Cryogenic Engineering Conference, Colorado Springs, CO, August 15-17, 1983 . New York, Plenum Press, 1984, p. 837-846. Previously announced in STAR as N83-33103. refs

Experimental and analytical results are presented for choked flows of fluid nitrogen over a range of reduced inlet stagnation temperatures (from 0.67 to ambient) and reduced inlet stagnation pressures to 2. Flow rate and pressure profile comparisons are made between N aligned sequential orifice inlets, a 33-tooth labyrinth seal, a 3-step seal, a cylindrical seal and the classic venturi. Seal effectiveness appears strongly dependent on upstream losses and geometry configuration. Author

A85-26911* Rensselaer Polytechnic Inst., Troy, N.Y.
CONVECTIVE INFLUENCE ON THE STABILITY OF A CYLINDRICAL SOLID-LIQUID INTERFACE
Q. T. FANG, M. E. GLICKSMAN (Rensselaer Polytechnic Institute, Troy, NY), S. R. CORIELL, G. B. MCFADDEN, and R. F. BOISVERT (National Bureau of Standards, Washington, DC) Journal of Fluid Mechanics (ISSN 0022-1120), vol. 151, Feb. 1985, p. 121-140. refs
(Contract NAG3-333)

Experiments in which a long vertical, heated wire is surrounded by concentric annuli of a melt and its crystalline solid show that the convection state changes from a stable unicell surrounded by a stationary cylindrical solid-liquid interface, to a complex time-dependent flow surrounded by a rotating, helical solid-liquid interface. This transition occurs at a Grashof number of approximately 150, which is an order of magnitude less than the critical Grashof number calculated for a liquid annulus surrounded by rigid walls. A linear stability analysis has been carried out for an infinitely tall vertical annulus. When the deformable nature of the crystal-melt interface is taken into account in the boundary conditions, two new modes of instability arise. The most dangerous mode is asymmetrical and corresponds to helical waves travelling vertically upwards. The critical Grashof number and the scaling properties of the eigenstate agree with experiments. The results clearly demonstrate the coupling of convection with crystal-melt interfacial instabilities. Author

A85-27096*# National Aeronautics and Space Administration. Lewis Research Center, Cleveland, Ohio.
AERODYNAMIC EFFECT OF COMBUSTOR INLET AIR PRESSURE ON FUEL JET ATOMIZATION
R. D. INGEBO (NASA, Lewis Research Center, Cleveland, OH) Journal of Propulsion and Power (ISSN 0748-4658), vol. 1, Mar.-Apr. 1985, p. 137-142. Previously cited in issue 17, p. 2468, Accession no. A84-36973. refs

A85-30075* National Aeronautics and Space Administration. Lewis Research Center, Cleveland, Ohio.
ANALYSIS OF THREE-DIMENSIONAL SOLIDIFICATION INTERFACE SHAPE
R. SIEGEL (NASA, Lewis Research Center, Cleveland, OH) International Journal of Heat and Mass Transfer (ISSN 0017-9310), vol. 28, March 1985, p. 701-705. refs

The determination of the shape of the solidification interface in a cooling melt by the thermal boundary conditions is investigated analytically, extending the analysis of Siegel (1982) and Siegel and Sosoka (1982) to the three-dimensional case. The solutions are generated by continuation into the solid region from conditions

at the cooled wall, and some numerical results are presented in tables and graphs. These findings and the analytical approach employed are applicable to crystallization and metal-forming processes. T.K.

A85-35596*# National Aeronautics and Space Administration. Lewis Research Center, Cleveland, Ohio.
ANALYSIS OF BUOYANCY EFFECT ON FULLY DEVELOPED LAMINAR HEAT TRANSFER IN A ROTATING TUBE
R. SIEGEL (NASA, Lewis Research Center, Cleveland, OH) ASME, Transactions, Journal of Heat Transfer (ISSN 0022-1481), vol. 107, May 1985, p. 338-344. refs

Laminar heat transfer is analyzed in a tube rotating about an axis perpendicular to the tube axis. The solution applies for flow that is either radially outward from the axis of rotation, or radially inward toward the axis of rotation. The conditions are fully developed, and there is uniform heat addition at the tube wall. The analysis is performed by expanding velocities and temperature in power series using the Taylor number as a perturbation parameter. Coriolis and buoyancy forces caused by tube rotation are included, and the solution is calculated through second-order terms. The secondary flow induced by the Coriolis terms always tends to increase the heat transfer coefficient; this effect can dominate for small wall heating. For radial inflow, buoyancy also tends to improve heat transfer. For radial outflow, however, buoyancy tends to reduce heat transfer; for large wall heating this effect can dominate, and there is a net reduction in heat transfer coefficient. Author

A85-37047* National Aeronautics and Space Administration. Lewis Research Center, Cleveland, Ohio.
CONTROL OF SOLIDIFICATION BOUNDARY IN CONTINUOUS CASTING BY ASYMMETRIC COOLING AND MOLD OFFSET
R. SIEGEL (NASA, Lewis Research Center, Cleveland, OH) International Journal of Heat and Mass Transfer (ISSN 0017-9310), vol. 28, Feb. 1985, p. 500-502.

A solution, developed to obtain solidification-interface shapes for complex situations in which both the ingot cooling and mold geometry are asymmetric, is analyzed. The effect of mold offsett and of unequal ingot side temperatures on the interface shapes is illustrated in graphs. The results of the analysis show how the solidification interface in continuous casting can be controlled by asymmetries in both mold geometry and cooling of the ingot sides. M.D.

A85-38999*# Nanjing Aeronautical Inst. (China).
STRUCTURE OF DUCTED PARTICLE-LADEN TURBULENT JETS
Q.-F. ZHANG (Nanjing Aeronautical Institute, Nanjing, People's Republic of China; Pennsylvania State University, University Park, PA), J.-S. SHUEN, A. S. P. SOLOMON, and G. M. FAETH (Pennsylvania State University, University Park, PA) AIAA Journal (ISSN 0001-1452), vol. 23, July 1985, p. 1123-1125. refs
(Contract NAG3-190)

New and existing measurements have been used to develop and evaluate models of particle-laden jets and sprays, yielding encouraging results for a stochastic separated flow (SSF) model which treats effects of interphase slip and turbulence on the basis of random walk computations of particle or drop motion. An evaluation of the SSF model using the measurements of Modarress et al. (1982, 1983) yielded results comparable to earlier work, suggesting that data from coflowing jets in ducts should be accompanied by static pressure measurements, since even small pressure gradients appreciably influence jet properties. O.C.

A85-39257* National Aeronautics and Space Administration. Lewis Research Center, Cleveland, Ohio.
APPLICATION OF VISCOUS AND INVISCID COMPUTATION METHODS FOR ROCKET TURBOPUMP SYSTEMS
L. A. POVINELLI, J. E. HAAS, K. L. MCLALLIN, J. R. SCHWAB, and R. V. CHIMA (NASA, Lewis Research Center, Cleveland, OH) IN: Space systems technology; Proceedings of the Aerospace Congress and Exposition, Long Beach, CA, October 15-18, 1984 . Warrendale, PA, Society of Automotive Engineers, Inc. (SAE SP-593), 1984, p. 39-57.
(SAE PAPER 841522)

This paper examines current research efforts underway at Lewis Research Center which have focused on improving the structural durability of the SSME turbodrive system through more fully examining the aerothermodynamics of the flow system. This objective was achieved by developing three-dimensional viscous and inviscid computer codes to predict the pressure and temperature distributions in the engine flow passages, particularly within the SSME turbines and turnaround ducts. Author

A85-39604*# Texas Technological Univ., Lubbock.
TURBULENCE MEASUREMENTS OF LATERAL JET INJECTION INTO CONFINED TUBULAR CROSSFLOW
G. B. FERRELL (Texas Tech University, Lubbock, TX) and D. G. LILLEY (Oklahoma State University, Stillwater, OK) AIAA, SAE, ASME, and ASEE, Joint Propulsion Conference, 21st, Monterey, CA, July 8-10, 1985. 13 p. refs
(Contract NAG3-549)
(AIAA PAPER 85-1102)

Experiments have been conducted to characterize the time-mean and turbulent flowfield of a deflected turbulent jet in a confining cylindrical crossflow. Jet-to-crossflow velocity ratios of 2, 4, and 6 were investigated, with no swirl in the crossflow. A six-position single hotwire technique was used to measure the velocities and all turbulent normal and shear stresses. Measurements confirmed that the deflected jet is symmetrical about the vertical plane passing through the crossflow axis, and the jet penetration was found to be reduced from that of comparable velocity-ratio infinite crossflow cases. Author

A85-39780*# National Aeronautics and Space Administration. Lewis Research Center, Cleveland, Ohio.
NUMERICAL CALCULATION OF SUBSONIC JETS IN CROSSFLOW WITH REDUCED NUMERICAL DIFFUSION
R. W. CLAUS (NASA, Lewis Research Center, Cleveland, OH) AIAA, SAE, ASME, and ASEE, Joint Propulsion Conference, 21st, Monterey, CA, July 8-10, 1985. 11 p. Previously announced in STAR as N85-25263. refs
(AIAA PAPER 85-1441)

A series of calculations are reported for two, subsonic jet in crossflow geometries. The parametric variation examined are the lateral spacing of a row of jets. The first series of calculations corresponds to a widely space jet geometry, S/D = 4, and the second series corresponds to closely spaced jets, S/D = 2. The calculations are done with alternate differencing schemes to illustrate the impact of numerical diffusion. The calculated jet trajectories agreed well with experimental data in the widely spaced jet geometry, but not in the closely spaced geometry. E.A.K.

A85-39894*# Case Western Reserve Univ., Cleveland, Ohio.
A NEW INTERPRETATION OF INTERNAL HEAT TRANSFER COEFFICIENTS OF POROUS MEDIA
A. DYBBS, K. KAR, M. GROENEWEG, J. X. LING, and M. NARAGHI (Case Western Reserve University, Cleveland, OH) American Society of Mechanical Engineers, Winter Annual Meeting, New Orleans, LA, Dec. 9-14, 1984. 7 p. refs
(Contract NAG3-97; NSG-3040; NSF CME-79-13389; NSF ENG-78-17782)
(ASME PAPER 84-WA/HT-51)

The results of laser anemometer and flow visualization based fluid mechanics studies of porous media are used to obtain heat transfer coefficients for porous materials. Average pore flow Re ranging from 0.16-700 were examined. Darcy, inertial steady

laminar, unsteady laminar and turbulent flow regimes were detected. A passage length model was devised to derive the heat transfer coefficient. Sample data from flows through porous metals composed of powders and fibers validated the passage length for Darcy and inertial flow regimes. Unsteady laminar and turbulent flow coefficients require the identification of new parameters. M.S.K.

A85-39898*# Rensselaer Polytechnic Inst., Troy, N.Y.
HEAT TRANSFER INVESTIGATION IN THE JUNCTION REGION OF CIRCULAR CYLINDER NORMAL TO A FLAT PLATE AT 90 DEG LOCATION
H. T. NAGAMATSU (Rensselaer Polytechnic Institute, Troy, NY) and J. N. HINCKEL (Instituto de Estudos Avancados, Sao Jose dos Campos, Sao Paulo, Brazil) American Society of Mechanical Engineers, Winter Annual Meeting, New Orleans, LA, Dec. 9-14, 1984. 7 p. refs
(Contract NSF MEA-80-06806; NAG3-292)
(ASME PAPER 84-WA/HT-70)

External heat-transfer rates were measured on a flat plate in the junction region of a circular cylinder mounted normal to the plate at a location 90 deg from the stagnation point. This configuration simulates the junction of the shroud with gas-turbine vanes. Heat-transfer results are presented for laminar, transition, and turbulent boundary layers for a Mach number of 0.14 with gas temperatures of approximately 750 deg R over a flat plate at room temperature. The measurements were made in air for a unit Reynolds number, Re/cm, range of 11,000 to 58,000. Heat-transfer measurements were conducted in the 70-ft long, 4-in. diameter shock tube. A shock-wave reflection technique was used to produce a flow Mach number of 0.14. Thin-film platinum heat gages were mounted on the flat plate and along the line of the stagnation point of the cylinder to measure the local heat flux in the junction region. The experimental heat-transfer data were correlated with the laminar and turbulent boundary-layer theories for the flat plate. With the cylinder the heat fluxes on the flat plate were greatly increased in the junction region compared to the heat flux for the plate alone. Author

A85-39900*# Texas A&M Univ., College Station.
HEAT TRANSFER ENHANCEMENT IN CHANNELS WITH TURBULENCE PROMOTERS
J. C. HAN, J. S. PARK, and C. K. LEI (Texas A&M University, College Station, TX) American Society of Mechanical Engineers, Winter Annual Meeting, New Orleans, LA, Dec. 9-14, 1984. 8 p. Army-supported research. refs
(Contract NAG3-311)
(ASME PAPER 84-WA/HT-72)

Repeated rib-roughness elements have been used in advanced turbine cooling designs to enhance the internal heat transfer. Often the ribs are perpendicular to the main flow direction so that they have an angle-of-attack of 90 degrees. The objective of this investigation was to determine the effect of rib angle-of-attack on the pressure drop and the average heat-transfer coefficients in the fully developed turbulent air flow in a square duct with two opposite rib-roughened walls for Reynolds numbers varied from 7,000 to 90,000. The rib height-to-equivalent diameter ratio was kept at a constant value of 0.063, the rib pitch-to-height ratio was varied from 10 to 20, and the rib angle-of-attack (alpha) was varied from 90 to 60 deg to 45 to 30 deg, respectively. The thermal-performance comparison indicated that the increased heat conductance for the rib with an oblique angle to the flow (alpha = 45 deg - 30 deg) was about 10-20 percent higher than the rib with a 90 deg angle to the flow, and the pumping power requirement for the angled rib was about 20-50 percent lower than the transverse rib. Semi-empirical correlations for friction factor and heat-transfer coefficients were developed to account for rib spacing and rib angle. The correlations can be used in the design of turbine-blade cooling passages. Author

A85-40701*# California Univ., Los Angeles.
VORTEX MODELING OF SINGLE AND MULTIPLE DILUTION JET MIXING IN A CROSSFLOW
A. R. KARAGOZIAN and C. N. KIM (California, University, Los Angeles) American Institute of Aeronautics and Astronautics, Fluid Dynamics and Plasmadynamics and Lasers Conference, 18th, Cincinnati, OH, July 16-18, 1985. 12 p. refs
(Contract NAG3-543)
(AIAA PAPER 85-1580)

An analytical model for the behavior of normally injected jets in a crossflow is developed and applied to fluids of differing densities. Central to the model are the dynamics of the vortex pair structure associated with the local jet cross-section and the entrainment of crossflow by jet fluid. Two specific cases are modeled: one involving a single dilution jet in a crossflow, in which trajectories are found to scale primarily with jet-to-crossflow momentum ratio, and the other involving a series of spanwise jets injected into a crossflow, which indicates scaling with momentum ratio and with the spacing-to-orifice-diameter ratio. In the case of multiple jet penetration, however, merging of the jets into an approximately two-dimensional jet downstream of injection is observed for low spacing-to-diameter ratios. Author

A85-40750*# National Aeronautics and Space Administration. Lewis Research Center, Cleveland, Ohio.
FLOW THROUGH VERY POROUS INCLINED SCREENS
K. K. MURAMOTO and P. A. DURBIN (NASA, Lewis Research Center, Cleveland, OH) American Institute of Aeronautics and Astronautics, Fluid Dynamics and Plasmadynamics and Lasers Conference, 18th, Cincinnati, OH, July 16-18, 1985. 7 p. Previously announced in STAR as N85-25761. refs
(AIAA PAPER 85-1650)

The steady, inviscid flow through and around a screen inclined at a uniform angle to the incoming flow was investigated. For a screen placed in an infinite flow field, an asymptotic analysis for small resistance coefficients was performed, and the effects of inclination were determined. The velocity at first order in the asymptotic expansion was nonuniform along the screen. This nonuniformity caused the wake behind the screen to contain distributed vorticity at second order. These effects therefore occurred at one order lower than for normal screens. M.G.

A85-40752*# Pennsylvania State Univ., University Park.
TURBULENCE MODELLING FOR COMPLEX SHEAR FLOWS
B. LAKSHMINARAYANA (Pennsylvania State University, University Park) American Institute of Aeronautics and Astronautics, Fluid Dynamics and Plasmadynamics and Lasers Conference, 18th, Cincinnati, OH, July 16-18, 1985. 38 p. refs
(Contract NSG-3266; NSG-3012; NSG-3212)
(AIAA PAPER 85-1652)

The turbulence models available for the prediction of complex turbulent shear layers are reviewed in this paper, concentrating mainly on three-dimensional flows, flows subjected to curvature and body rotation, separated flows, and vortex flows. A critical review of zero-equation, one-equation, two-equation, algebraic Reynolds stress, and full Reynolds stress models are carried out, with a specific emphasis on their applicability to complex flows. It is concluded that algebraic eddy viscosity models and kappa-epsilon/kappa-omega models, with a constant value of coefficients, are not adequate for complex flows. The models which include a description of stresses, either through an algebraic Reynolds stress model or a full Reynolds stress model, are essential for adequate prediction of these flows. It is recommended that systematic experimental investigations be carried out to isolate various complex interactions in order to understand and model the various effects and to carry out an extension of the present models to include complex flows. Author

A85-41326*# National Aeronautics and Space Administration. Lewis Research Center, Cleveland, Ohio.
SOLIDIFICATION INTERFACE SHAPE FOR CONTINUOUS CASTING IN AN OFFSET MOLD - TWO ANALYTICAL METHODS
R. SIEGEL (NASA, Lewis Research Center, Cleveland, OH) ASME, Transactions, Journal of Heat Transfer (ISSN 0022-1481), vol. 106, Feb. 1984, 4 p.

A solution method for finding the unknown solidification interface in manufacturing slab ingots as a continuous casting is presented, which involves a product solution in the potential plane and the use of conjugate harmonic functions. It is argued that the method may be more direct for some geometries than the Cauchy boundary value method. Moreover, the usefulness of the Cauchy boundary value method is demonstrated through the example of a nonsymmetric horizontal mold where the walls are offset to support the lower ingot boundary. L.T.

A85-41782* Cleveland State Univ., Ohio.
COMBINED INFLUENCE OF UNSTEADY FREE STREAM VELOCITY AND FREE STREAM TURBULENCE ON STAGNATION POINT HEAT TRANSFER
R. S. R. GORLA (Cleveland State University, OH) IN: 1983 Tokyo International Gas Turbine Congress, Tokyo, Japan, October 23-29, 1983, Proceedings. Volume 1 . Tokyo, Gas Turbine Society of Japan, 1984, p. 45-49. refs
(Contract NCC3-3)

An analysis is presented to study the combined effects of transient free stream velocity and free stream turbulence on heat transfer at a stagnation point over a cylinder situated in a crossflow. An expression for the eddy diffusivity has been formulated and the governing momentum and energy equations are integrated by means of the steepest descent method. The numerical results for the heat transfer rate are correlated by a turbulence parameter. It has been found that the stagnation point heat transfer rate increases with increasing free stream turbulence intensity. Author

A85-41787* Stanford Univ., Calif.
HEAT TRANSFER AND TURBULENCE MEASUREMENTS OF A FILM-COOLED FLOW OVER A CONVEXLY CURVED SURFACE
K. FURUHAMA, R. J. MOFFAT (Stanford University, CA), and M. N. FROTA (Rio de Janeiro, Pontificia Universidade Catolica, Brazil) IN: 1983 Tokyo International Gas Turbine Congress, Tokyo, Japan, October 23-29, 1983, Proceedings. Volume 1 . Tokyo, Gas Turbine Society of Japan, 1984, p. 119-126. refs
(Contract NAG3-3)

Heat transfer and hydrodynamic boundary layer measurements were made in a turbulent boundary layer on a convex surface with 13 rows of injection. Both full- and partial-coverage cases were tested for three blowing ratios: 0.2, 0.4, and 0.6. Heat transfer results are discussed in terms of Stanton number with injection air temperature equal to wall temperature. In the blown region, for both m (blowing ratio) = 0.2 and 0.4, the local response of the boundary layer is dominated by curvature, and m = 0.4 shows higher cooling effects than m = 0.2 or 0.6, as expected, based on flat-plate results. Hydrodynamic measurements with a triple-hot-wire suggest the existence of two streamwise lanes. Lanes containing injection holes are highly affected by injection and show a definite streamwise evolution. Lanes which do not contain holes are not affected much by injection and show little change in the streamwise direction. Author

A85-45282* Arizona State Univ., Tempe.
JET CHARACTERISTICS IN CONFINED SWIRLING FLOW
R. M. C. SO, S. A. AHMED, and H. C. MONGIA (Arizona State University, Tempe) Experiments in fluids (ISSN 0723-4864), vol. 3, no. 4, 1985, p. 221-230. refs
(Contract NAG3-260)

Jets in confined swirling flow are investigated in a facility where the swirling flow in the tube is produced by a vane-type swirler. The jet is located centrally in the swirler, and the diameter ratio of the tube to the jet is about 14. Both the jet and the swirling flow are fully turbulent. Results show that the confined jet is highly dissipative in nature. Consequently, the flow in the tube does not resemble a free jet with axial pressure gradient. The presence of swirl increases the rate of dissipation and the jet decays even faster. A fairly isotropic turbulence field is observed in the confined swirling flow. However, the introduction of the jet does not significantly affect this behavior, and near isotropy of the turbulence field is again observed at about 30 jet diameters downstream. Author

A85-45283* Arizona State Univ., Tempe.
DENSITY EFFECTS ON JET CHARACTERISTICS IN CONFINED SWIRLING FLOW
S. A. AHMED, R. M. C. SO, and H. C. MONGIA (Arizona State University, Tempe) Experiments in Fluids (ISSN 0723-4864), vol. 3, no. 4, 1985, p. 231-238. refs
(Contract NAG3-260)

Density effects on isothermal jet mixing in confined swirling flow are investigated. The experiment is carried out with helium/air as the jet fluid in the same facility as that used by So et al. (1984) and the test conditions are chosen to be the same as before. Contrary to the homogeneous mixing results, the helium jet is preserved up to 40 jet diameters downstream. The behavior of the mean and turbulence field depends highly on the initial jet velocity. Since the jets are fully turbulent and the jet momentum fluxes for inhomogeneous mixing are less than those for homogeneous mixing, the cause of this difference in behavior is directly attributed to the combined action of density difference and swirl. In spite of this, near isotropy of the turbulence field is again observed at about 40 jet diameters downstream. Author

A85-45856*# National Aeronautics and Space Administration. Lewis Research Center, Cleveland, Ohio.
INTERNAL COMBUSTION ENGINE COMBUSTION CHAMBER PROCESS STUDIES AT NASA LEWIS RESEARCH CENTER
H. J. SCHOCK (NASA, Lewis Research Center, Cleveland, OH) Journal of Propulsion and Power (ISSN 0748-4658), vol. 1, Sept.-Oct. 1985, p. 351-353. Previously cited in issue 19, p. 2749, Accession no. A84-40242. refs

A85-46484*# Pennsylvania State Univ., University Park.
MEASUREMENTS AND PREDICTIONS OF THE STRUCTURE OF EVAPORATING SPRAYS
A. S. P. SOLOMON, J.-S. SHUEN, Q.-F. ZHANG, and G. M. FAETH (Pennsylvania State University, University Park) ASME, Transactions, Journal of Heat Transfer (ISSN 0022-1481), vol. 107, Aug. 1985, p. 679-686. refs
(Contract NAG3-190)

In the present experimental and theoretical study of turbulent, evaporating sprays, round, Freon-11 sprays produced by an air-atomizing injector that is directed vertically downward in still air were subjected to structure measurements for mean and fluctuating gas velocities, total Freon-11 concentration, drop size and velocity contributions, mean gas temperature, and liquid flux distributions. An evaluation was then conducted of three spray models: (1) locally homogeneous flow, (2) deterministic separated flow, and (3) stochastic separated flow. The first two of these were found to perform poorly; the stochastic model yielded the best agreement between predictions and measurements. O.C.

A85-48538*# Pennsylvania State Univ., University Park.
STRUCTURE OF NONEVAPORATING SPRAYS. I - INITIAL CONDITIONS AND MEAN PROPERTIES
A. S. P. SOLOMON, J.-S. SHUEN, Q.-F. ZHANG, and G. M. FAETH (Pennsylvania State University, University Park) AIAA Journal (ISSN 0001-1452), vol. 23, Oct. 1985, p. 1548-1555. refs
(Contract NAG3-190)

Structure measurements were completed within the dilute portion of axisymmetric nonevaporating sprays. Measurements included: mean velocities, velocity fluctuations, and Reynolds stress of the gas phase; and mean velocities, fluctuating velocities, mass flux, and diameter distributions of the drop phase. The measurements were used to evaluate three typical methods of

analyzing sprays: (1) a locally homogeneous flow (LHF) analysis, where slip between the phases is neglected; (2) a deterministic separated flow (DSF) analysis, where slip is considered but effects of drop interactions with turbulence are ignored; and (3) a stochastic separated flow (SSF) analysis, where effects of both slip and turbulence are considered using random-walk computations for drop motion. Measurements of initial conditions of both phases near the injector, mean gas-phase properties, and liquid flux distributions are described herein. Best agreement between predictions and measurements was obtained with the SSF model, which provided a reasonable representation of turbulent dispersion of drops. A companion paper presents additional measurements of drop continuous phase properties. Author

A85-49354* Florida State Univ., Tallahassee.
A MULTIPLE-SCALES MODEL OF THE SHOCK-CELL STRUCTURE OF IMPERFECTLY EXPANDED SUPERSONIC JETS
C. K. W. TAM, J. A. JACKSON (Florida State University, Tallahassee), and J. M. SEINER (NASA, Langley Research Center, Hampton, VA) *Journal of Fluid Mechanics* (ISSN 0022-1120), vol. 153, April 1985, p. 123-149. refs
(Contract NAG3-182)

The present investigation is concerned with the development of an analytical model of the quasi-periodic shock-cell structure of an imperfectly expanded supersonic jet. The investigation represents a part of a program to develop a mathematical theory of broadband shock-associated noise of supersonic jets. Tam and Tanna (1982) have suggested that this type of noise is generated by the weak interaction between the quasi-periodic shock cells and the downstream-propagating large turbulence structures in the mixing layer of the jet. In the model developed in this paper, the effect of turbulence in the mixing layer of the jet is simulated by the addition of turbulent eddy-viscosity terms to the momentum equation. Attention is given to the mean-flow profile and the numerical solution, and a comparison of the numerical results with experimental data. G.R.

N85-10303*# National Aeronautics and Space Administration. Lewis Research Center, Cleveland, Ohio.
THE EFFECT OF CHANNEL CONVERGENCE ON HEAT TRANSFER IN A PASSAGE WITH SHORT PIN FINS
B. A. BRIGHAM Oct. 1984 17 p refs
(NASA-TM-83801; E-2306; NAS 1.15:83801) Avail: NTIS HC A02/MF A01 CSCL 20D

Array averaged heat transfer coefficients were obtained for two configurations of short pin fins in a converging channel and for two flat plate configurations in a converging channel. The effect of flow acceleration due to channel convergence and the effect of varying pin length on the heat transfer was determined. Results are presented in the form of Nusselt number versus Reynolds number for the four geometries tested. Author

N85-10306*# National Aeronautics and Space Administration. Lewis Research Center, Cleveland, Ohio.
A REVIEW AND ANALYSIS OF BOUNDARY LAYER TRANSITION DATA FOR TURBINE APPLICATION
R. E. GAUGLER Washington 1984 14 p refs Presented at the 13th Intern. Gas Turbine Conf. and Exhibit, Houston, Tex., 17-21 Mar. 1984; sponsored by the American Society of Mechanical Engineers
(NASA-TM-86880; E-2341; NAS 1.15:86880) Avail: NTIS HC A02/MF A01 CSCL 20D

A symposium on transition in turbines was held at the NASA Lewis Research Center. One recommendation of the working groups was the collection of existing transition data to provide standard cases against which models could be tested. A number of data sets from the open literature that include heat transfer data in apparently transitional boundary layers, with particular application to the turbine environment, were reviewed and analyzed to extract transition information from the heat transfer data. The data sets reviewed cover a wide range of flow conditions, from low speed, flat plate tests to full scale turbine airfoils operating at simulated turbine engine conditions. The results indicate that free stream turbulence and pressure gradient have strong, and opposite, effects on the location of the start of transition and on the length of the transition zone. R.S.F.

N85-11317*# National Aeronautics and Space Administration. Lewis Research Center, Cleveland, Ohio.
PRELIMINARY RESULTS OF A STUDY OF THE RELATIONSHIP BETWEEN FREE STREAM TURBULENCE AND STAGNATION REGION HEAT TRANSFER
G. J. VAANFOSSEN, JR. and R. J. SIMONEAU 1984 16 p refs Proposed for presentation at the 30th Intern. Gas Turbine Conf. and Exhibit, Houston, Tex., 17-21 Mar. 1985; sponsored by the American Society of Mechanical Engineers
(NASA-TM-86884; E-2346; NAS 1.15:86884) Avail: NTIS HC A02/MF A01 CSCL 20D

The mechanism that causes free stream turbulence to increase heat transfer in the stagnation region of turbine vanes and blades was studied. The work is being conducted in a wind tunnel at atmospheric conditions to facilitate measurements of turbulence and heat transfer. The model size is scaled up to simulate Reynolds numbers (based on leading edge diameter) that are to be expected on a turbine blade leading edge. Reynolds numbers from 13,000 to 177,000 were run in the present tests. Spanwise averaged heat transfer measurement with high and low turbulence were made with rough and smooth surface stagnation regions. Results of these measurements show that the boundary layer remains laminar in character even in the presence of free stream turbulence at the Reynolds numbers tested. If roughness is added the boundary layer becomes transitional as evidenced by the heat transfer increase with increasing distance from the stagnation line. Hot wire measurements near the stagnation region downstream of an array of parallel wires has shown that vorticity in the form of mean velocity gradients is amplified as flow approaches the stagnation region. Author

N85-12314*# National Aeronautics and Space Administration. Lewis Research Center, Cleveland, Ohio.
VORTEX-GENERATING COOLANT-FLOW-PASSAGE DESIGN FOR INCREASED FILM-COOLING EFFECTIVENESS AND SURFACE COVERAGE
S. S. PAPELL Nov. 1984 24 p refs
(NASA-TP-2388; E-2147; NAS 1.60:2388) Avail: NTIS HC A02/MF A01 CSCL 20D

The thermal film-cooling footprints observed by infrared imagery for three coolant-passage configurations embedded in adiabatic-test plates are discussed. The configurations included a standard round-hole cross section and two orientations of a vortex-generating flow passage. Both orientations showed up to factors of four increases in both film-cooling effectiveness and surface coverage over that obtained with the round coolant passage. The crossflow data covered a range of tunnel velocities from 15.5 to 45 m/sec with blowing rates from 0.20 to 2.05. A photographic streakline flow visualization technique supported the concept of the counterrotating apability of the flow passage design and gave visual credence to its role in inhibiting flow separation. M.G.

N85-14078*# National Aeronautics and Space Administration. Lewis Research Center, Cleveland, Ohio.
FLOW RATES AND PRESSURE PROFILES FOR ONE TO FOUR AXIALLY ALINED BORDA INLETS
R. C. HENDRICKS and T. T. STETZ Dec. 1984 32 p refs
(NASA-TP-2390; E-1979; NAS 1.60:2390) Avail: NTIS HC A03/MF A01 :b CSCL 20A

Choked flow rate and pressure profile data were taken on sequential, axially alined inlets of the Borda type. The configurations consisted of two to four inlets spaced 0.8 and 30 diameters apart. At a spacing of 30 diameters the reduced flow rate appeared to follow the simple empirical relation G sub r/G sub r,1 = N(-b), where G sub r,1 is the reduced flow rate for a single inlet; N is the number of inlets; and b, which is weakly temperature dependent, is approximately 0.4. The relation is in reasonable agreement with

an analysis of the N-inlet configuration. At a spacing of 30 diameters the pressure profiles dropped sharply at the entrance and partially recovered within each inlet somewhat independently of N. Jetting through the last Borda was common at low temperatures. At a spacing of 0.8 diameter fluid jetting was prevalent at low temperatures for each configuration studied and flow rates were the same as that for a single inlet. M.G.

N85-15133*# National Aeronautics and Space Administration. Lewis Research Center, Cleveland, Ohio.
HEAT TRANSFER RESULTS AND OPERATIONAL CHARACTERISTICS OF THE NASA LEWIS RESEARCH CENTER HOT SECTION CASCADE TEST FACILITY
H. J. GLADDEN, F. C. YEH, and D. L. FRONEK 1985 20 p refs Presented at the 30th Intern. Gas Turbine Conf. and Exhibit, Houston, Tex., 17-21 Mar. 1985; sponsored by ASME
(NASA-TM-86890; E-2357; NAS 1.15:86890) Avail: NTIS HC A02/MF A01 CSCL 20D

The NASA Lewis Research Center gas turbine hot section test facility has been developed to provide a real-engine environment with well known boundary conditions for the aerothermal performance evaluation/verification of computer design codes. The initial aerothermal research data obtained are presented and the operational characteristics of the facility are discussed. This facility is capable of testing at temperatures and pressures up to 1600 K and 18 atm which corresponds to a vane exit Reynolds number range of 0.5x10(6) to 2.5x10(6) based on vane chord. The component cooling air temperature can be independently modulated between 330 and 700 K providing gas-to-coolant temperature ratios similar to current engine application. Research instrumentation of the test components provide conventional pressure and temperature measurements as well as metal temperatures measured by IR-photography. The primary data acquisition mode is steady state through a 704 channel multiplexer/digitizer. The test facility was configured as an annular cascade of full coverage filmcooled vanes for the initial series of research tests. Author

N85-17324*# Wisconsin Univ., Milwaukee. Dept. of Mechanical Engineering.
A STUDY OF REYNOLDS-STRESS CLOSURE MODEL Semiannual Progress Report, 1 Jun. 1984 - 15 Jan. 1985
R. S. AMANO and P. GOEL Jan. 1985 50 p refs
(Contract NAG3-546)
(NASA-CR-174342; NAS 1.26:174342) Avail: NTIS HC A03/MF A01 CSCL 20D

A hybrid model of the Reynolds stress closure was developed. This model was tested for various sizes of step flow, and the computed Reynolds stress behavior was compared with experimental data. The third order closure model was reviewed. Transport equations for the triple velocity correlation were developed and implemented in a numerical code to evaluate the behavior of the triple velocity products in various regions of the flow field including recirculating, reattaching, and redeveloping flow domains. B.G.

N85-18291*# Massachusetts Inst. of Tech., Cambridge. Gas Turbine Lab.
RESEARCHED APPLIED TO TRANSONIC COMPRESSORS IN NUMERICAL FLUID MECHANICS OF INVISCID FLOW AND VISCOUS FLOW Final Report
W. T. THOMPKINS, JR. Feb. 1985 83 p refs
(Contract NAG3-9)
(NASA-CR-174353; NAS 1.26:174353) Avail: NTIS HC A05/MF A01 CSCL 20D

A streamline Euler solver which combines high accuracy and good convergence rates with capabilities for inverse or direct mode solution modes and an analysis technique for finite difference models of hyperbolic partial difference equations were developed. B.G.

N85-18292*# Pennsylvania State Univ., State College. Applied Research Lab.
THE BOUNDARY LAYER ON COMPRESSOR CASCADE BLADES Semiannual Progress Report, 1 Jun. - 1 Dec. 1984
S. DEUTSCH and W. C. ZIERKE 1984 47 p refs
(Contract NSG-3264)
(NASA-CR-174369; NAS 1.26:174369) Avail: NTIS HC A03/MF A01 CSCL 20D

The flow field about an airfoil in a cascade at chord Reynolds number (R sub C) near 50,000. The program is experimental and combines laser Doppler anemometry (LDA) with flow visualization techniques in order to obtain detailed flow data (e.g., boundary layer profiles, points of separation and the transition zone) on a cascade of highly-loaded compressor blades. The information provided is to serve as benchmark data for the evaluation of current and future compressor cascade predictive models, in this way aiding in the compressor design process. The completed pressure surface mean velocity profiles, as well as two detailed near wake velocity profiles, all at a single incidence angle are provided. B.G.

N85-19363*# National Aeronautics and Space Administration. Lewis Research Center, Cleveland, Ohio.
EXPERIMENTAL STUDY OF CERAMIC COATED TIP SEALS FOR TURBOJET ENGINES
T. J. BIESIADNY, G. A. KLANN (Army Research and Technology Labs., Cleveland), E. S. LASSOW (Howmet Corp., Whitehall, Mich.), M. MCHENRY (Army Aviation Logistics School, Fort Eustis, Va.), G. MCDONALD, and R. C. HENDRICKS 1985 22 p refs Presented at the 9th Ann. Conf. on Composites and Advan. Ceram. Mater., Cocoa Beach, Fla., 20-24 Jan. 1985; sponsored by the American Ceramic Society
(NASA-TM-86939; E-2457; NAS 1.15:86939; USAAVSCOM-TM-84-C-2) Avail: NTIS HC A02/MF A01 CSCL 20D

Ceramic gas-path seals were fabricated and successfully operated over 1000 cycles from flight idle to maximum power in a small turboshaft engine. The seals were fabricated by plasma spraying zirconia over a NiCoCrAlX bond boat on the Haynes 25 substrate. Coolant-side substrate temperatures and related engine parameters were recorded. Post-test inspection revealed mudflat surface cracking with penetration to the ceramic bond-coat interface. Author

N85-19364*# National Aeronautics and Space Administration. Lewis Research Center, Cleveland, Ohio.
RIBBON BURNER SIMULATION OF T-700 TURBINE SHROUD FOR CERAMIC LINED SEALS RESEARCH
J. K. LITTLE (Arnold Air Force Station, Tullahoma, Tenn.), G. P. ALLEN, G. MCDONALD, and R. C. HENDRICKS 1985 20 p refs Presented at the 9th Ann. Conf. on Composites and Advan. Ceram. Mater., Cocoa Beach, Fla., 20-24 Jan. 1985; sponsored by the American Ceramic Society
(NASA-TM-86940; E-2458; NAS 1.15:86940) Avail: NTIS HC A02/MF A01 CSCL 20D

Experimental and analytical studies were conducted to determine the acceptability of a ribbon-burner simulation of engine conditions for testing ceramic-lined turbine tip shrouds. The calculated values reveal that the ribbon burner establishes at least as harsh a thermal environment as is present at any time within the turbine shroud. Comparisons were made with ceramic components in a turboshaft engine. Author

N85-20269*# National Aeronautics and Space Administration. Lewis Research Center, Cleveland, Ohio.

FLOW VISUALIZATION STUDY OF THE EFFECT OF INJECTION HOLE GEOMETRY ON AN INCLINED JET IN CROSSFLOW

F. F. SIMON and M. L. CIANCONE 1985 26 p refs To be presented at the Symp. on Transport Phenomena in Rotating Machinery, held in Honolulu, Hi., 28 Apr. - 3 May 1985; sponsored in part by Michigan Univ., Hawaii Univ., ASME, Gas Turbine Society of Japan, and the Turbomachinery Society of Japan

(NASA-TM-86936; E-2450; NAS 1.15:86936) Avail: NTIS HC A03/MF A01 CSCL 20D

A flow visualization was studied by using neutrally buoyant, helium-filled soap bubbles, to determine the effect of injection hole geometry on the trajectory of an air jet in a crossflow and to investigate the mechanisms involved in jet deflection. Experimental variables were the blowing rate, and the injection hole geometry cusp facing upstream (CUS), cusp facing downstream (CDS), round, swirl passage, and oblong. It is indicated that jet deflection is governed by both the pressure drag forces and the entrainment of free-stream fluid into the jet flow. For injection hole geometries with similar cross-sectional areas and similar mass flow rates, the jet configuration with the larger aspect ratio experienced a greater deflection. Entrainment arises from lateral shearing forces on the sides of the jet, which set up a dual vortex motion within the jet and thereby cause some of the main-stream fluid momentum to be swept into the jet flow. This additional momentum forces the jet nearer the surface. Of the jet configurations, the oblong, CDS, and CUS configutations exhibited the largest deflections. The results correlate well with film cooling effectiveness data, which suggests a need to determine the jet exit configuration of optimum aspect ratio to provide maximum film cooling effectiveness. E.A.K.

N85-21569*# National Aeronautics and Space Administration. Lewis Research Center, Cleveland, Ohio.

ANALYSIS OF EXPERIMENTAL SHAFT SEAL DATA FOR HIGH-PERFORMANCE TURBOMACHINES, AS FOR SPACE SHUTTLE MAIN ENGINES

R. C. HENDRICKS, M. J. BRAUN (Akron, Univ., Ohio), R. L. MULLEN (Case Western Reserve Univ.), R. E. BURCHAM (Rocketdyne, Canoga Park, Calif.), and W. A. DIAMOND (Rocketdyne, Canoga Park, Calif.) 1985 19 p refs To be presented at the Symp. on Transport Phenomena in Rotating Machinery, Honolulu, Hawaii, 28 Apr. - 3 May 1985; sponsored in part by Michigan Univ., Hawaii Univ., ASME, Gas Turbine Soc. of Japan, and Turbomachinery Society of Japan

(NASA-TM-86928; E-2430; NAS 1.15:86928) Avail: NTIS HC A02/MF A01 CSCL 20D

High-pressure, high-temperature seal flow (leakage) data for nonrotating and rotating Raleigh-step and convergent-tapered-bore seals were characterized in terms of a normalized flow coefficient. The data for normalized Rayleigh-steip and nonrotating tapered-bore seals were in reasonable agreement with theory, but data for the rotating tapered-bore seals were not. The tapered-bore-seal operational clearances estimated from the flow data were significantly larger than calculated. Although clearances are influenced by wear from conical to cylindrical geometry and errors in clearance corrections, the problem was isolated to the shaft temperature - rotational speed clearance correction. The geometric changes support the use of some conical convergence in any seal. Under these conditions rotation reduced the normalized flow coefficiently by nearly 10 percent. Author

N85-21570*# National Aeronautics and Space Administration. Lewis Research Center, Cleveland, Ohio.

LIQUID FUEL SPRAY PROCESSES IN HIGH-PRESSURE GAS FLOW

R. D. INGEBO 1985 22 p refs Presented at 3rd Intern. Conf. on Liquid Atomization and Spray Systems, London, 8-10 Jul. 1985

(NASA-TM-86944; E-2463; NAS 1.15:86944) Avail: NTIS HC A02/MF A01 CSCL 20D

Atomization of single liquid jets injected downstream in high pressure and high velocity airflow was investigated to determine the effect of airstream pressure on mean drop size as measured with a scanning radiometer. For aerodynamic - wave breakup of liquid jets, the ratio of orifice diameter D sub o to measured mean drop diameter D sub m which is assumed equal to D sub 32 or Sauter mean diameter, was correlated with the product of the Weber and Reynolds numbers WeRe and the dimensionless group G1/square root of c, where G is the gravitational acceleration, 1 the mean free molecular path, and square root of C the root mean square velocity, as follows; D sub o/D sub 32 = 1.2 (WeRe) to the 0.4 (G1/square root of c) to the 0.15 for values of WeRe 1 million and an airstream pressure range of 0.10 to 2.10 MPa. G.L.C.

N85-21574*# National Aeronautics and Space Administration. Lewis Research Center, Cleveland, Ohio.

NESTED SUBCRITICAL FLOWS WITHIN SUPERCRITICAL SYSTEMS

R. C. HENDRICKS, M. J. BRAUN (Akron Univ.), R. L. WHEELER, III (Akron Univ.), and R. L. MULLEN 1985 12 p refs Proposed for presentation at the 20th Ann. Cavitation and Multiphase Flow Forum, Albuquerque, N. Mex., 24-26 Jun. 1985; sponsored by the American Society of Mechanical Engineers

(NASA-TM-86980; E-2518; NAS 1.15:86980) Avail: NTIS HC A02/MF A01 CSCL 20D

In supercritical systems the design inlet and outlet pressures are maintained above the thermaodynamic critical pressure P sub C. Designers rely on this simple rule of thumb to circumvent problems associated with a subcritical pressure regime nested within the supercritical pressure system along with the uncertainties in heat transfer, fluid mechanics, and thermophysical property variations. The simple rule of thumb is adequate in many low-power designs but is inadequate for high-performance turbomachines and linear systems, where nested two-phase regions can exist. Examples for a free-jet expansion with backpressure greater than P sub C and a rotor (bearing) with ambient pressure greater than P sub C illustrate the existence of subcritical pressure regimes nested within supercritical systems. Author

N85-24245*# National Aeronautics and Space Administration. Lewis Research Center, Cleveland, Ohio.

ADVANCED RADIATOR CONCEPTS

P. S. DIEM-KIRSOP 30 Jun. 1985 13 p refs Proposed for presentation at Soc. of Women Engr. Natl. Convention, Minneapolis, 27-30 Jun. 1985

(NASA-TM-87008; E-2552; NAS 1.15:87008) Avail: NTIS HC A02/MF A01 CSCL 20D

The liquid droplet radiator and the liquid belt radiator currently under study by the NASA LeRC are discussed. These advanced concepts offer benefits in reduced mass, compact stowage,. and ease of deployment. Operation and components of the radiators are described, heat transfer characteristics are discussed, and critical technologies are identified. The impact of the radiators on large power systems is also assessed. A.R.H.

N85-25760*# National Aeronautics and Space Administration. Lewis Research Center, Cleveland, Ohio.

THE INFLUENCE OF JET-GRID TURBULENCE ON HEAT TRANSFER FROM THE STAGNATION REGION OF A CYLINDER IN CROSSFLOW

J. E. OBRIEN (Pennsylvania State Univ., University Park) and G. J. VANFOSSEN, JR. 1985 13 p refs Proposed for presentation at the Natl. Heat Transfer Conf., Denver, 4-7 Aug. 1985; sponsored by ASME

(NASA-TM-87011; E-2555; NAS 1.15:87011) Avail: NTIS HC A02/MF A01 CSCL 20D

The effect of high-intensity turbulence on heat transfer from the stagnation region of a circular cylinder in crossflow was studied. The work was motivated by the desire to be able to more fully understand and predict the heat transfer to the leading edge of a turbine airfoil. In order to achieve high levels of turbulence with a reasonable degree of isotropy and homogeneity, a jet-injection turbulence grid was used. The jet grid provided turbulence intensities of 10 to 12 percent, measured at the test cylinder

location, for downstream blowing with the blowing rate adjusted to an optimal value for flow uniformity. Heat transfer augmentation above the zeroturbulence case ranged from 37 to 53 percent for the test cylinder behind the jet grid for a cylinder Reynolds number range of 48,000 to 180,000, respectively. The level of heat transfer augmentation was found to be fairly uniform with respect to circumferential distance from the stagnation line. Stagnation point heat transfer results (expressed in terms of the Frossling number) were found to be somewhat low with respect to previous studies, when compared on the basis of equal values of the parameter Tu Re(1/2), indicating an additional Reynolds number effect as observed by previous investigators. Consequently, for a specified value of Tu Re(1/2), data obtained with a relatively high turbulence intensity will have a lower value of the Frossling number. M.G.

N85-25761*# National Aeronautics and Space Administration. Lewis Research Center, Cleveland, Ohio.
FLOW THROUGH VERY POROUS INCLINED SCREENS
K. K. MURAMOTO and P. A. DURBIN 1985 10 p refs Proposed for presentation at the 18th Fluid Dyn. and Plasmadyn. and Lasers Conf., Cincinnati, 16-18 Jul. 1985; sponsored by AIAA
(NASA-TM-86979; E-2517; NAS 1.15:86979) Avail: NTIS HC A02/MF A01 CSCL 20D

The steady, inviscid flow through and around a screen inclined at a uniform angle to the incoming flow was investigated. For a screen placed in an infinite flow field, an asymptotic analysis for small resistance coefficients was performed, and the effects of inclination were determined. The velocity at first order in the asymptotic expansion was nonuniform along the screen. This nonuniformity caused the wake behind the screen to contain distributed vorticity at second order. These effects therefore occurred at one order lower than for normal screens. M.G.

N85-26902*# National Aeronautics and Space Administration. Lewis Research Center, Cleveland, Ohio.
ANALYTICAL STUDY OF FLOW PHENOMENA IN SSME TURNAROUND DUCT GEOMETRIES
K. L. MCLALLIN *In* NASA. Marshall Space Flight Center Advan. High Pressure O2/H2 Technol. p 579-598 Apr. 1985 refs
Avail: NTIS HC A99/MF E03; SOD HC CSCL 20D

The SSME fuel turbopump hot gas manifold was identified as a source of loss and flow distortion which significantly affects the performance and durability of both the drive turbine and the LOX injector area of the main combustion chamber. Two current SSME geometries were studied, the full power level (FPL) and the first manned orbital flight (FMOF) configuration. The effects of turnaround duct geometry on flow losses and distortions, by varying wall curvature and flow area variation in the 180 deg turnaround region were examined. The effects of the duct inlet flow phenomena such as the radial distortion of the inlet flow and inlet swirl level on turnaround duct performance were also investigated. It is shown that of the two current geometries, the FMOF configuration had lower pressure losses and generated less flow distortion, but had a small flow separation bubble at the 180 deg turnaround exit. It is found that by optimizing wall curvature and flow diffusion in the turnaround, improved duct performance can be achieved. E.A.K.

N85-27164*# Analex Corp., Cleveland, Ohio.
COMPUTER PROGRAM FOR THE CALCULATION OF MULTICOMPONENT CONVECTIVE DIFFUSION DEPOSITION RATES FROM CHEMICALLY FROZEN BOUNDARY LAYER THEORY Final Report
S. A. GOEKOGLU, B. K. CHEN, and D. E. ROSNER Washington Jan. 1984 35 p refs Prepared in cooperation with Yale Univ., New Haven, Conn.
(Contract NAS3-23293; NAG3-201)
(NASA-CR-168329; E-1971; NAS 1.26:168329) Avail: NTIS HC A03/MF A01 CSCL 20D

The computer program based on multicomponent chemically frozen boundary layer (CFBL) theory for calculating vapor and/or small particle deposition rates is documented. A specific application to perimter-averaged Na2SO4 deposition rate calculations on a cylindrical collector is demonstrated. The manual includes a typical program input and output for users. Author

N85-27165*# National Aeronautics and Space Administration. Lewis Research Center, Cleveland, Ohio.
FLOW RATE AND PRESSURE PROFILES FOR 1 TO 4 AXIALLY ALINED ORIFICE INLETS
R. C. HENDRICKS and T. T. STETZ May 1985 44 p refs
(NASA-TP-2460; E-1980; NAS 1.60:2460) Avail: NTIS HC A03/MF A01 CSCL 20D

Choked flow rate and pressure profile data were taken on sequential axially alined inlets of the orifice type, with an orifice length-to-diameter ratio of 0.5. The configuration consisted of two to four inlets spaced at 0.66 and 32 orifice diameters apart. At a spacing of 32 diameters the reduced flow rate appeared to follow the simple power-law relation G(sub r)/G(sub r,1) = N (sup-b), where G(sub r,1) is the reduced flow rate for a single inlet, N is the number of inlets, and b, although temperature dependent, is approximately 0.4. At this spacing the instrumented orifices and spacers gave pressure profiles that dropped sharply at the entrance and partially recovered within each inlet, somewhat independent of N. At low inlet temperature jetting through the last orifice was common. At a spacing of 0.66 diameter fluid jetting through all N inlets was prevalent at low temperatures for each configuration studied, as indicated by the flat pressure profiles and flow rates that were nearlly identical to those for a single orifice inlet. A simplifying relation was developed between the friction loss parameters for flow through N sequential tubes and N sequential inlets. The predicted flow rates for N tubes were in reasonable agreement with the N inlet analysis and followed the simple power-law relation. M.G.

N85-27168*# California Inst. of Tech., Pasadena.
FREE-SURFACE PHENOMENA UNDER LOW- AND ZERO-GRAVITY CONDITIONS Final Technical Report
D. COLES 6 Jun. 1985 16 p refs
(Contract NAG3-466)
(NASA-CR-175835; NAS 1.26:175835) Avail: NTIS HC A02/MF A01 CSCL 20D

An apparatus to measure contact angle was constructed to exploit the proposed internal-corner criterion. If 2 alfa is the internal angle between two intersecting vertical planes and gamma is the contact angle, a meniscus at the corner rises to a finite height if alfa + gamma pi/2 and to an infinite height if alfa + gamma pi/2. The apparatus operates by decreasing the angle alfa from pi/2 until the meniscus height changes abruptly. A number of liquids are tested on glass and plexiglas. E.A.K.

N85-27945*# National Aeronautics and Space Administration. Lewis Research Center, Cleveland, Ohio.
SIMULATION OF MULTISTAGE TURBINE FLOWS
M. L. CELESTINA (Sverdrup Technology, Inc., Middleburg Heights, Ohio), R. A. MULAC (Sverdrup Technology, Inc., Middleburg Heights, Ohio), and J. J. ADAMCZYK *In its* Struct. Integrity and Durability of Reusable Space Propulsion Systems p 27-36 May 1985
Avail: NTIS HC A09/MF A01 CSCL 20D

The numerical simulation of turbine flows serves to enhance the understanding of the flow phenomena within multistage turbomachinery components. The direct benefit of this activity is improved modeling capability, which can be used to improve component efficiency and durability. A hierarchy of equations was formulated to assess the difficulty in analyzing the flow field within multistage turbomachinery components. The Navier-Stokes equations provides the most complete description. The simplest description is given by a set of equations that govern the quasi-one-dimensional flow. The number of unknowns to be solved for increases monotonically above the number of equations. The development of the additional set of equations needed to mathematically close the system of equations forms the closure problem associated with that level of description. For the Navier-Stokes equation there is no closure problem. For the quasi-one-dimensional equation set random flow fluctuations,

unsteady fluctuations, nonaxisymmetric flow variations, and hub-to-shroud variations on the quasi-one-dimensional flow must be accounted for. E.A.K.

N85-27947*# National Aeronautics and Space Administration. Lewis Research Center, Cleveland, Ohio.
UNSTEADY HEAT TRANSFER DUE TO TIME-DEPENDENT FREE STREAM VELOCITY Abstract Only
R. S. R. GORLA and A. AMERI *In* NASA. Lewis Research Center Struct. Integrity and Durability of Reusable Space Propulsion Systems p 39-40 May 1985 refs
Avail: NTIS HC A09/MF A01 CSCL 20D

The present work was undertaken in order to study the unsteady combined convection from a horizontal circular cylinder to a transverse flow. A coordinate perturbation method is used to transform the governing set of partial differential equations into a system of ordinary differential equations. The free stream time-dependent velocity was assumed to be sinusoidal and the boundary layer response due to both low as well as high frequencies of oscillation will be studied. Currently numerical solutions are being obtained for the distribution of the unsteady Nusselt number and the friction factor. Author

N85-27948*# National Aeronautics and Space Administration. Lewis Research Center, Cleveland, Ohio.
NEW FACILITY TO STUDY UNSTEADY WAKE EFFECTS ON TURBINE AIRFOIL HEAT TRANSFER
R. J. SIMONEAU *In its* Struct. Integrity and Durability of Reusable Space Propulsion Systems p 41-47 May 1985
Avail: NTIS HC A09/MF A01 CSCL 20D

A significant portion of the SSME aerothermal loads program is directed at the heat transfer effects of the unsteady flows, particularly wakes, that occur naturally in turbomachinery. Although these phenomena occur in all turbomachines, we feel they will be more severe in the SSME turbines because of the high heat transfer associated with the very high Reynolds numbers over the SSME airfoils. G.L.C.

N85-29179* National Aeronautics and Space Administration. Lewis Research Center, Cleveland, Ohio.
HIGH THERMAL POWER DENSITY HEAT TRANSFER APPARATUS PROVIDING ELECTRICAL ISOLATION AT HIGH TEMPERATURE USING HEAT PIPES Patent
J. F. MORRIS, inventor (to NASA) 19 Mar. 1985 6 p Filed 24 Jun. 1983 Continuation-in-part of abandoned US Patent Appl-SN-202228, filed 30 Nov. 1980
(NASA-CASE-LEW-12950-2; US-PATENT-4,506,183; US-PATENT-APPL-SN-507626; US-PATENT-APPL-SN-202228; US-PATENT-CLASS-310-306; US-PATENT-CLASS-165-32; US-PATENT-CLASS-165-104.14) Avail: US Patent and Trademark Office CSCL 20D

This invention is directed to transferring heat from an extremely high temperature source to an electrically isolated lower temperature receiver. The invention is particularly concerned with supplying thermal power to a thermionic converter from a nuclear reactor with electric isolation. Heat from a high temperature heat pipe is transferred through a vacuum or a gap filled with electrically nonconducting gas to a cooler heat pipe. If the receiver requires gratr thermal power density, geometries are used with larger heat pipe areas for transmitting and receiving energy than the area for conducting the heat to the thermionic converter. In this way the heat pipe capability for increasing thermal power densities compensates for the comparative low thermal power densities through the electrically nonconducting gap between the two heat pipes. Official Gazette of the U.S. Patent and Trademark Office

N85-30242*# National Aeronautics and Space Administration. Lewis Research Center, Cleveland, Ohio.
FAST APPROACH FOR CALCULATING FILM THICKNESSES AND PRESSURES IN ELASTOHYDRODYNAMICALLY LUBRICATED CONTACTS AT HIGH LOADS
L. G. HOUPERT (SKF Engineering and Research Center) and B. J. HAMROCK 1985 31 p refs Proposed for presentation at the Joint Lubrication Conf., Atlanta, 8-10 Oct. 1985; sponsored by the American Society of Lubrication Engineers
(NASA-TM-87032; E-2581; NAS 1.15:87032) Avail: NTIS HC A03/MF A01 CSCL 20D

The film thicknesses and pressures in elastohydrodynamically lubricated contacts have been calculated for a line contact by using an improved version of Okamura's approach. The new approach allows for lubricant compressibility, the use of Roelands' viscosity, a general mesh (nonconstant step), and accurate calculations of the elastic deformation. The new approach is described, and the effects on film thickness, pressure, and pressure spike of each of the improvements are discussed. Successful runs have been obtained at high pressure (to 4.8 GPa) with low CPU times. Author

N85-30245*# United Technologies Research Center, East Hartford, Conn.
TURBULENT TRANSPORT AND LENGTH SCALE MEASUREMENT EXPERIMENTS WITH COMFINED COAXIAL JETS Interim Report, 1 Sep. 1983 - 16 Aug. 1984
B. V. JOHNSON and R. ROBACK Nov. 1984 74 p refs (Contract NAS3-2271)
(NASA-CR-174831; NAS 1.26:174831; UTRC-R84-915540-34)
Avail: NTIS HC A04/MF A01 CSCL 20D

A three phase experimental study of mixing downstream of swirling and nonswirling confined coaxial jets was conducted to obtain data for the evaluation and improvement of turbulent transport models currently employed in a variety of computational procedures. The present effort was directed toward the acquisition of length scale and dissipation rate data that provide more accurate inlet boundary conditions for the computational procedures and a data base to evaluate the turbulent transport models in the near jet region where recirculation does not occur, and the acquisition of mass and momentum turbulent transport data for a nonswirling flow condition with a blunt inner jet inlet configuration rather than the tapered inner jet inlet. A measurement technique, generally used to obtain approximate integral length and microscales of turbulence and dissipation rates, was computerized. Results showed the dissipation rate varied by 2 1/2 orders of magnitude across the inlet plane, by 2 orders of magnitude 51 mm from the inlet plane, and by 1 order of magnitude at 102 mm from the inlet plane for a nonswirling flow test conditions. Author

N85-30246*# National Aeronautics and Space Administration. Lewis Research Center, Cleveland, Ohio.
GENERATION OF CAPILLARY INSTABILITIES BY EXTERNAL DISTURBANCES IN A LIQUID JET Ph.D. Thesis - State Univ. of N.Y.
S. J. LEIB May 1985 77 p refs
(NASA-TM-87041; E-2503; NAS 1.15:87041) Avail: NTIS HC A05/MF A01 CSCL 20D

The receptivity problem in a circular liquid jet is considered. A time harmonic axial pressure gradient is imposed on the steady, parallel flow of a jet of liquid emerging from a circular duct. Using a technique developed in plasma physics a casual solution to the forced problem is obtained over certain ranges of Weber number for a number of mean velocity profiles. This solution contains a term which grows exponentially in the downstream direction and can be identified with a capillary instability wave. Hence, it is found that the externally imposed disturbances can indeed trigger instability waves in a liquid jet. The amplitude of the instability wave generated relative to the amplitude of the forcing is computed numerically for a number of cases. Author

N85-30247*# National Aeronautics and Space Administration. Lewis Research Center, Cleveland, Ohio.
APPLICATION OF COMPUTATIONAL FLUID DYNAMICS TO COMPLEX INLET DUCTS
C. E. TOWNE and E. F. SCHUM (Rockwell International Corp., Columbus, Ohio) 1985 15 p refs Presented at the 21st Joint Propulsion Conf., Monterey, Calif., 8-10 Jul. 1985; sponsored in part by AIAA, SAE, ASME, and ASEE
(NASA-TM-87060; E-2629; NAS 1.15:87060; AIAA-85-1213)
Avail: NTIS HC A02/MF A01 CSCL 20D

A three-dimensional parabolic Navier-Stokes code, PEPSIG, was used to analyze the flow in the subsonic diffuser section of a typical modern inlet design. The effect of curvature of the diffuser centerline and transitioning cross sections was studied to determine the primary cause of flow distortion in the duct. Total pressure values at the engine compressor face are reported. M.G.

N85-31433*# National Aeronautics and Space Administration. Lewis Research Center, Cleveland, Ohio.
TRANSITION IN TURBINES
Washington Jul. 1985 224 p refs Symp. held in Cleveland, 15-16 May 1984
(NASA-CP-2386; E-2456; NAS 1.55:2386) Avail: NTIS HC A10/MF A01 CSCL 20D

The concept of a large disturbance bypass mechanism for the initiation of transition is reviewed and studied. This mechanism, or some manifestation thereof, is suspected to be at work in the boundary layers present in a turbine flow passage. Discussion is presented on four relevant subtopics: (1) the effect of upstream disturbances and wakes on transition; (2) transition prediction models, code development, and verification; (3) transition and turbulence measurement techniques; and (4) the hydrodynamic condition of low Reynolds number boundary layers.

N85-31434*# National Aeronautics and Space Administration. Lewis Research Center, Cleveland, Ohio.
COMBUSTOR TURBULENCE
C. J. MAREK *In its* Transition in Turbines p 5-16 Jul. 1985 refs
Avail: NTIS HC A10/MF A01 CSCL 20D

The turbulence entering the turbine is produced in the combustor. High turbulence levels from the combustor can alter the location of the transition point on the turbine vane. The dynamics of turbulence and the progress being made in computing the flow are discussed. Author

N85-31435*# National Aeronautics and Space Administration. Lewis Research Center, Cleveland, Ohio.
PRELIMINARY RESULTS OF A STUDY OF THE RELATIONSHIP BETWEEN FREE-STREAM TURBULENCE AND STAGNATION REGION HEAT TRANSFER
G. J. VANFOSSEN, JR. and R. J. SIMONEAU *In its* Transition in Turbines p 17-34 Jul. 1985 refs Previously announced as N85-11317
Avail: NTIS HC A10/MF A01 CSCL 20D

Preliminary results of a study to investigate the relationship between free stream turbulence and heat transfer augmentation in the stagnation region is presented. The effects of free stream turbulence and surface roughness on spanwise averaged heat transfer were investigated. Turbulence was measured upstream of a cylinder placed in the wake of an array of parallel wires that were perpendicular to the cylinder axis. Finally, flow visualization and thermal visualization techniques were combined to show the relationship between vortices in the stagnation region and spanwise variations in heat transfer. Author

N85-31438*# National Aeronautics and Space Administration. Lewis Research Center, Cleveland, Ohio.
FLAT-PLATE TRANSITION
B. A. ERCEGOVIC *In its* Transition in Turbines p 61-68 Jul. 1985
Avail: NTIS HC A10/MF A01 CSCL 20D

A new research effort was undertaken to build a boundary-layer transition tunnel. This facility only recently became operational. The data obtained so far are merely qualitative. The main goal is to predict heat transfer given any combination of factors such as pressure gradient, turbulence level, Reynolds number, or intermittency factor. The boundary-layer transition tunnel is a closed-loop tunnel that controls the turbulence level, velocity and temperature of the air within it. Problems associated with the operation of this tunnel are examined. B.W.

N85-31439*# Clemson Univ., S.C.
HEAT TRANSFER AND FLUID MECHANICS MEASUREMENTS IN TRANSITIONAL BOUNDARY LAYER FLOWS
T. WANG, T. W. SIMON (Minnesota Univ., Minneapolis), and J. BUDDHAVARAPU (TSI, Inc., St. Paul, Minn.) *In* NASA. Lewis Research Center Transition in Turbines p 69-79 Jul. 1985 refs
(Contract NAG3-286)
Avail: NTIS HC A10/MF A01 CSCL 20D

Experimental results are presented to document hydrodynamic and thermal development of flat-plate boundary layers undergoing natural transition. Local heat transfer coefficients, skin friction coefficients and profiles of velocity, temperature and Reynolds normal and shear stresses are presented. A case with no transition and transitional cases with 0.68% and 2.0% free-stream disturbance intensities were investigated. The locations of transition are consistent with earlier data. A late-laminar state with significant levels of turbulence is documented. In late-transitional and early-turbulent flows, turbulent Prandtl number and conduction layer thickness values exceed, and the Reynolds analogy factor is less than, values previously measured in fully turbulent flows. Author

N85-31440*# National Aeronautics and Space Administration. Lewis Research Center, Cleveland, Ohio.
A REVIEW AND ANALYSIS OF BOUNDARY LAYER TRANSITION DATA FOR TURBINE APPLICATION
R. E. GAUGLER *In its* Transition in Turbines p 81-93 Jul. 1985 refs Previously announced as N85-10306
Avail: NTIS HC A10/MF A01 CSCL 20D

A number of data sets from the open literature that include heat transfer data in apparently transitional boundary layers, with particular application to the turbine environment, were reviewed and analyzed to extract transition information. The data were analyzed by using a version of the STAN5 two-dimensional boundary layer code. The transition starting and ending points were determined by adjusting parameters in STAN5 until the calculations matched the data. The results are presented as a table of the deduced transition location and length as functions of the test parameters. The data sets reviewed cover a wide range of flow conditions, from low-speed, flat-plate tests to full-scale turbine airfoils operating at simulated turbine engine conditions. The results indicate that free-stream turbulence and pressure gradient have strong, and opposite, effects on the location of the start of transition and on the length of the transition zone.
Author

N85-31441*# National Aeronautics and Space Administration. Lewis Research Center, Cleveland, Ohio.
TURBULENT SOLUTIONS OF EQUATIONS OF FLUID MOTION
R. G. DEISSLER *In its* Transition in Turbines p 95-160 Jul. 1985 refs Repr. from Rev. of Modern Phys., v. 56, no. 1, pt. 1, Apr. 1984 Previously announced in IAA as A84-41156
Avail: NTIS HC A10/MF A01 CSCL 20D

Some turbulent solutions of the unaveraged Navier-Stokes equations (equations of fluid motion) are reviewed. Those equations are solved numerically in order to study the nonlinear physics of incompressible turbulent flow. The three components of the

mean-square velocity fluctuations are initially equal for the conditions chosen. The resulting solutions show characteristics of turbulence, such as the linear and nonlinear excitation of small-scale fluctuations. For the stronger fluctuations the initially nonrandom flow develops into an apparently random turbulence. The cases considered include turbulence that is statistically homogeneous or inhomogeneous and isotropic or anisotropic. A statistically steady-state turbulence is obtained by using a spatially periodic body force. Various turbulence processes, including the transfer of energy between eddy sizes and between directional components and the production, dissipation, and spatial diffusion of turbulence, are considered. It is concluded that the physical processes occurring in turbulence can be profitably studied numerically. B.W.

N85-31443*# *National Aeronautics and Space Administration.* Lewis Research Center, Cleveland, Ohio.
REVERBERATION EFFECTS ON DIRECTIONALITY AND RESPONSE OF STATIONARY MONOPOLE AND DIPOLE SOURCES IN A WIND TUNNEL
K. J. BAUMEISTER 1985 38 p refs To be presented at the Winter Ann. Meeting of the ASME, Miami Beach, Fla., 17-21 Nov. 1985
(NASA-TM-87063; E-2432; NAS 1.15:87063) Avail: NTIS HC A03/MF A01 CSCL 20D

Analytical solutions for the three dimensional inhomogeneous wave equation with flow in a hardwall rectangular wind tunnel and in the free field are presented for a stationary monopole noise source. Dipole noise sources are calculated by combining two monopoles 180 deg out of phase. Numerical calculations for the modal content, spectral response and directivity for both monopole and dipole sources are presented. In addition, the effect of tunnel alterations, such as the addition of a mounting plate, on the tunnels reverberant response are considered. In the frequency range of practical importance for the turboprop response, important features of the free field directivity can be approximated in a hardwall wind tunnel with flow if the major lobe of the noise source is not directed upstream. However, for an omnidirectional source, such as a monopole, the hardwall wind tunnel and free field response are not comparable. Author

N85-31444*# National Aeronautics and Space Administration. Lewis Research Center, Cleveland, Ohio.
HEAT TRANSFER IN AEROPROPULSION SYSTEMS
R. J. SIMONEAU 1985 37 p refs To be presented at the 1985 US-Japan Heat Transfer Joint Seminar, San Diego, Calif., 17-20 Sep. 1985; sponsored in part by NSF and Japan Society for the Promotion of Science
(NASA-TM-87066; E-2634; NAS 1.15:87066) Avail: NTIS HC A03/MF A01 CSCL 20D

Aeropropulsion heat transfer is reviewed. A research methodology based on a growing synergism between computations and experiments is examined. The aeropropulsion heat transfer arena is identified as high Reynolds number forced convection in a highly disturbed environment subject to strong gradients, body forces, abrupt geometry changes and high three dimensionality - *all in an unsteady flow field. Numerous examples based on heat* transfer to the aircraft gas turbine blade are presented to illustrate the types of heat transfer problems which are generic to aeropropulsion systems. The research focus of the near future in aeropropulsion heat transfer is projected. E.A.K.

N85-31445*# Stanford Univ., Palo Alto, Calif. Dept. of Mechanical Engineering.
VELOCITY VISUALIZATION IN GASEOUS FLOWS Final Report
R. K. HANSON Jul. 1985 17 p refs
(Contract NAS3-285)
(NASA-CR-174954; NAS 1.26:174954) Avail: NTIS HC A02/MF A01 CSCL 20D

Techniques are established for visualizing velocity in gaseous flows. Two approaches are considered, both of which are capable of yielding velocity simultaneously at a large number of flowfield locations, thereby providing images of velocity. The first technique employs a laser to mark specific fluid elements and a camera to track their subsequent motion. Marking is done by laser-induced phosphorescence of biacetyl, added as a tracer species in a flow of N2, or by laser-induced formation of sulfur particulates in SF6-H2-N2 mixtures. The second technique is based on the Doppler effect, and uses an intensified photodiode array camera and a planar form of laser-induced fluorescence to detect 2-d velocities of I2 (in I2-N2 mixtures) via Doppler-shifted absorption of narrow-linewidth laser radiation at 514.5 nm. Author

N85-33433* *National Aeronautics and Space Administration.* Lewis Research Center, Cleveland, Ohio.
VORTEX GENERATING FLOW PASSAGE DESIGN FOR INCREASED FILM COOLING EFFECTIVENESS Patent
S. S. PAPELL, inventor (to NASA) 16 Jul. 1985 8 p Filed 15 Feb. 1984 Supersedes N84-20782 (22 - 11, p 1652)
(NASA-CASE-LEW-14039-1; US-PATENT-4,529,358; US-PATENT-APPL-SN-580419; US-PATENT-CLASS-416-97A; US-PATENT-CLASS-415-115) Avail: US Patent and Trademark Office CSCL 20D

It is an object of the invention to provide a film cooling apparatus of increased effectiveness and efficiency. In accordance with the invention, a cooling fluid is injected into a hot flowing gas through a passageway in a wall which contains and is subject to the hot gas. The passageway is slanted in a downstream direction at an acute angle to the wall. A cusp shape is provided in the passageway to generate vortices in the injected cooling fluid thereby reducing the energy extracted from the hot gas for that purpose. The cusp shape increases both film cooling effectiveness and wall area coverage. The cusp may be at either the downstream or upstream side of the passageway, the former substantially eliminating flow separation of the cooling fluid from the wall immediately downstream of the passageway.
Official Gazette of the U.S. Patent and Trademark Office

N85-33435*# National Aeronautics and Space Administration. Lewis Research Center, Cleveland, Ohio.
LOCAL HEAT-TRANSFER MEASUREMENTS ON A LARGE, SCALE-MODEL TURBINE BLADE AIRFOIL USING A COMPOSITE OF A HEATER ELEMENT AND LIQUID CRYSTALS
S. A. HIPPENSTEELE, L. M. RUSSELL, and F. J. TORRES 1985 21 p refs Presented at the 30th Intern. Gas Turbine Conf. and Exhibit, Houston, Tex., 17-21 Mar. 1985; sponsored by ASME
(NASA-TM-86900; E-2347; NAS 1.15:86900) Avail: NTIS HC A02/MF A01 CSCL 20D

Local heat transfer coefficients were experimentally mapped along the midchord of a five-time-size turbine blade airfoil in a static cascade operated at room temperature over a range of Reynolds numbers. The test surface consisted of a composite of commercially available materials: a mylar sheet with a layer of cholesteric liquid crystals, that change color with temperature, and a heater sheet made of a carbon-impregnated paper, that produces uniform heat flux. After the initial selection and calibration of the composite sheet, accurate, quantitative, and continuous heat transfer coefficients were mapped over the airfoil surface. The local heat transfer coefficients are presented for Reynolds numbers from 2.8 x 10 to the 5th power to 7.6 x 10 to the 5th power. Comparisons are made with analytical values of heat transfer coefficients obtained from the STAN5 boundary layer code. Also, a leading edge separation bubble was revealed by thermal and flow visualization. Author

N85-33453# Kentucky Univ., Lexington. Inst. for Mining and Minerals Research.
SOLIDS MIXING IN A THREE PHASE FLUIDIZED BED CONTAINING SPHERICALLY SHAPED-POROUS SOLID PARTICLES
G. J. SNELL and D. ZOPFF May 1984 53 p refs Sponsored by Kentucky Energy Cabinet
(PB85-187961; IMMR84-098) Avail: NTIS HC A04/MF A01
CSCL 07A

Solids mixing a 3 phase fluidized bed containing 1.8 mm nominal diameter porous spherically shaped solids was studied using a batch type tracer technique. High speed photography was used to determine concentration time traces of color code solid tracer in a region near the wall of a 2 in. i.d. fluidization tube, located at a vertical elevation about 7 in. above the distributor. An add mixture of water and gaseous nitrogen at room temperature and essentially ambient pressure was used to fluidize a spherically shaped, nickel molybdate on alumina solid phase throughout this study. An empirical steady state mixing time was defined in order to characterize top to bottom of bed solids mixing. This mixing index was in turn correlated with superficial liquid velocity, superficial gas velocity, and an axial characteristic dimension. GRA

35

INSTRUMENTATION AND PHOTOGRAPHY

Includes remote sensors; measuring instruments and gages; detectors; cameras and photographic supplies; and holography.

A85-10034* Aerodyne Research, Inc., Billerica, Mass.
AN APPROACH FOR AUTOMATED ANALYSIS OF PARTICLE HOLOGRAMS
A. C. STANTON, H. J. CAULFIELD, and G. W. STEWART (Aerodyne Research, Inc., Billerica, MA) Optical Engineering (ISSN 0091-3286), vol. 23, Sept.-Oct. 1984, p. 577-582. refs
(Contract NAS3-24094)

A simple method for analyzing droplet holograms is proposed that is readily adaptable to automation using modern image digitizers and analyzers for determination of the number, location, and size distributions of spherical or nearly spherical droplets. The method determines these parameters by finding the spatial location of best focus of the droplet images. With this location known, the particle size may be determined by direct measurement of image area in the focal plane. Particle velocity and trajectory may be determined by comparison of image locations at different instants in time. The method is tested by analyzing digitized images from a reconstructed in-line hologram, and the results show that the method is more accurate than a time-consuming plane-by-plane search for sharpest focus. C.D.

A85-10035* Aerometrics, Inc., Mountain View, Calif.
PHASE/DOPPLER SPRAY ANALYZER FOR SIMULTANEOUS MEASUREMENTS OF DROP SIZE AND VELOCITY DISTRIBUTIONS
W. D. BACHALO and M. J. HOUSER (Aerometrics, Inc., Mountain View, CA) Optical Engineering (ISSN 0091-3286), vol. 23, Sept.-Oct. 1984, p. 583-590. refs
(Contract NAS3-23684)

Research was conducted on a laser light scatter detection method for measuring the size and velocity of spherical particles. The method is based upon the measurement of the interference fringe pattern produced by spheres passing through the intersection of two laser beams. A theoretical analysis of the method was carried out using the geometrical optics theory. The instrument response function was determined to be linear with drop size. Experimental verification of the theory was obtained by using monodisperse droplet streams. Several optical configurations were tested to identify all of the parametric effects upon the size measurements. Both off-axis forward-scatter and back-scatter light detection were utilized. Simulated spray environments and fuel spray nozzles were used in the evaluation of the method. The measurements of the monodisperse drops showed complete agreement with the theoretical predictions. The method was demonstrated to be independent of the beam intensity and extinction resulting from the surrounding drops. An instrument based on the concept has been developed. Author

A85-10036* Spectron Development Labs., Inc., Costa Mesa, Calif.
SPRAY CHARACTERIZATION WITH A NONINTRUSIVE TECHNIQUE USING ABSOLUTE SCATTERED LIGHT
C. F. HESS and V. E. ESPINOSA (Spectron Development Laboratories, Inc., Costa Mesa, CA) Optical Engineering (ISSN 0091-3286), vol. 23, Sept.-Oct. 1984, p. 604-609. refs
(Contract F49620-83-C-0060; NAS3-23538)

A technique to measure the size and velocity of particles is discussed, and results are presented. In this technique two small laser beams of one color identify the center of a laser beam of a different color. This defines a region of almost uniform intensity where the light scattered by the individual particles can be related to their sizes. A variation of this technique that uses two polarizations of the same color of laser beam is also presented. Results are presented for monodisperse, bimodal, trimodal, and polydisperse sprays produced by the Berglund-Liu droplet generator and a pressure nozzle. Size distributions obtained at three different ranges for the same spray show excellent self-consistency in the overlapping regions. Measurements of a spray of known characteristics exhibit errors in the order of 10 percent. Author

A85-11100*# National Aeronautics and Space Administration. Lewis Research Center, Cleveland, Ohio.
EDDY CURRENT JET ENGINE DISK-CRACK MONITOR
J. P. BARRANGER (NASA, Lewis Research Center, Cleveland, OH) Materials Evaluation (ISSN 0025-5327), vol. 42, Oct. 1984, p. 1374-1378.

A disk-crack monitor is described that is suitable for use on the ground or in flight. The system consists of an engine-mounted eddy current sensor, a series capacitance in each leg of the sensor circuit, and a capacitance-conductance bridge followed by an oscilloscope capable of advanced signal processing. It was applied to the detection of service-induced cracks in the first-stage turbine wheel of a helicopter engine. A 3.5 mm long radial fatigue crack plus smaller cracks, all located in the blade root region of the wheel, were detected during engine test stand operation at ground idle speed and temperature. The calculation of the value of series capacitance is also presented. Author

A85-16794* Spectron Development Labs., Inc., Costa Mesa, Calif.
NONINTRUSIVE OPTICAL SINGLE-PARTICLE COUNTER FOR MEASURING THE SIZE AND VELOCITY OF DROPLETS IN A SPRAY
C. F. HESS (Spectron Development Laboratories, Inc., Costa Mesa, CA) Applied Optics (ISSN 0003-6935), vol. 23, Dec. 1, 1984, p. 4375-4382. refs
(Contract NAS3-23538; F49620-83-C-0060)

A technique for measuring nonintrusively, and in real time, the size and velocity of droplets in a spray is presented. A small beam identifies the center of a larger beam, thus defining a region of almost uniform intensity, and only droplets crossing through such a center are measured. The size is obtained from the absolute scattered light and the velocity from the modulated signal produced by the interferometric pattern. A self-calibrating algorithm is also discussed. Results are presented for a spray of predictable chracteristics. Author

A85-21695* Stanford Univ., Calif.
VELOCITY VISUALIZATION IN GAS FLOWS USING LASER-INDUCED PHOSPHORESCENCE OF BIACETYL
B. HILLER, R. A. BOOMAN, C. HASSA, and R. K. HANSON (Stanford University, Stanford, CA) Review of Scientific Instruments (ISSN 0034-6748), vol. 55, Dec. 1984, p. 1964-1967. refs
(Contract F49620-83-K-0004; NAG3-285)

Visualization of a two-dimensional velocity field by means of laser-induced phosphorescence is demonstrated in a nitrogen flow at room temperature. A pulsed dye laser is used to excite seeded biacetyl molecules along a line in the flow. Two successive exposures of the emitted phosphorescence are recorded with an intensified 100 x 100 element photodiode array camera. Velocities are determined from the distance traveled in the time interval between exposures. Important factors in connection with the phosphorescence of biacetyl are discussed. Author

A85-24464* National Aeronautics and Space Administration. Lewis Research Center, Cleveland, Ohio.
REMOTE DISPLACEMENT MEASUREMENTS USING A LASER DIODE
G. BEHEIM (NASA, Lewis Research Center, Cleveland, OH) and K. FRITSCH (John Carroll University, Cleveland, OH) Electronics Letters (ISSN 0013-5194), vol. 21, Jan. 31, 1985, p. 93, 94.

A technique for measuring displacements remotely to minimum distances of 8 mm with a resolution of 2 microns is described. A dynamic interferometer method is employed using a frequency-ramped laser diode. A direct measurement of the period of the resulting beat signal is used to determine the displacement. Author

A85-28820*# National Aeronautics and Space Administration. Lewis Research Center, Cleveland, Ohio.
RAINBOW SCHLIEREN VS MACH-ZEHNDER INTERFEROMETER - A COMPARISON
W. L. HOWES (NASA, Lewis Research Center, Cleveland, OH) Applied Optics (ISSN 0003-6935), vol. 24, March 15, 1985, p. 816-822. refs

The rainbow schlieren apparatus is simpler, cheaper, and more easily built to large scale than the interferometer. The accuracies of the two instruments are similar but only if refraction is properly accounted for in interferometry. The measurement thresholds of both instruments are similar. The rainbow schlieren device provides more detailed information because the detection threshold of the rainbow schlieren is an order of magnitude better than that of the interferometer. Author

A85-29562* Michigan State Univ., East Lansing.
CLOSED-LOOP STRAIN CONTROLLED TESTING AT ELEVATED TEMPERATURES WITH A NON-CONTACTING GAGE
J. F. MARTIN and B. E. SCHULTZ (Michigan State University, East Lansing, MI) IN: International Instrumentation Symposium, 29th, Albuquerque, NM, May 2-6, 1983, Proceedings . Research Triangle Park, NC, Instrument Society of America, 1983, p. 237-240.
(Contract NAG3-51)

Normal strains were measured over a 100 micron gage length at a distance of 50 microns from the edge of a notch using a non-contacting, laser-based interferometric technique. Tests were performed at 600 C under direct strain control from this interferometric 'micro-gage'. A minicomputer system, that produced a voltage analog of strain as a final output, controlled the strain measuring apparatus. This analog output was used directly as the feedback signal to a closed-loop, electrohydraulic mechanical test system. This allowed both strain rate and strain amplitude to be controlled at the notch root of the specimen. Author

A85-29563* United Technologies Research Center, East Hartford, Conn.
FIBER OPTIC TEMPERATURE SENSOR
W. W. MOREY, W. H. GLENN, and E. SNITZER (United Technologies Research Center, East Hartford, CT) IN: International Instrumentation Symposium, 29th, Albuquerque, NM, May 2-6, 1983, Proceedings . Research Triangle Park, NC, Instrument Society of America, 1983, p. 261-274.
(Contract NAS3-21841; N00163-81-C-0071)

A temperature sensor has been developed that utilizes the temperature dependent absorption of a rare earth doped optical fiber. The temperature measurement is localized at a remote position by splicing a short section of the rare earth fiber into a loop of commercial data communication fiber that sends and returns an optical probe signal to the temperature sensitive section of fiber. The optical probe signal is generated from two different wavelength filtered LED sources. A four port fiber optic coupler combines the two separate wavelength signals into the fiber sensing loop. Time multiplexing is used so that each signal wavelength is present at a different time. A reference signal level measurement is also made from the LED sources and a ratio taken with the sensor signal to produce a transmission measurement of the fiber loop. The transmission is affected differently at each wavelength by the rare earth temperature sensitive fiber. The temperature is determined from a ratio of the two transmission measurements. This method eliminates any ambiguity with respect to changes in signal level in the fiber loop such as mating and unmating optical connectors. The temperature range of the sensor is limited to about 800 C by the temperature limit fo the feed fibers. Author

A85-31113* Stanford Univ., Calif.
FAST LASER-INDUCED AEROSOL FORMATION FOR VISUALIZATION OF GAS FLOWS
C. HASSA and R. K. HANSON (Stanford University, Stanford, CA) Review of Scientific Instruments (ISSN 0034-6748), vol. 56, April 1985, p. 557-559. refs
(Contract NAG3-285; F49620-83-K-0004)

A technique for aerosol seeding of gas flows by laser-induced particle formation is demonstrated using a pulsed Nd:YAG laser (1.06 microns) for optical breakdown of a mixture of SF6 and H2 in an inert carrier gas. It is noted that, contrary to the smoke-wire approach, the laser-induced particles form first in zones of high turbulence, since mixing enhances coagulation. The method also allows seeding to be performed in locations hardly accessible otherwise and is mechanically nonintrusive. Finally, a study of the mixture and the breakdown effects indicates that for H2:SF6 ratios between 3:1 and 15:1 the particle formation is only limited by the physics of the gas/particle conversion. L.T.

A85-32294* Stanford Univ., Calif.
TWO-FREQUENCY LASER-INDUCED FLUORESCENCE TECHNIQUE FOR RAPID VELOCITY-FIELD MEASUREMENTS IN GAS FLOWS
B. HILLER and R. K. HANSON (Stanford University, Stanford, CA) Optics Letters (ISSN 0146-9592), vol. 10, May 1985, p. 206-208. refs
(Contract NAG3-285; F49620-83-K-0004)

A technique is presented for measurements of two-dimensional velocity fields in gas flows. The single-mode frequency of an argon-ion laser is fixed in the wing of an absorption line of iodine molecules that are seeded at low level in the flow of interest. The emitted fluorescence is detected with an image-intensified 100 x 100 photodiode-array camera. two pairs of counterpropagating laser sheets sequentially probe the flow to determine two velocity components. The frequency in one pair is shifted with respect to the other by an acousto-optic modulator. This two-frequency scheme eliminates the need to determine the slope of the line externally and offers the potential for combined pressure and velocity-field measurements. Author

A85-36726* National Aeronautics and Space Administration. Lewis Research Center, Cleveland, Ohio.
ELECTRONIC HETERODYNE READOUT OF FRINGES IN MOIRE DEFLECTOMETRY
J. STRICKER (NASA, Lewis Research Center, Cleveland, OH; Technion Israel Institute of Technology, Haifa, Israel) Optics Letters (ISSN 0146-9592), vol. 10, June 1985, p. 247-249. refs

An electronic heterodyne technique is described for the readout of fringes in moire deflectometry. The technique is based on phase measurements of signals generated by a photodetector observing the light transmitted through a traveling moire fringe pattern. The phase of the signal is proportional to the fringe deviation and thus to the deflection angle of the light ray. The phase is measured on line by a standard phase meter with an accuracy of 1 deg or 1:360 of a fringe. The technique, which is precise and sensitive, is demonstrated by detecting and measuring a fringe shift of 0.15 mm corresponding to 0.029 of a fringe. Author

A85-37704*# National Aeronautics and Space Administration. Lewis Research Center, Cleveland, Ohio.
THE INFINITE LINE PRESSURE PROBE
D. R. ENGLUND (NASA, Lewis Research Center, Cleveland, OH) and W. B. RICHARDS (Oberlin College, Oberlin, OH) (Instrument Society of America, International Instrumentation Symposium, 30th, Denver, CO, May 7-10, 1984) ISA Transactions (ISSN 0019-0578), vol. 24, no. 2, 1985, p. 11-19. Previously announced in STAR as N84-19787. refs

The infinite line pressure probe provides a means for measuring high frequency fluctuating pressures in difficult environments. A properly designed infinite line probe does not resonate; thus its frequency response is not limited by acoustic resonance in the probe tubing, as in conventional probes. The characteristics of infinite line pressure probes are reviewed and some applications in turbine engine research are described. A probe with a flat-oval cross section, permitting a constant-impedance pressure transducer installation, is described. Techniques for predicting the frequency response of probes with both circular and flat-oval cross sections are also cited. Author

A85-39796*# National Aeronautics and Space Administration. Lewis Research Center, Cleveland, Ohio.
TRANSIENT TECHNIQUE FOR MEASURING HEAT TRANSFER COEFFICIENTS ON STATOR AIRFOILS IN A JET ENGINE ENVIRONMENT
H. J. GLADDEN and M. P. PROCTOR (NASA, Lewis Research Center, Cleveland, OH) AIAA, SAE, ASME, and ASEE, Joint Propulsion Conference, 21st, Monterey, CA, July 8-10, 1985. 12 p. Previously announced in STAR as N85-25794. refs
(AIAA PAPER 85-1471)

A transient technique was used to measure heat transfer coefficients on stator airfoils in a high-temperature annular cascade at real engine conditions. The transient response of thin film thermocouples on the airfoil surface to step changes in the gas stream temperature was used to determine these coefficients. In addition, gardon gages and paired thermocouples were also utilized to measure heat flux on the airfoil pressure surface at steady state conditions. The tests were conducted at exit gas stream Reynolds numbers of one-half to 1.9 million based on true chord. The results from the transient technique show good comparison with the steady-state results in both trend and magnitude. In addition, comparison is made with the STAN5 boundary layer code and shows good comparison with the trends. However, the magnitude of the experimental data is consistently higher than the analysis. Author

A85-39835*# Cleveland State Univ., Ohio.
INCIDENT BEAM POLARIZATION FOR LASER DOPPLER VELOCIMETRY EMPLOYING A SAPPHIRE CYLINDRICAL WINDOW
J. A. LOCK (Cleveland State University, Cleveland, OH) and H. J. SCHOCK (NASA, Lewis Research Center, Cleveland, OH) Applied Optics (ISSN 0003-6935), vol. 24, July 1, 1985, p. 1987-1995. refs

For laser Doppler velocimetry studies employing sapphire windows as optical access ports, the birefringency of sapphire produces an extra beam intersection volume which serves to effectively smear the acquired velocity flow field data. It is shown that for a cylindrical window geometry, the extra beam intersection volume may be eliminated with minimal decrease in the fringe visibility of the remaining intersection volume by suitably orienting the polarizations of the initial laser beams. For horizontally incident beams, these polarizations were measured at three intersection locations within the cylinder. It was found that the measured polarization angles agreed with the theoretical predictions. Author

A85-41634* National Aeronautics and Space Administration. Lewis Research Center, Cleveland, Ohio.
CALIBRATION STABILITY OF SOME HOT-CATHODE ION GAUGES
I. WARSHAWSKY (NASA, Lewis Research Center, Cleveland, OH) Journal of Vacuum Science and Technology A (ISSN 0734-2101), vol. 3, Mar.-Apr. 1985, p. 430-432. refs

Data are presented on the stability of calibration of some hot-cathode ion gauges: a conventional triode used in the range of 0.0002-0.2 Pa, and Bayard-Alpert-type gauges used in the range of 0.0002-0.02 Pa. Numerical magnitudes are given of the systematic corrections that must be applied to the gauge indication in order to achieve the highest accuracy of pressure indication. The relative sensitivities of these gauges to Ar, N2, Ne, and He are also given. Author

A85-42854*# National Aeronautics and Space Administration. Lewis Research Center, Cleveland, Ohio.
MOIRE DEFLECTOMETRY WITH DEFERRED ELECTRONIC HETERODYNE READOUT
J. STRICKER (NASA, Lewis Research Center, Cleveland, OH) Applied Optics (ISSN 0003-6935), vol. 24, Aug. 1, 1985, p. 2298, 2299. refs

The electronic heterodyne technique is applied to the task of deferred readout of phase objects' moire fringes. In combination with the heterodyne readout technique, moire deflectometry constitutes a powerful tool for the study of phase objects, exhibiting high sensitivity, ease of automation and recording, low cost, use of incoherent illumination, and independence from fringe contrast variations. O.C.

A85-42857*# National Aeronautics and Space Administration. Lewis Research Center, Cleveland, Ohio.
REMOTE DISPLACEMENT MEASUREMENT USING A PASSIVE INTERFEROMETER WITH A FIBER-OPTIC LINK
G. BEHEIM (NASA, Lewis Research Center, Cleveland, OH) Applied Optics (ISSN 0003-6935), vol. 24, Aug. 1, 1985, p. 2335-2340. refs

Remote displacement measurement is demonstrated using a Fabry-Perot cavity with a multimode optical fiber link. The sensing cavity modulates, as a function of its length, the spectrum of a light-emitting diode (LED). The light returns via the fiber and is analyzed by a tunable reference cavity. A closed-loop control causes the reference cavity to track the sensing cavity length within 2 x 10 to the -12th m. Displacement range is 2 x 10 to the -6th m. The reference cavity length is measured interferometrically, using a laser, to obtain the sensing cavity length. Advantages of this sensing technique include compatibility with multimode fiber-optic components, high immunity to optical losses, and large dynamic range. Author

A85-46607* Babcock and Wilcox Co., Alliance, Ohio.
HIGH-TEMPERATURE FIBER OPTIC PRESSURE SENSOR
J. W. BERTHOLD (Babcock and Wilcox Co., Research and Development Div., Alliance, OH) IN: International Instrumentation Symposium, 30th, Denver, CO, May 7-10, 1984, Proceedings . Research Triangle Park, NC, ISA, 1984, p. 85-94. refs
(Contract NAS3-23712)

Attention is given to a program to develop fiber optic methods to measure diaphragm deflection. The end application is intended for pressure transducers capable of operating to 540 C. In this paper are reported the results of a laboratory study to characterize the performance of the fiber-optic microbend sensor. The data presented include sensitivity and spring constant. The advantages and limitations of the microbend sensor for static pressure measurement applications are described. A proposed design is presented for a 540 C pressure transducer using the fiber optic microbend sensor. Author

A85-46925* Yale Univ., New Haven, Conn.
POLARIZATION (ELLIPSOMETRIC) MEASUREMENTS OF LIQUID CONDENSATE DEPOSITION AND EVAPORATION RATES AND DEW POINTS IN FLOWING SALT/ASH-CONTAINING COMBUSTION GASES
K. SESHADRI and D. E. ROSNER (Yale University, New Haven, CT) Combustion and Flame (ISSN 0010-2180), vol. 61, Sept. 1985, p. 251-260. refs
(Contract NSG-3169; AF-AFOSR-84-0034)

An application of an optical polarization technique in a combustion environment is demonstrated by following, in real-time, growth rates of boric oxide condensate on heated platinum ribbons exposed to seeded propane-air combustion gases. The results obtained agree with the results of earlier interference measurements and also with theoretical chemical vapor deposition predictions. In comparison with the interference method, the polarization technique places less stringent requirements on surface quality, which may justify the added optical components needed for such measurements. V.L.

A85-48659* Minnesota Univ., Minneapolis.
HOLOGRAPHIC OPTICAL SYSTEM FOR ABERRATION CORRECTIONS IN LASER DOPPLER VELOCIMETRY
R. C. KIM, S. K. CASE (Minnesota, University, Minneapolis), and H. J. SCHOCK (NASA, Lewis Research Center, Cleveland, OH) Optical Engineering (ISSN 0091-3286), vol. 24, Sept.-Oct. 1985, p. 786-790. refs

An optical system containing multifaceted holographic optical elements (HOEs) has been developed to correct for aberrations introduced by nonflat windows in laser Doppler velocimetry. The multifacet aberration correction approach makes it possible to record on one plate many sets of adjacent HOEs that address different measurement volume locations. By using 5-mm-diameter facets, it is practical to place 10-20 sets of holograms on one 10 x 12.5-cm plate, so that the procedure of moving the entire optical system to examine different locations may not be necessary. The holograms are recorded in dichromated gelatin and therefore are nonabsorptive and suitable for use with high-power argon laser beams. Low f-number optics coupled with a 90-percent efficient distortion-correcting hologram in the collection side of the system yield high optical efficiency. V.L.

N85-16096*# National Aeronautics and Space Administration. Lewis Research Center, Cleveland, Ohio.
HIGH TEMPERATURE THERMOCOUPLE AND HEAT FLUX GAUGE USING A UNIQUE THIN FILM-HARDWARE HOT JUNCTURE
C. H. LIEBERT, R. HOLANDA, S. A. HIPPENSTEELE, and C. A. ANDRACCHIO Dec. 1984 29 p refs Proposed for presentation at 30th Intern. Gas Turbine Conf. and Exhibition, Houston, Tex., 17-21 Mar. 1985; sponsored by ASME
(NASA-TM-86898; E-2365; NAS 1.15:86898) Avail: NTIS HC A03/MF A01 CSCL 14B

A special thin film-hardware material thermocouple (TC) and heat flux gauge concept for a reasonably high temperature and high flux flat plate heat transfer experiment was fabricated and tested to gauge temperatures of 911 K. This concept was developed for minimal disturbance of boundary layer temperature and flow over the plates and minimal disturbance of heat flux through the plates. Comparison of special heat flux gauge Stanton number output at steady-state conditions with benchmark literature data was good and agreement was within a calculated uncertainty of the measurement system. Also, good agreement of special TC and standard TC outputs was obtained and the results are encouraging. Oxidation of thin film thermoelements was a primary failure mode after about 5 of operation. Author

N85-16099*# National Aeronautics and Space Administration. Lewis Research Center, Cleveland, Ohio.
EFFECT OF FIVE LUBRICANTS ON LIFE OF AISI 9310 SPUR GEARS
D. P. TOWNSEND and E. V. ZARETSKY Jan. 1985 15 p refs
(NASA-TP-2419; E-2183; NAS 1.60:2419) Avail: NTIS HC A02/MF A01 CSCL 13I

Spur-gear surface fatigue tests were conducted with five lubricants using a single lot of consumable-electrode vacuum melted (CVM) AISI 9310 spur gears. The lot of gears was divided into five groups, each of which was tested with a different lubricant. The test lubricants are classified as either a synthetic hydrocarbon, mineral oil, or ester-based lubricant. All five lubricants have imilar viscosity and pressure-viscosity coefficients. A pentaerythritol base stock without sufficient antiwear additives produced a surface fatigue life pproximately 22 percent that of the same base stock with chlorine and phosphorus type additives. The presence of sulfur type antiwear additives in the lubricant did not appear to affect the surface fatigue life of the gears tested. No statistical difference in the 10-percent surface fatigue life was produced with four of the five lubricants. Author

N85-16100*# National Aeronautics and Space Administration. Lewis Research Center, Cleveland, Ohio.
INTEGRATED EXHAUST GAS ANALYSIS SYSTEM FOR AIRCRAFT TURBINE ENGINE COMPONENT TESTING
R. L. SUMMERS and R. C. ANDERSON Jan. 1985 28 p refs
(NASA-TP-2424; E-2302; NAS 1.60:2424) Avail: NTIS HC A03/MF A01 CSCL 14B

An integrated exhaust gas analysis system was designed and installed in the hot-section facility at the Lewis Research Center. The system is designed to operate either manually or automatically and also to be operated from a remote station. The system measures oxygen, water vapor, total hydrocarbons, carbon monoxide, carbon dioxide, and oxides of nitrogen. Two microprocessors control the system and the analyzers, collect data and process them into engineering units, and present the data to the facility computers and the system operator. Within the design of this system there are innovative concepts and procedures that are of general interest and application to other gas analysis tasks. Author

N85-21604*# Spectron Development Labs., Inc., Costa Mesa, Calif.
RESEARCH STUDY OF DROPLET SIZING TECHNOLOGY LEADING TO THE DEVELOPMENT OF AN ADVANCED DROPLET SIZING SYSTEM Final Report
C. F. HESS, A. E. SMART, and V. E. ESPINOSA Jan. 1985 88 p refs
(Contract NAS3-23538)
(NASA-CR-174839; NAS 1.26:174839) Avail: NTIS HC A05/MF A01 CSCL 14B

An instrument to measure the size and velocity of droplets was developed. The instrument uses one of two techniques, as appropriate. In the first technique two small laser beams of one color identify the center of a larger laser beam of a different color. This defines a region of almost uniform intensity where the light scattered by the individual droplets can be related to their size. The first technique uses the visibility of a Doppler burst and validates it against the peak intensity of the signal's pedestal.

Results are presented for monodisperse, bimodal, trimodal, and polydisperse sprays produced by the Berglund-Liu droplet generator and a pressure nozzle. Size distributions of a given spray obtained using three different size ranges show excellent self-consistency in the overlapping region. Measurements of sprays of known characteristics exhibit errors in the order of 10%. The principles of operation and design criteria of the instrument are discussed in great detail. Author

N85-21605*# National Aeronautics and Space Administration. Lewis Research Center, Cleveland, Ohio.
EVALUATION RESULTS OF THE 700 DEG C CHINESE STRAIN GAUGES
H. F. HOBART 1985 11 p refs Presented at the High Temperature Measurements for Experimental Mechanics Conf., Knoxville, Tenn., 27-28 Mar. 1985
(NASA-TM-86973; E-2502; NAS 1.15:86973) Avail: NTIS HC A02/MF A01 CSCL 14B

Gauges fabricated from specially developed Fe-Cr-Al-V-Ti-Y alloy wire in the Republic of China were evaluated for use in static strain measurement of hot gas turbine engines. Gauge factor variation with temperature, apparent strain, and drift were included. Results of gauge factor versus temperature tests show gauge factor decreasing with increasing temperature. The average slope is -3-1/2 percent/100 K, with an uncertainty band of + or - 8 percent. Values of room temperature gauge factor for the Chinese and Kanthal A-1 gauges averaged 2.73 and 2.12, respectively. The room temperature gauge factor of the Chinese gauges was specified to be 2.62. The apparent strain data for both the Chinese alloy and Kanthal A-1 showed large cycle to cycle nonrepeatability. All apparent strain curves had a similar S-shape, first going negative and then rising to positive value with increasing temperatures. The mean curve for the Chinese gauges between room temperature and 100 K had a total apparent strain of 1500 microstrain. The equivalent value for Kanthal A-1 was about 9000 microstrain. Drift tests at 950 K for 50 hr show an average drift rate of about -9 microstrain/hr. Short-term (1 hr) rates are higher, averaging about -40 microstrain for the first hour. In the temperature range 700 to 870 K, however, short-term drift rates can be as high as 1700 microstrain for the first hour. Therefore, static strain measurements in this temperature range should be avoided. A.R.H.

N85-21607# National Bureau of Standards, Gaithersburg, Md.
ADVANCED THIN FILM THERMOCOUPLES
K. G. KREIDER, S. SEMANCIK, and C. OLSON Oct. 1984 85 p refs
(Contract NASA ORDER C-54715-D)
(NASA-CR-175541; NAS 1.26:175541; PB85-132322; NBSIR-84-2949) Avail: NTIS HC A05/MF A01 CSCL 14B

The fabrication, materials characterization, and performance of thin film platinum rhodium thermocouples on gas turbine alloys was investigated. The materials chosen for the study were the turbine blade alloy systems MAR M200+Hf with NiCoCrAlY and FeCrAlY coatings, and vane alloy systems MAR M509 with FeCrAlY. Research was focussed on making improvements in the problem areas of coating substrate stability, adhesion, and insulation reliability and durability. Diffusion profiles between the substrate and coating with and without barrier coatings of Al2O3 are reported. The relationships between fabrication parameters of thermal oxidation and sputtering of the insulator and its characterization and performance are described. The best thin film thermocouples were fabricated with the NiCoCrAlY coatings which were thermally oxidized and sputter coated with Al2O3. GRA

N85-25792*# General Electric Co., Schenectady, N. Y. Corporate Research and Development.
ADVANCED SMOKE METER DEVELOPMENT SURVEY AND ANALYSIS Final Report
R. W. PITZ, C. M. PENNEY, C. M. STANFORTH, and W. M. SHAFFERNOCKER Nov. 1984 59 p refs
(Contract NAS3-23532)
(NASA-CR-168287; NAS 1.26:168287) Avail: NTIS HC A04/MF A01 CSCL 14B

Ideal smoke meter characteristics are determined to provide a basis for evaluation of candidate systems. Five promising techniques are analyzed in detail to evaluate compilance with the practical smoke meter requirements. Four of the smoke measurement concepts are optical methods: Modulated Transmission (MODTRAN), Cross Beam Absorption Counter (CBAC), Laser Induced Incandescence (LIN), and Photoacoustic Spectroscopy (PAS). A rapid response filter instrument called a Taper Element Oscillating Microbalance (TEOM) is also evaluated. For each technique, the theoretical principles are described, the expected performance is determined, and the advantages and disadvantages are discussed The expected performance is evaluated against each of the smoke meter specifications, and the key questions for further study are given. The most promising smoke meter technique analyzed was MODTRAN, which is a variation on a direct transmission measurement. The soot-laden gas is passed through a transmission cell, and the gas pressure is modulated by a speaker. B.W.

N85-25794*# National Aeronautics and Space Administration. Lewis Research Center, Cleveland, Ohio.
TRANSIENT TECHNIQUE FOR MEASURING HEAT TRANSFER COEFFICIENTS ON STATOR AIRFOILS IN A JET ENGINE ENVIRONMENT
H. J. GLADDEN and M. P. PROCTOR 1985 17 p refs Proposed for presentation at the 21st Joint Propulsion Conf., Monterey, Calif., 8-10 Jul. 1985; sponsored by AIAA, SAE and ASME
(NASA-TM-87005; E-2501; NAS 1.15:87005) Avail: NTIS HC A02/MF A01 CSCL 14B

A transient technique was used to measure heat transfer coefficients on stator airfoils in a high-temperature annular cascade at real engine conditions. The transient response of thin film thermocouples on the airfoil surface to step changes in the gas stream temperature was used to determine these coefficients. In addition, gardon gages and paired thermocouples were also utilized to measure heat flux on the airfoil pressure surface at steady state conditions. The tests were conducted at exit gas stream Reynolds numbers of one-half to 1.9 million based on true chord. The results from the transient technique show good comparison with the steady-state results in both trend and magnitude. In addition, comparison is made with the STAN5 boundary layer code and shows good comparison with the trends. However, the magnitude of the experimental data is consistently higher than the analysis. Author

N85-26903*# National Aeronautics and Space Administration. Lewis Research Center, Cleveland, Ohio.
INSTRUMENTATION TECHNOLOGY OVERVIEW Abstract Only
W. C. NIEBERDING *In* NASA. Marshall Space Flight Center Advan. High Pressure O2/H2 Technol. p 599-602 Apr. 1985
Avail: NTIS HC A99/MF E03; SOD HC CSCL 14B

The Instrumentation Technology program advances the state of the art of instrumentation associated with the SSME to improve service life and performance by providing increased measurement capability. Two broad categories of instrumentation technology are sought. The first category includes sensors and systems destined to be used in and on the operational engine either during operation or between operations. These measurements supply information necessary for engine control and/or diagnostics throughout the life of the engine. The second category includes measurement systems and techniques whose application will be to engine component test stands and possibly to the test bed engine. The measurements provide the detailed information necessary to verify

computer models of the performance of the various engine subsystems. E.A.K.

N85-30288*# National Aeronautics and Space Administration. Lewis Research Center, Cleveland, Ohio.
FILTER INDUCED ERRORS IN LASER ANEMOMETER MEASUREMENTS USING COUNTER PROCESSORS
L. G. OBERLE and R. G. SEASHOLTZ 1985 15 p refs To be presented at the Intern. Laser Anemometry Symp., ASME Winter Ann. Meeting, Miami, Fla., 17-21 Nov. 1985
(NASA-TM-87047; E-2609; NAS 1.15:87047) Avail: NTIS HC A02/MF A01 CSCL 14B

Simulations of laser Doppler anemometer (LDA) systems have focused primarily on noise studies or biasing errors. Another possible source of error is the choice of filter types and filter cutoff frequencies. Before it is applied to the counter portion of the signal processor, a Doppler burst is filtered to remove the pedestal and to reduce noise in the frequency bands outside the region in which the signal occurs. Filtering, however, introduces errors into the measurement of the frequency of the input signal which leads to inaccurate results. Errors caused by signal filtering in an LDA counter-processor data acquisition system are evaluated and filters for a specific application which will reduce these errors are chosen. E.A.K.

N85-32302*# National Aeronautics and Space Administration. Lewis Research Center, Cleveland, Ohio.
A COMPARISON OF ELECTRONIC HETERODYNE MOIRE DEFLECTOMETRY AND ELECTRONIC HETERODYNE HOLOGRAPHIC INTERFEROMETRY FOR FLOW MEASUREMENTS
A. J. DECKER and J. STRICKER (Technion - Israel Inst. of Tech.) 1985 19 p refs Proposed for presentation at the Aerospace Technol. Conf. and Exposition, Long Beach, Calif., 14-17 Oct. 1985; sponsored by Society of Automotive Engineers
(NASA-TM-87071; E-2643; NAS 1.15:87071) Avail: NTIS HC A02/MF A01 CSCL 14B

Electronic heterodyne moire deflectometry and electronic heterodyne holographic interferometry are compared as methods for the accurate measurement of refractive index and density change distributions of phase objects. Experimental results are presented to show that the two methods have comparable accuracy for measuring the first derivative of the interferometric fringe shift. The phase object for the measurements is a large crystal of KD*P, whose refractive index distribution can be changed accurately and repeatably for the comparison. Although the refractive index change causes only about one interferometric fringe shift over the entire crystal, the derivative shows considerable detail for the comparison. As electronic phase measurement methods, both methods are very accurate and are intrinsically compatible with computer controlled readout and data processing. Heterodyne moire is relatively inexpensive and has high variable sensitivity. Heterodyne holographic interferometry is better developed, and can be used with poor quality optical access to the experiment. Author

N85-33454# Department of Energy, Washington, D. C.
APPARATUS AND METHOD FOR IDENTIFICATION OF MATRIX MATERIALS IN WHICH TRANSURANIC ELEMENTS ARE EMBEDDED USING THERMAL NEUTRON CAPTURE GAMMA-RAY EMISSION Patent Application
D. A. CLOSE (Los Alamos Scientific Lab.), L. A. FRANKS (Los Alamos Scientific Lab.), and S. M. KOCIMSKI, inventor (to DOE) (Los Alamos Scientific Lab.) 16 Aug. 1984 26 p
(Contract W-7405-ENG-36)
(DE85-011659) Avail: NTIS HC A03/MF A01

An invention is described that enables the quantitative simultaneous identification of the matrix materials in which fertile and fissile nuclides are embedded to be made along with the quantitative assay of the fertile and fissile materials. The invention also enables corrections for any absorption of neutrons by the matrix materials and by the measurement apparatus by the measurement of the prompt and delayed neutron flux emerging from a sample after the sample is interrogated by simultaneously applied neutrons and gamma radiation. High energy electrons are directed at a first target to produce gamma radiation. A second target receives the resulting pulsed gamma radiation and produces neutrons from the interaction with the gamma radiation. These neutrons are slowed by a moderator surrounding the sample and bathe the sample uniformly, generating second gamma radiation in the interaction. The gamma radiation is then resolved and quantitatively detected, providing a spectroscopic signature of the constituent elements contained in the matrix and in the materials within the vicinity of the sample. DOE

N85-33456*# Honeywell, Inc., Lexington, Mass. Aerospace and Defense Group.
MOSAIC INFRARED SENSOR FOR SPACE ASTRONOMY (MIRSSA) Interim Technical Report
Dec. 1983 39 p refs
(Contract NASW-3688)
(NASA-CR-176154; NAS 1.26:176154; H-8407-07) Avail: NTIS HC A03/MF A01 CSCL 14B

The development of mosaic infrared detector/focal plane arrays for space astronomy is reported. The Mosaic IR Sensor for Space Astronomy (MIRSSA) Program is an effort to develop PV HgCdTe detector arrays with the spectral response of up to 5 micron and silicon CCDs for low temperature applications. Desired background-limited performance (BLIP) for space applications requires an extremely high-R sub A product which can be achieved by selecting the detector materials and the operating temperature. The parameters were determined by measurement of HgCdTe PV detector arrays at various temperatures in the SW and MW spectral bands. It is demonstrated that high performance PV HgCdTe detectors can be fabricated for low temperature applications. E.A.K.

N85-33457# Army Armament Research and Development Command, Dover, N. J. Product Assurance Directorate.
AUTOMATIC SPHERICITY INTERFEROMETER FOR TESTING LENS RADII
J. SALERNO Jun. 1985 24 p
(AD-A155736; AD-E401352; ARPAD-TR-85001) Avail: NTIS HC A02/MF A01 CSCL 20F

The majority of lens radii measurements are made with test plates. This technique has the disadvantage of bringing the lens into direct contact with the test plate which can cause scratching of the surface and subsequent rejection of the test unit. In addition, test plate measurements are subjective because they depend on the experience and skill of the operator. As an alternative, an automated interferometric technique was evaluated for its ability to measure lens radii. This method uses a fizeau interferometer with the following accessories: transmission sphere, lens mount, and digital radius slide. This technique, chosen for its ease of operation and noncontact approach, proved to be a more suitable approach to radius measurement than the use of test plates, because it eliminated both the subjectivity and contact associated with the test plates. GRA

N85-35389*# Illinois Univ., Urbana. Dept. of Astronautics and Astronautical Engineering.
THE USE OF A LASER DOPPLER VELOCIMETER IN A STANDARD FLAMMABILITY TUBE Final Report, Jan. 1981 - May 1982
R. A. STREHLOW and E. M. FLYNN May 1985 101 p refs
(Contract NAS3-2266C)
(NASA-CR-174960; NAS 1.26:174960; TR-AAE-85-4; UILU-ENG-85-0504) Avail: NTIS HC A06/MF A01 CSCL 14B

The use of the Laser Doppler Velocimeter, (LDV), to measure the flow associated with the passage of a flame through a standard flammability limit tube (SFLT) was studied. Four major results are presented: (1) it is shown that by using standard ray tracing calculations, the displacement of the LDV volume and the fringe rotation within the experimental error of measurement can be predicted; (2) the flow velocity vector field associated with passage of an upward propagating flame in an SFLT is determined; (3) it is determined that the use of a light interruption technique to

track particles is not feasible; and (4) it is shown that a 25 mW laser is adequate for LDV measurements in the Shuttle or Spacelab. E.A.K.

N85-35391*# Pratt and Whitney Aircraft, East Hartford, Conn. Engineering Div.
DEVELOPMENT OF ADVANCED HIGH-TEMPERATURE HEAT FLUX SENSORS. PHASE 2: VERIFICATION TESTING Final Report
W. H. ATKINSON, M. A. CYR, and R. R. STRANGE Aug. 1985 69 p refs
(Contract NAS3-22133)
(NASA-CR-174973; NAS 1.26:174973; PWA-5914-39) Avail: NTIS HC A04/MF A01 CSCL 14B

A two-phase program is conducted to develop heat flux sensors capable of making heat flux measurements throughout the hot section of gas turbine engines. In Phase 1, three types of heat flux sensors are selected; embedded thermocouple, laminated, and Gardon gauge sensors. A demonstration of the ability of these sensors to operate in an actual engine environment is reported. A segmented liner of each of two combustors being used in the Broad Specification Fuels Combustor program is instrumented with the three types of heat flux sensors then tested in a high pressure combustor rig. Radiometer probes are also used to measure the radiant heat loads to more fully characterize the combustor environment. Test results show the heat flux sensors to be in good agreement with radiometer probes and the predicted data trends. In general, heat flux sensors have strong potential for use in combustor development programs. Author

36

LASERS AND MASERS

Includes parametric amplifiers.

N85-12341*# General Electric Co., Schenectady, N. Y. Corporate Research and Development.
LASER BALANCING SYSTEM FOR HIGH MATERIAL REMOVAL RATES Final Report
M. G. JONES, G. GEORGALAS, and A. L. ORTIZ Oct. 1984 28 p refs
(Contract NAS3-22814)
(NASA-CR-174731; NAS 1.26:174731; REPT-84-SRD-042) Avail: NTIS HC A03/MF A01 CSCL 20E

A laser technique to remove material in excess of 10 mg/sec from a spinning rotor is described. This material removal rate is 20 times greater than previously reported for a surface speed of 30 m/sec. Material removal enhancement was achieved by steering a focused laser beam with moving optics to increase the time of laser energy interaction with a particular location on the circumferential surface of a spinning rotor. A neodymium:yttrium aluminum garnet (Nd:YAG) pulse laser was used in this work to evaluate material removal for carbon steel, 347 stainless steel, Inconal 718, and titanium 6-4. This technique is applicable to dynamic laser balancing. Author

37

MECHANICAL ENGINEERING

Includes auxiliary systems (non-power); machine elements and processes; and mechanical equipment.

A85-11069* National Aeronautics and Space Administration. Lewis Research Center, Cleveland, Ohio.
ELASTOHYDRODYNAMIC LUBRICATION OF LINE CONTACTS
B. J. HAMROCK (NASA, Lewis Research Center, Cleveland, OH) and B. O. JACOBSON (Lulea, Hogskola, Lulea, Sweden) ASLE Transactions, vol. 27, Oct. 1984, p. 275-286; Discussion, p. 286, 287; Author's Closure, p. 287. Previously announced in STAR as N83-16759. refs

An isothermal elastohydrodynamically lubricated rectangular contact was evaluated numerically. This required the simultaneous solution of the elasticity and Reynolds equations. In the elasticity analysis the contact zone was divided into equal rectangular areas, and it was assumed that a uniform pressure was applied over each area. The elastohydrodynamic lubrication theory thus developed was used to investigate the influence of the dimensionless speed, load, and materials parameters on minimum film thickness. Ten cases were used in obtaining the minimum film thickness formula. Plots are shown that indicate the details of the pressure distribution, film shape, and flow. The characteristic pressure spike is clearly in evidence as is the parallel film shape through the central portion of the contact, with a minimum film thickness occurring near the outlet of the contact. S.L.

A85-11074* Akron Univ., Ohio.
AN ANALYSIS OF TEMPERATURE EFFECT IN A FINITE JOURNAL BEARING WITH SPATIAL TILT AND VISCOUS DISSIPATION
M. J. BRAUN (Akron, University, Akron, OH), R. L. MULLEN (Case Western Reserve University, Cleveland, OH), and R. C. HENDRICKS (NASA, Lewis Research Center, Cleveland, OH) ASLE Transactions, vol. 27, Oct. 1984, p. 405-412; Discussion, p. 412; Authors' Closure, p. 412. refs

The analysis presented herein deals with the evaluation of the pressure, velocity, and temperature profiles in a finite-length plane journal bearing. The geometry of the case under study consists of a spatially tilted shaft. The two-dimensional Reynolds equation accounts for the variation of the clearance gap h with x and z and is used to model the pressure field. The latter is solved for a variety of shaft tilt angles and then used to calculate the two-dimensional flow field. Finally, the flow field is used in the energy equation to solve for the film temperature profile, when the effect of viscous dissipation is taken into account. Author

A85-15972* Garrett Turbine Engine Co., Phoenix, Ariz.
CERAMIC COMPONENT DEVELOPMENT FOR THE AGT101 GAS TURBINE ENGINE
W. D. CARRUTHERS and J. R. SMITH (Garrett Turbine Engine Co., Phoenix, AZ) (University of Michigan, American Ceramic Society, General Motors Corp., et al., Automotive Materials Conference, 12th, Ann Arbor, MI, Mar. 14, 15, 1984) Ceramic Engineering and Science Proceedings (ISSN 0196-6219), vol. 5, May-June 1984, p. 350-368.
(Contract DEN3-167)

Under DOE/NASA sponsorship, a team is developing the AGT101, a highly efficient gas turbine engine for automotive application. The regenerated engine will operate at a maximum of 1370 C (2500 F) and 100,000 rpm, and will utilize a variety of Si3N4, SiC, lithium aluminum silicate and ceramic fiber insulation components. Engine design has been performed to consider the fabrication and material characteristics of these ceramic materials for both the static and rotating hot section components. Component fabrication has been performed, components have been screened in thermal and mechanical tests, and initial engine testing has been performed. Author

A85-15973* General Motors Corp., Indianapolis, Ind.
CERAMIC COMPONENTS FOR GAS TURBINE ENGINES
P. W. HEITMAN (General Motors Corp., Allison Gas Turbine Div., Indianapolis, IN) (University of Michigan, American Ceramic Society, General Motors Corp., et al., Automotive Materials Conference, 12th, Ann Arbor, MI, Mar. 14, 15, 1984) Ceramic Engineering and Science Proceedings (ISSN 0196-6219), vol. 5, May-June 1984, p. 369-378. Research supported by the U.S. Department of Energy.
(Contract DEN3-168)

The ceramic component design, manufacturing and inspection technologies under development for the AGT 100 automotive gas turbine promise to meet marketplace cost and performance criteria. Especially consequential developments are noted toward this goal in the case of net and near-net shape component fabrication. Integral turbine rotors, scrolls, combustors, support structures and heat exchangers have been successfully produced and evaluated. Consistency of material properties have yet to be achieved for the processing methods in question, however. O.C.

A85-19085* National Aeronautics and Space Administration. Lewis Research Center, Cleveland, Ohio.
FRICTIONAL AND MORPHOLOGICAL PROPERTIES OF AU-MOS2 FILMS SPUTTERED FROM A COMPACT TARGET
T. SPALVINS (NASA, Lewis Research Center, Cleveland, OH) Thin Solid Films (ISSN 0040-6090), vol. 118, 1984, p. 375-384. Previously announced in STAR as N84-20858. refs

AuMoS2 films 0.02 to 1.2 microns thick were sputtered from target compacted from 5 wt percent Au + 95 wt percent MoS2, to investigate the frictional and morphological film growth characteristics. The gold dispersion effects in MoS2 films are of interest to increase the densification and strengthening of the film structure. Three microstructural growth stages were identified on the nano-micro-macrostructural level. During sliding both sputtered Au-MoS2 and MoS2 films have a tendency to break within the columner region. The remaining or effective film, about 0.2 microns thick, performs the lubrication. The Au-MoS2 films displayed a lower friction coefficient with a high degree of frictional stability and less wear debris generation as compared to pure MoS2 films. The more favorable frictional characteristics of the Au-MoS2 films are attributed to the effective film thickness and the high density packed columner zone which has a reduced effect on the fragmentation of the tapered crystallites during fracture. M.G.

A85-21280*# National Aeronautics and Space Administration. Lewis Research Center, Cleveland, Ohio.
HYDRODYNAMIC LUBRICATION OF RIGID NONCONFORMAL CONTACTS IN COMBINED ROLLING AND NORMAL MOTION
M. K. GHOSH (NASA, Lewis Research Center, Cleveland, OH; Banaras Hindu University, Varanasi, India), B. J. HAMROCK (NASA, Lewis Research Center, Cleveland, OH), and D. BREWE (U.S. Army, Propulsion Laboratory, Cleveland, OH) ASME, Transactions, Journal of Tribology (ISSN 0742-4787), vol. 107, Jan. 1985, p. 97-103. Previously announced in STAR as N84-17592. refs
(ASME PAPER 84-TRIB-13)

A numerical solution to the problem of hydrodynamic lubrication of rigid point contacts with an isoviscous, incompressible lubricant was obtained. The hydrodynamic load-carrying capacity under unsteady (or dynamic) conditions arising from the combined effects of squeeze motion superposed upon the entraining motion was determined for both normal approach and separation. Superposed normal motion considerably increases net load-carrying capacity during normal approach and substantially reduces net load-carrying capacity during separation. Geometry was also found to have a significant influence on the dynamic load-carrying capacity. The ratio of dynamic to steady state load-carrying capacity increases with increasing geometry parameter for normal approach and decreases during separation. The cavitation (film rupture) boundary is also influenced significantly by the normal motion, moving downstream during approach and upstream during separation. For sufficiently high normal separation velocity the rupture boundary may even move upstream of the minimum-film-thickness position. Sixty-three cases were used to derive a functional relationship for the ratio of the dynamic to steady state load-carrying capacity in terms of the dimensionless normal velocity parameter (incorporating normal velocity, entraining velocity, and film thickness) and the geometry parameter. M.G.

A85-21289*# National Aeronautics and Space Administration. Lewis Research Center, Cleveland, Ohio.
FAST NUMERICAL CALCULATIONS OF EHD SLIDING TRACTION FORCES APPLICATION TO ROLLING BEARINGS
L. HOUPERT (NASA, Lewis Research Center, Cleveland, OH; SKF Nederland, Nieuwegein, Netherlands) American Society of Mechanical Engineers and American Society of Lubrication Engineers, Joint Lubrication Conference, San Diego, CA, Oct. 22-24, 1984. 6 p. refs
(ASME PAPER 84-TRIB-26)

Based on analytical calculations assuming isothermal elastohydrodynamic (EHD) lubrication conditions, and on curve-fitting of a thermal correction factor, a new formula is proposed to calculate the sliding traction force developed in a concentrated contact, assuming a nonlinear, viscoelastic lubricant and undirectional sliding. When sliding occurs in the rolling and transverse directions (bidimensional sliding), a simplified numerical method is outlined by which the components of the local shear stress are quickly calculated. The latter method is applied to the calculation of the shear stress and temperature distribution in the ball-raceway contacts of an angular-contact ball bearing. Because of the viscoelastic behavior of the lubricant, a nonzero lateral traction force is obtained. Author

A85-22281* Washington Univ., Seattle.
METALLURGICAL AND MECHANICAL PHENOMENA DUE TO RUBBING OF TITANIUM AGAINST SINTERED POWDER NICHROME
R. ZENAS, T. ARCHBOLD, J. WOLAK, A. F. EMERY, and S. ETEMAD (Washington, University, Seattle, WA) ASLE Transactions, vol. 28, Jan. 1985, p. 97-103. refs
(Contract NAG3-7)

Metallurgical and mechanical changes occurring during high-speed rubbing of Ti-6Al-4V blade specimens against an abradable Nichrome aircraft engine seal material were studied using optical microscopy, electron microscopy, and microhardness techniques. Evidence of temperatures above the beta transus of Ti-6Al-4V (1000 C) and of thermal hardening was found on blade tips that exhibited undesirable abrading characteristics resulting in high forces of interaction, high temperatures, and smearing. The material within the layer of the corresponding seals was found to be work-hardened to a depth of about 0.1 mm and showed evidence of densification extending to a depth of about 0.5 mm below the rubbed surface. Wear particles produced by rub interactions that generated cleanly abraded seal surfaces were found to be several times larger than those produced during interactions which showed evidence of surface smearing and seal densification. Author

A85-23838* Dartmouth Coll., Hanover, N.H.
THERMAL AND THERMOMECHANICAL EFFECTS IN DRY SLIDING
F. E. KENNEDY, JR. (Dartmouth College, Hanover, NH) Wear (ISSN 0043-1648), vol. 100, Dec. 1984, p. 453-476. refs
(Contract NSG-3253; N00014-81-K-0090)

Developments in the study of interrelated thermal and mechanical phenomena in sliding systems are reviewed. The topics reviewed include mechanisms of frictional heating and the distribution of heat during sliding friction, the experimental measurement and analysis of surface and near-surface temperatures resulting from frictional heating, thermal deformation around sliding contacts and the changes in contact geometry caused by thermal deformation and thermoelastic instability, and the thermomechanical stress distribution around the frictionally heated and thermally deformed contact spots. The influence of the thermal and thermomechanical contact phenomena on friction and wear, surface melting, softening, chemical deterioration, and thermocracking are discussed. The phenomena have important

implications in the design and application of sliding or sliding-rolling mechanical components such as dynamic seals, brakes, clutches, plastic bearings, solid or boundary-lubricated bearings, and gears. M.D.

A85-24497*# California State Univ., Long Beach.
INTO MESH LUBRICATION OF SPUR GEARS WITH ARBITRARY OFFSET OIL JET. I - FOR JET VELOCITY LESS THAN OR EQUAL TO GEAR VELOCITY
L. S. AKIN (California State University, Long Beach, CA) and D. P. TOWNSEND (NASA, Lewis Research Center, Cleveland, OH) ASME, Transactions, Journal of Mechanisms, Transmission, and Automation in Design, vol. 105, Dec. 1983, p. 713-718. refs

An analysis was conducted for into mesh oil jet lubrication with an arbitrary offset and inclination angle from the pitch point for the case where the oil jet velocity is equal to or less than pitch line velocity. The analysis includes the case for the oil jet offset from the pitch point in the direction of the pinion and where the oil jet is inclined to intersect the common pitch point. Equations were developed for the minimum oil jet velocity required to impinge on the pinion or gear and the optimum oil jet velocity to obtain the maximum impingement depth. Author

A85-31202* National Aeronautics and Space Administration. Lewis Research Center, Cleveland, Ohio.
THERMAL ELASTOHYDRODYNAMIC LUBRICATION OF LINE CONTACTS
M. K. GHOSH (NASA, Lewis Research Center, Cleveland, OH; Banaras Hindu University, Varanasi, India) and B. J. HAMROCK (NASA, Lewis Research Center, Cleveland, OH) ASLE Transactions, vol. 28, April 1985, p. 159-169; Discussion, p. 169, 170; Authors' Closure, p. 170, 171. Previously announced in STAR as N83-34326. refs

A numerical solution to the problem of thermal elastohydrodynamic lubrication of line contacts was obtained by using a finite difference formulation. The solution procedure consists of simultaneous solution of the thermal Reynolds equation, the elasticity equation, and the energy equation subject to appropriate boundary conditions. Pressure distribution, film shape, and temperature distribution were obtained for fully flooded conjunctions, a paraffinic lubricant, and various dimensionless speed parameters while the dimensionless load and materials parameters were held constant. Reduction in the minimum film thickness due to thermal effects (as a ratio of thermal to isothermal minimum film thickness) is given by a simple formula as a function of the thermal loading parameter Q: $H(min)/H(min, I) = 10/10 + Q(0.4)$. Plots of pressure distribution, film shape, temperature distribution, and flow are shown for some representative cases. M.G.

A85-31203* National Aeronautics and Space Administration. Lewis Research Center, Cleveland, Ohio.
FIRST-ORDER BALL-BEARING KINEMATICS
E. KINGSBURY (NASA, Lewis Research Center, Cleveland, OH; Charles Stark Draper Laboratory, Inc., Cambridge, MA) ASLE Transactions, vol. 28, April 1985, p. 239-243; Discussion, p. 243; Author's Closure, p. 243, 244. refs

Two first-order equations are given connecting geometry and internal motions in an angular-contact ball bearing. Total speed, kinematic equivalence, basic speed ratio, and modal speed ratio are defined and discussed; charts are given for the speed ratios covering all bearings and all rotational modes. Instances where specific first-order assumptions might fail are discussed, and the resulting effects on bearing performance reviewed. Author

A85-32960*# National Aeronautics and Space Administration. Lewis Research Center, Cleveland, Ohio.
DUAL CLEARANCE SQUEEZE FILM DAMPER FOR HIGH LOAD CONDITIONS
D. P. FLEMING (NASA, Lewis Research Center, Cleveland, OH) ASME, Transactions, Journal of Tribology (ISSN 0742-4787), vol. 107, April 1985, p. 274-278; Discussion, p. 278; Author's Closure, p. 278, 279. Previously announced in STAR as N84-25064. refs (ASME PAPER 84-TRIB-7)

Squeeze film dampers are widely used to control vibrations in aircraft turbine engines and other rotating machinery. However, if shaft unbalance rises appreciably above the design value (e.g., due to a turbine blade loss), a conventional squeeze film becomes overloaded, and is no longer effective in controlling vibration amplitudes and bearing forces. A damper concept characterized by two oil films is described. Under normal conditions, only one low-clearance film is active, allowing precise location of the shaft centerline. Under high unbalance conditions, both films are active, controlling shaft vibration in a near-optimum manner, and allowing continued operation until a safe shutdown can be made. Author

A85-33779*# Cincinnati Univ., Ohio.
A COMPUTER AIDED DESIGN PROCEDURE FOR GENERATING GEAR TEETH
S. H. CHANG, R. L. HUSTON (Cincinnati, University, Cincinnati, OH), and J. J. COY (U.S. Army, Propulsion Laboratory, Cleveland, OH) American Society of Mechanical Engineers, Design Engineering Technical Conference, Cambridge, MA, Oct. 7-10, 1984. 5 p.
(Contract NSG-3188)
(ASME PAPER 84-DET-184)

A procedure for computer aided design (CAD) of gear teeth is presented. It is developed for generated teeth fabricated by a hob cutter or a shaper. It provides a means for analytically and numerically determining the tooth profile, given the cutter profile. An illustrative example with involute tooth profiles is given. Application with non-standard profiles and with bevel, spiral bevel, and hypoid gears is discussed. Author

A85-33780*# Cincinnati Univ., Ohio.
DYNAMIC ANALYSIS OF STRAIGHT AND INVOLUTE TOOTH FORMS
H. H. LIN, R. L. HUSTON (Cincinnati, University, Cincinnati, OH), and J. J. COY (U.S. Army, Propulsion Laboratory, Cleveland, OH) American Society of Mechanical Engineers, Design Engineering Technical Conference, Cambridge, MA, Oct. 7-10, 1984. 10 p. refs
(Contract NSG-3188)
(ASME PAPER 84-DET-226)

The effect of load speed on straight and involute tooth forms is studied using several finite-element models. It is found that for rapidly rotating gears and sprockets, the load speed along the tooth surface can significantly affect the tooth vibration. Indeed, it is found that for sufficiently high load speeds and for sufficiently slender tooth forms, the tooth deflection can, at times, be directed opposite to the load direction. Comparisons are made of various dynamic models of gear and sprocket teeth. It is shown that for stubby tooth forms there is considerable difference between results obtained with finite element models and results obtained with Timoshenko beam models. Finally, it is shown that gear or sprocket vibrations can be induced by the shape of the tooth form itself. This effect becomes increasingly significant at higher speeds. Author

A85-33781*# Cleveland State Univ., Ohio.
GEAR MESH STIFFNESS AND LOAD SHARING IN PLANETARY GEARING
R. KASUBA (Cleveland State University, Cleveland, OH) and R. AUGUST (Sverdrup Technology, Inc., Tullahoma, TN) American Society of Mechanical Engineers, Design Engineering Technical Conference, Cambridge, MA, Oct. 7-10, 1984. 6 p. refs
(Contract NAG3-186)
(ASME PAPER 84-DET-229)

An interactive computerized analysis was developed for determining load sharing among planetary gears. The load sharing is established as a function of transmitted torque, degree of sun gear fixity, component flexibility, gear tooth quality, and phasing of individual planet gears. A nonlinear variable gear tooth mesh stiffness model was used to simulate the sun/plant and planet/ring gear meshes. The determined load sharing and gear mesh stiffness parameters then can be used for the subsequent assessment of dynamic load factors. Author

A85-35049*# California State Univ., Long Beach.
LUBRICANT JET FLOW PHENOMENA IN SPUR AND HELICAL GEARS WITH MODIFIED CENTER DISTANCES AND/OR ADDENDUMS - FOR OUT-OF-MESH CONDITIONS
L. S. AKIN (California State University, Long Beach, CA) and D. P. TOWNSEND (NASA, Lewis Research Center, Cleveland, OH) ASME, Transactions, Journal of Mechanisms, Transmission, and Automation in Design, vol. 107, March 1985, p. 24-30. Previously announced in STAR as N84-29224. refs
(ASME PAPER 84-DET-96)

Out-of-mesh jet lubrication of gears was examined. The pinion impingement cycle was described briefly. An analysis was developed for the lubricant jet flow in the out-of-mesh condition. The analysis provides for the inclusion of modified center distances and modified addendum. Equations were generated for the limit values of variables necessary to remove the severe limitations to facilitate computer analysis. A computer program was designed using these limit formulas to prevent negative impingement (missing) on the pinion. Author

A85-39938* Creare, Inc., Hanover, N.H.
AN EXPERIMENTAL INVESTIGATION OF RUBBING INTERACTION IN LABYRINTH SEALS AT CRYOGENIC TEMPERATURE
F. X. DOLAN (Creare, Inc., Hanover, NH), F. E. KENNEDY, and E. M. SCHULSON (Dartmouth College, Hanover, NH) (U.S. Navy, Workshop on Thermomechanical Effects in Sliding Systems, 3rd, Hanover, NH, June 18-20, 1984) Wear (ISSN 0043-1648), vol. 102, March 1985, p. 51-66. refs
(Contract NAS3-23276)

An experimental program was carried out to address issues related to the observed cracking of the titanium knife edges on the labyrinth seals of the high pressure fuel pump (HPFP) in the Space Shuttle main engine (SSME). Thermal shock experiments were carried out using a jet specimen with geometry similar to the knife edge geometry. These tests demonstrate that cracking of the titanium alloy is possible in a situation involving repeated thermal cycles over a wide temperature range, as might be realized during a rub in the liquid hydrogen fuel pump. High speed rub interaction tests were conducted using a representative knife edge and seal geometry over a broad range of interaction rates. Alternative materials were also experimentally evaluated. These tests provide information which can be used to design improved labyrinth seals for the HPFP of the SSME. In particular, plasma-sprayed aluminum-graphite was found to be significantly better than aluminum alloy seals used at present from the standpoint of rub performance. Ion nitriding of the titanium alloy knife edges was also found to improve rub performance compared with the untreated baseline knife edge material. Author

A85-42573*# Texas A&M Univ., College Station.
ROTORDYNAMIC COEFFICIENTS FOR COMPRESSIBLE FLOW IN TAPERED ANNULAR SEALS
C. C. NELSON (Texas A&M University, College Station) ASME, Transactions, Journal of Tribology (ISSN 0742-4787), vol. 107, July 1985, p. 318-325. refs
(Contract NAG3-181)

Derivation of the governing equations for compressible flow in a tapered annular seal is based on Hirs' turbulent bulk-flow model. Zeroth and first-order perturbation equations are developed by an expansion in the eccentricity ratio. These equations are numerically integrated to obtain the leakage, and the direct and cross-coupled stiffness and damping coefficients. Seal parameters similar to the Space Shuttle Main Engine High Pressure Oxidizer Turbopump are used to demonstrate output from the analysis procedure. The effects of preswirl and seal taper are shown for three different length-to-diameter ratios. Generally the results indicate that prerotating the fluid significantly increases the cross-coupled stiffness but has little effect on the other coefficients, and increasing the convergent taper increases the direct stiffness while decreasing the direct damping and cross-coupled stiffness. Author

A85-45466* National Aeronautics and Space Administration. Lewis Research Center, Cleveland, Ohio.
INITIAL RESULTS OF SENSITIVITY TESTS - PERFORMED ON THE RE-1000 FREE-PISTON STIRLING ENGINE
J. G. SCHREIBER (NASA, Lewis Research Center, Cleveland, OH) IN: IECEC '84: Advanced energy systems - Their role in our future; Proceedings of the Nineteenth Intersociety Energy Conversion Engineering Conference, San Francisco, CA, August 19-24, 1984. Volume 3 . La Grange Park, IL, American Nuclear Society, 1984, p. 1878-1885.

Tests have been performed over several years to investigate the dynamics of a free-piston Stirling engine for the purpose of computer code validation. Tests on the 1 kW (1.33 hp) single cylinder engine have involved the determination of the sensitivity of the engine performance to variations in working space pressure, heater and cooler temperatures, regenerator porosity, power piston mass, and displacer dynamics. Maps of engine performance have been recorded with the use of an 81.2 percent porosity regenerator. Both a high-efficiency displacer and a high-power displacer were tested; efficiencies up to 33 percent were recorded, and power output of approximately 1500 W was obtained. Preliminary results of the sensitivity tests are presented, and descriptions of future tests are given. B.J.

A85-45473* Mechanical Technology, Inc., Latham, N. Y.
MOD II ENGINE AND TECHNOLOGY DEVELOPMENT
W. D. ERNST (Mechanical Technology, Inc., Latham, NY) IN: IECEC '84: Advanced energy systems - Their role in our future; Proceedings of the Nineteenth Intersociety Energy Conversion Engineering Conference, San Francisco, CA, August 19-24, 1984. Volume 3 . La Grange Park, IL, American Nuclear Society, 1984, p. 1935-1941. DOE-supported research.
(Contract DEN3-32)

The second-generation automotive Stirling engine, known as the Mod II, will be used to accomplish the Automotive Stirling Engine (ASE) Program objectives. Preliminary design has advanced to the point of procuring long-lead components to evaluate manufacturability. The heater head castings of the Hot Engine System (working gas cycle) are being procured, while the V-block casting of the Cold Engine/Drive system is being sectioned for evaluation. The technology required for these designs, and their impact on Mod II performance, have progressed to the design substantiation stage, and successful accomplishment of the program objectives is expected. Author

A85-45474* Mechanical Technology, Inc., Latham, N. Y.
AUTOMOTIVE STIRLING ENGINE SYSTEMS DEVELOPMENT
A. E. RICHEY (Mechanical Technology, Inc., Latham, NY) IN: IECEC '84: Advanced energy systems - Their role in our future; Proceedings of the Nineteenth Intersociety Energy Conversion Engineering Conference, San Francisco, CA, August 19-24, 1984. Volume 3 . La Grange Park, IL, American Nuclear Society, 1984, p. 1942-1948. DOE-supported research.
(Contract DEN3-32)

The objective of the Automotive Stirling Engine (ASE) program is to develop a Stirling engine for automotive use that provides a 30 percent improvement in fuel economy relative to a comparable internal-combustion engine while meeting emissions goals. This paper traces the engine systems' development efforts focusing on: (1) a summary of engine system performance for all Mod I engines; (2) the development, program conducted for the upgraded Mod I; and (3) vehicle systems work conducted to enhance vehicle fuel economy. Problems encountered during the upgraded Mod I test program are discussed. The importance of the EPA driving cycle cold-start penalty and the measures taken to minimize that penalty with the Mod II are also addressed. Author

A85-45479* National Aeronautics and Space Administration. Lewis Research Center, Cleveland, Ohio.
OVERVIEW OF NASA LEWIS RESEARCH CENTER FREE-PISTON STIRLING ENGINE ACTIVITIES
J. G. SLABY (NASA, Lewis Research Center, Cleveland, OH) IN: IECEC '84: Advanced energy systems - Their role in our future; Proceedings of the Nineteenth Intersociety Energy Conversion Engineering Conference, San Francisco, CA, August 19-24, 1984. Volume 3 . La Grange Park, IL, American Nuclear Society, 1984, p. 1994-2008. Previously announced in STAR as N84-22512. refs

A generic free-piston Stirling technology project is being conducted to develop technologies generic to both space power and terrestrial heat pump applications in a cooperative, cost-shared effort. The generic technology effort includes extensive parametric testing of a 1 kW free-piston Stirling engine (RE-1000), development of a free-piston Stirling performance computer code, design and fabrication under contract of a hydraulic output modification for RE-1000 engine tests, and a 1000-hour endurance test, under contract, of a 3 kWe free-piston Stirling/alternator engine. A newly initiated space power technology feasibility demonstration effort addresses the capability of scaling a free-piston Stirling/alternator system to about 25 kWe; developing thermodynamic cycle efficiency or equal to 70 percent of Carnot at temperature ratios in the order of 1.5 to 2.0; achieving a power conversion unit specific weight of 6 kg/kWe; operating with noncontacting gas bearings; and dynamically balancing the system. Planned engine and component design and test efforts are described. A.R.H.

A85-45488* National Aeronautics and Space Administration. Lewis Research Center, Cleveland, Ohio.
COMPARISON OF FREE-PISTON STIRLING ENGINE MODEL PREDICTIONS WITH RE1000 ENGINE TEST DATA
R. C. TEW (NASA, Lewis Research Center, Cleveland, OH) IN: IECEC '84: Advanced energy systems - Their role in our future; Proceedings of the Nineteenth Intersociety Energy Conversion Engineering Conference, San Francisco, CA, August 19-24, 1984. Volume 3 . La Grange Park, IL, American Nuclear Society, 1984, p. 2073-2085. Previously announced in STAR as N84-24509. refs

Predictions of a free-piston Stirling engine model are compared with RE1000 engine test data taken at NASA-Lewis Research Center. The model validation and the engine testing are being done under a joint interagency agreement between the Department of Energy's Oak Ridge National Laboratory and NASA-Lewis. A kinematic code developed at Lewis was upgraded to permit simulation of free-piston engine performance; it was further upgraded and modified at Lewis and is currently being validated. The model predicts engine performance by numerical integration of equations for each control volume in the working space. Piston motions are determined by numerical integration of the force balance on each piston or can be specified as Fourier series. In addition, the model Fourier analyzes the various piston forces to permit the construction of phasor force diagrams. The paper compares predicted and experimental values of power and efficiency and shows phasor force diagrams for the RE1000 engine displacer and piston. Further development plans for the model are also discussed. Author

N85-13233*# National Aeronautics and Space Administration. Lewis Research Center, Cleveland, Ohio.
EFFECT OF TWO INNER-RING OIL-FLOW DISTRIBUTION SCHEMES ON THE OPERATING CHARACTERISTICS OF A 35 MILLIMETER BORE BALL BEARING TO 2.5 MILLION DN
F. T. SCHULLER, S. I. PINEL (Industrial Tectonics, Inc., Rancho Dominquez, Calif.), and H. R. SIGNER (Industrial Tectonics, Inc., Rancho Dominquez, Calif.) Jan. 1985 14 p refs
(Contract NAS3-19779)
(NASA-TP-2404; E-2127; NAS 1.60:2404) Avail: NTIS HC A02/MF A01 CSCL 13I

Parametric tests were conducted with a 35-mm-bore, split-inner-ring ball bearing with a double-inner-land-guided cage. Provisions were made for through-the-inner-ring lubrication. Test condictions were either a thrust load of 667 N (150 lb) or a combined load of 667 N (150 lb) thrust and 222 N (50 lb) radial, shaft speeds from 32000 to 72000 rpm, and an oil-inlet temperature of 394 K (250 deg F). Outer ring cooling was used in some tests. Tests were run with either 50 or 75 percent of the total oil flow distributed to the inner-ring raceway. Successful operation was experienced with both 50% and 75% flow patterns to 2.5 million DN. Cooling the outer ring had little effect on inner-ring temperature; however, the outer-ring temperature decreased as much as 7% at 2.5 million DN. Maximum recorded power loss was 3.1 kW (4.2 hp), and maximum cage slip was 8.7 percent. Both occurred at a shaft speed of 72000 rpm, a lubricant flow rate of 1900 cu/min (0.50 gal/min), a combined load, and no outer-ring cooling.
Author

N85-13234*# National Aeronautics and Space Administration. Lewis Research Center, Cleveland, Ohio.
EFFECT OF LUBRICANT EXTREME-PRESSURE ADDITIVES ON SURFACE FATIGUE LIFE OF AISI 9310 SPUR GEARS
H. W. SCIBBE, D. P. TOWNSEND, and P. R. ARON Dec. 1984 14 p refs
(NASA-TP-2408; E-2042; NAS 1.60:2408) Avail: NTIS HC A02/MF A01 CSCL 13I

Surface fatigue tests were conducted with AISI 9310 spur gears using a formulated synthetic tetraester oil (conforming to MIL-L-23699 specifications) as the lubricant containing either sulfur or phosphorus as the EP additive. Four groups of gears were tested. One group of gears tested without an additive in the lubricant acted as the reference oil. In the other three groups either a 0.1 wt % sulfur or phosphorus additive was added to the tetraester oil to enhance gear surface fatigue life. Test conditions included a gear temperature of 334 K (160 F), a maximum Hertz stress of 1.71 GPa (248 000 psi), and a speed of 10,000 rpm. The gears tested with a 0.1 wt % phosphorus additive showed pitting fatigue life 2.6 times the life of gears tested with the reference tetraester based oil. Although fatigue lives of two groups of gears tested with the sulfur additive in the oil showed improvement over the control group gear life, the results, unlike those obtained with the phosphorus oil, were not considered to be statistically significant.
R.J.F.

N85-13235*# Cummins Engine Co., Inc., Columbus, Ind.
ADVANCED AUTOMOTIVE DIESEL ASSESSMENT PROGRAM Final Report
R. SEKAR and L. TOZZI Dec. 1983 354 p refs
(Contract DEN3-261)
(NASA-CR-168285; DOE/NASA/0261-1; NAS 1.26:168285; CTR-0747-84003) Avail: NTIS HC A16/MF A01 CSCL 13I

Cummins Engine Company completed an analytical study to identify an advanced automotive (light duty) diesel (AAD) power plant for a 3,000-pound passenger car. The study resulted in the

definition of a revolutionary diesel engine with several novel features. A 3,000-pound car with this engine is predicted to give 96.3, 72.2, and 78.8 MPG in highway, city, and combined highway-city driving, respectively. This compares with current diesel powered cars yielding 41.7, 35.0, and 37.7 MPG. The time for 0-60 MPH acceleration is 13.9 sec. compared to the baseline of 15.2 sec. Four technology areas were identified as crucial in bringing this concept to fruition. They are: (1) part-load preheating, (2) positive displacement compounding, (3) spark assisted diesel combustion system, and (4) piston development for adiabatic, oilless diesel engine. Marketing and planning studies indicate that an aggressive program with significant commitment could result in a production car in 10 years from the date of commencement.

N85-14116*# National Aeronautics and Space Administration. Lewis Research Center, Cleveland, Ohio.
ROTORDYNAMIC INSTABILITY PROBLEMS IN HIGH-PERFORMANCE TURBOMACHINERY
Washington Dec. 1984 507 p refs Workshop held in College Station, Tex., 28-30 May 1984; sponsored by Texas A&M Univ., Army Research Office, and the Air Force Aeropropulsion Lab.
(NASA-CP-2338; E-2214; NAS 1.55:2338) Avail: NTIS HC A22/MF A01 CSCL 13I

Rotordynamics and predictions on the stability of characteristics of high performance turbomachinery were discussed. Resolutions of problems on experimental validation of the forces that influence rotordynamics were emphasized. The programs to predict or measure forces and force coefficients in high-performance turbomachinery are illustrated. Data to design new machines with enhanced stability characteristics or upgrading existing machines are presented.

N85-14122*# National Aeronautics and Space Administration. Lewis Research Center, Cleveland, Ohio.
INTERNAL HYSTERESIS EXPERIENCED ON A HIGH PRESSURE SYN GAS COMPRESSOR
F. Y. ZEIDAN (Qatar Fertiliser Co., Umm Said) *In its* Rotordynamic Instability Problems in High-Performance Turbomachinery p 97-108 Dec. 1984 refs
Avail: NTIS HC A22/MF A01 CSCL 13I

A vibration instability phenomenon experienced in operating high pressure syn gas centrifugal compressors in two ammonia plants is described. The compressors were monitored by orbit and spectrum analysis for changes from baseline readings. It is found that internal hysteresis was the major destabilizing force; however, the problem was further complicated by seal lockup at the suction end of the compressor. A coupling lockup problem and a coupling fit problem, which frettage of the shaft, are also considered as contributors to the self excited vibrations. E.A.K.

N85-15168*# National Aeronautics and Space Administration. Lewis Research Center, Cleveland, Ohio.
NITRIDING OF TITANIUM AND ITS ALLOYS BY N2, NH3 OR MIXTURES OF N2 + H2 IN A DC ARC PLASMA AT LOW PRESSURES (OR ≈ TO TORR)
R. AVNI Nov. 1984 23 p refs
(NASA-TM-83803; E-2254; NAS 1.15:83803) Avail: NTIS HC A02/MF A01 CSCL 11F

The dc glow discharges in different gas mixtures of Ar + N2, Ar + NH3 or Ar + N2 + H2 result in the surface nitriding of Ti metal and its alloy (Ti6Al4V). Various gas mixtures were used in order to establish the main active species governing the nitriding process, i.e., N, N2, NH, or NH2 as excited or ionized particles. The dc discharge was sampled and analyzed by quadruple mass spectrometry (QPMS) and optical emission spectroscopy (OES), and the nitrided samples were analyzed by scanning electron microscopy (SEM) with an EDAX attachment, microhardness, and Fourier transform infrared reflectance spectrometry (FTIR). It was found that the excited and ionized nitrogen and hydrogen atoms are the main species responsible for the nitriding process in a dc glow discharge. Author

N85-20368*# National Aeronautics and Space Administration. Lewis Research Center, Cleveland, Ohio.
REPORT OF THE CONSTELLATIONS PANEL
D. J. BENTS, G. VONTIESENHAUSEN (NASA. Marshall Space Flight Center), C. A. LUNDQUIST (Alabama Univ., Huntsville), P. SWAN (California Univ., Los Angeles), H. L. MAYER (Aerospace Corp.), M. J. MANGANO (JPL, California Inst. of Tech., Pasadean), S. BERGAMASUI (Padua Univ.), F. BEVILACQUA (Aeritalia), F. WILLIAMS (Martin Marietta, New Orleans), G. RUM (CNR, Italy) et al. *In* NASA. Marshall Space Flight Center Appl. of Tethers in Space, Vol. 2 16 p Mar. 1985
Avail: NTIS HC A14/MF A01 CSCL 13I

The purpose of a constellation is to provide a mode of distributing space systems in a method that could be advantageous and not eliminating the consolidation/aggregation advantages. The applicability of stabilization concepts to various orbital conditions was defined. B.G.

N85-20377*# National Aeronautics and Space Administration. Lewis Research Center, Cleveland, Ohio.
VARIABLE FRICTION SECONDARY SEAL FOR FACE SEALS Patent Application
E. DIRUSSO, inventor (to NASA) 16 Nov. 1984 8 p
(NASA-CASE-LEW-14170-1; NAS 1.71:LEW-14170-1; US-PATENT-APPL-SN-672224) Avail: NTIS HC A02/MF A01 CSCL 11A

Vibration and stability of a primary seal ring are controlled by a secondary seal system. An inflatable bladder which forms a portion of secondary seal varies the damping applied to this seal ring. The amplitude of vibration of the primary seal ring is sensed with a proximity probe that is connected to a microprocessor in a control system. The bladder pressure is changed by the control system to mitigate any sensed instability or vibration. NASA

N85-21657*# National Aeronautics and Space Administration. Lewis Research Center, Cleveland, Ohio.
TRIBOLOGICAL SYSTEMS AS APPLIED TO AIRCRAFT ENGINES
D. H. BUCKLEY 26 Apr. 1985 23 p refs To be presented at the 60th AGARD Struct. and Mater. Panel Meeting, San Antonio, 21-26 Apr. 1985
(NASA-TM-86965; E-2478; NAS 1.15:86965) Avail: NTIS HC A02/MF A01 CSCL 13I

Tribological systems as applied to aircraft are reviewed. The importance of understanding the fundamental concepts involved in such systems is discussed. Basic properties of materials which can be related to adhesion, friction and wear are presented and correlated with tribology. Surface processes including deposition and treatment are addressed in relation to their present and future application to aircraft components such as bearings, gears and seals. Lubrication of components with both liquids and solids is discussed. Advances in both new liquid molecular structures and additives for those structures are reviewed and related to the needs of advanced engines. Solids and polymer composites are suggested for increasing use and ceramic coatings containing fluoride compounds are offered for the extreme temperatures encountered in such components as advanced bearings and seals. M.G.

N85-21658*# National Aeronautics and Space Administration. Lewis Research Center, Cleveland, Ohio.
LUBRICATION AND PERFORMANCE OF HIGH-SPEED ROLLING-ELEMENT BEARINGS
E. V. ZARETSKY, F. T. SCHULLER, and H. H. COE 1985 19 p refs Proposed for presentation at the 1985 Ann. Meeting of the American Society of Lubrications Engineers, Las Vegas, Nev., 6-9 May 1985
(NASA-TM-86958; E-2362; NAS 1.15:86958) Avail: NTIS HC A02/MF A01 CSCL 13I

Trends in aircraft engine operating speeds have dictated the need for rolling-element bearings capable of speeds to 3 million DN. A review of high-speed rolling-element bearing state-of-the-art performance and lubrication is presented. Through the use of

under-race lubrication and bearing thermal management bearing operation can be obtained to speeds of 3 million DN. Jet lubricated ball bearings are limited to 2.5 million DN for large bore sizes and to 3 million DN for small bore sizes. Current computer programs are able to predict bearing thermal performance. Author

N85-21662*# Tuskegee Inst., Ala. Dept. of Mechanical Engineering.
ARC-DRIVEN RAIL GUN RESEARCH Annual Report
P. K. RAY Dec. 1984 69 p refs
(Contract NAG3-76)
(NASA-CR-174816; NAS 1.26:174816) Avail: NTIS HC A04/MF A01 CSCL 14B

The equations describing the performance of an inductively-driven rail gun are analyzed numerically. Friction between the projectile and rails is included through an empirical formulation. The equations are applied to the experiment of Rashleigh and Marshall to obtain an estimate of energy distribution in rail guns as a function of time. The effect of frictional heat dissipation on the bore of the gun is calculated. The mechanism of plasma and projectile acceleration in a dc rail gun is described from a microscopic point of view through the establishment of the Hall field. The plasma conductivity is shown to be a tensor indicating that there is a small component of current parallel to the direction of acceleration. The plasma characteristics are evaluated as a function of plasma mass through a simple fluid mechanical analysis of the plasma. By equating the energy dissipated in the plasma with the radiation heat loss, the properties of the plasma are determined. Author

N85-23085*# National Aeronautics and Space Administration. Lewis Research Center, Cleveland, Ohio.
FRICTIONAL AND STRUCTURAL CHARACTERIZATION OF ION-NITRIDED LOW AND HIGH CHROMIUM STEELS
T. SPALVINS 1985 17 p refs Presented at the 12th Intern. Conf. on Metallurgical Coatings, Los Angeles, 15-19 Apr. 1985
(NASA-TM-86991; E-2487; NAS 1.15:86991) Avail: NTIS HC A02/MF A01 CSCL 13I

Low Cr steels AISI 41410, AISI 4340, and high Cr austenitic stainless steels AISI 304, AISI 316 were ion nitrided in a dc glow discharge plasma consisting of a 75 percent H2 - 25 percent N2 mixture. Surface compound layer phases were identified, and compound layer microhardness and diffusion zone microhardness profiles were established. Distinct differences in surface compound layer hardness and diffusion zone profiles were determined between the low and high Cr alloy steels. The high Cr stainless steels after ion nitriding displayed a hard compound layer and an abrupt diffusion zone. The compound layers of the high Cr stainless steels had a columnar structure which accounts for brittleness when layers are exposed to contact stresses. The ion nitrided surfaces of high and low Cr steels displayed a low coefficient of friction with respect to the untreated surfaces when examined in a pin and disk tribotester. Author

N85-25847*# National Aeronautics and Space Administration. Lewis Research Center, Cleveland, Ohio.
EXPERIMENTAL STIFFNESS OF TAPERED BORE SEALS
D. P. FLEMING 1985 20 p refs Presented at the Design Eng. Tech. Conf., Cincinnati, 10-13 Sep. 1985; sponsored by ASME
(NASA-TM-86978; E-2515; NAS 1.15:86978) Avail: NTIS HC A02/MF A01 CSCL 11A

The stiffness of tapered-bore ring seals was measured with air as the sealed fluid. Static stiffness agreed fairly well with results of a previous analysis. Cross-coupled stiffness due to shaft rotation was much less than predicted. It is suggested that part of the disparity may be due to simplifying assumptions in the analysis; however, these do not appear to account for the entire difference observed. E.A.K.

N85-25848*# Transmission Research, Inc., Cleveland, Ohio.
THERMAL TRACTION CONTACT PERFORMANCE EVALUATION UNDER FULLY FLOODED AND STARVED CONDITIONS Interim Report
J. L. TEVAARWERK May 1985 132 p refs
(Contract DEN3-35)
(NASA-CR-168173; NAS 1.26:168173; IR-2) Avail: NTIS HC A07/MF A01 CSCL 13I

Ultra high speed traction tests were performed on two traction fluids commonly employed. Traction data on these fluids is required for purposes of traction drive design optimization techniques. To obtain the traction data, an existing twin disc traction test machine was employed. This machine was modified to accommodate the range of test variables. All the data reported was obtained under conditions of side slip, a technique whereby only low power levels are required to simulate real traction drive contacts. Theoretical traction predictions were performed for a representative number of curves that showed the influence of rolling velocity, of contact pressure and of aspect ratio. To establish the accuracy of the thermal model the predictions were performed ith increasing levels of independence of experimentally determined parameters. In the final resulting prediction only two non linear thermal parameters were used for the prediction of 15 different traction curves covering the entire range of variables as used in the investigation, with the exception of the influence of asperity traction. Comparison of these theoretical curves and corresponding experimental traces show very good agreement. Author

N85-26890*# National Aeronautics and Space Administration. Lewis Research Center, Cleveland, Ohio.
PRELIMINARY RESULTS ON PASSIVE EDDY CURRENT DAMPER TECHNOLOGY FOR SSME TURBOMACHINERY
R. E. CUNNINGHAM *In* NASA. Marshall Space Flight Center Advan. High Pressure O2/H2 Technol. p 366-380 Apr. 1985
Avail: NTIS HC A99/MF E03; SOD HC CSCL 13I

Some preliminary results have been obtained for the dynamic response of a rotor operating over a speed range of 800 to 10,000 rpm. Amplitude frequency plots show the lateral vibratory response of an unbalanced rotor with and without external damping. The mode of damping is by means of eddy currents generated with 4 c shaped permanent magnets installed at the lower bearing of a vertically oriented rotor. The lower ball bearing and its damper assembly are totally immersed in liquid nitrogen at a temperature of -197 deg C (-320 deg F). These preliminary results for a referenced or base line passive eddy current damper assembly show that the amplitude of synchronous vibration is reduced at the resonant frequency. Measured damping coefficients were calculated to phi = .086; this compares with a theoretically calculated value of phi = .079. Author

N85-27226*# National Aeronautics and Space Administration. Lewis Research Center, Cleveland, Ohio.
FATIGUE CRITERION TO SYSTEM DESIGN, LIFE AND RELIABILITY
E. V. ZARETSKY 10 Jul. 1985 22 p refs Presented at the 21st Joint Propulsion Conf., Monterey, Calif., 8-10 Jul. 1985; sponsored by AIAA, SAE and ASME
(NASA-TM-87017; E-2562; NAS 1.15:87017) Avail: NTIS HC A02/MF A01 CSCL 14D

A generalized methodology to structural life prediction, design, and reliability based upon a fatigue criterion is advanced. The life prediction methodology is based in part on work of W. Weibull and G. Lundberg and A. Palmgren. The approach incorporates the computed life of elemental stress volumes of a complex machine element to predict system life. The results of coupon fatigue testing can be incorporated into the analysis allowing for life prediction and component or structural renewal rates with reasonable statistical certainty. Author

N85-27227*# National Aeronautics and Space Administration. Lewis Research Center, Cleveland, Ohio.
LIFE AND RELIABILITY MODELING OF BEVEL GEAR REDUCTIONS
M. SAVAGE (Akron Univ., Ohio), C. K. BRIKMANIS (Akron Univ., Ohio), D. G. LEWICKI (Army Research and Technology Lab., Cleveland), and J. J. COY (Army Research and Technology Lab., Cleveland) 13 Mar. 1985 24 p refs Presented at the Natl. Design Eng. Conf., Chicago, 11-13 Mar. 1985; sponsored by ASME
(NASA-TM-87006; E-2549; NAS 1.15:87006; USAAVSCOM-TR-85-C-3) Avail: NTIS HC A02/MF A01 CSCL 13I

A reliability model is presented for bevel gear reductions with either a single input pinion or dual input pinions of equal size. The dual pinions may or may not have the same power applied for the analysis. The gears may be straddle mounted or supported in a bearing quill. The reliability model is based on the Weibull distribution. The reduction's basic dynamic capacity is defined as the output torque which may be applied for one million output rotations of the bevel gear with a 90 percent probability of reduction survival. Author

N85-27228*# National Aeronautics and Space Administration. Lewis Research Center, Cleveland, Ohio.
FATIGUE LIFE ANALYSIS OF A TURBOPROP REDUCTION GEARBOX
D. G. LEWICKI (Army Research and Technology Lab., Cleveland, Ohio), J. D. BLACK (Detroit Diesel Allison, Indianapolis, Ind.), M. SAVAGE (Akron Univ.), and J. J. COY (Army Research and Technology Lab., Cleveland, Ohio) 1985 25 p refs Prepared for presentation at the Design Tech. Conf., Cincinnati, 11-13 Sep. 1985; sponsored by ASME
(NASA-TM-87014; E-2559; NAS 1.15:87014; USAAVSCOM-TR-84-C-4) Avail: NTIS HC A02/MF A01 CSCL 13I

A fatigue life analysis of the Allison T56/501 turboprop reduction gearbox was developed. The life and reliability of the gearbox was based on the lives and reliabilities of the main power train bearings and gears. The bearing and gear lives were determined using the Lundberg-Palmgren theory and a mission profile. The five planet bearing set had the shortest calculated life among the various gearbox components, which agreed with field experience where the planet bearing had the greatest incidences of failure. The analytical predictions of relative lives among the various bearings were in reasonable agreement with field experience. The predicted gearbox life was in excellent agreement with field data when the material life adjustment factors alone were used. The gearbox had a lower predicted life in comparison with field data when no life adjustment factors were used or when lubrication life adjustment factors were used either alone or in combination with the material factors. Author

N85-28371*# National Aeronautics and Space Administration. Lewis Research Center, Cleveland, Ohio.
OPERATING CHARACTERISTICS OF A 0.87 KW-HR FLYWHEEL ENERGY STORAGE MODULE
S. H. LOEWENTHAL, H. W. SCIBBE, R. D. PARKER, and E. V. ZARETSKY 23 Aug. 1985 18 p refs Presented at 20th Intersoc. Energy Conversion Eng. Conf. (IECEC), Miami Beach, Fla., 18-23 Aug. 1985; sponsored by SAE, ANS, ASME, IEEE, AIAA, ACS and American Institute of Chemical Engineers
(NASA-TM-87038; E-2535; NAS 1.15:87038) Avail: NTIS HC A02/MF A01 CSCL 10C

Discussion is given of the design and loss characteristics of 0.87 kW-hr (peak) flywheel energy storage module suitable for aerospace and automotive applications. The maraging steel flywheel rotor, a 46-cm- (18-in-) diameter, 58-kg (128-lb) tapered disk, delivers 0.65 kW-hr of usable energy between operating speeds of 10,000 and 20,000 rpm. The rotor is supported by 20- and 25-mm bore diameter, deep-groove ball bearings, lubricated by a self-replenishing wick type lubrication system. To reduce aerodynamic losses, the rotor housing was evacuated to vacuum levels from 40 to 200 millitorr. Dynamic rotor instabilities uncovered during testing necessitated the use of an elastometric-bearing damper to limit shaft excursions. Spindown losses from bearing, seal, and aerodynamic drag at 50 millitorr typically ranged from 64 to 193 W at 10,000 and 20,000 rpm, respectively. Discharge efficiency of the flywheel system exceeded 96 percent at torque levels greater than 21 percent of rated torque. Author

N85-28372*# Hamilton Standard, Windsor Locks, Conn.
MULTI-MESH GEAR DYNAMICS PROGRAM EVALUATION AND ENHANCEMENTS Final Report
L. S. BOYD and J. PIKE May 1985 128 p refs
(Contract NAS3-23928)
(NASA-CR-174747; NAS 1.26:174747) Avail: NTIS HC A07/MF A01 CSCL 13I

A multiple mesh gear dynamics computer program was continually developed and modified during the last four years. The program can handle epicyclic gear systems as well as single mesh systems with internal, buttress, or helical tooth forms. The following modifications were added under the current funding: variable contact friction, planet cage and ring gear rim flexibility options, user friendly options, dynamic side bands, a speed survey option and the combining of the single and multiple mesh options into one general program. The modified program was evaluated by comparing calculated values to published test data and to test data taken on a Hamilton Standard turboprop reduction gear-box. In general, the correlation between the test data and the analytical data is good. R.J.F.

N85-28373*# National Aeronautics and Space Administration. Lewis Research Center, Cleveland, Ohio.
LUBRICANT AND ADDITIVE EFFECTS ON SPUR GEAR FATIGUE LIFE
D. P. TOWNSEND, E. V. ZARETSKY, and H. W. SCIBBE 1985 28 p refs To be presented at 1985 Lubrication Conf., Atlanta, 8-10 Oct. 1985, sponsored by ASME and American Society of Lubrication Engineers
(NASA-TM-87044; E-2482; NAS 1.15:87044) Avail: NTIS HC A03/MF A01 CSCL 13I

Spur gear endurance tests were conducted with six lubricants using a single lot of consumable-electrode vacuum melted (CVM) AISI 9310 spur gears. The sixth lubricant was divided into four batches each of which had a different additive content. Lubricants tested with a phosphorus-type load carrying additive showed a statistically significant improvement in life over lubricants without this type of additive. The presence of sulfur type antiwear additives in the lubricant did not appear to affect the surface fatigue life of the gears. No statistical difference in life was produced with those lubricants of different base stocks but with similar viscosity, pressure-viscosity coefficients and antiwear additives. Gears tested with a 0.1 wt % sulfur and 0.1 wt % phosphorus EP additives in the lubricant had reactive films that were 200 to 400 (0.8 to 1.6 microns) thick. Author

N85-29292*# National Aeronautics and Space Administration. Lewis Research Center, Cleveland, Ohio.
VIBRATION CONTROL OF ROTOR SHAFT
K. NONAMI 1985 19 p refs Proposed for presentation at Design Eng. Tech. Conf., Cincinnati, 10-13 Sep. 1985; sponsored by ASME
(NASA-TM-87053; E-2616; NAS 1.15:87053) Avail: NTIS HC A02/MF A01 CSCL 13I

Suppression of flexural forced vibration or the self-excited vibration of a rotating shaft system not by passive elements but by active elements is described. The distinctive feature of this method is not to dissipate the vibration energy but to provide the force cancelling the vibration displacement and the vibration velocity through the bearing housing in rotation. Therefore the bearings of this kind are appropriately named Active Control Bearings. A simple rotor system having one disk at the center of the span on flexible supports is investigated in this paper. The actuators of the electrodynamic transducer are inserted in the sections of the bearing housing. First, applying the optimal regulator

of optimal control theory, the flexural vibration control of the rotating shaft and the vibration control of support systems are performed by the optimal state feedback system using these actuators. Next, the quasi-modal control based on a modal analysis is applied to this rotor system. This quasi-modal control system is constructed by means of optimal velocity feedback loops. The differences between optimal control and quasi-modal control are discussed and their merits and demerits are made clear. Finally, the experiments are described concerning only the optimal regulator method. Author

N85-29295*# National Aeronautics and Space Administration. Lewis Research Center, Cleveland, Ohio.
POWDER METALLURGY FORGED GEAR DEVELOPMENT Final Report, Sep. 1980 - Jul. 1984
D. H. RO, B. L. FERGUSON, S. PILLAY, D. T. OSTBERG (Army Tank-Automotive Command), and D. P. TOWNSEND Mar. 1985 112 p refs
(Contract DAAE07-80-C-9115)
(NASA-TM-87483; NAS 1.15:87483; AD-A153479; TACOM-TR-13046) Avail: NTIS HC A06/MF A01 CSCL 13I

The purpose of this project is to investigate and develop powder forging methods for producing high-perfomance gears from sintered performs. Three gears have been forged from grade 4600 steel powder to which sufficient graphite was added to achieve the desired final carbon level. The first gear, referred to as the NASA test gear because it was designed specifically for gear testing at NASA Lewis Research Center, was forged from 4620 and 4640 steel powder preforms. This gear was a straight spur gear with 28 involute teeth, a 0.25 inch-(6.35 mm) thick web, and a top and bottom hub. Both net teeth and oversize teeth (0.004 inches grinding stock per side) were forged, with these gears being carburized after forging. Gears were then tested in a four square gear testing rig at NASA under the guidance of Dennis Townsend. Using a maximum Hertzian stress of 248,000 psi at pitch line and a gear rotational speed of 10,000 rpm, gear lives were obtained for these gears. GRA

N85-30333* National Aeronautics and Space Administration. Lewis Research Center, Cleveland, Ohio.
VARIABLE FORCE, EDDY-CURRENT OR MAGNETIC DAMPER Patent
R. E. CUNNINGHAM, inventor (to NASA) 14 May 1985 6 p Filed 3 Feb. 1983
(NASA-CASE-LEW-13717-1; US-PATENT-4,517,505; US-PATENT-APPL-SN-463456; US-PATENT-CLASS-318-611; US-PATENT-CLASS-310-77; US-PATENT-CLASS-310-93; US-PATENT-CLASS-335-100) Avail: US Patent and Trademark Office CSCL 13I

An object of the invention is to provide variable damping for resonant vibrations which may occur at different rotational speeds in the range of rpms in which a rotating machine is operated. A variable force damper in accordance with the invention includes a rotating mass carried on a shaft which is supported by a bearing in a resilient cage. The cage is attached to a support plate whose rim extends into an annular groove in a housing. Variable damping is effected by tabs of electrically conducting nonmagnetic material which extend radially from the cage. The tabs at an index position lie between the pole face of respective C shaped magnets. The magnets are attached by cantilever spring members to the housing. Author

N85-30342*# National Aeronautics and Space Administration. Lewis Research Center, Cleveland, Ohio.
CORRELATION OF RHEOLOGICAL CHARACTERISTICS OF LUBRICANTS WITH TRANSMISSION EFFICIENCY MEASUREMENTS
B. O. JACOBSON (Lulea Univ.), B. J. HAMROCK, and E. HOEGLUND (Lulea Univ.) 1985 15 p refs Presented at the Intern. Tribology Conf., Tokyo, 8-10 Jul. 1985; sponsored by Japan Society of Lubrication Engineers
(NASA-TM-86988; E-2531; NAS 1.15:86988) Avail: NTIS HC A02/MF A01 CSCL 11H

The power efficiency of a helicopter transmission has been analyzed for 11 lubricants by looking at the Newtonian and non-Newtonian properties of the lubricants. A non-Newtonian property of the lubricants was the limiting shear strength proportionality constant. The tests were performed on a high-pressure, short-time shear strength analyzer. A power efficiency formula that was obtained by analyzing the Newtonian and non-Newtonian properties of the lubricants is presented in detail. B.W.

N85-31511*# National Aeronautics and Space Administration. Lewis Research Center, Cleveland, Ohio.
EFFECT OF SPEED AND PRESS FIT ON FATIGUE LIFE OF ROLLER-BEARING INNER-RACE CONTACT
H. H. COE and E. V. ZARETSKY Jul. 1985 13 p refs
(NASA-TP-2496; E-2476; NAS 1.60:2496) Avail: NTIS HC A02/MF A01 CSCL 13I

An analysis was performed to determine the effects of inner ring speed and press fit on the rolling element fatigue life of a roller bearing inner race contact. The effects of the resultant hoop and radial stresses on the principal stresses were considered. The maximum shear stresses below the Hertzian contact were determined for different conditions of inner ring speed, load, and geometry and were applied to a conventional ring life analysis. The race contact fatigue life was reduced by more than 90 percent for some conditions when speed and press fit were considered. The depth of the maximum shear stress remained virtually unchanged. Author

N85-32329*# National Aeronautics and Space Administration. Lewis Research Center, Cleveland, Ohio.
SURFACE ROUGHNESS EFFECTS IN ELASTOHYDRODYNAMIC CONTACTS
J. H. TRIPP (Case Western Reserve Univ.) and B. J. HAMROCK Jul. 1985 14 p refs Presented at the 11th Leeds-Lyon Symp. on Mixed Lubrication and Lubricated Wear, Leeds, Engl., 4-7 Sep. 1984
(NASA-TP-2488; E-2524; NAS 1.60:2488) Avail: NTIS HC A02/MF A01 CSCL 20K

Surface roughness effects in full-film EHL contacts were studied. A flow factor modification to the Reynolds equation was applied to piezoviscous-elastic line contacts. Results for ensemble-averaged film shape, pressure distribution, and other mechanical quantities were obtained. Asperities elongated in the flow direction by a factor exceeding two decreased both film shape and pressure extrema at constant load; isotropic or transverse asperities increased these extrema. The largest effects are displayed by traction, which increased by over 5% for isotropic or transverse asperities and by slightly less for longitudinal roughness. E.A.K.

N85-32330*# National Aeronautics and Space Administration. Lewis Research Center, Cleveland, Ohio.
MECHANICS OF A GASEOUS FILM BARRIER TO LUBRICANT WETTING OF ELASTOHYDRODYNAMICALLY LUBRICATED CONJUNCTIONS
J. M. PRAHL (Case Western Reserve Univ.) and B. J. HAMROCK Aug. 1985 17 p refs Presented at the 11th Leeds-Lyon Symp. on Mixed Lubrication and Lubricated Wear, Leeds, Engl., 4-7 Sep. 1984
(Contract NCC3-30)
(NASA-TP-2500; E-2523; NAS 1.60:2500) Avail: NTIS HC A02/MF A01 CSCL 20K

Two analytical models, one based on simple hydrodynamic lubrication and the other on soft elastohydrodynamic lubrication, are presented and compared to delineate the dominant physical parameters that govern the mechanics of a gaseous film between a small droplet of lubricant and the outer race of a ball bearing. Both models are based on the balance of gravity forces, air drag forces, and air film lubrication forces and incorporate a drag coefficient C sub D and a lubrication coefficient C sub L to be determined from experiment. The soft elastohydrodynamic lubrication (EHL) model considers the effects of droplet deformation and solid-surface geometry; the simpler hydrodynamic lubrication (HL) model assumes that the droplet remains essentially spherical. The droplet's angular position depended primarily on the ratio of gas inertia to droplet gravity forces and on the gas Reynolds number and weakly on the ratio of droplet gravity forces to surface tension forces (Bond number) and geometric ratios for the soft EHL. An experimental configuration in which an oil droplet is supported by an air film on the rotating outer race of a ball bearing within a pressure-controlled chamber produced measurements of droplet angular position as a function of outer-race velocity droplet size and type, and chamber pressure. E.A.K.

N85-32331*# National Aeronautics and Space Administration. Lewis Research Center, Cleveland, Ohio.
HERTZIAN CONTACT IN TWO AND THREE DIMENSIONS
J. H. TRIPP (Case Western Reserve Univ.) Jul. 1985 27 p refs
(NASA-TP-2473; E-2256; NAS 1.60:2473) Avail: NTIS HC A03/MF A01 CSCL 20K

The basic solution to the problem of mechanical contact between elastically deforming solids was proposed by Hertz over a century ago and has been used by tribologists and others ever since in a steadily increasing number of applications. While the theoretical development is not conceptually difficult and treatments exist to suit all tastes, it is nonetheless interesting to trace the relationships among the solutions in different dimensions. Such an approach is used herein to shed light on the curious and sometimes perplexing behavior of line contacts. A number of the more frequently used contact expressions together as a convenient reference and for comparative purposes. Author

N85-32333*# National Aeronautics and Space Administration. Lewis Research Center, Cleveland, Ohio.
TAPE CASTING AS AN APPROACH TO AN ALL-CERAMIC TURBINE SHROUD SEAL
J. D. CAWLEY Jul. 1985 11 p refs
(NASA-TM-87078; E-2607; NAS 1.15:87078) Avail: NTIS HC A02/MF A01 CSCL 11A

Gas path seals have a one-dimensional variation in material requirement. Tape casting is a method which allows the fabrication of thin ceramic sheets, which may be laminated to accommodate these requirements. Using tape casting, thin sheets of zirconia (0.25 mm) were fabricated. These castings were successfully laminated and fired without bloating or delamination, demonstrating the feasibility of this approach. Author

N85-33489* National Aeronautics and Space Administration. Lewis Research Center, Cleveland, Ohio.
MULTISTAGE SPENT PARTICLE COLLECTOR AND A METHOD FOR MAKING SAME Patent
B. T. EBIHARA, inventor (to NASA) 2 Jul. 1985 7 p Filed 30 Sep. 1983 Supersedes N84-12447 (22 - 03, p 0376)
(NASA-CASE-LEW-13914-1; US-PATENT-4,527,092; US-PATENT-APPL-SN-537615; US-PATENT-CLASS-315-5.38; US-PATENT-CLASS-315-3.5; US-PATENT-CLASS-445-35) Avail: US Patent and Trademark Office CSCL 13I

A description is given of a spent particle collector which maintains structural integrity when raised to a high temperature although constructed of materials having widely different coefficients of expansion. The collector is comprised of one or more axisymmetric stages, each stage comprising a subassembly. A subassembly includes an inner pyrolytic graphite ring, a transition ring, a ceramic insulator ring and an outer metal ring which forms part of the wall of the collector. Each transition is of a ductile metal having high thermal conductivity and is provided with an annular sputter shield wall extending toward the source of spent particles and, where necessary, a trough in the other surface to enclose the sputter shield of the next adjacent transition ring. A plurality of radial extending slots are provided in a transition ring to form segments which are retained in their position by the sputter shield. Official Gazette of the U.S. Patent and Trademark Office

N85-33490* National Aeronautics and Space Administration. Lewis Research Center, Cleveland, Ohio.
DUAL CLEARANCE SQUEEZE FILM DAMPER Patent
D. P. FLEMING, inventor (to NASA) 9 Jul. 1985 8 p Filed 5 Apr. 1984 Supersedes N84-22562 (22 - 13, p 1932)
(NASA-CASE-LEW-13506-1; US-PATENT-4,527,910; US-PATENT-APPL-SN-596960; US-PATENT-CLASS-384-99; US-PATENT-CLASS-384-101) Avail: US Patent and Trademark Office CSCL 13I

A dual clearance hydrodynamic liquid squeeze film damper for a gas turbine engine is described. Under normal operating conditions, the device functions as a conventional squeeze film damper, using only one of its oil films. When an unbalance reaches abusive levels, as may occur with a blade loss or foreign object damage, a second, larger clearance film becomes active, controlling vibration amplitudes in a near optimum manner until the engine can be safely shut down and repaired.
Official Gazette of the U.S. Patent and Trademark Office

N85-33491*# Transmission Research, Inc., Cleveland, Ohio.
ROLLING, SLIP AND TRACTION MEASUREMENTS ON LOW MODULUS MATERIALS Interim Report
J. L. TEVAARWERK Jul. 1985 122 p refs
(Contract DEN3-35)
(NASA-CR-174909; NAS 1.26:174909; IR-3) Avail: NTIS HC A06/MF A01 CSCL 13I

Traction and wear tests were performed on six low modulus materials (LMM). Three different traction tests were performed to determine the suitability of the material for use as traction rollers. These were the rolling, slip and endurance traction tests. For each material the combination LMM on LMM and LMM on steel were evaluated. Rolling traction test were conducted to determine the load - velocity limits, the rolling traction coefficient of the materials and to establish the type of failures that would result when loading beyond the limit. It was found that in general a simple constant rolling traction coefficient was enough to describe the results of all the test. The slip traction tests revealed that the peak traction coefficients were considerably higher than for lubricated traction contacts. The endurance traction tests were performed to establish the durability of the LMM under conditions of prolonged traction. Wear measurements were performed during and after the test. Energetic wear rates were determined from the wear measurements conducted in the endurance traction tests. These values show that the roller wear is not severe when reasonable levels of traction are transmitted. Author

N85-33524*# National Aeronautics and Space Administration. Lewis Research Center, Cleveland, Ohio.
ADVANCES IN SPUTTERED AND ION PLATED SOLID FILM LUBRICATION
T. SPALVINS *In* NASA. Ames Research Center 19th Aerospace Mech. Symp. p 209-224 Aug. 1985 refs
Avail: NTIS HC A17/MF A01 CSCL 13M

The glow discharge or ion assisted vacuum deposition techniques, primarily sputtering and ion plating, have rapidly emerged and offer great potential to deposit solid lubricants. The increased energizing of these deposition processes lead to improved adherence and coherence, favorable morphological growth, higher density, and reduced residual stresses in the film. These techniques are of invaluable importance where high precision machines tribo-components require very thin, uniform lubricating films (0.2 m), which do not interface with component tolerances. The performance of sputtered MoS2 films and ion plated Au and Pb films are described in terms of film thickness, coefficient of friction, and wear lives. Author

N85-34402* National Aeronautics and Space Administration. Lewis Research Center, Cleveland, Ohio.
OXIDIZING SEAL FOR A TURBINE TIP GAS PATH Patent
J. D. CAWLEY, inventor (to NASA) 10 Sep. 1985 7 p Filed 19 Apr. 1984 Supersedes N84-22935 (22 - 13, p 1993)
(NASA-CASE-LEW-14053-1; US-PATENT-4,540,336; US-PATENT-APPL-SN-602050; US-PATENT-CLASS-415-174; US-PATENT-CLASS-415-170-R; US-PATENT-CLASS-415-196; US-PATENT-CLASS-415-200; US-PATENT-CLASS-416-174)
Avail: US Patent and Trademark Office CSCL 11A

The sealing of the gas path in a gas turbine engine at the blade tips is improved by maintaining a minimum clearance between the rotor blade tips and the gas path seal. This is accomplished by taking advantage of an increase in volume during controlled oxidation of certain intermetallic compounds which have high melting points. The increase in volume closes the clearance subsequent to a rub between the blades and the seal. Thus, these compounds re-form the tip seal surface to assure continued engine efficiency.
Official Gazette of the U.S. Patent and Trademark Office

N85-34404*# Ohio State Univ., Columbus. Dept. of Mechanical Engineering.
THE DESIGN AND ANALYSIS OF SINGLE FLANK TRANSMISSION ERROR TESTOR FOR LOADED GEARS Final Report, Apr. 1984 - Jul. 1985
D. R. HOUSER and D. E. BASSETT Sep. 1985 141 p refs
(Contract NAG3-541)
(NASA-CR-176163; NAS 1.26:176163; MPN-764038; ESL-716109)
Avail: NTIS HC A07/MF A01 CSCL 13I

Due to geometrical imperfections in gears and finite tooth stiffnesses, the motion transmitted from an input gear shaft to an output gear shaft will not have conjugate action. In order to strengthen the understanding of transmission error and to verify mathematical models of gear transmission error, a test stand that will measure the transmission error of a gear pair at operating loads, but at reduced speeds would be desirable. This document describes the design and development of a loaded transmission error tester. For a gear box with a gear ratio of one, few tooth meshing combinations will occur during a single test. In order to observe the effects of different tooth mesh combinations and to increase the ability to load test gear pairs with higher gear ratios, the system was designed around a gear box with a gear ratio of two. B.W.

N85-34405*# National Aeronautics and Space Administration. Lewis Research Center, Cleveland, Ohio.
GENERATED SPIRAL BEVEL GEARS: OPTIMAL MACHINE-TOOL SETTINGS AND TOOTH CONTACT ANALYSIS
F. L. LITVIN (Illinois Univ., Chicago), W. J. TSUNG (Illinois Univ., Chicago), J. J. COY, and C. HEINE (Dana Corp.) 1985 14 p refs Presented at the 1985 Off-Highway and Power Plant Congr. and Exposition, Milwaukee, 9-12 Sep. 1985; sponsored by the Society of Automotive Engineers Prepared in cooperation with Army Research and Technology Labs.
(Contract NSG3-48)
(NASA-TM-87075; E-2648; NAS 1.15:87075; USAAVSCOM-TR-85-C-9) Avail: NTIS HC A02/MF A01 CSCL 13I

Geometry and kinematic errors were studied for Gleason generated spiral bevel gears. A new method was devised for choosing optimal machine settings. These settings provide zero kinematic errors and an improved bearing contact. The kinematic errors are a major source of noise and vibration in spiral bevel gears. The improved bearing contact gives improved conditions for lubrication. A computer program for tooth contact analysis was developed, and thereby the new generation process was confirmed. The new process is governed by the requirement that during the generation process there is directional constancy of the common normal of the contacting surfaces for generator and generated surfaces of pinion and gear. E.A.K.

N85-34406*# National Aeronautics and Space Administration. Lewis Research Center, Cleveland, Ohio.
THERMAL STRESS ANALYSIS OF A NEW TURBINE SHROUD SEAL CONCEPT
R. F. HANDSCHUH Aug. 1985 16 p refs Prepared in cooperation with Army Aviation Research and Development Command, Cleveland
(NASA-TM-87082; E-2666; NAS 1.15:87082; USAAVSCOM-TR-85-C-16) Avail: NTIS HC A02/MF A01 CSCL 13I

The thermal stress field of a two piece turbine shroud seal concept was analyzed and results compared to one piece designs by finite element analysis. The two piece seal has independently formed structure (substrate) and ceramic components that are assembled at ambient conditions. The boundary conditions used for analysis were hot gas surface temperatures of 1370 and 1650 C (2500 and 3000 F) and cooled surface temperature of 700 C (1285 F). The resulting thermal stress field, of the two piece seal when compared to the one piece seals in the region of all ceramic material, was reduced substantially. Author

N85-34407*# National Aeronautics and Space Administration. Lewis Research Center, Cleveland, Ohio.
LUBRICATION AND COOLING FOR HIGH SPEED GEARS
D. P. TOWNSEND 1985 24 p refs Presented at the Lubrication Session of the Original Equipment Manuf. Design Conf., Philadelphia, 9-11 Sep. 1985
(NASA-TM-87096; E-2660; NAS 1.15:87096) Avail: NTIS HC A02/MF A01 CSCL 13I

The problems and failures occurring with the operation of high speed gears are discussed. The gearing losses associated with high speed gearing such as tooth mesh friction, bearing friction, churning, and windage are discussed with various ways shown to help reduce these losses and thereby improve efficiency. Several different methods of oil jet lubrication for high speed gearing are given such as into mesh, out of mesh, and radial jet lubrication. The experiments and analytical results for the various methods of oil jet lubrication are shown with the strengths and weaknesses of each method discussed. The analytical and experimental results of gear lubrication and cooling at various test conditions are presented. These results show the very definite need of improved methods of gear cooling at high speed and high load conditions. Author

N85-34408*# National Aeronautics and Space Administration. Lewis Research Center, Cleveland, Ohio.
ELASTOHYDRODYNAMIC LUBRICATION CALCULATIONS USED AS A TOOL TO STUDY SCUFFING
L. G. HOUPERT and B. J. HAMROCK 1985 20 p refs Presented at the 12th Leeds-Lyon Symp. on Tribology, Lyon, 3-6 Sep. 1985
(NASA-TM-87097; E-2658; NAS 1.15:87097) Avail: NTIS HC A02/MF A01 CSCL 11H

A new Reynolds equation was developed that takes into account the nonlinear viscous behavior of the fluid. The new Reynolds equation considers the nonlinear viscous fluid model of Eyring, the equilibrium equation, the constant mass flow, and the kinematic boundary condition. The new Reynolds equation and the elasticity equation are solved simultaneously by using a system approach and a Newton-Raphson technique. Comparisons are made with results obtained from the classical Reynolds equation. The effects of sliding speed and introducing a bump or a groove within the conjunction are studied. Results are shown for both moderate and heavy loads. E.A.K.

N85-34409*# National Aeronautics and Space Administration. Lewis Research Center, Cleveland, Ohio.
DESIGN AND LUBRICATION OF HIGH-SPEED ROLLING-ELEMENT BEARINGS
E. V. ZARETSKY 1985 19 p refs Presented at the Original Equipment Manuf. Design Conf., Philadelphia, 9-11 Sep. 1985
(NASA-TM-87107; E-2670; NAS 1.15:87107) Avail: NTIS HC A02/MF A01 CSCL 13I

The speed capability of rolling element bearings has increased from speeds of less than two million DN to speeds of three million DN. The life and reliability of these bearings also increased where they are equal to, or greater than, those of bearings with limited speed capability. Design parameters must be carefully chosen and optimized based upon sophisticated bearing computer programs. Material and lubricant selection must be integrated into the bearing design. Bearing thermal management must be implemented through proper lubrication and cooling. Parameters which can be used to design, specify, and lubricate high speed bearings are discussed. E.A.K.

38

QUALITY ASSURANCE AND RELIABILITY

Includes product sampling procedures and techniques; and quality control.

A85-42151*# National Aeronautics and Space Administration. Lewis Research Center, Cleveland, Ohio.
THE ROLE OF THE REFLECTION COEFFICIENT IN PRECISION MEASUREMENT OF ULTRASONIC ATTENUATION
E. R. GENERAZIO (NASA, Lewis Research Center, Cleveland, OH) (DARPA, Annual Review of Progress in Quantitative Nondestructive Evaluation, La Jolla, CA, July 8-13, 1984) Materials Evaluation (ISSN 0025-5327), vol. 43, July 1985, p. 995-1004. Previously announced in STAR as N84-32849. refs

Ultrasonic attenuation measurements using contact, pulse-echo techniques are sensitive to surface roughness and couplant thickness variations. This can reduce considerable inaccuracies in the measurement of the attenuation coefficient for broadband pulses. Inaccuracies arise from variations in the reflection coefficient at the buffer-couplant-sample interface. The reflection coefficient is examined as a function of the surface roughness and corresponding couplant thickness variations. Interrelations with ultrasonic frequency are illustrated. Reliable attenuation measurements are obtained only when the frequency dependence of the reflection coefficient is incorporated in signal analysis. Data are given for nickel 200 samples and a silicon nitride ceramic bar having surface roughness variations in the 0.3 to 3.0 microns range for signal bandwidths in the 50 to 100 MHz range. Author

N85-10371*# National Aeronautics and Space Administration. Lewis Research Center, Cleveland, Ohio.
ULTRASONIC NONDESTRUCTIVE EVALUATION, MICROSTRUCTURE, AND MECHANICAL PROPERTY INTERRELATIONS
A. VARY Washington Oct. 1984 30 p refs
(NASA-TM-86876; E-2337; NAS 1.15:86876) Avail: NTIS HC A03/MF A01 CSCL 14D

Ultrasonic techniques for mechanical property characterizations are reviewed and conceptual models are advanced for explaining and interpreting the empirically based results. At present, the technology is generally empirically based and is emerging from the research laboratory. Advancement of the technology will require establishment of theoretical foundations for the experimentally observed interrelations among ultrasonic measurements, mechanical properties, and microstructure. Conceptual models are applied to ultrasonic assessment of fracture toughness to illustrate an approach for predicting correlations found among ultrasonic measurements, microstructure, and mechanical properties. R.S.F.

N85-16195*# Ohio State Univ., Columbus.
FUNDAMENTALS OF MICROCRACK NUCLEATION MECHANICS Final Report
L. S. FU, Y. C. SHEU, C. M. CO, W. F. ZHONG, and H. D. SHEN NASA Washington Jan. 1985 86 p refs
(Contract NAG3-340)
(NASA-CR-3851; E-2296; NAS 1.26:3851; RFP763340/714952)
Avail: NTIS HC A05/MF A01 CSCL 20K

A foundation for ultrasonic evaluation of microcrack nucleation mechanics is identified in order to establish a basis for correlations between plane strain fracture toughness and ultrasonic factors through the interaction of elastic waves with material microstructures. Since microcracking is the origin of (brittle) fracture, it is appropriate to consider the role of stress waves in the dynamics of microcracking. Therefore, the following topics are discussed: (1) microstress distributions with typical microstructural defects located in the stress field; (2) elastic wave scattering from various idealized defects; and (3) dynamic effective-properties of media with randomly distributed inhomogeneities. R.S.F.

N85-20389*# National Aeronautics and Space Administration. Lewis Research Center, Cleveland, Ohio.
NDE FOR HEAT ENGINE CERAMICS
S. J. KLIMA 1984 13 p refs Presented at 22nd Automotive Technol. Develop. Contractors Coordination Meeting (ATD/CCM), 29 Oct. - 2 Nov. 1984, Dearborn, Mich.; sponsored by Society of Automotive Engineers
(NASA-TM-86949; E-2470; NAS 1.15:86949) Avail: NTIS HC A02/MF A01 CSCL 14B

Radiographic, ultrasonic, and scanning laser acoustic microscopy (SLAM) techniques were used to characterize silicon nitride and silicon carbide MOR bars in various stages of fabrication. Conventional and microfocus x-ray techniques were found capable of detecting minute high density inclusions in as-received powders, green compacts, and fully densified specimens. Significant density gradients in sintered bars were observed by radiography, ultrasonic velocity, and SLAM. Ultrasonic attenuation was found sensitive to microstructural variations due to grain and void morphology and distribution. SLAM was also capable of detecting voids, inclusions, and cracks in finished test bars. It was determined that thermoacoustic microscopy techniques have promise for application to green and densified ceramics. R.J.F.

N85-20390*# Massachusetts Inst. of Tech., Cambridge.
STRESS WAVES IN AN ISOTROPIC ELASTIC PLATE EXCITED BY A CIRCULAR TRANSDUCER Final Report
H. KARAGULLE, J. H. WILLIAMS, JR., and S. S. LEE Washington NASA Mar. 1985 52 p refs
(Contract NAG3-328)
(NASA-CR-3877; NAS 1.26:3877) Avail: NTIS HC A04/MF A01 CSCL 14D

Steady state harmonic stress waves in an isotropic elastic plate excited on one face by a circular transducer are analyzed theoretically. The transmitting transducer transforms an electrical voltage into a uniform normal stress at the top of the plate. To solve the boundary value problem, the radiation into a half-space is considered. The receiving transducer produces an electrical voltage proportional to the average spatially integrated normal stress over its face due to an incident wave. A numerical procedure is given to evaluate the frequency response at a receiving point due to a multiply reflected wave in the near field. Its stability and convergence are discussed. Parameterization plots which determine the particular wave whose frequency response has maximum magnitude compared with other multiple reflected waves are given for a range of values of dimensionless parameters. The effects of changes in the values of the parameters are discussed. B.G.

N85-21673*# Massachusetts Inst. of Tech., Cambridge. Dept. of Mechanical Engineering.
APPLICATION OF HOMOMORPHIC SIGNAL PROCESSING TO STRESS WAVE FACTOR ANALYSIS
H. KARAGULLE, J. H. WILLIAMS, JR., and S. S. LEE Feb. 1985 48 p refs
(Contract NSG-3328)
(NAS 1.26:174871; NASA-CR-174871) Avail: NTIS HC A03/MF A01 CSCL 14D

The stress wave factor (SWF) signal, which is the output of an ultrasonic testing system where the transmitting and receiving transducers are coupled to the same face of the test structure, is analyzed in the frequency domain. The SWF signal generated in an isotropic elastic plate is modelled as the superposition of successive reflections. The reflection which is generated by the stress waves which travel p times as a longitudinal (P) wave and s times as a shear (S) wave through the plate while reflecting back and forth between the bottom and top faces of the plate is designated as the reflection with p, s. Short-time portions of the SWF signal are considered for obtaining spectral information on individual reflections. If the significant reflections are not overlapped, the short-time Fourier analysis is used. A summary of the elevant points of homomorphic signal processing, which is also called cepstrum analysis, is given. Homomorphic signal processing is applied to short-time SWF signals to obtain estimates of the log spectra of individual reflections for cases in which the reflections are overlapped. Two typical SWF signals generated in aluminum plates (overlapping and non-overlapping reflections) are analyzed. M.G.

N85-21674*# National Aeronautics and Space Administration. Lewis Research Center, Cleveland, Ohio.
RADIOGRAPHIC DETECTABILITY LIMITS FOR SEEDED VOIDS IN SINTERED SILICON CARBIDE AND SILICON NITRIDE
G. Y. BAAKLINI (Cleveland State Univ.), J. D. KISER, and D. J. ROTH 1984 19 p refs Presented at the Regional Meeting of the American Ceramic Society, San Francisco, 28-31 Oct. 1984
(NASA-TM-86945; E-2464; NAS 1.15:86945) Avail: NTIS HC A02/MF A01 CSCL 14D

Conventional and microfocus X-radiographic techniques were compared to determine relative detectability limits for voids in green and sintered SiC and Si3N4. The relative sensitivity of the techniques was evaluated by comparing their ability to detect voids that were artificially introduced by a seeding process. For projection microfocus radiography the sensitivity of void detection at a 90/95 probability of detection/confidence level is 1.5% of specimen thickness in sintered SiC and Si3N4. For conventional contact radiography the sensitivity is 2.5% of specimen thickness. It appears that microfocus projection radiography is preferable to conventional contact radiography in cases where increased sensitivity is required and where the additional complexity of the technique can be tolerated. E.A.K.

N85-29307*# Massachusetts Inst. of Tech., Cambridge. Dept. of Mechanical Engineering.
ULTRASONIC TESTING OF PLATES CONTAINING EDGE CRACKS Final Report
J. H. WILLIAMS, JR., H. KARAGULLE, and S. S. LEE Washington NASA Jun. 1985 37 p refs
(Contract NAG3-328)
(NASA-CR-3904; E-2550; NAS 1.26:3904) Avail: NTIS HC A03/MF A01 CSCL 14D

The stress wave factor (SWF) signal is utilized for the nondestructive evaluation of plates containing perpendicular edge cracks. The effects of the existence lateral location and depth of the crack on the magnitude spectra of individual reflections in the SWF signal are studied. If the reflections in the SWF signal are not overlapped the short time Fourier analysis is applied. If the reflections are overlapped the short time homomorphic analysis (cepstrum analysis) is applied. Several reflections which have average resonant frequencies approximately at 0.9, 1.3, and 1.7 MHz are analyzed. It is observed that the magnitude ratios evaluated at average resonant frequencies decrease more with increasing d/h if the crack is located between the transducers, where h is plate thickness and d is crack depth. Moreover, for the plates, crack geometries, reflections, and frequencies considered, the average decibel drop depends mainly on the dimensionless parameter d/h and it is approximately -1 dB per 0.07 d/h. Changes in the average resonant frequencies of the magnitude spectra are also observed due to changes in the location of the crack. B.W.

N85-32337*# National Aeronautics and Space Administration. Lewis Research Center, Cleveland, Ohio.
RELIABILITY OF VOID DETECTION IN STRUCTURAL CERAMICS USING SCANNING LASER ACOUSTIC MICROSCOPY
D. J. ROTH, S. J. KLIMA, J. D. KISER, and G. Y. BAAKLINI (Cleveland State Univ.) 1985 54 p refs Presented at the Spring Meeting of the Am. Soc. for Nondestructive Testing, Washington, D.C., 11-14 Mar. 1985
(NASA-TM-87035; E-2591; NAS 1.15:87035) Avail: NTIS HC A04/MF A01 CSCL 14D

The reliability of scanning laser acoustic microscopy (SLAM) for detecting surface voids in structural ceramic test specimens was statistically evaluated. Specimens of sintered silicon nitride and sintered silicon carbide, seeded with surface voids, were examined by SLAM at an ultrasonic frequency of 100 MHz in the as fired condition and after surface polishing. It was observed that polishing substantially increased void detectability. Voids as small as 100 micrometers in diameter were detected in polished specimens with 0.90 probability at a 0.95 confidence level. In addition, inspection times were reduced up to a factor of 10 after polishing. The applicability of the SLAM technique for detection of naturally occurring flaws of similar dimensions to the seeded voids is discussed. A FORTRAN program listing is given for calculating and plotting flaw detection statistics. Author

39

STRUCTURAL MECHANICS

Includes structural element design and weight analysis; fatigue; and thermal stress.

A85-11125* Texas Univ., Austin.
ANALYSIS OF HOURGLASS INSTABILITIES AND CONTROL IN UNDERINTEGRATED FINITE ELEMENT METHODS
O.-P. JACQUOTTE and J. T. ODEN (Texas, University, Austin, TX) Computer Methods in Applied Mechanics and Engineering (ISSN 0045-7825), vol. 44, Aug. 1984, p. 339-363. refs
(Contract NAG3-329)

Belytschko et al. (1981, 1984) has developed stabilization methods for the treatment of underintegrated FEM problems; these methods involve the computation of an underintegrated stiffness matrix, which is rank-deficient, and the addition of a stabilization matrix which effectively eliminates the spurious modes. An attempt is presently made to give this a priori stabilization method a mathematical means of support. Attention is also given to an a posteriority stabilization method for hourglass control, in which an approximate solution of the underintegrated system is obtained and then subjected to a special projection in order to eliminate the hourglass modes. A proof is obtained for the convergence of this stabilized underintegrated approximation to the exact solution of a model problem at almost the same rate (as the mesh is refined) as the fully integrated solutions. O.C.

A85-12029* Massachusetts Inst. of Tech., Cambridge.
RATIONAL APPROACH FOR ASSUMED STRESS FINITE ELEMENTS
T. H. H. PIAN (MIT, Cambridge, MA) and K. SUMIHARA International Journal for Numerical Methods in Engineering (ISSN 0029-5981), vol. 20, Sept. 1984, p. 1685-1695. refs
(Contract NAG3-33)

A new method for the formulation of hybrid elements by the Hellinger-Reissner principle is established by expanding the essential terms of the assumed stresses as complete polynomials in the natural coordinates of the element. The equilibrium conditions are imposed in a variational sense through the internal displacements which are also expanded in the natural co-ordinates. The resulting element possesses all the ideal qualities, i.e. it is invariant, it is less sensitive to geometric distortion, it contains a minimum number of stress parameters and it provides accurate stress calculations. For the formulation of a 4-node plane stress element, a small perturbation method is used to determine the equilibrium constraint equations. The element has been proved to be always rank sufficient. Author

A85-12716*# National Aeronautics and Space Administration. Lewis Research Center, Cleveland, Ohio.
FLUTTER OF TURBOFAN ROTORS WITH MISTUNED BLADES
K. R. V. KAZA and R. E. KIELB (NASA, Lewis Research Center, Cleveland, OH) (Structures, Structural Dynamics and Materials Conference, 23rd, New Orleans, LA, May 10-12, 1982, Collection of Technical Papers. Part 2, p. 446-461) AIAA Journal (ISSN 0001-1452), vol. 22, Nov. 1984, p. 1618-1625. Previously cited in issue 13, p. 2111, Accession no. A82-30175. refs

A85-12721*# Massachusetts Inst. of Tech., Cambridge.
FLUTTER AND FORCED RESPONSE OF MISTUNED ROTORS USING STANDING WAVE ANALYSIS
J. DUGUNDJI and D. J. BUNDAS (MIT, Cambridge, MA) (Structures, Structural Dynamics and Materials Conference, 24th, Lake Tahoe, NV, May 2-4, 1983, Collection of Technical Papers. Part 2, p. 149-159) AIAA Journal (ISSN 0001-1452), vol. 22, Nov. 1984, p. 1652-1661. Previously cited in issue 12, p. 1742, Accession no. A83-29823. refs
(Contract NAG3-214)

A85-13942* Babcock and Wilcox Co., New York, N.Y.
EXTENSION OF CONSTRAINED INCREMENTAL NEWTON-RAPHSON SCHEME TO GENERALIZED LOADING FIELDS
J. PADOVAN (Akron, University, Akron, OH) and S. PAI (Babcok and Wilcox Co., New York, NY; Akron, University, Akron, OH) Franklin Institute, Journal (ISSN 0016-0032), vol. 318, Sept. 1984, p. 165-186. refs
(Contract NAG3-54)

This paper develops numerical strategies which enable the constrained incremental Newton-Raphson scheme to handle the static response of structure to loading fields with completely generalized histories. This is made possible through the use of specially warped hyperelliptic constraint surfaces which control successive or clustered load steps in the vicinity of loading events with specific timing schedules. Such an approach enables improved convergence and stability characteristics. Due to the generality of the methodology, pre- and postbuckling behavior caused by both kinematic and material nonlinearity can be handled. To demonstrate the scheme, the results of several bench-mark problems are also presented. These include situations involving nonlinear kinematics as well as highly history-dependent elastic-plastic and thermoelastic-plastic material behavior. Author

A85-15893* Massachusetts Inst. of Tech., Cambridge.
HYBRID SEMILOOF ELEMENTS FOR PLATES AND SHELLS BASED UPON A MODIFIED HU-WASHIZU PRINCIPLE
T. H. H. PIAN (MIT, Cambridge, MA) and K. SUMIHARA Computers and Structures (ISSN 0045-7949), vol. 19, no. 1-2, 1984, p. 165-173. refs
(Contract NAG3-33)

Hybrid SemiLoof elements for plates and shells are developed based upon modified Hu-Washizu principle. In the new version of the assumed stress hybrid formulation the equilibrium equations are satisfied through the introduction of internal displacement parameters as Lagrange multipliers. The inversion of the resulting H-matrices is simplified particularly when the stresses are expressed in terms of natural coordinates. A 24-DOF triangular element and a 32-DOF quadrilateral element based on shallow shell theory are derived and evaluated. Author

A85-15894* Georgia Inst. of Tech., Atlanta.
HYBRID STRESS FINITE ELEMENTS FOR LARGE DEFORMATIONS OF INELASTIC SOLIDS
K. W. REED and S. N. ATLURI (Georgia Institute of Technology, Atlanta, GA) Computers and Structures (ISSN 0045-7949), vol. 19, no. 1-2, 1984, p. 175-182. refs
(Contract NAG3-38)

A new hybrid stress finite element algorithm, based on a generalization of Fraeijs de Veubeke's complementary energy principle is presented. Analyses of large quasistatic deformation of inelastic solids (hypoelastic, plastic, viscoplastic) are within its capability. Principle variables in the formulation are the nominal stress rate and spin. A brief account is given of the boundary value problem in these variables, and the 'equivalent' variational principle. The finite element equation, along with initial positions and stresses, comprise an initial value problem. Factors affecting the choice of time integration schemes are discussed. Results found by application of the new algorithm are compared to those obtained by a velocity based finite element algorithm. Author

A85-16095*# National Aeronautics and Space Administration. Lewis Research Center, Cleveland, Ohio.
VIBRATION AND FLUTTER OF MISTUNED BLADED-DISK ASSEMBLIES
K. RAO, V. KAZA (NASA, Lewis Research Center, Cleveland, OH), and R. E. KIELB AIAA, ASME, ASCE, and AHS, Structures, Structural Dynamics and Materials Conference, 25th, Palm Springs, CA, May 14-16, 1984. 16 p. Previously announced in STAR as N84-23923. refs
(AIAA PAPER 84-0991)

An analytical model for investigating vibration and flutter of mistuned bladed disk assemblies is presented. This model accounts

for elastic, inertial and aerodynamic coupling between bending and torsional motions of each individual blade, elastic and inertial couplings between the blades and the disk, and aerodynamic coupling among the blades. The disk was modeled as a circular plate with constant thickness and each blade was represented by a twisted, slender, straight, nonuniform, elastic beam with a symmetric cross section. The elastic axis, inertia axis, and the tension axis were taken to be noncoincident and the structural warping of the section was explicitly considered. The blade aerodynamic loading in the subsonic and supersonic flow regimes was obtained from two-dimensional unsteady, cascade theories. All the possible standing wave modes of the disk and traveling wave modes of the blades were included. The equations of motion were derived by using the energy method in conjunction with the assumed mode shapes for the disk and the blades. Continuities of displacement and slope at the blade-disk junction were maintained. The equations were solved to investigate the effects of blade-disk coupling and blade frequency mistuning on vibration and flutter. Results showed that the flexibility of practical disks such as those used for current generation turbufans did not have a significant influence on either the tuned or mistuned flutter characteristics. However, the disk flexibility may have a strong influence on some of the system frequencies and on forced response. Author

A85-17039*# Rice Univ., Houston, Tex.
OSCILLATOR RESPONSE TO NONSTATIONARY EXCITATION
P.-T. D. SPANOS (Rice University, Houston, TX) and G. P. SOLOMOS ASME, Transactions, Journal of Applied Mechanics (ISSN 0021-8936), vol. 51, Dec. 1984, p. 907-912. refs
(Contract NAG3-210)
(ASME PAPER 84-WA/APM-38)

Analytical solutions are presented regarding probability density distributions of various response parameters of a lightly damped oscillator. The oscillator is subjected to a broad-band stochastic excitation which possesses a time-variant power spectrum. The analytical solutions are derived by utilizing appropriate Fokker-Planck equations which govern Markovian approximations of the response parameters considered. The reliability of the approximate analytical solution is tested by using pertinent data generated by a digital Monte Carlo study. Author

A85-17040*# National Aeronautics and Space Administration. Lewis Research Center, Cleveland, Ohio.
EFFECTS OF WARPING AND PRETWIST ON TORSIONAL VIBRATION OF ROTATING BEAMS
K. R. V. KAZA and R. E. KIELB (NASA, Lewis Research Center, Cleveland, OH) ASME, Transactions, Journal of Applied Mechanics (ISSN 0021-8936), vol. 51, Dec. 1984, p. 913-920. refs
(ASME PAPER 84-WA/APM-41)

The effect of pretwist and warping on the torsional vibration of short-aspect-ratio rotating beams is examined for application to the modeling of turbofan, turboprop, and compressor blades. The equations of motion and the associated boundary conditions by using both Wagner's hypothesis and Washizu's theory are derived and a few minor limitations of the Wagner's hypothesis, as applied to thick blades, are pointed out and discussed. The equations for several special cases are solved in a closed form. Results are presented indicating the effect of warping, pretwist, and rotation on torsional vibration of beams as aspect ratio is varied. The results show that the structural warping and pretwist terms have a significant effect on torsional frequency and mode shapes of short-aspect-ratio blades whereas the inertial warping terms have negligible effect. Since the torsional frequencies and mode shapes are very important in aeroelastic analyses by using modal methods, the structural warping terms should be included in modeling turbofan, turboprop, compressor, and turbine blades. Author

A85-18795*# Battelle Columbus Labs., Ohio.
A HISTORY DEPENDENT DAMAGE MODEL FOR LOW CYCLE FATIGUE
B. N. LEIS (Battelle Columbus Laboratories, Columbus, OH) American Society of Mechanical Engineers, Pressure Vessels and Piping Conference and Exhibition, San Antonio, TX, June 17-21, 1984. 10 p. Research supported by the Battelle Columbus Laboratories, and Battelle Memorial Institute. refs
(Contract NAS3-22825)
(ASME PAPER 84-PVP-112)

This paper examines damage assessment and accumulation. A nonlinear damage postulate is advanced that embodies the dependence of the damage rate on cycle-dependent changes in the bulk microstructure and the surface topography. The postulate is analytically formulated in terms of the deformation history dependence of the bulk behavior. This formulation is used in conjunction with baseline data in accordance with the damage postulate to predict the low cycle fatigue resistance of OFE copper. Close comparison of the predictions with observed behavior suggests the postulate offers a viable basis for nonlinear damage analysis. Author

A85-19433* Case Western Reserve Univ., Cleveland, Ohio.
STATISTICS AND THERMODYNAMICS OF FRACTURE
A. CHUDNOVSKY (Case Western Reserve University, Cleveland, OH) (Michigan Technological University, Workshop on Media with Microstructure and Wave Propagation, Michigan Technological University, Houghton, MI, Jan. 24, 25, 1983) International Journal of Engineering Science (ISSN 0020-7225), vol. 22, no. 8-10, 1984, p. 989-997. refs
(Contract NAG3-223)

A probabilistic model of the fracture processes unifying the phenomenological study of long term strength of materials, fracture mechanics and statistical approaches to fracture is briefly outlined. The general framework of irreversible thermodynamics is employed to model the deterministic side of the failure phenomenon. The stochastic calculus is used to account for thg failure mechanisms controlled by chance; particularly, the random roughness of fracture surfaces. Author

A85-19899* Georgia Inst. of Tech., Atlanta.
DEVELOPMENT AND TESTING OF STABLE, INVARIANT, ISOPARAMETRIC CURVILINEAR 2- AND 3-D HYBRID-STRESS ELEMENTS
E. F. PUNCH (Georgia Institute of Technology, Atlanta, GA; GM Research Laboratories, Warren, MI) and S. N. ATLURI (Georgia Institute of Technology, Atlanta, GA) Computer Methods in Applied Mechanics and Engineering (ISSN 0045-7825), vol. 47, Dec. 1984, p. 331-356. refs
(Contract NAG3-346)

Linear and quadratic Serendipity hybrid-stress elements are examined in respect of stability, coordinate invariance, and optimality. A formulation based upon symmetry group theory successfully addresses these issues in undistorted geometries and is fully detailed for plane elements. The resulting least-order stable invariant stress polynomials can be applied as astute approximations in distorted cases through a variety of tensor components and variational principles. A distortion sensitivity study for two- and three-dimensional elements provides favorable numerical comparisons with the assumed displacement method. Author

A85-22069* Ohio State Univ., Cleveland.
VIBRATIONS OF TWISTED CANTILEVERED PLATES - SUMMARY OF PREVIOUS AND CURRENT STUDIES
A. W. LEISSA (Ohio State University, Columbus, OH), J. C. MACBAIN (USAF, Aero Propulsion Laboratory, Wright-Patterson AFB, OH), and R. E. KIELB (NASA, Lewis Research Center, Structural and Mechanical Technology Div., Cleveland, OH) Journal of Sound and Vibration (ISSN 0022-460X), vol. 96, Sept. 22, 1984, p. 159-173. refs

This work summarizes a comprehensive study made of the free vibrations of twisted, cantilevered plates of rectangular

planform. Numerous theoretical and experimental investigations previously made by others have resulted in frequency results which disagree considerably. To clarify the problem a joint industry/government/university research effort was initiated to obtain comprehensive theoretical and experimental results for models having useful ranges of aspect ratios, thickness ratios and twist angles. Theoretical data came from 19 independent computer analyses, including finite element, shell theory and beam theory idealizations. Two independent sets of experimental data were also obtained. The theoretical and experimental results are summarized and compared. Author

A85-23150*# National Aeronautics and Space Administration. Lewis Research Center, Cleveland, Ohio.
A SIMPLIFIED METHOD FOR ELASTIC-PLASTIC-CREEP STRUCTURAL ANALYSIS
A. KAUFMAN (NASA, Lewis Research Center, Cleveland, OH) ASME, Transactions, Journal of Engineering for Gas Turbines and Power (ISSN 0022-0825), vol. 107, Jan. 1985, p. 231-237. refs
(ASME PAPER 84-GT-191)

A simplified inelastic analysis computer program (ANSYPM) was developed for predicting the stress-strain history at the critical location of a thermomechanically cycled structure from an elastic solution. The program uses an iterative and incremental procedure to estimate the plastic strains from the material stress-strain properties and a plasticity hardening model. Creep effects are calculated on the basis of stress relaxation at constant strain, creep at constant stress or a combination of stress relaxation and creep accumulation. The simplified method was exercised on a number of problems involving uniaxial and multiaxial loading, isothermal and nonisothermal conditions, dwell times at various points in the cycles, different materials and kinematic hardening. Good agreement was found between these analytical results and nonlinear finite element solutions for these problems. The simplified analysis program used less than 1 percent of the CPU time required for a nonlinear finite element analysis. Author

A85-24532* Northwestern Univ., Evanston, Ill.
ON STRESS FIELD NEAR A STATIONARY CRACK TIP
S. NEMAT-NASSER and M. OBATA (Northwestern University, Evanston, IL) Mechanics of Materials (ISSN 0167-6636), vol. 3, Sept. 1984, p. 235-243. refs
(Contract NAG3-134; DAAG29-82-K-0147)
(AD-A152863)

It is well known that the stress and elastic-plastic deformation fields near a crack tip have important roles in the corresponding fracture process. For elastic-perfectly-plastic solids, different solutions are given in the literature. In this work several of these solutions are examined and compared for Mode I (tension), Mode II (shear), and mixed Modes I and II loading conditions in plane strain. By consideration of the dynamic solution, it is shown that the assumption that the material is yielding all around a crack tip may not be reasonable in all cases. By admitting the existence of some elastic sectors, continuous stress fields are obtained even for mixed Modes I and II. Author

A85-27935* Materials Research Lab., Inc., Glenwood, Ill.
FRACTURE OF COMPOSITE-ADHESIVE-COMPOSITE SYSTEMS
E. J. RIPLING, J. S. SANTNER, and P. B. CROSLEY (Materials Research Laboratory, Inc., Glenwood, IL) IN: Adhesive joints: Formation, characteristics, and testing . New York, Plenum Press, 1984, p. 755-787. refs
(Contract NAS3-21824)

This program was undertaken to initiate the development of a test method for testing adhesive joints in metal-adhesive-composite systems. The uniform double cantilever beam (UDCB) and the width tapered beam (WTB) specimen geometries were evaluated for measuring Mode I fracture toughness in these systems. The WTB specimen is the preferred geometry in spite of the fact that it is more costly to machine than the UDCB specimen. The use of loading tabs attached to thin sheets of composites proved to be experimentally unsatisfactory. Consequently, a new system was developed to load thin sheets of adherends. This system allows for the direct measurement of displacement along the load line. In well made joints separation occurred between the plies rather than in the adhesive. Author

A85-30313*# Pratt and Whitney Aircraft Group, East Hartford, Conn.
FINITE ELEMENT ENGINE BLADE STRUCTURAL OPTIMIZATION
K. W. BROWN (United Technologies Corp., Pratt and Whitney Group, East Hartford, CT), M. S. HIRSCHBEIN, and C. C. CHAMIS (NASA, Lewis Research Center, Cleveland, OH) IN: Structures, Structural Dynamics, and Materials Conference, 26th, Orlando, FL, April 15-17, 1985, Technical Papers. Part 1 . New York, American Institute of Aeronautics and Astronautics, 1985, p. 793-803. refs
(Contract NAS3-22525)
(AIAA PAPER 85-0645)

The Structural Tailoring of Engine Blades (STAEBL) computer program was developed to perform engine fan blade numerical optimizations. These blade optimizations seek a minimum weight or cost design that satisfies realistic blade design constraints, by tuning one to twenty design variables. The STAEBL system has been generalized to include both fan and compressor blade numerical optimizations. The system analyses have been significantly improved through the inclusion of an efficient plate finite element analysis for blade stress and frequency determinations. Additionally, a finite element based approximate severe foreign object damage (FOD) analysis has been included. The new FOD analysis gives very accurate estimates of the full nonlinear bird ingestion solution. Optimizations of fan and compressor blades have been performed using the system, showing significant cost and weight reductions, while comparing very favorably with refined design validation procedures. Author

A85-32343* *Indian Inst. of Tech., Madras.*
NATURAL FREQUENCIES OF TWISTED ROTATING PLATES
V. RAMAMURTI (Indian Institute of Technology, Madras, India) and R. KIELB (NASA, Lewis Research Center, Cleveland, OH) Journal of Sound and Vibration (ISSN 0022-460X), vol. 97, Dec. 8, 1984, p. 429-449. refs

A detailed comparison is presented of the predicted eigenfrequencies of twisted rotating plates as obtained by using two different shape functions. Primarily, rotating twisted plates of two different aspect ratios and two different thickness ratios are considered. The effects of rotation are included by using a 'stress smoothing' technique when calculating the augmented stiffness matrix. In addition, the effects of Coriolis acceleration, contributions from membrane behavior, setting angle and sweep angle are considered. The effects of geometric nonlinearity are briefly discussed. Finally, results of a brief study of cambered plates are presented. Author

A85-32962*# National Aeronautics and Space Administration. Lewis Research Center, Cleveland, Ohio.
FLUTTER OF SWEPT FAN BLADES
R. E. KIELB and K. R. V. KAZA (NASA, Lewis Research Center, Cleveland, OH) ASME, Transactions, Journal of Engineering for Gas Turbines and Power (ISSN 0022-0825), vol. 107, April 1985, p. 394-398. Previously announced in STAR as N84-16587. refs
(ASME PAPER 84-GT-138)

The effect of sweep on fan blade flutter is studied by applying the analytical methods developed for aeroelastic analysis of advance turboprops. Two methods are used. The first method utilizes an approximate structural model in which the blade is represented by a swept, nonuniform beam. The second method utilizes a finite element technique to conduct modal flutter analysis. For both methods the unsteady aerodynamic loads are calculated using two dimensional cascade theories which are modified to account for sweep. An advanced fan stage is analyzed with 0, 15 and 30 degrees of sweep. It is shown that sweep has a beneficial effect on predominantly torsional flutter and a detrimental effect on predominantly bending flutter. This detrimental effect is shown to be significantly destabilizing for 30 degrees of sweep. M.G.

A85-33847* Georgia Inst. of Tech., Atlanta.
ON THE EXISTENCE AND STABILITY CONDITIONS FOR MIXED-HYBRID FINITE ELEMENT SOLUTIONS BASED ON REISSNER'S VARIATIONAL PRINCIPLE
L. A. KARLOVITZ, S. N. ATLURI (Georgia Institute of Technology, Atlanta, GA), and W.-M. XUE *International Journal of Solids and Structures* (ISSN 0020-7683), vol. 21, no. 1, 1985, p. 97-116. refs
(Contract NAG3-346)

The extensions of Reissner's two-field (stress and displacement) principle to the cases wherein the displacement field is discontinuous and/or the stress field results in unreciprocated tractions, at a finite number of surfaces ('interelement boundaries') in a domain (as, for instance, when the domain is discretized into finite elements), is considered. The conditions for the existence, uniqueness, and stability of mixed-hybrid finite element solutions based on such discontinuous fields, are summarized. The reduction of these global conditions to local ('element') level, and the attendant conditions on the ranks of element matrices, are discussed. Two examples of stable, invariant, least-order elements - a four-node square planar element and an eight-node cubic element - are discussed in detail. Author

A85-35046*# Massachusetts Inst. of Tech., Cambridge.
EVOLUTION OF ASSUMED STRESS HYBRID FINITE ELEMENT
T. H. H. PIAN (MIT, Cambridge, MA) World Congress and Exhibition on Finite Element Methods, 4th, Interlaken, Switzerland, Sept. 17-21, 1984, Preprint. 18 p. refs
(Contract NAG3-33; F33615-83-K-5016)

Early versions of the assumed stress hybrid finite elements were based on the a priori satisifaction of stress equilibrium conditions. In the new version such conditions are relaxed but are introduced through additional internal displacement functions as Lagrange multipliers. A rational procedure is to choose the displacement terms such that the resulting strains are now of complete polynomials up to the same degree as that of the assumed stresses. Several example problems indicate that optimal element properties are resulted by this method. Author

A85-35048*
PLASTICITY, VISCOPLASTICITY, AND CREEP OF SOLIDS BY MECHANICAL SUBELEMENT MODELS
T. H. H. PIAN IN: Numerical methods in coupled systems. Chichester, Sussex, England, John Wiley and Sons, Ltd., 1984, p. 119-126. refs
(Contract NAG3-33)

This paper discusses the modelling by mechanical subelements, the general plasticity, the viscoplasticity, and the creep behavior of solids under multiaxial loading conditions. The formulation of a time-independent elastic-plastic analysis is based on the viscoplasticity theory and the assumed stress finite element method. An example of an in-plane stress problem is included. Author

A85-37440* Akron Univ., Ohio.
PANTOGRAPHING SELF ADAPTIVE GAP ELEMENTS
J. PADOVAN, R. MOSCARELLO (Akron, University, Akron, OH), J. STAFFORD, and F. TABADDOR (B.F. Goodrich Co., Akron, OH) *Computers and Structures* (ISSN 0045-7949), vol. 20, no. 4, 1985, p. 745-758. refs
(Contract NAG3-54)

This paper develops a so-called pantographing self adaptive gap element type contact strategy. Due to the manner of formulation, the scheme has the capability to handle large deformations in the contact zone; contact initiation in structure exhibiting either positive or indefinite stiffness characteristics; kinematic and material nonlinearity as well as; self adaptively adjusts load/time stepping. In this context, contact in pre and postbuckling structure can be treated. To illustrate the scheme, several benchmark problems are presented. These include contacting structure involving large deformation kinematics, inelastic behavior as well as pre and postbuckling stiffness characteristics. Author

A85-38425*# Technion - Israel Inst. of Tech., Haifa.
THERMODYNAMICALLY CONSISTENT CONSTITUTIVE EQUATIONS FOR NONISOTHERMAL LARGE STRAIN, ELASTO-PLASTIC, CREEP BEHAVIOR
R. RIFF (Technion - Israel Institute of Technology, Haifa, Israel; Georgia Institute of Technology, Atlanta, GA), R. L. CARLSON, and G. J. SIMITSES (Georgia Institute of Technology, Atlanta, GA) American Institute of Aeronautics and Astronautics, Structures, Structural Dynamics and Materials Conference, 26th, Orlando, FL, Apr. 15-17, 1985. 11 p.
(Contract NAG3-534)
(AIAA PAPER 85-0621)

The paper is concerned with the development of constitutive relations for large nonisothermal elastic-viscoplastic deformations for metals. The kinematics of elastic-plastic deformation, valid for finite strains and rotations, is presented. The resulting elastic-plastic uncoupled equations for the deformation rate combined with use of the incremental elasticity law permits a precise and purely deductive development of elastic-viscoplastic theory. It is shown that a phenomenological thermodynamic theory in which the elastic deformation and the temperature are state variables, including few internal variables, can be utilized to construct elastic-viscoplastic constitutive equations, which are appropriate for metals. The limiting case of inviscid plasticity is examined. Author

A85-39769*# National Aeronautics and Space Administration. Lewis Research Center, Cleveland, Ohio.
UNIFIED CONSTITUTIVE MATERIAL MODELS FOR NONLINEAR FINITE-ELEMENT STRUCTURAL ANALYSIS
A. KAUFMAN (NASA, Lewis Research Center, Cleveland, OH), J. H. LAFLEN (General Electric Co., Cincinnati, OH), and U. S. LINDHOLM (Southwest Research Institute, San Antonio, TX) AIAA, SAE, ASME, and ASEE, Joint Propulsion Conference, 21st, Monterey, CA, July 8-10, 1985. 10 p. Previously announced in STAR as N85-24338. refs
(AIAA PAPER 85-1418)

Unified constitutive material models were developed for structural analyses of aircraft gas turbine engine components with particular application to isotropic materials used for high-pressure stage turbine blades and vanes. Forms or combinations of models independently proposed by Bodner and Walker were considered. These theories combine time-dependent and time-independent aspects of inelasticity into a continuous spectrum of behavior. This is in sharp contrast to previous classical approaches that partition inelastic strain into uncoupled plastic and creep components. Predicted stress-strain responses from these models were evaluated against monotonic and cyclic test results for uniaxial specimens of two cast nickel-base alloys, B1900+Hf and Rene 80. Previously obtained tension-torsion test results for Hastelloy X alloy were used to evaluate multiaxial stress-strain cycle predictions. The unified models, as well as appropriate algorithms for integrating the constitutive equations, were implemented in finite-element computer codes. Author

A85-39770*# South Carolina State Coll., Orangeburg.
ON LOCAL TOTAL STRAIN REDISTRIBUTION USING A SIMPLIFIED CYCLIC INELASTIC ANALYSIS BASED ON AN ELASTIC SOLUTION
S. Y. HWANG (South Carolina State College, Orangeburg, SC) and A. KAUFMAN (NASA, Lewis Research Center, Cleveland, OH) AIAA, SAE, ASME, and ASEE, Joint Propulsion Conference, 21st, Monterey, CA, July 8-10, 1985. 10 p. Previously announced in STAR as N85-21690. refs
(AIAA PAPER 85-1419)

Strain redistribution corrections were developed for a simplified inelastic analysis procedure to economically calculate material cyclic response at the critical location of a structure for life prediction purposes. The method was based on the assumption that the plastic region in the structure is local and the total strain history required for input can be defined from elastic finite element analyses. Cyclic stress-strain behavior was represented by a bilinear kinematic hardening model. The simplified procedure has been found to predict stress-strain response with reasonable accuracy

for thermally cycled problems but needs improvement for mechanically load cycled problems. This study derived and incorporated Neuber type corrections in the simplified procedure to account for local total strain redistribution under cyclic mechanical loading. The corrected simplified method was exercised on a mechanically load cycled benchmark notched plate problem. Excellent agreement was found between the predicted material response and nonlinear finite element solutions for the problem. The simplified analysis computer program used 0.3 percent of the CPU time required for a nonlinear finite element analysis. Author

A85-40814*# National Aeronautics and Space Administration. Lewis Research Center, Cleveland, Ohio.
FATIGUE CRITERION TO SYSTEM DESIGN, LIFE AND RELIABILITY
E. V. ZARETSKY (NASA, Lewis Research Center, Cleveland, OH) AIAA, SAE, ASME, and ASEE, Joint Propulsion Conference, 21st, Monterey, CA, July 8-10, 1985. 9 p. Previously announced in STAR as N85-27226. refs
(AIAA PAPER 85-1140)

A generalized methodology to structural life prediction, design, and reliability based upon a fatigue criterion is advanced. The life prediction methodology is based in part on work of Weibull and Lundberg and Palmgren. The approach incorporates the computed life of elemental stress volumes of a complex machine element to predict system life. The results of coupon fatigue testing can be incorporated into the analysis allowing for life prediction and component or structural renewal rates with reasonable statistical certainty. Author

A85-40910* Southwest Research Inst., San Antonio, Tex.
CONSTITUTIVE MODELING AND COMPUTATIONAL IMPLEMENTATION FOR FINITE STRAIN PLASTICITY
K. W. REED (Southwest Research Institute, San Antonio, TX) and S. N. ATLURI (Georgia Institute of Technology, Atlanta) International Journal of Plasticity (ISSN 0749-6419), vol. 1, no. 1, 1985, p. 63-87. refs
(Contract NAG3-346)

This paper describes a simple alternate approach to the difficult problem of modeling material behavior. Starting from a general representation for a rate-tpe constitutive equation, it is shown by example how sets of test data may be used to derive restrictions on the scalar functions appearing in the representation. It is not possible to determine these functions from experimental data, but the aforementioned restrictions serve as a guide in their eventual definition. The implications are examined for hypo-elastic, isotropically hardening plastic, and kinematically hardening plastic materials. A simple model for the evolution of the 'back-stress,' in a kinematic-hardening plasticity theory, that is entirely analogous to a hypoelastic stress-strain relation is postulated and examined in detail in modeling finitely plastic tension-torsion test. The implementation of rate-type material models in finite element algorithms is also discussed. Author

A85-41109* Massachusetts Inst. of Tech., Cambridge.
AXISYMMETRIC SOLID ELEMENTS BY A RATIONAL HYBRID STRESS METHOD
Z. TIAN and T. H. H. PIAN (MIT, Cambridge, MA) (George Washington University and NASA, Symposium on Advances and Trends in Structures and Dynamics, Washington, DC, Oct. 22-25, 1984) Computers and Structures (ISSN 0045-7949), vol. 20, no. 1-3, 1985, p. 141-149. refs
(Contract NAG3-33)

Four-node axisymmetric solid elements are derived by a new version of hybrid method for which the assumed stresses are expressed in complete polynomials in natural coordinates. The stress equilibrium conditions are introduced through the use of additional displacements as Lagrange multipliers. A rational procedure is to choose the displacement terms such that the resulting strains are also of complete polynomials of the same order. Example problems all indicate that elements obtained by this procedure lead to better results in displacements and stresses than that by other finite elements. Author

A85-41983* Akron Univ., Ohio.
QUASI-STATIC SOLUTION ALGORITHMS FOR KINEMATICALLY/MATERIALLY NONLINEAR THERMOMECHANICAL PROBLEMS
J. PADOVAN (Akron, University, OH) and S. S. PAI (Babcock and Wilcox Co., Akron, OH) Journal of Thermal Stresses (ISSN 0149-5739), vol. 7, no. 3-4, 1984, p. 227-257. Research supported by Babcock and Wilcox Corp. refs
(Contract NAG3-54)

This paper develops an algorithmic solution strategy which allows the handling of positive/indefinite stiffness characteristics associated with the pre- and post-buckling of structures subject to complex thermomechanical loading fields. The flexibility of the procedure is such that it can be applied to both finite difference and element-type simulations. Due to the generality of the algorithmic approach developed, both kinematic and thermal/mechanical type material nonlinearity including inelastic effects can be treated. This includes the possibility of handling completely general thermomechanical boundary conditions. To demonstrate the scheme, the results of several benchmark problems is presented. Author

A85-42047* National Aeronautics and Space Administration. Lewis Research Center, Cleveland, Ohio.
FINITE DIFFERENCE ANALYSIS OF TORSIONAL VIBRATIONS OF PRETWISTED, ROTATING, CANTILEVER BEAMS WITH EFFECTS OF WARPING
K. B. SUBRAHMANYAM and K. R. V. KAZA (NASA, Lewis Research Center, Cleveland, OH) Journal of Sound and Vibration (ISSN 0022-460X), vol. 99, March 22, 1985, p. 213-224. refs

Theoretical natural frequencies of the first three modes of torsional vibration of pretwisted, rotating cantilever beams are determined for various thickness and aspect ratios. Conclusions concerning individual and collective effects of warping, pretwist, tension-torsion coupling and tennis racket effect (twist-rotational coupling) terms on the natural frequencies are drawn from numerical results obtained by using a finite difference procedure with first order central differences. The relative importance of structural warping, inertial warping, pretwist, tension-torsion and twist-rotational coupling terms is discussed for various rotational speeds. The accuracy of results obtained by using the finite difference approach is verified by a comparison with the exact solution for specialized simple cases of the equation of motion used in this paper. Author

A85-42566*# Garrett Turbine Engine Co., Phoenix, Ariz.
CREEP-RUPTURE RELIABILITY ANALYSIS
A. PERALTA-DURAN (Garrett Turbine Engine Co., Phoenix, AZ) and P. H. WIRSCHING (Arizona, University, Phoenix) ASME, Transactions, Journal of Vibration, Acoustics, Stress, and Reliability in Design (ISSN 0739-3717), vol. 107, July 1985, p. 339-346. Previously announced in STAR as N84-19925. refs
(Contract NAG3-41)

A probabilistic approach to the correlation and extrapolation of creep-rupture data is presented. Time temperature parameters (TTP) are used to correlate the data, and an analytical expression for the master curve is developed. The expression provides a simple model for the statistical distribution of strength and fits neatly into a probabilistic design format. The analysis focuses on the Larson-Miller and on the Manson-Haferd parameters, but it can be applied to any of the TTP's. A method is developed for evaluating material dependent constants for TTP's. It is shown that optimized constants can provide a significant improvement in the correlation of the data, thereby reducing modelling error. Attempts were made to quantify the performance of the proposed method in predicting long term behavior. Uncertainty in predicting long term behavior from short term tests was derived for several sets of data. Examples are presented which illustrate the theory and demonstrate the application of state of the art reliability methods to the design of components under creep. Author

A85-47626* National Aeronautics and Space Administration. Lewis Research Center, Cleveland, Ohio.
VIBRATIONS OF TWISTED CANTILEVER PLATES - A COMPARISON OF THEORETICAL RESULTS
R. E. KIELB (NASA, Lewis Research Center, Cleveland, OH), A. W. LEISSA (Ohio State University, Columbus), and J. C. MACBAIN (USAF, Aero Propulsion Laboratory, Wright-Patterson AFB, OH) International Journal for Numerical Methods in Engineering (ISSN 0029-5981), vol. 21, Aug. 1985, p. 1365-1380. refs

As a result of significant differences in the published results for various methods of analysis involving the use of finite element techniques, there are now some questions regarding the adequacy of these methods to predict accurately the vibratory characteristics of highly twisted cantilever plates. In an attempt to help in a resolution of the arising problems, a joint government/industry/university research effort was initiated. The primary objective of the present paper is to summarize the theoretical methods used in the study and show samples of the obtained results. The study provided 19 sets of theoretical results which are derived from beam theory, shell theory, and finite element methods. G.R.

A85-48703* Air Force Flight Dynamics Lab., Wright-Patterson AFB, Ohio.
STRUCTURAL OPTIMIZATION USING OPTIMALITY CRITERIA METHODS
N. S. KHOT (USAF, Flight Dynamics Laboratory, Wright-Patterson AFB, OH) and L. BERKE (NASA, Lewis Research Center, Cleveland, OH) IN: New directions in optimum structural design . Chichester, England and New York, Wiley-Interscience, 1984, p. 47-74.

Optimality criteria methods take advantage of some concepts as those of statically determinate or indeterminate structures, and certain variational principles of structural dynamics, to develop efficient algorithms for the sizing of structures that are subjected to stiffness-related constraints. Some of the methods and iterative strategies developed over the last decade for calculations of the Lagrange multipliers in stressand displacement-limited problems, as well as for satisfying the appropriate optimality criterion, are discussed. The application of these methods are illustrated by solving problems with stress and displacement constraints. O.C.

N85-10384*# Stanford Univ., Calif.
AUGMENTED WEAK FORMS AND ELEMENT-BY-ELEMENT PRECONDITIONERS: EFFICIENT ITERATIVE STRATEGIES FOR STRUCTURAL FINITE ELEMENTS. A PRELIMINARY STUDY
A. MULLER and T. J. R. HUGHES *In* NASA. Langley Research Center Res. in Struct. and Dyn., 1984 p 95-109 Oct. 1984 refs
(Contract NAG3-319)
Avail: NTIS HC A18/MF A01 CSCL 20K

A weak formulation in structural analysis that provides well conditioned matrices suitable for iterative solutions is presented. A mixed formulation ensures the proper representation of the problem and the constitutive relations are added in a penalized form. The problem is solved by a double conjugate gradient algorithm combined with an element by element approximate factorization procedure. The double conjugate gradient strategy resembles Uzawa's variable-length type algorithms the main difference is the presence of quadratic terms in the mixed variables. In the case of shear deformable beams these terms ensure that the proper finite thickness solution is obtained. E.A.K.

N85-11380*# Arizona Univ., Tucson. Dept. of Aerospace and Mechanical Engineering.
RELIABILITY CONSIDERATIONS FOR THE TOTAL STRAIN RANGE VERSION OF STRAINRANGE PARTITIONING Final Report
P. H. WIRSCHING and Y. T. WU Sep. 1984 85 p refs
(Contract NAG3-41)
(NASA-CR-174757; NAS 1.26:174757) Avail: NTIS HC A05/MF A01 CSCL 20K

A proposed total strainrange version of strainrange partitioning (SRP) to enhance the manner in which SRP is applied to life prediction is considered with emphasis on how advanced reliability technology can be applied to perform risk analysis and to derive safety check expressions. Uncertainties existing in the design factors associated with life prediction of a component which experiences the combined effects of creep and fatigue can be identified. Examples illustrate how reliability analyses of such a component can be performed when all design factors in the SRP model are random variables reflecting these uncertainties. The Rackwitz-Fiessler and Wu algorithms are used and estimates of the safety index and the probablity of failure are demonstrated for a SRP problem. Methods of analysis of creep-fatigue data with emphasis on procedures for producing synoptic statistics are presented. An attempt to demonstrate the importance of the contribution of the uncertainties associated with small sample sizes (fatique data) to risk estimates is discussed. The procedure for deriving a safety check expression for possible use in a design criteria document is presented. A.R.H.

N85-15184*# National Aeronautics and Space Administration. Lewis Research Center, Cleveland, Ohio.
THE USE OF AN OPTICAL DATA ACQUISITION SYSTEM FOR BLADED DISK VIBRATION ANALYSIS
C. LAWRENCE and E. H. MEYN Dec. 1984 23 p refs
(NASA-TM-86891; E-2358; NAS 1.15:86891) Avail: NTIS HC A02/MF A01 CSCL 20K

A new concept in instrumentation was developed by engineers at NASA Lewis Research Center to collect vibration data from multi-bladed rotors. This new concept, known as the optical data acquisition system, uses optical transducers to measure bladed tip delections by reflection light beams off the tips of the blades as they pass in front of the optical transducer. By using an array of transducers around the perimeter of the rotor, detailed vibration signals can be obtained. In this study, resonant frequencies and mode shapes were determined for a 56 bladed rotor using the optical system. Frequency data from the optical system was also compared to data obtained from strain gauge measurements and finite element analysis and was found to be in good agreement. Author

N85-16205*# National Aeronautics and Space Administration. Lewis Research Center, Cleveland, Ohio.
EXPERIMENTAL COMPLIANCE CALIBRATION OF THE NASA LEWIS RESEARCH CENTER MODE 2 FATIGUE SPECIMEN
R. J. BUZZARD 1985 11 p refs Proposed for presentation at the 18th Natl. Symp. on Fracture Mech., Boulder, Colo., 24-27 Jun. 1985; sponsored by American Society for Testing and Materials
(NASA-TM-86908; E-2398; NAS 1.15:86908) Avail: NTIS HC A02/MF A01 CSCL 20K

Calibration of the mode II aluminum fatigue specimen was performed experimentally to provide displacement and stress intensity coefficients over crack length to specimen width ratios (a/W) of 0.5 to 0.9. Displacements were measured both at the specimen notch mouth and at the intersection of the notch with the centerline of the loading pin holes. R.S.F.

N85-18375*# *National Aeronautics and Space Administration.* Lewis Research Center, Cleveland, Ohio.

NASA LEWIS RESEARCH CENTER/UNIVERSITY GRADUATE RESEARCH PROGRAM ON ENGINE STRUCTURES

C. C. CHAMIS 1985 18 p Presented at the 30th Intern. Gas Turbine Conf. and Exhibit, Houston, Tex., 17-21 Mar. 1985; sponsored by ASME

(NASA-TM-86916; E-2393; NAS 1.15:86916) Avail: NTIS HC A02/MF A01 CSCL 20K

NASA Lewis Research Center established a graduate research program in support of the Engine Structures Research activities. This graduate research program focuses mainly on structural and dynamics analyses, computational mechanics, mechanics of composites and structural optimization. The broad objectives of the program, the specific program, the participating universities and the program status are briefly described. Author

N85-20396*# National Aeronautics and Space Administration. Lewis Research Center, Cleveland, Ohio.

LOCAL STRAIN REDISTRIBUTION CORRECTIONS FOR A SIMPLIFIED INELASTIC ANALYSIS PROCEDURE BASED ON AN ELASTIC FINITE-ELEMENT ANALYSIS

A. KAUFMAN and S. Y. HWANG (South Carolina State Coll., Orangeburg) Mar. 1985. 14 p refs To be presented at the 21st AIAA/SAE/ASME Joint Propulsion Conf., Monterey, Calif., 8-11 Jul. 1985

(NASA-TP-2421; E-2373; NAS 1.60:2421) Avail: NTIS HC A02/MF A01 CSCL 20K

Strain redistribution corrections were developed for a simplified inelastic analysis procedure to economically calculate material cyclic response at the critical location of a structure for life prediction proposes. The method was based on the assumption that the plastic region in the structure is local and the total strain history required for input can be defined from elastic finite-element analyses. Cyclic stress-strain behavior was represented by a bilinear kinematic hardening model. The simplified procedure predicts stress-strain response with reasonable accuracy for thermally cycled problems but needs improvement for mechanically load-cycled problems. Neuber-type corrections were derived and incorporated in the simplified procedure to account for local total strain redistribution under cyclic mechanical loading. The corrected simplified method was used on a mechanically load-cycled benchmark notched-plate problem. The predicted material response agrees well with the nonlinear finite-element solutions for the problem. The simplified analysis computer program was 0.3% of the central processor unit time required for a nonlinear finite-element analysis. E.A.K.

N85-21685*# Case Western Reserve Univ., Cleveland, Ohio. Dept. of Civil Engineering.

TRANSLATIONAL AND EXTENSIONAL ENERGY RELEASE RATES (THE J- AND M-INTEGRALS) FOR A CRACK LAYER IN THERMOELASTICITY Final Report

A. CHUDNOVSKY and B. GOMMERSTADT Mar. 1985 9 p refs

(Contract NAG3-223)

(NASA-CR-174872; NAS 1.26:174872) Avail: NTIS HC A02/MF A01 CSCL 20K

A number of papers have been presented on the evaluation of energy release rate for thermoelasticity and corresponding J integral. Two main approaches were developed to treat energy release rate in elasticity. The first is based on direct calculation of the potential energy rate with respect to crack length. The second makes use of Lagrangian formalism. The translational and expansional energy release rates in thermoelasticity are studied by employing the formalism of irreversible thermodynamics and the Crack Layer Approach. Author

N85-21686*# *Pratt and Whitney Aircraft, East Hartford, Conn.* Engineering Div.

3-D INELASTIC ANALYSIS METHODS FOR HOT SECTION COMPONENTS (BASE PROGRAM) Annual Status Report, 14 Feb. 1983 - 14 Feb. 1984

R. B. WILSON, M. J. BAK, S. NAKAZAWA, and P. K. BANERJEE Feb. 1984 167 p refs

(Contract NAS3-23697)

(NASA-CR-174700; NAS 1.26:174700; PWA-5940-19; ASR-1) Avail: NTIS HC A08/MF A01 CSCL 20K

A 3-D inelastic analysis methods program consists of a series of computer codes embodying a progression of mathematical models (mechanics of materials, special finite element, boundary element) for streamlined analysis of combustor liners, turbine blades, and turbine vanes. These models address the effects of high temperatures and thermal/mechanical loadings on the local (stress/strain) and global (dynamics, buckling) structural behavior of the three selected components. These models are used to solve 3-D inelastic problems using linear approximations in the sense that stresses/strains and temperatures in generic modeling regions are linear functions of the spatial coordinates, and solution increments for load, temperature and/or time are extrapolated linearly from previous information. Three linear formulation computer codes, referred to as MOMM (Mechanics of Materials Model), MHOST (MARC-Hot Section Technology), and BEST (Boundary Element Stress Technology), were developed and are described. Author

N85-21687*# Massachusetts Inst. of Tech., Cambridge. Dept. of Aeronautics and Astronautics.

RECENT ADVANCES IN HYBRID/MIXED FINITE ELEMENTS

T. H. H. PIAN 1985 8 p refs

(Contract NAG3-33)

(NASA-CR-175574; NAS 1.26:175574) Avail: NTIS HC A02/MF A01 CSCL 20K

In formulations of Hybrid/Mixed finite element methods respectively by the Hellinger-Reissner principle and the Hu-Washizu principle, the stress equilibrium equations are brought in as conditions of constraint through the introduction of additional internal displacement parameters. These two approaches are more flexible and have better computing efficiencies. A procedure for the choice of assumed stress terms for 3-D solids is suggested. Example solutions are given for plates and shells using the present formulations and the idea of semiloof elements. Author

N85-21690*# National Aeronautics and Space Administration. Lewis Research Center, Cleveland, Ohio.

ON LOCAL TOTAL STRAIN REDISTRIBUTION USING A SIMPLIFIED CYCLIC INELASTIC ANALYSIS BASED ON AN ELASTIC SOLUTION

S. Y. HWANG (South Carolina State Coll.) and A. KAUFMAN 1985 16 p refs Proposed for presentation at the 21st Joint Propulsion Conf., Monterey, Calif., 9-11 Jul. 1985; sponsored by the AIAA, SAE and ASME

(NASA-TM-86913; E-2406; NAS 1.15:86913) Avail: NTIS HC A02/MF A01 CSCL 20K

Strain redistribution corrections were developed for a simplified inelastic analysis procedure to economically calculate material cyclic response at the critical location of a structure for life prediction purposes. The method was based on the assumption that the plastic region in the structure is local and the total strain history required for input can be defined from elastic finite element analyses. Cyclic stress-strain behavior was represented by a bilinear kinematic hardening model. The simplified procedure has been found to predict stress-strain response with reasonable accuracy for thermally cycled problems but needs improvement for mechanically load cycled problems. This study derived and incorporated Neuber type corrections in the simplified procedure to account for local total strain redistribution under cyclic mechanical loading. The corrected simplified method was exercised on a mechanically load cycled benchmark notched plate problem. Excellent agreement was found between the predicted material response and nonlinear finite element solutions for the problem.

The simplified analysis computer program used 0.3 percent of the CPU time required for a nonlinear finite element analysis. Author

N85-21691*# Akron Univ., Ohio. Dept. of Civil Engineering.
VISCOPLASTIC CONSTITUTIVE RELATIONSHIPS WITH DEPENDENCE ON THERMOMECHANICAL HISTORY Final Report
D. N. ROBINSON and P. A. BARTOLOTTA Mar. 1985 42 p refs
(Contract NAG3-379)
(NASA-CR-174836; NAS 1.26:174836) Avail: NTIS HC A03/MF A01 CSCL 20K

Experimental evidence of thermomechanical history dependence in the cyclic hardening behavior of some common high-temperature structural alloys is presented with special emphasis on dynamic metallurgical changes. The inadequacy of formulating nonisothermal constitutive equations solely on the basis of isothermal testing is discussed. A representation of thermoviscoplasticity is proposed that qualitatively accounts for the observed hereditary behavior. This is achieved by formulating the scalar evolutionary equation in an established viscoplasticity theory to reflect thermomechanical path dependence. To assess the importance of accounting for thermomechanical history dependence in practical structural analyses, two qualitative models are specified: (1) formulated as if based entirely on isothermal information; (2) to reflect thermomechanical path dependence using the proposed thermoviscoplastic representation. Predictions of the two models are compared and the impact the calculated differences in deformation behavior may have on subsequent lifetime predictions is discussed. E.A.K.

N85-21720*# Virginia Polytechnic Inst. and State Univ., Blacksburg. Dept. of Engineering Science and Mechanics.
GEOMETRICALLY NONLINEAR ANALYSIS OF LAMINATED ELASTIC STRUCTURES Final Report
J. N. REDDY Nov. 1984 107 p refs
(Contract NAG3-208)
(NASA-CR-175609; NAS 1.26:175609; PB85-127173; VPI-E-84-36) Avail: NTIS HC A06/MF A01 CSCL 20K

Laminated composite plates and shells that can be used to model automobile bodies, aircraft wings and fuselages, and pressure vessels among many other were analyzed. The finite element method, a numerical technique for engineering analysis of structures, is used to model the geometry and approximate the solution. Various alternative formulations for analyzing laminated plates and shells are developed and their finite element models are tested for accuracy and economy in computation. These include the shear deformation laminate theory and degenerated 3-D elasticity theory for laminates. GRA

N85-23096*# Massachusetts Inst. of Tech., Cambridge.
ON HYBRID AND MIXED FINITE ELEMENT METHODS
T. H. H. PIAN 1981 19 p refs
(Contract NAG3-33)
(NASA-CR-175551; NAS 1.26:175551) Avail: NTIS HC A02/MF A01 CSCL 20K

Three versions of the assumed stress hybrid model in finite element methods and the corresponding variational principles for the formulation are presented. Examples of rank deficiency for stiffness matrices by the hybrid stress model are given and their corresponding kinematic deformation modes are identified. A discussion of the derivation of general semi-Loof elements for plates and shells by the hybrid stress method is given. It is shown that the equilibrium model by Fraeijs de Veubeke can be derived by the approach of the hybrid stress model as a special case of semi-Loof elements. Author

N85-24338*# National Aeronautics and Space Administration. Lewis Research Center, Cleveland, Ohio.
UNIFIED CONSTITUTIVE MATERIAL MODELS FOR NONLINEAR FINITE-ELEMENT STRUCTURAL ANALYSIS
A. KAUFMAN, J. H. LAFLEN (General Electric Co., Cincinnati), and U. S. LINDHOLM (Southwest Research Inst., San Antonio) 10 Jul. 1985 16 p refs Proposed for presentation at 21st Joint Propulsion Conf., Monterey, Calif., 8-10 Jul. 1985; sponsored by AIAA, SAE and ASME
(NASA-TM-86985; E-2529; NAS 1.15:86985) Avail: NTIS HC A02/MF A01 CSCL 20K

Unified constitutive material models were developed for structural analyses of aircraft gas turbine engine components with particular application to isotropic materials used for high-pressure stage turbine blades and vanes. Forms or combinations of models independently proposed by Bodner and Walker were considered. These theories combine time-dependent and time-independent aspects of inelasticity into a continuous spectrum of behavior. This is in sharp contrast to previous classical approaches that partition inelastic strain into uncoupled plastic and creep components. Predicted stress-strain responses from these models were evaluated against monotonic and cyclic test results for uniaxial specimens of two cast nickel-base alloys, B1900+Hf and Rene' 80. Previously obtained tension-torsion test results for Hastelloy X alloy were used to evaluate multiaxial stress-strain cycle predictions. The unified models, as well as appropriate algorithms for integrating the constitutive equations, were implemented in finite-element computer codes. Author

N85-24339*# National Aeronautics and Space Administration. Lewis Research Center, Cleveland, Ohio.
CYCLIC STRUCTURAL ANALYSES OF ANISOTROPIC TURBINE BLADES FOR REUSABLE SPACE PROPULSION SYSTEMS
J. M. MANDERSCHEID and A. KAUFMAN 12 Apr. 1985 13 p refs Presented at 1985 JANNAF Propulsion Meeting, San Diego, Calif., 9-12 Apr. 1985; sponsored by JANNAF
(NASA-TM-86990; E-2534; NAS 1.15:86990) Avail: NTIS HC A02/MF A01 CSCL 20K

Turbine blades for reusable space propulsion systems are subject to severe thermomechanical loading cycles that result in large inelastic strains and very short lives. These components require the use of anisotropic high-temperature alloys to meet the safety and durability requirements of such systems. To assess the effects on blade life of material anisotropy, cyclic structural analyses are being performed for the first stage high-pressure fuel turbopump blade of the space shuttle main engine. The blade alloy is directionally solidified MAR-M 246 alloy. The analyses are based on a typical test stand engine cycle. Stress-strain histories at the airfoil critical location are computed using the MARC nonlinear finite-element computer code. The MARC solutions are compared to cyclic response predictions from a simplified structural analysis procedure developed at the NASA Lewis Research Center. Author

N85-25893*# National Aeronautics and Space Administration. Lewis Research Center, Cleveland, Ohio.
VIBRATION AND BUCKLING OF ROTATING, PRETWISTED, PRECONED BEAMS INCLUDING COORIOLIS EFFECTS
K. B. SUBRAHMANYAM and K. R. V. KAZA 1985 21 p refs Proposed for presentation at the 10th Bien. Design Eng. Conf. and Exhibit on Mech. Vibration and Noise, Cincinnati, 10-13 Sep. 1985; sponsored by ASME
(NASA-TM-87004; E-2310; NAS 1.15:87004) Avail: NTIS HC A02/MF A01 CSCL 20K

The effects of pretwist, precone, setting angle and Coriolis forces on the vibration and buckling behavior of rotating, torsionally rigid, cantilevered beams were studied. The beam is considered to be clamped on the axis of rotation in one case, and off the axis of rotation in the other. Two methods are employed for the solution of the vibration problem: (1) one based upon a finite-difference approach using second order central differences for solution of the equations of motion, and (2) based upon the minimum of the total potential energy functional with a Ritz type

of solution procedure making use of complex forms of shape functions for the dependent variables. The individual and collective effects of pretwist, precone, setting angle, thickness ratio and Coriolis forces on the natural frequencies and the buckling boundaries are presented. It is shown that the inclusion of Coriolis effects is necessary for blades of moderate to large thickness ratios while these effects are not so important for small thickness ratio blades. The possibility of buckling due to centrifugal softening terms for large values of precone and rotation is shown. E.A.K.

N85-25894*# Akron Univ., Ohio. Dept. of Civil Engineering.
ON THERMOMECHANICAL TESTING IN SUPPORT OF CONSTITUTIVE EQUATION DEVELOPMENT FOR HIGH TEMPERATURE ALLOYS Final Report
D. N. ROBINSON May 1985 32 p refs
(Contract NAG3-379)
(NASA-CR-174879; NAS 1.26:174879) Avail: NTIS HC A03/MF A01 CSCL 11F

Three major categories of testing are identified that are necessary to provide support for the development of constitutive equations for high temperature alloys. These are exploratory, charactrization and verification tests. Each category is addressed and specific examples of each are given. An extensive, but not exhaustive, set of references is provided concerning pertinent experimental results and their relationships to theoretical development. This guide to formulating a meaningful testing effort in support of consitutive equation development can also aid in defining the necessary testing equipment and instrumentation for the establishment of a deformation and structures testing laboratory. Author

N85-25896*# Georgia Inst. of Tech., Atlanta.
ANALYSIS OF SHELL TYPE STRUCTURES SUBJECTED TO TIME DEPENDENT MECHANICAL AND THERMAL LOADING Semiannual Status Report, 15 Aug. 1984 - 14 Apr. 1985
G. J. SIMITSES, R. L. CARLSON, and R. RIFF May 1985 4 p
(Contract NAG3-534)
(NASA-CR-175747; NAS 1.26:175747) Avail: NTIS HC A02/MF A01 CSCL 20K

A general mathematical model and solution methodologies for analyzing structural response of thin, metallic shell-type structures under large transient, cyclic or static thermomechanical loads is considered. Among the system responses, which are associated with these load conditions, are thermal buckling, creep buckling and ratchetting. Thus, geometric as well as material-type nonlinearities (of high order) can be anticipated and must be considered in the development of the mathematical model. G.L.C.

N85-26885*# Wyle Labs., Inc., Huntsville, Ala.
FLOW DYNAMIC ENVIRONMENT DATA BASE DEVELOPMENT FOR THE SSME
C. V. SUNDARAM *In* NASA. Marshall Space Flight Center Advan. High Pressure O2/H2 Technol. p 277-288 Apr. 1985 refs
Avail: NTIS HC A99/MF E03; SOD HC CSCL 20K

The fluid flow-induced vibration of the Space Shuttle main engine (SSME) components are being studied with a view to correlating the frequency characteristics of the pressure fluctuations in a rocket engine to its operating conditions and geometry. An overview of the data base development for SSME test firing results and the interactive computer software used to access, retrieve, and plot or print the results selectively for given thrust levels, engine numbers, etc., is presented. The various statistical methods available in the computer code for data analysis are discussed. Plots of test data, nondimensionalized using parameters such as fluid flow velocities, densities, and pressures, are presented. Results are compared with those available in the literature. Correlations between the resonant peaks observed at higher frequencies in power spectral density plots with pump geometry and operating conditions are discussed. An overview of the status of the investigation is presented and future directions are discussed. A.R.H.

N85-26887*# National Aeronautics and Space Administration. Lewis Research Center, Cleveland, Ohio.
NONLINEAR STRUCTURAL ANALYSIS FOR FIBER-REINFORCED SUPERALLOY TURBINE BLADES
D. A. HOPKINS and C. C. CHAMIS *In* NASA. Marshall Space Flight Center Advan. High Pressure O2/H2 Technol. p 318-340 Apr. 1985 refs
Avail: NTIS HC A99/MF E03; SOD HC CSCL 20K

A computational capability for predicting the nonlinear thermomechanical structural response of fiber-reinforced superalloy (FRS) turbine blades is described. This capability is embedded in a special purpose computer code (COBSTRAN) developed at the NASA Lewis Research Center. Special features of this computational capability include accounting for: fiber/matrix reaction, nonlinear and anisotropic material behavior, complex stress distribution due to local and global heterogeneity, and residual stresses due to initial fabrication and/or inelastic behavior during subsequent missions. Numerical results are presented from analyses of a hypothetical FRS turbine blade subjected to a fabrication process and subsequent mission cycle. The results demonstrate the capabilities of this computational tool to; predict local stress/strain response and capture trends of local nonlinear and anisotropic material behavior, relate the effects of this local behavior to the global response of a multilayered fiber-composite turbine blade, and trace material history from fabrication through successive missions. Author

N85-27260*# Akron Univ., Ohio. Dept. of Civil Engineering.
SOME ADVANCES IN EXPERIMENTATION SUPPORTING DEVELOPMENT OF VISCOPLASTIC CONSTITUTIVE MODELS Final Report
J. R. ELLIS and D. N. ROBINSON May 1985 62 p refs
(Contract NAG3-379; W-7405-ENG-26)
(NASA-CR-174855; NAS 1.26:174855) Avail: NTIS HC A04/MF A01 CSCL 20K

The development of a biaxial extensometer capable of measuring axial, torsion, and diametral strains to near-microstrain resolution at elevated temperatures is discussed. An instrument with this capability was needed to provide experimental support to the development of viscoplastic constitutive models. The advantages gained when torsional loading is used to investigate inelastic material response at elevated temperatures are highlighted. The development of the biaxial extensometer was conducted in two stages. The first involved a series of bench calibration experiments performed at room temperature. The second stage involved a series of in-place calibration experiments conducted at room and elevated temperature. A review of the calibration data indicated that all performance requirements regarding resolution, range, stability, and crosstalk had been met by the subject instrument over the temperature range of interest, 21 C to 651 C. The scope of the in-place calibration experiments was expanded to investigate the feasibility of generating stress relaxation data under torsional loading. B.W.

N85-27261*# General Electric Co., Cincinnati, Ohio. Aircraft Engine Business Group.
COMPONENT-SPECIFIC MODELING Annual Status Report
R. L. MCKNIGHT 1984 115 p
(Contract NAS3-23687)
(NASA-CR-174765; NAS 1.26:174765; ASR-1) Avail: NTIS HC A06/MF A01 CSCL 20K

A series of interdisciplinary modeling and analysis techniques that were specialized to address three specific hot section components are presented. These techniques will incorporate data as well as theoretical methods from many diverse areas including cycle and performance analysis, heat transfer analysis, linear and nonlinear stress analysis, and mission analysis. Building on the proven techniques already available in these fields, the new methods developed will be integrated into computer codes to provide an accurate, efficient and unified approach to analyzing combustor burner liners, hollow air-cooled turbine blades and air-cooled turbine vanes. For these components, the methods

developed will predict temperature, deformation, stress and strain histories throughout a complete flight mission. Author

N85-27263*# Connecticut Univ., Storrs. Dept. of Mechanical Engineering.
ELEVATED TEMPERATURE BIAXIAL FATIGUE Final Report, 15 Feb. 1981 - 31 Oct. 1984
E. H. JORDAN 31 Oct. 1984 167 p refs
(Contract NAG3-160)
(NASA-CR-175795; NAS 1.26:175795) Avail: NTIS HC A09/MF A01 CSCL 20K

A three year experimental program for studying elevated temperature biaxial fatigue of a nickel based alloy Hastelloy-X has been completed. A new high temperature fatigue test facility with unique capabilities has been developed. Effort was directed toward understanding multiaxial fatigue and correlating the experimental data to the existing theories of fatigue failure. The difficult task of predicting fatigue lives for non-proportional loading was used as an ultimate test for various life prediction methods being considered. The primary means of reaching improved undertanding were through several critical non-proportional loading experiments. It was discovered that the cracking mode switched from primarily cracking on the maximum shear planes at room temperature to cracking on the maximum normal strain planes at 649 C. Author

N85-27264*# National Aeronautics and Space Administration. Lewis Research Center, Cleveland, Ohio.
A COMPUTER ANALYSIS PROGRAM FOR INTERFACING THERMAL AND STRUCTURAL CODES
R. L. THOMPSON and R. J. MAFFEO (GE, Cincinnati) 1985 17 p refs Proposed for presentation at the Intern. Computers in Eng. Conf. and Exhibition, Boston, 4-8 Aug. 1985; sponsored by ASME
(NASA-TM-87021; E-2571; NAS 1.15:87021) Avail: NTIS HC A02/MF A01 CSCL 20K

A software package has been developed to transfer three-dimensional transient thermal information accurately, efficiently, and automatically from a heat transfer analysis code to a structural analysis code. The code is called three-dimensional TRansfer ANalysis Code to Interface Thermal and Structural codes, or 3D TRANCITS. TRANCITS has the capability to couple finite difference and finite element heat transfer analysis codes to linear and nonlinear finite element structural analysis codes. TRANCITS currently supports the output of SINDA and MARC heat transfer codes directly. It will also format the thermal data output directly so that it is compatible with the input requirements of the NASTRAN and MARC structural analysis codes. Other thermal and structural codes can be interfaced using the transfer module with the neutral heat transfer input file and the neutral temperature output file. The transfer module can handle different elemental mesh densities for the heat transfer analysis and the structural analysis. Author

N85-27952*# National Aeronautics and Space Administration. Lewis Research Center, Cleveland, Ohio.
OVERVIEW OF STRUCTURAL RESPONSE: PROBABILISTIC STRUCTURAL ANALYSIS Abstract Only
C. C. CHAMIS *In its* Struct. Integrity and Durability of Reusable Space Propulsion Systems p 63-66 May 1985
Avail: NTIS HC A09/MF A01 CSCL 20K

Advanced analysis methods are required to predict accurately the structural response (static, transient, cyclic, etc.) and accompanying local stresses in space propulsion system components operating in a fatigue environment consisting of complex thermal and mechanical load spectra. The probabilistic approach to structural response consists of the following program elements: (1) composite load spectra, (2) probabilistic structural analysis methods development, (3) probabilitic finite element theory, (4) probabilistic structural analysis application, (5) structural tailoring of turbopump blades, (6) unified theory of dynamic creep buckling/ratcheting, (7) creep buckling/ratcheting analyzer, and (8) nonlinear COBSTRAN development. Research activities on all of these program elements (except the creep buckling/ratcheting analyzer) are under way. G.L.C.

N85-27953*# Rockwell International Corp., Canoga Park, Calif.
COMPOSITE LOADS SPECTRA FOR SELECT SPACE PROPULSION STRUCTURAL COMPONENTS Abstract Only
J. F. NEWELL *In* NASA. Lewis Research Center Struct. Integrity and Durability of Reusable Space Propulsion Systems p 67-75 May 1985
(Contract NAS3-24382)
Avail: NTIS HC A09/MF A01 CSCL 20K

Rocket engine technology continues to demand higher performance with lighter weight components that have man-rated reliability requirements. These requirements have yielded higher operating pressures, temperatures, and transient effects as well as markedly increased mechanical vibration and flow-related loads. The difficulty in installation, cost, and potential for destroying an engine severely limited the required instrumentation and measurements to adequately define loads of key components such as turbine blades. Also, accurate analytical methodologies for defining internal flow-related loads are just emerging for problems typically found in rocket engines. The difficulty of obtained measured data and verified analysis methodologies has led to the probabilistic load definition approach. G.L.C.

N85-27954*# Battelle Columbus Labs., Ohio.
COMPOSITE LOADS SPECTRA FOR SELECT SPACE PROPULSION STRUCTURAL COMPONENTS: PROBABILISTIC LOAD MODEL DEVELOPMENT Abstract Only
R. KURTH *In* NASA. Lewis Research Center Struct. Integrity and Durability of Reusable Space Propulsion Systems p 77-83 May 1985
(Contract NAS3-24382)
Avail: NTIS HC A09/MF A01 CSCL 20K

This effort is in support of the development of the expert system of computer codes to predict the loads on select structural components of a space propulsion engine. The development will be based primarily on the space shuttle main engine (SSME) test data base. Because of random variations of the many different sources of the loadings on the selected structural components and transients, a probabilistic approach to the problems was adopted. The goal of this task is to characterize all of the individual sources of loads at critical structural locations, such as the turbine blades, the transfer ducts, and liquid oxygen posts, using state-of-the-art probabilistic methods with varying levels of sophistication. The second phase of this work is the development of a composite load model based on a probabilistic synthesis of the individual load model previously developed. This model will be based on the stochastic combination of the load variables and not on the physical process for the combination of the individual loads to the composite load seen by the selected structural components. R.J.F.

N85-27955*# Southwest Research Inst., San Antonio, Tex.
PROBABILISTIC STRUCTURAL ANALYSIS THEORY DEVELOPMENT Abstract Only
O. H. BURNSIDE *In* NASA. Lewis Research Center Struct. Integrity and Durability of Reusable Space Propulsion Systems p 85-92 May 1985
(Contract NAS3-24389)
Avail: NTIS HC A09/MF A01 CSCL 20K

The objective of the Probabilistic Structural Analysis Methods (PSAM) project is to develop analysis techniques and computer programs for predicting the probabilistic response of critical structural components for current and future space propulsion systems. This technology will play a central role in establishing system performance and durability. The first year's technical activity is concentrating on probabilistic finite element formulation strategy and code development. Work is also in progress to survey critical materials and space shuttle mian engine components. The probabilistic finite element computer program NESSUS (Numerical Evaluation of Stochastic Structures Under Stress) is being developed. The final probabilistic code will have, in the general case, the capability of performing nonlinear dynamic of stochastic structures. It is the goal of the approximate methods effort to increase problem solving efficiency relative to finite element

methods by using energy methods to generate trial solutions which satisfy the structural boundary conditions. These approximate methods will be less computer intensive relative to the finite element approach. R.J.F.

N85-27956*# MARC Analysis Research Corp., Palo Alto, Calif.
PROBABILISTIC FINITE ELEMENT DEVELOPMENT Abstract Only
J. NAGTEGAAL *In* NASA. Lewis Research Center Struct. Integrity and Durability of Reusable Space Propulsion Systems p 93-98 May 1985
(Contract NAS3-24389)
Avail: NTIS HC A09/MF A01 CSCL 20K

The probabilistic finite element computer program known as Numerical Evaluation of Stochastic Structures Under Stress (NESSUS) is being developed for the analysis of critical structural components for reusable space propulsion systems. First year efforts involve the formulation of the probabilistic analysis strategy and the development of a probabilistic linear analysis code. The ultimate goal of the 3-year program is the development of a finite element code capable of performing nonlinear dynamic analysis of structures having stochastic material properties, geometry, and boundary conditions and subjected to random loading. Three levels of sophistication are envisioned for the stochastic description of the structural problem, namely: (1) homogeneous random variable for stiffness, mass, damping, and external loading; (2) stochastic characterization of variables at the element level, with specified interelement correlations; and (3) stochastic interpolation of variables within a finite element. Two alternative probabilistic analysis methods will be developed, allowing for all three levels of modeling sophistication. R.J.F.

N85-27957*# Northwestern Univ., Evanston, Ill.
PROBABILISTIC FINITE ELEMENT: VARIATIONAL THEORY Abstract Only
T. BELYTSCHKO and W. K. LIU *In* NASA. Lewis Research Center Struct. Integrity and Durability of Reusable Propulsion Systems p 99-107 May 1985
(Contract NAG3-535)
Avail: NTIS HC A09/MF A01 CSCL 20K

The goal of this research is to provide techniques which are cost-effective and enable the engineer to evaluate the effect of uncertainties in complex finite element models. Embedding the probabilistic aspects in a variational formulation is a natural approach. In addition, a variational approach to probabilistic finite elements enables it to be incorporated within standard finite element methodologies. Therefore, once the procedures are developed, they can easily be adapted to existing general purpose programs. Furthermore, the variational basis for these methods enables them to be adapted to a wide variety of structural elements and to provide a consistent basis for incorporating probabilistic features in many aspects of the structural problem. Tasks concluded include the theoretical development of probabilistic variational equations for structural dynamics, the development of efficient numerical algorithms for probabilistic sensitivity displacement and stress analysis, and integration of methodologies into a pilot computer code. R.J.F.

N85-27959*# Georgia Inst. of Tech., Atlanta.
DYNAMIC CREEP BUCKLING: ANALYSIS OF SHELL STRUCTURES SUBJECTED TO TIME-DEPENDENT MECHANICAL AND THERMAL LOADING Abstract Only
G. J. SIMITSES, R. L. CARLSON, and R. RIFF *In* NASA. Lewis Research Center Struct. Integrity and Durability of Reusable Space Propulsion Systems p 117-120 May 1985
(Contract NAG3-534)
Avail: NTIS HC A09/MF A01 CSCL 20K

The objective of the present research is to develop a general mathematical model and solution methodologies for analyzing the structural response of thin, metallic shell structures under large transient, cyclic, or static thermomechanical loads. Among the system responses associated with these loads and conditions are thermal buckling, creep buckling, and ratcheting. Thus geometric and material nonlinearities (of high order) can be anticipated and must be considered in developing the mathematical model. A complete, true ab-initio rate theory of kinematics and kinetics for continuum and curved thin structures, without any restriction on the magnitude of the strains or the deformations, was formulated. The time dependence and large strain behavior are incorporated through the introduction of the time rates of metric and curvature in two coordinate systems: fixed (spatial) and convected (material). The relations between the time derivative and the covariant derivative (gradient) were developed for curved space and motion, so the velocity components supply the connection between the equations of motion and the time rates of change of the metric and curvature tensors. R.J.F.

N85-27961*# National Aeronautics and Space Administration. Lewis Research Center, Cleveland, Ohio.
INTERACTION OF HIGH-CYCLE AND LOW-CYCLE FATIGUE OF HAYNES 188 ALLOY AT 1400 F DEG Abstract Only
P. T. BIZON, D. J. THOMA, and G. R. HALFORD *In its* Struct. Integrity and Durability of Reusable Space Propulsion Systems p 129-138 May 1985
Avail: NTIS HC A09/MF A01 CSCL 20K

The interaction of low-cycle fatigue (LCF) and high-cycle fatigue (HCF) was evaluated at the NASA Lewis Research Center on Haynes 188 alloy at 1400 F. Completely reversed, axial-load, strain-controlled fatigue tests were performed to determine the baseline data for this study. Additional specimens for interaction tests were cycled first at a high strain range for various small portions of expected LCF life followed by a step change to a low strain range to failure in HCF. Failure was defined as complete specimen separation. The resultant lives varied between 10 and 5000 cycles for the low-cycle fatigue tests and between 4500 and 3 million for the high-cycle fatigue tests. For the interaction tests the low-cycle-life portion ranged from 30 and 1000 applied cycles while the high-frequency life ranged from 300 and 300,000 cycles to failure. The step change results showed a significant nonlinear interaction in expected life. Application of a small part of the LCF life drastically decreased the available HCF life as compared with what would have been expected by the classical linear damage rule (LDR). B.W.

N85-27962*# National Aeronautics and Space Administration. Lewis Research Center, Cleveland, Ohio.
REEXAMINATION OF CUMULATIVE FATIGUE DAMAGE LAWS Abstract Only
G. R. HALFORD and S. S. MANSON (Case Western Reserve Univ.) *In its* Struct. Integrity and Durability of Reusable Space Propulsion Systems p 139-145 May 1985 refs
Avail: NTIS HC A09/MF A01 CSCL 20K

Treatment of accumulated fatigue damage in materials and structures subjected to a history of nonsimple repetitive loadings has received a large amount of attention in recent years. A method used for the treatment of complex loading is known as linear damage rule. It was recognized that, this method could result in unconservative predictions of material and structural behavior. An intense flurry of activity followed in the pursuit of alternative methods of analysis that would predict behavior more accurately. So many methods were introduced that it became necessary periodically to prepare review papers placing all the new methods into perspective. The current integrated view regarding the state of the art as it applies to this effort is discussed. The more recently proposed cumulative damage life prediction methods are reviewed. The double linear damage rule (DLDR), which has evolved over the past 20 years, is reexamined with the intent of improving its accuracy and applicability to engineering problems. Modifications are introduced to the analytical formulation to achieve greater compatibility between the DLDR and the so-called damage curve approach, which is an alternative continuous representation of the DLDR. B.W.

N85-27963*# National Aeronautics and Space Administration. Lewis Research Center, Cleveland, Ohio.
CYCLIC STRUCTURAL ANALYSES OF SSME TURBINE BLADES
A. KAUFMAN and J. M. MANDERSCHEID *In its* Struct. Integrity and Durability of Reusable Space Propulsion Systems p 147-154 May 1985 refs
Avail: NTIS HC A09/MF A01 CSCL 20K

The problems of calculating the structural response of high-temperature space propulsion components such as turbine blades for the fuel turbopump are addressed. The first high-pressure-stage fuel turbine blade (HPFTB) in the liquid-hydrogen turbopump of the space shuttle main engine (SSME) was selected for this study. In the past these blades have cracked in the blade shank region and at the airfoil leading edge adjacent to the platform. To achieve the necessary durability, these blades are currently being cast by using directional solidification. Single-crystal alloys are also being investigated for future SSME applications. The study evaluated the utility of advanced structural analysis methods in assessing the low-cycle fatigue lives of these anisotropic components. The turbine blade airfoil of the high-pressure stage of the SSME fuel turbopump was analyzed because it has a history of rapid crack initiation.
B.W.

N85-30361*# National Aeronautics and Space Administration. Lewis Research Center, Cleveland, Ohio.
STRUCTURAL ANALYSIS AND COST ESTIMATE OF AN EIGHT-LEG SPACE FRAME AS A SUPPORT STRUCTURE FOR HORIZONTAL AXIS WIND TURBINES Final Report
R. L. SIZEMORE, J. R. WINEMILLER, S. T. YEE, and G. R. FREDERICK (Toledo Univ.) Oct. 1983 27 p refs
(Contract DE-AI01-76ET-20320)
(NASA-TM-83470; E-1529; DOE/NASA/20320-49; NAS 1.15:83470) Avail: NTIS HC A03/MF A01 CSCL 20K

A structural analysis was performed and a cost estimate was prepared to determine if an eight-leg space frame tower in which the legs lie on the surface of a hyperboloid of revolution was a suitable alternative to the truss-type tower for application to an intermediate size horizontal axis wind turbine. This tower concept had eight straight pipe elements as its main structural members that lie on the surface of a hyperboloid of revolution. The structural analysis included: response to static loads, determination of vibration characteristics, and investigation of overall frame stability. The design was lighter than the four-leg truss-type tower used for the Mod-O and Mod-OA wind turbines. The estimated cost for fabrication and erection of the hyperboloid tower is less than that for any of the four Mod-OA towers constructed to date. It is concluded that the hyperboloid tower concept is a suitable alternative to the truss-type tower for application to horizontal axis wind turbines.
E.A.K.

N85-31530*# National Aeronautics and Space Administration. Lewis Research Center, Cleveland, Ohio.
NONLINEAR CONSTITUTIVE RELATIONS FOR HIGH TEMPERATURE APPLICATION, 1984
Jun. 1985 368 p refs Symp. held in Cleveland, 15-17 Jun. 1984
(NASA-CP-2369; E-2368; NAS 1.55:2369) Avail: NTIS HC A16/MF A01 CSCL 20K

Nonlinear constitutive relations for high temperature applications were discussed. The state of the art in nonlinear constitutive modeling of high temperature materials was reviewed and the need for future research and development efforts in this area was identified. Considerable research efforts are urgently needed in the development of nonlinear constitutive relations for high temperature applications prompted by recent advances in high temperature materials technology and new demands on material and component performance. Topics discussed include: constitutive modeling, numerical methods, material testing, and structural applications.

N85-31531*# Southwest Research Inst., San Antonio, Tex.
A SURVEY OF UNIFIED CONSTITUTIVE THEORIES
K. S. CHAN, U. S. LINDHOLM, S. R. BODNER (Technion - Israel Inst. of Tech., Haifa), and K. P. WALKER (Engineering Scientific Software, Inc., Smithfield, R.I.) *In* NASA. Lewis Research Center Nonlinear Constitutive Relations for High Temp. Appl., 1984 p 1-23 Jun. 1985 refs
(Contract NAS3-23925)
Avail: NTIS HC A16/MF A01 CSCL 20K

The state of the art of time temperature dependent elastic viscoplastic constitutive theories which are based on the unified approach werre assessed. This class of constitutive theories is characterized by the use of kinetic equations and internal variables with appropriate evolutionary equations for treating all aspects of inelastic deformation including plasticity, creep, and stress relaxation. More than 10 such unified theories which are shown to satisfy the uniqueness and stability criteria imposed by Drucker's postulate and Ponter's inequalities are identified. The theories are compared for the types of flow law, kinetic equation, evolutionary equation of the internal variables, and treatment of temperature dependence. The similarities and differences of these theories are outlined in terms of mathematical formulations and illustrated by comparisons of theoretical calculations with experimental results which include monotonic stress-strain curves, cyclic hysteresis loops, creep and stress relaxation rates, and thermomechanical loops. Numerical methods used for integrating these stiff time temperature dependent constitutive equations are reviewed.
E.A.K.

N85-31533*# Akron Univ., Ohio.
THERMOMECHANICAL DEFORMATION IN THE PRESENCE OF METALLURGICAL CHANGES
D. N. ROBINSON *In* NASA. Lewis Research Center Nonlinear Constitutive Relations for High Temp. Appl., 1984 p 51-54 Jun. 1985 refs
(Contract NAG3-379)
Avail: NTIS HC A16/MF A01 CSCL 20K

Nonisothermal testing that can be used as a basis of a nonisothermal representation is discussed. Related tests regarding metallurgical changes that occur in other high temperature structural alloys are discussed. A viscoplastic constitutive model capable of qualitatively representing the behavioral features was formulated. This model is used to assess the differences in ultimate life prediction in some typical nonisothermal structural problems when the constitutive model does or does not account for metallurgically induced thermomechanical history dependence.
E.A.K.

N85-31536*# Texas A&M Univ., College Station. Aerospace Engineering Dept.
ON THE USE OF INTERNAL STATE VARIABLES IN THERMOVISCOPLASTIC CONSTITUTIVE EQUATIONS
D. H. ALLEN and J. M. BEEK *In* NASA. Lewis Research Center Nonlinear Constitutive Relations for High Temp. Appl., 1984 p 83-102 Jun. 1985 refs
(Contract NAG3-491)
Avail: NTIS HC A16/MF A01 CSCL 20K

The general theory of internal state variables are reviewed to apply it to inelastic metals in use in high temperature environments. In this process, certain constraints and clarifications will be made regarding internal state variables. It is shown that the Helmholtz free energy can be utilized to construct constitutive equations which are appropriate for metallic superalloys. Internal state variables are shown to represent locally averaged measures of dislocation arrangement, dislocation density, and intergranular fracture. The internal state variable model is demonstrated to be a suitable framework for comparison of several currently proposed models for metals and can therefore be used to exhibit history dependence, nonlinearity, and rate as well as temperature sensitivity. E.A.K.

N85-31538*# National Aeronautics and Space Administration. Lewis Research Center, Cleveland, Ohio.
A COMPARISON OF TWO CONTEMPORARY CREEP-FATIGUE LIFE PREDICTION METHODS Abstract Only
M. A. MCGAW *In its* Nonlinear Constitutive Relations for High Temp. Appl., 1984 p 125 Jun. 1985
Avail: NTIS HC A16/MF A01 CSCL 20K

A comparison of two contemporary approaches to creep fatigue life prediction, the Continuous Damage Mechanics as developed at ONERA, and Strain Range Partitioning, is presented. The general framework of each of these approaches, both being crack initiation life prediction tools, are examined. The basis for, and implications of each predictive method are discussed, relative to the material class(es) for which each was developed, as well as to their general applicability. Evident is a need for critical experiments capable of discriminating among the models; to this end, the question of choice of experiment and material is addressed. Author

N85-31541*# Texas A&M Univ., College Station. Aerospace Engineering Dept.
NUMERICAL CONSIDERATIONS IN THE DEVELOPMENT AND IMPLEMENTATION OF CONSTITUTIVE MODELS
W. E. HAISLER and P. K. IMBRIE *In* NASA. Lewis Research Center Nonlinear Constitutive Relations for High Temp. Appl., 1984 p 169-185 Jun. 1985 refs
(Contract NAG3-491)
Avail: NTIS HC A16/MF A01 CSCL 20K

Several unified constitutive models were tested in uniaxial form by specifying input strain histories and comparing output stress histories. The purpose of the tests was to evaluate several time integration methods with regard to accuracy, stability, and computational economy. The sensitivity of the models to slight changes in input constants was also investigated. Results are presented for In100 at 1350 F and Hastelloy-X at 1800 F.
Author

N85-31542*# National Aeronautics and Space Administration. Lewis Research Center, Cleveland, Ohio.
ON NUMERICAL INTEGRATION AND COMPUTER IMPLEMENTATION OF VISCOPLASTIC MODELS
T. Y. CHANG (Akron Univ., Ohio), J. P. CHANG (Akron Univ., Ohio), and R. L. THOMPSON *In its* Nonlinear Constitutive Relations for High Temp. Appl., 1984 p 187-200 Jun. 1985 refs
Avail: NTIS HC A16/MF A01 CSCL 20K

Due to the stringent design requirement for aerospace or nuclear structural components, considerable research interests have been generated on the development of constitutive models for representing the inelastic behavior of metals at elevated temperatures. In particular, a class of unified theories (or viscoplastic constitutive models) have been proposed to simulate material responses such as cyclic plasticity, rate sensitivity, creep deformations, strain hardening or softening, etc. This approach differs from the conventional creep and plasticity theory in that both the creep and plastic deformations are treated as unified time-dependent quantities. Although most of viscoplastic models give better material behavior representation, the associated constitutive differential equations have stiff regimes which present numerical difficulties in time-dependent analysis. In this connection, appropriate solution algorithm must be developed for viscoplastic analysis via finite element method. G.L.C.

N85-31543*# National Aeronautics and Space Administration. Lewis Research Center, Cleveland, Ohio.
TWO SIMPLIFIED PROCEDURES FOR PREDICTING CYCLIC MATERIAL RESPONSE FROM A STRAIN HISTORY
A. KAUFMAN and V. MORENO (Pratt and Whitney Aircraft, East Hartford, Conn.) *In its* Nonlinear Constitutive Relations for High Temp. Appl., 1984 p 201-219 Jun. 1985 refs
Avail: NTIS HC A16/MF A01 CSCL 20K

Simplified inelastic analysis procedures were developed at NASA Lewis and Pratt & Whitney Aircraft for predicting the stress-strain response at the critical location of a thermomechanically cycled structure. These procedures are intended primarily for use as economical structural analysis tools in the early design stages of aircraft engine hot section components where nonlinear finite-element analyses would be prohibitively expensive. Both simplified methods use as input the total strain history calculated from a linear elastic analysis. The elastic results are modified to approximate the characteristics of the inelastic cycle by incremental solution techniques. A von Mises yield criterion is used to determine the onset of active plasticity. The fundamental assumption of these methods is that the inelastic strain is local and constrained from redistribution by the surrounding elastic material. G.L.C.

N85-31545*# Akron Univ., Ohio. Dept. of Civil Engineering.
SOME ADVANCES IN EXPERIMENTATION SUPPORTING DEVELOPMENT OF VISCOPLASTIC CONSTITUTIVE MODELS
J. R. ELLIS and D. N. ROBINSON *In* NASA. Lewis Research Center Nonlinear Constitutive Relations for High Temp. Appl., 1984 p 237-271 Jun. 1985 refs Previously announced as N85-27260
(Contract NAG3-379; W-7405-ENG-26)
Avail: NTIS HC A16/MF A01 CSCL 20K

The development of a biaxial extensometer capable of measuring axial, torsion, and diametral strains to near-microstrain resolution at elevated temperatures is discussed. An instrument with this capability was needed to provide experimental support to the development of viscoplastic constitutive models. The advantages gained when torsional loading is used to investigate inelastic material response at elevated temperatures are highlighted. The development of the biaxial extensometer was conducted in two stages. The first involved a series of bench calibration experiments performed at room temperature. The second stage involved a series of in-place calibration experiments performed at room temperature. A review of the calibration data indicated that all performance requirements regarding resolution, range, stability, and crosstalk had been met by the subject instrument over the temperature range of interest, 21 C to 651 C. The scope of the in-placed calibration experiments was expanded to investigate the feasibility of generating stress relaxation data under torsional loading. B.W. (IAA)

N85-31546*# Michigan State Univ., East Lansing. Dept. of Metallurgy, Mechanics, and Materials Science.
A COMPARISON OF SMOOTH SPECIMEN AND ANALYTICAL SIMULATION TECHNIQUES FOR NOTCHED MEMBERS AT ELEVATED TEMPERATURES
J. F. MARTIN *In* NASA. Lewis Research Center Nonlinear Constitutive Relations for High Temp. Appl., 1984 p 273-281 Jun. 1985 refs
(Contract NAG3-51)
Avail: NTIS HC A16/MF A01 CSCL 20K

Experimental strain measurements have been made at the highly strained regions on notched plate specimens that were made of Hastelloy X. Tests were performed at temperatures up to 1,600 F. Variable load patterns were chosen so as to produce plastic and creep strains. Were appropriate, notch root stresses were experimentally estimated by subjecting a smooth specimen to the measured notch root strains. The results of three analysis techniques are presented and compared to the experimental data. The most accurate results were obtained from an analysis procedure that used a smooth specimen and the Neuber relation to simulate the notch root stress-strain response. When a generalized constitutive relation was used with the Neuber relation, good results were also obtained, however, these results were not as accurate as those obtained when the smooth specimen was used directly. Finally, a general finite element program, ANYSIS, was used which resulted in acceptable solutions, but, these were the least accurate predictions. Author

N85-31548*# Cincinnati Univ., Ohio. Dept. of Aerospace Engineering and Applied Mechanics.
FINITE ELEMENT ANALYSIS OF NOTCH BEHAVIOR USING A STATE VARIABLE CONSTITUTIVE EQUATION
L. T. DAME, D. C. STOUFFER, and N. ABUELFOUTOUH *In* NASA. Lewis Research Center Nonlinear Constitutive Relations for High Temp. Appl., 1984 p 297-310 Jun. 1985 refs
(Contract NAS3-23698; NAS3-23927; NAG3-511)
Avail: NTIS HC A16/MF A01 CSCL 20K

The state variable constitutive equation of Bodner and Partom was used to calculate the load-strain response of Inconel 718 at 649 C in the root of a notch. The constitutive equation was used with the Bodner-Partom evolution equation and with a second evolution equation that was derived from a potential function of the stress and state variable. Data used in determining constants for the constitutive models was from one-dimensional smooth bar tests. The response was calculated for a plane stress condition at the root of the notch with a finite element code using constant strain triangular elements. Results from both evolution equations compared favorably with the observed experimental response. The accuracy and efficiency of the finite element calculations also compared favorably to existing methods. Author

N85-32340*# Akron Univ., Ohio. Dept. of Civil Engineering.
RESULTS OF AN INTERLABORATORY FATIGUE TEST PROGRAM CONDUCTED ON ALLOY 800H AT ROOM AND ELEVATED TEMPERATURES Final Report
J. R. ELLIS Jul. 1985 38 p refs Sponsored in part by General Atomic Co.
(Contract NAG3-379)
(NASA-CR-174940; NAS 1.26:174940) Avail: NTIS HC A03/MF A01 CSCL 20K

The experimental approach adopted for low cycle fatigue tests of alloy 800H involved the use of electrohydraulic test systems, hour glass geometry specimens, diametral extensometers, and axial strain computers. Attempts to identify possible problem areas were complicated by the lack of reliable data for the heat of Alloy 800H under investigation. The method adopted was to generate definitive test data in an Interlaboratory Fatigue Test Program. The laboratories participating in the program were Argonne National Laboratory, Battelle Columbus, Mar-Test, and NASA Lewis. Fatigue tests were conducted on both solid and turbular specimens at temperatures of 20, 593, and 760 C and strain ranges of 2.0, 1.0, and 0.5 percent. The subject test method can, under certain circumstances, produce fatigue data which are serious in error. This approach subsequently was abandoned at General Atomic Company in favor of parallel gage length specimens and axial extensiometers. F.M.R.

N85-32341*# Akron Univ., Ohio. Dept. of Civil Engineering.
A CONTINUOUS DAMAGE MODEL BASED ON STEPWISE-STRESS CREEP RUPTURE TESTS Final Report
D. N. ROBINSON Cleveland Jul. 1985 24 p refs
(Contract NAG3-379)
(NASA-CR-174941; NAS 1.26:174941) Avail: NTIS HC A02/MF A01 CSCL 20K

A creep damage accumulation model is presented that makes use of the Kachanov damage rate concept with a provision accounting for damage that results from a variable stress history. This is accomplished through the introduction of an additional term in the Kachanov rate equation that is linear in the stress rate. Specification of the material functions and parameters in the model requires two types of constituting a data base: (1) standard constant-stress creep rupture tests, and (2) a sequence of two-step creep rupture tests. Author

N85-33520*# National Aeronautics and Space Administration. Lewis Research Center, Cleveland, Ohio.
APPLICATION OF TRACTION DRIVES AS SERVO MECHANISMS
S. H. LOEWENTHAL, D. A. ROHN, and B. M. STEINETZ *In* NASA. Ames Research Center 19th Aerospace Mech. Symp. p 119-139 Aug. 1985 refs
Avail: NTIS HC A17/MF A01 CSCL 20K

The suitability of traction drives for a wide class of aerospace control mechanisms is examined. Potential applications include antenna or solar array drive positioners, robotic joints, control moment gyro (CMG) actuators and propeller pitch change mechanisms. In these and similar applications the zero backlash, high torsional stiffness, low hysteresis and torque ripple characteristics of traction drives are of particular interest, as is the ability to run without liquid lubrication in certain cases. Wear and fatigue considerations for wet and dry operation are examined along with the tribological performance of several promising self lubricating polymers for traction contracts. The speed regulation capabilities of variable ratio traction drives are reviewed. A torsional stiffness analysis described suggests that traction contacts are relatively stiff compared to gears and are significantly stiffer than the other structural elements in the prototype CMG traction drive analyzed. Discussion is also given of an advanced turboprop propeller pitch change mechanism that incorporates a traction drive. Author

N85-33541*# General Electric Co., Cincinnati, Ohio. Advanced Technology Programs Dept.
A REVIEW OF PATH-INDEPENDENT INTEGRALS IN ELASTIC-PLASTIC FRACTURE MECHANICS, TASK 4 Interim Report
K. S. KIM Aug. 1985 33 p refs
(Contract NAS3-23940)
(NASA-CR-174956; NAS 1.26:174956) Avail: NTIS HC A03/MF A01 CSCL 20K

The path independent (P-I) integrals in elastic plastic fracture mechanics which have been proposed in recent years to overcome the limitations imposed on the J integral are reviewed. The P-I integrals considered herein are the J integral by Rice, the thermoelastic P-I integrals by Wilson and Yu and by Gurtin, the J* integral by Blackburn, the J sub theta integral by Ainsworth et al., the J integral by Kishimoto et al., and the delta T sub p and delta T* sub p integrals by Atluri et al. The theoretical foundation of these P-I integrals is examined with emphasis on whether or not path independence is maintained in the presence of nonproportional loading and unloading in the plastic regime, thermal gradients, and material inhomogeneities. The similarities, differences, salient features, and limitations of these P-I integrals are discussed. Comments are also made with regard to the physical meaning, the possibility of experimental measurement, and computational aspects. Author

N85-34427*# National Aeronautics and Space Administration. Lewis Research Center, Cleveland, Ohio.
NONLINEAR FLAP-LAG-EXTENSIONAL VIBRATIONS OF ROTATING, PRETWISTED, PRECONED BEAMS INCLUDING CORIOLIS EFFECTS
K. B. SUBRAHMANYAM (NBKR Inst. of Science and Tech.) and K. R. V. KAZA 1985 35 p refs Presented at the 19th Midwestern Mech. Conf., Columbus, Ohio, 9-11 Sep. 1985; sponsored by the Ohio State Univ.
(NASA-TM-87102; E-2598; NAS 1.15:87102) Avail: NTIS HC A03/MF A01 CSCL 20K

The effects of pretwist, precone, setting angle, Coriolis forces and second degree geometric nonlinearities on the natural frequencies, steady state deflections and mode shapes of rotating, torsionally rigid, cantilevered beams were studied. The governing coupled equations of flap lag extensional motion are derived including the effects of large precone and retaining geometric nonlinearities up to second degree. The Galerkin method, with nonrotating normal modes, is used for the solution of both steady state nonlinear equations and linear perturbation equations.

Parametric indicating the individual and collective effects of pretwist, precone, Coriolis forces and second degree geometric nonlinearities on the steady state deflection, natural frequencies and mode shapes of rotating blades are presented. It is indicated that the second degree geometric nonlinear terms, which vanish for zero precone, can produce frequency changes of engineering significance. Further confirmation of the validity of including those generated by MSC NASTRAN. It is indicated that the linear and nonlinear Coriolis effects must be included in analyzing thick blades. The Coriolis effects are significant on the first flatwise and the first edgewise modes. E.A.K.

43

EARTH RESOURCES

Includes remote sensing of earth resources by aircraft and spacecraft; photogrammetry; and aerial photography.

A85-10244*# Environmental Research Inst. of Michigan, Ann Arbor.
COMPARISON OF ATMOSPHERIC CORRECTION ALGORITHMS FOR THE COASTAL ZONE COLOR SCANNER
F. J. TANIS (Michigan, Environmental Research Institute, Ann Arbor, MI) and S. C. JAIN (MONITEQ Ltd., Concord, Ontario, Canada) IN: International Symposium on Remote Sensing of Environment, 17th, Ann Arbor, MI, May 9-13, 1983, Proceedings. Volume 2 . Ann Arbor, MI, Environmental Research Institute of Michigan, 1984, p. 923-935. refs
(Contract NAS3-22892)

Before Nimbus-7 Costal Zone Color Scanner (CZC) data can be used to distinguish between coastal water types, methods must be developed for the removal of spatial variations in aerosol path radiance. These can dominate radiance measurements made by the satellite. An assessment is presently made of the ability of four different algorithms to quantitatively remove haze effects; each was adapted for the extraction of the required scene-dependent parameters during an initial pass through the data set The CZCS correction algorithms considered are (1) the Gordon (1981, 1983) algorithm; (2) the Smith and Wilson (1981) iterative algorityhm; (3) the pseudooptical depth method; and (4) the residual component algorithm. O.C.

44

ENERGY PRODUCTION AND CONVERSION

Includes specific energy conversion systems, e.g., fuel cells and batteries; global sources of energy; fossil fuels; geophysical conversion; hydroelectric power; and wind power.

A85-10652*# Westinghouse Electric Corp., Pittsburgh, Pa.
MEASURED EFFECTS OF WIND TURBINE GENERATION AT THE BLOCK ISLAND POWER COMPANY
V. F. WILREKER, R. F. SMITH, P. H. STILLER (Westinghouse Electric Corp., Pittsburgh, PA), G. W. SCOT (Enertech Corp., Norwich, VT), and R. K. SHALTENS (NASA, Lewis Research Center, Cleveland, OH) American Power Conference, Chicago, IL, Apr. 24-26, 1984, Paper. 10 p. Research supported by the U.S. Department of Energy. refs
(Contract DEN3-275; DEN3-354)

Data measurements made on the NASA MOD-OA 200-kw wind-turbine generator (WTG) installed on a utility grid form the basis for an overall performance analysis. Fuel displacement/-savings, dynamic interactions, and WTG excitation (reactive-power) control effects are studied. Continuous recording of a large number of electrical and mechanical variables on FM magnetic tape permit evaluation and correlation of phenomena over a bandwidth of at least 20 Hz. Because the wind-power penetration reached peaks of 60 percent, the impact of wind fluctuation and wind-turbine/diesel-utility interaction is evaluated in a worst-case scenario. The speed-governor dynamics of the diesel units exhibited an underdamped response, and the utility operation procedures were not altered to optimize overall WTG/utility performance. Primary findings over the data collection period are: a calculated 6.7-percent reduction in fuel consumption while generating 11 percent of the total electrical energy; acceptable system voltage and frequency fluctuations with WTG connected; and applicability of WTG excitation schemes using voltage, power, or VARS as the controlled variable. Author

A85-11345* Cleveland State Univ., Ohio.
CONTROL ALGORITHMS AND COMPUTER SIMULATION OF A STAND-ALONE PHOTOVOLTAIC VILLAGE POWER SYSTEM
P. P. GROUMPOS, J. E. CULLER (Cleveland State University, Cleveland, OH), R. DELOMBARD, A. F. RATAJCZAK (NASA, Lewis Research Center, Cleveland, OH), and R. CULL (NASA, Lewis Research Center; Standard Oil Company of Ohio, Cleveland, OH) IN: Photovoltaic Solar Energy Conference; Proceedings of the Fifth International Conference, Athens, Greece, October 17-21, 1983 . Dordrecht, D. Reidel Publishing Co., 1984, p. 353-357.
(Contract NCC3-16)

At Stand-Alone Photovoltaic (SAPV) power systems increase in size and load diversity, the design and simulation of control subsystems takes on added importance. These SAPV systems represent 'mini utilities' with commensurate controls requirements, albeit with the added complexity of the energy source (sunlight received) being an uncontrollable variable. This paper briefly describes a stand-alone photovoltaic power/load system computerized simulation model. The model was tested against operational data from the Schuchuli stand-alone village photovoltaic system and has achieved acceptable levels of simulation accuracy. The model can be used to simulate system designs although with probable battery modification. Author

A85-15800* Cleveland State Univ., Ohio.
NEAR-OPTIMUM DESIGN OF GAAS-BASED CONCENTRATOR SPACE SOLAR CELLS FOR 80 C OPERATION
C. GORADIA, M. GHALLA-GORADIA (Cleveland State University, Cleveland, OH), and H. CURTIS (NASA, Lewis Research Center, Cleveland, OH) Applied Physics Communications (ISSN 0277-9374), vol. 4, no. 2-3, 1984, p. 97-119. NASA-supported research. refs

Using a detailed computer simulation model and reasonable values of optical, geometrical and material parameters from current published literature, parameter optimization studies were performed on two cell geometries, namely, the circular geometry for a Cassegrainian concentrator with 100 AM0, 80 C operation and the rectangular geometry for a venetian blind concentrator with 20 AM0, 80 C operation. For each cell geometry, three cell configurations were considered: p/n AlGaAs/GaAs; n/p AlGaAs/GaAs; and, n/p GaAs shallow homojunction. The studies show the possibility of designing GaAs-based space solar cells with beginning-of-life efficiencies exceeding 22 percent at 20 to 100 AM0, 80 C and probable efficiency degradation of less than 15 percent after a 70 percent reduction in diffusion length in each cell region. Author

A85-18608* National Aeronautics and Space Administration. Lewis Research Center, Cleveland, Ohio.
CHARACTERISTICS OF ARC CURRENTS ON A NEGATIVELY BIASED SOLAR CELL ARRAY IN A PLASMA
D. B. SNYDER (NASA, Lewis Research Center, Cleveland, OH) (IEEE, U.S. Defense Nuclear Agency, U.S. Department of Energy, and NASA, Annual Conference on Nuclear and Space Radiation Effects, 21st, Colorado Springs, CO, July 23-25, 1984) IEEE Transactions on Nuclear Science (ISSN 0018-9499), vol. NS-31, Dec. 1984, p. 1584-1587. Previously announced in STAR as N84-27824. refs

The time dependence of the emitted currents during arcing on solar cell arrays is being studied. The arcs are characterized using three parameters: the voltage change of the array during the arc (i.e., the charge lost), the peak current during the arc, and the time constant describing the arc current. This paper reports the dependence of these characteristics on two array parameters, the interconnect bias voltage and the array capacitance to ground. It was found that the voltage change of the array during an arc is nearly equal to the bias voltage. The array capacitance, on the other hand, influences both the peak current and the decay time constant of the arc. Both of these characteristics increase with increasing capacitance. Author

A85-19948* Cleveland State Univ., Ohio.
APPLICABILITY OF THE MEYER-NELDEL RULE TO SOLAR CELLS
C. GORADIA (Cleveland State University, Cleveland, OH) and V. G. WEIZER (NASA, Lewis Research Center, Cleveland, OH) Applied Physics Letters (ISSN 0003-6951), vol. 45, Dec. 15, 1984, p. 1298-1300.

A comparison of data taken on high quality silicon, GaAs, and GaInAs solar cells with those taken on a variety of homojunction, heterojunction, and metal-insulator-semiconductor devices indicates that while the Meyer-Neldel rule may be applicable to certain types of solar cells it is not applicable to well-behaved, diffusion-controlled homojunction devices. It cannot be used, therefore, as a universal rule to predict maximum achievable solar cell voltages. Author

A85-21297*# Westinghouse Electric Corp., Pittsburgh, Pa.
FUEL CELL POWER PLANT ECONOMIC AND OPERATIONAL CONSIDERATIONS
J. R. LANCE (Westinghouse Electric Corp., Advanced Energy Systems Div., Pittsburgh, PA) American Society of Mechanical Engineers, Annual Energy Sources Technology Conference and Exhibit, 7th, New Orleans, LA, Feb. 11-17, 1984. 8 p. Research supported by the U.S. Department of Energy.
(Contract DEN3-290)
(ASME PAPER 84-AES-7)

Fuel cell power plants intended for electric utility and cogeneration applications are now in the design and construction stage. This paper describes economic and operational considerations being used in the development and design of plants utilizing air cooled phosphoric acid fuel cells. Fuel cell power plants have some unique characteristics relative to other types of power plants. As a result it was necessary to develop specific definitions of the fuel cell power plant characteristics in order to perform cost of electricity calculations. This paper describes these characteristics and describes the economic analyses used in the Westinghouse fuel cell power plant program. Author

A85-24668* Cincinnati Univ., Ohio.
HIGH-VOLTAGE SOLAR-CELL CHIP
V. J. KAPOOR, G. J. VALCO, G. G. SKEBE (Cincinnati, University, Cincinnati, OH), and J. C. EVANS, JR. (NASA, Lewis Research Center, Cleveland, OH) Journal of Applied Physics (ISSN 0021-8979), vol. 57, Feb. 15, 1985, p. 1343-1346. refs
(Contract NAG3-80)

Integrated circuit technology has been successfully applied to the design and fabrication of 0.5 x 0.5-cm planar multijunction solar-cell chips. Each of these solar cells consisted of six voltage-generating unit cells monolithically connected in series and fabricated on a 75-micron-thick, p-type, single crystal, silicon substrate. A contact photolithic process employing five photomask levels together with a standard microelectronics batch-processing technique were used to construct the solar-cell chip. The open-circuit voltage increased rapidly with increasing illumination up to 5 AM1 suns where it began to saturate at the sum of the individual unit-cell voltages at a maximum of 3.0 V. A short-circuit current density per unit cell of 240 mA/sq cm was observed at 10 AM1 suns. Author

A85-28080* National Aeronautics and Space Administration. Lewis Research Center, Cleveland, Ohio.
EFFECT OF SOLAR-CELL JUNCTION GEOMETRY ON OPEN-CIRCUIT VOLTAGE
V. G. WEIZER and M. P. GODLEWSKI (NASA, Lewis Research Center, Cleveland, OH) Journal of Applied Physics (ISSN 0021-8979), vol. 57, March 15, 1985, p. 2292-2294. refs

Simple analytical models have been found that adequately describe the voltage behavior of both the stripe junction and dot junction grating cells as a function of junction area. While the voltage in the former case is found to be insensitive to junction area reduction, significant voltage increases are shown to be possible for the dot junction cell. With regard to cells in which the junction area has been increased in a quest for better performance, it was found that (1) texturation does not affect the average saturation current density J0, indicating that the texturation process is equivalent to a simple extension of junction area by a factor of square root of 3 and (2) the vertical junction cell geometry produces a sizable decrease in J0 that, unfortunately, is more than offset by the effects of attendant areal increases. Author

A85-32639* Cleveland State Univ., Ohio.
THEORY OF THE HIGH BASE RESISTIVITY N(+)PP(+) SILICON SOLAR CELL AND ITS APPLICATION TO RADIATION DAMAGE EFFECTS
C. GORADIA (Cleveland State University, Cleveland, OH) and I. WEINBERG (NASA, Lewis Research Center, Cleveland, OH) Journal of Applied Physics (ISSN 0021-8979), vol. 57, May 15, 1985, p. 4752-4760. refs

Particulate radiation in space is a principal source of silicon solar cell degradation, and an investigation of cell radiation damage at higher base resistivities appears to have implication toward increasing solar cell and, therefore, useful satellite lifetimes in the space environment. However, contrary to expectations, it has been found that for cells with resistivities of 84 and 1250 ohm cm, the radiation resistance decreases as cell base resistivity increases. An analytical solar-cell computer model was developed with the objective to determine the reasons for this unexpected behavior. The present paper has the aim to describe the analytical model and its use in interpreting the behavior, under irradiation, of high-resistivity solar cells. Attention is given to boundary conditions at the space-charge region edges, cell currents, cell voltages, the generation of the theoretical I-V characteristic, experimental results, and computer calculations. G.R.

A85-35602*# National Aeronautics and Space Administration. Lewis Research Center, Cleveland, Ohio.
PHOTOVOLTAICS - THE ENDLESS SPRING
H. W. BRANDHORST, JR. (NASA, Lewis Research Center, Cleveland, OH) IN: Photovoltaic Specialists Conference, 17th, Kissimmee, FL, May 1-4, 1984, Conference Record . New York, Institute of Electrical and Electronics Engineers, 1984, p. 1-6. Previously announced in STAR as N84-31782.

An overview of the developments in the photovoltaic field over the past decade or two is presened. Accomplishments in the terrestrial field are reviewed along with projections and challenges toward meeting cost goals. The contrasts and commonality of space and terrestrial photovoltaics are presented. Finally, a strategic philosophy of photovoltaics research highlighting critical factors, appropriate directions, emerging opportunities, and challenges of the future is given. Author

A85-35604*# National Aeronautics and Space Administration, Washington, D.C.
THE NASA PHOTOVOLTAIC TECHNOLOGY PROGRAM
J. P. MULLIN, J. C. LORIA (NASA, Washington, DC), and H. W. BRANDHORST, JR. (NASA, Lewis Research Center, Cleveland, OH) IN: Photovoltaic Specialists Conference, 17th, Kissimmee, FL, May 1-4, 1984, Conference Record . New York, Institute of Electrical and Electronics Engineers, 1984, p. 12-16. Previously announced in STAR as N85-32426.

The NASA Office of Aeronautical and Space Technology OAST Program in space photovoltaics is reviewed. From the perspective of national landmark mission requirements and five year and 25-year long range plans, the texture of the program is revealed. Planar silicon and concentrator GaAs array technology advances are discussed. Advances in lightweight (50 micro cell) arrays and radiation tolerance research are presented. Recent progress in cascade cells and ultralightweight GaAs planar cells is noted. Progress in raising silicon cell voltage to its theoretical maximum is detailed. Advanced concepts such as plasmon converters and the Long Duration Exposure Facility LDEF flight experiments pertaining to solar cell and array technology are also shown.
M.A.C.

A85-35617*# National Aeronautics and Space Administration. Lewis Research Center, Cleveland, Ohio.
VOLTAGE CONTROLLING MECHANISMS IN LOW RESISTIVITY SILICON SOLAR CELLS - A UNIFIED APPROACH
V. G. WEIZER, C. K. SWARTZ, R. E. HART, and M. P. GODLEWSKI (NASA, Lewis Research Center, Cleveland, OH) IN: Photovoltaic Specialists Conference, 17th, Kissimmee, FL, May 1-4, 1984, Conference Record . New York, Institute of Electrical and Electronics Engineers, 1984, p. 117-122. Previously announced in STAR as N84-20916. refs

An experimental technique capable of resolving the dark saturation current into its base and emitter components is used as the basis of an analysis in which the voltage limiting mechanisms were determined for a variety of high voltage, low resistivity silicon solar cells. The cells studied include the University of Florida hi-low emitter cell, the NASA and the COMSAT multi-step diffused cells, the Spire Corporation ion-implanted emitter cell, and the University of New South Wales MINMIS and MINP cells. The results proved to be, in general, at variance with prior expectations. Most surprising was the finding that the MINP and the MINMIS voltage improvements are due, to a considerable extent, to a previously unrecognized optimization of the base component of the saturation current. This result is substantiated by an independent analysis of the material used to fabricate these devices. Author

A85-35707*# National Aeronautics and Space Administration. Lewis Research Center, Cleveland, Ohio.
STATUS OF DOE AND AID STAND-ALONE PHOTOVOLTAIC SYSTEM FIELD TESTS
W. J. BIFANO, R. DELOMBARD, A. F. RATAJCZAK, and L. R. SCUDDER (NASA, Lewis Research Center, Cleveland, OH) IN: Photovoltaic Specialists Conference, 17th, Kissimmee, FL, May 1-4, 1984, Conference Record . New York, Institute of Electrical and Electronics Engineers, 1984, p. 1159-1167. refs

The NASA Lewis Research Center (LeRC) is managing stand-alone photovoltaic (PV) system projects sponsored by the U.S. Department of Energy (DOE) and the U.S. Agency for International Development (AID). The DOE project includes village PV power demonstration projects in Gabon (four sites) and the Marshall Islands, and PV-powered vaccine refrigerator systems in six countries. The AID project includes a large village power system, a farmhouse system and two water pumping-irrigation systems in Tunisia, a water pumping/grain grinding system in Upper Volta, five medical clinic systems in four countries, PV-powered vaccine refrigerator systems in 18 countries and a PV-powered remote earth station in Indonesia. This paper reviews these PV projects and summarizes significant findings to date. Author

A85-36750* National Aeronautics and Space Administration. Lewis Research Center, Cleveland, Ohio.
METHOD FOR EVALUATING WIND TURBINE WAKE EFFECTS ON WIND FARM PERFORMANCE
H. E. NEUSTADTER and D. A. SPERA (NASA, Lewis Research Center, Cleveland, OH) IN: ASME Wind Energy Symposium, 3rd, Dallas, TX, February 18-20, 1985. New York, American Society of Mechanical Engineering, 1985, p. 61-67.

A method of testing the performance of a cluster of wind turbine units an data analysis equations are presented which together form a simple and direct procedure for determining the reduction in energy output caused by the wake of an upwind turbine. This method appears to solve the problems presented by data scatter and wind variability. Test data from the three-unit Mod-2 wind turbine cluster at Goldendale, Washington, are analyzed to illustrate the application of the proposed method. In this sample case the reduction in energy was found to be about 10 percent when the Mod-2 units were separated a distance equal to seven diameters and winds were below rated. Author

A85-45380* National Aeronautics and Space Administration. Lewis Research Center, Cleveland, Ohio.
DESIGN CONSIDERATIONS FOR A 10-KW INTEGRATED HYDROGEN-OXYGEN REGENERATIVE FUEL CELL SYSTEM
M. A. HOBERECHT, T. B. MILLER, L. L. RIEKER, and O. D. GONZALEZ-SANABRIA (NASA, Lewis Research Center, Cleveland, OH) IN: IECEC '84: Advanced energy systems - Their role in our future; Proceedings of the Nineteenth Intersociety Energy Conversion Engineering Conference, San Francisco, CA, August 19-24, 1984. Volume 1 . La Grange Park, IL, American Nuclear Society, 1984, p. 240-246. Previously announced in STAR as N84-23023.

Integration of an alkaline fuel cell subsystem with an alkaline electrolysis subsystem to form a regenerative fuel cell (RFC) system for low earth orbit (LEO) applications characterized by relatively high overall round trip electrical efficiency, long life, and high reliability is possible with present state of the art technology. A hypothetical 10 kW system computer modeled and studied based on data from ongoing contractual efforts in both the alkaline fuel cell and alkaline water electrolysis areas. The alkaline fuel cell technology is under development utilizing advanced cell components and standard Shuttle Orbiter system hardware. The alkaline electrolysis technology uses a static water vapor feed technique and scaled up cell hardware is developed. The computer aided study of the performance, operating, and design parameters of the hypothetical system is addressed. E.A.K.

A85-45384* National Aeronautics and Space Administration. Lewis Research Center, Cleveland, Ohio.
DESIGN OF A 1-KWH BIPOLAR NICKEL HYDROGEN BATTERY
R. L. CATALDO (NASA, Lewis Research Center, Cleveland, OH) IN: IECEC '84: Advanced energy systems - Their role in our future; Proceedings of the Nineteenth Intersociety Energy Conversion Engineering Conference, San Francisco, CA, August 19-24, 1984. Volume 1 . La Grange Park, IL, American Nuclear Society, 1984, p. 264-269. Previously announced in STAR as N84-23024. refs

The design of a nickel hydrogen battery utilizing bipolar construction in a common pressure vessel is discussed. Design features are as follows: 40 ampere-hour capacity, 1 kWh stored energy as a 24 cell battery, 1.8 kW delivered in a LEO Cycle and maximum pulse power of 18.0 kW. Author

A85-45385* National Aeronautics and Space Administration. Lewis Research Center, Cleveland, Ohio.
TEARDOWN ANALYSIS OF A TEN CELL BIPOLAR NICKEL-HYDROGEN BATTERY
M. A. MANZO, O. D. GONZALEZ-SANABRIA, J. S. HERZAU, and L. J. SCAGLIONE (NASA, Lewis Research Center, Cleveland, OH) IN: IECEC '84: Advanced energy systems - Their role in our future; Proceedings of the Nineteenth Intersociety Energy Conversion Engineering Conference, San Francisco, CA, August 19-24, 1984. Volume 1 . La Grange Park, IL, American Nuclear Society, 1984, p. 270-278. Previously announced in STAR as N84-23026. refs

Design studies have identified bipolar nickel-hydrogen batteries as an attractive storage option for high power, high voltage applications. A pre-prototype Ni-H2 battery was designed, assembled and tested in the early phases of a concept verification program. The initial stack was built with available hardware and components from past programs. The stack performed well. After 2000 low-earth-orbit cycles the stack was dismantled in order to allow evaluation and analysis of the design and components. The results of the teardown analysis and recommended modifications are discussed. Author

A85-45386* National Aeronautics and Space Administration. Lewis Research Center, Cleveland, Ohio.
SEPARATOR DEVELOPMENT AND TESTING OF NICKEL-HYDROGEN CELLS
O. D. GONZALEZ-SANABRIA and M. A. MANZO (NASA, Lewis Research Center, Cleveland, OH) IN: IECEC '84: Advanced energy systems - Their role in our future; Proceedings of the Nineteenth Intersociety Energy Conversion Engineering Conference, San Francisco, CA, August 19-24, 1984. Volume 1 . La Grange Park, IL, American Nuclear Society, 1984, p. 279-286. Previously announced in STAR as N84-22712.

The components, design, and operating characteristics of Ni-H2 cells and batteries were improved. A separator development program was designed to develop a separator that is resistant to penetration by oxygen and loose active material from the nickel electrode, while retaining the required chemical and thermal stability, reservoir capability, and high ionic conductivity. The performance of the separators in terms of cell operating voltage was to at least match that of state-of-the-art separators while eliminating the separator problems. The separators were submitted to initial screening tests and those which successfully completed the tests were built into Ni-H2 cells for short term testing. The separators with the best performance are tested for long term performance and life. S.L.

A85-45391* Hughes Research Labs., Malibu, Calif.
LONG LIFE NICKEL ELECTRODES FOR A NICKEL-HYDROGEN CELL. III - RESULTS OF AN ACCELERATED TEST AND FAILURE ANALYSES
H. S. LIM and S. A. VERZWYVELT (Hughes Research Laboratories, Malibu, CA) IN: IECEC '84: Advanced energy systems - Their role in our future; Proceedings of the Nineteenth Intersociety Energy Conversion Engineering Conference, San Francisco, CA, August 19-24, 1984. Volume 1 . La Grange Park, IL, American Nuclear Society, 1984, p. 312-318. refs
(Contract NAS3-22238)

Nineteen different designs of nickel electrodes were tested in Ni/H2 boiler plate cells in an accelerated low earth orbit cycle regime to the end of their life. The failure analyses of these cells showed that the major performance changes due to the cycling was a severe reduction of their high rate discharge capability rather than an absolute capacity reduction. Many physical changes of the nickel electrodes were observed after the cycling test. These changes include dimensional expansion, sinter rupture, loose black powdering of the active material, morphology changes, active material migration, increase of pore volume, change of pore distribution, and increase of surface area. All of these were caused by active material expansion with cycling. Among these changes, the morphology change which involves migration of active material away from the current collecting nickel sinter appears to be that most responsible for the reduction of the rate capability. Author

A85-45408* TriSolar Corp., Bedford, Mass.
MICROPROCESSOR CONTROL OF PHOTOVOLTAIC SYSTEMS
A. R. MILLNER and D. L. KAUFMAN (TriSolar Corp., Bedford, MA) IN: IECEC '84: Advanced energy systems - Their role in our future; Proceedings of the Nineteenth Intersociety Energy Conversion Engineering Conference, San Francisco, CA, August 19-24, 1984. Volume 1 . La Grange Park, IL, American Nuclear Society, 1984, p. 422-427.
(Contract DEN3-310)

The present low power CMOS microprocessor controller for photovoltaic power systems possesses three programs, which are respectively intended for (1) conventional battery-charging systems with state-of-charge estimation and sequential shedding of subarrays and loads, (2) maximum power-controlled battery-charging systems, and (3) variable speed dc motor drives. Attention is presently given to the development of this terrestrial equipment for spacecraft use. O.C.

A85-45438* National Aeronautics and Space Administration. Lewis Research Center, Cleveland, Ohio.
ADVANCED DESIGNS FOR IPV NICKEL-HYDROGEN CELLS
J. J. SMITHRICK, M. A. MANZO, and O. GONZALEZ-SANABRIA (NASA, Lewis Research Center, Cleveland, OH) IN: IECEC '84: Advanced energy systems - Their role in our future; Proceedings of the Nineteenth Intersociety Energy Conversion Engineering Conference, San Francisco, CA, August 19-24, 1984. Volume 1 . La Grange Park, IL, American Nuclear Society, 1984, p. 631-635. Previously announced in STAR as N84-23025. refs

Advanced designs for individual pressure vessel nickel-hydrogen cells have been conceived which should improve the cycle life at deep depths-of-discharge. Features of the designs which are new and not incorporated in either of the contemporary cells (Air Force/Hughes, Comsat) are: (1) use of alternate methods of oxygen recombination, (2) use of serrated edge separators to facilitate movement of gas within the cell while still maintaining required physical contact with the wall wick, and (3) use of an expandable stack to accommodate some of the nickel electrode expansion. The designs also consider electrolyte volume requirements over the life of the cells, and are fully compatible with the Air Force/Hughes design. Author

A85-45443* National Aeronautics and Space Administration. Lewis Research Center, Cleveland, Ohio.
RESULTS OF ELECTRIC-VEHICLE PROPULSION SYSTEM PERFORMANCE ON THREE LEAD-ACID BATTERY SYSTEMS
J. G. EWASHINKA (NASA, Lewis Research Center, Cleveland, OH) IN: IECEC '84: Advanced energy systems - Their role in our future; Proceedings of the Nineteenth Intersociety Energy Conversion Engineering Conference, San Francisco, CA, August 19-24, 1984. Volume 2 . La Grange Park, IL, American Nuclear Society, 1984, p. 727-735. Previously announced in STAR as N84-25166.

Three types of state of the art 6 V lead acid batteries were tested. The cycle life of lead acid batteries as a function of the electric vehicle propulsion system design was determined. Cycle life, degradation rate and failure modes with different battery types (baseline versus state of the art tubular and thin plate batteries) were compared. The effects of testing strings of three versus six series connected batteries on overall performance were investigated. All three types do not seem to have an economically feasible battery system for the propulsion systems. The tubular plate batteries on the load leveled profile attained 235 cycles with no signs of degradation and minimal capacity loss. E.A.K.

A85-45512* National Aeronautics and Space Administration. Lewis Research Center, Cleveland, Ohio.
MOD-2 WIND TURBINE FIELD OPERATIONS EXPERIENCE
L. H. GORDON (NASA, Lewis Research Center, Cleveland, OH) IN: IECEC '84: Advanced energy systems - Their role in our future; Proceedings of the Nineteenth Intersociety Energy Conversion Engineering Conference, San Francisco, CA, August 19-24, 1984. Volume 4 . La Grange Park, IL, American Nuclear Society, 1984, p. 2363-2368.

The Mod-2 wind turbine is now in a 2-year research/experimental operations phase which offers a unique opportunity to study the effects of single and multiple wind turbines interacting with each other, the power grid, and the environment. This paper addresses the field operations and research testing experienced at the Mod-2 Cluster Goodnoe Hills Research Test Site near Goldendale, WA. Field operation, both routine and nonroutine, are discussed as well as the role of the participating utility. Technical areas discussed pertain to system performance and loads. Specific research tests relating to acoustics, TV interference, and wake effects are also discussed. Author

A85-45513* National Aeronautics and Space Administration. Lewis Research Center, Cleveland, Ohio.
AILERON CONTROLS FOR WIND TURBINE APPLICATIONS
D. R. MILLER and R. L. PUTHOFF (NASA, Lewis Research Center, Cleveland, OH) IN: IECEC '84: Advanced energy systems - Their role in our future; Proceedings of the Nineteenth Intersociety Energy Conversion Engineering Conference, San Francisco, CA, August 19-24, 1984. Volume 4 . La Grange Park, IL, American Nuclear Society, 1984, p. 2369-2373. Previously announced in STAR as N85-11458.

Horizontal axis wind turbines which utilize partial or full variable blade pitch to regulate rotor speed were examined. The weight and costs of these systems indicated a need for alternate methods of rotor control. Aileron control is an alternative which has potential to meet this need. Aileron control rotors were tested on the Mod-O wind turbine to determine their power regulation and shutdown characteristics. Test results for a 20 and 38 percent chord aileron control rotor are presented. Test is shown that aileron control is a viable method for safety for safely controlling rotor speed, following a loss of general load. E.A.K.

A85-45517*# General Electric Co., Philadelphia, Pa.
ADVANCED MULTI-MEGAWATT WIND TURBINE DESIGN FOR UTILITY APPLICATION
W. C. PIJAWKA (General Electric Co., King of Prussia, PA) ANS, SAE, ACS, AIAA, ASME, et al., Intersociety Energy Conversion Engineering Conference on Advanced Energy Systems Their role in our future, 19th, San Francisco, CA, Aug. 19-24, 1984, Paper. 6 p. DOE-sponsored research.
(Contract DEN3-153)

A NASA/DOE program to develop a utility class multimegawatt wind turbine, the MOD-5A, is described. The MOD-5A features a 400 foot diameter rotor which is teetered and positioned upwind of the tower; a 7.3 megawatt power rating with a variable speed electric generating system; and a redundant rotor support and torque transmission structure. The rotor blades were fabricated from an epoxy-bonded wood laminate material which was a successful outgrowth of the MOD-OA airfoil design. Preliminary data from operational tests carried out at the NASA Plumbrook test facility are presented. I.H.

N85-10444*# Hughes Aircraft Co., El Segundo, Calif.
ADVANCED NICKEL-HYDROGEN CELL CONFIGURATION STUDY Final Report
E. ADLER and F. PEREZ Oct. 1984 74 p refs
(Contract NAS3-22249)
(NASA-CR-174775; NAS 1.26:174775; E9787) Avail: NTIS HC A04/MF A01 CSCL 10C

Three nickel hydrogen battery designs, individual pressure vessel (IPV), common pressure vessel (CPV), and a bipolar battery module were studied. Weight, system complexity and cost were compared for a satellite operating in a 6 hour, 5600 nautical mile orbit. The required energy storage is 52 kWh. A 25% improvement in specific energy is observed by employing a bipolar battery versus a battery comprised of hundreds of IPV's. Further weight benefits are realized by the development of light weight technologies in the bipolar design. E.A.K.

N85-10445*# Cleveland State Univ., Ohio.
MANUAL OF PHOSPHORIC ACID FUEL CELL POWER PLANT OPTIMIZATION MODEL AND COMPUTER PROGRAM Final Report
C. Y. LU and K. A. ALKASAB May 1984 66 p refs
(Contract NCC3-17; DE-AI21-80ET-17088)
(NASA-CR-174721; DOE/NASA/0017-3; NAS 1.26:174721)
Avail: NTIS HC A04/MF A01 CSCL 10B

An optimized cost and performance model for a phosphoric acid fuel cell power plant system was derived and developed into a modular FORTRAN computer code. Cost, energy, mass, and electrochemical analyses were combined to develop a mathematical model for optimizing the steam to methane ratio in the reformer, hydrogen utilization in the PAFC plates per stack. The nonlinear programming code, COMPUTE, was used to solve this model, in which the method of mixed penalty function combined with Hooke and Jeeves pattern search was chosen to evaluate this specific optimization problem. Author

N85-10447*# Cleveland State Univ., Ohio.
MANUAL OF PHOSPHORIC ACID FUEL CELL STACK THREE-DIMENSIONAL MODEL AND COMPUTER PROGRAM Final Report
C. Y. LU and K. A. ALKASAB May 1984 66 p refs
(Contract NCC3-17; DE-AI21-80ET-17088)
(NASA-CR-174722; DOE/NASA/0017-4; NAS 1.26:174722)
Avail: NTIS HC A04/MF A01 CSCL 10B

A detailed distributed mathematical model of phosphoric acid fuel cell stack have been developed, with the FORTRAN computer program, for analyzing the temperature distribution in the stack and the associated current density distribution on the cell plates. Energy, mass, and electrochemical analyses in the stack were combined to develop the model. Several reasonable assumptions were made to solve this mathematical model by means of the finite differences numerical method. Author

N85-11455*# Clarkson Coll. of Technology, Potsdam, N.Y.
ELECTROCATALYSIS OF FUEL CELL REACTIONS: INVESTIGATION OF ALTERNATE ELECTROLYTES Final Report
D. T. CHIN, K. L. HSUEH, and H. H. CHANG Jan. 1984 114 p refs
(Contract NAG3-238; DE-AI21-80ET-17088)
(NASA-CR-174753; DOE/NASA/0238-1; NAS 1.26:174753)
Avail: NTIS HC A06/MF A01 CSCL 10A

Oxygen reduction and transport properties of the electrolyte in the phosphoric acid fuel cell are studied. The areas covered were: (1) development of a theoretical expression for the rotating ring disk electrode technique; (2) determination of the intermediate reaction rate constants for oxygen reduction on platinum in phosphoric acid electrolyte; (3) determination of oxygen reduction mechanism in trifluoreomethanesulfonic acid (TFMSA) which was considered as an alternate electrolyte for the acid fuel cells; and (4) the measurement of transport properties of the phosphoric acid electrolyte at high concentrations and temperatures. Author

N85-11456*# Cleveland State Univ., Ohio.
PHOSPHORIC ACID FUEL CELL POWER PLANT SYSTEM PERFORMANCE MODEL AND COMPUTER PROGRAM Final Report
K. A. ALKASAB and C. Y. LU Jan. 1984 134 p refs
(Contract NCC3-17; DE-AI21-80ET-17088)
(NASA-CR-174638; DOE/NASA/0017-1; NAS 1.26:174638)
Avail: NTIS HC A07/MF A01 CSCL 10A

A FORTRAN computer program was developed for analyzing the performance of phosphoric acid fuel cell power plant systems. Energy mass and electrochemical analysis in the reformer, the

shaft converters, the heat exchangers, and the fuel cell stack were combined to develop a mathematical model for the power plant for both atmospheric and pressurized conditions, and for several commercial fuels. Author

N85-11457*# Rensselaer Polytechnic Inst., Troy, N.Y. Dept. of Electrical, Computer and Systems Engineering.
RESEARCH ON GALLIUM ARSENIDE DIFFUSED JUNCTION SOLAR CELLS Final Report, 1 Oct. 1982 - 30 Jun. 1984
J. M. BORREGO and S. K. GHANDI Oct. 1984 54 p refs
(Contract NAG3-188)
(NASA-CR-174057; NAS 1.26:174057) Avail: NTIS HC A04/MF A01 CSCL 10A

The feasibility of using bulk GaAs for the fabrication of diffused junction solar cells was determined. The effects of thermal processing of GaAs was studied, and the quality of starting bulk GaAs for this purpose was assessed. These cells are to be made by open tube diffusion techniques, and are to be tested for photovoltaic response under AMO conditions. B.G.

N85-11458*# National Aeronautics and Space Administration. Lewis Research Center, Cleveland, Ohio.
AILERON CONTROLS FOR WIND TURBINE APPLICATIONS
D. R. MILLER and R. L. PUTOFF Nov. 1984 14 p refs
Presented at the Intersociety Conversion Eng. Conf., San Francisco, 19-24 Aug. 1984
(Contract DE-AI01-76ET-20320)
(NASA-TM-86867; DOE/NASA/20320-60; E-2330; NAS 1.15:86867) Avail: NTIS HC A02/MF A01 CSCL 10A

Horizontal axis wind turbines which utilize partial or full variable blade pitch to regulate rotor speed were examined. The weight and costs of these systems indicated a need for alternate methods of rotor control. Aileron control is an alternative which has potential to meet this need. Aileron control rotors were tested on the Mod-O wind turbine to determine their power regulation and shutdown characteristics. Test results for a 20 and 38% chord aileron control rotor are presented. Test is shown that aileron control is a viable method for safety for safely controlling rotor speed, following a loss of general load. E.A.K.

N85-12465*# National Aeronautics and Space Administration. Lewis Research Center, Cleveland, Ohio.
NASA REDOX STORAGE SYSTEM DEVELOPMENT PROJECT *Final Report*
N. H. HAGEDORN Oct. 1984 48 p refs
(Contract DE-AI04-80AL-12726)
(NASA-TM-83677; E-2125; NAS 1.15:83677) Avail: NTIS HC A03/MF A01 CSCL 10C

The Redox Storage System Technology Project was jointly supported by the U.S. Department of Energy and NASA. The objectives of the project were to develop the Redox flow battery concept and to probe its technical and economic viability. The iron and chromium redox couples were selected as the reactants. Membranes and electrodes were developed for the original mode of operating at 25 C with the reactants separated by an ion-exchange membrane. Analytical capabilities and system-level operating concepts were developed and verified in a 1-kW, 13-kWh preprototype system. A subsequent change was made in operating mode, going to 65 C and using mixed reactants. New membranes and a new electrode catalyst were developed, resulting in single cell operation as high as 80 mA/sq cm with energy efficiencies greater than 80 percent. Studies indicate a likely system cost of about $75/kWh. Standard Oil of Ohio (Sohio) has undertaken further development of the Redox system. An exclusive patent license was obtained from NASA by Sohio. Transfer of Redox technology to Sohio is supported by the NASA Technology Utilization Office. Author

N85-13371*# United Technologies Corp., South Windsor, Conn. Power Systems Div.
REGENERATIVE FUEL CELL ENERGY STORAGE SYSTEM FOR A LOW EARTH ORBIT SPACE STATION
R. E. MARTIN, J. GAROW, and K. B. MICHAELS Aug. 1984 146 p refs
(Contract NAS3-22234)
(NASA-CR-174802; NAS 1.26:174802; FCR-6128) Avail: NTIS HC A07/MF A01 CSCL 10B

Results of a study to define the characteristics of a regenerative fuel cell energy storage system for a large space station operating in low earth orbit (LEO) are presented. The regenerative fuel cell system employs an alkaline electrolyte fuel cell with the option of employing either an alkaline or a solid polymer electrolyte electrolyzer. R.S.F.

N85-13892*# National Aeronautics and Space Administration. Lewis Research Center, Cleveland, Ohio.
DYNAMIC POWER SYSTEMS FOR POWER GENERATION
R. E. ENGLISH *In its* Space Power p 137-149 Apr. 1984 refs
Avail: NTIS HC A14/MF A01 CSCL 10B

The characteristics of dynamic power systems have considerable potential value, especially for the space station. The base of technology that makes these dynamic power systems practical is reviewed. The following types of power-generating systems are examined herein: organic Rankine cycle, potassium Rankine cycle, Brayton cycle, and Stirling cycle. R.S.F.

N85-16291*# Westinghouse Electric Corp., Pittsburgh, Pa. Advanced Energy Systems Div.
GAS COOLED FUEL CELL SYSTEMS TECHNOLOGY DEVELOPMENT Final Report
J. M. FERET Aug. 1983 329 p refs
(Contract DEN3-390; DE-AI01-80ET-17088)
(NASA-CR-174732; DOE/NASA/0290-1; NAS 1.26:174732)
Avail: NTIS HC A15/MF A01 CSCL 10B

The first phase of a planned multiphase program to develop a Phosphoric is addressed. This report describes the efforts performed that culminated in the: (1) Establishment of the preliminary design requirements and system conceptual design for the nominally rated 375 kW PAFC module and is interfacing power plant systems; (2) Establishment of PAFC component and stack performance, endurance, and design parameter data needed for design verification for power plant application; (3) Improvement of the existing PAFC materials data base and establishment of materials specifications and process procedes for the cell components; and (4) Testing of 122 subscale cell atmospheric test for 110,000 cumulative test hours, 12 subscale cell pressurized tests for 15,000 cumulative test hours, and 12 pressurized stack test for 10,000 cumulative test hours. B.W.

N85-16292*# Life Systems, Inc., Cleveland, Ohio.
ENGINEERING MODEL SYSTEM STUDY FOR A REGENERATIVE FUEL CELL: STUDY REPORT
B. J. CHANG, F. H. SCHUBERT, A. J. KOVACH, and R. A. WYNVEEN Sep. 1984 91 p refs
(Contract NAS3-21287)
(NASA-CR-174801; NAS 1.26:174801; LSI-TR-376-30) Avail: NTIS HC A05/MF A01 CSCL 10A

Key design issues of the regenerative fuel cell system concept were studied and a design definition of an alkaline electrolyte based engineering model system or low Earth orbit missions was completed. Definition of key design issues for a regenerative fuel cell system include gaseous reactant storage, shared heat exchangers and high pressure pumps. A power flow diagram for the 75 kW initial space station and the impact of different regenerative fuel cell modular sizes on the total 5 year to orbit weight and volume are determined. System characteristics, an isometric drawing, component sizes and mass and energy balances are determined for the 10 kW engineering model system. An open loop regenerative fuel cell concept is considered for integration of the energy storage system with the life support system of the

space station. Technical problems and their solutions, pacing technologies and required developments and demonstrations for the regenerative fuel cell system are defined. E.A.K.

N85-16293*# Georgia Tech Research Inst., Atlanta.
INFRARED TECHNOLOGY FOR SATELLITE POWER CONVERSION Semiannual Status Report
D. P. CAMPBELL, M. A. GOUKER, and J. J. GALLAGHER 11 Dec. 1984 26 p refs
(Contract NAG3-282)
(NASA-CR-174266; NAS 1.26:174266) Avail: NTIS HC A03/MF A01 CSCL 10A

Successful fabrication of bismuth bolometers led to the observation of antenna action rom array elements. Fabrication of the best antennas arrays was made more facile with finding that increased argon flow during the dc sputtering produced more uniform bismuth films and bonding to antennas must be done with the substrate temperaure below 100 C. Higher temperatures damaged the bolometers. During the testing of the antennas, it was found that the use of a quasi-optical system provided a uniform radiation field. Groups of antennas were bonded in series and in parallel with the parallel configuration showing the greater response. R.S.F.

N85-16299*# National Aeronautics and Space Administration. Lewis Research Center, Cleveland, Ohio.
SHUTDOWN CHARACTERISTICS OF THE MOD-O WIND TURBINE WITH AILERON CONTROLS Final Report
D. R. MILLER and R. D. CORRIGAN 1984 23 p refs Presented at the Horizontal-Axis Wind Turbine Technol. Workshop, Cleveland, 8-10 May 1984
(Contract DE-AI01-76ET-20320)
(NASA-TM-86918; DOE/NASA/20320-61; E-2410; NAS 1.15:86918) Avail: NTIS HC A02/MF A01 CSCL 10B

Horizontal-axis wind turbines utilize partial or full variable blade pitch to regulate rotor speed. The weight and costs of these systems indicated a need for alternate methods of rotor control. Aileron control is an alternative which has potential to meet this need. The NASA Lewis Research Center has been experimentally testing aileron control rotors on the Mod-U wind turbine to determine their power regulation and shutdown characteristics. Experimental and analytical shutdown test results are presented for a 38 percent chord aileron-control rotor. These results indicated that the 38 percent chord ailerons provided overspeed protection over the entire Mod-O operational windspeed range, and had a no-load equilibrium tip speed ratio of 1.9. Thus, the 38 percent chord ailerons had much improved aerodynamic braking capability when compared with the first aileron-control rotor having 20 percent chord ailerons. B.W.

N85-16300*# Garrett Turbine Engine Co., Phoenix, Ariz.
ADVANCED TECHNOLOGY COGENERATION SYSTEM CONCEPTUAL DESIGN STUDY: CLOSED CYCLE GAS TURBINES Final Report
E. A. T. MOCK and H. C. DAUDET Oct. 1983 296 p Prepared in cooperation with Gibbs and Hill, Inc., New York, N.Y., Foster-Wheeler Co., Houston, Tex., and Little (Arthur D.) Co., Santa Monica, Calif.
(Contract DEN3-215; DE-AI01-77ET-13111)
(NASA-CR-168222; DOE/NASA/0215-1; NAS 1.26:168222; GTEC31-4773) Avail: NTIS HC A13/MF A01 CSCL 10B

The results of a three task study performed for the Department of Energy under the direction of the NASA Lewis Research Center are documented. The thermal and electrical energy requirements of three specific industrial plants were surveyed and cost records for the energies consumed were compiled. Preliminary coal fired atmospheric fluidized bed heated closed cycle gas turbine and steam turbine cogeneration system designs were developed for each industrial plant. Preliminary cost and return-on-equity values were calculated and the results compared. The best of the three sites was selected for more detailed design and evaluation of both closed cycle gas turbine and steam turbine cogeneration systems during Task II. Task III involved characterizing the industrial sector electrical and thermal loads for the 48 contiguous states, applying a family of closed cycle gas turbine and steam turbine cogeneration systems to these loads, and conducting a market penetration analysis of the closed cycle gas turbine cogeneration system. Author

N85-17421*# Toledo Univ., Ohio.
THERMAL-STRESS ANALYSIS FOR A WOOD COMPOSITE BLADE Final Report
K. C. FU and A. HARB Jul. 1984 119 p refs
(Contract NAG3-373; DE-AI01-79ET-20320)
(NASA-CR-174794; DOE/NASA/0373-1; NAS 1.26:174794)
Avail: NTIS HC A06/MF A01 CSCL 20K

A thermal-stress analysis of a wind turbine blade made of wood composite material is reported. First, the governing partial differential equation on heat conduction is derived, then, a finite element procedure using variational approach is developed for the solution of the governing equation. Thus, the temperature distribution throughout the blade is determined. Next, based on the temperature distribution, a finite element procedure using potential energy approach is applied to determine the thermal-stress distribution. A set of results is obtained through the use of a computer, which is considered to be satisfactory. All computer programs are contained in the report. B.W.

N85-17422*# United Technologies Corp., South Windsor, Conn. Power Systems Div.
ELECTRIC UTILITY ACID FUEL CELL STACK TECHNOLOGY ADVANCEMENT Final Report
J. V. CONGDON, G. J. GOLLER, G. J. GREISING, J. J. OBRIEN, S. A. RANDALL, G. J. SANDELLI, R. D. BREAULT, G. W. AUSTIN, S. BOPSE, and R. D. COYKENDALL Nov. 1984 158 p refs
(Contract DEN3-191; DE-AI21-80ET-17088)
(NASA-CR-174804; DOE/NASA/0191-1; NAS 1.26:174804; FCR-4684F) Avail: NTIS HC A08/MF A01 CSCL 10A

The principal effort under this program was directed at the fuel cell stack technology required to accomplish the initial feasibility demonstrations of increased cell stack operating pressures and temperatures, increased cell active area, incorporation of the ribbed substrate cell configuration at the bove conditions, and the introduction of higher performance electrocatalysts. The program results were successful with the primary accomplishments being: (1) fabrication of 10 sq ft ribbed substrate, cell components including higher performing electrocatalysts; (2) assembly of a 10 sq ft, 30-cell short stack; and (3) initial test of this stack at 120 psia and 405 F. These accomplishments demonstrate the feasibility of fabricating and handling large area cells using materials and processes that are oriented to low cost manufacture. An additional accomplishment under the program was the testing of two 3.7 sq ft short stacks at 12 psia/405 F to 5400 and 4500 hours respectively. These tests demonstrate the durability of the components and the cell stack configuration to a nominal 5000 hours at the higher pressure and temperature condition planned for the next electric utility power plant. R.S.F.

N85-18451*# Georgia Inst. of Tech., Atlanta.
TECHNOLOGY FOR SATELLITE POWER CONVERSION Interim Technical Report
D. P. CAMPBELL, M. A. GOUKER, C. SUMMERS, and J. J. GALLAGHER 5 Oct. 1984 80 p refs
(Contract NAG3-282)
(NASA-CR-174335; NAS 1.26:174335) Avail: NTIS HC A05/MF A01 CSCL 10A

Techniques for satellite electromagnetic energy transfer and power conversion at millimeter and infrared wavelengths are discussed. The design requirements for rectenna receiving elements are reviewed for both coherent radiation sources and Earth thermal infrared emission. Potential power transmitters including gyrotrons, free electron lasers, and CO2 lasers are assessed along with the rectification properties of metal-oxide metal diode power converters. M.G.

N85-19511*# Stonehart Associates, Inc., Madison, Conn.
PREPARATION AND EVALUATION OF ADVANCED CATALYSTS FOR PHOSPHORIC ACID FUEL CELLS Final Report
P. STONEHART, J. BARIS, J. HOCKMUTH, and P. PAGLIARO Jun. 1984 138 p
(Contract DEN3-176; DE-AI21-80ET-17088)
(NASA-CR-168223; NAS 1.26:168223) Avail: NTIS HC A07/MF A01 CSCL 10A

The platinum electrocatalysts were characterized for their crystallite sizes and the degree of dispersion on the carbon supports. One application of these electrocatalysts was for anodic oxidation of hydrogen in hot phosphoric acid fuel cells, coupled with the influence of low concentrations of carbon monoxide in the fuel gas stream. In a similar way, these platinum on carbon electrocatalysts were evaluated for oxygen reduction in hot phosphoric acid. Binary noble metal alloys were prepared for anodic oxidation of hydrogen and noble metal-refractory metal mixtures were prepared for oxygen reduction. An exemplar alloy of platinum and palladium (50/50 atom %) was discovered for anodic oxidation of hydrogen in the presence of carbon monoxide, and patent disclosures were submitted. For the cathode, platinum-vanadium alloys were prepared showing improved performance over pure platinum. Preliminary experiments on electrocatalyst utilization in electrode structures showed low utilization of the noble metal when the electrocatalyst loading exceeded one weight percent on the carbon. A.R.H.

N85-20530* National Aeronautics and Space Administration. Lewis Research Center, Cleveland, Ohio.
SCREEN PRINTED INTERDIGITATED BACK CONTACT SOLAR CELL Patent
C. R. BARAONA, G. A. MAZARIS, and A. T. CHAI, inventors (to NASA) 23 Oct. 1984 6 p Filed 10 Feb. 1983 Supersedes N83-20374 (21 - 10, p 1557)
(NASA-CASE-LEW-13414-1; NAS 1.71:LEW-13414-1; US-PATENT-4,478,879; US-PATENT-APPL-SN-465364; US-PATENT-CLASS-427-85; US-PATENT-CLASS-136-256)
Avail: US Patent and Trademark Office CSCL 10A

Interdigitated back contact solar cells are made by screen printing dopant materials onto the back surface of a semiconductor substrate in a pair of interdigitated patterns. These dopant materials are then diffused into the substrate to form junctions having configurations corresponding to these patterns. Contacts having configurations which match the patterns are then applied over the junctions.
Official Gazette of the U.S. Patent and Trademark Office

N85-20535*# National Aeronautics and Space Administration. Lewis Research Center, Cleveland, Ohio.
LITHIUM COUNTERDOPED SILICON SOLAR CELL Patent Application
I. WEINBERG and H. W. BRANDHORST, JR., inventors (to NASA) 7 Nov. 1984 10 p
(NASA-CASE-LEW-14177-1; NAS 1.71:LEW-14177-1; US-PATENT-APPL-SN-669140) Avail: NTIS HC A02/MF A01 CSCL 10A

The resistance to radiation damage of an n(+)p boron doped silicon solar cell is improved by lithium counterdoping. Even though lithium is an n-dopant in silicon, the lithium is introduced in small enough quantities so that the cell base remains p-type. The lithium is introduced into the solar cell wafer by implantation of lithium ions whose energy is about 50 keV. After this lithium implantation, the wafer is annealed in a nitrogen atmosphere at 375 C for two hours. NASA

N85-20545*# Michigan State Univ., East Lansing. Div. of Engineering Research.
IMPROVED MODELS FOR INCREASING WIND PENETRATION, ECONOMICS AND OPERATING RELIABILITY Final Report
R. A. SCHLUETER, G. L. PARK, G. SIGARI, and T. COSTI Apr. 1984 198 p refs
(Contract NAG3-399)
(NASA-CR-175538; NAS 1.26:175538; DE85-000865; DOE/NBM-1077) Avail: NTIS HC A09/MF A01 CSCL 10A

The need for wind power prediction in order to enable larger wind power penetrations and improve the economics and reliability of power system operation is discussed. Methods for estimating turbulence and prediction of diurnal wind power prediction are reviewed. A method is presented to predict meteorological event induced wind power variation from measurements of wind speed at reference meteorological towers that encircle all wind turbine clusters and from sites within the wind turbine clusters. The methodology uses a recursive least squares model and requires: (1) detection of even propagation direction; and (2) determination of delays between groups of measurements at reference meteorological towers and those measurements at towers in the array. Proper filtering of the data and methods for switching reference sites and delays for the transition from one frontal system to another are also discussed. The performance of the prediction methodology on data sets from both sites was quite good and indicates one or more hour ahead prediction of wind power for meteorological events is feasible. DOE

N85-21768* National Aeronautics and Space Administration. *Lewis Research Center, Cleveland, Ohio.*
SOLAR ENERGY CONVERTER USING SURFACE PLASMA WAVES Patent
L. M. ANDERSON, inventor (to NASA) 13 Nov. 1984 7 p Filed 19 Apr. 1983 Supersedes N83-26258 (21 - 15, p 2430)
(NASA-CASE-LEW-13827-1; NAS 1.71:LEW-13827-1; US-PATENT-4,482,778; US-PATENT-APPL-SN-486470; US-PATENT-CLASS-136-246; US-PATENT-CLASS-136-225; US-PATENT-CLASS-357-30) Avail: US Patent and Trademark Office CSCL 10A

Sunlight is dispersed over a diffraction grating formed on the surface of a conducting film on a substrate. The angular dispersion controls the effective grating period so that a matching spectrum of surface plasmons is excited for parallel processing on the conducting film. The resulting surface plasmons carry energy to an array of inelastic tunnel diodes. This solar energy converter does not require different materials for each frequency band, and sunlight is directly converted to electricity in an efficient manner by extracting more energy from the more energetic photons.
Official Gazette of the U.S. Patent and Trademark Office

N85-22499*# National Aeronautics and Space Administration. Lewis Research Center, Cleveland, Ohio.
DISCHARGES ON A NEGATIVELY BIASED SOLAR CELL ARRAY IN A CHARGED-PARTICLE ENVIRONMENT
D. B. SNYDER *In its* Spacecraft Environ. Interactions Technol. p 379-388 Mar. 1985 refs Previously announced as N84-23690
Avail: NTIS HC A99/MF E03 CSCL 10A

The charging behavior of a negatively biased solar cell array when subjected to a charged particle environment is studied in the ion density range from 200 to 12,000 ions/sq cm with the applied bias range of -500 to -1400 V. The profile of the surface potentials across the array is related to the presence of discharges. At the low end of the ion density range the solar cell cover slides charge to from 0 to +5 volts independent of the applied voltage. No discharges are seen at bias voltages as large as -1400 V. At the higher ion densities the cover slide potential begins to fluctuate, and becomes significantly negative. Under these conditions discharges can occur. The threshold bias voltage for discharges decreases with increasing ion density. A condition for discharges emerging from the experimental observations is that the average coverslide potential must be more negative than -4 V. The observations presented suggest that the plasma potential near

the array becomes negative before a discharge occurs. This suggests that discharges are driven by an instability in the plasma. Author

N85-23242*# National Aeronautics and Space Administration. Lewis Research Center, Cleveland, Ohio.
DEVELOPMENT OF LARGE, HORIZONTAL-AXIS WIND TURBINES Final Report
D. H. BALDWIN and J. KENNARD (Sverdrup Technology, Inc., Middleburg Heights, Ohio) Mar. 1985 15 p refs
(Contract DE-AI01-76ET-20320)
(NASA-TM-86950; E-2471; DOE/NASA/20320-62; NAS 1.15:86950) Avail: NTIS HC A02/MF A01 CSCL 10B

A program to develop large, horizontal-axis wind turbines is discussed. The program is directed toward developing the technology for safe, reliable, environmentally acceptable large wind turbines that can generate a significant amount of electricity at costs competitive with those of conventional electricity-generating systems. In addition, these large wind turbines must be fully compatible with electric utility operations and interface requirements. Several ongoing projects in large-wind-turbine development are directed toward meeting the technology requirements for utility applications. The machines based on first-generation technology (Mod-OA and Mod-1) successfully completed their planned periods of experimental operation in June, 1982. The second-generation machines (Mod-2) are in operation at selected utility sites. A third-generation machine (Mod-5) is under contract. Erection and initial operation of the Mod-5 in Hawaii should take place in 1986. Each successive generation of technology increased reliability and energy capture while reducing the cost of electricity. These advances are being made by gaining a better understanding of the system-design drivers, improving the analytical design tools, verifying design methods with operating field data, and incorporating new technology and innovative designs. Information is given on the results from the first- and second-generation machines (Mod-OA, - 1, and -2), the status of the Department of Interior, and the status of the third-generation wind turbine (Mod-5). R.J.F.

N85-23243*# National Aeronautics and Space Administration. Lewis Research Center, Cleveland, Ohio.
OPERATIONAL PERFORMANCE OF THE PHOTOVOLTAIC-POWERED GRAIN MILL AND WATER PUMP AT TANGAYE, BURKINA FASO (FORMERLY UPPER VOLTA) Final Report
J. E. MARTZ and A. F. ROBERTS (Michigan Univ., Ann Arbor) Mar. 1985 28 p refs
(Contract NASA ORDER DSB-5710-2-79)
(NASA-TM-86970; E-2496; NAS 1.15:86970) Avail: NTIS HC A03/MF A01 CSCL 10B

A photovoltaic (PV) system powering a grain mill and water pump was installed in the remote African village of Tangaye, Burkina Faso (formerly Upper Volta) under the sponsorship of the U.S. Agency for International Development (AID) and by the National Aeronautics and Space Administration (NASA) Lewis Research Center (LeRC) in early 1979. The presence reports covers the second two years of operation from April 1981 through June 1983. During this time, the grain mill and water pump were operational 96 and 88 percent of the time respectively, and the PV system generated sufficient electricity to enable the grinding of about 111 metric tons of finely ground flow and the pumping of over 5000 cm sq of water from the 10 m deep well. The report includes a description of the current configuration of the system, a review of system performance, a discussion of the socioeconomic impact of the system on the villagers and a summary of results and conclusions covering the entire four-year period. Author

N85-25941*# Engelhard Industries, Inc., Edison, N.J. Specialty Chemicals Div.
DEVELOP AND TEST FUEL CELL POWERED ON-SITE INTEGRATED TOTAL ENERGY SYSTEMS. PHASE 3: FULL-SCALE POWER PLANT DEVELOPMENT Quarterly Technical Progress Report, May - Jul. 1984
A. KAUFMAN, S. PUDICK, C. L. WANG, J. WERTH, and J. A. WHELAN 6 Nov. 1984 20 p
(Contract DEN3-241; DE-AI01-80ET-17088)
(NASA-CR-174887; DOE/NASA/0241-14; NAS 1.26:174887)
Avail: NTIS HC A02/MF A01 CSCL 10A

Two 25-cell, 13 inch x 23 inch (4kW) stacks were started up to evaluate the reliability of component and stack technology developed through the end of 1983. Both stacks started up well and are running satisfactorily on hydrogen-air after 1900 hours and 800 hours, respectively. A synthetic-reformat mixing station is nearing completion, and both stacks will be operated on reformate fuel. A stack-protection control system was placed in operation for Stack No. 2, and a similar set-up is in preparation for Stack No. 1. This system serves to change operating conditions or shut the stack down to avoid deleterious effects from nonstack-related upsets. The capability will greatly improve changes of obtaining meaningful long-term test data. E.A.K.

N85-27377*# General Electric Co., Schenectady, N. Y. Advanced Energy Programs Dept.
PARAMETRIC STUDY OF POTENTIAL EARLY COMMERCIAL POWER PLANTS TASK 3-A MHD COST ANALYSIS Final Technical Report, Apr. 1983
Apr. 1983 51 p
(Contract DEN3-244)
(NASA-CR-175839; NAS 1.26:175839) Avail: NTIS HC A04/MF A01 CSCL 10B

The development of costs for an MHD Power Plant and the comparison of these costs to a conventional coal fired power plant are reported. The program is divided into three activities: (1) code of accounts review; (2) MHD pulverized coal power plant cost comparison; (3) operating and maintenance cost estimates. The scope of each NASA code of account item was defined to assure that the recently completed Task 3 capital cost estimates are consistent with the code of account scope. Improvement confidence in MHD plant capital cost estimates by identifying comparability with conventional pulverized coal fired (PCF) power plant systems is undertaken. The basis for estimating the MHD plant operating and maintenance costs of electricity is verified. E.A.K.

N85-27385*# National Aeronautics and Space Administration. Lewis Research Center, Cleveland, Ohio.
EFFECT OF PRECIPITATION ON WIND TURBINE PERFORMANCE Final Report
R. D. CORRIGAN and R. D. DEMIGLIO (Sverdrup, Inc.) May 1985 23 p refs
(Contract DE-AI01-76ET-20320)
(NASA-TM-86986; E-2530; DOE/NASA/20320-64; NAS 1.15:86986) Avail: NTIS HC A02/MF A01 CSCL 10A

The effects of precipitation on wind turbine power output was analyzed. The tests were conducted on the two bladed Mod-0 horizontal axis wind turbine with three different rotor configurations. Experimental data from these tests are presented which clearly indicate that the performance of the Mod-0 wind turbine is affected by rain. Light rainfall degraded performance by as much as 20 percent while heavy rainfall degraded performance by as much as 30 percent. Snow mixed with drizzle degraded performance by as much as 36 percent at low windspeeds. Also presented are the results of an analysis to predict the effect of rain on wind turbine performance. This analysis used a blade element/momentum code with modified airfoil characteristics to account for the effect of rain and predicted a loss in performance of 31 percent in high winds with moderate rainfall rates. These predicted results agreed well with experimental data. Author

N85-27387*# National Aeronautics and Space Administration. Lewis Research Center, Cleveland, Ohio.
CYCLING PERFORMANCE OF THE IRON-CHROMIUM REDOX ENERGY STORAGE SYSTEM
R. F. GAHN, N. H. HAGEDORN, and J. A. JOHNSON 1985 19 p refs Proposed for presentation at the 20th Intersoc. Energy Conversion Eng. Conf., Miami Beach, Fla., 18-23 Aug. 1985; sponsored by SAE, ANS, ASME, IEEE, AIAA, ACS, and AIChE
(Contract DE-AI04-80AL-12726)
(NASA-TM-87034; E-2590; DOE/NASA/12726-25; NAS 1.15:87034) Avail: NTIS HC A02/MF A01 CSCL 10C

Extended charge-discharge cycling of this electrochemical storage system at 65 C was performed on 14.5 sq cm single cells and a four cell, 867 sq cm bipolar stack. Both the anolyte and catholyte reactant fluids contained 1 molar concentrations of iron and chromium chlorides in hydrochloric acid and were separated by a low-selectivity, cation-exchange membrane. The effect of cycling on the chromium electrode and the cation-exchange membrane was determined. Bismuth and bismuth-lead catalyzed chromium electrodes and a radiation-grafted polyethylene membrane were evaluated by cycling between 5 and 85 percent state-of-charge at 80 mA/sq cm and by periodic charge-discharge polarization measurements to 140 mA/sq cm. Gradual performance losses were observed during cycling but were recoverable by completely discharging the system. Good scale-up to the 867 sq cm stack was achieved. The only difference appeared to be an unexplained resistive-type loss which resulted in a 75 percent W-hr efficiency (at 80 mA/sq cm versus 81 percent for the 14.5 sq cm cell). A new rebalance cell was developed to maintain reactant ionic balance. The cell successfully reduced ferric ions in the iron reactant stream to ferrous ions while chloride ions were oxidized to chlorine gas. Author

N85-28444*# National Aeronautics and Space Administration. Lewis Research Center, Cleveland, Ohio.
INITIAL PERFORMANCE OF ADVANCED DESIGNS FOR IPV NICKEL-HYDROGEN CELLS
J. J. SMITHRICK 23 Aug. 1985 11 p refs Presented at 20th Intersoc. Energy Conversion Eng. Conf. (IECEC), Miami Beach, Fla., 18-23 Aug. 1985; sponsored by SAE, ANS, ASME, IEEE, AIAA, ACS and American Institute of Chemical Engineers
(NASA-TM-87029; E-2585; NAS 1.15:87029) Avail: NTIS HC A02/MF A01 CSCL 10C

Advanced designs for individual pressure vessel nickel hydrogen cells were conceived which should improve the life cycle at deep depths of discharge and improve thermal management. Features of the designs which are new and not incorporated in either of the contemporary cells (Air Force/Hughes, Comsat) are: (1) the use of alternate methods of oxygen recombination, (2) use of serrated edge separators to facilitate movement of gas within the cell while still maintaining required physical contact with the wall wick, and (3) use of an expandable stack to accommodate some of the nickel electrode expansion. The designs also consider electrolyte volume requirements over the life of the cells, and are fully compatible with the Air Force/Hughes design. R.J.F.

N85-29363*# Cleveland State Univ., Ohio.
CONCEPTUAL DESIGN OF A FIXED-PITCH WIND TURBINE GENERATOR SYSTEM RATED AT 400 KILOWATTS Final Report
A. PINTZ, R. KASUBA, and J. SPRING Jun. 1984 86 p refs Sponsored in part by DOE
(Contract NCC3-6; DE-AI01-79ET-20320)
(NASA-CR-174877; NAS 1.26:174877; DOE/NASA/0006-1)
Avail: NTIS HC A05/MF A01 CSCL 10B

The design and cost aspects of a fixed pitch, 400 kW Wind Turbine Generator (WTG) concept are presented. Improvements in reliability and cost reductions were achieved with fixed pitch operation and by incorporating recent advances in WTG technology. The specifications for this WTG concept were as follows: (1) A fixed pitch, continuous wooden rotor was to be provided by the Gougeon Bros. Co. (2) An 8 leg hyperboloid tower that showed promise as a low cost structure was to be used. (3) Only commercially available components and parts that could be easily fabricated were to be considered. (4) Design features deemed desirable based on recent NASA research efforts were to be incorporated. Detailed costs and weight estimates were prepared for the second machine and a wind farm of 12 WTG's. The calculated cost of energy for the fixed pitch, twelve unit windfarm is 11.5 cents/kW hr not including the cost of land and access roads. The study shows feasibility of fixed pitch, intermediate power WTG operation. Author

N85-29364*# Toledo Univ., Ohio.
WAKE EFFECTS ON THE AERODYNAMIC PERFORMANCE OF HORIZONTAL AXIS WIND TURBINES
A. A. AFJEH Aug. 1984 176 p refs
(Contract NCC3-5; DE-AI01-76ET-20320)
(NASA-CR-174920; DOE/NASA/0005-1; NAS 1.26:174920)
Avail: NTIS HC A09/MF A01 CSCL 10A

Success of vortex theories in the performance analysis of horizontal axis wind turbines depends greatly upon accurate specification of the geometry of the vortex wake. Two analysis methods were developed, a new simplified free wake method (SFW) and a prescribed wake method. An earlier wake model of helicopter rotors is extended for wind turbine applications, the fast free wake method (FFW). The FFW was accomplished by partitioning the flow field downstream of the rotor into three regions: (1) the near wake, modeled as a series of straight vortex lines; (2) the intermediate wake, modeled as a number of vortex rings; and (3) the far wake, taken to be a semi-infinite cylindrical wake. In the SFW, a new wake model is proposed. The model assumes that the wake is composed of an intense tip vortex and a diffused inboard wake, consistent with the experimentally observed wake of hovering helicopters. It is assumed that the vortex formation was almost immediate as opposed to the actual gradual rolling-up of the tip vortex. The method is demonstrated by assuming that the wake expansion can be represented by an analytical expression. E.A.K.

N85-29365*# National Aeronautics and Space Administration. Lewis Research Center, Cleveland, Ohio.
GOVERNMENT REVIEW OF THE MOD-2 WIND TURBINE (AS-BUILT)
W. R. JOHNSON, A. G. BIRCHENOUGH, B. S. LINSCOTT, J. R. REAGAN, P. J. SIROCKY, R. L. SIZEMORE, T. L. SULLIVAN, and R. H. HOLEMAN Jun. 1985 76 p refs Prepared in cooperation with Bonneville Power Administration
(Contract DE-AI01-76ET-20320)
(NASA-TM-86983; E-2526; DOE/NASA/20320-63; NAS 1.15:86983) Avail: NTIS HC A05/MF A01 CSCL 10B

The findings and recommendations of the Government committee formed to conduct an as-built review of the three Mod-2 wind turbine units at Goldendale, Washington are given. The purpose of the review was to identify any critical deficiencies in machine components that could result in failure, and to recommend any necessary corrective action before resuming safe machine operation. The review concluded that one of the deficiencies identified would preclude planned attended or unattended operation, provided that certain corrective actions were implemented. R.J.F.

N85-30476*# National Aeronautics and Space Administration. Lewis Research Center, Cleveland, Ohio.
ANALYTICAL MODEL FOR PREDICTING EMERGENCY SHUTDOWN OF A TWO-BLADED HORIZONTAL AXIS WIND TURBINE
D. R. MILLER and C. B. F. ENSWORTH 1983 15 p refs Presented at the Wind Workshop 6, Minneapolis, 1-3 Jun. 1983; sponsored by American Solar Energy Society
(Contract DE-AI01-76ET-20320)
(NASA-TM-83472; E-1786; DOE/NASA/20320-50; NAS 1.15:83472) Avail: NTIS HC A02/MF A01 CSCL 10A

An analytical model was developed to predict the shutdown characteristics of a large two bladed horizontal-axis wind turbine following a sudden loss of generator load. The analytical model is

described and used to predict rotor speed time histories following a loss of load, for a tip-control rotor and an aileron control rotor. These shutdown predictions are compared with experimental results from full-scale tests conducted on the Mod-O 100 kW wind turbine with both a tip control rotor and an aileron-control rotor. Predicted and measured rotor speed time histories are compared based on peak overspeed rpm, time at which this peak rpm occurs, and the general shape of the time history curve. The results of this comparison indicated there was good agreement between predictions and the full scale test results, thus verifying the analytical shutdown model. In general, the best agreement between predictions and full-scale test results was obtained up to the time where the peak overspeed rpm occurred. Author

N85-30477*# National Aeronautics and Space Administration. Lewis Research Center, Cleveland, Ohio.
PERFORMANCE COMPARISON BETWEEN NACA 23024 AND NACA 64(3)-618 AIRFOIL CONFIGURATED ROTORS FOR HORIZONTAL-AXIS WIND TURBINES
R. D. CORRIGAN, C. B. F. ENSWORTH, and T. G. KEITH, JR. (Toledo Univ., Ohio) 1983 22 p refs Presented at the Wind Workshop 6, Minneapolis, 1-3 Jun. 1983; sponsored by American Solar Energy Society
(Contract DE-AI01-76ET-20320)
(NASA-TM-83471; DOE/NASA/20320-51; NAS 1.15:83471)
Avail: NTIS HC A02/MF A01 CSCL 10A

Wind turbine performance tests were conducted on the Mod-O 100-kW horizontal-axis wind turbine to compare a tip-controlled rotor having NACA 23024 airfoil tip sections with a similar rotor having NACA 64 sub 3-618 airfoil tip sections. The inboard portion of the blades had an NACA 23024 airfoil section. The wind turbine configuration consisted of the nacelle-rotor assembly mounted atop a tubular tower with the rotor axis 38 m above ground level. The rotor was 39 m in diameter, coned, and teetered and had 20 deg of pitch and flap coupling delta sub 3. The blades had 23 percent root cutout and the movable tip-control section covered the outer 31 percent of the blade. Testing was conducted at nominal rotor speeds of 20 and 31 rpm witth the rotor downwind of he tower. The tests indicate improved performance for the rotor with the NACA 64 sub 3-618 airfoil tip sections over the rotor with the NACA 23024 airfoil tip sections. In addition, performance was predicted for each rotor configuration by using two performance prediction codes. This report presents the test results and compares them with each other and with predicted performance for both rotor configurations. Author

N85-30478*# National Aeronautics and Space Administration. Lewis Research Center, Cleveland, Ohio.
THE FEDERAL WIND PROGRAM AT NASA LEWIS RESEARCH CENTER
D. H. BALDWIN and B. S. LINSCOTT 1983 22 p refs Presented at 6th Biennial Wind Energy Conf. and Workshop, Minneapolis, 1-3 Jun. 1983; sponsored by American Solar Energy Society
(Contract DE-AI01-76ET-20320)
(NASA-TM-83480; E-1798; DOE/NASA/20320-52; NAS 1.15:83480) Avail: NTIS HC A02/MF A01 CSCL 10A

There are several ongoing large wind system development projects directed toward meeting the technology requirements for utility applications. The first generation technology machines, Mod-OA and Mod-1, have successfully completed their planned periods of experimental operation. Disposition of these machines is nearly complete. The second generation machines, Mod-2's, continue experimental operation at Goodnoe Hills, WA, and Medicine Bow, Wy. Design and engineering development of third generation, Mod-5, machines is underway. Initial experimental operation of Mod-5 is planned for DOE in late 1984 or early 1985. An overview of these project activities is presented. In addition to these projects, NASA also is conducting research on large horizontal axis wind turbines. The four main areas of experimental research are: (1) aerodynamics; (2) structural dynamics and aeroelasticity; (3) composite and hybrid composite materials; and (4) multiple system interaction. Key research activities and results are described. The continuing need for future wind turbine research and technology development is explored. Author

N85-30479*# National Aeronautics and Space Administration. Lewis Research Center, Cleveland, Ohio.
OPERATIONAL RESULTS FOR THE EXPERIMENTAL DOE/NASA MOD-OA WIND TURBINE PROJECT
R. K. SHALTENS and A. G. BIRCHENOUGH 1983 29 p refs Presented at the 6th Wind Workshop, Minneapolis, 1-3 Jun. 1983; sponsored by American Solar Energy Society
(Contract DE-AI01-76ET-20320)
(NASA-TM-83517; E-1865; DOE/NASA/20320-55; NAS 1.15:83517) Avail: NTIS HC A03/MF A01 CSCL 10A

The Mod-OA wind turbine project which was to gain early experience in the operation of large wind turbines in a utility environment is discussed. The Mod-OA wind turbines were a first generation design, and even though not cost effective, the operating experience and performance characteristics had a significant effect on the design and development of the second and third generation machines. The Mod-OA machines were modified as a result of the operational experience, particularly the blade development and control system strategy. The results of study to investigate the interaction of a Mod-OA wind turbine with an isolated diesel generation system are discussed. The machine configuration, its advantages and disadvantages and the machine performance and availability are discussed. E.A.K.

N85-30480*# National Aeronautics and Space Administration. Lewis Research Center, Cleveland, Ohio.
LIFE CYCLE TEST RESULTS OF A BIPOLAR NICKEL HYDROGEN BATTERY
R. L. CATALDO 1985 14 p refs Presented at the 20th Intersociety Energy Conversion Eng. Conf. (IECEC), Miami Beach, Fla., 18-23 Aug. 1985; sponsored by SAE, ANS, ASME, IEEE, AIAA, ACS and AICHE
(NASA-TM-87046; E-2608; NAS 1.15:87056) Avail: NTIS HC A02/MF A01 CSCL 10C

A history of low Earth orbit laboratory test data on a 6.5 Ah bipolar nickel hydrogen battery designed and built at the NASA Lewis Research Center is presented. During the past several years the Storage and Thermal Branch has been deeply involved in the design, development, and optimization of nickel hydrogen devices. The bipolar concept is a means of achieving the goal of producing an acceptable battery of higher energy density, able to withstand the demands of low Earth orbit regimes. Author

N85-30481*# Mechanical Technology, Inc., Latham, N. Y.
FREE-PISTON STIRLING ENGINE/LINEAR ALTERNATOR 1000-HOUR ENDURANCE TEST Final Report
J. RAUCH and G. DOCHAT Mar. 1985 98 p
(Contract DEN3-333)
(NASA-CR-174771; DOE/NASA/0333-1; NAS 1.26:174771)
Avail: NTIS HC A05/MF A01 CSCL 10B

The Free Piston Stirling Engine (FPSE) has the potential to be a long lived, highly reliable, power conversion device attractive for many product applications such as space, residential or remote site power. The purpose of endurance testing the FPSE was to demonstrate its potential for long life. The endurance program was directed at obtaining 1000 operational hours under various test conditions: low power, full stroke, duty cycle and stop/start. Critical performance parameters were measured to note any change and/or trend. Inspections were conducted to measure and compare critical seal/bearing clearances. The engine performed well throughout the program, completing more than 1100 hours. Hardware inspection, including the critical clearances, showed no significant change in hardware or clearance dimensions. The performance parameters did not exhibit any increasing or decreasing trends. The test program confirms the potential for long life FPSE applications. Author

N85-30483*# Engelhard Industries, Inc., Edison, N.J.
DEVELOP AND TEST FUEL CELL POWERED ON-SITE INTEGRATED TOTAL ENERGY SYSTEMS. PHASE 3: FULL-SCALE POWER PLANT DEVELOPMENT Quarterly Report, Aug. - Oct. 1983
A. KAUFMAN, S. PUDICK, C. L. WANG, J. WERTH, and J. A. WHELAN 21 Dec. 1983 30 p
(Contract DEN3-241; DE-AI-01-80ET-17088)
(NASA-CR-168338; NAS 1.26:168338; DOE/NASA/0241-11; QR-11) Avail: NTIS HC A03/MF A01 CSCL 10C

On-going test experience with a 5kW methanol-air integrated system is described. Long-term successful operation of a semi-automated electrolyte-replenishment system and non-metallic cooling plates was sustained in a 24-cell, two sq. ft. (4kW) stack. Single-cell test results for two developmental cathode catalysts are reported. Corrosion-protection efforts for metallic current-collecting plates are described. Author

N85-31374*# National Aeronautics and Space Administration. Lewis Research Center, Cleveland, Ohio.
SOLAR DYNAMIC SYSTEMS
M. O. DUSTIN *In* NASA. Goddard Space Flight Center The 1984 Goddard Space Flight Center Battery Workshop p 53-68 Jul. 1985
Avail: NTIS HC A25/MF A01 CSCL 10A

The development of the solar dynamic system is discussed. The benefits of the solar dynamic system over pv systems are enumerated. The history of the solar dynamic development is recounted. The purpose and approach of the advanced development are outlined. Critical concentrator technology and critical heat recover technology are examined. E.A.K.

N85-31624*# National Aeronautics and Space Administration. Lewis Research Center, Cleveland, Ohio.
HIGH EFFICIENCY SOLAR CELL RESEARCH FOR SPACE APPLICATIONS
D. J. FLOOD *In* JPL Proc. of the Flat-Plate Solar Array Proj. Res. Forum on High-Efficiency Crystalline Silicon Solar Cells p 147-162 15 May 1985 refs
Avail: NTIS HC A21/MF A01 CSCL 10A

A review is given of NASA photovoltaic research with emphasis on the activities of the Lewis Research Center. High efficiency solar cell research is discussed, as well as solar arrays, multi-junction cell bandgaps, and plasmon coupling. R.J.F.

N85-31646*# National Aeronautics and Space Administration. Lewis Research Center, Cleveland, Ohio.
DESIGN PRINCIPLES FOR NICKEL-HYDROGEN CELLS AND BATTERIES
L. H. THALLER, M. A. MANZO, and O. D. GONZALEZ-SANABRIA 1985 13 p refs Presented at the 20th Intersoc. Energy Conversion Eng. Conf., Miami Beach, Fla., 18-23 Aug. 1985; sponsored in part by SAE, ANS, ASME, IEEE, AIAA, ACS and AIChE
(NASA-TM-87037; E-2594; NAS 1.15:87037) Avail: NTIS HC A02/MF A01 CSCL 10C

Nickel-hydrogen cells and, more recently, bipolar batteries have been built by a variety of organizations. The design principles that have been used by the technology group at the NASA Lewis Research Center draw upon their extensive background in separator technology, alkaline fuel cell technology, and several alkaline cell technology areas. These design principles have been incorporated into both the more contemporary individual pressure vessel (IPV) designs that were pioneered by other groups, as well as the more recent bipolar battery designs using active cooling that are being developed at NASA Lewis Research Center and under contract. These principles are rather straightforward applications of capillary force formalisms, coupled with the slowly developing data base resulting from careful post test analyses. The objective of this overall effort is directed towards the low-Earth-orbit (LEO) application where the cycle life requirements are much more severe than the geosynchronous-orbit (GEO) application. A summary of the design principles employed is presented along with a discussion of the recommendations for component pore sizes and pore size distributions, as well as suggested materials of construction. These will be made based on our experience in these areas to show how these design principles have been translated into operating hardware. Author

N85-33566*# Ohio State Univ., Columbus. Dept. of Welding Engineering.
DIFFUSION WELDING OF CASSEGRAINIAN CONCENTRATOR CELL STACK ASSEMBLIES M.S. Thesis Final Report, Jun. 1983 - Sep. 1985
K. J. GANGL Jul. 1985 137 p refs
(Contract NAG3-448)
(NASA-CR-176104; NAS 1.26:176104) Avail: NTIS HC A07/MF A01 CSCL 10B

Development of a procedure to join the components of the Cassegrainian concentrator photovoltaic cell stack assembly was studied. Diffusion welding was selected as the most promising process, and was concentrated on exclusively. All faying surfaces were coated with silver to promote welding. The first phase of the study consisted of developing the relationship between process parameters and joint strength using silver plated steel samples and an isostatic pressure system. In the second phase, mockups of the cell stack assembly were welded in a hot isostatic press. Excellent joint strength was achieved with parameters of 350 C and 10 ksi, but the delicate GaAs component could not survive the welding cycle without cracking. The tendency towards cracking was found to be affected by both temperature and pressure. Further work will be required in the future to solve this problem. Author

N85-34441* National Aeronautics and Space Administration. Lewis Research Center, Cleveland, Ohio.
THERMIONIC PHOTOVOLTAIC ENERGY CONVERTER Patent
D. L. CHUBB, inventor (to NASA) 9 Jul. 1985 7 p Filed 15 Feb. 1984 Supersedes N84-20918 (22 - 11, p 1673)
(NASA-CASE-LEW-14077-1; US-PATENT-4,528,417; US-PATENT-APPL-SN-580573; US-PATENT-CLASS-136-253)
Avail: US Patent and Trademark Office CSCL 10A

A thermionic photovoltaic energy conversion device comprises a thermionic diode mounted within a hollow tubular photovoltaic converter. The thermionic diode maintains a cesium discharge for producing excited atoms that emit line radiation in the wavelength region of 850 nm to 890 nm. The photovoltaic converter is a silicon or gallium arsenide photovoltaic cell having bandgap energies in this same wavelength region for optimum cell efficiency.
Official Gazette of the U.S. Patent and Trademark Office

N85-34443*# National Aeronautics and Space Administration. Lewis Research Center, Cleveland, Ohio.
EVALUATION OF DEVELOPMENTAL MEMBRANES FOR THE MIXED REACTANT IRON-CHROMIUM REDOX SYSTEM
J. S. LING 1984 13 p refs Presented at the 166th Meeting of the Electrochem. Soc., New Orleans, 7-12 Oct. 1984
(Contract DE-AI04-80AL-12726)
(NASA-TM-87074; E-2646; DOE/NASA/12726-26; NAS 1.15:87074) Avail: NTIS HC A02/MF A01 CSCL 10C

The operation of the redox storage system at 65 C with premixed ion has changed chromium reactant solutions membrane requirements. These new conditions allow the use of low resistivity membranes with relatively poor selectivity compared to membranes developed for system operation with separate reactants at 25 C. The results of in cell evaluations of developmental membranes for the new conditions are presented. Data include diffusion rate, area resistivity, and coulombic and energy efficiencies over a wide range of current densities. Use of these membranes results in peak round trip energy efficiencies greater than 80% at current densities as high as 80 mA/sq cm. E.A.K.

N85-34444*# National Aeronautics and Space Administration. Lewis Research Center, Cleveland, Ohio.
REFLECTION PLANE TESTS OF A WIND TURBINE BLADE TIP SECTION WITH AILERONS Final Report
J. M. SAVINO, T. W. NYLAND, A. G. BIRCHENOUGH, F. L. JORDAN (NASA, Langley Research Center), and N. K. CAMPBELL (NASA, Langley Research Center) Aug. 1985 57 p refs
(Contract DE-AI01-79ET-20320)
(NASA-TM-87018; E-2564; DOE/NASA/20320-65; NAS 1.15:87018) Avail: NTIS HC A04/MF A01 CSCL 10A

Tests were conducted in the NASA Langley 30 by 60 foot Wind Tunnel on a full scale 7.31 m (24 ft) long tip section of a wind turbine rotor blade. The blade tip section was built with ailerons on the trailing edge. The ailerons, which spanned a length of 6.1 m (20 ft), were designed so that two types could be evaluated: the plain and the balanced. The ailerons were hinged on the suction surface at the 0.62 X chord station behind the leading edge. The purpose of the tests was to measure the aerodynamic characteristics of the blade section for: an angle of attack range from 0 deg to 90 deg aileron deflections from 0 deg to -90 deg, and Reynolds numbers of 0.79 and 1.5 x 10 to the 6th power. These data were then used to determine which aileron configuration had the most desirable rotor control and aerodynamic braking characteristics. Tests were also run to determine the effects of vortex generators, leading edge roughness, and the gaps between the aileron sections on the lift, drag, and chordwise force coefficients of the blade tip section. Author

N85-35471*# Giner, Inc., Waltham, Mass.
DEVELOPMENT OF ELECTRODES FOR THE NASA IRON/CHROMIUM Final Report
L. SWETTE and V. JALAN Jun. 1984 285 p refs
(Contract DEN3-262; DE-AI04-80AL-12726)
(NASA-CR-174724; DOE/NASA/0262-1; NAS 1.26:174724)
Avail: NTIS HC A13/MF A01 CSCL 10A

This program was directed primarily to the development of the negative (Cr3+/Cr2+) electrode for the NASA chromous/ferric Redox battery. The investigation of the effects of substrate processing and gold/lead catalyzation parameters on electrochemical performance were continued. In addition, the effects of reactant cross-mixing, acidity level, and temperature were examined for both Redox couples. Finally, the performance of optimized electrodes was tested in system hardware (1/3 square foot single cell). The major findings are discussed: (1) The recommended processing temperature for the carbon felt, as a substrate for the negative electrode, is 1650 to 1750 C, (2) The recommended gold catalyzation procedure is essentially the published NASA procedure (NASA TM-82724, Nov. 1981) based on deposition from aqueous methanol solution, with the imposition of a few controls such as temperature (25 C) and precatalyzation pH of the felt (7), (3) Experimental observations of the gold catalyzation process and subsequent electron microscopy indicate that the gold is deposited from the colloidal state, induced by contact of the solution with the carbon felt, (4) Electrodeposited lead appears to be present as a thin uniform layer over the entire surface of the carbon fibers, rather than an discrete particles, and (5) Cross-mixing of reactants (Fe-2+ in negative electrode solution or Cr-3+ in the positive electrode solution) did not appear to produce significant interference at either electrode. Author

N85-35472*# Michigan Univ., Ann Arbor.
PRACTICAL ASPECTS OF PHOTOVOLTAIC TECHNOLOGY, APPLICATIONS AND COST (REVISED) Final Report
L. ROSENBLUM Aug. 1985 247 p refs Previously announced as N83-34450
(Contract NAG3-185)
(NASA-CR-174963; NAS 1.26:174963) Avail: NTIS HC A11/MF A01 CSCL 10A

The purpose of this text is to provide the reader with the background, understanding, and computational tools needed to master the practical aspects of photovoltaic (PV) technology, application, and cost. The focus is on stand-alone, silicon solar cell, flat-plate systems in the range of 1 to 25 kWh/day output. Technology topics covered include operation and performance of each of the major system components (e.g., modules, array, battery, regulators, controls, and instrumentation), safety, installation, operation and maintenance, and electrical loads. Application experience and trends are presented. Indices of electrical service performance - reliability, availability, and voltage control - are discussed, and the known service performance of central station electric grid, diesel-generator, and PV stand-alone systems are compared. PV system sizing methods are reviewed and compared, and a procedure for rapid sizing is described and illustrated by the use of several sample cases. The rapid sizing procedure yields an array and battery size that corresponds to a minimum cost system for a given load requirement, insulation condition, and desired level of service performance. PV system capital cost and levelized energy cost are derived as functions of service performance and insulation. Estimates of future trends in PV system costs are made. Author

45

ENVIRONMENT POLLUTION

Includes air, noise, thermal and water pollution; environment monitoring; and contamination control.

N85-23830*# National Aeronautics and Space Administration. Lewis Research Center, Cleveland, Ohio.
EXTREME PRECISION ANTENNA REFLECTOR STUDY RESULTS
G. R. SHARP, L. D. GILGER (Harris Corp., Melbourne, Fla.), and K. E. ARD (Harris Corp., Melbourne, Fla.) *In* NASA. Langley Research Center Large Space Antenna Systems Technol., 1984 p 279-300 Apr. 1985 refs
Avail: NTIS HC A20/MF A01 CSCL 22B

Thermal and mechanical distortion degrade the RF performance of antennas. The complexity of future communications antennas requires accurate, dimensionally stable antenna reflectors and structures built from materials other than those currently used. The advantages and disadvantages of using carbon fibers in an epoxy matrix are reviewed as well as current reflector fabrications technology and adjustment. The manufacturing sequence and coefficient of thermal expansion of carbon fiber/borosilicate glass composites is described. The construction of a parabolic reflector from this material and the assembling of both reflector and antenna are described. A 3M-aperture-diameter carbon/glass reflector that can be used as a subassembly for large reflectors is depicted. The deployment sequence for a 10.5M-aperture-diameter antenna, final reflector adjustment, and the deployment sequence for large reflectors are also illustrated. A.R.H.

46

GEOPHYSICS

Includes aeronomy; upper and lower atmosphere studies; ionospheric and magnetospheric physics; and geomagnetism.

A85-29538* Iowa Univ., Iowa City.
EFFECTS OF CHEMICAL RELEASES BY THE STS 3 ORBITER ON THE IONOSPHERE
J. S. PICKETT, G. B. MURPHY, W. S. KURTH, C. K. GOERTZ (Iowa, University, Iowa City, IA), and S. D. SHAWHAN (NASA, Washington, DC) Journal of Geophysical Research (ISSN 0148-0227), vol. 90, April 1, 1985, p. 3487-3497. Previously announced in STAR as N84-25204. refs
(Contract NAS8-32807; NAG3-449)

The Plasma Diagnostics Package, flown aboard STS-3 as part of the first Shuttle payload (OSS-1), recorded the effects of various chemical releases from the Orbiter. Changes in the plasma environment was observed during flash evaporator system releases, water dumps and maneuvering thruster operations. During flash evaporator operations, broadband Orbiter-generated electrostatic noise was enhanced and plasma density irregularities were observed to increase by 3 to 30 times with a spectrum which rose steeply and peaked below 6 Hz. In the case of water dumps, background electrostatic noise was enhanced at frequencies below about 3 kHz and suppressed at frequencies above 2 kHz. Thruster activity also stimulated electrostatic noise with a spectrum which peaked at approximately 0.5 kHz. In addition, ions with energies up to 1 keV were seen during some thruster events. Author

A85-37717* Iowa Univ., Iowa City.
DE-1 MEASUREMENTS OF AKR WAVE DIRECTIONS
W. CALVERT (Iowa, University, Iowa City, IA) Geophysical Research Letters (ISSN 0094-8276), vol. 12, June 1985, p. 381-384. refs
(Contract NAG3-10)

In addition to its wave rotation sense, the direction of auroral kilometric radiation (AKR) can also be measured with the plasma wave instrument on Dynamics Explorer 1, from the relative phase of the signals received by its orthogonal electric dipole antennas. By this method, which differs in principle from the previous spin-null method for measuring wave directions, it has been found possible to pinpoint the AKR source by triangulation, using measurements from different points along the DE-1 orbit. The resulting apparent source, in one instance, seemed to occupy a well-defined auroral-zone invariant magnetic latitude and showed the expected increase of altitude with decreasing frequency. An analysis of the method also confirmed the validity of the previous rotation sense measurements. Author

47

METEOROLOGY AND CLIMATOLOGY

Includes weather forecasting and modification.

A85-11979*# Control Data Corp., Minneapolis, Minn.
GASP CLOUD ENCOUNTER STATISTICS - IMPLICATIONS FOR LAMINAR FLOW CONTROL FLIGHT
W. H. JASPERSON, G. D. NASTROM (Control Data Corp., Minneapolis, MN), R. E. DAVIS (NASA, Langley Research Center, Flight Electronics Div., Hampton, VA), and J. D. HOLDEMAN (NASA, Lewis Research Center, Aerothermodynamics and Fuels Div., Cleveland, OH) Journal of Aircraft (ISSN 0021-8669), vol. 21, Nov. 1984, p. 851-857. refs

The cloud observation archive from the NASA Global Atmospheric Sampling Program (GASP) is analyzed in order to derive the probability of cloud encounter at altitudes normally flown by commercial airliners, for application to a determination of the feasability of Laminar Flow Control (LFC) on long-range routes. The probability of cloud encounter is found to vary significantly with season. Several meteorological circulation features are apparent in the latitudinal distribution of cloud cover. The cloud encounter data are shown to be consistent with the classical midlatitude cyclone model with more clouds encountered in highs than in lows. Aircraft measurements of route-averaged time-in-clouds fit a gamma probability distribution model which is applied to estimate the probability of extended cloud encounter, and the associated loss of LFC effectiveness along seven high-density routes. The probability is demonstrated to be low. I.H.

A85-21140* Control Data Corp., Minneapolis, Minn.
A COMPARISON OF NMC AND GWC ANALYSIS FIELD TEMPERATURES WITH AIRCRAFT MEASUREMENTS
W. H. JASPERSON and G. D. NASTROM (Control Data Corp., Minneapolis, MN) Journal of Climate and Applied Meteorology (ISSN 0733-3021), vol. 23, Oct. 1984, p. 1421-1426. refs
(Contract NAS3-21249)

Comparison between in situ aircraft observations of temperature and National Meteorological Center and Global Weather Central analysis fields of temperature is presented for a continental and oceanic flight route. The standard deviations of the temperature differences over several hundred flights are found to be 2.5 and 3.5 C for the continental and oceanic route, respectively. A bias towards warm temperatures of about 0.85 C for the analysis fields was found for the oceanic route. Only small differences are found between the NMC and GWC analysis field temperatures. Author

A85-31199* Control Data Corp., Minneapolis, Minn.
VARIABILITY OF CLOUDINESS AT AIRLINE CRUISE ALTITUDES FROM GASP MEASUREMENTS
W. H. JASPERSON, G. D. NASTROM (Control Data Corp., Minneapolis, MN), R. E. DAVIS (NASA, Langley Research Center, Hampton, VA), and J. D. HOLDEMAN (NASA, Lewis Research Center, Cleveland, OH) Journal of Climate and Applied Meteorology (ISSN 0733-3021), vol. 24, Jan. 1985, p. 74-82. refs

Additional statistics relating to the climatology of cloud cover at airline cruise altitudes are presented. The data were obtained between 1975 and 1979 from commercial airliners participating in the Global Atmospheric Sampling Program (GASP). The statistics describe the seasonal, latitudinal and altitudinal variation in cloudiness parameters as well as differences in the high-altitude cloud structure attributed to cyclone and convective-cloud generation processes. The latitudinal distribution of cloud cover derived form the GASP data was found to agree with high-altitude satellite observations. The relationships between three different measures of cloudiness and the relative vorticity at high altitudes is also discussed. I.H.

N85-10558*# National Aeronautics and Space Administration. Lewis Research Center, Cleveland, Ohio.
MERIT: A MAN/COMPUTER DATA MANAGEMENT AND ENHANCEMENT SYSTEM FOR UPPER AIR NOWCASTING/FORECASTING IN THE UNITED STATES
R. STEINBERG *In* ESA Nowcasting 2. Mesoscale Observations and Very-Short-Range Weather Forecasting p 465-471 Jun. 1984 refs
Avail: NTIS HC A23/MF A01

It is suggested that the very short range forecast problem for aviation is one of data management rather than model development and the possibility of improving the aviation forecast using current technology is underlined. The MERIT concept of modeling technology, and advanced man/computer interactive data management and enhancement techniques to provide a tailored, accurate and timely forecast for aviation is outlined. The MERIT includes utilization of the Langrangian approach, extensive use of the automated aircraft report to complement the present data base and provide the most current observations; and the concept that a 2 to 12 hour forecast provided every 3 hr can meet the domestic needs of aviation instead of the present 18 and 24 hr forecast provided every 12 hr. Author (ESA)

N85-21872*# National Aeronautics and Space Administration. Lewis Research Center, Cleveland, Ohio.
SIMULTANEOUS CABIN AND AMBIENT OZONE MEASUREMENTS ON TWO BOEING 747 AIRPLANES. VOLUME 3: OCTOBER 1978 - JULY 1979
J. D. HOLDEMAN and W. H. JASPERSON (Control Data Corp., Minneapolis) Feb. 1985 579 p refs
(Contract DOT-FA78WAI-893)
(NASA-TM-86883; E-2344; NAS 1.15:86883) Avail: NTIS HC A25/MF A01 CSCL 04B

Measurements of ozone concentrations at cruise altitudes both outside and in the cabin of a Boeing 747SP and Boeing 747-100 airliners in routine commercial service are presented. Plotted and tabulated data are identified by route and are arranged chronologically for each airplane. These data were taken at 5- or 10-min intervals by automated instruments used in the NASA Global Atmospheric Sampling Program (GASP). All GASP cabin ozone data obtained from October 1978 to early July 1979 are presented. R.J.F.

N85-35534*# PRC Planning and Economics, Inc., Lake Success, N.Y.
COMPARATIVE ANALYSIS OF OPERATIONAL FORECASTS VERSUS ACTUAL WEATHER CONDITIONS IN AIRLINE FLIGHT PLANNING, VOLUME 1
J. F. KEITZ Apr. 1982 83 p 5 Vol.
(Contract NAS3-22748)
(NASA-CR-167862; NAS 1.26:167862) Avail: NTIS HC A05/MF A01 CSCL 04B

The impact of more timely and accurate weather data on airline flight planning with the emphasis on fuel savings is studied. This volume of the report discusses the results of Task 1 of the four major tasks included in the study. Task 1 compares flight plans based on forecasts with plans based on the verifying analysis from 33 days during the summer and fall of 1979. The comparisons show that: (1) potential fuel savings conservatively estimated to be between 1.2 and 2.5 percent could result from using more timely and accurate weather data in flight planning and route selection; (2) the Suitland forecast generally underestimates wind speeds; and (3) the track selection methodology of many airlines operating on the North Atlantic may not be optimum resulting in their selecting other than the optimum North Atlantic Organized Track about 50 percent of the time. Author

N85-35535*# PRC Planning and Economics, Inc., Lake Success, N.Y.
COMPARATIVE ANALYSIS OF OPERATIONAL FORECASTS VERSUS ACTUAL WEATHER CONDITIONS IN AIRLINE FLIGHT PLANNING, VOLUME 2
J. F. KEITZ Apr. 1982 54 p 5 Vol.
(Contract NAS3-22748)
(NASA-CR-167863; NAS 1.26:167863) Avail: NTIS HC A04/MF A01 CSCL 04B

The impact of more timely and accurate weather data on airline flight planning with the emphasis on fuel savings is studied. This volume of the report discusses the results of Task 2 of the four major tasks included in the study. Task 2 compares various catagories of flight plans and flight tracking data produced by a simulation system developed for the Federal Aviation Administrations by SRI International. (Flight tracking data simulate actual flight tracks of all aircraft operating at a given time and provide for rerouting of flights as necessary to resolve traffic conflicts.) The comparisons of flight plans on the forecast to flight plans on the verifying analysis confirm Task 1 findings that wind speeds are generally underestimated. Comparisons involving flight tracking data indicate that actual fuel burn is always higher than planned, in either direction, and even when the same weather data set is used. Since the flight tracking model output results in more diversions than is known to be the case, it was concluded that there is an error in the flight tracking algorithm. Author

N85-35536*# PRC Planning and Economics, Inc., Lake Success, N.Y.
COMPARATIVE ANALYSIS OF OPERATIONAL FORECASTS VERSUS ACTUAL WEATHER CONDITIONS IN AIRLINE FLIGHT PLANNING, VOLUME 3
J. F. KEITZ Apr. 1982 96 p 5 Vol.
(Contract NAS3-22748)
(NASA-CR-167864; NAS 1.26:167864) Avail: NTIS HC A05/MF A01 CSCL 04B

The impact of more timely and accurate weather data on airline flight planning with the emphasis on fuel savings is studied. This volume of the report discusses the results of Task 3 of the four major tasks included in the study. Task 3 compares flight plans developed on the Suitland forecast with actual data observed by the aircraft (and averaged over 10 degree segments). The results show that the average difference between the forecast and observed wind speed is 9 kts. without considering direction, and the average difference in the component of the forecast wind parallel to the direction of the observed wind is 13 kts. - both indicating that the Suitland forecast underestimates the wind speeds. The Root Mean Square (RMS) vector error is 30.1 kts. The average absolute difference in direction between the forecast and observed wind is 26 degrees and the temperature difference is 3 degree Centigrade. These resuits indicate that the forecast model as well as the verifying analysis used to develop comparison flight plans in Tasks 1 and 2 is a limiting factor and that the average potential fuel savings or penalty are up to 3.6 percent depending on the direction of flight. Author

N85-35537*# PRC Planning and Economics, Inc., Lake Success, N.Y.
COMPARATIVE ANALYSIS OF OPERATIONAL FORECASTS VERSUS ACTUAL WEATHER CONDITIONS IN AIRLINE FLIGHT PLANNING, VOLUME 4
J. F. KEITZ Apr. 1982 93 p 5 Vol.
(Contract NAS3-22748)
(NASA-CR-167865; NAS 1.26:167865) Avail: NTIS HC A05/MF A01 CSCL 04B

The impact of more timely and accurate weather data on airline flight planning with the emphasis on fuel savings is studied. This volume of the report discusses the results of Task 4 of the four major tasks included in the study. Task 4 uses flight plan segment wind and temperature differences as indicators of dates and geographic areas for which significant forecast errors may have occurred. An in-depth analysis is then conducted for the days identified. The analysis show that significant errors occur in the

operational forecast on 15 of the 33 arbitrarily selected days included in the study. Wind speeds in an area of maximum winds are underestimated by at least 20 to 25 kts. on 14 of these days. The analysis also show that there is a tendency to repeat the same forecast errors from prog to prog. Also, some perceived forecast errors from the flight plan comparisons could not be verified by visual inspection of the corresponding National Meteorological Center forecast and analyses charts, and it is likely that they are the result of weather data interpolation techniques or some other data processing procedure in the airlines' flight planning systems. Author

N85-35538*# PRC Planning and Economics, Inc., Lake Success, N.Y.
COMPARATIVE ANALYSIS OF OPERATIONAL FORECASTS VERSUS ACTUAL WEATHER CONDITIONS IN AIRLINE FLIGHT PLANNING: SUMMARY REPORT
J. F. KEITZ Apr. 1982 47 p 5 Vol.
(Contract NAS3-22748)
(NASA-CR-167866; NAS 1.26:167866) Avail: NTIS HC A03/MF A01 CSCL 04B

The impact of more timely and accurate weather data on airline flight planning with the emphasis on fuel savings is studied. This summary report discusses the results of each of the four major tasks of the study. Task 1 compared airline flight plans based on operational forecasts to plans based on the verifying analyses and found that average fuel savings of 1.2 to 2.5 percent are possible with improved forecasts. Task 2 consisted of similar comparisons but used a model developed for the FAA by SRI International that simulated the impact of ATc diversions on the flight plans. While parts of Task 2 confirm the Task I findings, inconsistency with other data and the known impact of ATC suggests that other Task 2 findings are the result of errors in the model. Task 3 compares segment weather data from operational flight plans with the weather actually observed by the aircraft and finds the average error could result in fuel burn penalties (or savings) of up to 3.6 percent for the average 8747 flight. In Task 4 an in-depth analysis of the weather forecast for the 33 days included in the study finds that significant errors exist on 15 days. Wind speeds in the area of maximum winds are underestimated by 20 to 50 kts., a finding confirmed in the other three tasks. Author

51

LIFE SCIENCES (GENERAL)

Includes genetics.

N85-27508*# Applied Medical Technology, Inc., Brecksville, Ohio.
PERCUTANEOUS CONNECTORS Annual Report
G. J. PICHA and S. R. TAYLOR Sep. 1981 49 p refs
(Contract NAS3-22654)
(NASA-CR-175627; NAS 1.26:175627; AR-1) Avail: NTIS HC A03/MF A01 CSCL 06B

A surface possessing a regular array of micro-pillars was evaluated with regard to its ability to control epithelial downgrowth at the percutaneous interface. A range of pillar sizes were applied to the vertical segment of T shaped Biomer (R) implants. These percutaneous tabs were implanted into the dorsum of cats for a period of 6 weeks using a standardized surgical technique. Comments were made post-operatively and at the time of retrieval. A quantitative scoring system was applied to these observations as well as histological results. As observed, the pillar morphology used displayed the ability to control epithelial downgrowth. Collagen ingrowth into the interpillar spaces and possibly direct interactions of the epithelial cells with the morphology may account for the inhibition. The reproducibility of epithelial inhibition is, however, limited by other factors which are currently not well understood. These factors and potential methods of assessment are discussed. Author

54

MAN/SYSTEM TECHNOLOGY AND LIFE SUPPORT

Includes human engineering; biotechnology; and space suits and protective clothing.

A85-38444* National Aeronautics and Space Administration. Lewis Research Center, Cleveland, Ohio.
FRICTION AND WEAR PROPERTIES OF A CHARNLEY ARTIFICIAL HIP JOINT
W. R. JONES, JR. (NASA, Lewis Research Center, Cleveland, OH) American Society of Lubrication Engineers and American Society of Mechanical Engineers, Lubrication Conference, San Diego, CA, Oct. 22-24, 1984. 10 p. refs
(ASLE PREPRINT 84-LC-4A-4)

59

MATHEMATICAL AND COMPUTER SCIENCES (GENERAL)

N85-21990*# National Aeronautics and Space Administration. Lewis Research Center, Cleveland, Ohio.
A CONVERGENT SERIES EXPANSION FOR HYPERBOLIC SYSTEMS OF CONSERVATION LAWS Final Report
E. HARABETIAN Feb. 1985 90 p refs
(Contract NAS1-17070)
(NASA-CR-172557; ICASE-85-13; NAS 1.26:172557) Avail: NTIS HC A05/MF A01 CSCL 12A

The discontinuities piecewise analytic initial value problem for a wide class of conservation laws is considered which includes the full three-dimensional Euler equations. The initial interaction at an arbitrary curved surface is resolved in time by a convergent series. Among other features the solution exhibits shock, contact, and expansion waves as well as sound waves propagating on characteristic surfaces. The expansion waves correspond to he one-dimensional rarefactions but have a more complicated structure. The sound waves are generated in place of zero strength shocks, and they are caused by mismatches in derivatives. M.G.

60

COMPUTER OPERATIONS AND HARDWARE

Includes computer graphics and data processing.

A85-24526* Louisiana State Univ., Baton Rouge.
TRANSFERRING DATA OSCILLOSCOPE TO AN IBM USING AN APPLE II+
D. L. MILLER, M. Y. FRENKLACH, P. J. LAUGHLIN, and D. W. CLARY (Louisiana State University, Baton Rouge, LA) Computer Applications in the Laboratory, no. 4, 1984, p. 260-269.
(Contract DE-FG22-80PC-30247; NAS3-23542; NAG3-477)

A set of PASCAL programs permitting the use of a laboratory microcomputer to facilitate and control the transfer of data from a digital oscilloscope (used with photomultipliers in experiments on soot formation in hydrocarbon combustion) to a mainframe

computer and the subsequent mainframe processing of these data is presented. Advantages of this approach include the possibility of on-line computations, transmission flexibility, automatic transfer and selection, increased capacity and analysis options (such as smoothing, averaging, Fourier transformation, and high-quality plotting), and more rapid availability of results. The hardware and software are briefly characterized, the programs are discussed, and printouts of the listings are provided. T.K.

A85-28613* Arizona State Univ., Tempe.
MULTIBUS-BASED PARALLEL PROCESSOR FOR SIMULATION
E. P. OGRADY and C.-H. WANG (Arizona State University, Tempe, AZ) IN: Summer Computer Simulation Conference, 15th, Vancouver, Canada, July 11-13, 1983, Proceedings. Volume 1 . La Jolla, CA, Society for Computer Simulation, 1983, p. 371-375. refs
(Contract NAG3-112)

A Multibus-based parallel processor simulation system is described. The system is intended to serve as a vehicle for gaining hands-on experience, testing system and application software, and evaluating parallel processor performance during development of a larger system based on the horizontal/vertical-bus interprocessor communication mechanism. The prototype system consists of up to seven Intel iSBC 86/12A single-board computers which serve as processing elements, a multiple transmission controller (MTC) designed to support system operation, and an Intel Model 225 Microcomputer Development System which serves as the user interface and input/output processor. All components are interconnected by a Multibus/IEEE 796 bus. An important characteristic of the system is that it provides a mechanism for a processing element to broadcast data to other selected processing elements. This parallel transfer capability is provided through the design of the MTC and a minor modification to the iSBC 86/12A board. The operation of the MTC, the basic hardware-level operation of the system, and pertinent details about the iSBC 86/12A and the Multibus are described. Author

A85-28628* California Univ., Los Angeles.
GENERAL APPROACHES FOR ACHIEVING HIGH SPEED COMPUTATIONS
T. LANG and M. D. ERCEGOVAC (California, University, Los Angeles, CA) IN: Summer Computer Simulation Conference, 15th, Vancouver, Canada, July 11-13, 1983, Proceedings. Volume 2 . La Jolla, CA, Society for Computer Simulation, 1983, p. 992-1006. refs
(Contract NAG3-132)

The basic organizational approach to achieve high speed computations has been to execute several instructions concurrently. Various algorithmic structures and related computer organizations have been identified and used for this purpose. Each of them is better suited for some classes of applications, provides a potential speed-up with respect to the sequential computer, and suffers from degradation factors that reduce the effective speed-up obtained. The basic algorithmic structures are presented, the corresponding computer organizations described and the potential degradation factors identified. Also included are considerations related to the cost of the system and to the corresponding programming methodology. Author

A85-36727* Carnegie-Mellon Univ., Pittsburgh, Pa.
OPTICAL LINEAR ALGEBRA PROCESSORS - NOISE AND ERROR-SOURCE MODELING
D. CASASENT (Carnegie-Mellon University, Pittsburgh, PA) and A. GHOSH (AT&T Bell Laboratories, Allentown; Carnegie-Mellon University, Pittsburgh, PA) Optics Letters (ISSN 0146-9592), vol. 10, June 1985, p. 252-254. Research supported by the Unicorn Systems, Inc. refs
(Contract NAG3-5; AF-AFOSR-79-0091)

The modeling of system and component noise and error sources in optical linear algebra processors (OLAPs) are considered, with attention to the frequency-multiplexed OLAP. General expressions are obtained for the output produced as a function of various component errors and noise. A digital simulator for this model is discussed. Author

N85-10659*# National Aeronautics and Space Administration. Lewis Research Center, Cleveland, Ohio.
HARDWARE FOR A REAL-TIME MULTIPROCESSOR SIMULATOR
R. A. BLECH and D. J. ARPASI 1984 11 p refs To be presented at the SCS Multiconf. Distributed Simulation, San Diego, Calif., 24-26 Jan. 1985; sponsored by the Soc. for Computer Simulation
(NASA-TM-83805; E-2315; NAS 1.15:83805) Avail: NTIS HC A02/MF A01 CSCL 09B

The hardware for a real time multiprocessor simulator (RTMPS) developed at the NASA Lewis Research Center is described. The RTMPS is a multiple microprocessor system used to investigate the application of parallel processing concepts to real time simulation. It is designed to provide flexible data exchange paths between processors by using off the shelf microcomputer boards and minimal customized interfacing. A dedicated operator interface allows easy setup of the simulator and quick interpreting of simulation data. Simulations for the RTMPS are coded in a NASA designed real time multiprocessor language (RTMPL). This language is high level and geared to the multiprocessor environment. A real time multiprocessor operating system (RTMPOS) has also been developed that provides a user friendly operator interface. The RTMPS and supporting software are currently operational and are being evaluated at Lewis. The results of this evaluation will be used to specify the design of an optimized parallel processing system for real time simulation of dynamic systems. M.G.

61

COMPUTER PROGRAMMING AND SOFTWARE

Includes computer programs, routines, and algorithms.

A85-28612* College of William and Mary, Williamsburg, Va.
THE USE OF ADA IN DISTRIBUTED SIMULATIONS
W. R. COLLINS and S. FEYOCK (College of William and Mary, Williamsburg, VA) IN: Summer Computer Simulation Conference, 15th, Vancouver, Canada, July 11-13, 1983, Proceedings. Volume 1 . La Jolla, CA, Society for Computer Simulation, 1983, p. 364-370. refs
(Contract NAG3-232)

The increasing need for detailed information about systems of continually growing complexity enhances steadily the demands regarding the employed models. The present investigation is concerned with work related to the development of high-performance computer hardware intended for the support of the real-time simulation of jet engines. The hardware is structured in the form of a network of communicating microprocessors running in parallel. The need for a higher-order language capability for programming such a network has led to the research considered in this study. Attention is given to the hardware which is being developed, an abstract model, programming language considerations, research considerations, research objectives, Ada tasks, Ada packages, the Ada model, the mapping of the model to the hardware, a precompiler example, and the advantages of Ada. G.R.

A85-28615* California Univ., Los Angeles.
A FUNCTIONAL LANGUAGE APPROACH IN HIGH-SPEED DIGITAL SIMULATION
M. D. ERCEGOVAC and S.-L. LU (California, University, Los Angeles, CA) IN: Summer Computer Simulation Conference, 15th, Vancouver, Canada, July 11-13, 1983, Proceedings. Volume 1 . La Jolla, CA, Society for Computer Simulation, 1983, p. 383-387. refs
(Contract NAG3-132)

A functional programming approach for a multi-microprocessor architecture is presented. The language, based on Backus FP, its intermediate form and the translation process are discussed and illustrated with an example. The approach allows performance analysis to be performed at a high level as an aid in program partitioning. Author

A85-34131* College of William and Mary, Williamsburg, Va.
MOVING TARGET, DISTRIBUTED, REAL-TIME SIMULATION USING ADA
W. R. COLLINS, S. FEYOCK, L. A. KING, and L. J. MORELL (College of William and Mary, Williamsburg, VA) IN: Simulation in Ada; Proceedings of the Eastern Simulation Conference, Norfolk, VA, March 3-8, 1985 . San Diego, CA, Society for Computer Simulation, 1985, p. 27-32. refs
(Contract NAG3-232)

Research on a precompiler solution is described for the moving target compiler problem encountered when trying to run parallel simulation algorithms on several microcomputers. The precompiler is under development at NASA-Lewis for simulating jet engines. Since the behavior of any component of a jet engine, e.g., the fan inlet, rear duct, forward sensor, etc., depends on the previous behaviors and not the current behaviors of other components, the behaviors can be modeled on different processors provided the outputs of the processors reach other processors in appropriate time intervals. The simulator works in compute and transfer modes. The Ada procedure sets for the behaviors of different components are divided up and routed by the precompiler, which essentially receives a multitasking program. The subroutines are synchronized after each computation cycle. M.S.K.

N85-10683*# National Aeronautics and Space Administration. Lewis Research Center, Cleveland, Ohio.
FLOATING-POINT FUNCTION GENERATION ROUTINES FOR 16-BIT MICROCOMPUTERS
M. A. MACKIN and J. F. SOEDER Oct. 1984 55 p refs
(NASA-TM-83783; E-2279; NAS 1.15:83783) Avail: NTIS HC A04/MF A01 CSCL 09B

Several computer subroutines have been developed that interpolate three types of nonanalytic functions: univariate, bivariate, and map. The routines use data in floating-point form. However, because they are written for use on a 16-bit Intel 8086 system with an 8087 mathematical coprocessor, they execute as fast as routines using data in scaled integer form. Although all of the routines are written in assembly language, they have been implemented in a modular fashion so as to facilitate their use with high-level languages. Author

N85-17576*# National Aeronautics and Space Administration. Lewis Research Center, Cleveland, Ohio.
MINDS: A MICROCOMPUTER INTERACTIVE DATA SYSTEM FOR 8086-BASED CONTROLLERS
J. F. SOEDER Jan. 1985 41 p refs
(NASA-TP-2378; E-2172; NAS 1.60:2378) Avail: NTIS HC A03/MF A01 CSCL 09B

A microcomputer interactive data system (MINDS) software package for the 8086 family of microcomputers is described. To enhance program understandability and ease of code maintenance, the software is written in PL/M-86, Intel Corporation's high-level system implementation language. The MINDS software is intended to run in residence with real-time digital control software to provide displays of steady-state and transient data. In addition, the MINDS package provides classic monitor capabilities along with extended provisions for debugging an executing control system. The software uses the CP/M-86 operating system developed by Digital Research, Inc., to provide program load capabilities along with a uniform file structure for data and table storage. Finally, a library of input and output subroutines to be used with consoles equipped with PL/M-86 and assembly language is described. Author

N85-28610*# National Aeronautics and Space Administration. Lewis Research Center, Cleveland, Ohio.
REAL-TIME MULTIPROCESSOR PROGRAMMING LANGUAGE (RTMPL) USER'S MANUAL
D. J. ARPASI Jun. 1985 115 p refs
(NASA-TP-2422; E-1999; NAS 1.60:2422) Avail: NTIS HC A06/MF A01 CSCL 09B

A real-time multiprocessor programming language (RTMPL) has been developed to provide for high-order programming of real-time simulations on systems of distributed computers. RTMPL is a structured, engineering-oriented language. The RTMPL utility supports a variety of multiprocessor configurations and types by generating assembly language programs according to user-specified targeting information. Many programming functions are assumed by the utility (e.g., data transfer and scaling) to reduce the programming chore. This manual describes RTMPL from a user's viewpoint. Source generation, applications, utility operation, and utility output are detailed. An example simulation is generated to illustrate many RTMPL features. Author

62

COMPUTER SYSTEMS

Includes computer networks.

A85-28614* California Univ., Los Angeles.
DATA FLOW METHODS FOR DYNAMIC SYSTEM SIMULATION - A CSSL-IV MICROCOMPUTER NETWORK INTERFACE
A. MAKOUI and W. J. KARPLUS (California, University, Los Angeles, CA) IN: Summer Computer Simulation Conference, 15th, Vancouver, Canada, July 11-13, 1983, Proceedings. Volume 1 . La Jolla, CA, Society for Computer Simulation, 1983, p. 376-382. refs
(Contract NAG3-132)

A major problem in employing networks of microcomputers for the real-time simulation of complex systems is to allocate computational tasks to the various microcomputers in such a way that idle time and time lost in interprocess communication is minimized. The research reported in this paper is directed to the development of a software interface between a higher-level simulation language and a network of microcomputers. A CSSL-IV source program is translated to a data flow graph. This graph is then analyzed automatically so as to allocate computing tasks to the various processors. Author

A85-28629* California Univ., Los Angeles.
FUNCTIONAL LANGUAGE AND DATA FLOW ARCHITECTURES
M. D. ERCEGOVAC, D. R. PATEL, and T. LANG (California, University, Los Angeles, CA) IN: Summer Computer Simulation Conference, 15th, Vancouver, Canada, July 11-13, 1983, Proceedings. Volume 2 . La Jolla, CA, Society for Computer Simulation, 1983, p. 1007-1023. refs
(Contract NAG3-132)

This is a tutorial article about language and architecture approaches for highly concurrent computer systems based on the functional style of programming. The discussion concentrates on the basic aspects of functional languages, and sequencing models such as data-flow, demand-driven and reduction which are essential at the machine organization level. Several examples of highly concurrent machines are described. Author

N85-17596*# National Aeronautics and Space Administration. Lewis Research Center, Cleveland, Ohio.
OPERATING SYSTEM FOR A REAL-TIME MULTIPROCESSOR PROPULSION SYSTEM SIMULATOR. USER'S MANUAL
G. L. COLE Jan. 1985 42 p refs
(NASA-TP-2426; D-1998; NAS 1.60:2426) Avail: NTIS HC A03/MF A01 CSCL 09B

The NASA Lewis Research Center is developing and evaluating experimental hardware and software systems to help meet future needs for real-time, high-fidelity simulations of air-breathing propulsion systems. Specifically, the real-time multiprocessor simulator project focuses on the use of multiple microprocessors to achieve the required computing speed and accuracy at relatively low cost. Operating systems for such hardware configurations are generally not available. A real time multiprocessor operating system (RTMPOS) that supports a variety of multiprocessor configurations was developed at Lewis. With some modification, RTMPOS can also support various microprocessors. RTMPOS, by means of menus and prompts, provides the user with a versatile, user-friendly environment for interactively loading, running, and obtaining results from a multiprocessor-based simulator. The menu functions are described and an example simulation session is included to demonstrate the steps required to go from the simulation loading phase to the execution phase. R.S.F.

63

CYBERNETICS

Includes feedback and control theory.

A85-47704* National Aeronautics and Space Administration. Lewis Research Center, Cleveland, Ohio.
A REAL-TIME FORTRAN IMPLEMENTATION OF A SENSOR FAILURE DETECTION, ISOLATION AND ACCOMMODATION ALGORITHM
J. C. DELAAT (NASA, Lewis Research Center, Cleveland, OH) IN: 1984 American Control Conference, San Diego, CA, June 6-8, 1984, Proceedings. Volume 1 . New York, IEEE, 1984, p. 572, 573. refs

An advanced, sensor failure detection, isolation, and accomodation algorithm has been developed by NASA for the F100 turbofan engine. The algorithm takes advantage of the analytical redundancy of the sensors to improve the reliability of the sensor set. The method requires the controls computer, to determine when a sensor failure has occurred without the help of redundant hardware sensors in the control system. The controls computer provides an estimate of the correct value of the output of the failed sensor. The algorithm has been programmed in FORTRAN using a real-time microprocessor-based controls computer. A detailed description of the algorithm and its implementation on a microprocessor is given. I.H.

A85-47794* ALPHATECH, Inc., Burlington, Mass.
A DESIGN METHODOLOGY FOR ROBUST FAILURE DETECTION AND ISOLATION
K. R. PATTIPATI, A. S. WILLSKY, J. C. DECKERT, J. S. ETERNO, and J. S. WEISS (Alphatech, Inc., Burlington, MA) IN: 1984 American Control Conference, San Diego, CA, June 6-8, 1984, Proceedings. Volume 3 . New York, IEEE, 1984, p. 1755-1762. refs
(Contract NAS3-24078)

A decentralized failure detection and isolation (FDI) methodology, which is robust with respect to model uncertainties and noise, is presented Redundancy metrics are developed, and optimization problems are posed for the choices of robust parity relations. Closed-form solutions for some special failure cases are given. Connections are drawn with other disciplines, and the use of the metrics to evaluate alternative FDI schemes is discussed. Author

64

NUMERICAL ANALYSIS

Includes iteration, difference equations, and numerical approximation.

A85-21370* Concordia Univ., Montreal (Quebec).
RECENT ADVANCES IN METHODS FOR NUMERICAL SOLUTION OF O.D.E. INITIAL VALUE PROBLEMS
T. D. BUI (Concordia University, Montreal, Canada), A. K. OPPENHEIM (California, University, Berkeley, CA), and D. T. PRATT (Washington, University, Seattle, WA) Journal of Computational and Applied Mathematics (ISSN 0377-0427), vol. 11, Dec. 1984, p. 283-296. Research supported by the Ministere de l'Education du Quebec; Natural Sciences and Engineering Research Council of Canada. refs
(Contract NSERC-A-9265; NSF CPE-81-15163; NAG3-227; DE-AC03-76SF-00098)

In the mathematical modeling of physical systems, it is often necessary to solve an initial value problem (IVP), consisting of a system of ordinary differential equations (ODE). A typical program produces approximate solutions at certain mesh points. Almost all existing codes try to control the local truncation error, while the user is really interested in controlling the true or global error. The present investigation provides a review of recent advances regarding the solution of the IVP, giving particular attention to stiff systems. Stiff phenomena are customarily defined in terms of the eigenvalues of the Jacobian. There are, however, some difficulties connected with this approach. It is pointed out that an estimate of the Lipschitz constant proves to be a very practical way to determine the stiffness of a problem. G.R.

A85-21979* Akron Univ., Ohio.
ON THE DEVELOPMENT OF HIERARCHICAL SOLUTION STRATEGIES FOR NONLINEAR FINITE ELEMENT FORMULATIONS
J. PADOVAN and J. LACKNEY (Akron, University, Akron, OH) Computers and Structures (ISSN 0045-7949), vol. 19, no. 4, 1984, p. 535-544. refs
(Contract NSG-3283)

This paper develops a hierarchical type solution scheme which can handle the field equations associated with nonlinear finite element simulations. The overall procedure possesses various levels of application namely degree of freedom, nodal, elemental, substructural as well as global. In particular iteration, updating, assembly and solution control occurs at the various hierarchical levels. Due to the manner of formulation, the degree of matrix inversion depends on the size of the various hierarchical partitioned groups. In this context, degree of freedom partitioning requires no inversion. To benchmark the overall scheme, the results of several numerical examples are presented. Author

A85-28006* National Aeronautics and Space Administration. Lewis Research Center, Cleveland, Ohio.
A PROCEDURE FOR OBTAINING EXPLICIT SOLUTIONS TO A CLASS OF FREDHOLM INTEGRAL EQUATIONS
M. E. GOLDSTEIN (NASA, Lewis Research Center, Cleveland, OH) and M. J. LEITMAN (Case Western Reserve University, Cleveland, OH) Journal of Integral Equations (ISSN 0163-5549), vol. 8, 1985, p. 87-93.
(Contract NSF MCS-83-01844)

A Fredholm integral equation is solved in closed form by reducing it to a standard boundary value problem for a sectionally analytic function. The procedure maybe extended to more general classes of functions whose Fourier transforms only exist along certain lines in the complex k-plane. Examples are used to illustrate the results. M.D.

A85-28015* National Aeronautics and Space Administration. Lewis Research Center, Cleveland, Ohio.
CONSTRUCTIVE EXISTENCE AND UNIQUENESS FOR TWO-POINT BOUNDARY-VALUE PROBLEMS WITH A LINEAR GRADIENT TERM
J. A. PENNLINE (NASA, Lewis Research Center, Computer Services Div., Cleveland, OH) Applied Mathematics and Computation (ISSN 0096-3003), vol. 15, 1984, p. 233-260. refs

A85-50073* Texas Univ., Austin.
STABILITY, ACCURACY, AND EFFICIENCY OF SOME UNDERINTEGRATED METHODS IN FINITE ELEMENT COMPUTATIONS
O.-P. JACQUOTTE (Texas, University, Austin) Computer Methods in Applied Mechanics and Engineering (ISSN 0045-7825), vol. 50, Aug. 1985, p. 275-293. refs
(Contract NAG3-329)

In an attempt to increase computational efficiency in the numerical solution of highly nonlinear problems in solid and fluid mechanics, underintegrated finite element methods have been employed by many analysts. Underintegration refers to the use of a rule of an order lower than that required to integrate polynomial integrands exactly. The main drawback of this technique is related to the production of rank-deficient stiffness matrices, or equivalently an expanded kernel of the governing linear momentum operators. Such a development can introduce numerical instabilities. In order to overcome this difficulty, artificial stiffness or viscosity methods, or other stabilization methods have been proposed. One approach involves the elimination of spurious modes in a postprocessing operation. The present study is concerned with this a posteriori elimination method, taking into account the results which can be expected from it, and some of its possible extensions. G.R.

N85-19733*# National Aeronautics and Space Administration. Lewis Research Center, Cleveland, Ohio.
MODELING THE INTERNAL COMBUSTION ENGINE
F. J. ZELEZNIK and B. J. MCBRIDE Mar. 1985 309 p refs
(NASA-RP-1094; E-996; NAS 1.61:1094) Avail: NTIS HC A14/MF A01 CSCL 12A

A flexible and computationally economical model of the internal combustion engine was developed for use on large digital computer systems. It is based on a system of ordinary differential equations for cylinder-averaged properties. The computer program is capable of multicycle calculations, with some parameters varying from cycle to cycle, and has restart capabilities. It can accommodate a broad spectrum of reactants, permits changes in physical properties, and offers a wide selection of alternative modeling functions without any reprogramming. It readily adapts to the amount of information available in a particular case because the model is in fact a hierarchy of five models. The models range from a simple model requiring only thermodynamic properties to a complex model demanding full combustion kinetics, transport properties, and poppet valve flow characteristics. Among its many features the model includes heat transfer, valve timing, supercharging, motoring, finite burning rates, cycle-to-cycle variations in air-fuel ratio, humid air, residual and recirculated exhaust gas, and full combustion kinetics. Author

N85-27584*# Pratt and Whitney Aircraft, East Hartford, Conn. Engineering Div.
ERROR REDUCTION PROGRAM Final Report
S. A. SYED, L. M. CHIAPPETTA, and A. D. GOSMAN 11 Jan. 1985 246 p refs
(Contract NAS3-23686)
(NASA-CR-174776; NAS 1.26:174776; PWA-5928-25) Avail: NTIS HC A11/MF A01 CSCL 12A

The details of a study to select, incorporate and evaluate the best available finite difference scheme to reduce numerical error in combustor performance evaluation codes are described. The combustor performance computer programs chosen were the two dimensional and three dimensional versions of Pratt & Whitney's TEACH code. The criteria used to select schemes required that the difference equations mirror the properties of the governing differential equation, be more accurate than the current hybrid difference scheme, be stable and economical, be compatible with TEACH codes, use only modest amounts of additional storage, and be relatively simple. The methods of assessment used in the selection process consisted of examination of the difference equation, evaluation of the properties of the coefficient matrix, Taylor series analysis, and performance on model problems. Five schemes from the literature and three schemes developed during the course of the study were evaluated. This effort resulted in the incorporation of a scheme in 3D-TEACH which is usuallly more accurate than the hybrid differencing method and never less accurate. M.G.

71

ACOUSTICS

Includes sound generation, transmission, and attenuation.

A85-10869*# Virginia Polytechnic Inst. and State Univ., Blacksburg.
THE INFLUENCE OF COMBUSTION LINER HOLES ON NOISE PRODUCTION BY DUCTED BURNERS
J. R. MAHAN and J. D. JONES (Virginia Polytechnic Institute and State University, Blacksburg, VA) American Institute of Aeronautics and Astronautics and NASA, Aeroacoustics Conference, 9th, Williamsburg, VA, Oct. 15-17, 1984. 7 p. refs
(Contract NAG3-124)
(AIAA PAPER 84-2322)

The thermoacoustic energy conversion process in a turbulent flame is not yet sufficiently well understood to allow accurate prediction of the sound pressure field of even the simplest of laboratory burners. The present contribution is intended to be a step toward fuller understanding of this process. In particular, the possibility is explored that the source structure, in the form of the thermoacoustic efficiency spectrum, might be influenced by the acoustic response of the burner itself. Experimental results are presented which seem to establish that, at least for the gas-fueled laboratory burner studied, source activity is not affected by the addition of downstream combustion liner holes which otherwise alter the acoustic response of the burner. Author

A85-10882*# Lockheed-Georgia Co., Marietta.
AN EXPERIMENTAL STUDY OF TONE EXCITED HEATED JETS
J. LEPICOVSKY, K. K. AHUJA, and M. SALIKUDDIN (Lockheed-Georgia Co., Marietta, GA) American Institute of Aeronautics and Astronautics and NASA, Aeroacoustics Conference, 9th, Williamsburg, VA, Oct. 15-17, 1984. 11 p. refs
(Contract NAS3-23708)
(AIAA PAPER 84-2341)

The objective of this investigation was to obtain detailed experimental data on the effects of upstream acoustic excitation on the mixing of heated jets with the surrounding air. Based on the information gathered in the literature survey, a technical approach was developed to carry out a systematic set of mean flowfield measurements for a broad range of jet operating and acoustic excitation conditions. Most of the results were obtained at Mach numbers of 0.3 and 0.8 and total temperatures of up to 800 K. Some measurements were made also for the fully expanded supersonic jet of Mj = 1.15. The maximum level of excitation was Le equal to or less than 150 dB and a range of excitation frequencies up to fe = 4 kHz was used. The important results derived from this study can be summarized as follows: (1) the sensitivity of heated jets to upstream acoustic excitation varies strongly with the jet operating conditions, (2) the threshold excitation level increases with increasing jet temperature, and (3) the preferred Strouhal number does not change significantly with a change of the jet operating conditions. Author

A85-12301* Minnesota Univ., Minneapolis.
ACOUSTIC STRUCTURE AND PROPAGATION IN HIGHLY POROUS, LAYERED, FIBROUS MATERIALS
R. F. LAMBERT and J. S. TESAR (Minnesota, University, Minneapolis, MN) Acoustical Society of America, Journal (ISSN 0001-4966), vol. 76, Oct. 1984, p. 1231-1237. Previously announced in STAR as N84-27546. refs
(Contract NSF MEA-80-1136; NAG3-161)

The acoustic structure and propagation of sound in highly porous, layered, fine fiber materials is examined. Of particular interest is the utilization of the Kozeny number for determining the static flow resistance and the static structure factor based on flow permeability measurements. In this formulation the Kozeny number is a numerical constant independent of volume porosity at high porosities. The other essential parameters are then evaluated employing techniques developed earlier for open cell foams. The attenuation and progressive phase characteristics in bulk samples are measured and compared with predicted values. The agreements on the whole are very satisfactory. M.A.C.

A85-13955*# Arizona Univ., Tucson.
EFFECT OF AIRFOIL MEAN LOADING ON CONVECTED GUST INTERACTION NOISE
M. R. MYERS and E. J. KERSCHEN (Arizona, University, Tucson, AZ) American Institute of Aeronautics and Astronautics and NASA, Aeroacoustics Conference, 9th, Williamsburg, VA, Oct. 15-17, 1984. 13 p. refs
(Contract NAG3-357)
(AIAA PAPER 84-2324)

The present theoretical model for noise generation when a convected vortical or entropic gust encounters an airfoil at a nonzero angle-of-attack is based on a linearization of the Euler equations for the steady, subsonic flow past the airfoil. Noise generation is found to be concentrated at local regions which scale on the gust wavelength and are present at airfoil leading and trailing edges. Steady loading of the airfoil affects noise generation at the leading and trailing edges in significantly different ways. Parametric calculations are presented which illustrate that, at high frequencies, moderate levels of airfoil steady loading can drastically increase the noise level produced by airfoil-convected gust interactions. O.C.

A85-13956*# Arizona Univ., Tucson.
NOISE PRODUCED BY THE INTERACTION OF A ROTOR WAKE WITH A SWEPT STATOR BLADE
E. ENVIA and E. J. KERSCHEN (Arizona, University, Tucson, AZ) American Institute of Aeronautics and Astronautics and NASA, Aeroacoustics Conference, 9th, Williamsburg, VA, Oct. 15-17, 1984. 11 p. refs
(Contract NAG3-357)
(AIAA PAPER 84-2326)

An analysis is developed for the noise generated by the interaction of rotor viscous wakes and a single swept stator vane. The stator vane spans a channel with infinite parallel walls which contains a uniform subsonic mean flow. High frequency wakes, for which the noise generation is concentrated at the vane leading edge, are considered. The general wake pattern is expanded in spanwise modes and solutions for each mode are derived using the Wiener-Hopf technique applied to the equations in the nonorthogonal coordinates. Closed form expressions for the acoustic farfield are obtained. The results of the analysis are used in parametric calculations of rotor viscous wake-stator vane interactions in order to study the effectiveness of sweep as a noise reduction mechanism. For the cases studied, moderate stator sweep angles produce sizeable reductions in the level of the farfield noise. The presence of rotor wake circumferential lean actually increases the noise reduction produced by moderate stator sweep angles. Author

A85-16099*# National Aeronautics and Space Administration. Lewis Research Center, Cleveland, Ohio.
SUPERSONIC JET SHOCK NOISE REDUCTION
J. R. STONE (NASA, Lewis Research Center, Cleveland, OH) American Institute of Aeronautics and Astronautics, Aeroacoustics Conference, 9th, Williamsburg, VA, Oct. 15-17, 1984. 44 p. Previously announced in STAR as N84-35085. refs
(AIAA PAPER 84-2278)

Shock-cell noise is identified to be a potentially significant problem for advanced supersonic aircraft at takeoff. Therefore NASA conducted fundamental studies of the phenomena involved and model-scale experiments aimed at developing means of noise reduction. The results of a series of studies conducted to determine means by which supersonic jet shock noise can be reduced to acceptable levels for advanced supersonic cruise aircraft are reviewed. Theoretical studies were conducted on the shock associated noise of supersonic jets from convergent-divergent (C-D) nozzles. Laboratory studies were conducted on the influence of narrowband shock screech on broadband noise and on means of screech reduction. The usefulness of C-D nozzle passages was investigated at model scale for single-stream and dual-stream nozzles. The effect of off-design pressure ratio was determined under static and simulated flight conditions for jet temperatures up to 960 K. Annular and coannular flow passages with center plugs and multi-element suppressor nozzles were evaluated, and the effect of plug tip geometry was established. In addition to the far-field acoustic data, mean and turbulent velocity distributions were measured with a laser velocimeter, and shadowgraph images of the flow field were obtained. Author

A85-16102*# National Aeronautics and Space Administration. Lewis Research Center, Cleveland, Ohio.
TIME DEPENDENT WAVE ENVELOPE FINITE DIFFERENCE ANALYSIS OF SOUND PROPAGATION
K. J. BAUMEISTER (NASA, Lewis Research Center, Cleveland, OH) American Institute of Aeronautics and Astronautics and NASA, Aeroacoustics Conference, 9th, Williamsburg, VA, Oct. 15-17, 1984. 9 p. Previously announced in STAR as N84-32118. refs
(AIAA PAPER 84-2285)

A transient finite difference wave envelope formulation is presented for sound propagation, without steady flow. Before the finite difference equations are formulated, the governing wave equation is first transformed to a form whose solution tends not to oscillate along the propagation direction. This transformation reduces the required number of grid points by an order of magnitude. Physically, the transformed pressure represents the amplitude of the conventional sound wave. The derivation for the wave envelope transient wave equation and appropriate boundary conditions are presented as well as the difference equations and stability requirements. To illustrate the method, example solutions are presented for sound propagation in a straight hard wall duct and in a two dimensional straight soft wall duct. The numerical results are in good agreement with exact analytical results.
Author

A85-16103*# National Aeronautics and Space Administration. Lewis Research Center, Cleveland, Ohio.
ANALYSIS OF THE EFFECT ON COMBUSTOR NOISE MEASUREMENTS OF ACOUSTIC WAVES REFLECTED BY THE TURBINE AND COMBUSTOR INLET
R. G. HUFF (NASA, Lewis Research Center, Cleveland, OH) American Institute of Aeronautics and Astronautics and NASA, Aeroacoustics Conference, 9th, Williamsburg, VA, Oct. 15-17, 1984. 11 p. Previously announced in STAR as N84-32122. refs
(AIAA PAPER 84-2323)

Spectral analyses of static pressure fluctuations measured in turbine engine combustors at low engine speed show good agreement with theory. At idle speed the high pressure turbine is unchoked. Above idle speed the turbine chokes and a significant change in the shape of the measured combustor pressure spectrum is observed. A simplified theoretical model of the acoustic pressure generated in the combustor due to the turbulence-flame front

interaction did not account for acoustic waves reflected from the turbine. By retaining this simplified combustion noise source model and adding a partial reflecting plane at the turbine and combustor inlet, a simple theoretical model was developed that reproduces the undulations in the combustor fluctuating pressure spectra. Plots of the theoretical combustor fluctuating pressure spectra are compared to the measured pressure spectra obtained from the CF6-50 turbofan engine over a range of engine operating speeds. The simplified combustion noise theory when modified by a simple turbine reflecting plane adequately accounts for the changes in measured combustor pressure spectra. It is further concluded that the shape of the pressure spectra downstream of the turbine, neglecting noise generated by the turbine itself, will be the combustion noise spectra unchanged except for the level reduction due to the energy blocked by the turbine. Author

A85-16104*# Missouri Univ., Rolla.
MODELLING OF WIND TUNNEL WALL EFFECTS ON THE RADIATION CHARACTERISTICS OF ACOUSTIC SOURCES
W. EVERSMAN (Missouri-Rolla, University, Rolla, MO) and K. J. BAUMEISTER (NASA, Lewis Research Center, Cleveland, OH) American Institute of Aeronautics and Astronautics and NASA, Aeroacoustics Conference, 9th, Williamsburg, VA, Oct. 15-17, 1984. 12 p. refs
(AIAA PAPER 84-2364)

It is pointed out that the relatively high fuel economy available from propeller-driven aircraft has renewed interest in high speed, highly loaded multiple blade turboprop propulsion systems. Undesirable features related to community noise and the high intensity cabin noise have stimulated new research on the acoustic characteristics of turboprops. The present investigation has the objective to develop a mathematical model of the essential features of the radiation of acoustic disturbances from propellers in a duct and in free space in order to quantify the success with which duct testing can be expected to approximate free field conditions. In connection with the importance of source directionality, a detailed model is considered which consists of a finite element representation of the Gutin propeller theory valid in both the near and far field. G.R.

A85-20738* National Aeronautics and Space Administration. Lewis Research Center, Cleveland, Ohio.
SOUND GENERATION AND UPSTREAM INFLUENCE DUE TO INSTABILITY WAVES INTERACTING WITH NON-UNIFORM MEAN FLOWS
M. E. GOLDSTEIN (NASA, Lewis Research Center, Cleveland, OH) Journal of Fluid Mechanics (ISSN 0022-1120), vol. 149, Dec. 1984, p. 161-177. refs

Attention is given to the sound produced by artificially excited, spatially growing instability waves on subsonic shear layers. Real flows that always diverge in the downstream direction allow sound to be produced by the interaction of the instability waves with the resulting streamwise variations of the flow. The upstream influence, or feedback, can interact with the splitter plate lip to produce a downstream-propagating instability wave that may under certain conditions be the same instability wave that originally generated the upstream influence. The present treatment is restricted to very low Mach number flows, so that compressibility effects can only become important over large distances. O.C.

A85-25932*# Lockheed-Georgia Co., Marietta.
SOME UNIQUE EXPERIMENTS ON RECEPTIVITY
K. K. AHUJA (Lockheed-Georgia Co., Advanced Flight Sciences Dept., Marietta, GA) American Institute of Aeronautics and Astronautics, Shear Flow Control Conference, Boulder, CO, Mar. 12-14, 1985. 9 p. refs
(Contract NAS3-23286)
(AIAA PAPER 85-0533)

The objective of this study is to determine whether or not a solid trailing edge is required to produce efficient coupling between sound and instability waves in a shear layer. Instability waves in the shear layer of a subsonic jet, excited externally by a point sound source, were first visualized by using a phase-locked flow visualization technique. Various means were adopted to shield the sound reaching the nozzle lip. It was found that the low frequency sound couples more efficiently at distances downstream of the nozzle exit. To substantiate the findings further, a supersonic screeching jet was tested such that it passed through a small opening in a baffle placed parellel to the exit plane. The measured feedback or screech frequencies, and also the excited flow disturbances, were found to change drastically on traversing the baffle axially. Similar conclusions were reached when a second baffle was placed downstream of the first baffle, and the effects of moving the first baffle on the feedback frequency of sound generated by flow impingement on the second baffle were examined. It is argued that sound waves passing through the mixing layer of a jet can excite flow instability without the benefit of assistance and coupling at the trailing edge. Author

A85-26915* California Univ., Los Angeles.
THE RESPONSE OF HELMHOLTZ RESONATORS TO EXTERNAL EXCITATION. I - SINGLE RESONATORS
P. A. MONKEWITZ and N.-M. NGUYEN-VO (California, University, Los Angeles, CA) Journal of Fluid Mechanics (ISSN 0022-1120), vol. 151, Feb. 1985, p. 477-497. refs
(Contract NSG-3236)

The response of single two- and three-dimensional Helmholtz resonators subject to external excitation by a plane acoustic wave is studied. The inviscid linearized problem is solved by the matched-asymptotic-expansion technique in the low-frequency limit, i.e. when the characteristic neck dimension is small compared with the acoustic wavelength. The scale of the cavity is chosen such as to tune the system to the lowest Helmholtz mode. The results are compared with the classical lumped-element model, and refined expressions are derived for the effective mass (added length) and stiffness (effective cavity volume) of the resonator. Author

A85-36047* National Aeronautics and Space Administration. Lewis Research Center, Cleveland, Ohio.
THE SCATTERING OF ULTRASONIC THIRD SOUND FROM SUBSTRATE SURFACE DEFECTS
E. R. GENERAZIO (NASA, Lewis Research Center, Cleveland, OH; Pennsylvania State University, University Park, PA) and R. W. REED (United Technologies Research Center, East Hartford, CT; Pennsylvania State University, University Park, PA) Journal of Low Temperature Physics (ISSN 0022-2291), vol. 56, no. 3-4, 1984, p. 355-377. Navy-supported research. refs

The interaction of third sound with isolated surface defects is examined. Phase-inverted reflections are observed to occur at surface defects even when the wavelength of the third sound is much greater than the dimensions of the defect. The origin of the scattering mechanism is believed to be due to the change in the helium film thickness in the vicinity of the topological variations introduced by the presence of the surface defects. Data are obtained for ultrasonic frequencies in the 20-200 kHz range. Author

A85-39909*# National Aeronautics and Space Administration. Lewis Research Center, Cleveland, Ohio.
A THEORETICAL PREDICTION OF THE ACOUSTIC PRESSURE GENERATED BY TURBULENCE-FLAME FRONT INTERACTIONS
R. G. HUFF (NASA, Lewis Research Center, Cleveland, OH) American Society of Mechanical Engineers, Winter Annual Meeting, New Orleans, LA, Dec. 9-14, 1984. 8 p. Previously announced in STAR as N84-26383. refs
(ASME PAPER 84-WA/NCA-11)

The equations of momentum and continuity are combined and linearized yielding the one dimensional nonhomogeneous acoustic wave equation. Three terms in the non-homogeneous equation act as acoustic sources and are taken to be forcing functions acting on the homogeneous wave equation. The three source terms are: fluctuating entropy, turbulence gradients, and turbulence-flame interactions. Each source term is discussed. The turbulence-flame interaction source is used as the basis for

computing the source acoustic pressure from the Fourier transformed wave equation. Pressure fluctuations created in turbopump gas generators and turbines may act as a forcing function for turbine and propellant tube vibrations in earth to orbit space propulsion systems and could reduce their life expectancy. A preliminary assessment of the acoustic pressure fluctuations in such systems is presented. Author

A85-42563*# National Aeronautics and Space Administration. Lewis Research Center, Cleveland, Ohio.
THE PERFORMANCE OF JET NOISE SUPPRESSION DEVICES FOR INDUSTRIAL APPLICATIONS
M. D. DAHL (NASA, Lewis Research Center, Cleveland, OH) and O. H. MCDANIEL (Pennsylvania State University, University Park) ASME, *Transactions, Journal of Vibration, Acoustics, Stress, and* Reliability in Design (ISSN 0739-3717), vol. 107, July 1985, p. 303-309. Research supported by the Occupational Safety and Health Administration. refs

N85-10788*# National Aeronautics and Space Administration. Lewis Research Center, Cleveland, Ohio.
OBSERVATIONS FROM VARYING THE LIFT AND DRAG INPUTS TO A NOISE PREDICTION METHOD FOR SUPERSONIC HELICAL TIP SPEED PROPELLERS
J. H. DITTMAR Sep. 1984 21 p refs
(NASA-TM-83797; E-2295; NAS 1.15:83797) Avail: NTIS HC A02/MF A01 CSCL 20A

Previous comparisons between calculated and measured supersonic helical tip speed propeller noise show them to have different trends of peak blade passing tone versus helical tip Mach number. It was postulated that improvements in this comparison could be made first by including the drag force terms in the prediction and then by reducing the blade lift terms at the tip to allow the drag forces to dominate the noise prediction. Propeller hub to tip lift distributions were varied, but they did not yield sufficient change in the predicted lift noise to improve the comparison. This result indicates that some basic changes in the *theory may be needed. In addition, the noise predicted by the* drag forces did not exhibit the same curve shape as the measured data. So even if the drag force terms were to dominate, the trends with helical tip Mach number for theory and experiment would still not be the same. The effect of the blade shock wave pressure rise was approxmated by increasing the drag coefficient at the blade tip. Predictions using this shock wdave approximation did have a curve shape similar to the measured data. This result indicates that the shock pressure rise probably controls the noise at supersonic tip speed and that the linear prediction method can give the proper noise trend with Mach number. R.S.F.

N85-11791*# Bolt, Beranek, and Newman, Inc., Cambridge, Mass.
TURBOFAN NOISE GENERATION. VOLUME 2: COMPUTER PROGRAMS Final Report
C. S. VENTRES, M. A. THEOBALD, and W. D. MARK Jul. 1982 206 p 2 Vol.
(Contract NAS3-21252)
(NASA-CR-167952; NAS 1.26:167952; BBN-4770) Avail: NTIS HC A10/MF A01 CSCL 20A

The use of a package of computer programs developed to calculate the in duct acoustic mods excited by a fan/stator stage *operating at subsonic tip speed is described. The following three* noise source mechanisms are included: (1) sound generated by the rotor blades interacting with turbulence ingested into, or generated within, the inlet duct; (2) sound generated by the stator vanes interacting with the turbulent wakes of the rotor blades; and (3) sound generated by the stator vanes interacting with the velocity deficits in the mean wakes of the rotor blades. The computations for three different noise mechanisms are coded as three separate computer program packages. The computer codes are described by means of block diagrams, tables of data and variables, and example program executions; FORTRAN listings are included. M.G.

N85-13549*# General Electric Co., Cincinnati, Ohio. Aircraft Engine Business Group.
EXPERIMENTAL INVESTIGATION OF SHOCK-CELL NOISE REDUCTION FOR DUAL-STREAM NOZZLES IN SIMULATED FLIGHT Final Report
B. A. JANARDAN, K. YAMAMOTO, R. K. MAJJIGI, and J. F. BRAUSCH Washington NASA Nov. 1984 189 p refs
(Contract NAS3-23166)
(NASA-CR-3846; E-2283; NAS 1.26:3846; R83AEB358) Avail: NTIS HC A09/MF A01 CSCL 20A

Six scale-model nozzles were tested in an anechoic facility to evauate the effectiveness of convergent-divergent (C-D) terminations in reducing shock-cell noise of unsuppressed and mechanically suppressed coannular plug nozzles. One hundred fifty-three acoustic test points with inverted velocity profiles were conducted under static and simulated flight conditions. Diagnostic flow visualization with a shadowgraph and velocity measurements with a laser velocimeter were performed on selected plumes. Shock-cells were identified on the plug and downstream of the plug of the unsuppressed convergent coannular nozzle with truncated plug. Broadband peak frequencies predicted with the two shock-cell structures were correlated with the observed spectra using the measured shock-cell spacings. Relative to a convergent circular nozzle, the perceived noise level (PNL) data at an observer angle of 60 deg relative to inlet, indicated a reduction of (1) 6.5 dB and 9.2 dB with unsuppressed C-D coannular nozzle with truncated plug and (2) 7.7 dB and 8.3 dB with suppressed C-D coannular nozzle under static and simulated flight conditions, espectively. The unsuppressed C-D coannular nozzle with truncated plug, operating at the C-D design condition, had shock-cells downstream of the plug with no shock-cells on the plug. The downstream shock-cells were eliminated by replacing the truncated plug with a smooth extension to obtain an additional 2.4 dB and 3 dB front quadrant PNL reduction, under static and simulated flight conditions, respectively. Other results are discussed. M.G.

N85-13550*# General Electric Co., Cincinnati, Ohio.
EXPERIMENTAL INVESTIGATION OF SHOCK-CELL NOISE REDUCTION FOR SINGLE STREAM NOZZLES IN SIMULATED FLIGHT Final Report
K. YAMAMOTO, J. F. BRAUSCH, T. F. BALSA, B. A. JANARDAN, and P. R. KNOTT Washington NASA Dec. 1984 397 p refs
(Contract NAS3-22514)
(NASA-CR-3845; E-2282; NAS 1.26:3845; R82AEB492) Avail: NTIS HC A17/MF A01 CSCL 20A

Seven single stream model nozzles were tested in the Anechoic Free-Jet Acoustic Test Facility to evaluate the effectiveness of convergent divergent (C-D) flowpaths in the reduction of shock-cell noise under both static and mulated flight conditions. The test nozzles included a baseline convergent circular nozzle, a C-D circular nozzle, a convergent annular plug nozzle, a C-D annular plug nozzle, a convergent multi-element suppressor plug nozzle, and a C-D multi-element suppressor plug nozzle. Diagnostic flow visualization with a shadowgraph and aerodynamic plume measurements with a laser velocimeter were performed with the test nozzles. A theory of shock-cell noise for annular plug nozzles with shock-cells in the vicinity of the plug was developed. The benefit of these C-D nozzles was observed over a broad range of pressure ratiosin the vicinity of their design conditions. At the C-D design condition, the C-D annual nozzle was found to be free of shock-cells on the plug. R.S.F.

N85-13551*# National Aeronautics and Space Administration. Lewis Research Center, Cleveland, Ohio.
STATIC JET NOISE TEST RESULTS OF FOUR 0.35 SCALE-MODEL QCGAT MIXER NOZZLES
D. E. GROESBECK and C. A. WASSERBAUER Oct. 1984 47 p refs
(NASA-TM-86871; E-2333; NAS 1.15:86871) Avail: NTIS HC A03/MF A01 CSCL 20A

As part of the NASA Quiet Clean General Aviation Turbofan (QCGAT) engine mixer-nozzle exhaust system program, static jet

exhaust noise was recorded at microphone angles of 45 to 155 deg relative to the nozzle inlet for a conventional profile coaxial nozzle and three 12-lobed coaxial mixer nozzles. Both flows in all four nozzles are internally mixed before being discharged from a single exhaust nozzle. The conventional profile coaxial nozzle jet noise is compared to the current NASA Lewis coaxial jet noise prediction and after applying an adjustment to the predicted levels based on the ratio of the kinetic energy of the primary and secondary flows, the prediction is within a standard deviation of 0.9 dB of the measured data. The mass average (mixed flow) prediction is also compared to the noise data for the three mixer nozzles with a reasonably good fit after applying another kinetic energy ratio adjustment (standard deviation of 0.7 to 1.5 dB with the measured data). The tests included conditions for the full-scale engine at takeoff (T.O.), cutback (86% T.O.) and approach (67% T.O.). M.G.

N85-17667*# Cleveland State Univ., Ohio.
INVESTIGATION ON EXPERIMENTAL TECHNIQUES TO DETECT, LOCATE AND QUANTIFY GEAR NOISE IN HELICOPTER TRANSMISSIONS Final Report
P. M. FLANAGAN and W. J. ATHERTON Washington NASA Jan. 1985 101 p refs Original contains color illustrations
(Contract NAG3-315)
(NASA-CR-3847; E-2294; NAS 1.26:3847) Avail: NTIS HC A06/MF A01 CSCL 20A

A robotic system to automate the detection, location, and quantification of gear noise using acoustic intensity measurement techniques has been successfully developed. Major system components fabricated under this grant include an instrumentation robot arm, a robot digital control unit and system software. A commercial, desktop computer, spectrum analyzer and two microphone probe complete the equipment required for the Robotic Acoustic Intensity Measurement System (RAIMS). Large-scale acoustic studies of gear noise in helicopter transmissions cannot be performed accurately and reliably using presently available instrumentation and techniques. Operator safety is a major concern in certain gear noise studies due to the operating environment. The man-hours needed to document a noise field in situ is another shortcoming of present techniques. RAIMS was designed to reduce the labor and hazard in collecting data and to improve the accuracy and repeatability of characterizing the acoustic field by automating the measurement process. Using RAIMS a system operator can remotely control the instrumentation robot to scan surface areas and volumes generating acoustic intensity information using the two microphone technique. Acoustic intensity studies requiring hours of scan time can be performed automatically without operator assistance. During a scan sequence, the acoustic intensity probe is positioned by the robot and acoustic intensity data is collected, processed, and stored.

N85-19791*# General Electric Co., Schenectady, N. Y. Corporate Research and Development.
EFFECTS OF VANE/BLADE RATIO AND SPACING ON FAN NOISE, VOLUME 1 Final Technical Report
P. R. GLIEBE (GE, Cincinnati) and R. A. KANTOLA Dec. 1983 164 p refs 2 Vol.
(Contract NAS3-22062)
(NASA-CR-174664; NAS 1.26:174664; GE-84SRD006-VOL-1)
Avail: NTIS HC A08/MF A01 CSCL 20A

The noise characteristics of a high-speed fan were studied. The experimental investigation was carried out on a 50.8 cm (20 in.) diameter scale model fan stage in an anechoic chamber with an inflow turbulence control screen installed. The forty-four blade rotor was tested with forty-eight vane and eighty-six vane stator rows, over a range of aixal rotor-stator spacings from 0.5 to 2.3 rotor tip chords. A two-dimensional strip theory model of rotor-stator interaction noise was employed to predict the measured tone power level trends, and good overall agreement with measured trends was obtained. A.R.H.

N85-19792*# General Electric Co., Schenectady, N. Y.
EFFECTS OF VANE/BLADE RATIO AND SPACING ON FAN NOISE. VOLUME 2: DATA SUPPLEMENT Final Report
P. R. GLIEBE and R. A. KANTOLA Dec. 1983 359 p 2 Vol.
(Contract NAS3-22062)
(NASA-CR-174665; NAS 1.26:174665; GE-84SRD006-VOL-2; DS-3-VOL-2) Avail: NTIS HC A16/MF A01 CSCL 20A

Complete tabulations of 1/3-octave band acoustic measurements are given. Author

N85-22108*# National Aeronautics and Space Administration. Lewis Research Center, Cleveland, Ohio.
FURTHER COMPARISON OF WIND TUNNEL AND AIRPLANE ACOUSTIC DATA FOR ADVANCED DESIGN HIGH SPEED PROPELLER MODELS
J. H. DITTMAR 1985 23 p refs To be presented at the 109th Meeting of the Acoust. Soc. of Am., Austin, Tex., 8-12 Apr. 1985
(NASA-TM-86935; E-2448; NAS 1.15:86935) Avail: NTIS HC A02/MF A01 CSCL 20A

Comparisons were made between the SR-2 and SR-3 model propeller noise data taken in the NASA 8-by-6 wind tunnel, in the United Technologies Research Center (UTRC) anechoic tunnel, and with boom and fuselage microphones on the NASA Jetstar airplane. Plots of peak blade passage tone noise versus helical tip Mach number generally showed good agreement. The levels of the airplane fuselage data were somewhat lower than the boom data by an approximately uniform value. The curve shapes were similar except for the UTRC data which was flatter than the other sets. This was attributed to the UTRC data being taken at constant power while the other data were taken at constant advance ratio. General curves of the peak blade passage tone versus helical tip Mach number fit through all the data are also presented. Directivity shape comparisons at the cruise condition were similar for the airplane and 8-by-6 tunnel data. The UTRC data peaked farther forward but, when an angle correction was made for the different axial Mach number used in the UTRC tests, the shape was similar to the others. The general agreement of the data from the four configurations enables the formation of a good consensus of the noise from these propellers. Author

N85-22109*# National Aeronautics and Space Administration. Lewis Research Center, Cleveland, Ohio.
NOISE TRANSMISSION LOSS OF A RECTANGULAR PLATE IN AN INFINITE BAFFLE
L. A. ROUSSOS Mar. 1985 36 p refs Presented at the 107th Meeting of the Acoustical Society of America, Norfolk, Va., 7-10 May 1984
(NASA-TP-2398; L-15861; NAS 1.60:2398) Avail: NTIS HC A03/MF A01 CSCL 20A

An improved analytical procedure was developed that allows for the efficient calculation of the noise transmission characteristics of a finite rectangular plate. Both isotropic and symmetrically laminated composite plates are considered. The plate is modeled with classic thin-plate theory and is assumed to be simply supported on all four sides. The incident acoustic pressure is assumed to be a plane wave impinging on the plate at an arbitrary angle. The reradiated pressure is assumed to be negligible compared with the blocked pressure, and the plate vibrations are calculated by a normal-mode approach. A Green's function integral equation is used to link the plate vibrations to be transmitted far-field sound waves, and transmission loss is calculated from the ratio of incident to transmitted acoustic powers. The result is a versatile research and engineering analysis tool that predicts noise transmission loss and enables the determination of the modal behavior of the plate. E.A.K.

N85-27637*# Texas Univ., Austin.
INTERACTION OF FINITE-AMPLITUDE SOUND WITH AIR-FILLED POROUS MATERIALS Final Report, 1 Sep. 1981 - 28 Feb. 1985
D. A. NELSON Mar. 1985 177 p refs
(Contract NSG-3198; N00014-75-C-0867; N00014-84-K-0574)
(NASA-CR-174885; NAS 1.26:174885; ARL-TR-85-15) Avail: NTIS HC A09/MF A01 CSCL 20A

The propagation of high intensity sound waves through an air-filled porus material was studied. The material is assumed: (1) to be rigid, incompressible, and homogeneous, and (2) to be adequately described by two properties: resistivity r and porosity. The resulting wave equation is still nonlinear, however, because of the u sgn(u) term in the resistivity. The equation is solved in the frequency domain as an infinite set of coupled inhomogeneous Helmholtz equations, one for each harmonic. An approximate but analytical solution leads to predictions of excess attenuation, saturation, and phase speed reduction for the fundamental component. A more general numerical solution is used to calculate the propagation curves for the higher harmonics. The u sgn(u) nonlinearity produces a cubic distortion pattern; when the input signal is a pure tone, only odd harmonic distortion products are generated. G.L.C.

N85-30770*# National Aeronautics and Space Administration. Lewis Research Center, Cleveland, Ohio.
MEASURED ACOUSTIC PROPERTIES OF VARIABLE AND LOW DENSITY BULK ABSORBERS
M. D. DAHL and E. J. RICE 1985 18 p refs Presented at the Winter Ann. Meeting of the Am. Soc. of Mech. Engr., Miami Beach, Fla., 17-21 Nov. 1985
(NASA-TM-87065; E-2633; NAS 1.15:87065) Avail: NTIS HC A02/MF A01 CSCL 20A

Experimental data were taken to determine the acoustic absorbing properties of uniform low density and layered variable density samples using a bulk absober with a perforated plate facing to hold the material in place. In the layered variable density case, the bulk absorber was packed such that the lowest density layer began at the surface of the sample and progressed to higher density layers deeper inside. The samples were placed in a rectangular duct and measurements were taken using the two microphone method. The data were used to calculate specific acoustic impedances and normal incidence absorption coefficients. Results showed that for uniform density samples the absorption coefficient at low frequencies decreased with increasing density and resonances occurred in the absorption coefficient curve at lower densities. These results were confirmed by a model for uniform density bulk absorbers. Results from layered variable density samples showed that low frequency absorption was the highest when the lowest density possible was packed in the first layer near the exposed surface. The layers of increasing density within the sample had the effect of damping the resonances. Author

72

ATOMIC AND MOLECULAR PHYSICS

Includes atomic structure and molecular spectra.

N85-22477*# National Aeronautics and Space Administration. Lewis Research Center, Cleveland, Ohio.
LABORATORY STUDIES OF KAPTON DEGRADATION IN AN OXYGEN ION BEAM
D. C. FERGUSON *In its* Spacecraft Environ. Interactions Technol., 1983 p 81-90 Mar. 1985 refs
Avail: NTIS HC A99/MF E03 CSCL 18H

Results are presented from a preliminary laboratory investigation of the degradation of the widely used polyimide Kapton under oxygen ion bombardment. Recent space shuttle flights have shown that Kapton and some other materials exposed to the apparent ram flow of residual atmosphere (at orbital velocity in low Earth orbit) lose mass and change their optical properties. It was hypothesized that these changes are caused by chemical interaction with atomic oxygen, aided by the 5-eV impact energy of atmospheric oxygen atoms in the ram. The reaction rate under O(+) bombardment seemed to be independent of incident energy over a wide range of energies. Although the flux of thermal ions in this experiment was much greater than the accelerated flux, the observed Kapton degradation was limited to the beam area and ram flow direction. This is consistent with an activation energy above the thermal energies but well below the beam energies. The results reproduce well the material loss, optical changes, SEM surface structure, and ram directionality of the samples returned by the shuttle. These factors, along with the lack of degradation under argon ion bombardment, are convincing evidence for ram flow oxidation as the mechanism of degradation. B.G.

73

NUCLEAR AND HIGH-ENERGY PHYSICS

Includes elementary and nuclear particles; and reactor theory.

N85-35728*# Boeing Aerospace Co., Seattle, Wash. Electrical Power Systems Technology.
APPLICABILITY OF 100KWE-CLASS OF SPACE REACTOR POWER SYSTEMS TO NASA MANNED SPACE STATION MISSIONS Final Report
S. W. SILVERMAN, H. J. WILLENBERG, and C. ROBERTSON (General Electric Co., King of Prussia, Pa.) Aug. 1985 184 p refs
(Contract NAS3-23865)
(NASA-CR-174696; NAS 1.26:174696; D180-28461-1) Avail: NTIS HC A09/MF A01 CSCL 18I

An assessment is made of a manned space station operating with sufficiently high power demands to require a multihundred kilowatt range electrical power system. The nuclear reactor is a competitor for supplying this power level. Load levels were selected at 150kWe and 300kWe. Interactions among the reactor electrical power system, the manned space station, the space transportation system, and the mission were evaluated. The reactor shield and the conversion equipment were assumed to be in different positions with respect to the station; on board, tethered, and on a free flyer platform. Mission analyses showed that the free flyer concept resulted in unacceptable costs and technical problems. The tethered reactor providing power to an electrolyzer for regenerative fuel cells on the space station, results in a minimum weight shield and can be designed to release the reactor power section so that it moves to a high altitude orbit where the decay period is at least 300 years. Placing the reactor on the station, on a structural boom is an attractive design, but heavier than the long tethered reactor design because of the shield weight for manned activity near the reactor. Author

74

OPTICS

Includes light phenomena.

A85-23134* Stanford Univ., Calif.
OPTICAL COMPUTER SWITCHING NETWORK
B. CLYMER (Stanford University, Stanford, CA) and S. A. COLLINS, JR. (Ohio State University, Columbus, OH) (IEEE, ICO, and SPIE, International Optical Computing Conference, 10th, Cambridge, MA, Apr. 6-8, 1983) Optical Engineering (ISSN 0091-3286), vol. 24, Jan.-Feb. 1985, p. 74-81. Research supported by the Hughes Aircraft Co. and Ohio State University. refs
(Contract NSG-3302)

The design for an optical switching system for minicomputers that uses an optical spatial light modulator such as a Hughes liquid crystal light valve is presented. The switching system is designed to connect 80 minicomputers coupled to the switching system by optical fibers. The system has two major parts: the connection system that connects the data lines by which the computers communicate via a two-dimensional optical matrix array and the control system that controls which computers are connected. The basic system, the matrix-based connecting system, and some of the optical components to be used are described. Finally, the details of the control system are given and illustrated with a discussion of timing. Author

N85-13594*# Opcoa, Inc., Santa Ana, Calif.
FIBER OPTIC, FABRY-PEROT HIGH TEMPERATURE SENSOR Final Report
K. JAMES and B. QUICK Nov. 1984 28 p
(Contract NAS3-23522)
(NASA-CR-174712; NAS 1.26:174712) Avail: NTIS HC A03/MF A01 CSCL 20F

A digital, fiber optic temperature sensor using a variable Fabry-Perot cavity as the sensor element was analyzed, designed, fabricated, and tested. The fiber transmitted cavity reflection spectra is dispersed then converted from an optical signal to electrical information by a charged coupled device (CCD). A microprocessor-based color demodulation system converts the wavelength information to temperature. This general sensor concept not only utilizes an all-optical means of parameter sensing and transmitting, but also exploits microprocessor technology for automated control, calibration, and enhanced performance. The complete temperature sensor system was evaluated in the laboratory. Results show that the Fabry-Perot temperature sensor has good resolution (0.5% of full seale), high accuracy, and potential high temperature (1000 C) applications. Author

N85-28786*# National Aeronautics and Space Administration. Lewis Research Center, Cleveland, Ohio.
INCIDENT BEAM POLARIZATION FOR LASER DOPPLER VELOCIMETRY EMPLOYING A SAPPHIRE CYLINDRICAL WINDOW
J. A. LOCK (Clevelend State Univ.) and H. J. SCHOCK Jun. 1985 25 p refs
(NASA-TM-87064; E-2316-1; NAS 1.15:87064) Avail: NTIS HC A02/MF A01 CSCL 20F

For laser Doppler velocimetry studies employing sapphire windows as optical access ports, the birefringency of sapphire produces an extra beam intersection volume which serves to effectively smear the acquired velocity flow field data. It is shown that for a cylindrical window geometry, the extra beam intersection volume may be eliminated with minimal decrease in the fringe visibility of the remaining intersection volume by suitably orienting the polarizations of the initial laser beams. For horizontally incident beams, these polarizations were measured at three intersection locations within the cylinder. It was found that the measured polarization angles agreed with the theoretical predictions. Author

N85-34631*# National Aeronautics and Space Administration. Lewis Research Center, Cleveland, Ohio.
DIAMONDLIKE CARBON PROTECTIVE COATINGS FOR IR MATERIALS
M. J. MIRTICH, D. NIR, D. M. SWEC, and B. A. BANKS 1985 18 p refs Presented at the 12th Intern. Conf. on Met. Coatings, Los Angeles, 15-19 Apr. 1985; sponsored by the American Vacuum Society
(NASA-TM-87083; E-2506; NAS 1.15:87083) Avail: NTIS HC A02/MF A01 CSCL 20F

Diamondlike carbon (DLC) films have the potential to protect optical windows in applications where it is important to maintain the integrity of the specular transmittance of these films on ZnS and ZnSe infrared transmitting windows. The films must be adherent and durable such that they protect the windows from rain and particle erosion as well as chemical attack. In order to optimize the performance of these films, 0.1 micro m thick diamondlike carbon films were deposited on fused silica and silicon wafers, using three different methods of ion beam deposition. One method was sputter deposition from a carbon target using an 8 cm ion source. The merits of hydrogen addition were experimentally evaluated in conjunction with this method. The second method used a 30 cm hollow cathode ion source with hydrocarbon/Argon gases to deposit diamondlike carbon films from the primary beam at 90 to 250 eV. The third method used a dual beam system employing a hydrocarbon/Argon 30 cm ion source and an 8 cm ion source. Films were evaluated for adherence, intrinsic stress, infrared transmittance between 2.5 and 50 micro m, and protection from particle erosion. An erosion test using a sandblaster was used to give quantitative values of the protection afforded to the fused silica by the diamondlike carbon films. The fused silica surfaces protected by diamondlike carbon films were exposed to 100 micro m diameter SiO particles at 60 mi/hr (26.8/sec) in the sandblaster. B.W.

75

PLASMA PHYSICS

Includes magnetohydrodynamics and plasma fusion.

A85-12705*# Colorado State Univ., Fort Collins.
ION FLOW EXPERIMENTS IN A MULTIPOLE DISCHARGE CHAMBER
H. R. KAUFMAN, R. S. ROBINSON, and L. E. FRISA (Colorado State University, Fort Collins, CO) AIAA Journal (ISSN 0001-1452), vol. 22, Nov. 1984, p. 1544-1549. Previously cited in issue 03, p. 398, Accession no. A83-14398. refs
(Contract NSG-3011)

A85-16443*# Michigan State Univ., East Lansing.
MEASUREMENTS OF ENERGY DISTRIBUTION IN MICROWAVE PLASMAS OF N2 AND HE AND COMPARISONS WITH RESULTS FOR H2
R. CHAPMAN and M. C. HAWLEY (Michigan State University, East Lansing, MI) IN: International Electric Propulsion Conference, 17th, Tokyo, Japan, May 28-31, 1984, Proceedings . Tokyo, Japan Society for Aeronautical and Space Sciences, 1984, p. 547-550.
(Contract NSG-3299)

An electrothermal propulsion concept utilizing a microwave plasma system as the mechanism to convert electromagnetic energy into translational energy of the flowing gas is being investigated. Specifically, this study compares the energy transfer characteristics of three different gases, H2, N2, and He, to gain some insight as to the dominant energy transfer processes present in a microwave plasma. A calorimetric experimental system has been designed and built enclosing the microwave plasma system to accurately determine the net energy transferred to the flowing gas. Results are obtained for N2 and He discharges and compared with previously reported experimental results for H2. Author

A85-16444*# Michigan State Univ., East Lansing.
THE ENERGETICS OF HYDROGEN ATOM RECOMBINATION - ANALYSIS, EXPERIMENTS, AND MODELING
J. W. FILPUS and M. C. HAWLEY (Michigan State University, East Lansing, MI) IN: International Electric Propulsion Conference, 17th, Tokyo, Japan, May 28-31, 1984, Proceedings . Tokyo, Japan Society for Aeronautical and Space Sciences, 1984, p. 551-559. refs
(Contract NSG-3299)

A theoretical investigation of the effect of the microscopic energetics of the recombination reaction on the performance of a microwave-plasma electrothermal propulsion system is described, and the results of the analysis are presented. A series of experiments to test the concept is described and analyzed by comparison with a computer model of the recombination reaction. It is concluded that internal energy considerations are not likely to significantly affect the design of a microwave-plasma electrothermal rocket. The experimental results indicate that the microwave power is far higher than the capacity of the gas to absorb it; the cooling needed to control the energy dominates the experimental results. C.D.

A85-16455*# Michigan State Univ., East Lansing.
RECENT WORK ON A MICROWAVE ION SOURCE
J. ASMUSSEN and J. ROOT (Michigan State University, East Lansing, MI) IN: International Electric Propulsion Conference, 17th, Tokyo, Japan, May 28-31, 1984, Proceedings . Tokyo, Japan Society for Aeronautical and Space Sciences, 1984, p. 660-664. refs
(Contract NSG-3299)

The performance of a microwave (2.45 GHz) plasma-disk ion source using a cylindrical microwave cavity is described. The operating characteristics in argon and xenon gases with 50-200 W of input power and gas flow rates from 10-80 sccm are presented. In particular, extracted beam current versus accelerating voltage, and specific energy vs. mass utilization efficiency and extracted beam current are presented. Double Langmuir probe measurements indicate that electron densities in excess of 10 to the 12th per cu cm can be readily achieved in the microwave generated plasma. Author

A85-17262* Kansas Univ., Lawrence.
NUMERICAL SIMULATIONS OF POSITIVELY-BIASED PROBES AND DIELECTRIC-CONDUCTOR DISKS IN A PLASMA
S. T. BRANDON, R. L. KESSEL, J. ENOCH, and T. P. ARMSTRONG (Kansas, University, Lawrence, KS) Journal of Applied Physics (ISSN 0021-8979), vol. 56, Dec. 1, 1984, p. 3215-3222. refs
(Contract NSG-3290)

Plasma densities in the low-earth orbit range may be sufficient to cause difficulties for spacecraft operating at high voltages in this environment. The present investigation is concerned with the results of a continuing effort to develop a particle-in-cell (PIC), cylindrically-symmetric, 2-1/2 dimensional, self-consistent numerical simulation code. The simulation has the objective to explore the interactions of an ambient plasma with a conducting disk, which may be partially covered by a dielectric material. The disk and the surrounding dielectric material represent a hole in an insulator covering a conductor. Attention is given to a review of the simulation model, plain disk calculations, the disk and dielectric configuration, and the 'pinhole' effect. G.R.

A85-43552* Michigan State Univ., East Lansing.
EXPERIMENTAL PERFORMANCE OF A MICROWAVE CAVITY PLASMA DISK ION SOURCE
J. ROOT and J. ASMUSSEN (Michigan State University, East Lansing) Review of Scientific Instruments (ISSN 0034-6748), vol. 56, Aug. 1985, p. 1511-1519. *refs*
(Contract NSG-3299)

The detailed description and performance characteristics of a microwave ion source are presented. This ion source utilizes an internally tuned, single-mode (or selective multimode) cylindrical cavity applicator to focus and match microwave energy into a disk-shaped discharge zone. The combination of mode focus control and variable, internal cavity matching allows the efficient operation and beam extraction over a wide range of pressures, powers and gaseous inputs. Experimental measurements of ion beam current versus accelerating voltage and input microwave power in xenon and oxygen gas are presented. Ion source specific energy and mass utilization versus experimental variables are also determined. The experimental performance demonstrates the ability of this ion source to extract an ion beam with a well matched, stable, and continuous operation over a wide range of input gases, low pressures, and over input gas flow rates in excess of 100 to a few sccm. Double Langmuir probe measurements in xenon gas indicate high degrees of ionization, and electron and ion concentrations in excess of 100 critical densities in the microwave discharge zone. This ion source has many potential uses such as spacecraft electric propulsion, material ion beam processing, and neutral beam ion sources. Author

N85-22472*# National Aeronautics and Space Administration, Washington, D.C.
SUPRATHERMAL PLASMA OBSERVED ON STS-3 MISSION BY PLASMA DIAGNOSTICS PACKAGE
W. PATERSON, L. A. FRANK, H. OWENS, J. S. PICKETT, G. B. MURPHY, and S. D. SHAWHAN *In* NASA. Lewis Research Center Spacecraft Environ. Interactions Technol., 1983 p 13-17 Mar. 1985 refs Prepared in cooperation with Iowa Univ., Iowa City
(Contract NAG3-449)
Avail: NTIS HC A99/MF E03 CSCL 20I

Artificially produced electron beams were used extensively during the past decade as a means of probing the magnetosphere, and more recently as a means of actively controlling spacecraft potential. Experimentation in these areas has proven valuable, yet at times confusing, due to the interaction of the electron beam with the ambient plasma. The OSS-1/STS-3 Mission in March 1982 provided a unique opportunity to study beam-plasma interactions at an altitude of 240 km. On board for this mission was a Fast Pulse Electron Generator (FPEG). Measurements made by the Plasma Diagnostics Package (PDP) while extended on the Orbiter RMS show modifications of the ion and electron energy distributions during electron beam injection. Observations made by charged particle detectors are discussed and related to measurements of Orbiter potential. Several of the PDP instruments, the joint PDP/FPEG experiment, and observations made during electron beam injection are described. B.G.

N85-22494*# National Aeronautics and Space Administration. Lewis Research Center, Cleveland, Ohio.
THE PIX-2 EXPERIMENT: AN OVERVIEW
C. K. PURVIS *In its* Spacecraft Environ. Interactions Technol. p 321-332 Mar. 1985 refs
Avail: NTIS HC A99/MF E03 CSCL 20I

The second Plasma Interactions Experiment (PIX-2) was launched in January 1983 as a piggyback on the second stage of the Delta launch vehicle that carried IRAS into orbit. Placed in a 870 km circular polar orbit, it returned 18 hrs of data on the plasma current collection and arcing behavior of solar arrays biased to +/-1000 V in steps. The four 500 sq cm solar array segments were biased singly and in combinations. In addition to the array segments PIX-2 carried a Sun sensor, a Langmuir probe to measure electron currents, and a hot-wire filament electron emitter to control vehicle potential during positive array bias sequences. The PIX-2 experiment is reviewed from program and operational perspectives. M.G.

N85-22495*# National Aeronautics and Space Administration. Lewis Research Center, Cleveland, Ohio.
PLASMA INTERACTION EXPERIMENT 2 (PIX 2): LABORATORY AND FLIGHT RESULTS
N. T. GRIER *In its* Spacecraft Environ. Interactions Technol. p 333-347 Mar. 1985
Avail: NTIS HC A99/MF E03 CSCL 20I

The Plasma Interaction Experiments 1 and 2 (PIX 1 and 2) were designed as first steps toward understanding interactions between high-voltage solar arrays and the surrounding plasma. The PIX 2 consisted of an approximately 2000-sq cm array divided into four equal segments. Each of the segments could be biased independently and the current measured separately. In addition to the solar array segments, PIX 2 had a hot-wire-filament electron emitter and a spherical Langmuir probe. The emitter was operated when the array segments were biased positively bove 125 V. Thermal electrons from the emitter aided in balancing the electron currents collected by the array. Laboratory and flight results of PIX 2 are presented. At high positive voltages on the solar array segments, the flight currents were approximately an order of magnitude larger than the ground test currents. This is attributed to the tank walls in the laboratory interfering with the electron currents to the array segments. From previous tests it is known that the tank walls limit the electron currents at high voltages. This was the first verification of the extent of the laboratory tank effect on the plasma coupling current. M.G.

N85-22496*# National Aeronautics and Space Administration. Lewis Research Center, Cleveland, Ohio.
RAM-WAKE EFFECTS ON PLASMA CURRENT COLLECTION OF THE PIX 2 LANGMUIR PROBE
D. C. FERGUSON *In its* Spacecraft Environ. Interactions Technol. p 349-357 Mar. 1985 refs
Avail: NTIS HC A99/MF E03 CSCL 20I

The Plasma Interaction Experiment 2 (PIX 2) Langmuir probe readings of the same polar magnetospheric regions taken on consecutive orbits showed occasional apparent densities as much as 10 times lower than the average, although each pass clearly showed density structures related to the day/night boundary. At other points in the orbit, Langmuir probe currents varied by as much as a factor of 20 on a time scale of minutes. The hypothesis is advanced that these apparent inconsistencies in Langmuir probe current are the results of the probe's orientation relative to the body of the spacecraft and the velocity vector. Theoretical studies predict a possible depletion in collected electron current by a factor of 100 in the wake. Experimental results from other spacecraft indicate that a wake electron depletion by a factor of 10 or so is realistic. This amount of depletion is consistent with the PIX 2 data if the spacecraft was rotating. Both the Sun sensor and temperature sensor data on PIX 2 show a complex variation consistent with rotation of the Langmuir probe into and out of the spacecraft wake on a time scale of minutes. Furthermore, Langmuir probe data taken when the probe was not in the spacecraft wake are consistent from orbit to orbit. This supports the interpretation that ram/wake effects may be the source of apparent discrepancies at other orientations. M.G.

N85-22497*# National Aeronautics and Space Administration. Lewis Research Center, Cleveland, Ohio.
NASCAP SIMULATION OF PIX 2 EXPERIMENTS
J. C. ROCHE and M. J. MANDELL (Systems, Science and Software, San Diego) *In its* Spacecraft Environ. Interactions Technol. p 359-366 Mar. 1985
Avail: NTIS HC A99/MF E03 CSCL 20I

The latest version of the NASCAP/LEO digital computer code used to simulate the PIX 2 experiment is discussed. NASCAP is a finite-element code and previous versions were restricted to a single fixed mesh size. As a consequence the resolution was dictated by the largest physical dimension to be modeled. The latest version of NASCAP/LEO can subdivide selected regions. This permitted the modeling of the overall Delta launch vehicle in the primary computational grid at a coarse resolution, with subdivided regions at finer resolution being used to pick up the details of the experiment module configuration. Langmuir probe data from the flight were used to estimate the space plasma density and temperature and the Delta ground potential relative to the space plasma. This information is needed for input to NASCAP. Because of the uncertainty or variability in the values of these parameters, it was necessary to explore a range around the nominal value in order to determine the variation in current collection. The flight data from PIX 2 were also compared with the results of the NASCAP simulation. R.J.F.

N85-22498*# National Aeronautics and Space Administration. Lewis Research Center, Cleveland, Ohio.
AN INVESTIGATION OF ARC DISCHARGING ON NEGATIVELY BIASED DIELECTRIC CONDUCTOR SAMPLES IN A PLASMA
W. L. MILLER *In its* Spacecraft Environ. Interactions Technol. p 367-377 Mar. 1985 refs
Avail: NTIS HC A99/MF E03 CSCL 20I

Proposals are now being developed for the construction of high-power photovoltaic systems for operation in low Earth orbit, where the plasma number density is about 1,000 to 1,000,000 per cubic cm. Existing data indicate that interactions between the plasma and high-voltage surfaces of an orbiting power system will occur. In ground tests, where the applied voltage is increased negatively from ground, the array current collection shows an approximately linear rise until it terminates in arcing at greater than several hundred volts negative. This arcing may reduce the power generation efficiency and could possibly affect the low-level logic circuits of the spacecraft. Therefore it is important that the arcing phenomenon be well understood. This study is a survey of the behavior of different dielectric-conductor samples, including a solar cell module, that were biased negatively in a low-density plasma environment with the intent of defining arc discharge conditions and characteristics. Procedures and results are discussed. Author

76

SOLID-STATE PHYSICS

Includes superconductivity.

A85-11466* Varian Associates, Palo Alto, Calif..
MAGNESIUM DOPING OF EFFICIENT GAAS AND GA(0.75)IN(0.25)AS SOLAR CELLS GROWN BY METALORGANIC CHEMICAL VAPOR DEPOSITION
C. R. LEWIS, C. W. FORD, and J. G. WERTHEN (Varian Associates, Inc., Palo Alto, CA) Applied Physics Letters (ISSN 0003-6951), vol. 45, Oct. 15, 1984, p. 895-897. refs
(Contract NAS3-22232)

Magnesium has been substituted for zinc in GaAs and Ga(0.75)In(0.25)As solar cells grown by metalorganic chemical vapor deposition (MOCVD). Bis(cyclopentadienyl)magnesium (Cp2Mg) is used as the MOCVD transport agent for Mg. Full retention of excellent material quality and efficient cell performance results. The substitution of Mg for Zn would enhance the abruptness and reproducibility of doping profiles, and facilitate high temperature processing and operation, due to the much lower diffusion coefficient of Mg, relative to Zn, in these materials. Author

A85-18082* Michigan Technological Univ., Houghton.
THE MECHANISMS OF FORMATION AND PREVENTION OF CHANNEL SEGREGATION DURING ALLOY SOLIDIFICATION
A. HELLAWELL (Michigan Technological University, Houghton, MI) and A. K. SAMPLE Metallurgical Transactions A - Physical Metallurgy and Materials Science (ISSN 0360-2133), vol. 15A, Dec. 1984, p. 2163-2173. refs
(Contract NSF DMR-82-12115; NAG3-560; NAS8-33727)

Using a base chilled configuration, conditions for the formation and prevention of segregation channels are studied in the ammonium chloride-water and lead-tin systems. Such channels

develop when the rejected solute is less dense than the solvent and are therefore a result of density inversion, but slow (less than 5 rpm) rates of mold rotation, about axes inclined to the vertical by 20 to 30 deg, throughout the time of solidification, effectively prevent the formation or propagation of these channels. In experiments with artificially created or blocked channels, a simultaneous solute plume in the bulk liquid must be present in order for a channel to develop. The results indicate that channels originate not within the dendritic array, but immediately ahead of the growth front as a result of perturbation from the less dense boundary layer into the bulk liquid. The effect of mold movement is to translate laterally the bulk liquid relative to the growth front so that perturbations are sheared off. The nature of the liquid movement is considered and shown to be a function of the mold dimensions. M.D.

A85-21425* California Univ., Irvine.
PRISM-COUPLED LIGHT EMISSION FROM TUNNEL JUNCTIONS
S. USHIODA, J. E. RUTLEDGE, and R. M. PIERCE (California, University, Irvine, CA) Physical Review Letters (ISSN 0031-9007), vol. 54, Jan. 21, 1985, p. 224-226. refs
(Contract NAG3-524)

Completely p-polarized light emission has been observed from smooth Al-AlO(x)-Au tunnel junctions placed on a prism coupler. The angle and polarization dependence demonstrate unambiguously that the emitted light is radiated by the fast-mode surface plasmon polariton. The emission spectra suggest that the dominant process for the excitation of the fast mode is through conversion of the slow mode to the fast mode mediated by residual roughness on the junction surface. Author

A85-24649* *California Univ., Irvine.*
SUBSTRATE-INDUCED ORIENTATIONAL ORDER IN THE ISOTROPIC PHASE OF LIQUID CRYSTALS
A. MAUGER, G. ZRIBI, D. L. MILLS (California, University, Irvine, CA), and J. TONER (IBM Thomas J. Watson Research Center, Yorktown Heights, NY) Physical Review Letters (ISSN 0031-9007), vol. 53, Dec. 24, 1984, p. 2485-2488. refs
(Contract NAG3-250)

Nematic order induced near a solid boundary in an otherwise isotropic liquid crystal is studied theoretically, at temperatures just above the bulk nematic-isotropic phase transition. Three distinct regimes are found, depending on the strength of orientational torques at the boundary: (1) strong orientational order, (2) strong orientational order followed by a first-order transition to a state of weak orientational order as temperature is raised, and (3) a state of weak orientational order. Author

A85-32635* Perkin-Elmer Corp., Norwalk, Conn.
ELECTRICAL CHARACTERIZATION OF PLASMA-GROWN OXIDES ON GALLIUM ARSENIDE
F. I. HSHIEH (Perkin-Elmer Corp., Norwalk, CT; Rensselaer Polytechnic Institute, Troy, NY), K. N. BHAT, S. K. GHANDHI, and J. M. BORREGO (Rensselaer Polytechnic Institute, Troy, NY) Journal of Applied Physics (ISSN 0021-8979), vol. 57, May 15, 1985, p. 4657-4662. refs
(Contract NAG3-175)

Plasma-grown GaAs oxides and their interfaces have been characterized by measuring the electrical properties of metal-oxide-semiconductor capacitors and of Schottky junctions. The current transport mechanism in the oxide at high electrical field was found to be Frankel-Poole emission, with an electron trap center at 0.47 eV below the conduction band of the oxide. The interface-state density, evaluated from capacitance and conductance measurements, exhibits a U-shaped interface-state continuum extending over the entire band gap. Two discrete deep states with high concentration are superimposed on this continuum at 0.40 and 0.70 eV below the conduction band. The results obtained from measurements on Schottky junctions have excluded the possibility that these two deep states originate from plasma damage. Possible origins of these states are discussed in this paper. Author

A85-32636* Rensselaer Polytechnic Inst., Troy, N.Y.
HEAT TREATMENT OF BULK GALLIUM ARSENIDE USING A PHOSPHOSILICATE GLASS CAP
G. MATHUR, M. L. WHEATON, J. M. BORREGO, and S. K. GHANDHI (Rensselaer Polytechnic Institute, Troy, NY) Journal of Applied Physics (ISSN 0021-8979), vol. 57, May 15, 1985, p. 4711-4714. refs
(Contract NAG3-188)

n-type bulk GaAs crystals, capped with chemically vapor-deposited phosphosilicate glass, were heat treated at temperatures in the range of 600 to 950 C. Measurements on Schottky diodes and solar cells fabricated on the heat-treated material, after removal of a damaged surface layer, show an increase in free-carrier concentration, in minority-carrier-diffusion length, and in solar-cell short-circuit current. The observed changes are attributed to a removal of lifetime-reducing acceptorlike impurities, defects, or their complexes. Author

A85-33645* Rensselaer Polytechnic Inst., Troy, N.Y.
FABRICATION OF P(+)-N JUNCTION GAAS SOLAR CELLS BY A NOVEL METHOD
S. K. GHANDHI, G. MATHUR, H. RODE, and J. M. BORREGO (Rensselaer Polytechnic Institute, Troy, NY) Solid-State Electronics (ISSN 0038-1101), vol. 27, Dec. 1984, p. 1149-1151.
(Contract NAG3-188)

A novel method for making p(+)-n diffused junction GaAs solar cells, with the formation of a diffusion source, an anti-reflective coating, and a protective cover glass in a single chemical-vapor deposition operation is discussed. Consideration is given to device fabrication and to solar-cell characteristics. The advantages of the technique are that the number of process steps is kept to an absolute minimum, the fabrication procedure is low-cost, and the GaAs surface is protected during the entire operation. M.D.

A85-35308* National Aeronautics and Space Administration. Lewis Research Center, Cleveland, Ohio.
COMPUTER SIMULATION OF THIN FILM NUCLEATION AND GROWTH
J. SALIK (NASA, Lewis Research Center, Cleveland, OH) Journal of Applied Physics (ISSN 0021-8979), vol. 57, June 1, 1985, p. 5017-5023. refs

Some of the processes involved in thin film nucleation and growth were simulated by means of a digital computer. The main conclusions drawn from the simulation results are (1) Because of the random nature of the processes involved, a large variation in results is obtained. (2) Upon impingement, clusters are formed up to a coverage of ca. 0.2, and from there on growth of existing clusters, rather than formation of new ones, takes place. (3) Surface migration is responsible for the formation of most of the clusters at coverages smaller than 0.1, whereas at higher coverages most clusters are formed upon impingement. (4) Surface migration accelerates the growth and causes reduction in cluster density. (5) Reevaporation slows the growth and reduces the cluster density dramatically. Author

A85-35620*# National Aeronautics and Space Administration. Lewis Research Center, Cleveland, Ohio.
THE EFFECT OF DIFFUSION INDUCED LATTICE STRESS ON THE OPEN-CIRCUIT VOLTAGE IN SILICON SOLAR CELLS
V. G. WEIZER and M. P. GODLEWSKI (NASA, Lewis Research Center, Cleveland, OH) IN: Photovoltaic Specialists Conference, 17th, Kissimmee, FL, May 1-4, 1984, Conference Record . New York, Institute of Electrical and Electronics Engineers, 1984, p. 134-137. Previously announced in STAR as N84-23027. refs

It is demonstrated that diffusion induced stresses in low resistivity silicon solar cells can significantly reduce both the open-circuit voltage and collection efficiency. The degradation mechanism involves stress induced changes in both the minority carrier mobility and the diffusion length. Thermal recovery characteristics indicate that the stresses are relieved at higher temperatures by divacancy flow (silicon self diffusion). The level of residual stress in as-fabricated cells was found to be negligible in the cells tested. Author

A85-35698*# National Aeronautics and Space Administration. Lewis Research Center, Cleveland, Ohio.
RADIATION DAMAGE AND DEFECT BEHAVIOR IN ION-IMPLANTED, LITHIUM COUNTERDOPED SILICON SOLAR CELLS
I. WEINBERG, S. MEHTA, and C. K. SWARTZ (NASA, Lewis Research Center, Cleveland, OH) IN: Photovoltaic Specialists Conference, 17th, Kissimmee, FL, May 1-4, 1984, Conference Record . New York, Institute of Electrical and Electronics Engineers, 1984, p. 1088-1092. Previously announced in STAR as N84-22890. refs

Boron doped silicon n+p solar cells were counterdoped with lithium by ion implantation and the resuitant n+p cells irradiated by 1 MeV electrons. The function of fluence and a Deep Level Transient Spectroscopy (DLTS) was studied to correlate defect behavior with cell performance. It was found that the lithium counterdoped cells exhibited significantly increased radiation resistance when compared to boron doped control cells. It is concluded that the annealing behavior is controlled by dissociation and recombination of defects. The DLTS studies show that counterdoping with lithium eliminates at least three deep level defects and results in three new defects. It is speculated that the increased radiation resistance of the counterdoped cells is due primarily to the interaction of lithium with oxygen, single vacanies and divacancies and that the lithium-oxygen interaction is the most effective in contributing to the increased radiation resistance.
E.A.K.

A85-35699*# National Aeronautics and Space Administration. Lewis Research Center, Cleveland, Ohio.
EFFECTS OF 1 MEV ELECTRONS AND 10 MEV PROTONS ON THE PERFORMANCE AND REFLECTANCE OF THIN BSR CELLS
H. B. CURTIS, C. K. SWARTZ (NASA, Lewis Research Center, Cleveland, OH), and R. L. STATLER (U.S. Navy, Naval Research Laboratory, Washington, DC) IN: Photovoltaic Specialists Conference, 17th, Kissimmee, FL, May 1-4, 1984, Conference Record . New York, Institute of Electrical and Electronics Engineers, 1984, p. 1093-1096.
(Contract NAS3-22229)

Thin silicon cells with BSR's were irradiated with 1 MeV electrons on either the front or back side of the cell. There were two types of cells, a 10 ohm-cm with a BSF and a 0.15 ohm-cm without a BSF. Data on the electrical performance and reflectance are given for various fluence levels of 1 MeV electrons for both type cells and 10 MeV protons for the 10 ohm-cm cell. Author

A85-38019* National Aeronautics and Space Administration. Lewis Research Center, Cleveland, Ohio.
DENDRITIC SOLIDIFICATION. I - ANALYSIS OF CURRENT THEORIES AND MODELS. II - A MODEL FOR DENDRITIC GROWTH UNDER AN IMPOSED THERMAL GRADIENT
V. LAXMANN (NASA, Lewis Research Center; Case Western Reserve University, Cleveland, OH) Acta Metallurgica (ISSN 0001-6160), vol. 33, June 1985, p. 1023-1049. NASA-supported research. refs

A critical review of the present dendritic growth theories and models is presented. Mathematically rigorous solutions to dendritic growth are found to rely on an ad hoc assumption that dendrites grow at the maximum possible growth rate. This hypothesis is found to be in error and is replaced by stability criteria which consider the conditions under which a dendrite tip advances in a stable fashion in a liquid. The important elements of a satisfactory model for dendritic solidification are summarized and a theoretically consistent model for dendritic growth under an imposed thermal gradient is proposed and described. The model is based on the modification of an analysis due to Burden and Hunt (1974) and predicts correctly in all respects, the transition from a dendritic to a planar interface at both very low and very large growth rates.
M.D.

A85-38192* Nebraska Univ., Lincoln.
DIELECTRIC PROPERTIES OF 'DIAMONDLIKE' CARBON PREPARED BY RF PLASMA DEPOSITION
J. D. LAMB and J. A. WOOLLAM (Nebraska, University, Lincoln, NE) Journal of Applied Physics (ISSN 0021-8979), vol. 57, June 15, 1985, p. 5420-5423. Research supported by the University of Nebraska. refs
(Contract NAG3-154)

Metal-carbon-metal structures were fabricated using either gold or aluminum evaporated electrodes and RF plasma (methane) deposited 'diamondlike' carbon films. Alternating-current conductance and capacitance versus voltage and frequency (10 Hz to 13 MHz) data were taken to determine the dielectric properties of these films. Conductance versus frequency data fit a generalized power law, consistent with both dc and hopping conduction components. The capacitance versus frequency data are well matched to the conductance versus frequency data, as predicted by a Kramers-Kronig analysis. The dielectric loss tangent is nearly constant at 0.5 to 1.0 percent over the frequency range from 1 to 100 kHz. The dc resistivity is above 10 to the 13th ohm cm, and the dc breakdown strength is above 8 x 10 to the 6th V/cm is properly prepared samples. Author

A85-40386* National Aeronautics and Space Administration. Lewis Research Center, Cleveland, Ohio.
PLASMA DEPOSITED HYDROGENATED CARBON ON GAAS AND INP
J. D. WARNER, J. J. POUCH, S. A. ALTEROVITZ, D. C. LIU (NASA, Lewis Research Center, Cleveland, OH), and W. A. LANFORD (New York, State University, Albany) Journal of Vacuum Science and Technology A (ISSN 0734-2101), vol. 3, May-June 1985, pt. 1, p. 900-903. Army-supported research. Previously announced in STAR as N85-10844. refs

The properties of diamond like carbon films grown by RF flow discharge 30 kHz plasma using methane are reported. The Cis XPS line shape of films showed localized hybrid carbon bonds as low as 40 to as high as 95 percent. Infrared spectroscopy and N(15) nuclear reaction profiling data indicated 35 to 42 percent hydrogen, depending inversely on deposition temperature. The deposition rate of films on Si falls off exponentially with substrate temperature, and nucleation does not occur above 200 C on GaAs and InP. Optical data of the films showed bandgap values of 2.0 to 2.4 eV increasing monotonically with CH4 flow rate. Author

A85-41635* Minnesota Univ., Minneapolis.
CONE FORMATION AS A RESULT OF WHISKER GROWTH ON ION BOMBARDED METAL SURFACES
G. K. WEHNER (Minnesota, University, Minneapolis) Journal of Vacuum Science and Technology A (ISSN 0734-2101), vol. 3, July-Aug. 1985, p. 1821-1835. SERC-supported research. refs
(Contract NSG-3041)

It is shown experimentally that the seed metals which can cause cone development on ion bombarded metal targets need not to have a lower sputtering yield as widely believed but rather a higher melting point. By lowering the bombarding ion energy to near sputtering threshold values (less than 100 eV) the growth of genuine single crystal whiskers which point in all directions not related to the direction of ion incidence is observed. It is concluded that (intentional or unintentional) seed cones are the result of an interplay among whisker growth, surface movement of atoms, and the effects of sputtering. Author

A85-48516* National Aeronautics and Space Administration. Lewis Research Center, Cleveland, Ohio.
MONTE CARLO STUDY OF REVERSIBLE GROWTH OF CLUSTERS ON A SURFACE
J. SALIK (NASA, Lewis Research Center, Cleveland, OH) Physical Review B - Solid State, 3rd Series (ISSN 0556-2805), vol. 32, Aug. 1, 1985, p. 1824-1826. refs

The effect of binding energy on the growth of clusters on a two-dimensional square lattice was studied by a means of a Monte Carlo simulation. The results indicate that for binding energies higher than 0.5kT, clusters grow relative to the initial random

distribution, while for binding energies lower than 0.5 kT, clusters decompose. It was also found that at low binding energies the equilibrium percentage of atoms that are bound in clusters is linearly dependent on the binding energy. The cluster density behaved in a similar manner. This similarity reflects the fact that at low binding energies the growth proceeds mainly by the formation of new clusters rather than by an increase in the size of existing ones. Author

N85-10844*# National Aeronautics and Space Administration. Lewis Research Center, Cleveland, Ohio.
PLASMA DEPOSITED DIAMONDLIKE CARBON ON GAAS AND INP
J. D. WARNER, J. J. POUCH, S. A. ALTEROVITZ, D. C. LIU, and W. A. LANFORD (State Univ. of New York, Albany) 1984 15 p refs Proposed for presentation at the 31st Natl. Symp. of the Am. Vacuum Soc., Reno, Nev., 3-7 Dec. 1984
(NASA-TM-86870; E-2332; NAS 1.15:86870) Avail: NTIS HC A02/MF A01 CSCL 20L

The properties of diamond like carbon films grown by RF flow discharge 30 kHz plasma using methane are reported. The Cls XPS line shape of films showed localized hybrid carbon bonds as low as 40 to as high as 95 percent. Infrared spectroscopy and N(15) nuclear reaction profiling data indicated 35 to 42 percent hydrogen, depending inversely on deposition temperature. The deposition rate of films on Si falls off exponentially with substrate temperature, and nucleation does not occur above 200 C on GaAs and InP. Optical data of the films showed bandgap values of 2.0 to 2.4 eV increasing monotonically with CH4 flow rate. Author

N85-11862*# Connecticut Univ., Storrs. Dept. of Mechanical Engineering.
BIAXIAL CONSTITUTIVE EQUATION DEVELOPMENT FOR SINGLE CRYSTALS Semiannual Status Report, 6 Jan. - 6 Jul. 1984
E. H. JORDAN 1984 29 p
(Contract NAG3-512)
(NASA-CR-174056; NAS 1.26:174056) Avail: NTIS HC A03/MF A01 CSCL 20L

Current gas turbine engines utilize large single crystal superalloy components in the hot section. Structural analysis of these components requires a valid stress strain temperature constitutive equation. The goal of the program described is to create one or more models and verify these models. A constitutive equation based on an assumed slip behavior of a single slip system was formulated, programmed, and debugged. Specifically, the basic theory for a model based on aggravating slip behavior on individual slip systems was formulated and programmed and some simulations were run using assumed values of constants. In addition, a formulation allowing strain controlled simulations was completed. An approach to structural analysis of the specimen was developed. This approach uses long tube consistancy conditions and finite elements specially formulated to take advantage of the symmetry of 100 oriented specimens. R.S.F.

N85-23414*# Michigan Technological Univ., Houghton. Dept. of Chemistry and Chemical Engineering.
RAMAN STRUCTURAL STUDIES OF THE NICKEL ELECTRODE Progress Report, 20 Feb. 1984 - 20 Mar. 1985
B. C. CORNILSEN 1985 39 p refs
(Contract NAG3-519)
(NASA-CR-175619; NAS 1.26:175619) Avail: NTIS HC A03/MF A01 CSCL 20L

Raman spectroscopy is sensitive to empirically controlled nickel electrode structural variations, and has unique potential for structural characterization of these materials. How the structure relates to electrochemical properties is examined so that the latter can be more completely understood, controlled, and optimized. Electrodes were impregnated and cycled, and cyclic voltammetry is being used for electrochemical characterization. Structural variation was observed which has escaped detection using other methods. Structural changes are induced by: (1) cobalt doping, (2) the state of change or discharge, (3) the preparation conditions and type of buffer used, and (4) the formation process. Charged active mass has an NiOOH-type structure, agreeing with X-ray diffraction results. Discharged active mass, however, is not isostructural with beta-Ni(OH)2. Chemically prepared alpha phases are not isostructural either. A disordered structural model, containing point defects, is proposed for the cycled materials. This model explains K(+) incorporation. Band assignments were made and spectra interpreted for beta-Ni(OH)2, electrochemical NiOOH and chemically precipitated NiOOH. Author

N85-24961*# National Aeronautics and Space Administration. Lewis Research Center, Cleveland, Ohio.
MONTE CARLO LATTICE MODELS FOR ADSORBED POLYMER CONFORMATION
B. S. GOOD May 1985 12 p refs
(NASA-TP-2453; E-2400; NAS 1.60:2453) Avail: NTIS HC A02/MF A01 CSCL 20L

The adhesion between a polymer film and a metal surface is of great technological interest. However, the prediction of adhesion and wear properties of polymer coated metals is quite difficult because a fundamental understanding of the polymer surface interaction does not yet exist. A computer model for the conformation of a polymer molecule adsorbed on a surface is discussed. The chain conformation is assumed to be described by a partially directed random walk on a three dimensional simple cubic lattice. An attractive surface potential is incorporated into the model through the use of a random walk step probability distribution that is anisotropic in the direction normal to the attractive surface. The effects of variations in potential characteristics are qualitatively included by varying both the degree of anistropy of the step distribution and the range of the anisotropy. Polymer conformation is characterized by the average end to end distance, average radius of gyration, and average number of chain segments adsorbed on the surface. Author

N85-26406*# National Aeronautics and Space Administration. Lewis Research Center, Cleveland, Ohio.
OPTICAL PROPERTIES OF HYDROGENATED AMORPHOUS CARBON FILMS GROWN FROM METHANE PLASMA
J. J. POUCH, S. A. ALTEROVITZ, J. D. WARNER, D. C. LIU, and W. A. LANFORD (State Univ. of New York, Albany) 18 Apr. 1985 8 p refs Presented at Spring Meeting of the Mater. Res. Soc., San Francisco, 15-18 Apr. 1985
(NASA-TM-86995; E-2541; NAS 1.15:86995) Avail: NTIS HC A02/MF A01 CSCL 20L

A 30 kHz ac glow discharge formed from methane gas was used to grow carbon films on InP substrates. Both the growth rate, and the realitive Ar ion sputtering rate at 3 keV varied monotonically with deposition power. Results from the N-15 nuclear reaction profile experiments indicated a slight drop in the hydrogen concentration as more energy was dissipated in the ac discharge. Values for the index of refraction and extinction coefficient ranged from 1.721 to 1.910 and 0 to -0.188, respectively. Optical bandgaps as high as 2.34 eV were determined. Author

77

THERMODYNAMICS AND STATISTICAL PHYSICS

Includes quantum mechanics; and Bose and Fermi statistics.

N85-16663*# National Aeronautics and Space Administration. Lewis Research Center, Cleveland, Ohio.
COMPUTER PROGRAM FOR CALCULATION OF COMPLEX CHEMICAL EQUILIBRIUM COMPOSITIONS AND APPLICATIONS. SUPPLEMENT 1: TRANSPORT PROPERTIES
S. GORDON (Gordon (Sanford) and Associates), B. MCBRIDE, and F. J. ZELEZNIK Oct. 1984 26 p refs
(NASA-TM-86885; E-2348; NAS 1.15:86885) Avail: NTIS HC A03/MF A01 CSCL 20M

An addition to the computer program of NASA SP-273 is given that permits transport property calculations for the gaseous phase. Approximate mixture formulas are used to obtain viscosity and frozen thermal conductivity. Reaction thermal conductivity is obtained by the same method as in NASA TN D-7056. Transport properties for 154 gaseous species were selected for use with the program. Author

N85-22204*# National Aeronautics and Space Administration. Lewis Research Center, Cleveland, Ohio.
IDEAL GAS THERMODYNAMIC PROPERTIES FOR THE PHENYL, PHENOXY, AND O-BIPHENYL RADICALS
A. BURCAT, F. J. ZELEZNIK, and B. J. MCBRIDE Jan. 1985 22 p refs
(NASA-TM-83800; E-2303; NAS 1.15:83800) Avail: NTIS HC A02/MF A01 CSCL 20M

Ideal gas thermodynamic properties of the phenyl and o-biphenyl radicals, their deuterated analogs and the phenoxy radical were calculated to 5000 K using estimated vibrational frequencies and structures. The ideal gas thermodynamic properties of benzene, biphenyl, their deuterated analogs and phenyl were also calculated. Author

82

DOCUMENTATION AND INFORMATION SCIENCE

Includes information storage and retrieval technology; micrography; and library science.

N85-22255*# National Aeronautics and Space Administration. Lewis Research Center, Cleveland, Ohio.
BIBLIOGRAPHY OF LEWIS RESEARCH CENTER TECHNICAL PUBLICATIONS ANNOUNCED IN 1983
Jun. 1984 345 p
(NASA-TM-83693; E-2151; NAS 1.15:83693) Avail: NTIS HC A16/MF A01 CSCL 05B

This compilation of abstracts describes and indexes over 800 technical publications that resulted from the scientific and engineering work performed and managed by the Lewis Research Center in 1983. Announced in the 1983 issues of STAR (Scientific and Technical Aerospace Reports) and/or IAA (International Aerospace Abstracts), the documents cited include research reports, journal articles, conference presentations, patents and patent applications, and theses. A.R.H.

N85-28876*# National Aeronautics and Space Administration. Lewis Research Center, Cleveland, Ohio.
BIBLIOGRAPHY OF LEWIS RESEARCH CENTER TECHNICAL PUBLICATIONS ANNOUNCED IN 1984
May 1985 322 p
(NASA-TM-87012; E-2556; NAS 1.15:87012) Avail: NTIS HC A14/MF A01 CSCL 05B

This compilation of abstracts describes and indexes the technical reporting that resulted from the scientific and engineering work performed and managed by the Lewis Research Center in 1984. All the publications were announced in the 1984 issues of STAR (Scientific and Technical Aerospace Reports) and/or IAA (International Aerospace Abstracts). Included are research reports, journal articles, conference presentations, patents and patent applications, and theses. Author

85

URBAN TECHNOLOGY AND TRANSPORTATION

Includes applications of space technology to urban problems; technology transfer; technology assessment; and surface and mass transportation.

N85-12808*# Mechanical Technology, Inc., Latham, N. Y.
DEVELOPMENT OF GAS-LUBRICATED PISTONS FOR HEAVY DUTY DIESEL ENGINE TECHNOLOGY PROGRAM Final Report
W. SHAPIRO Jul. 1984 192 p refs
(Contract DEN3-309; DE-AI01-80CS-50194)
(NASA-CR-174746; NAS 1.26:174746; MTI-84TR58) Avail: NTIS HC A09/MF A01 CSCL 13F

Static testing of a segmented, gas-lubricated, piston-ring was accomplished. The ring utilizes high-pressure gas generated during the diesel cycle to energize a hydrostatic gas film between the piston and cylinder liner. The configuration was deficient in overall performance, because all segments of a ring set failed to form a fluid-film simultaneously, when exposed to internal preload. The difficulty was traced to the moment balance required to prevent the segments from overturning and contacting the cylinder walls. Some individual sectors formed a film and performed well in every respect including load capability to 6,000 N. These results produce optimism as to the ultimate feasibility of hydrostatic, gas-lubricated piston rings. In addition to test results, the principles of operation, and theoretical developments are presented. Breathable liner concepts are suggested for future consideration. In these configurations, solid hydrostatic pistons are coupled with flexible liners that elastically deform to form a gas-film under hydrostatic pressurization. Breathable liners afford the mechanical simplicity required for mass produced engines, and initial examination indicates satisfactory operation. Author

N85-13692*# National Aeronautics and Space Administration. Lewis Research Center, Cleveland, Ohio.
OVERVIEW OF WASTE HEAT UTILIZATION SYSTEMS
M. M. BAILEY 1984 12 p refs Presented at the 22nd Automotive Technol. Development Contractors' Coordination Meeting, Dearborn, Mich., 29 Oct. 1 Nov. 1984; sponsored by DOE
(NASA-TM-86901; DOE/NASA/50194-41; NAS 1.15:86901)
Avail: NTIS HC A02/MF A01 CSCL 10B

The heavy truck diesel engine rejects a significant fraction of its fuel energy in the form of waste heat. Historically, the Department of Energy has supported technology efforts for utilization of the diesel exhaust heat. Specifically, the Turbocompound and the Organic Rankine Cycle System (ORCS) have demonstrated that meaningful improvements in highway fuel economy can be realized through waste heat utilization. For heat recovery from the high temperature exhaust of future adiabatic diesel engines, the DOE/NASA are investigating a variety of alternatives based on the Rankine, Brayton, and Stirling power

cycles. Initial screening results indicate that systems of this type offer a fuel savings advantage over the turbocompound system. Capital and maintenance cost projections, however, indicate that the alternative power cycles are not competitive on an economic payback basis. Plans call for continued analysis in an attempt to identify a cost effective configuration with adequate fuel savings potential. Author

N85-16698*# General Electric Co., Philadelphia, Pa. Advanced Energy Programs Dept.
TRANSFORMATION TOUGHENED CERAMICS FOR THE HEAVY DUTY DIESEL ENGINE TECHNOLOGY PROGRAM Final Report
S. MUSIKANT, E. FEINGOLD, H. RAUCH, and S. SAMANTA Oct. 1984 34 p refs
(Contract DEN3-339; DE-AI01-80CS-5019)
(NASA-CR-174689; DOE/NASA/0339-1; NAS 1.26:174689)
Avail: NTIS HC A03/MF A01 CSCL 13F

The objective of this program is to develop an advanced high temperature oxide structural ceramic for application to the heavy duty diesel engine. The approach is to employ transformation toughening by additions of ZrO.5HfO.5O2 solid solution to the oxide ceramics, mullite (2Al2O3S2SiO2) and alumina (Al2O3). The study is planned for three phases, each 12 months in duration. This report covers Phase 1. During this period, processing techniques were developed to incorporate the ZrO.5HfO.5O2 solid solution in the matrices while retaining the necessary metastable tetragonal phase. Modulus of rupture and of elasticity, coefficient of thermal expansion, fracture toughness by indent technique and thermal diffusivity of representative specimens were measured. In Phase 2, the process will be improved to provide higher mechanical strength and to define the techniques for scale up to component size. In Phase 3, full scale component prototypes will be fabri-]cated. Author

N85-16699*# Integral Technologies, Inc., Westmont, Ill.
METHODS FOR HEAT TRANSFER AND TEMPERATURE FIELD ANALYSIS OF THE INSULATED DIESEL Interim Report
T. MOREL, P. N. BLUMBERG, E. F. FORT, and R. KERIBAR Aug. 1984 274 p refs
(Contract DEN3-342; DE-AI01-80CS-50194)
(NASA-CR-174783; DOE/NASA/0342-1; NAS 1.26:174783)
Avail: NTIS HC A12/MF A01 CSCL 13F

Work done during phase 1 of a three-year program aimed at developing a comprehensive heat transfer and thermal analysis methodology oriented specifically to the design requirements of insulated diesel engines is reported. The technology developed in this program makes possible a quantitative analysis of the low heat rejection concept. The program is comprehensive in that it addresses all the heat transfer issues that are critical to the successful development of the low heat rejection diesel engine: (1) in-cylinder convective and radiative heat transfer; (2) cyclic transient heat transfer in thin solid layers at component surfaces adjacent to the combustion chamber; and (3) steady-state heat conduction in the overall engine structure. The Integral Technologies, Inc. (ITI) program is comprised of a set of integrated analytical and experimental tasks. A detailed review of the ITI program approach is provided, including the technical issues which underlie it and a summay of the methods that were developed. R.S.F.

N85-18831*# Garrett Turbine Engine Co., Phoenix, Ariz. Engineering Staff.
ADVANCED GAS TURBINE (AGT) POWERTRAIN SYSTEM DEVELOPMENT FOR AUTOMOTIVE APPLICATIONS Semiannual Progress Report, Jul. - Dec. 1983
Jun. 1984 70 p refs
(Contract DEN3-167)
(NASA-CR-174809; DOE/NASA/0167-8; NAS 1.26:174809; GARRETT-31-3725(8); SAPR-8) Avail: NTIS HC A04/MF A01 CSCL 13F

Rotor dynamic instability investigations were conducted. Forward ball bearing hydraulic mount configurations were tested with little effect. Trial assembly of S/N 002 ceramic engine was initiated. Impeller design activities were completed on the straight line element (SLE) blade definition to address near-net-shape powder metal die forging. Performance characteristics of the Baseline Test 2A impeller were closely preserved. The modified blading design has been released for tooling procurement. Developmental testing of the diffusion flame combustor (DFC) for initial use in the S/N 002 2100 F ceramic structures engine was completed. A natural gas slave preheater was designed and fabricated. Preliminary regenerator static seal rig testing showed a significant reduction in leakage and sensitivity to stack height. Ceramic screening tests were completed and two complete sets of ceramic static structures were qualified for engine testing. Efforts on rotor dynamics development to resolve subsynchronous motion were continued. A.S.B.

N85-19894*# Kumm (Emerson L.), Tempe, Ariz.
FEASIBILITY DEMONSTRATION OF A NOVEL, FLAT-BELT, CONTINUOUSLY VARIABLE TRANSMISSION OR AUTOMOTIVE AND ELECTRIC-HYBRID VEHICLE APPLICATION Final Report
E. L. KUMM May 1984 138 p Prepared for JPL
(Contract DEN3-272; JPL-956602)
(NASA-CR-174430; JPL-9950-945; NAS 1.26:174430; DOE/CS-54209/20; KI-P-1008) Avail: NTIS HC A07/MF A01 CSCL 13F

The performance of a flat belt continuously variable transmission (CVT) over its design input speed, output torque, and speed ratio range was determined. The arrangement studied reduces the required width of the pulleys and their actuators as compared to pulleys whose sheaves are moved axially by actuators to vary the belt radius ratio or pulley speed ratio. Topics covered included: (1) flat belt transmission design; (2) variable speed assembly fabrication; (3) critical components; (4) variable speed assembly test stand; (5) test stand control rigs; (6) transmission tests; and (7) improvement assessment of the current design. Results show that the flat belt CVT appears to have significant advantages in reducing the size and weight of the automotive CVT as well as giving high operating efficiencies. A.R.H.

N85-19895*# National Aeronautics and Space Administration. Lewis Research Center, Cleveland, Ohio.
INITIAL TESTING OF A VARIABLE-STROKE STIRLING ENGINE Final Report
L. G. THIEME Feb. 1985 28 p refs Presented at the 21st Automotive Technol. Develop. Contractors' Coordination Meeting, Dearborn, Mich., 14-17 Nov. 1983
(Contract DE-AI01-77CS-51040)
(NASA-TM-86875; DOE/NASA/51040-58; E-2336; NAS 1.15:86875) Avail: NTIS HC A03/MF A01 CSCL 13F

In support of the U.S. Department of Energy's Stirling Engine Highway Vehicle Systems Program, NASA Lewis Research Center is evaluating variable-stroke control for Stirling engines. The engine being tested is the Advenco Stirling engine; this engine was manufactured by Philips Research Laboratories of the Netherlands and uses a variable-angle swash-plate drive to achieve variable stroke operation. The engine is described, initial steady-state test data taken at Lewis are presented, a major drive system failure and subsequent modifications are described. Computer simulation results are presented to show potential part-load efficiency gains with variable-stroke control. Author

N85-27769*# National Aeronautics and Space Administration. Lewis Research Center, Cleveland, Ohio.
OVERVIEW OF THE 1985 NASA LEWIS RESEARCH CENTER SP-100 FREE-PISTON STIRLING ENGINE ACTIVITIES
J. SLABY 1985 21 p refs Presented at the 20th Intersoc. Energy Conversion Engr. Conf., Miami Beach, Fla., 18-23 Aug. 1985; cosponsored by ASME, ANS, SAE, IEEE, AIAA, ACS, and AIChE
(Contract DE-AI05-82OR-1005)
(NASA-TM-87028; DOE/NASA/1005-5; NAS 1.15:87028; E-2584)
Avail: NTIS HC A02/MF A01 CSCL 10B

This effort is keyed on the design, fabrication, assembly, and testing of a 25 kWe Stirling space-power technology-feasibility

demonstrator engine. Another facet of the SP-100 project covers the status of a 9000-hr endurance test conducted on a 2 kWe free-piston Stirling/linear alternator system employing hydrostatic gas bearings. Dynamic balancing of the RE-1000 engine (a 1 kWe free-piston Stirling engine) using a passive dynamic absorber will be discussed along with the results of a parametric study showing the relationships of Stirling power converter specific weight and efficiency as functions of Stirling engine heater to cooler temperature ratio. Planned tests will be described covering a hydrodynamic gas bearing concept for potential SP-100 application. Author

N85-32043*# National Aeronautics and Space Administration. Lewis Research Center, Cleveland, Ohio.
COMPARATIVE EVALUATION OF THREE ALTERNATIVE POWER CYCLES FOR WASTE HEAT RECOVERY FROM THE EXHAUST OF ADIABATIC DIESEL ENGINES Final Report
M. M. BAILEY Jul. 1985 27 p refs
(Contract DE-AI01-80CS-50194)
(NASA-TM-86953; E-2196; DOE/NASA/50194-43; NAS 1.15:86953) Avail: NTIS HC A03/MF A01 CSCL 13F

Three alternative power cycles were compared in application as an exhaust-gas heat-recovery system for use with advanced adiabatic diesel engines. The power cycle alternatives considered were steam Rankine, organic Rankine with RC-1 as the working fluid, and variations of an air Brayton cycle. The comparison was made in terms of fuel economy and economic payback potential for heavy-duty trucks operating in line-haul service. The results indicate that, in terms of engine rated specific fuel consumption, a diesel/alternative-power-cycle engine offers a significant improvement over the turbocompound diesel used as the baseline for comparison. The maximum imporvement resulted from the use of a Rankine cycle heat-recovery system in series with turbocompounding. The air Brayton cycle alternatives studied, which included both simple-cycle and compression-intercooled configurations, were less effective and provided about half the fuel consumption improvement of the Rankine cycle alternatives under the same conditions. Capital and maintenance cost estimates were also developed for each of the heat-recovery power cycle systems. These costs were integrated with the fuel savings to identify the time required for net annual savings to pay back the initial capital investment. The sensitivity of capital payback time to arbitrary increases in fuel price, not accompanied by corresponding hardware cost inflation, was also examined. The results indicate that a fuel price increase is required for the alternative power cycles to pay back capital within an acceptable time period.
Author

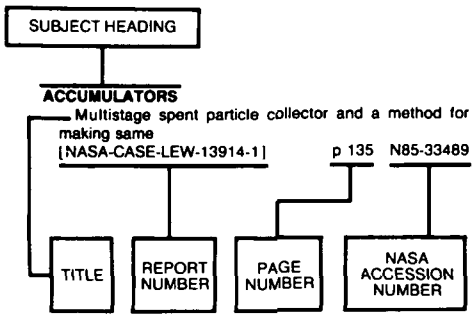
99

GENERAL

N85-17928*# National Aeronautics and Space Administration. Lewis Research Center, Cleveland, Ohio.
RESEARCH AND TECHNOLOGY HIGHLIGHTS OF THE LEWIS RESEARCH CENTER Annual Report, 1984
1984 52 p
(NASA-TM-86899; NAS 1.15:86899) Avail: NTIS HC A04/MF A01 CSCL 05A

Highlights of research accomplishments of the Lewis Research Center for fiscal year 1984 are presented. The report is divided into four major sections covering aeronautics, space communications, space technology, and materials and structures. Six articles on energy are included in the space technology section. B.W.

Typical Subject Index Listing



The subject heading is the key to the subject content of the document. Titles, report numbers, and accession numbers of pertinent documents are provided under each subject heading. When the title is insufficiently descriptive of the document content, a title extension has been added, separated from the title by three hyphens. The report number helps to indicate the type of document cited (e.g., NASA report, NASA translation, NASA contractor report). The NASA accession number is the number by which the document abstracts are arranged in this journal and by which the document is sold or requested. The titles, with title extensions if present, are arranged under each subject heading in ascending accession number order. The subject headings have been selected from the latest revision of the *NASA Thesaurus* (NASA SP-7051).

A

ABERRATION
Holographic optical system for aberration corrections in laser Doppler velocimetry p 123 A85-48659

ABSORBERS (MATERIALS)
Measured acoustic properties of variable and low density bulk absorbers
[NASA-TM-87065] p 177 N85-30770

ABSORPTIVITY
Aluminum work function: Effect of oxidation, mechanical scraping and ion bombardment
[NASA-TM-87079] p 78 N85-34265

ABSTRACTS
Bibliography of Lewis Research Center technical publications announced in 1984
[NASA-TM-87012] p 184 N85-28876

ACCELERATED LIFE TESTS
Long life nickel electrodes for a nickel-hydrogen cell. III - Results of an accelerated test and failure analyses p 156 A85-45391

ACCELERATION (PHYSICS)
A unified relation for cavitation erosion p 109 A85-24445

ACCUMULATORS
Multistage spent particle collector and a method for making same
[NASA-CASE-LEW-13914-1] p 135 N85-33489

ACCURACY
Strainrange partitioning - A total strain range version --- for creep fatigue life prediction by summing inelastic and elastic strain-range-life relations for two Ni base superalloys p 64 A85-11603
Assessment of three-dimensional inviscid codes and loss calculations for turbine aerodynamic computations
[ASME PAPER 84-GT-187] p 4 A85-32961
Stability, accuracy, and efficiency of some underintegrated methods in finite element computations p 172 A85-50073
Reducing numerical diffusion for incompressible flow calculations
[NASA-TM-83621] p 24 N85-14840

ACEE PROGRAM
Measurement and prediction of Energy Efficient Engine noise
[AIAA PAPER 84-2284] p 13 A85-13954
Energy efficient engine combustor test hardware detailed design report
[NASA-CR-167945] p 18 N85-10950
Energy efficient engine component development and integration program
[NASA-CR-170034] p 22 N85-10990
Energy efficient engine. Volume 2. Appendix A: Component development and integration program
[NASA-CR-173085] p 22 N85-10991
Energy efficient engine. Volume 1: Component development and integration program
[NASA-CR-173084] p 22 N85-10992
Energy efficient engine. Low pressure turbine test hardware detailed design report
[NASA-CR-167956] p 22 N85-10994
Energy efficient engine high pressure turbine test hardware detailed design report
[NASA-CR-167955] p 23 N85-10995
Energy efficient engine high pressure turbine ceramic shroud support technology report
[NASA-CR-168036] p 23 N85-10996
Energy efficient engine ICLS engine bearings, drives and configuration: Detail design report
[NASA-CR-167871] p 23 N85-10997
Energy efficient engine. High pressure compressor detail design report
[NASA-CR-165558] p 23 N85-10998
Energy efficient engine high-pressure turbine component rig performance test report
[NASA-CR-168189] p 30 N85-29955
Energy efficient engine integrated core/low spool test hardware design report
[NASA-CR-168137] p 31 N85-29956
Energy Efficient Engine (E3) controls and accessories detail design report
[NASA-CR-168017] p 31 N85-29957
Energy efficient engine component development and integration program
[NASA-CR-172846] p 31 N85-29958
Energy efficient engine. Fan and quarter-stage component performance report
[NASA-CR-168070] p 33 N85-34141
Energy efficient engine, high pressure turbine thermal barrier coating. Support technology report
[NASA-CR-168037] p 34 N85-35199

ACETYL COMPOUNDS
Velocity visualization in gas flows using laser-induced phosphorescence of biacetyl p 121 A85-21695

ACOUSTIC ATTENUATION
Interaction of finite-amplitude sound with air-filled porous materials
[NASA-CR-174885] p 177 N85-27637

ACOUSTIC EXCITATION
An experimental study of tone excited heated jets
[AIAA PAPER 84-2341] p 172 A85-10882
Some unique experiments on receptivity --- for forced disturbances entering shear flow
[AIAA PAPER 85-0533] p 174 A85-25932
Acoustic control of free jet mixing
[AIAA PAPER 85-0569] p 109 A85-25951
The response of Helmholtz resonators to external excitation. I - Single resonators p 174 A85-26915
Preliminary analysis of tone-excited two-stream jet velocity decay
[NASA-TM-86951] p 8 N85-21114

ACOUSTIC IMPEDANCE
Interaction of finite-amplitude sound with air-filled porous materials
[NASA-CR-174885] p 177 N85-27637

ACOUSTIC MEASUREMENT
Acoustic structure and propagation in highly porous, layered, fibrous materials p 173 A85-12301
Analytical and physical modeling program for the NASA Lewis Research Center's Altitude Wind Tunnel (AWT)
[NASA-TM-86919] p 35 N85-15757

ACOUSTIC MICROSCOPES
Reliability of void detection in structural ceramics using scanning laser acoustic microscopy
[NASA-TM-87035] p 138 N85-32337

ACOUSTIC PROPAGATION
Time dependent wave envelope finite difference analysis of sound propagation
[AIAA PAPER 84-2285] p 173 A85-16102
Oscillatory conductive heat transfer for a fiber in an ideal gas p 109 A85-26077

ACOUSTIC PROPERTIES
Acoustic structure and propagation in highly porous, layered, fibrous materials p 173 A85-12301
Measured acoustic properties of variable and low density bulk absorbers
[NASA-TM-87065] p 177 N85-30770

ACOUSTIC SCATTERING
The scattering of ultrasonic third sound from substrate surface defects p 174 A85-36047

ACOUSTO-OPTICS
Two-frequency laser-induced fluorescence technique for rapid velocity-field measurements in gas flows p 121 A85-32294
Optical linear algebra processors - Noise and error-source modeling p 169 A85-36727

ACTIVATION
CO adsorption on (111) and (100) surfaces of the Pt sub 3 Ti alloy. Evidence for parallel binding and strong activation of CO
[NASA-CR-176077] p 77 N85-32176

ACTIVE CONTROL
Energy efficient engine. Low pressure turbine test hardware detailed design report
[NASA-CR-167956] p 22 N85-10994
Vibration control of rotor shaft
[NASA-TM-87053] p 133 N85-29292

ADA (PROGRAMMING LANGUAGE)
The use of Ada in distributed simulations p 169 A85-28612
Moving target, distributed, real-time simulation using Ada p 170 A85-34131

ADDITIVES
Methanol as a soot reducer in a turbulent swirling burner
[ASME PAPER 84-JPGC-GT-2] p 61 A85-23192
Radiation damage and defect behavior in ion-implanted, lithium counterdoped silicon solar cells p 182 A85-35698
Dopant effect of yttrium and the growth and adherence of alumina on nickel-aluminum alloys p 82 A85-40973
Fracture of yttria-doped, sintered reaction-bonded silicon nitride
[ACS PAPER 7-J3-84] p 82 A85-42797
Effect of lubricant extreme-pressure additives on surface fatigue life of AISI 9310 spur gears
[NASA-TP-2408] p 130 N85-13234
Effect of five lubricants on life of AISI 9310 spur gears
[NASA-TP-2419] p 123 N85-16099
Characterization of lubricated bearing surfaces operated under high loads
[NASA-TM-86964] p 88 N85-21357
The effects of lithium counterdoping on radiation damage and annealing in n(+)p silicon solar cells p 50 N85-22586
Jet fuel instability mechanisms
[NASA-CR-175856] p 93 N85-28127
Lubricant and additive effects on spur gear fatigue life
[NASA-TM-87044] p 133 N85-28373

ADHESION
Universal binding energy relations in metallic adhesion
[NASA-TM-86889] p 72 N85-12132
Fundamental tribological properties of ceramics
[NASA-TM-86915] p 85 N85-15893
Humidity effects on adhesion of nickel-zinc ferrite in elastic contact with magnetic tape and itself
[NASA-TP-2449] p 88 N85-21359
Monte Carlo lattice models for adsorbed polymer conformation
[NASA-TP-2453] p 183 N85-24961

C-3

ADHESION TESTS
Mechanical property measurements of plasma-sprayed thermal-barrier coatings subjected to oxidation p 81 A85-29729

ADHESIVE BONDING
Fracture of composite-adhesive-composite systems p 141 A85-27935
Ceramic microstructure and adhesion p 82 A85-40384
Ceramic microstructure and adhesion [NASA-TM-83804] p 83 N85-10186
Molecular orbital studies in oxidation: Sulfate formation and metal-metal oxide adhesion [NASA-CR-176070] p 77 N85-32174

ADIABATIC EQUATIONS
An interactive computer code for calculation of gas-phase chemical equilibrium (EQLBRM) [NASA-CR-168337] p 18 N85-10948

ADSORPTION
Adsorption of O2, SO2, and SO3 on nickel oxide. Mechanism for sulfate formation [NASA-CR-176072] p 77 N85-32175
CO adsorption on (111) and (100) surfaces of the Pt sub 3 Ti alloy. Evidence for parallel binding and strong activation of CO *[NASA-CR-176077] p 77 N85-32176*

AEROACOUSTICS
Acoustic pressures emanating from a turbomachine stage [AIAA PAPER 84-2325] p 2 A85-10870
Effect of airfoil mean loading on convected gust interaction noise [AIAA PAPER 84-2324] p 173 A85-13955
Modelling of wind tunnel wall effects on the radiation characteristics of acoustic sources [AIAA PAPER 84-2364] p 174 A85-16104
A theoretical prediction of the acoustic pressure generated by turbulence-flame front interactions [ASME PAPER 84-WA/NCA-11] p 174 A85-39909
Turbofan noise generation. Volume 2: Computer programs [NASA-CR-167952] p 175 N85-11791

AEROASSIST
OTV Propulsion Issues [NASA-CP-2347] p 37 N85-16989

AERODYNAMIC CHARACTERISTICS
Progress in development of a Navier-Stokes solver for evaluation of iced airfoil performance *[AIAA PAPER 85-0410] p 3 A85-19731*
Analytical modeling of circuit aerodynamics in the new NASA Lewis Altitude Wind Tunnel [AIAA PAPER 85-0380] p 3 A85-26389
Icing flight research - Aerodynamic effects of ice and ice shape documentation with stereo photography [AIAA PAPER 85-0468] p 11 A85-30192
Low-speed aerodynamic test of an axisymmetric supersonic inlet with variable cowl slot [AIAA PAPER 85-1210] p 5 A85-40819
Noise constraints effecting optimal propeller designs [SAE PAPER 850871] p 7 A85-50106
Design and wind tunnel evaluation of a symmetric airfoil series for large wind turbine applications [NASA-CR-174764] p 7 N85-10919
Energy efficient engine ICLS Nacelle detail design report [NASA-CR-167870] p 22 N85-10993
Analytical modeling of circuit aerodynamics in the new NASA Lewis wind tunnel [NASA-TM-86912] p 8 N85-15688
Icing flight research: Aerodynamic effects of ice and ice shape documentation with stereo photography [NASA-TM-86906] p 12 N85-18049
The Altitude Wind Tunnel (AWT): A unique facility for propulsion system and adverse weather testing [NASA-TM-86921] p 35 N85-18067
Noise constraints effecting optimal propeller designs [NASA-TM-86967] p 8 N85-19923
Large-scale Advanced Propfan (LAP) performance, acoustic and weight estimation, January, 1984 [NASA-CR-174782] p 9 N85-22368
Low-speed aerodynamic test of an axisymmetric supersonic inlet with variable cowl slot [NASA-TM-87039] p 28 N85-26710
Wake effects on the aerodynamic performance of horizontal axis wind turbines [NASA-CR-174920] p 162 N85-29364
Heat transfer in aeropropulsion systems [NASA-TM-87066] p 119 N85-31444

AERODYNAMIC COEFFICIENTS
Analytical determination of propeller performance degradation due to ice accretion [AIAA PAPER 85-0339] p 14 A85-20867
Optimization of cascade blade mistuning. I - Equations of motion and basic inherent properties p 16 A85-42365

AERODYNAMIC CONFIGURATIONS
Energy efficient engine ICLS Nacelle detail design report [NASA-CR-167870] p 22 N85-10993
Performance comparison between NACA 23024 and NACA 64(3)-618 airfoil configurated rotors for horizontal-axis wind turbines [NASA-TM-83471] p 163 N85-30477

AERODYNAMIC DRAG
Preliminary assessment of power-generating tethers in space and of propulsion for their orbit maintenance p 37 N85-22520
Ice shapes and the resulting drag increase for a NACA 0012 airfoil [NASA-TM-83556] p 11 N85-27839

AERODYNAMIC HEATING
Unsteady heat transfer due to time-dependent free stream velocity p 117 N85-27947

AERODYNAMIC LOADS
Effect of airfoil mean loading on convected gust interaction noise [AIAA PAPER 84-2324] p 173 A85-13955
A linearized unsteady aerodynamic analysis for transonic cascades p 3 A85-20744
Overview of aerothermodynamic loads definition study p 51 N85-27942

AERODYNAMIC NOISE
Effect of airfoil mean loading on convected gust interaction noise [AIAA PAPER 84-2324] p 173 A85-13955
Noise constraints effecting optimal propeller designs [SAE PAPER 850871] p 7 A85-50106
Noise constraints effecting optimal propeller designs [NASA-TM-86967] p 8 N85-19923
Noise transmission loss of a rectangular plate in an infinite baffle [NASA-TP-2398] p 176 N85-22109
Large-scale Advanced Propfan (LAP) performance, acoustic and weight estimation, January, 1984 [NASA-CR-174782] p 9 N85-22368

AERODYNAMIC STABILITY
Effects of friction dampers on aerodynamically unstable rotor stages p 14 A85-21866
Optimization of cascade blade mistuning. II - Global optimum and numerical optimization p 16 A85-45715
Aerodynamic detuning analysis of an unstalled supersonic turbofan cascade [NASA-TM-87001] p 9 N85-26670

AERODYNAMIC STALLING
Stall recovery control strategy methodology and results [AIAA PAPER 85-1433] p 16 A85-40841

AERODYNAMICS
Energy efficient engine combustor test hardware detailed design report [NASA-CR-167945] p 18 N85-10950
Inverse design technique for cascades [NASA-CR-3836] p 7 N85-12008
Aerodynamic analysis of a horizontal axis wind turbine by use of helical vortex theory. Volume 1: Theory [NASA-CR-168054] p 9 N85-29916

AEROELASTICITY
Flutter of turbofan rotors with mistuned blades p 139 A85-12716
Flutter and forced response of mistuned rotors using standing wave analysis p 139 A85-12721
Flutter of swept fan blades [ASME PAPER 84-GT-138] p 141 A85-32962
Vibration and flutter of mistuned bladed-disk assemblies p 16 A85-45854
Structural response of a rotating bladed disk to rotor whirl [NASA-CR-175605] p 27 N85-22391

AERONAUTICAL ENGINEERING
Bibliography of Lewis Research Center technical publications announced in 1983 [NASA-TM-83693] p 184 N85-22255
Future directions in aeropropulsion technology [NASA-TM-87010] p 1 N85-23685
Alternatives for jet engine control [NASA-CR-175832] p 29 N85-26714
Alternatives for jet engine control [NASA-CR-175833] p 29 N85-26715

AERONAUTICS
Research and technology highlights of the Lewis Research Center [NASA-TM-86899] p 186 N85-17928

AEROSOLS
Fast laser-induced aerosol formation for visualization of gas flows p 121 A85-31113

AEROSPACE ENGINEERING
PMR polyimide composites for aerospace applications --- Polymerization of Monomer Reactants p 55 A85-21520
Bibliography of Lewis Research Center technical publications announced in 1983 [NASA-TM-83693] p 184 N85-22255

AEROSPACE ENVIRONMENTS
Ion beam sputter-deposited thin film coatings for protection of spacecraft polymers in low Earth orbit [NASA-TM-87051] p 91 N85-30137

AEROSPACE SYSTEMS
High temperature metal and ceramic composites p 55 A85-37483

AEROTHERMODYNAMICS
Application of viscous and inviscid computation methods for rocket turbopump systems [SAE PAPER 841522] p 110 A85-39257
Future fundamental combustion research for aeropropulsion systems [AIAA PAPER 85-1398] p 16 A85-42671
Heat transfer results and operational characteristics of the NASA Lewis Research Center Hot Section Cascade Test Facility [NASA-TM-86890] p 114 N85-15133
Analytical and physical modeling program for the NASA Lewis Research Center's Altitude Wind Tunnel (AWT) [NASA-TM-86919] p 35 N85-15757
Combustion research for gas turbine engines *[NASA-TM-86963] p 26 N85-21164*
Future fundamental combustion research for aeropropulsion systems [NASA-TM-87049] p 30 N85-27870
Structural Integrity and Durability of Reusable Space Propulsion Systems [NASA-CP-2381] p 51 N85-27941
Overview of aerothermodynamic loads definition study p 51 N85-27942

AGING (MATERIALS)
Ten year environmental test of glass fiber/epoxy pressure vessels [AIAA PAPER 85-1198] p 56 A85-47022
Ten year environmental test of glass fiber/epoxy pressure vessels [NASA-TM-87058] p 58 N85-30034
Thermomechanical deformation in the presence of metallurgical changes p 150 N85-31533

AILERONS
Aileron controls for wind turbine applications p 157 A85-45513
Aileron controls for wind turbine applications [NASA-TM-86867] p 158 N85-11458
Shutdown characteristics of the Mod-0 wind turbine with aileron controls [NASA-TM-86918] p 159 N85-16299
Reflection plane tests of a wind turbine blade tip section with ailerons [NASA-TM-87018] p 165 N85-34444

AIR FLOW
Swirling flows in typical combustor geometries [AIAA PAPER 85-0184] p 108 A85-19574
A stagnation pressure probe for droplet-laden air flow [AIAA PAPER 85-0330] p 108 A85-19672
Contingency power concepts for helicopter turboshaft engine p 15 A85-32005
Heat transfer enhancement in channels with turbulence promoters [ASME PAPER 84-WA/HT-72] p 111 A85-39900
Internal combustion engine combustion chamber process studies at NASA Lewis Research Center p 112 A85-45856
Turbine heat transfer p 19 N85-10964
Energy efficient engine. High pressure compressor detail design report [NASA-CR-165558] p 23 N85-10998
Liquid fuel spray processes in high-pressure gas flow [NASA-TM-86944] p 115 N85-21570

AIR INTAKES
Low-speed aerodynamic test of an axisymmetric supersonic inlet with variable cowl slot [AIAA PAPER 85-1210] p 5 A85-40819
Low-speed aerodynamic test of an axisymmetric supersonic inlet with variable cowl slot [NASA-TM-87039] p 28 N85-26710

AIR JETS
The performance of jet noise suppression devices for industrial applications p 175 A85-42563
Density effects on jet characteristics in confined swirling flow p 112 A85-45283
Flow visualization study of the effect of injection hole geometry on an inclined jet in crossflow [NASA-TM-86936] p 115 N85-20269

AIR TRAFFIC
MERIT: A man/computer data management and enhancement system for upper air nowcasting/forecasting in the United States --- Minimum Energy Routes using Interactive Techniques (MERIT) p 167 N85-10558

AIRBORNE/SPACEBORNE COMPUTERS
Satellite baseband processor test performance summary p 95 A85-14434

AIRCRAFT COMPARTMENTS
Simultaneous cabin and ambient ozone measurements on two Boeing 747 airplanes. Volume 3: October 1978 - July 1979
[NASA-TM-86883] p 167 N85-21872
AIRCRAFT CONTROL
High-temperature optically activated GaAs power switching for aircraft digital electronic control
[NASA-CR-174711] p 34 N85-12901
AIRCRAFT DESIGN
Noise constraints effecting optimal propeller designs
[SAE PAPER 850871] p 7 A85-50106
Observations from varying the lift and drag inputs to a noise prediction method for supersonic helical tip speed propellers
[NASA-TM-83797] p 175 N85-10788
Energy efficient engine component development and integration program
[NASA-CR-169496] p 22 N85-10989
Energy efficient engine component development and integration program
[NASA-CR-170034] p 22 N85-10990
Energy efficient engine. Volume 2. Appendix A: Component development and integration program
[NASA-CR-173085] p 22 N85-10991
Study of advanced fuel system concepts for commercial aircraft and engines
[NASA-CR-174752] p 93 N85-19176
Noise constraints effecting optimal propeller designs
[NASA-TM-86967] p 8 N85-19923
Lubrication and performance of high-speed rolling-element bearings
[NASA-TM-86958] p 131 N85-21658
AIRCRAFT ENGINES
The role of modern control theory in the design of controls for aircraft turbine engines p 13 A85-13627
Comparison of scaled model data to full size energy efficient engine test results
[AIAA PAPER 84-2281] p 13 A85-13953
Vibration and flutter of mistuned bladed-disk assemblies p 16 A85-45854
A real-time FORTRAN implementation of a sensor failure detection, isolation and accommodation algorithm p 171 A85-47704
Turbine Engine Hot Section Technology (HOST)
[NASA-TM-83022] p 18 N85-10951
Nonlinear structural and life analyses of a turbine blade p 19 N85-10954
Nonlinear structural and life analyses of a combustor liner p 19 N85-10955
Pre-HOST high temperature crack propagation p 19 N85-10956
Structural analysis p 20 N85-10969
Component-specific modeling p 20 N85-10971
The 3-D inelastic analysis methods for hot section components: Brief description p 20 N85-10972
Constitutive model development for isotropic materials p 20 N85-10975
Airfoil deposition model p 21 N85-10979
Effects of surface chemistry on hot corrosion life: Overview p 21 N85-10980
Combustion system for radiation investigations p 21 N85-10986
Energy efficient engine component development and integration program
[NASA-CR-170034] p 22 N85-10990
Energy efficient engine. Low pressure turbine test hardware detailed design report
[NASA-CR-167956] p 22 N85-10994
Energy efficient engine high pressure turbine test hardware detailed design report
[NASA-CR-167955] p 23 N85-10995
Energy efficient engine. High pressure compressor detail design report
[NASA-CR-165558] p 23 N85-10998
Static jet noise test results of four 0.35 scale-model QCGAT mixer nozzles
[NASA-TM-86871] p 175 N85-13551
Design description of a microprocessor based Engine Monitoring and Control unit (EMAC) for small turboshaft
[NASA-TM-86860] p 1 N85-17935
NASA Lewis Research Center/University Graduate Research Program on Engine Structures
[NASA-TM-86916] p 145 N85-18375
Analytical fuel property effects: Small combustors, phase 2
[NASA-CR-174848] p 93 N85-19175
Study of advanced fuel system concepts for commercial aircraft and engines
[NASA-CR-174752] p 93 N85-19176
Study of advanced fuel system concepts for commercial aircraft
[NASA-CR-174751] p 12 N85-19978
A theory of post-stall transients in multistage axial compression systems
[NASA-CR-3878] p 8 N85-21117
Stratified charge rotary aircraft engine technology enablement program
[NASA-CR-174812] p 25 N85-21163
Tribological systems as applied to aircraft engines
[NASA-TM-86965] p 131 N85-21657
Advanced smoke meter development survey and analysis
[NASA-CR-168287] p 124 N85-25792
Component-specific modeling
[NASA-CR-174925] p 32 N85-32119
AIRCRAFT EQUIPMENT
Icing tunnel tests of Electro-Impulse De-Icing of an engine inlet and high-speed wings
[AIAA PAPER 85-0466] p 10 A85-20872
Electro-impulse de-icing of a turbofan engine inlet
[AIAA PAPER 85-1118] p 12 A85-40811
AIRCRAFT FUEL SYSTEMS
Study of advanced fuel system concepts for commercial aircraft and engines
[NASA-CR-174752] p 93 N85-19176
Study of advanced fuel system concepts for commercial aircraft
[NASA-CR-174751] p 12 N85-19978
AIRCRAFT FUELS
Study of advanced fuel system concepts for commercial aircraft
[NASA-CR-174751] p 12 N85-19978
Applications of high pressure differential scanning calorimetry to aviation fuel thermal stability research
[NASA-TM-87002] p 63 N85-23941
Jet fuel property changes and their effect on producibility and cost in the U.S., Canada, and Europe
[NASA-CR-174840] p 93 N85-27012
Detailed studies of aviation fuel flowability
[NASA-CR-174938] p 94 N85-31308
Comparative analysis of operational forecasts versus actual weather conditions in airline flight planning, volume 1
[NASA-CR-167862] p 167 N85-35534
Comparative analysis of operational forecasts versus actual weather conditions in airline flight planning, volume 4
[NASA-CR-167865] p 167 N85-35537
Comparative analysis of operational forecasts versus actual weather conditions in airline flight planning: Summary report
[NASA-CR-167866] p 168 N85-35538
AIRCRAFT NOISE
Analysis of the effect on combustor noise measurements of acoustic waves reflected by the turbine and combustor inlet
[AIAA PAPER 84-2323] p 173 A85-16103
Static jet noise test results of four 0.35 scale-model QCGAT mixer nozzles
[NASA-TM-86871] p 175 N85-13551
AIRCRAFT PERFORMANCE
Comparative analysis of operational forecasts versus actual weather conditions in airline flight planning, volume 1
[NASA-CR-167862] p 167 N85-35534
AIRCRAFT POWER SUPPLIES
Advanced secondary power system for transport aircraft
[NASA-TP-2463] p 30 N85-28944
AIRCRAFT STRUCTURES
Icing flight research - Aerodynamic effects of ice and ice shape documentation with stereo photography
[AIAA PAPER 85-0468] p 11 A85-30192
Icing flight research: Aerodynamic effects of ice and ice shape documentation with stereo photography
[NASA-TM-86906] p 12 N85-18049
AIRCRAFT WAKES
Noise produced by the interaction of a rotor wake with a swept stator blade
[AIAA PAPER 84-2326] p 173 A85-13956
AIRFOIL PROFILES
Progress in development of a Navier-Stokes solver for evaluation of iced airfoil performance
[AIAA PAPER 85-0410] p 3 A85-19731
AIRFOILS
Effect of airfoil mean loading on convected gust interaction noise
[AIAA PAPER 84-2324] p 173 A85-13955
Predicting rime ice accretion on airfoils p 3 A85-25135
Feedback in separated flows over symmetric airfoils
[AIAA PAPER 84-2297] p 3 A85-28899
Transient technique for measuring heat transfer coefficients on stator airfoils in a jet engine environment
[AIAA PAPER 85-1471] p 122 A85-39796
The computation of viscid/inviscid interaction on airfoils with separated flow p 6 A85-42954
Design and wind tunnel evaluation of a symmetric airfoil series for large wind turbine applications
[NASA-CR-174764] p 7 N85-10919
Turbine heat transfer p 19 N85-10964
Unsteady pressure measurements on a biconvex airfoil in a transonic oscillating cascade
[NASA-TM-86914] p 8 N85-15689
High temperature thermocouple and heat flux gauge using a unique thin film-hardware hot juncture
[NASA-TM-86898] p 123 N85-16096
Study of controlled diffusion stator blading
[NASA-CR-167995] p 25 N85-18058
The boundary layer on compressor cascade blades
[NASA-CR-174369] p 114 N85-18292
Transient technique for measuring heat transfer coefficients on stator airfoils in a jet engine environment
[NASA-TM-87005] p 124 N85-25794
Ice shapes and the resulting drag increase for a NACA 0012 airfoil
[NASA-TM-83556] p 11 N85-27839
New facility to study unsteady wake effects on turbine airfoil heat transfer p 117 N85-27948
Performance comparison between NACA 23024 and NACA 64(3)-618 airfoil configurated rotors for horizontal-axis wind turbines
[NASA-TM-83471] p 163 N85-30477
Heat transfer in aeropropulsion systems
[NASA-TM-87066] p 119 N85-31444
Local heat-transfer measurements on a large, scale-model turbine blade airfoil using a composite of a heater element and liquid crystals
[NASA-TM-86900] p 119 N85-33435
ALCOHOLS
Alkaline battery containing a separator of a cross-linked copolymer of vinyl alcohol and unsaturated carboxylic acid
[NASA-CASE-LEW-13102-1] p 104 N85-29144
ALGEBRA
Alternatives for jet engine control
[NASA-CR-175831] p 29 N85-26713
ALGORITHMS
Hybrid stress finite elements for large deformations of inelastic solids p 139 A85-15894
Efficient solution of the Euler and Navier-Stokes equations with a vectorized multiple-grid algorithm p 2 A85-18679
Accelerated convergence for incompressible flow calculations
[AIAA PAPER 85-0058] p 2 A85-19489
Inviscid and viscous flows in cascades with an explicit multiple-grid algorithm p 7 A85-48539
Comparison of numerical techniques for integration of stiff ordinary differential equations arising in combustion chemistry
[NASA-TP-2372] p 17 N85-10065
CREKID: A computer code for transient, gas-phase combustion of kinetics
[NASA-TM-83806] p 17 N85-10068
Augmented weak forms and element-by-element preconditioners: Efficient iterative strategies for structural finite elements. A preliminary study p 144 N85-10384
Accelerated convergence for incompressible flow calculations
[NASA-TM-86863] p 18 N85-10949
A comparison of the efficiency of numerical methods for integrating chemical kinetic rate equations
[NASA-TM-83590] p 25 N85-21162
Linearization of digital derived rate algorithm for use in linear stability analysis
[NASA-TM-87000] p 41 N85-23904
Comparative analysis of operational forecasts versus actual weather conditions in airline flight planning, volume 2
[NASA-CR-167863] p 167 N85-35535
ALKALINE BATTERIES
Alkaline battery containing a separator of a cross-linked copolymer of vinyl alcohol and unsaturated carboxylic acid
[NASA-CASE-LEW-13102-1] p 104 N85-29144
ALKANES
Liquid phase products and solid deposit formation from thermally stressed model jet fuels
[NASA-TM-86874] p 92 N85-13066
ALLOYS
Effects of cobalt, boron, and zirconium on the microstructure of Udimet 738
[NASA-CR-174762] p 70 N85-10166
Characterization of erosion of metallic materials under cavitation attack in a mineral oil
[NASA-TM-86934] p 74 N85-19075
Alloys based on NiAl for high temperature applications
[NASA-TM-86976] p 75 N85-21322
Advanced thin film thermocouples
[NASA-CR-175541] p 124 N85-21607
Viscoplastic constitutive relationships with dependence on thermomechanical history
[NASA-CR-174836] p 146 N85-21691
Effects of surface chemistry on hot corrosion life
[NASA-CR-174915] p 28 N85-26711

Properties and microstructures for dual alloy combinations of three superalloys with alloy 901
[NASA-TM-86987] p 76 N85-26963
Thermomechanical deformation in the presence of metallurgical changes p 150 N85-31533
Results of an interlaboratory fatigue test program conducted on alloy 800H at room and elevated temperatures
[NASA-CR-174940] p 152 N85-32340

ALTITUDE
Analytical and physical modeling program for the NASA Lewis Research Center's Altitude Wind Tunnel (AWT)
[NASA-TM-86919] p 35 N85-15757

ALTITUDE SIMULATION
The Altitude Wind Tunnel (AWT) - A unique facility for propulsion system and adverse weather testing
[AIAA PAPER 85-0314] p 34 A85-19661
Analytical and physical modeling program for the NASA Lewis Research Center's Altitude Wind Tunnel (AWT)
[AIAA PAPER 85-0379] p 34 A85-19709
The NASA altitude wind tunnel - Its role in advanced icing research and development
[AIAA PAPER 85-0090] p 35 A85-26381
Analytical modeling of circuit aerodynamics in the new NASA Lewis Altitude Wind Tunnel
[AIAA PAPER 85-0380] p 3 A85-26389
Analytical modeling of circuit aerodynamics in the new NASA Lewis wind tunnel
[NASA-TM-86912] p 8 N85-15688
The NASA Altitude Wind Tunnel (AWT): Its role in advanced icing research and development
[NASA-TM-86920] p 35 N85-15758

ALTITUDE TESTS
Altitude testing of a flight weight, self-cooled, 2D thrust vectoring exhaust nozzle
[SAE PAPER 841557] p 14 A85-25984

ALUMINATES
Alloys based on NiAl for high temperature applications
[NASA-TM-86976] p 75 N85-21322

ALUMINUM
Universal binding energy relations in metallic adhesion
[NASA-TM-86889] p 72 N85-12132
Optimization of the NiCrAl-Y/ZrO-Y2O3 thermal barrier system
[NASA-TM-86905] p 72 N85-15878
Experimental compliance calibration of the NASA Lewis Research Center Mode 2 fatigue specimen
[NASA-TM-86908] p 144 N85-16205
High temperature properties of equiatomic FeAl with ternary additions
[NASA-TM-86938] p 73 N85-19072
Effects of chromium and aluminum on mechanical and oxidation properties of iron-nickel-base superalloys based on CG-27
[NASA-TP-2443] p 75 N85-21323
Aluminum work function: Effect of oxidation, mechanical scraping and ion bombardment
[NASA-TM-87079] p 78 N85-34265

ALUMINUM ALLOYS
Deformation and erosion of f.c.c. metals and alloys under cavitation attack p 65 A85-12789
Modeling of gamma/gamma-prime phase equilibrium in the nickel-aluminum system p 65 A85-14959
Ductility in rapidly solidified NiAl p 66 A85-26158
The transient oxidation of single crystal NiAl+Zr
[NASA-CR-174756] p 70 N85-11221
A study of spectrum fatigue crack propagation in two aluminum alloys. 1: Spectrum simplification
[NASA-TM-86929] p 72 N85-18124
A study of spectrum fatigue crack propagation in two aluminum alloys. 2: Influence of microstructures
[NASA-TM-86930] p 73 N85-18125
Rapidly solidified NiAl and FeAl
[NASA-TM-86941] p 74 N85-20042

ALUMINUM COATINGS
Microstructural development of protective Al2O3 scales p 80 A85-21650

ALUMINUM COMPOUNDS
The B2 aluminides as alternative materials
[NASA-TM-86937] p 74 N85-19076

ALUMINUM GRAPHITE COMPOSITES
Select fiber composites for space applications - A mechanistic assessment p 54 A85-16040

ALUMINUM OXIDES
Microstructural development of protective Al2O3 scales p 80 A85-21650
Dopant effect of yttrium and the growth and adherence of alumina on nickel-aluminum alloys p 82 A85-40973
The transient oxidation of single crystal NiAl+Zr
[NASA-CR-174756] p 70 N85-11221
Fundamental tribological properties of ceramics
[NASA-TM-86915] p 85 N85-15893
Dispersed metal-toughened ceramics and ceramic brazing
[NASA-CR-174284] p 86 N85-15916
Transformation toughened ceramics for the heavy duty diesel engine technology program
[NASA-CR-174689] p 185 N85-16698
Dispersed-metal-toughened alumina
[NASA-CR-174687] p 89 N85-22758

AMBIENT TEMPERATURE
Results of an interlaboratory fatigue test program conducted on alloy 800H at room and elevated temperatures
[NASA-CR-174940] p 152 N85-32340

AMMONIA
Performance characterization tests of a 1-kW resistojet using hydrogen, nitrogen and ammonia as propellants
[AIAA PAPER 85-1159] p 44 A85-39628

AMORPHOUS MATERIALS
Mechanical-contact-induced transformation from the amorphous to the partially crystalline state in metallic glass p 65 A85-19084
'Diamondlike' carbon films - Optical absorption, dielectric properties, and hardness dependence on deposition parameters p 82 A85-40383
Optical properties of hydrogenated amorphous carbon films grown from methane plasma
[NASA-TM-86995] p 183 N85-26406

AMPLIFICATION
Adaptive antenna arrays for weak interfering signals
[NASA-CR-174336] p 98 N85-17258

AMPLIFIER DESIGN
A 20 GHz, 75 watt, helix TWT for space communications p 101 A85-14433

AMPLIFIERS
The 30 GHz solid state amplifier for low cost low data rate ground terminals
[NASA-CR-174795] p 102 N85-12300

AMPLITUDES
The use of an optical data acquisition system for bladed disk vibration analysis
[NASA-TM-86891] p 144 N85-15184

ANEMOMETERS
Hot section laser anemometry p 19 N85-10962

ANGLE OF ATTACK
Performance and surge limits of a TF30-P-3 turbofan engine/axisymmetric mixed-compression inlet propulsion system at Mach 2.5
[NASA-TP-2461] p 27 N85-25261

ANGLES (GEOMETRY)
Free-surface phenomena under low- and zero-gravity conditions
[NASA-CR-175835] p 116 N85-27168

ANISOTROPY
Low cycle fatigue of MAR-M 200 single crystals at 760 and 870 deg C
[NASA-TM-86933] p 74 N85-19074
Orientation and temperature dependence of some mechanical properties of the single-crystal nickel-base superalloy Rene N4. 3: Tension-compression anisotropy
[NASA-TM-86982] p 76 N85-22660

ANNEALING
Heat treatment of bulk gallium arsenide using a phosphosilicate glass cap p 181 A85-32636
The effects of lithium counterdoping on radiation damage and annealing in n(+)p silicon solar cells p 50 N85-22586

ANNULAR DUCTS
Rotordynamic coefficients for compressible flow in tapered annular seals p 129 A85-42573

ANNULAR FLOW
Supersonic jet shock noise reduction
[AIAA PAPER 84-2278] p 173 A85-16099
An improved computer model for prediction of axial gas turbine performance losses
[NASA-CR-174246] p 24 N85-15724

ANNULAR NOZZLES
Experimental investigation of shock-cell noise reduction for single stream nozzles in simulated flight
[NASA-CR-3845] p 175 N85-13550

ANTENNA ARRAYS
On the calculation of the directivity of planar array feeds for satellite reflector applications p 97 A85-32249
The study of microstrip antenna arrays and related problems
[NASA-CR-174054] p 97 N85-11265
Characterization of MMIC devices for active array antennas
[NASA-TM-86907] p 38 N85-15779
Infrared technology for satellite power conversion --- antenna arrays and bolometers
[NASA-CR-174266] p 159 N85-16293
Adaptive antenna arrays for weak interfering signals
[NASA-CR-174336] p 98 N85-17258
Adaptive antenna arrays for satellite communications: Design and testing
[NASA-CR-176162] p 100 N85-34329

ANTENNA COMPONENTS
Characterization of MMIC devices for active array antennas
[NASA-TM-86907] p 38 N85-15779

ANTENNA DESIGN
Advanced 30/20 GHz multiple beam antenna for future communications satellites p 96 A85-14436
The 20 GHz proof-of-concept test model results for a multiple scan beam dual reflector antenna
[NASA-CR-174268] p 98 N85-15944
Configuration study for a 30 GHz monolithic receive array: Technical assessment
[NASA-CR-174697] p 98 N85-18238
Configuration study for a 30 GHz monolithic receive array, volume 1
[NASA-CR-174697-VOL-1] p 98 N85-18239
Configuration study for a 30 GHz monolithic receive array, volume 2
[NASA-CR-174697-VOL-2] p 99 N85-18240
Extreme precision antenna reflector study results p 165 N85-23830

ANTENNA FEEDS
Dual-mode coaxial feed with low crosspolarisation p 101 A85-20171
On the calculation of the directivity of planar array feeds for satellite reflector applications p 97 A85-32249

ANTENNA RADIATION PATTERNS
Dual-mode coaxial feed with low crosspolarisation p 101 A85-20171
Case study of sample spacing in planar near-field measurement of high gain antennas
[NASA-TM-86872] p 97 N85-10234
The 20 GHz proof-of-concept test model results for a multiple scan beam dual reflector antenna
[NASA-CR-174268] p 98 N85-15944
Adaptive antenna arrays for satellite communications: Design and testing
[NASA-CR-176162] p 100 N85-34329

ANTENNAS
Case study of sample spacing in planar near-field measurement of high gain antennas
[NASA-TM-86872] p 97 N85-10234
MMIC devices for active phased array antennas
[NASA-CR-174281] p 98 N85-15943

ANTIKNOCK ADDITIVES
Knock syndrome: Its cures and its victims
[NASA-CR-174395] p 93 N85-19185

APERTURES
Focal shifts in parabolic reflectors p 97 A85-39356
Characterization of MMIC devices for active array antennas
[NASA-TM-86907] p 38 N85-15779

ARC DISCHARGES
Cathode degradation and erosion in high pressure arc discharges p 43 A85-16445
Characteristics of arc currents on a negatively biased solar cell array in a plasma p 154 A85-18608
An investigation of arc discharging on negatively biased dielectric conductor samples in a plasma p 180 N85-22498
Hollow cathodes in high pressure arc discharges
[NASA-TM-87098] p 52 N85-34179

ARC JET ENGINES
Cathode degradation and erosion in high pressure arc discharges p 43 A85-16445
Electrode erosion in arc discharges at atmospheric pressure
[NASA-TM-87087] p 52 N85-34178
Hollow cathodes in high pressure arc discharges
[NASA-TM-87098] p 52 N85-34179

ARC SPRAYING
Arc spray fabrication of metal matrix composite monotape
[NASA-CASE-LEW-13828-1] p 58 N85-30027

ARCHITECTURE (COMPUTERS)
A functional language approach in high-speed digital simulation p 170 A85-28615
General approaches for achieving high speed computations p 169 A85-28628
Functional language and data flow architectures p 170 A85-28629

ARIZONA
Control aspects of the Schuchuli Village stand-alone photovoltaic power system
[NASA-TM-83790] p 103 N85-13157

AROMATIC COMPOUNDS
Liquid phase products and solid deposit formation from thermally stressed model jet fuels
[NASA-TM-86874] p 92 N85-13066

ARRAYS
Mosaic Infrared Sensor for Space Astronomy (MIRSSA)
[NASA-CR-176154] p 125 N85-33456

ASBESTOS
Separator development and testing of nickel-hydrogen cells p 156 A85-45386

ASSEMBLING
Extreme precision antenna reflector study results p 165 N85-23830
ATMOSPHERIC CORRECTION
Comparison of atmospheric correction algorithms for the Coastal Zone Color Scanner p 153 A85-10244
ATMOSPHERIC PRESSURE
Electrode erosion in arc discharges at atmospheric pressure
[NASA-TM-87087] p 52 N85-34178
ATMOSPHERIC TEMPERATURE
A comparison of NMC and GWC analysis field temperatures with aircraft measurements p 166 A85-21140
ATOMIC RECOMBINATION
Molecular orbital studies in oxidation: Sulfate formation and metal-metal oxide adhesion
[NASA-CR-176070] p 77 N85-32174
ATOMIC STRUCTURE
AES and LEED study of the zinc blende SiC(100) surface p 61 A85-41633
Mechanism for chelated sulfate formation from SO2 and bis (triphenylphosphine) platinum p 62 A85-48493
ATOMIZING
Liquid fuel spray processes in high-pressure gas flow
[NASA-TM-86944] p 115 N85-21570
ATTENUATION
Normal modes in an overmoded circular waveguide coated with lossy material
[NASA-CR-176186] p 100 N85-35320
ATTENUATORS
Design of low loss helix circuits for interference fitted and brazed circuits
[NASA-CR-168313] p 103 N85-19328
ATTITUDE CONTROL
Report of the Constellations Panel p 131 N85-20368
Operating characteristics of a 0.87 kW-hr flywheel energy storage module
[NASA-TM-87038] p 133 N85-28371
AURORAL ARCS
Circuit transients due to negative bias arcs on a high-voltage solar array in low Earth orbit
[NASA-TP-2407] p 39 N85-14858
AURORAL ELECTROJETS
Polar orbit electrostatic charging of objects in shuttle wake p 40 N85-22487
AURORAS
DE-1 measurements of AKR wave directions --- auroral kilometric radiation p 166 A85-37717
AUTOMATIC CONTROL
Fiber optic, Fabry-Perot high temperature sensor
[NASA-CR-174712] p 178 N85-13594
Automated testing of developmental satellite communications systems and subsystems
[NASA-TM-87070] p 100 N85-31348
AUTOMATIC TEST EQUIPMENT
An approach for automated analysis of particle holograms p 120 A85-10034
Satellite baseband processor test performance summary p 95 A85-14434
Closed-loop strain controlled testing at elevated temperatures with a non-contacting gage p 121 A85-29562
Automated testing of developmental satellite communications systems and subsystems
[NASA-TM-87070] p 100 N85-31348
AUTOMOBILE ENGINES
Ceramic component development for the AGT101 gas turbine engine p 126 A85-15972
Ceramic components for gas turbine engines p 127 A85-15973
Mod II engine and technology development p 129 A85-45473
Automotive Stirling engine systems development p 130 A85-45474
Advanced automotive diesel assessment program
[NASA-CR-168285] p 130 N85-13235
Advanced Gas Turbine (AGT) powertrain system development for automotive applications
[NASA-CR-174809] p 185 N85-18831
Knock syndrome: Its cures and its victims
[NASA-CR-174395] p 93 N85-19185
Advanced Gas Turbine (AGT) technology project
[NASA-CR-174798] p 31 N85-29961
AUTOMOBILES
Advanced automotive diesel assessment program
[NASA-CR-168285] p 130 N85-13235
Knock syndrome: Its cures and its victims
[NASA-CR-174395] p 93 N85-19185
Feasibility demonstration of a novel, flat-belt, continuously variable transmission or automotive and electric-hybrid vehicle application
[NASA-CR-174430] p 185 N85-19894
AUXILIARY POWER SOURCES
Ion thruster system (8-cm) cyclic endurance test
[NASA-CR-174745] p 47 N85-12937
Regenerative fuel cell systems for space station p 104 N85-31372
AUXILIARY PROPULSION
Ion thruster system (8-cm) cyclic endurance test
[NASA-CR-174745] p 47 N85-12937
AVALANCHE DIODES
The 30 GHz solid state amplifier for low cost low data rate ground terminals
[NASA-CR-174795] p 102 N85-12300
Sixty GHz IMPATT diode development
[NASA-CR-174969] p 105 N85-33293
AVERAGE
Model equation for simulating flows in multistage turbomachinery
[NASA-TM-86869] p 7 N85-12036
AXES OF ROTATION
Wake effects on the aerodynamic performance of horizontal axis wind turbines
[NASA-CR-174920] p 162 N85-29364
AXIAL FLOW
Rotor wake characteristics of a transonic axial flow fan
[AIAA PAPER 85-1133] p 6 A85-43974
AXIAL FLOW TURBINES
Predicted turbine stage performance using quasi-three-dimensional and boundary-layer analyses p 15 A85-34013
AXIAL LOADS
Plasticity, viscoplasticity, and creep of solids by mechanical subelement models p 142 A85-35048
AXIAL STRAIN
Results of an interlaboratory fatigue test program conducted on alloy 800H at room and elevated temperatures
[NASA-CR-174940] p 152 N85-32340
AXISYMMETRIC FLOW
Prediction of an axisymmetric combusting flow p 59 A85-12713
Analytical modeling of circuit aerodynamics in the new NASA Lewis Altitude Wind Tunnel
[AIAA PAPER 85-0380] p 3 A85-26389
A three-dimensional axisymmetric calculation procedure for turbulent flows in a radial vaneless diffuser
[NASA-TM-86903] p 7 N85-14798
Analytical modeling of circuit aerodynamics in the new NASA Lewis wind tunnel
[NASA-TM-86912] p 8 N85-15688

B

BALANCING
Laser balancing system for high material removal rates
[NASA-CR-174731] p 126 N85-12341
Development of a multiplane multispeed balancing system for turbine systems
[NASA-CR-174750] p 35 N85-22400
BALL BEARINGS
Topological reaction rate measurements related to scuffing p 64 A85-11070
First-order ball-bearing kinematics p 128 A85-31203
Effect of two inner-ring oil-flow distribution schemes on the operating characteristics of a 35 millimeter bore ball bearing to 2.5 million DN
[NASA-TP-2404] p 130 N85-13233
Operating characteristics of a 0.87 kW-hr flywheel energy storage module
[NASA-TM-87038] p 133 N85-28371
Mechanics of a gaseous film barrier to lubricant wetting of elastohydrodynamically lubricated conjunctions
[NASA-TP-2500] p 135 N85-32330
BARRIER LAYERS
Advanced thermal barrier system bond coatings for use on Ni, Co-, and Fe-base alloy substrates
[NASA-TM-87062] p 77 N85-31283
BARS
Thermal-mechanical fatigue crack growth in Inconel X-750
[NASA-CR-174740] p 72 N85-15877
NDE for heat engine ceramics
[NASA-TM-86949] p 137 N85-20389
BATCH PROCESSING
High-voltage solar-cell chip p 154 A85-24668
BEADS
Spherical microglass particle impingement studies of thermoplastic materials at normal incidence p 79 A85-11072
BEAMS (SUPPORTS)
Effects of warping and pretwist on torsional vibration of rotating beams
[ASME PAPER 84-WA/APM-41] p 140 A85-17040
BEARINGS
Characterization of lubricated bearing surfaces operated under high loads
[NASA-TM-86964] p 88 N85-21357
Reusable rocket engine turbopump condition monitoring p 51 N85-26907
Fatigue life analysis of a turboprop reduction gearbox
[NASA-TM-87014] p 133 N85-27228
BENDING MOMENTS
Nonlinear flap-lag-extensional vibrations of rotating, pretwisted, preconed beams including Coriolis effects
[NASA-TM-87102] p 152 N85-34427
BENZENE
Formation of high molecular weight products from benzene during boundary lubrication
[NASA-TM-86966] p 62 N85-22644
Fuel-rich catalytic combustion: A soot-free technique for in situ hydrogen-like enrichment
[NASA-TP-2498] p 63 N85-31244
BERYLLIUM
Fracture toughness of hot-pressed beryllium p 66 A85-25835
BIAS
Circuit transients due to negative bias arcs on a high-voltage solar array in low Earth orbit
[NASA-TP-2407] p 39 N85-14858
BIBLIOGRAPHIES
Bibliography of Lewis Research Center technical publications announced in 1983
[NASA-TM-83693] p 184 N85-22255
BINARY ALLOYS
Dendritic solidification. III - Some further refinements to the model for dendritic growth under an imposed thermal gradient p 69 A85-44703
BINARY SYSTEMS (MATERIALS)
Ultrasonic wave propagation in two-phase media - Spherical inclusions p 54 A85-11926
BINDING
Universal binding energy relations in metallic adhesion
[NASA-TM-86889] p 72 N85-12132
CO adsorption on (111) and (100) surfaces of the Pt sub 3 Ti alloy. Evidence for parallel binding and strong activation of CO
[NASA-CR-176077] p 77 N85-32176
BIPOLAR TRANSISTORS
Bipolar-FET combinational power transistors for power conversion applications p 100 A85-12669
High voltage-high power components for large space power distribution systems p 45 A85-45370
BIPOLARITY
Teardown analysis of a ten cell bipolar nickel-hydrogen battery p 156 A85-45385
Advanced nickel-hydrogen cell configuration study
[NASA-CR-174775] p 157 N85-10444
Life cycle test results of a bipolar nickel hydrogen battery
[NASA-TM-87046] p 163 N85-30480
BIREFRINGENCE
Incident beam polarization for laser Doppler velocimetry employing a sapphire cylindrical window p 122 A85-39835
Incident beam polarization for laser Doppler velocimetry employing a sapphire cylindrical window
[NASA-TM-87064] p 178 N85-28786
BIT ERROR RATE
Satellite baseband processor test performance summary p 95 A85-14434
BITS
Floating-point function generation routines for 16-bit microcomputers
[NASA-TM-83783] p 170 N85-10683
BLADE TIPS
Metallurgical and mechanical phenomena due to rubbing of titanium against sintered powder Nichrome p 127 A85-22281
An experimental investigation and numerical prediction of thermomechanical phenomena in high speed rotor tip rubbing p 14 A85-25442
Observations from varying the lift and drag inputs to a noise prediction method for supersonic helical tip speed propellers
[NASA-TM-83797] p 175 N85-10788
Oxidizing seal for a turbine tip gas path
[NASA-CASE-LEW-14053-1] p 136 N85-34402
BLOWING
Analytical study of blowing boundary layer control for subsonic V/STOL inlets p 2 A85-11646
BLUFF BODIES
The mechanisms of flame holding in the wake of a bluff body
[NASA-CR-3866] p 26 N85-21166
BOEING 747 AIRCRAFT
Simultaneous cabin and ambient ozone measurements on two Boeing 747 airplanes. Volume 3: October 1978 - July 1979
[NASA-TM-86883] p 167 N85-21872

BOLOMETERS
Infrared technology for satellite power conversion --- antenna arrays and bolometers
[NASA-CR-174266] p 159 N85-16293
BOREHOLES
Experimental stiffness of tapered bore seals
[NASA-TM-86978] p 132 N85-25847
BORIDES
Surface hardening of steel by boriding in a cold rf plasma p 68 A85-40275
BORON
Effects of cobalt, boron, and zirconium on the microstructure of Udimet 738
[NASA-CR-174762] p 70 N85-10166
BORON FIBERS
Fibers for structurally reliable metal and ceramic composites p 55 A85-37484
BORON NITRIDES
Tribological properties of boron nitride synthesized by ion beam deposition
[NASA-TM-86962] p 87 N85-21355
BOTTLES
Ten year environmental test of glass fiber/epoxy pressure vessels
[AIAA PAPER 85-1198] p 56 A85-47022
Ten year environmental test of glass fiber/epoxy pressure vessels
[NASA-TM-87058] p 58 N85-30034
BOUNDARY LAYER CONTROL
Analytical study of blowing boundary layer control for subsonic V/STOL inlets p 2 A85-11646
BOUNDARY LAYER EQUATIONS
A three-dimensional boundary-layer analysis including heat-transfer and blade-rotation effects
p 6 A85-42988
BOUNDARY LAYER FLOW
A note on blade wake interaction influence on compressor stator row aerodynamic performance
p 4 A85-32965
Design and wind tunnel evaluation of a symmetric airfoil series for large wind turbine applications
[NASA-CR-174764] p 7 N85-10919
BOUNDARY LAYER SEPARATION
Low-speed aerodynamic test of an axisymmetric supersonic inlet with variable cowl slot
[AIAA PAPER 85-1210] p 5 A85-40819
Low-speed aerodynamic test of an axisymmetric supersonic inlet with variable cowl slot
[NASA-TM-87039] p 28 N85-26710
BOUNDARY LAYER TRANSITION
A review and analysis of boundary layer transition data for turbine application
[NASA-TM-86880] p 113 N85-10306
Transition in Turbines
[NASA-CP-2386] p 118 N85-31433
Flat-plate transition p 118 N85-31438
Heat transfer and fluid mechanics measurements in transitional boundary layer flows p 118 N85-31439
A review and analysis of boundary layer transition data for turbine application p 118 N85-31440
BOUNDARY LAYERS
Free-surface phenomena under low- and zero-gravity conditions
[NASA-CR-175885] p 36 N85-27922
Unsteady flow in a supersonic cascade with two in-passage shocks
[NASA-CR-3925] p 10 N85-35158
BOUNDARY LUBRICATION
Hydrodynamic lubrication of rigid nonconformal contacts in combined rolling and normal motion
[ASME PAPER 84-TRIB-13] p 127 A85-21280
The influence of temperature on the lubricating effectiveness of MoS2 dispersed in mineral oils
[ASLE PREPRINT 84-LC-2A-2] p 80 A85-25963
Thermal elastohydrodynamic lubrication of line contacts p 128 A85-31202
Formation of high molecular weight products from benzene during boundary lubrication
[NASA-TM-86966] p 62 N85-22644
BOUNDARY VALUE PROBLEMS
Recent advances in methods for numerical solution of O.D.E. initial value problems p 171 A85-21370
A procedure for obtaining explicit solutions to a class of Fredholm integral equations p 171 A85-28006
Constructive existence and uniqueness for two-point boundary-value problems with a linear gradient term
p 172 A85-28015
Analysis of three-dimensional solidification interface shape p 109 A85-30075
Solidification interface shape for continuous casting in an offset mold - Two analytical methods
p 112 A85-41326
A convergent series expansion for hyperbolic systems of conservation laws
[NASA-CR-172557] p 168 N85-21990
BRANCHING (MATHEMATICS)
Nonlinear global stability analysis of compressor stall phenomena
[NASA-CR-174908] p 31 N85-29960
BRANCHING (PHYSICS)
Circular waveguide bifurcation for asymmetric modes
p 101 A85-20170
BRAYTON CYCLE
Dynamic power systems for power generation
p 158 N85-13892
Comparative evaluation of three alternative power cycles for waste heat recovery from the exhaust of adiabatic diesel engines
[NASA-TM-86953] p 186 N85-32043
BRAZING
Dispersed metal-toughened ceramics and ceramic brazing
[NASA-CR-174284] p 86 N85-15916
Design of low loss helix circuits for interference fitted and brazed circuits
[NASA-CR-168313] p 103 N85-19328
BREADBOARD MODELS
Design and analysis report for the RL10-2B breadboard low thrust engine
[NASA-CR-174857] p 48 N85-19020
BREATHING APPARATUS
Ten year environmental test of glass fiber/epoxy pressure vessels
[AIAA PAPER 85-1198] p 56 A85-47022
Ten year environmental test of glass fiber/epoxy pressure vessels
[NASA-TM-87058] p 58 N85-30034
BROADCASTING
Technical characteristics of the broadcasting satellite plan at 12 GHz for the Western Hemisphere
p 96 A85-28233
Development and use of the computer software package for planning the 12 GHz broadcasting-satellite service at RARC '83 p 96 A85-29605
Experimental results supporting the determination of service quality objectives for DBS systems
p 96 A85-29611
Alternatives for satellite sound broadcast systems at HF and VHF p 99 N85-23815
BROMIDES
Graphite fiber intercalation: Dynamics of the bromine intercalation process
[NASA-TM-87015] p 53 N85-26921
BROMINE
Stability of bromine intercalated graphite fibers
[NASA-TM-86859] p 84 N85-10187
Homogeneity of pristine and bromine intercalated graphite fibers
[NASA-TM-87016] p 89 N85-25521
Environmental stability of intercalated graphite fibers
[NASA-TM-87025] p 90 N85-26992
A micrographic and gravimetric study of intercalation and deintercalation of graphite fibers
[NASA-TM-87026] p 91 N85-28110
BUOYANCY
Analysis of buoyancy effect on fully developed laminar heat transfer in a rotating tube p 110 A85-35596
BURNERS
Ribbon burner simulation of T-700 turbine shroud for ceramic lined seals research
[NASA-TM-86940] p 114 N85-19364
Digital temperature and velocity control of mach 0.3 atmospheric pressure durability testing burner rigs in long time, unattended cyclic testing
[NASA-TM-86959] p 75 N85-21321
BUTT JOINTS
Diffusion welding of MA 6000 and a conventional nickel-base superalloy p 69 A85-43551
BYPASS RATIO
Effect of combined pressure and temperature distortion orientation on high-bypass-ratio turbofan engine stability
[NASA-TM-83771] p 17 N85-10067
Effect of steady-state temperature distortion on inlet flow to a high-bypass-ration turbofan engine
[NASA-TM-86896] p 24 N85-15725
Energy efficient engine. Fan and quarter-stage component performance report
[NASA-CR-168070] p 33 N85-34141
Energy Efficient Engine Program technology benefit/cost study, volume 1
[NASA-CR-174766-VOL-1] p 33 N85-35197
Energy Efficient Engine Program technology benefit/cost study, volume 2
[NASA-CR-174766-VOL-2] p 33 N85-35198

C

CABIN ATMOSPHERES
Simultaneous cabin and ambient ozone measurements on two Boeing 747 airplanes. Volume 3: October 1978 - July 1979
[NASA-TM-86883] p 167 N85-21872
CALIBRATING
Calibration stability of some hot-cathode ion gauges
p 122 A85-41634
Heat flux sensor calibrator p 41 N85-27970
CALORIMETERS
Applications of high pressure differential scanning calorimetry to aviation fuel thermal stability research
[NASA-TM-87002] p 63 N85-23941
CAMERA SHUTTERS
Initial feasibility ground test of a proposed photogrammetric system for measuring the shapes of ice accretions on helicopter rotor blades during forward flight
[NASA-TM-87391] p 12 N85-12887
CANS
Flame radiation and linear heat transfer in a tubular-can combustor p 15 A85-39580
CANTILEVER BEAMS
Finite difference analysis of torsional vibrations of pretwisted, rotating, cantilever beams with effects of warping p 143 A85-42047
Nonlinear flap-lag-extensional vibrations of rotating, pretwisted, preconed beams including Coriolis effects
[NASA-TM-87102] p 152 N85-34427
CANTILEVER PLATES
Vibrations of twisted cantilevered plates - Summary of previous and current studies p 140 A85-22069
Vibrations of twisted cantilever plates - A comparison of theoretical results p 144 A85-47626
CAPACITANCE
Characteristics of arc currents on a negatively biased solar cell array in a plasma p 154 A85-18608
Sixty GHz IMPATT diode development
[NASA-CR-174969] p 105 N85-33293
CAPACITORS
High voltage-high power components for large space power distribution systems p 45 A85-45370
CAPILLARY FLOW
Generation of capillary instabilities by external disturbances in a liquid jet
[NASA-TM-87041] p 117 N85-30246
CARBIDES
The effect of tantalum on the structure/properties of two polycrystalline nickel-base superalloys: B-1900 + Hf MAR-M247
[NASA-CR-174847] p 73 N85-18127
CARBON
Dielectric properties of 'diamondlike' carbon prepared by RF plasma deposition p 182 A85-38192
'Diamondlike' carbon films - Optical absorption, dielectric properties, and hardness dependence on deposition parameters p 82 A85-40383
Plasma deposited hydrogenated carbon on GaAs and InP p 182 A85-40386
Plasma deposited diamondlike carbon on GaAs and InP
[NASA-TM-86870] p 183 N85-10844
The effect of tantalum and carbon on the structure/properties of a single crystal nickel-base superalloy
[NASA-CR-174779] p 71 N85-11223
Deposition of diamondlike carbon films
[NASA-CASE-LEW-14080-1] p 95 N85-20153
Apparatus for producing diamond-like carbon flakes
[NASA-CASE-LEW-13837-3] p 95 N85-20155
Textured carbon surfaces on copper
[NASA-CASE-LEW-14130-1] p 95 N85-20156
Optical properties of hydrogenated amorphous carbon films grown from methane plasma
[NASA-TM-86995] p 183 N85-26406
Mechanical protection of DLC films on fused silica slides
[NASA-TM-87056] p 91 N85-30138
Diamondlike carbon protective coatings for IR materials
[NASA-TM-87083] p 178 N85-34631
CARBON ARCS
Diamondlike flakes
[NASA-CASE-LEW-13837-2] p 57 N85-21267
CARBON COMPOUNDS
Gas cooled fuel cell systems technology development
[NASA-CR-174732] p 158 N85-16291
CARBON DIOXIDE LASERS
Technology for satellite power conversion
[NASA-CR-174335] p 159 N85-18451
CARBON FIBERS
Environmental effects on the tensile strength of chemically vapor deposited silicon carbide fibers
[NASA-TM-86981] p 89 N85-24000

Graphite fiber intercalation: Dynamics of the bromine intercalation process
[NASA-TM-87015] p 53 N85-26921
Environmental stability of intercalated graphite fibers
[NASA-TM-87025] p 90 N85-26992

CARBON MONOXIDE
Shock tube measurements of growth constants in the branched-chain ethane-carbon monoxide-oxygen system
[NASA-TM-87068] p 64 N85-32156
Why CO bonds side-on at low coverage and both side-on and upright at high coverage on the Cr(110) surface
[NASA-CR-176071] p 77 N85-32173
CO adsorption on (111) and (100) surfaces of the Pt sub 3 Ti alloy. Evidence for parallel binding and strong activation of CO
[NASA-CR-176077] p 77 N85-32176

CARBON STEELS
Powder metallurgy forged gear development
[NASA-TM-87483] p 134 N85-29295

CARBOXYLIC ACIDS
Alkaline battery containing a separator of a cross-linked copolymer of vinyl alcohol and unsaturated carboxylic acid
[NASA-CASE-LEW-13102-1] p 104 N85-29144

CARRIER DENSITY (SOLID STATE)
Heat treatment of bulk gallium arsenide using a phosphosilicate glass cap p 181 A85-32636

CARRIER TO NOISE RATIOS
On the subjective evaluation of the interference protection ratios' measurements for co-channel FM-TV signals p 96 A85-28241

CASCADE FLOW
Computation of internal flows: Methods and applications; Proceedings of the Energy Sources Technology Conference, New Orleans, LA, February 12-16, 1984 p 106 A85-11630
Computation of viscous flows in turbomachinery cascades p 106 A85-11631
Two-dimensional internal compressible viscous flows using semi-elliptic analysis p 106 A85-11640
Flutter of turbofan rotors with mistuned blades p 139 A85-12716
A linearized unsteady aerodynamic analysis for transonic cascades p 3 A85-20744
Design and performance of a fixed, nonaccelerating guide vane cascade that operates over an inlet flow angle range of 60 deg
[ASME PAPER 84-GT-75] p 4 A85-32964
Application of Runge Kutta time marching scheme for the computation of transonic flows in turbomachines
[AIAA PAPER 85-1332] p 5 A85-39728
Time dependent computation of the Euler equations for designing 2-D cascades, including the case of transonic shock free design p 5 A85-41814
Optimization of cascade blade mistuning. II - Global optimum and numerical optimization p 16 A85-45715
Inviscid and viscous flows in cascades with an explicit multiple-grid algorithm p 7 A85-48539
Inverse design technique for cascades
[NASA-CR-3836] p 7 N85-12008
Incompressible lifting-surface aerodynamics for a rotor-stator combination
[NASA-TM-83767] p 7 N85-12039
Unsteady pressure measurements on a biconvex airfoil in a transonic oscillating cascade
[NASA-TM-86914] p 8 N85-15689
Unsteady flow in a supersonic cascade with two in-passage shocks
[NASA-CR-3925] p 10 N85-35158

CASCADE WIND TUNNELS
Inverse design technique for cascades
[NASA-CR-3836] p 7 N85-12008

CASSEGRAIN ANTENNAS
Configuration study for a 30 GHz monolithic receive array: Technical assessment
[NASA-CR-174697] p 98 N85-18238
Configuration study for a 30 GHz monolithic receive array, volume 1
[NASA-CR-174697-VOL-1] p 98 N85-18239

CASTING
Control of solidification boundary in continuous casting by asymmetric cooling and mold offset p 110 A85-37047
Solidification interface shape for continuous casting in an offset mold - Two analytical methods p 112 A85-41326
The effect of tantalum on the structure/properties of two polycrystalline nickel-base superalloys: B-1900 + Hf MAR-M247
[NASA-CR-174847] p 73 N85-18127
Tape casting as an approach to an all-ceramic turbine shroud seal
[NASA-TM-87078] p 135 N85-32333

CATALYSIS
Fuel-rich catalytic combustion: A soot-free technique *for in situ hydrogen-like enrichment*
[NASA-TP-2498] p 63 N85-31244

CATALYSTS
Imide modified epoxy matrix resins
[NASA-CR-174695] p 85 N85-15892
Electric utility acid fuel cell stack technology advancement
[NASA-CR-174804] p 159 N85-17422
Solids mixing in a three phase fluidized bed containing spherically shaped-porous solid particles
[PB85-187961] p 120 N85-33453

CATALYTIC ACTIVITY
The role of surface generated radicals in catalytic combustion p 30 N85-27869
Fuel rich catalytic comustion: The first stage of a two-stage combustor
[NASA-TM-87042] p 63 N85-28983

CATASTROPHE THEORY
Nonlinear global stability analysis of compressor stall phenomena
[NASA-CR-174908] p 31 N85-29960

CATHODES
Cathode degradation and erosion in high pressure arc *discharges* p 43 A85-16445
Electric utility acid fuel cell stack technology advancement
[NASA-CR-174804] p 159 N85-17422
Apparatus for mounting a field emission cathode
[NASA-CASE-LEW-14108-1] p 104 N85-29149
Electrode erosion in arc discharges at atmospheric pressure
[NASA-TM-87087] p 52 N85-34178

CATHODIC COATINGS
Cathode degradation and erosion in high pressure arc discharges p 43 A85-16445

CATS
Percutaneous connectors
[NASA-CR-175627] p 168 N85-27508

CAVITATION CORROSION
Cavitation erosion size scale effects p 65 A85-11935
Deformation and erosion of f.c.c. metals and alloys under cavitation attack p 65 A85-12789
A unified relation for cavitation erosion p 109 A85-24445
Characterization of erosion of metallic materials under cavitation attack in a mineral oil
[NASA-TM-86934] p 74 N85-19075

CELL ANODES
Moderate temperature sodium cells. V - Discharge reactions and rechargeability of NiS and NiS2 positive electrodes in molten NaAlCl4 p 59 A85-11892

CENTAUR LAUNCH VEHICLE
A high energy stage for the National Space Transportation System
[IAF PAPER 84-15] p 36 A85-23200
Shuttle/Centaur project perspective p 37 N85-16991
Linearization of digital derived rate algorithm for use in linear stability analysis
[NASA-TM-87000] p 41 N85-23904

CENTRIFUGAL COMPRESSORS
Internal hysteresis experienced on a high pressure syn gas compressor p 131 N85-14122

CENTRIFUGAL PUMPS
Small centrifugal pumps for low thrust rockets
[AIAA PAPER 85-1302] p 45 A85-43978

CERAMIC COATINGS
Oxidation-based model for thermal barrier coating life p 78 A85-10310
Performance of thermal barrier coatings in high heat flux environments p 79 A85-19087
A morphological study of silicon carbide prepared by chemical vapor deposition p 79 A85-20938
Plastic flow of plasma sprayed ceramics p 80 A85-24161
Life modeling of atmospheric and low pressure plasma-sprayed thermal-barrier coating p 81 A85-29728
Mechanical property measurements of plasma-sprayed thermal-barrier coatings subjected to oxidation p 81 A85-29729
Deposition of silicon nitride from SiCl4 and NH3 in a low pressure RF plasma p 81 A85-36229
Failure during thermal cycling of plasma-sprayed thermal barrier coatings p 81 A85-36246
An investigation of enhanced capability thermal barrier coating systems for diesel engine components
[NASA-CR-174820] p 86 N85-18154
Thermal barrier coating system
[NASA-CASE-LEW-13324-2] p 57 N85-21266
Tribological properties of boron nitride synthesized by ion beam deposition
[NASA-TM-86962] p 87 N85-21355
Metallic and metalloceramic coating by thermal decomposition
[NASA-TM-86992] p 88 N85-22755
Rocket thrust chamber thermal barrier coatings p 90 N85-26867

CERAMIC MATRIX COMPOSITES
High temperature metal and ceramic composites p 55 A85-37483
Fibers for structurally reliable metal and ceramic composites p 55 A85-37484
Factors influencing the ball milling of Si3N4 in water
[NASA-TM-86932] p 86 N85-19136
Film and interstitial formation of metals in plasma-sprayed ceramics
[NASA-TM-86993] p 89 N85-22756

CERAMICS
Ceramic component development for the AGT101 gas turbine engine p 126 A85-15972
Ceramic components for gas turbine engines p 127 A85-15973
Deposition stress effects on the life of thermal barrier coatings on burner rigs p 79 A85-19086
Friction and wear of ceramics p 80 A85-23833
Feasibility study of the welding of SiC p 81 A85-39339
Ceramic wear in indentation and sliding contact p 82 A85-39549
Ceramic microstructure and adhesion p 82 A85-40384
Photoacoustic microscopy of ceramic turbine blades p 83 A85-43930
Ceramic microstructure and adhesion
[NASA-TM-83804] p 83 N85-10186
Milling of Si3N4 with Si3N4 hardware
[NASA-TM-86864] p 84 N85-10191
Surface protection overview p 21 N85-10978
Energy efficient engine high pressure turbine ceramic shroud support technology report
[NASA-CR-168036] p 23 N85-10996
High performance fibers for structurally reliable metal and ceramic composites --- advanced gas turbine engine materials
[NASA-TM-86878] p 56 N85-12095
Fundamental tribological properties of ceramics
[NASA-TM-86915] p 85 N85-15893
Dispersed metal-toughened ceramics and ceramic brazing
[NASA-CR-174284] p 86 N85-15916
Transformation toughened ceramics for the heavy duty diesel engine technology program
[NASA-CR-174689] p 185 N85-16698
Experimental and analytical study of ceramic-coated turbine-tip shroud seals for small turbine engines
[NASA-TM-86881] p 25 N85-18057
Advanced Gas Turbine (AGT) powertrain system development for automotive applications
[NASA-CR-174809] p 185 N85-18831
Experimental study of ceramic coated tip seals for turbojet engines
[NASA-TM-86939] p 114 N85-19363
Ribbon burner simulation of T-700 turbine shroud for ceramic lined seals research
[NASA-TM-86940] p 114 N85-19364
NDE for heat engine ceramics
[NASA-TM-86949] p 137 N85-20389
Oxidation and hot corrosion of hot-pressed Si3N4 at 1000 deg C
[NASA-TM-86977] p 88 N85-21358
Fabrication of ceramic substrate-reinforced and free forms
[NASA-TM-86994] p 50 N85-23926
Effects of wear on structure-sensitive magnetic properties of ceramic ferrite in contact with magnetic tape
[NASA-TM-87007] p 90 N85-26991
Breakway friction and dynamic friction/wear measurements of various ceramic materials from 25 C (75 F) to 650 C (1200 F)
[NASA-CR-174803] p 90 N85-26994
Preparation of silicon carbide-silicon nitride fibers by the pyrolysis of polycarbosilazane precursors
[NASA-TM-86505] p 91 N85-28107
Ceramic applications in turbine engines
[NASA-CR-174715] p 91 N85-28109
Burner rig corrosion of SiC at 1000 deg C
[NASA-TM-87061] p 53 N85-30011
Tape casting as an approach to an all-ceramic turbine shroud seal
[NASA-TM-87078] p 135 N85-32333
Reliability of void detection in structural ceramics using scanning laser acoustic microscopy
[NASA-TM-87035] p 138 N85-32337

CH-47 HELICOPTER
Performance degradation of helicopter rotor in forward flight due to ice p 11 A85-42937

CHANNEL FLOW
Computation of internal flows: Methods and applications; Proceedings of the Energy Sources Technology Conference, New Orleans, LA, February 12-16, 1984 p 106 A85-11630
Heat transfer enhancement in channels with turbulence promoters [ASME PAPER 84-WA/HT-72] p 111 A85-39900
The effect of channel convergence on heat transfer in a passage with short pin fins [NASA-TM-83801] p 113 N85-10303
A study of Reynolds-stress closure model [NASA-CR-174342] p 114 N85-17324

CHANNELS (DATA TRANSMISSION)
Multibus-based parallel processor for simulation p 169 A85-28613

CHARGED PARTICLES
Suprathermal plasma observed on STS-3 Mission by plasma diagnostics package p 179 N85-22472
Discharges on a negatively biased solar cell array in a charged-particle environment p 160 N85-22499
Spacecraft environmental interactions: A joint Air Force and NASA research and technology program p 40 N85-22517
Multistage spent particle collector and a method for making same [NASA-CASE-LEW-13914-1] p 135 N85-33489

CHELATES
Mechanism for chelated sulfate formation from SO2 and bis (triphenylphosphine) platinum p 62 A85-48493

CHEMICAL ATTACK
Study of Kapton under simulated shuttle environment [NASA-CR-176003] p 41 N85-29997
Burner rig corrosion of SiC at 1000 deg C [NASA-TM-87061] p 53 N85-30011

CHEMICAL BONDS
Why CO bonds side-on at low coverage and both side-on and upright at high coverage on the Cr(110) surface [NASA-CR-176071] p 77 N85-32173

CHEMICAL CLOUDS
Effects of chemical releases by the STS 3 orbiter on the ionosphere p 166 A85-29538

CHEMICAL COMPOSITION
Milling of Si3N4 with Si3N4 hardware [NASA-TM-86864] p 84 N85-10191
Optimization of the NiCrAl-Y/ZrO-Y2O3 thermal barrier system [NASA-TM-86905] p 72 N85-15878

CHEMICAL EQUILIBRIUM
Effect of water on hydrogen permeability --- Stirling engines [NASA-TM-86904] p 53 N85-14864
Computer program for calculation of complex chemical equilibrium compositions and applications. Supplement 1: Transport properties [NASA-TM-86885] p 184 N85-16663
Combustion gas properties. Part 3: Hydrogen gas fuel and dry air [NASA-TP-2477] p 32 N85-31058

CHEMICAL PROPULSION
Preliminary assessment of power-generating tethers in space and of propulsion for their orbit maintenance p 37 N85-22520
Primary propulsion of electrothermal, ion and chemical systems for space-based radar orbit transfer [NASA-TM-87043] p 51 N85-27972

CHEMICAL REACTIONS
Reactions of NaCl with gaseous SO3, SO2, and O2 p 59 A85-11897
Direct numerical simulations of a reacting mixing layer with chemical heat release [AIAA PAPER 85-0143] p 60 A85-19548
Direct simulations of chemically reacting turbulent mixing layers [AIAA PAPER 85-0321] p 60 A85-19666
Chemical reactions involved in the initiation of hot corrosion of IN-738 p 66 A85-31688
Mechanism for forming hydrogen chloride and sodium sulfate from sulfur trioxide, water, and sodium chloride p 62 A85-48513
The reactions of cobalt, iron and nickel in SO-2 atmospheres: Similarities and differences [NASA-TM-86868] p 70 N85-11217
Integrating chemical kinetic rate equations by selective use of stiff and nonstiff methods [NASA-TM-86923] p 24 N85-15726
Imide modified epoxy matrix resins [NASA-CR-174695] p 85 N85-15892
Chemical approach for controlling nadimide cure temperature and rate [NASA-CASE-LEW-13770-5] p 87 N85-21352
Shock tube study of the fuel structure effects on the chemical kinetic mechanisms responsible for soot formation, part 2 [NASA-CR-174880] p 63 N85-25444

CHEMICAL TESTS
Chemical approach for controlling nadimide cure temperature and rate [NASA-CASE-LEW-13770-6] p 63 N85-30039

CHEMISORPTION
Why CO bonds side-on at low coverage and both side-on and upright at high coverage on the Cr(110) surface [NASA-CR-176071] p 77 N85-32173

CHIPS (ELECTRONICS)
High-voltage solar-cell chip p 154 A85-24668

CHLORIDES
Dynamics of graphite fiber intercalation: In situ resistivity measurements with a four point probe [NASA-TM-86858] p 53 N85-10105

CHROMIUM
Optimization of the NiCrAl-Y/ZrO-Y2O3 thermal barrier system [NASA-TM-86905] p 72 N85-15878
Effects of chromium and aluminum on mechanical and oxidation properties of iron-nickel-base superalloys based on CG-27 [NASA-TP-2443] p 75 N85-21323
Dispersed-metal-toughened alumina [NASA-CR-174687] p 89 N85-22758
Why CO bonds side-on at low coverage and both side-on and upright at high coverage on the Cr(110) surface [NASA-CR-176071] p 77 N85-32173
Development of electrodes for the NASA iron/chromium [NASA-CR-174724] p 165 N85-35471

CHROMIUM ALLOYS
Orientation and temperature dependence of some mechanical properties of the single-crystal nickel-base superalloy Rene N4. 3: Tension-compression anisotropy [NASA-TM-86982] p 76 N85-22660
Study of the effects of implantation on the high Fe-Ni-Cr and Ni-Cr-Al alloys [NASA-CR-175625] p 76 N85-22661

CHROMIUM CARBIDES
Effects of silver and group 2 fluorides addition to plasma sprayed chromium carbide high temperature solid lubricant for foil gas bearing to 650 deg C [NASA-TM-86895] p 84 N85-14928

CHROMIUM COMPOUNDS
Chemical and electrochemical behavior of the Cr(III)/Cr(II) half-cell in the iron-chromium redox energy storage system p 61 A85-33785

CHROMIUM STEELS
Frictional and structural characterization of ion-nitrided low and high chromium steels [NASA-TM-86991] p 132 N85-23085

CIRCUIT BREAKERS
High-voltage, high-power, solid-state remote power controllers for aerospace applications [NASA-TP-2437] p 49 N85-21263

CIRCUIT PROTECTION
Circuit transients due to negative bias arcs on a high-voltage solar array in low Earth orbit [NASA-TP-2407] p 39 N85-14858

CIRCUITS
Design of low loss helix circuits for interference fitted and brazed circuits [NASA-CR-168313] p 103 N85-19328

CIRCULAR CYLINDERS
Heat transfer investigation in the junction region of circular cylinder normal to a flat plate at 90 deg location [ASME PAPER 84-WA/HT-70] p 111 A85-39898
The influence of jet-grid turbulence on heat transfer from the stagnation region of a cylinder in crossflow [NASA-TM-87011] p 115 N85-25760

CIRCULAR PLATES
Vibration and flutter of mistuned bladed-disk assemblies [AIAA PAPER 84-0991] p 139 A85-16095
Vibration and flutter of mistuned bladed-disk assemblies p 16 A85-45854

CIRCULAR WAVEGUIDES
Circular waveguide bifurcation for asymmetric modes p 101 A85-20170
Plot of modal field distribution in rectangular and circular waveguides p 101 A85-25170

CIVIL AVIATION
Energy efficient engine. Volume 2. Appendix A: Component development and integration program [NASA-CR-173085] p 22 N85-10991

CLADDING
Manufacturing process to reduce large grain growth in zirconium alloys [DE85-011649] p 78 N85-34267

CLEAN ENERGY
Measured effects of wind turbine generation at the Block Island Power Company p 153 A85-10652

CLEARANCES
Dual clearance squeeze film damper for high load conditions [ASME PAPER 84-TRIB-7] p 128 A85-32960

CLIMATOLOGY
Variability of cloudiness at airline cruise altitudes from GASP measurements p 166 A85-31199

CLIMBING FLIGHT
Wind tunnel results of advanced high speed propellers in the takeoff, climb, and landing operating regimes [AIAA PAPER 85-1259] p 6 A85-47025
Wind tunnel results of advanced high speed propellers in the takeoff, climb and landing operating regimes [NASA-TM-87054] p 9 N85-29925

CLOSE PACKED LATTICES
Effect of hot isostatic pressing on the properties of sintered alpha silicon carbide p 83 A85-48757

CLOSED CYCLES
Advanced technology cogeneration system conceptual design study: Closed cycle gas turbines [NASA-CR-168222] p 159 N85-16300

CLOSURE LAW
A study of Reynolds-stress closure model [NASA-CR-174342] p 114 N85-17324

CLOUD COVER
Variability of cloudiness at airline cruise altitudes from GASP measurements p 166 A85-31199

CLOUDS (METEOROLOGY)
GASP cloud encounter statistics - Implications for laminar flow control flight p 166 A85-11979
Comparison of icing cloud instruments for 1982-1983 icing season flight program [AIAA PAPER 84-0020] p 13 A85-16098

COASTAL ZONE COLOR SCANNER
Comparison of atmospheric correction algorithms for the Coastal Zone Color Scanner p 153 A85-10244

COATING
Textured carbon surfaces on copper [NASA-CASE-LEW-14130-1] p 95 N85-20156

COATINGS
RF-sputtered silicon and hafnium nitrides - Properties and adhesion to 440C stainless steel p 81 A85-36240
Turbine Engine Hot Section Technology (HOST) [NASA-TM-83022] p 18 N85-10951
Plasma variables and tribological properties of coatings in low pressure (0.1 - 10.0 torr) plasma systems [NASA-TM-83798] p 94 N85-11261
Effect of water on hydrogen permeability — Stirling engines [NASA-TM-86904] p 53 N85-14864
Experimental test program for evaluation of solid lubricant coating as applied to compliant foil gas bearings to 315 deg C [NASA-CR-174837] p 85 N85-15895
Diamondlike flakes [NASA-CASE-LEW-13837-2] p 57 N85-21267
Numerical methods for analyzing electromagnetic scattering [NASA-CR-175507] p 99 N85-21438
Advanced thin film thermocouples [NASA-CR-175541] p 124 N85-21607

COAXIAL CABLES
Dual-mode coaxial feed with low crosspolarisation p 101 A85-20171

COAXIAL FLOW
Mass and momentum turbulent transport experiments with confined coaxial jets p 107 A85-14399
Turbulent transport and length scale measurement experiments with comfined coaxial jets [NASA-CR-174831] p 117 N85-30245

COBALT
Effects of cobalt, boron, and zirconium on the microstructure of Udimet 738 [NASA-CR-174762] p 70 N85-10166
The reactions of cobalt, iron and nickel in SO-2 atmospheres: Similarities and differences [NASA-TM-86868] p 70 N85-11217
The response of cobalt-free Udimet 700 type alloy to modified heat treatments [NASA-TM-86942] p 75 N85-20043

COBALT ALLOYS
Effects of cobalt on the hot workability of nickel-base superalloys p 67 A85-32412
Quasi-static solution algorithms for kinematically/materially nonlinear thermomechanical problems p 143 A85-41983
Creep-rupture behavior of iron superalloys in high-pressure hydrogen [NASA-CR-174411] p 74 N85-19078

COGENERATION
Advanced technology cogeneration system conceptual design study: Closed cycle gas turbines [NASA-CR-168222] p 159 N85-16300

COLLIMATION
Electronic heterodyne readout of fringes in moire deflectometry p 122 A85-36726

COLOR CODING
An allpass filter design for luminance and chrominance separation of NTSC signals p 102 A85-28230
COLOR PHOTOGRAPHY
Rainbow schlieren vs Mach-Zehnder interferometer - A comparison p 121 A85-28820
COLOR TELEVISION
An allpass filter design for luminance and chrominance separation of NTSC signals p 102 A85-28230
Experimental results supporting the determination of service quality objectives for DBS systems p 96 A85-29611
COMBINED STRESS
On stress field near a stationary crack tip [AD-A152863] p 141 A85-24532
COMBUSTIBLE FLOW
Prediction of an axisymmetric combusting flow p 59 A85-12713
Direct simulations of chemically reacting turbulent mixing layers [AIAA PAPER 85-0321] p 60 A85-19666
Growth of a diffusion flame in the field of a vortex p 61 A85-47320
Dilution zone mixing studies p 21 N85-10984
The mechanisms of flame holding in the wake of a bluff body [NASA-CR-3866] p 26 N85-21166
Investigation of flowfields found in typical combustor geometries [NASA-CR-3869] p 26 N85-21167
Error reduction program --- combustor performance evaluation codes [NASA-CR-174776] p 172 N85-27584
COMBUSTION
Integrating chemical kinetic rate equations by selective use of stiff and nonstiff methods [AIAA PAPER 85-0237] p 60 A85-19607
CREKID: A computer code for transient, gas-phase combustion of kinetics [NASA-TM-83806] p 17 N85-10068
Turbine Engine Hot Section Technology (HOST) [NASA-TM-83022] p 18 N85-10951
New integration techniques for chemical kinetic rate equations. 2: Accuracy comparison [NASA-TM-86893] p 23 N85-13798
Integrating chemical kinetic rate equations by selective use of stiff and nonstiff methods [NASA-TM-86923] p 24 N85-15726
The structure of dilute combusting sprays [NASA-CR-174838] p 24 N85-15728
Combustion gas properties. 2: Natural gas fuel and dry air [NASA-TP-2435] p 26 N85-21168
Fuel rich catalytic comustion: The first stage of a two-stage combustor [NASA-TM-87042] p 63 N85-28983
Combustion gas properties. Part 3: Hydrogen gas fuel and dry air [NASA-TP-2477] p 32 N85-31058
COMBUSTION CHAMBERS
The influence of combustion liner holes on noise production by ducted burners [AIAA PAPER 84-2322] p 172 A85-10869
Analysis of the effect on combustor noise measurements of acoustic waves reflected by the turbine and combustor inlet [AIAA PAPER 84-2323] p 173 A85-16103
Calculation of confined swirling flows [AIAA PAPER 85-0060] p 108 A85-19491
Flame flashback in a premixed dump combustor [AIAA PAPER 85-0145] p 60 A85-19550
Swirling flows in typical combustor geometries [AIAA PAPER 85-0184] p 108 A85-19574
Direct simulations of chemically reacting turbulent mixing layers [AIAA PAPER 85-0321] p 60 A85-19666
Aerodynamic effect of combustor inlet air pressure on fuel jet atomization p 109 A85-27096
Flame radiation and linear heat transfer in a tubular-can combustor p 15 A85-39580
Turbulence measurements of lateral jet injection into confined tubular crossflow [AIAA PAPER 85-1102] p 110 A85-39604
Experiments in dilution jet mixing - Effects of multiple rows and non-circular orifices [AIAA PAPER 85-1104] p 15 A85-39606
Advanced liner-cooling techniques for gas turbine combustors [AIAA PAPER 85-1290] p 15 A85-39703
Small gas turbine combustor study - Fuel injector performance in a transpiration-cooled liner [AIAA PAPER 85-1312] p 16 A85-39717
Progress report - Advanced cryogenic OTV engine technology [AIAA PAPER 85-1341] p 44 A85-39735
Combustion efficiency of a premixed continuous flow combustor p 61 A85-42571
Future fundamental combustion research for aeropropulsion systems [AIAA PAPER 85-1398] p 16 A85-42671
Internal combustion engine combustion chamber process studies at NASA Lewis Research Center p 112 A85-45856
Turbine Engine Hot Section Technology (HOST) [NASA-TM-83022] p 18 N85-10951
Nonlinear structural and life analyses of a combustor liner p 19 N85-10955
Effects of surface chemistry on hot corrosion life: Overview p 21 N85-10980
Dilution zone mixing studies p 21 N85-10984
Combustion system for radiation investigations p 21 N85-10986
Validation of structural analysis methods using the in-house liner cyclic rigs p 21 N85-10987
Energy efficient engine component development and integration program [NASA-CR-170034] p 22 N85-10990
The structure of dilute combusting sprays [NASA-CR-174838] p 24 N85-15728
Analytical fuel property effects: Small combustors, phase 2 [NASA-CR-174848] p 93 N85-19175
Advanced liner-cooling techniques for gas turbine combustors [NASA-TM-86952] p 8 N85-21115
Combustion research for gas turbine engines [NASA-TM-86963] p 26 N85-21164
Investigation of flowfields found in typical combustor geometries [NASA-CR-3869] p 26 N85-21167
Deflected jet experiments in a turbulent combustor flowfield [NASA-CR-174863] p 26 N85-22390
Dilution jet configurations in a reverse flow combustor [NASA-CR-174888] p 27 N85-22392
Small gas turbine combustor study: Fuel injector performance in a transpiration-cooled liner [NASA-TM-86989] p 27 N85-25264
Experiments in dilution jet mixing effects of multiple rows and non-circular orifices [NASA-TM-86996] p 28 N85-25266
Analytical fuel property effects--small combustors [NASA-CR-174738] p 28 N85-26709
Turbulence characteristics of swirling flowfields [NASA-CR-174918] p 29 N85-26717
Rocket thrust chamber thermal barrier coatings p 90 N85-26867
Error reduction program --- combustor performance evaluation codes [NASA-CR-174776] p 172 N85-27584
Predictions and measurements of isothermal flowfields in axisymmetric combustor geometries [NASA-CR-174916] p 29 N85-27867
The role of surface generated radicals in catalytic combustion p 30 N85-27869
Future fundamental combustion research for aeropropulsion systems [NASA-TM-87049] p 30 N85-27870
Fuel rich catalytic comustion: The first stage of a two-stage combustor [NASA-TM-87042] p 63 N85-28983
Combustor turbulence p 118 N85-31434
Flow modifying device [NASA-CASE-LEW-13562-2] p 33 N85-35195
Development of advanced high-temperature heat flux sensors. Phase 2: Verification testing [NASA-CR-174973] p 126 N85-35391
COMBUSTION CHEMISTRY
Comparison of numerical techniques for integration of stiff ordinary differential equations arising in combustion chemistry [NASA-TP-2372] p 17 N85-10065
COMBUSTION CONTROL
Energy efficient engine combustor test hardware detailed design report [NASA-CR-167945] p 18 N85-10950
The mechanisms of flame holding in the wake of a bluff body [NASA-CR-174058] p 62 N85-11149
COMBUSTION EFFICIENCY
Flame flashback in a premixed dump combustor [AIAA PAPER 85-0145] p 60 A85-19550
Aerodynamic effect of combustor inlet air pressure on fuel jet atomization p 109 A85-27096
Combustion efficiency of a premixed continuous flow combustor p 61 A85-42571
Comparison of numerical techniques for integration of stiff ordinary differential equations arising in combustion chemistry [NASA-TP-2372] p 17 N85-10065
An interactive computer code for calculation of gas-phase chemical equilibrium (EQLBRM) [NASA-CR-168337] p 18 N85-10948
The mechanisms of flame holding in the wake of a bluff body [NASA-CR-174058] p 62 N85-11149
Shock tube study of the fuel structure effects on the chemical kinetic mechanisms responsible for soot formation, part 2 [NASA-CR-174880] p 63 N85-25444
The role of surface generated radicals in catalytic combustion p 30 N85-27869
SSME fuel preburner two-dimensional analysis p 51 N85-27943
COMBUSTION PHYSICS
The mechanisms of flame holding in the wake of a bluff body [NASA-CR-174058] p 62 N85-11149
A comparison of the efficiency of numerical methods for integrating chemical kinetic rate equations [NASA-TM-83590] p 25 N85-21162
COMBUSTION PRODUCTS
Polarization (ellipsometric) measurements of liquid condensate deposition and evaporation rates and dew points in flowing salt/ash-containing combustion gases p 123 A85-46925
Combustion gas properties I-ASTM jet A fuel and dry air [NASA-TP-2359] p 17 N85-10064
Combustion gas properties. 2: Natural gas fuel and dry air [NASA-TP-2435] p 26 N85-21168
Digital temperature and velocity control of mach 0.3 atmospheric pressure durability testing burner rigs in long time, unattended cyclic testing [NASA-TM-86959] p 75 N85-21321
Jet fuel instability mechanisms [NASA-CR-175856] p 93 N85-28127
Fuel-rich catalytic combustion: A soot-free technique for in situ hydrogen-like enrichment [NASA-TP-2498] p 63 N85-31244
COMBUSTION STABILITY
A theoretical prediction of the acoustic pressure generated by turbulence-flame front interactions [ASME PAPER 84-WA/NCA-11] p 174 A85-39909
Chemistry of fuel deposits and sediments and their predursors [NASA-CR-174778] p 92 N85-10209
Combustor turbulence p 118 N85-31434
COMMERCIAL AIRCRAFT
Variability of cloudiness at airline cruise altitudes from GASP measurements p 166 A85-31199
Energy efficient engine component development and integration program [NASA-CR-170034] p 22 N85-10990
Study of advanced fuel system concepts for commercial aircraft and engines [NASA-CR-174752] p 93 N85-19176
Study of advanced fuel system concepts for commercial aircraft [NASA-CR-174751] p 12 N85-19978
COMMUNICATION SATELLITES
Status of NASA's multibeam communications technology program p 100 A85-14432
A 20 GHz, 75 watt, helix TWT for space communications p 101 A85-14433
Satellite baseband processor test performance summary p 95 A85-14434
The NASA satellite communication 20 x 20 matrix switches p 101 A85-14435
Advanced 30/20 GHz multiple beam antenna for future communications satellites p 96 A85-14436
Ion propulsion for communications satellites p 42 A85-16412
Technical characteristics of the broadcasting satellite plan at 12 GHz for the Western Hemisphere p 96 A85-28233
On the subjective evaluation of the interference protection ratios' measurements for co-channel FM-TV signals p 96 A85-28241
Development and use of the computer software package for planning the 12 GHz broadcasting-satellite service at RARC '83 p 96 A85-29605
Four-dimensional modulation and coding - An alternate to frequency-reuse p 97 A85-36653
Modeling of NASA's 30/20 GHz satellite communications system p 38 A85-36663
Demand for satellite-provided domestic communications services up to the year 2000 [NASA-TM-86894] p 97 N85-15099
Engineering calculations for communications satellite systems planning [NASA-CR-175552] p 37 N85-21233
Alternatives for satellite sound broadcast systems at HF and VHF p 99 N85-23815

Satellite provided customer promises services, a forecast of potential domestic demand through the year 2000. Volume 4: Sensitivity analysis
[NASA-CR-174662] p 99 N85-27092
Telecommunications forecast for ITU Region 2 to the year 1995
[NASA-TM-87077] p 38 N85-34150

COMPARISON
Predicted turbine stage performance using quasi-three-dimensional and boundary-layer analyses p 15 A85-34013

COMPENSATORS
A fast time domain digital simulation technique for power converters - Application to a buck converter with feedforward compensation p 101 A85-20900

COMPONENT RELIABILITY
Creep-rupture reliability analysis p 143 A85-42566
Engine cyclic durability by analysis and material testing p 25 N85-15744
Component-specific modeling
[NASA-CR-174765] p 147 N85-27261
Composite loads spectra for select space propulsion structural components p 148 N85-27953
High pressure compressor component performance report
[NASA-CR-168245] p 33 N85-34138

COMPOSITE MATERIALS
Advanced blade tip seal system, volume 2
[NASA-CR-167851] p 23 N85-10999
Chemical approach for controlling nadimide cure temperature and rate with maleimide
[NASA-CASE-LEW-13770-3] p 87 N85-21350
Chemical approach for controlling nadimide cure temperature and rate with maleimide
[NASA-CASE-LEW-13770-4] p 87 N85-21351
A study of the stress wave factor technique for the characterization of composite materials
[NASA-CR-174870] p 58 N85-30035

COMPOSITE STRUCTURES
Design procedures for fiber composite structural components - Rods, beams, and beam columns p 54 A85-15636
Fracture of composite-adhesive-composite systems p 141 A85-27935

COMPOSITION (PROPERTY)
The effects of Cr, Co, Al, Mo and Ta on the cyclic oxidation behavior of a prototype cast Ni-base superalloy based on a 2(5) composite statistically designed experiment
[NASA-TM-83784] p 71 N85-12131

COMPOUNDING
Milling of Si3N4 with Si3N4 hardware
[NASA-TM-86864] p 84 N85-10191

COMPRESSED GAS
Internal hysteresis experienced on a high pressure syn gas compressor p 131 N85-14122

COMPRESSIBLE FLOW
Acoustic pressures emanating from a turbomachine stage
[AIAA PAPER 84-2325] p 2 A85-10870
Two-dimensional internal compressible viscous flows using semi-elliptic analysis p 106 A85-11640
Calculation of compressible flow about three-dimensional inlets with auxiliary inlets, slats and vanes by means of a panel method
[AIAA PAPER 85-1196] p 5 A85-40817
The three-dimensional compressible flow in a radial inflow turbine scroll p 6 A85-41826
Rotordynamic coefficients for compressible flow in tapered annular seals p 129 A85-42573
Application of computational fluid dynamics to complex inlet ducts
[AIAA PAPER 85-1213] p 6 A85-47023
Application of computational fluid dynamics to complex inlet ducts
[NASA-TM-87060] p 118 N85-30247
Calculation of compressible flow about three-dimensional inlets with auxiliary inlets, slats and vanes by means of a panel method
[NASA-CR-174975] p 10 N85-35162

COMPRESSION LOADS
Design procedures for fiber composite structural components - Rods, beams, and beam columns p 54 A85-15636
Orientation and temperature dependence of some mechanical properties of the single-crystal nickel-base superalloy Rene N4. 3: Tension-compression anisotropy
[NASA-TM-86982] p 76 N85-22660

COMPRESSOR BLADES
Optimization of cascade blade mistuning. I - Equations of motion and basic inherent properties p 16 A85-42365
Rotor wake characteristics of a transonic axial flow fan
[AIAA PAPER 85-1133] p 6 A85-43974
Optimization of cascade blade mistuning. II - Global optimum and numerical optimization p 16 A85-45715
Unsteady flow in a supersonic cascade with two in-passage shocks
[NASA-CR-3925] p 10 N85-35158

COMPRESSOR ROTORS
Energy efficient engine component development and integration program
[NASA-CR-170034] p 22 N85-10990

COMPRESSORS
Energy efficient engine. High pressure compressor detail design report
[NASA-CR-165558] p 23 N85-10998
Nonlinear global stability analysis of compressor stall phenomena
[NASA-CR-174908] p 31 N85-29960
High pressure compressor component performance report
[NASA-CR-168245] p 33 N85-34138

COMPUTATION
Error reduction program --- combustor performance evaluation codes
[NASA-CR-174776] p 172 N85-27584

COMPUTATIONAL CHEMISTRY
Integrating chemical kinetic rate equations by selective use of stiff and nonstiff methods
[NASA-TM-86923] p 24 N85-15726

COMPUTATIONAL FLUID DYNAMICS
Computation of internal flows: Methods and applications; Proceedings of the Energy Sources Technology Conference, New Orleans, LA, February 12-16, 1984 p 106 A85-11630
Computation of viscous flows in turbomachinery cascades p 106 A85-11631
Two-dimensional internal compressible viscous flows using semi-elliptic analysis p 106 A85-11640
Analytical study of blowing boundary layer control for subsonic V/STOL inlets p 2 A85-11646
Development of finite analytic method for unsteady three-dimensional Navier-Stokes equation p 106 A85-11647
Prediction of an axisymmetric combusting flow p 59 A85-12713
Computation and turbulence closure models for shear flows in rotating curved bodies p 107 A85-14349
Efficient solution of the Euler and Navier-Stokes equations with a vectorized multiple-grid algorithm p 2 A85-18679
Finite difference methods for reducing numerical diffusion in TEACH-type calculations --- Teaching Elliptic Axisymmetric Characteristics Heuristically
[AIAA PAPER 85-0057] p 108 A85-19488
Calculation of confined swirling flows
[AIAA PAPER 85-0060] p 108 A85-19491
Computational thermo-fluid dynamics contributions to advanced gas turbine engine design
[AIAA PAPER 85-0083] p 14 A85-19509
Direct numerical simulations of a reacting mixing layer with chemical heat release
[AIAA PAPER 85-0143] p 60 A85-19548
A space-marching method for incompressible Navier-Stokes equations
[AIAA PAPER 85-0170] p 108 A85-19564
Swirling flows in typical combustor geometries
[AIAA PAPER 85-0184] p 108 A85-19574
Progress in development of a Navier-Stokes solver for evaluation of iced airfoil performance
[AIAA PAPER 85-0410] p 3 A85-19731
Assessment of discretization schemes to reduce numerical diffusion in the calculation of complex flows
[AIAA PAPER 85-0441] p 108 A85-19751
Computation of three-dimensional viscous flows using a space-marching method p 4 A85-29259
Lubricant jet flow phenomena in spur and helical gears with modified center distances and/or addendums - For out-of-mesh conditions
[ASME PAPER 84-DET-96] p 129 A85-35049
Application of viscous and inviscid computation methods for rocket turbopump systems
[SAE PAPER 841522] p 110 A85-39257
Application of Runge Kutta time marching scheme for the computation of transonic flows in turbomachines
[AIAA PAPER 85-1332] p 5 A85-39728
Turbulence modelling for complex shear flows
[AIAA PAPER 85-1652] p 111 A85-40752
Calculation of compressible flow about three-dimensional inlets with auxiliary inlets, slats and vanes by means of a panel method
[AIAA PAPER 85-1196] p 5 A85-40817
Time dependent computation of the Euler equations for designing 2-D cascades, including the case of transonic shock free design p 5 A85-41814
Future fundamental combustion research for aeropropulsion systems
[AIAA PAPER 85-1398] p 16 A85-42671
The computation of viscid/inviscid interaction on airfoils with separated flow p 6 A85-42954
A three-dimensional boundary-layer analysis including heat-transfer and blade-rotation effects p 6 A85-42988
Inviscid analysis of advanced turboprop propeller flow fields
[AIAA PAPER 85-1263] p 6 A85-43977
Application of computational fluid dynamics to complex inlet ducts
[AIAA PAPER 85-1213] p 6 A85-47023
A multiple-scales model of the shock-cell structure of imperfectly expanded supersonic jets p 113 A85-49354
Computational thermo-fluid dynamics contributions to advanced gas turbine engine design
[NASA-TM-86865] p 18 N85-10069
Inverse design technique for cascades
[NASA-CR-3836] p 7 N85-12008
Model equation for simulating flows in multistage turbomachinery
[NASA-TM-86869] p 7 N85-12036
Researched applied to transonic compressors in numerical fluid mechanics of inviscid flow and viscous flow
[NASA-CR-174353] p 114 N85-18291
NASA Lewis Research Center/University Graduate Research Program on Engine Structures
[NASA-TM-86916] p 145 N85-18375
Combustion research for gas turbine engines
[NASA-TM-86963] p 26 N85-21164
Future fundamental combustion research for aeropropulsion systems
[NASA-TM-87049] p 30 N85-27870
Application of computational fluid dynamics to complex inlet ducts
[NASA-TM-87060] p 118 N85-30247

COMPUTATIONAL GRIDS
Rational approach for assumed stress finite elements p 139 A85-12029
Efficient solution of the Euler and Navier-Stokes equations with a vectorized multiple-grid algorithm p 2 A85-18679
Finite difference methods for reducing numerical diffusion in TEACH-type calculations --- Teaching Elliptic Axisymmetric Characteristics Heuristically
[AIAA PAPER 85-0057] p 108 A85-19488
Inviscid and viscous flows in cascades with an explicit multiple-grid algorithm p 7 A85-48539

COMPUTER AIDED DESIGN
Interdisciplinary design analysis of a precision spacecraft antenna
[AIAA PAPER 85-0804] p 38 A85-30303
Finite element engine blade structural optimization
[AIAA PAPER 85-0645] p 141 A85-30313
A computer aided design procedure for generating gear teeth
[ASME PAPER 84-DET-184] p 128 A85-33779
Design considerations for a 10-kW integrated hydrogen-oxygen regenerative fuel cell system p 155 A85-45380
Advanced secondary power system for transport aircraft
[NASA-TP-2463] p 30 N85-28944
Design and lubrication of high-speed rolling-element bearings
[NASA-TM-87107] p 137 N85-34409

COMPUTER GRAPHICS
A computer aided design procedure for generating gear teeth
[ASME PAPER 84-DET-184] p 128 A85-33779

COMPUTER NETWORKS
Optical computer switching network p 178 A85-23134
Data flow methods for dynamic system simulation - A CSSL-IV microcomputer network interface p 170 A85-28614

COMPUTER PROGRAMS
Progress toward the development of an aircraft icing analysis capability
[AIAA PAPER 84-0105] p 10 A85-10653
ICAN - Integrated composites analyzer
[AIAA PAPER 84-0974] p 54 A85-16094
Analytical determination of propeller performance degradation due to ice accretion
[AIAA PAPER 85-0339] p 14 A85-20867
A simplified method for elastic-plastic-creep structural analysis
[ASME PAPER 84-GT-191] p 141 A85-23150
Assessment of three-dimensional inviscid codes and loss calculations for turbine aerodynamic computations
[ASME PAPER 84-GT-187] p 4 A85-32961
Design and performance of a fixed, nonaccelerating guide vane cascade that operates over an inlet flow angle range of 60 deg
[ASME PAPER 84-GT-75] p 4 A85-32964

Predicted turbine stage performance using quasi-three-dimensional and boundary-layer analyses p 15 A85-34013
A study of interply layer effects on the free edge stress field of angleplied laminates p 55 A85-41127
A generalized computer code for developing dynamic gas turbine engine models (DIGTEM) p 17 A85-49021
CREKID: A computer code for transient, gas-phase combustion of kinetics
[NASA-TM-83806] p 17 N85-10068
Manual of phosphoric acid fuel cell stack three-dimensional model and computer program
[NASA-CR-174722] p 157 N85-10447
Floating-point function generation routines for 16-bit microcomputers
[NASA-TM-83783] p 170 N85-10683
An interactive computer code for calculation of gas-phase chemical equilibrium (EQLBRM)
[NASA-CR-168337] p 18 N85-10948
Phosphoric acid fuel cell power plant system performance model and computer program
[NASA-CR-174638] p 157 N85-11456
Turbofan noise generation. Volume 2: Computer programs
[NASA-CR-167952] p 175 N85-11791
Development of gas-lubricated pistons for heavy duty diesel engine technology program
[NASA-CR-174746] p 184 N85-12808
Integrating chemical kinetic rate equations by selective use of stiff and nonstiff methods
[NASA-TM-86923] p 24 N85-15726
A study of interply layer effects on the free-edge stress field of angleplied laminates
[NASA-TM-86924] p 57 N85-15822
Computer program for calculation of complex chemical equilibrium compositions and applications. Supplement 1: Transport properties
[NASA-TM-86885] p 184 N85-16663
Modeling the internal combustion engine
[NASA-RP-1094] p 172 N85-19733
3-D inelastic analysis methods for hot section components (base program) --- turbine blades, turbine vanes, and combustor liners
[NASA-CR-174700] p 145 N85-21686
Three-dimensional calculation of shuttle charging in polar orbit p 40 N85-22486
NASCAP simulation of PIX 2 experiments p 180 N85-22497
Confined turbulent swirling recirculating flow predictions
[NASA-CR-174917] p 29 N85-26716
Computer program for the calculation of multicomponent convective diffusion deposition rates from chemically frozen boundary layer theory
[NASA-CR-168329] p 116 N85-27164
Component-specific modeling
[NASA-CR-174765] p 147 N85-27261
Error reduction program --- combustor performance evaluation codes
[NASA-CR-174776] p 172 N85-27584
Predictions and measurements of isothermal flowfields in axisymmetric combustor geometries
[NASA-CR-174916] p 29 N85-27867
Composite loads spectra for select space propulsion structural components: Probabilistic load model development p 148 N85-27954
Probabilistic finite element development p 149 N85-27956
Multi-mesh gear dynamics program evaluation and enhancements
[NASA-CR-174747] p 133 N85-28372
DEAN: A program for dynamic engine analysis
[NASA-TM-87033] p 30 N85-28945
Fast approach for calculating film thicknesses and pressures in elastohydrodynamically lubricated contacts at high loads
[NASA-TM-87032] p 117 N85-30242
Combustion gas properties. Part 3: Hydrogen gas fuel and dry air
[NASA-TP-2477] p 32 N85-31058
A comparison of smooth specimen and analytical simulation techniques for notched members at elevated temperatures p 151 N85-31546
Component-specific modeling
[NASA-CR-174925] p 32 N85-32119
Component-specific modeling
[NASA-CR-174765] p 33 N85-34140
General design method for 3-dimensional, potential flow fields. Part 2: Computer program DIN3D1 for simple, unbranched ducts
[NASA-CR-3926] p 10 N85-35159

COMPUTER SYSTEMS DESIGN
General approaches for achieving high speed computations p 169 A85-28628

COMPUTER SYSTEMS PERFORMANCE
General approaches for achieving high speed computations p 169 A85-28628

COMPUTER SYSTEMS PROGRAMS
Development and use of the computer software package for planning the 12 GHz broadcasting-satellite service at RARC '83 p 96 A85-29605
MINDS: A microcomputer interactive data system for 8086-based controllers
[NASA-TP-2378] p 170 N85-17576

COMPUTER SYSTEMS SIMULATION
Hardware for a real-time multiprocessor simulator
[NASA-TM-83805] p 169 N85-10659

COMPUTER TECHNIQUES
Recent advances in methods for numerical solution of O.D.E. initial value problems p 171 A85-21370
Closed-loop strain controlled testing at elevated temperatures with a non-contacting gage p 121 A85-29562

COMPUTERIZED SIMULATION
Control algorithms and computer simulation of a stand-alone photovoltaic village power system p 153 A85-11345
Numerical simulations of positively-biased probes and dielectric-conductor disks in a plasma --- for low earth orbit plasma densities p 179 A85-17262
Direct simulations of chemically reacting turbulent mixing layers
[AIAA PAPER 85-0321] p 60 A85-19666
Computer simulation of plasma electron collection by PIX-II --- solar array-space plasma interaction
[AIAA PAPER 85-0386] p 43 A85-19715
Circular waveguide bifurcation for asymmetric modes p 101 A85-20170
On the development of hierarchical solution strategies for nonlinear finite element formulations p 171 A85-21979
Moving target, distributed, real-time simulation using Ada p 170 A85-34131
Numerical simulation of positive-potential conductors in the presence of a plasma and a secondary-emitting dielectric p 102 A85-35306
Computer simulation of thin film nucleation and growth p 181 A85-35308
On local total strain redistribution using a simplified cyclic inelastic analysis based on an elastic solution
[AIAA PAPER 85-1419] p 142 A85-39770
The J3 SCR model applied to resonant converter simulation p 102 A85-42156
Comparison of free-piston Stirling engine model predictions with RE1000 engine test data p 130 A85-45488
A computer simulation of thin film nucleation and growth: The Volmer-Weber case
[NASA-TM-86968] p 53 N85-21264
On local total strain redistribution using a simplified cyclic inelastic analysis based on an elastic solution
[NASA-TM-86913] p 145 N85-21690
Three-dimensional calculation of shuttle charging in polar orbit p 40 N85-22486
NASCAP simulation of PIX 2 experiments p 180 N85-22497
Simulation of multistage turbine flows p 116 N85-27945
DEAN: A program for dynamic engine analysis
[NASA-TM-87033] p 30 N85-28945

CONCENTRATION (COMPOSITION)
Simultaneous cabin and ambient ozone measurements on two Boeing 747 airplanes. Volume 3: October 1978 - July 1979
[NASA-TM-86883] p 167 N85-21872

CONCENTRATORS
Near-optimum design of GaAs-based concentrator space solar cells for 80 C operation p 153 A85-15800

CONCURRENT PROCESSING
Functional language and data flow architectures p 170 A85-28629

CONDUCTIVE HEAT TRANSFER
Oscillatory conductive heat transfer for a fiber in an ideal gas p 109 A85-26077

CONFERENCES
Computation of internal flows: Methods and applications; Proceedings of the Energy Sources Technology Conference, New Orleans, LA, February 12-16, 1984 p 106 A85-11630
Turbine Engine Hot Section Technology (HOST)
[NASA-TM-83022] p 18 N85-10951
Space Power
[NASA-CP-2352] p 47 N85-13880
Rotordynamic Instability Problems in High-Performance Turbomachinery
[NASA-CP-2338] p 131 N85-14116
OTV Propulsion Issues
[NASA-CP-2347] p 37 N85-16989
Spacecraft Environmental Interactions Technology, 1983
[NASA-CP-2359] p 39 N85-22470
Structural Integrity and Durability of Reusable Space Propulsion Systems
[NASA-CP-2381] p 51 N85-27941
Nonlinear Constitutive Relations for High Temperature Application, 1984
[NASA-CP-2369] p 150 N85-31530

CONFINEMENT
Behavior of turbulent gas jets in an axisymmetric confinement
[NASA-CR-174829] p 28 N85-25265

CONSERVATION LAWS
A convergent series expansion for hyperbolic systems of conservation laws
[NASA-CR-172557] p 168 N85-21990

CONSTITUTIVE EQUATIONS
Thermodynamically consistent constitutive equations for nonisothermal large strain, elasto-plastic, creep behavior
[AIAA PAPER 85-0621] p 142 A85-38425
Unified constitutive material models for nonlinear finite-element structural analysis --- gas turbine engine blades and vanes
[AIAA PAPER 85-1418] p 142 A85-39769
Constitutive modeling and computational implementation for finite strain plasticity p 143 A85-40910
Biaxial constitutive equation development for single crystals
[NASA-CR-174056] p 183 N85-11862
Viscoplastic constitutive relationships with dependence on thermomechanical history
[NASA-CR-174836] p 146 N85-21691
Unified constitutive material models for nonlinear finite-element structural analysis --- gas turbine engine blades and vanes
[NASA-TM-86985] p 146 N85-24338
On thermomechanical testing in support of constitutive equation development for high temperature alloys
[NASA-CR-174879] p 147 N85-25894
Nonlinear Constitutive Relations for High Temperature Application, 1984
[NASA-CP-2369] p 150 N85-31530
A survey of unified constitutive theories p 150 N85-31531
Numerical considerations in the development and implementation of constitutive models p 151 N85-31541
On numerical integration and computer implementation of viscoplastic models p 151 N85-31542
Finite element analysis of notch behavior using a state variable constitutive equation p 152 N85-31548

CONTACTORS
Free-surface phenomena under low- and zero-gravity conditions
[NASA-CR-175835] p 116 N85-27168

CONTAINERS
Flame radiation and linear heat transfer in a tubular-can combustor p 15 A85-39580

CONTROL MOMENT GYROSCOPES
Application of traction drives as servo mechanisms p 152 N85-33520

CONTROL SIMULATION
The use of Ada in distributed simulations p 169 A85-28612
Multibus-based parallel processor for simulation p 169 A85-28613
A functional language approach in high-speed digital simulation p 170 A85-28615
Control aspects of the Schuchuli Village stand-alone photovoltaic power system
[NASA-TM-83790] p 103 N85-13157

CONTROL THEORY
The role of modern control theory in the design of controls for aircraft turbine engines p 13 A85-13627
Nonlinear global stability analysis of compressor stall phenomena
[NASA-CR-174908] p 31 N85-29960

CONVECTIVE FLOW
Effect of airfoil mean loading on convected gust interaction noise
[AIAA PAPER 84-2324] p 173 A85-13955
A numerical study of the steady scalar convective diffusion equation for small viscosity p 107 A85-16533
Convective influence on the stability of a cylindrical solid-liquid interface p 109 A85-26911

CONVECTIVE HEAT TRANSFER
Methods for heat transfer and temperature field analysis of the insulated diesel
[NASA-CR-174783] p 185 N85-16699
Unsteady heat transfer due to time-dependent free stream velocity p 117 N85-27947

CONVERGENCE
Accelerated convergence for incompressible flow calculations
[AIAA PAPER 85-0058] p 2 A85-19489
The effect of channel convergence on heat transfer in a passage with short pin fins
[NASA-TM-83801] p 113 N85-10303
Accelerated convergence for incompressible flow calculations
[NASA-TM-86863] p 18 N85-10949
CONVERGENT NOZZLES
Experimental investigation of shock-cell noise reduction for dual-stream nozzles in simulated flight
[NASA-CR-3846] p 175 N85-13549
Experimental investigation of shock-cell noise reduction for single stream nozzles in simulated flight
[NASA-CR-3845] p 175 N85-13550
CONVERGENT-DIVERGENT NOZZLES
Supersonic jet shock noise reduction
[AIAA PAPER 84-2278] p 173 A85-16099
Experimental investigation of shock-cell noise reduction for dual-stream nozzles in simulated flight
[NASA-CR-3846] p 175 N85-13549
Experimental investigation of shock-cell noise reduction for single stream nozzles in simulated flight
[NASA-CR-3845] p 175 N85-13550
Vacuum chamber pressure effects on thrust measurements of low Reynolds number nozzles
[NASA-TM-86955] p 49 N85-21259
CONVEXITY
Heat transfer and turbulence measurements of a film-cooled flow over a convexly curved surface
p 112 A85-41787
CONVOLUTION INTEGRALS
Convoluted nozzle design for the RL10 derivative 2B engine
[NASA-CR-174953] p 32 N85-29965
COOLANTS
Coolant passage heat transfer with rotation
p 20 N85-10968
COOLING
Small gas turbine combustor study - Fuel injector performance in a transpiration-cooled liner
[AIAA PAPER 85-1312] p 16 A85-39717
The effect of channel convergence on heat transfer in a passage with short pin fins
[NASA-TM-83801] p 113 N85-10303
Fabrication of ceramic substrate-reinforced and free forms
[NASA-TM-86994] p 50 N85-23926
Small gas turbine combustor study: Fuel injector performance in a transpiration-cooled liner
[NASA-TM-86989] p 27 N85-25264
Performance analysis of radiation cooled dc transmission lines for high power space systems
[NASA-TM-87040] p 104 N85-28222
Design principles for nickel-hydrogen cells and batteries
[NASA-TM-87037] p 164 N85-31646
Design and lubrication of high-speed rolling-element bearings
[NASA-TM-87107] p 137 N85-34409
COOLING SYSTEMS
High thermal power density heat transfer apparatus providing electrical isolation at high temperature using heat pipes
[NASA-CASE-LEW-12950-2] p 117 N85-29179
Vortex generating flow passage design for increased film cooling effectiveness
[NASA-CASE-LEW-14039-1] p 119 N85-33433
COPOLYMERIZATION
Chemical control of nadimide cure temperature and rate
[NASA-CASE-LEW-13770-2] p 63 N85-28982
COPOLYMERS
Chemical approach for controlling nadimide cure temperature and rate with maleimide
[NASA-CASE-LEW-13770-3] p 87 N85-21350
Chemical approach for controlling nadimide cure temperature and rate with maleimide
[NASA-CASE-LEW-13770-4] p 87 N85-21351
Alkaline battery containing a separator of a cross-linked copolymer of vinyl alcohol and unsaturated carboxylic acid
[NASA-CASE-LEW-13102-1] p 104 N85-29144
COPPER
Effect of interfacial characteristics of metal clad polymeric substrates on electrical high frequency interconnection performance
[NASA-TM-86948] p 99 N85-20223
COPPER ALLOYS
Deformation and erosion of f.c.c. metals and alloys under cavitation attack p 65 A85-12789
COPPER CHLORIDES
Environmental stability of intercalated graphite fibers
[NASA-TM-87025] p 90 N85-26992
COPPER OXIDES
Textured carbon surfaces on copper
[NASA-CASE-LEW-14130-1] p 95 N85-20156
CORIOLIS EFFECT
Vibration and buckling of rotating, pretwisted, preconed beams including Cooriolis effects
[NASA-TM-87004] p 146 N85-25893
Nonlinear flap-lag-extensional vibrations of rotating, pretwisted, preconed beams including Coriolis effects
[NASA-TM-87102] p 152 N85-34427
CORNERS
Free-surface phenomena under low- and zero-gravity conditions
[NASA-CR-175835] p 116 N85-27168
CORRELATION
Ground correlation investigation of thruster/spacecraft interactions to be measured on the IAPS flight test
p 42 A85-16408
Elevated temperature biaxial fatigue
[NASA-CR-175795] p 148 N85-27263
CORROSION
Reactions of NaCl with gaseous SO3, SO2, and O2
p 59 A85-11897
The reactions of cobalt, iron and nickel in SO-2 atmospheres: Similarities and differences
[NASA-TM-86868] p 70 N85-11217
Surface effects of corrosive media on hardness, friction, and wear of materials
[NASA-TM-83711] p 85 N85-15896
Replaceable blade turbine and stationary specimen corrosion testing facility
[NASA-TM-86931] p 73 N85-18126
CORROSION RESISTANCE
The transient oxidation of single crystal NiAl + Zr
[NASA-CR-174756] p 70 N85-11221
Study of the effects of implantation on the high Fe-Ni-Cr and Ni-Cr-Al alloys
[NASA-CR-175625] p 76 N85-22661
Mechanism of strength degradation for hot corrosion of alpha-SiC
[NASA-TM-87052] p 91 N85-30135
CORROSION TESTS
Replaceable blade turbine and stationary specimen corrosion testing facility
[NASA-TM-86931] p 73 N85-18126
Compatibility experiments of facilities, materials, and propellants for electrothermal thrusters
[NASA-TM-86956] p 49 N85-21260
Burner rig corrosion of SiC at 1000 deg C
[NASA-TM-87061] p 53 N85-30011
COST ANALYSIS
Space Station propulsion - The Advanced Development Program at Lewis
[AIAA PAPER 85-1154] p 44 A85-39626
Space station propulsion: The advanced development program at Lewis
[NASA-TM-86999] p 50 N85-25386
Conceptual design of a fixed-pitch wind turbine generator system rated at 400 kilowatts
[NASA-CR-174877] p 162 N85-29363
Energy Efficient Engine Program technology benefit/cost study, volume 1
[NASA-CR-174766-VOL-1] p 33 N85-35197
Energy Efficient Engine Program technology benefit/cost study, volume 2
[NASA-CR-174766-VOL-2] p 33 N85-35198
COST EFFECTIVENESS
Parametric study of potential early commercial power plants Task 3-A MHD cost analysis
[NASA-CR-175839] p 161 N85-27377
Energy efficient engine component development and integration program
[NASA-CR-172846] p 31 N85-29958
Operational results for the experimental DOE/NASA Mod-OA wind turbine project
[NASA-TM-83517] p 163 N85-30479
COST ESTIMATES
Structural analysis and cost estimate of an eight-leg space frame as a support structure for horizontal axis wind turbines
[NASA-TM-83470] p 150 N85-30361
COST REDUCTION
Energy efficient engine. Volume 1: Component development and integration program
[NASA-CR-173084] p 22 N85-10992
COSTS
Jet fuel property changes and their effect on producibility and cost in the U.S., Canada, and Europe
[NASA-CR-174840] p 93 N85-27012
COUPLED MODES
Vibration and flutter of mistuned bladed-disk assemblies
[AIAA PAPER 84-0991] p 139 A85-16095
Circular waveguide bifurcation for asymmetric modes
p 101 A85-20170
Nonlinear flap-lag-extensional vibrations of rotating, pretwisted, preconed beams including Coriolis effects
[NASA-TM-87102] p 152 N85-34427
COUPLING
Dilute plasma coupling currents to a high voltage solar array in weak magnetic fields p 46 A85-45388
COWLINGS
Low-speed aerodynamic test of an axisymmetric supersonic inlet with variable cowl slot
[AIAA PAPER 85-1210] p 5 A85-40819
Low-speed aerodynamic test of an axisymmetric supersonic inlet with variable cowl slot
[NASA-TM-87039] p 28 N85-26710
CRACK GEOMETRY
Eddy current jet engine disk-crack monitor
p 120 A85-11100
CRACK INITIATION
Development of coated single-crystal superalloy systems for gas turbine applications p 68 A85-32440
Application of two creep fatigue life models for the prediction of elevated temperature crack initiation of a nickel base alloy
[AIAA PAPER 85-1420] p 69 A85-43979
Nonlinear structural and life analyses of a combustor liner p 19 N85-10955
Pre-HOST high temperature crack propagation
p 19 N85-10956
Life prediction and constitutive behavior: Overview
p 20 N85-10973
Constitutive model development for isotropic materials
p 20 N85-10975
Creep fatigue life prediction for engine hot section materials (isotropic)
[NASA-CR-168228] p 32 N85-31057
CRACK PROPAGATION
Fracture toughness of hot-pressed beryllium
p 66 A85-25835
On the fatigue crack propagation behavior of superalloys at intermediate temperatures p 68 A85-32434
Pre-HOST high temperature crack propagation
p 19 N85-10956
HOST high temperature crack propagation
p 21 N85-10977
Thermal-mechanical fatigue crack growth in Inconel X-750
[NASA-CR-174740] p 72 N85-15877
A study of spectrum fatigue crack propagation in two aluminum alloys. 1: Spectrum simplification
[NASA-TM-86929] p 72 N85-18124
A study of spectrum fatigue crack propagation in two aluminum alloys. 2: Influence of microstructures
[NASA-TM-86930] p 73 N85-18125
Translational and extensional energy release rates (the J- and M-integrals) for a crack layer in thermoelasticity
[NASA-CR-174872] p 145 N85-21685
Ultrasonic testing of plates containing edge cracks
[NASA-CR-3904] p 138 N85-29307
CRACK TIPS
On stress field near a stationary crack tip
[AD-A152863] p 141 A85-24532
CRACKING (CHEMICAL ENGINEERING)
Jet fuel property changes and their effect on producibility and cost in the U.S., Canada, and Europe
[NASA-CR-174840] p 93 N85-27012
CRACKS
Ultrasonic testing of plates containing edge cracks
[NASA-CR-3904] p 138 N85-29307
CREEP ANALYSIS
Strainrange partitioning - A total strain range version --- for creep fatigue life prediction by summing inelastic and elastic strain-range-life relations for two Ni base superalloys p 64 A85-11603
Thermodynamically consistent constitutive equations for nonisothermal large strain, elasto-plastic, creep behavior
[AIAA PAPER 85-0621] p 142 A85-38425
CREEP BUCKLING
Dynamic creep buckling: Analysis of shell structures subjected to time-dependent mechanical and thermal loading p 149 N85-27959
CREEP PROPERTIES
Influence of composition on the microstructure and mechanical properties of a nickel-base superalloy single crystal p 66 A85-32387
Factors which influence directional coarsening of gamma-prime during creep in nickel-base superalloy single crystals p 67 A85-32388
The influence of hold times on LCF and FCG behavior in a P/M Ni-base superalloy --- Low Cycle Fatigue/Fatigue Crack Growth p 67 A85-32400
Plasticity, viscoplasticity, and creep of solids by mechanical subelement models p 142 A85-35048
Nonlinear structural and life analyses of a combustor liner p 19 N85-10955
Reliability considerations for the total strain range version of strainrange partitioning
[NASA-CR-174757] p 144 N85-11380

Creep fatigue life prediction for engine hot section materials (isotropic)
[NASA-CR-168228] p 32 N85-31057
A comparison of two contemporary creep-fatigue life prediction methods p 151 N85-31538

CREEP RUPTURE STRENGTH
Elevated temperature creep-rupture behavior of the single crystal nickel-base superalloy NASAIR 100 p 66 A85-27812
Development of coated single-crystal superalloy systems for gas turbine applications p 68 A85-32440
Creep-rupture reliability analysis p 143 A85-42566
Fracture of yttria-doped, sintered reaction-bonded silicon nitride
[ACS PAPER 7-J3-84] p 82 A85-42797
The effects of seven alloying elements on the microstructure and stress-rupture behavior of nickle-base superalloys
[NASA-TM-83791] p 70 N85-10168
Effects of tin on microstructure and mechanical behavior of Inconel 718
[NASA-TM-86866] p 71 N85-12129
Stirling material technology
[NASA-TM-86888] p 72 N85-13007
Creep-rupture behavior of iron superalloys in high-pressure hydrogen
[NASA-CR-174411] p 74 N85-19078

CREEP STRENGTH
Advanced stress analysis methods applicable to turbine engine structures
[NASA-CR-175573] p 26 N85-21165
Alloys based on NiAl for high temperature applications
[NASA-TM-86976] p 75 N85-21322

CREEP TESTS
A continuous damage model based on stepwise-stress creep rupture tests
[NASA-CR-174941] p 152 N85-32341

CRITICAL TEMPERATURE
External fuel vaporization study, phase 2
[NASA-CR-174079] p 92 N85-11252

CROSS FLOW
Flow visualization of lateral jet injection into swirling crossflow
[AIAA PAPER 85-0059] p 2 A85-19490
Turbulence measurements of lateral jet injection into confined tubular crossflow
[AIAA PAPER 85-1102] p 110 A85-39604
Numerical calculation of subsonic jets in crossflow with reduced numerical diffusion
[AIAA PAPER 85-1441] p 110 A85-39780
Vortex modeling of single and multiple dilution jet mixing in a crossflow
[AIAA PAPER 85-1580] p 111 A85-40701
Dilution zone mixing studies p 21 N85-10984
Flow visualization study of the effect of injection hole geometry on an inclined jet in crossflow
[NASA-TM-86936] p 115 N85-20269
Development of a temperature measurement system with application to a jet in a cross flow experiment
[NASA-CR-174896] p 27 N85-25262
Numerical calculation of subsonic jets in crossflow with reduced numerical diffusion
[NASA-TM-87003] p 27 N85-25263
The influence of jet-grid turbulence on heat transfer from the stagnation region of a cylinder in crossflow
[NASA-TM-87011] p 115 N85-25760

CROSS POLARIZATION
Dual-mode coaxial feed with low crosspolarisation p 101 A85-20171

CROSSLINKING
Chemical approach for controlling nadimide cure temperature and rate
[NASA-CASE-LEW-13770-5] p 87 N85-21352
Chemical control of nadimide cure temperature and rate
[NASA-CASE-LEW-13770-2] p 63 N85-28982
Development of a lithium secondary battery separator p 104 N85-31378

CRYOGENIC EQUIPMENT
Cryogenic upper stage test bed engine
[AIAA PAPER 85-1339] p 44 A85-39733

CRYOGENIC FLUID STORAGE
Technology requirements to be addressed by the NASA Lewis Research Center Cryogenic Fluid Management Facility program
[AIAA PAPER 85-1229] p 94 A85-47024
Technology requirements to be addressed by the NASA Lewis Research Center Cryogenic Fluid Management Facility program
[NASA-TM-87048] p 38 N85-29987

CRYOGENIC FLUIDS
Technology requirements to be addressed by the NASA Lewis Research Center Cryogenic Fluid Management Facility program
[AIAA PAPER 85-1229] p 94 A85-47024
OTV Propulsion Issues
[NASA-CP-2347] p 37 N85-16989
Technology requirements to be addressed by the NASA Lewis Research Center Cryogenic Fluid Management Facility program
[NASA-TM-87048] p 38 N85-29987

CRYOGENIC ROCKET PROPELLANTS
Progress report - Advanced cryogenic OTV engine technology
[AIAA PAPER 85-1341] p 44 A85-39735

CRYOGENICS
Select fiber composites for space applications - A mechanistic assessment p 54 A85-16040
An experimental investigation of rubbing interaction in labyrinth seals at cryogenic temperature p 129 A85-39938
Manrating orbital transfer vehicle propulsion
[NASA-TM-87019] p 50 N85-25385

CRYSTAL GROWTH
Analysis of three-dimensional solidification interface shape p 109 A85-30075
Electrical characterization of plasma-grown oxides on gallium arsenide p 181 A85-32635
Dendritic solidification. I - Analysis of current theories and models. II - A model for dendritic growth under an imposed thermal gradient p 182 A85-38019
Cone formation as a result of whisker growth on ion bombarded metal surfaces p 182 A85-41635
Dendritic solidification. III - Some further refinements to the model for dendritic growth under an imposed thermal gradient p 69 A85-44703
Monte Carlo study of reversible growth of clusters on a surface p 182 A85-48516
A computer simulation of thin film nucleation and growth: The Volmer-Weber case
[NASA-TM-86968] p 53 N85-21264
Manufacturing process to reduce large grain growth in zirconium alloys
[DE85-011649] p 78 N85-34267

CRYSTAL LATTICES
Monte Carlo study of reversible growth of clusters on a surface p 182 A85-48516
Monte Carlo lattice models for adsorbed polymer conformation
[NASA-TP-2453] p 183 N85-24961

CRYSTAL STRUCTURE
Frictional and morphological properties of Au-MoS2 films sputtered from a compact target p 127 A85-19085
Substrate-induced orientational order in the isotropic phase of liquid crystals p 181 A85-24649
Characterization of erosion of metallic materials under *cavitation attack in a mineral oil*
[NASA-TM-86934] p 74 N85-19075

CRYSTAL SURFACES
AES and LEED study of the zinc blende SiC(100) surface p 61 A85-41633

CRYSTALLIZATION
Mechanical-contact-induced transformation from the amorphous to the partially crystalline state in metallic glass p 65 A85-19084

CUMULATIVE DAMAGE
Considerations for damage analysis of gas turbine hot section components
[ASME PAPER 84-PVP-77] p 14 A85-18792
A history dependent damage model for low cycle fatigue
[ASME PAPER 84-PVP-112] p 140 A85-18795
A unified relation for cavitation erosion p 109 A85-24445

CURING
Chemical approach for controlling nadimide cure temperature and rate with maleimide
[NASA-CASE-LEW-13770-3] p 87 N85-21350
Chemical approach for controlling nadimide cure temperature and rate with maleimide
[NASA-CASE-LEW-13770-4] p 87 N85-21351
Chemical control of nadimide cure temperature and rate
[NASA-CASE-LEW-13770-2] p 63 N85-28982

CURRENT DENSITY
Manual of phosphoric acid fuel cell stack three-dimensional model and computer program
[NASA-CR-174722] p 157 N85-10447

CYCLIC LOADS
Hygrothermomechanical evaluation of transverse filament tape epoxy/polyester fiberglass composites p 54 A85-15632
A history dependent damage model for low cycle fatigue
[ASME PAPER 84-PVP-112] p 140 A85-18795
On local total strain redistribution using a simplified cyclic inelastic analysis based on an elastic solution
[AIAA PAPER 85-1419] p 142 A85-39770
Application of two creep fatigue life models for the prediction of elevated temperature crack initiation of a nickel base alloy
[AIAA PAPER 85-1420] p 69 A85-43979
Nonlinear structural and life analyses of a combustor liner p 19 N85-10955
Design procedures for fiber composite structural components: Panels subjected to combined in-plane loads
[NASA-TM-86909] p 57 N85-15823
Low cycle fatigue of MAR-M 200 single crystals at 760 and 870 deg C
[NASA-TM-86933] p 74 N85-19074
Local strain redistribution corrections for a simplified inelastic analysis procedure based on an elastic finite-element analysis
[NASA-TP-2421] p 145 N85-20396
On local total strain redistribution using a simplified cyclic inelastic analysis based on an elastic solution
[NASA-TM-86913] p 145 N85-21690
Cyclic structural analyses of anisotropic turbine blades for reusable space propulsion systems --- ssme fuel turbopump
[NASA-TM-86990] p 146 N85-24339
Long-life high performance fuel cell program
[NASA-CR-174874] p 50 N85-25384
Analysis of shell type structures subjected to time *dependent mechanical and thermal loading*
[NASA-CR-175747] p 147 N85-25896
Interaction of high-cycle and low-cycle fatigue of Haynes 188 alloy at 1400 F deg p 149 N85-27961
Thermomechanical deformation in the presence of metallurgical changes p 150 N85-31533
Results of an interlaboratory fatigue test program conducted on alloy 800H at room and elevated temperatures
[NASA-CR-174940] p 152 N85-32340

CYLINDRICAL BODIES
Combined influence of unsteady free stream velocity and free stream turbulence on stagnation point heat transfer p 112 A85-41782

CZOCHRALSKI METHOD
Research on gallium arsenide diffused junction solar cells
[NASA-CR-174057] p 158 N85-11457

D

DAMAGE
Reexamination of cumulative fatigue damage laws p 149 N85-27962
A continuous damage model based on stepwise-stress creep rupture tests
[NASA-CR-174941] p 152 N85-32341

DAMAGE ASSESSMENT
Spherical microglass particle impingement studies of thermoplastic materials at normal incidence p 79 A85-11072
A history dependent damage model for low cycle fatigue
[ASME PAPER 84-PVP-112] p 140 A85-18795

DAMPERS (VALVES)
Dual clearance squeeze film damper
[NASA-CASE-LEW-13506-1] p 135 N85-33490

DATA ACQUISITION
Development of a multiplane multispeed balancing system for turbine systems
[NASA-CR-174750] p 35 N85-22400

DATA BASE MANAGEMENT SYSTEMS
Flow dynamic environment data base development for the SSME p 147 N85-26885

DATA BASES
Flow dynamic environment data base development for the SSME p 147 N85-26885

DATA CORRELATION
Creep-rupture reliability analysis p 143 A85-42566

DATA FLOW ANALYSIS
Data flow methods for dynamic system simulation - A CSSL-IV microcomputer network interface p 170 A85-28614
Functional language and data flow architectures p 170 A85-28629

DATA MANAGEMENT
MERIT: A man/computer data management and enhancement system for upper air nowcasting/forecasting in the United States --- Minimum Energy Routes using Interactive Techniques (MERIT) p 167 N85-10558

DATA STORAGE
Transferring data oscilloscope to an IBM using an Apple II+ p 168 A85-24526

DATA TRANSMISSION
Transferring data oscilloscope to an IBM using an Apple II+ p 168 A85-24526

DECELERATION
A unified relation for cavitation erosion
p 109 A85-24445
DEFECTS
Radiation damage and defect behavior in ion-implanted, lithium counterdoped silicon solar cells
p 182 A85-35698
Reliability of void detection in structural ceramics using scanning laser acoustic microscopy
[NASA-TM-87035] p 138 N85-32337
DEFLECTION
A comparison of electronic heterodyne moire deflectometry and electronic heterodyne holographic interferometry for flow measurements
[NASA-TM-87071] p 125 N85-32302
DEFORMATION
Pantographing self adaptive gap elements
p 142 A85-37440
Creep of chemically vapor deposited SiC fibers
[NASA-TM-86897] p 56 N85-14878
Advanced stress analysis methods applicable to turbine engine structures
[NASA-CR-175573] p 26 N85-21165
On Hybrid and mixed finite element methods
[NASA-CR-175551] p 146 N85-23096
A comparison of electronic heterodyne moire deflectometry and electronic heterodyne holographic interferometry for flow measurements
[NASA-TM-87071] p 125 N85-32302
DEGRADATION
Laboratory degradation of Kapton in a low energy oxygen ion beam
[AIAA PAPER 83-2658] p 78 A85-10675
Interply layer degradation effects on composite structural response
[AIAA PAPER 84-0849] p 54 A85-16096
Cathode degradation and erosion in high pressure arc discharges p 43 A85-16445
Interply layer degradation effects on composite structural response p 55 A85-39215
Performance degradation of helicopter rotor in forward flight due to ice p 11 A85-42937
Study of Kapton under simulated shuttle environment
[NASA-CR-176003] p 41 N85-29997
DEICERS
Icing tunnel tests of Electro-Impulse De-Icing of an engine inlet and high-speed wings
[AIAA PAPER 85-0466] p 10 A85-20872
DEICING
Electro-impulse de-icing of a turbofan engine inlet
[AIAA PAPER 85-1118] p 12 A85-40811
Analytical and physical modeling program for the NASA Lewis Research Center's Altitude Wind Tunnel (AWT)
[NASA-TM-86919] p 35 N85-15757
DELAMINATING
Interply layer degradation effects on composite structural response
[AIAA PAPER 84-0849] p 54 A85-16096
Interply layer degradation effects on composite structural response p 55 A85-39215
DEMAND (ECONOMICS)
Demand for satellite-provided domestic communications services up to the year 2000
[NASA-TM-86894] p 97 N85-15099
Satellite provided customer promises services, a forecast of potential domestic demand through the year 2000. Volume 4: Sensitivity analysis
[NASA-CR-174662] p 99 N85-27092
DENDRITIC CRYSTALS
The mechanisms of formation and prevention of channel segregation during alloy solidification
p 180 A85-18082
Dendritic solidification. I - Analysis of current theories and models. II - A model for dendritic growth under an imposed thermal gradient p 182 A85-38019
Dendritic solidification. III - Some further refinements to the model for dendritic growth under an imposed thermal gradient p 69 A85-44703
DENSIFICATION
Evaluation of alpha-SiC sintering using statistical methods p 83 A85-42800
DENSITY DISTRIBUTION
Vortex modeling of single and multiple dilution jet mixing in a crossflow
[AIAA PAPER 85-1580] p 111 A85-40701
DEPOSITION
Plasma deposited hydrogenated carbon on GaAs and InP p 182 A85-40386
Analysis of glow discharges for understanding the process of film formation
[NASA-TM-83750] p 62 N85-10138
Plasma deposited diamondlike carbon on GaAs and InP
[NASA-TM-86870] p 183 N85-10844
Initial feasibility ground test of a proposed photogrammetric system for measuring the shapes of ice accretions on helicopter rotor blades during forward flight
[NASA-TM-87391] p 12 N85-12887
Liquid phase products and solid deposit formation from thermally stressed model jet fuels
[NASA-TM-86874] p 92 N85-13066
Deposition of diamondlike carbon films
[NASA-CASE-LEW-14080-1] p 95 N85-20153
Optical properties of hydrogenated amorphous carbon films grown from methane plasma
[NASA-TM-86995] p 183 N85-26406
Jet fuel instability mechanisms
[NASA-CR-175856] p 93 N85-28127
The structure of ion plated films in relation to coating properties
[NASA-TM-87055] p 95 N85-29085
Diamondlike carbon protective coatings for IR materials
[NASA-TM-87083] p 178 N85-34631
DESENSITIZING
Manufacturing process to reduce large grain growth in zirconium alloys
[DE85-011649] p 78 N85-34267
DESIGN ANALYSIS
Near-optimum design of GaAs-based concentrator space solar cells for 80 C operation p 153 A85-15800
A high energy stage for the National Space Transportation System
[IAF PAPER 84-15] p 36 A85-23200
Interdisciplinary design analysis of a precision spacecraft antenna
[AIAA PAPER 85-0804] p 38 A85-30303
Contingency power concepts for helicopter turboshaft engine p 15 A85-32005
Design and performance of a fixed, nonaccelerating guide vane cascade that operates over an inlet flow angle range of 60 deg
[ASME PAPER 84-GT-75] p 4 A85-32964
Preliminary design of a 10 kW thermophotovoltaic system for space applications p 45 A85-45371
A 37.5-kW point design comparison of the nickel-cadmium battery, bipolar nickel-hydrogen battery, and regenerative hydrogen-oxygen fuel cell energy storage subsystems for low earth orbit p 46 A85-45387
Advanced designs for IPV nickel-hydrogen cells
p 156 A85-45438
Advanced multi-megawatt wind turbine design for utility application p 157 A85-45517
Energy efficient engine flight propulsion system preliminary analysis and design report
[NASA-CR-174701] p 18 N85-10947
Energy efficient engine high pressure turbine test hardware detailed design report
[NASA-CR-167955] p 23 N85-10995
Inverse design technique for cascades
[NASA-CR-3836] p 7 N85-12008
Fuel and oxidizer turbine loss analysis
p 50 N85-26900
DETECTION
Sensor failure detection for jet engines using analytical redundancy
[AIAA PAPER 84-1452] p 13 A85-16097
Radiographic detectability limits for seeded voids in sintered silicon carbide and silicon nitride
[NASA-TM-86945] p 138 N85-21674
DIAMONDS
Apparatus for producing diamond-like carbon flakes
[NASA-CASE-LEW-13837-3] p 95 N85-20155
Diamondlike flakes
[NASA-CASE-LEW-13837-2] p 57 N85-21267
DIAPHRAGMS (MECHANICS)
Variable friction secondary seal for face seals
[NASA-CASE-LEW-14170-1] p 131 N85-20377
DIELECTRIC PROPERTIES
Dielectric properties of 'diamondlike' carbon prepared by RF plasma deposition p 182 A85-38192
DIELECTRICS
Numerical simulation of positive-potential conductors in the presence of a plasma and a secondary-emitting dielectric p 102 A85-35306
An investigation of arc discharging on negatively biased dielectric conductor samples in a plasma
p 180 N85-22498
DIELS-ALDER REACTIONS
Chemical approach for controlling nadimide cure temperature and rate
[NASA-CASE-LEW-13770-6] p 63 N85-30039
DIESEL ENGINES
Development of gas-lubricated pistons for heavy duty diesel engine technology program
[NASA-CR-174746] p 184 N85-12808
Advanced automotive diesel assessment program
[NASA-CR-168285] p 130 N85-13235
Overview of waste heat utilization systems
[NASA-TM-86901] p 184 N85-13692
Transformation toughened ceramics for the heavy duty diesel engine technology program
[NASA-CR-174689] p 185 N85-16698
Methods for heat transfer and temperature field analysis of the insulated diesel
[NASA-CR-174783] p 185 N85-16699
An investigation of enhanced capability thermal barrier coating systems for diesel engine components
[NASA-CR-174820] p 86 N85-18154
Sliding seal materials for adiabatic engines
[NASA-CR-174893] p 89 N85-22757
Breakway friction and dynamic friction/wear measurements of various ceramic materials from 25 C (75 F) to 650 C (1200 F)
[NASA-CR-174803] p 90 N85-26994
DIFFERENTIAL EQUATIONS
Integrating chemical kinetic rate equations by selective use of stiff and nonstiff methods
[AIAA PAPER 85-0237] p 60 A85-19607
Recent advances in methods for numerical solution of O.D.E. initial value problems p 171 A85-21370
New integration techniques for chemical kinetic rate equations. 2: Accuracy comparison
[NASA-TM-86893] p 23 N85-13798
Integrating chemical kinetic rate equations by selective use of stiff and nonstiff methods
[NASA-TM-86923] p 24 N85-15726
Modeling the internal combustion engine
[NASA-RP-1094] p 172 N85-19733
A comparison of the efficiency of numerical methods for integrating chemical kinetic rate equations
[NASA-TM-83590] p 25 N85-21162
Nonlinear flap-lag-extensional vibrations of rotating, pretwisted, preconed beams including Coriolis effects
[NASA-TM-87102] p 152 N85-34427
DIFFRACTION PATTERNS
Ion-beam nitriding of steels p 66 A85-24667
Electronic heterodyne readout of fringes in moire deflectometry p 122 A85-36726
DIFFUSION
A numerical study of the steady scalar convective diffusion equation for small viscosity
p 107 A85-16533
The effect of diffusion induced lattice stress on the open-circuit voltage in silicon solar cells
p 181 A85-35620
Analysis techniques for tracer studies of oxidation
[NASA-CR-174796] p 84 N85-12162
Reducing numerical diffusion for incompressible flow calculations
[NASA-TM-83621] p 24 N85-14840
The structure of dilute combusting sprays
[NASA-CR-174838] p 24 N85-15728
Study of controlled diffusion stator blading
[NASA-CR-167995] p 25 N85-18058
A study of interdiffusion in beta + gamma/gamma + gamma prime Ni-Cr-Al
[NASA-CR-174852] p 74 N85-20041
DIFFUSION FLAMES
Drop-turbulence interactions in a diffusion flame
[AIAA PAPER 85-0319] p 60 A85-19665
Growth of a diffusion flame in the field of a vortex
p 61 A85-47320
DIFFUSION WELDING
Diffusion welding of MA 6000 and a conventional nickel-base superalloy p 69 A85-43551
Diffusion welding of Cassegrainian concentrator cell stack assemblies
[NASA-CR-176104] p 164 N85-33566
DIFFUSIVITY
The reactions of cobalt, iron and nickel in SO-2 atmospheres: Similarities and differences
[NASA-TM-86868] p 70 N85-11217
DIGITAL FILTERS
An allpass filter design for luminance and chrominance separation of NTSC signals p 102 A85-28230
Linearization of digital derived rate algorithm for use in linear stability analysis
[NASA-TM-87000] p 41 N85-23904
DIGITAL SIMULATION
A fast time domain digital simulation technique for power converters - Application to a buck converter with feedforward compensation p 101 A85-20900
The use of Ada in distributed simulations
p 169 A85-28612
Multibus-based parallel processor for simulation
p 169 A85-28613
A functional language approach in high-speed digital simulation p 170 A85-28615
Optical linear algebra processors - Noise and error-source modeling p 169 A85-36727

DIGITAL SYSTEMS
High-temperature optically activated GaAs power switching for aircraft digital electronic control
[NASA-CR-174711] p 34 N85-12901
Energy Efficient Engine (E3) controls and accessories detail design report
[NASA-CR-168017] p 31 N85-29957
DILUTION
Dilution zone mixing studies p 21 N85-10984
Development of a temperature measurement system with application to a jet in a cross flow experiment
[NASA-CR-174896] p 27 N85-25262
DIODES
Remote displacement measurements using a laser diode p 121 A85-24464
High voltage-high power components for large space power distribution systems p 45 A85-45370
DIPOLE ANTENNAS
DE-1 measurements of AKR wave directions --- auroral kilometric radiation p 166 A85-37717
Infrared technology for satellite power conversion --- antenna arrays and bolometers
[NASA-CR-174266] p 159 N85-16293
DIRECT CURRENT
Nitriding of titanium and its alloys by N2, NH3 or mixtures of N2 + H2 in a dc arc plasma at low pressures (or = to torr)
[NASA-TM-83803] p 131 N85-15168
Performance analysis of radiation cooled dc transmission lines for high power space systems
[NASA-TM-87040] p 104 N85-28222
DIRECT POWER GENERATORS
Operational performance of the photovoltaic-powered grain mill and water pump at Tangaye, Burkina Faso (formerly Upper Volta)
[NASA-TM-86970] p 161 N85-23243
DIRECTIONAL SOLIDIFICATION (CRYSTALS)
Materials for advanced turbine engines. Project 2: Rene 150 directionally solidified superalloy turbine blades, volume 2
[NASA-CR-167993] p 23 N85-12059
DIRECTIVITY
On the calculation of the directivity of planar array feeds for satellite reflector applications p 97 A85-32249
DISCHARGERS
Extended performance technology study 30-cm thruster
[NASA-CR-168259] p 48 N85-15806
DISCONTINUITY
MMIC devices for active phased array antennas
[NASA-CR-174281] p 98 N85-15943
Characterization of microstrip discontinuities in the time and frequency domains
[NASA-CR-176190] p 106 N85-35342
DISCRETE FUNCTIONS
Assessment of discretization schemes to reduce numerical diffusion in the calculation of complex flows
[AIAA PAPER 85-0441] p 108 A85-19751
DISKS (SHAPES)
Hot isostatically pressed manufacture of high strength MERL 76 disk and seal shapes
[NASA-CR-165550] p 71 N85-11225
DISPERSION
An experimental investigation of microstrip properties on soft substrates from 2 to 40 GHz
[NASA-TM-86961] p 99 N85-20224
DISPLACEMENT
Experimental compliance calibration of the NASA Lewis Research Center Mode 2 fatigue specimen
[NASA-TM-86908] p 144 N85-16205
Recent advances in hybrid/mixed finite elements
[NASA-CR-175574] p 145 N85-21687
DISPLACEMENT MEASUREMENT
Remote displacement measurements using a laser diode p 121 A85-24464
Remote displacement measurement using a passive interferometer with a fiber-optic link p 122 A85-42857
DISTORTION
Temperature distortion generator for turboshaft engine testing
[SAE PAPER 841541] p 15 A85-39065
Effect of combined pressure and temperature distortion orientation on high-bypass-ratio turbofan engine stability
[NASA-TM-83771] p 17 N85-10067
Temperature distortion generator for turboshaft engine testing
[NASA-TM-83748] p 1 N85-15658
Effect of steady-state temperature distortion on inlet flow to a high-bypass-ration turbofan engine
[NASA-TM-86896] p 24 N85-15725
DISTRIBUTED PROCESSING
The use of Ada in distributed simulations
p 169 A85-28612
Real-Time Multiprocessor Programming Language (RTMPL) user's manual
[NASA-TP-2422] p 170 N85-28610
DOCUMENTATION
Bibliography of Lewis Research Center technical publications announced in 1984
[NASA-TM-87012] p 184 N85-28876
DOMESTIC ENERGY
Operational results for the experimental DOE/NASA Mod-OA wind turbine project
[NASA-TM-83517] p 163 N85-30479
DOMESTIC SATELLITE COMMUNICATIONS SYSTEMS
Experimental results supporting the determination of service quality objectives for DBS systems
p 96 A85-29611
DOPED CRYSTALS
Magnesium doping of efficient GaAs and Ga(0.75)In(0.25)As solar cells grown by metalorganic chemical vapor deposition p 180 A85-11466
The transient oxidation of single crystal NiAl + Zr
[NASA-CR-174756] p 70 N85-11221
DOPES
Lithium counterdoped silicon solar cell
[NASA-CASE-LEW-14177-1] p 160 N85-20535
Molecular orbital studies in oxidation: Sulfate formation and metal-metal oxide adhesion
[NASA-CR-176070] p 77 N85-32174
DOPPLER EFFECT
Filter induced errors in laser anemometer measurements using counter processors
[NASA-TM-87047] p 125 N85-30288
Velocity visualization in gaseous flows
[NASA-CR-174954] p 119 N85-31445
DRAG
Icing flight research - Aerodynamic effects of ice and ice shape documentation with stereo photography
[AIAA PAPER 85-0468] p 11 A85-30192
Observations from varying the lift and drag inputs to a noise prediction method for supersonic helical tip speed propellers
[NASA-TM-83797] p 175 N85-10788
Icing flight research: Aerodynamic effects of ice and ice shape documentation with stereo photography
[NASA-TM-86906] p 12 N85-18049
Report of the Constellations Panel
p 131 N85-20368
DROP SIZE
An approach for automated analysis of particle holograms p 120 A85-10034
Phase/doppler spray analyzer for simultaneous measurements of drop size and velocity distributions
p 120 A85-10035
Spray characterization with a nonintrusive technique using absolute scattered light p 120 A85-10036
Nonintrusive optical single-particle counter for measuring the size and velocity of droplets in a spray
p 120 A85-16794
Aerodynamic effect of combustor inlet air pressure on fuel jet atomization p 109 A85-27096
Structure of nonevaporating sprays. I - Initial conditions and mean properties p 112 A85-48538
Liquid fuel spray processes in high-pressure gas flow
[NASA-TM-86944] p 115 N85-21570
Research study of droplet sizing technology leading to the development of an advanced droplet sizing system
[NASA-CR-174839] p 123 N85-21604
DROP TESTS
Graphite/PMR polyimide composites with improved toughness
[NASA-TM-87081] p 58 N85-32148
DROPS (LIQUIDS)
Comparison of icing cloud instruments for 1982-1983 icing season flight program
[AIAA PAPER 84-0020] p 13 A85-16098
Drop-turbulence interactions in a diffusion flame
[AIAA PAPER 85-0319] p 60 A85-19665
Experimental study of the spray characteristics of a research airblast atomizer
[NASA-TM-86911] p 24 N85-15727
The structure of dilute combusting sprays
[NASA-CR-174838] p 24 N85-15728
Advanced radiator concepts
[NASA-TM-87008] p 115 N85-24245
DRY FRICTION
Effects of friction dampers on aerodynamically unstable rotor stages p 14 A85-21866
Metallurgical and mechanical phenomena due to rubbing of titanium against sintered powder Nichrome
p 127 A85-22281
Thermal and thermomechanical effects in dry sliding
p 127 A85-23838
DUCT GEOMETRY
Analytical study of flow phenomena in SSME turnaround duct geometries p 116 N85-26902
DUCTED FLOW
The influence of combustion liner holes on noise production by ducted burners
[AIAA PAPER 84-2322] p 172 A85-10869
A finite element solution of three-dimensional inviscid rotational flows through curved ducts
p 107 A85-11648
Mass and momentum turbulent transport experiments with confined coaxial jets p 107 A85-14399
Flow control in a diffusing S-Duct
[AIAA PAPER 85-0524] p 3 A85-25928
Review - Computational methods for internal flows with emphasis on turbomachinery p 4 A85-29126
Structure of ducted particle-laden turbulent jets
p 110 A85-38999
Application of viscous and inviscid computation methods for rocket turbopump systems
[SAE PAPER 841522] p 110 A85-39257
Heat transfer enhancement in channels with turbulence promoters
[ASME PAPER 84-WA/HT-72] p 111 A85-39900
Application of computational fluid dynamics to complex inlet ducts
[AIAA PAPER 85-1213] p 6 A85-47023
Application of computational fluid dynamics to complex inlet ducts
[NASA-TM-87060] p 118 N85-30247
DUCTILITY
Ductility in rapidly solidified NiAl p 66 A85-26158
Characterization of solid particle erosion resistance of ductile metals based on their properties
p 69 A85-42569
DUCTS
Vortex-generating coolant-flow-passage design for increased film-cooling effectiveness and surface coverage
[NASA-TP-2388] p 113 N85-12314
DURABILITY
Experimental test program for evaluation of solid lubricant coating as applied to compliant foil gas bearings to 315 deg C
[NASA-CR-174837] p 85 N85-15895
DYNAMIC CHARACTERISTICS
Rotordynamic coefficients for compressible flow in tapered annular seals p 129 A85-42573
High temperature static strain sensor development program p 19 N85-10959
DYNAMIC CONTROL
Alternatives for jet engine control
[NASA-CR-175831] p 29 N85-26713
Alternatives for jet engine control
[NASA-CR-175832] p 29 N85-26714
Alternatives for jet engine control
[NASA-CR-175833] p 29 N85-26715
DYNAMIC MODELS
Analytical modeling of circuit aerodynamics in the new NASA Lewis Altitude Wind Tunnel
[AIAA PAPER 85-0380] p 3 A85-26389
Small-signal model for the series resonant converter
p 102 A85-39453
Analytical modeling of circuit aerodynamics in the new NASA Lewis wind tunnel
[NASA-TM-86912] p 8 N85-15688
Mechanics of a gaseous film barrier to lubricant wetting of elastohydrodynamically lubricated conjunctions
[NASA-TP-2500] p 135 N85-32330
DYNAMIC PRESSURE
The infinite line pressure probe p 122 A85-37704
DYNAMIC RESPONSE
Flutter and forced response of mistuned rotors using standing wave analysis p 139 A85-12721
DYNAMIC STRUCTURAL ANALYSIS
Effects of warping and pretwist on torsional vibration of rotating beams
[ASME PAPER 84-WA/APM-41] p 140 A85-17040
Dynamic analysis of straight and involute tooth forms
[ASME PAPER 84-DET-226] p 128 A85-33780
Augmented weak forms and element-by-element preconditioners: Efficient iterative strategies for structural finite elements. A preliminary study p 144 N85-10384
Overview of structural response: Probabilistic structural analysis p 148 N85-27952
Probabilistic finite element development
p 149 N85-27956
Dynamic creep buckling: Analysis of shell structures subjected to time-dependent mechanical and thermal loading p 149 N85-27959
DYNAMICAL SYSTEMS
Data flow methods for dynamic system simulation - A CSSL-IV microcomputer network interface
p 170 A85-28614
Solar dynamic systems p 164 N85-31374
DYNAMICS EXPLORER 1 SATELLITE
DE-1 measurements of AKR wave directions --- auroral kilometric radiation p 166 A85-37717

E

EARTH ATMOSPHERE
Study of Kapton under simulated shuttle environment
[NASA-CR-176003] p 41 N85-29997
EARTH ORBITS
Laboratory degradation of Kapton in a low energy oxygen ion beam
[AIAA PAPER 83-2658] p 78 A85-10675
Teardown analysis of a ten cell bipolar nickel-hydrogen battery p 156 A85-45385
A 37.5-kW point design comparison of the nickel-cadmium battery, bipolar nickel-hydrogen battery, and regenerative hydrogen-oxygen fuel cell energy storage subsystems for low earth orbit p 46 A85-45387
Advanced designs for IPV nickel-hydrogen cells p 156 A85-45438
OTV propulsion tecnology programmatic overview p 37 N85-16997
Report of the Constellations Panel p 131 N85-20368
Radiation exposure and performance of multiple burn LEO-GEO orbit transfer trajectories
[NASA-TM-86946] p 36 N85-21228
Spacecraft Environmental Interactions Technology, 1983
[NASA-CP-2359] p 39 N85-22470
Study of Kapton under simulated shuttle environment
[NASA-CR-176003] p 41 N85-29997
Design principles for nickel hydrogen cells and batteries p 104 N85-31398
Life cycle test results of a bipolar nickel hydrogen battery p 105 N85-31406
ECONOMIC ANALYSIS
Fuel cell power plant economic and operational considerations
[ASME PAPER 84-AES-7] p 154 A85-21297
PM superalloys - A troubled adolescent? p 69 A85-44772
EDDY CURRENTS
Eddy current jet engine disk-crack monitor p 120 A85-11100
Preliminary results on passive eddy current damper technology for SSME turbomachinery p 132 N85-26890
EDDY VISCOSITY
SSME fuel preburner two-dimensional analysis p 51 N85-27943
EDGES
A study of interply layer effects on the free edge stress field of angleplied laminates p 55 A85-41127
A study of interply layer effects on the free-edge stress field of angleplied laminates
[NASA-TM-86924] p 57 N85-15822
Ultrasonic testing of plates containing edge cracks
[NASA-CR-3904] p 138 N85-29307
EDUCATION
NASA Lewis Research Center/University Graduate Research Program on Engine Structures
[NASA-TM-86916] p 145 N85-18375
EFFICIENCY
Component-specific modeling p 20 N85-10971
Energy efficient engine. High pressure compressor detail design report
[NASA-CR-165558] p 23 N85-10998
Sixty GHz IMPATT diode development
[NASA-CR-174969] p 105 N85-33293
Lubrication and cooling for high speed gears
[NASA-TM-87096] p 136 N85-34407
ELASTIC BODIES
Development and testing of stable, invariant, isoparametric curvilinear 2- and 3-D hybrid-stress elements p 140 A85-19899
ELASTIC DEFORMATION
Deformation and fracture behavior of Ni-Mo-Al(gamma/gamma prime-alpha) in situ composite p 64 A85-11058
On the existence and stability conditions for mixed-hybrid finite element solutions based on Reissner's variational principle p 142 A85-33847
Thermodynamically consistent constitutive equations for nonisothermal large strain, elasto-plastic, creep behavior
[AIAA PAPER 85-0621] p 142 A85-38425
On local total strain redistribution using a simplified cyclic inelastic analysis based on an elastic solution
[AIAA PAPER 85-1419] p 142 A85-39770
Fundamental tribological properties of ceramics
[NASA-TM-86915] p 85 N85-15893
On local total strain redistribution using a simplified cyclic inelastic analysis based on an elastic solution
[NASA-TM-86913] p 145 N85-21690
Hertzian contact in two and three dimensions
[NASA-TP-2473] p 135 N85-32331
ELASTIC MEDIA
Ultrasonic wave propagation in two-phase media - Spherical inclusions p 54 A85-11926
ELASTIC PROPERTIES
A survey of unified constitutive theories p 150 N85-31531
On the use of internal state variables in thermoviscoplastic constitutive equations p 150 N85-31536
ELASTIC SCATTERING
Fundamentals of microcrack nucleation mechanics
[NASA-CR-3851] p 137 N85-16195
ELASTIC WAVES
Fundamentals of microcrack nucleation mechanics
[NASA-CR-3851] p 137 N85-16195
ELASTOHYDRODYNAMICS
Elastohydrodynamic lubrication of line contacts p 126 A85-11069
Topological reaction rate measurements related to scuffing p 64 A85-11070
Fast numerical calculations of EHD sliding traction forces Application to rolling bearings
[ASME PAPER 84-TRIB-26] p 127 A85-21289
Thermal elastohydrodynamic lubrication of line contacts p 128 A85-31202
Fast approach for calculating film thicknesses and pressures in elastohydrodynamically lubricated contacts at high loads
[NASA-TM-87032] p 117 N85-30242
Surface roughness effects in elastohydrodynamic contacts
[NASA-TP-2488] p 134 N85-32329
Mechanics of a gaseous film barrier to lubricant wetting of elastohydrodynamically lubricated conjunctions
[NASA-TP-2500] p 135 N85-32330
ELASTOPLASTICITY
On stress field near a stationary crack tip
[AD-A152863] p 141 A85-24532
Plasticity, viscoplasticity, and creep of solids by mechanical subelement models p 142 A85-35048
Thermodynamically consistent constitutive equations for nonisothermal large strain, elasto-plastic, creep behavior
[AIAA PAPER 85-0621] p 142 A85-38425
Constitutive modeling and computational implementation for finite strain plasticity p 143 A85-40910
HOST high temperature crack propagation p 21 N85-10977
A review of path-independent integrals in elastic-plastic fracture mechanics, task 4
[NASA-CR-174956] p 152 N85-33541
ELECTRIC ARCS
Metal vapor arc switch electromagnetic accelerator technology
[NASA-CR-174380] p 103 N85-18259
Apparatus for producing diamond-like carbon flakes
[NASA-CASE-LEW-13837-3] p 95 N85-20155
ELECTRIC CONDUCTORS
Numerical simulation of positive-potential conductors in the presence of a plasma and a secondary-emitting dielectric p 102 A85-35306
An investigation of arc discharging on negatively biased dielectric conductor samples in a plasma p 180 N85-22498
ELECTRIC CONTACTS
Screen printed interdigitated back contact solar cell
[NASA-CASE-LEW-13414-1] p 160 N85-20530
ELECTRIC DISCHARGES
Mass spectra of neutral particles released during electrical breakdown of thin polymer films p 88 N85-22511
ELECTRIC ENERGY STORAGE
Cycling performance of the iron-chromium redox energy storage system
[NASA-TM-87034] p 162 N85-27387
ELECTRIC FILTERS
A fast time domain digital simulation technique for power converters - Application to a buck converter with feedforward compensation p 101 A85-20900
ELECTRIC GENERATORS
Preliminary assessment of power-generating tethers in space and of propulsion for their orbit maintenance p 37 N85-22520
Free-piston Stirling engine/linear alternator 1000-hour endurance test
[NASA-CR-174771] p 163 N85-30481
Experimental investigation of a variable speed constant frequency electric generating system from a utility perspective
[NASA-CR-174950] p 105 N85-32251
ELECTRIC HYBRID VEHICLES
Feasibility demonstration of a novel, flat-belt, continuously variable transmission or automotive and electric-hybrid vehicle application
[NASA-CR-174430] p 185 N85-19894
ELECTRIC MOTOR VEHICLES
Results of electric-vehicle propulsion system performance on three lead-acid battery systems p 156 A85-45443
ELECTRIC POTENTIAL
Voltage controlling mechanisms in low resistivity silicon solar cells - A unified approach p 155 A85-35617
The effect of diffusion induced lattice stress on the open-circuit voltage in silicon solar cells p 181 A85-35620
Teardown analysis of a ten cell bipolar nickel-hydrogen battery p 156 A85-45385
Discharges on a negatively biased solar cell array in a charged-particle environment p 160 N85-22499
ELECTRIC POWER
Measured effects of wind turbine generation at the Block Island Power Company p 153 A85-10652
ELECTRIC POWER PLANTS
Fuel cell power plant economic and operational considerations
[ASME PAPER 84-AES-7] p 154 A85-21297
Advanced multi-megawatt wind turbine design for utility application p 157 A85-45517
Manual of phosphoric acid fuel cell power plant optimization model and computer program
[NASA-CR-174721] p 157 N85-10445
Phosphoric acid fuel cell power plant system performance model and computer program
[NASA-CR-174638] p 157 N85-11456
ELECTRIC POWER SUPPLIES
High voltage-high power components for large space power distribution systems p 45 A85-45370
High voltage requirements and issues for the 1990's — for spacecraft power supplies p 46 A85-45429
Electric power - Photovoltaic or solar dynamic? p 46 A85-47042
A historical overview of the electrical power systems in the US manned and some US unmanned spacecraft
[NASA-CR-174806] p 47 N85-13910
Experimental investigation of a variable speed constant frequency electric generating system from a utility perspective
[NASA-CR-174950] p 105 N85-32251
Applicability of 100kWe-class of space reactor power systems to NASA manned space station missions
[NASA-CR-174696] p 177 N85-35728
ELECTRIC PROPULSION
Performance capabilities of the 12-centimeter Xenon ion thruster p 42 A85-16439
Extended performance technology study 30-cm thruster
[NASA-CR-168259] p 48 N85-15806
High frequency plasma generator for ion thrusters
[NASA-CR-174772] p 48 N85-17023
Preliminary assessment of power-generating tethers in space and of propulsion for their orbit maintenance p 37 N85-22520
Primary propulsion of electrothermal, ion and chemical systems for space-based radar orbit transfer
[NASA-TM-87043] p 51 N85-27972
ELECTRIC SWITCHES
Metal vapor arc switch electromagnetic accelerator technology
[NASA-CR-174380] p 103 N85-18259
High-voltage, high-power, solid-state remote power controllers for aerospace applications
[NASA-TP-2437] p 49 N85-21263
ELECTRICAL FAULTS
Mass analysis of neutral particles and ions released during electrical breakdowns on spacecraft surfaces
[NASA-CR-175585] p 39 N85-21250
Mass spectra of neutral particles released during electrical breakdown of thin polymer films p 88 N85-22511
ELECTRICAL MEASUREMENT
Electrical characterization of plasma-grown oxides on gallium arsenide p 181 A85-32635
The high voltage silicon cell: A comparative analysis p 49 N85-22569
ELECTRICAL RESISTIVITY
Theory of the high base resistivity n(+)pp(+) silicon solar cell and its application to radiation damage effects p 154 A85-32639
Voltage controlling mechanisms in low resistivity silicon solar cells - A unified approach p 155 A85-35617
The effect of diffusion induced lattice stress on the open-circuit voltage in silicon solar cells p 181 A85-35620
Dynamics of graphite fiber intercalation: In situ resistivity measurements with a four point probe
[NASA-TM-86858] p 53 N85-10105
Graphite fiber intercalation: Dynamics of the bromine intercalation process
[NASA-TM-87015] p 53 N85-26921
ELECTROCATALYSTS
Electrocatalyst advances for hydrogen oxidation in phosphoric acid fuel cells p 60 A85-15614
Preparation and evaluation of advanced catalysts for phosphoric acid fuel cells
[NASA-CR-168223] p 160 N85-19511

Regenerative fuel cell systems for space station p 104 N85-31372

ELECTROCHEMICAL CELLS
Advanced nickel-hydrogen cell configuration study [NASA-CR-174775] p 157 N85-10444
Cycling performance of the iron-chromium redox energy storage system [NASA-TM-87034] p 162 N85-27387

ELECTROCHEMISTRY
Chemical and electrochemical behavior of the Cr(III)/Cr(II) half-cell in the iron-chromium redox energy storage system p 61 A85-33785
NASA Redox Storage System Development Project [NASA-TM-83677] p 158 N85-12465
Electrochemistry and storage p 62 N85-13889
Raman structural studies of the nickel electrode [NASA-CR-175619] p 183 N85-23414
Regenerative fuel cell systems for space station p 104 N85-31372
System level electrochemical principles p 104 N85-31375

ELECTRODE MATERIALS
Chemical and electrochemical behavior of the Cr(III)/Cr(II) half-cell in the iron-chromium redox energy storage system p 61 A85-33785
Long life nickel electrodes for a nickel-hydrogen cell. III - Results of an accelerated test and failure analyses p 156 A85-45391
Preparation and evaluation of advanced catalysts for phosphoric acid fuel cells [NASA-CR-168223] p 160 N85-19511

ELECTRODEPOSITION
Film and interstitial formation of metals in plasma-sprayed ceramics [NASA-TM-86993] p 89 N85-22756

ELECTRODES
Advanced designs for IPV nickel-hydrogen cells p 156 A85-45438
Electric utility acid fuel cell stack technology advancement [NASA-CR-174804] p 159 N85-17422
Raman structural studies of the nickel electrode [NASA-CR-175619] p 183 N85-23414
The failure mechanism of a nickel electrode in a nickel-hydrogen cell p 105 N85-31408
Electrode erosion in arc discharges at atmospheric pressure [NASA-TM-87087] p 52 N85-34178
Development of electrodes for the NASA iron/chromium [NASA-CR-174724] p 165 N85-35471

ELECTRODYNAMICS
Spacecraft Environmental Interactions Technology, 1983 [NASA-CP-2359] p 39 N85-22470

ELECTROHYDRAULIC FORMING
Results of an interlaboratory fatigue test program conducted on alloy 800H at room and elevated temperatures [NASA-CR-174940] p 152 N85-32340

ELECTROHYDRODYNAMICS
Elastohydrodynamic lubrication calculations used as a tool to study scuffing [NASA-TM-87097] p 137 N85-34408

ELECTROLYSIS
Engineering model system study for a regenerative fuel cell: Study report [NASA-CR-174801] p 158 N85-16292

ELECTROLYTES
Develop and test fuel cell powered on-site integrated total energy systems. Phase 3: Full-scale power plant development [NASA-CR-168338] p 164 N85-30483

ELECTROLYTIC CELLS
Engineering model system study for a regenerative fuel cell: Study report [NASA-CR-174801] p 158 N85-16292

ELECTROMAGNETIC COMPATIBILITY
Design guidelines for assessing and controlling spacecraft charging effects p 40 N85-22500

ELECTROMAGNETIC INTERFERENCE
On the subjective evaluation of the interference protection ratios' measurements for co-channel FM-TV signals p 96 A85-28241
Adaptive antenna arrays for weak interfering signals [NASA-CR-174336] p 98 N85-17258

ELECTROMAGNETIC NOISE MEASUREMENT
On the subjective evaluation of the interference protection ratios' measurements for co-channel FM-TV signals p 96 A85-28241

ELECTROMAGNETIC PROPULSION
Preliminary analysis of space mission applications for electromagnetic launchers [NASA-CR-174067] p 35 N85-12071

ELECTROMAGNETIC PULSES
Electro-impulse de-icing of a turbofan engine inlet [AIAA PAPER 85-1118] p 12 A85-40811
Design guidelines for assessing and controlling spacecraft charging effects p 40 N85-22500

ELECTROMAGNETIC SCATTERING
Numerical methods for analyzing electromagnetic scattering [NASA-CR-175507] p 99 N85-21438
Analysis of the electromagnetic scattering from an inlet geometry with lossy walls [NASA-CR-175743] p 99 N85-25686

ELECTRON BEAMS
Electron beam charging of Space Shuttle thermal protection system tiles p 39 N85-22478
Electron yields from spacecraft materials p 40 N85-22512

ELECTRON BOMBARDMENT
Ground correlation investigation of thruster/spacecraft interactions to be measured on the IAPS flight test p 42 A85-16408
Performance capabilities of the 12-centimeter Xenon ion thruster p 42 A85-16439
Aluminum work function: Effect of oxidation, mechanical scraping and ion bombardment [NASA-TM-87079] p 78 N85-34265

ELECTRON CYCLOTRON HEATING
High frequency plasma generator for ion thrusters [NASA-CR-174772] p 48 N85-17023

ELECTRON EMISSION
Plasma variables and tribological properties of coatings in low pressure (0.1 - 10.0 torr) plasma systems [NASA-TM-83798] p 94 N85-11261
Textured carbon surfaces on copper [NASA-CASE-LEW-14130-1] p 95 N85-20156
Electron yields from spacecraft materials p 40 N85-22512
Hollow cathodes in high pressure arc discharges [NASA-TM-87098] p 52 N85-34179

ELECTRON FLUX DENSITY
Three-dimensional calculation of shuttle charging in polar orbit p 40 N85-22486
Polar orbit electrostatic charging of objects in shuttle wake p 40 N85-22487

ELECTRON IRRADIATION
Effects of 1 MeV electrons and 10 MeV protons on the performance and reflectance of thin BSR cells --- back surface reflector p 182 A85-35699
The effects of lithium counterdoping on radiation damage and annealing in n(+)p silicon solar cells p 50 N85-22586

ELECTRON MICROSCOPY
Friction and wear of some ferrous-base metallic glasses p 64 A85-11071
Microstructures in rapidly solidified Ni-Mo alloys [NASA-TM-87100] p 78 N85-34266

ELECTRON TRAJECTORIES
Theory of ion acceleration with closed electron drift --- in spacecraft plasma propulsion p 41 A85-15512

ELECTRON TUNNELING
Inelastic tunnel diodes [NASA-CASE-LEW-13833-1] p 103 N85-21492

ELECTRONIC CONTROL
A real-time FORTRAN implementation of a sensor failure detection, isolation and accommodation algorithm p 171 A85-47704

ELECTRONIC MODULES
The study of microstrip antenna arrays and related problems [NASA-CR-174054] p 97 N85-11265

ELECTRONIC RECORDING SYSTEMS
Moire deflectometry with deferred electronic heterodyne readout p 122 A85-42854

ELECTROSTATIC ENGINES
Precision tunable resonant microwave cavity [NASA-CASE-LEW-13935-1] p 103 N85-20248

ELECTROSTATIC PROBES
Numerical simulations of positively-biased probes and dielectric-conductor disks in a plasma --- for low earth orbit plasma densities p 179 A85-17262
Ram-wake effects on plasma current collection of the PIX 2 Langmuir probe p 180 N85-22496

ELECTROTHERMAL ENGINES
Electrothermal thruster diagnostics p 42 A85-16440
Experiments with a microwave electrothermal thruster concept p 42 A85-16441
The energetics of hydrogen atom recombination - Analysis, experiments, and modeling --- in electrothermal propulsion system p 179 A85-16444
Investigation of a pulsed electrothermal thruster system [NASA-CR-174768] p 46 N85-11132
Compatibility experiments of facilities, materials, and propellants for electrothermal thrusters [NASA-TM-86956] p 49 N85-21260

ELLIPTIC FUNCTIONS
Two-dimensional internal compressible viscous flows using semi-elliptic analysis p 106 A85-11640

ELLIPTICAL POLARIZATION
Polarization (ellipsometric) measurements of liquid condensate deposition and evaporation rates and dew points in flowing salt/ash-containing combustion gases p 123 A85-46925

ELONGATION
Spherical microglass particle impingement studies of thermoplastic materials at normal incidence p 79 A85-11072

EMISSION SPECTRA
Prism-coupled light emission from tunnel junctions p 181 A85-21425

EMITTERS
Voltage controlling mechanisms in low resistivity silicon solar cells - A unified approach p 155 A85-35617
Preliminary design of a 10 kW thermophotovoltaic system for space applications p 45 A85-45371

ENDURANCE
IAPS (8-cm) ion thruster cyclic endurance test --- Ion Auxiliary Propulsion System p 42 A85-16406

ENERGY ABSORPTION
Impact resistance of fiber composites Energy-absorbing mechanisms and environmental effects p 56 A85-46543

ENERGY CONSERVATION
Energy efficient engine flight propulsion system preliminary analysis and design report [NASA-CR-174701] p 18 N85-10947
Energy Efficient Engine Program technology benefit/cost study, volume 2 [NASA-CR-174766-VOL-2] p 33 N85-35198
Comparative analysis of operational forecasts versus actual weather conditions in airline flight planning, volume 1 [NASA-CR-167862] p 167 N85-35534
Comparative analysis of operational forecasts versus actual weather conditions in airline flight planning, volume 2 [NASA-CR-167863] p 167 N85-35535
Comparative analysis of operational forecasts versus actual weather conditions in airline flight planning, volume 3 [NASA-CR-167864] p 167 N85-35536
Comparative analysis of operational forecasts versus actual weather conditions in airline flight planning, volume 4 [NASA-CR-167865] p 167 N85-35537
Comparative analysis of operational forecasts versus actual weather conditions in airline flight planning: Summary report [NASA-CR-167866] p 168 N85-35538

ENERGY CONSUMPTION
Wind tunnel results of advanced high speed propellers in the takeoff, climb, and landing operating regimes [AIAA PAPER 85-1259] p 6 A85-47025
Wind tunnel results of advanced high speed propellers in the takeoff, climb and landing operating regimes [NASA-TM-87054] p 9 N85-29925

ENERGY CONVERSION EFFICIENCY
Magnesium doping of efficient GaAs and Ga(0.75)In(0.25)As solar cells grown by metalorganic chemical vapor deposition p 180 A85-11466
Measurements of energy distribution in microwave plasmas of N2 and He and comparisons with results for H2 p 178 A85-16443
Effect of solar-cell junction geometry on open-circuit voltage p 154 A85-28080
Fabrication of p(+)-n junction GaAs solar cells by a novel method p 181 A85-33645
The NASA photovoltaic technology program p 155 A85-35604
Method for evaluating wind turbine wake effects on wind farm performance p 155 A85-36750
Energy efficient engine high pressure turbine test hardware detailed design report [NASA-CR-167955] p 23 N85-10995
NASA Redox Storage System Development Project [NASA-TM-83677] p 158 N85-12465
Overview of the 1985 NASA Lewis Research Center SP-100 free-piston Stirling engine activities [NASA-TM-87028] p 185 N85-27769
Develop and test fuel cell powered on-site integrated total energy systems. Phase 3: Full-scale power plant development [NASA-CR-168338] p 164 N85-30483
Energy Efficient Engine Program technology benefit/cost study, volume 1 [NASA-CR-174766-VOL-1] p 33 N85-35197

ENERGY DISTRIBUTION
Measurements of energy distribution in microwave plasmas of N2 and He and comparisons with results for H2 p 178 A85-16443

ENERGY STORAGE
A rotating superconducting solenoid for 100 kWh energy storage --- in space p 44 A85-33144
Chemical and electrochemical behavior of the Cr(III)/Cr(II) half-cell in the iron-chromium redox energy storage system p 61 A85-33785
Design considerations for a 10-kW integrated hydrogen-oxygen regenerative fuel cell system p 155 A85-45380
Design of a 1-kWh bipolar nickel hydrogen battery p 155 A85-45384
NASA Redox Storage System Development Project [NASA-TM-83677] p 158 N85-12465
Regenerative fuel cell energy storage system for a low Earth orbit space station [NASA-CR-174802] p 158 N85-13371
Engineering model system study for a regenerative fuel cell: Study report [NASA-CR-174801] p 158 N85-16292
Operating characteristics of a 0.87 kW-hr flywheel energy storage module [NASA-TM-87038] p 133 N85-28371
Regenerative fuel cell systems for space station p 104 N85-31372
System level electrochemical principles p 104 N85-31375
Evaluation of developmental membranes for the mixed reactant iron-chromium redox system [NASA-TM-87074] p 164 N85-34443

ENERGY TECHNOLOGY
Measured effects of wind turbine generation at the Block Island Power Company p 153 A85-10652
Fuel cell power plant economic and operational considerations [ASME PAPER 84-AES-7] p 154 A85-21297
Status of DOE and AID stand-alone photovoltaic system field tests p 155 A85-35707
Parametric study of potential early commercial power plants Task 3-A MHD cost analysis [NASA-CR-175839] p 161 N85-27377

ENGINE AIRFRAME INTEGRATION
The Altitude Wind Tunnel (AWT) - A unique facility for propulsion system and adverse weather testing [AIAA PAPER 85-0314] p 34 A85-19661
Energy efficient engine component development and integration program [NASA-CR-172846] p 31 N85-29958

ENGINE ANALYZERS
DEAN: A program for dynamic engine analysis [NASA-TM-87033] p 30 N85-28945

ENGINE CONTROL
The role of modern control theory in the design of controls for aircraft turbine engines p 13 A85-13627
The use of Ada in distributed simulations p 169 A85-28612
Multibus-based parallel processor for simulation p 169 A85-28613
TF34 convertible engine control system design p 15 A85-32006
A real-time FORTRAN implementation of a sensor failure detection, isolation and accommodation algorithm p 171 A85-47704
Energy Efficient Engine (E3) controls and accessories detail design report [NASA-CR-168017] p 31 N85-29957

ENGINE COOLANTS
Vortex-generating coolant-flow-passage design for increased film-cooling effectiveness and surface coverage [NASA-TP-2388] p 113 N85-12314

ENGINE DESIGN
The role of modern control theory in the design of controls for aircraft turbine engines p 13 A85-13627
Ceramic component development for the AGT101 gas turbine engine p 126 A85-15972
Ceramic components for gas turbine engines p 127 A85-15973
Computational thermo-fluid dynamics contributions to advanced gas turbine engine design [AIAA PAPER 85-0083] p 14 A85-19509
Three-dimensional inviscid flow analysis of turbofan forced mixers [AIAA PAPER 85-0086] p 2 A85-19510
Predicted turbine stage performance using quasi-three-dimensional and boundary-layer analyses p 15 A85-34013
Main propulsion system design recommendations for an advanced Orbit Transfer Vehicle [AIAA PAPER 85-1336] p 36 A85-39730
Stall recovery control strategy methodology and results [AIAA PAPER 85-1433] p 16 A85-40841
Inviscid analysis of advanced turboprop propeller flow fields [AIAA PAPER 85-1263] p 6 A85-43977
Mod II engine and technology development p 129 A85-45473
Automotive Stirling engine systems development p 130 A85-45474
Overview of NASA Lewis Research Center free-piston Stirling engine activities p 130 A85-45479
Computational thermo-fluid dynamics contributions to advanced gas turbine engine design [NASA-TM-86865] p 18 N85-10069
Energy efficient engine flight propulsion system *preliminary analysis and design report* [NASA-CR-174701] p 18 N85-10947
Energy efficient engine component development and integration program [NASA-CR-170034] p 22 N85-10990
Energy efficient engine ICLS Nacelle detail design report [NASA-CR-167870] p 22 N85-10993
Energy efficient engine. Low pressure turbine test hardware detailed design report [NASA-CR-167956] p 22 N85-10994
Energy efficient engine ICLS engine bearings, drives and configuration: Detail design report [NASA-CR-167871] p 23 N85-10997
External fuel vaporization study, phase 2 [NASA-CR-174079] p 92 N85-11252
Stirling material technology [NASA-TM-86888] p 72 N85-13007
Advanced automotive diesel assessment program *[NASA-CR-168285] p 130 N85-13235*
Fabrication and quality assurance processes for superhybrid composite fan blades [NASA-TM-83354] p 57 N85-14882
Vehicle/engine integration --- orbit transfer vehicles p 37 N85-17008
Advanced Gas Turbine (AGT) powertrain system development for automotive applications [NASA-CR-174809] p 185 N85-18831
Creep-rupture behavior of iron superalloys in high-pressure hydrogen [NASA-CR-174411] p 74 N85-19078
Analytical fuel property effects: Small combustors, phase 2 [NASA-CR-174848] p 93 N85-19175
Initial testing of a variable-stroke Stirling engine [NASA-TM-86875] p 185 N85-19895
Lubrication and performance of high-speed rolling-element bearings [NASA-TM-86958] p 131 N85-21658
Ceramic applications in turbine engines [NASA-CR-174715] p 91 N85-28109
Energy efficient engine. Fan and quarter-stage component performance report [NASA-CR-168070] p 33 N85-34141

ENGINE FAILURE
Contingency power concepts for helicopter turboshaft engine p 15 A85-32005
Reusable rocket engine turbopump condition monitoring [SAE PAPER 841619] p 44 A85-39267
A theory of post-stall transients in multistage axial compression systems [NASA-CR-3878] p 8 N85-21117
Nonlinear global stability analysis of compressor stall phenomena [NASA-CR-174908] p 31 N85-29960

ENGINE INLETS
Icing tunnel tests of Electro-Impulse De-Icing of an *engine inlet and high-speed wings* [AIAA PAPER 85-0466] p 10 A85-20872
Electro-impulse de-icing of a turbofan engine inlet [AIAA PAPER 85-1118] p 12 A85-40811
Stall recovery control strategy methodology and results [AIAA PAPER 85-1433] p 16 A85-40841
Effect of steady-state temperature distortion on inlet flow to a high-bypass-ration turbofan engine [NASA-TM-86896] p 24 N85-15725
Calculation of compressible flow about three-dimensional inlets with auxiliary inlets, slats and vanes by means of a panel method [NASA-CR-174975] p 10 N85-35162

ENGINE MONITORING INSTRUMENTS
Eddy current jet engine disk-crack monitor p 120 A85-11100
Reusable rocket engine turbopump condition monitoring [SAE PAPER 841619] p 44 A85-39267

ENGINE NOISE
Comparison of scaled model data to full size energy efficient engine test results [AIAA PAPER 84-2281] p 13 A85-13953
Measurement and prediction of Energy Efficient Engine noise [AIAA PAPER 84-2284] p 13 A85-13954
Analysis of the effect on combustor noise measurements of acoustic waves reflected by the turbine and combustor inlet [AIAA PAPER 84-2323] p 173 A85-16103
Energy efficient engine component development and integration program [NASA-CR-169496] p 22 N85-10989
Turbofan noise generation. Volume 2: Computer programs [NASA-CR-167952] p 175 N85-11791
Experimental investigation of shock-cell noise reduction for dual-stream nozzles in simulated flight [NASA-CR-3846] p 175 N85-13549
Static jet noise test results of four 0.35 scale-model QCGAT mixer nozzles [NASA-TM-86871] p 175 N85-13551

ENGINE PARTS
Ceramic component development for the AGT101 gas turbine engine p 126 A85-15972
Ceramic components for gas turbine engines p 127 A85-15973
Considerations for damage analysis of gas turbine hot section components [ASME PAPER 84-PVP-77] p 14 A85-18792
Finite element engine blade structural optimization *[AIAA PAPER 85-0645] p 141 A85-30313*
Effect of low temperature on fatigue and fracture properties of Ti-5Al-2.5Sn(ELI) for use in engine components p 70 A85-47972
Component-specific modeling p 20 N85-10971
Constitutive model development for isotropic materials p 20 N85-10975
Energy efficient engine ICLS engine bearings, drives and configuration: Detail design report [NASA-CR-167871] p 23 N85-10997
An investigation of enhanced capability thermal barrier coating systems for diesel engine components [NASA-CR-174820] p 86 N85-18154
Advanced Gas Turbine (AGT) powertrain system development for automotive applications *[NASA-CR-174809] p 185 N85-18831*
Tribological systems as applied to aircraft engines [NASA-TM-86965] p 131 N85-21657
Properties and microstructures for dual alloy combinations of three superalloys with alloy 901 [NASA-TM-86987] p 76 N85-26963
Ceramic applications in turbine engines [NASA-CR-174715] p 91 N85-28109
Energy efficient engine component development and integration program [NASA-CR-172846] p 31 N85-29958
Creep fatigue life prediction for engine hot section materials (isotropic) [NASA-CR-168228] p 32 N85-31057
Component-specific modeling [NASA-CR-174925] p 32 N85-32119

ENGINE TESTING LABORATORIES
The Altitude Wind Tunnel (AWT) - A unique facility for propulsion system and adverse weather testing [AIAA PAPER 85-0314] p 34 A85-19661

ENGINE TESTS
Eddy current jet engine disk-crack monitor p 120 A85-11100
Comparison of scaled model data to full size energy efficient engine test results [AIAA PAPER 84-2281] p 13 A85-13953
IAPS (8-cm) ion thruster cyclic endurance test --- Ion Auxiliary Propulsion System p 42 A85-16406
Electrothermal thruster diagnostics p 42 A85-16440
Altitude testing of a flight weight, self-cooled, 2D thrust vectoring exhaust nozzle [SAE PAPER 841557] p 14 A85-25984
Inert gas test of two 12-cm magnetostatic thrusters p 43 A85-29310
Temperature distortion generator for turboshaft engine testing [SAE PAPER 841541] p 15 A85-39065
Performance characterization tests of a 1-kW resistojet using hydrogen, nitrogen and ammonia as propellants [AIAA PAPER 85-1159] p 44 A85-39628
Initial results of sensitivity tests - Performed on the RE-1000 free-piston Stirling engine p 129 A85-45466
Combustion system for radiation investigations p 21 N85-10986
HOST liner cyclic facilities: Facility description p 22 N85-10988
Energy efficient engine component development and *integration program* [NASA-CR-170034] p 22 N85-10990
Advanced blade tip seal system, volume 2 [NASA-CR-167851] p 23 N85-10999
Temperature distortion generator for turboshaft engine testing [NASA-TM-83748] p 1 N85-15658

Integrated exhaust gas analysis system for aircraft turbine engine component testing
[NASA-TP-2424] p 123 N85-16100
Study of advanced fuel system concepts for commercial aircraft
[NASA-CR-174751] p 12 N85-19978
Ceramic applications in turbine engines
[NASA-CR-174715] p 91 N85-28109
Energy efficient engine high-pressure turbine component rig performance test report
[NASA-CR-168189] p 30 N85-29955
Free-piston Stirling engine/linear alternator 1000-hour endurance test
[NASA-CR-174771] p 163 N85-30481
Energy efficient engine. Fan and quarter-stage component performance report
[NASA-CR-168070] p 33 N85-34141

ENGINES
Effect of water on hydrogen permeability --- Stirling engines
[NASA-TM-86904] p 53 N85-14864

ENTHALPY
External fuel vaporization study, phase 2
[NASA-CR-174079] p 92 N85-11252

ENVIRONMENT EFFECTS
High voltage requirements and issues for the 1990's --- for spacecraft power supplies p 46 A85-45429
Impact resistance of fiber composites - Energy-absorbing mechanisms and environmental effects p 56 A85-46543

ENVIRONMENT SIMULATION
The Altitude Wind Tunnel (AWT) - A unique facility for propulsion system and adverse weather testing
[AIAA PAPER 85-0314] p 34 A85-19661
Ribbon burner simulation of T-700 turbine shroud for ceramic lined seals research
[NASA-TM-86940] p 114 N85-19364

ENVIRONMENTAL TESTS
Ten year environmental test of glass fiber/epoxy pressure vessels
[AIAA PAPER 85-1198] p 56 A85-47022
Ten year environmental test of glass fiber/epoxy pressure vessels
[NASA-TM-87058] p 58 N85-30034

EPOXY COMPOUNDS
Ten year environmental test of glass fiber/epoxy pressure vessels
[AIAA PAPER 85-1198] p 56 A85-47022
Ten year environmental test of glass fiber/epoxy pressure vessels
[NASA-TM-87058] p 58 N85-30034

EPOXY MATRIX COMPOSITES
Imide modified epoxy matrix resins
[NASA-CR-174695] p 85 N85-15892

EPOXY RESINS
Fiberglass epoxy laminate fatigue properties at 300 and 20 K p 56 A85-47970
Imide modified epoxy matrix resins
[NASA-CR-174695] p 85 N85-15892

EQUATIONS OF MOTION
Flutter of turbofan rotors with mistuned blades p 139 A85-12716
Optimization of cascade blade mistuning. I - Equations of motion and basic inherent properties p 16 A85-42365
Transition in Turbines
[NASA-CP-2386] p 118 N85-31433

EQUATIONS OF STATE
Universal binding energy relations in metallic adhesion
[NASA-TM-86889] p 72 N85-12132

EQUILIBRIUM FLOW
Reducing numerical diffusion for incompressible flow calculations
[NASA-TM-83621] p 24 N85-14840
Elastohydrodynamic lubrication calculations used as a tool to study scuffing
[NASA-TM-87097] p 137 N85-34408

EROSION
Spherical microglass particle impingement studies of thermoplastic materials at normal incidence p 79 A85-11072
Deformation and erosion of f.c.c. metals and alloys under cavitation attack p 65 A85-12789
Cathode degradation and erosion in high pressure arc discharges p 43 A85-16445
A unified relation for cavitation erosion p 109 A85-24445
High-temperature erosion of plasma-sprayed, yttria-stabilized zirconia in a simulated turbine environment
[AIAA PAPER 85-1219] p 82 A85-39662
Effect of surface configuration during solid particle impingement erosion p 69 A85-42568
Characterization of solid particle erosion resistance of ductile metals based on their properties p 69 A85-42569
High-temperature erosion of plasma-sprayed, yttria-stabilized zirconia in a simulated turbine environment
[NASA-TP-2406] p 84 N85-13045
Characterization of erosion of metallic materials under cavitation attack in a mineral oil
[NASA-TM-86934] p 74 N85-19075
Mechanical protection of DLC films on fused silica slides
[NASA-TM-87056] p 91 N85-30138
Electrode erosion in arc discharges at atmospheric pressure
[NASA-TM-87087] p 52 N85-34178

ERROR ANALYSIS
Finite difference methods for reducing numerical diffusion in TEACH-type calculations --- Teaching Elliptic Axisymmetric Characteristics Heuristically
[AIAA PAPER 85-0057] p 108 A85-19488
Calculation of confined swirling flows
[AIAA PAPER 85-0060] p 108 A85-19491

ERRORS
Optical linear algebra processors - Noise and error-source modeling p 169 A85-36727
Error reduction program --- combustor performance evaluation codes
[NASA-CR-174776] p 172 N85-27584
Filter induced errors in laser anemometer measurements using counter processors
[NASA-TM-87047] p 125 N85-30288
Comparative analysis of operational forecasts versus actual weather conditions in airline flight planning, volume 4
[NASA-CR-167865] p 167 N85-35537
Comparative analysis of operational forecasts versus actual weather conditions in airline flight planning: Summary report
[NASA-CR-167866] p 168 N85-35538

ETHANE
Shock tube measurements of growth constants in the branched-chain ethane-carbon monoxide-oxygen system
[NASA-TM-87068] p 64 N85-32156

EULER EQUATIONS OF MOTION
Efficient solution of the Euler and Navier-Stokes equations with a vectorized multiple-grid algorithm p 2 A85-18679
Time dependent computation of the Euler equations for designing 2-D cascades, including the case of transonic shock free design p 5 A85-41814
Researched applied to transonic compressors in numerical fluid mechanics of inviscid flow and viscous flow
[NASA-CR-174353] p 114 N85-18291
A convergent series expansion for hyperbolic systems of conservation laws
[NASA-CR-172557] p 168 N85-21990
Redistribution of the inlet temperature profile through the SSME fuel turbine p 50 N85-26901

EUTECTIC ALLOYS
New eutectic alloys and their heats of transformation p 66 A85-27808

EUTECTIC COMPOSITES
Deformation and fracture behavior of Ni-Mo-Al(gamma/gamma prime-alpha) in situ composite p 64 A85-11058

EVALUATION
Operational performance of the photovoltaic-powered grain mill and water pump at Tangaye, Burkina Faso (formerly Upper Volta)
[NASA-TM-86970] p 161 N85-23243

EVAPORATION
Measurements and predictions of the structure of evaporating sprays p 112 A85-46484

EXHAUST DIFFUSERS
Energy efficient engine combustor test hardware detailed design report
[NASA-CR-167945] p 18 N85-10950

EXHAUST EMISSION
Energy efficient engine component development and integration program
[NASA-CR-169496] p 22 N85-10989

EXHAUST GASES
Overview of waste heat utilization systems
[NASA-TM-86901] p 184 N85-13692
Integrated exhaust gas analysis system for aircraft turbine engine component testing
[NASA-TP-2424] p 123 N85-16100
Comparative evaluation of three alternative power cycles for waste heat recovery from the exhaust of adiabatic diesel engines
[NASA-TM-86953] p 186 N85-32043

EXHAUST NOZZLES
Altitude testing of a flight weight, self-cooled, 2D thrust vectoring exhaust nozzle
[SAE PAPER 841557] p 14 A85-25984
The performance of jet noise suppression devices for industrial applications p 175 A85-42563
A multiple-scales model of the shock-cell structure of imperfectly expanded supersonic jets p 113 A85-49354
Static jet noise test results of four 0.35 scale-model QCGAT mixer nozzles
[NASA-TM-86871] p 175 N85-13551

EXISTENCE THEOREMS
Constructive existence and uniqueness for two-point boundary-value problems with a linear gradient term p 172 A85-28015

EXPERIMENTATION
On thermomechanical testing in support of constitutive equation development for high temperature alloys
[NASA-CR-174879] p 147 N85-25894

EXPERT SYSTEMS
Composite loads spectra for select space propulsion structural components: Probabilistic load model development p 148 N85-27954

EXTENSOMETERS
Some advances in experimentation supporting development of viscoplastic constitutive models
[NASA-CR-174855] p 147 N85-27260
Some advances in experimentation supporting development of viscoplastic constitutive models p 151 N85-31545
Results of an interlaboratory fatigue test program conducted on alloy 800H at room and elevated temperatures
[NASA-CR-174940] p 152 N85-32340

EXTERNAL COMBUSTION ENGINES
Stirling material technology
[NASA-TM-86888] p 72 N85-13007

EXTERNAL SURFACE CURRENTS
Surface interactions and high-voltage current collection p 40 N85-22493

EXTRUDING
High temperature properties of equiatomic FeAl with ternary additions
[NASA-TM-86938] p 73 N85-19072

F

FABRICATION
Ceramic components for gas turbine engines p 127 A85-15973
Fabrication and quality assurance processes for superhybrid composite fan blades
[NASA-TM-83354] p 57 N85-14882
Effect of substituted phenylnadimides on processing and properties of PMR polyimide composites
[NASA-TM-86902] p 85 N85-14929
Infrared technology for satellite power conversion --- antenna arrays and bolometers
[NASA-CR-174266] p 159 N85-16293
Investigation on experimental techniques to detect, locate and quantify gear noise in helicopter transmissions
[NASA-CR-3847] p 176 N85-17667
Extreme precision antenna reflector study results p 165 N85-23830
Tape casting as an approach to an all-ceramic turbine shroud seal
[NASA-TM-87078] p 135 N85-32333

FABRY-PEROT INTERFEROMETERS
Remote displacement measurement using a passive interferometer with a fiber-optic link p 122 A85-42857

FACE CENTERED CUBIC LATTICES
Deformation and erosion of f.c.c. metals and alloys under cavitation attack p 65 A85-12789
Modeling of gamma/gamma-prime phase equilibrium in the nickel-aluminum system p 65 A85-14959

FACTORIZATION
Augmented weak forms and element-by-element preconditioners: Efficient iterative strategies for structural finite elements. A preliminary study p 144 N85-10384

FAILURE ANALYSIS
Sensor failure detection for jet engines using analytical redundancy
[AIAA PAPER 84-1452] p 13 A85-16097
Deposition stress effects on the life of thermal barrier coatings on burner rigs p 79 A85-19086
Contingency power concepts for helicopter turboshaft engine p 15 A85-32005
Teardown analysis of a ten cell bipolar nickel-hydrogen battery p 156 A85-45385
Long life nickel electrodes for a nickel-hydrogen cell. III - Results of an accelerated test and failure analyses p 156 A85-45391
A design methodology for robust failure detection and isolation p 171 A85-47794
Airfoil deposition model p 21 N85-10979
Reusable rocket engine turbopump condition monitoring p 51 N85-26907
The failure mechanism of a nickel electrode in a nickel-hydrogen cell p 105 N85-31408

A comparison of two contemporary creep-fatigue life prediction methods p 151 N85-31538
FAILURE MODES
Failure during thermal cycling of plasma-sprayed thermal barrier coatings p 81 A85-36246
A design methodology for robust failure detection and isolation p 171 A85-47794
A continuous damage model based on stepwise-stress creep rupture tests
[NASA-CR-174941] p 152 N85-32341
FAN BLADES
Finite element engine blade structural optimization
[AIAA PAPER 85-0645] p 141 A85-30313
Flutter of swept fan blades
[ASME PAPER 84-GT-138] p 141 A85-32962
Rotor wake characteristics of a transonic axial flow fan
[AIAA PAPER 85-1133] p 6 A85-43974
Energy efficient engine. Volume 2. Appendix A: Component development and integration program
[NASA-CR-173085] p 22 N85-10991
Fabrication and quality assurance processes for superhybrid composite fan blades
[NASA-TM-83354] p 57 N85-14882
Effects of vane/blade ratio and spacing on fan noise, volume 1
[NASA-CR-174664] p 176 N85-19791
Effects of vane/blade ratio and spacing on fan noise. Volume 2: Data supplement
[NASA-CR-174665] p 176 N85-19792
Energy Efficient Engine Program technology benefit/cost study, volume 1
[NASA-CR-174766-VOL-1] p 33 N85-35197
FAR FIELDS
Case study of sample spacing in planar near-field measurement of high gain antennas
[NASA-TM-86872] p 97 N85-10234
FATIGUE (MATERIALS)
Spherical microglass particle impingement studies of thermoplastic materials at normal incidence p 79 A85-11072
Fatigue criterion to system design, life and reliability
[AIAA PAPER 85-1140] p 143 A85-40814
Turbine Engine Hot Section Technology (HOST)
[NASA-TM-83022] p 18 N85-10951
Experimental compliance calibration of the NASA Lewis Research Center Mode 2 fatigue specimen
[NASA-TM-86908] p 144 N85-16205
Fatigue criterion to system design, life and reliability
[NASA-TM-87017] p 132 N85-27226
Elevated temperature biaxial fatigue
[NASA-CR-175795] p 148 N85-27263
Structural Integrity and Durability of Reusable Space Propulsion Systems
[NASA-CP-2381] p 51 N85-27941
Interaction of high-cycle and low-cycle fatigue of Haynes 188 alloy at 1400 F deg p 149 N85-27961
Reexamination of cumulative fatigue damage laws p 149 N85-27962
Two simplified procedures for predicting cyclic material response from a strain history p 151 N85-31543
Application of traction drives as servo mechanisms p 152 N85-33520
FATIGUE LIFE
Strainrange partitioning - A total strain range version --- for creep fatigue life prediction by summing inelastic and elastic strain-range-life relations for two Ni base superalloys p 64 A85-11603
A study of fatigue damage mechanisms in Waspaloy from 25 to 800 C p 65 A85-12098
Considerations for damage analysis of gas turbine hot section components
[ASME PAPER 84-PVP-77] p 14 A85-18792
A history dependent damage model for low cycle fatigue
[ASME PAPER 84-PVP-112] p 140 A85-18795
Fracture toughness of hot-pressed beryllium p 66 A85-25835
Simplified design and life prediction of rocket thrust chambers p 44 A85-29314
On the fatigue crack propagation behavior of superalloys at intermediate temperatures p 68 A85-32434
Application of two creep fatigue life models for the prediction of elevated temperature crack initiation of a nickel base alloy
[AIAA PAPER 85-1420] p 69 A85-43979
Fiberglass epoxy laminate fatigue properties at 300 and 20 K p 56 A85-47970
Life prediction and constitutive behavior: Overview p 20 N85-10973
Effect of lubricant extreme-pressure additives on surface fatigue life of AISI 9310 spur gears
[NASA-TP-2408] p 130 N85-13234
Thermal-mechanical fatigue crack growth in Inconel X-750
[NASA-CR-174740] p 72 N85-15877
Fundamentals of microcrack nucleation mechanics
[NASA-CR-3851] p 137 N85-16195
Fatigue life analysis of a turboprop reduction gearbox
[NASA-TM-87014] p 133 N85-27228
Creep fatigue life prediction for engine hot section materials (isotropic)
[NASA-CR-168228] p 32 N85-31057
Effect of speed and press fit on fatigue life of roller-bearing inner-race contact
[NASA-TP-2496] p 134 N85-31511
A comparison of two contemporary creep-fatigue life prediction methods p 151 N85-31538
FATIGUE TESTS
Hygrothermomechanical evaluation of transverse filament tape epoxy/polyester fiberglass composites p 54 A85-15632
Engine cyclic durability by analysis and material testing p 25 N85-15744
Effect of five lubricants on life of AISI 9310 spur gears
[NASA-TP-2419] p 123 N85-16099
Low cycle fatigue of MAR-M 200 single crystals at 760 and 870 deg C
[NASA-TM-86933] p 74 N85-19074
Lubricant and additive effects on spur gear fatigue life
[NASA-TM-87044] p 133 N85-28373
Results of an interlaboratory fatigue test program conducted on alloy 800H at room and elevated temperatures
[NASA-CR-174940] p 152 N85-32340
FEASIBILITY
Initial feasibility ground test of a proposed photogrammetric system for measuring the shapes of ice accretions on helicopter rotor blades during forward flight
[NASA-TM-87391] p 12 N85-12887
FEASIBILITY ANALYSIS
Feasibility study of the welding of SiC p 81 A85-39339
Research on gallium arsenide diffused junction solar cells
[NASA-CR-174057] p 158 N85-11457
Diffusion welding of Cassegrainian concentrator cell stack assemblies
[NASA-CR-176104] p 164 N85-33566
FEEDBACK
Feedback in separated flows over symmetric airfoils
[AIAA PAPER 84-2297] p 3 A85-28899
FEEDBACK CONTROL
Identification of multivariable high-performance turbofan engine dynamics from closed-loop data p 13 A85-13630
Closed-loop strain controlled testing at elevated temperatures with a non-contacting gage p 121 A85-29562
Small-signal model for the series resonant converter p 102 A85-39453
FEEDFORWARD CONTROL
A fast time domain digital simulation technique for power converters - Application to a buck converter with feedforward compensation p 101 A85-20900
FERRIC IONS
Dynamics of graphite fiber intercalation: In situ resistivity measurements with a four point probe
[NASA-TM-86858] p 53 N85-10105
FERRITES
Fundamental tribological properties of ceramics
[NASA-TM-86915] p 85 N85-15893
Humidity effects on adhesion of nickel-zinc ferrite in elastic contact with magnetic tape and itself
[NASA-TP-2449] p 88 N85-21359
Effects of wear on structure-sensitive magnetic properties of ceramic ferrite in contact with magnetic tape
[NASA-TM-87007] p 90 N85-26991
FERROUS METALS
Friction and wear of some ferrous-base metallic glasses p 64 A85-11071
FIBER COMPOSITES
Acoustic structure and propagation in highly porous, layered, fibrous materials p 173 A85-12301
Select fiber composites for space applications - A mechanistic assessment p 54 A85-16040
ICAN - Integrated composites analyzer
[AIAA PAPER 84-0974] p 54 A85-16094
Interply layer degradation effects on composite structural response
[AIAA PAPER 84-0849] p 54 A85-16096
Interply layer degradation effects on composite structural response p 55 A85-39215
Impact resistance of fiber composites - Energy-absorbing mechanisms and environmental effects p 56 A85-46543
Fundamental studies of composite toughness p 56 N85-12948
Design procedures for fiber composite structural components: Panels subjected to combined in-plane loads
[NASA-TM-86909] p 57 N85-15823
Tribological properties of graphite-fiber-reinforced, partially fluorinated polyimide composites
[NASA-TM-86926] p 86 N85-18153
Homogeneity of pristine and bromine intercalated graphite fibers
[NASA-TM-87016] p 89 N85-25521
Designing for fiber composite structural durability in hygrothermomechanical environment
[NASA-TM-87045] p 58 N85-27978
Arc spray fabrication of metal matrix composite monotape
[NASA-CASE-LEW-13828-1] p 58 N85-30027
Structural characteristics of high temperature composites
[NASA-CR-175998] p 58 N85-30037
FIBER OPTICS
Fiber optic temperature sensor p 121 A85-29563
Remote displacement measurement using a passive interferometer with a fiber-optic link p 122 A85-42857
High-temperature fiber optic pressure sensor p 123 A85-46607
High-temperature optically activated GaAs power switching for aircraft digital electronic control
[NASA-CR-174711] p 34 N85-12901
Fiber optic, Fabry-Perot high temperature sensor
[NASA-CR-174712] p 178 N85-13594
Reusable rocket engine turbopump condition monitoring p 51 N85-26907
FIBER REINFORCED COMPOSITES
Use of statical indentation laws in the impact analysis of laminated composite plates p 55 A85-29133
Ten year environmental test of glass fiber/epoxy pressure vessels
[AIAA PAPER 85-1198] p 56 A85-47022
Nonlinear analysis for high-temperature multilayered fiber composite structures --- turbine blades
[NASA-TM-83754] p 57 N85-21273
Nonlinear structural analysis for fiber-reinforced superalloy turbine blades p 147 N85-26887
Ten year environmental test of glass fiber/epoxy pressure vessels
[NASA-TM-87058] p 58 N85-30034
Mechanical properties of SiC fiber-reinforced reaction-bonded Si3N4 composites
[NASA-TM-87085] p 59 N85-34223
FIBER STRENGTH
Fibers for structurally reliable metal and ceramic composites p 55 A85-37484
High performance fibers for structurally reliable metal and ceramic composites --- advanced gas turbine engine materials
[NASA-TM-86878] p 56 N85-12095
FIBERS
Oscillatory conductive heat transfer for a fiber in an ideal gas p 109 A85-26077
Dynamics of graphite fiber intercalation: In situ resistivity measurements with a four point probe
[NASA-TM-86858] p 53 N85-10105
Stability of bromine intercalated graphite fibers
[NASA-TM-86859] p 84 N85-10187
Creep of chemically vapor deposited SiC fibers
[NASA-TM-86897] p 56 N85-14878
A micrographic and gravimetric study of intercalation and deintercalation of graphite fibers
[NASA-TM-87026] p 91 N85-28110
FIELD EFFECT TRANSISTORS
Bipolar-FET combinational power transistors for power conversion applications p 100 A85-12669
High-temperature optically activated GaAs power switching for aircraft digital electronic control
[NASA-CR-174711] p 34 N85-12901
High-voltage, high-power, solid-state remote power controllers for aerospace applications
[NASA-TP-2437] p 49 N85-21263
FIELD EMISSION
Apparatus for mounting a field emission cathode
[NASA-CASE-LEW-14108-1] p 104 N85-29149
FILM COOLING
Advanced liner-cooling techniques for gas turbine combustors
[AIAA PAPER 85-1290] p 15 A85-39703
Heat transfer and turbulence measurements of a film-cooled flow over a convexly curved surface p 112 A85-41787
Vortex-generating coolant-flow-passage design for increased film-cooling effectiveness and surface coverage
[NASA-TP-2388] p 113 N85-12314
Heat transfer results and operational characteristics of the NASA Lewis Research Center Hot Section Cascade Test Facility
[NASA-TM-86890] p 114 N85-15133

Flow visualization study of the effect of injection hole geometry on an inclined jet in crossflow
[NASA-TM-86936] p 115 N85-20269
Advanced liner-cooling techniques for gas turbine combustors
[NASA-TM-86952] p 8 N85-21115
Vortex generating flow passage design for increased film cooling effectiveness
[NASA-CASE-LEW-14039-1] p 119 N85-33433

FILM THICKNESS
Thermal elastohydrodynamic lubrication of line contacts p 128 A85-31202
The scattering of ultrasonic third sound from substrate surface defects p 174 A85-36047
Fast approach for calculating film thicknesses and pressures in elastohydrodynamically lubricated contacts at high loads
[NASA-TM-87032] p 117 N85-30242

FINITE DIFFERENCE THEORY
Time dependent wave envelope finite difference analysis of sound propagation
[AIAA PAPER 84-2285] p 173 A85-16102
Finite difference methods for reducing numerical diffusion in TEACH-type calculations --- Teaching Elliptic Axisymmetric Characteristics Heuristically
[AIAA PAPER 85-0057] p 108 A85-19488
Finite difference analysis of torsional vibrations of pretwisted, rotating, cantilever beams with effects of warping p 143 A85-42047
Researched applied to transonic compressors in numerical fluid mechanics of inviscid flow and viscous flow
[NASA-CR-174353] p 114 N85-18291
Vibration and buckling of rotating, pretwisted, preconed beams including Cooriolis effects
[NASA-TM-87004] p 146 N85-25893
A computer analysis program for interfacing thermal and structural codes
[NASA-TM-87021] p 148 N85-27264
Error reduction program --- combustor performance evaluation codes
[NASA-CR-174776] p 172 N85-27584

FINITE ELEMENT METHOD
Analysis of hourglass instabilities and control in underintegrated finite element methods p 139 A85-11125
A finite element solution of three-dimensional inviscid rotational flows through curved ducts p 107 A85-11648
Rational approach for assumed stress finite elements p 139 A85-12029
Hybrid Semiloof elements for plates and shells based upon a modified Hu-Washizu principle p 139 A85-15893
Hybrid stress finite elements for large deformations of inelastic solids p 139 A85-15894
Development and testing of stable, invariant, isoparametric curvilinear 2- and 3-D hybrid-stress elements p 140 A85-19899
On the development of hierarchical solution strategies for nonlinear finite element formulations p 171 A85-21979
A simplified method for elastic-plastic-creep structural analysis
[ASME PAPER 84-GT-191] p 141 A85-23150
Finite element engine blade structural optimization
[AIAA PAPER 85-0645] p 141 A85-30313
Natural frequencies of twisted rotating plates p 141 A85-32343
On the existence and stability conditions for mixed-hybrid finite element solutions based on Reissner's variational principle p 142 A85-33847
Evolution of assumed stress hybrid finite element p 142 A85-35046
Plasticity, viscoplasticity, and creep of solids by mechanical subelement models p 142 A85-35048
Pantographing self adaptive gap elements p 142 A85-37440
Unified constitutive material models for nonlinear finite-element structural analysis --- gas turbine engine blades and vanes
[AIAA PAPER 85-1418] p 142 A85-39769
Axisymmetric solid elements by a rational hybrid stress method p 143 A85-41109
A study of interply layer effects on the free edge stress field of angleplied laminates p 55 A85-41127
Impact resistance of fiber composites - Energy-absorbing mechanisms and environmental effects p 56 A85-46543
Stability, accuracy, and efficiency of some underintegrated methods in finite element computations p 172 A85-50073
Augmented weak forms and element-by-element preconditioners: Efficient iterative strategies for structural finite elements. A preliminary study p 144 N85-10384
Constitutive model development for isotropic materials p 20 N85-10975
A study of interply layer effects on the free-edge stress field of angleplied laminates
[NASA-TM-86924] p 57 N85-15822
Analytical and experimental investigation of rubbing interaction in labyrinth seals for a liquid hydrogen fuel pump --- space shuttle main engine
[NASA-CR-174657] p 48 N85-18084
Local strain redistribution corrections for a simplified inelastic analysis procedure based on an elastic finite-element analysis
[NASA-TP-2421] p 145 N85-20396
Advanced stress analysis methods applicable to turbine engine structures
[NASA-CR-175573] p 26 N85-21165
Nonlinear analysis for high-temperature multilayered fiber composite structures --- turbine blades
[NASA-TM-83754] p 57 N85-21273
3-D inelastic analysis methods for hot section components (base program) --- turbine blades, turbine vanes, and combustor liners
[NASA-CR-174700] p 145 N85-21686
Recent advances in hybrid/mixed finite elements
[NASA-CR-175574] p 145 N85-21687
Geometrically nonlinear analysis of laminated elastic structures
[NASA-CR-175609] p 146 N85-21720
On Hybrid and mixed finite element methods
[NASA-CR-175551] p 146 N85-23096
Unified constitutive material models for nonlinear finite-element structural analysis --- gas turbine engine blades and vanes
[NASA-TM-86985] p 146 N85-24338
A computer analysis program for interfacing thermal and structural codes
[NASA-TM-87021] p 148 N85-27264
Probabilistic finite element development p 149 N85-27956
Probabilistic finite element: Variational theory p 149 N85-27957
Designing for fiber composite structural durability in hygrothermomechanical environment
[NASA-TM-87045] p 58 N85-27978
A review of path-independent integrals in elastic-plastic fracture mechanics, task 4
[NASA-CR-174956] p 152 N85-33541
Thermal stress analysis of a new turbine shroud seal concept
[NASA-TM-87082] p 136 N85-34406

FINITE VOLUME METHOD
Thermodynamic evaluation of transonic compressor rotors using the finite volume approach
[NASA-CR-175811] p 29 N85-26712

FINS
The effect of channel convergence on heat transfer in a passage with short pin fins
[NASA-TM-83801] p 113 N85-10303

FLAME HOLDERS
The mechanisms of flame holding in the wake of a bluff body
[NASA-CR-3866] p 26 N85-21166

FLAME PROPAGATION
The influence of combustion liner holes on noise production by ducted burners
[AIAA PAPER 84-2322] p 172 A85-10869
Gravitational effects on flames spreading over thick solid surfaces
[IAF PAPER 84-154] p 59 A85-13092
Flame flashback in a premixed dump combustor
[AIAA PAPER 85-0145] p 60 A85-19550
Drop-turbulence interactions in a diffusion flame
[AIAA PAPER 85-0319] p 60 A85-19665
Growth of a diffusion flame in the field of a vortex p 61 A85-47320
Behavior of the lean methane-air flame at zero-gravity
[NASA-CR-175586] p 62 N85-21283

FLAME SPECTROSCOPY
Flame radiation and linear heat transfer in a tubular-can combustor p 15 A85-39580
Polarization (ellipsometric) measurements of liquid condensate deposition and evaporation rates and dew points in flowing salt/ash-containing combustion gases p 123 A85-46925
Shock tube measurements of growth constants in the branched-chain ethane-carbon monoxide-oxygen system
[NASA-TM-87068] p 64 N85-32156

FLAME SPRAYING
Drop-turbulence interactions in a diffusion flame
[AIAA PAPER 85-0319] p 60 A85-19665
Thermal barrier coating system
[NASA-CASE-LEW-14057-1] p 59 N85-35233

FLAME STABILITY
The mechanisms of flame holding in the wake of a bluff body
[NASA-CR-3866] p 26 N85-21166

FLAMEOUT
The mechanisms of flame holding in the wake of a bluff body
[NASA-CR-174058] p 62 N85-11149

FLAMES
A theoretical prediction of the acoustic pressure generated by turbulence-flame front interactions
[ASME PAPER 84-WA/NCA-11] p 174 A85-39909
The structure of dilute combusting sprays
[NASA-CR-174838] p 24 N85-15728
Behavior of the lean methane-air flame at zero-gravity
[NASA-CR-175586] p 62 N85-21283

FLAMMABILITY
Effect of gravity on halogenated hydrocarbon flame retardant effectiveness
[IAF PAPER 84-156] p 61 A85-23199
The use of a laser Doppler velocimeter in a standard flammability tube
[NASA-CR-174960] p 125 N85-35389

FLASHBACK
Flame flashback in a premixed dump combustor
[AIAA PAPER 85-0145] p 60 A85-19550

FLAT PLATES
Resonance in flows with vortex sheets and edges p 1 A85-10357
Vortex induced lift on a flat plate with a curved forward-facing flap p 4 A85-30175
Heat transfer investigation in the junction region of circular cylinder normal to a flat plate at 90 deg location
[ASME PAPER 84-WA/HT-70] p 111 A85-39898

FLEXIBILITY
Vibration and flutter of mistuned bladed-disk assemblies
[AIAA PAPER 84-0991] p 139 A85-16095

FLEXING
Graphite/PMR polyimide composites with improved toughness
[NASA-TM-87081] p 58 N85-32148
Reliability of two sintered silicon nitride materials
[NASA-TM-87092] p 92 N85-34284

FLIGHT CHARACTERISTICS
Performance degradation of helicopter rotor in forward flight due to ice p 11 A85-42937

FLIGHT CONDITIONS
GASP cloud encounter statistics - Implications for laminar flow control flight p 166 A85-11979
The Altitude Wind Tunnel (AWT): A unique facility for propulsion system and adverse weather testing
[NASA-TM-86921] p 35 N85-18067

FLIGHT CONTROL
Advanced secondary power system for transport aircraft
[NASA-TP-2463] p 30 N85-28944

FLIGHT HAZARDS
Experimental aerodynamic characteristics of an NACA 0012 airfoil with simulated ice p 12 A85-21844

FLIGHT PATHS
Comparative analysis of operational forecasts versus actual weather conditions in airline flight planning, volume 2
[NASA-CR-167863] p 167 N85-35535
Comparative analysis of operational forecasts versus actual weather conditions in airline flight planning, volume 3
[NASA-CR-167864] p 167 N85-35536
Comparative analysis of operational forecasts versus actual weather conditions in airline flight planning, volume 4
[NASA-CR-167865] p 167 N85-35537
Comparative analysis of operational forecasts versus actual weather conditions in airline flight planning: Summary report
[NASA-CR-167866] p 168 N85-35538

FLIGHT PLANS
Comparative analysis of operational forecasts versus actual weather conditions in airline flight planning, volume 1
[NASA-CR-167862] p 167 N85-35534
Comparative analysis of operational forecasts versus actual weather conditions in airline flight planning, volume 2
[NASA-CR-167863] p 167 N85-35535
Comparative analysis of operational forecasts versus actual weather conditions in airline flight planning: Summary report
[NASA-CR-167866] p 168 N85-35538

FLIGHT SIMULATION
Comparative analysis of operational forecasts versus actual weather conditions in airline flight planning, volume 2
[NASA-CR-167863] p 167 N85-35535

FLIGHT TESTS
Ground correlation investigation of thruster/spacecraft interactions to be measured on the IAPS flight test p 42 A85-16408

The UH-1H helicopter icing flight test program - An overview
[AIAA PAPER 85-0338] p 11 A85-28898
The UH-1H helicopter icing flight test program: An overview
[NASA-TM-86925] p 11 N85-15702
FLOATING POINT ARITHMETIC
Floating-point function generation routines for 16-bit microcomputers
[NASA-TM-83783] p 170 N85-10683
FLOW CHARACTERISTICS
Acoustic structure and propagation in highly porous, layered, fibrous materials p 173 A85-12301
Analytical modeling of circuit aerodynamics in the new NASA Lewis Altitude Wind Tunnel
[AIAA PAPER 85-0380] p 3 A85-26389
Flow through very porous inclined screens
[AIAA PAPER 85-1650] p 111 A85-40750
Coolant passage heat transfer with rotation p 20 N85-10968
Vortex-generating coolant-flow-passage design for increased film-cooling effectiveness and surface coverage
[NASA-TP-2388] p 113 N85-12314
Analytical modeling of circuit aerodynamics in the new NASA Lewis wind tunnel
[NASA-TM-86912] p 8 N85-15688
Flow through very porous inclined screens
[NASA-TM-86979] p 116 N85-25761
Fuel and oxidizer turbine loss analysis p 50 N85-26900
Detailed studies of aviation fuel flowability
[NASA-CR-174938] p 94 N85-31308
Transition in Turbines
[NASA-CP-2386] p 118 N85-31433
FLOW COEFFICIENTS
Generation of instability waves in flows separating from smooth surfaces p 1 A85-10352
Analysis of experimental shaft seal data for high-performance turbomachines, as for Space Shuttle main engines
[NASA-TM-86928] p 115 N85-21569
FLOW DISTRIBUTION
An experimental study of tone excited heated jets
[AIAA PAPER 84-2341] p 172 A85-10882
Assessment of three-dimensional inviscid codes and loss calculations for turbine aerodynamic computations
[ASME PAPER 84-GT-187] p 4 A85-32961
Turbulence measurements of lateral jet injection into confined tubular crossflow
[AIAA PAPER 85-1102] p 110 A85-39604
Inviscid analysis of advanced turboprop propeller flow fields
[AIAA PAPER 85-1263] p 6 A85-43977
Inviscid and viscous flows in cascades with an explicit multiple-grid algorithm p 7 A85-48539
Hot section laser anemometry p 19 N85-10962
Energy efficient engine high pressure turbine test hardware detailed design report
[NASA-CR-167955] p 23 N85-10995
Effect of two inner-ring oil-flow distribution schemes on the operating characteristics of a 35 millimeter bore ball bearing to 2.5 million DN
[NASA-TP-2404] p 130 N85-13233
A three-dimensional axisymmetric calculation procedure for turbulent flows in a radial vaneless diffuser
[NASA-TM-86903] p 7 N85-14798
The boundary layer on compressor cascade blades
[NASA-CR-174369] p 114 N85-18292
Investigation of flowfields found in typical combustor geometries
[NASA-CR-3869] p 26 N85-21167
The influence of jet-grid turbulence on heat transfer from the stagnation region of a cylinder in crossflow
[NASA-TM-87011] p 115 N85-25760
Turbulence characteristics of swirling flowfields
[NASA-CR-174918] p 29 N85-26717
Predictions and measurements of isothermal flowfields in axisymmetric combustor geometries
[NASA-CR-174916] p 29 N85-27867
Simulation of multistage turbine flows p 116 N85-27945
Feasibility of mapping velocity flow fields in SSME powerhead by laser anemometry techniques p 41 N85-27971
General design method for 3-dimensional, potential flow fields. Part 2: Computer program DIN3D1 for simple, unbranched ducts
[NASA-CR-3926] p 10 N85-35159
Calculation of compressible flow about three-dimensional inlets with auxiliary inlets, slats and vanes by means of a panel method
[NASA-CR-174975] p 10 N85-35162
FLOW EQUATIONS
A two-equation turbulence model for two-phase jets p 107 A85-14376
FLOW GEOMETRY
Computation and turbulence closure models for shear flows in rotating curved bodies p 107 A85-14349
Flow control in a diffusing S-Duct
[AIAA PAPER 85-0524] p 3 A85-25928
Structure of ducted particle-laden turbulent jets p 110 A85-38999
Numerical calculation of subsonic jets in crossflow with reduced numerical diffusion
[AIAA PAPER 85-1441] p 110 A85-39780
Turbulence modelling for complex shear flows
[AIAA PAPER 85-1652] p 111 A85-40752
An improved computer model for prediction of axial gas turbine performance losses
[NASA-CR-174246] p 24 N85-15724
Numerical calculation of subsonic jets in crossflow with reduced numerical diffusion
[NASA-TM-87003] p 27 N85-25263
FLOW MEASUREMENT
An experimental study of tone excited heated jets
[AIAA PAPER 84-2341] p 172 A85-10882
Flow control in a diffusing S-Duct
[AIAA PAPER 85-0524] p 3 A85-25928
An experimental study of three-dimensional shock wave/turbulent boundary layer interactions in a supersonic flow
[AIAA PAPER 85-1566] p 5 A85-40691
Measurements and predictions of the structure of evaporating sprays p 112 A85-46484
Holographic optical system for aberration corrections in laser Doppler velocimetry p 123 A85-48659
Velocity visualization in gaseous flows
[NASA-CR-174954] p 119 N85-31445
FLOW REGULATORS
Flow through very porous inclined screens
[AIAA PAPER 85-1650] p 111 A85-40750
Flow through very porous inclined screens
[NASA-TM-86979] p 116 N85-25761
FLOW STABILITY
Generation of instability waves in flows separating from smooth surfaces p 1 A85-10352
The linear two-dimensional stability of inviscid vortex streets of finite-cored vortices
[AD-A153032] p 107 A85-14241
Some unique experiments on receptivity --- for forced disturbances entering shear flow
[AIAA PAPER 85-0533] p 174 A85-25932
Generation of capillary instabilities by external disturbances in a liquid jet
[NASA-TM-87041] p 117 N85-30246
FLOW VELOCITY
Velocity visualization in gas flows using laser-induced phosphorescence of biacetyl p 121 A85-21695
Into mesh lubrication of spur gears with arbitrary offset oil jet. I - For jet velocity less than or equal to gear velocity p 128 A85-24497
Structure of particle-laden jets - Measurements and predictions p 109 A85-25137
A comparison of flow rates and pressure profiles for N-sequential inlets and three related seal configurations p 109 A85-26526
Combined influence of unsteady free stream velocity and free stream turbulence on stagnation point heat transfer p 112 A85-41782
Structure of nonevaporating sprays. I - Initial conditions and mean properties p 112 A85-48538
Flow rates and pressure profiles for one to four axially alined Borda inlets
[NASA-TP-2390] p 113 N85-14078
Preliminary analysis of tone-excited two-stream jet velocity decay
[NASA-TM-86951] p 8 N85-21114
Fuel and oxidizer turbine loss analysis p 50 N85-26900
Flow rate and pressure profiles for 1 to 4 axially alined orifice inlets
[NASA-TP-2460] p 116 N85-27165
Burner rig corrosion of SiC at 1000 deg C
[NASA-TM-87061] p 53 N85-30011
Combustor turbulence p 118 N85-31434
Preliminary results of a study of the relationship between free-stream turbulence and stagnation region heat transfer p 118 N85-31435
Velocity visualization in gaseous flows
[NASA-CR-174954] p 119 N85-31445
Flow modifying device
[NASA-CASE-LEW-13562-2] p 33 N85-35195
The use of a laser Doppler velocimeter in a standard flammability tube
[NASA-CR-174960] p 125 N85-35389
FLOW VISUALIZATION
Flow visualization of lateral jet injection into swirling crossflow
[AIAA PAPER 85-0059] p 2 A85-19490
Velocity visualization in gas flows using laser-induced phosphorescence of biacetyl p 121 A85-21695
Some unique experiments on receptivity --- for forced disturbances entering shear flow
[AIAA PAPER 85-0533] p 174 A85-25932
Rainbow schlieren vs Mach-Zehnder interferometer - A comparison p 121 A85-28820
Fast laser-induced aerosol formation for visualization of gas flows p 121 A85-31113
Unsteady pressure measurements on a biconvex airfoil in a transonic oscillating cascade
[NASA-TM-86914] p 8 N85-15689
Flow visualization study of the effect of injection hole geometry on an inclined jet in crossflow
[NASA-TM-86936] p 115 N85-20269
Deflected jet experiments in a turbulent combustor flowfield
[NASA-CR-174863] p 26 N85-22390
Preliminary results of a study of the relationship between free-stream turbulence and stagnation region heat transfer p 118 N85-31435
Velocity visualization in gaseous flows
[NASA-CR-174954] p 119 N85-31445
FLUID DYNAMICS
Design and performance of a fixed, nonaccelerating guide vane cascade that operates over an inlet flow angle range of 60 deg
[ASME PAPER 84-GT-75] p 4 A85-32964
Researched applied to transonic compressors in numerical fluid mechanics of inviscid flow and viscous flow
[NASA-CR-174353] p 114 N85-18291
Advanced research and technology programs for advanced high-pressure oxygen-hydrogen rocket propulsion
[NASA-TM-86969] p 37 N85-21231
Flow dynamic environment data base development for the SSME p 147 N85-26885
Analytical study of flow phenomena in SSME turnaround duct geometries p 116 N85-26902
FLUID FILMS
Fast numerical calculations of EHD sliding traction forces Application to rolling bearings
[ASME PAPER 84-TRIB-26] p 127 A85-21289
FLUID FLOW
Thermal traction contact performance evaluation under fully flooded and starved conditions
[NASA-CR-168173] p 132 N85-25848
Flow modifying device
[NASA-CASE-LEW-13562-2] p 33 N85-35195
FLUID INJECTION
Vortex modeling of single and multiple dilution jet mixing in a crossflow
[AIAA PAPER 85-1580] p 111 A85-40701
FLUID JETS
Generation of capillary instabilities by external disturbances in a liquid jet
[NASA-TM-87041] p 117 N85-30246
FLUID MANAGEMENT
Technology requirements to be addressed by the NASA Lewis Research Center Cryogenic Fluid Management Facility program
[AIAA PAPER 85-1229] p 94 A85-47024
Technology requirements to be addressed by the NASA Lewis Research Center Cryogenic Fluid Management Facility program
[NASA-TM-87048] p 38 N85-29987
FLUID MECHANICS
A new interpretation of internal heat transfer coefficients of porous media
[ASME PAPER 84-WA/HT-51] p 110 A85-39894
Advanced research and technology programs for advanced high-pressure oxygen-hydrogen rocket propulsion
[NASA-TM-86969] p 37 N85-21231
Nested subcritical flows within supercritical systems
[NASA-TM-86980] p 115 N85-21574
Arc-driven rail gun research
[NASA-CR-174816] p 132 N85-21662
Transition in Turbines
[NASA-CP-2386] p 118 N85-31433
Heat transfer and fluid mechanics measurements in transitional boundary layer flows p 118 N85-31439
FLUID POWER
Rotordynamic Instability Problems in High-Performance Turbomachinery
[NASA-CP-2338] p 131 N85-14116
FLUIDIZED BED PROCESSORS
Advanced technology cogeneration system conceptual design study: Closed cycle gas turbines
[NASA-CR-168222] p 159 N85-16300
Solids mixing in a three phase fluidized bed containing spherically shaped-porous solid particles
[PB85-187961] p 120 N85-33453
FLUORESCENCE
Two-frequency laser-induced fluorescence technique for rapid velocity-field measurements in gas flows p 121 A85-32294

Velocity visualization in gaseous flows
[NASA-CR-174954] p 119 N85-31445

FLUORIDES
Effects of silver and group 2 fluorides addition to plasma sprayed chromium carbide high temperature solid lubricant for foil gas bearing to 650 deg C
[NASA-TM-86895] p 84 N85-14928

FLUTTER
Vibration and flutter of mistuned bladed-disk assemblies
[AIAA PAPER 84-0991] p 139 A85-16095
Flutter of swept fan blades
[ASME PAPER 84-GT-138] p 141 A85-32962
Vibration and flutter of mistuned bladed-disk assemblies p 16 A85-45854
Aerodynamic detuning analysis of an unstalled supersonic turbofan cascade
[NASA-TM-87001] p 9 N85-26670
Unsteady flow in a supersonic cascade with two in-passage shocks
[NASA-CR-3925] p 10 N85-35158

FLUTTER ANALYSIS
Flutter and forced response of mistuned rotors using standing wave analysis p 139 A85-12721
Flutter of swept fan blades
[ASME PAPER 84-GT-138] p 141 A85-32962

FLUX DENSITY
Mass analysis of neutral particles and ions released during electrical breakdowns on spacecraft surfaces
[NASA-CR-175585] p 39 N85-21250

FLYWHEELS
A rotating superconducting solenoid for 100 kWh energy storage --- in space p 44 A85-33144
Operating characteristics of a 0.87 kW-hr flywheel energy storage module
[NASA-TM-87038] p 133 N85-28371

FOCI
Focal shifts in parabolic reflectors p 97 A85-39356

FOIL BEARINGS
Effects of silver and group 2 fluorides addition to plasma sprayed chromium carbide high temperature solid lubricant for foil gas bearing to 650 deg C
[NASA-TM-86895] p 84 N85-14928

FORCED CONVECTION
Heat transfer in aeropropulsion systems
[NASA-TM-87066] p 119 N85-31444

FORCED VIBRATION
Flutter and forced response of mistuned rotors using standing wave analysis p 139 A85-12721
Vibration and flutter of mistuned bladed-disk assemblies
[AIAA PAPER 84-0991] p 139 A85-16095
A study of internal and distributed damping for vibrating turbomachiner blades
[NASA-CR-175901] p 30 N85-27868

FORECASTING
Satellite provided customer promises services, a forecast of potential domestic demand through the year 2000. Volume 4: Sensitivity analysis
[NASA-CR-174662] p 99 N85-27092

FORGING
Powder metallurgy forged gear development
[NASA-TM-87483] p 134 N85-29295

FORMING TECHNIQUES
Factors influencing the ball milling of Si3N4 in water
[NASA-TM-86932] p 86 N85-19136

FORTRAN
A generalized computer code for developing dynamic gas turbine engine models (DIGTEM) p 17 A85-49021
Manual of phosphoric acid fuel cell stack three-dimensional model and computer program
[NASA-CR-174722] p 157 N85-10447
Phosphoric acid fuel cell power plant system performance model and computer program
[NASA-CR-174638] p 157 N85-11456
Reliability of void detection in structural ceramics using scanning laser acoustic microscopy
[NASA-TM-87035] p 138 N85-32337

FRACTURE MECHANICS
Deformation and fracture behavior of Ni-Mo-Al(gamma/gamma prime-alpha) in situ composite p 64 A85-11058
A study of fatigue damage mechanisms in Waspaloy from 25 to 800 C p 65 A85-12098
Statistics and thermodynamics of fracture p 140 A85-19433
On stress field near a stationary crack tip
[AD-A152863] p 141 A85-24532
HOST high temperature crack propagation p 21 N85-10977
Rapidly solidified NiAl and FeAl
[NASA-TM-86941] p 74 N85-20042
Translational and extensional energy release rates (the J- and M-integrals) for a crack layer in thermoelasticity
[NASA-CR-174872] p 145 N85-21685
Multiaxial and thermomechanical fatigue considerations in damage tolerant design
[NASA-TM-87022] p 76 N85-26964
Interaction of high-cycle and low-cycle fatigue of Haynes 188 alloy at 1400 F deg p 149 N85-27961
A review of path-independent integrals in elastic-plastic fracture mechanics, task 4
[NASA-CR-174956] p 152 N85-33541

FRACTURE STRENGTH
Fracture toughness of hot-pressed beryllium p 66 A85-25835
Fracture of composite-adhesive-composite systems p 141 A85-27935
Effect of low temperature on fatigue and fracture properties of Ti-5Al-2.5Sn(ELI) for use in engine components p 70 A85-47972
Fundamental studies of composite toughness p 56 N85-12948
Dispersed metal-toughened ceramics and ceramic brazing
[NASA-CR-174284] p 86 N85-15916
Dispersed-metal-toughened alumina
[NASA-CR-174687] p 89 N85-22758
Mechanism of strength degradation for hot corrosion of alpha-SiC
[NASA-TM-87052] p 91 N85-30135

FRACTURES (MATERIALS)
Turbine Engine Hot Section Technology (HOST)
[NASA-TM-83022] p 18 N85-10951
Fundamental tribological properties of ceramics
[NASA-TM-86915] p 85 N85-15893

FRACTURING
Structural Integrity and Durability of Reusable Space Propulsion Systems
[NASA-CP-2381] p 51 N85-27941
Designing for fiber composite structural durability in hygrothermomechanical environment
[NASA-TM-87045] p 58 N85-27978

FREDHOLM EQUATIONS
A procedure for obtaining explicit solutions to a class of Fredholm integral equations p 171 A85-28006

FREE BOUNDARIES
Control of solidification boundary in continuous casting by asymmetric cooling and mold offset p 110 A85-37047

FREE ELECTRON LASERS
Technology for satellite power conversion
[NASA-CR-174335] p 159 N85-18451

FREE FLOW
Combined influence of unsteady free stream velocity and free stream turbulence on stagnation point heat transfer p 112 A85-41782
Preliminary results of a study of the relationship between free stream turbulence and stagnation region heat transfer
[NASA-TM-86884] p 113 N85-11317
Preliminary results of a study of the relationship between free-stream turbulence and stagnation region heat transfer p 118 N85-31435

FREE JETS
Acoustic control of free jet mixing
[AIAA PAPER 85-0569] p 109 A85-25951

FREE RADICALS
Analysis of glow discharges for understanding the process of film formation
[NASA-TM-83750] p 62 N85-10138
Shock tube measurements of growth constants in the branched-chain ethane-carbon monoxide-oxygen system
[NASA-TM-87068] p 64 N85-32156

FREE VIBRATION
Vibrations of twisted cantilevered plates - Summary of previous and current studies p 140 A85-22069
Vibrations of twisted cantilever plates - A comparison of theoretical results p 144 A85-47626
A study of internal and distributed damping for vibrating turbomachiner blades
[NASA-CR-175901] p 30 N85-27868

FREEZING
Jet fuel property changes and their effect on producibility and cost in the U.S., Canada, and Europe
[NASA-CR-174840] p 93 N85-27012

FREQUENCIES
Vibration and flutter of mistuned bladed-disk assemblies
[AIAA PAPER 84-0991] p 139 A85-16095

FREQUENCY ASSIGNMENT
The subjective effect of multiple co-channel frequency modulated television interference p 96 A85-28234
Development and use of the computer software package for planning the 12 GHz broadcasting-satellite service at RARC '83 p 96 A85-29605
Engineering calculations for communications satellite systems planning
[NASA-CR-175552] p 37 N85-21233

FREQUENCY DIVISION MULTIPLE ACCESS
A frequency-routed satellite system concept using multiple orthogonally-polarized beams for frequency reuse p 97 A85-34470

FREQUENCY MEASUREMENT
Characterization of microstrip discontinuities in the time and frequency domains
[NASA-CR-176190] p 106 N85-35342

FREQUENCY MODULATION
On the subjective evaluation of the interference protection ratios' measurements for co-channel FM-TV signals p 96 A85-28241
Four-dimensional modulation and coding - An alternate to frequency-reuse p 97 A85-36653

FREQUENCY RESPONSE
Experimental results supporting the determination of service quality objectives for DBS systems p 96 A85-29611

FREQUENCY REUSE
A frequency-routed satellite system concept using multiple orthogonally-polarized beams for frequency reuse p 97 A85-34470
Four-dimensional modulation and coding - An alternate to frequency-reuse p 97 A85-36653

FRESH WATER
Operational performance of the photovoltaic-powered grain mill and water pump at Tangaye, Burkina Faso (formerly Upper Volta)
[NASA-TM-86970] p 161 N85-23243

FRESNEL REFLECTORS
Focal shifts in parabolic reflectors p 97 A85-39356

FRETTING
Effect of humidity on fretting wear of several pure metals
[NASA-TP-2403] p 72 N85-13006

FRICTION
Friction in rail guns p 101 A85-16424
Frictional and morphological properties of Au-MoS2 films sputtered from a compact target p 127 A85-19085
Polyimides - Tribological properties and their use as lubricants p 79 A85-21524
Friction, wear, transfer, and wear surface morphology of ultrahigh-molecular-weight polyethylene p 80 A85-22276
Friction and wear of ceramics p 80 A85-23833
Effects of silver and group 2 fluorides addition to plasma sprayed chromium carbide high temperature solid lubricant for foil gas bearing to 650 deg C
[NASA-TM-86895] p 84 N85-14928
Fundamental tribological properties of ceramics
[NASA-TM-86915] p 85 N85-15893
Experimental test program for evaluation of solid lubricant coating as applied to compliant foil gas bearings to 315 deg C
[NASA-CR-174837] p 85 N85-15895
Surface effects of corrosive media on hardness, friction, and wear of materials
[NASA-TM-83711] p 85 N85-15896
Tribological properties of boron nitride synthesized by ion beam deposition
[NASA-TM-86962] p 87 N85-21355
Tribological systems as applied to aircraft engines
[NASA-TM-86965] p 131 N85-21657
Breakway friction and dynamic friction/wear measurements of various ceramic materials from 25 C (75 F) to 650 C (1200 F)
[NASA-CR-174803] p 90 N85-26994
Surface roughness effects in elastohydrodynamic contacts
[NASA-TP-2488] p 134 N85-32329
Lubrication and cooling for high speed gears
[NASA-TM-87096] p 136 N85-34407

FRICTION REDUCTION
Effects of friction dampers on aerodynamically unstable rotor stages p 14 A85-21866
Lubricant and additive effects on spur gear fatigue life
[NASA-TM-87044] p 133 N85-28373

FUEL CELL POWER PLANTS
Electric utility acid fuel cell stack technology advancement
[NASA-CR-174804] p 159 N85-17422

FUEL CELLS
Long-life high performance fuel cell program
[NASA-CR-174874] p 50 N85-25384
Evaluation of developmental membranes for the mixed reactant iron-chromium redox system
[NASA-TM-87074] p 164 N85-34443

FUEL COMBUSTION
Methanol as a soot reducer in a turbulent swirling burner
[ASME PAPER 84-JPGC-GT-2] p 61 A85-23192
Internal combustion engine combustion chamber process studies at NASA Lewis Research Center p 112 A85-45856
Growth of a diffusion flame in the field of a vortex p 61 A85-47320

Combustion gas properties I-ASTM jet A fuel and dry air
[NASA-TP-2359] p 17 N85-10064
The mechanisms of flame holding in the wake of a bluff body
[NASA-CR-174058] p 62 N85-11149
The mechanisms of flame holding in the wake of a bluff body
[NASA-CR-3866] p 26 N85-21166
Shock tube study of the fuel structure effects on the chemical kinetic mechanisms responsible for soot formation, part 2
[NASA-CR-174880] p 63 N85-25444
Analytical fuel property effects--small combustors
[NASA-CR-174738] p 28 N85-26709
Fuel-rich catalytic combustion: A soot-free technique for in situ hydrogen-like enrichment
[NASA-TP-2498] p 63 N85-31244

FUEL CONSUMPTION
Energy efficient engine flight propulsion system preliminary analysis and design report
[NASA-CR-174701] p 18 N85-10947
Energy efficient engine. Volume 1: Component development and integration program
[NASA-CR-173084] p 22 N85-10992
Energy efficient engine high-pressure turbine component rig performance test report
[NASA-CR-168189] p 30 N85-29955
Energy efficient engine integrated core/low spool test hardware design report
[NASA-CR-168137] p 31 N85-29956
Energy Efficient Engine (E3) controls and accessories detail design report
[NASA-CR-168017] p 31 N85-29957
Comparative analysis of operational forecasts versus actual weather conditions in airline flight planning, volume 1
[NASA-CR-167862] p 167 N85-35534
Comparative analysis of operational forecasts versus actual weather conditions in airline flight planning, volume 2
[NASA-CR-167863] p 167 N85-35535
Comparative analysis of operational forecasts versus actual weather conditions in airline flight planning, volume 3
[NASA-CR-167864] p 167 N85-35536
Comparative analysis of operational forecasts versus actual weather conditions in airline flight planning, volume 4
[NASA-CR-167865] p 167 N85-35537

FUEL CONTROL
Energy Efficient Engine (E3) controls and accessories detail design report
[NASA-CR-168017] p 31 N85-29957

FUEL FLOW
Energy efficient engine high-pressure turbine component rig performance test report
[NASA-CR-168189] p 30 N85-29955
Detailed studies of aviation fuel flowability
[NASA-CR-174938] p 94 N85-31308

FUEL INJECTION
Aerodynamic effect of combustor inlet air pressure on fuel jet atomization p 109 A85-27096
Turbulence measurements of lateral jet injection into confined tubular crossflow
[AIAA PAPER 85-1102] p 110 A85-39604
Small gas turbine combustor study - Fuel injector performance in a transpiration-cooled liner
[AIAA PAPER 85-1312] p 16 A85-39717
Experimental study of the spray characteristics of a research airblast atomizer
[NASA-TM-86911] p 24 N85-15727
Small gas turbine combustor study: Fuel injector performance in a transpiration-cooled liner
[NASA-TM-86989] p 27 N85-25264

FUEL PRODUCTION
Jet fuel property changes and their effect on producibility and cost in the U.S., Canada, and Europe
[NASA-CR-174840] p 93 N85-27012

FUEL PUMPS
An experimental investigation of rubbing interaction in labyrinth seals at cryogenic temperature p 129 A85-39938
Effect of low temperature on fatigue and fracture properties of Ti-5Al-2.5Sn(ELI) for use in engine components p 70 A85-47972
Analytical and experimental investigation of rubbing interaction in labyrinth seals for a liquid hydrogen fuel pump --- space shuttle main engine
[NASA-CR-174657] p 48 N85-18084

FUEL SPRAYS
Liquid fuel spray processes in high-pressure gas flow
[NASA-TM-86944] p 115 N85-21570

FUEL SYSTEMS
Energy Efficient Engine (E3) controls and accessories detail design report
[NASA-CR-168017] p 31 N85-29957

FUEL TESTS
Rapid estimation of concentration of aromatic classes in middistillate fuels by high-performance liquid chromatography
[NASA-TP-2495] p 93 N85-31307

FUEL-AIR RATIO
Combustion gas properties. 2: Natural gas fuel and dry air
[NASA-TP-2435] p 26 N85-21168
Behavior of the lean methane-air flame at zero-gravity
[NASA-CR-175586] p 62 N85-21283
Flow modifying device
[NASA-CASE-LEW-13562-2] p 33 N85-35195

FUELS
External fuel vaporization study, phase 2
[NASA-CR-174079] p 92 N85-11252

FULL SCALE TESTS
Comparison of scaled model data to full size energy efficient engine test results
[AIAA PAPER 84-2281] p 13 A85-13953

FUSION (MELTING)
New eutectic alloys and their heats of transformation p 66 A85-27808

G

GALERKIN METHOD
A study of internal and distributed damping for vibrating turbomachiner blades
[NASA-CR-175901] p 30 N85-27868

GALILEO PROJECT
A high energy stage for the National Space Transportation System
[IAF PAPER 84-15] p 36 A85-23200

GALLIUM ARSENIDES
Magnesium doping of efficient GaAs and Ga(0.75)In(0.25)As solar cells grown by metalorganic chemical vapor deposition p 180 A85-11466
Near-optimum design of GaAs-based concentrator space solar cells for 80 C operation p 153 A85-15800
Electrical characterization of plasma-grown oxides on gallium arsenide p 181 A85-32635
Heat treatment of bulk gallium arsenide using a phosphosilicate glass cap p 181 A85-32636
Fabrication of p(+)-n junction GaAs solar cells by a novel method p 181 A85-33645
Plasma deposited hydrogenated carbon on GaAs and InP p 182 A85-40386
Plasma deposited diamondlike carbon on GaAs and InP
[NASA-TM-86870] p 183 N85-10844
High-temperature optically activated GaAs power switching for aircraft digital electronic control
[NASA-CR-174711] p 34 N85-12901
Effect of barrier height on friction behavior of the semiconductors silicon and gallium arsenide in contact with pure metals
[NASA-TP-2405] p 84 N85-13044
GaAs and 3-5 compound solar cells status and prospects for use in space
[NASA-TM-86960] p 49 N85-21261
GaAs and 3-5 compound solar cells status and prospects for use in space p 49 N85-22580
Sixty GHz IMPATT diode development
[NASA-CR-174969] p 105 N85-33293
Diffusion welding of Cassegrainian concentrator cell stack assemblies
[NASA-CR-176104] p 164 N85-33566

GAMMA RAYS
Apparatus and method for identification of matrix materials in which transuranic elements are embedded using thermal neutron capture gamma-ray emission
[DE85-011659] p 125 N85-33454

GAS ANALYSIS
Integrated exhaust gas analysis system for aircraft turbine engine component testing
[NASA-TP-2424] p 123 N85-16100

GAS BEARINGS
Development of gas-lubricated pistons for heavy duty diesel engine technology program
[NASA-CR-174746] p 184 N85-12808
Experimental test program for evaluation of solid lubricant coating as applied to compliant foil gas bearings to 315 deg C
[NASA-CR-174837] p 85 N85-15895

GAS COMPOSITION
Combustion gas properties I-ASTM jet A fuel and dry air
[NASA-TP-2359] p 17 N85-10064
Combustion gas properties. Part 3: Hydrogen gas fuel and dry air
[NASA-TP-2477] p 32 N85-31058

GAS COOLING
Gas cooled fuel cell systems technology development
[NASA-CR-174732] p 158 N85-16291

GAS DENSITY
Density effects on jet characteristics in confined swirling flow p 112 A85-45283

GAS DYNAMICS
Time dependent wave envelope finite difference analysis of sound propagation
[AIAA PAPER 84-2285] p 173 A85-16102
Advanced research and technology programs for advanced high-pressure oxygen-hydrogen rocket propulsion
[NASA-TM-86969] p 37 N85-21231
Ideal gas thermodynamic properties for the phenyl, phenoxy, and o-biphenyl radicals
[NASA-TM-83800] p 184 N85-22204
Velocity visualization in gaseous flows
[NASA-CR-174954] p 119 N85-31445
Mechanics of a gaseous film barrier to lubricant wetting of elastohydrodynamically lubricated conjunctions
[NASA-TP-2500] p 135 N85-32330

GAS FLOW
Velocity visualization in gas flows using laser-induced phosphorescence of biacetyl p 121 A85-21695
Fast laser-induced aerosol formation for visualization of gas flows p 121 A85-31113
Two-frequency laser-induced fluorescence technique for rapid velocity-field measurements in gas flows p 121 A85-32294
Replaceable blade turbine and stationary specimen corrosion testing facility
[NASA-TM-86931] p 73 N85-18126
Vortex generating flow passage design for increased film cooling effectiveness
[NASA-CASE-LEW-14039-1] p 119 N85-33433

GAS IONIZATION
Frictional and structural characterization of ion-nitrided low and high chromium steels
[NASA-TM-86991] p 132 N85-23085

GAS LUBRICANTS
Dual clearance squeeze film damper
[NASA-CASE-LEW-13506-1] p 135 N85-33490

GAS MIXTURES
Combustion gas properties. Part 3: Hydrogen gas fuel and dry air
[NASA-TP-2477] p 32 N85-31058

GAS TEMPERATURE
HOST instrumentation R and D program overview p 19 N85-10957

GAS TURBINE ENGINES
Reactions of NaCl with gaseous SO3, SO2, and O2 p 59 A85-11897
Ceramic component development for the AGT101 gas turbine engine p 126 A85-15972
Ceramic components for gas turbine engines p 127 A85-15973
Sensor failure detection for jet engines using analytical redundancy
[AIAA PAPER 84-1452] p 13 A85-16097
Considerations for damage analysis of gas turbine hot section components
[ASME PAPER 84-PVP-77] p 14 A85-18792
Computational thermo-fluid dynamics contributions to advanced gas turbine engine design
[AIAA PAPER 85-0083] p 14 A85-19509
Effects of friction dampers on aerodynamically unstable rotor stages p 14 A85-21866
The effect of aerodynamic and structural detuning on turbomachine supersonic unstalled torsional flutter
[AIAA PAPER 85-0761] p 14 A85-30378
Progress in the utilization of an *oxide-dispersion-strengthened alloy for small engine* turbine blades
[SAE PAPER 841512] p 68 A85-39284
Experiments in dilution jet mixing - Effects of multiple rows and non-circular orifices
[AIAA PAPER 85-1104] p 15 A85-39606
High-temperature erosion of plasma-sprayed, yttria-stabilized zirconia in a simulated turbine environment
[AIAA PAPER 85-1219] p 82 A85-39662
Advanced liner-cooling techniques for gas turbine combustors
[AIAA PAPER 85-1290] p 15 A85-39703
Computational thermo-fluid dynamics contributions to advanced gas turbine engine design
[NASA-TM-86865] p 18 N85-10069
A review and analysis of boundary layer transition data for turbine application
[NASA-TM-86880] p 113 N85-10306

Energy efficient engine flight propulsion system preliminary analysis and design report
[NASA-CR-174701] p 18 N85-10947
Turbine Engine Hot Section Technology (HOST)
[NASA-TM-83022] p 18 N85-10951
Nonlinear structural and life analyses of a turbine blade p 19 N85-10954
Nonlinear structural and life analyses of a combustor liner p 19 N85-10955
Pre-HOST high temperature crack propagation p 19 N85-10956
High temperature static strain sensor development program p 19 N85-10959
Component-specific modeling p 20 N85-10971
The 3-D inelastic analysis methods for hot section components: Brief description p 20 N85-10972
Constitutive model development for isotropic materials p 20 N85-10975
Surface protection overview p 21 N85-10978
Airfoil deposition model p 21 N85-10979
Effects of surface chemistry on hot corrosion life: Overview p 21 N85-10980
Dilution zone mixing studies p 21 N85-10984
Studies on the hot corrosion of a nickel-base superalloy, Udimet 700
[NASA-TM-86882] p 71 N85-11224
Hot isostatically pressed manufacture of high strength MERL 76 disk and seal shapes
[NASA-CR-165550] p 71 N85-11225
External fuel vaporization study, phase 2
[NASA-CR-174079] p 92 N85-11252
Biaxial constitutive equation development for single crystals
[NASA-CR-174056] p 183 N85-11862
High performance fibers for structurally reliable metal and ceramic composites --- advanced gas turbine engine materials
[NASA-TM-86878] p 56 N85-12095
High-temperature erosion of plasma-sprayed, yttria-stabilized zirconia in a simulated turbine environment
[NASA-TP-2406] p 84 N85-13045
Fabrication and quality assurance processes for superhybrid composite fan blades
[NASA-TM-83354] p 57 N85-14882
Engine cyclic durability by analysis and material testing p 25 N85-15744
Integrated exhaust gas analysis system for aircraft turbine engine component testing
[NASA-TP-2424] p 123 N85-16100
Advanced Gas Turbine (AGT) powertrain system development for automotive applications
[NASA-CR-174809] p 185 N85-18831
Advanced liner-cooling techniques for gas turbine combustors
[NASA-TM-86952] p 8 N85-21115
Combustion research for gas turbine engines
[NASA-TM-86963] p 26 N85-21164
Evaluation results of the 700 deg C Chinese strain gauges --- for gas turbine engine
[NASA-TM-86973] p 124 N85-21605
Advanced thin film thermocouples
[NASA-CR-175541] p 124 N85-21607
Development of a multiplane multispeed balancing system for turbine systems
[NASA-CR-174750] p 35 N85-22400
Experiments in dilution jet mixing effects of multiple rows and non-circular orifices
[NASA-TM-86996] p 28 N85-25266
Analytical fuel property effects--small combustors
[NASA-CR-174738] p 28 N85-26709
Multiaxial and thermomechanical fatigue considerations in damage tolerant design
[NASA-TM-87022] p 76 N85-26964
Ceramic applications in turbine engines
[NASA-CR-174715] p 91 N85-28109
Energy efficient engine high-pressure turbine component rig performance test report
[NASA-CR-168189] p 30 N85-29955
Energy efficient engine integrated core/low spool test hardware design report
[NASA-CR-168137] p 31 N85-29956
Advanced Gas Turbine (AGT) technology project
[NASA-CR-174798] p 31 N85-29961
Creep fatigue life prediction for engine hot section materials (isotropic)
[NASA-CR-168228] p 32 N85-31057
Flat-plate transition p 118 N85-31438
A review and analysis of boundary layer transition data for turbine application p 118 N85-31440
Tape casting as an approach to an all-ceramic turbine shroud seal
[NASA-TM-87078] p 135 N85-32333
Dual clearance squeeze film damper
[NASA-CASE-LEW-13506-1] p 135 N85-33490
Oxidizing seal for a turbine tip gas path
[NASA-CASE-LEW-14053-1] p 136 N85-34402
Energy Efficient Engine Program technology benefit/cost study, volume 2
[NASA-CR-174766-VOL-2] p 33 N85-35198
Energy efficient engine, high pressure turbine thermal barrier coating. Support technology report
[NASA-CR-168037] p 34 N85-35199
Development of advanced high-temperature heat flux sensors. Phase 2: Verification testing
[NASA-CR-174973] p 126 N85-35391

GAS TURBINES
Predicted turbine stage performance using quasi-three-dimensional and boundary-layer analyses p 15 A85-34013
Small gas turbine combustor study - Fuel injector performance in a transpiration-cooled liner
[AIAA PAPER 85-1312] p 16 A85-39717
Effect of surface configuration during solid particle impingement erosion p 69 A85-42568
Future fundamental combustion research for aeropropulsion systems
[AIAA PAPER 85-1398] p 16 A85-42671
The effect of channel convergence on heat transfer in a passage with short pin fins
[NASA-TM-83801] p 113 N85-10303
Coolant passage heat transfer with rotation p 20 N85-10968
Structural analysis p 20 N85-10969
Heat transfer results and operational characteristics of the NASA Lewis Research Center Hot Section Cascade Test Facility
[NASA-TM-86890] p 114 N85-15133
An improved computer model for prediction of axial gas turbine performance losses
[NASA-CR-174246] p 24 N85-15724
Advanced technology cogeneration system conceptual design study: Closed cycle gas turbines
[NASA-CR-168222] p 159 N85-16300
NASA Lewis Research Center/University Graduate Research Program on Engine Structures
[NASA-TM-86916] p 145 N85-18375
Small gas turbine combustor study: Fuel injector performance in a transpiration-cooled liner
[NASA-TM-86989] p 27 N85-25264
Future fundamental combustion research for aeropropulsion systems
[NASA-TM-87049] p 30 N85-27870

GAS-LIQUID INTERACTIONS
Mechanics of a gaseous film barrier to lubricant wetting of elastohydrodynamically lubricated conjunctions
[NASA-TP-2500] p 135 N85-32330

GAS-METAL INTERACTIONS
Effects of SO2 and SO3 on the Na2SO4 induced corrosion of nickel p 65 A85-15603
Effects of MAR-M247 substrate (modified) composition on coating oxidation coating/substrate interdiffusion --- protective coatings for hot section components of gas turbine engines
[NASA-CR-174851] p 73 N85-19073
Oxidation and hot corrosion of hot-pressed Si3N4 at 1000 deg C
[NASA-TM-86977] p 88 N85-21358

GAS-SOLID INTERFACES
Gravitational effects on flames spreading over thick solid surfaces
[IAF PAPER 84-154] p 59 A85-13092

GASES
Combustion gas properties I-ASTM jet A fuel and dry air
[NASA-TP-2359] p 17 N85-10064

GATES (CIRCUITS)
A new very high voltage semiconductor switch
[NASA-TM-86957] p 103 N85-20246

GEAR TEETH
A computer aided design procedure for generating gear teeth
[ASME PAPER 84-DET-184] p 128 A85-33779
Dynamic analysis of straight and involute tooth forms
[ASME PAPER 84-DET-226] p 128 A85-33780
Gear mesh stiffness and load sharing in planetary gearing
[ASME PAPER 84-DET-229] p 129 A85-33781
Lubricant jet flow phenomena in spur and helical gears with modified center distances and/or addendums - For out-of-mesh conditions
[ASME PAPER 84-DET-96] p 129 A85-35049
Planetary-gear-support bearing test rig design
[NASA-CR-174927] p 12 N85-35185

GEARS
Into mesh lubrication of spur gears with arbitrary offset oil jet. I - For jet velocity less than or equal to gear velocity p 128 A85-24497
Lubricant jet flow phenomena in spur and helical gears with modified center distances and/or addendums - For out-of-mesh conditions
[ASME PAPER 84-DET-96] p 129 A85-35049
Energy efficient engine ICLS engine bearings, drives and configuration: Detail design report
[NASA-CR-167871] p 23 N85-10997
Effect of lubricant extreme-pressure additives on surface fatigue life of AISI 9310 spur gears
[NASA-TP-2408] p 130 N85-13234
Effect of five lubricants on life of AISI 9310 spur gears
[NASA-TP-2419] p 123 N85-16099
Life and reliability modeling of bevel gear reductions
[NASA-TM-87006] p 133 N85-27227
Fatigue life analysis of a turboprop reduction gearbox
[NASA-TM-87014] p 133 N85-27228
Multi-mesh gear dynamics program evaluation and enhancements
[NASA-CR-174747] p 133 N85-28372
Lubricant and additive effects on spur gear fatigue life
[NASA-TM-87044] p 133 N85-28373
Powder metallurgy forged gear development
[NASA-TM-87483] p 134 N85-29295
Spiral bevel and circular arc helical gears: Tooth contact analysis and the effect of misalignment on circular arc helical gears
[NASA-TM-87013] p 32 N85-31060
The design and analysis of single flank transmission error testor for loaded gears
[NASA-CR-176163] p 136 N85-34404
Generated spiral bevel gears: Optimal machine-tool settings and tooth contact analysis
[NASA-TM-87075] p 136 N85-34405
Lubrication and cooling for high speed gears
[NASA-TM-87096] p 136 N85-34407
Elastohydrodynamic lubrication calculations used as a tool to study scuffing
[NASA-TM-87097] p 137 N85-34408
Planetary-gear-support bearing test rig design
[NASA-CR-174927] p 12 N85-35185

GEOMAGNETISM
DE-1 measurements of AKR wave directions --- auroral kilometric radiation p 166 A85-37717

GEOMETRY
A comparison of flow rates and pressure profiles for N-sequential inlets and three related seal configurations p 109 A85-26526

GEOSYNCHRONOUS ORBITS
Experiments in charge control at geosynchronous orbit - ATS-5 and ATS-6 p 39 A85-35379
OTV propulsion tecnology programmatic overview p 37 N85-16997
Radiation exposure and performance of multiple burn LEO-GEO orbit transfer trajectories
[NASA-TM-86946] p 36 N85-21228
Design guidelines for assessing and controlling spacecraft charging effects p 40 N85-22500

GLASS
Spherical microglass particle impingement studies of thermoplastic materials at normal incidence p 79 A85-11072
Structural characteristics of high temperature composites
[NASA-CR-175998] p 58 N85-30037

GLASS FIBER REINFORCED PLASTICS
Hygrothermomechanical evaluation of transverse filament tape epoxy/polyester fiberglass composites p 54 A85-15632
Fiberglass epoxy laminate fatigue properties at 300 and 20 K p 56 A85-47970

GLASS FIBERS
Ten year environmental test of glass fiber/epoxy pressure vessels
[AIAA PAPER 85-1198] p 56 A85-47022
Ten year environmental test of glass fiber/epoxy pressure vessels
[NASA-TM-87058] p 58 N85-30034

GLOBAL AIR SAMPLING PROGRAM
GASP cloud encounter statistics - Implications for laminar flow control flight p 166 A85-11979
Variability of cloudiness at airline cruise altitudes from GASP measurements p 166 A85-31199

GLOW DISCHARGES
Analysis of glow discharges for understanding the process of film formation
[NASA-TM-83750] p 62 N85-10138
Nitriding of titanium and its alloys by N2, NH3 or mixtures of N2 + H2 in a dc arc plasma at low pressures (or = to torr)
[NASA-TM-83803] p 131 N85-15168
Frictional and structural characterization of ion-nitrided low and high chromium steels
[NASA-TM-86991] p 132 N85-23085
The structure of ion plated films in relation to coating properties
[NASA-TM-87055] p 95 N85-29085

GOLD COATINGS
Frictional and morphological properties of Au-MoS2 films sputtered from a compact target p 127 A85-19085
GRAIN BOUNDARIES
Oxidation of silicon nitride sintered with rare-earth oxide additions p 83 A85-42798
Analysis techniques for tracer studies of oxidation [NASA-CR-174796] p 84 N85-12162
High temperature properties of equiatomic FeAl with ternary additions [NASA-TM-86938] p 73 N85-19072
GRAIN SIZE
On the fatigue crack propagation behavior of superalloys at intermediate temperatures p 68 A85-32434
Evaluation of alpha-SiC sintering using statistical methods p 83 A85-42800
GRAINS (FOOD)
Operational performance of the photovoltaic-powered grain mill and water pump at Tangaye, Burkina Faso (formerly Upper Volta) [NASA-TM-86970] p 161 N85-23243
GRAPHITE
Dynamics of graphite fiber intercalation: In situ resistivity measurements with a four point probe [NASA-TM-86858] p 53 N85-10105
Stability of bromine intercalated graphite fibers [NASA-TM-86859] p 84 N85-10187
Experimental test program for evaluation of solid lubricant coating as applied to compliant foil gas bearings to 315 deg C [NASA-CR-174837] p 85 N85-15895
Tribological properties of graphite-fiber-reinforced, partially fluorinated polyimide composites [NASA-TM-86926] p 86 N85-18153
Homogeneity of pristine and bromine intercalated graphite fibers [NASA-TM-87016] p 89 N85-25521
Graphite fiber intercalation: Dynamics of the bromine intercalation process [NASA-TM-87015] p 53 N85-26921
Environmental stability of intercalated graphite fibers [NASA-TM-87025] p 90 N85-26992
A micrographic and gravimetric study of intercalation and deintercalation of graphite fibers [NASA-TM-87026] p 91 N85-28110
Multistage spent particle collector and a method for making same [NASA-CASE-LEW-13914-1] p 135 N85-33489
GRAPHITE-EPOXY COMPOSITES
Select fiber composites for space applications - A mechanistic assessment p 54 A85-16040
GRAPHITE-POLYIMIDE COMPOSITES
PMR polyimide composites for aerospace applications --- Polymerization of Monomer Reactants p 55 A85-21520
Effect of counterface material type and its topography on the tribological properties of polyimide composites [NASA-TM-87036] p 90 N85-26993
Graphite/PMR polyimide composites with improved toughness [NASA-TM-87081] p 58 N85-32148
GRASHOF NUMBER
Convective influence on the stability of a cylindrical solid-liquid interface p 109 A85-26911
GRATINGS (SPECTRA)
Solar energy converter using surface plasma waves [NASA-CASE-LEW-13827-1] p 160 N85-21768
GRAVIMETRY
A micrographic and gravimetric study of intercalation and deintercalation of graphite fibers [NASA-TM-87026] p 91 N85-28110
GRAVITATIONAL EFFECTS
Gravitational effects on flames spreading over thick solid surfaces [IAF PAPER 84-154] p 59 A85-13092
Effect of gravity on halogenated hydrocarbon flame retardant effectiveness [IAF PAPER 84-156] p 61 A85-23199
GREAT LAKES (NORTH AMERICA)
Comparison of atmospheric correction algorithms for the Coastal Zone Color Scanner p 153 A85-10244
GREEN'S FUNCTIONS
Noise transmission loss of a rectangular plate in an infinite baffle [NASA-TP-2398] p 176 N85-22109
GRINDING (COMMINUTION)
Milling of Si3N4 with Si3N4 hardware [NASA-TM-86864] p 84 N85-10191
GRINDING (MATERIAL REMOVAL)
Factors influencing the ball milling of Si3N4 in water [NASA-TM-86932] p 86 N85-19136
Parametric evaluation of ball milling of SiC in water [NASA-TM-86974] p 88 N85-21356
GRINDING MILLS
Milling of Si3N4 with Si3N4 hardware [NASA-TM-86864] p 84 N85-10191
Operational performance of the photovoltaic-powered grain mill and water pump at Tangaye, Burkina Faso (formerly Upper Volta) [NASA-TM-86970] p 161 N85-23243
GROUND TESTS
Spacecraft environmental interactions: A joint Air Force and NASA research and technology program p 40 N85-22517
GUIDE VANES
Design and performance of a fixed, nonaccelerating guide vane cascade that operates over an inlet flow angle range of 60 deg [ASME PAPER 84-GT-75] p 4 A85-32964
GUST LOADS
Effect of airfoil mean loading on convected gust interaction noise [AIAA PAPER 84-2324] p 173 A85-13955

H

HAFNIUM ALLOYS
RF-sputtered silicon and hafnium nitrides - Properties and adhesion to 440C stainless steel p 81 A85-36240
HALL ACCELERATORS
Theory of ion acceleration with closed electron drift --- in spacecraft plasma propulsion p 41 A85-15512
HARDENING (MATERIALS)
Metallurgical and mechanical phenomena due to rubbing of titanium against sintered powder Nichrome p 127 A85-22281
Surface hardening of steel by boriding in a cold rf plasma p 68 A85-40275
HARDNESS
Creep-rupture behavior of iron superalloys in high-pressure hydrogen [NASA-CR-174411] p 74 N85-19078
Deposition of diamondlike carbon films [NASA-CASE-LEW-14080-1] p 95 N85-20153
HARDWARE
Energy efficient engine integrated core/low spool test hardware design report [NASA-CR-168137] p 31 N85-29956
HARMONIC ANALYSIS
Effects of vane/blade ratio and spacing on fan noise, volume 1 [NASA-CR-174664] p 176 N85-19791
HASTELLOY (TRADEMARK)
Elevated temperature biaxial fatigue [NASA-CR-175795] p 148 N85-27263
A comparison of smooth specimen and analytical simulation techniques for notched members at elevated temperatures p 151 N85-31546
HEAT EXCHANGERS
Advanced radiator concepts [NASA-TM-87008] p 115 N85-24245
HEAT FLUX
Performance of thermal barrier coatings in high heat flux environments p 79 A85-19087
Heat transfer investigation in the junction region of circular cylinder normal to a flat plate at 90 deg location [ASME PAPER 84-WA/HT-70] p 111 A85-39898
High temperature thermocouple and heat flux gauge using a unique thin film-hardware hot juncture [NASA-TM-86898] p 123 N85-16096
Heat flux sensor calibrator p 41 N85-27970
Development of advanced high-temperature heat flux sensors. Phase 2: Verification testing [NASA-CR-174973] p 126 N85-35391
HEAT GENERATION
An experimental investigation and numerical prediction of thermomechanical phenomena in high speed rotor tip rubbing p 14 A85-25442
Generated spiral bevel gears: Optimal machine-tool settings and tooth contact analysis [NASA-TM-87075] p 136 N85-34405
HEAT MEASUREMENT
Transient technique for measuring heat transfer coefficients on stator airfoils in a jet engine environment [AIAA PAPER 85-1471] p 122 A85-39796
Transient technique for measuring heat transfer coefficients on stator airfoils in a jet engine environment [NASA-TM-87005] p 124 N85-25794
Heat flux sensor calibrator p 41 N85-27970
HEAT OF FORMATION
Direct numerical simulations of a reacting mixing layer with chemical heat release [AIAA PAPER 85-0143] p 60 A85-19548
HEAT OF FUSION
New eutectic alloys and their heats of transformation p 66 A85-27808
HEAT PIPES
High thermal power density heat transfer apparatus providing electrical isolation at high temperature using heat pipes [NASA-CASE-LEW-12950-2] p 117 N85-29179
HEAT PUMPS
Overview of NASA Lewis Research Center free-piston Stirling engine activities p 130 A85-45479
HEAT RADIATORS
Methods for heat transfer and temperature field analysis of the insulated diesel [NASA-CR-174783] p 185 N85-16699
HEAT RESISTANT ALLOYS
Microstructural development of protective Al2O3 scales p 80 A85-21650
Elevated temperature creep-rupture behavior of the single crystal nickel-base superalloy NASAIR 100 p 66 A85-27812
Chemical reactions involved in the initiation of hot corrosion of IN-738 p 66 A85-31688
Influence of composition on the microstructure and mechanical properties of a nickel-base superalloy single crystal p 66 A85-32387
Factors which influence directional coarsening of gamma-prime during creep in nickel-base superalloy single crystals p 67 A85-32388
The influence of hold times on LCF and FCG behavior in a P/M Ni-base superalloy --- Low Cycle Fatigue/Fatigue Crack Growth p 67 A85-32400
Effects of cobalt on the hot workability of nickel-base superalloys p 67 A85-32412
Rapid solidification and dynamic compaction of Ni-base superalloy powders p 67 A85-32414
On the fatigue crack propagation behavior of superalloys at intermediate temperatures p 68 A85-32434
Development of coated single-crystal superalloy systems for gas turbine applications p 68 A85-32440
Dopant effect of yttrium and the growth and adherence of alumina on nickel-aluminum alloys p 82 A85-40973
Diffusion welding of MA 6000 and a conventional nickel-base superalloy p 69 A85-43551
PM superalloys - A troubled adolescent? p 69 A85-44772
Morphological changes of gamma prime precipitates in nickel-base superalloy single crystals [NASA-TM-83698] p 70 N85-10165
The effects of seven alloying elements on the microstructure and stress-rupture behavior of nickle-base superalloys [NASA-TM-83791] p 70 N85-10168
High temperature static strain sensor development program p 19 N85-10959
The transient oxidation of single crystal NiAl+Zr [NASA-CR-174756] p 70 N85-11221
The effect of tantalum and carbon on the structure/properties of a single crystal nickel-base superalloy [NASA-CR-174779] p 71 N85-11223
Studies on the hot corrosion of a nickel-base superalloy, Udimet 700 [NASA-TM-86882] p 71 N85-11224
Materials for advanced turbine engines. Project 2: Rene 150 directionally solidified superalloy turbine blades, volume 2 [NASA-CR-167993] p 23 N85-12059
Effects of tin on microstructure and mechanical behavior of Inconel 718 [NASA-TM-86866] p 71 N85-12129
The effects of Cr, Co, Al, Mo and Ta on the cyclic oxidation behavior of a prototype cast Ni-base superalloy based on a 2(5) composite statistically designed experiment [NASA-TM-83784] p 71 N85-12131
Analysis techniques for tracer studies of oxidation [NASA-CR-174796] p 84 N85-12162
The effect of tantalum on the structure/properties of two polycrystalline nickel-base superalloys: B-1900 + Hf MAR-M247 [NASA-CR-174847] p 73 N85-18127
Effects of MAR-M247 substrate (modified) composition on coating oxidation coating/substrate interdiffusion --- protective coatings for hot section components of gas turbine engines [NASA-CR-174851] p 73 N85-19073
Low cycle fatigue of MAR-M 200 single crystals at 760 and 870 deg C [NASA-TM-86933] p 74 N85-19074
Creep-rupture behavior of iron superalloys in high-pressure hydrogen [NASA-CR-174411] p 74 N85-19078
Effect of reduction of strategic Columbium addition in 718 Alloy on the structure and properties [NASA-CR-174841] p 75 N85-21320
Orientation and temperature dependence of some mechanical properties of the single-crystal nickel-base superalloy Rene N4. 3: Tension-compression anisotropy [NASA-TM-86982] p 76 N85-22660
On thermomechanical testing in support of constitutive equation development for high temperature alloys [NASA-CR-174879] p 147 N85-25894

Nonlinear structural analysis for fiber-reinforced superalloy turbine blades p 147 N85-26887
Iron rich low cost superalloys
[NASA-CR-174900] p 76 N85-26962
On the use of internal state variables in thermoviscoplastic constitutive equations p 150 N85-31536

HEAT TRANSFER
Flame radiation and linear heat transfer in a tubular-can combustor p 15 A85-39580
Advanced liner-cooling techniques for gas turbine combustors
[AIAA PAPER 85-1290] p 15 A85-39703
Transient technique for measuring heat transfer coefficients on stator airfoils in a jet engine environment
[AIAA PAPER 85-1471] p 122 A85-39796
Heat transfer investigation in the junction region of circular cylinder normal to a flat plate at 90 deg location
[ASME PAPER 84-WA/HT-70] p 111 A85-39898
Solidification interface shape for continuous casting in an offset mold - Two analytical methods p 112 A85-41326
Future fundamental combustion research for aeropropulsion systems
[AIAA PAPER 85-1398] p 16 A85-42671
The effect of channel convergence on heat transfer in a passage with short pin fins
[NASA-TM-83801] p 113 N85-10303
A review and analysis of boundary layer transition data for turbine application
[NASA-TM-86880] p 113 *N85-10306*
Turbine Engine Hot Section Technology (HOST)
[NASA-TM-83022] p 18 N85-10951
Turbine heat transfer p 19 N85-10964
Coolant passage heat transfer with rotation p 20 N85-10968
Preliminary results of a study of the relationship between free stream turbulence and stagnation region heat transfer
[NASA-TM-86884] p 113 N85-11317
Heat transfer results and operational characteristics of the NASA Lewis Research Center Hot Section Cascade *Test Facility*
[NASA-TM-86890] p 114 N85-15133
High temperature thermocouple and heat flux gauge using a unique thin film-hardware hot juncture
[NASA-TM-86898] p 123 N85-16096
Design of low loss helix circuits for interference fitted and brazed circuits
[NASA-CR-168313] p 103 N85-19328
Experimental study of ceramic coated tip seals for turbojet engines
[NASA-TM-86939] p 114 N85-19363
Ribbon burner simulation of T-700 turbine shroud for ceramic lined seals research
[NASA-TM-86940] p 114 N85-19364
Advanced liner-cooling techniques for gas turbine combustors
[NASA-TM-86952] p 8 N85-21115
Nested subcritical flows within supercritical systems
[NASA-TM-86980] p 115 N85-21574
Manrating orbital transfer vehicle propulsion
[NASA-TM-87019] p 50 N85-25385
The influence of jet-grid turbulence on heat transfer from the stagnation region of a cylinder in crossflow
[NASA-TM-87011] p 115 N85-25760
Transient technique for measuring heat transfer coefficients on stator airfoils in a jet engine environment
[NASA-TM-87005] p 124 N85-25794
Component-specific modeling
[NASA-CR-174765] p 147 N85-27261
A computer analysis program for interfacing thermal and structural codes
[NASA-TM-87021] p 148 N85-27264
Future fundamental combustion research for aeropropulsion systems
[NASA-TM-87049] p 30 N85-27870
Overview of aerothermodynamic loads definition study p 51 N85-27942
High thermal power density heat transfer apparatus providing electrical isolation at high temperature using heat pipes
[NASA-CASE-LEW-12950-2] p 117 N85-29179
Turbulent transport and length scale measurement experiments with comfined coaxial jets
[NASA-CR-174831] p 117 *N85-30245*
Transition in Turbines
[NASA-CP-2386] p 118 N85-31433
Preliminary results of a study of the relationship between free-stream turbulence and stagnation region heat transfer p 118 N85-31435
Flat-plate transition p 118 N85-31438
Heat transfer and fluid mechanics measurements in transitional boundary layer flows p 118 N85-31439
A review and analysis of boundary layer transition data for turbine application p 118 N85-31440
Heat transfer in aeropropulsion systems
[NASA-TM-87066] p 119 N85-31444
Local heat-transfer measurements on a large, scale-model turbine blade airfoil using a composite of a heater element and liquid crystals
[NASA-TM-86900] p 119 N85-33435
Component-specific modeling
[NASA-CR-174765] p 33 N85-34140

HEAT TRANSFER COEFFICIENTS
A new interpretation of internal heat transfer coefficients of porous media
[ASME PAPER 84-WA/HT-51] p 110 A85-39894
Combined influence of unsteady free stream velocity and free stream turbulence on stagnation point heat transfer p 112 A85-41782
Heat transfer and turbulence measurements of a film-cooled flow over a convexly curved surface p 112 A85-41787
Local heat-transfer measurements on a large, scale-model turbine blade airfoil using a composite of a heater element and liquid crystals
[NASA-TM-86900] p 119 N85-33435

HEAT TREATMENT
Heat treatment of bulk gallium arsenide using a phosphosilicate glass cap p 181 A85-32636
Creep of chemically vapor deposited SiC fibers
[NASA-TM-86897] p 56 N85-14878
The response of cobalt-free Udimet 700 type alloy to modified heat treatments
[NASA-TM-86942] p 75 N85-20043
Properties and microstructures for dual alloy combinations of three superalloys with alloy 901
[NASA-TM-86987] p 76 N85-26963

HELICAL WINDINGS
A 20 GHz, 75 watt, helix TWT for space communications p 101 A85-14433

HELICOPTER DESIGN
Transmission efficiency measurements and correlations *with physical characteristics of the lubricant* p 89 N85-23781

HELICOPTER PERFORMANCE
Experimental aerodynamic characteristics of an NACA 0012 airfoil with simulated ice p 12 A85-21844

HELICOPTERS
The UH-1H helicopter icing flight test program - An overview
[AIAA PAPER 85-0338] p 11 *A85-26898*
Contingency power concepts for helicopter turboshaft engine p 15 A85-32005
Initial feasibility ground test of a proposed photogrammetric system for measuring the shapes of ice accretions on helicopter rotor blades during forward flight
[NASA-TM-87391] p 12 N85-12887
The UH-1H helicopter icing flight test program: An overview
[NASA-TM-86925] p 11 N85-15702
Investigation on experimental techniques to detect, locate and quantify gear noise in helicopter transmissions
[NASA-CR-3847] p 176 N85-17667
Correlation of rheological characteristics of lubricants with transmission efficiency measurements
[NASA-TM-86988] p 134 N85-30342

HELIUM
Density effects on jet characteristics in confined swirling flow p 112 A85-45283

HELIUM PLASMA
Measurements of energy distribution in microwave plasmas of N2 and He and comparisons with results for H2 p 178 A85-16443

HELMHOLTZ RESONATORS
The response of Helmholtz resonators to external excitation. I - Single resonators p 174 A85-26915

HELMHOLTZ VORTICITY EQUATION
On the use of internal state variables in thermoviscoplastic constitutive equations p 150 N85-31536

HERMETIC SEALS
Experimental stiffness of tapered bore seals
[NASA-TM-86978] p 132 N85-25847

HETERODYNING
A comparison of electronic heterodyne moire deflectometry and electronic heterodyne holographic interferometry for flow measurements
[NASA-TM-87071] p 125 *N85-32302*

HETEROJUNCTION DEVICES
GaAs and 3-5 compound solar cells status and prospects for use in space p 49 N85-22580

HIERARCHIES
On the development of hierarchical solution strategies for nonlinear finite element formulations p 171 A85-21979

HIGH ALTITUDE
Variability of cloudiness at airline cruise altitudes from GASP measurements p 166 A85-31199

HIGH CURRENT
Surface interactions and high-voltage current collection p 40 N85-22493

HIGH FREQUENCIES
Development of high frequency low weight power magnetics for aerospace power systems p 102 A85-45373
Effect of Interfacial characteristics of metal clad polymeric substrates on electrical high frequency interconnection performance
[NASA-TM-86948] p 99 N85-20223
Alternatives for satellite sound broadcast systems at HF and VHF p 99 N85-23815

HIGH GAIN
Case study of sample spacing in planar near-field measurement of high gain antennas
[NASA-TM-86872] p 97 N85-10234

HIGH LEVEL LANGUAGES
Data flow methods for dynamic system simulation - A CSSL-IV microcomputer network interface p 170 A85-28614
A functional language approach in high-speed digital simulation p 170 A85-28615
Functional language and data flow architectures p 170 A85-28629
Floating-point function generation routines for 16-bit microcomputers
[NASA-TM-83783] p 170 N85-10683

HIGH PRESSURE
Cathode degradation and erosion in high pressure arc discharges p 43 A85-16445
Energy efficient engine high pressure turbine ceramic shroud support technology report
[NASA-CR-168036] p 23 N85-10996
Energy efficient engine. High pressure compressor detail design report
[NASA-CR-165558] p 23 N85-10998
Liquid fuel spray processes in high-pressure gas flow
[NASA-TM-86944] p 115 N85-21570
Applications of high pressure differential scanning calorimetry to aviation fuel thermal stability research
[NASA-TM-87002] p 63 N85-23941
Graphite fiber intercalation: Dynamics of the bromine intercalation process
[NASA-TM-87015] p 53 *N85-26921*
Energy efficient engine high-pressure turbine component rig performance test report
[NASA-CR-168189] p 30 N85-29955
High pressure compressor component performance report
[NASA-CR-168245] p 33 N85-34138
Hollow cathodes in high pressure arc discharges
[NASA-TM-87098] p 52 N85-34179

HIGH SPEED
Wind tunnel results of advanced high speed propellers in the takeoff, climb, and landing operating regimes
[AIAA PAPER 85-1259] p 6 A85-47025
Effect of two inner-ring oil-flow distribution schemes on the operating characteristics of a 35 millimeter bore ball bearing to 2.5 million DN
[NASA-TP-2404] p 130 N85-13233
Lubrication and performance of high-speed rolling-element bearings
[NASA-TM-86958] p 131 N85-21658
Development of a multiplane multispeed balancing system for turbine systems
[NASA-CR-174750] p 35 N85-22400
Wind tunnel results of advanced high speed propellers in the takeoff, climb and landing operating regimes
[NASA-TM-87054] p 9 N85-29925

HIGH SPEED PHOTOGRAPHY
Solids mixing in a three phase fluidized bed containing spherically shaped-porous solid particles
[PB85-187961] p 120 N85-33453

HIGH STRENGTH ALLOYS
Hot isostatically pressed manufacture of high strength MERL 76 disk and seal shapes
[NASA-CR-165550] p 71 N85-11225

HIGH TEMPERATURE
High temperature oxidation of propene p 61 A85-33570
High-temperature fiber optic pressure sensor p 123 A85-46607
Stability of bromine intercalated graphite fibers
[NASA-TM-86859] p 84 N85-10187
Pre-HOST high temperature crack propagation p 19 N85-10956
Effects of tin on microstructure and mechanical behavior of Inconel 718
[NASA-TM-86866] p 71 N85-12129
High-temperature optically activated GaAs power switching for aircraft digital electronic control
[NASA-CR-174711] p 34 N85-12901

Effects of silver and group 2 fluorides addition to plasma sprayed chromium carbide high temperature solid lubricant for foil gas bearing to 650 deg C
[NASA-TM-86895] p 84 N85-14928
Dispersed metal-toughened ceramics and ceramic brazing
[NASA-CR-174284] p 86 N85-15916
Transformation toughened ceramics for the heavy duty diesel engine technology program
[NASA-CR-174689] p 185 N85-16698
High temperature properties of equiatomic FeAl with ternary additions
[NASA-TM-86938] p 73 N85-19072
Chemical approach for controlling nadimide cure temperature and rate
[NASA-CASE-LEW-13770-5] p 87 N85-21352
3-D inelastic analysis methods for hot section components (base program) --- turbine blades, turbine vanes, and combustor liners
[NASA-CR-174700] p 145 N85-21686
Multiaxial and thermomechanical fatigue considerations in damage tolerant design
[NASA-TM-87022] p 76 N85-26964
Structural characteristics of high temperature composites
[NASA-CR-175998] p 58 N85-30037
Creep fatigue life prediction for engine hot section materials (isotropic)
[NASA-CR-168228] p 32 N85-31057
On numerical integration and computer implementation of viscoplastic models p 151 N85-31542
A comparison of smooth specimen and analytical simulation techniques for notched members at elevated temperatures p 151 N85-31546
Shock tube measurements of growth constants in the branched-chain ethane-carbon monoxide-oxygen system
[NASA-TM-87068] p 64 N85-32156
Results of an interlaboratory fatigue test program conducted on alloy 800H at room and elevated temperatures
[NASA-CR-174940] p 152 N85-32340
Multistage spent particle collector and a method for making same
[NASA-CASE-LEW-13914-1] p 135 N85-33489

HIGH TEMPERATURE ENVIRONMENTS
Performance of thermal barrier coatings in high heat flux environments p 79 A85-19087
Component-specific modeling p 20 N85-10971
The 3-D inelastic analysis methods for hot section components: Brief description p 20 N85-10972
Life prediction and constitutive behavior: Overview p 20 N85-10973
HOST high temperature crack propagation p 21 N85-10977
Surface protection overview p 21 N85-10978
Airfoil deposition model p 21 N85-10979
Evaluation results of the 700 deg C Chinese strain gauges --- for gas turbine engine
[NASA-TM-86973] p 124 N85-21605
Thermal barrier coating system
[NASA-CASE-LEW-14057-1] p 59 N85-35233

HIGH TEMPERATURE TESTS
Ceramic component development for the AGT101 gas turbine engine p 126 A85-15972
Plastic flow of plasma sprayed ceramics p 80 A85-24161
Strength and microstructure of sintered Si3N4 with rare-earth-oxide additions
[ACS PAPER 130-13-84] p 80 A85-25271
Closed-loop strain controlled testing at elevated temperatures with a non-contacting gage p 121 A85-29562
On the fatigue crack propagation behavior of superalloys at intermediate temperatures p 68 A85-32434
Analysis of stress-strain, fracture, and ductility behavior of aluminum maxtrix composites containing discontinuous silicon carbide reinforcement p 55 A85-37421
Fracture of yttria-doped, sintered reaction-bonded silicon nitride
[ACS PAPER 7-J3-84] p 82 A85-42797
Compatibility experiments of facilities, materials, and propellants for electrothermal thrusters
[NASA-TM-86956] p 49 N85-21260
Analysis of experimental shaft seal data for high-performance turbomachines, as for Space Shuttle main engines
[NASA-TM-86928] p 115 N85-21569
Burner rig corrosion of SiC at 1000 deg C
[NASA-TM-87061] p 53 N85-30011
Nonlinear Constitutive Relations for High Temperature Application, 1984
[NASA-CP-2369] p 150 N85-31530

HIGH VACUUM
Vacuum chamber pressure effects on thrust measurements of low Reynolds number nozzles
[NASA-TM-86955] p 49 N85-21259

HIGH VOLTAGES
High-voltage solar-cell chip p 154 A85-24668
Dilute plasma coupling currents to a high voltage solar array in weak magnetic fields p 46 A85-45388
High voltage requirements and issues for the 1990's --- for spacecraft power supplies p 46 A85-45429
Circuit transients due to negative bias arcs on a high-voltage solar array in low Earth orbit
[NASA-TP-2407] p 39 N85-14858
A new very high voltage semiconductor switch
[NASA-TM-86957] p 103 N85-20246
Spacecraft Environmental Interactions Technology, 1983
[NASA-CP-2359] p 39 N85-22470

HISTORIES
A historical overview of the electrical power systems in the US manned and some US unmanned spacecraft
[NASA-CR-174806] p 47 N85-13910

HOLDERS
Apparatus for mounting a field emission cathode
[NASA-CASE-LEW-14108-1] p 104 N85-29149

HOLE GEOMETRY (MECHANICS)
Flow visualization study of the effect of injection hole geometry on an inclined jet in crossflow
[NASA-TM-86936] p 115 N85-20269

HOLLOW CATHODES
Extended performance technology study 30-cm thruster
[NASA-CR-168259] p 48 N85-15806
Heaterless ignition of inert gas ion thruster hollow cathodes
[NASA-TM-87086] p 52 N85-34177
Hollow cathodes in high pressure arc discharges
[NASA-TM-87098] p 52 N85-34179

HOLOGRAPHIC INTERFEROMETRY
A comparison of electronic heterodyne moire deflectometry and electronic heterodyne holographic interferometry for flow measurements
[NASA-TM-87071] p 125 N85-32302

HOLOGRAPHY
An approach for automated analysis of particle holograms p 120 A85-10034

HOMOGENEITY
Homogeneity of pristine and bromine intercalated graphite fibers
[NASA-TM-87016] p 89 N85-25521

HOMOJUNCTIONS
GaAs and 3-5 compound solar cells status and prospects for use in space p 49 N85-22580

HORIZONTAL ORIENTATION
Wake effects on the aerodynamic performance of horizontal axis wind turbines
[NASA-CR-174920] p 162 N85-29364

HOT CATHODES
Calibration stability of some hot-cathode ion gauges p 122 A85-41634

HOT CORROSION
Effects of SO2 and SO3 on the Na2SO4 induced corrosion of nickel p 65 A85-15603
Chemical reactions involved in the initiation of hot corrosion of IN-738 p 66 A85-31688
Hot corrosion of sintered alpha-SiC at 1000 C
[ACS PAPER 19-B-84P] p 83 A85-45302
Effects of surface chemistry on hot corrosion life: Overview p 21 N85-10980
Studies on the hot corrosion of a nickel-base superalloy, Udimet 700
[NASA-TM-86882] p 71 N85-11224
Digital temperature and velocity control of mach 0.3 atmospheric pressure durability testing burner rigs in long time, unattended cyclic testing
[NASA-TM-86959] p 75 N85-21321
Oxidation and hot corrosion of hot-pressed Si3N4 at 1000 deg C
[NASA-TM-86977] p 88 N85-21358
Effects of surface chemistry on hot corrosion life
[NASA-CR-174915] p 28 N85-26711
Burner rig corrosion of SiC at 1000 deg C
[NASA-TM-87061] p 53 N85-30011
Mechanism of strength degradation for hot corrosion of alpha-SiC
[NASA-TM-87052] p 91 N85-30135
A multiple linear regression analysis of hot corrosion attack on a series of nickel base turbine alloys
[NASA-TM-87020] p 77 N85-31284

HOT PRESSING
Effect of hot isostatic pressing on reaction-bonded silicon nitride p 79 A85-15195
Fracture toughness of hot-pressed beryllium p 66 A85-25835
The effect of microstructure, temperature, and hold-time on low-cycle fatigue of As HIP P/M Rene 95 p 67 A85-32399
The substitution of nickel for cobalt in hot isostatically pressed powder metallurgy UDIMET 700 alloys p 68 A85-37415
Microstructure of reaction-bonded silicon nitride consolidated by isostatic hot-pressing p 83 A85-45304
Effect of hot isostatic pressing on the properties of sintered alpha silicon carbide p 83 A85-48757
Hot isostatically pressed manufacture of high strength MERL 76 disk and seal shapes
[NASA-CR-165550] p 71 N85-11225
Oxidation and hot corrosion of hot-pressed Si3N4 at 1000 deg C
[NASA-TM-86977] p 88 N85-21358
Dispersed-metal-toughened alumina
[NASA-CR-174687] p 89 N85-22758

HOT SURFACES
Component-specific modeling
[NASA-CR-174765] p 33 N85-34140

HOT WORKING
Effects of cobalt on the hot workability of nickel-base superalloys p 67 A85-32412

HUMIDITY
Effect of humidity on fretting wear of several pure metals
[NASA-TP-2403] p 72 N85-13006
Humidity effects on adhesion of nickel-zinc ferrite in elastic contact with magnetic tape and itself
[NASA-TP-2449] p 88 N85-21359

HYBRID STRUCTURES
Evolution of assumed stress hybrid finite element p 142 A85-35046
Axisymmetric solid elements by a rational hybrid stress method p 143 A85-41109

HYDROCARBON COMBUSTION
Transferring data oscilloscope to an IBM using an Apple II+ p 168 A85-24526

HYDROCARBON FUELS
Chemistry of fuel deposits and sediments and their predursors
[NASA-CR-174778] p 92 N85-10209
Combustion gas properties. 2: Natural gas fuel and dry air
[NASA-TP-2435] p 26 N85-21168
Fuel-rich catalytic combustion: A soot-free technique for in situ hydrogen-like enrichment
[NASA-TP-2498] p 63 N85-31244
Rapid estimation of concentration of aromatic classes in middistillate fuels by high-performance liquid chromatography
[NASA-TP-2495] p 93 N85-31307

HYDROCARBONS
Effect of gravity on halogenated hydrocarbon flame retardant effectiveness
[IAF PAPER 84-156] p 61 A85-23199
Plasma deposited hydrogenated carbon on GaAs and InP p 182 A85-40386
Plasma deposited diamondlike carbon on GaAs and InP
[NASA-TM-86870] p 183 N85-10844
Applications of high pressure differential scanning calorimetry to aviation fuel thermal stability research
[NASA-TM-87002] p 63 N85-23941
Fuel rich catalytic comustion: The first stage of a two-stage combustor
[NASA-TM-87042] p 63 N85-28983

HYDRODYNAMICS
Hydrodynamic lubrication of rigid nonconformal contacts in combined rolling and normal motion
[ASME PAPER 84-TRIB-13] p 127 A85-21280
Rotordynamic Instability Problems in High-Performance Turbomachinery
[NASA-CP-2338] p 131 N85-14116
Mechanics of a gaseous film barrier to lubricant wetting of elastohydrodynamically lubricated conjunctions
[NASA-TP-2500] p 135 N85-32330
Dual clearance squeeze film damper
[NASA-CASE-LEW-13506-1] p 135 N85-33490

HYDROGEN
Effect of water on hydrogen permeability --- Stirling engines
[NASA-TM-86904] p 53 N85-14864

HYDROGEN CHLORIDES
Mechanism for forming hydrogen chloride and sodium sulfate from sulfur trioxide, water, and sodium chloride p 62 A85-48513

HYDROGEN FUELS
Electrocatalyst advances for hydrogen oxidation in phosphoric acid fuel cells p 60 A85-15614
Performance characterization tests of a 1-kW resistojet using hydrogen, nitrogen and ammonia as propellants
[AIAA PAPER 85-1159] p 44 A85-39628
Combustion gas properties. Part 3: Hydrogen gas fuel and dry air
[NASA-TP-2477] p 32 N85-31058

HYDROGEN IONS
Three-dimensional calculation of shuttle charging in polar orbit p 40 N85-22486

HYDROGEN OXYGEN ENGINES
An evaluation of oxygen/hydrogen propulsion systems for the Space Station
[AIAA PAPER 85-1156] p 45 A85-43976
Advanced research and technology programs for advanced high-pressure oxygen-hydrogen rocket propulsion
[NASA-TM-86969] p 37 N85-21231
An evaluation of oxygen-hydrogen propulsion systems for the Space Station
[NASA-TM-87059] p 52 N85-28971
Status of advanced orbital transfer propulsion
[NASA-TM-87069] p 52 N85-35225
HYDROGEN OXYGEN FUEL CELLS
Design considerations for a 10-kW integrated hydrogen-oxygen regenerative fuel cell system p 155 A85-45380
HYDROGEN PLASMA
Frictional and structural characterization of ion-nitrided low and high chromium steels
[NASA-TM-86991] p 132 N85-23085
HYDROGEN RECOMBINATIONS
The energetics of hydrogen atom recombination - Analysis, experiments, and modeling --- in electrothermal propulsion system p 179 A85-16444
HYDROGEN-BASED ENERGY
Design principles for nickel hydrogen cells and batteries p 104 N85-31398
HYDROGENATION
Optical properties of hydrogenated amorphous carbon films grown from methane plasma
[NASA-TM-86995] p 183 N85-26406
HYDROSTATICS
Development of gas-lubricated pistons for heavy duty diesel engine technology program
[NASA-CR-174746] p 184 N85-12808
HYDROTHERMAL STRESS ANALYSIS
Designing for fiber composite structural durability in hygrothermomechanical environment
[NASA-TM-87045] p 58 N85-27978
HYGRAL PROPERTIES
Hygrothermomechanical evaluation of transverse filament tape epoxy/polyester fiberglass composites p 54 A85-15632
ICAN - Integrated composites analyzer
[AIAA PAPER 84-0974] p 54 A85-16094
Designing for fiber composite structural durability in hygrothermomechanical environment
[NASA-TM-87045] p 58 N85-27978
HYPERBOLIC DIFFERENTIAL EQUATIONS
A convergent series expansion for hyperbolic systems of conservation laws
[NASA-CR-172557] p 168 N85-21990
HYPERVELOCITY LAUNCHERS
Preliminary analysis of space mission applications for electromagnetic launchers
[NASA-CR-174067] p 35 N85-12071
HYPERVELOCITY PROJECTILES
Rail accelerator technology and applications
[NASA-TM-86947] p 48 N85-21258
Arc-driven rail gun research
[NASA-CR-174816] p 132 N85-21662
HYSTERESIS
Internal hysteresis experienced on a high pressure syn gas compressor p 131 N85-14122
Application of traction drives as servo mechanisms p 152 N85-33520

I

IBM 370 COMPUTER
Transferring data oscilloscope to an IBM using an Apple II+ p 168 A85-24526
ICE
Comparison of icing cloud instruments for 1982-1983 icing season flight program
[AIAA PAPER 84-0020] p 13 A85-16098
Initial feasibility ground test of a proposed photogrammetric system for measuring the shapes of ice accretions on helicopter rotor blades during forward flight
[NASA-TM-87391] p 12 N85-12887
ICE FORMATION
Progress toward the development of an aircraft icing analysis capability
[AIAA PAPER 84-0105] p 10 A85-10653
Progress in development of a Navier-Stokes solver for evaluation of iced airfoil performance
[AIAA PAPER 85-0410] p 3 A85-19731
Analytical determination of propeller performance degradation due to ice accretion
[AIAA PAPER 85-0339] p 14 A85-20867
Icing tunnel tests of Electro-Impulse De-Icing of an engine inlet and high-speed wings
[AIAA PAPER 85-0466] p 10 A85-20872
Experimental aerodynamic characteristics of an NACA 0012 airfoil with simulated ice p 12 A85-21844
Predicting rime ice accretion on airfoils p 3 A85-25135
The NASA altitude wind tunnel - Its role in advanced icing research and development
[AIAA PAPER 85-0090] p 35 A85-26381
The UH-1H helicopter icing flight test program - An overview
[AIAA PAPER 85-0338] p 11 A85-28898
Icing flight research - Aerodynamic effects of ice and ice shape documentation with stereo photography
[AIAA PAPER 85-0468] p 11 A85-30192
Performance degradation of helicopter rotor in forward flight due to ice p 11 A85-42937
The UH-1H helicopter icing flight test program: An overview
[NASA-TM-86925] p 11 N85-15702
The NASA Altitude Wind Tunnel (AWT): Its role in advanced icing research and development
[NASA-TM-86920] p 35 N85-15758
Icing flight research: Aerodynamic effects of ice and ice shape documentation with stereo photography
[NASA-TM-86906] p 12 N85-18049
Ice shapes and the resulting drag increase for a NACA 0012 airfoil
[NASA-TM-83556] p 11 N85-27839
ICE PREVENTION
Progress toward the development of an aircraft icing analysis capability
[AIAA PAPER 84-0105] p 10 A85-10653
Analytical and physical modeling program for the NASA Lewis Research Center's Altitude Wind Tunnel (AWT)
[NASA-TM-86919] p 35 N85-15757
IDEAL GAS
Oscillatory conductive heat transfer for a fiber in an ideal gas p 109 A85-26077
Ideal gas thermodynamic properties for the phenyl, phenoxy, and o-biphenyl radicals
[NASA-TM-83800] p 184 N85-22204
IGNITION LIMITS
Systematic optimization of a detailed kinetic model using a methane ignition example p 59 A85-12890
Effect of gravity on halogenated hydrocarbon flame retardant effectiveness
[IAF PAPER 84-156] p 61 A85-23199
High temperature oxidation of propene p 61 A85-33570
Behavior of the lean methane-air flame at zero-gravity
[NASA-CR-175586] p 62 N85-21283
The use of a laser Doppler velocimeter in a standard flammability tube
[NASA-CR-174960] p 125 N85-35389
ILLUMINATION
Focal shifts in parabolic reflectors p 97 A85-39356
IMAGE ANALYSIS
An approach for automated analysis of particle holograms p 120 A85-10034
IMAGE PROCESSING
An allpass filter design for luminance and chrominance separation of NTSC signals p 102 A85-28230
Free-surface phenomena under low- and zero-gravity conditions
[NASA-CR-175885] p 36 N85-27922
IMIDES
Imide modified epoxy matrix resins
[NASA-CR-174695] p 85 N85-15892
IMPACT RESISTANCE
Impact resistance of fiber composites - Energy-absorbing mechanisms and environmental effects p 56 A85-46543
Fundamental studies of composite toughness p 56 N85-12948
IMPACT TESTS
Characterization of solid particle erosion resistance of ductile metals based on their properties p 69 A85-42569
IMPEDANCE
Characterization of microstrip discontinuities in the time and frequency domains
[NASA-CR-176190] p 106 N85-35342
IMPINGEMENT
Into mesh lubrication of spur gears with arbitrary offset oil jet. I - For jet velocity less than or equal to gear velocity p 128 A85-24497
Lubricant jet flow phenomena in spur and helical gears with modified center distances and/or addendums - For out-of-mesh conditions
[ASME PAPER 84-DET-96] p 129 A85-35049
Effect of surface configuration during solid particle impingement erosion p 69 A85-42568
Characterization of solid particle erosion resistance of ductile metals based on their properties p 69 A85-42569
IMPLANTATION
Percutaneous connectors
[NASA-CR-175627] p 168 N85-27508
IMPURITIES
Milling of Si3N4 with Si3N4 hardware
[NASA-TM-86864] p 84 N85-10191
INCIDENT RADIATION
Incident beam polarization for laser Doppler velocimetry employing a sapphire cylindrical window p 122 A85-39835
INCLUSIONS
Ultrasonic wave propagation in two-phase media - Spherical inclusions p 54 A85-11926
INCOMPRESSIBLE FLOW
Approximate analysis for resonance of an incompressible shear layer plus edges p 107 A85-19377
Accelerated convergence for incompressible flow calculations
[AIAA PAPER 85-0058] p 2 A85-19489
A space-marching method for incompressible Navier-Stokes equations
[AIAA PAPER 85-0170] p 108 A85-19564
Vortex induced lift on a flat plate with a curved forward-facing flap p 4 A85-30175
Accelerated convergence for incompressible flow calculations
[NASA-TM-86863] p 18 N85-10949
Incompressible lifting-surface aerodynamics for a rotor-stator combination
[NASA-TM-83767] p 7 N85-12039
Reducing numerical diffusion for incompressible flow calculations
[NASA-TM-83621] p 24 N85-14840
Turbulent solutions of equations of fluid motion p 118 N85-31441
General design method for 3-dimensional, potential flow fields. Part 2: Computer program DIN3D1 for simple, unbranched ducts
[NASA-CR-3926] p 10 N85-35159
INCONEL (TRADEMARK)
Effects of tin on microstructure and mechanical behavior of Inconel 718
[NASA-TM-86866] p 71 N85-12129
Thermal-mechanical fatigue crack growth in Inconel X-750
[NASA-CR-174740] p 72 N85-15877
Effect of reduction of strategic Columbium addition in 718 Alloy on the structure and properties
[NASA-CR-174841] p 75 N85-21320
Finite element analysis of notch behavior using a state variable constitutive equation p 152 N85-31548
INDENTATION
Use of statical indentation laws in the impact analysis of laminated composite plates p 55 A85-29133
Ceramic wear in indentation and sliding contact p 82 A85-39549
INDEXES (DOCUMENTATION)
Bibliography of Lewis Research Center technical publications announced in 1984
[NASA-TM-87012] p 184 N85-28876
INDIUM PHOSPHIDES
Plasma deposited hydrogenated carbon on GaAs and InP p 182 A85-40386
Plasma deposited diamondlike carbon on GaAs and InP
[NASA-TM-86870] p 183 N85-10844
INDUCTION HEATING
High frequency plasma generator for ion thrusters
[NASA-CR-174772] p 48 N85-17023
INDUSTRIAL ENERGY
Advanced technology cogeneration system conceptual design study: Closed cycle gas turbines
[NASA-CR-168222] p 159 N85-16300
INDUSTRIAL PLANTS
Advanced technology cogeneration system conceptual design study: Closed cycle gas turbines
[NASA-CR-168222] p 159 N85-16300
INELASTIC STRESS
Strainrange partitioning - A total strain range version --- for creep fatigue life prediction by summing inelastic and elastic strain-range-life relations for two Ni base superalloys p 64 A85-11603
A history dependent damage model for low cycle fatigue
[ASME PAPER 84-PVP-112] p 140 A85-18795
Unified constitutive material models for nonlinear finite-element structural analysis --- gas turbine engine blades and vanes
[AIAA PAPER 85-1418] p 142 A85-39769
The 3-D inelastic analysis methods for hot section components: Brief description p 20 N85-10972
Local strain redistribution corrections for a simplified inelastic analysis procedure based on an elastic finite-element analysis
[NASA-TP-2421] p 145 N85-20396

3-D inelastic analysis methods for hot section components (base program) --- turbine blades, turbine vanes, and combustor liners
[NASA-CR-174700] p 145 N85-21686
Unified constitutive material models for nonlinear finite-element structural analysis --- gas turbine engine blades and vanes
[NASA-TM-86985] p 146 N85-24338
A survey of unified constitutive theories p 150 N85-31531

INFRARED ASTRONOMY
Mosaic Infrared Sensor for Space Astronomy (MIRSSA)
[NASA-CR-176154] p 125 N85-33456

INFRARED DETECTORS
Mosaic Infrared Sensor for Space Astronomy (MIRSSA)
[NASA-CR-176154] p 125 N85-33456

INFRARED SPECTRA
Nitriding of titanium and its alloys by N2, NH3 or mixtures of N2 + H2 in a dc arc plasma at low pressures (or = to torr)
[NASA-TM-83803] p 131 N85-15168

INGESTION (ENGINES)
Temperature distortion generator for turboshaft engine testing
[SAE PAPER 841541] p 15 A85-39065
Temperature distortion generator for turboshaft engine testing
[NASA-TM-83748] p 1 N85-15658

INGOTS
Control of solidification boundary in continuous casting by asymmetric cooling and mold offset p 110 A85-37047

INJECTION
A new very high voltage semiconductor switch
[NASA-TM-86957] p 103 N85-20246

INLET AIRFRAME CONFIGURATIONS
Performance and surge limits of a TF30-P-3 turbofan engine/axisymmetric mixed-compression inlet propulsion system at Mach 2.5
[NASA-TP-2461] p 27 N85-25261

INLET FLOW
Analytical study of blowing boundary layer control for subsonic V/STOL inlets p 2 A85-11646
Calculation of compressible flow about three-dimensional inlets with auxiliary inlets, slats and vanes by means of a panel method
[AIAA PAPER 85-1196] p 5 A85-40817
The three-dimensional compressible flow in a radial inflow turbine scroll p 6 A85-41826
Application of computational fluid dynamics to complex inlet ducts
[AIAA PAPER 85-1213] p 6 A85-47023
Flow rates and pressure profiles for one to four axially alined Borda inlets
[NASA-TP-2390] p 113 N85-14078
Effect of steady-state temperature distortion on inlet flow to a high-bypass-ration turbofan engine
[NASA-TM-86896] p 24 N85-15725
Aerodynamic detuning analysis of an unstalled supersonic turbofan cascade
[NASA-TM-87001] p 9 N85-26670
Flow rate and pressure profiles for 1 to 4 axially alined orifice inlets
[NASA-TP-2460] p 116 N85-27165
Application of computational fluid dynamics to complex inlet ducts
[NASA-TM-87060] p 118 N85-30247

INLET PRESSURE
A comparison of flow rates and pressure profiles for N-sequential inlets and three related seal configurations p 109 A85-26526
Flow rates and pressure profiles for one to four axially alined Borda inlets
[NASA-TP-2390] p 113 N85-14078

INLET TEMPERATURE
Redistribution of the inlet temperature profile through the SSME fuel turbine p 50 N85-26901
SSME fuel preburner two-dimensional analysis p 51 N85-27943

INSPECTION
Advanced blade tip seal system, volume 2
[NASA-CR-167851] p 23 N85-10999

INSTRUMENT ERRORS
Fiber optic temperature sensor p 121 A85-29563

INSTRUMENTS
HOST instrumentation R and D program overview p 19 N85-10957
Instrumentation technology overview p 124 N85-26903

INSULATORS
Dispersed metal-toughened ceramics and ceramic brazing
[NASA-CR-174284] p 86 N85-15916

INTAKE SYSTEMS
A comparison of flow rates and pressure profiles for N-sequential inlets and three related seal configurations p 109 A85-26526
Flow rates and pressure profiles for one to four axially alined Borda inlets
[NASA-TP-2390] p 113 N85-14078
Performance and surge limits of a TF30-P-3 turbofan engine/axisymmetric mixed-compression inlet propulsion system at Mach 2.5
[NASA-TP-2461] p 27 N85-25261
Calculation of compressible flow about three-dimensional inlets with auxiliary inlets, slats and vanes by means of a panel method
[NASA-CR-174975] p 10 N85-35162

INTEGRAL EQUATIONS
Noise transmission loss of a rectangular plate in an infinite baffle
[NASA-TP-2398] p 176 N85-22109

INTEGRALS
Translational and extensional energy release rates (the J- and M-integrals) for a crack layer in thermoelasticity
[NASA-CR-174872] p 145 N85-21685

INTEGRATED CIRCUITS
High-voltage solar-cell chip p 154 A85-24668
Characterization of MMIC devices for active array antennas
[NASA-TM-86907] p 38 N85-15779
Configuration study for a 30 GHz monolithic receive array: Technical assessment
[NASA-CR-174697] p 98 N85-18238

INTEGRATED ENERGY SYSTEMS
Develop and test fuel cell powered on-site integrated total energy systems. Phase 3: Full-scale power plant development
[NASA-CR-174887] p 161 N85-25941

INTERACTIONAL AERODYNAMICS
Noise produced by the interaction of a rotor wake with a swept stator blade
[AIAA PAPER 84-2326] p 173 A85-13956
A linearized unsteady aerodynamic analysis for transonic cascades p 3 A85-20744
A note on blade wake interaction influence on compressor stator row aerodynamic performance p 4 A85-32965
The computation of viscid/inviscid interaction on airfoils with separated flow p 6 A85-42954

INTERACTIVE CONTROL
MINDS: A microcomputer interactive data system for 8086-based controllers
[NASA-TP-2378] p 170 N85-17576

INTERCALATION
Dynamics of graphite fiber intercalation: In situ resistivity measurements with a four point probe
[NASA-TM-86858] p 53 N85-10105
Stability of bromine intercalated graphite fibers
[NASA-TM-86859] p 84 N85-10187
Homogeneity of pristine and bromine intercalated graphite fibers
[NASA-TM-87016] p 89 N85-25521
Graphite fiber intercalation: Dynamics of the bromine intercalation process
[NASA-TM-87015] p 53 N85-26921
Environmental stability of intercalated graphite fibers
[NASA-TM-87025] p 90 N85-26992
A micrographic and gravimetric study of intercalation and deintercalation of graphite fibers
[NASA-TM-87026] p 91 N85-28110

INTERFACE STABILITY
Convective influence on the stability of a cylindrical solid-liquid interface p 109 A85-26911

INTERFACES
Effect of Interfacial characteristics of metal clad polymeric substrates on electrical high frequency interconnection performance
[NASA-TM-86948] p 99 N85-20223

INTERFACIAL TENSION
Contact angle and surface tension measurements of a five-ring polyphenyl ether
[NASA-TM-86927] p 86 N85-15897
Tribological properties of boron nitride synthesized by ion beam deposition
[NASA-TM-86962] p 87 N85-21355
Hertzian contact in two and three dimensions
[NASA-TP-2473] p 135 N85-32331

INTERFEROMETERS
Automatic sphericity interferometer for testing lens radii
[AD-A155736] p 125 N85-33457

INTERLAYERS
Graphite fiber intercalation: Dynamics of the bromine intercalation process
[NASA-TM-87015] p 53 N85-26921

INTERMETALLICS
Ductility in rapidly solidified NiAl p 66 A85-26158
New eutectic alloys and their heats of transformation p 66 A85-27808
High temperature properties of equiatomic FeAl with ternary additions
[NASA-TM-86938] p 73 N85-19072
The B2 aluminides as alternative materials
[NASA-TM-86937] p 74 N85-19076
Alloys based on NiAl for high temperature applications
[NASA-TM-86976] p 75 N85-21322
Oxidizing seal for a turbine tip gas path
[NASA-CASE-LEW-14053-1] p 136 N85-34402

INTERNAL COMBUSTION ENGINES
Internal combustion engine combustion chamber process studies at NASA Lewis Research Center p 112 A85-45856
Knock syndrome: Its cures and its victims
[NASA-CR-174395] p 93 N85-19185
Modeling the internal combustion engine
[NASA-RP-1094] p 172 N85-19733
NDE for heat engine ceramics
[NASA-TM-86949] p 137 N85-20389
Stratified charge rotary aircraft engine technology enablement program
[NASA-CR-174812] p 25 N85-21163

INTERNAL ENERGY
On the use of internal state variables in thermoviscoplastic constitutive equations p 150 N85-31536

INTERNATIONAL COOPERATION
Development and use of the computer software package for planning the 12 GHz broadcasting-satellite service at RARC '83 p 96 A85-29605

INTERORBITAL TRAJECTORIES
Radiation exposure and performance of multiple burn LEO-GEO orbit transfer trajectories
[NASA-TM-86946] p 36 N85-21228

INTERPOLATION
Floating-point function generation routines for 16-bit microcomputers
[NASA-TM-83783] p 170 N85-10683

INTERSTELLAR RADIATION
Radiation exposure and performance of multiple burn LEO-GEO orbit transfer trajectories
[NASA-TM-86946] p 36 N85-21228

INVERTERS
The J3 SCR model applied to resonant converter simulation p 102 A85-42156

INVISCID FLOW
Progress toward the development of an aircraft icing analysis capability
[AIAA PAPER 84-0105] p 10 A85-10653
Comparison of secondary flows predicted by a viscous code and an inviscid code with experimental data for a turning duct p 106 A85-11634
A finite element solution of three-dimensional inviscid rotational flows through curved ducts p 107 A85-11648
The linear two-dimensional stability of inviscid vortex streets of finite-cored vortices
[AD-A153032] p 107 A85-14241
Three-dimensional inviscid flow analysis of turbofan forced mixers
[AIAA PAPER 85-0086] p 2 A85-19510
Vortex induced lift on a flat plate with a curved forward-facing flap p 4 A85-30175
Assessment of three-dimensional inviscid codes and loss calculations for turbine aerodynamic computations
[ASME PAPER 84-GT-187] p 4 A85-32961
Application of viscous and inviscid computation methods for rocket turbopump systems
[SAE PAPER 841522] p 110 A85-39257
Flow through very porous inclined screens
[AIAA PAPER 85-1650] p 111 A85-40750
Inviscid analysis of advanced turboprop propeller flow fields
[AIAA PAPER 85-1263] p 6 A85-43977
Inviscid and viscous flows in cascades with an explicit multiple-grid algorithm p 7 A85-48539
Flow through very porous inclined screens
[NASA-TM-86979] p 116 N85-25761

IODINE COMPOUNDS
Environmental stability of intercalated graphite fibers
[NASA-TM-87025] p 90 N85-26992

ION ACCELERATORS
Theory of ion acceleration with closed electron drift --- in spacecraft plasma propulsion p 41 A85-15512

ION BEAMS
Laboratory degradation of Kapton in a low energy oxygen ion beam
[AIAA PAPER 83-2658] p 78 A85-10675
Ion-beam nitriding of steels p 66 A85-24667
Properties of coated and modified surfaces p 53 A85-36694
Experimental performance of a microwave cavity plasma disk ion source p 179 A85-43552

Extended performance technology study 30-cm thruster
[NASA-CR-168259] p 48 N85-15806
Deposition of diamondlike carbon films
[NASA-CASE-LEW-14080-1] p 95 N85-20153
Diamondlike flakes
[NASA-CASE-LEW-13837-2] p 57 N85-21267
Ion-beam nitriding of steels
[NASA-CASE-LEW-14104-1] p 75 N85-21324
Ion beam sputter-deposited thin film coatings for protection of spacecraft polymers in low Earth orbit
[NASA-TM-87051] p 91 N85-30137
Diamondlike carbon protective coatings for IR materials
[NASA-TM-87083] p 178 N85-34631

ION ENGINES
Ion flow experiments in a multipole discharge chamber p 178 A85-12705
Performance capabilities of the 12-centimeter Xenon ion thruster p 42 A85-16439
Cathode degradation and erosion in high pressure arc discharges p 43 A85-16445
Inert gas test of two 12-cm magnetostatic thrusters p 43 A85-29310
Development of a large insert gas ion thruster p 45 A85-42922
Investigation of a pulsed electrothermal thruster system
[NASA-CR-174768] p 46 N85-11132
Precision tunable resonant microwave cavity
[NASA-CASE-LEW-13935-1] p 103 N85-20248
Heaterless ignition of inert gas ion thruster hollow cathodes
[NASA-TM-87086] p 52 N85-34177

ION EXCHANGE MEMBRANE ELECTROLYTES
Development of a lithium secondary battery separator p 104 N85-31378
Evaluation of developmental membranes for the mixed reactant iron-chromium redox system
[NASA-TM-87074] p 164 N85-34443

ION EXTRACTION
Extended performance technology study 30-cm thruster
[NASA-CR-168259] p 48 N85-15806

ION IMPLANTATION
Radiation damage and defect behavior in ion-implanted, lithium counterdoped silicon solar cells p 182 A85-35698
Study of the effects of implantation on the high Fe-Ni-Cr and Ni-Cr-Al alloys
[NASA-CR-175625] p 76 N85-22661

ION IRRADIATION
Cone formation as a result of whisker growth on ion bombarded metal surfaces p 182 A85-41635

ION MOTION
Ion flow.experiments in a multipole discharge chamber p 178 A85-12705

ION PLATING
Tribological properties of boron nitride synthesized by ion beam deposition
[NASA-TM-86962] p 87 N85-21355
The structure of ion plated films in relation to coating properties
[NASA-TM-87055] p 95 N85-29085
Advances in sputtered and ion plated solid film lubrication p 136 N85-33524

ION PROPULSION
Theory of ion acceleration with closed electron drift --- in spacecraft plasma propulsion p 41 A85-15512
Ground correlation investigation of thruster/spacecraft interactions to be measured on the IAPS flight test p 42 A85-16408
Ion propulsion for communications satellites p 42 A85-16412
Characterization of 8-cm engineering model thruster
[NASA-CR-174673] p 46 N85-11131
Ring-cusp ion thruster with shell anode
[NASA-CASE-LEW-13881-1] p 48 N85-21256

ION SOURCES
Recent work on a microwave ion source p 179 A85-16455
Plasma deposited hydrogenated carbon on GaAs and InP p 182 A85-40386
Experimental performance of a microwave cavity plasma disk ion source p 179 A85-43552
Plasma deposited diamondlike carbon on GaAs and InP
[NASA-TM-86870] p 183 N85-10844

IONIZATION GAGES
Calibration stability of some hot-cathode ion gauges p 122 A85-41634

IONOSPHERIC CURRENTS
Three-dimensional calculation of shuttle charging in polar orbit p 40 N85-22486

IRON
The reactions of cobalt, iron and nickel in SO-2 atmospheres: Similarities and differences
[NASA-TM-86868] p 70 N85-11217
Surface effects of corrosive media on hardness, friction, and wear of materials
[NASA-TM-83711] p 85 N85-15896
High temperature properties of equiatomic FeAl with ternary additions
[NASA-TM-86938] p 73 N85-19072
Development of electrodes for the NASA iron/chromium
[NASA-CR-174724] p 165 N85-35471

IRON ALLOYS
Stirling material technology
[NASA-TM-86888] p 72 N85-13007
Creep-rupture behavior of iron superalloys in high-pressure hydrogen
[NASA-CR-174411] p 74 N85-19078
Effects of chromium and aluminum on mechanical and oxidation properties of iron-nickel-base superalloys based on CG-27
[NASA-TP-2443] p 75 N85-21323
Study of the effects of implantation on the high Fe-Ni-Cr and Ni-Cr-Al alloys
[NASA-CR-175625] p 76 N85-22661
Iron rich low cost superalloys
[NASA-CR-174900] p 76 N85-26962
Thermal barrier coating system
[NASA-CASE-LEW-14057-1] p 59 N85-35233

IRON CHLORIDES
Environmental stability of intercalated graphite fibers
[NASA-TM-87025] p 90 N85-26992

ISOPARAMETRIC FINITE ELEMENTS
Development and testing of stable, invariant, isoparametric curvilinear 2- and 3-D hybrid-stress elements p 140 A85-19899
Use of statical indentation laws in the impact analysis of laminated composite plates p 55 A85-29133

ISOSTATIC PRESSURE
Effect of hot isostatic pressing on reaction-bonded silicon nitride p 79 A85-15195
The substitution of nickel for cobalt in hot isostatically pressed powder metallurgy UDIMET 700 alloys p 68 A85-37415
Microstructure of reaction-bonded silicon nitride consolidated by isostatic hot-pressing p 83 A85-45304
Effect of hot isostatic pressing on the properties of sintered alpha silicon carbide p 83 A85-48757

ISOTHERMAL FLOW
Predictions and measurements of isothermal flowfields in axisymmetric combustor geometries
[NASA-CR-174916] p 29 N85-27867

ISOTHERMAL PROCESSES
Elastohydrodynamic lubrication of line contacts p 126 A85-11069

ISOTROPIC MEDIA
Unified constitutive material models for nonlinear finite-element structural analysis --- gas turbine engine blades and vanes
[AIAA PAPER 85-1418] p 142 A85-39769
Unified constitutive material models for nonlinear finite-element structural analysis --- gas turbine engine blades and vanes
[NASA-TM-86985] p 146 N85-24338

ISOTROPY
Substrate-induced orientational order in the isotropic phase of liquid crystals p 181 A85-24649
Constitutive model development for isotropic materials p 20 N85-10975

ITERATION
Perturbation-iteration theory for analyzing microwave striplines
[NASA-CR-176189] p 100 N85-35321

ITERATIVE SOLUTION
Augmented weak forms and element-by-element preconditioners: Efficient iterative strategies for structural finite elements. A preliminary study p 144 N85-10384

J

J INTEGRAL
Translational and extensional energy release rates (the J- and M-integrals) for a crack layer in thermoelasticity
[NASA-CR-174872] p 145 N85-21685
A review of path-independent integrals in elastic-plastic fracture mechanics, task 4
[NASA-CR-174956] p 152 N85-33541

JET AIRCRAFT
Observations from varying the lift and drag inputs to a noise prediction method for supersonic helical tip speed propellers
[NASA-TM-83797] p 175 N85-10788

JET AIRCRAFT NOISE
Supersonic jet shock noise reduction
[AIAA PAPER 84-2278] p 173 A85-16099
Experimental investigation of shock-cell noise reduction for dual-stream nozzles in simulated flight
[NASA-CR-3846] p 175 N85-13549

JET ENGINE FUELS
Combustion gas properties I-ASTM jet A fuel and dry air
[NASA-TP-2359] p 17 N85-10064
Lubricity of well-characterized jet and broad-cut fuels by ball-on-cylinder machine
[NASA-TM-83807] p 92 N85-12183
Liquid phase products and solid deposit formation from thermally stressed model jet fuels
[NASA-TM-86874] p 92 N85-13066
Study of advanced fuel system concepts for commercial aircraft and engines
[NASA-CR-174752] p 93 N85-19176
Jet fuel property changes and their effect on producibility and cost in the U.S., Canada, and Europe
[NASA-CR-174840] p 93 N85-27012
Jet fuel instability mechanisms
[NASA-CR-175856] p 93 N85-28127
Measurement and correlation of jet fuel viscosities at low temperatures
[NASA-CR-174911] p 94 N85-34295

JET ENGINES
Eddy current jet engine disk-crack monitor p 120 A85-11100
The use of Ada in distributed simulations p 169 A85-28612
Multibus-based parallel processor for simulation p 169 A85-28613
Fabrication of ceramic substrate-reinforced and free forms
[NASA-TM-86994] p 50 N85-23926
Advanced smoke meter development survey and analysis
[NASA-CR-168287] p 124 N85-25792
Alternatives for jet engine control
[NASA-CR-175831] p 29 N85-26713
Alternatives for jet engine control
[NASA-CR-175832] p 29 N85-26714
Alternatives for jet engine control
[NASA-CR-175833] p 29 N85-26715
Component-specific modeling
[NASA-CR-174765] p 33 N85-34140

JET FLOW
Into mesh lubrication of spur gears with arbitrary offset oil jet. I - For jet velocity less than or equal to gear velocity p 128 A85-24497
Some unique experiments on receptivity --- for forced disturbances entering shear flow
[AIAA PAPER 85-0533] p 174 A85-25932
Lubricant jet flow phenomena in spur and helical gears with modified center distances and/or addendums - For out-of-mesh conditions
[ASME PAPER 84-DET-96] p 129 A85-35049
Experiments in dilution jet mixing - Effects of multiple rows and non-circular orifices
[AIAA PAPER 85-1104] p 15 A85-39606
Numerical calculation of subsonic jets in crossflow with reduced numerical diffusion
[AIAA PAPER 85-1441] p 110 A85-39780
Flow visualization study of the effect of injection hole geometry on an inclined jet in crossflow
[NASA-TM-86936] p 115 N85-20269
Preliminary analysis of tone-excited two-stream jet velocity decay
[NASA-TM-86951] p 8 N85-21114
Liquid fuel spray processes in high-pressure gas flow
[NASA-TM-86944] p 115 N85-21570
Numerical calculation of subsonic jets in crossflow with reduced numerical diffusion
[NASA-TM-87003] p 27 N85-25263
Experiments in dilution jet mixing effects of multiple rows and non-circular orifices
[NASA-TM-86996] p 28 N85-25266
The influence of jet-grid turbulence on heat transfer from the stagnation region of a cylinder in crossflow
[NASA-TM-87011] p 115 N85-25760
Turbulent transport and length scale measurement experiments with comfined coaxial jets
[NASA-CR-174831] p 117 N85-30245

JET IMPINGEMENT
Spherical microglass particle impingement studies of thermoplastic materials at normal incidence p 79 A85-11072

JET MIXING FLOW
An experimental study of tone excited heated jets
[AIAA PAPER 84-2341] p 172 A85-10882
Mass and momentum turbulent transport experiments with confined coaxial jets p 107 A85-14399
Acoustic control of free jet mixing
[AIAA PAPER 85-0569] p 109 A85-25951

Experiments in dilution jet mixing - Effects of multiple rows and non-circular orifices
[AIAA PAPER 85-1104] p 15 A85-39606
Vortex modeling of single and multiple dilution jet mixing in a crossflow
[AIAA PAPER 85-1580] p 111 A85-40701
Jet characteristics in confined swirling flow p 112 A85-45282
Density effects on jet characteristics in confined swirling flow p 112 A85-45283
Dilution zone mixing studies p 21 N85-10984
Development of a temperature measurement system with application to a jet in a cross flow experiment
[NASA-CR-174896] p 27 N85-25262
Experiments in dilution jet mixing effects of multiple rows and non-circular orifices
[NASA-TM-86996] p 28 N85-25266

JET NOZZLES
Lubricant jet flow phenomena in spur and helical gears with modified center distances and/or addendums - For out-of-mesh conditions
[ASME PAPER 84-DET-96] p 129 A85-35049

JOINING
Effect of Interfacial characteristics of metal clad polymeric substrates on electrical high frequency interconnection performance
[NASA-TM-86948] p 99 N85-20223

JOINTS (ANATOMY)
Friction and wear properties of a Charnley artificial hip joint
[ASLE PREPRINT 84-LC-4A-4] p 168 A85-38444

JOINTS (JUNCTIONS)
Fracture of composite-adhesive-composite systems p 141 A85-27935

JOURNAL BEARINGS
An analysis of temperature effect in a finite journal bearing with spatial tilt and viscous dissipation p 126 A85-11074
Vibration control of rotor shaft
[NASA-TM-87053] p 133 N85-29292

JUNCTION TRANSISTORS
The study of microstrip antenna arrays and related problems
[NASA-CR-174054] p 97 N85-11265

K

KALMAN FILTERS
A design methodology for robust failure detection and isolation p 171 A85-47794

KAPTON (TRADEMARK)
Laboratory studies of Kapton degradation in an oxygen ion beam p 177 N85-22477
Study of Kapton under simulated shuttle environment
[NASA-CR-176003] p 41 N85-29997

KARMAN VORTEX STREET
The linear two-dimensional stability of inviscid vortex streets of finite-cored vortices
[AD-A153032] p 107 A85-14241

KELVIN-HELMHOLTZ INSTABILITY
Feedback in separated flows over symmetric airfoils
[AIAA PAPER 84-2297] p 3 A85-28899

KILOMETRIC WAVES
DE-1 measurements of AKR wave directions --- auroral kilometric radiation p 166 A85-37717

KINEMATIC EQUATIONS
First-order ball-bearing kinematics p 128 A85-31203

KINEMATICS
Advanced stress analysis methods applicable to turbine engine structures
[NASA-CR-175573] p 26 N85-21165
On Hybrid and mixed finite element methods
[NASA-CR-175551] p 146 N85-23096
Dynamic creep buckling: Analysis of shell structures subjected to time-dependent mechanical and thermal loading p 149 N85-27959
Spiral bevel and circular arc helical gears: Tooth contact analysis and the effect of misalignment on circular arc helical gears
[NASA-TM-87013] p 32 N85-31060
Generated spiral bevel gears: Optimal machine-tool settings and tooth contact analysis
[NASA-TM-87075] p 136 N85-34405

KINETIC FRICTION
Friction and wear properties of a Charnley artificial hip joint
[ASLE PREPRINT 84-LC-4A-4] p 168 A85-38444

KINETICS
Future fundamental combustion research for aeropropulsion systems
[AIAA PAPER 85-1398] p 16 A85-42671
Nitriding of titanium and its alloys by N2, NH3 or mixtures of N2 + H2 in a dc arc plasma at low pressures (or = to torr)
[NASA-TM-83803] p 131 N85-15168
Shock tube study of the fuel structure effects on the chemical kinetic mechanisms responsible for soot formation, part 2
[NASA-CR-174880] p 63 N85-25444
Future fundamental combustion research for aeropropulsion systems
[NASA-TM-87049] p 30 N85-27870
Dynamic creep buckling: Analysis of shell structures subjected to time-dependent mechanical and thermal loading p 149 N85-27959

L

LABYRINTH SEALS
An experimental investigation of rubbing interaction in labyrinth seals at cryogenic temperature p 129 A85-39938
Analytical and experimental investigation of rubbing interaction in labyrinth seals for a liquid hydrogen fuel pump --- space shuttle main engine
[NASA-CR-174657] p 48 N85-18084

LAGRANGE MULTIPLIERS
Recent advances in hybrid/mixed finite elements
[NASA-CR-175574] p 145 N85-21687

LAMINAR FLOW
GASP cloud encounter statistics - Implications for laminar flow control flight p 166 A85-11979
A review and analysis of boundary layer transition data for turbine application
[NASA-TM-86880] p 113 N85-10306
Thermodynamic evaluation of transonic compressor rotors using the finite volume approach
[NASA-CR-175811] p 29 N85-26712

LAMINAR HEAT TRANSFER
Analysis of buoyancy effect on fully developed laminar heat transfer in a rotating tube p 110 A85-35596

LAMINAR WAKES
The mechanisms of flame holding in the wake of a bluff body
[NASA-CR-3866] p 26 N85-21166

LAMINATES
Interply layer degradation effects on composite structural response
[AIAA PAPER 84-0849] p 54 A85-16096
Use of statical indentation laws in the impact analysis of laminated composite plates p 55 A85-29133
Interply layer degradation effects on composite structural response p 55 A85-39215
A study of interply layer effects on the free edge stress field of angleplied laminates p 55 A85-41127
Fiberglass epoxy laminate fatigue properties at 300 and 20 K p 56 A85-47970
Energy efficient engine. Volume 2. Appendix A: Component development and integration program
[NASA-CR-173085] p 22 N85-10991
A study of interply layer effects on the free-edge stress field of angleplied laminates
[NASA-TM-86924] p 57 N85-15822
Design procedures for fiber composite structural components: Panels subjected to combined in-plane loads
[NASA-TM-86909] p 57 N85-15823

LANDING
Wind tunnel results of advanced high speed propellers in the takeoff, climb, and landing operating regimes
[AIAA PAPER 85-1259] p 6 A85-47025
Wind tunnel results of advanced high speed propellers in the takeoff, climb and landing operating regimes
[NASA-TM-87054] p 9 N85-29925

LARGE SPACE STRUCTURES
Environmentally-induced voltage limitations in large space power systems p 43 A85-18584
Research and technology highlights of the Lewis Research Center
[NASA-TM-86899] p 186 N85-17928
Spacecraft environmental interactions: A joint Air Force and NASA research and technology program p 40 N85-22517
Alternatives for satellite sound broadcast systems at HF and VHF p 99 N85-23815
Extreme precision antenna reflector study results p 165 N85-23830

LASER ANEMOMETERS
Two-frequency laser-induced fluorescence technique for rapid velocity-field measurements in gas flows p 121 A85-32294
Investigation of flow phenomena in a transonic fan rotor using laser anemometry
[ASME PAPER 84-GT-199] p 4 A85-32963
Feasibility of mapping velocity flow fields in SSME powerhead by laser anemometry techniques p 41 N85-27971
Filter induced errors in laser anemometer measurements using counter processors
[NASA-TM-87047] p 125 N85-30288

LASER APPLICATIONS
Velocity visualization in gas flows using laser-induced phosphorescence of biacetyl p 121 A85-21695
Fast laser-induced aerosol formation for visualization of gas flows p 121 A85-31113
Laser balancing system for high material removal rates
[NASA-CR-174731] p 126 N85-12341
Velocity visualization in gaseous flows
[NASA-CR-174954] p 119 N85-31445

LASER DOPPLER VELOCIMETERS
Phase/doppler spray analyzer for simultaneous measurements of drop size and velocity distributions p 120 A85-10035
Incident beam polarization for laser Doppler velocimetry employing a sapphire cylindrical window p 122 A85-39835
Jet characteristics in confined swirling flow p 112 A85-45282
Internal combustion engine combustion chamber process studies at NASA Lewis Research Center p 112 A85-45856
Holographic optical system for aberration corrections in laser Doppler velocimetry p 123 A85-48659
Hot section laser anemometry p 19 N85-10962
The boundary layer on compressor cascade blades
[NASA-CR-174369] p 114 N85-18292
Incident beam polarization for laser Doppler velocimetry employing a sapphire cylindrical window
[NASA-TM-87064] p 178 N85-28786
Velocity visualization in gaseous flows
[NASA-CR-174954] p 119 N85-31445
The use of a laser Doppler velocimeter in a standard flammability tube
[NASA-CR-174960] p 125 N85-35389

LASER INDUCED FLUORESCENCE
Two-frequency laser-induced fluorescence technique for rapid velocity-field measurements in gas flows p 121 A85-32294

LASER INTERFEROMETRY
Phase/doppler spray analyzer for simultaneous measurements of drop size and velocity distributions p 120 A85-10035
Spray characterization with a nonintrusive technique using absolute scattered light p 120 A85-10036
Remote displacement measurements using a laser diode p 121 A85-24464

LASER OUTPUTS
Research study of droplet sizing technology leading to the development of an advanced droplet sizing system
[NASA-CR-174839] p 123 N85-21604

LASER WINDOWS
Incident beam polarization for laser Doppler velocimetry employing a sapphire cylindrical window p 122 A85-39835
Incident beam polarization for laser Doppler velocimetry employing a sapphire cylindrical window
[NASA-TM-87064] p 178 N85-28786

LASERS
Hot section laser anemometry p 19 N85-10962

LATERAL CONTROL
Aileron controls for wind turbine applications p 157 A85-45513
Aileron controls for wind turbine applications
[NASA-TM-86867] p 158 N85-11458

LEAD ACID BATTERIES
Results of electric-vehicle propulsion system performance on three lead-acid battery systems p 156 A85-45443

LEADING EDGE SLATS
Calculation of compressible flow about three-dimensional inlets with auxiliary inlets, slats and vanes by means of a panel method
[AIAA PAPER 85-1196] p 5 A85-40817

LEADING EDGES
Progress in development of a Navier-Stokes solver for evaluation of iced airfoil performance
[AIAA PAPER 85-0410] p 3 A85-19731

LEAKAGE
A comparison of flow rates and pressure profiles for N-sequential inlets and three related seal configurations p 109 A85-26526
Analysis of experimental shaft seal data for high-performance turbomachines, as for Space Shuttle main engines
[NASA-TM-86928] p 115 N85-21569

LEAST SQUARES METHOD
Improved models for increasing wind penetration, economics and operating reliability
[NASA-CR-175538] p 160 N85-20545

LENSES
Automatic sphericity interferometer for testing lens radii
[AD-A155736] p 125 N85-33457
LIFE (DURABILITY)
Turbine Engine Hot Section Technology (HOST)
[NASA-TM-83022] p 18 N85-10951
Nonlinear structural and life analyses of a turbine blade p 19 N85-10954
Nonlinear structural and life analyses of a combustor liner p 19 N85-10955
Constitutive model development for isotropic materials p 20 N85-10975
Surface protection overview p 21 N85-10978
Effects of surface chemistry on hot corrosion life: Overview p 21 N85-10980
Reliability considerations for the total strain range version of strainrange partitioning
[NASA-CR-174757] p 144 N85-11380
Engine cyclic durability by analysis and material testing p 25 N85-15744
A study of interdiffusion in beta + gamma/gamma + gamma prime Ni-Cr-Al
[NASA-CR-174852] p 74 N85-20041
Fabrication of ceramic substrate-reinforced and free forms
[NASA-TM-86994] p 50 N85-23926
Effects of surface chemistry on hot corrosion life
[NASA-CR-174915] p 28 N85-26711
Life and reliability modeling of bevel gear reductions
[NASA-TM-87006] p 133 N85-27227
Fatigue life analysis of a turboprop reduction gearbox
[NASA-TM-87014] p 133 N85-27228
Reexamination of cumulative fatigue damage laws p 149 N85-27962
Heat flux sensor calibrator p 41 N85-27970
Feasibility of mapping velocity flow fields in SSME powerhead by laser anemometry techniques p 41 N85-27971
LIFE CYCLE COSTS
Main propulsion system design recommendations for an advanced Orbit Transfer Vehicle
[AIAA PAPER 85-1336] p 36 A85-39730
LIFT
Vortex induced lift on a flat plate with a curved forward-facing flap p 4 A85-30175
Icing flight research - Aerodynamic effects of ice and ice shape documentation with stereo photography
[AIAA PAPER 85-0468] p 11 A85-30192
Observations from varying the lift and drag inputs to a noise prediction method for supersonic helical tip speed propellers
[NASA-TM-83797] p 175 N85-10788
Icing flight research: Aerodynamic effects of ice and ice shape documentation with stereo photography
[NASA-TM-86906] p 12 N85-18049
LIFT DEVICES
Incompressible lifting-surface aerodynamics for a rotor-stator combination
[NASA-TM-83767] p 7 N85-12039
LIGHT EMISSION
Prism-coupled light emission from tunnel junctions p 181 A85-21425
LIGHT SCATTERING
Spray characterization with a nonintrusive technique using absolute scattered light p 120 A85-10036
Research study of droplet sizing technology leading to the development of an advanced droplet sizing system
[NASA-CR-174839] p 123 N85-21604
LIGHT VALVES
Optical computer switching network p 178 A85-23134
LIMNOLOGY
Comparison of atmospheric correction algorithms for the Coastal Zone Color Scanner p 153 A85-10244
LINEAR EQUATIONS
A multiple linear regression analysis of hot corrosion attack on a series of nickel base turbine alloys
[NASA-TM-87020] p 77 N85-31284
LINEAR FILTERS
Linearization of digital derived rate algorithm for use in linear stability analysis
[NASA-TM-87000] p 41 N85-23904
LINEAR TRANSFORMATIONS
Optical linear algebra processors - Noise and error-source modeling p 169 A85-36727
LINEAR VIBRATION
Oscillator response to nonstationary excitation
[ASME PAPER 84-WA/APM-38] p 140 A85-17039
LININGS
Advanced liner-cooling techniques for gas turbine combustors
[AIAA PAPER 85-1290] p 15 A85-39703
Nonlinear structural and life analyses of a combustor liner p 19 N85-10955
Validation of structural analysis methods using the in-house liner cyclic rigs p 21 N85-10987
HOST liner cyclic facilities: Facility description p 22 N85-10988
Advanced liner-cooling techniques for gas turbine combustors
[NASA-TM-86952] p 8 N85-21115
Development of advanced high-temperature heat flux sensors. Phase 2: Verification testing
[NASA-CR-174973] p 126 N85-35391
LIQUID CHROMATOGRAPHY
Rapid estimation of concentration of aromatic classes in middistillate fuels by high-performance liquid chromatography
[NASA-TP-2495] p 93 N85-31307
LIQUID CRYSTALS
Substrate-induced orientational order in the isotropic phase of liquid crystals p 181 A85-24649
LIQUID INJECTION
Vortex generating flow passage design for increased film cooling effectiveness
[NASA-CASE-LEW-14039-1] p 119 N85-33433
LIQUID METALS
Arc spray fabrication of metal matrix composite monotape
[NASA-CASE-LEW-13828-1] p 58 N85-30027
LIQUID PROPELLANT ROCKET ENGINES
Cryogenic upper stage test bed engine
[AIAA PAPER 85-1339] p 44 A85-39733
LIQUID-LIQUID INTERFACES
Free-surface phenomena under low- and zero-gravity conditions
[NASA-CR-175885] p 36 N85-27922
LIQUID-SOLID INTERFACES
The mechanisms of formation and prevention of channel segregation during alloy solidification p 180 A85-18082
Convective influence on the stability of a cylindrical solid-liquid interface p 109 A85-26911
Analysis of three-dimensional solidification interface shape p 109 A85-30075
Control of solidification boundary in continuous casting by asymmetric cooling and mold offset p 110 A85-37047
Dendritic solidification. I - Analysis of current theories and models. II - A model for dendritic growth under an imposed thermal gradient p 182 A85-38019
LITHIUM
Radiation damage and defect behavior in ion-implanted, lithium counterdoped silicon solar cells p 182 A85-35698
Lithium counterdoped silicon solar cell
[NASA-CASE-LEW-14177-1] p 160 N85-20535
The effects of lithium counterdoping on radiation damage and annealing in n(+)p silicon solar cells p 50 N85-22586
LITHIUM SULFUR BATTERIES
Development of a lithium secondary battery separator p 104 N85-31378
LOAD DISTRIBUTION (FORCES)
Extension of constrained incremental Newton-Raphson scheme to generalized loading fields p 139 A85-13942
Gear mesh stiffness and load sharing in planetary gearing
[ASME PAPER 84-DET-229] p 129 A85-33781
LOAD TESTS
Use of statical indentation laws in the impact analysis of laminated composite plates p 55 A85-29133
A study of spectrum fatigue crack propagation in two aluminum alloys. 1: Spectrum simplification
[NASA-TM-86929] p 72 N85-18124
A study of spectrum fatigue crack propagation in two aluminum alloys. 2: Influence of microstructures
[NASA-TM-86930] p 73 N85-18125
Composite loads spectra for select space propulsion structural components p 148 N85-27953
LOADS (FORCES)
Dual clearance squeeze film damper for high load conditions
[ASME PAPER 84-TRIB-7] p 128 A85-32960
Structural analysis p 20 N85-10969
Characterization of lubricated bearing surfaces operated under high loads
[NASA-TM-86964] p 88 N85-21357
Breakway friction and dynamic friction/wear measurements of various ceramic materials from 25 C (75 F) to 650 C (1200 F)
[NASA-CR-174803] p 90 N85-26994
Some advances in experimentation supporting development of viscoplastic constitutive models
[NASA-CR-174855] p 147 N85-27260
Structural Integrity and Durability of Reusable Space Propulsion Systems
[NASA-CP-2381] p 51 N85-27941
Composite loads spectra for select space propulsion structural components: Probabilistic load model development p 148 N85-27954
Dynamic creep buckling: Analysis of shell structures subjected to time-dependent mechanical and thermal loading p 149 N85-27959
A study of the stress wave factor technique for the characterization of composite materials
[NASA-CR-174870] p 58 N85-30035
Some advances in experimentation supporting development of viscoplastic constitutive models p 151 N85-31545
A comparison of smooth specimen and analytical simulation techniques for notched members at elevated temperatures p 151 N85-31546
The design and analysis of single flank transmission error testor for loaded gears
[NASA-CR-176163] p 136 N85-34404
LOSSES
An improved computer model for prediction of axial gas turbine performance losses
[NASA-CR-174246] p 24 N85-15724
Fuel and oxidizer turbine loss analysis p 50 N85-26900
Study of Kapton under simulated shuttle environment
[NASA-CR-176003] p 41 N85-29997
LOSSY MEDIA
Numerical methods for analyzing electromagnetic scattering
[NASA-CR-175507] p 99 N85-21438
Normal modes in an overmoded circular waveguide coated with lossy material
[NASA-CR-176186] p 100 N85-35320
LOUVERS
Pre-HOST high temperature crack propagation p 19 N85-10956
LOW ASPECT RATIO
Study of controlled diffusion stator blading
[NASA-CR-167995] p 25 N85-18058
LOW COST
Replaceable blade turbine and stationary specimen corrosion testing facility
[NASA-TM-86931] p 73 N85-18126
Iron rich low cost superalloys
[NASA-CR-174900] p 76 N85-26962
LOW FREQUENCIES
Design of low loss helix circuits for interference fitted and brazed circuits
[NASA-CR-168313] p 103 N85-19328
Automated testing of developmental satellite communications systems and subsystems
[NASA-TM-87070] p 100 N85-31348
LOW PRESSURE
Energy efficient engine. Low pressure turbine test hardware detailed design report
[NASA-CR-167956] p 22 N85-10994
Nitriding of titanium and its alloys by N2, NH3 or mixtures of N2 + H2 in a dc arc plasma at low pressures (or = to torr)
[NASA-TM-83803] p 131 N85-15168
LOW TEMPERATURE
Detailed studies of aviation fuel flowability
[NASA-CR-174938] p 94 N85-31308
Measurement and correlation of jet fuel viscosities at low temperatures
[NASA-CR-174911] p 94 N85-34295
LOW TEMPERATURE TESTS
Fiberglass epoxy laminate fatigue properties at 300 and 20 K p 56 A85-47970
Effect of low temperature on fatigue and fracture properties of Ti-5Al-2.5Sn(ELI) for use in engine components p 70 A85-47972
LOW THRUST
Small centrifugal pumps for low thrust rockets
[AIAA PAPER 85-1302] p 45 A85-43978
LOW THRUST PROPULSION
Design and analysis report for the RL10-2B breadboard low thrust engine
[NASA-CR-174857] p 48 N85-19020
LOW WEIGHT
Free-surface phenomena under low- and zero-gravity conditions
[NASA-CR-175835] p 116 N85-27168
LUBRICANTS
Fast numerical calculations of EHD sliding traction forces Application to rolling bearings
[ASME PAPER 84-TRIB-26] p 127 A85-21289
Effect of lubricant extreme-pressure additives on surface fatigue life of AISI 9310 spur gears
[NASA-TP-2408] p 130 N85-13234
Effects of silver and group 2 fluorides addition to plasma sprayed chromium carbide high temperature solid lubricant for foil gas bearing to 650 deg C
[NASA-TM-86895] p 84 N85-14928

Contact angle and surface tension measurements of a five-ring polyphenyl ether
[NASA-TM-86927] p 86 N85-15897
Effect of five lubricants on life of AISI 9310 spur gears
[NASA-TP-2419] p 123 N85-16099
Tribological properties of graphite-fiber-reinforced, partially fluorinated polyimide composites
[NASA-TM-86926] p 86 N85-18153
Characterization of lubricated bearing surfaces operated under high loads
[NASA-TM-86964] p 88 N85-21357
Formation of high molecular weight products from benzene during boundary lubrication
[NASA-TM-86966] p 62 N85-22644
Transmission efficiency measurements and correlations with physical characteristics of the lubricant
p 89 N85-23781
Thermal traction contact performance evaluation under fully flooded and starved conditions
[NASA-CR-168173] p 132 N85-25848
Lubricant and additive effects on spur gear fatigue life
[NASA-TM-87044] p 133 N85-28373
Correlation of rheological characteristics of lubricants with transmission efficiency measurements
[NASA-TM-86988] p 134 N85-30342

LUBRICATING OILS
Into mesh lubrication of spur gears with arbitrary offset oil jet. I - For jet velocity less than or equal to gear velocity p 128 A85-24497
The influence of temperature on the lubricating effectiveness of MoS2 dispersed in mineral oils
[ASLE PREPRINT 84-LC-2A-2] p 80 A85-25963
Effect of two inner-ring oil-flow distribution schemes on the operating characteristics of a 35 millimeter bore ball bearing to 2.5 million DN
[NASA-TP-2404] p 130 N85-13233

LUBRICATION
Elastohydrodynamic lubrication of line contacts
p 126 A85-11069
An analysis of temperature effect in a finite journal *bearing with spatial tilt and viscous dissipation*
p 126 A85-11074
Lubricant jet flow phenomena in spur and helical gears with modified center distances and/or addendums - For out-of-mesh conditions
[ASME PAPER 84-DET-96] p 129 A85-35049
Lubricity of well-characterized jet and broad-cut fuels by ball-on-cylinder machine
[NASA-TM-83807] p 92 N85-12183
Development of gas-lubricated pistons for heavy duty diesel engine technology program
[NASA-CR-174746] p 184 N85-12808
Fundamental tribological properties of ceramics
[NASA-TM-86915] p 85 N85-15893
Study of advanced fuel system concepts for commercial aircraft
[NASA-CR-174751] p 12 N85-19978
Tribological systems as applied to aircraft engines
[NASA-TM-86965] p 131 N85-21657
Lubrication and performance of high-speed rolling-element bearings
[NASA-TM-86958] p 131 N85-21658
Development of a multiplane multispeed balancing system for turbine systems
[NASA-CR-174750] p 35 N85-22400
Fast approach for calculating film thicknesses and pressures in elastohydrodynamically lubricated contacts at high loads
[NASA-TM-87032] p 117 N85-30242
Surface roughness effects in elastohydrodynamic contacts
[NASA-TP-2488] p 134 N85-32329
Mechanics of a gaseous film barrier to lubricant wetting of elastohydrodynamically lubricated conjunctions
[NASA-TP-2500] p 135 N85-32330
Lubrication and cooling for high speed gears
[NASA-TM-87096] p 136 N85-34407
Elastohydrodynamic lubrication calculations used as a tool to study scuffing
[NASA-TM-87097] p 137 N85-34408
Design and lubrication of high-speed rolling-element bearings
[NASA-TM-87107] p 137 N85-34409

LUMINANCE
An allpass filter design for luminance and chrominance separation of NTSC signals p 102 A85-28230

LUMINOUS INTENSITY
Research study of droplet sizing technology leading to the development of an advanced droplet sizing system
[NASA-CR-174839] p 123 N85-21604

M

MACH NUMBER
Unsteady flow in a supersonic cascade with two in-passage shocks
[NASA-CR-3925] p 10 N85-35158

MACH-ZEHNDER INTERFEROMETERS
Rainbow schlieren vs Mach-Zehnder interferometer - A comparison p 121 A85-28820

MACHINE TOOLS
Spiral bevel and circular arc helical gears: Tooth contact analysis and the effect of misalignment on circular arc helical gears
[NASA-TM-87013] p 32 N85-31060
Generated spiral bevel gears: Optimal machine-tool settings and tooth contact analysis
[NASA-TM-87075] p 136 N85-34405

MAGNESIUM
Magnesium doping of efficient GaAs and Ga(0.75)In(0.25)As solar cells grown by metalorganic chemical vapor deposition p 180 A85-11466
Select fiber composites for space applications - A mechanistic assessment p 54 A85-16040
Universal binding energy relations in metallic adhesion
[NASA-TM-86889] p 72 N85-12132

MAGNESIUM OXIDES
Surface effects of corrosive media on hardness, friction, and wear of materials
[NASA-TM-83711] p 85 N85-15896

MAGNETIC FIELD CONFIGURATIONS
High frequency plasma generator for ion thrusters
[NASA-CR-174772] p 48 N85-17023

MAGNETIC FLUX
Dilute plasma coupling currents to a high voltage solar array in weak magnetic fields p 46 A85-45388

MAGNETIC PROPERTIES
Effects of wear on structure-sensitive magnetic properties of ceramic ferrite in contact with magnetic tape
[NASA-TM-87007] p 90 N85-26991

MAGNETIC RESONANCE
Analysis of glow discharges for understanding the process of film formation
[NASA-TM-83750] p 62 N85-10138

MAGNETIC TAPES
Humidity effects on adhesion of nickel-zinc ferrite in elastic contact with magnetic tape and itself
[NASA-TP-2449] p 88 N85-21359
Effects of wear on structure-sensitive magnetic properties of ceramic ferrite in contact with magnetic tape
[NASA-TM-87007] p 90 N85-26991

MAGNETIZATION
Development of high frequency low weight power magnetics for aerospace power systems
p 102 A85-45373

MAGNETOHYDRODYNAMIC GENERATORS
Parametric study of potential early commercial power plants Task 3-A MHD cost analysis
[NASA-CR-175839] p 161 N85-27377

MAGNETOHYDRODYNAMIC STABILITY
Discharges on a negatively biased solar cell array in a charged-particle environment *p 160 N85-22499*

MAN MACHINE SYSTEMS
MERIT: A man/computer data management and enhancement system for upper air nowcasting/forecasting in the United States --- Minimum Energy Routes using Interactive Techniques (MERIT) p 167 N85-10558

MANNED SPACECRAFT
A historical overview of the electrical power systems in the US manned and some US unmanned spacecraft
[NASA-CR-174806] p 47 N85-13910

MANUFACTURING
Manufacturing process to reduce large grain growth in *zirconium alloys*
[DE85-011649] p 78 N85-34267

MARTENSITIC STAINLESS STEELS
Deposition of silicon nitride from SiCl4 and NH3 in a low pressure RF plasma p 81 A85-36229

MASERS
Technology for satellite power conversion
[NASA-CR-174335] p 159 N85-18451

MASS SPECTRA
Nitriding of titanium and its alloys by N2, NH3 or mixtures of N2 + H2 in a dc arc plasma at low pressures (or = to torr)
[NASA-TM-83803] p 131 N85-15168
Mass analysis of neutral particles and ions released during electrical breakdowns on spacecraft surfaces
[NASA-CR-175585] p 39 N85-21250

MASS SPECTROMETERS
Mass spectra of neutral particles released during electrical breakdown of thin polymer films
p 88 N85-22511

MASS TRANSFER
Density effects on jet characteristics in confined swirling flow p 112 A85-45283
Turbulent transport and length scale measurement experiments with comfined coaxial jets
[NASA-CR-174831] p 117 N85-30245

MATERIALS SCIENCE
Research and technology highlights of the Lewis *Research Center*
[NASA-TM-86899] p 186 N85-17928

MATHEMATICAL MODELS
Identification of multivariable high-performance turbofan engine dynamics from closed-loop data
p 13 A85-13630
Modeling of gamma/gamma-prime phase equilibrium in the nickel-aluminum system p 65 A85-14959
Vortex modeling of single and multiple dilution jet mixing in a crossflow
[AIAA PAPER 85-1580] p 111 A85-40701
Constitutive modeling and computational implementation for finite strain plasticity
p 143 A85-40910
Comparison of free-piston Stirling engine model predictions with RE1000 engine test data
p 130 A85-45488
A study of Reynolds-stress closure model
[NASA-CR-174342] p 114 N85-17324
Analysis of shell type structures subjected to time dependent mechanical and thermal loading
[NASA-CR-175747] p 147 N85-25896
Composite loads spectra for select space propulsion structural components: Probabilistic load model development p 148 N85-27954
Turbulent transport and length scale measurement experiments with comfined coaxial jets
[NASA-CR-174831] p 117 N85-30245
Numerical considerations in the development and implementation of constitutive models
p 151 N85-31541
On numerical integration and computer implementation of viscoplastic models p 151 N85-31542
A continuous damage model based on stepwise-stress *creep rupture tests*
[NASA-CR-174941] p 152 N85-32341
Component-specific modeling
[NASA-CR-174765] p 33 N85-34140

MATHEMATICAL PROGRAMMING
Structural optimization using optimality criteria methods p 144 A85-48703

MATRIX MATERIALS
Resin selection criteria for 'tough' composite structures p 81 A85-35139
High performance fibers for structurally reliable metal and ceramic composites --- advanced gas turbine engine materials
[NASA-TM-86878] p 56 N85-12095
Chemical approach for controlling nadimide cure temperature and rate with maleimide
[NASA-CASE-LEW-13770-3] p 87 N85-21350
Chemical approach for controlling nadimide cure temperature and rate with maleimide
[NASA-CASE-LEW-13770-4] p 87 N85-21351
Chemical approach for controlling nadimide cure temperature and rate
[NASA-CASE-LEW-13770-6] p 63 N85-30039
Apparatus and method for identification of matrix materials in which transuranic elements are embedded using thermal neutron capture gamma-ray emission
[DE85-011659] p 125 N85-33454
Mechanical properties of SiC fiber-reinforced reaction-bonded Si3N4 composites
[NASA-TM-87085] p 59 N85-34223

MATRIX METHODS
Analysis of hourglass instabilities and control in underintegrated finite element methods
p 139 A85-11125

MEASURING INSTRUMENTS
Comparison of icing cloud instruments for 1982-1983 icing season flight program
[AIAA PAPER 84-0020] p 13 A85-16098
High temperature thermocouple and heat flux gauge using a unique thin film-hardware hot juncture
[NASA-TM-86898] p 123 N85-16096
Advanced smoke meter development survey and *analysis*
[NASA-CR-168287] p 124 N85-25792
Free-surface phenomena under low- and zero-gravity conditions
[NASA-CR-175835] p 116 N85-27168
Development of advanced high-temperature heat flux sensors. Phase 2: Verification testing
[NASA-CR-174973] p 126 N85-35391

MECHANICAL DEVICES
Apparatus for mounting a field emission cathode
[NASA-CASE-LEW-14108-1] p 104 N85-29149

MECHANICAL DRIVES
Thermal traction contact performance evaluation under fully flooded and starved conditions
[NASA-CR-168173] p 132 N85-25848
Application of traction drives as servo mechanisms
p 152 N85-33520
MECHANICAL OSCILLATORS
Oscillator response to nonstationary excitation
[ASME PAPER 84-WA/APM-38] p 140 A85-17039
MECHANICAL PROPERTIES
ICAN - Integrated composites analyzer
[AIAA PAPER 84-0974] p 54 A85-16094
Effects of cobalt on the hot workability of nickel-base superalloys p 67 A85-32412
Analysis of stress-strain, fracture, and ductility behavior of aluminum maxtrix composites containing discontinuous silicon carbide reinforcement p 55 A85-37421
Quasi-static solution algorithms for kinematically/materially nonlinear thermomechanical problems p 143 A85-41983
Evaluation of alpha-SiC sintering using statistical methods p 83 A85-42800
Diffusion welding of MA 6000 and a conventional nickel-base superalloy p 69 A85-43551
Microstructure of reaction-bonded silicon nitride consolidated by isostatic hot-pressing
p 83 A85-45304
Effect of hot isostatic pressing on the properties of sintered alpha silicon carbide p 83 A85-48757
Ultrasonic nondestructive evaluation, microstructure, and mechanical property interrelations
[NASA-TM-86876] p 137 N85-10371
Effect of substituted phenylnadimides on processing and properties of PMR polyimide composites
[NASA-TM-86902] p 85 N85-14929
Effect of reduction of strategic Columbium addition in 718 Alloy on the structure and properties
[NASA-CR-174841] p 75 N85-21320
Effects of chromium and aluminum on mechanical and oxidation properties of iron-nickel-base superalloys based on CG-27
[NASA-TP-2443] p 75 N85-21323
Extreme precision antenna reflector study results
p 165 N85-23830
Mechanical protection of DLC films on fused silica slides
[NASA-TM-87056] p 91 N85-30138
Mechanical properties of SiC fiber-reinforced reaction-bonded Si3N4 composites
[NASA-TM-87085] p 59 N85-34223
Generated spiral bevel gears: Optimal machine-tool settings and tooth contact analysis
[NASA-TM-87075] p 136 N85-34405
MELT SPINNING
Rapidly solidified NiAl and FeAl
[NASA-TM-86941] p 74 N85-20042
Microstructures in rapidly solidified Ni-Mo alloys
[NASA-TM-87100] p 78 N85-34266
MELTING POINTS
Study of advanced fuel system concepts for commercial aircraft and engines
[NASA-CR-174752] p 93 N85-19176
Jet fuel property changes and their effect on producibility and cost in the U.S., Canada, and Europe
[NASA-CR-174840] p 93 N85-27012
Measurement and correlation of jet fuel viscosities at low temperatures
[NASA-CR-174911] p 94 N85-34295
MELTS (CRYSTAL GROWTH)
The mechanisms of formation and prevention of channel segregation during alloy solidification
p 180 A85-18082
MEMBRANE STRUCTURES
Evaluation of developmental membranes for the mixed reactant iron-chromium redox system
[NASA-TM-87074] p 164 N85-34443
MENISCI
Advanced radiator concepts
[NASA-TM-87008] p 115 N85-24245
MERCURY CADMIUM TELLURIDES
Mosaic Infrared Sensor for Space Astronomy (MIRSSA)
[NASA-CR-176154] p 125 N85-33456
MERCURY ION ENGINES
IAPS (8-cm) ion thruster cyclic endurance test --- Ion Auxiliary Propulsion System p 42 A85-16406
Ring-cusp ion thrusters p 42 A85-16438
Ion thruster system (8-cm) cyclic endurance test
[NASA-CR-174745] p 47 N85-12937
MESH
Into mesh lubrication of spur gears with arbitrary offset oil jet. I - For jet velocity less than or equal to gear velocity p 128 A85-24497
Flow through very porous inclined screens
[AIAA PAPER 85-1650] p 111 A85-40750
Flow through very porous inclined screens
[NASA-TM-86979] p 116 N85-25761
METAL BONDING
Advanced thermal barrier system bond coatings for use on Ni, Co-, and Fe-base alloy substrates
[NASA-TM-87062] p 77 N85-31283
METAL COATINGS
Effects of MAR-M247 substrate (modified) composition on coating oxidation coating/substrate interdiffusion --- protective coatings for hot section components of gas turbine engines
[NASA-CR-174851] p 73 N85-19073
The role of silver in self-lubricating coatings for use at extreme temperatures
[NASA-TM-86943] p 87 N85-20127
Metallic and metalloceramic coating by thermal decomposition
[NASA-TM-86992] p 88 N85-22755
Film and interstitial formation of metals in plasma-sprayed ceramics
[NASA-TM-86993] p 89 N85-22756
Effects of surface chemistry on hot corrosion life
[NASA-CR-174915] p 28 N85-26711
METAL CRYSTALS
Deformation and erosion of f.c.c. metals and alloys under cavitation attack p 65 A85-12789
Dendritic solidification. III - Some further refinements to the model for dendritic growth under an imposed thermal gradient p 69 A85-44703
METAL FATIGUE
Strainrange partitioning - A total strain range version --- for creep fatigue life prediction by summing inelastic and elastic strain-range-life relations for two Ni base superalloys p 64 A85-11603
A history dependent damage model for low cycle fatigue
[ASME PAPER 84-PVP-112] p 140 A85-18795
The effect of microstructure, temperature, and hold-time on low-cycle fatigue of As HIP P/M Rene 95
p 67 A85-32399
The influence of hold times on LCF and FCG behavior in a P/M Ni-base superalloy --- Low Cycle Fatigue/Fatigue Crack Growth p 67 A85-32400
Effect of low temperature on fatigue and fracture properties of Ti-5Al-2.5Sn(ELI) for use in engine components p 70 A85-47972
Reliability considerations for the total strain range version of strainrange partitioning
[NASA-CR-174757] p 144 N85-11380
Thermal-mechanical fatigue crack growth in Inconel X-750
[NASA-CR-174740] p 72 N85-15877
A study of spectrum fatigue crack propagation in two aluminum alloys. 1: Spectrum simplification
[NASA-TM-86929] p 72 N85-18124
A study of spectrum fatigue crack propagation in two aluminum alloys. 2: Influence of microstructures
[NASA-TM-86930] p 73 N85-18125
METAL FILMS
Effect of Interfacial characteristics of metal clad polymeric substrates on electrical high frequency interconnection performance
[NASA-TM-86948] p 99 N85-20223
METAL MATRIX COMPOSITES
Analysis of stress-strain, fracture, and ductility behavior of aluminum maxtrix composites containing discontinuous silicon carbide reinforcement p 55 A85-37421
High temperature metal and ceramic composites
p 55 A85-37483
Fibers for structurally reliable metal and ceramic composites p 55 A85-37484
High performance fibers for structurally reliable metal and ceramic composites --- advanced gas turbine engine materials
[NASA-TM-86878] p 56 N85-12095
Nonlinear structural analysis for fiber-reinforced superalloy turbine blades p 147 N85-26887
Arc spray fabrication of metal matrix composite monotape
[NASA-CASE-LEW-13828-1] p 58 N85-30027
METAL OXIDES
Thermal barrier coating system
[NASA-CASE-LEW-13324-2] p 57 N85-21266
Molecular orbital studies in oxidation: Sulfate formation and metal-metal oxide adhesion
[NASA-CR-176070] p 77 N85-32174
METAL POWDER
Rapid solidification and dynamic compaction of Ni-base superalloy powders p 67 A85-32414
A new interpretation of internal heat transfer coefficients of porous media
[ASME PAPER 84-WA/HT-51] p 110 A85-39894
Powder metallurgy forged gear development
[NASA-TM-87483] p 134 N85-29295
METAL SHELLS
Dynamic creep buckling: Analysis of shell structures subjected to time-dependent mechanical and thermal loading p 149 N85-27959
METAL SURFACES
Surface hardening of steel by boriding in a cold rf plasma p 68 A85-40275
Cone formation as a result of whisker growth on ion bombarded metal surfaces p 182 A85-41635
Effect of surface configuration during solid particle impingement erosion p 69 A85-42568
Characterization of solid particle erosion resistance of ductile metals based on their properties
p 69 A85-42569
Surface effects of corrosive media on hardness, friction, and wear of materials
[NASA-TM-83711] p 85 N85-15896
Characterization of erosion of metallic materials under cavitation attack in a mineral oil
[NASA-TM-86934] p 74 N85-19075
Mass analysis of neutral particles and ions released during electrical breakdowns on spacecraft surfaces
[NASA-CR-175585] p 39 N85-21250
Ion-beam nitriding of steels
[NASA-CASE-LEW-14104-1] p 75 N85-21324
Study of the effects of implantation on the high Fe-Ni-Cr and Ni-Cr-Al alloys
[NASA-CR-175625] p 76 N85-22661
Why CO bonds side-on at low coverage and both side-on and upright at high coverage on the Cr(110) surface
[NASA-CR-176071] p 77 N85-32173
METAL VAPORS
Metal vapor arc switch electromagnetic accelerator technology
[NASA-CR-174380] p 103 N85-18259
METAL WORKING
Thermomechanical deformation in the presence of metallurgical changes p 150 N85-31533
METAL-METAL BONDING
Molecular orbital studies in oxidation: Sulfate formation and metal-metal oxide adhesion
[NASA-CR-176070] p 77 N85-32174
METALLIC GLASSES
Friction and wear of some ferrous-base metallic glasses p 64 A85-11071
Mechanical-contact-induced transformation from the amorphous to the partially crystalline state in metallic glass p 65 A85-19084
METALLOGRAPHY
Properties and microstructures for dual alloy combinations of three superalloys with alloy 901
[NASA-TM-86987] p 76 N85-26963
METALS
Universal binding energy relations in metallic adhesion
[NASA-TM-86889] p 72 N85-12132
Effect of humidity on fretting wear of several pure metals
[NASA-TP-2403] p 72 N85-13006
Effect of barrier height on friction behavior of the semiconductors silicon and gallium arsenide in contact with pure metals
[NASA-TP-2405] p 84 N85-13044
Characterization of erosion of metallic materials under cavitation attack in a mineral oil
[NASA-TM-86934] p 74 N85-19075
Monte Carlo lattice models for adsorbed polymer conformation
[NASA-TP-2453] p 183 N85-24961
On the use of internal state variables in thermoviscoplastic constitutive equations
p 150 N85-31536
On numerical integration and computer implementation of viscoplastic models p 151 N85-31542
METEOROLOGICAL FLIGHT
A comparison of NMC and GWC analysis field temperatures with aircraft measurements
p 166 A85-21140
METEOROLOGICAL SERVICES
GASP cloud encounter statistics - Implications for laminar flow control flight p 166 A85-11979
METHANE
Systematic optimization of a detailed kinetic model using a methane ignition example p 59 A85-12890
Effect of gravity on halogenated hydrocarbon flame retardant effectiveness
[IAF PAPER 84-156] p 61 A85-23199
Plasma deposited hydrogenated carbon on GaAs and InP p 182 A85-40386
Plasma deposited diamondlike carbon on GaAs and InP
[NASA-TM-86870] p 183 N85-10844
The structure of dilute combusting sprays
[NASA-CR-174838] p 24 N85-15728
Optical properties of hydrogenated amorphous carbon films grown from methane plasma
[NASA-TM-86995] p 183 N85-26406

METHYL ALCOHOLS
Methanol as a soot reducer in a turbulent swirling burner
[ASME PAPER 84-JPGC-GT-2] p 61 A85-23192
METHYL CHLOROSILANES
A morphological study of silicon carbide prepared by chemical vapor deposition p 79 A85-20938
MICROCOMPUTERS
Data flow methods for dynamic system simulation - A CSSL-IV microcomputer network interface p 170 A85-28614
Floating-point function generation routines for 16-bit microcomputers
[NASA-TM-83783] p 170 N85-10683
MINDS: A microcomputer interactive data system for 8086-based controllers
[NASA-TP-2378] p 170 N85-17576
MICROCRACKS
Fundamentals of microcrack nucleation mechanics
[NASA-CR-3851] p 137 N85-16195
Experimental and analytical study of ceramic-coated turbine-tip shroud seals for small turbine engines
[NASA-TM-86881] p 25 N85-18057
MICROHARDNESS
Nitriding of titanium and its alloys by N2, NH3 or mixtures of N2 + H2 in a dc arc plasma at low pressures (or = to torr)
[NASA-TM-83803] p 131 N85-15168
Surface effects of corrosive media on hardness, friction, and wear of materials
[NASA-TM-83711] p 85 N85-15896
Ion-beam nitriding of steels
[NASA-CASE-LEW-14104-1] p 75 N85-21324
Frictional and structural characterization of ion-nitrided low and high chromium steels
[NASA-TM-86991] p 132 N85-23085
MICROPROCESSORS
A functional language approach in high-speed digital simulation p 170 A85-28615
Microprocessor control of photovoltaic systems p 156 A85-45408
A generalized computer code for developing dynamic gas turbine engine models (DIGTEM) p 17 A85-49021
Fiber optic, Fabry-Perot high temperature sensor
[NASA-CR-174712] p 178 N85-13594
Design description of a microprocessor based Engine Monitoring and Control unit (EMAC) for small turboshaft
[NASA-TM-86860] p 1 N85-17935
MICROSCOPY
A micrographic and gravimetric study of intercalation and deintercalation of graphite fibers
[NASA-TM-87026] p 91 N85-28110
MICROSTRIP TRANSMISSION LINES
The study of microstrip antenna arrays and related problems
[NASA-CR-174054] p 97 N85-11265
Effect of Interfacial characteristics of metal clad polymeric substrates on electrical high frequency interconnection performance
[NASA-TM-86948] p 99 N85-20223
An experimental investigation of microstrip properties on soft substrates from 2 to 40 GHz
[NASA-TM-86961] p 99 N85-20224
Perturbation-iteration theory for analyzing microwave striplines
[NASA-CR-176189] p 100 N85-35321
Characterization of microstrip discontinuities in the time and frequency domains
[NASA-CR-176190] p 106 N85-35342
MICROSTRUCTURE
Frictional and morphological properties of Au-MoS2 films sputtered from a compact target p 127 A85-19085
Strength and microstructure of sintered Si3N4 with rare-earth-oxide additions
[ACS PAPER 130-13-84] p 80 A85-25271
Ductility in rapidly solidified NiAl p 66 A85-26158
Influence of composition on the microstructure and mechanical properties of a nickel-base superalloy single crystal p 66 A85-32387
Feasibility study of the welding of SiC p 81 A85-39339
Ceramic microstructure and adhesion p 82 A85-40384
The role of the reflection coefficient in precision measurement of ultrasonic attenuation p 137 A85-42151
Microstructure of reaction-bonded silicon nitride consolidated by isostatic hot-pressing p 83 A85-45304
Effects of cobalt, boron, and zirconium on the microstructure of Udimet 738
[NASA-CR-174762] p 70 N85-10166
The effects of seven alloying elements on the microstructure and stress-rupture behavior of nickle-base superalloys
[NASA-TM-83791] p 70 N85-10168
Ceramic microstructure and adhesion
[NASA-TM-83804] p 83 N85-10186
Ultrasonic nondestructive evaluation, microstructure, and mechanical property interrelations
[NASA-TM-86876] p 137 N85-10371
Effects of tin on microstructure and mechanical behavior of Inconel 718
[NASA-TM-86866] p 71 N85-12129
Fundamentals of microcrack nucleation mechanics
[NASA-CR-3851] p 137 N85-16195
A study of spectrum fatigue crack propagation in two aluminum alloys. 2: Influence of microstructures
[NASA-TM-86930] p 73 N85-18125
The effect of tantalum on the structure/properties of two polycrystalline nickel-base superalloys: B-1900 + Hf MAR-M247
[NASA-CR-174847] p 73 N85-18127
Creep-rupture behavior of iron superalloys in high-pressure hydrogen
[NASA-CR-174411] p 74 N85-19078
Effect of reduction of strategic Columbium addition in 718 Alloy on the structure and properties
[NASA-CR-174841] p 75 N85-21320
Properties and microstructures for dual alloy combinations of three superalloys with alloy 901
[NASA-TM-86987] p 76 N85-26963
Manufacturing process to reduce large grain growth in zirconium alloys
[DE85-011649] p 78 N85-34267
MICROWAVE AMPLIFIERS
A 20 GHz, 75 watt, helix TWT for space communications p 101 A85-14433
MICROWAVE ANTENNAS
Advanced 30/20 GHz multiple beam antenna for future communications satellites p 96 A85-14436
Characterization of MMIC devices for active array antennas
[NASA-TM-86907] p 38 N85-15779
The 20 GHz proof-of-concept test model results for a multiple scan beam dual reflector antenna
[NASA-CR-174268] p 98 N85-15944
MICROWAVE CIRCUITS
Characterization of MMIC devices for active array antennas
[NASA-TM-86907] p 38 N85-15779
Configuration study for a 30 GHz monolithic receive array, volume 1
[NASA-CR-174697-VOL-1] p 98 N85-18239
MICROWAVE EQUIPMENT
Status of NASA's multibeam communications technology program p 100 A85-14432
Experiments with a microwave electrothermal thruster concept p 42 A85-16441
Measurements of energy distribution in microwave plasmas of N2 and He and comparisons with results for H2 p 178 A85-16443
MICROWAVE OSCILLATORS
The energetics of hydrogen atom recombination - Analysis, experiments, and modeling --- in electrothermal propulsion system p 179 A85-16444
MICROWAVE PLASMA PROBES
Recent work on a microwave ion source p 179 A85-16455
Experimental performance of a microwave cavity plasma disk ion source p 179 A85-43552
MICROWAVE SWITCHING
The NASA satellite communication 20 x 20 matrix switches p 101 A85-14435
MICROWAVE TRANSMISSION
Plot of modal field distribution in rectangular and circular waveguides p 101 A85-25170
Modeling of NASA's 30/20 GHz satellite communications system p 38 A85-36663
Perturbation-iteration theory for analyzing microwave striplines
[NASA-CR-176189] p 100 N85-35321
MICROWAVES
Laboratory degradation of Kapton in a low energy oxygen ion beam
[AIAA PAPER 83-2658] p 78 A85-10675
Effect of Interfacial characteristics of metal clad polymeric substrates on electrical high frequency interconnection performance
[NASA-TM-86948] p 99 N85-20223
Precision tunable resonant microwave cavity
[NASA-CASE-LEW-13935-1] p 103 N85-20248
MIE SCATTERING
Fast laser-induced aerosol formation for visualization of gas flows p 121 A85-31113
MILLIMETER WAVES
MMIC devices for active phased array antennas
[NASA-CR-174281] p 98 N85-15943
MILLING (MACHINING)
Factors influencing the ball milling of Si3N4 in water
[NASA-TM-86932] p 86 N85-19136
Parametric evaluation of ball milling of SiC in water
[NASA-TM-86974] p 88 N85-21356
MILLING MACHINES
Demonstration of a silicon nitride attrition mill for production of fine pure Si and Si3N4 powders p 78 A85-10825
MIM (SEMICONDUCTORS)
Dielectric properties of 'diamondlike' carbon prepared by RF plasma deposition p 182 A85-38192
MINERAL OILS
The influence of temperature on the lubricating effectiveness of MoS2 dispersed in mineral oils
[ASLE PREPRINT 84-LC-2A-2] p 80 A85-25963
Characterization of erosion of metallic materials under cavitation attack in a mineral oil
[NASA-TM-86934] p 74 N85-19075
MISSION PLANNING
Missions/planning panel p 36 N85-13886
Tethered nuclear power for the Space Station
[NASA-TM-87023] p 51 N85-26912
Component-specific modeling
[NASA-CR-174765] p 147 N85-27261
MIXED OXIDES
Plastic flow of plasma sprayed ceramics p 80 A85-24161
MIXERS
Three-dimensional inviscid flow analysis of turbofan forced mixers
[AIAA PAPER 85-0086] p 2 A85-19510
MODELS
Effects of surface chemistry on hot corrosion life: Overview p 21 N85-10980
Three-dimensional calculation of shuttle charging in polar orbit p 40 N85-22486
Composite loads spectra for select space propulsion structural components p 148 N85-27953
Comparative analysis of operational forecasts versus actual weather conditions in airline flight planning, volume 2
[NASA-CR-167863] p 167 N85-35535
Comparative analysis of operational forecasts versus actual weather conditions in airline flight planning: Summary report
[NASA-CR-167866] p 168 N85-35538
MODULES
Operating characteristics of a 0.87 kW-hr flywheel energy storage module
[NASA-TM-87038] p 133 N85-28371
MODULUS OF ELASTICITY
Spherical microglass particle impingement studies of thermoplastic materials at normal incidence p 79 A85-11072
Transformation toughened ceramics for the heavy duty diesel engine technology program
[NASA-CR-174689] p 185 N85-16698
Rolling, slip and traction measurements on low modulus materials
[NASA-CR-174909] p 135 N85-33491
MOIRE EFFECTS
A comparison of electronic heterodyne moire deflectometry and electronic heterodyne holographic interferometry for flow measurements
[NASA-TM-87071] p 125 N85-32302
MOIRE FRINGES
Electronic heterodyne readout of fringes in moire deflectometry p 122 A85-36726
Moire deflectometry with deferred electronic heterodyne readout p 122 A85-42854
MOLECULAR BEAM EPITAXY
Sixty GHz IMPATT diode development
[NASA-CR-174969] p 105 N85-33293
MOLECULAR ORBITALS
Mechanism for chelated sulfate formation from SO2 and bis (triphenylphosphine) platinum p 62 A85-48493
Mechanism for forming hydrogen chloride and sodium sulfate from sulfur trioxide, water, and sodium chloride p 62 A85-48513
Why CO bonds side-on at low coverage and both side-on and upright at high coverage on the Cr(110) surface
[NASA-CR-176071] p 77 N85-32173
Molecular orbital studies in oxidation: Sulfate formation and metal-metal oxide adhesion
[NASA-CR-176070] p 77 N85-32174
MOLECULAR SPECTRA
Mass analysis of neutral particles and ions released during electrical breakdowns on spacecraft surfaces
[NASA-CR-175585] p 39 N85-21250
MOLTEN SALT ELECTROLYTES
Moderate temperature sodium cells. V - Discharge reactions and rechargeability of NiS and NiS2 positive electrodes in molten NaAlCl4 p 59 A85-11892
MOLTEN SALTS
Mechanism of strength degradation for hot corrosion of alpha-SiC
[NASA-TM-87052] p 91 N85-30135

MOLYBDENUM ALLOYS
Deformation and fracture behavior of Ni-Mo-Al(gamma/gamma prime-alpha) in situ composite p 64 A85-11058
Microstructures in rapidly solidified Ni-Mo alloys [NASA-TM-87100] p 78 N85-34266
MOLYBDENUM DISULFIDES
Frictional and morphological properties of Au-MoS2 films sputtered from a compact target p 127 A85-19085
The influence of temperature on the lubricating effectiveness of MoS2 dispersed in mineral oils [ASLE PREPRINT 84-LC-2A-2] p 80 A85-25963
MOM (SEMICONDUCTORS)
Prism-coupled light emission from tunnel junctions p 181 A85-21425
MONITORS
Design description of a microprocessor based Engine Monitoring and Control unit (EMAC) for small turboshaft [NASA-TM-86860] p 1 N85-17935
Reusable rocket engine turbopump condition monitoring p 51 N85-26907
MONOMERS
PMR polyimide composites for aerospace applications — Polymerization of Monomer Reactants p 55 A85-21520
Graphite/PMR polyimide composites with improved toughness [NASA-TM-87081] p 58 N85-32148
MONTE CARLO METHOD
Monte Carlo study of reversible growth of clusters on a surface p 182 A85-48516
Monte Carlo lattice models for adsorbed polymer conformation [NASA-TP-2453] p 183 N85-24961
MORPHOLOGY
Frictional and morphological properties of Au-MoS2 films sputtered from a compact target p 127 A85-19085
Morphological changes of gamma prime precipitates in nickel-base superalloy single crystals [NASA-TM-83698] p 70 N85-10165
Tribological properties of graphite-fiber-reinforced, partially fluorinated polyimide composites [NASA-TM-86926] p 86 N85-18153
Percutaneous connectors [NASA-CR-175627] p 168 N85-27508
The structure of ion plated films in relation to coating properties [NASA-TM-87055] p 95 N85-29085
MOSAICS
Mosaic Infrared Sensor for Space Astronomy (MIRSSA) [NASA-CR-176154] p 125 N85-33456
MOTION STABILITY
Linearization of digital derived rate algorithm for use in linear stability analysis [NASA-TM-87000] p 41 N85-23904
MOVING TARGET INDICATORS
Moving target, distributed, real-time simulation using Ada p 170 A85-34131
MULLITES
Transformation toughened ceramics for the heavy duty diesel engine technology program [NASA-CR-174689] p 185 N85-16698
MULTIBEAM ANTENNAS
Status of NASA's multibeam communications technology program p 100 A85-14432
Advanced 30/20 GHz multiple beam antenna for future communications satellites p 96 A85-14436
A frequency-routed satellite system concept using multiple orthogonally-polarized beams for frequency reuse p 97 A85-34470
Configuration study for a 30 GHz monolithic receive array: Technical assessment [NASA-CR-174697] p 98 N85-18238
Configuration study for a 30 GHz monolithic receive array, volume 1 [NASA-CR-174697-VOL-1] p 98 N85-18239
MULTIPLE BEAM INTERVAL SCANNERS
The 20 GHz proof-of-concept test model results for a multiple scan beam dual reflector antenna [NASA-CR-174268] p 98 N85-15944
MULTIPROCESSING (COMPUTERS)
A functional language approach in high-speed digital simulation p 170 A85-28615
Hardware for a real-time multiprocessor simulator [NASA-TM-83805] p 169 N85-10659
Operating system for a real-time multiprocessor propulsion system simulator. User's manual [NASA-TP-2426] p 171 N85-17596
Real-Time Multiprocessor Programming Language (RTMPL) user's manual [NASA-TP-2422] p 170 N85-28610
MULTIVARIATE STATISTICAL ANALYSIS
Identification of multivariable high-performance turbofan engine dynamics from closed-loop data p 13 A85-13630

N

N-TYPE SEMICONDUCTORS
Heat treatment of bulk gallium arsenide using a phosphosilicate glass cap p 181 A85-32636
Fabrication of p(+)-n junction GaAs solar cells by a novel method p 181 A85-33645
NACELLES
Electro-impulse de-icing of a turbofan engine inlet [AIAA PAPER 85-1118] p 12 A85-40811
Energy efficient engine ICLS Nacelle detail design report [NASA-CR-167870] p 22 N85-10993
NASA PROGRAMS
Status of NASA's multibeam communications technology program p 100 A85-14432
Analytical and physical modeling program for the NASA Lewis Research Center's Altitude Wind Tunnel (AWT) [AIAA PAPER 85-0379] p 34 A85-19709
Overview of NASA Lewis Research Center free-piston Stirling engine activities p 130 A85-45479
Bibliography of Lewis Research Center technical publications announced in 1983 [NASA-TM-83693] p 184 N85-22255
NATURAL GAS
Combustion gas properties. 2: Natural gas fuel and dry air [NASA-TP-2435] p 26 N85-21168
NAVIER-STOKES EQUATION
Development of finite analytic method for unsteady three-dimensional Navier-Stokes equation p 106 A85-11647
Efficient solution of the Euler and Navier-Stokes equations with a vectorized multiple-grid algorithm p 2 A85-18679
Accelerated convergence for incompressible flow calculations [AIAA PAPER 85-0058] p 2 A85-19489
A space-marching method for incompressible Navier-Stokes equations [AIAA PAPER 85-0170] p 108 A85-19564
Progress in development of a Navier-Stokes solver for evaluation of iced airfoil performance [AIAA PAPER 85-0410] p 3 A85-19731
Assessment of discretization schemes to reduce numerical diffusion in the calculation of complex flows [AIAA PAPER 85-0441] p 108 A85-19751
Application of computational fluid dynamics to complex inlet ducts [AIAA PAPER 85-1213] p 6 A85-47023
Accelerated convergence for incompressible flow calculations [NASA-TM-86863] p 18 N85-10949
Model equation for simulating flows in multistage turbomachinery [NASA-TM-86869] p 7 N85-12036
Reducing numerical diffusion for incompressible flow calculations [NASA-TM-83621] p 24 N85-14840
Researched applied to transonic compressors in numerical fluid mechanics of inviscid flow and viscous flow [NASA-CR-174353] p 114 N85-18291
Application of computational fluid dynamics to complex inlet ducts [NASA-TM-87060] p 118 N85-30247
Turbulent solutions of equations of fluid motion p 118 N85-31441
NEAR FIELDS
On stress field near a stationary crack tip [AD-A152863] p 141 A85-24532
Case study of sample spacing in planar near-field measurement of high gain antennas [NASA-TM-86872] p 97 N85-10234
NEGATIVE CONDUCTANCE
Circuit transients due to negative bias arcs on a high-voltage solar array in low Earth orbit [NASA-TP-2407] p 39 N85-14858
NEODYMIUM LASERS
Laser balancing system for high material removal rates [NASA-CR-174731] p 126 N85-12341
NETWORK ANALYSIS
Small-signal model for the series resonant converter p 102 A85-39453
The J3 SCR model applied to resonant converter simulation p 102 A85-42156
NETWORK CONTROL
Optical computer switching network p 178 A85-23134
A frequency-routed satellite system concept using multiple orthogonally-polarized beams for frequency reuse p 97 A85-34470
NETWORK SYNTHESIS
Bipolar-FET combinational power transistors for power conversion applications p 100 A85-12669
The NASA satellite communication 20 x 20 matrix switches p 101 A85-14435
NEUTRAL PARTICLES
Mass analysis of neutral particles and ions released during electrical breakdowns on spacecraft surfaces [NASA-CR-175585] p 39 N85-21250
Mass spectra of neutral particles released during electrical breakdown of thin polymer films p 88 N85-22511
NEUTRON EMISSION
Apparatus and method for identification of matrix materials in which transuranic elements are embedded using thermal neutron capture gamma-ray emission [DE85-011659] p 125 N85-33454
NEWTON-RAPHSON METHOD
Extension of constrained incremental Newton-Raphson scheme to generalized loading fields p 139 A85-13942
On the development of hierarchical solution strategies for nonlinear finite element formulations p 171 A85-21979
NICHROME (TRADEMARK)
Metallurgical and mechanical phenomena due to rubbing of titanium against sintered powder Nichrome p 127 A85-22281
NICKEL
Effects of SO2 and SO3 on the Na2SO4 induced corrosion of nickel p 65 A85-15603
The substitution of nickel for cobalt in hot isostatically pressed powder metallurgy UDIMET 700 alloys p 68 A85-37415
The effects of seven alloying elements on the microstructure and stress-rupture behavior of nickle-base superalloys [NASA-TM-83791] p 70 N85-10168
The reactions of cobalt, iron and nickel in SO-2 atmospheres: Similarities and differences [NASA-TM-86868] p 70 N85-11217
Optimization of the NiCrAl-Y/ZrO-Y2O3 thermal barrier system [NASA-TM-86905] p 72 N85-15878
Surface effects of corrosive media on hardness, friction, and wear of materials [NASA-TM-83711] p 85 N85-15896
Humidity effects on adhesion of nickel-zinc ferrite in elastic contact with magnetic tape and itself [NASA-TP-2449] p 88 N85-21359
NICKEL ALLOYS
Deformation and fracture behavior of Ni-Mo-Al(gamma/gamma prime-alpha) in situ composite p 64 A85-11058
Modeling of gamma/gamma-prime phase equilibrium in the nickel-aluminum system p 65 A85-14959
Ductility in rapidly solidified NiAl p 66 A85-26158
Elevated temperature creep-rupture behavior of the single crystal nickel-base superalloy NASAIR 100 p 66 A85-27812
Chemical reactions involved in the initiation of hot corrosion of IN-738 p 66 A85-31688
Factors which influence directional coarsening of gamma-prime during creep in nickel-base superalloy single crystals p 67 A85-32388
The influence of hold times on LCF and FCG behavior in a P/M Ni-base superalloy --- Low Cycle Fatigue/Fatigue Crack Growth p 67 A85-32400
Effects of cobalt on the hot workability of nickel-base superalloys p 67 A85-32412
Rapid solidification and dynamic compaction of Ni-base superalloy powders p 67 A85-32414
Cyclic oxidation behavior of beta+gamma overlay coatings on gamma and gamma+gamma-prime alloys p 68 A85-32431
On the fatigue crack propagation behavior of superalloys at intermediate temperatures p 68 A85-32434
Progress in the utilization of an oxide-dispersion-strengthened alloy for small engine turbine blades [SAE PAPER 841512] p 68 A85-39284
Dopant effect of yttrium and the growth and adherence of alumina on nickel-aluminum alloys p 82 A85-40973
Diffusion welding of MA 6000 and a conventional nickel-base superalloy p 69 A85-43551
Application of two creep fatigue life models for the prediction of elevated temperature crack initiation of a nickel base alloy [AIAA PAPER 85-1420] p 69 A85-43979
Morphological changes of gamma prime precipitates in nickel-base superalloy single crystals [NASA-TM-83698] p 70 N85-10165
The transient oxidation of single crystal NiAl+Zr [NASA-CR-174756] p 70 N85-11221
The effect of tantalum and carbon on the structure/properties of a single crystal nickel-base superalloy [NASA-CR-174779] p 71 N85-11223

Studies on the hot corrosion of a nickel-base superalloy, Udimet 700
[NASA-TM-86882] p 71 N85-11224
The effects of Cr, Co, Al, Mo and Ta on the cyclic oxidation behavior of a prototype cast Ni-base superalloy based on a 2(5) composite statistically designed experiment
[NASA-TM-83784] p 71 N85-12131
The effect of tantalum on the structure/properties of two polycrystalline nickel-base superalloys: B-1900 + Hf MAR-M247
[NASA-CR-174847] p 73 N85-18127
Low cycle fatigue of MAR-M 200 single crystals at 760 and 870 deg C
[NASA-TM-86933] p 74 N85-19074
Study of the effects of implantation on the high Fe-Ni-Cr and Ni-Cr-Al alloys
[NASA-CR-175625] p 76 N85-22661
A multiple linear regression analysis of hot corrosion attack on a series of nickel base turbine alloys
[NASA-TM-87020] p 77 N85-31284
Microstructures in rapidly solidified Ni-Mo alloys
[NASA-TM-87100] p 78 N85-34266

NICKEL CADMIUM BATTERIES
A 37.5-kW point design comparison of the nickel-cadmium battery, bipolar nickel-hydrogen battery, and regenerative hydrogen-oxygen fuel cell energy storage subsystems for low earth orbit p 46 A85-45387

NICKEL COMPOUNDS
Moderate temperature sodium cells. V - Discharge reactions and rechargeability of NiS and NiS2 positive electrodes in molten NaAlCl4 p 59 A85-11892
Alloys based on NiAl for high temperature applications
[NASA-TM-86976] p 75 N85-21322
Raman structural studies of the nickel electrode
[NASA-CR-175619] p 183 N85-23414

NICKEL HYDROGEN BATTERIES
Design of a 1-kWh bipolar nickel hydrogen battery p 155 A85-45384
Teardown analysis of a ten cell bipolar nickel-hydrogen battery p 156 A85-45385
Separator development and testing of nickel-hydrogen cells p 156 A85-45386
A 37.5-kW point design comparison of the nickel-cadmium battery, bipolar nickel-hydrogen battery, and regenerative hydrogen-oxygen fuel cell energy storage subsystems for low earth orbit p 46 A85-45387
Long life nickel electrodes for a nickel-hydrogen cell. III - Results of an accelerated test and failure analyses p 156 A85-45391
Advanced designs for IPV nickel-hydrogen cells p 156 A85-45438
Advanced nickel-hydrogen cell configuration study
[NASA-CR-174775] p 157 N85-10444
Initial performance of advanced designs for IPV nickel-hydrogen cells
[NASA-TM-87029] p 162 N85-28444
Life cycle test results of a bipolar nickel hydrogen battery
[NASA-TM-87046] p 163 N85-30480
Design principles for nickel hydrogen cells and batteries p 104 N85-31398
Initial performance of advanced designs for IPV nickel-hydrogen cells p 105 N85-31404
Life cycle test results of a bipolar nickel hydrogen battery p 105 N85-31406
The failure mechanism of a nickel electrode in a nickel-hydrogen cell p 105 N85-31408
Design principles for nickel-hydrogen cells and batteries
[NASA-TM-87037] p 164 N85-31646

NICKEL OXIDES
Adsorption of O2, SO2, and SO3 on nickel oxide. Mechanism for sulfate formation
[NASA-CR-176072] p 77 N85-32175

NIOBIUM ALLOYS
Effect of reduction of strategic Columbium addition in 718 Alloy on the structure and properties
[NASA-CR-174841] p 75 N85-21320

NITRIDING
Ion-beam nitriding of steels p 66 A85-24667
Nitriding of titanium and its alloys by N2, NH3 or mixtures of N2 + H2 in a dc arc plasma at low pressures (or = to torr)
[NASA-TM-83803] p 131 N85-15168
Ion-beam nitriding of steels
[NASA-CASE-LEW-14104-1] p 75 N85-21324

NITROGEN
Performance characterization tests of a 1-kW resistojet using hydrogen, nitrogen and ammonia as propellants
[AIAA PAPER 85-1159] p 44 A85-39628
Lubricity of well-characterized jet and broad-cut fuels by ball-on-cylinder machine
[NASA-TM-83807] p 92 N85-12183
Electrode erosion in arc discharges at atmospheric pressure
[NASA-TM-87087] p 52 N85-34178

NITROGEN PLASMA
Measurements of energy distribution in microwave plasmas of N2 and He and comparisons with results for H2 p 178 A85-16443
Frictional and structural characterization of ion-nitrided low and high chromium steels
[NASA-TM-86991] p 132 N85-23085

NOBLE METALS
Electrocatalyst advances for hydrogen oxidation in phosphoric acid fuel cells p 60 A85-15614

NOISE (SOUND)
Further comparison of wind tunnel and airplane acoustic data for advanced design high speed propeller models
[NASA-TM-86935] p 176 N85-22108
Generated spiral bevel gears: Optimal machine-tool settings and tooth contact analysis
[NASA-TM-87075] p 136 N85-34405

NOISE INTENSITY
Acoustic pressures emanating from a turbomachine stage
[AIAA PAPER 84-2325] p 2 A85-10870
Investigation on experimental techniques to detect, locate and quantify gear noise in helicopter transmissions
[NASA-CR-3847] p 176 N85-17667

NOISE MEASUREMENT
Comparison of scaled model data to full size energy efficient engine test results
[AIAA PAPER 84-2281] p 13 A85-13953
Measurement and prediction of Energy Efficient Engine noise
[AIAA PAPER 84-2284] p 13 A85-13954
Analysis of the effect on combustor noise measurements of acoustic waves reflected by the turbine and combustor inlet
[AIAA PAPER 84-2323] p 173 A85-16103

NOISE PREDICTION
A theoretical prediction of the acoustic pressure generated by turbulence-flame front interactions
[ASME PAPER 84-WA/NCA-11] p 174 A85-39909

NOISE PREDICTION (AIRCRAFT)
Measurement and prediction of Energy Efficient Engine noise
[AIAA PAPER 84-2284] p 13 A85-13954
Noise produced by the interaction of a rotor wake with a swept stator blade
[AIAA PAPER 84-2326] p 173 A85-13956
Modelling of wind tunnel wall effects on the radiation characteristics of acoustic sources
[AIAA PAPER 84-2364] p 174 A85-16104
Observations from varying the lift and drag inputs to a noise prediction method for supersonic helical tip speed propellers
[NASA-TM-83797] p 175 N85-10788

NOISE PROPAGATION
Noise transmission loss of a rectangular plate in an infinite baffle
[NASA-TP-2398] p 176 N85-22109
Interaction of finite-amplitude sound with air-filled porous materials
[NASA-CR-174885] p 177 N85-27637

NOISE REDUCTION
Supersonic jet shock noise reduction
[AIAA PAPER 84-2278] p 173 A85-16099
A high-speed implementation of the random decrement algorithm p 94 A85-29556
The performance of jet noise suppression devices for industrial applications p 175 A85-42563
Noise constraints effecting optimal propeller designs
[SAE PAPER 850871] p 7 A85-50106
Experimental investigation of shock-cell noise reduction for dual-stream nozzles in simulated flight
[NASA-CR-3846] p 175 N85-13549
Experimental investigation of shock-cell noise reduction for single stream nozzles in simulated flight
[NASA-CR-3845] p 175 N85-13550
Noise constraints effecting optimal propeller designs
[NASA-TM-86967] p 8 N85-19923
Interaction of finite-amplitude sound with air-filled porous materials
[NASA-CR-174885] p 177 N85-27637

NOISE SPECTRA
Effects of vane/blade ratio and spacing on fan noise, volume 1
[NASA-CR-174664] p 176 N85-19791
Effects of vane/blade ratio and spacing on fan noise. Volume 2: Data supplement
[NASA-CR-174665] p 176 N85-19792

NONDESTRUCTIVE TESTS
Eddy current jet engine disk-crack monitor p 120 A85-11100
Ultrasonic nondestructive evaluation, microstructure, and mechanical property interrelations
[NASA-TM-86876] p 137 N85-10371
NDE for heat engine ceramics
[NASA-TM-86949] p 137 N85-20389
Stress waves in an isotropic elastic plate excited by a circular transducer
[NASA-CR-3877] p 138 N85-20390
Structural Integrity and Durability of Reusable Space Propulsion Systems
[NASA-CP-2381] p 51 N85-27941
Ultrasonic testing of plates containing edge cracks
[NASA-CR-3904] p 138 N85-29307
A study of the stress wave factor technique for the characterization of composite materials
[NASA-CR-174870] p 58 N85-30035
Reliability of void detection in structural ceramics using scanning laser acoustic microscopy
[NASA-TM-87035] p 138 N85-32337

NONISOTHERMAL PROCESSES
Thermodynamically consistent constitutive equations for nonisothermal large strain, elasto-plastic, creep behavior
[AIAA PAPER 85-0621] p 142 A85-38425
Thermomechanical deformation in the presence of metallurgical changes p 150 N85-31533

NONLINEAR EQUATIONS
On the development of hierarchical solution strategies for nonlinear finite element formulations p 171 A85-21979
Local strain redistribution corrections for a simplified inelastic analysis procedure based on an elastic finite-element analysis
[NASA-TP-2421] p 145 N85-20396
Nonlinear flap-lag-extensional vibrations of rotating, pretwisted, preconed beams including Coriolis effects
[NASA-TM-87102] p 152 N85-34427

NONLINEAR SYSTEMS
Alternatives for jet engine control
[NASA-CR-175831] p 29 N85-26713
Alternatives for jet engine control
[NASA-CR-175832] p 29 N85-26714
Alternatives for jet engine control
[NASA-CR-175833] p 29 N85-26715

NONLINEARITY
A simplified method for elastic-plastic-creep structural analysis
[ASME PAPER 84-GT-191] p 141 A85-23150
On local total strain redistribution using a simplified cyclic inelastic analysis based on an elastic solution
[AIAA PAPER 85-1419] p 142 A85-39770
Nonlinear analysis for high-temperature multilayered fiber composite structures --- turbine blades
[NASA-TM-83754] p 57 N85-21273
On local total strain redistribution using a simplified cyclic inelastic analysis based on an elastic solution
[NASA-TM-86913] p 145 N85-21690
Nonlinear Constitutive Relations for High Temperature Application, 1984
[NASA-CP-2369] p 150 N85-31530
Elastohydrodynamic lubrication calculations used as a tool to study scuffing
[NASA-TM-87097] p 137 N85-34408

NONSTABILIZED OSCILLATION
Oscillator response to nonstationary excitation
[ASME PAPER 84-WA/APM-38] p 140 A85-17039

NONUNIFORM FLOW
Sound generation and upstream influence due to instability waves interacting with non-uniform mean flows p 174 A85-20738

NOTCH STRENGTH
Finite element analysis of notch behavior using a state variable constitutive equation p 152 N85-31548

NOTCH TESTS
Finite element analysis of notch behavior using a state variable constitutive equation p 152 N85-31548

NOWCASTING
MERIT: A man/computer data management and enhancement system for upper air nowcasting/forecasting in the United States --- Minimum Energy Routes using Interactive Techniques (MERIT) p 167 N85-10558

NOZZLE DESIGN
Supersonic jet shock noise reduction
[AIAA PAPER 84-2278] p 173 A85-16099
Experimental investigation of shock-cell noise reduction for single stream nozzles in simulated flight
[NASA-CR-3845] p 175 N85-13550
Convoluted nozzle design for the RL10 derivative 2B engine
[NASA-CR-174953] p 32 N85-29965

NOZZLE EFFICIENCY
Altitude testing of a flight weight, self-cooled, 2D thrust vectoring exhaust nozzle
[SAE PAPER 841557] p 14 A85-25984

NOZZLE FLOW
The three-dimensional compressible flow in a radial inflow turbine scroll p 6 A85-41826

A multiple-scales model of the shock-cell structure of imperfectly expanded supersonic jets
p 113 A85-49354
Experimental investigation of shock-cell noise reduction for single stream nozzles in simulated flight
[NASA-CR-3845] p 175 N85-13550

NOZZLE GEOMETRY
Supersonic jet shock noise reduction
[AIAA PAPER 84-2278] p 173 A85-16099
Preliminary analysis of tone-excited two-stream jet velocity decay
[NASA-TM-86951] p 8 N85-21114

NUCLEAR BINDING ENERGY
Monte Carlo study of reversible growth of clusters on a surface p 182 A85-48516

NUCLEAR ELECTRIC PROPULSION
An evaluation of oxygen/hydrogen propulsion systems for the Space Station
[AIAA PAPER 85-1156] p 45 A85-43976
Tethered nuclear power for the Space Station
[NASA-TM-87023] p 51 N85-26912
An evaluation of oxygen-hydrogen propulsion systems for the Space Station
[NASA-TM-87059] p 52 N85-28971

NUCLEAR POWER REACTORS
Applicability of 100kWe-class of space reactor power systems to NASA manned space station missions
[NASA-CR-174696] p 177 N85-35728

NUCLEAR REACTORS
High thermal power density heat transfer apparatus providing electrical isolation at high temperature using heat pipes
[NASA-CASE-LEW-12950-2] p 117 N85-29179

NUCLEATION
Computer simulation of thin film nucleation and growth
p 181 A85-35308
Fundamentals of microcrack nucleation mechanics
[NASA-CR-3851] p 137 N85-16195
A computer simulation of thin film nucleation and growth: The Volmer-Weber case
[NASA-TM-86968] p 53 N85-21264

NUMERICAL ANALYSIS
Comparison of numerical techniques for integration of stiff ordinary differential equations arising in combustion chemistry
[NASA-TP-2372] p 17 N85-10065
Nonlinear structural analysis for fiber-reinforced superalloy turbine blades p 147 N85-26887

NUMERICAL CONTROL
Microprocessor control of photovoltaic systems
p 156 A85-45408
Design description of a microprocessor based Engine Monitoring and Control unit (EMAC) for small turboshaft
[NASA-TM-86860] p 1 N85-17935
Digital temperature and velocity control of mach 0.3 atmospheric pressure durability testing burner rigs in long time, unattended cyclic testing
[NASA-TM-86959] p 75 N85-21321

NUMERICAL INTEGRATION
Analysis of hourglass instabilities and control in underintegrated finite element methods
p 139 A85-11125
Integrating chemical kinetic rate equations by selective use of stiff and nonstiff methods
[AIAA PAPER 85-0237] p 60 A85-19607
Recent advances in methods for numerical solution of O.D.E. initial value problems p 171 A85-21370
A comparison of the efficiency of numerical methods for integrating chemical kinetic rate equations
[NASA-TM-83590] p 25 N85-21162

NUMERICAL STABILITY
Analysis of hourglass instabilities and control in underintegrated finite element methods
p 139 A85-11125
Extension of constrained incremental Newton-Raphson scheme to generalized loading fields
p 139 A85-13942
Assessment of discretization schemes to reduce numerical diffusion in the calculation of complex flows
[AIAA PAPER 85-0441] p 108 A85-19751
Development and testing of stable, invariant, isoparametric curvilinear 2- and 3-D hybrid-stress elements p 140 A85-19899
Recent advances in methods for numerical solution of O.D.E. initial value problems p 171 A85-21370
Stability, accuracy, and efficiency of some underintegrated methods in finite element computations
p 172 A85-50073

O

O RING SEALS
Analysis of experimental shaft seal data for high-performance turbomachines, as for Space Shuttle main engines
[NASA-TM-86928] p 115 N85-21569
Experimental stiffness of tapered bore seals
[NASA-TM-86978] p 132 N85-25847

ONBOARD DATA PROCESSING
Satellite baseband processor test performance summary p 95 A85-14434

ONE DIMENSIONAL FLOW
Unsteady flow in a supersonic cascade with two in-passage shocks
[NASA-CR-3925] p 10 N85-35158

OPEN CHANNEL FLOW
Behavior of turbulent gas jets in an axisymmetric confinement
[NASA-CR-174829] p 28 N85-25265

OPEN CIRCUIT VOLTAGE
High-voltage solar-cell chip p 154 A85-24668
Effect of solar-cell junction geometry on open-circuit voltage p 154 A85-28080

OPERATING COSTS
Energy efficient engine flight propulsion system preliminary analysis and design report
[NASA-CR-174701] p 18 N85-10947
Energy efficient engine component development and integration program
[NASA-CR-169496] p 22 N85-10989
Energy efficient engine. Volume 1: Component development and integration program
[NASA-CR-173084] p 22 N85-10992

OPERATORS (MATHEMATICS)
Model equation for simulating flows in multistage turbomachinery
[NASA-TM-86869] p 7 N85-12036

OPTICAL COMPUTERS
Optical computer switching network
p 178 A85-23134
Optical linear algebra processors - Noise and error-source modeling p 169 A85-36727

OPTICAL CORRECTION PROCEDURE
Holographic optical system for aberration corrections in laser Doppler velocimetry p 123 A85-48659

OPTICAL DATA PROCESSING
Optical computer switching network
p 178 A85-23134
Optical linear algebra processors - Noise and error-source modeling p 169 A85-36727

OPTICAL FILTERS
Filter induced errors in laser anemometer measurements using counter processors
[NASA-TM-87047] p 125 N85-30288

OPTICAL HETERODYNING
Electronic heterodyne readout of fringes in moire deflectometry p 122 A85-36726
Moire deflectometry with deferred electronic heterodyne readout p 122 A85-42854

OPTICAL MEASURING INSTRUMENTS
An approach for automated analysis of particle holograms p 120 A85-10034
Nonintrusive optical single-particle counter for measuring the size and velocity of droplets in a spray
p 120 A85-16794
Remote displacement measurements using a laser diode p 121 A85-24464
Fiber optic temperature sensor p 121 A85-29563

OPTICAL POLARIZATION
Incident beam polarization for laser Doppler velocimetry employing a sapphire cylindrical window
p 122 A85-39835

OPTICAL PROPERTIES
Laboratory degradation of Kapton in a low energy oxygen ion beam
[AIAA PAPER 83-2658] p 78 A85-10675
Optical properties of hydrogenated amorphous carbon films grown from methane plasma
[NASA-TM-86995] p 183 N85-26406

OPTICS
The use of an optical data acquisition system for bladed disk vibration analysis
[NASA-TM-86891] p 144 N85-15184

OPTIMIZATION
Optimization of cascade blade mistuning. I - Equations of motion and basic inherent properties
p 16 A85-42365
Optimization of cascade blade mistuning. II - Global optimum and numerical optimization p 16 A85-45715
Structural optimization using optimality criteria methods p 144 A85-48703
Noise constraints effecting optimal propeller designs
[SAE PAPER 850871] p 7 A85-50106
Manual of phosphoric acid fuel cell power plant optimization model and computer program
[NASA-CR-174721] p 157 N85-10445
Energy efficient engine. High pressure compressor detail design report
[NASA-CR-165558] p 23 N85-10998
An improved computer model for prediction of axial gas turbine performance losses
[NASA-CR-174246] p 24 N85-15724
Optimization of the NiCrAl-Y/ZrO-Y2O3 thermal barrier system
[NASA-TM-86905] p 72 N85-15878
Noise constraints effecting optimal propeller designs
[NASA-TM-86967] p 8 N85-19923
Alternatives for jet engine control
[NASA-CR-175831] p 29 N85-26713
Alternatives for jet engine control
[NASA-CR-175833] p 29 N85-26715
High pressure compressor component performance report
[NASA-CR-168245] p 33 N85-34138

OPTIONS
Space station propulsion options
[AIAA PAPER 85-1155] p 45 A85-43975

ORBIT SPECTRUM UTILIZATION
Engineering calculations for communications satellite systems planning
[NASA-CR-175552] p 37 N85-21233

ORBIT TRANSFER VEHICLES
Main propulsion system design recommendations for an advanced Orbit Transfer Vehicle
[AIAA PAPER 85-1336] p 36 A85-39730
Cryogenic upper stage test bed engine
[AIAA PAPER 85-1339] p 44 A85-39733
Progress report - Advanced cryogenic OTV engine technology
[AIAA PAPER 85-1341] p 44 A85-39735
OTV Propulsion Issues
[NASA-CP-2347] p 37 N85-16989
OTV propulsion tecnology programmatic overview
p 37 N85-16997
Vehicle/engine integration --- orbit transfer vehicles
p 37 N85-17008
Design and analysis report for the RL10-2B breadboard low thrust engine
[NASA-CR-174857] p 48 N85-19020
Convoluted nozzle design for the RL10 derivative 2B engine
[NASA-CR-174953] p 32 N85-29965
Status of advanced orbital transfer propulsion
[NASA-TM-87069] p 52 N85-35225

ORBITAL MANEUVERING VEHICLES
Status of advanced orbital transfer propulsion
[NASA-TM-87069] p 52 N85-35225

ORBITAL SERVICING
OTV propulsion tecnology programmatic overview
p 37 N85-16997

ORBITAL SPACE STATIONS
Engineering model system study for a regenerative fuel cell: Study report
[NASA-CR-174801] p 158 N85-16292
Manrating orbital transfer vehicle propulsion
[NASA-TM-87019] p 50 N85-25385
Applicability of 100kWe-class of space reactor power systems to NASA manned space station missions
[NASA-CR-174696] p 177 N85-35728

ORGANIC SILICON COMPOUNDS
Preparation of silicon carbide-silicon nitride fibers by the pyrolysis of polycarbosilazane precursors
[NASA-TM-86505] p 91 N85-28107

ORGANOMETALLIC COMPOUNDS
Magnesium doping of efficient GaAs and Ga(0.75)In(0.25)As solar cells grown by metalorganic chemical vapor deposition p 180 A85-11466

ORIFICE FLOW
Experiments in dilution jet mixing - Effects of multiple rows and non-circular orifices
[AIAA PAPER 85-1104] p 15 A85-39606
Experiments in dilution jet mixing effects of multiple rows and non-circular orifices
[NASA-TM-86996] p 28 N85-25266
Flow rate and pressure profiles for 1 to 4 axially alined orifice inlets
[NASA-TP-2460] p 116 N85-27165

ORIFICES
Flow rate and pressure profiles for 1 to 4 axially alined orifice inlets
[NASA-TP-2460] p 116 N85-27165

OSCILLATING FLOW
Resonance in flows with vortex sheets and edges
p 1 A85-10357
Approximate analysis for resonance of an incompressible shear layer plus edges
p 107 A85-19377

OSCILLATION DAMPERS
Variable force, eddy-current or magnetic damper
[NASA-CASE-LEW-13717-1] p 134 N85-30333
OSCILLOSCOPES
Transferring data oscilloscope to an IBM using an Apple II+ p 168 A85-24526
OXIDATION
Systematic optimization of a detailed kinetic model using a methane ignition example p 59 A85-12890
Electrocatalyst advances for hydrogen oxidation in phosphoric acid fuel cells p 60 A85-15614
Performance of thermal barrier coatings in high heat flux environments p 79 A85-19087
Cyclic oxidation behavior of beta+gamma overlay coatings on gamma and gamma+gamma-prime alloys p 68 A85-32431
High temperature oxidation of propene p 61 A85-33570
The transient oxidation of single crystal NiAl+Zr
[NASA-CR-174756] p 70 N85-11221
Analysis techniques for tracer studies of oxidation
[NASA-CR-174796] p 84 N85-12162
Optimization of the NiCrAl-Y/ZrO-Y2O3 thermal barrier system
[NASA-TM-86905] p 72 N85-15878
Effects of chromium and aluminum on mechanical and oxidation properties of iron-nickel-base superalloys based on CG-27
[NASA-TP-2443] p 75 N85-21323
Oxidation and hot corrosion of hot-pressed Si3N4 at 1000 deg C
[NASA-TM-86977] p 88 N85-21358
Shock tube study of the fuel structure effects on the chemical kinetic mechanisms responsible for soot formation, part 2
[NASA-CR-174880] p 63 N85-25444
Effects of surface chemistry on hot corrosion life
[NASA-CR-174915] p 28 N85-26711
Burner rig corrosion of SiC at 1000 deg C
[NASA-TM-87061] p 53 N85-30011
Ion beam sputter-deposited thin film coatings for protection of spacecraft polymers in low Earth orbit
[NASA-TM-87051] p 91 N85-30137
Fuel-rich catalytic combustion: A soot-free technique for in situ hydrogen-like enrichment
[NASA-TP-2498] p 63 N85-31244
Shock tube measurements of growth constants in the branched-chain ethane-carbon monoxide-oxygen system
[NASA-TM-87068] p 64 N85-32156
Molecular orbital studies in oxidation: Sulfate formation and metal-metal oxide adhesion
[NASA-CR-176070] p 77 N85-32174
Aluminum work function: Effect of oxidation, mechanical scraping and ion bombardment
[NASA-TM-87079] p 78 N85-34265
OXIDATION RESISTANCE
Oxidation-based model for thermal barrier coating life p 78 A85-10310
Oxidation of silicon nitride sintered with rare-earth oxide additions p 83 A85-42798
The effects of Cr, Co, Al, Mo and Ta on the cyclic oxidation behavior of a prototype cast Ni-base superalloy based on a 2(5) composite statistically designed experiment
[NASA-TM-83784] p 71 N85-12131
Effects of MAR-M247 substrate (modified) composition on coating oxidation coating/substrate interdiffusion --- protective coatings for hot section components of gas turbine engines
[NASA-CR-174851] p 73 N85-19073
Thermal barrier coating system
[NASA-CASE-LEW-14057-1] p 59 N85-35233
OXIDATION-REDUCTION REACTIONS
NASA Redox Storage System Development Project
[NASA-TM-83677] p 158 N85-12465
Cycling performance of the iron-chromium redox energy storage system
[NASA-TM-87034] p 162 N85-27387
OXIDE FILMS
Cyclic oxidation behavior of beta+gamma overlay coatings on gamma and gamma+gamma-prime alloys p 68 A85-32431
Electrical characterization of plasma-grown oxides on gallium arsenide p 181 A85-32635
Ion beam sputter-deposited thin film coatings for protection of spacecraft polymers in low Earth orbit
[NASA-TM-87051] p 91 N85-30137
Thermal barrier coating system
[NASA-CASE-LEW-14057-1] p 59 N85-35233
OXYGEN
Separator development and testing of nickel-hydrogen cells p 156 A85-45386
Electrocatalysis of fuel cell reactions: Investigation of alternate electrolytes
[NASA-CR-174753] p 157 N85-11455
Study of Kapton under simulated shuttle environment
[NASA-CR-176003] p 41 N85-29997
Shock tube measurements of growth constants in the branched-chain ethane-carbon monoxide-oxygen system
[NASA-TM-87068] p 64 N85-32156
OXYGEN ATOMS
Adsorption of O2, SO2, and SO3 on nickel oxide. Mechanism for sulfate formation
[NASA-CR-176072] p 77 N85-32175
OXYGEN IONS
Three-dimensional calculation of shuttle charging in polar orbit p 40 N85-22486
OXYGENATION
Jet fuel instability mechanisms
[NASA-CR-175856] p 93 N85-28127
OXYNITRIDES
Strength and microstructure of sintered Si3N4 with rare-earth-oxide additions
[ACS PAPER 130-13-84] p 80 A85-25271
Oxidation of silicon nitride sintered with rare-earth oxide additions p 83 A85-42798
OZONE
Simultaneous cabin and ambient ozone measurements on two Boeing 747 airplanes. Volume 3: October 1978 - July 1979
[NASA-TM-86883] p 167 N85-21872

P

P-N JUNCTIONS
Theory of the high base resistivity n(+)pp(+) silicon solar cell and its application to radiation damage effects p 154 A85-32639
Fabrication of p(+)-n junction GaAs solar cells by a novel method p 181 A85-33645
PANEL METHOD (FLUID DYNAMICS)
Calculation of compressible flow about three-dimensional inlets with auxiliary inlets, slats and vanes by means of a panel method
[AIAA PAPER 85-1196] p 5 A85-40817
Calculation of compressible flow about three-dimensional inlets with auxiliary inlets, slats and vanes by means of a panel method
[NASA-CR-174975] p 10 N85-35162
PANELS
Design procedures for fiber composite structural components: Panels subjected to combined in-plane loads
[NASA-TM-86909] p 57 N85-15823
PARABOLIC REFLECTORS
Focal shifts in parabolic reflectors p 97 A85-39356
Optical analysis of parabolic dish concentrators for solar dynamic power systems in space
[NASA-TM-87080] p 52 N85-34176
PARALLEL PLATES
Analysis of the electromagnetic scattering from an inlet geometry with lossy walls
[NASA-CR-175743] p 99 N85-25686
PARALLEL PROCESSING (COMPUTERS)
Multibus-based parallel processor for simulation p 169 A85-28613
General approaches for achieving high speed computations p 169 A85-28628
Hardware for a real-time multiprocessor simulator
[NASA-TM-83805] p 169 N85-10659
PARAMETER IDENTIFICATION
Identification of multivariable high-performance turbofan engine dynamics from closed-loop data p 13 A85-13630
PARAMETERIZATION
Stress waves in an isotropic elastic plate excited by a circular transducer
[NASA-CR-3877] p 138 N85-20390
PARTIAL DIFFERENTIAL EQUATIONS
Thermal-stress analysis for a wood composite blade
[NASA-CR-174794] p 159 N85-17421
PARTICLE IN CELL TECHNIQUE
Numerical simulations of positively-biased probes and dielectric-conductor disks in a plasma --- for low earth orbit plasma densities p 179 A85-17262
PARTICLE LADEN JETS
A two-equation turbulence model for two-phase jets p 107 A85-14376
Structure of particle-laden jets - Measurements and predictions p 109 A85-25137
Structure of ducted particle-laden turbulent jets p 110 A85-38999
Effect of surface configuration during solid particle impingement erosion p 69 A85-42568
Characterization of solid particle erosion resistance of ductile metals based on their properties p 69 A85-42569
PARTICLE SIZE DISTRIBUTION
An approach for automated analysis of particle holograms p 120 A85-10034
Phase/doppler spray analyzer for simultaneous measurements of drop size and velocity distributions p 120 A85-10035
Spray characterization with a nonintrusive technique using absolute scattered light p 120 A85-10036
Predicting rime ice accretion on airfoils p 3 A85-25135
Milling of Si3N4 with Si3N4 hardware
[NASA-TM-86864] p 84 N85-10191
Research study of droplet sizing technology leading to the development of an advanced droplet sizing system
[NASA-CR-174839] p 123 N85-21604
PARTICULATE SAMPLING
Fuel-rich catalytic combustion: A soot-free technique for in situ hydrogen-like enrichment
[NASA-TP-2498] p 63 N85-31244
PASCAL (PROGRAMMING LANGUAGE)
Transferring data oscilloscope to an IBM using an Apple II+ p 168 A85-24526
PASSAGEWAYS
Vortex-generating coolant-flow-passage design for increased film-cooling effectiveness and surface coverage
[NASA-TP-2388] p 113 N85-12314
PAYLOADS
Rail accelerator technology and applications
[NASA-TM-86947] p 48 N85-21258
PELVIS
Friction and wear properties of a Charnley artificial hip joint
[ASLE PREPRINT 84-LC-4A-4] p 168 A85-38444
PERFORMANCE
Life cycle test results of a bipolar nickel hydrogen battery
[NASA-TM-87046] p 163 N85-30480
PERFORMANCE PREDICTION
Progress toward the development of an aircraft icing analysis capability
[AIAA PAPER 84-0105] p 10 A85-10653
Predicted turbine stage performance using quasi-three-dimensional and boundary-layer analyses p 15 A85-34013
Comparison of free-piston Stirling engine model predictions with RE1000 engine test data p 130 A85-45488
Phosphoric acid fuel cell power plant system performance model and computer program
[NASA-CR-174638] p 157 N85-11456
Analytical fuel property effects--small combustors
[NASA-CR-174738] p 28 N85-26709
Aerodynamic analysis of a horizontal axis wind turbine by use of helical vortex theory. Volume 1: Theory
[NASA-CR-168054] p 9 N85-29916
Analytical model for predicting emergency shutdown of a two-bladed horizontal axis wind turbine
[NASA-TM-83472] p 162 N85-30476
Performance comparison between NACA 23024 and NACA 64(3)-618 airfoil configurated rotors for horizontal-axis wind turbines
[NASA-TM-83471] p 163 N85-30477
PERFORMANCE TESTS
Satellite baseband processor test performance summary p 95 A85-14434
IAPS (8-cm) ion thruster cyclic endurance test --- Ion Auxiliary Propulsion System p 42 A85-16406
Performance capabilities of the 12-centimeter Xenon ion thruster p 42 A85-16439
Recent work on a microwave ion source p 179 A85-16455
Altitude testing of a flight weight, self-cooled, 2D thrust vectoring exhaust nozzle
[SAE PAPER 841557] p 14 A85-25984
Status of DOE and AID stand-alone photovoltaic system field tests p 155 A85-35707
Method for evaluating wind turbine wake effects on wind farm performance p 155 A85-36750
Space Station propulsion - The Advanced Development Program at Lewis
[AIAA PAPER 85-1154] p 44 A85-39626
Performance characterization tests of a 1-kW resistojet using hydrogen, nitrogen and ammonia as propellants
[AIAA PAPER 85-1159] p 44 A85-39628
Small centrifugal pumps for low thrust rockets
[AIAA PAPER 85-1302] p 45 A85-43978
Advanced blade tip seal system, volume 2
[NASA-CR-167851] p 23 N85-10999
Space station propulsion: The advanced development program at Lewis
[NASA-TM-86999] p 50 N85-25386
Instrumentation technology overview p 124 N85-26903
Effect of precipitation on wind turbine performance
[NASA-TM-86986] p 161 N85-27385
Free-piston Stirling engine/linear alternator 1000-hour endurance test
[NASA-CR-174771] p 163 N85-30481

Develop and test fuel cell powered on-site integrated total energy systems. Phase 3: Full-scale power plant development
[NASA-CR-168338] p 164 N85-30483
Rolling, slip and traction measurements on low modulus materials
[NASA-CR-174909] p 135 N85-33491
Planetary-gear-support bearing test rig design
[NASA-CR-174927] p 12 N85-35185

PERMEABILITY
Acoustic structure and propagation in highly porous, layered, fibrous materials p 173 A85-12301
Effect of water on hydrogen permeability --- Stirling engines
[NASA-TM-86904] p 53 N85-14864

PERMITTIVITY
An experimental investigation of microstrip properties on soft substrates from 2 to 40 GHz
[NASA-TM-86961] p 99 N85-20224

PERTURBATION THEORY
Perturbation-iteration theory for analyzing microwave striplines
[NASA-CR-176189] p 100 N85-35321

PHASE DIAGRAMS
Modeling of gamma/gamma-prime phase equilibrium in the nickel-aluminum system p 65 A85-14959

PHASE ERROR
Dual-mode coaxial feed with low crosspolarisation p 101 A85-20171

PHASE TRANSFORMATIONS
Rapid solidification and dynamic compaction of Ni-base superalloy powders p 67 A85-32414
A study of interdiffusion in beta + gamma/gamma + gamma prime Ni-Cr-Al
[NASA-CR-174852] p 74 N85-20041

PHASED ARRAYS
MMIC devices for active phased array antennas
[NASA-CR-174281] p 98 N85-15943
Configuration study for a 30 GHz monolithic receive array: Technical assessment
[NASA-CR-174697] p 98 N85-18238
Configuration study for a 30 GHz monolithic receive array, volume 1
[NASA-CR-174697-VOL-1] p 98 N85-18239

PHENYLS
Effect of substituted phenylnadimides on processing and properties of PMR polyimide composites
[NASA-TM-86902] p 85 N85-14929
Ideal gas thermodynamic properties for the phenyl, phenoxy, and o-biphenyl radicals
[NASA-TM-83800] p 184 N85-22204

PHOSPHORESCENCE
Velocity visualization in gas flows using laser-induced phosphorescence of biacetyl p 121 A85-21695

PHOSPHORIC ACID FUEL CELLS
Electrocatalyst advances for hydrogen oxidation in phosphoric acid fuel cells p 60 A85-15614
Fuel cell power plant economic and operational considerations
[ASME PAPER 84-AES-7] p 154 A85-21297
Manual of phosphoric acid fuel cell power plant optimization model and computer program
[NASA-CR-174721] p 157 N85-10445
Manual of phosphoric acid fuel cell stack three-dimensional model and computer program
[NASA-CR-174722] p 157 N85-10447
Electrocatalysis of fuel cell reactions: Investigation of alternate electrolytes
[NASA-CR-174753] p 157 N85-11455
Phosphoric acid fuel cell power plant system performance model and computer program
[NASA-CR-174638] p 157 N85-11456
Gas cooled fuel cell systems technology development
[NASA-CR-174732] p 158 N85-16291
Electric utility acid fuel cell stack technology advancement
[NASA-CR-174804] p 159 N85-17422
Preparation and evaluation of advanced catalysts for phosphoric acid fuel cells
[NASA-CR-168223] p 160 N85-19511
Develop and test fuel cell powered on-site integrated total energy systems. Phase 3: Full-scale power plant development
[NASA-CR-174887] p 161 N85-25941

PHOTOACOUSTIC MICROSCOPY
Photoacoustic microscopy of ceramic turbine blades p 83 A85-43930

PHOTOELECTRIC MATERIALS
Practical aspects of photovoltaic technology, applications and cost (revised)
[NASA-CR-174963] p 165 N85-35472

PHOTOGRAMMETRY
Initial feasibility ground test of a proposed photogrammetric system for measuring the shapes of ice accretions on helicopter rotor blades during forward flight
[NASA-TM-87391] p 12 N85-12887

PHOTOGRAPHS
Initial feasibility ground test of a proposed photogrammetric system for measuring the shapes of ice accretions on helicopter rotor blades during forward flight
[NASA-TM-87391] p 12 N85-12887

PHOTONS
Preliminary design of a 10 kW thermophotovoltaic system for space applications p 45 A85-45371

PHOTOTRANSISTORS
High-temperature optically activated GaAs power switching for aircraft digital electronic control
[NASA-CR-174711] p 34 N85-12901

PHOTOVOLTAIC CELLS
Photovoltaics - The endless spring p 154 A85-35602
The NASA photovoltaic technology program p 155 A85-35604
Preliminary design of a 10 kW thermophotovoltaic system for space applications p 45 A85-45371
Microprocessor control of photovoltaic systems p 156 A85-45408
Control aspects of the Schuchuli Village stand-alone photovoltaic power system
[NASA-TM-83790] p 103 N85-13157
GaAs and 3-5 compound solar cells status and prospects for use in space
[NASA-TM-86960] p 49 N85-21261
The high voltage silicon cell: A comparative analysis p 49 N85-22569
GaAs and 3-5 compound solar cells status and prospects for use in space p 49 N85-22580
Operational performance of the photovoltaic-powered grain mill and water pump at Tangaye, Burkina Faso (formerly Upper Volta)
[NASA-TM-86970] p 161 N85-23243
Thermionic photovoltaic energy converter
[NASA-CASE-LEW-14077-1] p 164 N85-34441
Practical aspects of photovoltaic technology, applications and cost (revised)
[NASA-CR-174963] p 165 N85-35472

PHOTOVOLTAIC CONVERSION
Control algorithms and computer simulation of a stand-alone photovoltaic village power system p 153 A85-11345
Status of DOE and AID stand-alone photovoltaic system field tests p 155 A85-35707

PHOTOVOLTAIC EFFECT
Preliminary design of a 10 kW thermophotovoltaic system for space applications p 45 A85-45371
Research on gallium arsenide diffused junction solar cells
[NASA-CR-174057] p 158 N85-11457
High efficiency solar cell research for space applications p 164 N85-31624
Thermionic photovoltaic energy converter
[NASA-CASE-LEW-14077-1] p 164 N85-34441

PHYSIOLOGICAL EFFECTS
Percutaneous connectors
[NASA-CR-175627] p 168 N85-27508

PIPE FLOW
Analysis of buoyancy effect on fully developed laminar heat transfer in a rotating tube p 110 A85-35596
Behavior of turbulent gas jets in an axisymmetric confinement
[NASA-CR-174829] p 28 N85-25265

PISTON ENGINES
Initial results of sensitivity tests - Performed on the RE-1000 free-piston Stirling engine p 129 A85-45466
Mod II engine and technology development p 129 A85-45473
Overview of NASA Lewis Research Center free-piston Stirling engine activities p 130 A85-45479
Overview of the 1985 NASA Lewis Research Center SP-100 free-piston Stirling engine activities
[NASA-TM-87028] p 185 N85-27769

PISTONS
Comparison of free-piston Stirling engine model predictions with RE1000 engine test data p 130 A85-45488
Development of gas-lubricated pistons for heavy duty diesel engine technology program
[NASA-CR-174746] p 184 N85-12808
Sliding seal materials for adiabatic engines
[NASA-CR-174893] p 89 N85-22757

PITCH (INCLINATION)
Conceptual design of a fixed-pitch wind turbine generator system rated at 400 kilowatts
[NASA-CR-174877] p 162 N85-29363

PITTING
Mechanism of strength degradation for hot corrosion of alpha-SiC
[NASA-TM-87052] p 91 N85-30135

PLANE STRAIN
Fundamentals of microcrack nucleation mechanics
[NASA-CR-3851] p 137 N85-16195

PLANE WAVES
The response of Helmholtz resonators to external excitation. I - Single resonators p 174 A85-26915
Analysis of the electromagnetic scattering from an inlet geometry with lossy walls
[NASA-CR-175743] p 99 N85-25686

PLASMA CURRENTS
Ion flow experiments in a multipole discharge chamber p 178 A85-12705
Dilute plasma coupling currents to a high voltage solar array in weak magnetic fields p 46 A85-45388
Ram-wake effects on plasma current collection of the PIX 2 Langmuir probe p 180 N85-22496

PLASMA DENSITY
Ram-wake effects on plasma current collection of the PIX 2 Langmuir probe p 180 N85-22496
NASCAP simulation of PIX 2 experiments p 180 N85-22497

PLASMA DIAGNOSTICS
Effects of chemical releases by the STS 3 orbiter on the ionosphere p 166 A85-29538
Analysis of glow discharges for understanding the process of film formation
[NASA-TM-83750] p 62 N85-10138
Nitriding of titanium and its alloys by N2, NH3 or mixtures of N2 + H2 in a dc arc plasma at low pressures (or = to torr)
[NASA-TM-83803] p 131 N85-15168
Arc-driven rail gun research
[NASA-CR-174816] p 132 N85-21662
Suprathermal plasma observed on STS-3 Mission by plasma diagnostics package p 179 N85-22472
Electron and ion density depletions measured in the STS-3 orbiter wake p 39 N85-22474
Ram-wake effects on plasma current collection of the PIX 2 Langmuir probe p 180 N85-22496

PLASMA DISPLAY DEVICES
Frictional and structural characterization of ion-nitrided low and high chromium steels
[NASA-TM-86991] p 132 N85-23085

PLASMA DYNAMICS
Ion flow experiments in a multipole discharge chamber p 178 A85-12705
Rail accelerator technology and applications
[NASA-TM-86947] p 48 N85-21258

PLASMA ENGINES
Ring-cusp ion thrusters p 42 A85-16438

PLASMA GENERATORS
Recent work on a microwave ion source p 179 A85-16455
High frequency plasma generator for ion thrusters
[NASA-CR-174772] p 48 N85-17023

PLASMA HEATING
High frequency plasma generator for ion thrusters
[NASA-CR-174772] p 48 N85-17023

PLASMA INTERACTION EXPERIMENT
Computer simulation of plasma electron collection by PIX-II --- solar array-space plasma interaction
[AIAA PAPER 85-0386] p 43 A85-19715
The PIX-2 experiment: An overview p 179 N85-22494
Plasma interaction experiment 2 (PIX 2): Laboratory and flight results p 180 N85-22495
Ram-wake effects on plasma current collection of the PIX 2 Langmuir probe p 180 N85-22496

PLASMA INTERACTIONS
Characteristics of arc currents on a negatively biased solar cell array in a plasma p 154 A85-18608
The effect of plasma on solar cell array arc characteristics
[AIAA PAPER 85-0384] p 43 A85-19713
Numerical simulation of positive-potential conductors in the presence of a plasma and a secondary-emitting dielectric p 102 A85-35306
The effect of plasma on solar cell array arc characteristics
[NASA-TM-86887] p 47 N85-11133
Spacecraft Environmental Interactions Technology, 1983
[NASA-CP-2359] p 39 N85-22470
Surface interactions and high-voltage current collection p 40 N85-22493
The PIX-2 experiment: An overview p 179 N85-22494
Plasma interaction experiment 2 (PIX 2): Laboratory and flight results p 180 N85-22495
Discharges on a negatively biased solar cell array in a charged-particle environment p 160 N85-22499

Spacecraft environmental interactions: A joint Air Force and NASA research and technology program p 40 N85-22517

PLASMA JETS
Ion flow experiments in a multipole discharge chamber p 178 A85-12705
Deposition stress effects on the life of thermal barrier coatings on burner rigs p 79 A85-19086
The effect of plasma on solar cell array arc characteristics
[AIAA PAPER 85-0384] p 43 A85-19713
Properties of coated and modified surfaces p 53 A85-36694
Experimental performance of a microwave cavity plasma disk ion source p 179 A85-43552
The effect of plasma on solar cell array arc characteristics
[NASA-TM-86887] p 47 N85-11133

PLASMA LAYERS
Plasma variables and tribological properties of coatings in low pressure (0.1 - 10.0 torr) plasma systems
[NASA-TM-83798] p 94 N85-11261

PLASMA PHYSICS
Plasma deposited hydrogenated carbon on GaAs and InP p 182 A85-40386
Plasma deposited diamondlike carbon on GaAs and InP
[NASA-TM-86870] p 183 N85-10844

PLASMA PROPULSION
The energetics of hydrogen atom recombination - Analysis, experiments, and modeling --- in electrothermal propulsion system p 179 A85-16444
Ring-cusp ion thruster with shell anode
[NASA-CASE-LEW-13881-1] p 48 N85-21256

PLASMA SPRAYING
Deposition stress effects on the life of thermal barrier coatings on burner rigs p 79 A85-19086
Plastic flow of plasma sprayed ceramics p 80 A85-24161
Cyclic oxidation behavior of beta+gamma overlay coatings on gamma and gamma+gamma-prime alloys p 68 A85-32431
Electrical characterization of plasma-grown oxides on gallium arsenide p 181 A85-32635
Deposition of silicon nitride from SiCl4 and NH3 in a low pressure RF plasma p 81 A85-36229
Failure during thermal cycling of plasma-sprayed thermal barrier coatings p 81 A85-36246
Dielectric properties of 'diamondlike' carbon prepared by RF plasma deposition p 182 A85-38192
High-temperature erosion of plasma-sprayed, yttria-stabilized zirconia in a simulated turbine environment
[AIAA PAPER 85-1219] p 82 A85-39662
Surface hardening of steel by boriding in a cold rf plasma p 68 A85-40275
'Diamondlike' carbon films - Optical absorption, dielectric properties, and hardness dependence on deposition parameters p 82 A85-40383
Energy efficient engine high pressure turbine ceramic shroud support technology report
[NASA-CR-168036] p 23 N85-10996
High-temperature erosion of plasma-sprayed, yttria-stabilized zirconia in a simulated turbine environment
[NASA-TP-2406] p 84 N85-13045
Film and interstitial formation of metals in plasma-sprayed ceramics
[NASA-TM-86993] p 89 N85-22756
Thermal barrier coating system
[NASA-CASE-LEW-14057-1] p 59 N85-35233

PLASMAS (PHYSICS)
Plasma variables and tribological properties of coatings in low pressure (0.1 - 10.0 torr) plasma systems
[NASA-TM-83798] p 94 N85-11261

PLASMONS
Inelastic tunnel diodes
[NASA-CASE-LEW-13833-1] p 103 N85-21492
Solar energy converter using surface plasma waves
[NASA-CASE-LEW-13827-1] p 160 N85-21768

PLASTIC DEFORMATION
Deformation and erosion of f.c.c. metals and alloys under cavitation attack p 65 A85-12789
Hybrid stress finite elements for large deformations of inelastic solids p 139 A85-15894
Simplified design and life prediction of rocket thrust chambers p 44 A85-29314

PLASTIC FLOW
Plastic flow of plasma sprayed ceramics p 80 A85-24161

PLATE THEORY
Hybrid Semiloof elements for plates and shells based upon a modified Hu-Washizu principle p 139 A85-15893
Vibrations of twisted cantilevered plates - Summary of previous and current studies p 140 A85-22069
Vibrations of twisted cantilever plates - A comparison of theoretical results p 144 A85-47626

PLATES (STRUCTURAL MEMBERS)
Stress waves in an isotropic elastic plate excited by a circular transducer
[NASA-CR-3877] p 138 N85-20390
Geometrically nonlinear analysis of laminated elastic structures
[NASA-CR-175609] p 146 N85-21720
Ultrasonic testing of plates containing edge cracks
[NASA-CR-3904] p 138 N85-29307

PLATINUM
Mechanism for chelated sulfate formation from SO2 and bis (triphenylphosphine) platinum p 62 A85-48493
Dispersed metal-toughened ceramics and ceramic brazing
[NASA-CR-174284] p 86 N85-15916
Advanced thin film thermocouples
[NASA-CR-175541] p 124 N85-21607

PLATINUM ALLOYS
Compatibility experiments of facilities, materials, and propellants for electrothermal thrusters
[NASA-TM-86956] p 49 N85-21260
CO adsorption on (111) and (100) surfaces of the Pt sub 3 Ti alloy. Evidence for parallel binding and strong activation of CO
[NASA-CR-176077] p 77 N85-32176

PLOTTING
Plot of modal field distribution in rectangular and circular waveguides p 101 A85-25170

PLUG NOZZLES
Experimental investigation of shock-cell noise reduction for dual-stream nozzles in simulated flight
[NASA-CR-3846] p 175 N85-13549
Experimental investigation of shock-cell noise reduction for single stream nozzles in simulated flight
[NASA-CR-3845] p 175 N85-13550

PLUMES
Preliminary analysis of tone-excited two-stream jet velocity decay
[NASA-TM-86951] p 8 N85-21114

POLAR ORBITS
Three-dimensional calculation of shuttle charging in polar orbit p 40 N85-22486
Polar orbit electrostatic charging of objects in shuttle wake p 40 N85-22487

POLARIZATION (WAVES)
Incident beam polarization for laser Doppler velocimetry employing a sapphire cylindrical window
[NASA-TM-87064] p 178 N85-28786

POLARIZED ELECTROMAGNETIC RADIATION
A frequency-routed satellite system concept using multiple orthogonally-polarized beams for frequency reuse p 97 A85-34470

POLARIZED LIGHT
Prism-coupled light emission from tunnel junctions p 181 A85-21425

POLLUTION CONTROL
Methanol as a soot reducer in a turbulent swirling burner
[ASME PAPER 84-JPGC-GT-2] p 61 A85-23192

POLYCRYSTALS
The effect of tantalum on the structure/properties of two polycrystalline nickel-base superalloys: B-1900 + Hf MAR-M247
[NASA-CR-174847] p 73 N85-18127
Aluminum work function: Effect of oxidation, mechanical scraping and ion bombardment
[NASA-TM-87079] p 78 N85-34265

POLYETHYLENES
Friction, wear, transfer, and wear surface morphology of ultrahigh-molecular-weight polyethylene p 80 A85-22276

POLYIMIDE RESINS
Polyimides - Tribological properties and their use as lubricants p 79 A85-21524
Chemical approach for controlling nadimide cure temperature and rate with maleimide
[NASA-CASE-LEW-13770-3] p 87 N85-21350
Chemical approach for controlling nadimide cure temperature and rate with maleimide
[NASA-CASE-LEW-13770-4] p 87 N85-21351
Chemical approach for controlling nadimide cure temperature and rate
[NASA-CASE-LEW-13770-5] p 87 N85-21352
Chemical control of nadimide cure temperature and rate
[NASA-CASE-LEW-13770-2] p 63 N85-28982
Chemical approach for controlling nadimide cure temperature and rate
[NASA-CASE-LEW-13770-6] p 63 N85-30039
Graphite/PMR polyimide composites with improved toughness
[NASA-TM-87081] p 58 N85-32148

POLYIMIDES
Effect of substituted phenylnadimides on processing and properties of PMR polyimide composites
[NASA-TM-86902] p 85 N85-14929
Tribological properties of graphite-fiber-reinforced, partially fluorinated polyimide composites
[NASA-TM-86926] p 86 N85-18153
Ion beam sputter-deposited thin film coatings for protection of spacecraft polymers in low Earth orbit
[NASA-TM-87051] p 91 N85-30137
Graphite/PMR polyimide composites with improved toughness
[NASA-TM-87081] p 58 N85-32148

POLYMER CHEMISTRY
PMR polyimide composites for aerospace applications --- Polymerization of Monomer Reactants p 55 A85-21520
Chemical approach for controlling nadimide cure temperature and rate
[NASA-CASE-LEW-13770-6] p 63 N85-30039

POLYMER MATRIX COMPOSITES
PMR polyimide composites for aerospace applications --- Polymerization of Monomer Reactants p 55 A85-21520
Effect of counterface material type and its topography on the tribological properties of polyimide composites
[NASA-TM-87036] p 90 N85-26993

POLYMERIC FILMS
Effect of Interfacial characteristics of metal clad polymeric substrates on electrical high frequency interconnection performance
[NASA-TM-86948] p 99 N85-20223
Mass analysis of neutral particles and ions released during electrical breakdowns on spacecraft surfaces
[NASA-CR-175585] p 39 N85-21250
Mass spectra of neutral particles released during electrical breakdown of thin polymer films p 88 N85-22511
Monte Carlo lattice models for adsorbed polymer conformation
[NASA-TP-2453] p 183 N85-24961

POLYMERIZATION
PMR polyimide composites for aerospace applications --- Polymerization of Monomer Reactants p 55 A85-21520
Development of a lithium secondary battery separator p 104 N85-31378
Graphite/PMR polyimide composites with improved toughness
[NASA-TM-87081] p 58 N85-32148

POLYMERS
Tribological properties of graphite-fiber-reinforced, partially fluorinated polyimide composites
[NASA-TM-86926] p 86 N85-18153

POLYPHENYL ETHER
Contact angle and surface tension measurements of a five-ring polyphenyl ether
[NASA-TM-86927] p 86 N85-15897
Formation of high molecular weight products from benzene during boundary lubrication
[NASA-TM-86966] p 62 N85-22644

POROUS MATERIALS
Acoustic structure and propagation in highly porous, layered, fibrous materials p 173 A85-12301
A new interpretation of internal heat transfer coefficients of porous media
[ASME PAPER 84-WA/HT-51] p 110 A85-39894
Flow through very porous inclined screens
[AIAA PAPER 85-1650] p 111 A85-40750
Flow through very porous inclined screens
[NASA-TM-86979] p 116 N85-25761
Interaction of finite-amplitude sound with air-filled porous materials
[NASA-CR-174885] p 177 N85-27637

POTENTIAL ENERGY
Translational and extensional energy release rates (the J- and M-integrals) for a crack layer in thermoelasticity
[NASA-CR-174872] p 145 N85-21685

POTENTIAL FLOW
A linearized unsteady aerodynamic analysis for transonic cascades p 3 A85-20744
Calculation of compressible flow about three-dimensional inlets with auxiliary inlets, slats and vanes by means of a panel method
[NASA-CR-174975] p 10 N85-35162

POWDER (PARTICLES)
Milling of Si3N4 with Si3N4 hardware
[NASA-TM-86864] p 84 N85-10191
Factors influencing the ball milling of Si3N4 in water
[NASA-TM-86932] p 86 N85-19136

POWDER METALLURGY
Demonstration of a silicon nitride attrition mill for production of fine pure Si and Si3N4 powders p 78 A85-10825

The effect of microstructure, temperature, and hold-time on low-cycle fatigue of As HIP P/M Rene 95 p 67 A85-32399
The influence of hold times on LCF and FCG behavior in a P/M Ni-base superalloy --- Low Cycle Fatigue/Fatigue Crack Growth p 67 A85-32400
The substitution of nickel for cobalt in hot isostatically pressed powder metallurgy UDIMET 700 alloys p 68 A85-37415
PM superalloys - A troubled adolescent? p 69 A85-44772
Hot isostatically pressed manufacture of high strength MERL 76 disk and seal shapes [NASA-CR-165550] p 71 N85-11225
Alloys based on NiAl for high temperature applications [NASA-TM-86976] p 75 N85-21322
Fabrication of ceramic substrate-reinforced and free forms [NASA-TM-86994] p 50 N85-23926
Powder metallurgy forged gear development [NASA-TM-87483] p 134 N85-29295

POWER
Development of high frequency low weight power magnetics for aerospace power systems p 102 A85-45373

POWER CONDITIONING
Control algorithms and computer simulation of a stand-alone photovoltaic village power system p 153 A85-11345
A 20 GHz, 75 watt, helix TWT for space communications p 101 A85-14433
Inelastic tunnel diodes [NASA-CASE-LEW-13833-1] p 103 N85-21492

POWER CONVERTERS
Bipolar-FET combinational power transistors for power conversion applications p 100 A85-12669
A fast time domain digital simulation technique for power converters - Application to a buck converter with feedforward compensation p 101 A85-20900

POWER EFFICIENCY
Development of high frequency low weight power magnetics for aerospace power systems p 102 A85-45373
Automotive Stirling engine systems development p 130 A85-45474
Wind tunnel results of advanced high speed propellers in the takeoff, climb, and landing operating regimes [AIAA PAPER 85-1259] p 6 A85-47025
Effect of precipitation on wind turbine performance [NASA-TM-86986] p 161 N85-27385
Wind tunnel results of advanced high speed propellers in the takeoff, climb and landing operating regimes [NASA-TM-87054] p 9 N85-29925
Free-piston Stirling engine/linear alternator 1000-hour endurance test [NASA-CR-174771] p 163 N85-30481

POWER FACTOR CONTROLLERS
Advanced in solid state switchgear technology for large space power systems p 102 A85-45362
Microprocessor control of photovoltaic systems p 156 A85-45408

POWER REACTORS
Applicability of 100kWe-class of space reactor power systems to NASA manned space station missions [NASA-CR-174696] p 177 N85-35728

POWER SUPPLIES
Development of high frequency low weight power magnetics for aerospace power systems p 102 A85-45373

POWER SUPPLY CIRCUITS
Small-signal model for the series resonant converter p 102 A85-39453
Development of high frequency low weight power magnetics for aerospace power systems p 102 A85-45373
Control aspects of the Schuchuli Village stand-alone photovoltaic power system [NASA-TM-83790] p 103 N85-13157
Developments in space power components for power management and distribution p 47 N85-13877
High-voltage, high-power, solid-state remote power controllers for aerospace applications [NASA-TP-2437] p 49 N85-21263

POWER TRANSMISSION (LASERS)
Technology for satellite power conversion [NASA-CR-174335] p 159 N85-18451

PREBURNERS
SSME fuel preburner two-dimensional analysis p 51 N85-27943

PRECIPITATION (METEOROLOGY)
Effect of precipitation on wind turbine performance [NASA-TM-86986] p 161 N85-27385

PRECIPITATION HARDENING
Progress in the utilization of an oxide-dispersion-strengthened alloy for small engine turbine blades [SAE PAPER 841512] p 68 A85-39284
Diffusion welding of MA 6000 and a conventional nickel-base superalloy p 69 A85-43551
Thermomechanical deformation in the presence of metallurgical changes p 150 N85-31533

PREDICTION ANALYSIS TECHNIQUES
Computation of viscous flows in turbomachinery cascades p 106 A85-11631
Predicting rime ice accretion on airfoils p 3 A85-25135
A theoretical prediction of the acoustic pressure generated by turbulence-flame front interactions [ASME PAPER 84-WA/NCA-11] p 174 A85-39909
Nonlinear structural and life analyses of a turbine blade p 19 N85-10954
Nonlinear structural and life analyses of a combustor liner p 19 N85-10955
Life prediction and constitutive behavior: Overview p 20 N85-10973
Validation of structural analysis methods using the in-house liner cyclic rigs p 21 N85-10987
Reliability considerations for the total strain range version of strainrange partitioning [NASA-CR-174757] p 144 N85-11380
Confined turbulent swirling recirculating flow predictions [NASA-CR-174917] p 29 N85-26716
Elevated temperature biaxial fatigue [NASA-CR-175795] p 148 N85-27263
Predictions and measurements of isothermal flowfields in axisymmetric combustor geometries [NASA-CR-174916] p 29 N85-27867
Reexamination of cumulative fatigue damage laws p 149 N85-27962
Analytical model for predicting emergency shutdown of a two-bladed horizontal axis wind turbine [NASA-TM-83472] p 162 N85-30476
Heat transfer and fluid mechanics measurements in transitional boundary layer flows p 118 N85-31439
A review and analysis of boundary layer transition data for turbine application p 118 N85-31440
A comparison of two contemporary creep-fatigue life prediction methods p 151 N85-31538
Two simplified procedures for predicting cyclic material response from a strain history p 151 N85-31543
Lubrication and cooling for high speed gears [NASA-TM-87096] p 136 N85-34407

PREDICTIONS
Effects of surface chemistry on hot corrosion life: Overview p 21 N85-10980

PREMIXED FLAMES
Flame flashback in a premixed dump combustor [AIAA PAPER 85-0145] p 60 A85-19550
Combustion efficiency of a premixed continuous flow combustor p 61 A85-42571

PRESSURE DISTRIBUTION
Effect of combined pressure and temperature distortion orientation on high-bypass-ratio turbofan engine stability [NASA-TM-83771] p 17 N85-10067
Flow rate and pressure profiles for 1 to 4 axially alined orifice inlets [NASA-TP-2460] p 116 N85-27165

PRESSURE EFFECTS
Fast approach for calculating film thicknesses and pressures in elastohydrodynamically lubricated contacts at high loads [NASA-TM-87032] p 117 N85-30242

PRESSURE GRADIENTS
Nested subcritical flows within supercritical systems [NASA-TM-86980] p 115 N85-21574

PRESSURE MEASUREMENT
A stagnation pressure probe for droplet-laden air flow [AIAA PAPER 85-0330] p 108 A85-19672
The infinite line pressure probe p 122 A85-37704
Unsteady pressure measurements on a biconvex airfoil in a transonic oscillating cascade [NASA-TM-86914] p 8 N85-15689

PRESSURE OSCILLATIONS
Approximate analysis for resonance of an incompressible shear layer plus edges p 107 A85-19377
Oscillatory conductive heat transfer for a fiber in an ideal gas p 109 A85-26077

PRESSURE PULSES
Flow dynamic environment data base development for the SSME p 147 N85-26885

PRESSURE RATIO
High pressure compressor component performance report [NASA-CR-168245] p 33 N85-34138

PRESSURE SENSORS
A stagnation pressure probe for droplet-laden air flow [AIAA PAPER 85-0330] p 108 A85-19672
The infinite line pressure probe p 122 A85-37704
High-temperature fiber optic pressure sensor p 123 A85-46607

PRESSURE VESSEL DESIGN
Advanced nickel-hydrogen cell configuration study [NASA-CR-174775] p 157 N85-10444

PRESSURE VESSELS
Ten year environmental test of glass fiber/epoxy pressure vessels [AIAA PAPER 85-1198] p 56 A85-47022
Initial performance of advanced designs for IPV nickel-hydrogen cells [NASA-TM-87029] p 162 N85-28444
Ten year environmental test of glass fiber/epoxy pressure vessels [NASA-TM-87058] p 58 N85-30034
Initial performance of advanced designs for IPV nickel-hydrogen cells p 105 N85-31404

PRESTRESSING
Effects of warping and pretwist on torsional vibration of rotating beams [ASME PAPER 84-WA/APM-41] p 140 A85-17040
Vibration and buckling of rotating, pretwisted, preconed beams including Cooriolis effects [NASA-TM-87004] p 146 N85-25893

PRIMARY BATTERIES
Electrochemistry and storage p 62 N85-13889

PRINTED CIRCUITS
MMIC devices for active phased array antennas [NASA-CR-174281] p 98 N85-15943

PRINTING
Screen printed interdigitated back contact solar cell [NASA-CASE-LEW-13414-1] p 160 N85-20530

PROBABILITY THEORY
Creep-rupture reliability analysis p 143 A85-42566
Probabilistic structural analysis theory development p 148 N85-27955
Probabilistic finite element development p 149 N85-27956
Reliability of void detection in structural ceramics using scanning laser acoustic microscopy [NASA-TM-87035] p 138 N85-32337

PROBES
Precision tunable resonant microwave cavity [NASA-CASE-LEW-13935-1] p 103 N85-20248

PROBLEM SOLVING
New integration techniques for chemical kinetic rate equations. 2: Accuracy comparison [NASA-TM-86893] p 23 N85-13798

PROCESS CONTROL (INDUSTRY)
Chemical approach for controlling nadimide cure temperature and rate with maleimide [NASA-CASE-LEW-13770-3] p 87 N85-21350
Chemical approach for controlling nadimide cure temperature and rate with maleimide [NASA-CASE-LEW-13770-4] p 87 N85-21351

PRODUCT DEVELOPMENT
Conceptual design of a fixed-pitch wind turbine generator system rated at 400 kilowatts [NASA-CR-174877] p 162 N85-29363

PROFILOMETERS
Characterization of lubricated bearing surfaces operated under high loads [NASA-TM-86964] p 88 N85-21357

PROGRAM VERIFICATION (COMPUTERS)
Comparison of free-piston Stirling engine model predictions with RE1000 engine test data p 130 A85-45488

PROGRAMMING LANGUAGES
Functional language and data flow architectures p 170 A85-28629

PROJECT MANAGEMENT
Life prediction and constitutive behavior: Overview p 20 N85-10973

PROP-FAN TECHNOLOGY
Large-scale advanced propfan (LAP) program progress report [AIAA PAPER 85-1187] p 17 A85-47021
Large-scale Advanced Propfan (LAP) performance, acoustic and weight estimation, January, 1984 [NASA-CR-174782] p 9 N85-22368
Large-scale Advanced Propfan (LAP) program [NASA-TM-87067] p 32 N85-29964

PROPAGATION MODES
Circular waveguide bifurcation for asymmetric modes p 101 A85-20170
Dual-mode coaxial feed with low crosspolarisation p 101 A85-20171
Plot of modal field distribution in rectangular and circular waveguides p 101 A85-25170
Turbofan noise generation. Volume 2: Computer programs [NASA-CR-167952] p 175 N85-11791

PROPELLANT TANKS
Ion thruster system (8-cm) cyclic endurance test
[NASA-CR-174745] p 47 N85-12937
PROPELLANT TESTS
Electrothermal thruster diagnostics p 42 A85-16440
Compatibility experiments of facilities, materials, and propellants for electrothermal thrusters
[NASA-TM-86956] p 49 N85-21260
PROPELLER BLADES
Large-scale advanced propfan (LAP) program progress report
[AIAA PAPER 85-1187] p 17 A85-47021
Noise constraints effecting optimal propeller designs
[SAE PAPER 850871] p 7 A85-50106
Noise constraints effecting optimal propeller designs
[NASA-TM-86967] p 8 N85-19923
Large-scale Advanced Propfan (LAP) program
[NASA-TM-87067] p 32 N85-29964
PROPELLER EFFICIENCY
Analytical determination of propeller performance degradation due to ice accretion
[AIAA PAPER 85-0339] p 14 A85-20867
Large-scale advanced propfan (LAP) program progress report
[AIAA PAPER 85-1187] p 17 A85-47021
Large-scale Advanced Propfan (LAP) program
[NASA-TM-87067] p 32 N85-29964
PROPELLER FANS
Wind tunnel results of advanced high speed propellers in the takeoff, climb, and landing operating regimes
[AIAA PAPER 85-1259] p 6 A85-47025
Large-scale Advanced Propfan (LAP) performance, acoustic and weight estimation, January, 1984
[NASA-CR-174782] p 9 N85-22368
Wind tunnel results of advanced high speed propellers in the takeoff, climb and landing operating regimes
[NASA-TM-87054] p 9 N85-29925
PROPELLERS
Modelling of wind tunnel wall effects on the radiation characteristics of acoustic sources
[AIAA PAPER 84-2364] p 174 A85-16104
Inviscid analysis of advanced turboprop propeller flow fields
[AIAA PAPER 85-1263] p 6 A85-43977
Wind tunnel results of advanced high speed propellers in the takeoff, climb, and landing operating regimes
[AIAA PAPER 85-1259] p 6 A85-47025
Further comparison of wind tunnel and airplane acoustic data for advanced design high speed propeller models
[NASA-TM-86935] p 176 N85-22108
Wind tunnel results of advanced high speed propellers in the takeoff, climb and landing operating regimes
[NASA-TM-87054] p 9 N85-29925
PROPULSION
Energy efficient engine. Volume 1: Component development and integration program
[NASA-CR-173084] p 22 N85-10992
Future directions in aeropropulsion technology
[NASA-TM-87010] p 1 N85-23685
Heat transfer in aeropropulsion systems
[NASA-TM-87066] p 119 N85-31444
Status of advanced orbital transfer propulsion
[NASA-TM-87069] p 52 N85-35225
PROPULSION SYSTEM CONFIGURATIONS
The energetics of hydrogen atom recombination - Analysis, experiments, and modeling --- in electrothermal propulsion system p 179 A85-16444
Aerodynamic effect of combustor inlet air pressure on fuel jet atomization p 109 A85-27096
Review - Computational methods for internal flows with emphasis on turbomachinery p 4 A85-29126
Main propulsion system design recommendations for an advanced Orbit Transfer Vehicle
[AIAA PAPER 85-1336] p 36 A85-39730
Future fundamental combustion research for aeropropulsion systems
[AIAA PAPER 85-1398] p 16 A85-42671
Space station propulsion options
[AIAA PAPER 85-1155] p 45 A85-43975
Investigation of a pulsed electrothermal thruster system
[NASA-CR-174768] p 46 N85-11132
OTV Propulsion Issues
[NASA-CP-2347] p 37 N85-16989
Manrating orbital transfer vehicle propulsion
[NASA-TM-87019] p 50 N85-25385
Future fundamental combustion research for aeropropulsion systems
[NASA-TM-87049] p 30 N85-27870
PROPULSION SYSTEM PERFORMANCE
IAPS (8-cm) ion thruster cyclic endurance test --- Ion Auxiliary Propulsion System p 42 A85-16406
Ion propulsion for communications satellites p 42 A85-16412
Ring-cusp ion thrusters p 42 A85-16438
Experiments with a microwave electrothermal thruster concept p 42 A85-16441
Aerodynamic effect of combustor inlet air pressure on fuel jet atomization p 109 A85-27096
Development of a large insert gas ion thruster p 45 A85-42922
An evaluation of oxygen/hydrogen propulsion systems for the Space Station
[AIAA PAPER 85-1156] p 45 A85-43976
Results of electric-vehicle propulsion system performance on three lead-acid battery systems p 156 A85-45443
Energy efficient engine component development and integration program
[NASA-CR-169496] p 22 N85-10989
Investigation of a pulsed electrothermal thruster system
[NASA-CR-174768] p 46 N85-11132
The Altitude Wind Tunnel (AWT): A unique facility for propulsion system and adverse weather testing
[NASA-TM-86921] p 35 N85-18067
Performance and surge limits of a TF30-P-3 turbofan engine/axisymmetric mixed-compression inlet propulsion system at Mach 2.5
[NASA-TP-2461] p 27 N85-25261
Error reduction program --- combustor performance evaluation codes
[NASA-CR-174776] p 172 N85-27584
An evaluation of oxygen-hydrogen propulsion systems for the Space Station
[NASA-TM-87059] p 52 N85-28971
Energy efficient engine integrated core/low spool test hardware design report
[NASA-CR-168137] p 31 N85-29956
PROPULSIVE EFFICIENCY
Inert gas test of two 12-cm magnetostatic thrusters p 43 A85-29310
Manrating orbital transfer vehicle propulsion
[NASA-TM-87019] p 50 N85-25385
PROPYLENE
High temperature oxidation of propene p 61 A85-33570
PROSTHETIC DEVICES
Friction and wear properties of a Charnley artificial hip joint
[ASLE PREPRINT 84-LC-4A-4] p 168 A85-38444
PROTECTIVE COATINGS
Oxidation-based model for thermal barrier coating life p 78 A85-10310
Performance of thermal barrier coatings in high heat flux environments p 79 A85-19087
Microstructural development of protective Al2O3 scales p 80 A85-21650
Cyclic oxidation behavior of beta+gamma overlay coatings on gamma and gamma+gamma-prime alloys p 68 A85-32431
Development of coated single-crystal superalloy systems for gas turbine applications p 68 A85-32440
Properties of coated and modified surfaces p 53 A85-36694
Dopant effect of yttrium and the growth and adherence of alumina on nickel-aluminum alloys p 82 A85-40973
Surface protection overview p 21 N85-10978
Energy efficient engine high pressure turbine ceramic shroud support technology report
[NASA-CR-168036] p 23 N85-10996
Experimental and analytical study of ceramic-coated turbine-tip shroud seals for small turbine engines
[NASA-TM-86881] p 25 N85-18057
Effects of MAR-M247 substrate (modified) composition on coating oxidation coating/substrate interdiffusion --- protective coatings for hot section components of gas turbine engines
[NASA-CR-174851] p 73 N85-19073
Effects of surface chemistry on hot corrosion life
[NASA-CR-174915] p 28 N85-26711
Ion beam sputter-deposited thin film coatings for protection of spacecraft polymers in low Earth orbit
[NASA-TM-87051] p 91 N85-30137
Mechanical protection of DLC films on fused silica slides
[NASA-TM-87056] p 91 N85-30138
Diamondlike carbon protective coatings for IR materials
[NASA-TM-87083] p 178 N85-34631
PROTON IRRADIATION
Effects of 1 MeV electrons and 10 MeV protons on the performance and reflectance of thin BSR cells --- back surface reflector p 182 A85-35699
PULLEYS
Feasibility demonstration of a novel, flat-belt, continuously variable transmission or automotive and electric-hybrid vehicle application
[NASA-CR-174430] p 185 N85-19894
PULSED JET ENGINES
Investigation of a pulsed electrothermal thruster system
[NASA-CR-174768] p 46 N85-11132
PULSED LASERS
Laser balancing system for high material removal rates
[NASA-CR-174731] p 126 N85-12341
PUMPS
Operational performance of the photovoltaic-powered grain mill and water pump at Tangaye, Burkina Faso (formerly Upper Volta)
[NASA-TM-86970] p 161 N85-23243
PYROELECTRICITY
Pyroelectric conversion in space p 45 A85-45377
PYROLYSIS
Shock tube study of the fuel structure effects on the chemical kinetic mechanisms responsible for soot formation, part 2
[NASA-CR-174880] p 63 N85-25444
Preparation of silicon carbide-silicon nitride fibers by the pyrolysis of polycarbosilazane precursors
[NASA-TM-86505] p 91 N85-28107
Fuel-rich catalytic combustion: A soot-free technique for in situ hydrogen-like enrichment
[NASA-TP-2498] p 63 N85-31244

Q

QUALITY CONTROL
Fabrication and quality assurance processes for superhybrid composite fan blades
[NASA-TM-83354] p 57 N85-14882
QUANTITATIVE ANALYSIS
Rapid estimation of concentration of aromatic classes in middistillate fuels by high-performance liquid chromatography
[NASA-TP-2495] p 93 N85-31307

R

RADAR CROSS SECTIONS
Numerical methods for analyzing electromagnetic scattering
[NASA-CR-175507] p 99 N85-21438
Normal modes in an overmoded circular waveguide coated with lossy material
[NASA-CR-176186] p 100 N85-35320
RADIAL FLOW
Analysis of buoyancy effect on fully developed laminar heat transfer in a rotating tube p 110 A85-35596
The three-dimensional compressible flow in a radial inflow turbine scroll p 6 A85-41826
RADIANT HEATING
Development of advanced high-temperature heat flux sensors. Phase 2: Verification testing
[NASA-CR-174973] p 126 N85-35391
RADIATION CHEMISTRY
Fast laser-induced aerosol formation for visualization of gas flows p 121 A85-31113
RADIATION DAMAGE
Theory of the high base resistivity n(+)pp(+) silicon solar cell and its application to radiation damage effects p 154 A85-32639
Radiation damage and defect behavior in ion-implanted, lithium counterdoped silicon solar cells p 182 A85-35698
Lithium counterdoped silicon solar cell
[NASA-CASE-LEW-14177-1] p 160 N85-20535
The effects of lithium counterdoping on radiation damage and annealing in n(+)p silicon solar cells p 50 N85-22586
RADIATION DISTRIBUTION
Numerical methods for analyzing electromagnetic scattering
[NASA-CR-175507] p 99 N85-21438
RADIATION DOSAGE
Radiation exposure and performance of multiple burn LEO-GEO orbit transfer trajectories
[NASA-TM-86946] p 36 N85-21228
RADIATION EFFECTS
Effects of 1 MeV electrons and 10 MeV protons on the performance and reflectance of thin BSR cells --- back surface reflector p 182 A85-35699
RADIATION MEASUREMENT
Flame radiation and linear heat transfer in a tubular-can combustor p 15 A85-39580
Combustion system for radiation investigations p 21 N85-10986
RADIATION SHIELDING
Applicability of 100kWe-class of space reactor power systems to NASA manned space station missions
[NASA-CR-174696] p 177 N85-35728

RADIATION TOLERANCE
Lithium counterdoped silicon solar cell
[NASA-CASE-LEW-14177-1] p 160 N85-20535
RADIATIVE HEAT TRANSFER
Methods for heat transfer and temperature field analysis of the insulated diesel
[NASA-CR-174783] p 185 N85-16699
Performance analysis of radiation cooled dc transmission lines for high power space systems
[NASA-TM-87040] p 104 N85-28222
RADICALS
Ideal gas thermodynamic properties for the phenyl, phenoxy, and o-biphenyl radicals
[NASA-TM-83800] p 184 N85-22204
RADII
Automatic sphericity interferometer for testing lens radii
[AD-A155736] p 125 N85-33457
RADIO FREQUENCIES
Precision tunable resonant microwave cavity
[NASA-CASE-LEW-13935-1] p 103 N85-20248
Automated testing of developmental satellite communications systems and subsystems
[NASA-TM-87070] p 100 N85-31348
RADIO FREQUENCY DISCHARGE
Deposition of silicon nitride from SiCl4 and NH3 in a low pressure RF plasma p 81 A85-36229
Dielectric properties of 'diamondlike' carbon prepared by RF plasma deposition p 182 A85-38192
Experimental performance of a microwave cavity plasma disk ion source p 179 A85-43552
RADIO FREQUENCY HEATING
High frequency plasma generator for ion thrusters
[NASA-CR-174772] p 48 N85-17023
RADIO FREQUENCY INTERFERENCE
Adaptive antenna arrays for satellite communications: Design and testing
[NASA-CR-176162] p 100 N85-34329
RADIOGRAPHY
Radiographic detectability limits for seeded voids in sintered silicon carbide and silicon nitride
[NASA-TM-86945] p 138 N85-21674
RADIOMETERS
Liquid fuel spray processes in high-pressure gas flow
[NASA-TM-86944] p 115 N85-21570
Development of advanced high-temperature heat flux sensors. Phase 2: Verification testing
[NASA-CR-174973] p 126 N85-35391
RAILGUN ACCELERATORS
Friction in rail guns p 101 A85-16424
Preliminary analysis of space mission applications for electromagnetic launchers
[NASA-CR-174067] p 35 N85-12071
Rail accelerator technology and applications
[NASA-TM-86947] p 48 N85-21258
Arc-driven rail gun research
[NASA-CR-174816] p 132 N85-21662
RAMAN SPECTROSCOPY
Raman structural studies of the nickel electrode
[NASA-CR-175619] p 183 N85-23414
RANDOM NOISE
A high-speed implementation of the random decrement algorithm p 94 A85-29556
RANDOM VIBRATION
Oscillator response to nonstationary excitation
[ASME PAPER 84-WA/APM-38] p 140 A85-17039
RANDOM WALK
Monte Carlo lattice models for adsorbed polymer conformation
[NASA-TP-2453] p 183 N85-24961
RANKINE CYCLE
Overview of waste heat utilization systems
[NASA-TM-86901] p 184 N85-13692
Dynamic power systems for power generation p 158 N85-13892
Comparative evaluation of three alternative power cycles for waste heat recovery from the exhaust of adiabatic diesel engines
[NASA-TM-86953] p 186 N85-32043
RAPID QUENCHING (METALLURGY)
Rapid solidification and dynamic compaction of Ni-base superalloy powders p 67 A85-32414
Rapidly solidified NiAl and FeAl
[NASA-TM-86941] p 74 N85-20042
RARE EARTH COMPOUNDS
Strength and microstructure of sintered Si3N4 with rare-earth-oxide additions
[ACS PAPER 130-13-84] p 80 A85-25271
Oxidation of silicon nitride sintered with rare-earth oxide additions p 83 A85-42798
RARE GASES
Inert gas test of two 12-cm magnetostatic thrusters p 43 A85-29310
Development of a large insert gas ion thruster p 45 A85-42922
Heaterless ignition of inert gas ion thruster hollow cathodes
[NASA-TM-87086] p 52 N85-34177
RATIONAL FUNCTIONS
Axisymmetric solid elements by a rational hybrid stress method p 143 A85-41109
REACTION BONDING
Effect of hot isostatic pressing on reaction-bonded silicon nitride p 79 A85-15195
Microstructure of reaction-bonded silicon nitride consolidated by isostatic hot-pressing p 83 A85-45304
Radiographic detectability limits for seeded voids in sintered silicon carbide and silicon nitride
[NASA-TM-86945] p 138 N85-21674
REACTION KINETICS
Moderate temperature sodium cells. V - Discharge reactions and rechargeability of NiS and NiS2 positive electrodes in molten NaAlCl4 p 59 A85-11892
Systematic optimization of a detailed kinetic model using a methane ignition example p 59 A85-12890
Integrating chemical kinetic rate equations by selective use of stiff and nonstiff methods
[AIAA PAPER 85-0237] p 60 A85-19607
Chemical reactions involved in the initiation of hot corrosion of IN-738 p 66 A85-31688
Polarization (ellipsometric) measurements of liquid condensate deposition and evaporation rates and dew points in flowing salt/ash-containing combustion gases p 123 A85-46925
Comparison of numerical techniques for integration of stiff ordinary differential equations arising in combustion chemistry
[NASA-TP-2372] p 17 N85-10065
CREKID: A computer code for transient, gas-phase combustion of kinetics
[NASA-TM-83806] p 17 N85-10068
New integration techniques for chemical kinetic rate equations. 2: Accuracy comparison
[NASA-TM-86893] p 23 N85-13798
Integrating chemical kinetic rate equations by selective use of stiff and nonstiff methods
[NASA-TM-86923] p 24 N85-15726
A study of interdiffusion in beta + gamma/gamma + gamma prime Ni-Cr-Al
[NASA-CR-174852] p 74 N85-20041
A comparison of the efficiency of numerical methods for integrating chemical kinetic rate equations
[NASA-TM-83590] p 25 N85-21162
READOUT
Electronic heterodyne readout of fringes in moire deflectometry p 122 A85-36726
REAL TIME OPERATION
Moving target, distributed, real-time simulation using Ada p 170 A85-34131
A generalized computer code for developing dynamic gas turbine engine models (DIGTEM) p 17 A85-49021
Hardware for a real-time multiprocessor simulator
[NASA-TM-83805] p 169 N85-10659
Operating system for a real-time multiprocessor propulsion system simulator. User's manual
[NASA-TP-2426] p 171 N85-17596
Real-Time Multiprocessor Programming Language (RTMPL) user's manual
[NASA-TP-2422] p 170 N85-28610
RECIRCULATIVE FLUID FLOW
Calculation of confined swirling flows
[AIAA PAPER 85-0060] p 108 A85-19491
Confined turbulent swirling recirculating flow predictions
[NASA-CR-174917] p 29 N85-26716
RECRYSTALLIZATION
Rapid solidification and dynamic compaction of Ni-base superalloy powders p 67 A85-32414
RECTANGLES
Elastohydrodynamic lubrication of line contacts p 126 A85-11069
RECTANGULAR PANELS
Noise transmission loss of a rectangular plate in an infinite baffle
[NASA-TP-2398] p 176 N85-22109
RECTANGULAR PLATES
Vibrations of twisted cantilevered plates - Summary of previous and current studies p 140 A85-22069
RECTANGULAR WAVEGUIDES
Plot of modal field distribution in rectangular and circular waveguides p 101 A85-25170
RECTENNAS
Technology for satellite power conversion
[NASA-CR-174335] p 159 N85-18451
REDOX CELLS
Chemical and electrochemical behavior of the Cr(III)/Cr(II) half-cell in the iron-chromium redox energy storage system p 61 A85-33785
Cycling performance of the iron-chromium redox energy storage system
[NASA-TM-87034] p 162 N85-27387
Evaluation of developmental membranes for the mixed reactant iron-chromium redox system
[NASA-TM-87074] p 164 N85-34443
Development of electrodes for the NASA iron/chromium
[NASA-CR-174724] p 165 N85-35471
REDUCED GRAVITY
Free-surface phenomena under low- and zero-gravity conditions
[NASA-CR-175885] p 36 N85-27922
REDUCTION
Life and reliability modeling of bevel gear reductions
[NASA-TM-87006] p 133 N85-27227
REDUCTION (CHEMISTRY)
Electrocatalysis of fuel cell reactions: Investigation of alternate electrolytes
[NASA-CR-174753] p 157 N85-11455
Effect of water on hydrogen permeability --- Stirling engines
[NASA-TM-86904] p 53 N85-14864
REDUNDANCY
Sensor failure detection for jet engines using analytical redundancy
[AIAA PAPER 84-1452] p 13 A85-16097
REFINING
Jet fuel property changes and their effect on producibility and cost in the U.S., Canada, and Europe
[NASA-CR-174840] p 93 N85-27012
REFLECTANCE
Nitriding of titanium and its alloys by N2, NH3 or mixtures of N2 + H2 in a dc arc plasma at low pressures (or = to torr)
[NASA-TM-83803] p 131 N85-15168
REFLECTION
Preliminary design of a 10 kW thermophotovoltaic system for space applications p 45 A85-45371
REFRACTIVITY
A comparison of electronic heterodyne moire deflectometry and electronic heterodyne holographic interferometry for flow measurements
[NASA-TM-87071] p 125 N85-32302
The use of a laser Doppler velocimeter in a standard flammability tube
[NASA-CR-174960] p 125 N85-35389
REFRACTORY COATINGS
Thermal barrier coating system
[NASA-CASE-LEW-13324-2] p 57 N85-21266
REFRACTORY MATERIALS
Milling of Si3N4 with Si3N4 hardware
[NASA-TM-86864] p 84 N85-10191
Nonlinear analysis for high-temperature multilayered fiber composite structures --- turbine blades
[NASA-TM-83754] p 57 N85-21273
Viscoplastic constitutive relationships with dependence on thermomechanical history.
[NASA-CR-174836] p 146 N85-21691
Convoluted nozzle design for the RL10 derivative 2B engine
[NASA-CR-174953] p 32 N85-29965
REFRACTORY METAL ALLOYS
Application of two creep fatigue life models for the prediction of elevated temperature crack initiation of a nickel base alloy
[AIAA PAPER 85-1420] p 69 A85-43979
REFRACTORY METALS
High temperature metal and ceramic composites p 55 A85-37483
REGENERATION (ENGINEERING)
Initial results of sensitivity tests - Performed on the RE-1000 free-piston Stirling engine p 129 A85-45466
REGENERATIVE FUEL CELLS
Design considerations for a 10-kW integrated hydrogen-oxygen regenerative fuel cell system p 155 A85-45380
Regenerative fuel cell energy storage system for a low Earth orbit space station
[NASA-CR-174802] p 158 N85-13371
Engineering model system study for a regenerative fuel cell: Study report
[NASA-CR-174801] p 158 N85-16292
Develop and test fuel cell powered on-site integrated total energy systems. Phase 3: Full-scale power plant development
[NASA-CR-168338] p 164 N85-30483
Regenerative fuel cell systems for space station p 104 N85-31372
System level electrochemical principles p 104 N85-31375
REGIONAL PLANNING
Development and use of the computer software package for planning the 12 GHz broadcasting-satellite service at RARC '83 p 96 A85-29605

REGRESSION ANALYSIS
The effects of seven alloying elements on the microstructure and stress-rupture behavior of nickle-base superalloys
[NASA-TM-83791] p 70 N85-10168
Thermal traction contact performance evaluation under fully flooded and starved conditions
[NASA-CR-168173] p 132 N85-25848
A multiple linear regression analysis of hot corrosion attack on a series of nickel base turbine alloys
[NASA-TM-87020] p 77 N85-31284
REINFORCING FIBERS
Fibers for structurally reliable metal and ceramic composites p 55 A85-37484
High performance fibers for structurally reliable metal and ceramic composites --- advanced gas turbine engine materials
[NASA-TM-86878] p 56 N85-12095
Preparation of silicon carbide-silicon nitride fibers by the pyrolysis of polycarbosilazane precursors
[NASA-TM-86505] p 91 N85-28107
REISSNER THEORY
Rational approach for assumed stress finite elements p 139 A85-12029
On the existence and stability conditions for mixed-hybrid finite element solutions based on Reissner's variational principle p 142 A85-33847
RELIABILITY
The 30 GHz solid state amplifier for low cost low data rate ground terminals
[NASA-CR-174795] p 102 N85-12300
Life and reliability modeling of bevel gear reductions
[NASA-TM-87006] p 133 N85-27227
RELIABILITY ANALYSIS
Fatigue criterion to system design, life and reliability
[AIAA PAPER 85-1140] p 143 A85-40814
Reliability considerations for the total strain range version of strainrange partitioning
[NASA-CR-174757] p 144 N85-11380
Improved models for increasing wind penetration, economics and operating reliability
[NASA-CR-175538] p 160 N85-20545
Fatigue criterion to system design, life and reliability
[NASA-TM-87017] p 132 N85-27226
REMOTE CONTROL
Advanced in solid state switchgear technology for large space power systems p 102 A85-45362
REMOTE SENSORS
Fiber optic temperature sensor p 121 A85-29563
Remote displacement measurement using a passive interferometer with a fiber-optic link p 122 A85-42857
RENE 95
The effect of microstructure, temperature, and hold-time on low-cycle fatigue of As HIP P/M Rene 95 p 67 A85-32399
The influence of hold times on LCF and FCG behavior in a P/M Ni-base superalloy --- Low Cycle Fatigue/Fatigue Crack Growth p 67 A85-32400
REPORTS
Research and technology highlights of the Lewis Research Center
[NASA-TM-86899] p 186 N85-17928
RESEARCH
Bibliography of Lewis Research Center technical publications announced in 1983
[NASA-TM-83693] p 184 N85-22255
RESEARCH AND DEVELOPMENT
The role of modern control theory in the design of controls for aircraft turbine engines p 13 A85-13627
Recent work on a microwave ion source p 179 A85-16455
Environmentally-induced voltage limitations in large space power systems p 43 A85-18584
High temperature metal and ceramic composites p 55 A85-37483
The trend of future gas turbine technology p 16 A85-41778
Development of a large insert gas ion thruster p 45 A85-42922
Research and technology highlights of the Lewis Research Center
[NASA-TM-86899] p 186 N85-17928
Bibliography of Lewis Research Center technical publications announced in 1984
[NASA-TM-87012] p 184 N85-28876
RESEARCH FACILITIES
Research and technology highlights of the Lewis Research Center
[NASA-TM-86899] p 186 N85-17928
High efficiency solar cell research for space applications p 164 N85-31624
RESEARCH MANAGEMENT
The NASA photovoltaic technology program p 155 A85-35604
RESIN MATRIX COMPOSITES
Resin selection criteria for 'tough' composite structures p 81 A85-35139
Fundamental studies of composite toughness p 56 N85-12948
RESINS
Resin selection criteria for 'tough' composite structures p 81 A85-35139
RESISTANCE THERMOMETERS
High temperature static strain sensor development program p 19 N85-10959
RESISTOJET ENGINES
Space Station propulsion - The Advanced Development Program at Lewis
[AIAA PAPER 85-1154] p 44 A85-39626
Performance characterization tests of a 1-kW resistojet using hydrogen, nitrogen and ammonia as propellants
[AIAA PAPER 85-1159] p 44 A85-39628
An evaluation of oxygen/hydrogen propulsion systems for the Space Station
[AIAA PAPER 85-1156] p 45 A85-43976
Compatibility experiments of facilities, materials, and propellants for electrothermal thrusters
[NASA-TM-86956] p 49 N85-21260
Space station propulsion: The advanced development program at Lewis
[NASA-TM-86999] p 50 N85-25386
An evaluation of oxygen-hydrogen propulsion systems for the Space Station
[NASA-TM-87059] p 52 N85-28971
RESONANCE
Precision tunable resonant microwave cavity
[NASA-CASE-LEW-13935-1] p 103 N85-20248
RESONANT FREQUENCIES
The response of Helmholtz resonators to external excitation. I - Single resonators p 174 A85-26915
Natural frequencies of twisted rotating plates p 141 A85-32343
The use of an optical data acquisition system for bladed disk vibration analysis
[NASA-TM-86891] p 144 N85-15184
REUSABLE HEAT SHIELDING
Electron beam charging of Space Shuttle thermal protection system tiles p 39 N85-22478
REUSABLE ROCKET ENGINES
Reusable rocket engine turbopump condition monitoring
[SAE PAPER 841619] p 44 A85-39267
Structural Integrity and Durability of Reusable Space Propulsion Systems
[NASA-CP-2381] p 51 N85-27941
REUSABLE SPACECRAFT
Advanced research and technology programs for advanced high-pressure oxygen-hydrogen rocket propulsion
[NASA-TM-86969] p 37 N85-21231
REVERBERATION
Reverberation effects on directionality and response of stationary monopole and dipole sources in a wind tunnel
[NASA-TM-87063] p 119 N85-31443
REVERSED FLOW
Small gas turbine combustor study - Fuel injector performance in a transpiration-cooled liner
[AIAA PAPER 85-1312] p 16 A85-39717
Dilution jet configurations in a reverse flow combustor
[NASA-CR-174888] p 27 N85-22392
Small gas turbine combustor study: Fuel injector performance in a transpiration-cooled liner
[NASA-TM-86989] p 27 N85-25264
REYNOLDS NUMBER
A review and analysis of boundary layer transition data for turbine application
[NASA-TM-86880] p 113 N85-10306
Heat transfer in aeropropulsion systems
[NASA-TM-87066] p 119 N85-31444
REYNOLDS STRESS
A study of Reynolds-stress closure model
[NASA-CR-174342] p 114 N85-17324
RHENIUM
Compatibility experiments of facilities, materials, and propellants for electrothermal thrusters
[NASA-TM-86956] p 49 N85-21260
RHODIUM
Advanced thin film thermocouples
[NASA-CR-175541] p 124 N85-21607
RIGGING
Behavior of the lean methane-air flame at zero-gravity
[NASA-CR-175586] p 62 N85-21283
RITZ AVERAGING METHOD
A study of internal and distributed damping for vibrating turbomachiner blades
[NASA-CR-175901] p 30 N85-27868
RL-10 ENGINES
Convoluted nozzle design for the RL10 derivative 2B engine
[NASA-CR-174953] p 32 N85-29965
ROBOTICS
Investigation on experimental techniques to detect, locate and quantify gear noise in helicopter transmissions
[NASA-CR-3847] p 176 N85-17667
ROBUSTNESS (MATHEMATICS)
A design methodology for robust failure detection and isolation p 171 A85-47794
ROCKET ENGINE DESIGN
Electrothermal thruster diagnostics p 42 A85-16440
The energetics of hydrogen atom recombination - Analysis, experiments, and modeling --- in electrothermal propulsion system p 179 A85-16444
Simplified design and life prediction of rocket thrust chambers p 44 A85-29314
Reusable rocket engine turbopump condition monitoring
[SAE PAPER 841619] p 44 A85-39267
Progress report - Advanced cryogenic OTV engine technology
[AIAA PAPER 85-1341] p 44 A85-39735
Development of a large insert gas ion thruster p 45 A85-42922
Design and analysis report for the RL10-2B breadboard low thrust engine
[NASA-CR-174857] p 48 N85-19020
ROCKET ENGINES
Electrothermal thruster diagnostics p 42 A85-16440
Small centrifugal pumps for low thrust rockets
[AIAA PAPER 85-1302] p 45 A85-43978
Characterization of 8-cm engineering model thruster
[NASA-CR-174673] p 46 N85-11131
Design and analysis report for the RL10-2B breadboard low thrust engine
[NASA-CR-174857] p 48 N85-19020
Ring-cusp ion thruster with shell anode
[NASA-CASE-LEW-13881-1] p 48 N85-21256
ROCKET EXHAUST
Effects of chemical releases by the STS 3 orbiter on the ionosphere p 166 A85-29538
ROCKET THRUST
Heaterless ignition of inert gas ion thruster hollow cathodes
[NASA-TM-87086] p 52 N85-34177
ROLLER BEARINGS
Fast numerical calculations of EHD sliding traction forces Application to rolling bearings
[ASME PAPER 84-TRIB-26] p 127 A85-21289
Effect of two inner-ring oil-flow distribution schemes on the operating characteristics of a 35 millimeter bore ball bearing to 2.5 million DN
[NASA-TP-2404] p 130 N85-13233
Lubrication and performance of high-speed rolling-element bearings
[NASA-TM-86958] p 131 N85-21658
Effect of speed and press fit on fatigue life of roller-bearing inner-race contact
[NASA-TP-2496] p 134 N85-31511
Elastohydrodynamic lubrication calculations used as a tool to study scuffing
[NASA-TM-87097] p 137 N85-34408
Design and lubrication of high-speed rolling-element bearings
[NASA-TM-87107] p 137 N85-34409
Planetary-gear-support bearing test rig design
[NASA-CR-174927] p 12 N85-35185
ROLLING
Hydrodynamic lubrication of rigid nonconformal contacts in combined rolling and normal motion
[ASME PAPER 84-TRIB-13] p 127 A85-21280
ROLLING CONTACT LOADS
Hydrodynamic lubrication of rigid nonconformal contacts in combined rolling and normal motion
[ASME PAPER 84-TRIB-13] p 127 A85-21280
Fast numerical calculations of EHD sliding traction forces Application to rolling bearings
[ASME PAPER 84-TRIB-26] p 127 A85-21289
Pantographing self adaptive gap elements p 142 A85-37440
Effect of speed and press fit on fatigue life of roller-bearing inner-race contact
[NASA-TP-2496] p 134 N85-31511
Rolling, slip and traction measurements on low modulus materials
[NASA-CR-174909] p 135 N85-33491
ROOT-MEAN-SQUARE ERRORS
Comparative analysis of operational forecasts versus actual weather conditions in airline flight planning, volume 3
[NASA-CR-167864] p 167 N85-35536
ROTARY ENGINES
Stratified charge rotary aircraft engine technology enablement program
[NASA-CR-174812] p 25 N85-21163

ROTARY STABILITY
The effect of aerodynamic and structural detuning on turbomachine supersonic unstalled torsional flutter
[AIAA PAPER 85-0761] p 14 A85-30378
Dynamic analysis of straight and involute tooth forms
[ASME PAPER 84-DET-226] p 128 A85-33780
Structural response of a rotating bladed disk to rotor whirl
[NASA-CR-175605] p 27 N85-22391
ROTARY WINGS
Experimental aerodynamic characteristics of an NACA 0012 airfoil with simulated ice p 12 A85-21844
Performance degradation of helicopter rotor in forward flight due to ice p 11 A85-42937
Initial feasibility ground test of a proposed photogrammetric system for measuring the shapes of ice accretions on helicopter rotor blades during forward flight
[NASA-TM-87391] p 12 N85-12887
ROTATING BODIES
Effects of warping and pretwist on torsional vibration of rotating beams
[ASME PAPER 84-WA/APM-41] p 140 A85-17040
Finite difference analysis of torsional vibrations of pretwisted, rotating, cantilever beams with effects of warping p 143 A85-42047
ROTATING CYLINDERS
Computation and turbulence closure models for shear flows in rotating curved bodies p 107 A85-14349
Convective influence on the stability of a cylindrical solid-liquid interface p 109 A85-26911
Analysis of buoyancy effect on fully developed laminar heat transfer in a rotating tube p 110 A85-35596
ROTATING DISKS
Vibration and flutter of mistuned bladed-disk assemblies
[AIAA PAPER 84-0991] p 139 A85-16095
ROTATING FLUIDS
Computation and turbulence closure models for shear flows in rotating curved bodies p 107 A85-14349
ROTATING SHAFTS
Rotordynamic coefficients for compressible flow in tapered annular seals p 129 A85-42573
Analysis of experimental shaft seal data for high-performance turbomachines, as for Space Shuttle main engines
[NASA-TM-86928] p 115 N85-21569
Variable force, eddy-current or magnetic damper
[NASA-CASE-LEW-13717-1] p 134 N85-30333
ROTATING STALLS
Stall recovery control strategy methodology and results
[AIAA PAPER 85-1433] p 16 A85-40841
A theory of post-stall transients in multistage axial compression systems
[NASA-CR-3878] p 8 N85-21117
ROTATION
Linearization of digital derived rate algorithm for use in linear stability analysis
[NASA-TM-87000] p 41 N85-23904
ROTOR AERODYNAMICS
Flutter and forced response of mistuned rotors using standing wave analysis p 139 A85-12721
Effects of friction dampers on aerodynamically unstable rotor stages p 14 A85-21866
The UH-1H helicopter icing flight test program - An overview
[AIAA PAPER 85-0338] p 11 A85-28898
Investigation of flow phenomena in a transonic fan rotor using laser anemometry
[ASME PAPER 84-GT-199] p 4 A85-32963
Rotordynamic Instability Problems in High-Performance Turbomachinery
[NASA-CP-2338] p 131 N85-14116
The UH-1H helicopter icing flight test program: An overview
[NASA-TM-86925] p 11 N85-15702
Operating characteristics of a 0.87 kW-hr flywheel energy storage module
[NASA-TM-87038] p 133 N85-28371
Vibration control of rotor shaft
[NASA-TM-87053] p 133 N85-29292
ROTOR BLADES
Noise produced by the interaction of a rotor wake with a swept stator blade
[AIAA PAPER 84-2326] p 173 A85-13956
An experimental investigation and numerical prediction of thermomechanical phenomena in high speed rotor tip rubbing p 14 A85-25442
Turbofan noise generation. Volume 2: Computer programs
[NASA-CR-167952] p 175 N85-11791
ROTOR BLADES (TURBOMACHINERY)
Acoustic pressures emanating from a turbomachine stage
[AIAA PAPER 84-2325] p 2 A85-10870
Review - Computational methods for internal flows with emphasis on turbomachinery p 4 A85-29126
Natural frequencies of twisted rotating plates p 141 A85-32343
Calculation of three-dimensional, viscous flow through turbomachinery blade passages by parabolic marching
[AIAA PAPER 85-1408] p 5 A85-39767
A three-dimensional boundary-layer analysis including heat-transfer and blade-rotation effects p 6 A85-42988
Coolant passage heat transfer with rotation p 20 N85-10968
Structural analysis p 20 N85-10969
Incompressible lifting-surface aerodynamics for a rotor-stator combination
[NASA-TM-83767] p 7 N85-12039
Structural response of a rotating bladed disk to rotor whirl
[NASA-CR-175605] p 27 N85-22391
Calculation of three-dimensional, viscous flow through turbomachinery blade passages by parabolic marching
[NASA-TM-86984] p 9 N85-23711
Vibration and buckling of rotating, pretwisted, preconed beams including Cooriolis effects
[NASA-TM-87004] p 146 N85-25893
Development of a rotor wake-vortex model, volume 1
[NASA-CR-174849] p 9 N85-26668
Aerodynamic detuning analysis of an unstalled supersonic turbofan cascade
[NASA-TM-87001] p 9 N85-26670
Ice shapes and the resulting drag increase for a NACA 0012 airfoil
[NASA-TM-83556] p 11 N85-27839
Reflection plane tests of a wind turbine blade tip section with ailerons
[NASA-TM-87018] p 165 N85-34444
ROTOR SPEED
Shutdown characteristics of the Mod-O wind turbine with aileron controls
[NASA-TM-86918] p 159 N85-16299
Development of a rotor wake-vortex model, volume 1
[NASA-CR-174849] p 9 N85-26668
ROTORS
Aileron controls for wind turbine applications p 157 A85-45513
Aileron controls for wind turbine applications
[NASA-TM-86867] p 158 N85-11458
Laser balancing system for high material removal rates
[NASA-CR-174731] p 126 N85-12341
The use of an optical data acquisition system for bladed disk vibration analysis
[NASA-TM-86891] p 144 N85-15184
Reusable rocket engine turbopump condition monitoring p 51 N85-26907
RUNGE-KUTTA METHOD
Recent advances in methods for numerical solution of O.D.E. initial value problems p 171 A85-21370
Application of Runge Kutta time marching scheme for the computation of transonic flows in turbomachines
[AIAA PAPER 85-1332] p 5 A85-39728
RUPTURING
A continuous damage model based on stepwise-stress creep rupture tests
[NASA-CR-174941] p 152 N85-32341

S

S MATRIX THEORY
Circular waveguide bifurcation for asymmetric modes p 101 A85-20170
SALTS
Airfoil deposition model p 21 N85-10979
SAPPHIRE
Incident beam polarization for laser Doppler velocimetry employing a sapphire cylindrical window p 122 A85-39835
Incident beam polarization for laser Doppler velocimetry employing a sapphire cylindrical window
[NASA-TM-87064] p 178 N85-28786
SATELLITE ANTENNAS
Status of NASA's multibeam communications technology program p 100 A85-14432
Advanced 30/20 GHz multiple beam antenna for future communications satellites p 96 A85-14436
Technical characteristics of the broadcasting satellite plan at 12 GHz for the Western Hemisphere p 96 A85-28233
On the calculation of the directivity of planar array feeds for satellite reflector applications p 97 A85-32249
Configuration study for a 30 GHz monolithic receive array, volume 2
[NASA-CR-174697-VOL-2] p 99 N85-18240
Alternatives for satellite sound broadcast systems at HF and VHF p 99 N85-23815
SATELLITE NETWORKS
A frequency-routed satellite system concept using multiple orthogonally-polarized beams for frequency reuse p 97 A85-34470
Modeling of NASA's 30/20 GHz satellite communications system p 38 A85-36663
Demand for satellite-provided domestic communications services up to the year 2000
[NASA-TM-86894] p 97 N85-15099
SATELLITE ORBITS
Engineering calculations for communications satellite systems planning
[NASA-CR-175552] p 37 N85-21233
SATELLITE TELEVISION
On the subjective evaluation of the interference protection ratios' measurements for co-channel FM-TV signals p 96 A85-28241
Experimental results supporting the determination of service quality objectives for DBS systems p 96 A85-29611
SATELLITE TEMPERATURE
Interdisciplinary design analysis of a precision spacecraft antenna
[AIAA PAPER 85-0804] p 38 A85-30303
SATELLITE TRANSMISSION
Adaptive antenna arrays for satellite communications: Design and testing
[NASA-CR-176162] p 100 N85-34329
SCALE (CORROSION)
Cavitation erosion size scale effects p 65 A85-11935
Microstructural development of protective Al2O3 scales p 80 A85-21650
SCALE MODELS
Comparison of scaled model data to full size energy efficient engine test results
[AIAA PAPER 84-2281] p 13 A85-13953
SCALING
Universal binding energy relations in metallic adhesion
[NASA-TM-86889] p 72 N85-12132
SCHLIEREN PHOTOGRAPHY
Rainbow schlieren vs Mach-Zehnder interferometer - A comparison p 121 A85-28820
SCHOTTKY DIODES
Effect of barrier height on friction behavior of the semiconductors silicon and gallium arsenide in contact with pure metals
[NASA-TP-2405] p 84 N85-13044
SCINTILLATION
Unsteady pressure measurements on a biconvex airfoil in a transonic oscillating cascade
[NASA-TM-86914] p 8 N85-15689
SCREENS
Flow through very porous inclined screens
[AIAA PAPER 85-1650] p 111 A85-40750
Flow through very porous inclined screens
[NASA-TM-86979] p 116 N85-25761
SEALS (STOPPERS)
Metallurgical and mechanical phenomena due to rubbing of titanium against sintered powder Nichrome p 127 A85-22281
An experimental investigation and numerical prediction of thermomechanical phenomena in high speed rotor tip rubbing p 14 A85-25442
A comparison of flow rates and pressure profiles for N-sequential inlets and three related seal configurations p 109 A85-26526
High-temperature erosion of plasma-sprayed, yttria-stabilized zirconia in a simulated turbine *environment*
[AIAA PAPER 85-1219] p 82 A85-39662
Rotordynamic coefficients for compressible flow in tapered annular seals p 129 A85-42573
High-temperature erosion of plasma-sprayed, yttria-stabilized zirconia in a simulated turbine environment
[NASA-TP-2406] p 84 N85-13045
Experimental study of ceramic coated tip seals for turbojet engines
[NASA-TM-86939] p 114 N85-19363
Ribbon burner simulation of T-700 turbine shroud for ceramic lined seals research
[NASA-TM-86940] p 114 N85-19364
Variable friction secondary seal for face seals
[NASA-CASE-LEW-14170-1] p 131 N85-20377
Sliding seal materials for adiabatic engines
[NASA-CR-174893] p 89 N85-22757
Experimental stiffness of tapered bore seals
[NASA-TM-86978] p 132 N85-25847
Tape casting as an approach to an all-ceramic turbine shroud seal
[NASA-TM-87078] p 135 N85-32333
Oxidizing seal for a turbine tip gas path
[NASA-CASE-LEW-14053-1] p 136 N85-34402

Thermal stress analysis of a new turbine shroud seal concept
[NASA-TM-87082] p 136 N85-34406

SECONDARY EMISSION
Numerical simulation of positive-potential conductors in the presence of a plasma and a secondary-emitting dielectric p 102 A85-35306
Textured carbon surfaces on copper
[NASA-CASE-LEW-14130-1] p 95 N85-20156
Electron yields from spacecraft materials
p 40 N85-22512

SECONDARY FLOW
Comparison of secondary flows predicted by a viscous code and an inviscid code with experimental data for a turning duct p 106 A85-11634
Flow control in a diffusing S-Duct
[AIAA PAPER 85-0524] p 3 A85-25928

SEDIMENTS
Chemistry of fuel deposits and sediments and their predursors
[NASA-CR-174778] p 92 N85-10209

SELECTION
Resin selection criteria for 'tough' composite structures p 81 A85-35139

SELF EXCITATION
Internal hysteresis experienced on a high pressure syn gas compressor p 131 N85-14122

SELF SEALING
Experimental stiffness of tapered bore seals
[NASA-TM-86978] p 132 N85-25847

SEMICONDUCTING FILMS
Dielectric properties of 'diamondlike' carbon prepared by RF plasma deposition p 182 A85-38192

SEMICONDUCTOR DEVICES
A new very high voltage semiconductor switch
[NASA-TM-86957] p 103 N85-20246
Inelastic tunnel diodes
[NASA-CASE-LEW-13833-1] p 103 N85-21492

SEMICONDUCTOR JUNCTIONS
Prism-coupled light emission from tunnel junctions
p 181 A85-21425
Effect of solar-cell junction geometry on open-circuit voltage p 154 A85-28080
Screen printed interdigitated back contact solar cell
[NASA-CASE-LEW-13414-1] p 160 N85-20530

SEMICONDUCTOR LASERS
Remote displacement measurements using a laser diode p 121 A85-24464

SEMICONDUCTORS (MATERIALS)
AES and LEED study of the zinc blende SiC(100) surface p 61 A85-41633
Advanced in solid state switchgear technology for large space power systems p 102 A85-45362
Effect of barrier height on friction behavior of the semiconductors silicon and gallium arsenide in contact with pure metals
[NASA-TP-2405] p 84 N85-13044
GaAs and 3-5 compound solar cells status and prospects for use in space
[NASA-TM-86960] p 49 N85-21261

SENSITIVITY
Radiographic detectability limits for seeded voids in sintered silicon carbide and silicon nitride
[NASA-TM-86945] p 138 N85-21674

SENSORS
Sensor failure detection for jet engines using analytical redundancy
[AIAA PAPER 84-1452] p 13 A85-16097
A real-time FORTRAN implementation of a sensor failure detection, isolation and accommodation algorithm
p 171 A85-47704

SEPARATED FLOW
Generation of instability waves in flows separating from smooth surfaces p 1 A85-10352
Feedback in separated flows over symmetric airfoils
[AIAA PAPER 84-2297] p 3 A85-28899
Structure of ducted particle-laden turbulent jets
p 110 A85-38999
The computation of viscid/inviscid interaction on airfoils with separated flow p 6 A85-42954
The structure of dilute combusting sprays
[NASA-CR-174838] p 24 N85-15728
Vacuum chamber pressure effects on thrust measurements of low Reynolds number nozzles
[NASA-TM-86955] p 49 N85-21259

SEPARATION
The mechanisms of formation and prevention of channel segregation during alloy solidification
p 180 A85-18082

SEPARATORS
Separator development and testing of nickel-hydrogen cells p 156 A85-45386
Electric utility acid fuel cell stack technology advancement
[NASA-CR-174804] p 159 N85-17422
Alkaline battery containing a separator of a cross-linked copolymer of vinyl alcohol and unsaturated carboxylic acid
[NASA-CASE-LEW-13102-1] p 104 N85-29144
Development of a lithium secondary battery separator
p 104 N85-31378

SERIES EXPANSION
A convergent series expansion for hyperbolic systems of conservation laws
[NASA-CR-172557] p 168 N85-21990

SERVICE LIFE
Life modeling of atmospheric and low pressure plasma-sprayed thermal-barrier coating
p 81 A85-29728
Fatigue criterion to system design, life and reliability
[AIAA PAPER 85-1140] p 143 A85-40814
Long-life high performance fuel cell program
[NASA-CR-174874] p 50 N85-25384
Fatigue criterion to system design, life and reliability
[NASA-TM-87017] p 132 N85-27226
Life cycle test results of a bipolar nickel hydrogen battery
[NASA-TM-87046] p 163 N85-30480
Free-piston Stirling engine/linear alternator 1000-hour endurance test
[NASA-CR-174771] p 163 N85-30481
Design principles for nickel-hydrogen cells and batteries
[NASA-TM-87037] p 164 N85-31646

SERVICES
Demand for satellite-provided domestic communications services up to the year 2000
[NASA-TM-86894] p 97 N85-15099

SERVOMECHANISMS
Application of traction drives as servo mechanisms
p 152 N85-33520

SHAFTS (MACHINE ELEMENTS)
An analysis of temperature effect in a finite journal bearing with spatial tilt and viscous dissipation
p 126 A85-11074
Vibration control of rotor shaft
[NASA-TM-87053] p 133 N85-29292

SHALE OIL
Lubricity of well-characterized jet and broad-cut fuels by ball-on-cylinder machine
[NASA-TM-83807] p 92 N85-12183

SHEAR FLOW
Computation and turbulence closure models for shear flows in rotating curved bodies p 107 A85-14349
Approximate analysis for resonance of an incompressible shear layer plus edges
p 107 A85-19377
Some unique experiments on receptivity --- for forced disturbances entering shear flow
[AIAA PAPER 85-0533] p 174 A85-25932
Turbulence modelling for complex shear flows
[AIAA PAPER 85-1652] p 111 A85-40752

SHEAR LAYERS
Generation of instability waves in flows separating from smooth surfaces p 1 A85-10352
Approximate analysis for resonance of an incompressible shear layer plus edges
p 107 A85-19377
Sound generation and upstream influence due to instability waves interacting with non-uniform mean flows
p 174 A85-20738
Turbulent solutions of equations of fluid motion
p 118 N85-31441

SHEAR PROPERTIES
Structural characteristics of high temperature composites
[NASA-CR-175998] p 58 N85-30037

SHEAR STRENGTH
Imide modified epoxy matrix resins
[NASA-CR-174695] p 85 N85-15892
Graphite/PMR polyimide composites with improved toughness
[NASA-TM-87081] p 58 N85-32148

SHEAR STRESS
A study of Reynolds-stress closure model
[NASA-CR-174342] p 114 N85-17324

SHELL ANODES
Ring-cusp ion thruster with shell anode
[NASA-CASE-LEW-13881-1] p 48 N85-21256

SHELL STABILITY
Analysis of shell type structures subjected to time dependent mechanical and thermal loading
[NASA-CR-175747] p 147 N85-25896
Dynamic creep buckling: Analysis of shell structures subjected to time-dependent mechanical and thermal loading p 149 N85-27959

SHELL THEORY
Hybrid Semiloof elements for plates and shells based upon a modified Hu-Washizu principle
p 139 A85-15893
Dynamic creep buckling: Analysis of shell structures subjected to time-dependent mechanical and thermal loading p 149 N85-27959

SHELLS (STRUCTURAL FORMS)
Geometrically nonlinear analysis of laminated elastic structures
[NASA-CR-175609] p 146 N85-21720

SHOCK RESISTANCE
Dispersed-metal-toughened alumina
[NASA-CR-174687] p 89 N85-22758

SHOCK TUBES
Shock tube measurements of growth constants in the branched-chain ethane-carbon monoxide-oxygen system
[NASA-TM-87068] p 64 N85-32156

SHOCK WAVE ATTENUATION
Time dependent computation of the Euler equations for designing 2-D cascades, including the case of transonic shock free design p 5 A85-41814

SHOCK WAVE INTERACTION
Heat transfer investigation in the junction region of circular cylinder normal to a flat plate at 90 deg location
[ASME PAPER 84-WA/HT-70] p 111 A85-39898
An experimental study of three-dimensional shock wave/turbulent boundary layer interactions in a supersonic flow
[AIAA PAPER 85-1566] p 5 A85-40691

SHOCK WAVES
A multiple-scales model of the shock-cell structure of imperfectly expanded supersonic jets
p 113 A85-49354
Observations from varying the lift and drag inputs to a noise prediction method for supersonic helical tip speed propellers
[NASA-TM-83797] p 175 N85-10788
Experimental investigation of shock-cell noise reduction for dual-stream nozzles in simulated flight
[NASA-CR-3846] p 175 N85-13549
Unsteady flow in a supersonic cascade with two in-passage shocks
[NASA-CR-3925] p 10 N85-35158

SHROUDED TURBINES
Ribbon burner simulation of T-700 turbine shroud for ceramic lined seals research
[NASA-TM-86940] p 114 N85-19364
Thermal stress analysis of a new turbine shroud seal concept
[NASA-TM-87082] p 136 N85-34406

SHROUDS
Energy efficient engine high pressure turbine ceramic shroud support technology report
[NASA-CR-168036] p 23 N85-10996
Experimental and analytical study of ceramic-coated turbine-tip shroud seals for small turbine engines
[NASA-TM-86881] p 25 N85-18057

SHUTDOWNS
Shutdown characteristics of the Mod-O wind turbine with aileron controls
[NASA-TM-86918] p 159 N85-16299
Analytical model for predicting emergency shutdown of a two-bladed horizontal axis wind turbine
[NASA-TM-83472] p 162 N85-30476

SIDELOBE REDUCTION
Configuration study for a 30 GHz monolithic receive array, volume 2
[NASA-CR-174697-VOL-2] p 99 N85-18240

SIDELOBES
The 20 GHz proof-of-concept test model results for a multiple scan beam dual reflector antenna
[NASA-CR-174268] p 98 N85-15944

SIGNAL ANALYSIS
The role of the reflection coefficient in precision measurement of ultrasonic attenuation
p 137 A85-42151

SIGNAL PROCESSING
A high-speed implementation of the random decrement algorithm p 94 A85-29556
Application of homomorphic signal processing to stress wave factor analysis
[NAS 1.26:174871] p 138 N85-21673

SIGNAL TO NOISE RATIOS
Experimental results supporting the determination of service quality objectives for DBS systems
p 96 A85-29611
Configuration study for a 30 GHz monolithic receive array, volume 2
[NASA-CR-174697-VOL-2] p 99 N85-18240

SIGNAL TRANSMISSION
Four-dimensional modulation and coding - An alternate to frequency-reuse p 97 A85-36653
Effect of Interfacial characteristics of metal clad polymeric substrates on electrical high frequency interconnection performance
[NASA-TM-86948] p 99 N85-20223

SILENCERS
The performance of jet noise suppression devices for industrial applications p 175 A85-42563

SILICON
Voltage controlling mechanisms in low resistivity silicon solar cells - A unified approach p 155 A85-35617
The effect of diffusion induced lattice stress on the open-circuit voltage in silicon solar cells p 181 A85-35620
Effect of barrier height on friction behavior of the semiconductors silicon and gallium arsenide in contact with pure metals
[NASA-TP-2405] p 84 N85-13044
The effects of lithium counterdoping on radiation damage and annealing in n(+)p silicon solar cells p 50 N85-22586

SILICON CARBIDES
A morphological study of silicon carbide prepared by chemical vapor deposition p 79 A85-20938
Fibers for structurally reliable metal and ceramic composites p 55 A85-37484
Feasibility study of the welding of SiC p 81 A85-39339
AES and LEED study of the zinc blende SiC(100) surface p 61 A85-41633
Evaluation of alpha-SiC sintering using statistical methods p 83 A85-42800
Hot corrosion of sintered alpha-SiC at 1000 C
[ACS PAPER 19-B-84P] p 83 A85-45302
Effect of hot isostatic pressing on the properties of sintered alpha silicon carbide p 83 A85-48757
Creep of chemically vapor deposited SiC fibers
[NASA-TM-86897] p 56 N85-14878
Fundamental tribological properties of ceramics
[NASA-TM-86915] p 85 N85-15893
Gas cooled fuel cell systems technology development
[NASA-CR-174732] p 158 N85-16291
NDE for heat engine ceramics
[NASA-TM-86949] p 137 N85-20389
Parametric evaluation of ball milling of SiC in water
[NASA-TM-86974] p 88 N85-21356
Radiographic detectability limits for seeded voids in sintered silicon carbide and silicon nitride
[NASA-TM-86945] p 138 N85-21674
Environmental effects on the tensile strength of chemically vapor deposited silicon carbide fibers
[NASA-TM-86981] p 89 N85-24000
Preparation of silicon carbide-silicon nitride fibers by the pyrolysis of polycarbosilazane precursors
[NASA-TM-86505] p 91 N85-28107
Burner rig corrosion of SiC at 1000 deg C
[NASA-TM-87061] p 53 N85-30011
Mechanism of strength degradation for hot corrosion of alpha-SiC
[NASA-TM-87052] p 91 N85-30135
Reliability of void detection in structural ceramics using scanning laser acoustic microscopy
[NASA-TM-87035] p 138 N85-32337
Mechanical properties of SiC fiber-reinforced reaction-bonded Si3N4 composites
[NASA-TM-87085] p 59 N85-34223

SILICON CONTROLLED RECTIFIERS
The J3 SCR model applied to resonant converter simulation p 102 A85-42156

SILICON DIOXIDE
Mechanical protection of DLC films on fused silica slides
[NASA-TM-87056] p 91 N85-30138

SILICON JUNCTIONS
Theory of the high base resistivity n(+)pp(+) silicon solar cell and its application to radiation damage effects p 154 A85-32639
Effects of 1 MeV electrons and 10 MeV protons on the performance and reflectance of thin BSR cells --- back surface reflector p 182 A85-35699

SILICON NITRIDES
Demonstration of a silicon nitride attrition mill for production of fine pure Si and Si3N4 powders p 78 A85-10825
Effect of hot isostatic pressing on reaction-bonded silicon nitride p 79 A85-15195
Strength and microstructure of sintered Si3N4 with rare-earth-oxide additions
[ACS PAPER 130-13-84] p 80 A85-25271
Deposition of silicon nitride from SiCl4 and NH3 in a low pressure RF plasma p 81 A85-36229
RF-sputtered silicon and hafnium nitrides - Properties and adhesion to 440C stainless steel p 81 A85-36240
Fracture of yttria-doped, sintered reaction-bonded silicon nitride
[ACS PAPER 7-J3-84] p 82 A85-42797
Oxidation of silicon nitride sintered with rare-earth oxide additions p 83 A85-42798
Microstructure of reaction-bonded silicon nitride consolidated by isostatic hot-pressing p 83 A85-45304
Milling of Si3N4 with Si3N4 hardware
[NASA-TM-86864] p 84 N85-10191
Factors influencing the ball milling of Si3N4 in water
[NASA-TM-86932] p 86 N85-19136
NDE for heat engine ceramics
[NASA-TM-86949] p 137 N85-20389
Oxidation and hot corrosion of hot-pressed Si3N4 at 1000 deg C
[NASA-TM-86977] p 88 N85-21358
Radiographic detectability limits for seeded voids in sintered silicon carbide and silicon nitride
[NASA-TM-86945] p 138 N85-21674
Preparation of silicon carbide-silicon nitride fibers by the pyrolysis of polycarbosilazane precursors
[NASA-TM-86505] p 91 N85-28107
Reliability of void detection in structural ceramics using scanning laser acoustic microscopy
[NASA-TM-87035] p 138 N85-32337
Mechanical properties of SiC fiber-reinforced reaction-bonded Si3N4 composites
[NASA-TM-87085] p 59 N85-34223
Reliability of two sintered silicon nitride materials
[NASA-TM-87092] p 92 N85-34284

SILICON POLYMERS
Preparation of silicon carbide-silicon nitride fibers by the pyrolysis of polycarbosilazane precursors
[NASA-TM-86505] p 91 N85-28107

SILVER
Effects of silver and group 2 fluorides addition to plasma sprayed chromium carbide high temperature solid lubricant for foil gas bearing to 650 deg C
[NASA-TM-86895] p 84 N85-14928
The role of silver in self-lubricating coatings for use at extreme temperatures
[NASA-TM-86943] p 87 N85-20127

SIMULATORS
Hardware for a real-time multiprocessor simulator
[NASA-TM-83805] p 169 N85-10659
Operating system for a real-time multiprocessor propulsion system simulator. User's manual
[NASA-TP-2426] p 171 N85-17596

SINGLE CRYSTALS
Elevated temperature creep-rupture behavior of the single crystal nickel-base superalloy NASAIR 100 p 66 A85-27812
Influence of composition on the microstructure and mechanical properties of a nickel-base superalloy single crystal p 66 A85-32387
Factors which influence directional coarsening of gamma-prime during creep in nickel-base superalloy single crystals p 67 A85-32388
Development of coated single-crystal superalloy systems for gas turbine applications p 68 A85-32440
Morphological changes of gamma prime precipitates in nickel-base superalloy single crystals
[NASA-TM-83698] p 70 N85-10165
The transient oxidation of single crystal NiAl+Zr
[NASA-CR-174756] p 70 N85-11221
The effect of tantalum and carbon on the structure/properties of a single crystal nickel-base superalloy
[NASA-CR-174779] p 71 N85-11223
Biaxial constitutive equation development for single crystals
[NASA-CR-174056] p 183 N85-11862
Low cycle fatigue of MAR-M 200 single crystals at 760 and 870 deg C
[NASA-TM-86933] p 74 N85-19074
Diamondlike flakes
[NASA-CASE-LEW-13837-2] p 57 N85-21267
Orientation and temperature dependence of some mechanical properties of the single-crystal nickel-base superalloy Rene N4. 3: Tension-compression anisotropy
[NASA-TM-86982] p 76 N85-22660
Effects of wear on structure-sensitive magnetic properties of ceramic ferrite in contact with magnetic tape
[NASA-TM-87007] p 90 N85-26991

SINTERING
Strength and microstructure of sintered Si3N4 with rare-earth-oxide additions
[ACS PAPER 130-13-84] p 80 A85-25271
Fracture of yttria-doped, sintered reaction-bonded silicon nitride
[ACS PAPER 7-J3-84] p 82 A85-42797
Oxidation of silicon nitride sintered with rare-earth oxide additions p 83 A85-42798
Evaluation of alpha-SiC sintering using statistical methods p 83 A85-42800
Hot corrosion of sintered alpha-SiC at 1000 C
[ACS PAPER 19-B-84P] p 83 A85-45302
Effect of hot isostatic pressing on the properties of sintered alpha silicon carbide p 83 A85-48757
Powder metallurgy forged gear development
[NASA-TM-87483] p 134 N85-29295
Reliability of void detection in structural ceramics using scanning laser acoustic microscopy
[NASA-TM-87035] p 138 N85-32337
Reliability of two sintered silicon nitride materials
[NASA-TM-87092] p 92 N85-34284

SIZE (DIMENSIONS)
Cavitation erosion size scale effects p 65 A85-11935
Effect of solar-cell junction geometry on open-circuit voltage p 154 A85-28080

SIZE DETERMINATION
Spray characterization with a nonintrusive technique using absolute scattered light p 120 A85-10036
Nonintrusive optical single-particle counter for measuring the size and velocity of droplets in a spray p 120 A85-16794
Research study of droplet sizing technology leading to the development of an advanced droplet sizing system
[NASA-CR-174839] p 123 N85-21604

SIZE DISTRIBUTION
Experimental study of the spray characteristics of a research airblast atomizer
[NASA-TM-86911] p 24 N85-15727

SKIN TEMPERATURE (NON-BIOLOGICAL)
Turbine heat transfer p 19 N85-10964

SLIDING
Hydrodynamic lubrication of rigid nonconformal contacts in combined rolling and normal motion
[ASME PAPER 84-TRIB-13] p 127 A85-21280

SLIDING CONTACT
Hydrodynamic lubrication of rigid nonconformal contacts in combined rolling and normal motion
[ASME PAPER 84-TRIB-13] p 127 A85-21280
Fast numerical calculations of EHD sliding traction forces Application to rolling bearings
[ASME PAPER 84-TRIB-26] p 127 A85-21289
Friction and wear of ceramics p 80 A85-23833

SLIDING FRICTION
Elastohydrodynamic lubrication of line contacts p 126 A85-11069
Friction and wear of some ferrous-base metallic glasses p 64 A85-11071
Mechanical-contact-induced transformation from the amorphous to the partially crystalline state in metallic glass p 65 A85-19084
Thermal and thermomechanical effects in dry sliding p 127 A85-23838
Ceramic wear in indentation and sliding contact p 82 A85-39549
An experimental investigation of rubbing interaction in labyrinth seals at cryogenic temperature p 129 A85-39938
Effect of barrier height on friction behavior of the semiconductors silicon and gallium arsenide in contact with pure metals
[NASA-TP-2405] p 84 N85-13044
Analytical and experimental investigation of rubbing interaction in labyrinth seals for a liquid hydrogen fuel pump --- space shuttle main engine
[NASA-CR-174657] p 48 N85-18084
Sliding seal materials for adiabatic engines
[NASA-CR-174893] p 89 N85-22757
Rolling, slip and traction measurements on low modulus materials
[NASA-CR-174909] p 135 N85-33491

SMOKE
Analytical fuel property effects: Small combustors, phase 2
[NASA-CR-174848] p 93 N85-19175
Advanced smoke meter development survey and analysis
[NASA-CR-168287] p 124 N85-25792

SODIUM CARBONATES
Hot corrosion of sintered alpha-SiC at 1000 C
[ACS PAPER 19-B-84P] p 83 A85-45302

SODIUM CHLORIDES
Reactions of NaCl with gaseous SO3, SO2, and O2 p 59 A85-11897
Mechanism for forming hydrogen chloride and sodium sulfate from sulfur trioxide, water, and sodium chloride p 62 A85-48513

SODIUM SULFATES
Reactions of NaCl with gaseous SO3, SO2, and O2 p 59 A85-11897
Effects of SO2 and SO3 on the Na2SO4 induced corrosion of nickel p 65 A85-15603
Hot corrosion of sintered alpha-SiC at 1000 C
[ACS PAPER 19-B-84P] p 83 A85-45302
Mechanism for forming hydrogen chloride and sodium sulfate from sulfur trioxide, water, and sodium chloride p 62 A85-48513

SODIUM SULFUR BATTERIES
Moderate temperature sodium cells. V - Discharge reactions and rechargeability of NiS and NiS2 positive electrodes in molten NaAlCl4 p 59 A85-11892

SOLAR ARRAYS
Control algorithms and computer simulation of a stand-alone photovoltaic village power system p 153 A85-11345
Characteristics of arc currents on a negatively biased solar cell array in a plasma p 154 A85-18608
Computer simulation of plasma electron collection by PIX-II --- solar array-space plasma interaction [AIAA PAPER 85-0386] p 43 A85-19715
The NASA photovoltaic technology program p 155 A85-35604
A 37.5-kW point design comparison of the nickel-cadmium battery, bipolar nickel-hydrogen battery, and regenerative hydrogen-oxygen fuel cell energy storage subsystems for low earth orbit p 46 A85-45387
Dilute plasma coupling currents to a high voltage solar array in weak magnetic fields p 46 A85-45388
Electric power - Photovoltaic or solar dynamic? p 46 A85-47042
A historical overview of the electrical power systems in the US manned and some US unmanned spacecraft [NASA-CR-174806] p 47 N85-13910
Circuit transients due to negative bias arcs on a high-voltage solar array in low Earth orbit [NASA-TP-2407] p 39 N85-14858
The PIX-2 experiment: An overview p 179 N85-22494
Plasma interaction experiment 2 (PIX 2): Laboratory and flight results p 180 N85-22495
Discharges on a negatively biased solar cell array in a charged-particle environment p 160 N85-22499
GaAs and 3-5 compound solar cells status and prospects for use in space p 49 N85-22580

SOLAR CELLS
Magnesium doping of efficient GaAs and Ga(0.75)In(0.25)As solar cells grown by metalorganic chemical vapor deposition p 180 A85-11466
Near-optimum design of GaAs-based concentrator space solar cells for 80 C operation p 153 A85-15800
Characteristics of arc currents on a negatively biased solar cell array in a plasma p 154 A85-18608
The effect of plasma on solar cell array arc characteristics [AIAA PAPER 85-0384] p 43 A85-19713
Applicability of the Meyer-Neldel rule to solar cells p 154 A85-19948
High-voltage solar-cell chip p 154 A85-24668
Effect of solar-cell junction geometry on open-circuit voltage p 154 A85-28080
Theory of the high base resistivity n(+)pp(+) silicon solar cell and its application to radiation damage effects p 154 A85-32639
Fabrication of p(+)-n junction GaAs solar cells by a novel method p 181 A85-33645
Voltage controlling mechanisms in low resistivity silicon solar cells - A unified approach p 155 A85-35617
The effect of diffusion induced lattice stress on the open-circuit voltage in silicon solar cells p 181 A85-35620
Radiation damage and defect behavior in ion-implanted, lithium counterdoped silicon solar cells p 182 A85-35698
Effects of 1 MeV electrons and 10 MeV protons on the performance and reflectance of thin BSR cells --- back surface reflector p 182 A85-35699
Microprocessor control of photovoltaic systems p 156 A85-45408
The effect of plasma on solar cell array arc characteristics [NASA-TM-86887] p 47 N85-11133
Research on gallium arsenide diffused junction solar cells [NASA-CR-174057] p 158 N85-11457
Screen printed interdigitated back contact solar cell [NASA-CASE-LEW-13414-1] p 160 N85-20530
Lithium counterdoped silicon solar cell [NASA-CASE-LEW-14177-1] p 160 N85-20535
GaAs and 3-5 compound solar cells status and prospects for use in space [NASA-TM-86960] p 49 N85-21261
An investigation of arc discharging on negatively biased dielectric conductor samples in a plasma p 180 N85-22498
Discharges on a negatively biased solar cell array in a charged-particle environment p 160 N85-22499
The high voltage silicon cell: A comparative analysis p 49 N85-22569
The effects of lithium counterdoping on radiation damage and annealing in n(+)p silicon solar cells p 50 N85-22586
High efficiency solar cell research for space applications p 164 N85-31624
Diffusion welding of Cassegrainian concentrator cell stack assemblies [NASA-CR-176104] p 164 N85-33566
Practical aspects of photovoltaic technology, applications and cost (revised) [NASA-CR-174963] p 165 N85-35472

SOLAR COLLECTORS
Solar dynamic systems p 164 N85-31374
Optical analysis of parabolic dish concentrators for solar dynamic power systems in space [NASA-TM-87080] p 52 N85-34176

SOLAR ENERGY
Optical analysis of parabolic dish concentrators for solar dynamic power systems in space [NASA-TM-87080] p 52 N85-34176

SOLAR ENERGY ABSORBERS
Solar dynamic systems p 164 N85-31374

SOLAR ENERGY CONVERSION
The NASA photovoltaic technology program p 155 A85-35604
Pyroelectric conversion in space p 45 A85-45377
Electric power - Photovoltaic or solar dynamic? p 46 A85-47042
Solar energy converter using surface plasma waves [NASA-CASE-LEW-13827-1] p 160 N85-21768
Practical aspects of photovoltaic technology, applications and cost (revised) [NASA-CR-174963] p 165 N85-35472

SOLAR GENERATORS
Environmentally-induced voltage limitations in large *space power systems* p 43 A85-18584

SOLAR THERMAL PROPULSION
Measurements of energy distribution in microwave plasmas of N2 and He and comparisons with results for H2 p 178 A85-16443

SOLENOIDS
A rotating superconducting solenoid for 100 kWh energy storage --- in space p 44 A85-33144

SOLID LUBRICANTS
Polyimides - Tribological properties and their use as lubricants p 79 A85-21524
Experimental test program for evaluation of solid lubricant coating as applied to compliant foil gas bearings to 315 deg C [NASA-CR-174837] p 85 N85-15895
The role of silver in self-lubricating coatings for use at extreme temperatures [NASA-TM-86943] p 87 N85-20127
Effect of counterface material type and its topography on the tribological properties of polyimide composites [NASA-TM-87036] p 90 N85-26993
Advances in sputtered and ion plated solid film lubrication p 136 N85-33524

SOLID SOLUTIONS
Solids mixing in a three phase fluidized bed containing spherically shaped-porous solid particles [PB85-187961] p 120 N85-33453

SOLID STATE DEVICES
Advanced in solid state switchgear technology for large space power systems p 102 A85-45362
The 30 GHz solid state amplifier for low cost low data rate ground terminals [NASA-CR-174795] p 102 N85-12300
A new very high voltage semiconductor switch [NASA-TM-86957] p 103 N85-20246
Solar energy converter using surface plasma waves [NASA-CASE-LEW-13827-1] p 160 N85-21768

SOLID SURFACES
Gravitational effects on flames spreading over thick solid surfaces [IAF PAPER 84-154] p 59 A85-13092

SOLID-SOLID INTERFACES
On the existence and stability conditions for mixed-hybrid finite element solutions based on Reissner's variational principle p 142 A85-33847
Solidification interface shape for continuous casting in an offset mold - Two analytical methods p 112 A85-41326

SOLIDIFICATION
The mechanisms of formation and prevention of channel segregation during alloy solidification p 180 A85-18082
Analysis of three-dimensional solidification interface shape p 109 A85-30075
Control of solidification boundary in continuous casting by asymmetric cooling and mold offset p 110 A85-37047
Dendritic solidification. I - Analysis of current theories and models. II - A model for dendritic growth under an imposed thermal gradient p 182 A85-38019
Solidification interface shape for continuous casting in an offset mold - Two analytical methods p 112 A85-41326
Dendritic solidification. III - Some further refinements to the model for dendritic growth under an imposed thermal gradient p 69 A85-44703
Microstructures in rapidly solidified Ni-Mo alloys [NASA-TM-87100] p 78 N85-34266

SOLIDS
Hybrid stress finite elements for large deformations of inelastic solids p 139 A85-15894

SOOT
Methanol as a soot reducer in a turbulent swirling burner [ASME PAPER 84-JPGC-GT-2] p 61 A85-23192
Ideal gas thermodynamic properties for the phenyl, *phenoxy, and o-biphenyl radicals* [NASA-TM-83800] p 184 N85-22204
Shock tube study of the fuel structure effects on the chemical kinetic mechanisms responsible for soot formation, part 2 [NASA-CR-174880] p 63 N85-25444
Fuel-rich catalytic combustion: A soot-free technique for in situ hydrogen-like enrichment [NASA-TP-2498] p 63 N85-31244

SOUND GENERATORS
Sound generation and upstream influence due to *instability waves interacting with non-uniform mean flows* p 174 A85-20738
A theoretical prediction of the acoustic pressure generated by turbulence-flame front interactions [ASME PAPER 84-WA/NCA-11] p 174 A85-39909

SOUND PRESSURE
The influence of combustion liner holes on noise production by ducted burners [AIAA PAPER 84-2322] p 172 A85-10869
Effects of vane/blade ratio and spacing on fan noise, volume 1 [NASA-CR-174664] p 176 N85-19791

SOUND PROPAGATION
Acoustic structure and propagation in highly porous, layered, fibrous materials p 173 A85-12301
Analysis of the effect on combustor noise measurements of acoustic waves reflected by the turbine and combustor inlet [AIAA PAPER 84-2323] p 173 A85-16103

SOUND TRANSMISSION
Measured acoustic properties of variable and low density bulk absorbers [NASA-TM-87065] p 177 N85-30770

SOUND WAVES
Analysis of the effect on combustor noise measurements of acoustic waves reflected by the turbine and combustor inlet [AIAA PAPER 84-2323] p 173 A85-16103
The response of Helmholtz resonators to external excitation. I - Single resonators p 174 A85-26915

SPACE BASED RADAR
Primary propulsion of electrothermal, ion and chemical systems for space-based radar orbit transfer [NASA-TM-87043] p 51 N85-27972

SPACE ENVIRONMENT SIMULATION
Numerical simulations of positively-biased probes and dielectric-conductor disks in a plasma --- for low earth orbit plasma densities p 179 A85-17262

SPACE MISSIONS
Preliminary analysis of space mission applications for electromagnetic launchers [NASA-CR-174067] p 35 N85-12071

SPACE PLASMAS
Numerical simulations of positively-biased probes and dielectric-conductor disks in a plasma --- for low earth orbit plasma densities p 179 A85-17262
Computer simulation of plasma electron collection by PIX-II --- solar array-space plasma interaction [AIAA PAPER 85-0386] p 43 A85-19715
Dilute plasma coupling currents to a high voltage solar array in weak magnetic fields p 46 A85-45388
Three-dimensional calculation of shuttle charging in polar orbit p 40 N85-22486
Surface interactions and high-voltage current collection p 40 N85-22493
The PIX-2 experiment: An overview p 179 N85-22494
Plasma interaction experiment 2 (PIX 2): Laboratory and flight results p 180 N85-22495
Ram-wake effects on plasma current collection of the PIX 2 Langmuir probe p 180 N85-22496
NASCAP simulation of PIX 2 experiments p 180 N85-22497
An investigation of arc discharging on negatively biased dielectric conductor samples in a plasma p 180 N85-22498

SPACE POWER REACTORS
Design of a 1-kWh bipolar nickel hydrogen battery p 155 A85-45384

SPACE POWER UNIT REACTORS
Overview of the 1985 NASA Lewis Research Center SP-100 free-piston Stirling engine activities [NASA-TM-87028] p 185 N85-27769

SPACE SHUTTLE MAIN ENGINE
Application of viscous and inviscid computation methods for rocket turbopump systems [SAE PAPER 841522] p 110 A85-39257

An experimental investigation of rubbing interaction in labyrinth seals at cryogenic temperature p 129 A85-39938
Analytical and experimental investigation of rubbing interaction in labyrinth seals for a liquid hydrogen fuel pump --- space shuttle main engine [NASA-CR-174657] p 48 N85-18084
Cyclic structural analyses of anisotropic turbine blades for reusable space propulsion systems --- ssme fuel turbopump [NASA-TM-86990] p 146 N85-24339
Flow dynamic environment data base development for the SSME p 147 N85-26885
Preliminary results on passive eddy current damper technology for SSME turbomachinery p 132 N85-26890
Redistribution of the inlet temperature profile through the SSME fuel turbine p 50 N85-26901
Analytical study of flow phenomena in SSME turnaround duct geometries p 116 N85-26902
Instrumentation technology overview p 124 N85-26903
Structural Integrity and Durability of Reusable Space Propulsion Systems [NASA-CP-2381] p 51 N85-27941
Overview of aerothermodynamic loads definition study p 51 N85-27942
SSME fuel preburner two-dimensional analysis p 51 N85-27943
Simulation of multistage turbine flows p 116 N85-27945
New facility to study unsteady wake effects on turbine airfoil heat transfer p 117 N85-27948
Overview of structural response: Probabilistic structural analysis p 148 N85-27952
Composite loads spectra for select space propulsion structural components p 148 N85-27953
Cyclic structural analyses of SSME turbine blades p 150 N85-27963
Thin-film sensors for space propulsion technology p 41 N85-27968
Heat flux sensor calibrator p 41 N85-27970
Feasibility of mapping velocity flow fields in SSME powerhead by laser anemometry techniques p 41 N85-27971

SPACE SHUTTLE PAYLOADS
Effects of chemical releases by the STS 3 orbiter on the ionosphere p 166 A85-29538
Shuttle/Centaur project perspective p 37 N85-16991
Suprathermal plasma observed on STS-3 Mission by plasma diagnostics package p 179 N85-22472
Electron and ion density depletions measured in the STS-3 orbiter wake p 39 N85-22474

SPACE SHUTTLES
Laboratory degradation of Kapton in a low energy oxygen ion beam [AIAA PAPER 83-2658] p 78 A85-10675
A high energy stage for the National Space Transportation System [IAF PAPER 84-15] p 36 A85-23200
Advanced research and technology programs for advanced high-pressure oxygen-hydrogen rocket propulsion [NASA-TM-86969] p 37 N85-21231
Spacecraft Environmental Interactions Technology, 1983 [NASA-CP-2359] p 39 N85-22470
Laboratory studies of Kapton degradation in an oxygen ion beam p 177 N85-22477
Electron beam charging of Space Shuttle thermal protection system tiles p 39 N85-22478
Study of Kapton under simulated shuttle environment [NASA-CR-176003] p 41 N85-29997

SPACE STATIONS
Space Station propulsion - The Advanced Development Program at Lewis [AIAA PAPER 85-1154] p 44 A85-39626
Space station propulsion options [AIAA PAPER 85-1155] p 45 A85-43975
An evaluation of oxygen/hydrogen propulsion systems for the Space Station [AIAA PAPER 85-1156] p 45 A85-43976
Electric power - Photovoltaic or solar dynamic? p 46 A85-47042
Regenerative fuel cell energy storage system for a low Earth orbit space station [NASA-CR-174802] p 158 N85-13371
Space Power [NASA-CP-2352] p 47 N85-13880
Advanced research and technology programs for advanced high-pressure oxygen-hydrogen rocket propulsion [NASA-TM-86969] p 37 N85-21231
Long-life high performance fuel cell program [NASA-CR-174874] p 50 N85-25384
Space station propulsion: The advanced development program at Lewis [NASA-TM-86999] p 50 N85-25386
Tethered nuclear power for the Space Station [NASA-TM-87023] p 51 N85-26912
Performance analysis of radiation cooled dc transmission lines for high power space systems [NASA-TM-87040] p 104 N85-28222
An evaluation of oxygen-hydrogen propulsion systems for the Space Station [NASA-TM-87059] p 52 N85-28971
Regenerative fuel cell systems for space station p 104 N85-31372
Optical analysis of parabolic dish concentrators for solar dynamic power systems in space [NASA-TM-87080] p 52 N85-34176

SPACE TRANSPORTATION SYSTEM
A high energy stage for the National Space Transportation System [IAF PAPER 84-15] p 36 A85-23200
Progress report - Advanced cryogenic OTV engine technology [AIAA PAPER 85-1341] p 44 A85-39735

SPACEBORNE ASTRONOMY
Mosaic Infrared Sensor for Space Astronomy (MIRSSA) [NASA-CR-176154] p 125 N85-33456

SPACEBORNE EXPERIMENTS
Experiments in charge control at geosynchronous orbit - ATS-5 and ATS-6 p 39 A85-35379

SPACECRAFT ANTENNAS
Interdisciplinary design analysis of a precision spacecraft antenna [AIAA PAPER 85-0804] p 38 A85-30303

SPACECRAFT CHARGING
Experiments in charge control at geosynchronous orbit - ATS-5 and ATS-6 p 39 A85-35379
Spacecraft Environmental Interactions Technology, 1983 [NASA-CP-2359] p 39 N85-22470
Electron and ion density depletions measured in the STS-3 orbiter wake p 39 N85-22474
Laboratory studies of Kapton degradation in an oxygen ion beam p 177 N85-22477
Electron beam charging of Space Shuttle thermal protection system tiles p 39 N85-22478
Three-dimensional calculation of shuttle charging in polar orbit p 40 N85-22486
Polar orbit electrostatic charging of objects in shuttle wake p 40 N85-22487
Surface interactions and high-voltage current collection p 40 N85-22493
The PIX-2 experiment: An overview p 179 N85-22494
Plasma interaction experiment 2 (PIX 2): Laboratory and flight results p 180 N85-22495
Design guidelines for assessing and controlling spacecraft charging effects p 40 N85-22500
Electron yields from spacecraft materials p 40 N85-22512
Spacecraft environmental interactions: A joint Air Force and NASA research and technology program p 40 N85-22517

SPACECRAFT COMMUNICATION
Demand for satellite-provided domestic communications services up to the year 2000 [NASA-TM-86894] p 97 N85-15099
Research and technology highlights of the Lewis Research Center [NASA-TM-86899] p 186 N85-17928
Automated testing of developmental satellite communications systems and subsystems [NASA-TM-87070] p 100 N85-31348

SPACECRAFT COMPONENTS
High voltage-high power components for large space power distribution systems p 45 A85-45370

SPACECRAFT CONFIGURATIONS
Vehicle/engine integration --- orbit transfer vehicles p 37 N85-17008
Report of the Constellations Panel p 131 N85-20368

SPACECRAFT CONSTRUCTION MATERIALS
Ion beam sputter-deposited thin film coatings for protection of spacecraft polymers in low Earth orbit [NASA-TM-87051] p 91 N85-30137

SPACECRAFT DESIGN
Main propulsion system design recommendations for an advanced Orbit Transfer Vehicle [AIAA PAPER 85-1336] p 36 A85-39730
Design guidelines for assessing and controlling spacecraft charging effects p 40 N85-22500

SPACECRAFT ENVIRONMENTS
High voltage requirements and issues for the 1990's --- for spacecraft power supplies p 46 A85-45429

SPACECRAFT EQUIPMENT
Developments in space power components for power management and distribution p 47 N85-13877
High-voltage, high-power, solid-state remote power controllers for aerospace applications [NASA-TP-2437] p 49 N85-21263

SPACECRAFT MAINTENANCE
Technology requirements to be addressed by the NASA Lewis Research Center Cryogenic Fluid Management Facility program [AIAA PAPER 85-1229] p 94 A85-47024
Technology requirements to be addressed by the NASA Lewis Research Center Cryogenic Fluid Management Facility program [NASA-TM-87048] p 38 N85-29987

SPACECRAFT MODULES
Mass analysis of neutral particles and ions released during electrical breakdowns on spacecraft surfaces [NASA-CR-175585] p 39 N85-21250

SPACECRAFT ORBITS
Life cycle test results of a bipolar nickel hydrogen battery p 105 N85-31406

SPACECRAFT POWER SUPPLIES
Environmentally-induced voltage limitations in large space power systems p 43 A85-18584
A rotating superconducting solenoid for 100 kWh energy storage --- in space p 44 A85-33144
Advanced in solid state switchgear technology for large space power systems p 102 A85-45362
Pyroelectric conversion in space p 45 A85-45377
Microprocessor control of photovoltaic systems p 156 A85-45408
High voltage requirements and issues for the 1990's --- for spacecraft power supplies p 46 A85-45429
Overview of NASA Lewis Research Center free-piston Stirling engine activities p 130 A85-45479
Electric power - Photovoltaic or solar dynamic? p 46 A85-47042
Space Power [NASA-CP-2352] p 47 N85-13880
Missions/planning panel p 36 N85-13886
Electrochemistry and storage p 62 N85-13889
Dynamic power systems for power generation p 158 N85-13892
Engineering model system study for a regenerative fuel cell: Study report [NASA-CR-174801] p 158 N85-16292
Technology for satellite power conversion [NASA-CR-174335] p 159 N85-18451
GaAs and 3-5 compound solar cells status and prospects for use in space [NASA-TM-86960] p 49 N85-21261
GaAs and 3-5 compound solar cells status and prospects for use in space p 49 N85-22580
Long-life high performance fuel cell program [NASA-CR-174874] p 50 N85-25384
Tethered nuclear power for the Space Station [NASA-TM-87023] p 51 N85-26912
Performance analysis of radiation cooled dc transmission lines for high power space systems [NASA-TM-87040] p 104 N85-28222
Solar dynamic systems p 164 N85-31374
System level electrochemical principles p 104 N85-31375
Design principles for nickel hydrogen cells and batteries p 104 N85-31398
Life cycle test results of a bipolar nickel hydrogen battery p 105 N85-31406
The failure mechanism of a nickel electrode in a nickel-hydrogen cell p 105 N85-31408
High efficiency solar cell research for space applications p 164 N85-31624
Design principles for nickel-hydrogen cells and batteries [NASA-TM-87037] p 164 N85-31646
Optical analysis of parabolic dish concentrators for solar dynamic power systems in space [NASA-TM-87080] p 52 N85-34176

SPACECRAFT PROPULSION
Ground correlation investigation of thruster/spacecraft interactions to be measured on the IAPS flight test p 42 A85-16408
Ion propulsion for communications satellites p 42 A85-16412
Friction in rail guns p 101 A85-16424
Electrothermal thruster diagnostics p 42 A85-16440
Inert gas test of two 12-cm magnetostatic thrusters p 43 A85-29310
Space Station propulsion - The Advanced Development Program at Lewis [AIAA PAPER 85-1154] p 44 A85-39626
Progress report - Advanced cryogenic OTV engine technology [AIAA PAPER 85-1341] p 44 A85-39735
Space station propulsion options [AIAA PAPER 85-1155] p 45 A85-43975

A historical overview of the electrical power systems in the US manned and some US unmanned spacecraft
[NASA-CR-174806] p 47 N85-13910
OTV propulsion tecnology programmatic overview
p 37 N85-16997
Vehicle/engine integration --- orbit transfer vehicles
p 37 N85-17008
Space station propulsion: The advanced development program at Lewis
[NASA-TM-86999] p 50 N85-25386
Structural Integrity and Durability of Reusable Space Propulsion Systems
[NASA-CP-2381] p 51 N85-27941
Composite loads spectra for select space propulsion structural components: Probabilistic load model development p 148 N85-27954
Probabilistic structural analysis theory development
p 148 N85-27955
Probabilistic finite element development
p 149 N85-27956
Thin-film sensors for space propulsion technology
p 41 N85-27968

SPACECRAFT RADIATORS
Preliminary evaluation of a liquid belt radiator for space applications
[NASA-CR-174807] p 47 N85-15804
Advanced radiator concepts
[NASA-TM-87008] p 115 N85-24245

SPACING
Effects of vane/blade ratio and spacing on fan noise, *volume 1*
[NASA-CR-174664] p 176 N85-19791
Effects of vane/blade ratio and spacing on fan noise. Volume 2: Data supplement
[NASA-CR-174665] p 176 N85-19792

SPATIAL DISTRIBUTION
Plot of modal field distribution in rectangular and circular waveguides p 101 A85-25170

SPATIAL MARCHING
Computation of viscous flows in turbomachinery cascades p 106 A85-11631
A space-marching method for incompressible Navier-Stokes equations
[AIAA PAPER 85-0170] p 108 A85-19564
Computation of three-dimensional viscous flows using a space-marching method p 4 A85-29259

SPECIFICATIONS
Spacecraft environmental interactions: A joint Air Force and NASA research and technology program
p 40 N85-22517

SPECIMEN GEOMETRY
Results of an interlaboratory fatigue test program conducted on alloy 800H at room and elevated temperatures
[NASA-CR-174940] p 152 N85-32340

SPEED CONTROL
Feasibility demonstration of a novel, flat-belt, continuously variable transmission or automotive and electric-hybrid vehicle application
[NASA-CR-174430] p 185 N85-19894
Experimental investigation of a variable speed constant frequency electric generating system from a utility perspective
[NASA-CR-174950] p 105 N85-32251

SPHERES
Ultrasonic wave propagation in two-phase media - Spherical inclusions p 54 A85-11926

SPIN
Thermal traction contact performance evaluation under fully flooded and starved conditions
[NASA-CR-168173] p 132 N85-25848

SPIRAL WRAPPING
Generated spiral bevel gears: Optimal machine-tool settings and tooth contact analysis
[NASA-TM-87075] p 136 N85-34405

SPRAY CHARACTERISTICS
Phase/doppler spray analyzer for simultaneous measurements of drop size and velocity distributions
p 120 A85-10035
Spray characterization with a nonintrusive technique using absolute scattered light p 120 A85-10036
Structure of nonevaporating sprays. I - Initial conditions and mean properties p 112 A85-48538

SPRAY NOZZLES
Experimental study of the spray characteristics of a *research airblast atomizer*
[NASA-TM-86911] p 24 N85-15727

SPRAYED COATINGS
Plastic flow of plasma sprayed ceramics
p 80 A85-24161
Life modeling of atmospheric and low pressure plasma-sprayed thermal-barrier coating
p 81 A85-29728
Mechanical property measurements of plasma-sprayed thermal-barrier coatings subjected to oxidation
p 81 A85-29729
Cyclic oxidation behavior of beta+gamma overlay coatings on gamma and gamma+gamma-prime alloys
p 68 A85-32431
An investigation of enhanced capability thermal barrier coating systems for diesel engine components
[NASA-CR-174820] p 86 N85-18154
Rocket thrust chamber thermal barrier coatings
p 90 N85-26867

SPRAYERS
Nonintrusive optical single-particle counter for *measuring the size and velocity of droplets in a spray*
p 120 A85-16794
Measurements and predictions of the structure of evaporating sprays p 112 A85-46484
The structure of dilute combusting sprays
[NASA-CR-174838] p 24 N85-15728
Research study of droplet sizing technology leading to the development of an advanced droplet sizing system
[NASA-CR-174839] p 123 N85-21604

SPUTTERING
Frictional and morphological properties of Au-MoS2 films sputtered from a compact target p 127 A85-19085
RF-sputtered silicon and hafnium nitrides - Properties and adhesion to 440C stainless steel p 81 A85-36240
Properties of coated and modified surfaces
p 53 A85-36694
Textured carbon surfaces on copper
[NASA-CASE-LEW-14130-1] p 95 N85-20156
Diamondlike flakes
[NASA-CASE-LEW-13837-2] p 57 N85-21267
Ion beam sputter-deposited thin film coatings for protection of spacecraft polymers in low Earth orbit
[NASA-TM-87051] p 91 N85-30137
Advances in sputtered and ion plated solid film lubrication p 136 N85-33524

SPUTTERING GAGES
Thin-film sensors for space propulsion technology
p 41 N85-27968

SQUEEZE FILMS
Dual clearance squeeze film damper for high load conditions
[ASME PAPER 84-TRIB-7] p 128 A85-32960
Dual clearance squeeze film damper
[NASA-CASE-LEW-13506-1] p 135 N85-33490

STABILITY
Effect of combined pressure and temperature distortion orientation on high-bypass-ratio turbofan engine stability
[NASA-TM-83771] p 17 N85-10067
Rotordynamic Instability Problems in High-Performance Turbomachinery
[NASA-CP-2338] p 131 N85-14116
Internal hysteresis experienced on a high pressure syn -gas compressor p 131 N85-14122

STABILITY TESTS
Environmental stability of intercalated graphite fibers
[NASA-TM-87025] p 90 N85-26992

STACKS
Gas cooled fuel cell systems technology development
[NASA-CR-174732] p 158 N85-16291
Develop and test fuel cell powered on-site integrated total energy systems. Phase 3: Full-scale power plant development
[NASA-CR-174887] p 161 N85-25941

STAGNATION POINT
Combined influence of unsteady free stream velocity and free stream turbulence on stagnation point heat transfer p 112 A85-41782
Preliminary results of a study of the relationship between free stream turbulence and stagnation region heat transfer
[NASA-TM-86884] p 113 N85-11317
The influence of jet-grid turbulence on heat transfer from the stagnation region of a cylinder in crossflow
[NASA-TM-87011] p 115 N85-25760
Preliminary results of a study of the relationship between free-stream turbulence and stagnation region heat transfer p 118 N85-31435

STAGNATION PRESSURE
A stagnation pressure probe for droplet-laden air flow
[AIAA PAPER 85-0330] p 108 A85-19672
A comparison of flow rates and pressure profiles for N-sequential inlets and three related seal configurations
p 109 A85-26526

STAINLESS STEELS
Topological reaction rate measurements related to scuffing p 64 A85-11070
RF-sputtered silicon and hafnium nitrides - Properties and adhesion to 440C stainless steel p 81 A85-36240

STANDING WAVES
Flutter and forced response of mistuned rotors using standing wave analysis p 139 A85-12721
Vibration and flutter of mistuned bladed-disk assemblies
[AIAA PAPER 84-0991] p 139 A85-16095

STATIC LOADS
Hygrothermomechanical evaluation of transverse filament tape epoxy/polyester fiberglass composites
p 54 A85-15632
Design procedures for fiber composite structural components - Rods, beams, and beam columns
p 54 A85-15636

STATIC PRESSURE
Effect of combined pressure and temperature distortion orientation on high-bypass-ratio turbofan engine stability
[NASA-TM-83771] p 17 N85-10067
High temperature static strain sensor development program p 19 N85-10959

STATIC TESTS
Static jet noise test results of four 0.35 scale-model QCGAT mixer nozzles
[NASA-TM-86871] p 175 N85-13551

STATISTICAL ANALYSIS
Evaluation of alpha-SiC sintering using statistical methods p 83 A85-42800
Factors influencing the ball milling of Si3N4 in water
[NASA-TM-86932] p 86 N85-19136
Reliability of void detection in structural ceramics using scanning laser acoustic microscopy
[NASA-TM-87035] p 138 N85-32337

STATISTICAL DISTRIBUTIONS
Creep-rupture reliability analysis p 143 A85-42566

STATISTICAL MECHANICS
Statistics and thermodynamics of fracture
p 140 A85-19433

STATISTICAL WEATHER FORECASTING
GASP cloud encounter statistics - Implications for laminar flow control flight p 166 A85-11979

STATOR BLADES
Noise produced by the interaction of a rotor wake with a swept stator blade
[AIAA PAPER 84-2326] p 173 A85-13956
A note on blade wake interaction influence on compressor stator row aerodynamic performance
p 4 A85-32965
Study of controlled diffusion stator blading
[NASA-CR-167995] p 25 N85-18058
Development of a rotor wake-vortex model, volume 1
[NASA-CR-174849] p 9 N85-26668

STATORS
Transient technique for measuring heat transfer coefficients on stator airfoils in a jet engine environment
[AIAA PAPER 85-1471] p 122 A85-39796
Energy efficient engine component development and integration program
[NASA-CR-170034] p 22 N85-10990
Transient technique for measuring heat transfer coefficients on stator airfoils in a jet engine environment
[NASA-TM-87005] p 124 N85-25794

STEADY STATE
Effect of steady-state temperature distortion on inlet flow to a high-bypass-ration turbofan engine
[NASA-TM-86896] p 24 N85-15725
Initial testing of a variable-stroke Stirling engine
[NASA-TM-86875] p 185 N85-19895

STEAM TURBINES
Advanced technology cogeneration system conceptual design study: Closed cycle gas turbines
[NASA-CR-168222] p 159 N85-16300

STEELS
Ion-beam nitriding of steels p 66 A85-24667
Surface hardening of steel by boriding in a cold rf plasma p 68 A85-40275
Effect of lubricant extreme-pressure additives on surface fatigue life of AISI 9310 spur gears
[NASA-TP-2408] p 130 N85-13234
Ion-beam nitriding of steels
[NASA-CASE-LEW-14104-1] p 75 N85-21324
Characterization of lubricated bearing surfaces operated under high loads
[NASA-TM-86964] p 88 N85-21357

STELLITE (TRADEMARK)
Interaction of high-cycle and low-cycle fatigue of Haynes 188 alloy at 1400 F deg p 149 N85-27961

STIFFNESS
Gear mesh stiffness and load sharing in planetary gearing
[ASME PAPER 84-DET-229] p 129 A85-33781
Comparison of numerical techniques for integration of stiff ordinary differential equations arising in combustion chemistry
[NASA-TP-2372] p 17 N85-10065
Experimental stiffness of tapered bore seals
[NASA-TM-86978] p 132 N85-25847
Application of traction drives as servo mechanisms
p 152 N85-33520

STIFFNESS MATRIX
Analysis of hourglass instabilities and control in underintegrated finite element methods
p 139 A85-11125

Stability, accuracy, and efficiency of some underintegrated methods in finite element computations p 172 A85-50073

STIRLING CYCLE
Initial results of sensitivity tests - Performed on the RE-1000 free-piston Stirling engine p 129 A85-45466
Mod II engine and technology development p 129 A85-45473
Automotive Stirling engine systems development p 130 A85-45474
Overview of NASA Lewis Research Center free-piston Stirling engine activities p 130 A85-45479
Comparison of free-piston Stirling engine model predictions with RE1000 engine test data p 130 A85-45488
Stirling material technology [NASA-TM-86888] p 72 N85-13007
Overview of waste heat utilization systems [NASA-TM-86901] p 184 N85-13692
Dynamic power systems for power generation p 158 N85-13892
Effect of water on hydrogen permeability --- Stirling engines [NASA-TM-86904] p 53 N85-14864
Initial testing of a variable-stroke Stirling engine [NASA-TM-86875] p 185 N85-19895
Overview of the 1985 NASA Lewis Research Center SP-100 free-piston Stirling engine activities [NASA-TM-87028] p 185 N85-27769
Free-piston Stirling engine/linear alternator 1000-hour endurance test [NASA-CR-174771] p 163 N85-30481

STOCHASTIC PROCESSES
A design methodology for robust failure detection and isolation p 171 A85-47794
Probabilistic finite element development p 149 N85-27956

STORAGE BATTERIES
Electrochemistry and storage p 62 N85-13889
Regenerative fuel cell systems for space station p 104 N85-31372
System level electrochemical principles p 104 N85-31375

STRAIN GAGES
Closed-loop strain controlled testing at elevated temperatures with a non-contacting gage p 121 A85-29562
High temperature static strain sensor development program p 19 N85-10959
Evaluation results of the 700 deg C Chinese strain gauges --- for gas turbine engine [NASA-TM-86973] p 124 N85-21605

STRAIN MEASUREMENT
Some advances in experimentation supporting development of viscoplastic constitutive models [NASA-CR-174855] p 147 N85-27260
Some advances in experimentation supporting development of viscoplastic constitutive models p 151 N85-31545

STRAIN RATE
Reliability considerations for the total strain range version of strainrange partitioning [NASA-CR-174757] p 144 N85-11380

STRATEGIC MATERIALS
The B2 aluminides as alternative materials [NASA-TM-86937] p 74 N85-19076

STRATIFICATION
Stratified charge rotary aircraft engine technology enablement program [NASA-CR-174812] p 25 N85-21163

STRATIFIED FLOW
Direct simulations of chemically reacting turbulent mixing layers [AIAA PAPER 85-0321] p 60 A85-19666

STREAM FUNCTIONS (FLUIDS)
Review - Computational methods for internal flows with emphasis on turbomachinery p 4 A85-29126

STRENGTH
Fundamentals of microcrack nucleation mechanics [NASA-CR-3851] p 137 N85-16195

STRESS ANALYSIS
Rational approach for assumed stress finite elements p 139 A85-12029
Hybrid stress finite elements for large deformations of inelastic solids p 139 A85-15894
Interply layer degradation effects on composite structural response [AIAA PAPER 84-0849] p 54 A85-16096
Development and testing of stable, invariant, isoparametric curvilinear 2- and 3-D hybrid-stress elements p 140 A85-19899
Simplified design and life prediction of rocket thrust chambers p 44 A85-29314
Evolution of assumed stress hybrid finite element p 142 A85-35046
Interply layer degradation effects on composite structural response p 55 A85-39215
Axisymmetric solid elements by a rational hybrid stress method p 143 A85-41109
A study of interply layer effects on the free edge stress field of angleplied laminates p 55 A85-41127
The 3-D inelastic analysis methods for hot section components: Brief description p 20 N85-10972
A study of interply layer effects on the free-edge stress field of angleplied laminates [NASA-TM-86924] p 57 N85-15822
Thermal-stress analysis for a wood composite blade [NASA-CR-174794] p 159 N85-17421
Advanced stress analysis methods applicable to turbine engine structures [NASA-CR-175573] p 26 N85-21165
3-D inelastic analysis methods for hot section components (base program) --- turbine blades, turbine vanes, and combustor liners [NASA-CR-174700] p 145 N85-21686
Component-specific modeling [NASA-CR-174765] p 147 N85-27261
Effect of speed and press fit on fatigue life of roller-bearing inner-race contact [NASA-TP-2496] p 134 N85-31511
Thermal stress analysis of a new turbine shroud seal concept [NASA-TM-87082] p 136 N85-34406

STRESS CONCENTRATION
Development and testing of stable, invariant, isoparametric curvilinear 2- and 3-D hybrid-stress elements p 140 A85-19899
On stress field near a stationary crack tip [AD-A152863] p 141 A85-24532
On local total strain redistribution using a simplified cyclic inelastic analysis based on an elastic solution [AIAA PAPER 85-1419] p 142 A85-39770
Fundamentals of microcrack nucleation mechanics [NASA-CR-3851] p 137 N85-16195
Local strain redistribution corrections for a simplified inelastic analysis procedure based on an elastic finite-element analysis [NASA-TP-2421] p 145 N85-20396
On local total strain redistribution using a simplified cyclic inelastic analysis based on an elastic solution [NASA-TM-86913] p 145 N85-21690
On Hybrid and mixed finite element methods [NASA-CR-175551] p 146 N85-23096
Two simplified procedures for predicting cyclic material response from a strain history p 151 N85-31543

STRESS CYCLES
Two simplified procedures for predicting cyclic material response from a strain history p 151 N85-31543

STRESS FUNCTIONS
Recent advances in hybrid/mixed finite elements [NASA-CR-175574] p 145 N85-21687

STRESS INTENSITY FACTORS
Experimental compliance calibration of the NASA Lewis Research Center Mode 2 fatigue specimen [NASA-TM-86908] p 144 N85-16205

STRESS MEASUREMENT
Deposition stress effects on the life of thermal barrier coatings on burner rigs p 79 A85-19086

STRESS WAVES
Stress waves in an isotropic elastic plate excited by a circular transducer [NASA-CR-3877] p 138 N85-20390
Application of homomorphic signal processing to stress wave factor analysis [NAS 1.26:174871] p 138 N85-21673
A study of the stress wave factor technique for the characterization of composite materials [NASA-CR-174870] p 58 N85-30035

STRESS-STRAIN DIAGRAMS
Analysis of stress-strain, fracture, and ductility behavior of aluminum maxtrix composites containing discontinuous silicon carbide reinforcement p 55 A85-37421
Constitutive modeling and computational implementation for finite strain plasticity p 143 A85-40910

STRESS-STRAIN RELATIONSHIPS
A simplified method for elastic-plastic-creep structural analysis [ASME PAPER 84-GT-191] p 141 A85-23150
Plasticity, viscoplasticity, and creep of solids by mechanical subelement models p 142 A85-35048
Application of two creep fatigue life models for the prediction of elevated temperature crack initiation of a nickel base alloy [AIAA PAPER 85-1420] p 69 A85-43979
A study of Reynolds-stress closure model [NASA-CR-174342] p 114 N85-17324
Local strain redistribution corrections for a simplified inelastic analysis procedure based on an elastic finite-element analysis [NASA-TP-2421] p 145 N85-20396
On thermomechanical testing in support of constitutive equation development for high temperature alloys [NASA-CR-174879] p 147 N85-25894
Cyclic structural analyses of SSME turbine blades p 150 N85-27963
Finite element analysis of notch behavior using a state variable constitutive equation p 152 N85-31548
Component-specific modeling [NASA-CR-174925] p 32 N85-32119
Hertzian contact in two and three dimensions [NASA-TP-2473] p 135 N85-32331

STRUCTURAL ANALYSIS
Extension of constrained incremental Newton-Raphson scheme to generalized loading fields p 139 A85-13942
Hybrid Semiloof elements for plates and shells based upon a modified Hu-Washizu principle p 139 A85-15893
ICAN - Integrated composites analyzer [AIAA PAPER 84-0974] p 54 A85-16094
Interply layer degradation effects on composite structural response [AIAA PAPER 84-0849] p 54 A85-16096
Considerations for damage analysis of gas turbine hot section components [ASME PAPER 84-PVP-77] p 14 A85-18792
On the development of hierarchical solution strategies for nonlinear finite element formulations p 171 A85-21979
Evolution of assumed stress hybrid finite element p 142 A85-35046
Interply layer degradation effects on composite structural response p 55 A85-39215
Unified constitutive material models for nonlinear finite-element structural analysis --- gas turbine engine blades and vanes [AIAA PAPER 85-1418] p 142 A85-39769
On local total strain redistribution using a simplified cyclic inelastic analysis based on an elastic solution [AIAA PAPER 85-1419] p 142 A85-39770
Turbine Engine Hot Section Technology (HOST) [NASA-TM-83022] p 18 N85-10951
Nonlinear structural and life analyses of a turbine blade p 19 N85-10954
Nonlinear structural and life analyses of a combustor liner p 19 N85-10955
Component-specific modeling p 20 N85-10971
The 3-D inelastic analysis methods for hot section components: Brief description p 20 N85-10972
Constitutive model development for isotropic materials p 20 N85-10975
Validation of structural analysis methods using the in-house liner cyclic rigs p 21 N85-10987
Biaxial constitutive equation development for single crystals [NASA-CR-174056] p 183 N85-11862
Engine cyclic durability by analysis and material testing p 25 N85-15744
NASA Lewis Research Center/University Graduate Research Program on Engine Structures [NASA-TM-86916] p 145 N85-18375
Nonlinear analysis for high-temperature multilayered fiber composite structures --- turbine blades [NASA-TM-83754] p 57 N85-21273
3-D inelastic analysis methods for hot section components (base program) --- turbine blades, turbine vanes, and combustor liners [NASA-CR-174700] p 145 N85-21686
On local total strain redistribution using a simplified cyclic inelastic analysis based on an elastic solution [NASA-TM-86913] p 145 N85-21690
Geometrically nonlinear analysis of laminated elastic structures [NASA-CR-175609] p 146 N85-21720
Raman structural studies of the nickel electrode [NASA-CR-175619] p 183 N85-23414
Unified constitutive material models for nonlinear finite-element structural analysis --- gas turbine engine blades and vanes [NASA-TM-86985] p 146 N85-24338
Cyclic structural analyses of anisotropic turbine blades for reusable space propulsion systems --- ssme fuel turbopump [NASA-TM-86990] p 146 N85-24339
Vibration and buckling of rotating, pretwisted, preconed beams including Cooriolis effects [NASA-TM-87004] p 146 N85-25893
Nonlinear structural analysis for fiber-reinforced superalloy turbine blades p 147 N85-26887
A computer analysis program for interfacing thermal and structural codes [NASA-TM-87021] p 148 N85-27264
Probabilistic structural analysis theory development p 148 N85-27955
Probabilistic finite element: Variational theory p 149 N85-27957

Cyclic structural analyses of SSME turbine blades p 150 N85-27963
Structural analysis and cost estimate of an eight-leg space frame as a support structure for horizontal axis wind turbines
[NASA-TM-83470] p 150 N85-30361
Two simplified procedures for predicting cyclic material response from a strain history p 151 N85-31543

STRUCTURAL DESIGN
Finite element engine blade structural optimization
[AIAA PAPER 85-0645] p 141 A85-30313
Design procedures for fiber composite structural components: Panels subjected to combined in-plane loads
[NASA-TM-86909] p 57 N85-15823
Operational results for the experimental DOE/NASA Mod-OA wind turbine project
[NASA-TM-83517] p 163 N85-30479

STRUCTURAL DESIGN CRITERIA
Design procedures for fiber composite structural components - Rods, beams, and beam columns p 54 A85-15636
Structural optimization using optimality criteria methods p 144 A85-48703
Energy efficient engine combustor test hardware detailed design report
[NASA-CR-167945] p 18 N85-10950
Structural analysis p 20 N85-10969
Overview of structural response: Probabilistic structural analysis p 148 N85-27952

STRUCTURAL MEMBERS
Viscoplastic constitutive relationships with dependence on thermomechanical history
[NASA-CR-174836] p 146 N85-21691
A comparison of smooth specimen and analytical simulation techniques for notched members at elevated temperatures p 151 N85-31546

STRUCTURAL RELIABILITY
Overview of structural response: Probabilistic structural analysis p 148 N85-27952

STRUCTURAL STABILITY
On the existence and stability conditions for mixed-hybrid finite element solutions based on Reissner's variational principle p 142 A85-33847
Effects of cobalt, boron, and zirconium on the microstructure of Udimet 738
[NASA-CR-174762] p 70 N85-10166

STRUCTURAL VIBRATION
Vibration and flutter of mistuned bladed-disk assemblies
[AIAA PAPER 84-0991] p 139 A85-16095
Natural frequencies of twisted rotating plates p 141 A85-32343
Vibration and flutter of mistuned bladed-disk assemblies p 16 A85-45854
Vibrations of twisted cantilever plates - A comparison of theoretical results p 144 A85-47626

SUBASSEMBLIES
Multistage spent particle collector and a method for making same
[NASA-CASE-LEW-13914-1] p 135 N85-33489

SUBSONIC AIRCRAFT
Energy efficient engine component development and integration program
[NASA-CR-170034] p 22 N85-10990

SUBSONIC FLOW
Analytical study of blowing boundary layer control for subsonic V/STOL inlets p 2 A85-11646
Sound generation and upstream influence due to instability waves interacting with non-uniform mean flows p 174 A85-20738

SUBSONIC FLUTTER
Flutter of turbofan rotors with mistuned blades p 139 A85-12716

SUBSONIC WIND TUNNELS
The Altitude Wind Tunnel (AWT) - A unique facility for propulsion system and adverse weather testing
[AIAA PAPER 85-0314] p 34 A85-19661
Analytical modeling of circuit aerodynamics in the new NASA Lewis Altitude Wind Tunnel
[AIAA PAPER 85-0380] p 3 A85-26389
Analytical modeling of circuit aerodynamics in the new NASA Lewis wind tunnel
[NASA-TM-86912] p 8 N85-15688

SUBSTITUTES
The B2 aluminides as alternative materials
[NASA-TM-86937] p 74 N85-19076

SUBSTRATES
Laboratory degradation of Kapton in a low energy oxygen ion beam
[AIAA PAPER 83-2658] p 78 A85-10675
Deposition stress effects on the life of thermal barrier coatings on burner rigs p 79 A85-19086
The scattering of ultrasonic third sound from substrate surface defects p 174 A85-36047
Effects of MAR-M247 substrate (modified) composition on coating oxidation coating/substrate interdiffusion --- protective coatings for hot section components of gas turbine engines
[NASA-CR-174851] p 73 N85-19073
The structure of ion plated films in relation to coating properties
[NASA-TM-87055] p 95 N85-29085
Thermal barrier coating system
[NASA-CASE-LEW-14057-1] p 59 N85-35233

SULFATION
Molecular orbital studies in oxidation: Sulfate formation and metal-metal oxide adhesion
[NASA-CR-176070] p 77 N85-32174
Adsorption of O2, SO2, and SO3 on nickel oxide. Mechanism for sulfate formation
[NASA-CR-176072] p 77 N85-32175

SULFUR DIOXIDES
Mechanism for chelated sulfate formation from SO2 and bis (triphenylphosphine) platinum p 62 A85-48493

SULFUR OXIDES
Effects of SO2 and SO3 on the Na2SO4 induced corrosion of nickel p 65 A85-15603
Mechanism for forming hydrogen chloride and sodium sulfate from sulfur trioxide, water, and sodium chloride p 62 A85-48513
Adsorption of O2, SO2, and SO3 on nickel oxide. Mechanism for sulfate formation
[NASA-CR-176072] p 77 N85-32175

SULFURIC ACID
Rapid estimation of concentration of aromatic classes in middistillate fuels by high-performance liquid chromatography
[NASA-TP-2495] p 93 N85-31307

SUPERCOMPUTERS
General approaches for achieving high speed computations p 169 A85-28628
Functional language and data flow architectures p 170 A85-28629

SUPERCONDUCTORS
A rotating superconducting solenoid for 100 kWh energy storage --- in space p 44 A85-33144

SUPERCOOLING
Dendritic solidification. I - Analysis of current theories and models. II - A model for dendritic growth under an imposed thermal gradient p 182 A85-38019

SUPERCRITICAL FLOW
Nested subcritical flows within supercritical systems
[NASA-TM-86980] p 115 N85-21574

SUPERHYBRID MATERIALS
Fabrication and quality assurance processes for superhybrid composite fan blades
[NASA-TM-83354] p 57 N85-14882

SUPERSONIC AIRCRAFT
Supersonic jet shock noise reduction
[AIAA PAPER 84-2278] p 173 A85-16099

SUPERSONIC BOUNDARY LAYERS
An experimental study of three-dimensional shock wave/turbulent boundary layer interactions in a supersonic flow
[AIAA PAPER 85-1566] p 5 A85-40691

SUPERSONIC FLOW
Numerical calculation of subsonic jets in crossflow with reduced numerical diffusion
[AIAA PAPER 85-1441] p 110 A85-39780
Numerical calculation of subsonic jets in crossflow with reduced numerical diffusion
[NASA-TM-87003] p 27 N85-25263
Unsteady flow in a supersonic cascade with two in-passage shocks
[NASA-CR-3925] p 10 N85-35158

SUPERSONIC FLUTTER
The effect of aerodynamic and structural detuning on turbomachine supersonic unstalled torsional flutter
[AIAA PAPER 85-0761] p 14 A85-30378

SUPERSONIC JET FLOW
A multiple-scales model of the shock-cell structure of imperfectly expanded supersonic jets p 113 A85-49354

SUPERSONIC SPEEDS
Observations from varying the lift and drag inputs to a noise prediction method for supersonic helical tip speed propellers
[NASA-TM-83797] p 175 N85-10788

SURFACE COOLING
Heat transfer and turbulence measurements of a film-cooled flow over a convexly curved surface p 112 A85-41787
Unsteady heat transfer due to time-dependent free stream velocity p 117 N85-27947

SURFACE DEFECTS
The scattering of ultrasonic third sound from substrate surface defects p 174 A85-36047

SURFACE ENERGY
Mechanism for chelated sulfate formation from SO2 and bis (triphenylphosphine) platinum p 62 A85-48493

SURFACE FINISHING
Laser balancing system for high material removal rates
[NASA-CR-174731] p 126 N85-12341
Textured carbon surfaces on copper
[NASA-CASE-LEW-14130-1] p 95 N85-20156
Diamondlike flakes
[NASA-CASE-LEW-13837-2] p 57 N85-21267
Ion-beam nitriding of steels
[NASA-CASE-LEW-14104-1] p 75 N85-21324
Reliability of void detection in structural ceramics using scanning laser acoustic microscopy
[NASA-TM-87035] p 138 N85-32337

SURFACE GEOMETRY
Effect of surface configuration during solid particle impingement erosion p 69 A85-42568

SURFACE PROPERTIES
Topological reaction rate measurements related to scuffing p 64 A85-11070
Surface hardening of steel by boriding in a cold rf plasma p 68 A85-40275
Effect of five lubricants on life of AISI 9310 spur gears
[NASA-TP-2419] p 123 N85-16099
Tribological properties of boron nitride synthesized by ion beam deposition
[NASA-TM-86962] p 87 N85-21355
Monte Carlo lattice models for adsorbed polymer conformation
[NASA-TP-2453] p 183 N85-24961
Free-surface phenomena under low- and zero-gravity conditions
[NASA-CR-175835] p 116 N85-27168
Interaction of high-cycle and low-cycle fatigue of Haynes 188 alloy at 1400 F deg p 149 N85-27961

SURFACE REACTIONS
Cathode degradation and erosion in high pressure arc discharges p 43 A85-16445
Mechanical-contact-induced transformation from the amorphous to the partially crystalline state in metallic glass p 65 A85-19084
A morphological study of silicon carbide prepared by chemical vapor deposition p 79 A85-20938
Characterization of erosion of metallic materials under cavitation attack in a mineral oil
[NASA-TM-86934] p 74 N85-19075
Three-dimensional calculation of shuttle charging in polar orbit p 40 N85-22486
Effects of surface chemistry on hot corrosion life
[NASA-CR-174915] p 28 N85-26711
The role of surface generated radicals in catalytic combustion p 30 N85-27869

SURFACE ROUGHNESS
The role of the reflection coefficient in precision measurement of ultrasonic attenuation p 137 A85-42151
An experimental investigation of microstrip properties on soft substrates from 2 to 40 GHz
[NASA-TM-86961] p 99 N85-20224
Surface roughness effects in elastohydrodynamic contacts
[NASA-TP-2488] p 134 N85-32329

SURFACE TEMPERATURE
Analytical fuel property effects: Small combustors, phase 2
[NASA-CR-174848] p 93 N85-19175
Fabrication of ceramic substrate-reinforced and free forms
[NASA-TM-86994] p 50 N85-23926

SURFACE WAVES
Solar energy converter using surface plasma waves
[NASA-CASE-LEW-13827-1] p 160 N85-21768

SURFACES
Incompressible lifting-surface aerodynamics for a rotor-stator combination
[NASA-TM-83767] p 7 N85-12039

SURGES
Circuit transients due to negative bias arcs on a high-voltage solar array in low Earth orbit
[NASA-TP-2407] p 39 N85-14858
A theory of post-stall transients in multistage axial compression systems
[NASA-CR-3878] p 8 N85-21117

SWEAT COOLING
Advanced liner-cooling techniques for gas turbine combustors
[AIAA PAPER 85-1290] p 15 A85-39703
Advanced liner-cooling techniques for gas turbine combustors
[NASA-TM-86952] p 8 N85-21115

SWEEP EFFECT
Flutter of swept fan blades
[ASME PAPER 84-GT-138] p 141 A85-32962

SWEPT WINGS
Computation of three-dimensional viscous flows using a space-marching method p 4 A85-29259

SWIRLING
Flow visualization of lateral jet injection into swirling crossflow
[AIAA PAPER 85-0059] p 2 A85-19490
Calculation of confined swirling flows
[AIAA PAPER 85-0060] p 108 A85-19491
Swirling flows in typical combustor geometries
[AIAA PAPER 85-0184] p 108 A85-19574
Jet characteristics in confined swirling flow
p 112 A85-45282
Density effects on jet characteristics in confined swirling flow p 112 A85-45283
Turbulence characteristics of swirling flowfields
[NASA-CR-174918] p 29 N85-26717
Flow modifying device
[NASA-CASE-LEW-13562-2] p 33 N85-35195
SWITCHES
Advanced in solid state switchgear technology for large space power systems p 102 A85-45362
High-temperature optically activated GaAs power switching for aircraft digital electronic control
[NASA-CR-174711] p 34 N85-12901
A new very high voltage semiconductor switch
[NASA-TM-86957] p 103 N85-20246
SWITCHING
High voltage-high power components for large space power distribution systems p 45 A85-45370
SWITCHING CIRCUITS
The NASA satellite communication 20 x 20 matrix switches p 101 A85-14435
A fast time domain digital simulation technique for power converters - Application to a buck converter with feedforward compensation p 101 A85-20900
Optical computer switching network
p 178 A85-23134
The J3 SCR model applied to resonant converter simulation p 102 A85-42156
SYNTHESIS (CHEMISTRY)
Ideal gas thermodynamic properties for the phenyl, phenoxy, and o-biphenyl radicals
[NASA-TM-83800] p 184 N85-22204
Preparation of silicon carbide-silicon nitride fibers by the pyrolysis of polycarbosilazane precursors
[NASA-TM-86505] p 91 N85-28107
SYNTHETIC RESINS
Fundamental studies of composite toughness
p 56 N85-12948
SYSTEM EFFECTIVENESS
Mod-2 wind turbine field operations experience
p 157 A85-45512
NASA Redox Storage System Development Project
[NASA-TM-83677] p 158 N85-12465
Transmission efficiency measurements and correlations with physical characteristics of the lubricant
p 89 N85-23781
SYSTEM FAILURES
A real-time FORTRAN implementation of a sensor failure detection, isolation and accommodation algorithm
p 171 A85-47704
SYSTEM GENERATED ELECTROMAGNETIC PULSES
Electron yields from spacecraft materials
p 40 N85-22512
SYSTEMS ANALYSIS
Energy efficient engine. Volume 1: Component development and integration program
[NASA-CR-173084] p 22 N85-10992
Preliminary analysis of space mission applications for electromagnetic launchers
[NASA-CR-174067] p 35 N85-12071
SYSTEMS ENGINEERING
The role of modern control theory in the design of controls for aircraft turbine engines p 13 A85-13627
Status of DOE and AID stand-alone photovoltaic system field tests p 155 A85-35707
Fatigue criterion to system design, life and reliability
[AIAA PAPER 85-1140] p 143 A85-40814
Combustion system for radiation investigations
p 21 N85-10986
Fatigue criterion to system design, life and reliability
[NASA-TM-87017] p 132 N85-27226
SYSTEMS INTEGRATION
An evaluation of oxygen/hydrogen propulsion systems for the Space Station
[AIAA PAPER 85-1156] p 45 A85-43976
An evaluation of oxygen-hydrogen propulsion systems for the Space Station
[NASA-TM-87059] p 52 N85-28971
SYSTEMS SIMULATION
Data flow methods for dynamic system simulation - A CSSL-IV microcomputer network interface
p 170 A85-28614
Moving target, distributed, real-time simulation using Ada p 170 A85-34131

T

TAKEOFF
Wind tunnel results of advanced high speed propellers in the takeoff, climb, and landing operating regimes
[AIAA PAPER 85-1259] p 6 A85-47025
Wind tunnel results of advanced high speed propellers in the takeoff, climb and landing operating regimes
[NASA-TM-87054] p 9 N85-29925
TANTALUM
The effect of tantalum on the structure/properties of two polycrystalline nickel-base superalloys: B-1900 + Hf MAR-M247
[NASA-CR-174847] p 73 N85-18127
TANTALUM ALLOYS
Effects of MAR-M247 substrate (modified) composition on coating oxidation coating/substrate interdiffusion --- protective coatings for hot section components of gas turbine engines
[NASA-CR-174851] p 73 N85-19073
TAPERING
Rotordynamic coefficients for compressible flow in tapered annular seals p 129 A85-42573
TARGET SIMULATORS
Moving target, distributed, real-time simulation using Ada p 170 A85-34131
TECHNOLOGICAL FORECASTING
The trend of future gas turbine technology
p 16 A85-41778
PM superalloys - A troubled adolescent?
p 69 A85-44772
Telecommunications forecast for ITU Region 2 to the year 1995
[NASA-TM-87077] p 38 N85-34150
TECHNOLOGY ASSESSMENT
Status of NASA's multibeam communications technology program p 100 A85-14432
The NASA photovoltaic technology program
p 155 A85-35604
PM superalloys - A troubled adolescent?
p 69 A85-44772
Mod II engine and technology development
p 129 A85-45473
Preliminary analysis of space mission applications for electromagnetic launchers
[NASA-CR-174067] p 35 N85-12071
Missions/planning panel p 36 N85-13886
Configuration study for a 30 GHz monolithic receive array: Technical assessment
[NASA-CR-174697] p 98 N85-18238
The high voltage silicon cell: A comparative analysis
p 49 N85-22569
Instrumentation technology overview
p 124 N85-26903
The Federal Wind Program at NASA Lewis Research Center
[NASA-TM-83480] p 163 N85-30478
A survey of unified constitutive theories
p 150 N85-31531
Energy Efficient Engine Program technology benefit/cost study, volume 2
[NASA-CR-174766-VOL-2] p 33 N85-35198
Practical aspects of photovoltaic technology, applications and cost (revised)
[NASA-CR-174963] p 165 N85-35472
TECHNOLOGY TRANSFER
Energy efficient engine. Volume 2. Appendix A: Component development and integration program
[NASA-CR-173085] p 22 N85-10991
TECHNOLOGY UTILIZATION
Status of DOE and AID stand-alone photovoltaic system field tests p 155 A85-35707
Progress in the utilization of an oxide-dispersion-strengthened alloy for small engine turbine blades
[SAE PAPER 841512] p 68 A85-39284
Solar dynamic systems p 164 N85-31374
Energy Efficient Engine Program technology benefit/cost study, volume 1
[NASA-CR-174766-VOL-1] p 33 N85-35197
TEETH
Spiral bevel and circular arc helical gears: Tooth contact analysis and the effect of misalignment on circular arc helical gears
[NASA-TM-87013] p 32 N85-31060
TEFLON (TRADEMARK)
An experimental investigation of microstrip properties on soft substrates from 2 to 40 GHz
[NASA-TM-86961] p 99 N85-20224
TELECOMMUNICATION
The subjective effect of multiple co-channel frequency modulated television interference p 96 A85-28234
Satellite provided customer promises services, a forecast of potential domestic demand through the year 2000. Volume 4: Sensitivity analysis
[NASA-CR-174662] p 99 N85-27092
TELEVISION TRANSMISSION
An allpass filter design for luminance and chrominance separation of NTSC signals p 102 A85-28230
The subjective effect of multiple co-channel frequency modulated television interference p 96 A85-28234
TEMPERATURE
Digital temperature and velocity control of mach 0.3 atmospheric pressure durability testing burner rigs in long time, unattended cyclic testing
[NASA-TM-86959] p 75 N85-21321
TEMPERATURE CONTROL
Advanced thermal barrier system bond coatings for use on Ni, Co-, and Fe-base alloy substrates
[NASA-TM-87062] p 77 N85-31283
TEMPERATURE DEPENDENCE
Heat treatment of bulk gallium arsenide using a phosphosilicate glass cap p 181 A85-32636
A 37.5-kW point design comparison of the nickel-cadmium battery, bipolar nickel-hydrogen battery, and regenerative hydrogen-oxygen fuel cell energy storage subsystems for low earth orbit p 46 A85-45387
Orientation and temperature dependence of some mechanical properties of the single-crystal nickel-base superalloy Rene N4. 3: Tension-compression anisotropy
[NASA-TM-86982] p 76 N85-22660
A survey of unified constitutive theories
p 150 N85-31531
TEMPERATURE DISTRIBUTION
A comparison of NMC and GWC analysis field temperatures with aircraft measurements
p 166 A85-21140
Manual of phosphoric acid fuel cell stack three-dimensional model and computer program
[NASA-CR-174722] p 157 N85-10447
Dilution jet configurations in a reverse flow combustor
[NASA-CR-174888] p 27 N85-22392
Development of a temperature measurement system with application to a jet in a cross flow experiment
[NASA-CR-174896] p 27 N85-25262
TEMPERATURE EFFECTS
An experimental study of tone excited heated jets
[AIAA PAPER 84-2341] p 172 A85-10882
Design procedures for fiber composite structural components - Rods, beams, and beam columns
p 54 A85-15636
The influence of temperature on the lubricating effectiveness of MoS2 dispersed in mineral oils
[ASLE PREPRINT 84-LC-2A-2] p 80 A85-25963
Oscillatory conductive heat transfer for a fiber in an ideal gas p 109 A85-26077
Thermal elastohydrodynamic lubrication of line contacts p 128 A85-31202
Stability of bromine intercalated graphite fibers
[NASA-TM-86859] p 84 N85-10187
Burner rig corrosion of SiC at 1000 deg C
[NASA-TM-87061] p 53 N85-30011
Nonlinear Constitutive Relations for High Temperature Application, 1984
[NASA-CP-2369] p 150 N85-31530
On the use of internal state variables in thermoviscoplastic constitutive equations
p 150 N85-31536
TEMPERATURE GRADIENTS
Temperature distortion generator for turboshaft engine testing
[SAE PAPER 841541] p 15 A85-39065
Dendritic solidification. III - Some further refinements to the model for dendritic growth under an imposed thermal gradient p 69 A85-44703
Temperature distortion generator for turboshaft engine testing
[NASA-TM-83748] p 1 N85-15658
Comparative analysis of operational forecasts versus actual weather conditions in airline flight planning, volume 4
[NASA-CR-167865] p 167 N85-35537
TEMPERATURE INVERSIONS
Effect of steady-state temperature distortion on inlet flow to a high-bypass-ration turbofan engine
[NASA-TM-86896] p 24 N85-15725
TEMPERATURE MEASUREMENT
Effect of combined pressure and temperature distortion orientation on high-bypass-ratio turbofan engine stability
[NASA-TM-83771] p 17 N85-10067
An interactive computer code for calculation of gas-phase chemical equilibrium (EQLBRM)
[NASA-CR-168337] p 18 N85-10948
Dilution jet configurations in a reverse flow combustor
[NASA-CR-174888] p 27 N85-22392
Development of a temperature measurement system with application to a jet in a cross flow experiment
[NASA-CR-174896] p 27 N85-25262
Measurement and correlation of jet fuel viscosities at low temperatures
[NASA-CR-174911] p 94 N85-34295

TEMPERATURE SENSORS
Fiber optic temperature sensor p 121 A85-29563
Fiber optic, Fabry-Perot high temperature sensor
[NASA-CR-174712] p 178 N85-13594
TENSILE CREEP
Morphological changes of gamma prime precipitates in nickel-base superalloy single crystals
[NASA-TM-83698] p 70 N85-10165
TENSILE STRENGTH
Design procedures for fiber composite structural components - Rods, beams, and beam columns p 54 A85-15636
Effects of tin on microstructure and mechanical behavior of Inconel 718
[NASA-TM-86866] p 71 N85-12129
Imide modified epoxy matrix resins
[NASA-CR-174695] p 85 N85-15892
Effects of chromium and aluminum on mechanical and oxidation properties of iron-nickel-base superalloys based on CG-27
[NASA-TP-2443] p 75 N85-21323
Environmental effects on the tensile strength of chemically vapor deposited silicon carbide fibers
[NASA-TM-86981] p 89 N85-24000
TENSILE STRESS
Orientation and temperature dependence of some mechanical properties of the single-crystal nickel-base superalloy Rene N4. 3: Tension-compression anisotropy
[NASA-TM-86982] p 76 N85-22660
A continuous damage model based on stepwise-stress creep rupture tests
[NASA-CR-174941] p 152 N85-32341
TENSILE TESTS
Deformation and fracture behavior of Ni-Mo-Al(gamma/gamma prime-alpha) in situ composite p 64 A85-11058
Fracture toughness of hot-pressed beryllium p 66 A85-25835
Mechanical property measurements of plasma-sprayed thermal-barrier coatings subjected to oxidation p 81 A85-29729
Constitutive modeling and computational implementation for finite strain plasticity p 143 A85-40910
Graphite/PMR polyimide composites with improved toughness
[NASA-TM-87081] p 58 N85-32148
TENSOR ANALYSIS
Alternatives for jet engine control
[NASA-CR-175831] p 29 N85-26713
Alternatives for jet engine control
[NASA-CR-175832] p 29 N85-26714
Alternatives for jet engine control
[NASA-CR-175833] p 29 N85-26715
TERNARY ALLOYS
High temperature properties of equiatomic FeAl with ternary additions
[NASA-TM-86938] p 73 N85-19072
TERNARY SYSTEMS
High temperature properties of equiatomic FeAl with ternary additions
[NASA-TM-86938] p 73 N85-19072
A study of interdiffusion in beta + gamma/gamma + gamma prime Ni-Cr-Al
[NASA-CR-174852] p 74 N85-20041
TEST EQUIPMENT
Flame flashback in a premixed dump combustor
[AIAA PAPER 85-0145] p 60 A85-19550
Cryogenic upper stage test bed engine
[AIAA PAPER 85-1339] p 44 A85-39733
The design and analysis of single flank transmission error testor for loaded gears
[NASA-CR-176163] p 136 N85-34404
TEST FACILITIES
HOST liner cyclic facilities: Facility description p 22 N85-10988
Heat transfer results and operational characteristics of the NASA Lewis Research Center Hot Section Cascade Test Facility
[NASA-TM-86890] p 114 N85-15133
TEST STANDS
HOST liner cyclic facilities: Facility description p 22 N85-10988
The design and analysis of single flank transmission error testor for loaded gears
[NASA-CR-176163] p 136 N85-34404
TEST VEHICLES
Energy efficient engine ICLS Nacelle detail design report
[NASA-CR-167870] p 22 N85-10993
TETHERING
Report of the Constellations Panel p 131 N85-20368
Preliminary assessment of power-generating tethers in space and of propulsion for their orbit maintenance p 37 N85-22520
TETRAHYDROFURAN
Development of a lithium secondary battery separator p 104 N85-31378
TF-34 ENGINE
TF34 convertible engine control system design p 15 A85-32006
Nonlinear global stability analysis of compressor stall phenomena
[NASA-CR-174908] p 31 N85-29960
THERMAL ANALYSIS
Energy efficient engine combustor test hardware detailed design report
[NASA-CR-167945] p 18 N85-10950
Applications of high pressure differential scanning calorimetry to aviation fuel thermal stability research
[NASA-TM-87002] p 63 N85-23941
THERMAL BUCKLING
Quasi-static solution algorithms for kinematically/materially nonlinear thermomechanical problems p 143 A85-41983
THERMAL CONTROL COATINGS
Oxidation-based model for thermal barrier coating life p 78 A85-10310
Life modeling of atmospheric and low pressure plasma-sprayed thermal-barrier coating p 81 A85-29728
Mechanical property measurements of plasma-sprayed thermal-barrier coatings subjected to oxidation p 81 A85-29729
Failure during thermal cycling of plasma-sprayed thermal barrier coatings p 81 A85-36246
Optimization of the NiCrAl-Y/ZrO-Y2O3 thermal barrier system
[NASA-TM-86905] p 72 N85-15878
An investigation of enhanced capability thermal barrier coating systems for diesel engine components
[NASA-CR-174820] p 86 N85-18154
Rocket thrust chamber thermal barrier coatings p 90 N85-26867
Advanced thermal barrier system bond coatings for use on Ni, Co-, and Fe-base alloy substrates
[NASA-TM-87062] p 77 N85-31283
Energy efficient engine, high pressure turbine thermal barrier coating. Support technology report
[NASA-CR-168037] p 34 N85-35199
THERMAL CYCLING TESTS
Simplified design and life prediction of rocket thrust chambers p 44 A85-29314
Failure during thermal cycling of plasma-sprayed thermal barrier coatings p 81 A85-36246
HOST instrumentation R and D program overview p 19 N85-10957
Validation of structural analysis methods using the in-house liner cyclic rigs p 21 N85-10987
HOST liner cyclic facilities: Facility description p 22 N85-10988
Rocket thrust chamber thermal barrier coatings p 90 N85-26867
THERMAL DECOMPOSITION
Metallic and metalloceramic coating by thermal decomposition
[NASA-TM-86992] p 88 N85-22755
THERMAL DEGRADATION
Liquid phase products and solid deposit formation from thermally stressed model jet fuels
[NASA-TM-86874] p 92 N85-13066
Laboratory studies of Kapton degradation in an oxygen ion beam p 177 N85-22477
THERMAL DISSOCIATION
Jet fuel property changes and their effect on producibility and cost in the U.S., Canada, and Europe
[NASA-CR-174840] p 93 N85-27012
THERMAL EXPANSION
Extreme precision antenna reflector study results p 165 N85-23830
THERMAL FATIGUE
A study of fatigue damage mechanisms in Waspaloy from 25 to 800 C p 65 A85-12098
Considerations for damage analysis of gas turbine hot section components
[ASME PAPER 84-PVP-77] p 14 A85-18792
Engine cyclic durability by analysis and material testing p 25 N85-15744
Thermal-mechanical fatigue crack growth in Inconel X-750
[NASA-CR-174740] p 72 N85-15877
Analytical and experimental investigation of rubbing interaction in labyrinth seals for a liquid hydrogen fuel pump --- space shuttle main engine
[NASA-CR-174657] p 48 N85-18084
THERMAL NEUTRONS
Apparatus and method for identification of matrix materials in which transuranic elements are embedded using thermal neutron capture gamma-ray emission
[DE85-011659] p 125 N85-33454
THERMAL NOISE
The influence of combustion liner holes on noise production by ducted burners
[AIAA PAPER 84-2322] p 172 A85-10869
Adaptive antenna arrays for weak interfering signals
[NASA-CR-174336] p 98 N85-17258
THERMAL PROTECTION
Electron beam charging of Space Shuttle thermal protection system tiles p 39 N85-22478
THERMAL RESISTANCE
Performance of thermal barrier coatings in high heat flux environments p 79 A85-19087
An experimental investigation and numerical prediction of thermomechanical phenomena in high speed rotor tip rubbing p 14 A85-25442
Thermal barrier coating system
[NASA-CASE-LEW-13324-2] p 57 N85-21266
THERMAL SHOCK
Dispersed-metal-toughened alumina
[NASA-CR-174687] p 89 N85-22758
THERMAL STABILITY
Stability of bromine intercalated graphite fibers
[NASA-TM-86859] p 84 N85-10187
External fuel vaporization study, phase 2
[NASA-CR-174079] p 92 N85-11252
Study of advanced fuel system concepts for commercial aircraft and engines
[NASA-CR-174752] p 93 N85-19176
Applications of high pressure differential scanning calorimetry to aviation fuel thermal stability research
[NASA-TM-87002] p 63 N85-23941
Graphite/PMR polyimide composites with improved toughness
[NASA-TM-87081] p 58 N85-32148
THERMAL STRESSES
Liquid phase products and solid deposit formation from thermally stressed model jet fuels
[NASA-TM-86874] p 92 N85-13066
Thermal-stress analysis for a wood composite blade
[NASA-CR-174794] p 159 N85-17421
Thermal stress analysis of a new turbine shroud seal concept
[NASA-TM-87082] p 136 N85-34406
THERMIONIC POWER GENERATION
High thermal power density heat transfer apparatus providing electrical isolation at high temperature using heat pipes
[NASA-CASE-LEW-12950-2] p 117 N85-29179
Thermionic photovoltaic energy converter
[NASA-CASE-LEW-14077-1] p 164 N85-34441
THERMOCOUPLE PYROMETERS
Thin-film sensors for space propulsion technology p 41 N85-27968
THERMOCOUPLES
High temperature thermocouple and heat flux gauge using a unique thin film-hardware hot juncture
[NASA-TM-86898] p 123 N85-16096
Advanced thin film thermocouples
[NASA-CR-175541] p 124 N85-21607
Development of a temperature measurement system with application to a jet in a cross flow experiment
[NASA-CR-174896] p 27 N85-25262
THERMODYNAMIC CYCLES
Initial testing of a variable-stroke Stirling engine
[NASA-TM-86875] p 185 N85-19895
THERMODYNAMIC EFFICIENCY
Overview of NASA Lewis Research Center free-piston Stirling engine activities p 130 A85-45479
THERMODYNAMIC EQUILIBRIUM
An interactive computer code for calculation of gas-phase chemical equilibrium (EQLBRM)
[NASA-CR-168337] p 18 N85-10948
THERMODYNAMIC PROPERTIES
ICAN - Integrated composites analyzer
[AIAA PAPER 84-0974] p 54 A85-16094
Combustion gas properties I-ASTM jet A fuel and dry air
[NASA-TP-2359] p 17 N85-10064
Computer program for calculation of complex chemical equilibrium compositions and applications. Supplement 1: Transport properties
[NASA-TM-86885] p 184 N85-16663
Chemical approach for controlling nadimide cure temperature and rate
[NASA-CASE-LEW-13770-5] p 87 N85-21352
Ideal gas thermodynamic properties for the phenyl, phenoxy, and o-biphenyl radicals
[NASA-TM-83800] p 184 N85-22204
On thermomechanical testing in support of constitutive equation development for high temperature alloys
[NASA-CR-174879] p 147 N85-25894

Computer program for the calculation of multicomponent convective diffusion deposition rates from chemically frozen boundary layer theory
[NASA-CR-168329] p 116 N85-27164
Design and lubrication of high-speed rolling-element bearings
[NASA-TM-87107] p 137 N85-34409

THERMODYNAMICS
Statistics and thermodynamics of fracture
p 140 A85-19433
Review - Computational methods for internal flows with emphasis on turbomachinery p 4 A85-29126
Thermodynamically consistent constitutive equations for nonisothermal large strain, elasto-plastic, creep behavior
[AIAA PAPER 85-0621] p 142 A85-38425
Viscoplastic constitutive relationships with dependence on thermomechanical history
[NASA-CR-174836] p 146 N85-21691
Analytical fuel property effects--small combustors
[NASA-CR-174738] p 28 N85-26709
Dynamic creep buckling: Analysis of shell structures subjected to time-dependent mechanical and thermal loading p 149 N85-27959
Designing for fiber composite structural durability in hygrothermomechanical environment
[NASA-TM-87045] p 58 N85-27978

THERMOELASTICITY
Quasi-static solution algorithms for kinematically/materially nonlinear thermomechanical problems p 143 A85-41983
Translational and extensional energy release rates (the J- and M-integrals) for a crack layer in thermoelasticity
[NASA-CR-174872] p 145 N85-21685
A review of path-independent integrals in elastic-plastic fracture mechanics, task 4
[NASA-CR-174956] p 152 N85-33541

THERMOGRAVIMETRY
Applications of high pressure differential scanning calorimetry to aviation fuel thermal stability research
[NASA-TM-87002] p 63 N85-23941

THERMOMECHANICAL TREATMENT
Select fiber composites for space applications - A mechanistic assessment p 54 A85-16040
Quasi-static solution algorithms for kinematically/materially nonlinear thermomechanical problems p 143 A85-41983
Analysis of shell type structures subjected to time dependent mechanical and thermal loading
[NASA-CR-175747] p 147 N85-25896
Multiaxial and thermomechanical fatigue considerations in damage tolerant design
[NASA-TM-87022] p 76 N85-26964
Thermomechanical deformation in the presence of metallurgical changes p 150 N85-31533

THERMOPHYSICAL PROPERTIES
Thermal and thermomechanical effects in dry sliding
p 127 A85-23838
Nested subcritical flows within supercritical systems
[NASA-TM-86980] p 115 N85-21574

THERMOPLASTICITY
Spherical microglass particle impingement studies of thermoplastic materials at normal incidence
p 79 A85-11072
Nonlinear structural and life analyses of a combustor liner p 19 N85-10955

THIN FILMS
Frictional and morphological properties of Au-MoS2 films sputtered from a compact target p 127 A85-19085
Computer simulation of thin film nucleation and growth
p 181 A85-35308
Properties of coated and modified surfaces
p 53 A85-36694
'Diamondlike' carbon films - Optical absorption, dielectric properties, and hardness dependence on deposition parameters p 82 A85-40383
Hot corrosion of sintered alpha-SiC at 1000 C
[ACS PAPER 19-B-84P] p 83 A85-45302
Monte Carlo study of reversible growth of clusters on a surface p 182 A85-48516
Analysis of glow discharges for understanding the process of film formation
[NASA-TM-83750] p 62 N85-10138
High temperature thermocouple and heat flux gauge using a unique thin film-hardware hot juncture
[NASA-TM-86898] p 123 N85-16096
Deposition of diamondlike carbon films
[NASA-CASE-LEW-14080-1] p 95 N85-20153
A computer simulation of thin film nucleation and growth: The Volmer-Weber case
[NASA-TM-86968] p 53 N85-21264
Advanced thin film thermocouples
[NASA-CR-175541] p 124 N85-21607
Mass spectra of neutral particles released during electrical breakdown of thin polymer films
p 88 N85-22511
Thin-film sensors for space propulsion technology
p 41 N85-27968
The structure of ion plated films in relation to coating properties
[NASA-TM-87055] p 95 N85-29085
Ion beam sputter-deposited thin film coatings for protection of spacecraft polymers in low Earth orbit
[NASA-TM-87051] p 91 N85-30137
Mechanical protection of DLC films on fused silica slides
[NASA-TM-87056] p 91 N85-30138
Advances in sputtered and ion plated solid film lubrication p 136 N85-33524

THIN WALLED SHELLS
Fabrication of ceramic substrate-reinforced and free forms
[NASA-TM-86994] p 50 N85-23926
Dynamic creep buckling: Analysis of shell structures subjected to time-dependent mechanical and thermal loading p 149 N85-27959

THIOLS
Formation of high molecular weight products from benzene during boundary lubrication
[NASA-TM-86966] p 62 N85-22644

THREE DIMENSIONAL BODIES
Recent advances in hybrid/mixed finite elements
[NASA-CR-175574] p 145 N85-21687

THREE DIMENSIONAL BOUNDARY LAYER
A three-dimensional boundary-layer analysis including heat-transfer and blade-rotation effects
p 6 A85-42988

THREE DIMENSIONAL FLOW
Development of finite analytic method for unsteady three-dimensional Navier-Stokes equation
p 106 A85-11647
A finite element solution of three-dimensional inviscid rotational flows through curved ducts
p 107 A85-11648
Three-dimensional inviscid flow analysis of turbofan forced mixers
[AIAA PAPER 85-0086] p 2 A85-19510
Computation of three-dimensional viscous flows using *a space-marching method* p 4 A85-29259
Calculation of three-dimensional, viscous flow through turbomachinery blade passages by parabolic marching
[AIAA PAPER 85-1408] p 5 A85-39767
An experimental study of three-dimensional shock wave/turbulent boundary layer interactions in a supersonic flow
[AIAA PAPER 85-1566] p 5 A85-40691
Calculation of compressible flow about three-dimensional inlets with auxiliary inlets, slats and vanes by means of a panel method
[AIAA PAPER 85-1196] p 5 A85-40817
The three-dimensional compressible flow in a radial inflow turbine scroll p 6 A85-41826
Inviscid analysis of advanced turboprop propeller flow fields
[AIAA PAPER 85-1263] p 6 A85-43977
Calculation of three-dimensional, viscous flow through turbomachinery blade passages by parabolic marching
[NASA-TM-86984] p 9 N85-23711
Turbulence characteristics of swirling flowfields
[NASA-CR-174918] p 29 N85-26717
Fuel and oxidizer turbine loss analysis
p 50 N85-26900
Redistribution of the inlet temperature profile through the SSME fuel turbine p 50 N85-26901
Unsteady flow in a supersonic cascade with two in-passage shocks
[NASA-CR-3925] p 10 N85-35158
General design method for 3-dimensional, potential flow fields. Part 2: Computer program DIN3D1 for simple, unbranched ducts
[NASA-CR-3926] p 10 N85-35159

THRUST
Energy efficient engine ICLS engine bearings, drives and configuration: Detail design report
[NASA-CR-167871] p 23 N85-10997

THRUST CHAMBERS
Simplified design and life prediction of rocket thrust chambers p 44 A85-29314
Extended performance technology study 30-cm thruster
[NASA-CR-168259] p 48 N85-15806

THRUST MEASUREMENT
Vacuum chamber pressure effects on thrust measurements of low Reynolds number nozzles
[NASA-TM-86955] p 49 N85-21259

THRUST VECTOR CONTROL
Altitude testing of a flight weight, self-cooled, 2D thrust vectoring exhaust nozzle
[SAE PAPER 841557] p 14 A85-25984

THRUSTORS
IAPS (8-cm) ion thruster cyclic endurance test --- Ion Auxiliary Propulsion System p 42 A85-16406
Ring-cusp ion thrusters p 42 A85-16438
Experiments with a microwave electrothermal thruster concept p 42 A85-16441

THYRISTORS
High-voltage, high-power, solid-state remote power controllers for aerospace applications
[NASA-TP-2437] p 49 N85-21263

TILES
Electron beam charging of Space Shuttle thermal protection system tiles p 39 N85-22478

TIME CONSTANT
Development of a temperature measurement system with application to a jet in a cross flow experiment
[NASA-CR-174896] p 27 N85-25262

TIME DEPENDENCE
Time dependent wave envelope finite difference analysis of sound propagation
[AIAA PAPER 84-2285] p 173 A85-16102
Some advances in experimentation supporting development of viscoplastic constitutive models
[NASA-CR-174855] p 147 N85-27260
Some advances in experimentation supporting development of viscoplastic constitutive models
p 151 N85-31545

TIME DIVISION MULTIPLE ACCESS
The NASA satellite communication 20 x 20 matrix switches p 101 A85-14435
Advanced 30/20 GHz multiple beam antenna for future communications satellites p 96 A85-14436
Modeling of NASA's 30/20 GHz satellite communications system p 38 A85-36663

TIME MARCHING
Application of Runge Kutta time marching scheme for the computation of transonic flows in turbomachines
[AIAA PAPER 85-1332] p 5 A85-39728
Thermodynamic evaluation of transonic compressor rotors using the finite volume approach
[NASA-CR-175811] p 29 N85-26712

TIME MEASUREMENT
Characterization of microstrip discontinuities in the time and frequency domains
[NASA-CR-176190] p 106 N85-35342

TIME SERIES ANALYSIS
Identification of multivariable high-performance turbofan engine dynamics from closed-loop data
p 13 A85-13630
Numerical considerations in the development and implementation of constitutive models
p 151 N85-31541

TIN
Effects of tin on microstructure and mechanical behavior of Inconel 718
[NASA-TM-86866] p 71 N85-12129

TIP DRIVEN ROTORS
Performance comparison between NACA 23024 and NACA 64(3)-618 airfoil configurated rotors for horizontal-axis wind turbines
[NASA-TM-83471] p 163 N85-30477

TIP SPEED
Shutdown characteristics of the Mod-O wind turbine with aileron controls
[NASA-TM-86918] p 159 N85-16299
Study of controlled diffusion stator blading
[NASA-CR-167995] p 25 N85-18058
Further comparison of wind tunnel and airplane acoustic data for advanced design high speed propeller models
[NASA-TM-86935] p 176 N85-22108
Energy efficient engine. Fan and quarter-stage component performance report
[NASA-CR-168070] p 33 N85-34141

TITANIUM
Nitriding of titanium and its alloys by N2, NH3 or mixtures of N2 + H2 in a dc arc plasma at low pressures (or = to torr)
[NASA-TM-83803] p 131 N85-15168

TITANIUM ALLOYS
Metallurgical and mechanical phenomena due to rubbing of titanium against sintered powder Nichrome
p 127 A85-22281
An experimental investigation of rubbing interaction in labyrinth seals at cryogenic temperature
p 129 A85-39938
Effect of low temperature on fatigue and fracture properties of Ti-5Al-2.5Sn(ELI) for use in engine components p 70 A85-47972
Nitriding of titanium and its alloys by N2, NH3 or mixtures of N2 + H2 in a dc arc plasma at low pressures (or = to torr)
[NASA-TM-83803] p 131 N85-15168
CO adsorption on (111) and (100) surfaces of the Pt sub 3 Ti alloy. Evidence for parallel binding and strong activation of CO
[NASA-CR-176077] p 77 N85-32176

TOLERANCES (MECHANICS)
Multiaxial and thermomechanical fatigue considerations in damage tolerant design
[NASA-TM-87022] p 76 N85-26964
TORQUE
Application of traction drives as servo mechanisms p 152 N85-33520
TORSION
Application of traction drives as servo mechanisms p 152 N85-33520
TORSIONAL STRESS
Constitutive modeling and computational implementation for finite strain plasticity p 143 A85-40910
TORSIONAL VIBRATION
Flutter of turbofan rotors with mistuned blades p 139 A85-12716
Effects of warping and pretwist on torsional vibration of rotating beams
[ASME PAPER 84-WA/APM-41] p 140 A85-17040
The effect of aerodynamic and structural detuning on turbomachine supersonic unstalled torsional flutter
[AIAA PAPER 85-0761] p 14 A85-30378
Finite difference analysis of torsional vibrations of pretwisted, rotating, cantilever beams with effects of warping p 143 A85-42047
Optimization of cascade blade mistuning. I - Equations of motion and basic inherent properties p 16 A85-42365
TOTAL ENERGY SYSTEMS
Measured effects of wind turbine generation at the Block Island Power Company p 153 A85-10652
Develop and test fuel cell powered on-site integrated total energy systems. Phase 3: Full-scale power plant development
[NASA-CR-174887] p 161 N85-25941
TOUGHNESS
Resin selection criteria for 'tough' composite structures p 81 A85-35139
Fundamental studies of composite toughness p 56 N85-12948
Imide modified epoxy matrix resins
[NASA-CR-174695] p 85 N85-15892
Graphite/PMR polyimide composites with improved toughness
[NASA-TM-87081] p 58 N85-32148
TOWERS
Structural analysis and cost estimate of an eight-leg space frame as a support structure for horizontal axis wind turbines
[NASA-TM-83470] p 150 N85-30361
TRACERS
Analysis techniques for tracer studies of oxidation
[NASA-CR-174796] p 84 N85-12162
TRACKING (POSITION)
Comparative analysis of operational forecasts versus actual weather conditions in airline flight planning, volume 1
[NASA-CR-167862] p 167 N85-35534
Comparative analysis of operational forecasts versus actual weather conditions in airline flight planning, volume 2
[NASA-CR-167863] p 167 N85-35535
TRACTION
Thermal traction contact performance evaluation under fully flooded and starved conditions
[NASA-CR-168173] p 132 N85-25848
Rolling, slip and traction measurements on low modulus materials
[NASA-CR-174909] p 135 N85-33491
Application of traction drives as servo mechanisms p 152 N85-33520
TRAILING EDGES
Reflection plane tests of a wind turbine blade tip section with ailerons
[NASA-TM-87018] p 165 N85-34444
TRAJECTORIES
Numerical calculation of subsonic jets in crossflow with reduced numerical diffusion
[AIAA PAPER 85-1441] p 110 A85-39780
Numerical calculation of subsonic jets in crossflow with reduced numerical diffusion
[NASA-TM-87003] p 27 N85-25263
TRAJECTORY ANALYSIS
Flow visualization study of the effect of injection hole geometry on an inclined jet in crossflow
[NASA-TM-86936] p 115 N85-20269
TRANSDUCERS
Unsteady pressure measurements on a biconvex airfoil in a transonic oscillating cascade
[NASA-TM-86914] p 8 N85-15689
Stress waves in an isotropic elastic plate excited by a circular transducer
[NASA-CR-3877] p 138 N85-20390
TRANSFER ORBITS
Radiation exposure and performance of multiple burn LEO-GEO orbit transfer trajectories
[NASA-TM-86946] p 36 N85-21228
Manrating orbital transfer vehicle propulsion
[NASA-TM-87019] p 50 N85-25385
Primary propulsion of electrothermal, ion and chemical systems for space-based radar orbit transfer
[NASA-TM-87043] p 51 N85-27972
TRANSFORMERS
Development of high frequency low weight power magnetics for aerospace power systems p 102 A85-45373
Developments in space power components for power management and distribution p 47 N85-13877
TRANSIENT LOADS
Analysis of shell type structures subjected to time dependent mechanical and thermal loading
[NASA-CR-175747] p 147 N85-25896
TRANSISTOR CIRCUITS
Bipolar-FET combinational power transistors for power conversion applications p 100 A85-12669
TRANSISTORS
Developments in space power components for power management and distribution p 47 N85-13877
TRANSITION TEMPERATURE
Effects of cobalt on the hot workability of nickel-base superalloys p 67 A85-32412
TRANSMISSION EFFICIENCY
Correlation of rheological characteristics of lubricants with transmission efficiency measurements
[NASA-TM-86988] p 134 N85-30342
TRANSMISSION LINES
Effect of Interfacial characteristics of metal clad polymeric substrates on electrical high frequency interconnection performance
[NASA-TM-86948] p 99 N85-20223
Performance analysis of radiation cooled dc transmission lines for high power space systems
[NASA-TM-87040] p 104 N85-28222
TRANSMISSION LOSS
Noise transmission loss of a rectangular plate in an infinite baffle
[NASA-TP-2398] p 176 N85-22109
TRANSMISSIONS (MACHINE ELEMENTS)
Gear mesh stiffness and load sharing in planetary gearing
[ASME PAPER 84-DET-229] p 129 A85-33781
Investigation on experimental techniques to detect, locate and quantify gear noise in helicopter transmissions
[NASA-CR-3847] p 176 N85-17667
Feasibility demonstration of a novel, flat-belt, continuously variable transmission or automotive and electric-hybrid vehicle application
[NASA-CR-174430] p 185 N85-19894
Transmission efficiency measurements and correlations with physical characteristics of the lubricant p 89 N85-23781
Correlation of rheological characteristics of lubricants with transmission efficiency measurements
[NASA-TM-86988] p 134 N85-30342
The design and analysis of single flank transmission error testor for loaded gears
[NASA-CR-176163] p 136 N85-34404
TRANSONIC COMPRESSORS
Study of controlled diffusion stator blading
[NASA-CR-167995] p 25 N85-18058
TRANSONIC FLOW
A linearized unsteady aerodynamic analysis for transonic cascades p 3 A85-20744
Investigation of flow phenomena in a transonic fan rotor using laser anemometry
[ASME PAPER 84-GT-199] p 4 A85-32963
Application of Runge Kutta time marching scheme for the computation of transonic flows in turbomachines
[AIAA PAPER 85-1332] p 5 A85-39728
Time dependent computation of the Euler equations for designing 2-D cascades, including the case of transonic shock free design p 5 A85-41814
Rotor wake characteristics of a transonic axial flow fan
[AIAA PAPER 85-1133] p 6 A85-43974
Inverse design technique for cascades
[NASA-CR-3836] p 7 N85-12008
TRANSPIRATION
Small gas turbine combustor study - Fuel injector performance in a transpiration-cooled liner
[AIAA PAPER 85-1312] p 16 A85-39717
Small gas turbine combustor study: Fuel injector performance in a transpiration-cooled liner
[NASA-TM-86989] p 27 N85-25264
TRANSPONDERS
Modeling of NASA's 30/20 GHz satellite communications system p 38 A85-36663
TRANSPORT AIRCRAFT
Advanced secondary power system for transport aircraft
[NASA-TP-2463] p 30 N85-28944
TRANSPORT PROPERTIES
Electrocatalysis of fuel cell reactions: Investigation of alternate electrolytes
[NASA-CR-174753] p 157 N85-11455
Computer program for calculation of complex chemical equilibrium compositions and applications. Supplement 1: Transport properties
[NASA-TM-86885] p 184 N85-16663
Computer program for the calculation of multicomponent convective diffusion deposition rates from chemically frozen boundary layer theory
[NASA-CR-168329] p 116 N85-27164
Turbulent transport and length scale measurement experiments with comfined coaxial jets
[NASA-CR-174831] p 117 N85-30245
TRANSPORT THEORY
Mass and momentum turbulent transport experiments with confined coaxial jets p 107 A85-14399
TRANSURANIUM ELEMENTS
Apparatus and method for identification of matrix materials in which transuranic elements are embedded using thermal neutron capture gamma-ray emission
[DE85-011659] p 125 N85-33454
TRAVELING WAVE TUBES
A 20 GHz, 75 watt, helix TWT for space communications p 101 A85-14433
Design of low loss helix circuits for interference fitted and brazed circuits
[NASA-CR-168313] p 103 N85-19328
TRAVELING WAVES
Vibration and flutter of mistuned bladed-disk assemblies
[AIAA PAPER 84-0991] p 139 A85-16095
TRIBOLOGY
Polyimides - Tribological properties and their use as lubricants p 79 A85-21524
Friction and wear of ceramics p 80 A85-23833
Thermal and thermomechanical effects in dry sliding p 127 A85-23838
Thermal elastohydrodynamic lubrication of line contacts p 128 A85-31202
Properties of coated and modified surfaces p 53 A85-36694
Plasma variables and tribological properties of coatings in low pressure (0.1 - 10.0 torr) plasma systems
[NASA-TM-83798] p 94 N85-11261
Tribological properties of graphite-fiber-reinforced, partially fluorinated polyimide composites
[NASA-TM-86926] p 86 N85-18153
The role of silver in self-lubricating coatings for use at extreme temperatures
[NASA-TM-86943] p 87 N85-20127
Tribological properties of boron nitride synthesized by ion beam deposition
[NASA-TM-86962] p 87 N85-21355
Tribological systems as applied to aircraft engines
[NASA-TM-86965] p 131 N85-21657
Effect of counterface material type and its topography on the tribological properties of polyimide composites
[NASA-TM-87036] p 90 N85-26993
Hertzian contact in two and three dimensions
[NASA-TP-2473] p 135 N85-32331
Aluminum work function: Effect of oxidation, mechanical scraping and ion bombardment
[NASA-TM-87079] p 78 N85-34265
TRIODES
Textured carbon surfaces on copper
[NASA-CASE-LEW-14130-1] p 95 N85-20156
TUBES
Flame radiation and linear heat transfer in a tubular-can combustor p 15 A85-39580
Apparatus for producing diamond-like carbon flakes
[NASA-CASE-LEW-13837-3] p 95 N85-20155
TUNING
Vibration and flutter of mistuned bladed-disk assemblies
[AIAA PAPER 84-0991] p 139 A85-16095
The effect of aerodynamic and structural detuning on turbomachine supersonic unstalled torsional flutter
[AIAA PAPER 85-0761] p 14 A85-30378
Optimization of cascade blade mistuning. I - Equations of motion and basic inherent properties p 16 A85-42365
Optimization of cascade blade mistuning. II - Global optimum and numerical optimization p 16 A85-45715
Precision tunable resonant microwave cavity
[NASA-CASE-LEW-13935-1] p 103 N85-20248
TURBINE BLADES
Hygrothermomechanical evaluation of transverse filament tape epoxy/polyester fiberglass composites p 54 A85-15632

The effect of aerodynamic and structural detuning on turbomachine supersonic unstalled torsional flutter
[AIAA PAPER 85-0761] p 14 A85-30378
Development of coated single-crystal superalloy systems for gas turbine applications p 68 A85-32440
A note on blade wake interaction influence on compressor stator row aerodynamic performance p 4 A85-32965
Progress in the utilization of an oxide-dispersion-strengthened alloy for small engine turbine blades
[SAE PAPER 841512] p 68 A85-39284
Unified constitutive material models for nonlinear finite-element structural analysis --- gas turbine engine blades and vanes
[AIAA PAPER 85-1418] p 142 A85-39769
Heat transfer investigation in the junction region of circular cylinder normal to a flat plate at 90 deg location
[ASME PAPER 84-WA/HT-70] p 111 A85-39898
Effect of surface configuration during solid particle impingement erosion p 69 A85-42568
Photoacoustic microscopy of ceramic turbine blades p 83 A85-43930
The effect of channel convergence on heat transfer in a passage with short pin fins
[NASA-TM-83801] p 113 N85-10303
Nonlinear structural and life analyses of a turbine blade p 19 N85-10954
Studies on the hot corrosion of a nickel-base superalloy, Udimet 700
[NASA-TM-86882] p 71 N85-11224
Preliminary results of a study of the relationship between free stream turbulence and stagnation region heat transfer
[NASA-TM-86884] p 113 N85-11317
Materials for advanced turbine engines. Project 2: Rene 150 directionally solidified superalloy turbine blades, volume 2
[NASA-CR-167993] p 23 N85-12059
Thermal-stress analysis for a wood composite blade
[NASA-CR-174794] p 159 N85-17421
Replaceable blade turbine and stationary specimen corrosion testing facility
[NASA-TM-86931] p 73 N85-18126
Nonlinear analysis for high-temperature multilayered fiber composite structures --- turbine blades
[NASA-TM-83754] p 57 N85-21273
Unified constitutive material models for nonlinear finite-element structural analysis --- gas turbine engine blades and vanes
[NASA-TM-86985] p 146 N85-24338
Cyclic structural analyses of anisotropic turbine blades for reusable space propulsion systems --- ssme fuel turbopump
[NASA-TM-86990] p 146 N85-24339
Nonlinear structural analysis for fiber-reinforced superalloy turbine blades p 147 N85-26887
Redistribution of the inlet temperature profile through the SSME fuel turbine p 50 N85-26901
Reusable rocket engine turbopump condition monitoring p 51 N85-26907
Cyclic structural analyses of SSME turbine blades p 150 N85-27963
Preliminary results of a study of the relationship between free-stream turbulence and stagnation region heat transfer p 118 N85-31435
Component-specific modeling
[NASA-CR-174925] p 32 N85-32119
Local heat-transfer measurements on a large, scale-model turbine blade airfoil using a composite of a heater element and liquid crystals
[NASA-TM-86900] p 119 N85-33435

TURBINE ENGINES

The role of modern control theory in the design of controls for aircraft turbine engines p 13 A85-13627
A generalized computer code for developing dynamic gas turbine engine models (DIGTEM) p 17 A85-49021
Chemistry of fuel deposits and sediments and their predursors
[NASA-CR-174778] p 92 N85-10209
HOST instrumentation R and D program overview p 19 N85-10957
Hot section laser anemometry p 19 N85-10962
Turbine heat transfer p 19 N85-10964
Life prediction and constitutive behavior: Overview p 20 N85-10973
Combustion system for radiation investigations p 21 N85-10986
Validation of structural analysis methods using the in-house liner cyclic rigs p 21 N85-10987
HOST liner cyclic facilities: Facility description p 22 N85-10988
Energy efficient engine. Low pressure turbine test hardware detailed design report
[NASA-CR-167956] p 22 N85-10994
Materials for advanced turbine engines. Project 2: Rene 150 directionally solidified superalloy turbine blades, volume 2
[NASA-CR-167993] p 23 N85-12059
Design description of a microprocessor based Engine Monitoring and Control unit (EMAC) for small turboshaft
[NASA-TM-86860] p 1 N85-17935
Experimental and analytical study of ceramic-coated turbine-tip shroud seals for small turbine engines
[NASA-TM-86881] p 25 N85-18057
Advanced stress analysis methods applicable to turbine engine structures
[NASA-CR-175573] p 26 N85-21165
New facility to study unsteady wake effects on turbine airfoil heat transfer p 117 N85-27948
Component-specific modeling
[NASA-CR-174925] p 32 N85-32119
Energy efficient engine, high pressure turbine thermal barrier coating. Support technology report
[NASA-CR-168037] p 34 N85-35199

TURBINE INSTRUMENTS

A real-time FORTRAN implementation of a sensor failure detection, isolation and accommodation algorithm p 171 A85-47704

TURBINE PUMPS

Application of viscous and inviscid computation methods for rocket turbopump systems
[SAE PAPER 841522] p 110 A85-39257
Reusable rocket engine turbopump condition monitoring
[SAE PAPER 841619] p 44 A85-39267
Cyclic structural analyses of anisotropic turbine blades for reusable space propulsion systems --- ssme fuel turbopump
[NASA-TM-86990] p 146 N85-24339
Preliminary results on passive eddy current damper technology for SSME turbomachinery p 132 N85-26890
Analytical study of flow phenomena in SSME turnaround duct geometries p 116 N85-26902
Reusable rocket engine turbopump condition monitoring p 51 N85-26907
SSME fuel preburner two-dimensional analysis p 51 N85-27943
Cyclic structural analyses of SSME turbine blades p 150 N85-27963

TURBINE WHEELS

Properties and microstructures for dual alloy combinations of three superalloys with alloy 901
[NASA-TM-86987] p 76 N85-26963
Unsteady heat transfer due to time-dependent free stream velocity p 117 N85-27947

TURBINES

Assessment of three-dimensional inviscid codes and loss calculations for turbine aerodynamic computations
[ASME PAPER 84-GT-187] p 4 A85-32961
The three-dimensional compressible flow in a radial inflow turbine scroll p 6 A85-41826
Energy efficient engine high pressure turbine ceramic shroud support technology report
[NASA-CR-168036] p 23 N85-10996
Fuel and oxidizer turbine loss analysis p 50 N85-26900
Combustor turbulence p 118 N85-31434
Heat transfer in aeropropulsion systems
[NASA-TM-87066] p 119 N85-31444

TURBOCOMPRESSORS

Energy efficient engine component development and integration program
[NASA-CR-170034] p 22 N85-10990
A theory of post-stall transients in multistage axial compression systems
[NASA-CR-3878] p 8 N85-21117
Simulation of multistage turbine flows p 116 N85-27945

TURBOFAN AIRCRAFT

Aerodynamic detuning analysis of an unstalled supersonic turbofan cascade
[NASA-TM-87001] p 9 N85-26670

TURBOFAN ENGINES

Identification of multivariable high-performance turbofan engine dynamics from closed-loop data p 13 A85-13630
Three-dimensional inviscid flow analysis of turbofan forced mixers
[AIAA PAPER 85-0086] p 2 A85-19510
TF34 convertible engine control system design p 15 A85-32006
Transient technique for measuring heat transfer coefficients on stator airfoils in a jet engine environment
[AIAA PAPER 85-1471] p 122 A85-39796
Stall recovery control strategy methodology and results
[AIAA PAPER 85-1433] p 16 A85-40841
The trend of future gas turbine technology p 16 A85-41778
Effect of combined pressure and temperature distortion orientation on high-bypass-ratio turbofan engine stability
[NASA-TM-83771] p 17 N85-10067
Energy efficient engine. Volume 1: Component development and integration program
[NASA-CR-173084] p 22 N85-10992
Energy efficient engine ICLS engine bearings, drives and configuration: Detail design report
[NASA-CR-167871] p 23 N85-10997
Turbofan noise generation. Volume 2: Computer programs
[NASA-CR-167952] p 175 N85-11791
Static jet noise test results of four 0.35 scale-model QCGAT mixer nozzles
[NASA-TM-86871] p 175 N85-13551
Effect of steady-state temperature distortion on inlet flow to a high-bypass-ration turbofan engine
[NASA-TM-86896] p 24 N85-15725
Performance and surge limits of a TF30-P-3 turbofan engine/axisymmetric mixed-compression inlet propulsion system at Mach 2.5
[NASA-TP-2461] p 27 N85-25261
Transient technique for measuring heat transfer coefficients on stator airfoils in a jet engine environment
[NASA-TM-87005] p 124 N85-25794
DEAN: A program for dynamic engine analysis
[NASA-TM-87033] p 30 N85-28945
Energy efficient engine component development and integration program
[NASA-CR-172846] p 31 N85-29958
Energy Efficient Engine Program technology benefit/cost study, volume 1
[NASA-CR-174766-VOL-1] p 33 N85-35197
Energy Efficient Engine Program technology benefit/cost study, volume 2
[NASA-CR-174766-VOL-2] p 33 N85-35198

TURBOFANS

Vibration and flutter of mistuned bladed-disk assemblies
[AIAA PAPER 84-0991] p 139 A85-16095
Electro-impulse de-icing of a turbofan engine inlet
[AIAA PAPER 85-1118] p 12 A85-40811
Energy efficient engine component development and integration program
[NASA-CR-170034] p 22 N85-10990
Turbofan noise generation. Volume 2: Computer programs
[NASA-CR-167952] p 175 N85-11791
Structural response of a rotating bladed disk to rotor whirl
[NASA-CR-175605] p 27 N85-22391
Energy efficient engine. Fan and quarter-stage component performance report
[NASA-CR-168070] p 33 N85-34141

TURBOGENERATORS

Conceptual design of a fixed-pitch wind turbine generator system rated at 400 kilowatts
[NASA-CR-174877] p 162 N85-29363

TURBOJET ENGINE CONTROL

Stall recovery control strategy methodology and results
[AIAA PAPER 85-1433] p 16 A85-40841

TURBOJET ENGINES

Transient technique for measuring heat transfer coefficients on stator airfoils in a jet engine environment
[AIAA PAPER 85-1471] p 122 A85-39796
The trend of future gas turbine technology p 16 A85-41778
Experimental study of ceramic coated tip seals for turbojet engines
[NASA-TM-86939] p 114 N85-19363
Transient technique for measuring heat transfer coefficients on stator airfoils in a jet engine environment
[NASA-TM-87005] p 124 N85-25794

TURBOMACHINE BLADES

Flutter of turbofan rotors with mistuned blades p 139 A85-12716
Vibration and flutter of mistuned bladed-disk assemblies
[AIAA PAPER 84-0991] p 139 A85-16095
Vibration and flutter of mistuned bladed-disk assemblies p 16 A85-45854
Vibrations of twisted cantilever plates - A comparison of theoretical results p 144 A85-47626
Model equation for simulating flows in multistage turbomachinery
[NASA-TM-86869] p 7 N85-12036
An improved computer model for prediction of axial gas turbine performance losses
[NASA-CR-174246] p 24 N85-15724
A study of internal and distributed damping for vibrating turbomachiner blades
[NASA-CR-175901] p 30 N85-27868
Unsteady heat transfer due to time-dependent free stream velocity p 117 N85-27947

Composite loads spectra for select space propulsion structural components p 148 N85-27953

TURBOMACHINERY

Computation of viscous flows in turbomachinery cascades p 106 A85-11631

Application of Runge Kutta time marching scheme for the computation of transonic flows in turbomachines [AIAA PAPER 85-1332] p 5 A85-39728

Inviscid and viscous flows in cascades with an explicit multiple-grid algorithm p 7 A85-48539

Advanced blade tip seal system, volume 2 [NASA-CR-167851] p 23 N85-10999

Model equation for simulating flows in multistage turbomachinery [NASA-TM-86869] p 7 N85-12036

Rotordynamic Instability Problems in High-Performance Turbomachinery [NASA-CP-2338] p 131 N85-14116

The use of an optical data acquisition system for bladed disk vibration analysis [NASA-TM-86891] p 144 N85-15184

Analysis of experimental shaft seal data for high-performance turbomachines, as for Space Shuttle main engines [NASA-TM-86928] p 115 N85-21569

Future directions in aeropropulsion technology [NASA-TM-87010] p 1 N85-23685

Simulation of multistage turbine flows p 116 N85-27945

TURBOPROP AIRCRAFT

Inviscid analysis of advanced turboprop propeller flow fields [AIAA PAPER 85-1263] p 6 A85-43977

Observations from varying the lift and drag inputs to a noise prediction method for supersonic helical tip speed propellers [NASA-TM-83797] p 175 N85-10788

TURBOPROP ENGINES

Large-scale advanced propfan (LAP) program progress report [AIAA PAPER 85-1187] p 17 A85-47021

Wind tunnel results of advanced high speed propellers in the takeoff, climb, and landing operating regimes [AIAA PAPER 85-1259] p 6 A85-47025

Analytical fuel property effects: Small combustors, phase 2 [NASA-CR-174848] p 93 N85-19175

Fatigue life analysis of a turboprop reduction gearbox [NASA-TM-87014] p 133 N85-27228

Wind tunnel results of advanced high speed propellers in the takeoff, climb and landing operating regimes [NASA-TM-87054] p 9 N85-29925

Large-scale Advanced Propfan (LAP) program [NASA-TM-87067] p 32 N85-29964

TURBOSHAFTS

TF34 convertible engine control system design p 15 A85-32006

Dual clearance squeeze film damper for high load conditions [ASME PAPER 84-TRIB-7] p 128 A85-32960

Temperature distortion generator for turboshaft engine testing [SAE PAPER 841541] p 15 A85-39065

Temperature distortion generator for turboshaft engine testing [NASA-TM-83748] p 1 N85-15658

TURBULENCE

The structure of dilute combusting sprays [NASA-CR-174838] p 24 N85-15728

Transition in Turbines [NASA-CP-2386] p 118 N85-31433

Preliminary results of a study of the relationship between free-stream turbulence and stagnation region heat transfer p 118 N85-31435

Flat-plate transition p 118 N85-31438

TURBULENCE METERS

Heat transfer and turbulence measurements of a film-cooled flow over a convexly curved surface p 112 A85-41787

TURBULENT BOUNDARY LAYER

An experimental study of three-dimensional shock wave/turbulent boundary layer interactions in a supersonic flow [AIAA PAPER 85-1566] p 5 A85-40691

Heat transfer and turbulence measurements of a film-cooled flow over a convexly curved surface p 112 A85-41787

Thermodynamic evaluation of transonic compressor rotors using the finite volume approach [NASA-CR-175811] p 29 N85-26712

Transition in Turbines [NASA-CP-2386] p 118 N85-31433

TURBULENT FLOW

The influence of combustion liner holes on noise production by ducted burners [AIAA PAPER 84-2322] p 172 A85-10869

Prediction of an axisymmetric combusting flow p 59 A85-12713

Computation and turbulence closure models for shear flows in rotating curved bodies p 107 A85-14349

Mass and momentum turbulent transport experiments with confined coaxial jets p 107 A85-14399

Accelerated convergence for incompressible flow calculations [AIAA PAPER 85-0058] p 2 A85-19489

Swirling flows in typical combustor geometries [AIAA PAPER 85-0184] p 108 A85-19574

Drop-turbulence interactions in a diffusion flame [AIAA PAPER 85-0319] p 60 A85-19665

Turbulence modelling for complex shear flows [AIAA PAPER 85-1652] p 111 A85-40752

Combustion efficiency of a premixed continuous flow combustor p 61 A85-42571

Jet characteristics in confined swirling flow p 112 A85-45282

Internal combustion engine combustion chamber process studies at NASA Lewis Research Center p 112 A85-45856

Measurements and predictions of the structure of evaporating sprays p 112 A85-46484

A review and analysis of boundary layer transition data for turbine application [NASA-TM-86880] p 113 N85-10306

Accelerated convergence for incompressible flow calculations [NASA-TM-86863] p 18 N85-10949

Preliminary results of a study of the relationship between free stream turbulence and stagnation region heat transfer [NASA-TM-86884] p 113 N85-11317

A three-dimensional axisymmetric calculation procedure for turbulent flows in a radial vaneless diffuser [NASA-TM-86903] p 7 N85-14798

Investigation of flowfields found in typical combustor geometries [NASA-CR-3869] p 26 N85-21167

The influence of jet-grid turbulence on heat transfer from the stagnation region of a cylinder in crossflow [NASA-TM-87011] p 115 N85-25760

Thermodynamic evaluation of transonic compressor rotors using the finite volume approach [NASA-CR-175811] p 29 N85-26712

Confined turbulent swirling recirculating flow predictions [NASA-CR-174917] p 29 N85-26716

Turbulence characteristics of swirling flowfields [NASA-CR-174918] p 29 N85-26717

Turbulent transport and length scale measurement experiments with comfined coaxial jets [NASA-CR-174831] p 117 N85-30245

Combustor turbulence p 118 N85-31434

Heat transfer and fluid mechanics measurements in transitional boundary layer flows p 118 N85-31439

A review and analysis of boundary layer transition data for turbine application p 118 N85-31440

Turbulent solutions of equations of fluid motion p 118 N85-31441

TURBULENT HEAT TRANSFER

Heat transfer enhancement in channels with turbulence promoters [ASME PAPER 84-WA/HT-72] p 111 A85-39900

TURBULENT JETS

A two-equation turbulence model for two-phase jets p 107 A85-14376

Flow visualization of lateral jet injection into swirling crossflow [AIAA PAPER 85-0059] p 2 A85-19490

Calculation of confined swirling flows [AIAA PAPER 85-0060] p 108 A85-19491

Structure of particle-laden jets - Measurements and predictions p 109 A85-25137

Structure of ducted particle-laden turbulent jets p 110 A85-38999

Turbulence measurements of lateral jet injection into confined tubular crossflow [AIAA PAPER 85-1102] p 110 A85-39604

Jet characteristics in confined swirling flow p 112 A85-45282

Deflected jet experiments in a turbulent combustor flowfield [NASA-CR-174863] p 26 N85-22390

Behavior of turbulent gas jets in an axisymmetric confinement [NASA-CR-174829] p 28 N85-25265

TURBULENT MIXING

Direct simulations of chemically reacting turbulent mixing layers [AIAA PAPER 85-0321] p 60 A85-19666

A theoretical prediction of the acoustic pressure generated by turbulence-flame front interactions [ASME PAPER 84-WA/NCA-11] p 174 A85-39909

The performance of jet noise suppression devices for industrial applications p 175 A85-42563

Behavior of turbulent gas jets in an axisymmetric confinement [NASA-CR-174829] p 28 N85-25265

TURBULENT WAKES

Development of a rotor wake-vortex model, volume 1 [NASA-CR-174849] p 9 N85-26668

New facility to study unsteady wake effects on turbine airfoil heat transfer p 117 N85-27948

TWISTING

Vibrations of twisted cantilevered plates - Summary of previous and current studies p 140 A85-22069

Natural frequencies of twisted rotating plates p 141 A85-32343

Finite difference analysis of torsional vibrations of pretwisted, rotating, cantilever beams with effects of warping p 143 A85-42047

Vibrations of twisted cantilever plates - A comparison of theoretical results p 144 A85-47626

TWO DIMENSIONAL FLOW

Resonance in flows with vortex sheets and edges p 1 A85-10357

Two-dimensional internal compressible viscous flows using semi-elliptic analysis p 106 A85-11640

The linear two-dimensional stability of inviscid vortex streets of finite-cored vortices [AD-A153032] p 107 A85-14241

Assessment of discretization schemes to reduce numerical diffusion in the calculation of complex flows [AIAA PAPER 85-0441] p 108 A85-19751

Vortex induced lift on a flat plate with a curved forward-facing flap p 4 A85-30175

Time dependent computation of the Euler equations for designing 2-D cascades, including the case of transonic shock free design p 5 A85-41814

Unsteady flow in a supersonic cascade with two in-passage shocks [NASA-CR-3925] p 10 N85-35158

TWO PHASE FLOW

A two-equation turbulence model for two-phase jets p 107 A85-14376

A stagnation pressure probe for droplet-laden air flow [AIAA PAPER 85-0330] p 108 A85-19672

Structure of particle-laden jets - Measurements and predictions p 109 A85-25137

Structure of ducted particle-laden turbulent jets p 110 A85-38999

Structure of nonevaporating sprays. I - Initial conditions and mean properties p 112 A85-48538

TWO REFLECTOR ANTENNAS

The 20 GHz proof-of-concept test model results for a multiple scan beam dual reflector antenna [NASA-CR-174268] p 98 N85-15944

TWO-WAVELENGTH LASERS

Two-frequency laser-induced fluorescence technique for rapid velocity-field measurements in gas flows p 121 A85-32294

U

UDIMET ALLOYS

The substitution of nickel for cobalt in hot isostatically pressed powder metallurgy UDIMET 700 alloys p 68 A85-37415

The response of cobalt-free Udimet 700 type alloy to modified heat treatments [NASA-TM-86942] p 75 N85-20043

ULTRASONIC RADIATION

Ultrasonic wave propagation in two-phase media - Spherical inclusions p 54 A85-11926

The scattering of ultrasonic third sound from substrate surface defects p 174 A85-36047

ULTRASONIC TESTS

Ultrasonic nondestructive evaluation, microstructure, and mechanical property interrelations [NASA-TM-86876] p 137 N85-10371

Application of homomorphic signal processing to stress wave factor analysis [NAS 1.26:174871] p 138 N85-21673

ULTRASONICS

The role of the reflection coefficient in precision measurement of ultrasonic attenuation p 137 A85-42151

Stress waves in an isotropic elastic plate excited by a circular transducer [NASA-CR-3877] p 138 N85-20390

Ultrasonic testing of plates containing edge cracks [NASA-CR-3904] p 138 N85-29307

Reliability of void detection in structural ceramics using scanning laser acoustic microscopy [NASA-TM-87035] p 138 N85-32337

UNIQUENESS THEOREM
Constructive existence and uniqueness for two-point boundary-value problems with a linear gradient term p 172 A85-28015
UNIVERSITIES
NASA Lewis Research Center/University Graduate Research Program on Engine Structures [NASA-TM-86916] p 145 N85-18375
UNSTEADY FLOW
Development of finite analytic method for unsteady three-dimensional Navier-Stokes equation p 106 A85-11647
A linearized unsteady aerodynamic analysis for transonic cascades p 3 A85-20744
Combined influence of unsteady free stream velocity and free stream turbulence on stagnation point heat transfer p 112 A85-41782
New facility to study unsteady wake effects on turbine airfoil heat transfer p 117 N85-27948
Unsteady flow in a supersonic cascade with two in-passage shocks [NASA-CR-3925] p 10 N85-35158
UPPER ATMOSPHERE
MERIT: A man/computer data management and enhancement system for upper air nowcasting/forecasting in the United States --- Minimum Energy Routes using Interactive Techniques (MERIT) p 167 N85-10558
UPPER STAGE ROCKET ENGINES
Cryogenic upper stage test bed engine [AIAA PAPER 85-1339] p 44 A85-39733
Shuttle/Centaur project perspective p 37 N85-16991
USER MANUALS (COMPUTER PROGRAMS)
Manual of phosphoric acid fuel cell power plant optimization model and computer program [NASA-CR-174721] p 157 N85-10445
Operating system for a real-time multiprocessor propulsion system simulator. User's manual [NASA-TP-2426] p 171 N85-17596
Real-Time Multiprocessor Programming Language (RTMPL) user's manual [NASA-TP-2422] p 170 N85-28610
USER REQUIREMENTS
Shuttle/Centaur project perspective p 37 N85-16991
UTILITIES
Experimental investigation of a variable speed constant frequency electric generating system from a utility perspective [NASA-CR-174950] p 105 N85-32251
UTILIZATION
Space Station propulsion - The Advanced Development Program at Lewis [AIAA PAPER 85-1154] p 44 A85-39626
Space station propulsion: The advanced development program at Lewis [NASA-TM-86999] p 50 N85-25386

V

V/STOL AIRCRAFT
Analytical study of blowing boundary layer control for subsonic V/STOL inlets p 2 A85-11646
VACUUM APPARATUS
Metal vapor arc switch electromagnetic accelerator technology [NASA-CR-174380] p 103 N85-18259
VACUUM DEPOSITION
Apparatus for producing diamond-like carbon flakes [NASA-CASE-LEW-13837-3] p 95 N85-20155
Diamondlike flakes [NASA-CASE-LEW-13837-2] p 57 N85-21267
Advances in sputtered and ion plated solid film lubrication p 136 N85-33524
VANELESS DIFFUSERS
A three-dimensional axisymmetric calculation procedure for turbulent flows in a radial vaneless diffuser [NASA-TM-86903] p 7 N85-14798
VANES
Studies on the hot corrosion of a nickel-base superalloy, Udimet 700 [NASA-TM-86882] p 71 N85-11224
Preliminary results of a study of the relationship between free stream turbulence and stagnation region heat transfer [NASA-TM-86884] p 113 N85-11317
Replaceable blade turbine and stationary specimen corrosion testing facility [NASA-TM-86931] p 73 N85-18126
Effects of vane/blade ratio and spacing on fan noise, volume 1 [NASA-CR-174664] p 176 N85-19791
Effects of vane/blade ratio and spacing on fan noise. Volume 2: Data supplement [NASA-CR-174665] p 176 N85-19792
Preliminary results of a study of the relationship between free-stream turbulence and stagnation region heat transfer p 118 N85-31435
VAPOR DEPOSITION
Magnesium doping of efficient GaAs and Ga(0.75)In(0.25)As solar cells grown by metalorganic chemical vapor deposition p 180 A85-11466
A morphological study of silicon carbide prepared by chemical vapor deposition p 79 A85-20938
Fabrication of p(+)-n junction GaAs solar cells by a novel method p 181 A85-33645
'Diamondlike' carbon films - Optical absorption, dielectric properties, and hardness dependence on deposition parameters p 82 A85-40383
Polarization (ellipsometric) measurements of liquid condensate deposition and evaporation rates and dew points in flowing salt/ash-containing combustion gases p 123 A85-46925
Creep of chemically vapor deposited SiC fibers [NASA-TM-86897] p 56 N85-14878
Environmental effects on the tensile strength of chemically vapor deposited silicon carbide fibers [NASA-TM-86981] p 89 N85-24000
Computer program for the calculation of multicomponent convective diffusion deposition rates from chemically frozen boundary layer theory [NASA-CR-168329] p 116 N85-27164
VAPOR PHASES
CREKID: A computer code for transient, gas-phase combustion of kinetics [NASA-TM-83806] p 17 N85-10068
VAPOR PRESSURE
Metal vapor arc switch electromagnetic accelerator technology [NASA-CR-174380] p 103 N85-18259
VARIATIONAL PRINCIPLES
Rational approach for assumed stress finite elements p 139 A85-12029
On Hybrid and mixed finite element methods [NASA-CR-175551] p 146 N85-23096
VARIATIONS
Probabilistic finite element: Variational theory p 149 N85-27957
VELOCITY
Digital temperature and velocity control of mach 0.3 atmospheric pressure durability testing burner rigs in long time, unattended cyclic testing [NASA-TM-86959] p 75 N85-21321
Design and lubrication of high-speed rolling-element bearings [NASA-TM-87107] p 137 N85-34409
VELOCITY DISTRIBUTION
Phase/doppler spray analyzer for simultaneous measurements of drop size and velocity distributions p 120 A85-10035
Dilution jet configurations in a reverse flow combustor [NASA-CR-174888] p 27 N85-22392
Feasibility of mapping velocity flow fields in SSME powerhead by laser anemometry techniques p 41 N85-27971
Generation of capillary instabilities by external disturbances in a liquid jet [NASA-TM-87041] p 117 N85-30246
VELOCITY MEASUREMENT
Nonintrusive optical single-particle counter for measuring the size and velocity of droplets in a spray p 120 A85-16794
Structure of particle-laden jets - Measurements and predictions p 109 A85-25137
Two-frequency laser-induced fluorescence technique for rapid velocity-field measurements in gas flows p 121 A85-32294
Hot section laser anemometry p 19 N85-10962
Dilution jet configurations in a reverse flow combustor [NASA-CR-174888] p 27 N85-22392
Velocity visualization in gaseous flows [NASA-CR-174954] p 119 N85-31445
VENTURI TUBES
A unified relation for cavitation erosion p 109 A85-24445
VERTICAL TAKEOFF AIRCRAFT
TF34 convertible engine control system design p 15 A85-32006
VERY HIGH FREQUENCIES
Alternatives for satellite sound broadcast systems at HF and VHF p 99 N85-23815
VIBRATION
Internal hysteresis experienced on a high pressure syn gas compressor p 131 N85-14122
Flow dynamic environment data base development for the SSME p 147 N85-26885
Generated spiral bevel gears: Optimal machine-tool settings and tooth contact analysis [NASA-TM-87075] p 136 N85-34405
Nonlinear flap-lag-extensional vibrations of rotating, pretwisted, preconed beams including Coriolis effects [NASA-TM-87102] p 152 N85-34427
VIBRATION DAMPING
Dual clearance squeeze film damper for high load conditions [ASME PAPER 84-TRIB-7] p 128 A85-32960
Variable friction secondary seal for face seals [NASA-CASE-LEW-14170-1] p 131 N85-20377
Preliminary results on passive eddy current damper technology for SSME turbomachinery p 132 N85-26890
A study of internal and distributed damping for vibrating turbomachiner blades [NASA-CR-175901] p 30 N85-27868
Vibration control of rotor shaft [NASA-TM-87053] p 133 N85-29292
Variable force, eddy-current or magnetic damper [NASA-CASE-LEW-13717-1] p 134 N85-30333
VIBRATION ISOLATORS
Preliminary results on passive eddy current damper technology for SSME turbomachinery p 132 N85-26890
Variable force, eddy-current or magnetic damper [NASA-CASE-LEW-13717-1] p 134 N85-30333
VIBRATION MODE
The use of an optical data acquisition system for bladed disk vibration analysis [NASA-TM-86891] p 144 N85-15184
VIBRATIONAL SPECTRA
Investigation on experimental techniques to detect, locate and quantify gear noise in helicopter transmissions [NASA-CR-3847] p 176 N85-17667
VISCOPLASTICITY
Plasticity, viscoplasticity, and creep of solids by mechanical subelement models p 142 A85-35048
Thermodynamically consistent constitutive equations for nonisothermal large strain, elasto-plastic, creep behavior [AIAA PAPER 85-0621] p 142 A85-38425
Viscoplastic constitutive relationships with dependence on thermomechanical history [NASA-CR-174836] p 146 N85-21691
On thermomechanical testing in support of constitutive equation development for high temperature alloys [NASA-CR-174879] p 147 N85-25894
Some advances in experimentation supporting development of viscoplastic constitutive models [NASA-CR-174855] p 147 N85-27260
Nonlinear Constitutive Relations for High Temperature Application, 1984 [NASA-CP-2369] p 150 N85-31530
On the use of internal state variables in thermoviscoplastic constitutive equations p 150 N85-31536
Some advances in experimentation supporting development of viscoplastic constitutive models p 151 N85-31545
VISCOSITY
A numerical study of the steady scalar convective diffusion equation for small viscosity p 107 A85-16533
External fuel vaporization study, phase 2 [NASA-CR-174079] p 92 N85-11252
Measurement and correlation of jet fuel viscosities at low temperatures [NASA-CR-174911] p 94 N85-34295
VISCOUS DAMPING
An analysis of temperature effect in a finite journal bearing with spatial tilt and viscous dissipation p 126 A85-11074
Effects of friction dampers on aerodynamically unstable rotor stages p 14 A85-21866
VISCOUS FLOW
Computation of viscous flows in turbomachinery cascades p 106 A85-11631
Comparison of secondary flows predicted by a viscous code and an inviscid code with experimental data for a turning duct p 106 A85-11634
Two-dimensional internal compressible viscous flows using semi-elliptic analysis p 106 A85-11640
Analytical modeling of circuit aerodynamics in the new NASA Lewis Altitude Wind Tunnel [AIAA PAPER 85-0380] p 3 A85-26389
Review - Computational methods for internal flows with emphasis on turbomachinery p 4 A85-29126
Computation of three-dimensional viscous flows using a space-marching method p 4 A85-29259
A note on blade wake interaction influence on compressor stator row aerodynamic performance p 4 A85-32965
Application of viscous and inviscid computation methods for rocket turbopump systems [SAE PAPER 841522] p 110 A85-39257

Calculation of three-dimensional, viscous flow through turbomachinery blade passages by parabolic marching
[AIAA PAPER 85-1408] p 5 A85-39767
Numerical calculation of subsonic jets in crossflow with reduced numerical diffusion
[AIAA PAPER 85-1441] p 110 A85-39780
A three-dimensional boundary-layer analysis including heat-transfer and blade-rotation effects
p 6 A85-42988
Application of computational fluid dynamics to complex inlet ducts
[AIAA PAPER 85-1213] p 6 A85-47023
Inviscid and viscous flows in cascades with an explicit multiple-grid algorithm p 7 A85-48539
Model equation for simulating flows in multistage turbomachinery
[NASA-TM-86869] p 7 N85-12036
Analytical modeling of circuit aerodynamics in the new NASA Lewis wind tunnel
[NASA-TM-86912] p 8 N85-15688
Calculation of three-dimensional, viscous flow through turbomachinery blade passages by parabolic marching
[NASA-TM-86984] p 9 N85-23711
Numerical calculation of subsonic jets in crossflow with reduced numerical diffusion
[NASA-TM-87003] p 27 N85-25263
Application of computational fluid dynamics to complex inlet ducts
[NASA-TM-87060] p 118 N85-30247
Elastohydrodynamic lubrication calculations used as a tool to study scuffing
[NASA-TM-87097] p 137 N85-34408

VOIDS
Reliability of void detection in structural ceramics using scanning laser acoustic microscopy
[NASA-TM-87035] p 138 N85-32337

VOLT-AMPERE CHARACTERISTICS
Environmentally-induced voltage limitations in large space power systems p 43 A85-18584
Applicability of the Meyer-Neldel rule to solar cells
p 154 A85-19948
Electrical characterization of plasma-grown oxides on gallium arsenide p 181 A85-32635
Theory of the high base resistivity n(+)pp(+) silicon solar cell and its application to radiation damage effects
p 154 A85-32639

VOLTAGE CONVERTERS (DC TO DC)
Small-signal model for the series resonant converter
p 102 A85-39453
The J3 SCR model applied to resonant converter simulation p 102 A85-42156

VOLTAGE REGULATORS
Small-signal model for the series resonant converter
p 102 A85-39453

VORTEX ALLEVIATION
Wake effects on the aerodynamic performance of horizontal axis wind turbines
[NASA-CR-174920] p 162 N85-29364

VORTEX GENERATORS
Flow control in a diffusing S-Duct
[AIAA PAPER 85-0524] p 3 A85-25928
Vortex generating flow passage design for increased film cooling effectiveness
[NASA-CASE-LEW-14039-1] p 119 N85-33433

VORTEX SHEDDING
Rotor wake characteristics of a transonic axial flow fan
[AIAA PAPER 85-1133] p 6 A85-43974

VORTEX SHEETS
Resonance in flows with vortex sheets and edges
p 1 A85-10357

VORTICES
A finite element solution of three-dimensional inviscid rotational flows through curved ducts
p 107 A85-11648
Vortex induced lift on a flat plate with a curved forward-facing flap p 4 A85-30175
Vortex modeling of single and multiple dilution jet mixing in a crossflow
[AIAA PAPER 85-1580] p 111 A85-40701
Growth of a diffusion flame in the field of a vortex
p 61 A85-47320
Vortex-generating coolant-flow-passage design for increased film-cooling effectiveness and surface coverage
[NASA-TP-2388] p 113 N85-12314
Deflected jet experiments in a turbulent combustor flowfield
[NASA-CR-174863] p 26 N85-22390
Development of a rotor wake-vortex model, volume 1
[NASA-CR-174849] p 9 N85-26668
Aerodynamic analysis of a horizontal axis wind turbine by use of helical vortex theory. Volume 1: Theory
[NASA-CR-168054] p 9 N85-29916

W

WAFERS
Lithium counterdoped silicon solar cell
[NASA-CASE-LEW-14177-1] p 160 N85-20535
Sixty GHz IMPATT diode development
[NASA-CR-174969] p 105 N85-33293

WAKES
A note on blade wake interaction influence on compressor stator row aerodynamic performance
p 4 A85-32965
Method for evaluating wind turbine wake effects on wind farm performance p 155 A85-36750
Rotor wake characteristics of a transonic axial flow fan
[AIAA PAPER 85-1133] p 6 A85-43974
Turbofan noise generation. Volume 2: Computer programs
[NASA-CR-167952] p 175 N85-11791
Electron and ion density depletions measured in the STS-3 orbiter wake p 39 N85-22474
Polar orbit electrostatic charging of objects in shuttle wake p 40 N85-22487
Ram-wake effects on plasma current collection of the PIX 2 Langmuir probe p 180 N85-22496
Wake effects on the aerodynamic performance of horizontal axis wind turbines
[NASA-CR-174920] p 162 N85-29364

WALL FLOW
A three-dimensional boundary-layer analysis including heat-transfer and blade-rotation effects
p 6 A85-42988

WALL TEMPERATURE
High temperature thermocouple and heat flux gauge using a unique thin film-hardware hot juncture
[NASA-TM-86898] p 123 N85-16096

WARNING SYSTEMS
Reusable rocket engine turbopump condition monitoring p 51 N85-26907

WARPAGE
Finite difference analysis of torsional vibrations of pretwisted, rotating, cantilever beams with effects of warping p 143 A85-42047

WASPALOY
A study of fatigue damage mechanisms in Waspaloy from 25 to 800 C p 65 A85-12098

WASTE ENERGY UTILIZATION
Overview of waste heat utilization systems
[NASA-TM-86901] p 184 N85-13692
Comparative evaluation of three alternative power cycles for waste heat recovery from the exhaust of adiabatic diesel engines
[NASA-TM-86953] p 186 N85-32043

WASTE HEAT
Comparative evaluation of three alternative power cycles for waste heat recovery from the exhaust of adiabatic diesel engines
[NASA-TM-86953] p 186 N85-32043

WATER
Mechanism for forming hydrogen chloride and sodium sulfate from sulfur trioxide, water, and sodium chloride
p 62 A85-48513
Effect of water on hydrogen permeability --- Stirling engines
[NASA-TM-86904] p 53 N85-14864
Factors influencing the ball milling of Si3N4 in water
[NASA-TM-86932] p 86 N85-19136
Parametric evaluation of ball milling of SiC in water
[NASA-TM-86974] p 88 N85-21356

WAVE ATTENUATION
The role of the reflection coefficient in precision measurement of ultrasonic attenuation
p 137 A85-42151

WAVE EQUATIONS
Reverberation effects on directionality and response of stationary monopole and dipole sources in a wind tunnel
[NASA-TM-87063] p 119 N85-31443

WAVE EXCITATION
The response of Helmholtz resonators to external excitation. I - Single resonators p 174 A85-26915

WAVE INTERACTION
Sound generation and upstream influence due to instability waves interacting with non-uniform mean flows
p 174 A85-20738

WAVE PROPAGATION
Generation of instability waves in flows separating from smooth surfaces p 1 A85-10352
Ultrasonic wave propagation in two-phase media - Spherical inclusions p 54 A85-11926
Feedback in separated flows over symmetric airfoils
[AIAA PAPER 84-2297] p 3 A85-28899
Perturbation-iteration theory for analyzing microwave striplines
[NASA-CR-176189] p 100 N85-35321

WAVE REFLECTION
Application of homomorphic signal processing to stress wave factor analysis
[NAS 1.26:174871] p 138 N85-21673

WAVEGUIDES
MMIC devices for active phased array antennas
[NASA-CR-174281] p 98 N85-15943
Design of low loss helix circuits for interference fitted and brazed circuits
[NASA-CR-168313] p 103 N85-19328
Numerical methods for analyzing electromagnetic scattering
[NASA-CR-175507] p 99 N85-21438
Analysis of the electromagnetic scattering from an inlet geometry with lossy walls
[NASA-CR-175743] p 99 N85-25686
Normal modes in an overmoded circular waveguide coated with lossy material
[NASA-CR-176186] p 100 N85-35320

WEAR
Friction and wear of some ferrous-base metallic glasses p 64 A85-11071
Mechanical-contact-induced transformation from the amorphous to the partially crystalline state in metallic glass p 65 A85-19084
Frictional and morphological properties of Au-MoS2 films sputtered from a compact target p 127 A85-19085
Polyimides - Tribological properties and their use as lubricants p 79 A85-21524
Friction, wear, transfer, and wear surface morphology of ultrahigh-molecular-weight polyethylene
p 80 A85-22276
Friction and wear of ceramics p 80 A85-23833
Ceramic wear in indentation and sliding contact
p 82 A85-39549
Lubricity of well-characterized jet and broad-cut fuels by ball-on-cylinder machine
[NASA-TM-83807] p 92 N85-12183
Effect of humidity on fretting wear of several pure metals
[NASA-TP-2403] p 72 N85-13006
Effects of silver and group 2 fluorides addition to plasma sprayed chromium carbide high temperature solid lubricant for foil gas bearing to 650 deg C
[NASA-TM-86895] p 84 N85-14928
Fundamental tribological properties of ceramics
[NASA-TM-86915] p 85 N85-15893
Surface effects of corrosive media on hardness, friction, and wear of materials
[NASA-TM-83711] p 85 N85-15896
Effect of five lubricants on life of AISI 9310 spur gears
[NASA-TP-2419] p 123 N85-16099
Ion-beam nitriding of steels
[NASA-CASE-LEW-14104-1] p 75 N85-21324
Tribological systems as applied to aircraft engines
[NASA-TM-86965] p 131 N85-21657
Sliding seal materials for adiabatic engines
[NASA-CR-174893] p 89 N85-22757
Reusable rocket engine turbopump condition monitoring p 51 N85-26907
Effects of wear on structure-sensitive magnetic properties of ceramic ferrite in contact with magnetic tape
[NASA-TM-87007] p 90 N85-26991
Effect of counterface material type and its topography on the tribological properties of polyimide composites
[NASA-TM-87036] p 90 N85-26993
Breakway friction and dynamic friction/wear measurements of various ceramic materials from 25 C (75 F) to 650 C (1200 F)
[NASA-CR-174803] p 90 N85-26994
Rolling, slip and traction measurements on low modulus materials
[NASA-CR-174909] p 135 N85-33491
Application of traction drives as servo mechanisms
p 152 N85-33520

WEAR INHIBITORS
Lubricant and additive effects on spur gear fatigue life
[NASA-TM-87044] p 133 N85-28373

WEAR TESTS
Friction and wear properties of a Charnley artificial hip joint
[ASLE PREPRINT 84-LC-4A-4] p 168 A85-38444
Lubricant and additive effects on spur gear fatigue life
[NASA-TM-87044] p 133 N85-28373
Mechanical protection of DLC films on fused silica slides
[NASA-TM-87056] p 91 N85-30138

WEATHER
Effect of precipitation on wind turbine performance
[NASA-TM-86986] p 161 N85-27385

WEATHER FORECASTING
Improved models for increasing wind penetration, economics and operating reliability
[NASA-CR-175538] p 160 N85-20545

Comparative analysis of operational forecasts versus actual weather conditions in airline flight planning, volume 1
[NASA-CR-167862] p 167 N85-35534
Comparative analysis of operational forecasts versus actual weather conditions in airline flight planning, volume 2
[NASA-CR-167863] p 167 N85-35535
Comparative analysis of operational forecasts versus actual weather conditions in airline flight planning, volume 3
[NASA-CR-167864] p 167 N85-35536
Comparative analysis of operational forecasts versus actual weather conditions in airline flight planning, volume 4
[NASA-CR-167865] p 167 N85-35537
Comparative analysis of operational forecasts versus actual weather conditions in airline flight planning: Summary report
[NASA-CR-167866] p 168 N85-35538

WEIBULL DENSITY FUNCTIONS
Reliability of two sintered silicon nitride materials
[NASA-TM-87092] p 92 N85-34284

WEIGHT (MASS)
Study of Kapton under simulated shuttle environment
[NASA-CR-176003] p 41 N85-29997

WEIGHTLESSNESS
Free-surface phenomena under low- and zero-gravity conditions
[NASA-CR-175835] p 116 N85-27168
Free-surface phenomena under low- and zero-gravity conditions
[NASA-CR-175885] p 36 N85-27922
The use of a laser Doppler velocimeter in a standard flammability tube
[NASA-CR-174960] p 125 N85-35389

WELD STRENGTH
Diffusion welding of Cassegrainian concentrator cell stack assemblies
[NASA-CR-176104] p 164 N85-33566

WELDED JOINTS
Feasibility study of the welding of SiC
p 81 A85-39339

WETTABILITY
Preliminary evaluation of a liquid belt radiator for space applications
[NASA-CR-174807] p 47 N85-15804
Contact angle and surface tension measurements of a five-ring polyphenyl ether
[NASA-TM-86927] p 86 N85-15897

WETTING
Factors influencing the ball milling of Si3N4 in water
[NASA-TM-86932] p 86 N85-19136
Mechanics of a gaseous film barrier to lubricant wetting of elastohydrodynamically lubricated conjunctions
[NASA-TP-2500] p 135 N85-32330

WHISKER COMPOSITES
Analysis of stress-strain, fracture, and ductility behavior of aluminum maxtrix composites containing discontinuous silicon carbide reinforcement p 55 A85-37421

WHISKERS (CRYSTALS)
Cone formation as a result of whisker growth on ion bombarded metal surfaces p 182 A85-41635

WIND EFFECTS
Comparative analysis of operational forecasts versus actual weather conditions in airline flight planning, volume 4
[NASA-CR-167865] p 167 N85-35537

WIND MEASUREMENT
Improved models for increasing wind penetration, economics and operating reliability
[NASA-CR-175538] p 160 N85-20545

WIND TUNNEL APPARATUS
The NASA altitude wind tunnel - Its role in advanced icing research and development
[AIAA PAPER 85-0090] p 35 A85-26381
Analytical and physical modeling program for the NASA Lewis Research Center's Altitude Wind Tunnel (AWT)
[NASA-TM-86919] p 35 N85-15757
The NASA Altitude Wind Tunnel (AWT): Its role in advanced icing research and development
[NASA-TM-86920] p 35 N85-15758

WIND TUNNEL MODELS
Analytical and physical modeling program for the NASA Lewis Research Center's Altitude Wind Tunnel (AWT)
[AIAA PAPER 85-0379] p 34 A85-19709

WIND TUNNEL TESTS
Modelling of wind tunnel wall effects on the radiation characteristics of acoustic sources
[AIAA PAPER 84-2364] p 174 A85-16104
The Altitude Wind Tunnel (AWT) - A unique facility for propulsion system and adverse weather testing
[AIAA PAPER 85-0314] p 34 A85-19661
The NASA altitude wind tunnel - Its role in advanced icing research and development
[AIAA PAPER 85-0090] p 35 A85-26381
Analytical modeling of circuit aerodynamics in the new NASA Lewis Altitude Wind Tunnel
[AIAA PAPER 85-0380] p 3 A85-26389
The UH-1H helicopter icing flight test program - An overview
[AIAA PAPER 85-0338] p 11 A85-28898
Design and performance of a fixed, nonaccelerating guide vane cascade that operates over an inlet flow angle range of 60 deg
[ASME PAPER 84-GT-75] p 4 A85-32964
Experiments in dilution jet mixing - Effects of multiple rows and non-circular orifices
[AIAA PAPER 85-1104] p 15 A85-39606
Design and wind tunnel evaluation of a symmetric airfoil series for large wind turbine applications
[NASA-CR-174764] p 7 N85-10919
Analytical modeling of circuit aerodynamics in the new NASA Lewis wind tunnel
[NASA-TM-86912] p 8 N85-15688
The UH-1H helicopter icing flight test program: An overview
[NASA-TM-86925] p 11 N85-15702
Analytical and physical modeling program for the NASA Lewis Research Center's Altitude Wind Tunnel (AWT)
[NASA-TM-86919] p 35 N85-15757
The NASA Altitude Wind Tunnel (AWT): Its role in advanced icing research and development
[NASA-TM-86920] p 35 N85-15758
The Altitude Wind Tunnel (AWT): A unique facility for propulsion system and adverse weather testing
[NASA-TM-86921] p 35 N85-18067
Further comparison of wind tunnel and airplane acoustic data for advanced design high speed propeller models
[NASA-TM-86935] p 176 N85-22108
Deflected jet experiments in a turbulent combustor flowfield
[NASA-CR-174863] p 26 N85-22390
Behavior of turbulent gas jets in an axisymmetric confinement
[NASA-CR-174829] p 28 N85-25265
Experiments in dilution jet mixing effects of multiple rows and non-circular orifices
[NASA-TM-86996] p 28 N85-25266
Reverberation effects on directionality and response of stationary monopole and dipole sources in a wind tunnel
[NASA-TM-87063] p 119 N85-31443
Reflection plane tests of a wind turbine blade tip section with ailerons
[NASA-TM-87018] p 165 N85-34444

WIND TUNNEL WALLS
Modelling of wind tunnel wall effects on the radiation characteristics of acoustic sources
[AIAA PAPER 84-2364] p 174 A85-16104
Reverberation effects on directionality and response of stationary monopole and dipole sources in a wind tunnel
[NASA-TM-87063] p 119 N85-31443

WIND TUNNELS
Analytical and physical modeling program for the NASA Lewis Research Center's Altitude Wind Tunnel (AWT)
[AIAA PAPER 85-0379] p 34 A85-19709

WIND TURBINES
Measured effects of wind turbine generation at the Block Island Power Company p 153 A85-10652
Method for evaluating wind turbine wake effects on wind farm performance p 155 A85-36750
Mod-2 wind turbine field operations experience p 157 A85-45512
Aileron controls for wind turbine applications p 157 A85-45513
Advanced multi-megawatt wind turbine design for utility application p 157 A85-45517
Design and wind tunnel evaluation of a symmetric airfoil series for large wind turbine applications
[NASA-CR-174764] p 7 N85-10919
Aileron controls for wind turbine applications
[NASA-TM-86867] p 158 N85-11458
Shutdown characteristics of the Mod-O wind turbine with aileron controls
[NASA-TM-86918] p 159 N85-16299
Improved models for increasing wind penetration, economics and operating reliability
[NASA-CR-175538] p 160 N85-20545
Development of large, horizontal-axis wind turbines
[NASA-TM-86950] p 161 N85-23242
Effect of precipitation on wind turbine performance
[NASA-TM-86986] p 161 N85-27385
Conceptual design of a fixed-pitch wind turbine generator system rated at 400 kilowatts
[NASA-CR-174877] p 162 N85-29363
Wake effects on the aerodynamic performance of horizontal axis wind turbines
[NASA-CR-174920] p 162 N85-29364
Government review of the Mod-2 wind turbine (as-built)
[NASA-TM-86983] p 162 N85-29365
Aerodynamic analysis of a horizontal axis wind turbine by use of helical vortex theory. Volume 1: Theory
[NASA-CR-168054] p 9 N85-29916
Structural analysis and cost estimate of an eight-leg space frame as a support structure for horizontal axis wind turbines
[NASA-TM-83470] p 150 N85-30361
Analytical model for predicting emergency shutdown of a two-bladed horizontal axis wind turbine
[NASA-TM-83472] p 162 N85-30476
Performance comparison between NACA 23024 and NACA 64(3)-618 airfoil configurated rotors for horizontal-axis wind turbines
[NASA-TM-83471] p 163 N85-30477
The Federal Wind Program at NASA Lewis Research Center
[NASA-TM-83480] p 163 N85-30478
Operational results for the experimental DOE/NASA Mod-OA wind turbine project
[NASA-TM-83517] p 163 N85-30479
Experimental investigation of a variable speed constant frequency electric generating system from a utility perspective
[NASA-CR-174950] p 105 N85-32251
Reflection plane tests of a wind turbine blade tip section with ailerons
[NASA-TM-87018] p 165 N85-34444

WIND VELOCITY
Comparative analysis of operational forecasts versus actual weather conditions in airline flight planning, volume 1
[NASA-CR-167862] p 167 N85-35534
Comparative analysis of operational forecasts versus actual weather conditions in airline flight planning, volume 2
[NASA-CR-167863] p 167 N85-35535
Comparative analysis of operational forecasts versus actual weather conditions in airline flight planning, volume 3
[NASA-CR-167864] p 167 N85-35536
Comparative analysis of operational forecasts versus actual weather conditions in airline flight planning, volume 4
[NASA-CR-167865] p 167 N85-35537
Comparative analysis of operational forecasts versus actual weather conditions in airline flight planning: Summary report
[NASA-CR-167866] p 168 N85-35538

WINDMILLS (WINDPOWERED MACHINES)
Government review of the Mod-2 wind turbine (as-built)
[NASA-TM-86983] p 162 N85-29365
Aerodynamic analysis of a horizontal axis wind turbine by use of helical vortex theory. Volume 1: Theory
[NASA-CR-168054] p 9 N85-29916

WINDOWS (APERTURES)
Diamondlike carbon protective coatings for IR materials
[NASA-TM-87083] p 178 N85-34631

WINDPOWER UTILIZATION
Mod-2 wind turbine field operations experience p 157 A85-45512
Aileron controls for wind turbine applications p 157 A85-45513
Aileron controls for wind turbine applications
[NASA-TM-86867] p 158 N85-11458
Improved models for increasing wind penetration, economics and operating reliability
[NASA-CR-175538] p 160 N85-20545
Government review of the Mod-2 wind turbine (as-built)
[NASA-TM-86983] p 162 N85-29365
Aerodynamic analysis of a horizontal axis wind turbine by use of helical vortex theory. Volume 1: Theory
[NASA-CR-168054] p 9 N85-29916
The Federal Wind Program at NASA Lewis Research Center
[NASA-TM-83480] p 163 N85-30478

WINDPOWERED GENERATORS
Development of large, horizontal-axis wind turbines
[NASA-TM-86950] p 161 N85-23242
Government review of the Mod-2 wind turbine (as-built)
[NASA-TM-86983] p 162 N85-29365
Structural analysis and cost estimate of an eight-leg space frame as a support structure for horizontal axis wind turbines
[NASA-TM-83470] p 150 N85-30361
The Federal Wind Program at NASA Lewis Research Center
[NASA-TM-83480] p 163 N85-30478
Operational results for the experimental DOE/NASA Mod-OA wind turbine project
[NASA-TM-83517] p 163 N85-30479

WINGS
Icing tunnel tests of Electro-Impulse De-Icing of an engine inlet and high-speed wings
[AIAA PAPER 85-0466] p 10 A85-20872
WOOD
Thermal-stress analysis for a wood composite blade
[NASA-CR-174794] p 159 N85-17421
WORKING FLUIDS
Preliminary evaluation of a liquid belt radiator for space applications
[NASA-CR-174807] p 47 N85-15804
Advanced radiator concepts
[NASA-TM-87008] p 115 N85-24245

X

X RAY ANALYSIS
Laboratory degradation of Kapton in a low energy oxygen ion beam
[AIAA PAPER 83-2658] p 78 A85-10675
XENON
Performance capabilities of the 12-centimeter Xenon ion thruster p 42 A85-16439

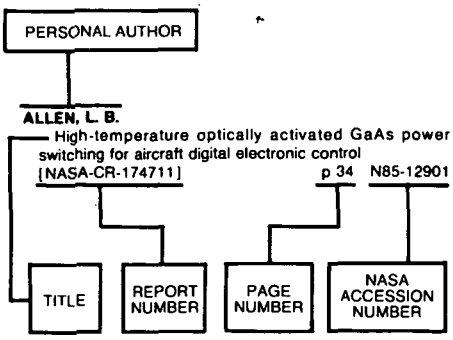
Y

YAG LASERS
Laser balancing system for high material removal rates
[NASA-CR-174731] p 126 N85-12341
YIELD
Electron yields from spacecraft materials
p 40 N85-22512
YTTERBIUM
Optimization of the NiCrAl-Y/ZrO-Y2O3 thermal barrier system
[NASA-TM-86905] p 72 N85-15878
Thermal barrier coating system
[NASA-CASE-LEW-14057-1] p 59 N85-35233
YTTRIUM
High-temperature erosion of plasma-sprayed, yttria-stabilized zirconia in a simulated turbine environment
[AIAA PAPER 85-1219] p 82 A85-39662
Dopant effect of yttrium and the growth and adherence of alumina on nickel-aluminum alloys p 82 A85-40973
High-temperature erosion of plasma-sprayed, yttria-stabilized zirconia in a simulated turbine environment
[NASA-TP-2406] p 84 N85-13045
Compatibility experiments of facilities, materials, and propellants for electrothermal thrusters
[NASA-TM-86956] p 49 N85-21260
YTTRIUM OXIDES
Progress in the utilization of an oxide-dispersion-strengthened alloy for small engine turbine blades
[SAE PAPER 841512] p 68 A85-39284
Fracture of yttria-doped, sintered reaction-bonded silicon nitride
[ACS PAPER 7-J3-84] p 82 A85-42797

Z

ZINC
AES and LEED study of the zinc blende SiC(100) surface p 61 A85-41633
Universal binding energy relations in metallic adhesion
[NASA-TM-86889] p 72 N85-12132
Humidity effects on adhesion of nickel-zinc ferrite in elastic contact with magnetic tape and itself
[NASA-TP-2449] p 88 N85-21359
ZIRCONIUM
High-temperature erosion of plasma-sprayed, yttria-stabilized zirconia in a simulated turbine environment
[AIAA PAPER 85-1219] p 82 A85-39662
Effects of cobalt, boron, and zirconium on the microstructure of Udimet 738
[NASA-CR-174762] p 70 N85-10166
High-temperature erosion of plasma-sprayed, yttria-stabilized zirconia in a simulated turbine environment
[NASA-TP-2406] p 84 N85-13045
Thermal barrier coating system
[NASA-CASE-LEW-14057-1] p 59 N85-35233
ZIRCONIUM ALLOYS
Manufacturing process to reduce large grain growth in zirconium alloys
[DE85-011649] p 78 N85-34267
ZIRCONIUM OXIDES
Separator development and testing of nickel-hydrogen cells p 156 A85-45386
An investigation of enhanced capability thermal barrier coating systems for diesel engine components
[NASA-CR-174820] p 86 N85-18154
Rocket thrust chamber thermal barrier coatings
p 90 N85-26867

Typical Personal Author Index Listing



Listings in this index are arranged alphabetically by personal author. The NASA accession number denotes the number by which the citation is identified.

A

ABBOTT, J. M.
Analytical and physical modeling program for the NASA Lewis Research Center's Altitude Wind Tunnel (AWT)
[AIAA PAPER 85-0379] p 34 A85-19709
Analytical and physical modeling program for the NASA Lewis Research Center's Altitude Wind Tunnel (AWT)
[NASA-TM-86919] p 35 N85-15757

ABOU-ARAB, T.
A two-equation turbulence model for two-phase jets
p 107 A85-14376

ABRAHAM, K. M.
Moderate temperature sodium cells. V - Discharge reactions and rechargeability of NiS and NiS2 positive electrodes in molten NaAlCl4 p 59 A85-11892

ABUELFOUTOUH, N.
Finite element analysis of notch behavior using a state variable constitutive equation p 152 N85-31548

ABUJELALA, M. T.
Confined turbulent swirling recirculating flow predictions
[NASA-CR-174917] p 29 N85-26716

ACOSTA, R. J.
Case study of sample spacing in planar near-field measurement of high gain antennas
[NASA-TM-86872] p 97 N85-10234

ACOSTA, W. A.
Experimental study of the spray characteristics of a research airblast atomizer
[NASA-TM-86911] p 24 N85-15727

ADAMCZYK, J. J.
Computational thermo-fluid dynamics contributions to advanced gas turbine engine design
[AIAA PAPER 85-0083] p 14 A85-19509
Computational thermo-fluid dynamics contributions to advanced gas turbine engine design
[NASA-TM-86865] p 18 N85-10069
Model equation for simulating flows in multistage turbomachinery
[NASA-TM-86869] p 7 N85-12036
Simulation of multistage turbine flows
p 116 N85-27945

ADLER, E.
Advanced nickel-hydrogen cell configuration study
[NASA-CR-174775] p 157 N85-10444

AFJEH, A. A.
Wake effects on the aerodynamic performance of horizontal axis wind turbines
[NASA-CR-174920] p 162 N85-29364

AGARWAL, P.
Energy efficient engine, high pressure turbine thermal barrier coating. Support technology report
[NASA-CR-168037] p 34 N85-35199

AHMED, S. A.
Jet characteristics in confined swirling flow
p 112 A85-45282
Density effects on jet characteristics in confined swirling flow p 112 A85-45283
Behavior of turbulent gas jets in an axisymmetric confinement
[NASA-CR-174829] p 28 N85-25265

AHUJA, K. K.
An experimental study of tone excited heated jets
[AIAA PAPER 84-2341] p 172 A85-10882
Some unique experiments on receptivity
[AIAA PAPER 85-0533] p 174 A85-25932
Acoustic control of free jet mixing
[AIAA PAPER 85-0569] p 109 A85-25951

AKAY, H. U.
A finite element solution of three-dimensional inviscid rotational flows through curved ducts
p 107 A85-11648

AKIN, L. S.
Into mesh lubrication of spur gears with arbitrary offset oil jet. I - For jet velocity less than or equal to gear velocity p 128 A85-24497
Lubricant jet flow phenomena in spur and helical gears with modified center distances and/or addendums - For out-of-mesh conditions
[ASME PAPER 84-DET-96] p 129 A85-35049

AL-KINANI, G.
Satellite provided customer promises services, a forecast of potential domestic demand through the year 2000. Volume 4: Sensitivity analysis
[NASA-CR-174662] p 99 N85-27092

ALIAKBARKHANAFJEH, A.
Aerodynamic analysis of a horizontal axis wind turbine by use of helical vortex theory. Volume 1: Theory
[NASA-CR-168054] p 9 N85-29916

ALKASAB, K. A.
Manual of phosphoric acid fuel cell power plant optimization model and computer program
[NASA-CR-174721] p 157 N85-10445
Manual of phosphoric acid fuel cell stack three-dimensional model and computer program
[NASA-CR-174722] p 157 N85-10447
Phosphoric acid fuel cell power plant system performance model and computer program
[NASA-CR-174638] p 157 N85-11456

ALLEN, D. H.
On the use of internal state variables in thermoviscoplastic constitutive equations
p 150 N85-31536

ALLEN, G. P.
Ribbon burner simulation of T-700 turbine shroud for ceramic lined seals research
[NASA-TM-86940] p 114 N85-19364

ALLEN, L. B.
High-temperature optically activated GaAs power switching for aircraft digital electronic control
[NASA-CR-174711] p 34 N85-12901

ALSTON, W. B.
Effect of substituted phenylnadimides on processing and properties of PMR polyimide composites
[NASA-TM-86902] p 85 N85-14929

ALTENKIRCH, R. A.
Gravitational effects on flames spreading over thick solid surfaces
[IAF PAPER 84-154] p 59 A85-13092

ALTEROVITZ, S. A.
Plasma deposited hydrogenated carbon on GaAs and InP p 182 A85-40386
Plasma deposited diamondlike carbon on GaAs and InP
[NASA-TM-86870] p 183 N85-10844
Optical properties of hydrogenated amorphous carbon films grown from methane plasma
[NASA-TM-86995] p 183 N85-26406

AMANO, R. S.
A study of Reynolds-stress closure model
[NASA-CR-174342] p 114 N85-17324

AMERI, A.
Unsteady heat transfer due to time-dependent free stream velocity p 117 N85-27947

ANAND, M. S.
Combustion efficiency of a premixed continuous flow combustor p 61 A85-42571

ANDERSON, A. B.
Dopant effect of yttrium and the growth and adherence of alumina on nickel-aluminum alloys p 82 A85-40973
Mechanism for chelated sulfate formation from SO2 and bis (triphenylphosphine) platinum p 62 A85-48493
Mechanism for forming hydrogen chloride and sodium sulfate from sulfur trioxide, water, and sodium chloride p 62 A85-48513
Why CO bonds side-on at low coverage and both side-on and upright at high coverage on the Cr(110) surface
[NASA-CR-176071] p 77 N85-32173
Molecular orbital studies in oxidation: Sulfate formation and metal-metal oxide adhesion
[NASA-CR-176070] p 77 N85-32174
Adsorption of O2, SO2, and SO3 on nickel oxide. Mechanism for sulfate formation
[NASA-CR-176072] p 77 N85-32175
CO adsorption on (111) and (100) surfaces of the Pt sub 3 Ti alloy. Evidence for parallel binding and strong activation of CO
[NASA-CR-176077] p 77 N85-32176

ANDERSON, D. N.
Flame flashback in a premixed dump combustor
[AIAA PAPER 85-0145] p 60 A85-19550

ANDERSON, G. G.
High temperature properties of equiatomic FeAl with ternary additions
[NASA-TM-86938] p 73 N85-19072

ANDERSON, L. M.
Inelastic tunnel diodes
[NASA-CASE-LEW-13833-1] p 103 N85-21492
Solar energy converter using surface plasma waves
[NASA-CASE-LEW-13827-1] p 160 N85-21768

ANDERSON, R. C.
Integrated exhaust gas analysis system for aircraft turbine engine component testing
[NASA-TP-2424] p 123 N85-16100

ANDRACCHIO, C. A.
High temperature thermocouple and heat flux gauge using a unique thin film-hardware hot juncture
[NASA-TM-86898] p 123 N85-16096

ANTOLOVICH, S. D.
A study of fatigue damage mechanisms in Waspaloy from 25 to 800 C p 65 A85-12098
The effect of microstructure, temperature, and hold-time on low-cycle fatigue of As HIP P/M Rene 95 p 67 A85-32399
A study of spectrum fatigue crack propagation in two aluminum alloys. 1: Spectrum simplification
[NASA-TM-86929] p 72 N85-18124
A study of spectrum fatigue crack propagation in two aluminum alloys. 2: Influence of microstructures
[NASA-TM-86930] p 73 N85-18125

AOKI, K.
Flow visualization of lateral jet injection into swirling crossflow
[AIAA PAPER 85-0059] p 2 A85-19490

ARCHBOLD, T.
Metallurgical and mechanical phenomena due to rubbing of titanium against sintered powder Nichrome p 127 A85-22281

ARD, K. E.
Extreme precision antenna reflector study results
p 165 N85-23830

ARGARWAL, P.
Life modeling of atmospheric and low pressure plasma-sprayed thermal-barrier coating
p 81 A85-29728

ARMSTRONG, R. S.
Detailed studies of aviation fuel flowability
[NASA-CR-174938] p 94 N85-31308
ARMSTRONG, T. P.
Numerical simulations of positively-biased probes and dielectric-conductor disks in a plasma
p 179 A85-17262
Numerical simulation of positive-potential conductors in the presence of a plasma and a secondary-emitting dielectric p 102 A85-35306
ARON, P. R.
RF-sputtered silicon and hafnium nitrides - Properties and adhesion to 440C stainless steel p 81 A85-36240
Effect of lubricant extreme-pressure additives on surface fatigue life of AISI 9310 spur gears
[NASA-TP-2408] p 130 N85-13234
ARPASI, D. J.
Hardware for a real-time multiprocessor simulator
[NASA-TM-83805] p 169 N85-10659
Real-Time Multiprocessor Programming Language (RTMPL) user's manual
[NASA-TP-2422] p 170 N85-28610
ASLANIDIS, I.
Alloys based on NiAl for high temperature applications
[NASA-TM-86976] p 75 N85-21322
ASMUSSEN, J.
Experiments with a microwave electrothermal thruster concept p 42 A85-16441
Recent work on a microwave ion source
p 179 A85-16455
Experimental performance of a microwave cavity plasma disk ion source p 179 A85-43552
ATASSI, H. M.
Feedback in separated flows over symmetric airfoils
[AIAA PAPER 84-2297] p 3 A85-28899
ATHERTON, W. J.
Investigation on experimental techniques to detect, locate and quantify gear noise in helicopter transmissions
[NASA-CR-3847] p 176 N85-17667
ATKINSON, W. H.
Development of advanced high-temperature heat flux sensors. Phase 2: Verification testing
[NASA-CR-174973] p 126 N85-35391
ATLURI, S. N.
Hybrid stress finite elements for large deformations of inelastic solids p 139 A85-15894
Development and testing of stable, invariant, *isoparametric curvilinear 2- and 3-D hybrid-stress* elements p 140 A85-19899
On the existence and stability conditions for mixed-hybrid finite element solutions based on Reissner's variational principle p 142 A85-33847
Constitutive modeling and computational implementation for finite strain plasticity
p 143 A85-40910
ATTWOOD, S. W.
Satellite baseband processor test performance summary p 95 A85-14434
AUGUST, R.
Gear mesh stiffness and load sharing in planetary gearing
[ASME PAPER 84-DET-229] p 129 A85-33781
AUSTIN, G. W.
Electric utility acid fuel cell stack technology advancement
[NASA-CR-174804] p 159 N85-17422
AVANT, R. L.
The J3 SCR model applied to resonant converter simulation p 102 A85-42156
AVELLA, A. J., JR.
Jet fuel property changes and their effect on producibility and cost in the U.S., Canada, and Europe
[NASA-CR-174840] p 93 N85-27012
AVNI, R.
Deposition of silicon nitride from SiCl4 and NH3 in a low pressure RF plasma p 81 A85-36229
Surface hardening of steel by boriding in a cold rf plasma p 68 A85-40275
Analysis of glow discharges for understanding the process of film formation
[NASA-TM-83750] p 62 N85-10138
Plasma variables and tribological properties of coatings *in low pressure (0.1 - 10.0 torr) plasma systems*
[NASA-TM-83798] p 94 N85-11261
Nitriding of titanium and its alloys by N2, NH3 or mixtures of N2 + H2 in a dc arc plasma at low pressures (or = to torr)
[NASA-TM-83803] p 131 N85-15168
AYDELOTT, J. C.
Technology requirements to be addressed by the NASA *Lewis Research Center Cryogenic Fluid Management* Facility program
[AIAA PAPER 85-1229] p 94 A85-47024
Technology requirements to be addressed by the NASA Lewis Research Center Cryogenic Fluid Management Facility program
[NASA-TM-87048] p 38 N85-29987

B

BAAKLINI, G. Y.
Radiographic detectability limits for seeded voids in sintered silicon carbide and silicon nitride
[NASA-TM-86945] p 138 N85-21674
Reliability of void detection in structural ceramics using scanning laser acoustic microscopy
[NASA-TM-87035] p 138 N85-32337
BACHALO, W. D.
Phase/doppler spray analyzer for simultaneous measurements of drop size and velocity distributions
p 120 A85-10035
BADGLEY, P. R.
Stratified charge rotary aircraft engine technology enablement program
[NASA-CR-174812] p 25 N85-21163
BADLANI, M. L.
Simplified design and life prediction of rocket thrust chambers p 44 A85-29314
BAER, J. R.
Fracture of yttria-doped, sintered reaction-bonded silicon nitride
[ACS PAPER 7-J3-84] p 82 A85-42797
BAEZ, A. N.
Design description of a microprocessor based Engine Monitoring and Control unit (EMAC) for small turboshaft
[NASA-TM-86860] p 1 N85-17935
BAGWELL, J. W.
Status of NASA's multibeam communications technology program p 100 A85-14432
BAILEY, M. M.
Overview of waste heat utilization systems
[NASA-TM-86901] p 184 N85-13692
Comparative evaluation of three alternative power cycles for waste heat recovery from the exhaust of adiabatic diesel engines
[NASA-TM-86953] p 186 N85-32043
BAILEY, R.
High temperature static strain sensor development program p 19 N85-10959
BAILEY, W. J.
Fiberglass epoxy laminate fatigue properties at 300 and 20 K p 56 A85-47970
BAK, M. J.
3-D inelastic analysis methods for hot section components (base program)
[NASA-CR-174700] p 145 N85-21686
BALDWIN, D. H.
Development of large, horizontal-axis wind turbines
[NASA-TM-86950] p 161 N85-23242
The Federal Wind Program at NASA Lewis Research Center
[NASA-TM-83480] p 163 N85-30478
BALSA, T. F.
Experimental investigation of shock-cell noise reduction for single stream nozzles in simulated flight
[NASA-CR-3845] p 175 N85-13550
BANERJEE, P. K.
3-D inelastic analysis methods for hot section components (base program)
[NASA-CR-174700] p 145 N85-21686
BANKS, B. A.
Deposition of diamondlike carbon films
[NASA-CASE-LEW-14080-1] p 95 N85-20153
Apparatus for producing diamond-like carbon flakes
[NASA-CASE-LEW-13837-3] p 95 N85-20155
Diamondlike flakes
[NASA-CASE-LEW-13837-2] p 57 N85-21267
Ion beam sputter-deposited thin film coatings for protection of spacecraft polymers in low Earth orbit
[NASA-TM-87051] p 91 N85-30137
Diamondlike carbon protective coatings for IR materials
[NASA-TM-87083] p 178 N85-34631
BARAONA, C. R.
Screen printed interdigitated back contact solar cell
[NASA-CASE-LEW-13414-1] p 160 N85-20530
BARBER, T. J.
Three-dimensional inviscid flow analysis of turbofan forced mixers
[AIAA PAPER 85-0086] p 2 A85-19510
BAREFOOT, J. R.
Modeling of gamma/gamma-prime phase equilibrium in the nickel-aluminum system p 65 A85-14959
BARGER, M. J.
Sixty GHz IMPATT diode development
[NASA-CR-174969] p 105 N85-33293
BARIS, J.
Preparation and evaluation of advanced catalysts for phosphoric acid fuel cells
[NASA-CR-168223] p 160 N85-19511
BARKHOUDARIAN, S.
Reusable rocket engine turbopump condition monitoring p 51 N85-26907
BARRANGER, J. P.
Eddy current jet engine disk-crack monitor
p 120 A85-11100
BARRETT, C. A.
The effects of seven alloying elements on the microstructure and stress-rupture behavior of nickle-base superalloys
[NASA-TM-83791] p 70 N85-10168
The effects of Cr, Co, Al, Mo and Ta on the cyclic oxidation behavior of a prototype cast Ni-base superalloy based on a 2(5) composite statistically designed experiment
[NASA-TM-83784] p 71 N85-12131
A multiple linear regression analysis of hot corrosion attack on a series of nickel base turbine alloys
[NASA-TM-87020] p 77 N85-31284
BARTH, R. L.
Temperature distortion generator for turboshaft engine testing
[SAE PAPER 841541] p 15 A85-39065
Temperature distortion generator for turboshaft engine testing
[NASA-TM-83748] p 1 N85-15658
BARTOLOTTA, P. A.
Viscoplastic constitutive relationships with dependence *on thermomechanical history*
[NASA-CR-174836] p 146 N85-21691
BARTON, J. M.
Inviscid analysis of advanced turboprop propeller flow *fields*
[AIAA PAPER 85-1263] p 6 A85-43977
BASHIR, S.
The effect of microstructure, temperature, and hold-time *on low-cycle fatigue of As HIP P/M Rene 95*
p 67 A85-32399
BASSETT, D. E.
The design and analysis of single flank transmission *error testor for loaded gears*
[NASA-CR-176163] p 136 N85-34404
BASU, S. N.
Analysis techniques for tracer studies of oxidation
[NASA-CR-174796] p 84 N85-12162
BAUMEISTER, K. J.
Time dependent wave envelope finite difference analysis of sound propagation
[AIAA PAPER 84-2285] p 173 A85-16102
Modelling of wind tunnel wall effects on the radiation characteristics of acoustic sources
[AIAA PAPER 84-2364] p 174 A85-16104
Reverberation effects on directionality and response of stationary monopole and dipole sources in a wind tunnel
[NASA-TM-87063] p 119 N85-31443
BEACH, R. F.
Advanced secondary power system for transport aircraft
[NASA-TP-2463] p 30 N85-28944
BEATTIE, J. R.
IAPS (8-cm) ion thruster cyclic endurance test
p 42 A85-16406
Ring-cusp ion thrusters p 42 A85-16438
Ion thruster system (8-cm) cyclic endurance test
[NASA-CR-174745] p 47 N85-12937
Extended performance technology study 30-cm thruster
[NASA-CR-168259] p 48 N85-15806
BEATTY, T. G.
Progress in the utilization of an oxide-dispersion-strengthened alloy for small engine turbine blades
[SAE PAPER 841512] p 68 A85-39284
BEEK, J. M.
On the use of internal state variables in thermoviscoplastic constitutive equations
p 150 N85-31536
BEHEIM, G.
Remote displacement measurements using a laser diode p 121 A85-24464
Remote displacement measurement using a passive *interferometer with a fiber-optic link* p 122 A85-42857
BEHLKE, R. F.
Study of controlled diffusion stator blading
[NASA-CR-167995] p 25 N85-18058
BEITLER, R. S.
Energy Efficient Engine (E3) controls and accessories detail design report
[NASA-CR-168017] p 31 N85-29957
BELYTSCHKO, T.
Probabilistic finite element: Variational theory
p 149 N85-27957

BENKO, E.
Sixty GHz IMPATT diode development
[NASA-CR-174969] p 105 N85-33293
BENNETT, J. C.
Mass and momentum turbulent transport experiments with confined coaxial jets p 107 A85-14399
BENTS, D. J.
Report of the Constellations Panel
p 131 N85-20368
Tethered nuclear power for the Space Station
[NASA-TM-87023] p 51 N85-26912
BERAK, J. M.
High-temperature optically activated GaAs power switching for aircraft digital electronic control
[NASA-CR-174711] p 34 N85-12901
BERGAMASUI, S.
Report of the Constellations Panel
p 131 N85-20368
BERGERON, R. P.
Vehicle/engine integration p 37 N85-17008
BERKE, L.
Structural optimization using optimality criteria methods p 144 A85-48703
BERNDT, C. C.
Performance of thermal barrier coatings in high heat flux environments p 79 A85-19087
Mechanical property measurements of plasma-sprayed thermal-barrier coatings subjected to oxidation
p 81 A85-29729
Failure during thermal cycling of plasma-sprayed thermal barrier coatings p 81 A85-36246
BERTHOLD, J. W.
High-temperature fiber optic pressure sensor
p 123 A85-46607
BEVILACQUA, F.
Report of the Constellations Panel
p 131 N85-20368
BEYERLE, R. A.
Combustion gas properties. Part 3: Hydrogen gas fuel and dry air
[NASA-TP-2477] p 32 N85-31058
BHASIN, K. B.
Effect of Interfacial characteristics of metal clad polymeric substrates on electrical high frequency interconnection performance
[NASA-TM-86948] p 99 N85-20223
An experimental investigation of microstrip properties on soft substrates from 2 to 40 GHz
[NASA-TM-86961] p 99 N85-20224
BHAT, K. N.
Electrical characterization of plasma-grown oxides on gallium arsenide p 181 A85-32635
BHAT, M. K.
Flow control in a diffusing S-Duct
[AIAA PAPER 85-0524] p 3 A85-25928
BHATT, R. T.
Environmental effects on the tensile strength of chemically vapor deposited silicon carbide fibers
[NASA-TM-86981] p 89 N85-24000
Mechanical properties of SiC fiber-reinforced reaction-bonded Si3N4 composites
[NASA-TM-87085] p 59 N85-34223
BHATTACHARYYA, S.
Creep-rupture behavior of iron superalloys in high-pressure hydrogen
[NASA-CR-174411] p 74 N85-19078
BHUSHAN, C.
Satellite provided customer promises services, a forecast of potential domestic demand through the year 2000. Volume 4: Sensitivity analysis
[NASA-CR-174662] p 99 N85-27092
BIESIADNY, T. J.
Temperature distortion generator for turboshaft engine testing
[SAE PAPER 841541] p 15 A85-39065
Temperature distortion generator for turboshaft engine testing
[NASA-TM-83748] p 1 N85-15658
Experimental and analytical study of ceramic-coated turbine-tip shroud seals for small turbine engines
[NASA-TM-86881] p 25 N85-18057
Experimental study of ceramic coated tip seals for turbojet engines
[NASA-TM-86939] p 114 N85-19363
BIFANO, W. J.
Status of DOE and AID stand-alone photovoltaic system field tests p 155 A85-35707
BILL, R. C.
Low cycle fatigue of MAR-M 200 single crystals at 760 and 870 deg C
[NASA-TM-86933] p 74 N85-19074
Multiaxial and thermomechanical fatigue considerations in damage tolerant design
[NASA-TM-87022] p 76 N85-26964
BIRCHENALL, C. E.
New eutectic alloys and their heats of transformation
p 66 A85-27808
BIRCHENOUGH, A. G.
Government review of the Mod-2 wind turbine (as-built)
[NASA-TM-86983] p 162 N85-29365
Operational results for the experimental DOE/NASA Mod-OA wind turbine project
[NASA-TM-83517] p 163 N85-30479
Reflection plane tests of a wind turbine blade tip section with ailerons
[NASA-TM-87018] p 165 N85-34444
BISSET, J. W.
Energy efficient engine flight propulsion system preliminary analysis and design report
[NASA-CR-174701] p 18 N85-10947
Energy efficient engine integrated core/low spool test hardware design report
[NASA-CR-168137] p 31 N85-29956
BITTKER, D. A.
Liquid phase products and solid deposit formation from thermally stressed model jet fuels
[NASA-TM-86874] p 92 N85-13066
BIZON, P. T.
Interaction of high-cycle and low-cycle fatigue of Haynes 188 alloy at 1400 F deg p 149 N85-27961
BLACK, J. D.
Fatigue life analysis of a turboprop reduction gearbox
[NASA-TM-87014] p 133 N85-27228
BLACK, J. F.
High-temperature optically activated GaAs power switching for aircraft digital electronic control
[NASA-CR-174711] p 34 N85-12901
BLAHA, B. J.
The NASA altitude wind tunnel - Its role in advanced icing research and development
[AIAA PAPER 85-0090] p 35 A85-26381
The NASA Altitude Wind Tunnel (AWT): Its role in advanced icing research and development
[NASA-TM-86920] p 35 N85-15758
BLECH, R. A.
Hardware for a real-time multiprocessor simulator
[NASA-TM-83805] p 169 N85-10659
BLOZY, J. T.
Altitude testing of a flight weight, self-cooled, 2D thrust vectoring exhaust nozzle
[SAE PAPER 841557] p 14 A85-25984
BLUMBERG, P. N.
Methods for heat transfer and temperature field analysis of the insulated diesel
[NASA-CR-174783] p 185 N85-16699
BOBER, L. J.
Inviscid analysis of advanced turboprop propeller flow fields
[AIAA PAPER 85-1263] p 6 A85-43977
BODNER, S. R.
A survey of unified constitutive theories
p 150 N85-31531
BOES, D. J.
Breakway friction and dynamic friction/wear measurements of various ceramic materials from 25 C (75 F) to 650 C (1200 F)
[NASA-CR-174803] p 90 N85-26994
BOISVERT, R. F.
Convective influence on the stability of a cylindrical solid-liquid interface p 109 A85-26911
BOLDMAN, D. R.
Unsteady pressure measurements on a biconvex airfoil in a transonic oscillating cascade
[NASA-TM-86914] p 8 N85-15689
BOOMAN, R. A.
Velocity visualization in gas flows using laser-induced phosphorescence of biacetyl p 121 A85-21695
BOPSE, S.
Electric utility acid fuel cell stack technology advancement
[NASA-CR-174804] p 159 N85-17422
BORDER, D. A.
An allpass filter design for luminance and chrominance separation of NTSC signals p 102 A85-28230
BORREGO, J. M.
Electrical characterization of plasma-grown oxides on gallium arsenide p 181 A85-32635
Heat treatment of bulk gallium arsenide using a phosphosilicate glass cap p 181 A85-32636
Fabrication of p(+)-n junction GaAs solar cells by a novel method p 181 A85-33645
Research on gallium arsenide diffused junction solar cells
[NASA-CR-174057] p 158 N85-11457
BOWEN, R. R.
Development and use of the computer software package for planning the 12 GHz broadcasting-satellite service at RARC '83 p 96 A85-29605
BOWLES, K. J.
Fundamental studies of composite toughness
p 56 N85-12948
Graphite/PMR polyimide composites with improved toughness
[NASA-TM-87081] p 58 N85-32148
BOWYER, J.
Satellite provided customer promises services, a forecast of potential domestic demand through the year 2000. Volume 4: Sensitivity analysis
[NASA-CR-174662] p 99 N85-27092
BOYCE, D. A.
Fiberglass epoxy laminate fatigue properties at 300 and 20 K p 56 A85-47970
BOYD, L. S.
Multi-mesh gear dynamics program evaluation and enhancements
[NASA-CR-174747] p 133 N85-28372
BOYLE, R. J.
Predicted turbine stage performance using quasi-three-dimensional and boundary-layer analyses
p 15 A85-34013
BOZZOLA, R.
Application of Runge Kutta time marching scheme for the computation of transonic flows in turbomachines
[AIAA PAPER 85-1332] p 5 A85-39728
BRABBS, T. A.
Fuel rich catalytic comustion: The first stage of a two-stage combustor
[NASA-TM-87042] p 63 N85-28983
Fuel-rich catalytic combustion: A soot-free technique for in situ hydrogen-like enrichment
[NASA-TP-2498] p 63 N85-31244
Shock tube measurements of growth constants in the branched-chain ethane-carbon monoxide-oxygen system
[NASA-TM-87068] p 64 N85-32156
BRAGG, M. B.
Predicting rime ice accretion on airfoils
p 3 A85-25135
BRANDHORST, H. W., JR.
Photovoltaics - The endless spring
p 154 A85-35602
The NASA photovoltaic technology program
p 155 A85-35604
Lithium counterdoped silicon solar cell
[NASA-CASE-LEW-14177-1] p 160 N85-20535
The effects of lithium counterdoping on radiation damage and annealing in n(+)p silicon solar cells
p 50 N85-22586
BRANDON, S. T.
Numerical simulations of positively-biased probes and dielectric-conductor disks in a plasma
p 179 A85-17262
BRAUN, M. J.
An analysis of temperature effect in a finite journal bearing with spatial tilt and viscous dissipation
p 126 A85-11074
Plastic flow of plasma sprayed ceramics
p 80 A85-24161
Analysis of experimental shaft seal data for high-performance turbomachines, as for Space Shuttle main engines
[NASA-TM-86928] p 115 N85-21569
Nested subcritical flows within supercritical systems
[NASA-TM-86980] p 115 N85-21574
BRAUN, W. H.
Unsteady flow in a supersonic cascade with two in-passage shocks
[NASA-CR-3925] p 10 N85-35158
BRAUSCH, J. F.
Experimental investigation of shock-cell noise reduction for dual-stream nozzles in simulated flight
[NASA-CR-3846] p 175 N85-13549
Experimental investigation of shock-cell noise reduction for single stream nozzles in simulated flight
[NASA-CR-3845] p 175 N85-13550
BREAULT, R. D.
Electric utility acid fuel cell stack technology advancement
[NASA-CR-174804] p 159 N85-17422
BRENNAN, S. M.
Space station propulsion options
[AIAA PAPER 85-1155] p 45 A85-43975
BREWE, D.
Hydrodynamic lubrication of rigid nonconformal contacts in combined rolling and normal motion
[ASME PAPER 84-TRIB-13] p 127 A85-21280
BREWER, G. D.
Study of advanced fuel system concepts for commercial aircraft and engines
[NASA-CR-174752] p 93 N85-19176
BRIGHAM, B. A.
The effect of channel convergence on heat transfer in a passage with short pin fins
[NASA-TM-83801] p 113 N85-10303

BRIKMANIS, C. K.
Life and reliability modeling of bevel gear reductions
[NASA-TM-87006] p 133 N85-27227
BRINKER, D. J.
GaAs and 3-5 compound solar cells status and prospects for use in space
[NASA-TM-86960] p 49 N85-21261
GaAs and 3-5 compound solar cells status and prospects for use in space p 49 N85-22580
BROKAW, R. S.
Shock tube measurements of growth constants in the branched-chain ethane-carbon monoxide-oxygen system
[NASA-TM-87068] p 64 N85-32156
BROMAN, C. L.
Energy efficient engine ICLS engine bearings, drives and configuration: Detail design report
[NASA-CR-167871] p 23 N85-10997
BROOK, J. W.
The computation of viscid/inviscid interaction on airfoils with separated flow p 6 A85-42954
BROOKY, J. D.
Study of controlled diffusion stator blading
[NASA-CR-167995] p 25 N85-18058
BROWN, J. R.
Vehicle/engine integration p 37 N85-17008
Design and analysis report for the RL10-2B breadboard low thrust engine
[NASA-CR-174857] p 48 N85-19020
BROWN, K. E.
Development and use of the computer software package for planning the 12 GHz broadcasting-satellite service at RARC '83 *p 96 A85-29605*
BROWN, K. W.
Finite element engine blade structural optimization
[AIAA PAPER 85-0645] p 141 A85-30313
BROWN, W. F., JR.
Fracture toughness of hot-pressed beryllium p 66 A85-25835
BROWN, W. H.
Acoustic control of free jet mixing
[AIAA PAPER 85-0569] p 109 A85-25951
BUCKLEY, D. H.
Friction and wear of some ferrous-base metallic glasses p 64 A85-11071
Spherical microglass particle impingement studies of thermoplastic materials at normal incidence p 79 A85-11072
Cavitation erosion size scale effects p 65 A85-11935
Deformation and erosion of f.c.c. metals and alloys under cavitation attack p 65 A85-12789
Mechanical-contact-induced transformation from the amorphous to the partially crystalline state in metallic glass p 65 A85-19084
Friction and wear of ceramics p 80 A85-23833
A unified relation for cavitation erosion p 109 A85-24445
Properties of coated and modified surfaces p 53 A85-36694
Ceramic wear in indentation and sliding contact p 82 A85-39549
Surface hardening of steel by boriding in a cold rf plasma p 68 A85-40275
Ceramic microstructure and adhesion p 82 A85-40384
Effect of surface configuration during solid particle impingement erosion p 69 A85-42568
Characterization of solid particle erosion resistance of ductile metals based on their properties p 69 A85-42569
Ceramic microstructure and adhesion
[NASA-TM-83804] *p 83 N85-10186*
Effect of humidity on fretting wear of several pure metals
[NASA-TP-2403] p 72 N85-13006
Effect of barrier height on friction behavior of the semiconductors silicon and gallium arsenide in contact with pure metals
[NASA-TP-2405] *p 84 N85-13044*
Fundamental tribological properties of ceramics
[NASA-TM-86915] p 85 N85-15893
Surface effects of corrosive media on hardness, friction, and wear of materials
[NASA-TM-83711] p 85 N85-15896
Characterization of erosion of metallic materials under cavitation attack in a mineral oil
[NASA-TM-86934] p 74 N85-19075
Tribological properties of boron nitride synthesized by ion beam deposition
[NASA-TM-86962] p 87 N85-21355
Humidity effects on adhesion of nickel-zinc ferrite in elastic contact with magnetic tape and itself
[NASA-TP-2449] *p 88 N85-21359*
Tribological systems as applied to aircraft engines
[NASA-TM-86965] p 131 N85-21657
Effects of wear on structure-sensitive magnetic properties of ceramic ferrite in contact with magnetic tape
[NASA-TM-87007] p 90 N85-26991
BUDDHAVARAPU, J.
Heat transfer and fluid mechanics measurements in transitional boundary layer flows p 118 N85-31439
BUFFUM, D. H.
Unsteady pressure measurements on a biconvex airfoil *in a transonic oscillating cascade*
[NASA-TM-86914] p 8 N85-15689
BUGGELE, A. E.
Unsteady pressure measurements on a biconvex airfoil in a transonic oscillating cascade
[NASA-TM-86914] p 8 N85-15689
BUI, T. D.
Recent advances in methods for numerical solution of O.D.E. initial value problems p 171 A85-21370
BUNDAS, D. J.
Flutter and forced response of mistuned rotors using standing wave analysis p 139 A85-12721
BURCAT, A.
High temperature oxidation of propene p 61 *A85-33570*
Ideal gas thermodynamic properties for the phenyl, phenoxy, and o-biphenyl radicals
[NASA-TM-83800] p 184 N85-22204
BURCHAM, R. E.
Analysis of experimental shaft seal data for high-performance turbomachines, as for Space Shuttle *main engines*
[NASA-TM-86928] p 115 N85-21569
BURGESS, R. M.
Small centrifugal pumps for low thrust rockets
[AIAA PAPER 85-1302] p 45 A85-43978
BURNSIDE, O. H.
Probabilistic structural analysis theory development p 148 *N85-27955*
BURTON, R. L.
Investigation of a pulsed electrothermal thruster system
[NASA-CR-174768] p 46 N85-11132
BUTTRILL, S. E., JR.
Chemistry of fuel deposits and sediments and their *predursors*
[NASA-CR-174778] p 92 N85-10209
BUZZARD, R. J.
Experimental compliance calibration of the NASA Lewis Research Center Mode 2 fatigue specimen
[NASA-TM-86908] p 144 N85-16205
BYERS, W. D.
Study of advanced fuel system concepts for commercial aircraft and engines
[NASA-CR-174752] p 93 N85-19176

C

CALCO, F. S.
Precision tunable resonant microwave cavity
[NASA-CASE-LEW-13935-1] p 103 N85-20248
CALFO, F. D.
Replaceable blade turbine and stationary specimen corrosion testing facility
[NASA-TM-86931] p 73 N85-18126
CALVERT, W.
DE-1 measurements of AKR wave directions p 166 A85-37717
CAMPBELL, D. P.
Infrared technology for satellite power conversion
[NASA-CR-174266] p 159 N85-16293
Technology for satellite power conversion
[NASA-CR-174335] p 159 N85-18451
CAMPBELL, N. K.
Reflection plane tests of a wind turbine blade tip section with ailerons
[NASA-TM-87018] p 165 N85-34444
CANAL, E.
Study of controlled diffusion stator blading
[NASA-CR-167995] p 25 N85-18058
CARLSON, R. G.
Energy efficient engine high pressure turbine ceramic shroud support technology report
[NASA-CR-168036] p 23 N85-10996
CARLSON, R. L.
Thermodynamically consistent constitutive equations for nonisothermal large strain, elasto-plastic, creep behavior
[AIAA PAPER 85-0621] p 142 A85-38425
Analysis of shell type structures subjected to time dependent mechanical and thermal loading
[NASA-CR-175747] p 147 N85-25896
Dynamic creep buckling: Analysis of shell structures subjected to time-dependent mechanical and thermal loading p 149 N85-27959
CARMI, U.
Deposition of silicon nitride from SiCl4 and NH3 in a *low pressure RF plasma* p 81 A85-36229
CAROL, L. A.
Cyclic oxidation behavior of beta+gamma overlay coatings on gamma and gamma+gamma-prime alloys p 68 A85-32431
A study of interdiffusion in beta + gamma/gamma + gamma prime Ni-Cr-Al
[NASA-CR-174852] p 74 N85-20041
CARROLL, D. R.
Satellite baseband processor test performance summary p 95 A85-14434
CARRUTHERS, W. D.
Ceramic component development for the AGT101 gas turbine engine p 126 A85-15972
CASASENT, D.
Optical linear algebra processors - Noise and error-source modeling p 169 A85-36727
CASE, S. K.
Holographic optical system for aberration corrections in laser Doppler velocimetry p 123 A85-48659
CASPAR, J. R.
A linearized unsteady aerodynamic analysis for transonic cascades p 3 A85-20744
CASSADY, P. L.
Initial feasibility ground test of a proposed photogrammetric system for measuring the shapes of ice accretions on helicopter rotor blades during forward flight
[NASA-TM-87391] p 12 N85-12887
CATALDO, R. L.
Design of a 1-kWh bipolar nickel hydrogen battery p 155 A85-45384
Life cycle test results of a bipolar nickel hydrogen battery
[NASA-TM-87046] p 163 N85-30480
Life cycle test results of a bipolar nickel hydrogen battery p 105 N85-31406
CAULEY, M. A.
The subjective effect of multiple co-channel frequency modulated television interference p 96 A85-28234
CAULFIELD, H. J.
An approach for automated analysis of particle holograms p 120 A85-10034
CAVICCHI, R. H.
Design and performance of a fixed, nonaccelerating guide vane cascade that operates over an inlet flow angle range of 60 deg
[ASME PAPER 84-GT-75] p 4 A85-32964
CAWLEY, J. D.
Tape casting as an approach to an all-ceramic turbine shroud seal
[NASA-TM-87078] p 135 N85-32333
Oxidizing seal for a turbine tip gas path
[NASA-CASE-LEW-14053-1] p 136 N85-34402
CELESTINA, M. L.
Simulation of multistage turbine flows p 116 N85-27945
CHAI, A. T.
Screen printed interdigitated back contact solar cell
[NASA-CASE-LEW-13414-1] p 160 N85-20530
CHAMBERLIN, R.
Comparison of scaled model data to full size energy efficient engine test results
[AIAA PAPER 84-2281] p 13 A85-13953
Measurement and prediction of Energy Efficient Engine noise
[AIAA PAPER 84-2284] p 13 A85-13954
The Altitude Wind Tunnel (AWT) - A unique facility for propulsion system and adverse weather testing
[AIAA PAPER 85-0314] *p 34 A85-19661*
The Altitude Wind Tunnel (AWT): A unique facility for propulsion system and adverse weather testing
[NASA-TM-86921] p 35 N85-18067
CHAMIS, C. C.
Hygrothermomechanical evaluation of transverse filament tape epoxy/polyester fiberglass composites p 54 A85-15632
Design procedures for fiber composite structural components - Rods, beams, and beam columns p 54 A85-15636
Select fiber composites for space applications - A mechanistic assessment p 54 A85-16040
ICAN - Integrated composites analyzer
[AIAA PAPER 84-0974] *p 54 A85-16094*
Interply layer degradation effects on composite structural response
[AIAA PAPER 84-0849] p 54 A85-16096
Finite element engine blade structural optimization
[AIAA PAPER 85-0645] p 141 A85-30313
Resin selection criteria for 'tough' composite structures p 81 A85-35139
Interply layer degradation effects on composite structural response p 55 A85-39215

A study of interply layer effects on the free edge stress field of angleplied laminates p 55 A85-41127
Impact resistance of fiber composites Energy-absorbing mechanisms and environmental effects p 56 A85-46543
The 3-D inelastic analysis methods for hot section components: Brief description p 20 N85-10972
Fabrication and quality assurance processes for superhybrid composite fan blades [NASA-TM-83354] p 57 N85-14882
A study of interply layer effects on the free-edge stress field of angleplied laminates [NASA-TM-86924] p 57 N85-15822
Design procedures for fiber composite structural components: Panels subjected to combined in-plane loads [NASA-TM-86909] p 57 N85-15823
NASA Lewis Research Center/University Graduate Research Program on Engine Structures [NASA-TM-86916] p 145 N85-18375
Nonlinear structural analysis for fiber-reinforced superalloy turbine blades p 147 N85-26887
Overview of structural response: Probabilistic structural analysis p 148 N85-27952
Designing for fiber composite structural durability in hygrothermomechanical environment [NASA-TM-87045] p 58 N85-27978

CHAN, K. S.
A survey of unified constitutive theories p 150 N85-31531

CHANG, B. J.
Engineering model system study for a regenerative fuel cell: Study report [NASA-CR-174801] p 158 N85-16292

CHANG, H. H.
Electrocatalysis of fuel cell reactions: Investigation of alternate electrolytes [NASA-CR-174753] p 157 N85-11455

CHANG, J. P.
On numerical integration and computer implementation of viscoplastic models p 151 N85-31542

CHANG, S. H.
A computer aided design procedure for generating gear teeth [ASME PAPER 84-DET-184] p 128 A85-33779

CHANG, T. Y.
On numerical integration and computer implementation of viscoplastic models p 151 N85-31542

CHAPMAN, R.
Measurements of energy distribution in microwave plasmas of N2 and He and comparisons with results for H2 p 178 A85-16443

CHEN, B. K.
Computer program for the calculation of multicomponent convective diffusion deposition rates from chemically frozen boundary layer theory [NASA-CR-168329] p 116 N85-27164

CHEN, C. C.
Advanced 30/20 GHz multiple beam antenna for future communications satellites p 96 A85-14436

CHEN, C.-J.
Development of finite analytic method for unsteady three-dimensional Navier-Stokes equation p 106 A85-11647

CHEN, D. Y.
Bipolar-FET combinational power transistors for power conversion applications p 100 A85-12669

CHEN, H.-C.
Development of finite analytic method for unsteady three-dimensional Navier-Stokes equation p 106 A85-11647

CHEN, J.
Sixty GHz IMPATT diode development [NASA-CR-174969] p 105 N85-33293

CHERRY, D. G.
Energy efficient engine. Low pressure turbine test hardware detailed design report [NASA-CR-167956] p 22 N85-10994

CHIAPPETTA, L.
External fuel vaporization study, phase 2 [NASA-CR-174079] p 92 N85-11252

CHIAPPETTA, L. M.
Finite difference methods for reducing numerical diffusion in TEACH-type calculations [AIAA PAPER 85-0057] p 108 A85-19488
Error reduction program [NASA-CR-174776] p 172 N85-27584

CHILDS, M. E.
An experimental study of three-dimensional shock wave/turbulent boundary layer interactions in a supersonic flow [AIAA PAPER 85-1566] p 5 A85-40691

CHIMA, R. C.
Efficient solution of the Euler and Navier-Stokes equations with a vectorized multiple-grid algorithm p 2 A85-18679

CHIMA, R. V.
Application of viscous and inviscid computation methods for rocket turbopump systems [SAE PAPER 841522] p 110 A85-39257
Inviscid and viscous flows in cascades with an explicit multiple-grid algorithm p 7 A85-48539

CHIN, D. T.
Electrocatalysis of fuel cell reactions: Investigation of alternate electrolytes [NASA-CR-174753] p 157 N85-11455

CHIN, S. A.
Bipolar-FET combinational power transistors for power conversion applications p 100 A85-12669

CHIRIVELLA, J.
Study of advanced fuel system concepts for commercial aircraft and engines [NASA-CR-174752] p 93 N85-19176

CHOE, S. J.
The influence of hold times on LCF and FCG behavior in a P/M Ni-base superalloy p 67 A85-32400

CHOI, S. R.
An experimental investigation and numerical prediction of thermomechanical phenomena in high speed rotor tip rubbing p 14 A85-25442

CHOU, J. H.
An experimental study of three-dimensional shock wave/turbulent boundary layer interactions in a supersonic flow [AIAA PAPER 85-1566] p 5 A85-40691

CHOUINARD, G.
Experimental results supporting the determination of service quality objectives for DBS systems p 96 A85-29611

CHUANG, S. L.
Plot of modal field distribution in rectangular and circular waveguides p 101 A85-25170
Numerical methods for analyzing electromagnetic scattering [NASA-CR-175507] p 99 N85-21438
Normal modes in an overmoded circular waveguide coated with lossy material [NASA-CR-176186] p 100 N85-35320

CHUBB, D. L.
Thermionic photovoltaic energy converter [NASA-CASE-LEW-14077-1] p 164 N85-34441

CHUDNOVSKY, A.
Statistics and thermodynamics of fracture p 140 A85-19433
Translational and extensional energy release rates (the J- and M-integrals) for a crack layer in thermoelasticity [NASA-CR-174872] p 145 N85-21685

CHUNANG, C. D.
Analysis of the electromagnetic scattering from an inlet geometry with lossy walls [NASA-CR-175743] p 99 N85-25686

CHUNG, B. T. F.
Plastic flow of plasma sprayed ceramics p 80 A85-24161

CIANCONE, M. L.
Flow visualization study of the effect of injection hole geometry on an inclined jet in crossflow [NASA-TM-86936] p 115 N85-20269

CLARK, R. W.
Calculation of compressible flow about three-dimensional inlets with auxiliary inlets, slats and vanes by means of a panel method [AIAA PAPER 85-1196] p 5 A85-40817
Calculation of compressible flow about three-dimensional inlets with auxiliary inlets, slats and vanes by means of a panel method [NASA-CR-174975] p 10 N85-35162

CLARY, D. W.
Transferring data oscilloscope to an IBM using an Apple II+ p 168 A85-24526
Shock tube study of the fuel structure effects on the chemical kinetic mechanisms responsible for soot formation, part 2 [NASA-CR-174880] p 63 N85-25444

CLAUS, R. W.
Accelerated convergence for incompressible flow calculations [AIAA PAPER 85-0058] p 2 A85-19489
Flame radiation and linear heat transfer in a tubular-can combustor p 15 A85-39580
Numerical calculation of subsonic jets in crossflow with reduced numerical diffusion [AIAA PAPER 85-1441] p 110 A85-39780
Accelerated convergence for incompressible flow calculations [NASA-TM-86863] p 18 N85-10949
Reducing numerical diffusion for incompressible flow calculations [NASA-TM-83621] p 24 N85-14840
Combustion research for gas turbine engines [NASA-TM-86963] p 26 N85-21164
Numerical calculation of subsonic jets in crossflow with reduced numerical diffusion [NASA-TM-87003] p 27 N85-25263

CLEAVELAND, B.
Configuration study for a 30 GHz monolithic receive array: Technical assessment [NASA-CR-174697] p 98 N85-18238
Configuration study for a 30 GHz monolithic receive array, volume 1 [NASA-CR-174697-VOL-1] p 98 N85-18239
Configuration study for a 30 GHz monolithic receive array, volume 2 [NASA-CR-174697-VOL-2] p 99 N85-18240

CLEMONS, J. M.
Preparation of silicon carbide-silicon nitride fibers by the pyrolysis of polycarbosilazane precursors [NASA-TM-86505] p 91 N85-28107

CLINE, S. J.
High pressure compressor component performance report [NASA-CR-168245] p 33 N85-34138
Energy efficient engine. Fan and quarter-stage component performance report [NASA-CR-168070] p 33 N85-34141

CLOSE, D. A.
Apparatus and method for identification of matrix materials in which transuranic elements are embedded using thermal neutron capture gamma-ray emission [DE85-011659] p 125 N85-33454

CLYMER, B.
Optical computer switching network p 178 A85-23134

CO, C. M.
Fundamentals of microcrack nucleation mechanics [NASA-CR-3851] p 137 N85-16195

COE, H. H.
Lubrication and performance of high-speed rolling-element bearings [NASA-TM-86958] p 131 N85-21658
Effect of speed and press fit on fatigue life of roller-bearing inner-race contact [NASA-TP-2496] p 134 N85-31511

COFFINBERRY, G. A.
Study of advanced fuel system concepts for commercial aircraft [NASA-CR-174751] p 12 N85-19978

COHEN, S.
Large-scale Advanced Propfan (LAP) performance, acoustic and weight estimation, January, 1984 [NASA-CR-174782] p 9 N85-22368

COLE, G. L.
Operating system for a real-time multiprocessor propulsion system simulator. User's manual [NASA-TP-2426] p 171 N85-17596

COLEMAN, E. B.
Experiments in dilution jet mixing - Effects of multiple rows and non-circular orifices [AIAA PAPER 85-1104] p 15 A85-39606
Experiments in dilution jet mixing effects of multiple rows and non-circular orifices [NASA-TM-86996] p 28 N85-25266

COLES, D.
Free-surface phenomena under low- and zero-gravity conditions [NASA-CR-175835] p 116 N85-27168

COLLIER, J. P.
Effects of cobalt on the hot workability of nickel-base superalloys p 67 A85-32412

COLLIN, R. E.
Circular waveguide bifurcation for asymmetric modes p 101 A85-20170
Dual-mode coaxial feed with low crosspolarisation p 101 A85-20171

COLLINS, S. A., JR.
Optical computer switching network p 178 A85-23134

COLLINS, W. R.
The use of Ada in distributed simulations p 169 A85-28612
Moving target, distributed, real-time simulation using Ada p 170 A85-34131

CONGDON, J. V.
Electric utility acid fuel cell stack technology advancement [NASA-CR-174804] p 159 N85-17422

CONLON, R. J.
Preliminary analysis of space mission applications for electromagnetic launchers [NASA-CR-174067] p 35 N85-12071

CONNOLLY, D. J.
An experimental investigation of microstrip properties on soft substrates from 2 to 40 GHz [NASA-TM-86961] p 99 N85-20224

COOK, C. R.
Energy efficient engine. Volume 2. Appendix A: Component development and integration program
[NASA-CR-173085] p 22 N85-10991
COOK, T. S.
Considerations for damage analysis of gas turbine hot section components
[ASME PAPER 84-PVP-77] p 14 A85-18792
COOKE, D. L.
Three-dimensional calculation of shuttle charging in polar orbit p 40 N85-22486
Polar orbit electrostatic charging of objects in shuttle wake p 40 N85-22487
COOPER, L. P.
OTV propulsion tecnology programmatic overview p 37 N85-16997
Vehicle/engine integration p 37 N85-17008
Manrating orbital transfer vehicle propulsion
[NASA-TM-87019] p 50 N85-25385
Status of advanced orbital transfer propulsion
[NASA-TM-87069] p 52 N85-35225
CORIELL, S. R.
Convective influence on the stability of a cylindrical solid-liquid interface p 109 A85-26911
CORNELL, C. C.
Experimental aerodynamic characteristics of an NACA *0012 airfoil with simulated ice* p 12 *A85-21844*
CORNILSEN, B. C.
Raman structural studies of the nickel electrode
[NASA-CR-175619] p 183 N85-23414
CORREA, S. M.
Prediction of an axisymmetric combusting flow p 59 A85-12713
CORRIGAN, R. D.
Shutdown characteristics of the Mod-O wind turbine with aileron controls
[NASA-TM-86918] p 159 N85-16299
Effect of precipitation on wind turbine performance
[NASA-TM-86986] p 161 N85-27385
Performance comparison between NACA 23024 and NACA 64(3)-618 airfoil configurated rotors for horizontal-axis wind turbines
[NASA-TM-83471] p 163 N85-30477
COSTI, T.
Improved models for increasing wind penetration, economics and operating reliability
[NASA-CR-175538] p 160 N85-20545
COY, J. J.
A computer aided design procedure for generating gear teeth
[ASME PAPER 84-DET-184] p 128 A85-33779
Dynamic analysis of straight and involute tooth forms
[ASME PAPER 84-DET-226] p 128 A85-33780
Transmission efficiency measurements and correlations with physical characteristics of the lubricant p 89 N85-23781
Life and reliability modeling of bevel gear reductions
[NASA-TM-87006] p 133 N85-27227
Fatigue life analysis of a turboprop reduction gearbox
[NASA-TM-87014] p 133 N85-27228
Spiral bevel and circular arc helical gears: Tooth contact analysis and the effect of misalignment on circular arc helical gears
[NASA-TM-87013] p 32 N85-31060
Generated spiral bevel gears: Optimal machine-tool settings and tooth contact analysis
[NASA-TM-87075] p 136 N85-34405
COYKENDALL, R. D.
Electric utility acid fuel cell stack technology advancement
[NASA-CR-174804] p 159 N85-17422
CRAWLEY, E. F.
Structural response of a rotating bladed disk to rotor whirl
[NASA-CR-175605] p 27 N85-22391
CRIMP, M. A.
Rapidly solidified NiAl and FeAl
[NASA-TM-86941] p 74 N85-20042
CROSLEY, P. B.
Fracture of composite-adhesive-composite systems p 141 A85-27935
CROSS, E. J., JR.
Experimental aerodynamic characteristics of an NACA 0012 airfoil with simulated ice p 12 A85-21844
CULL, R.
Control algorithms and computer simulation of a stand-alone photovoltaic village power system p 153 A85-11345
CULLER, J. E.
Control algorithms and computer simulation of a stand-alone photovoltaic village power system p 153 A85-11345
Control aspects of the Schuchuli Village stand-alone photovoltaic power system
[NASA-TM-83790] p 103 N85-13157
CUNNINGHAM, A. R.
Jet fuel property changes and their effect on producibility and cost in the U.S., Canada, and Europe
[NASA-CR-174840] p 93 N85-27012
CUNNINGHAM, R. E.
Preliminary results on passive eddy current damper technology for SSME turbomachinery p 132 N85-26890
Variable force, eddy-current or magnetic damper
[NASA-CASE-LEW-13717-1] p 134 N85-30333
CURRAN, F. M.
Hollow cathodes in high pressure arc discharges
[NASA-TM-87098] p 52 N85-34179
CURREN, A. N.
Textured carbon surfaces on copper
[NASA-CASE-LEW-14130-1] p 95 N85-20156
CURTIS, H.
Near-optimum design of GaAs-based concentrator space solar cells for 80 C operation p 153 A85-15800
CURTIS, H. B.
Effects of 1 MeV electrons and 10 MeV protons on the performance and reflectance of thin BSR cells p 182 A85-35699
CUSANO, C.
The influence of temperature on the lubricating *effectiveness of MoS2 dispersed in mineral oils*
[ASLE PREPRINT 84-LC-2A-2] p 80 A85-25963
CYR, M. A.
Development of advanced high-temperature heat flux sensors. Phase 2: Verification testing
[NASA-CR-174973] p 126 N85-35391

D

DADONE, L.
Performance degradation of helicopter rotor in forward flight due to ice p 11 A85-42937
DAHL, M. D.
The performance of jet noise suppression devices for industrial applications p 175 A85-42563
Measured acoustic properties of variable and low density bulk absorbers
[NASA-TM-87065] p 177 N85-30770
DAME, L. T.
Finite element analysis of notch behavior using a state variable constitutive equation p 152 N85-31548
DANIEL, S. R.
Jet fuel instability mechanisms
[NASA-CR-175856] p 93 N85-28127
DANIELE, C. J.
A generalized computer code for developing dynamic gas turbine engine models (DIGTEM) p 17 A85-49021
DANIELS, J. G.
Preparation of silicon carbide-silicon nitride fibers by the pyrolysis of polycarbosilazane precursors
[NASA-TM-86505] p 91 N85-28107
DAUDET, H. C.
Advanced technology cogeneration system conceptual design study: Closed cycle gas turbines
[NASA-CR-168222] p 159 N85-16300
DAVIS, R. E.
GASP cloud encounter statistics - Implications for laminar flow control flight p 166 A85-11979
Variability of cloudiness at airline cruise altitudes from GASP measurements p 166 A85-31199
DAVIS, R. H.
Contingency power concepts for helicopter turboshaft engine p 15 A85-32005
DAYAN, M.
AES and LEED study of the zinc blende SiC(100) surface p 61 A85-41633
DEADMORE, D. L.
Digital temperature and velocity control of mach 0.3 atmospheric pressure durability testing burner rigs in long time, unattended cyclic testing
[NASA-TM-86959] p 75 N85-21321
DEBOER, G. J.
Materials for advanced turbine engines. Project 2: Rene 150 directionally solidified superalloy turbine blades, volume 2
[NASA-CR-167993] p 23 N85-12059
DECKER, A. J.
A comparison of electronic heterodyne moire deflectometry and electronic heterodyne holographic *interferometry for flow measurements*
[NASA-TM-87071] p 125 N85-32302
DECKERT, J. C.
A design methodology for robust failure detection and isolation p 171 A85-47794
DEGAETANO, E.
Cryogenic upper stage test bed engine
[AIAA PAPER 85-1339] p 44 A85-39733
DEIDRICH, J. H.
Analytical and physical modeling program for the NASA Lewis Research Center's Altitude Wind Tunnel (AWT)
[NASA-TM-86919] p 35 N85-15757
DEISSLER, R. G.
Turbulent solutions of equations of fluid motion p 118 N85-31441
DELAAT, J. C.
A real-time FORTRAN implementation of a sensor failure detection, isolation and accommodation algorithm p 171 A85-47704
DELOMBARD, R.
Control algorithms and computer simulation of a stand-alone photovoltaic village power system p 153 A85-11345
Status of DOE and AID stand-alone photovoltaic system field tests p 155 A85-35707
Control aspects of the Schuchuli Village stand-alone photovoltaic power system
[NASA-TM-83790] p 103 N85-13157
DEMIGLIO, R. D.
Effect of precipitation on wind turbine performance
[NASA-TM-86986] p 161 N85-27385
DENGLER, R. P.
Advanced secondary power system for transport aircraft
[NASA-TP-2463] p 30 N85-28944
DEUTSCH, S.
The boundary layer on compressor cascade blades
[NASA-CR-174369] p 114 N85-18292
DIAMOND, W. A.
Analysis of experimental shaft seal data for high-performance turbomachines, as for Space Shuttle main engines
[NASA-TM-86928] p 115 N85-21569
DICARLO, J. A.
High temperature metal and ceramic composites p 55 A85-37483
Fibers for structurally reliable metal and ceramic composites p 55 A85-37484
High performance fibers for structurally reliable metal and ceramic composites
[NASA-TM-86878] p 56 N85-12095
Creep of chemically vapor deposited SiC fibers
[NASA-TM-86897] p 56 N85-14878
DIEDRICH, J. H.
Analytical and physical modeling program for the NASA Lewis Research Center's Altitude Wind Tunnel (AWT)
[AIAA PAPER 85-0379] p 34 A85-19709
DIEM-KIRSOP, P. S.
Advanced radiator concepts
[NASA-TM-87008] p 115 N85-24245
DIRUSSO, E.
Variable friction secondary seal for face seals
[NASA-CASE-LEW-14170-1] p 131 N85-20377
DITTMAR, J. H.
Observations from varying the lift and drag inputs to a noise prediction method for supersonic helical tip speed propellers
[NASA-TM-83797] p 175 N85-10788
Further comparison of wind tunnel and airplane acoustic data for advanced design high speed propeller models
[NASA-TM-86935] p 176 N85-22108
DIVERGILIO, W. F.
High frequency plasma generator for ion thrusters
[NASA-CR-174772] p 48 N85-17023
DOCHAT, G.
Free-piston Stirling engine/linear alternator 1000-hour endurance test
[NASA-CR-174771] p 163 N85-30481
DOLAN, F. X.
An experimental investigation of rubbing interaction in labyrinth seals at cryogenic temperature p 129 A85-39938
Analytical and experimental investigation of rubbing interaction in labyrinth seals for a liquid hydrogen fuel pump
[NASA-CR-174657] p 48 N85-18084
DOWNEY, A. N.
An experimental investigation of microstrip properties on soft substrates from 2 to 40 GHz
[NASA-TM-86961] p 99 N85-20224
DOYCHAK, J. K.
The transient oxidation of single crystal NiAl+Zr
[NASA-CR-174756] p 70 N85-11221
DRESHFIELD, R. L.
PM superalloys - A troubled adolescent? p 69 A85-44772
Effects of tin on microstructure and mechanical behavior of Inconel 718
[NASA-TM-86866] p 71 N85-12129
DUBIEL, D. J.
Energy efficient engine combustor test hardware detailed design report
[NASA-CR-167945] p 18 N85-10950

DUDERSTADT, E. C.
Life modeling of atmospheric and low pressure plasma-sprayed thermal-barrier coating p 81 A85-29728
Energy efficient engine, high pressure turbine thermal barrier coating. Support technology report [NASA-CR-168037] p 34 N85-35199
DUGUNDJI, J.
Flutter and forced response of mistuned rotors using standing wave analysis p 139 A85-12721
DUKE, J. C., JR.
A study of the stress wave factor technique for the characterization of composite materials [NASA-CR-174870] p 58 N85-30035
DULGEROFF, C. R.
IAPS (8-cm) ion thruster cyclic endurance test p 42 A85-16406
Ion thruster system (8-cm) cyclic endurance test [NASA-CR-174745] p 47 N85-12937
DUNBAR, W. G.
High voltage requirements and issues for the 1990's p 46 A85-45429
DUQUETTE, D. J.
The influence of hold times on LCF and FCG behavior in a P/M Ni-base superalloy p 67 A85-32400
DURBIN, P. A.
Resonance in flows with vortex sheets and edges p 1 A85-10357
Approximate analysis for resonance of an incompressible shear layer plus edges p 107 A85-19377
Flow through very porous inclined screens [AIAA PAPER 85-1650] p 111 A85-40750
Flow through very porous inclined screens [NASA-TM-86979] p 116 N85-25761
DUSTIN, M. O.
Solar dynamic systems p 164 N85-31374
DYBBS, A.
A new interpretation of internal heat transfer coefficients of porous media [ASME PAPER 84-WA/HT-51] p 110 A85-39894

E

EARHART, R. W.
Preliminary analysis of space mission applications for electromagnetic launchers [NASA-CR-174067] p 35 N85-12071
EBERT, L. J.
Elevated temperature creep-rupture behavior of the single crystal nickel-base superalloy NASAIR 100 p 66 A85-27812
Influence of composition on the microstructure and mechanical properties of a nickel-base superalloy single crystal p 66 A85-32387
Factors which influence directional coarsening of gamma-prime during creep in nickel-base superalloy single crystals p 67 A85-32388
EBIHARA, B. T.
Apparatus for mounting a field emission cathode [NASA-CASE-LEW-14108-1] p 104 N85-29149
Multistage spent particle collector and a method for making same [NASA-CASE-LEW-13914-1] p 135 N85-33489
ECER, A.
A finite element solution of three-dimensional inviscid rotational flows through curved ducts p 107 A85-11648
ECK, T. G.
Study of Kapton under simulated shuttle environment [NASA-CR-176003] p 41 N85-29997
EDWARD, B.
Configuration study for a 30 GHz monolithic receive array: Technical assessment [NASA-CR-174697] p 98 N85-18238
Configuration study for a 30 GHz monolithic receive array, volume 1 [NASA-CR-174697-VOL-1] p 98 N85-18239
Configuration study for a 30 GHz monolithic receive array, volume 2 [NASA-CR-174697-VOL-2] p 99 N85-18240
EHRESMAN, C. M.
A stagnation pressure probe for droplet-laden air flow [AIAA PAPER 85-0330] p 108 A85-19672
ELGHOBASHI, S.
A two-equation turbulence model for two-phase jets p 107 A85-14376
ELLIOT, J. E.
Moderate temperature sodium cells. V - Discharge reactions and rechargeability of NiS and NiS2 positive electrodes in molten NaAlCl4 p 59 A85-11892
ELLIS, J. R.
Some advances in experimentation supporting development of viscoplastic constitutive models [NASA-CR-174855] p 147 N85-27260
Some advances in experimentation supporting development of viscoplastic constitutive models p 151 N85-31545
Results of an interlaboratory fatigue test program conducted on alloy 800H at room and elevated temperatures [NASA-CR-174940] p 152 N85-32340
EMERY, A. F.
Metallurgical and mechanical phenomena due to rubbing of titanium against sintered powder Nichrome p 127 A85-22281
An experimental investigation and numerical prediction of thermomechanical phenomena in high speed rotor tip rubbing p 14 A85-25442
ENGLISH, R. E.
Dynamic power systems for power generation p 158 N85-13892
Preliminary assessment of power-generating tethers in space and of propulsion for their orbit maintenance p 37 N85-22520
ENGLUND, D. R.
The infinite line pressure probe p 122 A85-37704
Thin-film sensors for space propulsion technology p 41 N85-27968
ENOCH, J.
Numerical simulations of positively-biased probes and dielectric-conductor disks in a plasma p 179 A85-17262
ENSWORTH, C. B. F.
Analytical model for predicting emergency shutdown of a two-bladed horizontal axis wind turbine [NASA-TM-83472] p 162 N85-30476
Performance comparison between NACA 23024 and NACA 64(3)-618 airfoil configurated rotors for horizontal-axis wind turbines [NASA-TM-83471] p 163 N85-30477
ENVIA, E.
Noise produced by the interaction of a rotor wake with a swept stator blade [AIAA PAPER 84-2326] p 173 A85-13956
EPSTEIN, A.
Rotor wake characteristics of a transonic axial flow fan [AIAA PAPER 85-1133] p 6 A85-43974
ERCEGOVAC, M. D.
A functional language approach in high-speed digital simulation p 170 A85-28615
General approaches for achieving high speed computations p 169 A85-28628
Functional language and data flow architectures p 170 A85-28629
ERCEGOVIC, B. A.
Flat-plate transition p 118 N85-31438
ERNST, W. D.
Mod II engine and technology development p 129 A85-45473
ESKRIDGE, R. R.
Energy efficient engine ICLS Nacelle detail design report [NASA-CR-167870] p 22 N85-10993
ESPINOSA, V. E.
Spray characterization with a nonintrusive technique using absolute scattered light p 120 A85-10036
Research study of droplet sizing technology leading to the development of an advanced droplet sizing system [NASA-CR-174839] p 123 N85-21604
ETEMAD, S.
Metallurgical and mechanical phenomena due to rubbing of titanium against sintered powder Nichrome p 127 A85-22281
An experimental investigation and numerical prediction of thermomechanical phenomena in high speed rotor tip rubbing p 14 A85-25442
ETERNO, J. S.
A design methodology for robust failure detection and isolation p 171 A85-47794
EVANS, D. J.
Hot isostatically pressed manufacture of high strength MERL 76 disk and seal shapes [NASA-CR-165550] p 71 N85-11225
EVANS, J. C., JR.
High-voltage solar-cell chip p 154 A85-24668
EVERSMAN, W.
Modelling of wind tunnel wall effects on the radiation characteristics of acoustic sources [AIAA PAPER 84-2364] p 174 A85-16104
EWASHINKA, J. G.
Results of electric-vehicle propulsion system performance on three lead-acid battery systems p 156 A85-45443
EYSSA, Y. M.
A rotating superconducting solenoid for 100 kWh energy storage p 44 A85-33144

F

FADDOUL, J. R.
Ten year environmental test of glass fiber/epoxy pressure vessels [AIAA PAPER 85-1198] p 56 A85-47022
Ten year environmental test of glass fiber/epoxy pressure vessels [NASA-TM-87058] p 58 N85-30034
FAETH, F. M.
The structure of dilute combusting sprays [NASA-CR-174838] p 24 N85-15728
FAETH, G. M.
Drop-turbulence interactions in a diffusion flame [AIAA PAPER 85-0319] p 60 A85-19665
Structure of particle-laden jets - Measurements and predictions p 109 A85-25137
Structure of ducted particle-laden turbulent jets p 110 A85-38999
Measurements and predictions of the structure of evaporating sprays p 112 A85-46484
Structure of nonevaporating sprays. I - Initial conditions and mean properties p 112 A85-48538
FAIRBANKS, N. P.
Advanced blade tip seal system, volume 2 [NASA-CR-167851] p 23 N85-10999
FANG, Q. T.
Convective influence on the stability of a cylindrical solid-liquid interface p 109 A85-26911
FARKAS, D.
New eutectic alloys and their heats of transformation p 66 A85-27808
FARR, E.
Characterization of MMIC devices for active array antennas [NASA-TM-86907] p 38 N85-15779
FAYMON, K. A.
High voltage requirements and issues for the 1990's p 46 A85-45429
FEATHERSTON, C. D.
Jet fuel property changes and their effect on producibility and cost in the U.S., Canada, and Europe [NASA-CR-174840] p 93 N85-27012
FEINGOLD, E.
Transformation toughened ceramics for the heavy duty diesel engine technology program [NASA-CR-174689] p 185 N85-16698
FELDMAN, U.
Characterization of microstrip discontinuities in the time and frequency domains [NASA-CR-176190] p 106 N85-35342
FENG, Z.
A rotating superconducting solenoid for 100 kWh energy storage p 44 A85-33144
FERET, J. M.
Gas cooled fuel cell systems technology development [NASA-CR-174732] p 158 N85-16291
FERGUSON, B. L.
Powder metallurgy forged gear development [NASA-TM-87483] p 134 N85-29295
FERGUSON, D. C.
Laboratory degradation of Kapton in a low energy oxygen ion beam [AIAA PAPER 83-2658] p 78 A85-10675
Laboratory studies of Kapton degradation in an oxygen ion beam p 177 N85-22477
Ram-wake effects on plasma current collection of the PIX 2 Langmuir probe p 180 N85-22496
FERGUSON, T. V.
Feasibility of mapping velocity flow fields in SSME powerhead by laser anemometry techniques p 41 N85-27971
FERRANTE, J.
Universal binding energy relations in metallic adhesion [NASA-TM-86889] p 72 N85-12132
FERRELL, G. B.
Flow visualization of lateral jet injection into swirling crossflow [AIAA PAPER 85-0059] p 2 A85-19490
Turbulence measurements of lateral jet injection into confined tubular crossflow [AIAA PAPER 85-1102] p 110 A85-39604
Deflected jet experiments in a turbulent combustor flowfield [NASA-CR-174863] p 26 N85-22390
FESLER, W.
High pressure compressor component performance report [NASA-CR-168245] p 33 N85-34138
FEYOCK, S.
The use of Ada in distributed simulations p 169 A85-28612
Moving target, distributed, real-time simulation using Ada p 170 A85-34131

FIELD, R. D.
Rapid solidification and dynamic compaction of Ni-base superalloy powders p 67 A85-32414
FIELDER, W. L.
Reactions of NaCl with gaseous SO3, SO2, and O2 p 59 A85-11897
Oxidation and hot corrosion of hot-pressed Si3N4 at 1000 deg C
[NASA-TM-86977] p 88 N85-21358
FILPUS, J. W.
The energetics of hydrogen atom recombination - Analysis, experiments, and modeling p 179 A85-16444
FINBERG, I.
Surface hardening of steel by boriding in a cold rf plasma p 68 A85-40275
FINNEGAN, P. M.
Preliminary assessment of power-generating tethers in space and of propulsion for their orbit maintenance p 37 N85-22520
FITZGERALD, K.
Preliminary evaluation of a liquid belt radiator for space applications
[NASA-CR-174807] p 47 N85-15804
FLANAGAN, P. M.
Investigation on experimental techniques to detect, locate and quantify gear noise in helicopter transmissions
[NASA-CR-3847] p 176 N85-17667
FLEETER, S.
The effect of aerodynamic and structural detuning on turbomachine supersonic unstalled torsional flutter
[AIAA PAPER 85-0761] p 14 A85-30378
Aerodynamic detuning analysis of an unstalled supersonic turbofan cascade
[NASA-TM-87001] p 9 N85-26670
FLEMING, D. P.
Dual clearance squeeze film damper for high load conditions
[ASME PAPER 84-TRIB-7] p 128 A85-32960
Experimental stiffness of tapered bore seals
[NASA-TM-86978] p 132 N85-25847
Dual clearance squeeze film damper
[NASA-CASE-LEW-13506-1] p 135 N85-33490
FLOOD, D. J.
GaAs and 3-5 compound solar cells status and prospects for use in space
[NASA-TM-86960] p 49 N85-21261
GaAs and 3-5 compound solar cells status and prospects for use in space p 49 N85-22580
High efficiency solar cell research for space applications p 164 N85-31624
FLORENCE, D. E.
Vehicle/engine integration p 37 N85-17008
FLYNN, E. M.
The use of a laser Doppler velocimeter in a standard flammability tube
[NASA-CR-174960] p 125 N85-35389
FOGG, H. W.
Study of advanced fuel system concepts for commercial aircraft and engines
[NASA-CR-174752] p 93 N85-19176
FORD, C. W.
Magnesium doping of efficient GaAs and Ga(0.75)In(0.25)As solar cells grown by metalorganic chemical vapor deposition p 180 A85-11466
FORDYCE, J. S.
Missions/planning panel p 36 N85-13886
FORMAN, R.
Apparatus for mounting a field emission cathode
[NASA-CASE-LEW-14108-1] p 104 N85-29149
FORT, E. F.
Methods for heat transfer and temperature field analysis of the insulated diesel
[NASA-CR-174783] p 185 N85-16699
FOSNIGHT, V. V.
High frequency plasma generator for ion thrusters
[NASA-CR-174772] p 48 N85-17023
FOSS, J. F.
Development of a temperature measurement system with application to a jet in a cross flow experiment
[NASA-CR-174896] p 27 N85-25262
FOUST, R. R.
Design and analysis report for the RL10-2B breadboard low thrust engine
[NASA-CR-174857] p 48 N85-19020
FRANK, L. A.
Suprathermal plasma observed on STS-3 Mission by plasma diagnostics package p 179 N85-22472
FRANKS, L. A.
Apparatus and method for identification of matrix materials in which transuranic elements are embedded using thermal neutron capture gamma-ray emission
[DE85-011659] p 125 N85-33454
FRASER, H. L.
Rapid solidification and dynamic compaction of Ni-base superalloy powders p 67 A85-32414
FREDERICK, G. R.
Structural analysis and cost estimate of an eight-leg space frame as a support structure for horizontal axis wind turbines
[NASA-TM-83470] p 150 N85-30361
FREEDMAN, M. R.
Milling of Si3N4 with Si3N4 hardware
[NASA-TM-86864] p 84 N85-10191
Factors influencing the ball milling of Si3N4 in water
[NASA-TM-86932] p 86 N85-19136
Parametric evaluation of ball milling of SiC in water
[NASA-TM-86974] p 88 N85-21356
FREEDMAN, R. J.
Initial feasibility ground test of a proposed photogrammetric system for measuring the shapes of ice accretions on helicopter rotor blades during forward flight
[NASA-TM-87391] p 12 N85-12887
FRENKLACH, M.
Systematic optimization of a detailed kinetic model using a methane ignition example p 59 A85-12890
Shock tube study of the fuel structure effects on the chemical kinetic mechanisms responsible for soot formation, part 2
[NASA-CR-174880] p 63 N85-25444
FRENKLACH, M. Y.
Transferring data oscilloscope to an IBM using an Apple II+ p 168 A85-24526
FRIEDMAN, D. M.
Calculation of compressible flow about three-dimensional inlets with auxiliary inlets, slats and vanes by means of a panel method
[AIAA PAPER 85-1196] p 5 A85-40817
Calculation of compressible flow about three-dimensional inlets with auxiliary inlets, slats and vanes by means of a panel method
[NASA-CR-174975] p 10 N85-35162
FRISA, L. E.
Ion flow experiments in a multipole discharge chamber p 178 A85-12705
FRITSCH, K.
Remote displacement measurements using a laser diode p 121 A85-24464
FRONEK, D. L.
Heat transfer results and operational characteristics of the NASA Lewis Research Center Hot Section Cascade Test Facility
[NASA-TM-86890] p 114 N85-15133
FROTA, M. N.
Heat transfer and turbulence measurements of a film-cooled flow over a convexly curved surface p 112 A85-41787
FRYBURG, G. C.
Chemical reactions involved in the initiation of hot corrosion of IN-738 p 66 A85-31688
FRYE, R. J.
Advanced secondary power system for transport aircraft
[NASA-TP-2463] p 30 N85-28944
FRYXELL, R. E.
Effects of surface chemistry on hot corrosion life
[NASA-CR-174915] p 28 N85-26711
FU, K. C.
Thermal-stress analysis for a wood composite blade
[NASA-CR-174794] p 159 N85-17421
FU, L. S.
Ultrasonic wave propagation in two-phase media - Spherical inclusions p 54 A85-11926
Fundamentals of microcrack nucleation mechanics
[NASA-CR-3851] p 137 N85-16195
FUJII, M.
Development of coated single-crystal superalloy systems for gas turbine applications p 68 A85-32440
FUNG, S. S.
Topological reaction rate measurements related to scuffing p 64 A85-11070
FURST, R. B.
Small centrifugal pumps for low thrust rockets
[AIAA PAPER 85-1302] p 45 A85-43978
FURUHAMA, K.
Heat transfer and turbulence measurements of a film-cooled flow over a convexly curved surface p 112 A85-41787
FUSARO, R. L.
Polyimides - Tribological properties and their use as lubricants p 79 A85-21524
Friction, wear, transfer, and wear surface morphology of ultrahigh-molecular-weight polyethylene p 80 A85-22276
Tribological properties of graphite-fiber-reinforced, partially fluorinated polyimide composites
[NASA-TM-86926] p 86 N85-18153
Effect of counterface material type and its topography on the tribological properties of polyimide composites
[NASA-TM-87036] p 90 N85-26993

G

GAAB, T. P.
Orientation and temperature dependence of some mechanical properties of the single-crystal nickel-base superalloy Rene N4. 3: Tension-compression anisotropy
[NASA-TM-86982] p 76 N85-22660
GABB, T. P.
On the fatigue crack propagation behavior of superalloys at intermediate temperatures p 68 A85-32434
GAHN, R. F.
Cycling performance of the iron-chromium redox energy storage system
[NASA-TM-87034] p 162 N85-27387
GAIER, J. R.
Stability of bromine intercalated graphite fibers
[NASA-TM-86859] p 84 N85-10187
Homogeneity of pristine and bromine intercalated graphite fibers
[NASA-TM-87016] p 89 N85-25521
Environmental stability of intercalated graphite fibers
[NASA-TM-87025] p 90 N85-26992
GALLAGHER, J. J.
Infrared technology for satellite power conversion
[NASA-CR-174266] p 159 N85-16293
Technology for satellite power conversion
[NASA-CR-174335] p 159 N85-18451
GALLER, D. E.
Design and analysis report for the RL10-2B breadboard low thrust engine
[NASA-CR-174857] p 48 N85-19020
GANGL, K. J.
Diffusion welding of Cassegrainian concentrator cell stack assemblies
[NASA-CR-176104] p 164 N85-33566
GARDNER, W. B.
Energy Efficient Engine Program technology benefit/cost study, volume 1
[NASA-CR-174766-VOL-1] p 33 N85-35197
Energy Efficient Engine Program technology benefit/cost study, volume 2
[NASA-CR-174766-VOL-2] p 33 N85-35198
GAROW, J.
Regenerative fuel cell energy storage system for a low Earth orbit space station
[NASA-CR-174802] p 158 N85-13371
GARRETT, H. B.
Design guidelines for assessing and controlling spacecraft charging effects p 40 N85-22500
GARRISON, P. W.
An evaluation of oxygen/hydrogen propulsion systems for the Space Station
[AIAA PAPER 85-1156] p 45 A85-43976
An evaluation of oxygen-hydrogen propulsion systems for the Space Station
[NASA-TM-87059] p 52 N85-28971
GAUGLER, R. E.
A review and analysis of boundary layer transition data for turbine application
[NASA-TM-86880] p 113 N85-10306
A review and analysis of boundary layer transition data for turbine application p 118 N85-31440
GAUNTNER, J. W.
Contingency power concepts for helicopter turboshaft engine p 15 A85-32005
GAY, C. H.
Energy efficient engine. Low pressure turbine test hardware detailed design report
[NASA-CR-167956] p 22 N85-10994
GAYDA, J.
On the fatigue crack propagation behavior of superalloys at intermediate temperatures p 68 A85-32434
Orientation and temperature dependence of some mechanical properties of the single-crystal nickel-base superalloy Rene N4. 3: Tension-compression anisotropy
[NASA-TM-86982] p 76 N85-22660
GAYDOSH, D. J.
Ductility in rapidly solidified NiAl p 66 A85-26158
Rapidly solidified NiAl and FeAl
[NASA-TM-86941] p 74 N85-20042
GELDER, T. F.
Design and performance of a fixed, nonaccelerating guide vane cascade that operates over an inlet flow angle range of 60 deg
[ASME PAPER 84-GT-75] p 4 A85-32964
GENERAZIO, E. R.
The scattering of ultrasonic third sound from substrate surface defects p 174 A85-36047

The role of the reflection coefficient in precision measurement of ultrasonic attenuation p 137 A85-42151

GEORGALAS, G.
Laser balancing system for high material removal rates
[NASA-CR-174731] p 126 N85-12341

GERHART, P. M.
Progress in development of a Navier-Stokes solver for evaluation of iced airfoil performance
[AIAA PAPER 85-0410] p 3 A85-19731

GERTZ, J.
Rotor wake characteristics of a transonic axial flow fan
[AIAA PAPER 85-1133] p 6 A85-43974

GHALLA-GORADIA, M.
Near-optimum design of GaAs-based concentrator space solar cells for 80 C operation p 153 A85-15800
Preliminary design of a 10 kW thermophotovoltaic system for space applications p 45 A85-45371

GHANDHI, S. K.
Electrical characterization of plasma-grown oxides on gallium arsenide p 181 A85-32635
Heat treatment of bulk gallium arsenide using a phosphosilicate glass cap p 181 A85-32636
Fabrication of p(+)-n junction GaAs solar cells by a novel method p 181 A85-33645

GHANDI, S. K.
Research on gallium arsenide diffused junction solar cells
[NASA-CR-174057] p 158 N85-11457

GHIA, K. N.
Computation of internal flows: Methods and applications; Proceedings of the Energy Sources Technology Conference, New Orleans, LA, February 12-16, 1984 p 106 A85-11630
Two-dimensional internal compressible viscous flows using semi-elliptic analysis p 106 A85-11640

GHIA, U.
Two-dimensional internal compressible viscous flows using semi-elliptic analysis p 106 A85-11640

GHOSE, H. M.
A computer simulation of thin film nucleation and growth: The Volmer-Weber case
[NASA-TM-86968] p 53 N85-21264

GHOSH, A.
Optical linear algebra processors - Noise and error-source modeling p 169 A85-36727

GHOSH, M. K.
Hydrodynamic lubrication of rigid nonconformal contacts in combined rolling and normal motion
[ASME PAPER 84-TRIB-13] p 127 A85-21280
Thermal elastohydrodynamic lubrication of line contacts p 128 A85-31202

GILES, M. B.
A numerical study of the steady scalar convective diffusion equation for small viscosity p 107 A85-16533

GILGER, L. D.
Extreme precision antenna reflector study results p 165 N85-23830

GILMORE, D. R., JR.
TF34 convertible engine control system design p 15 A85-32006

GINTY, C. A.
Select fiber composites for space applications - A mechanistic assessment p 54 A85-16040

GLADDEN, H. J.
Transient technique for measuring heat transfer coefficients on stator airfoils in a jet engine environment
[AIAA PAPER 85-1471] p 122 A85-39796
Heat transfer results and operational characteristics of the NASA Lewis Research Center Hot Section Cascade Test Facility
[NASA-TM-86890] p 114 N85-15133
Transient technique for measuring heat transfer coefficients on stator airfoils in a jet engine environment
[NASA-TM-87005] p 124 N85-25794

GLASGOW, T. K.
Demonstration of a silicon nitride attrition mill for production of fine pure Si and Si3N4 powders p 78 A85-10825
Diffusion welding of MA 6000 and a conventional nickel-base superalloy p 69 A85-43551
Microstructures in rapidly solidified Ni-Mo alloys
[NASA-TM-87100] p 78 N85-34266

GLASSMAN, A. J.
Future directions in aeropropulsion technology
[NASA-TM-87010] p 1 N85-23685

GLENN, W. H.
Fiber optic temperature sensor p 121 A85-29563

GLICKSMAN, M. E.
Convective influence on the stability of a cylindrical solid-liquid interface p 109 A85-26911

GLIEBE, P. R.
Effects of vane/blade ratio and spacing on fan noise, volume 1
[NASA-CR-174664] p 176 N85-19791
Effects of vane/blade ratio and spacing on fan noise. Volume 2: Data supplement
[NASA-CR-174665] p 176 N85-19792
Development of a rotor wake-vortex model, volume 1
[NASA-CR-174849] p 9 N85-26668

GODLEWSKI, M. P.
Effect of solar-cell junction geometry on open-circuit voltage p 154 A85-28080
Voltage controlling mechanisms in low resistivity silicon solar cells - A unified approach p 155 A85-35617
The effect of diffusion induced lattice stress on the open-circuit voltage in silicon solar cells p 181 A85-35620
The high voltage silicon cell: A comparative analysis p 49 N85-22569

GOEDE, H.
High frequency plasma generator for ion thrusters
[NASA-CR-174772] p 48 N85-17023

GOEKOGLU, S. A.
Computer program for the calculation of multicomponent convective diffusion deposition rates from chemically frozen boundary layer theory
[NASA-CR-168329] p 116 N85-27164

GOEL, P.
A study of Reynolds-stress closure model
[NASA-CR-174342] p 114 N85-17324

GOERTZ, C. K.
Effects of chemical releases by the STS 3 orbiter on the ionosphere p 166 A85-29538

GOLDBERG, A. A.
Experimental results supporting the determination of service quality objectives for DBS systems p 96 A85-29611

GOLDSTEIN, D. N.
Contingency power concepts for helicopter turboshaft engine p 15 A85-32005

GOLDSTEIN, M. E.
Generation of instability waves in flows separating from smooth surfaces p 1 A85-10352
Sound generation and upstream influence due to instability waves interacting with non-uniform mean flows p 174 A85-20738
A procedure for obtaining explicit solutions to a class of Fredholm integral equations p 171 A85-28006

GOLDSTEIN, S. A.
Investigation of a pulsed electrothermal thruster system
[NASA-CR-174768] p 46 N85-11132

GOLLER, G. J.
Electric utility acid fuel cell stack technology advancement
[NASA-CR-174804] p 159 N85-17422

GOLWALKER, S. V.
The influence of hold times on LCF and FCG behavior in a P/M Ni-base superalloy p 67 A85-32400

GOMMERSTADT, B.
Translational and extensional energy release rates (the J- and M-integrals) for a crack layer in thermoelasticity
[NASA-CR-174872] p 145 N85-21685

GONSALVEZ, D. J.
Engineering calculations for communications satellite systems planning
[NASA-CR-175552] p 37 N85-21233

GONZALEZ-SANABRIA, O.
Advanced designs for IPV nickel-hydrogen cells p 156 A85-45438

GONZALEZ-SANABRIA, O. D.
Design considerations for a 10-kW integrated hydrogen-oxygen regenerative fuel cell system p 155 A85-45380
Teardown analysis of a ten cell bipolar nickel-hydrogen battery p 156 A85-45385
Separator development and testing of nickel-hydrogen cells p 156 A85-45386
Alkaline battery containing a separator of a cross-linked copolymer of vinyl alcohol and unsaturated carboxylic acid
[NASA-CASE-LEW-13102-1] p 104 N85-29144
Initial performance of advanced designs for IPV nickel-hydrogen cells p 105 N85-31404
Design principles for nickel-hydrogen cells and batteries
[NASA-TM-87037] p 164 N85-31646

GOOD, B. S.
Monte Carlo lattice models for adsorbed polymer conformation
[NASA-TP-2453] p 183 N85-24961

GORADIA, C.
Near-optimum design of GaAs-based concentrator space solar cells for 80 C operation p 153 A85-15800
Applicability of the Meyer-Neldel rule to solar cells p 154 A85-19948
Theory of the high base resistivity n(+)pp(+) silicon solar cell and its application to radiation damage effects p 154 A85-32639

GORDON, L. H.
Mod-2 wind turbine field operations experience p 157 A85-45512

GORDON, S.
Computer program for calculation of complex chemical equilibrium compositions and applications. Supplement 1: Transport properties
[NASA-TM-86885] p 184 N85-16663

GORDON, W. L.
Electron yields from spacecraft materials p 40 N85-22512

GORGOL, J. F.
Jet fuel property changes and their effect on producibility and cost in the U.S., Canada, and Europe
[NASA-CR-174840] p 93 N85-27012

GORLA, R. S. R.
Combined influence of unsteady free stream velocity and free stream turbulence on stagnation point heat transfer p 112 A85-41782
Unsteady heat transfer due to time-dependent free stream velocity p 117 N85-27947

GORLAND, S. H.
Radiation exposure and performance of multiple burn LEO-GEO orbit transfer trajectories
[NASA-TM-86946] p 36 N85-21228

GOSMAN, A. D.
Assessment of discretization schemes to reduce numerical diffusion in the calculation of complex flows
[AIAA PAPER 85-0441] p 108 A85-19751
Error reduction program
[NASA-CR-174776] p 172 N85-27584

GOTKIS, S.
Configuration study for a 30 GHz monolithic receive array: Technical assessment
[NASA-CR-174697] p 98 N85-18238
Configuration study for a 30 GHz monolithic receive array, volume 1
[NASA-CR-174697-VOL-1] p 98 N85-18239
Configuration study for a 30 GHz monolithic receive array, volume 2
[NASA-CR-174697-VOL-2] p 99 N85-18240

GOTO, H.
Effect of humidity on fretting wear of several pure metals
[NASA-TP-2403] p 72 N85-13006

GOUKER, M. A.
Infrared technology for satellite power conversion
[NASA-CR-174266] p 159 N85-16293
Technology for satellite power conversion
[NASA-CR-174335] p 159 N85-18451

GOULDIN, F. C.
Combustion efficiency of a premixed continuous flow combustor p 61 A85-42571

GOVADA, A. K.
A study of the stress wave factor technique for the characterization of composite materials
[NASA-CR-174870] p 58 N85-30035

GOVILA, R. K.
Fracture of yttria-doped, sintered reaction-bonded silicon nitride
[ACS PAPER 7-J3-84] p 82 A85-42797

GOVINDAN, T. R.
Computation of viscous flows in turbomachinery cascades p 106 A85-11631

GRAF, A. J.
Jet fuel property changes and their effect on producibility and cost in the U.S., Canada, and Europe
[NASA-CR-174840] p 93 N85-27012

GRAHAM, R. E.
Linearization of digital derived rate algorithm for use in linear stability analysis
[NASA-TM-87000] p 41 N85-23904

GRAHAM, R. W.
Computational thermo-fluid dynamics contributions to advanced gas turbine engine design
[AIAA PAPER 85-0083] p 14 A85-19509
Computational thermo-fluid dynamics contributions to advanced gas turbine engine design
[NASA-TM-86865] p 18 N85-10069

GRANT, H.
High temperature static strain sensor development program p 19 N85-10959

GRANTHAM, D. H.
High-temperature optically activated GaAs power switching for aircraft digital electronic control
[NASA-CR-174711] p 34 N85-12901

GRAY, D. E.
Energy Efficient Engine Program technology benefit/cost study, volume 1
[NASA-CR-174766-VOL-1] p 33 N85-35197
Energy Efficient Engine Program technology benefit/cost study, volume 2
[NASA-CR-174766-VOL-2] p 33 N85-35198

GRAY, H. R.
PM superalloys - A troubled adolescent? p 69 A85-44772
GREENE, J. E.
Properties of coated and modified surfaces p 53 A85-36694
GREENE, W.
Energy efficient engine combustor test hardware detailed design report
[NASA-CR-167945] p 18 N85-10950
GREGOREK, G. M.
Design and wind tunnel evaluation of a symmetric airfoil series for large wind turbine applications
[NASA-CR-174764] p 7 N85-10919
GREISING, G. J.
Electric utility acid fuel cell stack technology advancement
[NASA-CR-174804] p 159 N85-17422
GREITZER, E. M.
A theory of post-stall transients in multistage axial compression systems
[NASA-CR-3878] p 8 N85-21117
GRIER, N. T.
Dilute plasma coupling currents to a high voltage solar array in weak magnetic fields p 46 A85-45388
Plasma interaction experiment 2 (PIX 2): Laboratory and flight results p 180 N85-22495
GRIFFIN, J. H.
Effects of friction dampers on aerodynamically unstable rotor stages p 14 A85-21866
GRILL, A.
RF-sputtered silicon and hafnium nitrides - Properties and adhesion to 440C stainless steel p 81 A85-36240
Surface hardening of steel by boriding in a cold rf plasma p 68 A85-40275
GRISNIK, S. P.
Vacuum chamber pressure effects on thrust measurements of low Reynolds number nozzles
[NASA-TM-86955] p 49 N85-21259
Compatibility experiments of facilities, materials, and propellants for electrothermal thrusters
[NASA-TM-86956] p 49 N85-21260
GROENEWEG, J. F.
Analytical and physical modeling program for the NASA Lewis Research Center's Altitude Wind Tunnel (AWT)
[AIAA PAPER 85-0379] p 34 A85-19709
Analytical and physical modeling program for the NASA Lewis Research Center's Altitude Wind Tunnel (AWT)
[NASA-TM-86919] p 35 N85-15757
GROENEWEG, M.
A new interpretation of internal heat transfer coefficients of porous media
[ASME PAPER 84-WA/HT-51] p 110 A85-39894
GROESBECK, D. E.
Static jet noise test results of four 0.35 scale-model QCGAT mixer nozzles
[NASA-TM-86871] p 175 N85-13551
GROUMPOS, P. P.
Control algorithms and computer simulation of a stand-alone photovoltaic village power system p 153 A85-11345
The subjective effect of multiple co-channel frequency modulated television interference p 96 A85-28234
On the subjective evaluation of the interference protection ratios' measurements for co-channel FM-TV signals p 96 A85-28241
Control aspects of the Schuchuli Village stand-alone photovoltaic power system
[NASA-TM-83790] p 103 N85-13157
GULBRANDSEN, N. C.
Small centrifugal pumps for low thrust rockets
[AIAA PAPER 85-1302] p 45 A85-43978
GULINO, D. A.
'Diamondlike' carbon films - Optical absorption, dielectric properties, and hardness dependence on deposition parameters p 82 A85-40383
GUPTA, I. J.
Adaptive antenna arrays for weak interfering signals
[NASA-CR-174336] p 98 N85-17258
Adaptive antenna arrays for satellite communications: Design and testing
[NASA-CR-176162] p 100 N85-34329

H

HAAS, J. E.
Predicted turbine stage performance using quasi-three-dimensional and boundary-layer analyses p 15 A85-34013
Application of viscous and inviscid computation methods for rocket turbopump systems
[SAE PAPER 841522] p 110 A85-39257
Fuel and oxidizer turbine loss analysis p 50 N85-26900
HADY, W. F.
Tribological properties of graphite-fiber-reinforced, partially fluorinated polyimide composites
[NASA-TM-86926] p 86 N85-18153
HAFTKA, R. T.
Optimization of cascade blade mistuning. II - Global optimum and numerical optimization p 16 A85-45715
HAGEDORN, N. H.
NASA Redox Storage System Development Project
[NASA-TM-83677] p 158 N85-12465
Cycling performance of the iron-chromium redox energy *storage system*
[NASA-TM-87034] p 162 N85-27387
HAISLER, W. E.
Numerical considerations in the development and *implementation of constitutive models* p 151 N85-31541
HALES, S. J.
Rapid solidification and dynamic compaction of Ni-base *superalloy powders* p 67 A85-32414
HALFORD, G. R.
Strainrange partitioning - A total strain range version p 64 A85-11603
Application of two creep fatigue life models for the prediction of elevated temperature crack initiation of a nickel base alloy
[AIAA PAPER 85-1420] p 69 A85-43979
Life prediction and constitutive behavior: Overview p 20 N85-10973
Engine cyclic durability by analysis and material testing p 25 N85-15744
Interaction of high-cycle and low-cycle fatigue of Haynes 188 alloy at 1400 F deg p 149 N85-27961
Reexamination of cumulative fatigue damage laws p 149 N85-27962
HALILA, E. E.
Energy efficient engine high pressure turbine test hardware detailed design report
[NASA-CR-167955] p 23 N85-10995
HALLINAN, G. J.
Electric power - Photovoltaic or solar dynamic? p 46 A85-47042
HALTER, P. H.
Energy efficient engine. Fan and quarter-stage component performance report
[NASA-CR-168070] p 33 N85-34141
HAMED, A.
The three-dimensional compressible flow in a radial inflow turbine scroll p 6 A85-41826
HAMPSON, M. E.
Reusable rocket engine turbopump condition monitoring
[SAE PAPER 841619] p 44 A85-39267
Reusable rocket engine turbopump condition monitoring p 51 N85-26907
HAMROCK, B. J.
Elastohydrodynamic lubrication of line contacts p 126 A85-11069
Hydrodynamic lubrication of rigid nonconformal contacts in combined rolling and normal motion
[ASME PAPER 84-TRIB-13] p 127 A85-21280
Thermal elastohydrodynamic lubrication of line contacts p 128 A85-31202
Transmission efficiency measurements and correlations with physical characteristics of the lubricant p 89 N85-23781
Fast approach for calculating film thicknesses and pressures in elastohydrodynamically lubricated contacts at high loads
[NASA-TM-87032] p 117 N85-30242
Correlation of rheological characteristics of lubricants with transmission efficiency measurements
[NASA-TM-86988] p 134 N85-30342
Surface roughness effects in elastohydrodynamic contacts
[NASA-TP-2488] p 134 N85-32329
Mechanics of a gaseous film barrier to lubricant wetting *of elastohydrodynamically lubricated conjunctions*
[NASA-TP-2500] p 135 N85-32330
Elastohydrodynamic lubrication calculations used as a tool to study scuffing
[NASA-TM-87097] p 137 N85-34408
HAN, J. C.
Heat transfer enhancement in channels with turbulence promoters
[ASME PAPER 84-WA/HT-72] p 111 A85-39900
HANDSCHUH, R. F.
High-temperature erosion of plasma-sprayed, yttria-stabilized zirconia in a simulated turbine environment
[AIAA PAPER 85-1219] p 82 A85-39662
Spiral bevel and circular arc helical gears: Tooth contact analysis and the effect of misalignment on circular arc helical gears
[NASA-TM-87013] p 32 N85-31060
Thermal stress analysis of a new turbine shroud seal concept
[NASA-TM-87082] p 136 N85-34406
HANKS, D. E.
Study of advanced fuel system concepts for commercial aircraft and engines
[NASA-CR-174752] p 93 N85-19176
HANNUM, N. P.
An evaluation of oxygen/hydrogen propulsion systems for the Space Station
[AIAA PAPER 85-1156] p 45 A85-43976
An evaluation of oxygen-hydrogen propulsion systems for the Space Station
[NASA-TM-87059] p 52 N85-28971
HANSCHUH, R. F.
High-temperature erosion of plasma-sprayed, yttria-stabilized zirconia in a simulated turbine environment
[NASA-TP-2406] p 84 N85-13045
HANSEN, I. G.
Advanced secondary power system for transport aircraft
[NASA-TP-2463] p 30 N85-28944
HANSEN, J. L.
A note on blade wake interaction influence on compressor stator row aerodynamic performance p 4 A85-32965
HANSON, R. K.
Velocity visualization in gas flows using laser-induced phosphorescence of biacetyl p 121 A85-21695
Fast laser-induced aerosol formation for visualization of gas flows p 121 A85-31113
Two-frequency laser-induced fluorescence technique for rapid velocity-field measurements in gas flows p 121 A85-32294
Velocity visualization in gaseous flows
[NASA-CR-174954] p 119 N85-31445
HARABETIAN, E.
A convergent series expansion for hyperbolic systems of conservation laws
[NASA-CR-172557] p 168 N85-21990
HARB, A.
Thermal-stress analysis for a wood composite blade
[NASA-CR-174794] p 159 N85-17421
HARDY, T. L.
Cathode degradation and erosion in high pressure arc discharges p 43 A85-16445
Electrode erosion in arc discharges at atmospheric pressure
[NASA-TM-87087] p 52 N85-34178
Hollow cathodes in high pressure arc discharges
[NASA-TM-87098] p 52 N85-34179
HARF, F. H.
The substitution of nickel for cobalt in hot isostatically pressed powder metallurgy UDIMET 700 alloys p 68 A85-37415
The response of cobalt-free Udimet 700 type alloy to modified heat treatments
[NASA-TM-86942] p 75 N85-20043
Properties and microstructures for dual alloy combinations of three superalloys with alloy 901
[NASA-TM-86987] p 76 N85-26963
HART, R. E.
Voltage controlling mechanisms in low resistivity silicon solar cells - A unified approach p 155 A85-35617
The high voltage silicon cell: A comparative analysis p 49 N85-22569
HARTMANN, M. J.
The trend of future gas turbine technology p 16 A85-41778
HASSA, C.
Velocity visualization in gas flows using laser-induced phosphorescence of biacetyl p 121 A85-21695
Fast laser-induced aerosol formation for visualization of gas flows p 121 A85-31113
HATHAWAY, M. D.
A note on blade wake interaction influence on compressor stator row aerodynamic performance p 4 A85-32965
Rotor wake characteristics of a transonic axial flow fan
[AIAA PAPER 85-1133] p 6 A85-43974
HAWLEY, M. C.
Measurements of energy distribution in microwave plasmas of N2 and He and comparisons with results for H2 p 178 A85-16443
The energetics of hydrogen atom recombination - Analysis, experiments, and modeling p 179 A85-16444
HAYNES, J. F.
Contingency power concepts for helicopter turboshaft engine p 15 A85-32005
HECKEL, R. W.
Cyclic oxidation behavior of beta+gamma overlay coatings on gamma and gamma+gamma-prime alloys p 68 A85-32431

HEINE, C.
Generated spiral bevel gears: Optimal machine-tool settings and tooth contact analysis
[NASA-TM-87075] p 136 N85-34405
HEITMAN, P. W.
Ceramic components for gas turbine engines
p 127 A85-15973
Photoacoustic microscopy of ceramic turbine blades
p 83 A85-43930
Ceramic applications in turbine engines
[NASA-CR-174715] p 91 N85-28109
HELLAWELL, A.
The mechanisms of formation and prevention of channel segregation during alloy solidification
p 180 A85-18082
HELMS, H. E.
Ceramic applications in turbine engines
[NASA-CR-174715] p 91 N85-28109
HEMKER, K. J.
Orientation and temperature dependence of some mechanical properties of the single-crystal nickel-base superalloy Rene N4. 3: Tension-compression anisotropy
[NASA-TM-86982] p 76 N85-22660
Microstructures in rapidly solidified Ni-Mo alloys
[NASA-TM-87100] p 78 N85-34266
HENDRICKS, R. C.
An analysis of temperature effect in a finite journal bearing with spatial tilt and viscous dissipation
p 126 A85-11074
Plastic flow of plasma sprayed ceramics
p 80 A85-24161
A comparison of flow rates and pressure profiles for N-sequential inlets and three related seal configurations
p 109 A85-26526
Flow rates and pressure profiles for one to four axially alined Borda inlets
[NASA-TP-2390] p 113 N85-14078
Experimental and analytical study of ceramic-coated turbine-tip shroud seals for small turbine engines
[NASA-TM-86881] p 25 N85-18057
Experimental study of ceramic coated tip seals for turbojet engines
[NASA-TM-86939] p 114 N85-19363
Ribbon burner simulation of T-700 turbine shroud for ceramic lined seals research
[NASA-TM-86940] p 114 N85-19364
Analysis of experimental shaft seal data for high-performance turbomachines, as for Space Shuttle main engines
[NASA-TM-86928] p 115 N85-21569
Nested subcritical flows within supercritical systems
[NASA-TM-86980] p 115 N85-21574
Metallic and metalloceramic coating by thermal decomposition
[NASA-TM-86992] p 88 N85-22755
Film and interstitial formation of metals in plasma-sprayed ceramics
[NASA-TM-86993] p 89 N85-22756
Fabrication of ceramic substrate-reinforced and free forms
[NASA-TM-86994] p 50 N85-23926
Flow rate and pressure profiles for 1 to 4 axially alined orifice inlets
[NASA-TP-2460] p 116 N85-27165
HENEY, J. F.
A 20 GHz, 75 watt, helix TWT for space communications p 101 A85-14433
HENNEKE, E. G., II
A study of the stress wave factor technique for the characterization of composite materials
[NASA-CR-174870] p 58 N85-30035
HERBELL, T. P.
Demonstration of a silicon nitride attrition mill for production of fine pure Si and Si3N4 powders
p 78 A85-10825
Milling of Si3N4 with Si3N4 hardware
[NASA-TM-86864] p 84 N85-10191
Factors influencing the ball milling of Si3N4 in water
[NASA-TM-86932] p 86 N85-19136
Parametric evaluation of ball milling of SiC in water
[NASA-TM-86974] p 88 N85-21356
HERMAN, H.
Failure during thermal cycling of plasma-sprayed thermal barrier coatings p 81 A85-36246
HERRERA, J. I.
Experimental investigation of a variable speed constant frequency electric generating system from a utility perspective
[NASA-CR-174950] p 105 N85-32251
HERZAU, J. S.
Teardown analysis of a ten cell bipolar nickel-hydrogen battery p 156 A85-45385
HESS, C. F.
Spray characterization with a nonintrusive technique using absolute scattered light p 120 A85-10036
Nonintrusive optical single-particle counter for measuring the size and velocity of droplets in a spray
p 120 A85-16794
Research study of droplet sizing technology leading to the development of an advanced droplet sizing system
[NASA-CR-174839] p 123 N85-21604
HESS, J. L.
Calculation of compressible flow about three-dimensional inlets with auxiliary inlets, slats and vanes by means of a panel method
[AIAA PAPER 85-1196] p 5 A85-40817
Calculation of compressible flow about three-dimensional inlets with auxiliary inlets, slats and vanes by means of a panel method
[NASA-CR-174975] p 10 N85-35162
HESSELINK, L.
Free-surface phenomena under low- and zero-gravity conditions
[NASA-CR-175885] p 36 N85-27922
HESSERBACKER, G.
Configuration study for a 30 GHz monolithic receive array: Technical assessment
[NASA-CR-174697] p 98 N85-18238
Configuration study for a 30 GHz monolithic receive array, volume 1
[NASA-CR-174697-VOL-1] p 98 N85-18239
Configuration study for a 30 GHz monolithic receive array, volume 2
[NASA-CR-174697-VOL-2] p 99 N85-18240
HETZEL, R.
Numerical simulation of positive-potential conductors in the presence of a plasma and a secondary-emitting dielectric p 102 A85-35306
HIEATT, J. L.
Electric power - Photovoltaic or solar dynamic?
p 46 A85-47042
HILKO, B. K.
Investigation of a pulsed electrothermal thruster system
[NASA-CR-174768] p 46 N85-11132
HILL, T. G.
Analytical fuel property effects: Small combustors, phase 2
[NASA-CR-174848] p 93 N85-19175
HILLER, B.
Velocity visualization in gas flows using laser-induced phosphorescence of biacetyl p 121 A85-21695
Two-frequency laser-induced fluorescence technique for rapid velocity-field measurements in gas flows
p 121 A85-32294
HINCKEL, J. N.
Heat transfer investigation in the junction region of circular cylinder normal to a flat plate at 90 deg location
[ASME PAPER 84-WA/HT-70] p 111 A85-39898
HIPPENSTEELE, S. A.
High temperature thermocouple and heat flux gauge using a unique thin film-hardware hot juncture
[NASA-TM-86898] p 123 N85-16096
Local heat-transfer measurements on a large, scale-model turbine blade airfoil using a composite of a heater element and liquid crystals
[NASA-TM-86900] p 119 N85-33435
HIRSCHBEIN, M. S.
Finite element engine blade structural optimization
[AIAA PAPER 85-0645] p 141 A85-30313
Component-specific modeling p 20 N85-10971
HIRSCHKRON, R.
Contingency power concepts for helicopter turboshaft engine p 15 A85-32005
HO, P. Y.
Comparison of scaled model data to full size energy efficient engine test results
[AIAA PAPER 84-2281] p 13 A85-13953
Measurement and prediction of Energy Efficient Engine noise
[AIAA PAPER 84-2284] p 13 A85-13954
HOBART, H. F.
Evaluation results of the 700 deg C Chinese strain gauges
[NASA-TM-86973] p 124 N85-21605
HOBERECHT, M. A.
Design considerations for a 10-kW integrated hydrogen-oxygen regenerative fuel cell system
p 155 A85-45380
A 37.5-kW point design comparison of the nickel-cadmium battery, bipolar nickel-hydrogen battery, and regenerative hydrogen-oxygen fuel cell energy storage subsystems for low earth orbit p 46 A85-45387
Regenerative fuel cell systems for space station
p 104 N85-31372
HOCKMUTH, J.
Preparation and evaluation of advanced catalysts for phosphoric acid fuel cells
[NASA-CR-168223] p 160 N85-19511
HOEGLUND, E.
Correlation of rheological characteristics of lubricants with transmission efficiency measurements
[NASA-TM-86988] p 134 N85-30342
HOFFMAN, A. C.
Advanced secondary power system for transport aircraft
[NASA-TP-2463] p 30 N85-28944
HOFFMAN, R. W.
Electron yields from spacecraft materials
p 40 N85-22512
Study of Kapton under simulated shuttle environment
[NASA-CR-176003] p 41 N85-29997
HOLANDA, R.
High temperature thermocouple and heat flux gauge using a unique thin film-hardware hot juncture
[NASA-TM-86898] p 123 N85-16096
HOLDEMAN, J. D.
GASP cloud encounter statistics - Implications for laminar flow control flight p 166 A85-11979
Variability of cloudiness at airline cruise altitudes from GASP measurements p 166 A85-31199
Experiments in dilution jet mixing - Effects of multiple rows and non-circular orifices
[AIAA PAPER 85-1104] p 15 A85-39606
Dilution zone mixing studies p 21 N85-10984
Simultaneous cabin and ambient ozone measurements on two Boeing 747 airplanes. Volume 3: October 1978 - July 1979
[NASA-TM-86883] p 167 N85-21872
Experiments in dilution jet mixing effects of multiple rows and non-circular orifices
[NASA-TM-86996] p 28 N85-25266
HOLEMAN, R. H.
Government review of the Mod-2 wind turbine (as-built)
[NASA-TM-86983] p 162 N85-29365
HOLLANSWORTH, J. E.
Telecommunications forecast for ITU Region 2 to the year 1995
[NASA-TM-87077] p 38 N85-34150
HOLLOWAY, P. R.
Energy efficient engine. High pressure compressor detail design report
[NASA-CR-165558] p 23 N85-10998
HOLTZMAN, R. L.
An investigation of enhanced capability thermal barrier coating systems for diesel engine components
[NASA-CR-174820] p 86 N85-18154
HOPF, W. R.
Stall recovery control strategy methodology and results
[AIAA PAPER 85-1433] p 16 A85-40841
HOPKINS, D. A.
Nonlinear analysis for high-temperature multilayered fiber composite structures
[NASA-TM-83754] p 57 N85-21273
Nonlinear structural analysis for fiber-reinforced superalloy turbine blades p 147 N85-26887
HOTHI, H. S.
Development and use of the computer software package for planning the 12 GHz broadcasting-satellite service at RARC '83 p 96 A85-29605
HOULT, D. P.
Methanol as a soot reducer in a turbulent swirling burner
[ASME PAPER 84-JPGC-GT-2] p 61 A85-23192
HOUPERT, L.
Fast numerical calculations of EHD sliding traction forces Application to rolling bearings
[ASME PAPER 84-TRIB-26] p 127 A85-21289
HOUPERT, L. G.
Fast approach for calculating film thicknesses and pressures in elastohydrodynamically lubricated contacts at high loads
[NASA-TM-87032] p 117 N85-30242
Elastohydrodynamic lubrication calculations used as a tool to study scuffing
[NASA-TM-87097] p 137 N85-34408
HOUSER, D. R.
The design and analysis of single flank transmission error testor for loaded gears
[NASA-CR-176163] p 136 N85-34404
HOUSER, M. J.
Phase/doppler spray analyzer for simultaneous measurements of drop size and velocity distributions
p 120 A85-10035
HOWE, D. C.
Energy efficient engine flight propulsion system preliminary analysis and design report
[NASA-CR-174701] p 18 N85-10947
Energy efficient engine integrated core/low spool test hardware design report
[NASA-CR-168137] p 31 N85-29956

HOWES, W. L.
Rainbow schlieren vs Mach-Zehnder interferometer - A comparison p 121 A85-28820
HOYNIAK, D.
The effect of aerodynamic and structural detuning on turbomachine supersonic unstalled torsional flutter
[AIAA PAPER 85-0761] p 14 A85-30378
Aerodynamic detuning analysis of an unstalled supersonic turbofan cascade
[NASA-TM-87001] p 9 N85-26670
HSHIEH, F. I.
Electrical characterization of plasma-grown oxides on gallium arsenide p 181 A85-32635
HSU, L. C.
Alkaline battery containing a separator of a cross-linked copolymer of vinyl alcohol and unsaturated carboxylic acid
[NASA-CASE-LEW-13102-1] p 104 N85-29144
HSUEH, K. L.
Electrocatalysis of fuel cell reactions: Investigation of alternate electrolytes
[NASA-CR-174753] p 157 N85-11455
HUBBELL, T. E., JR.
Ion-beam nitriding of steels
[NASA-CASE-LEW-14104-1] p 75 N85-21324
HUDSON, W. R.
Spacecraft environmental interactions: A joint Air Force and NASA research and technology program
p 40 N85-22517
HUFF, R. G.
Analysis of the effect on combustor noise measurements of acoustic waves reflected by the turbine and combustor inlet
[AIAA PAPER 84-2323] p 173 A85-16103
A theoretical prediction of the acoustic pressure generated by turbulence-flame front interactions
[ASME PAPER 84-WA/NCA-11] p 174 A85-39909
HUGHES, C. E.
Analytical modeling of circuit aerodynamics in the new NASA Lewis Altitude Wind Tunnel
[AIAA PAPER 85-0380] p 3 A85-26389
Analytical modeling of circuit aerodynamics in the new NASA Lewis wind tunnel
[NASA-TM-86912] p 8 N85-15688
HUGHES, T. J. R.
Augmented weak forms and element-by-element preconditioners: Efficient iterative strategies for structural finite elements. A preliminary study p 144 N85-10384
HULL, D. R.
The effects of seven alloying elements on the microstructure and stress-rupture behavior of nickle-base superalloys
[NASA-TM-83791] p 70 N85-10168
HULLIGAN, D. D.
Effect of water on hydrogen permeability
[NASA-TM-86904] p 53 N85-14864
HULSE, C.
High temperature static strain sensor development program p 19 N85-10959
HUMENIK, F. M.
Flame radiation and linear heat transfer in a tubular-can combustor p 15 A85-39580
HUNG, C. C.
A micrographic and gravimetric study of intercalation and deintercalation of graphite fibers
[NASA-TM-87026] p 91 N85-28110
HURST, J. B.
Evaluation of alpha-SiC sintering using statistical methods p 83 A85-42800
HUSTON, R. L.
A computer aided design procedure for generating gear teeth
[ASME PAPER 84-DET-184] p 128 A85-33779
Dynamic analysis of straight and involute tooth forms
[ASME PAPER 84-DET-226] p 128 A85-33780
HWANG, D. P.
Analytical study of blowing boundary layer control for subsonic V/STOL inlets p 2 A85-11646
HWANG, S. Y.
On local total strain redistribution using a simplified cyclic inelastic analysis based on an elastic solution
[AIAA PAPER 85-1419] p 142 A85-39770
Local strain redistribution corrections for a simplified inelastic analysis procedure based on an elastic finite-element analysis
[NASA-TP-2421] p 145 N85-20396
On local total strain redistribution using a simplified cyclic inelastic analysis based on an elastic solution
[NASA-TM-86913] p 145 N85-21690
HYMAN, J., JR.
IAPS (8-cm) ion thruster cyclic endurance test
p 42 A85-16406
Ion thruster system (8-cm) cyclic endurance test
[NASA-CR-174745] p 47 N85-12937

I

IDE, R. F.
Comparison of icing cloud instruments for 1982-1983 icing season flight program
[AIAA PAPER 84-0020] p 13 A85-16098
IMBRIE, P. K.
Numerical considerations in the development and implementation of constitutive models
p 151 N85-31541
INGEBO, R. D.
Aerodynamic effect of combustor inlet air pressure on fuel jet atomization p 109 A85-27096
Liquid fuel spray processes in high-pressure gas flow
[NASA-TM-86944] p 115 N85-21570
INSPEKTOR, A.
Deposition of silicon nitride from SiCl4 and NH3 in a low pressure RF plasma p 81 A85-36229
IRION, C. E.
Stratified charge rotary aircraft engine technology enablement program
[NASA-CR-174812] p 25 N85-21163
ISHIGAKI, H.
Surface effects of corrosive media on hardness, friction, and wear of materials
[NASA-TM-83711] p 85 N85-15896
IZQUIERDO, A. J.
Methanol as a soot reducer in a turbulent swirling burner
[ASME PAPER 84-JPGC-GT-2] p 61 A85-23192

J

JACKSON, J. A.
A multiple-scales model of the shock-cell structure of imperfectly expanded supersonic jets
p 113 A85-49354
JACKSON, T. W.
Turbulence characteristics of swirling flowfields
[NASA-CR-174918] p 29 N85-26717
JACOBSON, B. O.
Elastohydrodynamic lubrication of line contacts
p 126 A85-11069
Correlation of rheological characteristics of lubricants with transmission efficiency measurements
[NASA-TM-86988] p 134 N85-30342
JACOBSON, N. S.
Hot corrosion of sintered alpha-SiC at 1000 C
[ACS PAPER 19-B-84P] p 83 A85-45302
The reactions of cobalt, iron and nickel in SO-2 atmospheres: Similarities and differences
[NASA-TM-86868] p 70 N85-11217
Burner rig corrosion of SiC at 1000 deg C
[NASA-TM-87061] p 53 N85-30011
Mechanism of strength degradation for hot corrosion of alpha-SiC
[NASA-TM-87052] p 91 N85-30135
JACQUEZ, A.
Design of low loss helix circuits for interference fitted and brazed circuits
[NASA-CR-168313] p 103 N85-19328
JACQUOTTE, O.-P.
Analysis of hourglass instabilities and control in underintegrated finite element methods
p 139 A85-11125
Stability, accuracy, and efficiency of some underintegrated methods in finite element computations
p 172 A85-50073
JAIN, S. C.
Comparison of atmospheric correction algorithms for the Coastal Zone Color Scanner p 153 A85-10244
JALAN, V.
Development of electrodes for the NASA iron/chromium
[NASA-CR-174724] p 165 N85-35471
JAMES, K.
Fiber optic, Fabry-Perot high temperature sensor
[NASA-CR-174712] p 178 N85-13594
JANARDAN, B. A.
Experimental investigation of shock-cell noise reduction for dual-stream nozzles in simulated flight
[NASA-CR-3846] p 175 N85-13549
Experimental investigation of shock-cell noise reduction for single stream nozzles in simulated flight
[NASA-CR-3845] p 175 N85-13550
JANOWSKI, G. M.
The effect of tantalum on the structure/properties of two polycrystalline nickel-base superalloys: B-1900 + Hf MAR-M247
[NASA-CR-174847] p 73 N85-18127
JARRETT, R. N.
Modeling of gamma/gamma-prime phase equilibrium in the nickel-aluminum system p 65 A85-14959
Effects of cobalt on the hot workability of nickel-base superalloys p 67 A85-32412
JASPERSON, W. H.
GASP cloud encounter statistics - Implications for laminar flow control flight p 166 A85-11979
A comparison of NMC and GWC analysis field temperatures with aircraft measurements
p 166 A85-21140
Variability of cloudiness at airline cruise altitudes from GASP measurements p 166 A85-31199
Simultaneous cabin and ambient ozone measurements on two Boeing 747 airplanes. Volume 3: October 1978 - July 1979
[NASA-TM-86883] p 167 N85-21872
JAWORSKE, D. A.
Dynamics of graphite fiber intercalation: In situ resistivity measurements with a four point probe
[NASA-TM-86858] p 53 N85-10105
Graphite fiber intercalation: Dynamics of the bromine intercalation process
[NASA-TM-87015] p 53 N85-26921
Environmental stability of intercalated graphite fibers
[NASA-TM-87025] p 90 N85-26992
JAYARAMAN, N.
A study of fatigue damage mechanisms in Waspaloy from 25 to 800 C p 65 A85-12098
Low cycle fatigue of MAR-M 200 single crystals at 760 and 870 deg C
[NASA-TM-86933] p 74 N85-19074
Microstructures in rapidly solidified Ni-Mo alloys
[NASA-TM-87100] p 78 N85-34266
JECH, R. W.
Ductility in rapidly solidified NiAl p 66 A85-26158
JEFFERIES, K. S.
Advanced secondary power system for transport aircraft
[NASA-TP-2463] p 30 N85-28944
Optical analysis of parabolic dish concentrators for solar dynamic power systems in space
[NASA-TM-87080] p 52 N85-34176
JENG, D. R.
Aerodynamic analysis of a horizontal axis wind turbine by use of helical vortex theory. Volume 1: Theory
[NASA-CR-168054] p 9 N85-29916
JENKINS, R. M.
An improved computer model for prediction of axial gas turbine performance losses
[NASA-CR-174246] p 24 N85-15724
JENSEN, K. A.
Textured carbon surfaces on copper
[NASA-CASE-LEW-14130-1] p 95 N85-20156
JERACKI, R. J.
Wind tunnel results of advanced high speed propellers in the takeoff, climb, and landing operating regimes
[AIAA PAPER 85-1259] p 6 A85-47025
Wind tunnel results of advanced high speed propellers in the takeoff, climb and landing operating regimes
[NASA-TM-87054] p 9 N85-29925
JOHNS, R. H.
Structural analysis p 20 N85-10969
JOHNSON, B. V.
Mass and momentum turbulent transport experiments with confined coaxial jets p 107 A85-14399
Turbulent transport and length scale measurement experiments with comfined coaxial jets
[NASA-CR-174831] p 117 N85-30245
JOHNSON, D. A.
Chemical and electrochemical behavior of the Cr(III)/Cr(II) half-cell in the iron-chromium redox energy storage system p 61 A85-33785
JOHNSON, G. M.
Efficient solution of the Euler and Navier-Stokes equations with a vectorized multiple-grid algorithm
p 2 A85-18679
JOHNSON, J. A.
Cycling performance of the iron-chromium redox energy storage system
[NASA-TM-87034] p 162 N85-27387
JOHNSON, W. A.
Effects of tin on microstructure and mechanical behavior of Inconel 718
[NASA-TM-86866] p 71 N85-12129
JOHNSON, W. R.
Government review of the Mod-2 wind turbine (as-built)
[NASA-TM-86983] p 162 N85-29365
JONES, B. L.
Experimental results supporting the determination of service quality objectives for DBS systems
p 96 A85-29611
JONES, J. D.
The influence of combustion liner holes on noise production by ducted burners
[AIAA PAPER 84-2322] p 172 A85-10869
JONES, M. G.
Laser balancing system for high material removal rates
[NASA-CR-174731] p 126 N85-12341

JONES, R. E.
Space Station propulsion - The Advanced Development Program at Lewis
[AIAA PAPER 85-1154] p 44 A85-39626
Combustion gas properties I-ASTM jet A fuel and dry air
[NASA-TP-2359] p 17 N85-10064
Combustion gas properties. 2: Natural gas fuel and dry air
[NASA-TP-2435] p 26 N85-21168
Space station propulsion: The advanced development program at Lewis
[NASA-TM-86999] p 50 N85-25386
Combustion gas properties. Part 3: Hydrogen gas fuel and dry air
[NASA-TP-2477] p 32 N85-31058
JONES, W. R., JR.
Topological reaction rate measurements related to scuffing p 64 A85-11070
Friction and wear properties of a Charnley artificial hip joint
[ASLE PREPRINT 84-LC-4A-4] p 168 A85-38444
Contact angle and surface tension measurements of a five-ring polyphenyl ether
[NASA-TM-86927] p 86 N85-15897
Characterization of lubricated bearing surfaces operated under high loads
[NASA-TM-86964] p 88 N85-21357
JONGEWARD, G. A.
Computer simulation of plasma electron collection by PIX-II
[AIAA PAPER 85-0386] p 43 A85-19715
JORDAN, E. H.
Biaxial constitutive equation development for single crystals
[NASA-CR-174056] p 183 N85-11862
Elevated temperature biaxial fatigue
[NASA-CR-175795] p 148 N85-27263
JORDAN, F. L.
Reflection plane tests of a wind turbine blade tip section with ailerons
[NASA-TM-87018] p 165 N85-34444
JOU, W.-H.
Direct numerical simulations of a reacting mixing layer with chemical heat release
[AIAA PAPER 85-0143] p 60 A85-19548

K

KANIC, P. G.
Design and analysis report for the RL10-2B breadboard low thrust engine
[NASA-CR-174857] p 48 N85-19020
KANTOLA, R. A.
Effects of vane/blade ratio and spacing on fan noise, volume 1
[NASA-CR-174664] p 176 N85-19791
Effects of vane/blade ratio and spacing on fan noise, Volume 2: Data supplement
[NASA-CR-174665] p 176 N85-19792
KAPOOR, V. J.
High-voltage solar-cell chip p 154 A85-24668
KAR, K.
A new interpretation of internal heat transfer coefficients of porous media
[ASME PAPER 84-WA/HT-51] p 110 A85-39894
KARAGOZIAN, A. R.
Vortex modeling of single and multiple dilution jet mixing in a crossflow
[AIAA PAPER 85-1580] p 111 A85-40701
KARAGULLE, H.
Stress waves in an isotropic elastic plate excited by a circular transducer
[NASA-CR-3877] p 138 N85-20390
Application of homomorphic signal processing to stress wave factor analysis
[NAS 1.26:174871] p 138 N85-21673
Ultrasonic testing of plates containing edge cracks
[NASA-CR-3904] p 138 N85-29307
KARLOVITZ, L. A.
On the existence and stability conditions for mixed-hybrid finite element solutions based on Reissner's variational principle p 142 A85-33847
KARPLUS, W. J.
Data flow methods for dynamic system simulation - A CSSL-IV microcomputer network interface p 170 A85-28614
KASPER, H. J.
Simplified design and life prediction of rocket thrust chambers p 44 A85-29314
KASRAIE, B.
Simplified design and life prediction of rocket thrust chambers p 44 A85-29314
KASUBA, R.
Gear mesh stiffness and load sharing in planetary gearing
[ASME PAPER 84-DET-229] p 129 A85-33781
Conceptual design of a fixed-pitch wind turbine generator system rated at 400 kilowatts
[NASA-CR-174877] p 162 N85-29363
KATSANIS, T.
Predicted turbine stage performance using quasi-three-dimensional and boundary-layer analyses p 15 A85-34013
Calculation of three-dimensional, viscous flow through turbomachinery blade passages by parabolic marching
[AIAA PAPER 85-1408] p 5 A85-39767
Calculation of three-dimensional, viscous flow through turbomachinery blade passages by parabolic marching
[NASA-TM-86984] p 9 N85-23711
KATZ, I.
Computer simulation of plasma electron collection by PIX-II
[AIAA PAPER 85-0386] p 43 A85-19715
Three-dimensional calculation of shuttle charging in polar orbit p 40 N85-22486
Polar orbit electrostatic charging of objects in shuttle wake p 40 N85-22487
Surface interactions and high-voltage current *collection* *p 40 N85-22493*
KAUFMAN, A.
A simplified method for elastic-plastic-creep structural analysis
[ASME PAPER 84-GT-191] p 141 A85-23150
Unified constitutive material models for nonlinear finite-element structural analysis
[AIAA PAPER 85-1418] p 142 A85-39769
On local total strain redistribution using a simplified cyclic inelastic analysis based on an elastic solution
[AIAA PAPER 85-1419] p 142 A85-39770
Nonlinear structural and life analyses of a turbine blade p 19 N85-10954
Nonlinear structural and life analyses of a combustor liner p 19 N85-10955
Constitutive model development for isotropic materials p 20 N85-10975
Engine cyclic durability by analysis and material testing p 25 N85-15744
Local strain redistribution corrections for a simplified inelastic analysis procedure based on an elastic finite-element analysis
[NASA-TP-2421] p 145 N85-20396
On local total strain redistribution using a simplified cyclic inelastic analysis based on an elastic solution
[NASA-TM-86913] p 145 N85-21690
Unified constitutive material models for nonlinear finite-element structural analysis
[NASA-TM-86985] p 146 N85-24338
Cyclic structural analyses of anisotropic turbine blades for reusable space propulsion systems
[NASA-TM-86990] p 146 N85-24339
Develop and test fuel cell powered on-site integrated total energy systems. Phase 3: Full-scale power plant development
[NASA-CR-174887] p 161 N85-25941
Cyclic structural analyses of SSME turbine blades p 150 N85-27963
Develop and test fuel cell powered on-site integrated total energy systems. Phase 3: Full-scale power plant development
[NASA-CR-168338] p 164 N85-30483
Two simplified procedures for predicting cyclic material response from a strain history p 151 N85-31543
KAUFMAN, D. L.
Microprocessor control of photovoltaic systems p 156 A85-45408
KAUFMAN, H. R.
Ion flow experiments in a multipole discharge chamber p 178 A85-12705
Theory of ion acceleration with closed electron drift p 41 A85-15512
KAUSHAL, D.
Satellite provided customer promises services, a forecast of potential domestic demand through the year 2000. Volume 4: Sensitivity analysis
[NASA-CR-174662] p 99 N85-27092
KAY, P. K.
Friction in rail guns *p 101 A85-16424*
KAZA, K. R. V.
Flutter of turbofan rotors with mistuned blades p 139 A85-12716
Effects of warping and pretwist on torsional vibration of rotating beams
[ASME PAPER 84-WA/APM-41] p 140 A85-17040
Flutter of swept fan blades
[ASME PAPER 84-GT-138] p 141 A85-32962
Finite difference analysis of torsional vibrations of pretwisted, rotating, cantilever beams with effects of warping p 143 A85-42047
Vibration and flutter of mistuned bladed-disk assemblies p 16 A85-45854
Vibration and buckling of rotating, pretwisted, preconed *beams including Coriolis effects*
[NASA-TM-87004] p 146 N85-25893
Nonlinear flap-lag-extensional vibrations of rotating, pretwisted, preconed beams including Coriolis effects
[NASA-TM-87102] p 152 N85-34427
KAZA, V.
Vibration and flutter of mistuned bladed-disk assemblies
[AIAA PAPER 84-0991] p 139 A85-16095
KEITH, T. G., JR.
Aerodynamic analysis of a horizontal axis wind turbine by use of helical vortex theory. Volume 1: Theory
[NASA-CR-168054] p 9 N85-29916
Performance comparison between NACA 23024 and NACA 64(3)-618 airfoil configurated rotors for horizontal-axis wind turbines
[NASA-TM-83471] p 163 N85-30477
KEITZ, J. F.
Comparative analysis of operational forecasts versus actual weather conditions in airline flight planning, volume 1
[NASA-CR-167862] p 167 N85-35534
Comparative analysis of operational forecasts versus actual weather conditions in airline flight planning, volume 2
[NASA-CR-167863] p 167 N85-35535
Comparative analysis of operational forecasts versus actual weather conditions in airline flight planning, volume 3
[NASA-CR-167864] p 167 N85-35536
Comparative analysis of operational forecasts versus actual weather conditions in airline flight planning, volume 4
[NASA-CR-167865] p 167 N85-35537
Comparative analysis of operational forecasts versus actual weather conditions in airline flight planning: Summary report
[NASA-CR-167866] p 168 N85-35538
KELKAR, S. S.
A fast time domain digital simulation technique for power converters - Application to a buck converter with feedforward compensation p 101 A85-20900
KELM, J. S.
Flow modifying device
[NASA-CASE-LEW-13562-2] p 33 N85-35195
KENDALL, B. R. F.
Mass analysis of neutral particles and ions released during electrical breakdowns on spacecraft surfaces
[NASA-CR-175585] p 39 N85-21250
Mass spectra of neutral particles released during electrical breakdown of thin polymer films p 88 N85-22511
KENNARD, J.
Development of large, horizontal-axis wind turbines
[NASA-TM-86950] p 161 N85-23242
KENNEDY, F. E.
An experimental investigation of rubbing interaction in labyrinth seals at cryogenic temperature p 129 A85-39938
Analytical and experimental investigation of rubbing interaction in labyrinth seals for a liquid hydrogen fuel pump
[NASA-CR-174657] p 48 N85-18084
KENNEDY, F. E., JR.
Thermal and thermomechanical effects in dry sliding p 127 A85-23838
KERCZEWSKI, R. J.
Automated testing of developmental satellite communications systems and subsystems
[NASA-TM-87070] p 100 N85-31348
KERIBAR, R.
Methods for heat transfer and temperature field analysis of the insulated diesel
[NASA-CR-174783] p 185 N85-16699
KERSCHEN, E. J.
Effect of airfoil mean loading on convected gust interaction noise
[AIAA PAPER 84-2324] p 173 A85-13955
Noise produced by the interaction of a rotor wake with a swept stator blade
[AIAA PAPER 84-2326] p 173 A85-13956
KERSLAKE, W. R.
Rail accelerator technology and applications
[NASA-TM-86947] p 48 N85-21258
KESSEL, R. L.
Numerical simulations of positively-biased probes and dielectric-conductor disks in a plasma p 179 A85-17262
Numerical simulation of positive-potential conductors in the presence of a plasma and a secondary-emitting dielectric p 102 A85-35306

KHANDELWAL, P. K.
Photoacoustic microscopy of ceramic turbine blades p 83 A85-43930
KHOT, N. S.
Structural optimization using optimality criteria methods p 144 A85-48703
KIELB, R.
Natural frequencies of twisted rotating plates p 141 A85-32343
KIELB, R. E.
Flutter of turbofan rotors with mistuned blades p 139 A85-12716
Vibration and flutter of mistuned bladed-disk assemblies
[AIAA PAPER 84-0991] p 139 A85-16095
Effects of warping and pretwist on torsional vibration of rotating beams
[ASME PAPER 84-WA/APM-41] p 140 A85-17040
Vibrations of twisted cantilevered plates - Summary of previous and current studies p 140 A85-22069
Flutter of swept fan blades
[ASME PAPER 84-GT-138] p 141 A85-32962
Vibration and flutter of mistuned bladed-disk assemblies p 16 A85-45854
Vibrations of twisted cantilever plates - A comparison of theoretical results p 144 A85-47626
KIM, C. N.
Vortex modeling of single and multiple dilution jet mixing in a crossflow
[AIAA PAPER 85-1580] p 111 A85-40701
KIM, K. S.
A review of path-independent integrals in elastic-plastic fracture mechanics, task 4
[NASA-CR-174956] p 152 N85-33541
KIM, R. C.
Holographic optical system for aberration corrections in laser Doppler velocimetry p 123 A85-48659
KIM, W. S.
Lubricity of well-characterized jet and broad-cut fuels by ball-on-cylinder machine
[NASA-TM-83807] p 92 N85-12183
Liquid phase products and solid deposit formation from thermally stressed model jet fuels
[NASA-TM-86874] p 92 N85-13066
Thin-film sensors for space propulsion technology p 41 N85-27968
KING, L. A.
Moving target, distributed, real-time simulation using Ada p 170 A85-34131
KING, R. J.
Small-signal model for the series resonant converter p 102 A85-39453
KINGSBURY, E.
First-order ball-bearing kinematics p 128 A85-31203
KINNICK, R. R.
Photoacoustic microscopy of ceramic turbine blades p 83 A85-43930
KIRALY, L. J.
A high-speed implementation of the random decrement algorithm p 94 A85-29556
KISER, J. D.
Milling of Si3N4 with Si3N4 hardware
[NASA-TM-86864] p 84 N85-10191
Factors influencing the ball milling of Si3N4 in water
[NASA-TM-86932] p 86 N85-19136
Parametric evaluation of ball milling of SiC in water
[NASA-TM-86974] p 88 N85-21356
Radiographic detectability limits for seeded voids in sintered silicon carbide and silicon nitride
[NASA-TM-86945] p 138 N85-21674
Reliability of void detection in structural ceramics using scanning laser acoustic microscopy
[NASA-TM-87035] p 138 N85-32337
KLANN, G. A.
Temperature distortion generator for turboshaft engine testing
[SAE PAPER 841541] p 15 A85-39065
Temperature distortion generator for turboshaft engine testing
[NASA-TM-83748] p 1 N85-15658
Experimental and analytical study of ceramic-coated turbine-tip shroud seals for small turbine engines
[NASA-TM-86881] p 25 N85-18057
Experimental study of ceramic coated tip seals for turbojet engines
[NASA-TM-86939] p 114 N85-19363
KLEMETSON, R. W.
An evaluation of oxygen/hydrogen propulsion systems for the Space Station
[AIAA PAPER 85-1156] p 45 A85-43976
An evaluation of oxygen-hydrogen propulsion systems for the Space Station
[NASA-TM-87059] p 52 N85-28971
KLIMA, S. J.
NDE for heat engine ceramics
[NASA-TM-86949] p 137 N85-20389
Reliability of void detection in structural ceramics using scanning laser acoustic microscopy
[NASA-TM-87035] p 138 N85-32337
KMIEC, T. D.
Design and analysis report for the RL10-2B breadboard low thrust engine
[NASA-CR-174857] p 48 N85-19020
KNIGHT, G. L.
Energy efficient engine. High pressure compressor detail design report
[NASA-CR-165558] p 23 N85-10998
KNOTT, P. R.
Experimental investigation of shock-cell noise reduction for single stream nozzles in simulated flight
[NASA-CR-3845] p 175 N85-13550
KOCH, C. C.
Energy efficient engine. High pressure compressor detail design report
[NASA-CR-165558] p 23 N85-10998
KOCIMSKI, S. M.
Apparatus and method for identification of matrix materials in which transuranic elements are embedded using thermal neutron capture gamma-ray emission
[DE85-011659] p 125 N85-33454
KOHL, F. J.
Reactions of NaCl with gaseous SO3, SO2, and O2 p 59 A85-11897
Chemical reactions involved in the initiation of hot corrosion of IN-738 p 66 A85-31688
Airfoil deposition model p 21 N85-10979
KOMATSU, G.
High frequency plasma generator for ion thrusters
[NASA-CR-174772] p 48 N85-17023
KORKAN, K. D.
Analytical determination of propeller performance degradation due to ice accretion
[AIAA PAPER 85-0339] p 14 A85-20867
Experimental aerodynamic characteristics of an NACA 0012 airfoil with simulated ice p 12 A85-21844
Performance degradation of helicopter rotor in forward flight due to ice p 11 A85-42937
KOVACH, A. J.
Engineering model system study for a regenerative fuel cell: Study report
[NASA-CR-174801] p 158 N85-16292
KRAITCHMAN, M. D.
Environmental effects on the tensile strength of chemically vapor deposited silicon carbide fibers
[NASA-TM-86981] p 89 N85-24000
KRATOCHVIL, D.
Satellite provided customer promises services, a forecast of potential domestic demand through the year 2000. Volume 4: Sensitivity analysis
[NASA-CR-174662] p 99 N85-27092
KREIDER, K. G.
Advanced thin film thermocouples
[NASA-CR-175541] p 124 N85-21607
KRETCH, B. E.
Perturbation-iteration theory for analyzing microwave striplines
[NASA-CR-176189] p 100 N85-35321
KUCHAR, A. P.
Energy efficient engine ICLS Nacelle detail design report
[NASA-CR-167870] p 22 N85-10993
KUMM, E. L.
Feasibility demonstration of a novel, flat-belt, continuously variable transmission or automotive and electric-hybrid vehicle application
[NASA-CR-174430] p 185 N85-19894
KUNG, J.
Sixty GHz IMPATT diode development
[NASA-CR-174969] p 105 N85-33293
KUNIK, W. G.
Analytical modeling of circuit aerodynamics in the new NASA Lewis Altitude Wind Tunnel
[AIAA PAPER 85-0380] p 3 A85-26389
Analytical modeling of circuit aerodynamics in the new NASA Lewis wind tunnel
[NASA-TM-86912] p 8 N85-15688
KUNTZ, H. L.
Oscillatory conductive heat transfer for a fiber in an ideal gas p 109 A85-26077
KURTH, R.
Composite loads spectra for select space propulsion structural components: Probabilistic load model development p 148 N85-27954
KURTH, W. S.
Effects of chemical releases by the STS 3 orbiter on the ionosphere p 166 A85-29538
KUSAKA, T.
Humidity effects on adhesion of nickel-zinc ferrite in elastic contact with magnetic tape and itself
[NASA-TP-2449] p 88 N85-21359
KUTNEY, J. T., JR.
Energy efficient engine. Fan and quarter-stage component performance report
[NASA-CR-168070] p 33 N85-34141
KWATRA, S. C.
An allpass filter design for luminance and chrominance separation of NTSC signals p 102 A85-28230
Modeling of NASA's 30/20 GHz satellite communications system p 38 A85-36663

L

LACKNEY, J.
On the development of hierarchical solution strategies for nonlinear finite element formulations p 171 A85-21979
LAFLEN, J. H.
Considerations for damage analysis of gas turbine hot section components
[ASME PAPER 84-PVP-77] p 14 A85-18792
Unified constitutive material models for nonlinear finite-element structural analysis
[AIAA PAPER 85-1418] p 142 A85-39769
Unified constitutive material models for nonlinear finite-element structural analysis
[NASA-TM-86985] p 146 N85-24338
LAKSHMINARAYANA, B.
Computation of viscous flows in turbomachinery cascades p 106 A85-11631
Computation and turbulence closure models for shear flows in rotating curved bodies p 107 A85-14349
A space-marching method for incompressible Navier-Stokes equations
[AIAA PAPER 85-0170] p 108 A85-19564
Computation of three-dimensional viscous flows using a space-marching method p 4 A85-29259
Turbulence modelling for complex shear flows
[AIAA PAPER 85-1652] p 111 A85-40752
LAM, P. T.
On the calculation of the directivity of planar array feeds for satellite reflector applications p 97 A85-32249
LAM, P. T. C.
Focal shifts in parabolic reflectors p 97 A85-39356
LAMB, J. D.
Dielectric properties of 'diamondlike' carbon prepared by RF plasma deposition p 182 A85-38192
'Diamondlike' carbon films - Optical absorption, dielectric properties, and hardness dependence on deposition parameters p 82 A85-40383
LAMBERT, R. F.
Acoustic structure and propagation in highly porous, layered, fibrous materials p 173 A85-12301
LAN, B. Y.
Chemistry of fuel deposits and sediments and their predursors
[NASA-CR-174778] p 92 N85-10209
LANCE, J. R.
Fuel cell power plant economic and operational considerations
[ASME PAPER 84-AES-7] p 154 A85-21297
LANFORD, W. A.
Plasma deposited hydrogenated carbon on GaAs and InP p 182 A85-40386
Plasma deposited diamondlike carbon on GaAs and InP
[NASA-TM-86870] p 183 N85-10844
Optical properties of hydrogenated amorphous carbon films grown from methane plasma
[NASA-TM-86995] p 183 N85-26406
LANG, T.
General approaches for achieving high speed computations p 169 A85-28628
Functional language and data flow architectures p 170 A85-28629
LANKFORD, J.
Sliding seal materials for adiabatic engines
[NASA-CR-174893] p 89 N85-22757
LARK, R. F.
Hygrothermomechanical evaluation of transverse filament tape epoxy/polyester fiberglass composites p 54 A85-15632
Fabrication and quality assurance processes for superhybrid composite fan blades
[NASA-TM-83354] p 57 N85-14882
LASSOW, E. S.
Experimental and analytical study of ceramic-coated turbine-tip shroud seals for small turbine engines
[NASA-TM-86881] p 25 N85-18057
Experimental study of ceramic coated tip seals for turbojet engines
[NASA-TM-86939] p 114 N85-19363

LAUER, J. L.
Topological reaction rate measurements related to scuffing p 64 A85-11070
Characterization of lubricated bearing surfaces operated under high loads
[NASA-TM-86964] p 88 N85-21357
LAUF, R. J.
Dispersed metal-toughened ceramics and ceramic brazing
[NASA-CR-174284] p 86 N85-15916
LAUGHLIN, P. J.
Transferring data oscilloscope to an IBM using an Apple II+ p 168 A85-24526
LAUVER, R. W.
Effect of substituted phenylnadimides on processing and properties of PMR polyimide composites
[NASA-TM-86902] p 85 N85-14929
Chemical approach for controlling nadimide cure temperature and rate with maleimide
[NASA-CASE-LEW-13770-3] p 87 N85-21350
Chemical approach for controlling nadimide cure temperature and rate with maleimide
[NASA-CASE-LEW-13770-4] p 87 N85-21351
Chemical approach for controlling nadimide cure temperature and rate
[NASA-CASE-LEW-13770-5] p 87 N85-21352
Chemical control of nadimide cure temperature and rate
[NASA-CASE-LEW-13770-2] p 63 N85-28982
Chemical approach for controlling nadimide cure temperature and rate
[NASA-CASE-LEW-13770-6] p 63 N85-30039
LAVASH, J. P.
Energy Efficient Engine (E3) controls and accessories detail design report
[NASA-CR-168017] p 31 N85-29957
LAVIN, S. P.
Comparison of scaled model data to full size energy efficient engine test results
[AIAA PAPER 84-2281] p 13 A85-13953
Measurement and prediction of Energy Efficient Engine noise
[AIAA PAPER 84-2284] p 13 A85-13954
LAWLER, J. S.
Experimental investigation of a variable speed constant frequency electric generating system from a utility perspective
[NASA-CR-174950] p 105 N85-32251
LAWRENCE, C.
The use of an optical data acquisition system for bladed disk vibration analysis
[NASA-TM-86891] p 144 N85-15184
LAXMANAN, V.
Dendritic solidification. III - Some further refinements to the model for dendritic growth under an imposed thermal gradient p 69 A85-44703
LAXMANN, V.
Dendritic solidification. I - Analysis of current theories and models. II - A model for dendritic growth under an imposed thermal gradient p 182 A85-38019
LAYNE, J. L.
An investigation of enhanced capability thermal barrier coating systems for diesel engine components
[NASA-CR-174820] p 86 N85-18154
LEACH, K. P.
Energy efficient engine high-pressure turbine component rig performance test report
[NASA-CR-168189] p 30 N85-29955
LEDBETTER, F. E., III
Preparation of silicon carbide-silicon nitride fibers by the pyrolysis of polycarbosilazane precursors
[NASA-TM-86505] p 91 N85-28107
LEE, C. S.
Plot of modal field distribution in rectangular and circular waveguides p 101 A85-25170
Numerical methods for analyzing electromagnetic scattering
[NASA-CR-175507] p 99 N85-21438
Normal modes in an overmoded circular waveguide coated with lossy material
[NASA-CR-176186] p 100 N85-35320
LEE, F. C.
A fast time domain digital simulation technique for power converters - Application to a buck converter with feedforward compensation p 101 A85-20900
LEE, F. C. Y.
The J3 SCR model applied to resonant converter simulation p 102 A85-42156
LEE, R. Q.
Case study of sample spacing in planar near-field measurement of high gain antennas
[NASA-TM-86872] p 97 N85-10234
LEE, S. S.
Stress waves in an isotropic elastic plate excited by a circular transducer
[NASA-CR-3877] p 138 N85-20390
Application of homomorphic signal processing to stress wave factor analysis
[NAS 1.26:174871] p 138 N85-21673
Ultrasonic testing of plates containing edge cracks
[NASA-CR-3904] p 138 N85-29307
LEE, S. W.
Plot of modal field distribution in rectangular and circular waveguides p 101 A85-25170
Numerical methods for analyzing electromagnetic scattering
[NASA-CR-175507] p 99 N85-21438
Normal modes in an overmoded circular waveguide coated with lossy material
[NASA-CR-176186] p 100 N85-35320
LEE, S.-W.
Focal shifts in parabolic reflectors p 97 A85-39356
LEESE, G. E.
Multiaxial and thermomechanical fatigue considerations in damage tolerant design
[NASA-TM-87022] p 76 N85-26964
LEHTINEN, B.
The role of modern control theory in the design of controls for aircraft turbine engines p 13 A85-13627
LEI, C. K.
Heat transfer enhancement in channels with turbulence promoters
[ASME PAPER 84-WA/HT-72] p 111 A85-39900
LEIB, S. J.
Generation of capillary instabilities by external disturbances in a liquid jet
[NASA-TM-87041] p 117 N85-30246
LEIS, B. N.
A history dependent damage model for low cycle fatigue
[ASME PAPER 84-PVP-112] p 140 A85-18795
LEISSA, A. W.
Vibrations of twisted cantilevered plates - Summary of previous and current studies p 140 A85-22069
Vibrations of twisted cantilever plates - A comparison of theoretical results p 144 A85-47626
A study of internal and distributed damping for vibrating turbomachiner blades
[NASA-CR-175901] p 30 N85-27868
LEITMAN, M. J.
A procedure for obtaining explicit solutions to a class of Fredholm integral equations p 171 A85-28006
LEKAN, J.
Demand for satellite-provided domestic communications services up to the year 2000
[NASA-TM-86894] p 97 N85-15099
LEMKEY, F.
High temperature static strain sensor development program p 19 N85-10959
LEMOGNE, T.
Aluminum work function: Effect of oxidation, mechanical scraping and ion bombardment
[NASA-TM-87079] p 78 N85-34265
LEMON, D. D.
Fracture toughness of hot-pressed beryllium p 66 A85-25835
LENAHAN, D. T.
Energy efficient engine. Low pressure turbine test hardware detailed design report
[NASA-CR-167956] p 22 N85-10994
Energy efficient engine high pressure turbine test hardware detailed design report
[NASA-CR-167955] p 23 N85-10995
LEONARDO, M.
A stagnation pressure probe for droplet-laden air flow
[AIAA PAPER 85-0330] p 108 A85-19672
LEPICOVSKY, J.
An experimental study of tone excited heated jets
[AIAA PAPER 84-2341] p 172 A85-10882
Acoustic control of free jet mixing
[AIAA PAPER 85-0569] p 109 A85-25951
LERCH, B. A.
A study of fatigue damage mechanisms in Waspaloy from 25 to 800 C p 65 A85-12098
LEROY, B. E.
Alternatives for satellite sound broadcast systems at HF and VHF p 99 N85-23815
LEVINE, S. R.
Deposition stress effects on the life of thermal barrier coatings on burner rigs p 79 A85-19086
Surface protection overview p 21 N85-10978
LEVIS, C. A.
Engineering calculations for communications satellite systems planning
[NASA-CR-175552] p 37 N85-21233
LEVY, R.
Analytical modeling of circuit aerodynamics in the new NASA Lewis Altitude Wind Tunnel
[AIAA PAPER 85-0380] p 3 A85-26389
Analytical modeling of circuit aerodynamics in the new NASA Lewis wind tunnel
[NASA-TM-86912] p 8 N85-15688
LEWICKI, D. G.
Life and reliability modeling of bevel gear reductions
[NASA-TM-87006] p 133 N85-27227
Fatigue life analysis of a turboprop reduction gearbox
[NASA-TM-87014] p 133 N85-27228
LEWIS, C. R.
Magnesium doping of efficient GaAs and Ga(0.75)In(0.25)As solar cells grown by metalorganic chemical vapor deposition p 180 A85-11466
LIEBERMAN, M.
Jet fuel property changes and their effect on producibility and cost in the U.S., Canada, and Europe
[NASA-CR-174840] p 93 N85-27012
LIEBERT, C. H.
High temperature thermocouple and heat flux gauge using a unique thin film-hardware hot juncture
[NASA-TM-86898] p 123 N85-16096
Heat flux sensor calibrator p 41 N85-27970
LILLEY, D. G.
Flow visualization of lateral jet injection into swirling crossflow
[AIAA PAPER 85-0059] p 2 A85-19490
Swirling flows in typical combustor geometries
[AIAA PAPER 85-0184] p 108 A85-19574
Turbulence measurements of lateral jet injection into confined tubular crossflow
[AIAA PAPER 85-1102] p 110 A85-39604
Investigation of flowfields found in typical combustor geometries
[NASA-CR-3869] p 26 N85-21167
Deflected jet experiments in a turbulent combustor flowfield
[NASA-CR-174863] p 26 N85-22390
Confined turbulent swirling recirculating flow predictions
[NASA-CR-174917] p 29 N85-26716
Turbulence characteristics of swirling flowfields
[NASA-CR-174918] p 29 N85-26717
Predictions and measurements of isothermal flowfields in axisymmetric combustor geometries
[NASA-CR-174916] p 29 N85-27867
LILLEY, J. R., JR.
Three-dimensional calculation of shuttle charging in polar orbit p 40 N85-22486
LIM, H. S.
Long life nickel electrodes for a nickel-hydrogen cell. III - Results of an accelerated test and failure analyses p 156 A85-45391
The failure mechanism of a nickel electrode in a nickel-hydrogen cell p 105 N85-31408
LIMERICK, C. D.
Design and analysis report for the RL10-2B breadboard low thrust engine
[NASA-CR-174857] p 48 N85-19020
LIN, H. H.
Dynamic analysis of straight and involute tooth forms
[ASME PAPER 84-DET-226] p 128 A85-33780
LINDGREN, L. C.
Ceramic applications in turbine engines
[NASA-CR-174715] p 91 N85-28109
LINDHOLM, U. S.
Unified constitutive material models for nonlinear finite-element structural analysis
[AIAA PAPER 85-1418] p 142 A85-39769
Unified constitutive material models for nonlinear finite-element structural analysis
[NASA-TM-86985] p 146 N85-24338
A survey of unified constitutive theories p 150 N85-31531
LING, H.
Focal shifts in parabolic reflectors p 97 A85-39356
LING, J. S.
Evaluation of developmental membranes for the mixed reactant iron-chromium redox system
[NASA-TM-87074] p 164 N85-34443
LING, J. X.
A new interpretation of internal heat transfer coefficients of porous media
[ASME PAPER 84-WA/HT-51] p 110 A85-39894
LINSCOTT, B. S.
Government review of the Mod-2 wind turbine (as-built)
[NASA-TM-86983] p 162 N85-29365
The Federal Wind Program at NASA Lewis Research Center
[NASA-TM-83480] p 163 N85-30478
LITTLE, J. K.
Experimental and analytical study of ceramic-coated turbine-tip shroud seals for small turbine engines
[NASA-TM-86881] p 25 N85-18057
Ribbon burner simulation of T-700 turbine shroud for ceramic lined seals research
[NASA-TM-86940] p 114 N85-19364

LITVIN, F. L.
Spiral bevel and circular arc helical gears: Tooth contact analysis and the effect of misalignment on circular arc helical gears
[NASA-TM-87013] p 32 N85-31060
Generated spiral bevel gears: Optimal machine-tool settings and tooth contact analysis
[NASA-TM-87075] p 136 N85-34405
LIU, D. C.
'Diamondlike' carbon films - Optical absorption, dielectric properties, and hardness dependence on deposition parameters p 82 A85-40383
Plasma deposited hydrogenated carbon on GaAs and InP p 182 A85-40386
Plasma deposited diamondlike carbon on GaAs and InP
[NASA-TM-86870] p 183 N85-10844
Effect of interfacial characteristics of metal clad polymeric substrates on electrical high frequency interconnection performance
[NASA-TM-86948] p 99 N85-20223
Optical properties of hydrogenated amorphous carbon films grown from methane plasma
[NASA-TM-86995] p 183 N85-26406
LIU, H. S.
High pressure compressor component performance report
[NASA-CR-168245] p 33 N85-34138
LIU, W. K.
Probabilistic finite element: Variational theory p 149 N85-27957
LIVER, P.
Flow control in a diffusing S-Duct
[AIAA PAPER 85-0524] p 3 A85-25928
LO, Y. T.
The study of microstrip antenna arrays and related problems
[NASA-CR-174054] p 97 N85-11265
Numerical methods for analyzing electromagnetic scattering
[NASA-CR-175507] p 99 N85-21438
LOCK, J. A.
Incident beam polarization for laser Doppler velocimetry employing a sapphire cylindrical window p 122 A85-39835
Incident beam polarization for laser Doppler velocimetry employing a sapphire cylindrical window
[NASA-TM-87064] p 178 N85-28786
LOEWENTHAL, S. H.
Operating characteristics of a 0.87 kW-hr flywheel energy storage module
[NASA-TM-87038] p 133 N85-28371
Application of traction drives as servo mechanisms p 152 N85-33520
LOH, J.
Configuration study for a 30 GHz monolithic receive array: Technical assessment
[NASA-CR-174697] p 98 N85-18238
Configuration study for a 30 GHz monolithic receive array, volume 1
[NASA-CR-174697-VOL-1] p 98 N85-18239
Configuration study for a 30 GHz monolithic receive array, volume 2
[NASA-CR-174697-VOL-2] p 99 N85-18240
LORIA, J. C.
The NASA photovoltaic technology program p 155 A85-35604
LOTTIG, R. A.
Altitude testing of a flight weight, self-cooled, 2D thrust vectoring exhaust nozzle
[SAE PAPER 841557] p 14 A85-25984
LOVELL, R. C.
High pressure compressor component performance report
[NASA-CR-168245] p 33 N85-34138
LU, C. Y.
Manual of phosphoric acid fuel cell power plant optimization model and computer program
[NASA-CR-174721] p 157 N85-10445
Manual of phosphoric acid fuel cell stack three-dimensional model and computer program
[NASA-CR-174722] p 157 N85-10447
Phosphoric acid fuel cell power plant system performance model and computer program
[NASA-CR-174638] p 157 N85-11456
LU, S.-L.
A functional language approach in high-speed digital simulation p 170 A85-28615
LUDEMANN, S. G.
Large-scale advanced propfan (LAP) program progress report
[AIAA PAPER 85-1187] p 17 A85-47021
Large-scale Advanced Propfan (LAP) program
[NASA-TM-87067] p 32 N85-29964
LUH, H.
The 20 GHz proof-of-concept test model results for a multiple scan beam dual reflector antenna
[NASA-CR-174268] p 98 N85-15944
LUNDQUIST, C. A.
Report of the Constellations Panel p 131 N85-20368

M

MA, Y. E.
Sixty GHz IMPATT diode development
[NASA-CR-174969] p 105 N85-33293
MACBAIN, J. C.
Vibrations of twisted cantilevered plates - Summary of previous and current studies p 140 A85-22069
Vibrations of twisted cantilever plates - A comparison of theoretical results p 144 A85-47626
MACKAY, R. A.
Factors which influence directional coarsening of gamma-prime during creep in nickel-base superalloy single crystals p 67 A85-32388
Morphological changes of gamma prime precipitates in nickel-base superalloy single crystals
[NASA-TM-83698] p 70 N85-10165
MACKIN, M. A.
Floating-point function generation routines for 16-bit microcomputers
[NASA-TM-83783] p 170 N85-10683
MAEDA, C.
Humidity effects on adhesion of nickel-zinc ferrite in elastic contact with magnetic tape and itself
[NASA-TP-2449] p 88 N85-21359
MAFFEO, R. J.
A computer analysis program for interfacing thermal and structural codes
[NASA-TM-87021] p 148 N85-27264
MAHAN, J. R.
The influence of combustion liner holes on noise production by ducted burners
[AIAA PAPER 84-2322] p 172 A85-10869
MAISEL, J. E.
A historical overview of the electrical power systems in the US manned and some US unmanned spacecraft
[NASA-CR-174806] p 47 N85-13910
MAJJIGI, R. K.
Experimental investigation of shock-cell noise reduction for dual-stream nozzles in simulated flight
[NASA-CR-3846] p 175 N85-13549
Development of a rotor wake-vortex model, volume 1
[NASA-CR-174849] p 9 N85-26668
MAKOUI, A.
Data flow methods for dynamic system simulation - A CSSL-IV microcomputer network interface p 170 A85-28614
MALAK, M.
The three-dimensional compressible flow in a radial inflow turbine scroll p 6 A85-41826
MALIK, S.
The mechanisms of flame holding in the wake of a bluff body
[NASA-CR-174058] p 62 N85-11149
The mechanisms of flame holding in the wake of a bluff body
[NASA-CR-3866] p 26 N85-21166
MANDELL, J. F.
Structural characteristics of high temperature composites
[NASA-CR-175998] p 58 N85-30037
MANDELL, M. J.
Computer simulation of plasma electron collection by PIX-II
[AIAA PAPER 85-0386] p 43 A85-19715
Three-dimensional calculation of shuttle charging in polar orbit p 40 N85-22486
Polar orbit electrostatic charging of objects in shuttle wake p 40 N85-22487
Surface interactions and high-voltage current collection p 40 N85-22493
NASCAP simulation of PIX 2 experiments p 180 N85-22497
MANDERSCHEID, J. M.
Cyclic structural analyses of anisotropic turbine blades for reusable space propulsion systems
[NASA-TM-86990] p 146 N85-24339
Cyclic structural analyses of SSME turbine blades p 150 N85-27963
MANGANO, M. J.
Report of the Constellations Panel p 131 N85-20368
MANGELS, J. A.
Fracture of yttria-doped, sintered reaction-bonded silicon nitride
[ACS PAPER 7-J3-84] p 82 A85-42797
MANSON, S. S.
Reexamination of cumulative fatigue damage laws p 149 N85-27962
MANTENIEKS, M.
Performance capabilities of the 12-centimeter Xenon ion thruster p 42 A85-16439
MANZO, M. A.
Teardown analysis of a ten cell bipolar nickel-hydrogen battery p 156 A85-45385
Separator development and testing of nickel-hydrogen cells p 156 A85-45386
A 37.5-kW point design comparison of the nickel-cadmium battery, bipolar nickel-hydrogen battery, and regenerative hydrogen-oxygen fuel cell energy storage subsystems for low earth orbit p 46 A85-45387
Advanced designs for IPV nickel-hydrogen cells p 156 A85-45438
Initial performance of advanced designs for IPV nickel-hydrogen cells p 105 N85-31404
Design principles for nickel-hydrogen cells and batteries
[NASA-TM-87037] p 164 N85-31646
MAPLES, B. W.
Modeling of NASA's 30/20 GHz satellite communications system p 38 A85-36663
MARAM, J. M.
Feasibility of mapping velocity flow fields in SSME powerhead by laser anemometry techniques p 41 N85-27971
MARBLE, F. E.
Growth of a diffusion flame in the field of a vortex p 61 A85-47320
MARCHAND, N.
Thermal-mechanical fatigue crack growth in Inconel X-750
[NASA-CR-174740] p 72 N85-15877
MAREK, C. J.
Combustor turbulence p 118 N85-31434
MARINO, D.
Homogeneity of pristine and bromine intercalated graphite fibers
[NASA-TM-87016] p 89 N85-25521
MARK, W. D.
Turbofan noise generation. Volume 2: Computer programs
[NASA-CR-167952] p 175 N85-11791
MARSIK, S. J.
Advanced research and technology programs for advanced high-pressure oxygen-hydrogen rocket propulsion
[NASA-TM-86969] p 37 N85-21231
MARTIN, C. H.
Engineering calculations for communications satellite systems planning
[NASA-CR-175552] p 37 N85-21233
MARTIN, J. F.
Closed-loop strain controlled testing at elevated temperatures with a non-contacting gage p 121 A85-29562
A comparison of smooth specimen and analytical simulation techniques for notched members at elevated temperatures p 151 N85-31546
MARTIN, M. R.
Development of a multiplane multispeed balancing system for turbine systems
[NASA-CR-174750] p 35 N85-22400
MARTIN, R. E.
Regenerative fuel cell energy storage system for a low Earth orbit space station
[NASA-CR-174802] p 158 N85-13371
Long-life high performance fuel cell program
[NASA-CR-174874] p 50 N85-25384
MARTZ, J. E.
Operational performance of the photovoltaic-powered grain mill and water pump at Tangaye, Burkina Faso (formerly Upper Volta)
[NASA-TM-86970] p 161 N85-23243
MARXER, N.
Characterization of lubricated bearing surfaces operated under high loads
[NASA-TM-86964] p 88 N85-21357
MATHUR, G.
Heat treatment of bulk gallium arsenide using a phosphosilicate glass cap p 181 A85-32636
Fabrication of p(+)-n junction GaAs solar cells by a novel method p 181 A85-33645
MATSUMURA, M.
A unified relation for cavitation erosion p 109 A85-24445
MATTHEWS, E. W.
The 20 GHz proof-of-concept test model results for a multiple scan beam dual reflector antenna
[NASA-CR-174268] p 98 N85-15944
MATTOX, D. M.
Properties of coated and modified surfaces p 53 A85-36694

MAUGER, A.
Substrate-induced orientational order in the isotropic phase of liquid crystals p 181 A85-24649
MAURER, G. A.
Effects of tin on microstructure and mechanical behavior of Inconel 718
[NASA-TM-86866] p 71 N85-12129
MAYER, H. L.
Report of the Constellations Panel
p 131 N85-20368
MAYO, F. R.
Chemistry of fuel deposits and sediments and their predursors
[NASA-CR-174778] p 92 N85-10209
MAZARIS, G. A.
Screen printed interdigitated back contact solar cell
[NASA-CASE-LEW-13414-1] p 160 N85-20530
MCBRIDE, B.
Computer program for calculation of complex chemical equilibrium compositions and applications. Supplement 1: Transport properties
[NASA-TM-86885] p 184 N85-16663
MCBRIDE, B. J.
Combustion gas properties I-ASTM jet A fuel and dry air
[NASA-TP-2359] p 17 N85-10064
Modeling the internal combustion engine
[NASA-RP-1094] p 172 N85-19733
Combustion gas properties. 2: Natural gas fuel and dry air
[NASA-TP-2435] p 26 N85-21168
Ideal gas thermodynamic properties for the phenyl, phenoxy, and o-biphenyl radicals
[NASA-TM-83800] p 184 N85-22204
Combustion gas properties. Part 3: Hydrogen gas fuel and dry air
[NASA-TP-2477] p 32 N85-31058
MCDANELS, D. L.
Analysis of stress-strain, fracture, and ductility behavior of aluminum maxtrix composites containing discontinuous silicon carbide reinforcement p 55 A85-37421
MCDANIEL, O. H.
The performance of jet noise suppression devices for industrial applications p 175 A85-42563
MCDONALD, G.
Plastic flow of plasma sprayed ceramics
p 80 A85-24161
Experimental study of ceramic coated tip seals for turbojet engines
[NASA-TM-86939] p 114 N85-19363
Ribbon burner simulation of T-700 turbine shroud for ceramic lined seals research
[NASA-TM-86940] p 114 N85-19364
Metallic and metalloceramic coating by thermal decomposition
[NASA-TM-86992] p 88 N85-22755
Film and interstitial formation of metals in plasma-sprayed ceramics
[NASA-TM-86993] p 89 N85-22756
Fabrication of ceramic substrate-reinforced and free forms
[NASA-TM-86994] p 50 N85-23926
MCDONALD, G. E.
Experimental and analytical study of ceramic-coated turbine-tip shroud seals for small turbine engines
[NASA-TM-86881] p 25 N85-18057
MCFADDEN, G. B.
Convective influence on the stability of a cylindrical solid-liquid interface p 109 A85-26911
MCFARLAND, E. R.
Design and performance of a fixed, nonaccelerating guide vane cascade that operates over an inlet flow angle range of 60 deg
[ASME PAPER 84-GT-75] p 4 A85-32964
MCGAW, M. A.
A comparison of two contemporary creep-fatigue life prediction methods p 151 N85-31538
MCHENRY, M.
Experimental study of ceramic coated tip seals for turbojet engines
[NASA-TM-86939] p 114 N85-19363
MCINTOSH, G. E.
A rotating superconducting solenoid for 100 kWh energy storage p 44 A85-33144
MCKEVITT, F. X.
Performance characterization tests of a 1-kW resistojet using hydrogen, nitrogen and ammonia as propellants
[AIAA PAPER 85-1159] p 44 A85-39628
MCKNIGHT, R. C.
Icing flight research - Aerodynamic effects of ice and ice shape documentation with stereo photography
[AIAA PAPER 85-0468] p 11 A85-30192
Initial feasibility ground test of a proposed photogrammetric system for measuring the shapes of ice accretions on helicopter rotor blades during forward flight
[NASA-TM-87391] p 12 N85-12887
Icing flight research: Aerodynamic effects of ice and ice shape documentation with stereo photography
[NASA-TM-86906] p 12 N85-18049
MCKNIGHT, R. L.
Component-specific modeling
[NASA-CR-174765] p 147 N85-27261
Component-specific modeling
[NASA-CR-174925] p 32 N85-32119
Component-specific modeling
[NASA-CR-174765] p 33 N85-34140
MCLALLIN, K. L.
Application of viscous and inviscid computation methods for rocket turbopump systems
[SAE PAPER 841522] p 110 A85-39257
Analytical study of flow phenomena in SSME turnaround duct geometries p 116 N85-26902
MCMURTRY, P. A.
Direct numerical simulations of a reacting mixing layer with chemical heat release
[AIAA PAPER 85-0143] p 60 A85-19548
MCNALLY, W. D.
Review - Computational methods for internal flows with emphasis on turbomachinery p 4 A85-29126
MEHALIC, C. M.
Effect of combined pressure and temperature distortion orientation on high-bypass-ratio turbofan engine stability
[NASA-TM-83771] p 17 N85-10067
Effect of steady-state temperature distortion on inlet flow to a high-bypass-ration turbofan engine
[NASA-TM-86896] p 24 N85-15725
MEHANDRU, S. P.
Dopant effect of yttrium and the growth and adherence of alumina on nickel-aluminum alloys p 82 A85-40973
Mechanism for chelated sulfate formation from SO2 and bis (triphenylphosphine) platinum p 62 A85-48493
Why CO bonds side-on at low coverage and both side-on and upright at high coverage on the Cr(110) surface
[NASA-CR-176071] p 77 N85-32173
Adsorption of O2, SO2, and SO3 on nickel oxide. Mechanism for sulfate formation
[NASA-CR-176072] p 77 N85-32175
CO adsorption on (111) and (100) surfaces of the Pt sub 3 Ti alloy. Evidence for parallel binding and strong activation of CO
[NASA-CR-176077] p 77 N85-32176
MEHTA, H. K.
Detailed studies of aviation fuel flowability
[NASA-CR-174938] p 94 N85-31308
MEHTA, S.
Radiation damage and defect behavior in ion-implanted, lithium counterdoped silicon solar cells
p 182 A85-35698
The effects of lithium counterdoping on radiation damage and annealing in n(+)p silicon solar cells
p 50 N85-22586
MEIRON, D. I.
The linear two-dimensional stability of inviscid vortex streets of finite-cored vortices
[AD-A153032] p 107 A85-14241
MELCHER, K. J.
DEAN: A program for dynamic engine analysis
[NASA-TM-87033] p 30 N85-28945
MELNIK, R. E.
The computation of viscid/inviscid interaction on airfoils with separated flow p 6 A85-42954
MERRILL, W.
The role of modern control theory in the design of controls for aircraft turbine engines p 13 A85-13627
Identification of multivariable high-performance turbofan engine dynamics from closed-loop data
p 13 A85-13630
MERRILL, W. C.
Sensor failure detection for jet engines using analytical redundancy
[AIAA PAPER 84-1452] p 13 A85-16097
MERUTKA, J.
Effects of surface chemistry on hot corrosion life: Overview p 21 N85-10980
METCALFE, R. W.
Direct numerical simulations of a reacting mixing layer with chemical heat release
[AIAA PAPER 85-0143] p 60 A85-19548
Direct simulations of chemically reacting turbulent mixing layers
[AIAA PAPER 85-0321] p 60 A85-19666
METZ, R. N.
Circuit transients due to negative bias arcs on a high-voltage solar array in low Earth orbit
[NASA-TP-2407] p 39 N85-14858
MEYERS, G. D.
Experiments in dilution jet mixing - Effects of multiple rows and non-circular orifices
[AIAA PAPER 85-1104] p 15 A85-39606
Experiments in dilution jet mixing effects of multiple rows and non-circular orifices
[NASA-TM-86996] p 28 N85-25266
MEYN, E. H.
The use of an optical data acquisition system for bladed disk vibration analysis
[NASA-TM-86891] p 144 N85-15184
MICHAELS, K. B.
Regenerative fuel cell energy storage system for a low Earth orbit space station
[NASA-CR-174802] p 158 N85-13371
MICHEL, R. W.
Vehicle/engine integration p 37 N85-17008
MIESKOWSKI, D. M.
Strength and microstructure of sintered Si3N4 with rare-earth-oxide additions
[ACS PAPER 130-13-84] p 80 A85-25271
Oxidation of silicon nitride sintered with rare-earth oxide additions p 83 A85-42798
Microstructure of reaction-bonded silicon nitride consolidated by isostatic hot-pressing
p 83 A85-45304
Reliability of two sintered silicon nitride materials
[NASA-TM-87092] p 92 N85-34284
MIKKELSEN, K. L.
Icing flight research - Aerodynamic effects of ice and ice shape documentation with stereo photography
[AIAA PAPER 85-0468] p 11 A85-30192
Icing flight research: Aerodynamic effects of ice and ice shape documentation with stereo photography
[NASA-TM-86906] p 12 N85-18049
MILES, G. A.
Analytical fuel property effects--small combustors
[NASA-CR-174738] p 28 N85-26709
MILLAN, P. P.
Progress in the utilization of an oxide-dispersion-strengthened alloy for small engine turbine blades
[SAE PAPER 841512] p 68 A85-39284
MILLARD, M. L.
Effect of hot isostatic pressing on reaction-bonded silicon nitride p 79 A85-15195
Evaluation of alpha-SiC sintering using statistical methods p 83 A85-42800
Effect of hot isostatic pressing on the properties of sintered alpha silicon carbide p 83 A85-48757
MILLER, C. J.
Noise constraints effecting optimal propeller designs
[SAE PAPER 850871] p 7 A85-50106
Noise constraints effecting optimal propeller designs
[NASA-TM-86967] p 8 N85-19923
MILLER, D. L.
Transferring data oscilloscope to an IBM using an Apple II+ p 168 A85-24526
MILLER, D. R.
Aileron controls for wind turbine applications
p 157 A85-45513
Aileron controls for wind turbine applications
[NASA-TM-86867] p 158 N85-11458
Shutdown characteristics of the Mod-O wind turbine with aileron controls
[NASA-TM-86918] p 159 N85-16299
Analytical model for predicting emergency shutdown of a two-bladed horizontal axis wind turbine
[NASA-TM-83472] p 162 N85-30476
MILLER, E. F.
Technical characteristics of the broadcasting satellite plan at 12 GHz for the Western Hemisphere
p 96 A85-28233
Development and use of the computer software package for planning the 12 GHz broadcasting-satellite service at RARC '83 p 96 A85-29605
MILLER, L. A.
Preliminary analysis of space mission applications for electromagnetic launchers
[NASA-CR-174067] p 35 N85-12071
MILLER, R. A.
Oxidation-based model for thermal barrier coating life
p 78 A85-10310
Performance of thermal barrier coatings in high heat flux environments p 79 A85-19087
Life modeling of atmospheric and low pressure plasma-sprayed thermal-barrier coating
p 81 A85-29728
Mechanical property measurements of plasma-sprayed thermal-barrier coatings subjected to oxidation
p 81 A85-29729
MILLER, T. B.
Design considerations for a 10-kW integrated hydrogen-oxygen regenerative fuel cell system
p 155 A85-45380

MILLER, T. L.
Analytical determination of propeller performance degradation due to ice accretion
[AIAA PAPER 85-0339] p 14 A85-20867
MILLER, W. L.
An investigation of arc discharging on negatively biased dielectric conductor samples in a plasma
p 180 N85-22498
MILLIGAN, W. W.
Low cycle fatigue of MAR-M 200 single crystals at 760 and 870 deg C
[NASA-TM-86933] p 74 N85-19074
MILLNER, A. R.
Microprocessor control of photovoltaic systems
p 156 A85-45408
MILLS, D. L.
Substrate-induced orientational order in the isotropic phase of liquid crystals p 181 A85-24649
MINER, R. V.
On the fatigue crack propagation behavior of superalloys at intermediate temperatures p 68 A85-32434
The effects of seven alloying elements on the microstructure and stress-rupture behavior of nickle-base superalloys
[NASA-TM-83791] p 70 N85-10168
Orientation and temperature dependence of some mechanical properties of the single-crystal nickel-base superalloy Rene N4. 3: Tension-compression anisotropy
[NASA-TM-86982] p 76 N85-22660
MINNIN, W. A.
Advanced 30/20 GHz multiple beam antenna for future communications satellites p 96 A85-14436
MIRTICH, M. J.
Deposition of diamondlike carbon films
[NASA-CASE-LEW-14080-1] p 95 N85-20153
Ion beam sputter-deposited thin film coatings for protection of spacecraft polymers in low Earth orbit
[NASA-TM-87051] p 91 N85-30137
Diamondlike carbon protective coatings for IR materials
[NASA-TM-87083] p 178 N85-34631
MISHINA, H.
Effect of barrier height on friction behavior of the semiconductors silicon and gallium arsenide in contact with pure metals
[NASA-TP-2405] p 84 N85-13044
MISRA, A. K.
Effects of SO2 and SO3 on the Na2SO4 induced corrosion of nickel p 65 A85-15603
Studies on the hot corrosion of a nickel-base superalloy, Udimet 700
[NASA-TM-86882] p 71 N85-11224
MITCHELL, A. M.
Transmission efficiency measurements and correlations with physical characteristics of the lubricant
p 89 N85-23781
MITCHELL, B.
Configuration study for a 30 GHz monolithic receive array: Technical assessment
[NASA-CR-174697] p 98 N85-18238
Configuration study for a 30 GHz monolithic receive array, volume 1
[NASA-CR-174697-VOL-1] p 98 N85-18239
Configuration study for a 30 GHz monolithic receive array, volume 2
[NASA-CR-174697-VOL-2] p 99 N85-18240
MITTRA, R.
Characterization of MMIC devices for active array antennas
[NASA-TM-86907] p 38 N85-15779
MMIC devices for active phased array antennas
[NASA-CR-174281] p 98 N85-15943
Characterization of microstrip discontinuities in the time and frequency domains
[NASA-CR-176190] p 106 N85-35342
MIYAKE, C. I.
Performance characterization tests of a 1-kW resistojet using hydrogen, nitrogen and ammonia as propellants
[AIAA PAPER 85-1159] p 44 A85-39628
MIYOSHI, K.
Friction and wear of some ferrous-base metallic glasses p 64 A85-11071
Mechanical-contact-induced transformation from the amorphous to the partially crystalline state in metallic glass p 65 A85-19084
Friction and wear of ceramics p 80 A85-23833
Ceramic wear in indentation and sliding contact
p 82 A85-39549
Fundamental tribological properties of ceramics
[NASA-TM-86915] p 85 N85-15893
Surface effects of corrosive media on hardness, friction, and wear of materials
[NASA-TM-83711] p 85 N85-15896
Tribological properties of boron nitride synthesized by ion beam deposition
[NASA-TM-86962] p 87 N85-21355
Humidity effects on adhesion of nickel-zinc ferrite in elastic contact with magnetic tape and itself
[NASA-TP-2449] p 88 N85-21359
Effects of wear on structure-sensitive magnetic properties of ceramic ferrite in contact with magnetic tape
[NASA-TM-87007] p 90 N85-26991
MOCK, E. A. T.
Advanced technology cogeneration system conceptual design study: Closed cycle gas turbines
[NASA-CR-168222] p 159 N85-16300
MOFFAT, R. J.
Heat transfer and turbulence measurements of a film-cooled flow over a convexly curved surface
p 112 A85-41787
MONGEAU, P. P.
Metal vapor arc switch electromagnetic accelerator technology
[NASA-CR-174380] p 103 N85-18259
MONGIA, H. C.
Jet characteristics in confined swirling flow
p 112 A85-45282
Density effects on jet characteristics in confined swirling flow p 112 A85-45283
MONKEWITZ, P. A.
The response of Helmholtz resonators to external excitation. I - Single resonators p 174 A85-26915
MONTES, H.
Aluminum work function: Effect of oxidation, mechanical scraping and ion bombardment
[NASA-TM-87079] p 78 N85-34265
MONTY, J. D.
Analytical fuel property effects: Small combustors, phase 2
[NASA-CR-174848] p 93 N85-19175
MOORE, F. K.
A theory of post-stall transients in multistage axial compression systems
[NASA-CR-3878] p 8 N85-21117
MOORE, J.
Thermodynamic evaluation of transonic compressor rotors using the finite volume approach
[NASA-CR-175811] p 29 N85-26712
MOORE, J. A.
Development of a lithium secondary battery separator
p 104 N85-31378
MOORE, T. J.
Effect of hot isostatic pressing on reaction-bonded silicon nitride p 79 A85-15195
Feasibility study of the welding of SiC
p 81 A85-39339
Diffusion welding of MA 6000 and a conventional nickel-base superalloy p 69 A85-43551
Effect of hot isostatic pressing on the properties of sintered alpha silicon carbide p 83 A85-48757
MOORHEAD, A. J.
Dispersed metal-toughened ceramics and ceramic brazing
[NASA-CR-174284] p 86 N85-15916
Dispersed-metal-toughened alumina
[NASA-CR-174687] p 89 N85-22758
MORACZ, D. J.
Energy efficient engine. Volume 2. Appendix A: Component development and integration program
[NASA-CR-173085] p 22 N85-10991
MORALES, W.
Formation of high molecular weight products from benzene during boundary lubrication
[NASA-TM-86966] p 62 N85-22644
MOREA, S. F.
Advanced research and technology programs for advanced high-pressure oxygen-hydrogen rocket propulsion
[NASA-TM-86969] p 37 N85-21231
MOREL, T.
Methods for heat transfer and temperature field analysis of the insulated diesel
[NASA-CR-174783] p 185 N85-16699
MORELL, L. J.
Moving target, distributed, real-time simulation using Ada p 170 A85-34131
MORENO, V.
Application of two creep fatigue life models for the prediction of elevated temperature crack initiation of a nickel base alloy
[AIAA PAPER 85-1420] p 69 A85-43979
Creep fatigue life prediction for engine hot section materials (isotropic)
[NASA-CR-168228] p 32 N85-31057
Two simplified procedures for predicting cyclic material response from a strain history p 151 N85-31543
MOREY, W. W.
Fiber optic temperature sensor p 121 A85-29563
MORRIS, J. F.
High thermal power density heat transfer apparatus providing electrical isolation at high temperature using heat pipes
[NASA-CASE-LEW-12950-2] p 117 N85-29179
MORRIS, P. J.
Acoustic control of free jet mixing
[AIAA PAPER 85-0569] p 109 A85-25951
MORTON, H. L.
Analytical fuel property effects: Small combustors, phase 2
[NASA-CR-174848] p 93 N85-19175
MOSCARELLO, R.
Pantographing self adaptive gap elements
p 142 A85-37440
MOSTAFA, A.
A two-equation turbulence model for two-phase jets
p 107 A85-14376
MUCKLEY, E. T.
Shuttle/Centaur project perspective
p 37 N85-16991
MULAC, R. A.
Simulation of multistage turbine flows
p 116 N85-27945
MULARZ, E. J.
Future fundamental combustion research for aeropropulsion systems
[AIAA PAPER 85-1398] p 16 A85-42671
Combustion research for gas turbine engines
[NASA-TM-86963] p 26 N85-21164
Future fundamental combustion research for aeropropulsion systems
[NASA-TM-87049] p 30 N85-27870
MULLEN, R. L.
An analysis of temperature effect in a finite journal bearing with spatial tilt and viscous dissipation
p 126 A85-11074
Plastic flow of plasma sprayed ceramics
p 80 A85-24161
Analysis of experimental shaft seal data for high-performance turbomachines, as for Space Shuttle main engines
[NASA-TM-86928] p 115 N85-21569
Nested subcritical flows within supercritical systems
[NASA-TM-86980] p 115 N85-21574
Film and interstitial formation of metals in plasma-sprayed ceramics
[NASA-TM-86993] p 89 N85-22756
MULLER, A.
Augmented weak forms and element-by-element preconditioners: Efficient iterative strategies for structural finite elements. A preliminary study p 144 N85-10384
MULLER, G. L.
Three-dimensional inviscid flow analysis of turbofan forced mixers
[AIAA PAPER 85-0086] p 2 A85-19510
MULLIN, J. P.
The NASA photovoltaic technology program
p 155 A85-35604
MURAMOTI, K. K.
Analytical modeling of circuit aerodynamics in the new NASA Lewis Altitude Wind Tunnel
[AIAA PAPER 85-0380] p 3 A85-26389
MURAMOTO, K. K.
Flow through very porous inclined screens
[AIAA PAPER 85-1650] p 111 A85-40750
Analytical modeling of circuit aerodynamics in the new NASA Lewis wind tunnel
[NASA-TM-86912] p 8 N85-15688
Flow through very porous inclined screens
[NASA-TM-86979] p 116 N85-25761
MURMAN, E. M.
Three-dimensional inviscid flow analysis of turbofan forced mixers
[AIAA PAPER 85-0086] p 2 A85-19510
MURPHY, G. B.
Effects of chemical releases by the STS 3 orbiter on the ionosphere p 166 A85-29538
Suprathermal plasma observed on STS-3 Mission by plasma diagnostics package p 179 N85-22472
Electron and ion density depletions measured in the STS-3 orbiter wake p 39 N85-22474
MURRAY, R. A.
Numerical simulation of positive-potential conductors in the presence of a plasma and a secondary-emitting dielectric p 102 A85-35306
MURTHY, K. N. S.
Computation of three-dimensional viscous flows using a space-marching method p 4 A85-29259
MURTHY, P. L. N.
ICAN - Integrated composites analyzer
[AIAA PAPER 84-0974] p 54 A85-16094
A study of interply layer effects on the free edge stress field of angleplied laminates p 55 A85-41127

A study of interply layer effects on the free-edge stress field of angleplied laminates
[NASA-TM-86924] p 57 N85-15822

MURTHY, S. N. B.
A stagnation pressure probe for droplet-laden air flow
[AIAA PAPER 85-0330] p 108 A85-19672

MUSIKANT, S.
Transformation toughened ceramics for the heavy duty diesel engine technology program
[NASA-CR-174689] p 185 N85-16698

MYERS, D. M.
Stratified charge rotary aircraft engine technology enablement program
[NASA-CR-174812] p 25 N85-21163

MYERS, M. R.
Effect of airfoil mean loading on convected gust interaction noise
[AIAA PAPER 84-2324] p 173 A85-13955

MYUNG, N. H.
Analysis of the electromagnetic scattering from an inlet geometry with lossy walls
[NASA-CR-175743] p 99 N85-25686

N

NAGAMATSU, H. T.
Heat transfer investigation in the junction region of circular cylinder normal to a flat plate at 90 deg location
[ASME PAPER 84-WA/HT-70] p 111 A85-39898

NAGTEGAAL, J.
Probabilistic finite element development
p 149 N85-27956

NAHRA, H. K.
Ion beam sputter-deposited thin film coatings for protection of spacecraft polymers in low Earth orbit
[NASA-TM-87051] p 91 N85-30137

NAKANISHI, S.
Experiments with a microwave electrothermal thruster concept p 42 A85-16441
Cathode degradation and erosion in high pressure arc discharges p 43 A85-16445
Precision tunable resonant microwave cavity
[NASA-CASE-LEW-13935-1] p 103 N85-20248

NAKANISHI, T. G.
Effects of cobalt, boron, and zirconium on the microstructure of Udimet 738
[NASA-CR-174762] p 70 N85-10166

NAKAZAWA, S.
3-D inelastic analysis methods for hot section components (base program)
[NASA-CR-174700] p 145 N85-21686

NARAGHI, M.
A new interpretation of internal heat transfer coefficients of porous media
[ASME PAPER 84-WA/HT-51] p 110 A85-39894

NASTROM, G. D.
GASP cloud encounter statistics - Implications for laminar flow control flight p 166 A85-11979
A comparison of NMC and GWC analysis field temperatures with aircraft measurements
p 166 A85-21140
Variability of cloudiness at airline cruise altitudes from GASP measurements p 166 A85-31199

NATARAJAN, V.
'Diamondlike' carbon films - Optical absorption, dielectric properties, and hardness dependence on deposition parameters p 82 A85-40383

NATHAL, M. V.
Elevated temperature creep-rupture behavior of the single crystal nickel-base superalloy NASAIR 100
p 66 A85-27812
Influence of composition on the microstructure and mechanical properties of a nickel-base superalloy single crystal p 66 A85-32387

NEELY, G. M.
Accelerated convergence for incompressible flow calculations
[AIAA PAPER 85-0058] p 2 A85-19489
Flame radiation and linear heat transfer in a tubular-can combustor p 15 A85-39580
Accelerated convergence for incompressible flow calculations
[NASA-TM-86863] p 18 N85-10949
Reducing numerical diffusion for incompressible flow calculations
[NASA-TM-83621] p 24 N85-14840

NELSON, C. C.
Rotordynamic coefficients for compressible flow in tapered annular seals p 129 A85-42573

NELSON, D. A.
Interaction of finite-amplitude sound with air-filled porous materials
[NASA-CR-174885] p 177 N85-27637

NELSON, W. A.
Energy efficient engine high pressure turbine ceramic shroud support technology report
[NASA-CR-168036] p 23 N85-10996

NEMAT-NASSER, S.
On stress field near a stationary crack tip
[AD-A152863] p 141 A85-24532

NESBITT, J. A.
Cyclic oxidation behavior of beta+gamma overlay coatings on gamma and gamma+gamma-prime alloys
p 68 A85-32431

NESTER, W. H.
Configuration study for a 30 GHz monolithic receive array: Technical assessment
[NASA-CR-174697] p 98 N85-18238
Configuration study for a 30 GHz monolithic receive array, volume 1
[NASA-CR-174697-VOL-1] p 98 N85-18239
Configuration study for a 30 GHz monolithic receive array, volume 2
[NASA-CR-174697-VOL-2] p 99 N85-18240

NEUMANN, H. E.
Performance and surge limits of a TF30-P-3 turbofan engine/axisymmetric mixed-compression inlet propulsion system at Mach 2.5
[NASA-TP-2461] p 27 N85-25261

NEUSTADTER, H. E.
Method for evaluating wind turbine wake effects on wind farm performance p 155 A85-36750

NEVEU, M. C.
Applications of high pressure differential scanning calorimetry to aviation fuel thermal stability research
[NASA-TM-87002] p 63 N85-23941

NEWELL, J. F.
Composite loads spectra for select space propulsion structural components p 148 N85-27953

NEWTON, J.
Ice shapes and the resulting drag increase for a NACA 0012 airfoil
[NASA-TM-83556] p 11 N85-27839

NGAN, Y. C.
The 30 GHz solid state amplifier for low cost low data rate ground terminals
[NASA-CR-174795] p 102 N85-12300

NGHIEM, H.
Sixty GHz IMPATT diode development
[NASA-CR-174969] p 105 N85-33293

NGUYEN-DINH, X.
Development of coated single-crystal superalloy systems for gas turbine applications p 68 A85-32440

NGUYEN-VO, N.-M.
The response of Helmholtz resonators to external excitation. I - Single resonators p 174 A85-26915

NGUYEN, H. C.
The effect of tantalum and carbon on the structure/properties of a single crystal nickel-base superalloy
[NASA-CR-174779] p 71 N85-11223

NICHOLSON, S.
Thermodynamic evaluation of transonic compressor rotors using the finite volume approach
[NASA-CR-175811] p 29 N85-26712

NIEBERDING, W. C.
Hot section laser anemometry p 19 N85-10962
Instrumentation technology overview
p 124 N85-26903

NIR, D.
Mechanical protection of DLC films on fused silica slides
[NASA-TM-87056] p 91 N85-30138
Diamondlike carbon protective coatings for IR materials
[NASA-TM-87083] p 178 N85-34631

NISSIM, E.
Optimization of cascade blade mistuning. I - Equations of motion and basic inherent properties
p 16 A85-42365
Optimization of cascade blade mistuning. II - Global optimum and numerical optimization p 16 A85-45715

NISSLEY, D. M.
Application of two creep fatigue life models for the prediction of elevated temperature crack initiation of a nickel base alloy
[AIAA PAPER 85-1420] p 69 A85-43979

NOE, K. A.
Behavior of the lean methane-air flame at zero-gravity
[NASA-CR-175586] p 62 N85-21283

NONAMI, K.
Vibration control of rotor shaft
[NASA-TM-87053] p 133 N85-29292

NORGREN, C. T.
Advanced liner-cooling techniques for gas turbine combustors
[AIAA PAPER 85-1290] p 15 A85-39703
Small gas turbine combustor study - Fuel injector performance in a transpiration-cooled liner
[AIAA PAPER 85-1312] p 16 A85-39717
Advanced liner-cooling techniques for gas turbine combustors
[NASA-TM-86952] p 8 N85-21115
Small gas turbine combustor study: Fuel injector performance in a transpiration-cooled liner
[NASA-TM-86989] p 27 N85-25264

NYLAND, T. W.
Reflection plane tests of a wind turbine blade tip section with ailerons
[NASA-TM-87018] p 165 N85-34444

O

OBATA, M.
On stress field near a stationary crack tip
[AD-A152863] p 141 A85-24532

OBERLE, L. G.
Filter induced errors in laser anemometer measurements using counter processors
[NASA-TM-87047] p 125 N85-30288

OBRIEN, J. E.
The influence of jet-grid turbulence on heat transfer from the stagnation region of a cylinder in crossflow
[NASA-TM-87011] p 115 N85-25760

OBRIEN, J. J.
Electric utility acid fuel cell stack technology advancement
[NASA-CR-174804] p 159 N85-17422

ODEN, J. T.
Analysis of hourglass instabilities and control in underintegrated finite element methods
p 139 A85-11125

ODONNELL, W. J.
Simplified design and life prediction of rocket thrust chambers p 44 A85-29314

OGRADY, E. P.
Multibus-based parallel processor for simulation
p 169 A85-28613

OKIISHI, T. H.
A note on blade wake interaction influence on compressor stator row aerodynamic performance
p 4 A85-32965

OLIVER, G. A.
Jet fuel property changes and their effect on producibility and cost in the U.S., Canada, and Europe
[NASA-CR-174840] p 93 N85-27012

OLSEN, R. B.
Pyroelectric conversion in space p 45 A85-45377

OLSEN, R. C.
Experiments in charge control at geosynchronous orbit - ATS-5 and ATS-6 p 39 A85-35379

OLSEN, W.
Ice shapes and the resulting drag increase for a NACA 0012 airfoil
[NASA-TM-83556] p 11 N85-27839

OLSON, C.
Advanced thin film thermocouples
[NASA-CR-175541] p 124 N85-21607

OLSON, S. L.
Fuel rich catalytic comustion: The first stage of a two-stage combustor
[NASA-TM-87042] p 63 N85-28983
Fuel-rich catalytic combustion: A soot-free technique for in situ hydrogen-like enrichment
[NASA-TP-2498] p 63 N85-31244

OPPENHEIM, A. K.
Recent advances in methods for numerical solution of O.D.E. initial value problems p 171 A85-21370
Knock syndrome: Its cures and its victims
[NASA-CR-174395] p 93 N85-19185

ORANGE, T. W.
Pre-HOST high temperature crack propagation
p 19 N85-10956
HOST high temperature crack propagation
p 21 N85-10977

ORTH, N. W.
Demonstration of a silicon nitride attrition mill for production of fine pure Si and Si3N4 powders
p 78 A85-10825

ORTIZ, A. L.
Laser balancing system for high material removal rates
[NASA-CR-174731] p 126 N85-12341

OSTBERG, D. T.
Powder metallurgy forged gear development
[NASA-TM-87483] p 134 N85-29295

OTTERSON, D. A.
Rapid estimation of concentration of aromatic classes in middistillate fuels by high-performance liquid chromatography
[NASA-TP-2495] p 93 N85-31307

OWENS, H.
Suprathermal plasma observed on STS-3 Mission by plasma diagnostics package p 179 N85-22472

P

PADOVAN, J.
Extension of constrained incremental Newton-Raphson scheme to generalized loading fields p 139 A85-13942
On the development of hierarchical solution strategies for nonlinear finite element formulations p 171 A85-21979
Plastic flow of plasma sprayed ceramics p 80 A85-24161
Pantographing self adaptive gap elements p 142 A85-37440
Quasi-static solution algorithms for kinematically/materially nonlinear thermomechanical problems p 143 A85-41983
PAGLIARO, P.
Preparation and evaluation of advanced catalysts for phosphoric acid fuel cells
[NASA-CR-168223] p 160 N85-19511
PAI, S.
Extension of constrained incremental Newton-Raphson scheme to generalized loading fields p 139 A85-13942
PAI, S. S.
Quasi-static solution algorithms for kinematically/materially nonlinear thermomechanical problems p 143 A85-41983
PALKO, R. L.
Initial feasibility ground test of a proposed photogrammetric system for measuring the shapes of ice accretions on helicopter rotor blades during forward flight
[NASA-TM-87391] p 12 N85-12887
PANDOLFI, M.
Inverse design technique for cascades
[NASA-CR-3836] p 7 N85-12008
PAPELL, S. S.
Vortex-generating coolant-flow-passage design for increased film-cooling effectiveness and surface coverage
[NASA-TP-2388] p 113 N85-12314
Vortex generating flow passage design for increased film cooling effectiveness
[NASA-CASE-LEW-14039-1] p 119 N85-33433
PARK, G. L.
Improved models for increasing wind penetration, *economics and operating reliability*
[NASA-CR-175538] p 160 N85-20545
PARK, J. S.
Heat transfer enhancement in channels with turbulence promoters
[ASME PAPER 84-WA/HT-72] p 111 A85-39900
PARKER, R. D.
Operating characteristics of a 0.87 kW-hr flywheel energy storage module
[NASA-TM-87038] p 133 N85-28371
PARKS, D. E.
Polar orbit electrostatic charging of objects in shuttle wake p 40 N85-22487
PARZYCH, D.
Large-scale Advanced Propfan (LAP) performance, acoustic and weight estimation, January, 1984
[NASA-CR-174782] p 9 N85-22368
PATEL, D. R.
Functional language and data flow architectures p 170 A85-28629
PATERSON, W.
Suprathermal plasma observed on STS-3 Mission by plasma diagnostics package p 179 N85-22472
PATHAK, P. H.
Analysis of the electromagnetic scattering from an inlet geometry with lossy walls
[NASA-CR-175743] p 99 N85-25686
PATHARE, V.
Alloys based on NiAl for high temperature applications
[NASA-TM-86976] p 75 N85-21322
PATTIPATI, K. R.
A design methodology for robust failure detection and isolation p 171 A85-47794
PAUCKERT, R.
Cryogenic upper stage test bed engine
[AIAA PAPER 85-1339] p 44 A85-39733
PECKHAM, R. J.
Design and analysis report for the RL10-2B breadboard low thrust engine
[NASA-CR-174857] p 48 N85-19020
PELACCIO, D. G.
Feasibility of mapping velocity flow fields in SSME powerhead by laser anemometry techniques p 41 N85-27971
PELLOUX, R. M.
Thermal-mechanical fatigue crack growth in Inconel X-750
[NASA-CR-174740] p 72 N85-15877
PENKO, P. F.
Vacuum chamber pressure effects on thrust measurements of low Reynolds number nozzles
[NASA-TM-86955] p 49 N85-21259
PENN, B. G.
Preparation of silicon carbide-silicon nitride fibers by the pyrolysis of polycarbosilazane precursors
[NASA-TM-86505] p 91 N85-28107
PENNEY, C. M.
Advanced smoke meter development survey and analysis
[NASA-CR-168287] p 124 N85-25792
PENNLINE, J. A.
Constructive existence and uniqueness for two-point boundary-value problems with a linear gradient term p 172 A85-28015
PERALTA-DURAN, A.
Creep-rupture *reliability analysis* p 143 *A85-42566*
PEREZ, F.
Advanced nickel-hydrogen cell configuration study
[NASA-CR-174775] p 157 N85-10444
PERIC, M.
Assessment of discretization schemes to reduce numerical diffusion in the calculation of complex flows
[AIAA PAPER 85-0441] p 108 A85-19751
PERKINS, P. J., JR.
Icing flight research - Aerodynamic effects of ice and ice shape documentation with stereo photography
[AIAA PAPER 85-0468] p 11 A85-30192
Icing flight research: Aerodynamic effects of ice and ice shape documentation with stereo photography
[NASA-TM-86906] p 12 N85-18049
PERREIRA, N. D.
Oscillatory conductive heat transfer for a fiber in an ideal gas p 109 A85-26077
PETERMAN, W.
Creep-rupture behavior of iron superalloys in *high-pressure hydrogen*
[NASA-CR-174411] p 74 N85-19078
PHILIPP, W. H.
Alkaline battery containing a separator of a cross-linked copolymer of vinyl alcohol and unsaturated carboxylic acid
[NASA-CASE-LEW-13102-1] p 104 N85-29144
PIAN, T. H. H.
Rational approach for assumed stress finite elements p 139 *A85-12029*
Hybrid Semiloof elements for plates and shells based upon a modified Hu-Washizu principle p 139 A85-15893
Evolution of assumed stress hybrid finite element p 142 A85-35046
Plasticity, viscoplasticity, and creep of solids by mechanical subelement models p 142 A85-35048
Axisymmetric solid elements by a rational hybrid stress method p 143 A85-41109
Advanced stress analysis methods applicable to turbine engine structures
[NASA-CR-175573] p 26 N85-21165
Recent advances in hybrid/mixed finite elements
[NASA-CR-175574] p 145 N85-21687
On Hybrid and mixed finite element methods
[NASA-CR-175551] p 146 N85-23096
PICHA, G. J.
Percutaneous connectors
[NASA-CR-175627] p 168 N85-27508
PICKETT, J. S.
Effects of chemical releases by the STS 3 orbiter on the ionosphere p 166 A85-29538
Suprathermal plasma observed on STS-3 Mission by plasma diagnostics package p 179 N85-22472
Electron and ion density depletions measured in the STS-3 orbiter wake p 39 N85-22474
PIERCE, L. A.
Reliability of two sintered silicon nitride materials
[NASA-TM-87092] p 92 N85-34284
PIERCE, R. M.
Prism-coupled light emission from tunnel junctions p 181 A85-21425
PIJAWKA, W. C.
Advanced multi-megawatt wind turbine design for utility application p 157 A85-45517
PIKE, C. P.
Spacecraft environmental interactions: A joint Air Force and NASA research and technology program p 40 N85-22517
PIKE, J.
Multi-mesh gear dynamics program evaluation and enhancements
[NASA-CR-174747] p 133 N85-28372
PILLAY, S.
Powder metallurgy forged gear development
[NASA-TM-87483] p 134 N85-29295
PILSNER, B. H.
Cyclic oxidation behavior of beta+gamma overlay coatings on gamma and gamma+gamma-prime alloys p 68 A85-32431
Effects of MAR-M247 substrate (modified) composition on coating oxidation coating/substrate interdiffusion
[NASA-CR-174851] p 73 N85-19073
PINEL, S. I.
Effect of two inner-ring oil-flow distribution schemes on the operating characteristics of a 35 millimeter bore ball bearing to 2.5 million DN
[NASA-TP-2404] p 130 N85-13233
PINKOWSKI, S.
Feasibility of mapping velocity flow fields in SSME powerhead by laser anemometry techniques p 41 N85-27971
PINTZ, A.
Conceptual design of a fixed-pitch wind turbine generator system rated at 400 kilowatts
[NASA-CR-174877] p 162 N85-29363
PISZCZOR, M. F., JR.
Preliminary design of a 10 kW thermophotovoltaic system for space applications p 45 A85-45371
PITZ, R. W.
Advanced smoke meter development survey and analysis
[NASA-CR-168287] p 124 N85-25792
PLENCNER, R. M.
Advanced secondary power system for transport aircraft
[NASA-TP-2463] p 30 N85-28944
POESCHEL, R. L.
IAPS (8-cm) ion thruster cyclic endurance test p 42 A85-16406
Ion propulsion for communications satellites p 42 A85-16412
Ring-cusp ion thrusters p 42 A85-16438
Ion thruster system (8-cm) cyclic endurance test
[NASA-CR-174745] p 47 N85-12937
POLEY, W.
Demand for satellite-provided domestic communications services up to the year 2000
[NASA-TM-86894] p 97 N85-15099
PONCHAK, G. E.
Effect of Interfacial characteristics of metal clad polymeric substrates on electrical high frequency interconnection performance
[NASA-TM-86948] p 99 N85-20223
An experimental investigation of microstrip properties on soft substrates from 2 to 40 GHz
[NASA-TM-86961] p 99 N85-20224
PORADA, T. W.
Linearization of digital derived rate algorithm for use in linear stability analysis
[NASA-TM-87000] p 41 N85-23904
POROWSKI, J. S.
Simplified design and life prediction of rocket thrust chambers p 44 A85-29314
POTAPCZUK, M. G.
Progress in development of a Navier-Stokes solver for evaluation of iced airfoil performance
[AIAA PAPER 85-0410] p 3 A85-19731
POUAGARE, M.
Computation of viscous flows in turbomachinery cascades p 106 A85-11631
Computation and turbulence closure models for shear flows in rotating curved bodies p 107 A85-14349
A space-marching method for incompressible Navier-Stokes equations
[AIAA PAPER 85-0170] p 108 A85-19564
POUCH, J. J.
Plasma deposited hydrogenated carbon on GaAs and InP p 182 A85-40386
Plasma deposited diamondlike carbon on GaAs and InP
[NASA-TM-86870] p 183 N85-10844
Optical properties of hydrogenated amorphous carbon films grown from methane plasma
[NASA-TM-86995] p 183 N85-26406
POVINELLI, L. A.
Comparison of secondary flows predicted by a viscous code and an inviscid code with experimental data for a turning duct p 106 A85-11634
Analytical and physical modeling program for the NASA Lewis Research Center's Altitude Wind Tunnel (AWT)
[AIAA PAPER 85-0379] p 34 A85-19709
Analytical modeling of circuit aerodynamics in the new NASA Lewis Altitude Wind Tunnel
[AIAA PAPER 85-0380] p 3 A85-26389
Assessment of three-dimensional inviscid codes and loss calculations for turbine aerodynamic computations
[ASME PAPER 84-GT-187] p 4 A85-32961

Application of viscous and inviscid computation methods for rocket turbopump systems
[SAE PAPER 841522] p 110 A85-39257
Analytical modeling of circuit aerodynamics in the new NASA Lewis wind tunnel
[NASA-TM-86912] p 8 N85-15688
Analytical and physical modeling program for the NASA Lewis Research Center's Altitude Wind Tunnel (AWT)
[NASA-TM-86919] p 35 N85-15757
Overview of aerothermodynamic loads definition study p 51 N85-27942

POWELL, A. G.
Low-speed aerodynamic test of an axisymmetric supersonic inlet with variable cowl slot
[AIAA PAPER 85-1210] p 5 A85-40819
Low-speed aerodynamic test of an axisymmetric supersonic inlet with variable cowl slot
[NASA-TM-87039] p 28 N85-26710

POWER, J. L.
Ground correlation investigation of thruster/spacecraft interactions to be measured on the IAPS flight test p 42 A85-16408

POWERS, W. O.
Rapid solidification and dynamic compaction of Ni-base superalloy powders p 67 A85-32414

PRAHL, J. M.
Mechanics of a gaseous film barrier to lubricant wetting of elastohydrodynamically lubricated conjunctions
[NASA-TP-2500] p 135 N85-32330

PRATT, B. S.
An interactive computer code for calculation of gas-phase chemical equilibrium (EQLBRM)
[NASA-CR-168337] p 18 N85-10948

PRATT, D. T.
Recent advances in methods for numerical solution of O.D.E. initial value problems p 171 A85-21370
CREKID: A computer code for transient, gas-phase combustion of kinetics
[NASA-TM-83806] p 17 N85-10068
An interactive computer code for calculation of gas-phase chemical equilibrium (EQLBRM)
[NASA-CR-168337] p 18 N85-10948

PROCTOR, M. P.
Flame flashback in a premixed dump combustor
[AIAA PAPER 85-0145] p 60 A85-19550
Transient technique for measuring heat transfer coefficients on stator airfoils in a jet engine environment
[AIAA PAPER 85-1471] p 122 A85-39796
Transient technique for measuring heat transfer coefficients,on stator airfoils in a jet engine environment
[NASA-TM-87005] p 124 N85-25794

PROK, G. M.
Lubricity of well-characterized jet and broad-cut fuels by ball-on-cylinder machine
[NASA-TM-83807] p 92 N85-12183

PUDICK, S.
Develop and test fuel cell powered on-site integrated total energy systems. Phase 3: Full-scale power plant development
[NASA-CR-174887] p 161 N85-25941
Develop and test fuel cell powered on-site integrated total energy systems. Phase 3: Full-scale power plant development
[NASA-CR-168338] p 164 N85-30483

PUNCH, E. F.
Development and testing of stable, invariant, isoparametric curvilinear 2- and 3-D hybrid-stress elements p 140 A85-19899

PURVIS, C. K.
The PIX-2 experiment: An overview p 179 N85-22494
Design guidelines for assessing and controlling spacecraft charging effects p 40 N85-22500
Spacecraft environmental interactions: A joint Air Force and NASA research and technology program p 40 N85-22517

PUTHOFF, R. L.
Aileron controls for wind turbine applications p 157 A85-45513

PUTOFF, R. L.
Aileron controls for wind turbine applications
[NASA-TM-86867] p 158 N85-11458

Q

QUENTMEYER, R. J.
Fabrication of ceramic substrate-reinforced and free forms
[NASA-TM-86994] p 50 N85-23926
Rocket thrust chamber thermal barrier coatings p 90 N85-26867

QUICK, B.
Fiber optic, Fabry-Perot high temperature sensor
[NASA-CR-174712] p 178 N85-13594

QUIJIJE, M. A.
The 30 GHz solid state amplifier for low cost low data rate ground terminals
[NASA-CR-174795] p 102 N85-12300

R

RADHAKRISHNAN, K.
Integrating chemical kinetic rate equations by selective use of stiff and nonstiff methods
[AIAA PAPER 85-0237] p 60 A85-19607
High temperature oxidation of propene p 61 A85-33570
Comparison of numerical techniques for integration of stiff ordinary differential equations arising in combustion chemistry
[NASA-TP-2372] p 17 N85-10065
CREKID: A computer code for transient, gas-phase combustion of kinetics
[NASA-TM-83806] p 17 N85-10068
New integration techniques for chemical kinetic rate equations. 2: Accuracy comparison
[NASA-TM-86893] p 23 N85-13798
Integrating chemical kinetic rate equations by selective use of stiff and nonstiff methods
[NASA-TM-86923] p 24 N85-15726
A comparison of the efficiency of numerical methods for integrating chemical kinetic rate equations
[NASA-TM-83590] p 25 N85-21162

RAITT, W. S.
Electron and ion density depletions measured in the STS-3 orbiter wake p 39 N85-22474

RAMACHANDRA, M. K.
Shock tube study of the fuel structure effects on the chemical kinetic mechanisms responsible for soot formation, part 2
[NASA-CR-174880] p 63 N85-25444

RAMACHANDRA, S. M.
Acoustic pressures emanating from a turbomachine stage
[AIAA PAPER 84-2325] p 2 A85-10870
Incompressible lifting-surface aerodynamics for a rotor-stator combination
[NASA-TM-83767] p 7 N85-12039

RAMAMURTI, R.
Two-dimensional internal compressible viscous flows using semi-elliptic analysis p 106 A85-11640

RAMAMURTI, V.
Natural frequencies of twisted rotating plates p 141 A85-32343

RAMLER, J. R.
Telecommunications forecast for ITU Region 2 to the year 1995
[NASA-TM-87077] p 38 N85-34150

RAMSAY, S. M.
Three-dimensional inviscid flow analysis of turbofan forced mixers
[AIAA PAPER 85-0086] p 2 A85-19510

RAMSEY, W. D.
Inert gas test of two 12-cm magnetostatic thrusters p 43 A85-29310

RANAUDO, R. J.
Icing flight research - Aerodynamic effects of ice and ice shape documentation with stereo photography
[AIAA PAPER 85-0468] p 11 A85-30192
Icing flight research: Aerodynamic effects of ice and ice shape documentation with stereo photography
[NASA-TM-86906] p 12 N85-18049

RANDALL, S. A.
Electric utility acid fuel cell stack technology advancement
[NASA-CR-174804] p 159 N85-17422

RAO, B. C. S.
Deformation and erosion of f.c.c. metals and alloys under cavitation attack p 65 A85-12789
Characterization of erosion of metallic materials under cavitation attack in a mineral oil
[NASA-TM-86934] p 74 N85-19075

RAO, K.
Vibration and flutter of mistuned bladed-disk assemblies
[AIAA PAPER 84-0991] p 139 A85-16095

RAO, P. V.
Cavitation erosion size scale effects p 65 A85-11935
Effect of surface configuration during solid particle impingement erosion p 69 A85-42568
Characterization of solid particle erosion resistance of ductile metals based on their properties p 69 A85-42569

RATAJCZAK, A. F.
Control algorithms and computer simulation of a stand-alone photovoltaic village power system p 153 A85-11345
Status of DOE and AID stand-alone photovoltaic system field tests p 155 A85-35707

RAUCH, H.
Transformation toughened ceramics for the heavy duty diesel engine technology program
[NASA-CR-174689] p 185 N85-16698

RAUCH, J.
Free-piston Stirling engine/linear alternator 1000-hour endurance test
[NASA-CR-174771] p 163 N85-30481

RAVEH, A.
Deposition of silicon nitride from SiCl4 and NH3 in a low pressure RF plasma p 81 A85-36229

RAWLIN, V. K.
Ring-cusp ion thruster with shell anode
[NASA-CASE-LEW-13881-1] p 48 N85-21256

RAY, P. K.
Arc-driven rail gun research
[NASA-CR-174816] p 132 N85-21662

RAZAVI, H.
Nonlinear global stability analysis of compressor stall phenomena
[NASA-CR-174908] p 31 N85-29960

REAGAN, J. R.
Government review of the Mod-2 wind turbine (as-built)
[NASA-TM-86983] p 162 N85-29365

REDD, L.
Main propulsion system design recommendations for an advanced Orbit Transfer Vehicle
[AIAA PAPER 85-1336] p 36 A85-39730

REDDOCH, T. W.
Experimental investigation of a variable speed constant frequency electric generating system from a utility perspective
[NASA-CR-174950] p 105 N85-32251

REDDY, J. N.
Geometrically nonlinear analysis of laminated elastic structures
[NASA-CR-175609] p 146 N85-21720

REED, K. W.
Hybrid stress finite elements for large deformations of inelastic solids p 139 A85-15894
Constitutive modeling and computational implementation for finite strain plasticity p 143 A85-40910

REED, R. W.
The scattering of ultrasonic third sound from substrate surface defects p 174 A85-36047

REID, L.
Analytical and physical modeling program for the NASA Lewis Research Center's Altitude Wind Tunnel (AWT)
[AIAA PAPER 85-0379] p 34 A85-19709
Analytical and physical modeling program for the NASA Lewis Research Center's Altitude Wind Tunnel (AWT)
[NASA-TM-86919] p 35 N85-15757

REID, M. A.
Chemical and electrochemical behavior of the Cr(III)/Cr(II) half-cell in the iron-chromium redox energy storage system p 61 A85-33785

REILLY, C. H.
Engineering calculations for communications satellite systems planning
[NASA-CR-175552] p 37 N85-21233

REINMANN, J. J.
Analytical and physical modeling program for the NASA Lewis Research Center's Altitude Wind Tunnel (AWT)
[AIAA PAPER 85-0379] p 34 A85-19709
Analytical and physical modeling program for the NASA Lewis Research Center's Altitude Wind Tunnel (AWT)
[NASA-TM-86919] p 35 N85-15757

RENGSTORFF, G. W. P.
Surface effects of corrosive media on hardness, friction, and wear of materials
[NASA-TM-83711] p 85 N85-15896

RENZ, D. D.
High voltage-high power components for large space power distribution systems p 45 A85-45370
Developments in space power components for power management and distribution p 47 N85-13877

RHODES, D. L.
Predictions and measurements of isothermal flowfields in axisymmetric combustor geometries
[NASA-CR-174916] p 29 N85-27867

RIBARSKY, M. W.
Study of the effects of implantation on the high Fe-Ni-Cr and Ni-Cr-Al alloys
[NASA-CR-175625] p 76 N85-22661

RICE, E. E.
Preliminary analysis of space mission applications for electromagnetic launchers
[NASA-CR-174067] p 35 N85-12071

RICE, E. J.
Measured acoustic properties of variable and low density bulk absorbers
[NASA-TM-87065] p 177 N85-30770

RICHARDS, W. B.
The infinite line pressure probe p 122 A85-37704
RICHEY, A. E.
Automotive Stirling engine systems development p 130 A85-45474
RICHTER, G. P.
Comparison of icing cloud instruments for 1982-1983 icing season flight program
[AIAA PAPER 84-0020] p 13 A85-16098
The UH-1H helicopter icing flight test program - An overview
[AIAA PAPER 85-0338] p 11 A85-28898
The UH-1H helicopter icing flight test program: An overview
[NASA-TM-86925] p 11 N85-15702
RIDDLEBAUGH, S. M.
Advanced liner-cooling techniques for gas turbine combustors
[AIAA PAPER 85-1290] p 15 A85-39703
Small gas turbine combustor study - Fuel injector performance in a transpiration-cooled liner
[AIAA PAPER 85-1312] p 16 A85-39717
Advanced liner-cooling techniques for gas turbine combustors
[NASA-TM-86952] p 8 N85-21115
Small gas turbine combustor study: Fuel injector performance in a transpiration-cooled liner
[NASA-TM-86989] p 27 N85-25264
RIEKER, L. L.
Design considerations for a 10-kW integrated hydrogen-oxygen regenerative fuel cell system p 155 A85-45380
RIFF, R.
Thermodynamically consistent constitutive equations for nonisothermal large strain, elasto-plastic, creep behavior
[AIAA PAPER 85-0621] p 142 A85-38425
Analysis of shell type structures subjected to time dependent mechanical and thermal loading
[NASA-CR-175747] p 147 N85-25896
Dynamic creep buckling: Analysis of shell structures subjected to time-dependent mechanical and thermal loading p 149 N85-27959
RILEY, J. J.
Direct numerical simulations of a reacting mixing layer with chemical heat release
[AIAA PAPER 85-0143] p 60 A85-19548
Direct simulations of chemically reacting turbulent mixing layers
[AIAA PAPER 85-0321] p 60 A85-19666
RIPLING, E. J.
Fracture of composite-adhesive-composite systems p 141 A85-27935
RIZK, M.
A two-equation turbulence model for two-phase jets p 107 A85-14376
RO, D. H.
Powder metallurgy forged gear development
[NASA-TM-87483] p 134 N85-29295
ROBACK, R.
Turbulent transport and length scale measurement experiments with comfined coaxial jets
[NASA-CR-174831] p 117 N85-30245
ROBERTS, A. F.
Operational performance of the photovoltaic-powered grain mill and water pump at Tangaye, Burkina Faso (formerly Upper Volta)
[NASA-TM-86970] p 161 N85-23243
ROBERTS, T.
The 20 GHz proof-of-concept test model results for a multiple scan beam dual reflector antenna
[NASA-CR-174268] p 98 N85-15944
ROBERTSON, C.
Applicability of 100kWe-class of space reactor power systems to NASA manned space station missions
[NASA-CR-174696] p 177 N85-35728
ROBINSON, D. N.
Viscoplastic constitutive relationships with dependence on thermomechanical history
[NASA-CR-174836] p 146 N85-21691
On thermomechanical testing in support of constitutive equation development for high temperature alloys
[NASA-CR-174879] p 147 N85-25894
Some advances in experimentation supporting development of viscoplastic constitutive models
[NASA-CR-174855] p 147 N85-27260
Thermomechanical deformation in the presence of metallurgical changes p 150 N85-31533
Some advances in experimentation supporting development of viscoplastic constitutive models p 151 N85-31545
A continuous damage model based on stepwise-stress creep rupture tests
[NASA-CR-174941] p 152 N85-32341
ROBINSON, R. A.
Experimental and analytical study of ceramic-coated turbine-tip shroud seals for small turbine engines
[NASA-TM-86881] p 25 N85-18057
ROBINSON, R. S.
Ion flow experiments in a multipole discharge chamber p 178 A85-12705
ROCHE, J. C.
Computer simulation of plasma electron collection by PIX-II
[AIAA PAPER 85-0386] p 43 A85-19715
NASCAP simulation of PIX 2 experiments p 180 N85-22497
RODE, H.
Fabrication of p(+)-n junction GaAs solar cells by a novel method p 181 A85-33645
ROHDE, J. E.
Turbine heat transfer p 19 N85-10964
Coolant passage heat transfer with rotation p 20 N85-10968
ROHLIK, H. E.
Computational thermo-fluid dynamics contributions to advanced gas turbine engine design
[AIAA PAPER 85-0083] p 14 A85-19509
Computational thermo-fluid dynamics contributions to advanced gas turbine engine design
[NASA-TM-86865] p 18 N85-10069
ROHN, D. A.
Application of traction drives as servo mechanisms p 152 N85-33520
ROLEK, R. J.
The influence of temperature on the lubricating effectiveness of MoS2 dispersed in mineral oils
[ASLE PREPRINT 84-LC-2A-2] p 80 A85-25963
ROMAN, R. F.
Textured carbon surfaces on copper
[NASA-CASE-LEW-14130-1] p 95 N85-20156
Ring-cusp ion thruster with shell anode
[NASA-CASE-LEW-13881-1] p 48 N85-21256
ROMANOFSKY, R. R.
Effect of Interfacial characteristics of metal clad polymeric substrates on electrical high frequency interconnection performance
[NASA-TM-86948] p 99 N85-20223
An experimental investigation of microstrip properties on soft substrates from 2 to 40 GHz
[NASA-TM-86961] p 99 N85-20224
RON, Y.
Deposition of silicon nitride from SiCl4 and NH3 in a low pressure RF plasma p 81 A85-36229
RONNEY, P. D.
Effect of gravity on halogenated hydrocarbon flame retardant effectiveness
[IAF PAPER 84-156] p 61 A85-23199
ROOT, J.
Recent work on a microwave ion source p 179 A85-16455
Experimental performance of a microwave cavity plasma disk ion source p 179 A85-43552
ROSE, J. J.
Universal binding energy relations in metallic adhesion
[NASA-TM-86889] p 72 N85-12132
ROSE, M. E.
A numerical study of the steady scalar convective diffusion equation for small viscosity p 107 A85-16533
ROSECRANS, P. M.
Manufacturing process to reduce large grain growth in zirconium alloys
[DE85-011649] p 78 N85-34267
ROSENBLUM, L.
Practical aspects of photovoltaic technology, applications and cost (revised)
[NASA-CR-174963] p 165 N85-35472
ROSENLIEB, J. W.
Planetary-gear-support bearing test rig design
[NASA-CR-174927] p 12 N85-35185
ROSNER, D. E.
Polarization (ellipsometric) measurements of liquid condensate deposition and evaporation rates and dew points in flowing salt/ash-containing combustion gases p 123 A85-46925
Computer program for the calculation of multicomponent convective diffusion deposition rates from chemically frozen boundary layer theory
[NASA-CR-168329] p 116 N85-27164
ROSS, P. N.
CO adsorption on (111) and (100) surfaces of the Pt sub 3 Ti alloy. Evidence for parallel binding and strong activation of CO
[NASA-CR-176077] p 77 N85-32176
ROTH, D. J.
Radiographic detectability limits for seeded voids in sintered silicon carbide and silicon nitride
[NASA-TM-86945] p 138 N85-21674
Reliability of void detection in structural ceramics using scanning laser acoustic microscopy
[NASA-TM-87035] p 138 N85-32337
ROTHOLZ, E.
A frequency-routed satellite system concept using multiple orthogonally-polarized beams for frequency reuse p 97 A85-34470
ROUSSOS, L. A.
Noise transmission loss of a rectangular plate in an infinite baffle
[NASA-TP-2398] p 176 N85-22109
ROYCE, B. S. H.
The role of surface generated radicals in catalytic combustion p 30 N85-27869
RUBIN, A. J.
Three-dimensional calculation of shuttle charging in polar orbit p 40 N85-22486
Polar orbit electrostatic charging of objects in shuttle wake p 40 N85-22487
RUDLAND, R. S.
Technology requirements to be addressed by the NASA Lewis Research Center Cryogenic Fluid Management Facility program
[AIAA PAPER 85-1229] p 94 A85-47024
Technology requirements to be addressed by the NASA Lewis Research Center Cryogenic Fluid Management Facility program
[NASA-TM-87048] p 38 N85-29987
RUM, G.
Report of the Constellations Panel p 131 N85-20368
RUSCH, W. V. T.
Focal shifts in parabolic reflectors p 97 A85-39356
RUSSELL, L. M.
Local heat-transfer measurements on a large, scale-model turbine blade airfoil using a composite of a heater element and liquid crystals
[NASA-TM-86900] p 119 N85-33435
RUTLEDGE, J. E.
Prism-coupled light emission from tunnel junctions p 181 A85-21425
RUTLEDGE, S. K.
Ion beam sputter-deposited thin film coatings for protection of spacecraft polymers in low Earth orbit
[NASA-TM-87051] p 91 N85-30137
RYDER, J. T.
Effect of low temperature on fatigue and fracture properties of Ti-5Al-2.5Sn(ELI) for use in engine components p 70 A85-47972

S

SADLER, G. G.
DEAN: A program for dynamic engine analysis
[NASA-TM-87033] p 30 N85-28945
SAFFMAN, P. G.
The linear two-dimensional stability of inviscid vortex streets of finite-cored vortices
[AD-A153032] p 107 A85-14241
SAGERSER, D. A.
Large-scale advanced propfan (LAP) program progress report
[AIAA PAPER 85-1187] p 17 A85-47021
Large-scale Advanced Propfan (LAP) program
[NASA-TM-87067] p 32 N85-29964
SAIN, M. K.
Alternatives for jet engine control
[NASA-CR-175831] p 29 N85-26713
Alternatives for jet engine control
[NASA-CR-175832] p 29 N85-26714
Alternatives for jet engine control
[NASA-CR-175833] p 29 N85-26715
SALERNO, J.
Automatic sphericity interferometer for testing lens radii
[AD-A155736] p 125 N85-33457
SALIK, J.
Ion-beam nitriding of steels p 66 A85-24667
Computer simulation of thin film nucleation and growth p 181 A85-35308
Monte Carlo study of reversible growth of clusters on a surface p 182 A85-48516
A computer simulation of thin film nucleation and growth: The Volmer-Weber case
[NASA-TM-86968] p 53 N85-21264
Ion-beam nitriding of steels
[NASA-CASE-LEW-14104-1] p 75 N85-21324
SALIKUDDIN, M.
An experimental study of tone excited heated jets
[AIAA PAPER 84-2341] p 172 A85-10882
SALTSMAN, J. F.
Strainrange partitioning - A total strain range version p 64 A85-11603

Application of two creep fatigue life models for the prediction of elevated temperature crack initiation of a nickel base alloy
[AIAA PAPER 85-1420] p 69 A85-43979
SALZMAN, J. A.
Demand for satellite-provided domestic communications services up to the year 2000
[NASA-TM-86894] p 97 N85-15099
Telecommunications forecast for ITU Region 2 to the year 1995
[NASA-TM-87077] p 38 N85-34150
SAMANTA, S.
Transformation toughened ceramics for the heavy duty diesel engine technology program
[NASA-CR-174689] p 185 N85-16698
SAMPLE, A. K.
The mechanisms of formation and prevention of channel segregation during alloy solidification
p 180 A85-18082
SANCHEZ, J. M.
Modeling of gamma/gamma-prime phase equilibrium in the nickel-aluminum system p 65 A85-14959
SANDELLI, G. J.
Electric utility acid fuel cell stack technology advancement
[NASA-CR-174804] p 159 N85-17422
SANDERS, W. A.
Strength and microstructure of sintered Si3N4 with rare-earth-oxide additions
[ACS PAPER 130-13-84] p 80 A85-25271
Oxidation of silicon nitride sintered with rare-earth oxide additions p 83 A85-42798
Microstructure of reaction-bonded silicon nitride consolidated by isostatic hot-pressing
p 83 A85-45304
Reliability of two sintered silicon nitride materials
[NASA-TM-87092] p 92 N85-34284
SANGER, N. L.
Design and performance of a fixed, nonaccelerating guide vane cascade that operates over an inlet flow angle range of 60 deg
[ASME PAPER 84-GT-75] p 4 A85-32964
SANTARPIA, D. E.
Status of NASA's multibeam communications technology program p 100 A85-14432
SANTAVICCA, D. A.
The role of surface generated radicals in catalytic combustion p 30 N85-27869
SANTNER, J. S.
Fracture of composite-adhesive-composite systems
p 141 A85-27935
SANTORO, G. J.
Replaceable blade turbine and stationary specimen corrosion testing facility
[NASA-TM-86931] p 73 N85-18126
SANZ, J. M.
Design and performance of a fixed, nonaccelerating guide vane cascade that operates over an inlet flow angle range of 60 deg
[ASME PAPER 84-GT-75] p 4 A85-32964
SAUNDERS, A. L.
The NASA satellite communication 20 x 20 matrix switches p 101 A85-14435
SAUNDERS, N. T.
Future directions in aeropropulsion technology
[NASA-TM-87010] p 1 N85-23685
SAVAGE, M.
Life and reliability modeling of bevel gear reductions
[NASA-TM-87006] p 133 N85-27227
Fatigue life analysis of a turboprop reduction gearbox
[NASA-TM-87014] p 133 N85-27228
SAVINO, J. M.
Reflection plane tests of a wind turbine blade tip section with ailerons
[NASA-TM-87018] p 165 N85-34444
SCAGLIONE, L. J.
Teardown analysis of a ten cell bipolar nickel-hydrogen battery p 156 A85-45385
SCARPELLI, A. R.
Precision tunable resonant microwave cavity
[NASA-CASE-LEW-13935-1] p 103 N85-20248
SCHATZ, M.
Performance capabilities of the 12-centimeter Xenon ion thruster p 42 A85-16439
SCHATZ, M. F.
Heaterless ignition of inert gas ion thruster hollow cathodes
[NASA-TM-87086] p 52 N85-34177
SCHATZMAN, J. C.
The linear two-dimensional stability of inviscid vortex streets of finite-cored vortices
[AD-A153032] p 107 A85-14241
SCHECHTER, B.
An investigation of enhanced capability thermal barrier coating systems for diesel engine components
[NASA-CR-174820] p 86 N85-18154
SCHEER, D. D.
Small centrifugal pumps for low thrust rockets
[AIAA PAPER 85-1302] p 45 A85-43978
SCHEUERMANN, C. M.
Stirling material technology
[NASA-TM-86888] p 72 N85-13007
SCHILLING, H. W.
Circular waveguide bifurcation for asymmetric modes
p 101 A85-20170
Dual-mode coaxial feed with low crosspolarisation
p 101 A85-20171
SCHLUETER, R. A.
Improved models for increasing wind penetration, economics and operating reliability
[NASA-CR-175538] p 160 N85-20545
SCHOCK, H. J.
Incident beam polarization for laser Doppler velocimetry employing a sapphire cylindrical window
p 122 A85-39835
Internal combustion engine combustion chamber process studies at NASA Lewis Research Center
p 112 A85-45856
Holographic optical system for aberration corrections in laser Doppler velocimetry p 123 A85-48659
Incident beam polarization for laser Doppler velocimetry employing a sapphire cylindrical window
[NASA-TM-87064] p 178 N85-28786
SCHOENMAN, L.
Progress report - Advanced cryogenic OTV engine technology
[AIAA PAPER 85-1341] p 44 A85-39735
SCHREIBER, J. G.
Initial results of sensitivity tests - Performed on the RE-1000 free-piston Stirling engine p 129 A85-45466
SCHRUBEN, D. L.
Measurement and correlation of jet fuel viscosities at low temperatures
[NASA-CR-174911] p 94 N85-34295
SCHUBERT, F. H.
Engineering model system study for a regenerative fuel cell: Study report
[NASA-CR-174801] p 158 N85-16292
SCHULLER, F. T.
Effect of two inner-ring oil-flow distribution schemes on the operating characteristics of a 35 millimeter bore ball bearing to 2.5 million DN
[NASA-TP-2404] p 130 N85-13233
Lubrication and performance of high-speed rolling-element bearings
[NASA-TM-86958] p 131 N85-21658
SCHULSON, E. M.
An experimental investigation of rubbing interaction in labyrinth seals at cryogenic temperature
p 129 A85-39938
Analytical and experimental investigation of rubbing interaction in labyrinth seals for a liquid hydrogen fuel pump
[NASA-CR-174657] p 48 N85-18084
SCHULTZ, B. E.
Closed-loop strain controlled testing at elevated temperatures with a non-contacting gage
p 121 A85-29562
SCHULTZ, D.
HOST liner cyclic facilities: Facility description
p 22 N85-10988
SCHUM, E. F.
Application of computational fluid dynamics to complex inlet ducts
[AIAA PAPER 85-1213] p 6 A85-47023
Application of computational fluid dynamics to complex inlet ducts
[NASA-TM-87060] p 118 N85-30247
SCHUMANN, L. F.
A three-dimensional axisymmetric calculation procedure for turbulent flows in a radial vaneless diffuser
[NASA-TM-86903] p 7 N85-14798
SCHUON, S. R.
Effects of chromium and aluminum on mechanical and oxidation properties of iron-nickel-base superalloys based on CG-27
[NASA-TP-2443] p 75 N85-21323
SCHWAB, J. R.
Comparison of secondary flows predicted by a viscous code and an inviscid code with experimental data for a turning duct p 106 A85-11634
Application of viscous and inviscid computation methods for rocket turbopump systems
[SAE PAPER 841522] p 110 A85-39257
Redistribution of the inlet temperature profile through the SSME fuel turbine p 50 N85-26901
SCHWARZE, G. E.
Development of high frequency low weight power magnetics for aerospace power systems
p 102 A85-45373
Performance analysis of radiation cooled dc transmission lines for high power space systems
[NASA-TM-87040] p 104 N85-28222
SCIBBE, H. W.
Effect of lubricant extreme-pressure additives on surface fatigue life of AISI 9310 spur gears
[NASA-TP-2408] p 130 N85-13234
Operating characteristics of a 0.87 kW-hr flywheel energy storage module
[NASA-TM-87038] p 133 N85-28371
Lubricant and additive effects on spur gear fatigue life
[NASA-TM-87044] p 133 N85-28373
SCOLA, D. A.
Imide modified epoxy matrix resins
[NASA-CR-174695] p 85 N85-15892
SCOT, G. W.
Measured effects of wind turbine generation at the Block Island Power Company p 153 A85-10652
SCOTT, W. G.
The 20 GHz proof-of-concept test model results for a multiple scan beam dual reflector antenna
[NASA-CR-174268] p 98 N85-15944
SCUDDER, L. R.
Status of DOE and AID stand-alone photovoltaic system field tests p 155 A85-35707
SEASHOLTZ, R. G.
Filter induced errors in laser anemometer measurements using counter processors
[NASA-TM-87047] p 125 N85-30288
SEINER, J. M.
A multiple-scales model of the shock-cell structure of imperfectly expanded supersonic jets
p 113 A85-49354
SEKAR, R.
Advanced automotive diesel assessment program
[NASA-CR-168285] p 130 N85-13235
SEMANCIK, S.
Advanced thin film thermocouples
[NASA-CR-175541] p 124 N85-21607
SENER, B.
A finite element solution of three-dimensional inviscid rotational flows through curved ducts
p 107 A85-11648
SENG, G. T.
Rapid estimation of concentration of aromatic classes in middistillate fuels by high-performance liquid chromatography
[NASA-TP-2495] p 93 N85-31307
SERAFINI, T. T.
PMR polyimide composites for aerospace applications
p 55 A85-21520
SESHADRI, K.
Polarization (ellipsometric) measurements of liquid condensate deposition and evaporation rates and dew points in flowing salt/ash-containing combustion gases
p 123 A85-46925
SHAFFER, S. J.
High pressure compressor component performance report
[NASA-CR-168245] p 33 N85-34138
SHAFFER, S. L.
Energy efficient engine. High pressure compressor detail design report
[NASA-CR-165558] p 23 N85-10998
SHAFFERNOCKER, W. M.
Advanced smoke meter development survey and analysis
[NASA-CR-168287] p 124 N85-25792
SHALKHAUSER, K. A.
Automated testing of developmental satellite communications systems and subsystems
[NASA-TM-87070] p 100 N85-31348
SHALTENS, R. K.
Measured effects of wind turbine generation at the Block Island Power Company p 153 A85-10652
Operational results for the experimental DOE/NASA Mod-OA wind turbine project
[NASA-TM-83517] p 163 N85-30479
SHANEYFELT, J. T.
Satellite baseband processor test performance summary p 95 A85-14434
SHAPIRO, W.
Development of gas-lubricated pistons for heavy duty diesel engine technology program
[NASA-CR-174746] p 184 N85-12808
SHARMA, L. K.
Feasibility of mapping velocity flow fields in SSME powerhead by laser anemometry techniques
p 41 N85-27971
SHARP, G. R.
Extreme precision antenna reflector study results
p 165 N85-23830
SHAW, L. M.
Unsteady pressure measurements on a biconvex airfoil in a transonic oscillating cascade
[NASA-TM-86914] p 8 N85-15689

SHAW, R. J.
Progress toward the development of an aircraft icing analysis capability
[AIAA PAPER 84-0105] p 10 A85-10653
Analytical determination of propeller performance degradation due to ice accretion
[AIAA PAPER 85-0339] p 14 A85-20867
The NASA altitude wind tunnel - Its role in advanced icing research and development
[AIAA PAPER 85-0090] p 35 A85-26381
The UH-1H helicopter icing flight test program - An overview
[AIAA PAPER 85-0338] p 11 A85-28898
Performance degradation of helicopter rotor in forward flight due to ice p 11 A85-42937
The UH-1H helicopter icing flight test program: An overview
[NASA-TM-86925] p 11 N85-15702
The NASA Altitude Wind Tunnel (AWT): Its role in advanced icing research and development
[NASA-TM-86920] p 35 N85-15758
Performance and surge limits of a TF30-P-3 turbofan engine/axisymmetric mixed-compression inlet propulsion system at Mach 2.5
[NASA-TP-2461] p 27 N85-25261
Ice shapes and the resulting drag increase for a NACA 0012 airfoil
[NASA-TM-83556] p 11 N85-27839

SHAWHAN, S. D.
Effects of chemical releases by the STS 3 orbiter on the ionosphere p 166 A85-29538
Suprathermal plasma observed on STS-3 Mission by plasma diagnostics package p 179 N85-22472
Electron and ion density depletions measured in the STS-3 orbiter wake p 39 N85-22474

SHEIBLEY, D. W.
Alkaline battery containing a separator of a cross-linked copolymer of vinyl alcohol and unsaturated carboxylic acid
[NASA-CASE-LEW-13102-1] p 104 N85-29144
Regenerative fuel cell systems for space station p 104 N85-31372

SHEN, H. D.
Fundamentals of microcrack nucleation mechanics
[NASA-CR-3851] p 137 N85-16195

SHENKMAN, A.
Large-scale Advanced Propfan (LAP) performance, acoustic and weight estimation, January, 1984
[NASA-CR-174782] p 9 N85-22368

SHEU, Y. C.
Ultrasonic wave propagation in two-phase media - Spherical inclusions p 54 A85-11926
Fundamentals of microcrack nucleation mechanics
[NASA-CR-3851] p 137 N85-16195

SHUEN, J. S.
The structure of dilute combusting sprays
[NASA-CR-174838] p 24 N85-15728

SHUEN, J.-S.
Drop-turbulence interactions in a diffusion flame
[AIAA PAPER 85-0319] p 60 A85-19665
Structure of particle-laden jets - Measurements and predictions p 109 A85-25137
Structure of ducted particle-laden turbulent jets p 110 A85-38999
Measurements and predictions of the structure of evaporating sprays p 112 A85-46484
Structure of nonevaporating sprays. I - Initial conditions and mean properties p 112 A85-48538

SIEGEL, R.
Analysis of three-dimensional solidification interface shape p 109 A85-30075
Analysis of buoyancy effect on fully developed laminar heat transfer in a rotating tube p 110 A85-35596
Control of solidification boundary in continuous casting by asymmetric cooling and mold offset p 110 A85-37047
Solidification interface shape for continuous casting in an offset mold - Two analytical methods p 112 A85-41326

SIGARI, G.
Improved models for increasing wind penetration, economics and operating reliability
[NASA-CR-175538] p 160 N85-20545

SIGNER, H. R.
Effect of two inner-ring oil-flow distribution schemes on the operating characteristics of a 35 millimeter bore ball bearing to 2.5 million DN
[NASA-TP-2404] p 130 N85-13233

SIGNORELLI, R. A.
High temperature metal and ceramic composites p 55 A85-37483

SILVERMAN, S. W.
Applicability of 100kWe-class of space reactor power systems to NASA manned space station missions
[NASA-CR-174696] p 177 N85-35728

SIMITSES, G. J.
Thermodynamically consistent constitutive equations for nonisothermal large strain, elasto-plastic, creep behavior
[AIAA PAPER 85-0621] p 142 A85-38425
Analysis of shell type structures subjected to time dependent mechanical and thermal loading
[NASA-CR-175747] p 147 N85-25896
Dynamic creep buckling: Analysis of shell structures subjected to time-dependent mechanical and thermal loading p 149 N85-27959

SIMON, F. F.
Flow visualization study of the effect of injection hole geometry on an inclined jet in crossflow
[NASA-TM-86936] p 115 N85-20269

SIMON, T. W.
Heat transfer and fluid mechanics measurements in transitional boundary layer flows p 118 N85-31439

SIMONEAU, R. J.
Preliminary results of a study of the relationship between free stream turbulence and stagnation region heat transfer
[NASA-TM-86884] p 113 N85-11317
New facility to study unsteady wake effects on turbine airfoil heat transfer p 117 N85-27948
Preliminary results of a study of the relationship between free-stream turbulence and stagnation region heat transfer p 118 N85-31435
Heat transfer in aeropropulsion systems
[NASA-TM-87066] p 119 N85-31444

SINCLAIR, J. H.
Impact resistance of fiber composites - Energy-absorbing mechanisms and environmental effects p 56 A85-46543

SINHA, A.
Effects of friction dampers on aerodynamically unstable rotor stages p 14 A85-21866

SIROCKY, P. J.
Government review of the Mod-2 wind turbine (as-built)
[NASA-TM-86983] p 162 N85-29365

SIZEMORE, R. L.
Government review of the Mod-2 wind turbine (as-built)
[NASA-TM-86983] p 162 N85-29365
Structural analysis and cost estimate of an eight-leg space frame as a support structure for horizontal axis wind turbines
[NASA-TM-83470] p 150 N85-30361

SKEBE, G. G.
High-voltage solar-cell chip p 154 A85-24668

SLABY, J.
Overview of the 1985 NASA Lewis Research Center SP-100 free-piston Stirling engine activities
[NASA-TM-87028] p 185 N85-27769

SLABY, J. G.
Overview of NASA Lewis Research Center free-piston Stirling engine activities p 130 A85-45479

SLEEPER, H. A.
Four-dimensional modulation and coding - An alternate to frequency-reuse p 97 A85-36653

SLINEY, H. E.
The influence of temperature on the lubricating effectiveness of MoS2 dispersed in mineral oils
[ASLE PREPRINT 84-LC-2A-2] p 80 A85-25963
Effects of silver and group 2 fluorides addition to plasma sprayed chromium carbide high temperature solid lubricant for foil gas bearing to 650 deg C
[NASA-TM-86895] p 84 N85-14928
The role of silver in self-lubricating coatings for use at extreme temperatures
[NASA-TM-86943] p 87 N85-20127

SMART, A. E.
Research study of droplet sizing technology leading to the development of an advanced droplet sizing system
[NASA-CR-174839] p 123 N85-21604

SMETANA, J.
Characterization of MMIC devices for active array antennas
[NASA-TM-86907] p 38 N85-15779

SMIALEK, J. L.
Microstructural development of protective Al2O3 scales p 80 A85-21650
Dopant effect of yttrium and the growth and adherence of alumina on nickel-aluminum alloys p 82 A85-40973
Hot corrosion of sintered alpha-SiC at 1000 C
[ACS PAPER 19-B-84P] p 83 A85-45302
Burner rig corrosion of SiC at 1000 deg C
[NASA-TM-87061] p 53 N85-30011
Mechanism of strength degradation for hot corrosion of alpha-SiC
[NASA-TM-87052] p 91 N85-30135

SMITH, G. T.
Resin selection criteria for 'tough' composite structures p 81 A85-35139

SMITH, J. R.
Ceramic component development for the AGT101 gas turbine engine p 126 A85-15972
Universal binding energy relations in metallic adhesion
[NASA-TM-86889] p 72 N85-12132

SMITH, R. F.
Measured effects of wind turbine generation at the Block Island Power Company p 153 A85-10652

SMITHRICK, J. J.
Advanced designs for IPV nickel-hydrogen cells p 156 A85-45438
Initial performance of advanced designs for IPV nickel-hydrogen cells
[NASA-TM-87029] p 162 N85-28444
Initial performance of advanced designs for IPV nickel-hydrogen cells p 105 N85-31404

SMOLL, A.
The 20 GHz proof-of-concept test model results for a multiple scan beam dual reflector antenna
[NASA-CR-174268] p 98 N85-15944

SNELL, G. J.
Solids mixing in a three phase fluidized bed containing spherically shaped-porous solid particles
[PB85-187961] p 120 N85-33453

SNITZER, E.
Fiber optic temperature sensor p 121 A85-29563

SNYDER, C. A.
Shock tube measurements of growth constants in the branched-chain ethane-carbon monoxide-oxygen system
[NASA-TM-87068] p 64 N85-32156

SNYDER, D. B.
Characteristics of arc currents on a negatively biased solar cell array in a plasma p 154 A85-18608
The effect of plasma on solar cell array arc characteristics
[AIAA PAPER 85-0384] p 43 A85-19713
The effect of plasma on solar cell array arc characteristics
[NASA-TM-86887] p 47 N85-11133
Discharges on a negatively biased solar cell array in a charged-particle environment p 160 N85-22499

SO, R. M. C.
Jet characteristics in confined swirling flow p 112 A85-45282
Density effects on jet characteristics in confined swirling flow p 112 A85-45283
Behavior of turbulent gas jets in an axisymmetric confinement
[NASA-CR-174829] p 28 N85-25265

SOCKOL, P. M.
Computation of internal flows: Methods and applications; Proceedings of the Energy Sources Technology Conference, New Orleans, LA, February 12-16, 1984 p 106 A85-11630
Review - Computational methods for internal flows with emphasis on turbomachinery p 4 A85-29126

SOEDER, J. F.
Floating-point function generation routines for 16-bit microcomputers
[NASA-TM-83783] p 170 N85-10683
MINDS: A microcomputer interactive data system for 8086-based controllers
[NASA-TP-2378] p 170 N85-17576

SOEDER, R. H.
Effect of combined pressure and temperature distortion orientation on high-bypass-ratio turbofan engine stability
[NASA-TM-83771] p 17 N85-10067
Effect of steady-state temperature distortion on inlet flow to a high-bypass-ration turbofan engine
[NASA-TM-86896] p 24 N85-15725

SOLOMON, A. S. P.
Drop-turbulence interactions in a diffusion flame
[AIAA PAPER 85-0319] p 60 A85-19665
Structure of particle-laden jets - Measurements and predictions p 109 A85-25137
Structure of ducted particle-laden turbulent jets p 110 A85-38999
Measurements and predictions of the structure of evaporating sprays p 112 A85-46484
Structure of nonevaporating sprays. I - Initial conditions and mean properties p 112 A85-48538
The structure of dilute combusting sprays
[NASA-CR-174838] p 24 N85-15728

SOLOMOS, G. P.
Oscillator response to nonstationary excitation
[ASME PAPER 84-WA/APM-38] p 140 A85-17039

SOMORJAI, G. A.
Properties of coated and modified surfaces p 53 A85-36694

SOVEY, J. S.
Deposition of diamondlike carbon films
[NASA-CASE-LEW-14080-1] p 95 N85-20153
Ring-cusp ion thruster with shell anode
[NASA-CASE-LEW-13881-1] p 48 N85-21256

Vacuum chamber pressure effects on thrust measurements of low Reynolds number nozzles
[NASA-TM-86955] p 49 N85-21259
Compatibility experiments of facilities, materials, and propellants for electrothermal thrusters
[NASA-TM-86956] p 49 N85-21260
SPALVINS, T.
Frictional and morphological properties of Au-MoS2 films sputtered from a compact target p 127 A85-19085
Surface hardening of steel by boriding in a cold rf plasma p 68 A85-40275
Plasma variables and tribological properties of coatings in low pressure (0.1 - 10.0 torr) plasma systems
[NASA-TM-83798] p 94 N85-11261
Tribological properties of boron nitride synthesized by ion beam deposition
[NASA-TM-86962] p 87 N85-21355
Frictional and structural characterization of ion-nitrided low and high chromium steels
[NASA-TM-86991] p 132 N85-23085
The structure of ion plated films in relation to coating properties
[NASA-TM-87055] p 95 N85-29085
Advances in sputtered and ion plated solid film lubrication p 136 N85-33524
SPANOS, P.-T. D.
Oscillator response to nonstationary excitation
[ASME PAPER 84-WA/APM-38] p 140 A85-17039
SPEAR, K. E.
A morphological study of silicon carbide prepared by chemical vapor deposition p 79 A85-20938
SPEIR, D. W.
Altitude testing of a flight weight, self-cooled, 2D thrust vectoring exhaust nozzle
[SAE PAPER 841557] p 14 A85-25984
SPERA, D. A.
Method for evaluating wind turbine wake effects on wind farm performance p 155 A85-36750
SPRING, J.
Conceptual design of a fixed-pitch wind turbine generator system rated at 400 kilowatts
[NASA-CR-174877] p 162 N85-29363
SRINATH, N. K.
Four-dimensional modulation and coding - An alternate to frequency-reuse p 97 A85-36653
SRINIVASAN, R.
Experiments in dilution jet mixing - Effects of multiple rows and non-circular orifices
[AIAA PAPER 85-1104] p 15 A85-39606
Experiments in dilution jet mixing effects of multiple rows and non-circular orifices
[NASA-TM-86996] p 28 N85-25266
SRIRAMAMURTHY, A. M.
Deformation and fracture behavior of Ni-Mo-Al(gamma/gamma prime-alpha) in situ composite p 64 A85-11058
ST.JOHN, G. A.
Chemistry of fuel deposits and sediments and their predursors
[NASA-CR-174778] p 92 N85-10209
STAFFORD, J.
Pantographing self adaptive gap elements p 142 A85-37440
STAIGER, P. J.
Primary propulsion of electrothermal, ion and chemical systems for space-based radar orbit transfer
[NASA-TM-87043] p 51 N85-27972
STANCIK, K.
Effect of steady-state temperature distortion on inlet flow to a high-bypass-ration turbofan engine
[NASA-TM-86896] p 24 N85-15725
STANFORTH, C. M.
Advanced smoke meter development survey and analysis
[NASA-CR-168287] p 124 N85-25792
STANITZ, J. D.
General design method for 3-dimensional, potential flow fields. Part 2: Computer program DIN3D1 for simple, unbranched ducts
[NASA-CR-3926] p 10 N85-35159
STANTON, A. C.
An approach for automated analysis of particle holograms p 120 A85-10034
STASKUS, J. V.
Electron beam charging of Space Shuttle thermal protection system tiles p 39 N85-22478
STATLER, R. L.
Effects of 1 MeV electrons and 10 MeV protons on the performance and reflectance of thin BSR cells p 182 A85-35699
STEARNS, C. A.
Reactions of NaCl with gaseous SO3, SO2, and O2 p 59 A85-11897
Chemical reactions involved in the initiation of hot corrosion of IN-738 p 66 A85-31688
Burner rig corrosion of SiC at 1000 deg C
[NASA-TM-87061] p 53 N85-30011
STECURA, S.
Optimization of the NiCrAl-Y/ZrO-Y2O3 thermal barrier system
[NASA-TM-86905] p 72 N85-15878
Thermal barrier coating system
[NASA-CASE-LEW-13324-2] p 57 N85-21266
Advanced thermal barrier system bond coatings for use on Ni, Co-, and Fe-base alloy substrates
[NASA-TM-87062] p 77 N85-31283
Thermal barrier coating system
[NASA-CASE-LEW-14057-1] p 59 N85-35233
STEENKEN, W. G.
Stall recovery control strategy methodology and results
[AIAA PAPER 85-1433] p 16 A85-40841
STEFKO, G. L.
Wind tunnel results of advanced high speed propellers in the takeoff, climb, and landing operating regimes
[AIAA PAPER 85-1259] p 6 A85-47025
Wind tunnel results of advanced high speed propellers in the takeoff, climb and landing operating regimes
[NASA-TM-87054] p 9 N85-29925
STEIN, Y.
The role of surface generated radicals in catalytic combustion p 30 N85-27869
STEINBACH, R. E.
Interdisciplinary design analysis of a precision spacecraft antenna
[AIAA PAPER 85-0804] p 38 A85-30303
STEINBERG, R.
MERIT: A man/computer data management and enhancement system for upper air nowcasting/forecasting in the United States p 167 N85-10558
STEINER, G.
Development of a large insert gas ion thruster p 45 A85-42922
STEINETZ, B. M.
Application of traction drives as servo mechanisms p 152 N85-33520
STEINNAGEL, K.
Satellite provided customer promises services, a forecast of potential domestic demand through the year 2000. Volume 4: Sensitivity analysis
[NASA-CR-174662] p 99 N85-27092
STEPHENS, J. R.
Stirling material technology
[NASA-TM-86888] p 72 N85-13007
The B2 aluminides as alternative materials
[NASA-TM-86937] p 74 N85-19076
STETZ, T. T.
Flow rates and pressure profiles for one to four axially alined Borda inlets
[NASA-TP-2390] p 113 N85-14078
Flow rate and pressure profiles for 1 to 4 axially alined orifice inlets
[NASA-TP-2460] p 116 N85-27165
STEVENS, G. A.
Modeling of NASA's 30/20 GHz satellite communications system p 38 A85-36663
STEVENS, N. J.
Environmentally-induced voltage limitations in large space power systems p 43 A85-18584
Design guidelines for assessing and controlling spacecraft charging effects p 40 N85-22500
STEVENSON, S.
Demand for satellite-provided domestic communications services up to the year 2000
[NASA-TM-86894] p 97 N85-15099
STEWART, G. W.
An approach for automated analysis of particle holograms p 120 A85-10034
STILLER, P. H.
Measured effects of wind turbine generation at the Block Island Power Company p 153 A85-10652
STINCHCOMB, W. W.
A study of the stress wave factor technique for the characterization of composite materials
[NASA-CR-174870] p 58 N85-30035
STOCKER, D. P.
Applications of high pressure differential scanning calorimetry to aviation fuel thermal stability research
[NASA-TM-87002] p 63 N85-23941
STOFAN, A. J.
A high energy stage for the National Space Transportation System
[IAF PAPER 84-15] p 36 A85-23200
STOLOFF, N. S.
The influence of hold times on LCF and FCG behavior in a P/M Ni-base superalloy p 67 A85-32400
STONE, J. R.
Supersonic jet shock noise reduction
[AIAA PAPER 84-2278] p 173 A85-16099
STONEHART, P.
Electrocatalyst advances for hydrogen oxidation in phosphoric acid fuel cells p 60 A85-15614
Preparation and evaluation of advanced catalysts for phosphoric acid fuel cells
[NASA-CR-168223] p 160 N85-19511
STOTLER, C. L.
Energy efficient engine ICLS Nacelle detail design report
[NASA-CR-167870] p 22 N85-10993
STOUFFER, D. C.
Finite element analysis of notch behavior using a state variable constitutive equation p 152 N85-31548
STRANGE, R. R.
Development of advanced high-temperature heat flux sensors. Phase 2: Verification testing
[NASA-CR-174973] p 126 N85-35391
STRANGMAN, T. E.
Development of coated single-crystal superalloy systems for gas turbine applications p 68 A85-32440
STRAZISAR, A. J.
Investigation of flow phenomena in a transonic fan rotor using laser anemometry
[ASME PAPER 84-GT-199] p 4 A85-32963
Rotor wake characteristics of a transonic axial flow fan
[AIAA PAPER 85-1133] p 6 A85-43974
STREHLOW, R. A.
The mechanisms of flame holding in the wake of a bluff body
[NASA-CR-174058] p 62 N85-11149
The mechanisms of flame holding in the wake of a bluff body
[NASA-CR-3866] p 26 N85-21166
Behavior of the lean methane-air flame at zero-gravity
[NASA-CR-175586] p 62 N85-21283
The use of a laser Doppler velocimeter in a standard flammability tube
[NASA-CR-174960] p 125 N85-35389
STRICKER, J.
Electronic heterodyne readout of fringes in moire deflectometry p 122 A85-36726
Moire deflectometry with deferred electronic heterodyne readout p 122 A85-42854
A comparison of electronic heterodyne moire deflectometry and electronic heterodyne holographic interferometry for flow measurements
[NASA-TM-87071] p 125 N85-32302
STUART, T. A.
Small-signal model for the series resonant converter p 102 A85-39453
STURGESS, G. J.
Calculation of confined swirling flows
[AIAA PAPER 85-0060] p 108 A85-19491
STURMAN, J. C.
High-voltage, high-power, solid-state remote power controllers for aerospace applications
[NASA-TP-2437] p 49 N85-21263
SUBRAHMANYAM, K. B.
Finite difference analysis of torsional vibrations of pretwisted, rotating, cantilever beams with effects of warping p 143 A85-42047
Vibration and buckling of rotating, pretwisted, preconed beams including Cooriolis effects
[NASA-TM-87004] p 146 N85-25893
Nonlinear flap-lag-extensional vibrations of rotating, pretwisted, preconed beams including Coriolis effects
[NASA-TM-87102] p 152 N85-34427
SUBRAMANIAN, S. V.
Application of Runge Kutta time marching scheme for the computation of transonic flows in turbomachines
[AIAA PAPER 85-1332] p 5 A85-39728
SULLIVAN, J. P.
Noise constraints effecting optimal propeller designs
[SAE PAPER 850871] p 7 A85-50106
Noise constraints effecting optimal propeller designs
[NASA-TM-86967] p 8 N85-19923
SULLIVAN, T. J.
Energy efficient engine. Fan and quarter-stage component performance report
[NASA-CR-168070] p 33 N85-34141
SULLIVAN, T. L.
Government review of the Mod-2 wind turbine (as-built)
[NASA-TM-86983] p 162 N85-29365
SUMIHARA, K.
Rational approach for assumed stress finite elements p 139 A85-12029
Hybrid Semiloof elements for plates and shells based upon a modified Hu-Washizu principle p 139 A85-15893
SUMMERS, C.
Technology for satellite power conversion
[NASA-CR-174335] p 159 N85-18451

SUMMERS, R. L.
Integrated exhaust gas analysis system for aircraft turbine engine component testing
[NASA-TP-2424] p 123 N85-16100
SUN, C. T.
Use of statical indentation laws in the impact analysis of laminated composite plates p 55 A85-29133
SUNDARAM, C. V.
Flow dynamic environment data base development for the SSME p 147 N85-26885
SUNDBERG, G. R.
Advanced in solid state switchgear technology for large space power systems p 102 A85-45362
A new very high voltage semiconductor switch
[NASA-TM-86957] p 103 N85-20246
SUTTON, R.
Cryogenic upper stage test bed engine
[AIAA PAPER 85-1339] p 44 A85-39733
SUTTON, R. D.
Analytical fuel property effects--small combustors
[NASA-CR-174738] p 28 N85-26709
SWAN, P.
Report of the Constellations Panel
p 131 N85-20368
SWARNER, W. G.
Adaptive antenna arrays for satellite communications: Design and testing
[NASA-CR-176162] p 100 N85-34329
SWARTWOUT, T.
Design and analysis report for the RL10-2B breadboard low thrust engine
[NASA-CR-174857] p 48 N85-19020
SWARTZ, C. K.
Voltage controlling mechanisms in low resistivity silicon solar cells - A unified approach p 155 A85-35617
Radiation damage and defect behavior in ion-implanted, lithium counterdoped silicon solar cells
p 182 A85-35698
Effects of 1 MeV electrons and 10 MeV protons on the performance and reflectance of thin BSR cells
p 182 A85-35699
The high voltage silicon cell: A comparative analysis
p 49 N85-22569
The effects of lithium counterdoping on radiation damage and annealing in n(+)p silicon solar cells
p 50 N85-22586
SWEC, D. M.
Ion beam sputter-deposited thin film coatings for protection of spacecraft polymers in low Earth orbit
[NASA-TM-87051] p 91 N85-30137
Diamondlike carbon protective coatings for IR materials
[NASA-TM-87083] p 178 N85-34631
SWETTE, L.
Development of electrodes for the NASA iron/chromium
[NASA-CR-174724] p 165 N85-35471
SWINDAL, J. L.
High-temperature optically activated GaAs power switching for aircraft digital electronic control
[NASA-CR-174711] p 34 N85-12901
SYED, S. A.
Finite difference methods for reducing numerical diffusion in TEACH-type calculations
[AIAA PAPER 85-0057] p 108 A85-19488
Calculation of confined swirling flows
[AIAA PAPER 85-0060] p 108 A85-19491
Assessment of discretization schemes to reduce numerical diffusion in the calculation of complex flows
[AIAA PAPER 85-0441] p 108 A85-19751
Reducing numerical diffusion for incompressible flow calculations
[NASA-TM-83621] p 24 N85-14840
Error reduction program
[NASA-CR-174776] p 172 N85-27584
SZETELA, E. J.
External fuel vaporization study, phase 2
[NASA-CR-174079] p 92 N85-11252
SZUCH, J. R.
Analytical and physical modeling program for the NASA Lewis Research Center's Altitude Wind Tunnel (AWT)
[AIAA PAPER 85-0379] p 34 A85-19709
Analytical and physical modeling program for the NASA Lewis Research Center's Altitude Wind Tunnel (AWT)
[NASA-TM-86919] p 35 N85-15757

T

TABADDOR, F.
Pantographing self adaptive gap elements
p 142 A85-37440
TABAKOFF, W.
The three-dimensional compressible flow in a radial inflow turbine scroll p 6 A85-41826
TAM, C. K. W.
A multiple-scales model of the shock-cell structure of imperfectly expanded supersonic jets
p 113 A85-49354
TAMASHIRO, R. N.
A 20 GHz, 75 watt, helix TWT for space communications p 101 A85-14433
TAN, T. M.
Use of statical indentation laws in the impact analysis of laminated composite plates p 55 A85-29133
TANAKA, K.
Effects of wear on structure-sensitive magnetic properties of ceramic ferrite in contact with magnetic tape
[NASA-TM-87007] p 90 N85-26991
TANIS, F. J.
Comparison of atmospheric correction algorithms for the Coastal Zone Color Scanner p 153 A85-10244
TANVEER, S.
Vortex induced lift on a flat plate with a curved forward-facing flap p 4 A85-30175
TAYLOR, J. R.
Flow modifying device
[NASA-CASE-LEW-13562-2] p 33 N85-35195
TAYLOR, S. R.
Percutaneous connectors
[NASA-CR-175627] p 168 N85-27508
TEAGAN, W. P.
Preliminary evaluation of a liquid belt radiator for space applications
[NASA-CR-174807] p 47 N85-15804
TELESMAN, J.
A study of spectrum fatigue crack propagation in two aluminum alloys. 1: Spectrum simplification
[NASA-TM-86929] p 72 N85-18124
A study of spectrum fatigue crack propagation in two aluminum alloys. 2: Influence of microstructures
[NASA-TM-86930] p 73 N85-18125
TESAR, J. S.
Acoustic structure and propagation in highly porous, layered, fibrous materials p 173 A85-12301
TEVAARWERK, J. L.
Thermal traction contact performance evaluation under fully flooded and starved conditions
[NASA-CR-168173] p 132 N85-25848
Rolling, slip and traction measurements on low modulus materials
[NASA-CR-174909] p 135 N85-33491
TEW, R. C.
Comparison of free-piston Stirling engine model predictions with RE1000 engine test data
p 130 A85-45488
TEWARI, S. N.
Deformation and fracture behavior of Ni-Mo-Al(gamma/gamma prime-alpha) in situ composite
p 64 A85-11058
Microstructures in rapidly solidified Ni-Mo alloys
[NASA-TM-87100] p 78 N85-34266
THALLER, L. H.
Electrochemistry and storage p 62 N85-13889
System level electrochemical principles
p 104 N85-31375
Design principles for nickel hydrogen cells and batteries p 104 N85-31398
Design principles for nickel-hydrogen cells and batteries
[NASA-TM-87037] p 164 N85-31646
THEOBALD, M. A.
Turbofan noise generation. Volume 2: Computer programs
[NASA-CR-167952] p 175 N85-11791
THIEME, L. G.
Initial testing of a variable-stroke Stirling engine
[NASA-TM-86875] p 185 N85-19895
THOMA, D. J.
Interaction of high-cycle and low-cycle fatigue of Haynes 188 alloy at 1400 F deg p 149 N85-27961
THOMAS, R. L.
Electric power - Photovoltaic or solar dynamic?
p 46 A85-47042
THOMAS, T. T.
Energy efficient engine high pressure turbine test hardware detailed design report
[NASA-CR-167955] p 23 N85-10995
THOMPKINS, W. T., JR.
Researched applied to transonic compressors in numerical fluid mechanics of inviscid flow and viscous flow
[NASA-CR-174353] p 114 N85-18291
THOMPSON, R. L.
Validation of structural analysis methods using the in-house liner cyclic rigs p 21 N85-10987
A computer analysis program for interfacing thermal and structural codes
[NASA-TM-87021] p 148 N85-27264
On numerical integration and computer implementation of viscoplastic models p 151 N85-31542
THRASHER, S. R.
Ceramic applications in turbine engines
[NASA-CR-174715] p 91 N85-28109
TIAN, Z.
Axisymmetric solid elements by a rational hybrid stress method p 143 A85-41109
TIDMAN, D. A.
Investigation of a pulsed electrothermal thruster system
[NASA-CR-174768] p 46 N85-11132
TIEGS, T. N.
Dispersed metal-toughened ceramics and ceramic brazing
[NASA-CR-174284] p 86 N85-15916
Dispersed-metal-toughened alumina
[NASA-CR-174687] p 89 N85-22758
TIEN, J. K.
Modeling of gamma/gamma-prime phase equilibrium in the nickel-aluminum system p 65 A85-14959
Effects of cobalt on the hot workability of nickel-base superalloys p 67 A85-32412
TIEN, J. S.
Flame flashback in a premixed dump combustor
[AIAA PAPER 85-0145] p 60 A85-19550
TITRAN, R. H.
Ductility in rapidly solidified NiAl p 66 A85-26158
Stirling material technology
[NASA-TM-86888] p 72 N85-13007
High temperature properties of equiatomic FeAl with ternary additions
[NASA-TM-86938] p 73 N85-19072
Alloys based on NiAl for high temperature applications
[NASA-TM-86976] p 75 N85-21322
TOMAZIC, W. A.
Effect of water on hydrogen permeability
[NASA-TM-86904] p 53 N85-14864
TONER, J.
Substrate-induced orientational order in the isotropic phase of liquid crystals p 181 A85-24649
TORRES, F. J.
Local heat-transfer measurements on a large, scale-model turbine blade airfoil using a composite of a heater element and liquid crystals
[NASA-TM-86900] p 119 N85-33435
TOTH, J. M., JR.
Fiberglass epoxy laminate fatigue properties at 300 and 20 K p 56 A85-47970
TOWNE, C. E.
Analytical modeling of circuit aerodynamics in the new NASA Lewis Altitude Wind Tunnel
[AIAA PAPER 85-0380] p 3 A85-26389
Application of computational fluid dynamics to complex inlet ducts
[AIAA PAPER 85-1213] p 6 A85-47023
Analytical modeling of circuit aerodynamics in the new NASA Lewis wind tunnel
[NASA-TM-86912] p 8 N85-15688
Application of computational fluid dynamics to complex inlet ducts
[NASA-TM-87060] p 118 N85-30247
TOWNSEND, D. P.
Into mesh lubrication of spur gears with arbitrary offset oil jet. I - For jet velocity less than or equal to gear velocity p 128 A85-24497
Lubricant jet flow phenomena in spur and helical gears with modified center distances and/or addendums - For out-of-mesh conditions
[ASME PAPER 84-DET-96] p 129 A85-35049
Effect of lubricant extreme-pressure additives on surface fatigue life of AISI 9310 spur gears
[NASA-TP-2408] p 130 N85-13234
Effect of five lubricants on life of AISI 9310 spur gears
[NASA-TP-2419] p 123 N85-16099
Lubricant and additive effects on spur gear fatigue life
[NASA-TM-87044] p 133 N85-28373
Powder metallurgy forged gear development
[NASA-TM-87483] p 134 N85-29295
Lubrication and cooling for high speed gears
[NASA-TM-87096] p 136 N85-34407
TOZZI, L.
Advanced automotive diesel assessment program
[NASA-CR-168285] p 130 N85-13235
TREFNY, C. J.
Low-speed aerodynamic test of an axisymmetric supersonic inlet with variable cowl slot
[AIAA PAPER 85-1210] p 5 A85-40819
Low-speed aerodynamic test of an axisymmetric supersonic inlet with variable cowl slot
[NASA-TM-87039] p 28 N85-26710
TRINH, T. Q.
Sixty GHz IMPATT diode development
[NASA-CR-174969] p 105 N85-33293

TRIPP, J. H.
Surface roughness effects in elastohydrodynamic contacts
[NASA-TP-2488] p 134 N85-32329
Hertzian contact in two and three dimensions
[NASA-TP-2473] p 135 N85-32331
TROTH, D. L.
Analytical fuel property effects--small combustors
[NASA-CR-174738] p 28 N85-26709
TROUT, A. M.
Combustion gas properties I-ASTM jet A fuel and dry air
[NASA-TP-2359] p 17 N85-10064
Combustion gas properties. 2: Natural gas fuel and dry air
[NASA-TP-2435] p 26 N85-21168
TSAY, C. B.
Spiral bevel and circular arc helical gears: Tooth contact analysis and the effect of misalignment on circular arc helical gears
[NASA-TM-87013] p 32 N85-31060
TSUI, P.
A morphological study of silicon carbide prepared by chemical vapor deposition p 79 A85-20938
TSUNG, W. J.
Generated spiral bevel gears: Optimal machine-tool settings and tooth contact analysis
[NASA-TM-87075] p 136 N85-34405
TSUNG, W. T.
Spiral bevel and circular arc helical gears: Tooth contact analysis and the effect of misalignment on circular arc helical gears
[NASA-TM-87013] p 32 N85-31060
TYREE, E.
The effect of plasma on solar cell array arc characteristics
[AIAA PAPER 85-0384] p 43 A85-19713
The effect of plasma on solar cell array arc characteristics
[NASA-TM-86887] p 47 N85-11133

U

USHIODA, S.
Prism-coupled light emission from tunnel junctions
p 181 A85-21425

V

VAANFOSSEN, G. J., JR.
Preliminary results of a study of the relationship between free stream turbulence and stagnation region heat transfer
[NASA-TM-86884] p 113 N85-11317
VAKILI, A. D.
Flow control in a diffusing S-Duct
[AIAA PAPER 85-0524] p 3 A85-25928
VALCO, G. J.
High-voltage solar-cell chip p 154 A85-24668
VALGORA, M. E.
Space station propulsion options
[AIAA PAPER 85-1155] p 45 A85-43975
VANFOSSEN, G. J., JR.
The influence of jet-grid turbulence on heat transfer from the stagnation region of a cylinder in crossflow
[NASA-TM-87011] p 115 N85-25760
Preliminary results of a study of the relationship between free-stream turbulence and stagnation region heat transfer p 118 N85-31435
VANNUCCI, R. D.
Graphite/PMR polyimide composites with improved toughness
[NASA-TM-87081] p 58 N85-32148
VANOVERBEKE, T. J.
SSME fuel preburner two-dimensional analysis
p 51 N85-27943
VARGA, G. M., JR.
Jet fuel property changes and their effect on producibility and cost in the U.S., Canada, and Europe
[NASA-CR-174840] p 93 N85-27012
VARY, A.
Ultrasonic nondestructive evaluation, microstructure, and mechanical property interrelations
[NASA-TM-86876] p 137 N85-10371
VATSA, V. N.
A three-dimensional boundary-layer analysis including heat-transfer and blade-rotation effects
p 6 A85-42988
VEDHA-NAYAGAM, M.
Gravitational effects on flames spreading over thick solid surfaces
[IAF PAPER 84-154] p 59 A85-13092
VEDULA, K. M.
High temperature properties of equiatomic FeAl with ternary additions
[NASA-TM-86938] p 73 N85-19072
Alloys based on NiAl for high temperature applications
[NASA-TM-86976] p 75 N85-21322
VEERABHADRA RAO, P.
Spherical microglass particle impingement studies of thermoplastic materials at normal incidence
p 79 A85-11072
A unified relation for cavitation erosion
p 109 A85-24445
VENTRES, C. S.
Turbofan noise generation. Volume 2: Computer programs
[NASA-CR-167952] p 175 N85-11791
VENUGOPALAN, M.
Analysis of glow discharges for understanding the process of film formation
[NASA-TM-83750] p 62 N85-10138
VERDON, J. M.
A linearized unsteady aerodynamic analysis for transonic cascades p 3 A85-20744
VERSAW, E. F.
Study of advanced fuel system concepts for commercial aircraft and engines
[NASA-CR-174752] p 93 N85-19176
VERZWYVELT, S. A.
Long life nickel electrodes for a nickel-hydrogen cell. III - Results of an accelerated test and failure analyses
p 156 A85-45391
The failure mechanism of a nickel electrode in a nickel-hydrogen cell p 105 N85-31408
VICKERS, E. C.
Flow modifying device
[NASA-CASE-LEW-13562-2] p 33 N85-35195
VINET, P.
Aluminum work function: Effect of oxidation, mechanical scraping and ion bombardment
[NASA-TM-87079] p 78 N85-34265
VINOPAL, T. J.
Vehicle/engine integration p 37 N85-17008
VONGLAHN, U. H.
Preliminary analysis of tone-excited two-stream jet velocity decay
[NASA-TM-86951] p 8 N85-21114
VONTIESENHAUSEN, G.
Report of the Constellations Panel
p 131 N85-20368

W

WAGNER, R. C.
Effects of silver and group 2 fluorides addition to plasma sprayed chromium carbide high temperature solid lubricant for foil gas bearing to 650 deg C
[NASA-TM-86895] p 84 N85-14928
Experimental test program for evaluation of solid lubricant coating as applied to compliant foil gas bearings to 315 deg C
[NASA-CR-174837] p 85 N85-15895
WALKER, K. P.
A survey of unified constitutive theories
p 150 N85-31531
WALLACE, J. F.
Effect of reduction of strategic Columbium addition in 718 Alloy on the structure and properties
[NASA-CR-174841] p 75 N85-21320
WALTON, E. K.
Adaptive antenna arrays for satellite communications: Design and testing
[NASA-CR-176162] p 100 N85-34329
WANG, C. L.
Develop and test fuel cell powered on-site integrated total energy systems. Phase 3: Full-scale power plant development
[NASA-CR-174887] p 161 N85-25941
Develop and test fuel cell powered on-site integrated total energy systems. Phase 3: Full-scale power plant development
[NASA-CR-168338] p 164 N85-30483
WANG, C.-H.
Multibus-based parallel processor for simulation
p 169 A85-28613
WANG, S. Y.
Primary propulsion of electrothermal, ion and chemical systems for space-based radar orbit transfer
[NASA-TM-87043] p 51 N85-27972
WANG, T.
Heat transfer and fluid mechanics measurements in transitional boundary layer flows p 118 N85-31439
WARK, C.
Development of a temperature measurement system with application to a jet in a cross flow experiment
[NASA-CR-174896] p 27 N85-25262
WARNER, J. D.
Plasma deposited hydrogenated carbon on GaAs and InP p 182 A85-40386
Plasma deposited diamondlike carbon on GaAs and InP
[NASA-TM-86870] p 183 N85-10844
Optical properties of hydrogenated amorphous carbon films grown from methane plasma
[NASA-TM-86995] p 183 N85-26406
WARSHAWSKY, I.
Calibration stability of some hot-cathode ion gauges
p 122 A85-41634
WASSERBAUER, C. A.
Static jet noise test results of four 0.35 scale-model QCGAT mixer nozzles
[NASA-TM-86871] p 175 N85-13551
WASSERBAUER, J. F.
Performance and surge limits of a TF30-P-3 turbofan engine/axisymmetric mixed-compression inlet propulsion system at Mach 2.5
[NASA-TP-2461] p 27 N85-25261
WATSON, G. K.
Effect of hot isostatic pressing on reaction-bonded silicon nitride p 79 A85-15195
Effect of hot isostatic pressing on the properties of sintered alpha silicon carbide p 83 A85-48757
WATSON, J. W.
Deposition stress effects on the life of thermal barrier coatings on burner rigs p 79 A85-19086
WAYNE, S. F.
Iron rich low cost superalloys
[NASA-CR-174900] p 76 N85-26962
WAYNERT, J.
A rotating superconducting solenoid for 100 kWh energy storage p 44 A85-33144
WEAR, J. D.
Combustion gas properties I-ASTM jet A fuel and dry air
[NASA-TP-2359] p 17 N85-10064
Combustion system for radiation investigations
p 21 N85-10986
Combustion gas properties. 2: Natural gas fuel and dry air
[NASA-TP-2435] p 26 N85-21168
Combustion gas properties. Part 3: Hydrogen gas fuel and dry air
[NASA-TP-2477] p 32 N85-31058
WEHNER, G. K.
Cone formation as a result of whisker growth on ion bombarded metal surfaces p 182 A85-41635
WEINBERG, I.
Theory of the high base resistivity n(+)pp(+) silicon solar cell and its application to radiation damage effects
p 154 A85-32639
Radiation damage and defect behavior in ion-implanted, lithium counterdoped silicon solar cells
p 182 A85-35698
Lithium counterdoped silicon solar cell
[NASA-CASE-LEW-14177-1] p 160 N85-20535
The effects of lithium counterdoping on radiation damage and annealing in n(+)p silicon solar cells
p 50 N85-22586
WEISS, J. S.
A design methodology for robust failure detection and isolation p 171 A85-47794
WEIZER, V. G.
Applicability of the Meyer-Neldel rule to solar cells
p 154 A85-19948
Effect of solar-cell junction geometry on open-circuit voltage p 154 A85-28080
Voltage controlling mechanisms in low resistivity silicon solar cells - A unified approach p 155 A85-35617
The effect of diffusion induced lattice stress on the open-circuit voltage in silicon solar cells
p 181 A85-35620
The high voltage silicon cell: A comparative analysis
p 49 N85-22569
WELDON, V. A.
Vehicle/engine integration p 37 N85-17008
WELGE, H. R.
Low-speed aerodynamic test of an axisymmetric supersonic inlet with variable cowl slot
[AIAA PAPER 85-1210] p 5 A85-40819
Low-speed aerodynamic test of an axisymmetric supersonic inlet with variable cowl slot
[NASA-TM-87039] p 28 N85-26710
WENGER, N. C.
HOST instrumentation R and D program overview
p 19 N85-10957
WERTH, J.
Develop and test fuel cell powered on-site integrated total energy systems. Phase 3: Full-scale power plant development
[NASA-CR-174887] p 161 N85-25941

Develop and test fuel cell powered on-site integrated total energy systems. Phase 3: Full-scale power plant development
[NASA-CR-168338] p 164 N85-30483
WERTHEN, J. G.
Magnesium doping of efficient GaAs and Ga(0.75)In(0.25)As solar cells grown by metalorganic chemical vapor deposition p 180 A85-11466
WESTFALL, L. J.
Arc spray fabrication of metal matrix composite monotape
[NASA-CASE-LEW-13828-1] p 58 N85-30027
WHALEN, M. V.
Vacuum chamber pressure effects on thrust measurements of low Reynolds number nozzles
[NASA-TM-86955] p 49 N85-21259
Compatibility experiments of facilities, materials, and propellants for electrothermal thrusters
[NASA-TM-86956] p 49 N85-21260
WHEATON, M. L.
Heat treatment of bulk gallium arsenide using a phosphosilicate glass cap p 181 A85-32636
WHEELER, R. L., III
Nested subcritical flows within supercritical systems
[NASA-TM-86980] p 115 N85-21574
WHELAN, J. A.
Develop and test fuel cell powered on-site integrated total energy systems. Phase 3: Full-scale power plant development
[NASA-CR-174887] p 161 N85-25941
Develop and test fuel cell powered on-site integrated total energy systems. Phase 3: Full-scale power plant development
[NASA-CR-168338] p 164 N85-30483
WHITE, B. E.
A frequency-routed satellite system concept using multiple orthogonally-polarized beams for frequency reuse p 97 A85-34470
WHITE, C. D.
Experiments in dilution jet mixing - Effects of multiple rows and non-circular orifices
[AIAA PAPER 85-1104] p 15 A85-39606
Experiments in dilution jet mixing effects of multiple rows and non-circular orifices
[NASA-TM-86996] p 28 N85-25266
WHITEHAIR, S.
Experiments with a microwave electrothermal thruster concept p 42 A85-16441
WHITTLE, D. P.
Effects of SO2 and SO3 on the Na2SO4 induced corrosion of nickel p 65 A85-15603
WHITTLESEY, A.
Design guidelines for assessing and controlling spacecraft charging effects p 40 N85-22500
WHYTE, W.
On the subjective evaluation of the interference protection ratios' measurements for co-channel FM-TV signals p 96 A85-28241
WHYTE, W. A.
The subjective effect of multiple co-channel frequency modulated television interference p 96 A85-28234
WHYTE, W. A., JR.
Experimental results supporting the determination of service quality objectives for DBS systems p 96 A85-29611
WILKINSON, C. L.
Space station propulsion options
[AIAA PAPER 85-1155] p 45 A85-43975
WILLENBERG, H. J.
Applicability of 100kWe-class of space reactor power systems to NASA manned space station missions
[NASA-CR-174696] p 177 N85-35728
WILLIAMS, F.
Report of the Constellations Panel p 131 N85-20368
WILLIAMS, G. C.
Interply layer degradation effects on composite structural response
[AIAA PAPER 84-0849] p 54 A85-16096
Interply layer degradation effects on composite structural response p 55 A85-39215
WILLIAMS, J. H., JR.
Stress waves in an isotropic elastic plate excited by a circular transducer
[NASA-CR-3877] p 138 N85-20390
Application of homomorphic signal processing to stress wave factor analysis
[NAS 1.26:174871] p 138 N85-21673
Ultrasonic testing of plates containing edge cracks
[NASA-CR-3904] p 138 N85-29307
WILLIAMS, J. J.
Flow modifying device
[NASA-CASE-LEW-13562-2] p 33 N85-35195
WILLIAMSON, W. S.
Characterization of 8-cm engineering model thruster
[NASA-CR-174673] p 46 N85-11131
WILLIE, R.
Development of a lithium secondary battery separator p 104 N85-31378
WILLSKY, A. S.
A design methodology for robust failure detection and isolation p 171 A85-47794
WILREKER, V. F.
Measured effects of wind turbine generation at the Block Island Power Company p 153 A85-10652
WILSON, R. B.
3-D inelastic analysis methods for hot section components (base program)
[NASA-CR-174700] p 145 N85-21686
WILSON, S. G.
Four-dimensional modulation and coding - An alternate to frequency-reuse p 97 A85-36653
WINEGAR, S. R.
Interdisciplinary design analysis of a precision spacecraft antenna
[AIAA PAPER 85-0804] p 38 A85-30303
WINEMILLER, J. R.
Structural analysis and cost estimate of an eight-leg space frame as a support structure for horizontal axis wind turbines
[NASA-TM-83470] p 150 N85-30361
WINSOR, N. K.
Investigation of a pulsed electrothermal thruster system
[NASA-CR-174768] p 46 N85-11132
WIRSCHING, P. H.
Creep-rupture reliability analysis p 143 A85-42566
Reliability considerations for the total strain range version of strainrange partitioning
[NASA-CR-174757] p 144 N85-11380
WITZELL, W. E.
Effect of low temperature on fatigue and fracture properties of Ti-5Al-2.5Sn(ELI) for use in engine components p 70 A85-47972
WOLAK, J.
Metallurgical and mechanical phenomena due to rubbing of titanium against sintered powder Nichrome p 127 A85-22281
An experimental investigation and numerical prediction of thermomechanical phenomena in high speed rotor tip rubbing p 14 A85-25442
WONG, R. S.
An experimental study of three-dimensional shock wave/turbulent boundary layer interactions in a supersonic flow
[AIAA PAPER 85-1566] p 5 A85-40691
WOOLLAM, J. A.
Dielectric properties of 'diamondlike' carbon prepared by RF plasma deposition p 182 A85-38192
'Diamondlike' carbon films - Optical absorption, dielectric properties, and hardness dependence on deposition parameters p 82 A85-40383
WOOTEN, W. H.
Altitude testing of a flight weight, self-cooled, 2D thrust vectoring exhaust nozzle
[SAE PAPER 841557] p 14 A85-25984
WORRELL, W. L.
The reactions of cobalt, iron and nickel in SO-2 atmospheres: Similarities and differences
[NASA-TM-86868] p 70 N85-11217
WU, J. M.
Flow control in a diffusing S-Duct
[AIAA PAPER 85-0524] p 3 A85-25928
WU, Y. T.
Reliability considerations for the total strain range version of strainrange partitioning
[NASA-CR-174757] p 144 N85-11380
WYNVEEN, R. A.
Engineering model system study for a regenerative fuel cell: Study report
[NASA-CR-174801] p 158 N85-16292

X

XUE, W.-M.
On the existence and stability conditions for mixed-hybrid finite element solutions based on Reissner's variational principle p 142 A85-33847

Y

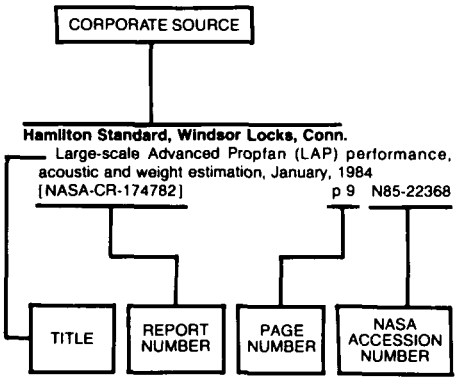
YAMAMOTO, K.
Experimental investigation of shock-cell noise reduction for dual-stream nozzles in simulated flight
[NASA-CR-3846] p 175 N85-13549
Experimental investigation of shock-cell noise reduction for single stream nozzles in simulated flight
[NASA-CR-3845] p 175 N85-13550
YAMAMOTO, O.
Inviscid analysis of advanced turboprop propeller flow fields
[AIAA PAPER 85-1263] p 6 A85-43977
YAMAURA, Y.
Engineering calculations for communications satellite systems planning
[NASA-CR-175552] p 37 N85-21233
YANG, K.
Electron yields from spacecraft materials p 40 N85-22512
YEE, S. T.
Structural analysis and cost estimate of an eight-leg space frame as a support structure for horizontal axis wind turbines
[NASA-TM-83470] p 150 N85-30361
YEH, F. C.
Heat transfer results and operational characteristics of the NASA Lewis Research Center Hot Section Cascade Test Facility
[NASA-TM-86890] p 114 N85-15133

Z

ZACHARY, A.
Cryogenic upper stage test bed engine
[AIAA PAPER 85-1339] p 44 A85-39733
ZAFRAN, S.
Electrothermal thruster diagnostics p 42 A85-16440
ZANA, L. M.
Rail accelerator technology and applications
[NASA-TM-86947] p 48 N85-21258
ZANNETTI, L.
Time dependent computation of the Euler equations for designing 2-D cascades, including the case of transonic shock free design p 5 A85-41814
Inverse design technique for cascades
[NASA-CR-3836] p 7 N85-12008
ZARETSKY, E. V.
Fatigue criterion to system design, life and reliability
[AIAA PAPER 85-1140] p 143 A85-40814
Effect of five lubricants on life of AISI 9310 spur gears
[NASA-TP-2419] p 123 N85-16099
Lubrication and performance of high-speed rolling-element bearings
[NASA-TM-86958] p 131 N85-21658
Fatigue criterion to system design, life and reliability
[NASA-TM-87017] p 132 N85-27226
Operating characteristics of a 0.87 kW-hr flywheel energy storage module
[NASA-TM-87038] p 133 N85-28371
Lubricant and additive effects on spur gear fatigue life
[NASA-TM-87044] p 133 N85-28373
Effect of speed and press fit on fatigue life of roller-bearing inner-race contact
[NASA-TP-2496] p 134 N85-31511
Design and lubrication of high-speed rolling-element bearings
[NASA-TM-87107] p 137 N85-34409
ZEIDAN, F. Y.
Internal hysteresis experienced on a high pressure syn gas compressor p 131 N85-14122
ZEISSER, M. H.
Energy efficient engine combustor test hardware detailed design report
[NASA-CR-167945] p 18 N85-10950
ZELAHY, J. W.
Advanced blade tip seal system, volume 2
[NASA-CR-167851] p 23 N85-10999
ZELEZNIK, F. J.
Computer program for calculation of complex chemical equilibrium compositions and applications. Supplement 1: Transport properties
[NASA-TM-86885] p 184 N85-16663
Modeling the internal combustion engine
[NASA-RP-1094] p 172 N85-19733
Ideal gas thermodynamic properties for the phenyl, phenoxy, and o-biphenyl radicals
[NASA-TM-83800] p 184 N85-22204
ZELLER, J.
The role of modern control theory in the design of controls for aircraft turbine engines p 13 A85-13627
ZENAS, R.
Metallurgical and mechanical phenomena due to rubbing of titanium against sintered powder Nichrome p 127 A85-22281
ZHANG, Q.-F.
Structure of particle-laden jets - Measurements and predictions p 109 A85-25137
Structure of ducted particle-laden turbulent jets p 110 A85-38999
Measurements and predictions of the structure of evaporating sprays p 112 A85-46484
Structure of nonevaporating sprays. I - Initial conditions and mean properties p 112 A85-48538

ZHONG, W. F.
Fundamentals of microcrack nucleation mechanics
[NASA-CR-3851] p 137 N85-16195
ZIEGLER, K. R.
Effect of reduction of strategic Columbium addition in 718 Alloy on the structure and properties
[NASA-CR-174841] p 75 N85-21320
ZIERKE, W. C.
The boundary layer on compressor cascade blades
[NASA-CR-174369] p 114 N85-18292
ZINOLABEDINI, R.
Graphite fiber intercalation: Dynamics of the bromine intercalation process
[NASA-TM-87015] p 53 N85-26921
ZIZELMAN, J.
Dilution jet configurations in a reverse flow combustor
[NASA-CR-174888] p 27 N85-22392
ZOPFF, D.
Solids mixing in a three phase fluidized bed containing spherically shaped-porous solid particles
[PB85-187961] p 120 N85-33453
ZRIBI, G.
Substrate-induced orientational order in the isotropic phase of liquid crystals p 181 A85-24649
ZUMWALT, G. W.
Icing tunnel tests of Electro-Impulse De-Icing of an engine inlet and high-speed wings
[AIAA PAPER 85-0466] p 10 A85-20872
Electro-impulse de-icing of a turbofan engine inlet
[AIAA PAPER 85-1118] p 12 A85-40811

Typical Corporate Source Index Listing



Listings in this index are arranged alphabetically by corporate source. The title of the document provides the user with a brief description of the subject matter. The report number helps to indicate the type of document cited (e.g., NASA report, translation, NASA contractor report). The NASA accession number denotes the number by which the citation is identified. The titles are arranged *under each corporate source in ascending* accession number order.

A

Aerodyne Research, Inc., Billerica, Mass.
An approach for automated analysis of particle holograms p 120 A85-10034
Aerojet Techsystems Co., Sacramento, Calif.
Progress report - Advanced cryogenic OTV engine *technology*
[AIAA PAPER 85-1341] p 44 A85-39735
Aerometrics, Inc., Mountain View, Calif.
Phase/doppler spray analyzer for simultaneous measurements of drop size and velocity distributions p 120 A85-10035
Air Force Aero Propulsion Lab., Wright-Patterson AFB, Ohio.
Vibrations of twisted cantilevered plates - Summary of previous and current studies p 140 A85-22069
Vibrations of twisted cantilever plates - A comparison of theoretical results p 144 A85-47626
Air Force Flight Dynamics Lab., Wright-Patterson AFB, Ohio.
Structural optimization using optimality criteria methods p 144 A85-48703
Air Force Geophysics Lab., Hanscom AFB, Mass.
Spacecraft Environmental Interactions Technology, 1983
[NASA-CP-2359] p 39 N85-22470
Akron Univ., Ohio.
An analysis of temperature effect in a finite journal bearing with spatial tilt and viscous dissipation p 126 A85-11074
Extension of constrained incremental Newton-Raphson scheme to generalized loading fields p 139 A85-13942
Progress in development of a Navier-Stokes solver for evaluation of iced airfoil performance
[AIAA PAPER 85-0410] p 3 A85-19731
On the development of hierarchical solution strategies for nonlinear finite element formulations p 171 A85-21979
Plastic flow of plasma sprayed ceramics p 80 A85-24161
Pantographing self adaptive gap elements p 142 A85-37440
Quasi-static solution algorithms for *kinematically/materially nonlinear thermomechanical* problems p 143 A85-41983
Viscoplastic constitutive relationships with dependence on thermomechanical history
[NASA-CR-174836] p 146 N85-21691
On thermomechanical testing in support of constitutive equation development for high temperature alloys
[NASA-CR-174879] p 147 N85-25894
Some advances in experimentation supporting development of viscoplastic constitutive models
[NASA-CR-174855] p 147 N85-27260
Thermomechanical deformation in the presence of metallurgical changes p 150 N85-31533
Some advances in experimentation supporting development of viscoplastic constitutive models p 151 N85-31545
Results of an interlaboratory fatigue test program conducted on alloy 800H at room and elevated temperatures
[NASA-CR-174940] p 152 N85-32340
A continuous damage model based on stepwise-stress creep rupture tests
[NASA-CR-174941] p 152 N85-32341
Measurement and correlation of jet fuel viscosities at low temperatures
[NASA-CR-174911] p 94 N85-34295
Alabama Univ., Huntsville.
Experiments in charge control at geosynchronous orbit - ATS-5 and ATS-6 p 39 A85-35379
ALPHATECH, Inc., Burlington, Mass.
A design methodology for robust failure detection and isolation p 171 A85-47794
Analex Corp., Cleveland, Ohio.
Interdisciplinary design analysis of a precision spacecraft antenna
[AIAA PAPER 85-0804] p 38 A85-30303
Computer program for the calculation of multicomponent convective diffusion deposition rates from chemically frozen boundary layer theory
[NASA-CR-168329] p 116 N85-27164
Applied Medical Technology, Inc., Brecksville, Ohio.
Percutaneous connectors
[NASA-CR-175627] p 168 N85-27508
Arizona State Univ., Tempe.
Multibus-based parallel processor for simulation p 169 A85-28613
Jet characteristics in confined swirling flow p 112 A85-45282
Density effects on jet characteristics in confined swirling flow p 112 A85-45283
Behavior of turbulent gas jets in an axisymmetric confinement
[NASA-CR-174829] p 28 N85-25265
Arizona Univ., Phoenix.
Creep-rupture reliability analysis p 143 A85-42566
Arizona Univ., Tucson.
Effect of airfoil mean loading on convected gust interaction noise
[AIAA PAPER 84-2324] p 173 A85-13955
Noise produced by the interaction of a rotor wake with a swept stator blade
[AIAA PAPER 84-2326] p 173 A85-13956
The linear two-dimensional stability of inviscid vortex streets of finite-cored vortices
[AD-A153032] p 107 A85-14241
Interply layer degradation effects on composite structural response
[AIAA PAPER 84-0849] p 54 A85-16096
Reliability considerations for the total strain range version of strainrange partitioning
[NASA-CR-174757] p 144 N85-11380
Army Armament Research and Development Command, Dover, N. J.
Automatic sphericity interferometer for testing lens radii
[AD-A155736] p 125 N85-33457
Army Aviation Research and Development Command, Cleveland, Ohio.
Mechanical properties of SiC fiber-reinforced reaction-bonded Si3N4 composites
[NASA-TM-87085] p 59 N85-34223
Generated spiral bevel gears: Optimal machine-tool settings and tooth contact analysis
[NASA-TM-87075] p 136 N85-34405
Thermal stress analysis of a new turbine shroud seal concept
[NASA-TM-87082] p 136 N85-34406
Army Propulsion Lab., Cleveland, Ohio.
Comparison of icing cloud instruments for 1982-1983 icing season flight program
[AIAA PAPER 84-0020] p 13 A85-16098
Hydrodynamic lubrication of rigid nonconformal contacts in combined rolling and normal motion
[ASME PAPER 84-TRIB-13] p 127 A85-21280
A note on blade wake interaction influence on compressor stator row aerodynamic performance p 4 A85-32965
A computer aided design procedure for generating gear teeth
[ASME PAPER 84-DET-184] p 128 A85-33779
Dynamic analysis of straight and involute tooth forms
[ASME PAPER 84-DET-226] p 128 A85-33780
Temperature distortion generator for turboshaft engine testing
[SAE PAPER 841541] p 15 A85-39065
High-temperature erosion of plasma-sprayed, yttria-stabilized zirconia in a simulated turbine environment
[AIAA PAPER 85-1219] p 82 A85-39662
Rotor wake characteristics of a transonic axial flow *fan*
[AIAA PAPER 85-1133] p 6 A85-43974
Army Research and Technology Labs., Cleveland, Ohio.
Predicted turbine stage performance using quasi-three-dimensional and boundary-layer analyses p 15 A85-34013
Future fundamental combustion research for aeropropulsion systems
[AIAA PAPER 85-1398] p 16 A85-42671
High-temperature erosion of plasma-sprayed, yttria-stabilized zirconia in a simulated turbine *environment*
[NASA-TP-2406] p 84 N85-13045
Low cycle fatigue of MAR-M 200 single crystals at 760 and 870 deg C
[NASA-TM-86933] p 74 N85-19074
Transmission efficiency measurements and correlations *with physical characteristics of the lubricant* p 89 N85-23781
Environmental effects on the tensile strength of chemically vapor deposited silicon carbide fibers
[NASA-TM-86981] p 89 N85-24000
Multiaxial and thermomechanical fatigue considerations in damage tolerant design
[NASA-TM-87022] p 76 N85-26964
DEAN: A program for dynamic engine analysis
[NASA-TM-87033] p 30 N85-28945
Avco Lycoming Div., Stratford, Conn.
Application of Runge Kutta time marching scheme for the computation of transonic flows in turbomachines
[AIAA PAPER 85-1332] p 5 A85-39728

B

Babcock and Wilcox Co., Akron, Ohio.
Quasi-static solution algorithms for kinematically/materially nonlinear thermomechanical problems p 143 A85-41983
Babcock and Wilcox Co., Alliance, Ohio.
High-temperature fiber optic pressure sensor p 123 A85-46607
Babcock and Wilcox Co., New York, N.Y.
Extension of constrained incremental Newton-Raphson scheme to generalized loading fields p 139 A85-13942

SOURCE

Ball Aerospace Systems Div., Boulder, Colo.
Fracture toughness of hot-pressed beryllium p 66 A85-25835
Banaras Hindu Univ., Varanasi (India).
Hydrodynamic lubrication of rigid nonconformal contacts in combined rolling and normal motion
[ASME PAPER 84-TRIB-13] p 127 A85-21280
Thermal elastohydrodynamic lubrication of line contacts p 128 A85-31202
Battelle Columbus Labs., Ohio.
A history dependent damage model for low cycle fatigue
[ASME PAPER 84-PVP-112] p 140 A85-18795
Preliminary analysis of space mission applications for electromagnetic launchers
[NASA-CR-174067] p 35 N85-12071
Composite loads spectra for select space propulsion structural components: Probabilistic load model development p 148 N85-27954
Bell Telephone Labs., Inc., Allentown, Pa.
Optical linear algebra processors - Noise and error-source modeling p 169 A85-36727
Bell Telephone Labs., Inc., Whippany, N. J.
A fast time domain digital simulation technique for power converters - Application to a buck converter with feedforward compensation p 101 A85-20900
Boeing Aerospace Co., Seattle, Wash.
Space station propulsion options
[AIAA PAPER 85-1155] p 45 A85-43975
High voltage requirements and issues for the 1990's p 46 A85-45429
Applicability of 100kWe-class of space reactor power systems to NASA manned space station missions
[NASA-CR-174696] p 177 N85-35728
Boeing Commercial Airplane Co., Seattle, Wash.
Detailed studies of aviation fuel flowability
[NASA-CR-174938] p 94 N85-31308
Boeing Vertol Co., Philadelphia, Pa.
Performance degradation of helicopter rotor in forward flight due to ice p 11 A85-42937
Bolt, Beranek, and Newman, Inc., Cambridge, Mass.
Turbofan noise generation. Volume 2: Computer programs
[NASA-CR-167952] p 175 N85-11791
Bonneville Power Administration, Portland, Oreg.
Government review of the Mod-2 wind turbine (as-built)
[NASA-TM-86983] p 162 N85-29365
Braun (Willis H.), Berea, Ohio.
Unsteady flow in a supersonic cascade with two in-passage shocks
[NASA-CR-3925] p 10 N85-35158

C

California Inst. of Tech., Pasadena.
The linear two-dimensional stability of inviscid vortex streets of finite-cored vortices
[AD-A153032] p 107 A85-14241
Vortex induced lift on a flat plate with a curved forward-facing flap p 4 A85-30175
Growth of a diffusion flame in the field of a vortex p 61 A85-47320
Free-surface phenomena under low- and zero-gravity conditions
[NASA-CR-175835] p 116 N85-27168
California State Univ., Long Beach.
Into mesh lubrication of spur gears with arbitrary offset oil jet. I - For jet velocity less than or equal to gear velocity p 128 A85-24497
Lubricant jet flow phenomena in spur and helical gears with modified center distances and/or addendums - For out-of-mesh conditions
[ASME PAPER 84-DET-96] p 129 A85-35049
California Univ., Berkeley.
Effects of SO2 and SO3 on the Na2SO4 induced corrosion of nickel p 65 A85-15603
Recent advances in methods for numerical solution of O.D.E. initial value problems p 171 A85-21370
Properties of coated and modified surfaces p 53 A85-36694
California Univ., Berkeley. Lawrence Berkeley Lab.
Knock syndrome: Its cures and its victims
[NASA-CR-174395] p 93 N85-19185
California Univ., Irvine.
A two-equation turbulence model for two-phase jets p 107 A85-14376
Prism-coupled light emission from tunnel junctions p 181 A85-21425
Substrate-induced orientational order in the isotropic phase of liquid crystals p 181 A85-24649
California Univ., Los Angeles.
The response of Helmholtz resonators to external excitation. I - Single resonators p 174 A85-26915
Data flow methods for dynamic system simulation - A CSSL-IV microcomputer network interface p 170 A85-28614
A functional language approach in high-speed digital simulation p 170 A85-28615
General approaches for achieving high speed computations p 169 A85-28628
Functional language and data flow architectures p 170 A85-28629
Vortex modeling of single and multiple dilution jet mixing in a crossflow
[AIAA PAPER 85-1580] p 111 A85-40701
Carnegie-Mellon Univ., Pittsburgh, Pa.
Effects of friction dampers on aerodynamically unstable rotor stages p 14 A85-21866
Optical linear algebra processors - Noise and error-source modeling p 169 A85-36727
Case Western Reserve Univ., Cleveland, Ohio.
An analysis of temperature effect in a finite journal bearing with spatial tilt and viscous dissipation p 126 A85-11074
Statistics and thermodynamics of fracture p 140 A85-19433
Flame flashback in a premixed dump combustor
[AIAA PAPER 85-0145] p 60 A85-19550
The effect of plasma on solar cell array arc characteristics
[AIAA PAPER 85-0384] p 43 A85-19713
Circular waveguide bifurcation for asymmetric modes p 101 A85-20170
Dual-mode coaxial feed with low crosspolarisation p 101 A85-20171
Plastic flow of plasma sprayed ceramics p 80 A85-24161
Elevated temperature creep-rupture behavior of the single crystal nickel-base superalloy NASAIR 100 p 66 A85-27812
A procedure for obtaining explicit solutions to a class of Fredholm integral equations p 171 A85-28006
Influence of composition on the microstructure and mechanical properties of a nickel-base superalloy single crystal p 66 A85-32387
Factors which influence directional coarsening of gamma-prime during creep in nickel-base superalloy single crystals p 67 A85-32388
Dendritic solidification. I - Analysis of current theories and models. II - A model for dendritic growth under an imposed thermal gradient p 182 A85-38019
A new interpretation of internal heat transfer coefficients of porous media
[ASME PAPER 84-WA/HT-51] p 110 A85-39894
Dopant effect of yttrium and the growth and adherence of alumina on nickel-aluminum alloys p 82 A85-40973
Mechanism for chelated sulfate formation from SO2 and bis (triphenylphosphine) platinum p 62 A85-48493
Mechanism for forming hydrogen chloride and sodium sulfate from sulfur trioxide, water, and sodium chloride p 62 A85-48513
The transient oxidation of single crystal NiAl+Zr
[NASA-CR-174756] p 70 N85-11221
Analysis techniques for tracer studies of oxidation
[NASA-CR-174796] p 84 N85-12162
Experimental test program for evaluation of solid lubricant coating as applied to compliant foil gas bearings to 315 deg C
[NASA-CR-174837] p 85 N85-15895
Effect of reduction of strategic Columbium addition in 718 Alloy on the structure and properties
[NASA-CR-174841] p 75 N85-21320
Translational and extensional energy release rates (the J- and M-integrals) for a crack layer in thermoelasticity
[NASA-CR-174872] p 145 N85-21685
Dilution jet configurations in a reverse flow combustor
[NASA-CR-174888] p 27 N85-22392
Electron yields from spacecraft materials p 40 N85-22512
Study of Kapton under simulated shuttle environment
[NASA-CR-176003] p 41 N85-29997
Why CO bonds side-on at low coverage and both side-on and upright at high coverage on the Cr(110) surface
[NASA-CR-176071] p 77 N85-32173
Molecular orbital studies in oxidation: Sulfate formation and metal-metal oxide adhesion
[NASA-CR-176070] p 77 N85-32174
Adsorption of O2, SO2, and SO3 on nickel oxide. Mechanism for sulfate formation
[NASA-CR-176072] p 77 N85-32175
CO adsorption on (111) and (100) surfaces of the Pt sub 3 Ti alloy. Evidence for parallel binding and strong activation of CO
[NASA-CR-176077] p 77 N85-32176
Perturbation-iteration theory for analyzing microwave striplines
[NASA-CR-176189] p 100 N85-35321
CBS Labs., Stamford, Conn.
Experimental results supporting the determination of service quality objectives for DBS systems p 96 A85-29611
Chevron Oil Field Research Co., La Habra, Calif.
The linear two-dimensional stability of inviscid vortex streets of finite-cored vortices
[AD-A153032] p 107 A85-14241
Chronos Research Labs., Inc., Olivehain, Calif.
Pyroelectric conversion in space p 45 A85-45377
Cincinnati Univ., Ohio.
Computation of internal flows: Methods and applications; Proceedings of the Energy Sources Technology Conference, New Orleans, LA, February 12-16, 1984 p 106 A85-11630
Two-dimensional internal compressible viscous flows using semi-elliptic analysis p 106 A85-11640
A study of fatigue damage mechanisms in Waspaloy from 25 to 800 C p 65 A85-12098
High-voltage solar-cell chip p 154 A85-24668
A computer aided design procedure for generating gear teeth
[ASME PAPER 84-DET-184] p 128 A85-33779
Dynamic analysis of straight and involute tooth forms
[ASME PAPER 84-DET-226] p 128 A85-33780
The three-dimensional compressible flow in a radial inflow turbine scroll p 6 A85-41826
Finite element analysis of notch behavior using a state variable constitutive equation p 152 N85-31548
Clarkson Coll. of Technology, Potsdam, N.Y.
Electrocatalysis of fuel cell reactions: Investigation of alternate electrolytes
[NASA-CR-174753] p 157 N85-11455
Clemson Univ., S.C.
Heat transfer and fluid mechanics measurements in transitional boundary layer flows p 118 N85-31439
Cleveland State Univ., Ohio.
Control algorithms and computer simulation of a stand-alone photovoltaic village power system p 153 A85-11345
Near-optimum design of GaAs-based concentrator space solar cells for 80 C operation p 153 A85-15800
Applicability of the Meyer-Neldel rule to solar cells p 154 A85-19948
A unified relation for cavitation erosion p 109 A85-24445
The subjective effect of multiple co-channel frequency modulated television interference p 96 A85-28234
On the subjective evaluation of the interference protection ratios' measurements for co-channel FM-TV signals p 96 A85-28241
Theory of the high base resistivity n(+)pp(+) silicon solar cell and its application to radiation damage effects p 154 A85-32639
Gear mesh stiffness and load sharing in planetary gearing
[ASME PAPER 84-DET-229] p 129 A85-33781
Incident beam polarization for laser Doppler velocimetry employing a sapphire cylindrical window p 122 A85-39835
Combined influence of unsteady free stream velocity and free stream turbulence on stagnation point heat transfer p 112 A85-41782
Preliminary design of a 10 kW thermophotovoltaic system for space applications p 45 A85-45371
Manual of phosphoric acid fuel cell power plant optimization model and computer program
[NASA-CR-174721] p 157 N85-10445
Manual of phosphoric acid fuel cell stack three-dimensional model and computer program
[NASA-CR-174722] p 157 N85-10447
Phosphoric acid fuel cell power plant system performance model and computer program
[NASA-CR-174638] p 157 N85-11456
A historical overview of the electrical power systems in the US manned and some US unmanned spacecraft
[NASA-CR-174806] p 47 N85-13910
Investigation on experimental techniques to detect, locate and quantify gear noise in helicopter transmissions
[NASA-CR-3847] p 176 N85-17667
Conceptual design of a fixed-pitch wind turbine generator system rated at 400 kilowatts
[NASA-CR-174877] p 162 N85-29363
College of William and Mary, Williamsburg, Va.
The use of Ada in distributed simulations p 169 A85-28612
Moving target, distributed, real-time simulation using Ada p 170 A85-34131
Colorado School of Mines, Golden.
Jet fuel instability mechanisms
[NASA-CR-175856] p 93 N85-28127
Colorado State Univ., Fort Collins.
Ion flow experiments in a multipole discharge chamber p 178 A85-12705

Theory of ion acceleration with closed electron drift
p 41 A85-15512
Efficient solution of the Euler and Navier-Stokes equations with a vectorized multiple-grid algorithm
p 2 A85-18679

Columbia Univ., New York.
Modeling of gamma/gamma-prime phase equilibrium in the nickel-aluminum system p 65 A85-14959
Effects of cobalt on the hot workability of nickel-base superalloys p 67 A85-32412

Concordia Univ., Montreal (Quebec).
Recent advances in methods for numerical solution of O.D.E. initial value problems p 171 A85-21370

Connecticut Univ., Storrs.
Mass and momentum turbulent transport experiments with confined coaxial jets p 107 A85-14399
Biaxial constitutive equation development for single crystals
[NASA-CR-174056] p 183 N85-11862
Iron rich low cost superalloys
[NASA-CR-174900] p 76 N85-26962
Elevated temperature biaxial fatigue
[NASA-CR-175795] p 148 N85-27263

Control Data Corp., Minneapolis, Minn.
GASP cloud encounter statistics - Implications for laminar flow control flight p 166 A85-11979
A comparison of NMC and GWC analysis field temperatures with aircraft measurements
p 166 A85-21140
Variability of cloudiness at airline cruise altitudes from GASP measurements p 166 A85-31199

Cornell Univ., Ithaca, N.Y.
Combustion efficiency of a premixed continuous flow combustor p 61 A85-42571
A theory of post-stall transients in multistage axial compression systems
[NASA-CR-3878] p 8 N85-21117

Creare, Inc., Hanover, N.H.
An experimental investigation of rubbing interaction in labyrinth seals at cryogenic temperature
p 129 A85-39938
Analytical and experimental investigation of rubbing interaction in labyrinth seals for a liquid hydrogen fuel pump
[NASA-CR-174657] p 48 N85-18084

Cummins Engine Co., Inc., Columbus, Ind.
Advanced automotive diesel assessment program
[NASA-CR-168285] p 130 N85-13235

D

Dartmouth Coll., Hanover, N.H.
Thermal and thermomechanical effects in dry sliding
p 127 A85-23838
An experimental investigation of rubbing interaction in labyrinth seals at cryogenic temperature
p 129 A85-39938

Defence Metallurgical Research Lab., Hyderabad (India).
Deformation and fracture behavior of Ni-Mo-Al(gamma/gamma prime-alpha) in situ composite
p 64 A85-11058

Delaware Univ., Newark.
New eutectic alloys and their heats of transformation
p 66 A85-27808

Department of Communications, Ottawa (Ontario).
Development and use of the computer software package for planning the 12 GHz broadcasting-satellite service at RARC '83 p 96 A85-29605
Experimental results supporting the determination of service quality objectives for DBS systems
p 96 A85-29611

Department of Energy, Washington, D. C.
Apparatus and method for identification of matrix materials in which transuranic elements are embedded using thermal neutron capture gamma-ray emission
[DE85-011659] p 125 N85-33454
Manufacturing process to reduce large grain growth in zirconium alloys
[DE85-011649] p 78 N85-34267

Detroit Diesel Allison, Indianapolis, Ind.
Analytical fuel property effects--small combustors
[NASA-CR-174738] p 28 N85-26709
Advanced Gas Turbine (AGT) technology project
[NASA-CR-174798] p 31 N85-29961

Douglas Aircraft Co., Inc., Long Beach, Calif.
Calculation of compressible flow about three-dimensional inlets with auxiliary inlets, slats and vanes by means of a panel method
[AIAA PAPER 85-1196] p 5 A85-40817
Low-speed aerodynamic test of an axisymmetric supersonic inlet with variable cowl slot
[AIAA PAPER 85-1210] p 5 A85-40819
Calculation of compressible flow about three-dimensional inlets with auxiliary inlets, slats and vanes by means of a panel method
[NASA-CR-174975] p 10 N85-35162

Draper (Charles Stark) Lab., Inc., Cambridge, Mass.
First-order ball-bearing kinematics
p 128 A85-31203

Drexel Univ., Philadelphia, Pa.
Use of statical indentation laws in the impact analysis of laminated composite plates p 55 A85-29133

Duke Univ., Durham, N. C.
A space-marching method for incompressible Navier-Stokes equations
[AIAA PAPER 85-0170] p 108 A85-19564

E

EIC, Inc., Norwood, Mass.
Moderate temperature sodium cells. V - Discharge reactions and rechargeability of NiS and NiS2 positive electrodes in molten NaAlCl4 p 59 A85-11892

Electrotek Concepts, Inc., Knoxville, Tenn.
Experimental investigation of a variable speed constant frequency electric generating system from a utility perspective
[NASA-CR-174950] p 105 N85-32251

Enertech Corp., Norwich, Vt.
Measured effects of wind turbine generation at the Block Island Power Company p 153 A85-10652

Engelhard Industries, Inc., Edison, N.J.
Develop and test fuel cell powered on-site integrated total energy systems. Phase 3: Full-scale power plant development
[NASA-CR-174887] p 161 N85-25941
Develop and test fuel cell powered on-site integrated total energy systems. Phase 3: Full-scale power plant development
[NASA-CR-168338] p 164 N85-30483

Environmental Research Inst. of Michigan, Ann Arbor.
Comparison of atmospheric correction algorithms for the Coastal Zone Color Scanner p 153 A85-10244

Exxon Research and Engineering Co., Linden, N.J.
Jet fuel property changes and their effect on producibility and cost in the U.S., Canada, and Europe
[NASA-CR-174840] p 93 N85-27012

F

Florida State Univ., Tallahassee.
A multiple-scales model of the shock-cell structure of imperfectly expanded supersonic jets
p 113 A85-49354

Flow Research, Inc., Kent, Wash.
Direct numerical simulations of a reacting mixing layer with chemical heat release
[AIAA PAPER 85-0143] p 60 A85-19548
Direct simulations of chemically reacting turbulent mixing layers
[AIAA PAPER 85-0321] p 60 A85-19666

Ford Aerospace and Communications Corp., Palo Alto, Calif.
The 20 GHz proof-of-concept test model results for a multiple scan beam dual reflector antenna
[NASA-CR-174268] p 98 N85-15944

Ford Motor Co., Dearborn, Mich.
Fracture of yttria-doped, sintered reaction-bonded silicon nitride
[ACS PAPER 7-J3-84] p 82 A85-42797

Foster Wheeler Corp., Houston, Tex.
Advanced technology cogeneration system conceptual design study: Closed cycle gas turbines
[NASA-CR-168222] p 159 N85-16300

G

Garrett Turbine Engine Co., Phoenix, Ariz.
Ceramic component development for the AGT101 gas turbine engine p 126 A85-15972
Life modeling of atmospheric and low pressure plasma-sprayed thermal-barrier coating
p 81 A85-29728
Development of coated single-crystal superalloy systems for gas turbine applications p 68 A85-32440
Progress in the utilization of an oxide-dispersion-strengthened alloy for small engine turbine blades
[SAE PAPER 841512] p 68 A85-39284
Experiments in dilution jet mixing - Effects of multiple rows and non-circular orifices
[AIAA PAPER 85-1104] p 15 A85-39606
Creep-rupture reliability analysis p 143 A85-42566
Advanced technology cogeneration system conceptual design study: Closed cycle gas turbines
[NASA-CR-168222] p 159 N85-16300
Advanced Gas Turbine (AGT) powertrain system development for automotive applications
[NASA-CR-174809] p 185 N85-18831

General Dynamics/Convair, San Diego, Calif.
Effect of low temperature on fatigue and fracture properties of Ti-5Al-2.5Sn(ELI) for use in engine components p 70 A85-47972

General Electric Co., Cincinnati, Ohio.
Comparison of scaled model data to full size energy efficient engine test results
[AIAA PAPER 84-2281] p 13 A85-13953
Measurement and prediction of Energy Efficient Engine noise
[AIAA PAPER 84-2284] p 13 A85-13954
Considerations for damage analysis of gas turbine hot section components
[ASME PAPER 84-PVP-77] p 14 A85-18792
Altitude testing of a flight weight, self-cooled, 2D thrust vectoring exhaust nozzle
[SAE PAPER 841557] p 14 A85-25984
Life modeling of atmospheric and low pressure plasma-sprayed thermal-barrier coating
p 81 A85-29728
Unified constitutive material models for nonlinear finite-element structural analysis
[AIAA PAPER 85-1418] p 142 A85-39769
Stall recovery control strategy methodology and results
[AIAA PAPER 85-1433] p 16 A85-40841
Energy efficient engine component development and integration program
[NASA-CR-169496] p 22 N85-10989
Energy efficient engine component development and integration program
[NASA-CR-170034] p 22 N85-10990
Energy efficient engine ICLS Nacelle detail design report
[NASA-CR-167870] p 22 N85-10993
Energy efficient engine. Low pressure turbine test hardware detailed design report
[NASA-CR-167956] p 22 N85-10994
Energy efficient engine high pressure turbine test hardware detailed design report
[NASA-CR-167955] p 23 N85-10995
Energy efficient engine high pressure turbine ceramic shroud support technology report
[NASA-CR-168036] p 23 N85-10996
Energy efficient engine ICLS engine bearings, drives and configuration: Detail design report
[NASA-CR-167871] p 23 N85-10997
Energy efficient engine. High pressure compressor detail design report
[NASA-CR-165558] p 23 N85-10998
Advanced blade tip seal system, volume 2
[NASA-CR-167851] p 23 N85-10999
Materials for advanced turbine engines. Project 2: Rene 150 directionally solidified superalloy turbine blades, volume 2
[NASA-CR-167993] p 23 N85-12059
Experimental investigation of shock-cell noise reduction for dual-stream nozzles in simulated flight
[NASA-CR-3846] p 175 N85-13549
Experimental investigation of shock-cell noise reduction for single stream nozzles in simulated flight
[NASA-CR-3845] p 175 N85-13550
Study of advanced fuel system concepts for commercial aircraft
[NASA-CR-174751] p 12 N85-19978
Development of a rotor wake-vortex model, volume 1
[NASA-CR-174849] p 9 N85-26668
Effects of surface chemistry on hot corrosion life
[NASA-CR-174915] p 28 N85-26711
Component-specific modeling
[NASA-CR-174765] p 147 N85-27261
Energy Efficient Engine (E3) controls and accessories detail design report
[NASA-CR-168017] p 31 N85-29957
Component-specific modeling
[NASA-CR-174925] p 32 N85-32119
A review of path-independent integrals in elastic-plastic fracture mechanics, task 4
[NASA-CR-174956] p 152 N85-33541
High pressure compressor component performance report
[NASA-CR-168245] p 33 N85-34138
Component-specific modeling
[NASA-CR-174765] p 33 N85-34140
Energy efficient engine. Fan and quarter-stage component performance report
[NASA-CR-168070] p 33 N85-34141
Flow modifying device
[NASA-CASE-LEW-13562-2] p 33 N85-35195
Energy efficient engine, high pressure turbine thermal barrier coating. Support technology report
[NASA-CR-168037] p 34 N85-35199

General Electric Co., Lynn, Mass.
Contingency power concepts for helicopter turboshaft engine p 15 A85-32005
TF34 convertible engine control system design p 15 A85-32006
Analytical fuel property effects: Small combustors, phase 2
[NASA-CR-174848] p 93 N85-19175
General Electric Co., Philadelphia, Pa.
Advanced multi-megawatt wind turbine design for utility application p 157 A85-45517
Transformation toughened ceramics for the heavy duty diesel engine technology program
[NASA-CR-174689] p 185 N85-16698
General Electric Co., Schenectady, N. Y.
Prediction of an axisymmetric combusting flow p 59 A85-12713
Laser balancing system for high material removal rates
[NASA-CR-174731] p 126 N85-12341
Effects of vane/blade ratio and spacing on fan noise, volume 1
[NASA-CR-174664] p 176 N85-19791
Effects of vane/blade ratio and spacing on fan noise. Volume 2: Data supplement
[NASA-CR-174665] p 176 N85-19792
Advanced smoke meter development survey and analysis
[NASA-CR-168287] p 124 N85-25792
Parametric study of potential early commercial power plants Task 3-A MHD cost analysis
[NASA-CR-175839] p 161 N85-27377
Manufacturing process to reduce large grain growth in zirconium alloys
[DE85-011649] p 78 N85-34267
General Electric Co., Syracuse, N.Y.
Configuration study for a 30 GHz monolithic receive array: Technical assessment
[NASA-CR-174697] p 98 N85-18238
Configuration study for a 30 GHz monolithic receive array, volume 1
[NASA-CR-174697-VOL-1] p 98 N85-18239
Configuration study for a 30 GHz monolithic receive array, volume 2
[NASA-CR-174697-VOL-2] p 99 N85-18240
General Motors Corp., Indianapolis, Ind.
Ceramic components for gas turbine engines p 127 A85-15973
Photoacoustic microscopy of ceramic turbine blades p 83 A85-43930
An investigation of enhanced capability thermal barrier coating systems for diesel engine components
[NASA-CR-174820] p 86 N85-18154
Ceramic applications in turbine engines
[NASA-CR-174715] p 91 N85-28109
General Motors Research Labs., Warren, Mich.
Drop-turbulence interactions in a diffusion flame
[AIAA PAPER 85-0319] p 60 A85-19665
Development and testing of stable, invariant, isoparametric curvilinear 2- and 3-D hybrid-stress elements p 140 A85-19899
Georgia Inst. of Tech., Atlanta.
A study of fatigue damage mechanisms in Waspaloy from 25 to 800 C p 65 A85-12098
Hybrid stress finite elements for large deformations of inelastic solids p 139 A85-15894
Development and testing of stable, invariant, isoparametric curvilinear 2- and 3-D hybrid-stress elements p 140 A85-19899
The effect of microstructure, temperature, and hold-time on low-cycle fatigue of As HIP P/M Rene 95 p 67 A85-32399
On the existence and stability conditions for mixed-hybrid finite element solutions based on Reissner's variational principle p 142 A85-33847
Thermodynamically consistent constitutive equations for nonisothermal large strain, elasto-plastic, creep behavior
[AIAA PAPER 85-0621] p 142 A85-38425
Constitutive modeling and computational implementation for finite strain plasticity p 143 A85-40910
Technology for satellite power conversion
[NASA-CR-174335] p 159 N85-18451
Study of the effects of implantation on the high Fe-Ni-Cr and Ni-Cr-Al alloys
[NASA-CR-175625] p 76 N85-22661
Analysis of shell type structures subjected to time dependent mechanical and thermal loading
[NASA-CR-175747] p 147 N85-25896
Dynamic creep buckling: Analysis of shell structures subjected to time-dependent mechanical and thermal loading p 149 N85-27959
Georgia Tech Research Inst., Atlanta.
Infrared technology for satellite power conversion
[NASA-CR-174266] p 159 N85-16293
Gibbs and Hill, Inc., New York.
Advanced technology cogeneration system conceptual design study: Closed cycle gas turbines
[NASA-CR-168222] p 159 N85-16300
Giner, Inc., Waltham, Mass.
Development of electrodes for the NASA iron/chromium
[NASA-CR-174724] p 165 N85-35471
GMAF, Inc., Freeport, N.Y.
Inverse design technique for cascades
[NASA-CR-3836] p 7 N85-12008
Goodrich (B. F.) Co., Akron, Ohio.
Pantographing self adaptive gap elements p 142 A85-37440
Grumman Aerospace Corp., Bethpage, N.Y.
The computation of viscid/inviscid interaction on airfoils with separated flow p 6 A85-42954
GT-Devices, Alexandria, Va.
Investigation of a pulsed electrothermal thruster system
[NASA-CR-174768] p 46 N85-11132

H

Hamilton Standard, Windsor Locks, Conn.
Large-scale Advanced Propfan (LAP) performance, *acoustic and weight estimation, January, 1984*
[NASA-CR-174782] p 9 N85-22368
Multi-mesh gear dynamics program evaluation and enhancements
[NASA-CR-174747] p 133 N85-28372
Hamilton Standard Div., United Aircraft Corp., Windsor Locks, Conn.
Large-scale advanced propfan (LAP) program progress report
[AIAA PAPER 85-1187] p 17 A85-47021
Hiroshima Univ. (Japan).
A unified relation for cavitation erosion p 109 A85-24445
Honeywell, Inc., Lexington, Mass.
Mosaic Infrared Sensor for Space Astronomy (MIRSSA)
[NASA-CR-176154] p 125 N85-33456
Hughes Aircraft Co., El Segundo, Calif.
Environmentally-induced voltage limitations in large space power systems p 43 A85-18584
Advanced nickel-hydrogen cell configuration study
[NASA-CR-174775] p 157 N85-10444
Hughes Aircraft Co., Torrance, Calif.
A 20 GHz, 75 watt, helix TWT for space communications p 101 A85-14433
Sixty GHz IMPATT diode development
[NASA-CR-174969] p 105 N85-33293
Hughes Research Labs., Malibu, Calif.
IAPS (8-cm) ion thruster cyclic endurance test p 42 A85-16406
Ion propulsion for communications satellites p 42 A85-16412
Ring-cusp ion thrusters p 42 A85-16438
Long life nickel electrodes for a nickel-hydrogen cell. III - Results of an accelerated test and failure analyses p 156 A85-45391
Characterization of 8-cm engineering model thruster
[NASA-CR-174673] p 46 N85-11131
Ion thruster system (8-cm) cyclic endurance test
[NASA-CR-174745] p 47 N85-12937
Extended performance technology study 30-cm thruster
[NASA-CR-168259] p 48 N85-15806
The failure mechanism of a nickel electrode in a nickel-hydrogen cell p 105 N85-31408

I

IBM Watson Research Center, Yorktown Heights, N.Y.
Substrate-induced orientational order in the isotropic phase of liquid crystals p 181 A85-24649
IIT Research Inst., Chicago, Ill.
Creep-rupture behavior of iron superalloys in high-pressure hydrogen
[NASA-CR-174411] p 74 N85-19078
Illinois Univ., Urbana.
Plot of modal field distribution in rectangular and circular waveguides p 101 A85-25170
The influence of temperature on the lubricating effectiveness of MoS2 dispersed in mineral oils
[ASLE PREPRINT 84-LC-2A-2] p 80 A85-25963
On the calculation of the directivity of planar array feeds for satellite reflector applications p 97 A85-32249
Rapid solidification and dynamic compaction of Ni-base superalloy powders p 67 A85-32414
Properties of coated and modified surfaces p 53 A85-36694
Focal shifts in parabolic reflectors p 97 A85-39356
MMIC devices for active phased array antennas
[NASA-CR-174281] p 98 N85-15943
Behavior of the lean methane-air flame at zero-gravity
[NASA-CR-175586] p 62 N85-21283
Numerical methods for analyzing electromagnetic scattering
[NASA-CR-175507] p 99 N85-21438
Normal modes in an overmoded circular waveguide coated with lossy material
[NASA-CR-176186] p 100 N85-35320
Characterization of microstrip discontinuities in the time and frequency domains
[NASA-CR-176190] p 106 N85-35342
The use of a laser Doppler velocimeter in a standard flammability tube
[NASA-CR-174960] p 125 N85-35389
Illinois Univ., Urbana-Champaign.
The mechanisms of flame holding in the wake of a bluff body
[NASA-CR-174058] p 62 N85-11149
The study of microstrip antenna arrays and related problems
[NASA-CR-174054] p 97 N85-11265
The mechanisms of flame holding in the wake of a bluff body
[NASA-CR-3866] p 26 N85-21166
Imperial Coll. of Science and Technology, London (England).
Assessment of discretization schemes to reduce numerical diffusion in the calculation of complex flows
[AIAA PAPER 85-0441] p 108 A85-19751
Indian Inst. of Tech., Madras.
Natural frequencies of twisted rotating plates p 141 A85-32343
Integral Technologies, Inc., Westmont, Ill.
Methods for heat transfer and temperature field analysis of the insulated diesel
[NASA-CR-174783] p 185 N85-16699
Iowa State Univ. of Science and Technology, Ames.
A note on blade wake interaction influence on compressor stator row aerodynamic performance p 4 A85-32965
Iowa Univ., Iowa City.
Development of finite analytic method for unsteady three-dimensional Navier-Stokes equation p 106 A85-11647
Effects of chemical releases by the STS 3 orbiter on the ionosphere p 166 A85-29538
DE-1 measurements of AKR wave directions p 166 A85-37717
Suprathermal plasma observed on STS-3 Mission by plasma diagnostics package p 179 N85-22472

J

Jet Propulsion Lab., California Inst. of Tech., Pasadena.
An evaluation of oxygen/hydrogen propulsion systems for the Space Station
[AIAA PAPER 85-1156] p 45 A85-43976
Feasibility demonstration of a novel, flat-belt, continuously variable transmission or automotive and electric-hybrid vehicle application
[NASA-CR-174430] p 185 N85-19894
An evaluation of oxygen-hydrogen propulsion systems for the Space Station
[NASA-TM-87059] p 52 N85-28971
John Carroll Univ., Cleveland, Ohio.
Remote displacement measurements using a laser diode p 121 A85-24464
John Deere Technologies International, Inc., Wood-Ridge, N.J.
Stratified charge rotary aircraft engine technology enablement program
[NASA-CR-174812] p 25 N85-21163

K

Kansas Univ., Lawrence.
Numerical simulations of positively-biased probes and dielectric-conductor disks in a plasma p 179 A85-17262
Numerical simulation of positive-potential conductors in the presence of a plasma and a secondary-emitting dielectric p 102 A85-35306
Kentucky Univ., Lexington.
Gravitational effects on flames spreading over thick solid surfaces
[IAF PAPER 84-154] p 59 A85-13092
Solids mixing in a three phase fluidized bed containing spherically shaped-porous solid particles
[PB85-187961] p 120 N85-33453

Kumm (Emerson L.), Tempe, Ariz.
Feasibility demonstration of a novel, flat-belt, continuously variable transmission or automotive and electric-hybrid vehicle application
[NASA-CR-174430] p 185 N85-19894

L

Life Systems, Inc., Cleveland, Ohio.
Engineering model system study for a regenerative fuel cell: Study report
[NASA-CR-174801] p 158 N85-16292
Little (Arthur D.), Inc., Cambridge, Mass.
Preliminary evaluation of a liquid belt radiator for space applications
[NASA-CR-174807] p 47 N85-15804
Little (Arthur D.), Inc., Santa Monica, Calif.
Advanced technology cogeneration system conceptual design study: Closed cycle gas turbines
[NASA-CR-168222] p 159 N85-16300
Lockheed-California Co., Burbank.
Effect of low temperature on fatigue and fracture properties of Ti-5Al-2.5Sn(ELI) for use in engine components p 70 A85-47972
Study of advanced fuel system concepts for commercial aircraft and engines
[NASA-CR-174752] p 93 N85-19176
Lockheed-Georgia Co., Marietta.
An experimental study of tone excited heated jets
[AIAA PAPER 84-2341] p 172 A85-10882
Some unique experiments on receptivity
[AIAA PAPER 85-0533] p 174 A85-25932
Acoustic control of free jet mixing
[AIAA PAPER 85-0569] p 109 A85-25951
Loral Electro-Optical Systems, Inc., Pasadena, Calif.
Inert gas test of two 12-cm magnetostatic thrusters p 43 A85-29310
Louisiana State Univ., Baton Rouge.
Systematic optimization of a detailed kinetic model using a methane ignition example p 59 A85-12890
Transferring data oscilloscope to an IBM using an Apple II+ p 168 A85-24526
Shock tube study of the fuel structure effects on the chemical kinetic mechanisms responsible for soot formation, part 2
[NASA-CR-174880] p 63 N85-25444
Lulea Univ. (Sweden).
Elastohydrodynamic lubrication of line contacts p 126 A85-11069

M

MARC Analysis Research Corp., Palo Alto, Calif.
Probabilistic finite element development p 149 N85-27956
Martin Marietta Aerospace, Denver, Colo.
Main propulsion system design recommendations for an advanced Orbit Transfer Vehicle
[AIAA PAPER 85-1336] p 36 A85-39730
Technology requirements to be addressed by the NASA Lewis Research Center Cryogenic Fluid Management Facility program
[AIAA PAPER 85-1229] p 94 A85-47024
Fiberglass epoxy laminate fatigue properties at 300 and 20 K p 56 A85-47970
Massachusetts Inst. of Tech., Cambridge.
Rational approach for assumed stress finite elements p 139 A85-12029
Flutter and forced response of mistuned rotors using standing wave analysis p 139 A85-12721
Hybrid Semiloof elements for plates and shells based upon a modified Hu-Washizu principle p 139 A85-15893
A numerical study of the steady scalar convective diffusion equation for small viscosity p 107 A85-16533
Three-dimensional inviscid flow analysis of turbofan forced mixers
[AIAA PAPER 85-0086] p 2 A85-19510
Methanol as a soot reducer in a turbulent swirling burner
[ASME PAPER 84-JPGC-GT-2] p 61 A85-23192
Evolution of assumed stress hybrid finite element p 142 A85-35046
Axisymmetric solid elements by a rational hybrid stress method p 143 A85-41109
Rotor wake characteristics of a transonic axial flow fan
[AIAA PAPER 85-1133] p 6 A85-43974
Thermal-mechanical fatigue crack growth in Inconel X-750
[NASA-CR-174740] p 72 N85-15877
Metal vapor arc switch electromagnetic accelerator technology
[NASA-CR-174380] p 103 N85-18259
Researched applied to transonic compressors in numerical fluid mechanics of inviscid flow and viscous flow
[NASA-CR-174353] p 114 N85-18291
Stress waves in an isotropic elastic plate excited by a circular transducer
[NASA-CR-3877] p 138 N85-20390
A theory of post-stall transients in multistage axial compression systems
[NASA-CR-3878] p 8 N85-21117
Advanced stress analysis methods applicable to turbine engine structures
[NASA-CR-175573] p 26 N85-21165
Application of homomorphic signal processing to stress wave factor analysis
[NAS 1.26:174871] p 138 N85-21673
Recent advances in hybrid/mixed finite elements
[NASA-CR-175574] p 145 N85-21687
Structural response of a rotating bladed disk to rotor whirl
[NASA-CR-175605] p 27 N85-22391
On Hybrid and mixed finite element methods
[NASA-CR-175551] p 146 N85-23096
Ultrasonic testing of plates containing edge cracks
[NASA-CR-3904] p 138 N85-29307
Structural characteristics of high temperature composites
[NASA-CR-175998] p 58 N85-30037
Materials Research Lab., Inc., Glenwood, Ill.
Fracture of composite-adhesive-composite systems p 141 A85-27935
Max-Planck-Inst. fuer Metallforschung, Stuttgart (West Germany).
A study of fatigue damage mechanisms in Waspaloy from 25 to 800 C p 65 A85-12098
Mechanical Technology, Inc., Latham, N. Y.
Mod II engine and technology development p 129 A85-45473
Automotive Stirling engine systems development p 130 A85-45474
Development of gas-lubricated pistons for heavy duty diesel engine technology program
[NASA-CR-174746] p 184 N85-12808
Development of a multiplane multispeed balancing system for turbine systems
[NASA-CR-174750] p 35 N85-22400
Free-piston Stirling engine/linear alternator 1000-hour endurance test
[NASA-CR-174771] p 163 N85-30481
Michigan State Univ., East Lansing.
Experiments with a microwave electrothermal thruster concept p 42 A85-16441
Measurements of energy distribution in microwave plasmas of N2 and He and comparisons with results for H2 p 178 A85-16443
The energetics of hydrogen atom recombination - Analysis, experiments, and modeling p 179 A85-16444
Recent work on a microwave ion source p 179 A85-16455
Closed-loop strain controlled testing at elevated temperatures with a non-contacting gage p 121 A85-29562
Experimental performance of a microwave cavity plasma disk ion source p 179 A85-43552
Improved models for increasing wind penetration, economics and operating reliability
[NASA-CR-175538] p 160 N85-20545
Development of a temperature measurement system with application to a jet in a cross flow experiment
[NASA-CR-174896] p 27 N85-25262
A comparison of smooth specimen and analytical simulation techniques for notched members at elevated temperatures p 151 N85-31546
Michigan Technological Univ., Houghton.
The mechanisms of formation and prevention of channel segregation during alloy solidification p 180 A85-18082
Cyclic oxidation behavior of beta+gamma overlay coatings on gamma and gamma+gamma-prime alloys p 68 A85-32431
The effect of tantalum and carbon on the structure/properties of a single crystal nickel-base superalloy
[NASA-CR-174779] p 71 N85-11223
The effect of tantalum on the structure/properties of two polycrystalline nickel-base superalloys: B-1900 + Hf MAR-M247
[NASA-CR-174847] p 73 N85-18127
Effects of MAR-M247 substrate (modified) composition on coating oxidation coating/substrate interdiffusion
[NASA-CR-174851] p 73 N85-19073
A study of interdiffusion in beta + gamma/gamma + gamma prime Ni-Cr-Al
[NASA-CR-174852] p 74 N85-20041
Raman structural studies of the nickel electrode
[NASA-CR-175619] p 183 N85-23414
Michigan Univ., Ann Arbor.
Integrating chemical kinetic rate equations by selective use of stiff and nonstiff methods
[AIAA PAPER 85-0237] p 60 A85-19607
High temperature oxidation of propene p 61 A85-33570
Practical aspects of photovoltaic technology, applications and cost (revised)
[NASA-CR-174963] p 165 N85-35472
Minnesota Univ., Minneapolis.
Acoustic structure and propagation in highly porous, layered, fibrous materials p 173 A85-12301
Cone formation as a result of whisker growth on ion bombarded metal surfaces p 182 A85-41635
Holographic optical system for aberration corrections in laser Doppler velocimetry p 123 A85-48659
Missouri Univ., Rolla.
Modelling of wind tunnel wall effects on the radiation characteristics of acoustic sources
[AIAA PAPER 84-2364] p 174 A85-16104
Mitre Corp., Bedford, Mass.
A frequency-routed satellite system concept using multiple orthogonally-polarized beams for frequency reuse p 97 A85-34470
Motorola, Inc., Scottsdale, Ariz.
Satellite baseband processor test performance summary p 95 A85-14434

N

Nanjing Aeronautical Inst. (China).
Structure of particle-laden jets - Measurements and predictions p 109 A85-25137
Structure of ducted particle-laden turbulent jets p 110 A85-38999
National Aeronautics and Space Administration, Washington, D.C.
Status of NASA's multibeam communications technology program p 100 A85-14432
Effects of chemical releases by the STS 3 orbiter on the ionosphere p 166 A85-29538
The NASA photovoltaic technology program p 155 A85-35604
Suprathermal plasma observed on STS-3 Mission by plasma diagnostics package p 179 N85-22472
Electron and ion density depletions measured in the STS-3 orbiter wake p 39 N85-22474
National Aeronautics and Space Administration. Langley Research Center, Hampton, Va.
GASP cloud encounter statistics - Implications for laminar flow control flight p 166 A85-11979
A numerical study of the steady scalar convective diffusion equation for small viscosity p 107 A85-16533
Variability of cloudiness at airline cruise altitudes from GASP measurements p 166 A85-31199
A three-dimensional boundary-layer analysis including heat-transfer and blade-rotation effects p 6 A85-42988
A multiple-scales model of the shock-cell structure of imperfectly expanded supersonic jets p 113 A85-49354
National Bureau of Standards, Gaithersburg, Md.
Advanced thin film thermocouples
[NASA-CR-175541] p 124 N85-21607
National Bureau of Standards, Washington, D.C.
Convective influence on the stability of a cylindrical solid-liquid interface p 109 A85-26911
Naval Research Lab., Washington, D. C.
Effects of 1 MeV electrons and 10 MeV protons on the performance and reflectance of thin BSR cells p 182 A85-35699
The J3 SCR model applied to resonant converter simulation p 102 A85-42156
Nebraska Univ., Lincoln.
Dielectric properties of 'diamondlike' carbon prepared by RF plasma deposition p 182 A85-38192
'Diamondlike' carbon films - Optical absorption, dielectric properties, and hardness dependence on deposition parameters p 82 A85-40383
Negev Univ., Beersheva (Israel).
RF-sputtered silicon and hafnium nitrides - Properties and adhesion to 440C stainless steel p 81 A85-36240
Surface hardening of steel by boriding in a cold rf plasma p 68 A85-40275
Nevada Univ., Reno.
Oscillatory conductive heat transfer for a fiber in an ideal gas p 109 A85-26077

Northwestern Univ., Evanston, Ill.
Deposition stress effects on the life of thermal barrier coatings on burner rigs p 79 A85-19086
On stress field near a stationary crack tip
[AD-A152863] p 141 A85-24532
Probabilistic finite element: Variational theory p 149 N85-27957

Notre Dame Univ., Ind.
Feedback in separated flows over symmetric airfoils
[AIAA PAPER 84-2297] p 3 A85-28899
Alternatives for jet engine control
[NASA-CR-175831] p 29 N85-26713
Alternatives for jet engine control
[NASA-CR-175832] p 29 N85-26714
Alternatives for jet engine control
[NASA-CR-175833] p 29 N85-26715

O

O'Donnell and Associates, Inc., Pittsburgh, Pa.
Simplified design and life prediction of rocket thrust chambers p 44 A85-29314

Oak Ridge National Lab., Tenn.
Dispersed metal-toughened ceramics and ceramic brazing
[NASA-CR-174284] p 86 N85-15916
Dispersed-metal-toughened alumina
[NASA-CR-174687] p 89 N85-22758

Oberlin Coll., Ohio.
The infinite line pressure probe p 122 A85-37704

Ohio State Univ., Cleveland.
Vibrations of twisted cantilevered plates - Summary of previous and current studies p 140 A85-22069

Ohio State Univ., Columbus.
Ultrasonic wave propagation in two-phase media - Spherical inclusions p 54 A85-11926
Optical computer switching network p 178 A85-23134
Predicting rime ice accretion on airfoils p 3 *A85-25135*
Vibrations of twisted cantilever plates - A comparison of theoretical results p 144 A85-47626
Design and wind tunnel evaluation of a symmetric airfoil series for large wind turbine applications
[NASA-CR-174764] p 7 N85-10919
Fundamentals of microcrack nucleation mechanics
[NASA-CR-3851] p 137 N85-16195
Adaptive antenna arrays for weak interfering signals
[NASA-CR-174336] p 98 N85-17258
Engineering calculations for communications satellite systems planning
[NASA-CR-175552] p 37 N85-21233
Analysis of the electromagnetic scattering from an inlet geometry with lossy walls
[NASA-CR-175743] p 99 N85-25686
A study of internal and distributed damping for vibrating turbomachiner blades
[NASA-CR-175901] p 30 N85-27868
Diffusion welding of Cassegrainian concentrator cell stack assemblies
[NASA-CR-176104] p 164 N85-33566
Adaptive antenna arrays for satellite communications: Design and testing
[NASA-CR-176162] p 100 N85-34329
The design and analysis of single flank transmission error testor for loaded gears
[NASA-CR-176163] p 136 N85-34404

Oklahoma State Univ., Stillwater.
Flow visualization of lateral jet injection into swirling crossflow
[AIAA PAPER 85-0059] p 2 A85-19490
Swirling flows in typical combustor geometries
[AIAA PAPER 85-0184] p 108 A85-19574
Turbulence measurements of lateral jet injection into confined tubular crossflow
[AIAA PAPER 85-1102] p 110 A85-39604
Investigation of flowfields found in typical combustor geometries
[NASA-CR-3869] p 26 N85-21167
Deflected jet experiments in a turbulent combustor flowfield
[NASA-CR-174863] p 26 N85-22390
Confined turbulent swirling recirculating flow predictions
[NASA-CR-174917] p 29 N85-26716
Turbulence characteristics of swirling flowfields
[NASA-CR-174918] p 29 N85-26717
Predictions and measurements of isothermal flowfields in axisymmetric combustor geometries
[NASA-CR-174916] p 29 N85-27867

Opcoa, Inc., Santa Ana, Calif.
Fiber optic, Fabry-Perot high temperature sensor
[NASA-CR-174712] p 178 N85-13594

P

Pennsylvania State Univ., State College.
The boundary layer on compressor cascade blades
[NASA-CR-174369] p 114 N85-18292

Pennsylvania State Univ., University Park.
Computation of viscous flows in turbomachinery cascades p 106 A85-11631
Computation and turbulence closure models for shear flows in rotating curved bodies p 107 A85-14349
A space-marching method for incompressible Navier-Stokes equations
[AIAA PAPER 85-0170] p 108 A85-19564
Drop-turbulence interactions in a diffusion flame
[AIAA PAPER 85-0319] *p 60 A85-19665*
A morphological study of silicon carbide prepared by chemical vapor deposition p 79 A85-20938
Effects of friction dampers on aerodynamically unstable rotor stages p 14 A85-21866
Structure of particle-laden jets - Measurements and predictions p 109 A85-25137
Acoustic control of free jet mixing
[AIAA PAPER 85-0569] p 109 A85-25951
Computation of three-dimensional viscous flows using a space-marching method p 4 A85-29259
The scattering of ultrasonic third sound from substrate surface defects p 174 A85-36047
Structure of ducted particle-laden turbulent jets p 110 A85-38999
Turbulence modelling for complex shear flows
[AIAA PAPER 85-1652] p 111 A85-40752
The performance of jet noise suppression devices for industrial applications p 175 A85-42563
Measurements and predictions of the structure of evaporating sprays p 112 A85-46484
Structure of nonevaporating sprays. I - Initial conditions and mean properties p 112 A85-48538
The structure of dilute combusting sprays
[NASA-CR-174838] p 24 N85-15728
Mass analysis of neutral particles and ions released during electrical breakdowns on spacecraft surfaces
[NASA-CR-175585] p 39 N85-21250
Mass spectra of neutral particles released during electrical breakdown of thin polymer films p 88 N85-22511

Perkin-Elmer Corp., Norwalk, Conn.
Electrical characterization of plasma-grown oxides on gallium arsenide p 181 A85-32635

Politecnico di Torino (Italy).
Time dependent computation of the Euler equations for designing 2-D cascades, including the case of transonic shock free design p 5 A85-41814

Pontifica Univ. Catolica do Rio de Janeiro (Brazil).
Heat transfer and turbulence measurements of a film-cooled flow over a convexly curved surface p 112 A85-41787

Pratt and Whitney Aircraft, East Hartford, Conn.
Energy efficient engine. Volume 1: Component development and integration program
[NASA-CR-173084] p 22 N85-10992
Hot isostatically pressed manufacture of high strength MERL 76 disk and seal shapes
[NASA-CR-165550] p 71 N85-11225
3-D inelastic analysis methods for hot section components (base program)
[NASA-CR-174700] p 145 N85-21686
Error reduction program
[NASA-CR-174776] p 172 N85-27584
Energy efficient engine component development and integration program
[NASA-CR-172846] p 31 N85-29958
Creep fatigue life prediction for engine hot section materials (isotropic)
[NASA-CR-168228] p 32 N85-31057
Energy Efficient Engine Program technology benefit/cost study, volume 1
[NASA-CR-174766-VOL-1] p 33 N85-35197
Energy Efficient Engine Program technology benefit/cost study, volume 2
[NASA-CR-174766-VOL-2] p 33 N85-35198
Development of advanced high-temperature heat flux sensors. Phase 2: Verification testing
[NASA-CR-174973] p 126 N85-35391

Pratt and Whitney Aircraft, West Palm Beach, Fla.
Design and analysis report for the RL10-2B breadboard low thrust engine
[NASA-CR-174857] p 48 N85-19020
Convoluted nozzle design for the RL10 derivative 2B engine
[NASA-CR-174953] p 32 N85-29965

Pratt and Whitney Aircraft Group, East Hartford, Conn.
Assessment of discretization schemes to reduce numerical diffusion in the calculation of complex flows
[AIAA PAPER 85-0441] p 108 A85-19751
Finite element engine blade structural optimization
[AIAA PAPER 85-0645] p 141 A85-30313
Application of two creep fatigue life models for the prediction of elevated temperature crack initiation of a nickel base alloy
[AIAA PAPER 85-1420] p 69 A85-43979
Study of controlled diffusion stator blading
[NASA-CR-167995] p 25 N85-18058
Energy efficient engine high-pressure turbine component *rig performance test report*
[NASA-CR-168189] p 30 N85-29955
Energy efficient engine integrated core/low spool test hardware design report
[NASA-CR-168137] p 31 N85-29956

PRC Planning and Economics, Inc., Lake Success, N.Y.
Comparative analysis of operational forecasts versus actual weather conditions in airline flight planning, volume 1
[NASA-CR-167862] p 167 N85-35534
Comparative analysis of operational forecasts versus actual weather conditions in airline flight planning, volume 2
[NASA-CR-167863] p 167 N85-35535
Comparative analysis of operational forecasts versus actual weather conditions in airline flight planning, volume 3
[NASA-CR-167864] p 167 N85-35536
Comparative analysis of operational forecasts versus actual weather conditions in airline flight planning, volume 4
[NASA-CR-167865] p 167 N85-35537
Comparative analysis of operational forecasts versus *actual weather conditions in airline flight planning:* Summary report
[NASA-CR-167866] p 168 N85-35538

Princeton Univ., N. J.
The role of surface generated radicals in catalytic combustion p 30 N85-27869

Purdue Univ., West Lafayette, Ind.
A stagnation pressure probe for droplet-laden air flow
[AIAA PAPER 85-0330] p 108 A85-19672
Use of statical indentation laws in the impact analysis of laminated composite plates p 55 A85-29133
The effect of aerodynamic and structural detuning on turbomachine supersonic unstalled torsional flutter
[AIAA PAPER 85-0761] p 14 A85-30378
Noise constraints effecting optimal propeller designs
[SAE PAPER 850871] p 7 A85-50106
Effects of cobalt, boron, and zirconium on the microstructure of Udimet 738
[NASA-CR-174762] p 70 N85-10166

Purdue Univ. School of Science at Indianapolis, Ind.
A finite element solution of three-dimensional inviscid rotational flows through curved ducts p 107 A85-11648

R

Rensselaer Polytechnic Inst., Troy, N.Y.
Topological reaction rate measurements related to scuffing p 64 A85-11070
Convective influence on the stability of a cylindrical solid-liquid interface p 109 A85-26911
The influence of hold times on LCF and FCG behavior in a P/M Ni-base superalloy p 67 A85-32400
Electrical characterization of plasma-grown oxides on gallium arsenide p 181 A85-32635
Heat treatment of bulk gallium arsenide using a phosphosilicate glass cap p 181 A85-32636
Fabrication of p(+)-n junction GaAs solar cells by a novel method p 181 A85-33645
Heat transfer investigation in the junction region of circular cylinder normal to a flat plate at 90 deg location
[ASME PAPER 84-WA/HT-70] p 111 A85-39898
Research on gallium arsenide diffused junction solar cells
[NASA-CR-174057] p 158 N85-11457
Development of a lithium secondary battery separator p 104 N85-31378

Rice Univ., Houston, Tex.
Oscillator response to nonstationary excitation
[ASME PAPER 84-WA/APM-38] p 140 A85-17039

Rocket Research Corp., Redmond, Wash.
Performance characterization tests of a 1-kW resistojet using hydrogen, nitrogen and ammonia as propellants
[AIAA PAPER 85-1159] p 44 A85-39628

Rockwell International Corp., Canoga Park, Calif.
The effect of microstructure, temperature, and hold-time on low-cycle fatigue of As HIP P/M Rene 95 p 67 A85-32399
Reusable rocket engine turbopump condition monitoring
[SAE PAPER 841619] p 44 A85-39267
Cryogenic upper stage test bed engine

[AIAA PAPER 85-1339] p 44 A85-39733
Small centrifugal pumps for low thrust rockets
[AIAA PAPER 85-1302] p 45 A85-43978
Electric power - Photovoltaic or solar dynamic?
p 46 A85-47042
Reusable rocket engine turbopump condition monitoring p 51 N85-26907
Composite loads spectra for select space propulsion structural components p 148 N85-27953
Feasibility of mapping velocity flow fields in SSME powerhead by laser anemometry techniques
p 41 N85-27971

Rockwell International Corp., Columbus, Ohio.
Application of computational fluid dynamics to complex inlet ducts
[AIAA PAPER 85-1213] p 6 A85-47023

S

Sandia National Labs., Albuquerque, N. Mex.
Properties of coated and modified surfaces
p 53 A85-36694

Scientific Research Associates, Inc., Glastonbury, Conn.
Analytical modeling of circuit aerodynamics in the new NASA Lewis Altitude Wind Tunnel
[AIAA PAPER 85-0380] p 3 A85-26389

Scientific Systems, Inc., Cambridge, Mass.
Nonlinear global stability analysis of compressor stall phenomena
[NASA-CR-174908] p 31 N85-29960

Signatron, Inc., Lexington, Mass.
A frequency-routed satellite system concept using multiple orthogonally-polarized beams for frequency reuse p 97 A85-34470

SKF Engineering and Research Centre, Nieuwegein (Netherlands).
Fast numerical calculations of EHD sliding traction forces Application to rolling bearings
[ASME PAPER 84-TRIB-26] p 127 A85-21289

SKF Industries, Inc., King of Prussia, Pa.
Planetary-gear-support bearing test rig design
[NASA-CR-174927] p 12 N85-35185

South Carolina State Coll., Orangeburg.
On local total strain redistribution using a simplified cyclic inelastic analysis based on an elastic solution
[AIAA PAPER 85-1419] p 142 A85-39770

Southwest Research Inst., San Antonio, Tex.
Unified constitutive material models for nonlinear finite-element structural analysis
[AIAA PAPER 85-1418] p 142 A85-39769
Constitutive modeling and computational *implementation for finite strain plasticity*
p 143 A85-40910
Sliding seal materials for adiabatic engines
[NASA-CR-174893] p 89 N85-22757
Probabilistic structural analysis theory development
p 148 N85-27955
A survey of unified constitutive theories
p 150 N85-31531

Spectron Development Labs., Inc., Costa Mesa, Calif.
Spray characterization with a nonintrusive technique using absolute scattered light p 120 A85-10036
Nonintrusive optical single-particle counter for measuring the size and velocity of droplets in a spray
p 120 A85-16794
Research study of droplet sizing technology leading to the development of an advanced droplet sizing system
[NASA-CR-174839] p 123 N85-21604

Spring Arbor Coll., Mich.
Chemical and electrochemical behavior of the Cr(III)/Cr(II) half-cell in the iron-chromium redox energy storage system p 61 A85-33785

SRI International Corp., Menlo Park, Calif.
Chemistry of fuel deposits and sediments and their predursors
[NASA-CR-174778] p 92 N85-10209

Standard Oil Co., Cleveland, Ohio.
Control algorithms and computer simulation of a stand-alone photovoltaic village power system
p 153 A85-11345

Stanford Univ., Calif.
Velocity visualization in gas flows using laser-induced phosphorescence of biacetyl p 121 A85-21695
Optical computer switching network
p 178 A85-23134
Fast laser-induced aerosol formation for visualization of gas flows p 121 A85-31113
Two-frequency laser-induced fluorescence technique for rapid velocity-field measurements in gas flows
p 121 A85-32294
Heat transfer and turbulence measurements of a film-cooled flow over a convexly curved surface
p 112 A85-41787
Augmented weak forms and element-by-element preconditioners: Efficient iterative strategies for structural finite elements. A preliminary study p 144 N85-10384
Free-surface phenomena under low- and zero-gravity conditions
[NASA-CR-175885] p 36 N85-27922

Stanford Univ., Palo Alto, Calif.
Velocity visualization in gaseous flows
[NASA-CR-174954] p 119 N85-31445

Stanitz (John D.), University Heights, Ohio.
General design method for 3-dimensional, potential flow fields. Part 2: Computer program DIN3D1 for simple, unbranched ducts
[NASA-CR-3926] p 10 N85-35159

State Univ. of New York, Albany.
Plasma deposited hydrogenated carbon on GaAs and InP p 182 A85-40386

State Univ. of New York, Stony Brook.
Failure during thermal cycling of plasma-sprayed thermal barrier coatings p 81 A85-36246

Stonehart Associates, Inc., Madison, Conn.
Electrocatalyst advances for hydrogen oxidation in phosphoric acid fuel cells p 60 A85-15614
Preparation and evaluation of advanced catalysts for phosphoric acid fuel cells
[NASA-CR-168223] p 160 N85-19511

Sverdrup Technology, Inc., Arnold Air Force Station, Tenn.
Gear mesh stiffness and load sharing in planetary gearing
[ASME PAPER 84-DET-229] p 129 A85-33781

Sverdrup Technology, Inc., Cleveland, Ohio.
Flame flashback in a premixed dump combustor
[AIAA PAPER 85-0145] p 60 A85-19550

System Science and Software, San Diego, Calif.
Computer simulation of plasma electron collection by PIX-II
[AIAA PAPER 85-0386] p 43 A85-19715

Systems Science and Software, La Jolla, Calif.
Surface interactions and high-voltage current collection p 40 N85-22493

T

Technion - Israel Inst. of Tech., Haifa.
High temperature oxidation of propene
p 61 A85-33570
Electronic heterodyne readout of fringes in moire deflectometry p 122 A85-36726
Thermodynamically consistent constitutive equations for nonisothermal large strain, elasto-plastic, creep behavior
[AIAA PAPER 85-0621] p 142 A85-38425

Tennessee Univ. Space Inst., Tullahoma.
Flow control in a diffusing S-Duct
[AIAA PAPER 85-0524] p 3 A85-25928

Texas A&M Univ., College Station.
Analytical determination of propeller performance degradation due to ice accretion
[AIAA PAPER 85-0339] p 14 A85-20867
Experimental aerodynamic characteristics of an NACA 0012 airfoil with simulated ice p 12 A85-21844
Heat transfer enhancement in channels with turbulence promoters
[ASME PAPER 84-WA/HT-72] p 111 A85-39900
Rotordynamic coefficients for compressible flow in tapered annular seals p 129 A85-42573
Performance degradation of helicopter rotor in forward flight due to ice p 11 A85-42937
On the use of internal state variables in thermoviscoplastic constitutive equations
p 150 N85-31536
Numerical considerations in the development and implementation of constitutive models
p 151 N85-31541

Texas Technological Univ., Lubbock.
Flow visualization of lateral jet injection into swirling crossflow
[AIAA PAPER 85-0059] p 2 A85-19490
Turbulence measurements of lateral jet injection into confined tubular crossflow
[AIAA PAPER 85-1102] p 110 A85-39604

Texas Univ., Austin.
Analysis of hourglass instabilities and control in underintegrated finite element methods
p 139 A85-11125
Stability, accuracy, and efficiency of some underintegrated methods in finite element computations
p 172 A85-50073
Interaction of finite-amplitude sound with air-filled porous materials
[NASA-CR-174885] p 177 N85-27637

Textron Bell Aerospace Co., Buffalo, N. Y.
Convoluted nozzle design for the RL10 derivative 2B engine
[NASA-CR-174953] p 32 N85-29965

Tokai Univ., Hiratsuka (Japan).
Flow visualization of lateral jet injection into swirling crossflow
[AIAA PAPER 85-0059] p 2 A85-19490

Toledo Univ., Ohio.
An allpass filter design for luminance and chrominance separation of NTSC signals p 102 A85-28230
Modeling of NASA's 30/20 GHz satellite communications system p 38 A85-36663
Small-signal model for the series resonant converter
p 102 A85-39453
Thermal-stress analysis for a wood composite blade
[NASA-CR-174794] p 159 N85-17421
Wake effects on the aerodynamic performance of horizontal axis wind turbines
[NASA-CR-174920] p 162 N85-29364
Aerodynamic analysis of a horizontal axis wind turbine by use of helical vortex theory. Volume 1: Theory
[NASA-CR-168054] p 9 N85-29916

Transmission Research, Inc., Cleveland, Ohio.
Thermal traction contact performance evaluation under fully flooded and starved conditions
[NASA-CR-168173] p 132 N85-25848
Rolling, slip and traction measurements on low modulus materials
[NASA-CR-174909] p 135 N85-33491

TriSolar Corp., Bedford, Mass.
Microprocessor control of photovoltaic systems
p 156 A85-45408

TRW Electronic Systems Group, Redondo Beach, Calif.
The 30 GHz solid state amplifier for low cost low data rate ground terminals
[NASA-CR-174795] p 102 N85-12300

TRW, Inc., Cleveland, Ohio.
Energy efficient engine. Volume 2. Appendix A: *Component development and integration program*
[NASA-CR-173085] p 22 N85-10991

TRW, Inc., Redondo Beach, Calif.
Advanced 30/20 GHz multiple beam antenna for future communications satellites p 96 A85-14436
Electrothermal thruster diagnostics p 42 A85-16440
An experimental study of three-dimensional shock wave/turbulent boundary layer interactions in a supersonic flow
[AIAA PAPER 85-1566] p 5 A85-40691
Electric power - Photovoltaic or solar dynamic?
p 46 A85-47042

TRW Space Technology Labs., Redondo Beach, Calif.
High frequency plasma generator for ion thrusters
[NASA-CR-174772] p 48 N85-17023

Tuskegee Inst., Ala.
Friction in rail guns p 101 A85-16424
An improved computer model for prediction of axial gas turbine performance losses
[NASA-CR-174246] p 24 N85-15724
Arc-driven rail gun research
[NASA-CR-174816] p 132 N85-21662

U

United Technologies Corp., East Hartford, Conn.
Finite difference methods for reducing numerical diffusion in TEACH-type calculations
[AIAA PAPER 85-0057] p 108 A85-19488
Calculation of confined swirling flows
[AIAA PAPER 85-0060] p 108 A85-19491
A linearized unsteady aerodynamic analysis for transonic cascades p 3 A85-20744
Energy efficient engine flight propulsion system preliminary analysis and design report
[NASA-CR-174701] p 18 N85-10947
Energy efficient engine combustor test hardware detailed design report
[NASA-CR-167945] p 18 N85-10950

United Technologies Corp., South Windsor, Conn.
Regenerative fuel cell energy storage system for a low Earth orbit space station
[NASA-CR-174802] p 158 N85-13371
Electric utility acid fuel cell stack technology advancement
[NASA-CR-174804] p 159 N85-17422
Long-life high performance fuel cell program
[NASA-CR-174874] p 50 N85-25384

United Technologies Research Center, East Hartford, Conn.
Mass and momentum turbulent transport experiments with confined coaxial jets p 107 A85-14399
Finite difference methods for reducing numerical diffusion in TEACH-type calculations
[AIAA PAPER 85-0057] p 108 A85-19488
Three-dimensional inviscid flow analysis of turbofan forced mixers

[AIAA PAPER 85-0086] p 2 A85-19510
Fiber optic temperature sensor p 121 A85-29563
The scattering of ultrasonic third sound from substrate surface defects p 174 A85-36047
High temperature static strain sensor development program p 19 N85-10959
External fuel vaporization study, phase 2
[NASA-CR-174079] p 92 N85-11252
High-temperature optically activated GaAs power switching for aircraft digital electronic control
[NASA-CR-174711] p 34 N85-12901
Imide modified epoxy matrix resins
[NASA-CR-174695] p 85 N85-15892
Turbulent transport and length scale measurement experiments with comfined coaxial jets
[NASA-CR-174831] p 117 N85-30245
Universities Space Research Association, Columbia, Md.
Design and performance of a fixed, nonaccelerating guide vane cascade that operates over an inlet flow angle range of 60 deg
[ASME PAPER 84-GT-75] p 4 A85-32964
University of Southern California, Los Angeles.
Focal shifts in parabolic reflectors p 97 A85-39356

V

Varian Associates, Palo Alto, Calif.
Magnesium doping of efficient GaAs and Ga(0.75)In(0.25)As solar cells grown by metalorganic chemical vapor deposition p 180 A85-11466
Design of low loss helix circuits for interference fitted and brazed circuits
[NASA-CR-168313] p 103 N85-19328
Virginia Polytechnic Inst. and State Univ., Blacksburg.
The influence of combustion liner holes on noise production by ducted burners
[AIAA PAPER 84-2322] p 172 A85-10869
Bipolar-FET combinational power transistors for power conversion applications p 100 A85-12669
A fast time domain digital simulation technique for power converters - Application to a buck converter with feedforward compensation p 101 A85-20900
New eutectic alloys and their heats of transformation p 66 A85-27808
Vortex induced lift on a flat plate with a curved forward-facing flap p 4 A85-30175
The J3 SCR model applied to resonant converter simulation p 102 A85-42156
Optimization of cascade blade mistuning. I - Equations of motion and basic inherent properties p 16 A85-42365
Optimization of cascade blade mistuning. II - Global optimum and numerical optimization p 16 A85-45715
Geometrically nonlinear analysis of laminated elastic structures
[NASA-CR-175609] p 146 N85-21720
Thermodynamic evaluation of transonic compressor rotors using the finite volume approach
[NASA-CR-175811] p 29 N85-26712
A study of the stress wave factor technique for the characterization of composite materials
[NASA-CR-174870] p 58 N85-30035
Virginia Univ., Charlottesville.
Four-dimensional modulation and coding - An alternate to frequency-reuse p 97 A85-36653

W

Washington Univ., Seattle.
Direct numerical simulations of a reacting mixing layer with chemical heat release
[AIAA PAPER 85-0143] p 60 A85-19548
Direct simulations of chemically reacting turbulent mixing layers
[AIAA PAPER 85-0321] p 60 A85-19666
Recent advances in methods for numerical solution of O.D.E. initial value problems p 171 A85-21370
Metallurgical and mechanical phenomena due to rubbing of titanium against sintered powder Nichrome p 127 A85-22281
An experimental investigation and numerical prediction of thermomechanical phenomena in high speed rotor tip rubbing p 14 A85-25442
An experimental study of three-dimensional shock wave/turbulent boundary layer interactions in a supersonic flow
[AIAA PAPER 85-1566] p 5 A85-40691
An interactive computer code for calculation of gas-phase chemical equilibrium (EQLBRM)
[NASA-CR-168337] p 18 N85-10948
Western Union Telegraph Co., McLean, Va.
Satellite provided customer promises services, a forecast of potential domestic demand through the year 2000. Volume 4: Sensitivity analysis
[NASA-CR-174662] p 99 N85-27092
Westinghouse Electric Corp., Pittsburgh, Pa.
Measured effects of wind turbine generation at the Block Island Power Company p 153 A85-10652
Fuel cell power plant economic and operational considerations
[ASME PAPER 84-AES-7] p 154 A85-21297
Gas cooled fuel cell systems technology development
[NASA-CR-174732] p 158 N85-16291
Westinghouse Research Labs., Pittsburgh, Pa.
Breakway friction and dynamic friction/wear measurements of various ceramic materials from 25 C (75 F) to 650 C (1200 F)
[NASA-CR-174803] p 90 N85-26994
Wichita State Univ., Kans.
Icing tunnel tests of Electro-Impulse De-Icing of an engine inlet and high-speed wings
[AIAA PAPER 85-0466] p 10 A85-20872
Electro-impulse de-icing of a turbofan engine inlet
[AIAA PAPER 85-1118] p 12 A85-40811
Wisconsin Univ., Madison.
A rotating superconducting solenoid for 100 kWh energy storage p 44 A85-33144
Wisconsin Univ., Milwaukee.
A study of Reynolds-stress closure model
[NASA-CR-174342] p 114 N85-17324
Wyle Labs., Inc., Huntsville, Ala.
Flow dynamic environment data base development for the SSME p 147 N85-26885

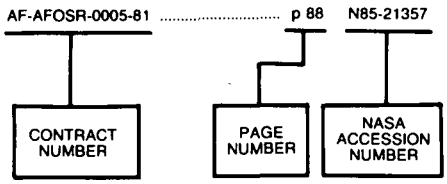
X

Xerox Electro-Optical Systems, Pasadena, Calif.
Development of a large insert gas ion thruster p 45 A85-42922

Y

Yale Univ., New Haven, Conn.
Polarization (ellipsometric) measurements of liquid condensate deposition and evaporation rates and dew points in flowing salt/ash-containing combustion gases p 123 A85-46925
Computer program for the calculation of multicomponent convective diffusion deposition rates from chemically frozen boundary layer theory
[NASA-CR-168329] p 116 N85-27164

Typical Contract Number Index Listing



Listings in this index are arranged alphanumerically by contract number. Under each contract number the NASA accession numbers denoting documents that have been produced as a result of research done under that contract are arranged in ascending order. The NASA accession number denotes the number by which the citation is identified.

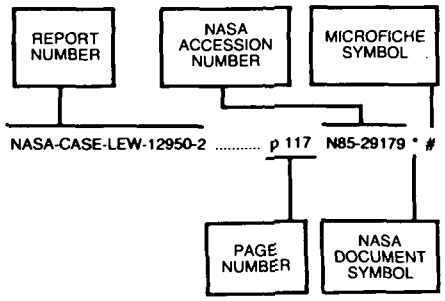
AF-AFOSR-0005-81 p 88 N85-21357
AF-AFOSR-79-0091 p 169 A85-36727
AF-AFOSR-80-0265 p 61 A85-47320
AF-AFOSR-81-0005 p 64 A85-11070
AF-AFOSR-84-0034 p 123 A85-46925
DA PROJ. 1L1-61101-AH-45 p 74 N85-19074
DAAE07-80-C-9115 p 134 N85-29295
DAAG24-83-K-0058 p 88 N85-21357
DAAG29-82-K-0147 p 141 A85-24532
DE-AC03-76SF-00098 p 65 A85-15603
p 171 A85-21370
p 93 N85-19185
p 77 N85-32176
DE-AC03-78ET-15365 p 60 A85-15614
DE-AC05-84OR-21400 p 86 N85-15916
p 89 N85-22758
DE-AC12-76SN-00052 p 78 N85-34267
DE-AE01-77CS-51040 p 31 N85-29961
DE-AI-01-80ET-17088 p 164 N85-30483
DE-AI01-76ET-20320 p 7 N85-10919
p 158 N85-11458
p 159 N85-16299
p 161 N85-23242
p 161 N85-27385
p 162 N85-29364
p 162 N85-29365
p 9 N85-29916
p 150 N85-30361
p 162 N85-30476
p 163 N85-30477
p 163 N85-30478
p 163 N85-30479
p 105 N85-32251
DE-AI01-77CS-1040 p 79 A85-15195
DE-AI01-77CS-51040 p 83 A85-48757
p 72 N85-13007
p 53 N85-14864
p 185 N85-19895
p 91 N85-28109
DE-AI01-77ET-13111 p 159 N85-16300
DE-AI01-79ET-20320 p 159 N85-17421
p 162 N85-29363
p 165 N85-34444
DE-AI01-79ET-20485 p 103 N85-13157
DE-AI01-80CS-50194 p 184 N85-12808
p 84 N85-14928
p 85 N85-15895
p 185 N85-16699
p 86 N85-18154
p 89 N85-22757
p 90 N85-26994
p 186 N85-32043
DE-AI01-80CS-5019 p 185 N85-16698
DE-AI01-80ET-17088 p 158 N85-16291
p 161 N85-25941
DE-AI04-80AL-12726 p 61 A85-33785
p 158 N85-12465
p 162 N85-27387
p 164 N85-34443
p 165 N85-35471
DE-AI05-82OR-1005 p 185 N85-27769
DE-AI21-80ET-17088 p 157 N85-10445
p 157 N85-10447
p 157 N85-11455
p 157 N85-11456
p 159 N85-17422
p 160 N85-19511
DE-FG22-80PC-30247 p 168 A85-24526
DE-FG22-80PC-30303 p 107 A85-14376
DEN3-153 p 157 A85-45517
DEN3-167 p 126 A85-15972
p 82 A85-42797
p 185 N85-18831
DEN3-168 p 127 A85-15973
p 31 N85-29961
DEN3-176 p 60 A85-15614
p 160 N85-19511
DEN3-17 p 83 A85-43930
p 91 N85-28109
DEN3-191 p 159 N85-17422
DEN3-215 p 159 N85-16300
DEN3-241 p 161 N85-25941
p 164 N85-30483
DEN3-244 p 161 N85-27377
DEN3-261 p 130 N85-13235
DEN3-262 p 165 N85-35471
DEN3-272 p 185 N85-19894
DEN3-275 p 153 A85-10652
DEN3-290 p 154 A85-21297
DEN3-303 p 74 N85-19078
DEN3-309 p 184 N85-12808
DEN3-310 p 156 A85-45408
DEN3-326 p 86 N85-18154
DEN3-32 p 129 A85-45473
p 130 A85-45474
DEN3-333 p 163 N85-30481
DEN3-339 p 185 N85-16698
DEN3-342 p 185 N85-16699
DEN3-346 p 90 N85-26994
DEN3-352 p 89 N85-22757
DEN3-354 p 153 A85-10652
DEN3-35 p 132 N85-25848
p 135 N85-33491
DEN3-390 p 158 N85-16291
DOT-FA78WAI-893 p 167 N85-21872
F19628-82-C-0081 p 40 N85-22486
p 40 N85-22487
F33615-78-C-2401 p 108 A85-19672
F33615-83-K-5016 p 142 A85-35046
F49620-83-C-0060 p 120 A85-10036
p 120 A85-16794
F49620-83-K-0004 p 121 A85-21695
p 121 A85-31113
p 121 A85-32294
F49620-83-K-0023 p 4 A85-32965
JPL-956602 p 185 N85-19894
NAG3-10 p 166 A85-37717
NAG3-112 p 169 A85-28613
NAG3-124 p 172 A85-10869
NAG3-132 p 170 A85-28614
p 170 A85-28615
p 169 A85-28628
p 170 A85-28629
NAG3-133 p 93 N85-19185
NAG3-134 p 141 A85-24532
NAG3-137 p 93 N85-19185
NAG3-141 p 97 A85-36653
NAG3-147 p 61 A85-33570
p 17 N85-10065
p 17 N85-10068
p 25 N85-21162
NAG3-153 p 80 A85-25963
NAG3-154 p 182 A85-38192
p 82 A85-40383
NAG3-156 p 96 A85-28234
p 96 A85-28241
NAG3-157 p 38 A85-36663
NAG3-159 p 2 A85-19490
p 37 N85-21233
NAG3-160 p 148 N85-27263
NAG3-161 p 173 A85-12301
NAG3-164 p 81 A85-36246
NAG3-172 p 58 N85-30035
NAG3-175 p 181 A85-32635
NAG3-176 p 107 A85-14376
NAG3-177 p 79 A85-20938
NAG3-179 p 107 A85-14241
p 4 A85-30175
NAG3-181 p 129 A85-42573
NAG3-182 p 113 A85-49354
NAG3-185 p 165 N85-35472
NAG3-186 p 129 A85-33781
NAG3-188 p 181 A85-32636
p 181 A85-33645
p 158 N85-11457
NAG3-190 p 60 A85-19665
p 109 A85-25137
p 110 A85-38999
p 112 A85-46484
p 112 A85-48538
p 24 N85-15728
NAG3-194 p 106 A85-11640
NAG3-197 p 93 N85-28127
NAG3-199 p 104 N85-31378
NAG3-200 p 27 N85-22391
NAG3-201 p 116 N85-27164
NAG3-208 p 146 N85-21720
NAG3-210 p 140 A85-17039
NAG3-214 p 139 A85-12721
NAG3-216 p 68 A85-32431
p 71 N85-11223
p 73 N85-18127
p 73 N85-19073
NAG3-220 p 101 A85-20900
NAG3-223 p 140 A85-19433
p 145 N85-21685
NAG3-227 p 171 A85-21370
NAG3-22 p 67 A85-32400
NAG3-231 p 14 A85-21866
NAG3-232 p 169 A85-28612
p 170 A85-34131
NAG3-238 p 157 N85-11455
NAG3-242 p 14 A85-20867
p 12 A85-21844
p 11 A85-42937
NAG3-244 p 68 A85-32431
p 74 N85-20041
NAG3-245 p 27 N85-25262
NAG3-250 p 181 A85-24649
NAG3-255 p 76 N85-22661
NAG3-256 p 5 A85-40691
NAG3-258 p 59 A85-13092
NAG3-260 p 112 A85-45282
p 112 A85-45283
p 28 N85-25265
NAG3-268 p 75 N85-21320
NAG3-26 p 6 A85-41826
NAG3-271 p 76 N85-26962
NAG3-277 p 18 N85-10948
NAG3-280 p 72 N85-15877
NAG3-282 p 159 N85-16293
p 159 N85-18451
NAG3-283 p 103 N85-18259
NAG3-284 p 10 A85-20872
p 12 A85-40811
NAG3-285 p 121 A85-21695
p 121 A85-31113
p 121 A85-32294
NAG3-286 p 118 N85-31439
NAG3-28 p 3 A85-25135
NAG3-290 p 60 A85-19550
NAG3-292 p 111 A85-39898
NAG3-294 p 61 A85-33570
p 17 N85-10065
NAG3-305 p 42 A85-16441
NAG3-311 p 111 A85-39900
NAG3-315 p 176 N85-17667

NAG3-319 p 144 N85-10384
NAG3-324 p 84 N85-12162
NAG3-325 p 67 A85-32414
NAG3-328 p 138 N85-20390
p 138 N85-29307
NAG3-329 p 139 A85-11125
p 172 A85-50073
NAG3-330 p 7 N85-10919
NAG3-333 p 109 A85-26911
NAG3-33 p 139 A85-12029
p 139 A85-15893
p 142 A85-35046
p 142 A85-35048
p 143 A85-41109
p 26 N85-21165
p 145 N85-21687
p 146 N85-23096
NAG3-340 p 54 A85-11926
p 137 N85-16195
NAG3-341 p 82 A85-40973
p 62 A85-48493
p 62 A85-48513
p 77 N85-32173
p 77 N85-32174
p 77 N85-32175
p 77 N85-32176
NAG3-346 p 140 A85-19899
p 142 A85-33847
p 143 A85-40910
NAG3-347 p 16 A85-42365
p 16 A85-45715
NAG3-34 p 8 N85-21117
NAG3-353 p 30 N85-27869
NAG3-356 p 4 A85-32965
NAG3-357 p 173 A85-13955
p 173 A85-13956
NAG3-359 p 44 A85-33144
NAG3-364 p 3 A85-25928
NAG3-373 p 159 N85-17421
NAG3-377 p 58 N85-30037
NAG3-379 p 146 N85-21691
p 147 N85-25894
p 147 N85-27260
p 150 N85-31533
p 151 N85-31545
p 152 N85-32340
p 152 N85-32341
NAG3-38 p 139 A85-15894
NAG3-399 p 160 N85-20545
NAG3-3 p 112 A85-41787
NAG3-40 p 100 A85-12669
NAG3-416 p 3 A85-19731
NAG3-417 p 69 A85-44703
NAG3-418 p 97 N85-11265
NAG3-419 p 97 A85-32249
p 97 A85-39356
NAG3-41 p 143 A85-42566
p 144 N85-11380
NAG3-424 p 30 N85-27868
NAG3-425 p 102 A85-42156
NAG3-426 p 41 N85-29997
NAG3-42 p 102 A85-28230
NAG3-448 p 164 N85-33566
NAG3-449 p 166 A85-29538
p 179 N85-22472
p 39 N85-22474
NAG3-466 p 116 N85-27168
NAG3-475 p 101 A85-25170
p 99 N85-21438
p 100 N85-35320
NAG3-476 p 99 N85-25686
NAG3-477 p 59 A85-12890
p 168 A85-24526
p 63 N85-25444
NAG3-488 p 94 N85-34295
NAG3-491 p 150 N85-31536
p 151 N85-31541
NAG3-511 p 152 N85-31548
NAG3-512 p 183 N85-11862
NAG3-519 p 183 N85-23414
NAG3-51 p 121 A85-29562
p 151 N85-31546
NAG3-524 p 181 A85-21425
NAG3-52 p 6 A85-41826
NAG3-534 p 142 A85-38425
p 147 N85-25896
p 149 N85-27959
NAG3-535 p 149 N85-27957
NAG3-536 p 98 N85-17258
p 100 N85-34329
NAG3-541 p 136 N85-34404
NAG3-543 p 111 A85-40701
NAG3-546 p 114 N85-17324
NAG3-547 p 47 N85-13910
NAG3-549 p 110 A85-39604
p 26 N85-22390
NAG3-54 p 139 A85-13942
p 142 A85-37440
p 143 A85-41983
NAG3-557 p 36 N85-27922
NAG3-560 p 180 A85-18082
NAG3-57 p 65 A85-14959
p 67 A85-32412
NAG3-58 p 70 N85-11221
NAG3-593 p 29 N85-26712
NAG3-59 p 70 N85-10166
NAG3-5 p 169 A85-36727
NAG3-60 p 62 N85-11149
p 26 N85-21166
NAG3-62 p 108 A85-19672
NAG3-70 p 61 A85-47320
NAG3-74 p 108 A85-19574
p 26 N85-21167
p 29 N85-26716
p 29 N85-26717
p 29 N85-27867
NAG3-76 p 101 A85-16424
p 132 N85-21662
NAG3-7 p 127 A85-22281
p 14 A85-25442
NAG3-80 p 154 A85-24668
NAG3-95 p 82 A85-40383
NAG3-97 p 110 A85-39894
NAG3-9 p 107 A85-16533
p 114 N85-18291
NASA ORDER C-49029-D p 97 A85-34470
NASA ORDER C-54715-D p 124 N85-21607
NASA ORDER C-72801-D p 86 N85-15916
p 89 N85-22758
NASA ORDER C-74148-D p 86 N85-15916
NASA ORDER DSB-5710-2-79 p 161 N85-23243
NASW-3688 p 125 N85-33456
NAS1-16147 p 28 N85-26710
NAS1-17070 p 107 A85-16533
p 168 N85-21990
NAS1-17130 p 107 A85-16533
NAS3-18896 p 70 A85-47972
NAS3-19779 p 130 N85-13233
NAS3-20072 p 71 N85-11225
NAS3-20073 p 68 A85-32440
p 68 A85-39284
NAS3-20074 p 23 N85-10999
p 23 N85-12059
NAS3-20609 p 35 N85-22400
NAS3-20643 p 13 A85-13953
p 22 N85-10989
p 22 N85-10990
p 22 N85-10993
p 22 N85-10994
p 23 N85-10995
p 23 N85-10996
p 23 N85-10997
p 23 N85-10998
p 31 N85-29957
p 33 N85-34138
p 33 N85-34141
p 34 N85-35199
NAS3-20646 p 18 N85-10947
p 18 N85-10950
p 22 N85-10991
p 22 N85-10992
p 30 N85-29955
p 31 N85-29956
p 31 N85-29958
p 33 N85-35197
p 33 N85-35198
NAS3-21036 p 46 N85-11131
NAS3-21249 p 166 A85-21140
NAS3-21252 p 175 N85-11791
NAS3-21287 p 158 N85-16292
NAS3-21358 p 46 N85-11131
NAS3-21509 p 103 N85-19328
NAS3-21726 p 59 A85-11892
NAS3-21741 p 42 A85-16406
p 47 N85-12937
NAS3-21824 p 141 A85-27935
NAS3-21841 p 121 A85-29563
NAS3-21943 p 42 A85-16438
p 48 N85-15806
NAS3-21971 p 92 N85-11252
NAS3-21991 p 10 N85-35159
NAS3-22008 p 25 N85-18058
NAS3-22062 p 176 N85-19791
p 176 N85-19792
NAS3-22133 p 126 N85-35391
NAS3-22229 p 182 A85-35699
NAS3-22232 p 180 A85-11466
NAS3-22234 p 158 N85-13371
p 50 N85-25384
NAS3-22238 p 156 A85-45391
p 105 N85-31408
NAS3-22249 p 157 N85-10444
NAS3-22250 p 5 A85-40817
p 10 N85-35162
NAS3-22253 p 47 N85-15804
NAS3-22342 p 101 A85-20170
p 101 A85-20171
NAS3-22441 p 103 N85-19328
NAS3-22444 p 45 A85-42922
NAS3-22473 p 48 N85-17023
NAS3-22498 p 98 N85-15944
NAS3-22499 p 96 A85-14436
NAS3-22502 p 95 A85-14434
NAS3-22510 p 92 N85-10209
NAS3-22514 p 175 N85-13550
NAS3-22525 p 141 A85-30313
NAS3-22534 p 14 A85-18792
NAS3-22535 p 34 N85-12901
NAS3-22654 p 168 N85-27508
NAS3-2266C p 125 N85-35389
NAS3-2271 p 117 N85-30245
NAS3-22748 p 167 N85-35534
p 167 N85-35535
p 167 N85-35536
p 167 N85-35537
p 168 N85-35538
NAS3-22752 p 15 A85-32006
NAS3-22769 p 93 N85-27012
NAS3-22771 p 107 A85-14399
NAS3-22772 p 5 A85-41814
p 7 N85-12008
NAS3-22814 p 126 N85-12341
NAS3-22825 p 140 A85-18795
NAS3-22829 p 93 N85-19175
NAS3-22876 p 43 A85-29310
NAS3-22892 p 153 A85-10244
NAS3-22902 p 32 N85-29965
NAS3-23039 p 2 A85-19510
NAS3-23051 p 9 N85-22368
NAS3-23052 p 45 A85-45377
NAS3-23056 p 25 N85-21163
NAS3-23058 p 40 N85-22493
NAS3-23164 p 45 A85-43978
NAS3-23165 p 28 N85-26709
NAS3-23166 p 175 N85-13549
NAS3-23169 p 19 N85-10959
NAS3-23245 p 56 A85-47970
NAS3-23253 p 105 N85-33293
NAS3-23255 p 99 N85-27092
NAS3-23258 p 42 A85-16412
NAS3-23265 p 42 A85-16440
NAS3-23266 p 102 N85-12300
NAS3-23267 p 12 N85-19978
NAS3-23271 p 93 N85-19176
NAS3-23276 p 129 A85-39938
p 48 N85-18084
NAS3-23286 p 174 A85-25932
NAS3-23288 p 69 A85-43979
p 32 N85-31057
NAS3-23293 p 116 N85-27164
NAS3-23349 p 44 A85-39267
p 51 N85-26907
NAS3-23351 p 101 A85-14433
NAS3-23353 p 45 A85-43975
NAS3-23354 p 35 N85-12071
NAS3-23522 p 178 N85-13594
NAS3-23525 p 59 A85-12713
NAS3-23528 p 85 N85-15892
NAS3-23531 p 60 A85-19666
NAS3-23532 p 124 N85-25792
NAS3-23538 p 120 A85-10036
p 120 A85-16794
p 123 N85-21604
NAS3-23540 p 16 A85-40841
NAS3-23542 p 168 A85-24526
NAS3-235924 p 108 A85-19491
NAS3-23681 p 9 N85-26668
NAS3-23684 p 120 A85-10035
NAS3-23686 p 108 A85-19491
p 172 N85-27584
NAS3-23687 p 147 N85-27261
p 32 N85-32119
p 33 N85-34140
NAS3-2368 p 108 A85-19488
p 108 A85-19751
NAS3-23696 p 3 A85-20744
NAS3-23697 p 145 N85-21686
NAS3-23698 p 152 N85-31548
NAS3-23702 p 12 N85-35185
NAS3-23705 p 15 A85-32005
NAS3-23708 p 172 A85-10882
p 109 A85-25951
NAS3-23712 p 123 A85-46607
NAS3-23716 p 6 A85-42988
NAS3-23772 p 44 A85-39735
NAS3-23773 p 44 A85-39733
NAS3-23780 p 98 N85-18238
p 98 N85-18239

	p 99	N85-18240
NAS3-23858	p 36	A85-39730
NAS3-23865	p 177	N85-35728
NAS3-23866	p 46	N85-11132
NAS3-23868	p 44	A85-39628
NAS3-23869	p 43	A85-18584
NAS3-23881	p 43	A85-19715
NAS3-23925	p 150	N85-31531
NAS3-23926	p 28	N85-26711
NAS3-23927	p 152	N85-31548
NAS3-23928	p 133	N85-28372
NAS3-23940	p 152	N85-33541
NAS3-24078	p 171	A85-47794
NAS3-24081	p 94	N85-31308
NAS3-24082	p 6	A85-42954
NAS3-24089	p 31	N85-29960
NAS3-24094	p 120	A85-10034
NAS3-24100	p 10	N85-35158
NAS3-24105	p 6	A85-43977
	p 32	N85-31058
	p 105	N85-32251
NAS3-24229	p 60	A85-19548
NAS3-24238	p 48	N85-19020
NAS3-24356	p 41	N85-27971
NAS3-24382	p 148	N85-27953
	p 148	N85-27954
NAS3-24389	p 148	N85-27955
	p 149	N85-27956
NAS3-285	p 119	N85-31445
NAS5-23481	p 39	A85-35379
NAS8-32807	p 166	A85-29538
NAS8-33727	p 180	A85-18082
NAS8-33982	p 39	A85-35379
NCC3-15	p 61	A85-23192
NCC3-16	p 153	A85-11345
NCC3-17	p 157	N85-10445
	p 157	N85-10447
	p 157	N85-11456
NCC3-21	p 65	A85-11935
NCC3-29	p 100	N85-35321
NCC3-30	p 85	N85-15895
	p 135	N85-32330
NCC3-35	p 62	N85-21283
NCC3-38	p 98	N85-15943
	p 106	N85-35342
NCC3-3	p 112	A85-41782
NCC3-43	p 71	N85-11224
NCC3-5	p 162	N85-29364
	p 9	N85-29916
NCC3-6	p 162	N85-29363
NSERC-A-9265	p 171	A85-21370
NSF CME-79-13389	p 110	A85-39894
NSF CPE-81-15163	p 171	A85-21370
NSF CPF-81-15163	p 93	N85-19185
NSF DMR-79-23647	p 70	N85-11217
NSF DMR-82-06195	p 65	A85-14959
NSF DMR-82-12115	p 180	A85-18082
NSF ECS-79-10269	p 101	A85-20170
	p 101	A85-20171
NSF ECS-81-20305	p 97	A85-39356
NSF ENG-78-17782	p 110	A85-39894
NSF MCS-83-01844	p 171	A85-28006
NSF MEA-80-06806	p 111	A85-39898
NSF MEA-80-1136	p 173	A85-12301
NSG-3011	p 178	A85-12705
	p 41	A85-15512
NSG-3012	p 111	A85-40752
NSG-3019	p 61	A85-42571
NSG-3040	p 110	A85-39894
NSG-3041	p 182	A85-41635
NSG-3048	p 29	N85-26713
	p 29	N85-26714
	p 29	N85-26715
NSG-3147	p 67	A85-32399
NSG-3150	p 39	A85-35379
NSG-3169	p 123	A85-46925
NSG-3180	p 64	A85-11070
NSG-3184	p 66	A85-27808
NSG-3185	p 55	A85-29133
NSG-3188	p 128	A85-33779
	p 128	A85-33780
NSG-3197	p 40	N85-22512
NSG-3198	p 109	A85-26077
	p 177	N85-27637
NSG-3206	p 27	N85-22392
NSG-3208	p 8	N85-21117
NSG-3212	p 111	A85-40752
NSG-3236	p 174	A85-26915
NSG-3246	p 67	A85-32388
	p 70	N85-10165
NSG-3253	p 127	A85-23838
NSG-3263	p 65	A85-12098
NSG-3264	p 114	N85-18292
NSG-3266	p 106	A85-11631
	p 107	A85-14349
	p 108	A85-19564
	p 4	A85-29259
	p 111	A85-40752
NSG-3281	p 102	A85-39453
NSG-3283	p 171	A85-21979
NSG-3290	p 179	A85-17262
	p 102	A85-35306
NSG-3294	p 107	A85-11648
NSG-3295	p 24	N85-15724
NSG-3299	p 178	A85-16443
	p 179	A85-16444
	p 179	A85-16455
	p 179	A85-43552
NSG-3301	p 39	N85-21250
	p 88	N85-22511
NSG-3302	p 178	A85-23134
NSG-3305	p 106	A85-11647
NSG-330	p 66	A85-32387
NSG-3328	p 138	N85-21673
NSG3-48	p 136	N85-34405
N00014-75-C-0867	p 177	N85-27637
N00014-81-K-0090	p 127	A85-23838
N00014-84-K-0574	p 177	N85-27637
N00163-81-C-0071	p 121	A85-29563
USIBSF-2813/82	p 68	A85-40275
W-7405-ENG-26	p 86	N85-15916
	p 147	N85-27260
	p 151	N85-31545
W-7405-ENG-36	p 125	N85-33454
141-20-17	p 162	N85-27387
146-20-1A	p 38	N85-34150
384-55-62	p 52	N85-34176
481-01-02	p 49	N85-21259
481-59-12	p 47	N85-11133
482-50-22	p 50	N85-25386
485-49-02	p 58	N85-30034
501-31-3B	p 175	N85-13549
505-23-72	p 133	N85-28373
505-31-0A	p 7	N85-12036
505-31-0A	p 7	N85-12008
505-31-04	p 113	N85-10306
	p 7	N85-14798
	p 24	N85-14840
	p 115	N85-20269
	p 26	N85-21164
	p 27	N85-25263
	p 28	N85-25265
	p 63	N85-25444
	p 115	N85-25760
	p 116	N85-25761
	p 124	N85-25794
	p 30	N85-27870
	p 63	N85-28983
	p 63	N85-31244
	p 119	N85-31445
	p 64	N85-32156
505-31-3A	p 8	N85-15689
505-31-3B	p 175	N85-13550
	p 175	N85-13551
505-31-32	p 175	N85-10788
505-31-42	p 17	N85-10065
	p 17	N85-10068
	p 18	N85-10069
	p 92	N85-10209
	p 113	N85-10303
	p 18	N85-10948
	p 18	N85-10949
	p 92	N85-12183
	p 92	N85-13066
	p 24	N85-15728
	p 184	N85-16663
	p 184	N85-22204
	p 93	N85-27012
	p 30	N85-27869
	p 119	N85-33435
505-31-52	p 124	N85-25792
505-32-32	p 24	N85-15726
505-32-42	p 131	N85-14116
505-32-52	p 113	N85-14078
	p 116	N85-27165
505-32-6A	p 1	N85-15658
505-32-72	p 172	N85-19733
505-33-1A	p 70	N85-10165
	p 71	N85-12129
	p 84	N85-12162
	p 74	N85-20042
	p 75	N85-21322
	p 76	N85-22660
505-33-1B	p 86	N85-15897
	p 76	N85-26962
	p 90	N85-26993
505-33-12	p 134	N85-32329
505-33-22	p 144	N85-11380
505-33-32	p 23	N85-13798
	p 85	N85-14929
505-33-42	p 146	N85-25893
505-33-5B	p 57	N85-15822
	p 57	N85-21273
505-33-52	p 84	N85-13045
	p 57	N85-14882
505-33-53	p 176	N85-22109
505-33-62	p 71	N85-11223
	p 73	N85-18127
	p 86	N85-18153
	p 73	N85-19072
	p 73	N85-19073
	p 74	N85-19076
	p 74	N85-20041
	p 75	N85-20043
	p 75	N85-21323
	p 88	N85-21357
	p 131	N85-21657
	p 62	N85-22644
	p 76	N85-26963
	p 117	N85-30242
	p 134	N85-30342
	p 77	N85-31283
	p 77	N85-31284
	p 58	N85-32148
	p 135	N85-32331
	p 78	N85-34266
	p 137	N85-34408
505-33-7A	p 57	N85-15823
	p 145	N85-18375
	p 58	N85-27978
	p 133	N85-28371
505-33-7B	p 144	N85-15184
	p 132	N85-25847
	p 133	N85-29292
	p 152	N85-34427
505-33-7C	p 144	N85-16205
	p 72	N85-18124
	p 73	N85-18125
	p 74	N85-19074
	p 131	N85-21658
	p 145	N85-21685
	p 134	N85-31511
	p 137	N85-34409
505-33-72	p 132	N85-27226
505-33-78	p 135	N85-32333
505-36-12	p 70	N85-11221
505-36-22	p 58	N85-30035
505-40-1B	p 123	N85-16100
505-40-14	p 30	N85-28945
	p 125	N85-32302
505-40-22	p 24	N85-15727
	p 94	N85-31308
	p 94	N85-34295
505-40-42	p 130	N85-13233
	p 130	N85-13234
	p 176	N85-17667
505-40-5A	p 17	N85-10067
	p 7	N85-12039
	p 25	N85-18057
	p 114	N85-19363
	p 114	N85-19364
505-40-5B	p 169	N85-10659
	p 178	N85-13594
505-40-68	p 25	N85-21163
	p 178	N85-28786
505-40-74	p 8	N85-15688
	p 24	N85-15725
	p 35	N85-15758
	p 171	N85-17596
	p 35	N85-18067
	p 177	N85-30770
505-40-84	p 1	N85-23685
505-40-90	p 8	N85-21114
	p 63	N85-23941
505-41-32	p 113	N85-11317
	p 113	N85-12314
505-42-92	p 136	N85-34406
505-42-94	p 123	N85-16099
	p 133	N85-27227
	p 133	N85-28372
	p 136	N85-34405
	p 136	N85-34407
505-43-3	p 170	N85-17576
505-43-4	p 170	N85-10683
505-43-52	p 26	N85-21168
	p 27	N85-25261
	p 28	N85-26710
	p 32	N85-31058
505-45-12	p 11	N85-27839
505-45-45	p 11	N85-15702
505-45-54	p 12	N85-18049
505-45-58	p 8	N85-19923
	p 176	N85-22108
	p 9	N85-29925
505-45-72	p 30	N85-28944
505-53-1A	p 137	N85-16195
505-53-1B	p 94	N85-11261
505-55-52	p 157	N85-10444

505-90-22 p 10 N85-35158
506-36-22 p 117 N85-30246
506-53-1A p 137 N85-10371
p 137 N85-20389
p 138 N85-21673
p 138 N85-29307
p 138 N85-32337
506-53-1B p 83 N85-10186
p 72 N85-12132
p 72 N85-13006
p 84 N85-13044
p 131 N85-15168
p 85 N85-15893
p 74 N85-19075
p 53 N85-21264
p 87 N85-21355
p 88 N85-21359
p 132 N85-23085
p 183 N85-24961
p 90 N85-26991
p 78 N85-34265
506-53-18 p 95 N85-29085
506-55-22 p 48 N85-21258
p 49 N85-21263
p 132 N85-21662
p 51 N85-27972
p 52 N85-34177
p 52 N85-34178
p 52 N85-34179
506-55-24 p 49 N85-21260
506-55-42 p 49 N85-21261
506-55-52 p 50 N85-25384
p 162 N85-28444
p 163 N85-30480
506-55-62 p 51 N85-26912
506-55-72 p 53 N85-10105
p 84 N85-10187
p 47 N85-13910
p 39 N85-14858
p 103 N85-20246
p 89 N85-25521
p 53 N85-26921
p 90 N85-26992
p 91 N85-28110
p 104 N85-28222
p 91 N85-30137
p 91 N85-30138
p 178 N85-34631
506-55-8A p 115 N85-24245
506-55-82A p 47 N85-15804
506-58-22 p 97 N85-10234
p 183 N85-10844
p 38 N85-15779
p 99 N85-20224
p 183 N85-26406
p 105 N85-33293
506-60-12 p 145 N85-20396
p 37 N85-21231
p 88 N85-22755
p 89 N85-22756
p 50 N85-23926
p 146 N85-24339
506-60-22 p 52 N85-28971
506-60-42 p 36 N85-21228
p 115 N85-21574
p 50 N85-25385
p 52 N85-35225
506-62-42 p 38 N85-29987
533-04-1A p 18 N85-10951
p 123 N85-16096
p 124 N85-21605
p 145 N85-21686
p 26 N85-22390
p 146 N85-24338
p 28 N85-25266
p 29 N85-26716
p 29 N85-26717
p 29 N85-27867
p 125 N85-30288
p 32 N85-32119
p 33 N85-34140
533-04-1B p 71 N85-12131
533-04-1C p 84 N85-10191
p 70 N85-11217
p 88 N85-21358
533-04-1E p 70 N85-10168
p 71 N85-11224
533-04-12 p 73 N85-18126
p 75 N85-21321
p 146 N85-21691
p 27 N85-25262
p 147 N85-25894
p 148 N85-27264
p 152 N85-32340
p 152 N85-32341
533-05-12 p 56 N85-12095
p 86 N85-19136
p 87 N85-20127
p 88 N85-21356
p 138 N85-21674
p 89 N85-24000
p 53 N85-30011
p 91 N85-30135
p 59 N85-34223
p 92 N85-34284
533-14-12 p 147 N85-27260
535-03-12 p 9 N85-22368
p 32 N85-29964
535-05-12 p 27 N85-22392
p 9 N85-26670
535-06-12 p 8 N85-21115
p 27 N85-25264
542-05-12 p 46 N85-11131
p 164 N85-34443
553-13-00 p 51 N85-27941
650-60-23 p 100 N85-31348
650-60-26 p 97 N85-15099
776-31-41 p 161 N85-23242
p 162 N85-29365
776-33-41 p 158 N85-11458
p 159 N85-16299
p 161 N85-27385
p 150 N85-30361
p 162 N85-30476
p 163 N85-30478
p 165 N85-34444
776-54-01 p 161 N85-23243
p 165 N85-35472
776-72-41 p 158 N85-12465
778-17-01 p 159 N85-17422
778-34-12 p 130 N85-13235
p 84 N85-14928
p 186 N85-32043
778-35-03 p 72 N85-13007
p 53 N85-14864
p 185 N85-19895

Typical Report Number Index Listing



Listings in this index are arranged alphanumerically by report number. The NASA accession number denotes the number by which the citation is identified. An asterisk (*) indicates that the item is a NASA report. A pound sign (#) indicates that the item is available on microfiche.

AAE-85-2 p 62 N85-21283 * #

ACS PAPER 130-13-84 p 80 A85-25271 * #
ACS PAPER 19-B-84P p 83 A85-45302 * #
ACS PAPER 7-J3-84 p 82 A85-42797 * #

AD-A146051 p 12 N85-12887 * #
AD-A152863 p 141 A85-24532 * #
AD-A153032 p 107 A85-14241 * #
AD-A153479 p 134 N85-29295 * #
AD-A153977 p 26 N85-21164 * #
AD-A155736 p 125 N85-33457 #
AD-A157111 p 89 N85-24000 * #
AD-A157112 p 76 N85-26964 * #
AD-A157113 p 7 N85-14798 * #

AD-E401352 p 125 N85-33457 #

AEDC-TR-84-10 p 12 N85-12887 * #

AFGL-TR-85-0018 p 39 N85-22470 * #

AIAA PAPER 83-2658 p 78 A85-10675 * #
AIAA PAPER 84-0020 p 13 A85-16098 * #
AIAA PAPER 84-0105 p 10 A85-10653 * #
AIAA PAPER 84-0849 p 54 A85-16096 * #
AIAA PAPER 84-0974 p 54 A85-16094 * #
AIAA PAPER 84-0991 p 139 A85-16095 * #
AIAA PAPER 84-1452 p 13 A85-16097 * #
AIAA PAPER 84-2278 p 173 A85-16099 * #
AIAA PAPER 84-2281 p 13 A85-13953 * #
AIAA PAPER 84-2284 p 13 A85-13954 * #
AIAA PAPER 84-2285 p 173 A85-16102 * #
AIAA PAPER 84-2297 p 3 A85-28899 * #
AIAA PAPER 84-2322 p 172 A85-10869 * #
AIAA PAPER 84-2323 p 173 A85-16103 * #
AIAA PAPER 84-2324 p 173 A85-13955 * #
AIAA PAPER 84-2325 p 2 A85-10870 * #
AIAA PAPER 84-2326 p 173 A85-13956 * #
AIAA PAPER 84-2341 p 172 A85-10882 * #
AIAA PAPER 84-2364 p 174 A85-16104 * #
AIAA PAPER 85-0057 p 108 A85-19488 * #
AIAA PAPER 85-0058 p 2 A85-19489 * #
AIAA PAPER 85-0059 p 2 A85-19490 * #
AIAA PAPER 85-0060 p 108 A85-19491 * #
AIAA PAPER 85-0083 p 14 A85-19509 * #
AIAA PAPER 85-0086 p 2 A85-19510 * #
AIAA PAPER 85-0090 p 35 A85-26381 * #
AIAA PAPER 85-0143 p 60 A85-19548 * #
AIAA PAPER 85-0145 p 60 A85-19550 * #
AIAA PAPER 85-0170 p 108 A85-19564 * #
AIAA PAPER 85-0184 p 108 A85-19574 * #
AIAA PAPER 85-0237 p 60 A85-19607 * #
AIAA PAPER 85-0314 p 34 A85-19661 * #
AIAA PAPER 85-0319 p 60 A85-19665 * #
AIAA PAPER 85-0321 p 60 A85-19666 * #
AIAA PAPER 85-0330 p 108 A85-19672 * #
AIAA PAPER 85-0338 p 11 A85-28898 * #
AIAA PAPER 85-0339 p 14 A85-20867 * #
AIAA PAPER 85-0379 p 34 A85-19709 * #
AIAA PAPER 85-0380 p 3 A85-26389 * #
AIAA PAPER 85-0384 p 43 A85-19713 * #
AIAA PAPER 85-0386 p 43 A85-19715 * #
AIAA PAPER 85-0410 p 3 A85-19731 * #
AIAA PAPER 85-0441 p 108 A85-19751 * #
AIAA PAPER 85-0466 p 10 A85-20872 * #
AIAA PAPER 85-0468 p 11 A85-30192 * #
AIAA PAPER 85-0524 p 3 A85-25928 * #
AIAA PAPER 85-0533 p 174 A85-25932 * #
AIAA PAPER 85-0569 p 109 A85-25951 * #
AIAA PAPER 85-0621 p 142 A85-38425 * #
AIAA PAPER 85-0645 p 141 A85-30313 * #
AIAA PAPER 85-0761 p 14 A85-30378 * #
AIAA PAPER 85-0804 p 38 A85-30303 * #
AIAA PAPER 85-1102 p 110 A85-39604 * #
AIAA PAPER 85-1104 p 15 A85-39606 * #
AIAA PAPER 85-1118 p 12 A85-40811 * #
AIAA PAPER 85-1133 p 6 A85-43974 * #
AIAA PAPER 85-1140 p 143 A85-40814 * #
AIAA PAPER 85-1154 p 44 A85-39626 * #
AIAA PAPER 85-1155 p 45 A85-43975 * #
AIAA PAPER 85-1156 p 45 A85-43976 * #
AIAA PAPER 85-1159 p 44 A85-39628 * #
AIAA PAPER 85-1187 p 17 A85-47021 * #
AIAA PAPER 85-1196 p 5 A85-40817 * #
AIAA PAPER 85-1198 p 56 A85-47022 * #
AIAA PAPER 85-1210 p 5 A85-40819 * #
AIAA PAPER 85-1213 p 6 A85-47023 * #
AIAA PAPER 85-1219 p 82 A85-39662 * #
AIAA PAPER 85-1229 p 94 A85-47024 * #
AIAA PAPER 85-1259 p 6 A85-47025 * #
AIAA PAPER 85-1263 p 6 A85-43977 * #
AIAA PAPER 85-1290 p 15 A85-39703 * #
AIAA PAPER 85-1302 p 45 A85-43978 * #
AIAA PAPER 85-1312 p 16 A85-39717 * #
AIAA PAPER 85-1332 p 5 A85-39728 * #
AIAA PAPER 85-1336 p 36 A85-39730 * #
AIAA PAPER 85-1339 p 44 A85-39733 * #
AIAA PAPER 85-1341 p 44 A85-39735 * #
AIAA PAPER 85-1398 p 16 A85-42671 * #
AIAA PAPER 85-1408 p 5 A85-39767 * #
AIAA PAPER 85-1418 p 142 A85-39769 * #
AIAA PAPER 85-1419 p 142 A85-39770 * #
AIAA PAPER 85-1420 p 69 A85-43979 * #
AIAA PAPER 85-1433 p 16 A85-40841 * #
AIAA PAPER 85-1441 p 110 A85-39780 * #
AIAA PAPER 85-1471 p 122 A85-39796 * #
AIAA PAPER 85-1566 p 5 A85-40691 * #
AIAA PAPER 85-1580 p 111 A85-40701 * #
AIAA PAPER 85-1650 p 111 A85-40750 * #
AIAA PAPER 85-1652 p 111 A85-40752 * #

AIAA-85-0090 p 35 N85-15758 * #
AIAA-85-0237 p 24 N85-15726 * #
AIAA-85-0314 p 35 N85-18067 * #
AIAA-85-0338 p 11 N85-15702 * #
AIAA-85-0379 p 35 N85-15757 * #
AIAA-85-0380 p 8 N85-15688 * #
AIAA-85-0468 p 12 N85-18049 * #
AIAA-85-1187 p 32 N85-29964 * #
AIAA-85-1213 p 118 N85-30247 * #
AIAA-85-1229 p 38 N85-29987 * #
AIAA-85-1259 p 9 N85-29925 * #
AIAA-85-1398 p 30 N85-27870 * #

AR-1 p 168 N85-27508 * #
AR-1 p 32 N85-31057 * #
AR-2 p 28 N85-26711 * #

ARL-TR-85-15 p 177 N85-27637 * #

ARPAD-TR-85001 p 125 N85-33457 #

ASLE PREPRINT 84-LC-2A-2 p 80 A85-25963 * #
ASLE PREPRINT 84-LC-4A-4 p 168 A85-38444 * #

ASME PAPER 84-AES-7 p 154 A85-21297 * #
ASME PAPER 84-DET-184 p 128 A85-33779 * #
ASME PAPER 84-DET-226 p 128 A85-33780 * #
ASME PAPER 84-DET-229 p 129 A85-33781 * #
ASME PAPER 84-DET-96 p 129 A85-35049 * #
ASME PAPER 84-GT-138 p 141 A85-32962 * #
ASME PAPER 84-GT-187 p 4 A85-32961 * #
ASME PAPER 84-GT-191 p 141 A85-23150 * #
ASME PAPER 84-GT-199 p 4 A85-32963 * #
ASME PAPER 84-GT-75 p 4 A85-32964 * #
ASME PAPER 84-JPGC-GT-2 p 61 A85-23192 * #
ASME PAPER 84-PVP-112 p 140 A85-18795 * #
ASME PAPER 84-PVP-77 p 14 A85-18792 * #
ASME PAPER 84-TRIB-13 p 127 A85-21280 * #
ASME PAPER 84-TRIB-26 p 127 A85-21289 * #
ASME PAPER 84-TRIB-7 p 128 A85-32960 * #
ASME PAPER 84-WA/APM-38 p 140 A85-17039 * #
ASME PAPER 84-WA/APM-41 p 140 A85-17040 * #
ASME PAPER 84-WA/HT-51 p 110 A85-39894 * #
ASME PAPER 84-WA/HT-70 p 111 A85-39898 * #
ASME PAPER 84-WA/HT-72 p 111 A85-39900 * #
ASME PAPER 84-WA/NCA-11 p 174 A85-39909 * #

ASR-1 p 145 N85-21686 * #
ASR-1 p 147 N85-27261 * #
ASR-1 p 33 N85-34140 * #
ASR-2 p 32 N85-32119 * #

AT85T004 p 12 N85-35185 * #

AVSCOM-TR-84-C-14 p 28 N85-26709 * #
AVSCOM-TR-84-C-17 p 84 N85-13045 * #

BBN-4770 p 175 N85-11791 * #

CCMS-84-13 p 58 N85-30035 * #

CONF-831142-3 p 86 N85-15916 * #
CONF-8410138-1 p 93 N85-19185 * #

CR-R-84041 p 28 N85-25265 * #

CREARE-TN-371 p 48 N85-18084 * #

CTR-0747-84003 p 130 N85-13235 * #

D-1998 p 171 N85-17596 * #

DE84-016884 p 93 N85-19185 * #
DE85-000865 p 160 N85-20545 * #
DE85-001552 p 86 N85-15916 * #
DE85-011649 p 78 N85-34267 #
DE85-011659 p 125 N85-33454 #

DOE/CS-54209/20 p 185 N85-19894 * #

DOE/NASA/0005-1 p 162 N85-29364 * #
DOE/NASA/0005-1 p 9 N85-29916 * #
DOE/NASA/0006-1 p 162 N85-29363 * #
DOE/NASA/0017-1 p 157 N85-11456 * #
DOE/NASA/0017-3 p 157 N85-10445 * #
DOE/NASA/0017-4 p 157 N85-10447 * #
DOE/NASA/0017-6 p 91 N85-28109 * #
DOE/NASA/0030-1 p 85 N85-15895 * #
DOE/NASA/0167-8 p 185 N85-18831 * #
DOE/NASA/0168-8 p 31 N85-29961 #
DOE/NASA/0191-1 p 159 N85-17422 * #
DOE/NASA/0215-1 p 159 N85-16300 * #
DOE/NASA/0238-1 p 157 N85-11455 * #
DOE/NASA/0241-11 p 164 N85-30483 * #
DOE/NASA/0241-14 p 161 N85-25941 * #
DOE/NASA/0261-1 p 130 N85-13235 * #
DOE/NASA/0262-1 p 165 N85-35471 * #
DOE/NASA/0290-1 p 158 N85-16291 * #
DOE/NASA/0326-1 p 86 N85-18154 * #
DOE/NASA/0330-1 p 7 N85-10919 * #
DOE/NASA/0333-1 p 163 N85-30481 * #
DOE/NASA/0339-1 p 185 N85-16698 * #
DOE/NASA/0342-1 p 185 N85-16699 * #
DOE/NASA/0346-1 p 90 N85-26994 * #
DOE/NASA/0352-1 p 89 N85-22757 * #
DOE/NASA/0373-1 p 159 N85-17421 * #
DOE/NASA/1005-5 p 185 N85-27769 * #
DOE/NASA/12726-25 p 162 N85-27387 * #
DOE/NASA/12726-26 p 164 N85-34443 * #

DOE/NASA/20320-49 p 150 N85-30361 * #
DOE/NASA/20320-50 p 162 N85-30476 * #
DOE/NASA/20320-51 p 163 N85-30477 * #
DOE/NASA/20320-52 p 163 N85-30478 * #
DOE/NASA/20320-55 p 163 N85-30479 * #
DOE/NASA/20320-60 p 158 N85-11458 * #
DOE/NASA/20320-61 p 159 N85-16299 * #
DOE/NASA/20320-62 p 161 N85-23242 * #
DOE/NASA/20320-63 p 162 N85-29365 * #
DOE/NASA/20320-64 p 161 N85-27385 * #
DOE/NASA/20320-65 p 165 N85-34444 * #
DOE/NASA/20485-17 p 103 N85-13157 * #
DOE/NASA/2801-1 p 89 N85-22758 * #
DOE/NASA/4105-1 p 105 N85-32251 * #
DOE/NASA/50194-40 p 84 N85-14928 * #
DOE/NASA/50194-41 p 184 N85-13692 * #
DOE/NASA/50194-43 p 186 N85-32043 * #
DOE/NASA/51040-57 p 72 N85-13007 * #
DOE/NASA/51040-58 p 185 N85-19895 * #
DOE/NASA/51040-59 p 53 N85-14864 * #

DOE/NBM-1077 p 160 N85-20545 * #

DOUGLAS-PAPER-7551 p 28 N85-26710 * #

DS-3-VOL-2 p 176 N85-19792 * #

D180-28461-1 p 177 N85-35728 * #
D6-52996 p 94 N85-31308 * #

E-1458 p 18 N85-10951 * #
E-1529 p 150 N85-30361 * #
E-1611 p 57 N85-14882 * #
E-1786 p 162 N85-30476 * #
E-1798 p 163 N85-30478 * #
E-1865 p 163 N85-30479 * #
E-1935 p 11 N85-27839 * #
E-1971 p 116 N85-27164 * #
E-1979 p 113 N85-14078 * #
E-1980 p 116 N85-27165 * #
E-1988 p 25 N85-21162 * #
E-1999 p 170 N85-28610 * #
E-2042 p 130 N85-13234 * #
E-2049-1 p 74 N85-19075 * #
E-2055 p 24 N85-14840 * #
E-2088 p 85 N85-15896 * #
E-2125 p 158 N85-12465 * #
E-2127 p 130 N85-13233 * #
E-2129 p 10 N85-35158 * #
E-2147 p 113 N85-12314 * #
E-2149 p 17 N85-10065 * #
E-2151 p 184 N85-22255 * #
E-2156 p 70 N85-10165 * #
E-2171 p 37 N85-16989 * #
E-2172 p 170 N85-17576 * #
E-2176 p 17 N85-10068 * #
E-2183 p 123 N85-16099 * #
E-2184 p 72 N85-13006 * #
E-2186 p 39 N85-22470 * #
E-2194 p 18 N85-10069 * #
E-2196 p 186 N85-32043 * #
E-2197 p 1 N85-15658 * #
E-2201 p 57 N85-15822 * #
E-2214 p 131 N85-14116 * #
E-2219 p 84 N85-13044 * #
E-2231 p 62 N85-10138 * #
E-2238 p 94 N85-11261 * #
E-2239 p 39 N85-14858 * #
E-2242 p 57 N85-21273 * #
E-2254 p 131 N85-15168 * #
E-2256 p 135 N85-32331 * #
E-2258 p 7 N85-12039 * #
E-2262 p 17 N85-10067 * #
E-2271 p 84 N85-13045 * #
E-2275 p 7 N85-12008 * #
E-2279 p 170 N85-10683 * #
E-2280 p 71 N85-12131 * #
E-2282 p 175 N85-13550 * #
E-2283 p 175 N85-13549 * #
E-2286 p 103 N85-13157 * #
E-2287 p 70 N85-10168 * #
E-2289 p 74 N85-20042 * #
E-2291 p 7 N85-12036 * #
E-2294 p 176 N85-17667 * #
E-2295 p 175 N85-10788 * #
E-2296 p 137 N85-16195 * #
E-2301 p 97 N85-10234 * #
E-2302 p 123 N85-16100 * #
E-2303 p 184 N85-22204 * #
E-2305 p 47 N85-13880 * #
E-2306 p 113 N85-10303 * #
E-2308 p 92 N85-12183 * #
E-2310 p 146 N85-25893 * #
E-2311 p 83 N85-10186 * #
E-2313 p 86 N85-15897 * #
E-2314 p 71 N85-11224 * #
E-2315 p 169 N85-10659 * #
E-2316-1 p 178 N85-28786 * #
E-2317 p 84 N85-14928 * #
E-2319 p 57 N85-15823 * #
E-2320 p 75 N85-21323 * #
E-2321 p 53 N85-10105 * #
E-2322 p 84 N85-10187 * #
E-2324 p 1 N85-17935 * #
E-2325-1 p 92 N85-34284 * #
E-2327 p 18 N85-10949 * #
E-2328 p 84 N85-10191 * #
E-2329 p 71 N85-12129 * #
E-2330 p 158 N85-11458 * #
E-2331 p 70 N85-11217 * #
E-2332 p 183 N85-10844 * #
E-2333 p 175 N85-13551 * #
E-2334 p 92 N85-13066 * #
E-2335 p 75 N85-20043 * #
E-2336 p 185 N85-19895 * #
E-2337 p 137 N85-10371 * #
E-2339 p 56 N85-12095 * #
E-2341 p 113 N85-10306 * #
E-2343 p 25 N85-18057 * #
E-2344 p 167 N85-21872 * #
E-2346 p 113 N85-11317 * #
E-2347 p 119 N85-33435 * #
E-2348 p 184 N85-16663 * #
E-2348 p 72 N85-18124 * #
E-2351 p 47 N85-11133 * #
E-2352 p 72 N85-13007 * #
E-2354 p 72 N85-12132 * #
E-2357 p 114 N85-15133 * #
E-2358 p 144 N85-15184 * #
E-2359 p 49 N85-21263 * #
E-2361 p 88 N85-21359 * #
E-2362 p 131 N85-21658 * #
E-2365 p 123 N85-16096 * #
E-2366 p 23 N85-13798 * #
E-2367 p 97 N85-15099 * #
E-2368 p 150 N85-31530 * #
E-2369 p 24 N85-15725 * #
E-2371 p 73 N85-18126 * #
E-2372 p 56 N85-14878 * #
E-2373 p 145 N85-20396 * #
E-2376 p 93 N85-31307 * #
E-2380 p 85 N85-14929 * #
E-2386 p 85 N85-15893 * #
E-2387 p 7 N85-14798 * #
E-2388 p 10 N85-35159 * #
E-2389 p 53 N85-14864 * #
E-2393 p 145 N85-18375 * #
E-2394 p 72 N85-15878 * #
E-2395 p 12 N85-18049 * #
E-2396 p 38 N85-15779 * #
E-2397 p 76 N85-26963 * #
E-2398 p 144 N85-16205 * #
E-2399 p 88 N85-21356 * #
E-2400 p 183 N85-24961 * #
E-2404 p 24 N85-15727 * #
E-2405 p 8 N85-15688 * #
E-2406 p 145 N85-21690 * #
E-2408 p 8 N85-15689 * #
E-2410 p 159 N85-16299 * #
E-2412 p 27 N85-25261 * #
E-2413 p 35 N85-15757 * #
E-2414 p 35 N85-15758 * #
E-2415 p 35 N85-18067 * #
E-2416 p 85 N85-15895 * #
E-2418 p 24 N85-15726 * #
E-2419 p 88 N85-21358 * #
E-2420 p 86 N85-19136 * #
E-2421 p 11 N85-15702 * #
E-2422 p 86 N85-18153 * #
E-2423 p 91 N85-30138 * #
E-2428 p 87 N85-20127 * #
E-2430 p 115 N85-21569 * #
E-2432 p 119 N85-31443 * #
E-2433 p 62 N85-22644 * #
E-2434 p 30 N85-28944 * #
E-2435 p 26 N85-21168 * #
E-2437 p 77 N85-31283 * #
E-2439 p 73 N85-18125 * #
E-2440 p 49 N85-21259 * #
E-2441 p 53 N85-26921 * #
E-2444 p 74 N85-19074 * #
E-2448 p 176 N85-22108 * #
E-2449 p 8 N85-19923 * #
E-2450 p 115 N85-20269 * #
E-2451 p 74 N85-19076 * #
E-2452 p 73 N85-19072 * #
E-2454 p 91 N85-30137 * #
E-2456 p 118 N85-31433 * #
E-2457 p 114 N85-19363 * #
E-2458 p 114 N85-19364 * #
E-2459 p 87 N85-21355 * #
E-2462 p 88 N85-21357 * #
E-2463 p 115 N85-21570 * #
E-2464 p 138 N85-21674 * #
E-2465 p 36 N85-21228 * #
E-2466 p 48 N85-21258 * #
E-2469 p 99 N85-20223 * #
E-2470 p 137 N85-20389 * #
E-2471 p 161 N85-23242 * #
E-2473 p 8 N85-21114 * #
E-2475 p 8 N85-21115 * #
E-2476 p 134 N85-31511 * #
E-2478 p 131 N85-21657 * #
E-2479 p 49 N85-21260 * #
E-2480 p 103 N85-20246 * #
E-2482 p 133 N85-28373 * #
E-2483 p 90 N85-26991 * #
E-2484 p 75 N85-21321 * #
E-2485 p 49 N85-21261 * #
E-2487 p 132 N85-23085 * #
E-2489 p 99 N85-20224 * #
E-2490 p 26 N85-21164 * #
E-2491 p 77 N85-31284 * #
E-2493 p 53 N85-21264 * #
E-2495 p 37 N85-21231 * #
E-2496 p 161 N85-23243 * #
E-2501 p 124 N85-25794 * #
E-2502 p 124 N85-21605 * #
E-2503 p 117 N85-30246 * #
E-2506 p 178 N85-34631 * #
E-2507 p 91 N85-30135 * #
E-2512 p 53 N85-30011 * #
E-2513 p 75 N85-21322 * #
E-2514 p 76 N85-26964 * #
E-2515 p 132 N85-25847 * #
E-2517 p 116 N85-25761 * #
E-2518 p 115 N85-21574 * #
E-2519 p 89 N85-24000 * #
E-2522 p 41 N85-23904 * #
E-2523 p 135 N85-32330 * #
E-2524 p 134 N85-32329 * #
E-2525 p 76 N85-22660 * #
E-2526 p 162 N85-29365 * #
E-2527 p 9 N85-23711 * #
E-2529 p 146 N85-24338 * #
E-2530 p 161 N85-27385 * #
E-2531 p 134 N85-30342 * #
E-2533 p 27 N85-25264 * #
E-2534 p 146 N85-24339 * #
E-2535 p 133 N85-28371 * #
E-2538 p 88 N85-22755 * #
E-2539 p 89 N85-22756 * #
E-2540 p 50 N85-23926 * #
E-2541 p 183 N85-26406 * #
E-2542 p 28 N85-25266 * #
E-2544 p 50 N85-25386 * #
E-2545 p 32 N85-31058 * #
E-2546 p 9 N85-26670 * #
E-2547 p 63 N85-23941 * #
E-2548 p 27 N85-25263 * #
E-2549 p 133 N85-27227 * #
E-2550 p 138 N85-29307 * #
E-2552 p 115 N85-24245 * #
E-2553 p 1 N85-23685 * #
E-2554 p 51 N85-27941 * #
E-2555 p 115 N85-25760 * #
E-2556 p 184 N85-28876 * #
E-2557 p 32 N85-31060 * #
E-2559 p 133 N85-27228 * #
E-2560 p 89 N85-25521 * #
E-2562 p 132 N85-27226 * #
E-2564 p 165 N85-34444 * #
E-2570 p 50 N85-25385 * #
E-2571 p 148 N85-27264 * #
E-2572 p 51 N85-26912 * #
E-2574 p 64 N85-32156 * #
E-2580 p 90 N85-26992 * #
E-2581 p 117 N85-30242 * #
E-2582 p 91 N85-28110 * #
E-2584 p 185 N85-27769 * #
E-2585 p 162 N85-28444 * #
E-2588 p 30 N85-28945 * #
E-2590 p 162 N85-27387 * #
E-2591 p 138 N85-32337 * #
E-2592 p 90 N85-26993 * #
E-2594 p 164 N85-31646 * #
E-2595 p 28 N85-26710 * #
E-2596 p 104 N85-28222 * #
E-2598 p 152 N85-34427 * #
E-2599 p 95 N85-29085 * #
E-2601 p 63 N85-28983 * #
E-2603 p 51 N85-27972 * #
E-2604 p 63 N85-31244 * #
E-2606 p 58 N85-27978 * #
E-2607 p 135 N85-32333 * #
E-2608 p 163 N85-30480 * #
E-2609 p 125 N85-30288 * #
E-2610 p 38 N85-29987 * #

E-2612 p 30 N85-27870 * #
E-2616 p 133 N85-29292 * #
E-2621 p 9 N85-29925 * #
E-2625 p 58 N85-30034 * #
E-2628 p 52 N85-28971 * #
E-2629 p 118 N85-30247 * #
E-2633 p 177 N85-30770 * #
E-2634 p 119 N85-31444 * #
E-2637 p 32 N85-29964 * #
E-2638 p 52 N85-35225 * #
E-2642 p 100 N85-31348 * #
E-2643 p 125 N85-32302 * #
E-2646 p 164 N85-34443 * #
E-2648 p 136 N85-34405 * #
E-2653 p 38 N85-34150 * #
E-2657 p 78 N85-34265 * #
E-2658 p 137 N85-34408 * #
E-2659 p 52 N85-34176 * #
E-2660 p 136 N85-34407 * #
E-2661 p 58 N85-32148 * #
E-2666 p 136 N85-34406 * #
E-2670 p 137 N85-34409 * #
E-2671 p 59 N85-34223 * #
E-2672 p 52 N85-34177 * #
E-2673 p 52 N85-34178 * #
E-2689 p 52 N85-34179 * #
E-2694 p 78 N85-34266 * #
E-996 p 172 N85-19733 * #

EDR-11442 p 91 N85-28109 * #
EDR-11682 p 31 N85-29961 #
EDR-11683 p 28 N85-26709 * #
EDR-11869 p 86 N85-18154 * #

ER-8050-F-VOL-2-APP-A p 22 N85-10991 * #

ESL-713533-5 p 37 N85-21233 * #
ESL-716109 p 136 N85-34404 * #
ESL-716111-2 p 98 N85-17258 * #
ESL-716111-3 p 100 N85-34329 * #

E9787 p 157 N85-10444 * #

FCR-4684F p 159 N85-17422 * #
FCR-6128 p 158 N85-13371 * #
FCR-6853 p 50 N85-25384 * #

FR-18046-3 p 48 N85-19020 * #

FSFL-R-85-002 p 27 N85-25262 * #

GARRETT-31-3725(8) p 185 N85-18831 * #

GE-84SRD006-VOL-1 p 176 N85-19791 * #
GE-84SRD006-VOL-2 p 176 N85-19792 * #

GTD-84-4 p 46 N85-11132 * #

GTEC31-4773 p 159 N85-16300 * #

H-8407-07 p 125 N85-33456 * #

IAF PAPER 84-154 p 59 A85-13092 * #
IAF PAPER 84-156 p 61 A85-23199 * #
IAF PAPER 84-15 p 36 A85-23200 * #

IAF-85-164 p 52 N85-35225 * #

ICASE-85-13 p 168 N85-21990 * #

IITRI-M06116-3 p 74 N85-19078 * #

IMMR84-098 p 120 N85-33453 #

IR-2 p 132 N85-25848 * #
IR-3 p 135 N85-33491 * #

JDTI-RED-85-1 p 25 N85-21163 * #

JM/85-6 p 29 N85-26712 * #

JPL-9950-945 p 185 N85-19894 * #

KI-P-1008 p 185 N85-19894 * #

L-15861 p 176 N85-22109 * #

LBL-18163 p 93 N85-19185 * #

LSI-TR-376-30 p 158 N85-16292 * #

MAI-R4 p 47 N85-13910 * #

MDC-J3789 p 10 N85-35162 * #

MPN-764038 p 136 N85-34404 * #

MTI-84TR39 p 35 N85-22400 * #
MTI-84TR58 p 184 N85-12808 * #

NAS 1.15:83022 p 18 N85-10951 * #
NAS 1.15:83354 p 57 N85-14882 * #
NAS 1.15:83470 p 150 N85-30361 * #
NAS 1.15:83471 p 163 N85-30477 * #
NAS 1.15:83472 p 162 N85-30476 * #
NAS 1.15:83480 p 163 N85-30478 * #
NAS 1.15:83517 p 163 N85-30479 * #
NAS 1.15:83556 p 11 N85-27839 * #
NAS 1.15:83590 p 25 N85-21162 * #
NAS 1.15:83621 p 24 N85-14840 * #
NAS 1.15:83677 p 158 N85-12465 * #
NAS 1.15:83693 p 184 N85-22255 * #
NAS 1.15:83698 p 70 N85-10165 * #
NAS 1.15:83711 p 85 N85-15896 * #
NAS 1.15:83748 p 1 N85-15658 * #
NAS 1.15:83750 p 62 N85-10138 * #
NAS 1.15:83754 p 57 N85-21273 * #
NAS 1.15:83767 p 7 N85-12039 * #
NAS 1.15:83771 p 17 N85-10067 * #
NAS 1.15:83783 p 170 N85-10683 * #
NAS 1.15:83784 p 71 N85-12131 * #
NAS 1.15:83790 p 103 N85-13157 * #
NAS 1.15:83791 p 70 N85-10168 * #
NAS 1.15:83797 p 175 N85-10788 * #
NAS 1.15:83798 p 94 N85-11261 * #
NAS 1.15:83800 p 184 N85-22204 * #
NAS 1.15:83801 p 113 N85-10303 * #
NAS 1.15:83803 p 131 N85-15168 * #
NAS 1.15:83804 p 83 N85-10186 * #
NAS 1.15:83805 p 169 N85-10659 * #
NAS 1.15:83806 p 17 N85-10068 * #
NAS 1.15:83807 p 92 N85-12183 * #
NAS 1.15:86505 p 91 N85-28107 * #
NAS 1.15:86858 p 53 N85-10105 * #
NAS 1.15:86859 p 84 N85-10187 * #
NAS 1.15:86860 p 1 N85-17935 * #
NAS 1.15:86863 p 18 N85-10949 * #
NAS 1.15:86864 p 84 N85-10191 * #
NAS 1.15:86865 p 18 N85-10069 * #
NAS 1.15:86866 p 71 N85-12129 * #
NAS 1.15:86867 p 158 N85-11458 * #
NAS 1.15:86868 p 70 N85-11217 * #
NAS 1.15:86869 p 7 N85-12036 * #
NAS 1.15:86870 p 183 N85-10844 * #
NAS 1.15:86871 p 175 N85-13551 * #
NAS 1.15:86872 p 97 N85-10234 * #
NAS 1.15:86874 p 92 N85-13066 * #
NAS 1.15:86875 p 185 N85-19895 * #
NAS 1.15:86876 p 137 N85-10371 * #
NAS 1.15:86878 p 56 N85-12095 * #
NAS 1.15:86880 p 113 N85-10306 * #
NAS 1.15:86881 p 25 N85-18057 * #
NAS 1.15:86882 p 71 N85-11224 * #
NAS 1.15:86883 p 167 N85-21872 * #
NAS 1.15:86884 p 113 N85-11317 * #
NAS 1.15:86885 p 184 N85-16663 * #
NAS 1.15:86887 p 47 N85-11133 * #
NAS 1.15:86888 p 72 N85-13007 * #
NAS 1.15:86889 p 72 N85-12132 * #
NAS 1.15:86890 p 114 N85-15133 * #
NAS 1.15:86891 p 144 N85-15184 * #
NAS 1.15:86893 p 23 N85-13798 * #
NAS 1.15:86894 p 97 N85-15099 * #
NAS 1.15:86895 p 84 N85-14928 * #
NAS 1.15:86896 p 24 N85-15725 * #
NAS 1.15:86897 p 56 N85-14878 * #
NAS 1.15:86898 p 123 N85-16096 * #
NAS 1.15:86899 p 186 N85-17928 * #
NAS 1.15:86900 p 119 N85-33435 * #
NAS 1.15:86901 p 184 N85-13692 * #
NAS 1.15:86902 p 85 N85-14929 * #
NAS 1.15:86903 p 7 N85-14798 * #
NAS 1.15:86904 p 53 N85-14864 * #
NAS 1.15:86905 p 72 N85-15878 * #
NAS 1.15:86906 p 12 N85-18049 * #
NAS 1.15:86907 p 38 N85-15779 * #
NAS 1.15:86908 p 144 N85-16205 * #
NAS 1.15:86909 p 57 N85-15823 * #
NAS 1.15:86911 p 24 N85-15727 * #
NAS 1.15:86912 p 8 N85-15688 * #
NAS 1.15:86913 p 145 N85-21690 * #
NAS 1.15:86914 p 8 N85-15689 * #
NAS 1.15:86915 p 85 N85-15893 * #
NAS 1.15:86916 p 145 N85-18375 * #
NAS 1.15:86918 p 159 N85-16299 * #
NAS 1.15:86919 p 35 N85-15757 * #
NAS 1.15:86920 p 35 N85-15758 * #
NAS 1.15:86921 p 35 N85-18067 * #
NAS 1.15:86923 p 24 N85-15726 * #
NAS 1.15:86924 p 57 N85-15822 * #
NAS 1.15:86925 p 11 N85-15702 * #
NAS 1.15:86926 p 86 N85-18153 * #
NAS 1.15:86927 p 86 N85-15897 * #

NAS 1.15:86928 p 115 N85-21569 * #
NAS 1.15:86929 p 72 N85-18124 * #
NAS 1.15:86930 p 73 N85-18125 * #
NAS 1.15:86931 p 73 N85-18126 * #
NAS 1.15:86932 p 86 N85-19136 * #
NAS 1.15:86933 p 74 N85-19074 * #
NAS 1.15:86934 p 74 N85-19075 * #
NAS 1.15:86935 p 176 N85-22108 * #
NAS 1.15:86936 p 115 N85-20269 * #
NAS 1.15:86937 p 74 N85-19076 * #
NAS 1.15:86938 p 73 N85-19072 * #
NAS 1.15:86939 p 114 N85-19363 * #
NAS 1.15:86940 p 114 N85-19364 * #
NAS 1.15:86941 p 74 N85-20042 * #
NAS 1.15:86942 p 75 N85-20043 * #
NAS 1.15:86943 p 87 N85-20127 * #
NAS 1.15:86944 p 115 N85-21570 * #
NAS 1.15:86945 p 138 N85-21674 * #
NAS 1.15:86946 p 36 N85-21228 * #
NAS 1.15:86947 p 48 N85-21258 * #
NAS 1.15:86948 p 99 N85-20223 * #
NAS 1.15:86949 p 137 N85-20389 * #
NAS 1.15:86950 p 161 N85-23242 * #
NAS 1.15:86951 p 8 N85-21114 * #
NAS 1.15:86952 p 8 N85-21115 * #
NAS 1.15:86953 p 186 N85-32043 * #
NAS 1.15:86955 p 49 N85-21259 * #
NAS 1.15:86956 p 49 N85-21260 * #
NAS 1.15:86957 p 103 N85-20246 * #
NAS 1.15:86958 p 131 N85-21658 * #
NAS 1.15:86959 p 75 N85-21321 * #
NAS 1.15:86960 p 49 N85-21261 * #
NAS 1.15:86961 p 99 N85-20224 * #
NAS 1.15:86962 p 87 N85-21355 * #
NAS 1.15:86963 p 26 N85-21164 * #
NAS 1.15:86964 p 88 N85-21357 * #
NAS 1.15:86965 p 131 N85-21657 * #
NAS 1.15:86966 p 62 N85-22644 * #
NAS 1.15:86967 p 8 N85-19923 * #
NAS 1.15:86968 p 53 N85-21264 * #
NAS 1.15:86969 p 37 N85-21231 * #
NAS 1.15:86970 p 161 N85-23243 * #
NAS 1.15:86973 p 124 N85-21605 * #
NAS 1.15:86974 p 88 N85-21356 * #
NAS 1.15:86976 p 75 N85-21322 * #
NAS 1.15:86977 p 88 N85-21358 * #
NAS 1.15:86978 p 132 N85-25847 * #
NAS 1.15:86979 p 116 N85-25761 * #
NAS 1.15:86980 p 115 N85-21574 * #
NAS 1.15:86981 p 89 N85-24000 * #
NAS 1.15:86982 p 76 N85-22660 * #
NAS 1.15:86983 p 162 N85-29365 * #
NAS 1.15:86984 p 9 N85-23711 * #
NAS 1.15:86985 p 146 N85-24338 * #
NAS 1.15:86986 p 161 N85-27385 * #
NAS 1.15:86987 p 76 N85-26963 * #
NAS 1.15:86988 p 134 N85-30342 * #
NAS 1.15:86989 p 27 N85-25264 * #
NAS 1.15:86990 p 146 N85-24339 * #
NAS 1.15:86991 p 132 N85-23085 * #
NAS 1.15:86992 p 88 N85-22755 * #
NAS 1.15:86993 p 89 N85-22756 * #
NAS 1.15:86994 p 50 N85-23926 * #
NAS 1.15:86995 p 183 N85-26406 * #
NAS 1.15:86996 p 28 N85-25266 * #
NAS 1.15:86999 p 50 N85-25386 * #
NAS 1.15:87000 p 41 N85-23904 * #
NAS 1.15:87001 p 9 N85-26670 * #
NAS 1.15:87002 p 63 N85-23941 * #
NAS 1.15:87003 p 27 N85-25263 * #
NAS 1.15:87004 p 146 N85-25893 * #
NAS 1.15:87005 p 124 N85-25794 * #
NAS 1.15:87006 p 133 N85-27227 * #
NAS 1.15:87007 p 90 N85-26991 * #
NAS 1.15:87008 p 115 N85-24245 * #
NAS 1.15:87010 p 1 N85-23685 * #
NAS 1.15:87011 p 115 N85-25760 * #
NAS 1.15:87012 p 184 N85-28876 * #
NAS 1.15:87013 p 32 N85-31060 * #
NAS 1.15:87014 p 133 N85-27228 * #
NAS 1.15:87015 p 53 N85-26921 * #
NAS 1.15:87016 p 89 N85-25521 * #
NAS 1.15:87017 p 132 N85-27226 * #
NAS 1.15:87018 p 165 N85-34444 * #
NAS 1.15:87019 p 50 N85-25385 * #
NAS 1.15:87020 p 77 N85-31284 * #
NAS 1.15:87021 p 148 N85-27264 * #
NAS 1.15:87022 p 76 N85-26964 * #
NAS 1.15:87023 p 51 N85-26912 * #
NAS 1.15:87025 p 90 N85-26992 * #
NAS 1.15:87026 p 91 N85-28110 * #
NAS 1.15:87028 p 185 N85-27769 * #
NAS 1.15:87029 p 162 N85-28444 * #
NAS 1.15:87032 p 117 N85-30242 * #
NAS 1.15:87033 p 30 N85-28945 * #
NAS 1.15:87034 p 162 N85-27387 * #

NAS 1.15:87035 p 138 N85-32337 * #
NAS 1.15:87036 p 90 N85-26993 * #
NAS 1.15:87037 p 164 N85-31646 * #
NAS 1.15:87038 p 133 N85-28371 * #
NAS 1.15:87039 p 28 N85-26710 * #
NAS 1.15:87040 p 104 N85-28222 * #
NAS 1.15:87041 p 117 N85-30246 * #
NAS 1.15:87042 p 63 N85-28983 * #
NAS 1.15:87043 p 51 N85-27972 * #
NAS 1.15:87044 p 133 N85-28373 * #
NAS 1.15:87045 p 58 N85-27978 * #
NAS 1.15:87047 p 125 N85-30288 * #
NAS 1.15:87048 p 38 N85-29987 * #
NAS 1.15:87049 p 30 N85-27870 * #
NAS 1.15:87051 p 91 N85-30137 * #
NAS 1.15:87052 p 91 N85-30135 * #
NAS 1.15:87053 p 133 N85-29292 * #
NAS 1.15:87054 p 9 N85-29925 * #
NAS 1.15:87055 p 95 N85-29085 * #
NAS 1.15:87056 p 91 N85-30138 * #
NAS 1.15:87056 p 163 N85-30480 * #
NAS 1.15:87058 p 58 N85-30034 * #
NAS 1.15:87059 p 52 N85-28971 * #
NAS 1.15:87060 p 118 N85-30247 * #
NAS 1.15:87061 p 53 N85-30011 * #
NAS 1.15:87062 p 77 N85-31283 * #
NAS 1.15:87063 p 119 N85-31443 * #
NAS 1.15:87064 p 178 N85-28786 * #
NAS 1.15:87065 p 177 N85-30770 * #
NAS 1.15:87066 p 119 N85-31444 * #
NAS 1.15:87067 p 32 N85-29964 * #
NAS 1.15:87068 p 64 N85-32156 * #
NAS 1.15:87069 p 52 N85-35225 * #
NAS 1.15:87070 p 100 N85-31348 * #
NAS 1.15:87071 p 125 N85-32302 * #
NAS 1.15:87074 p 164 N85-34443 * #
NAS 1.15:87075 p 136 N85-34405 * #
NAS 1.15:87077 p 38 N85-34150 * #
NAS 1.15:87078 p 135 N85-32333 * #
NAS 1.15:87079 p 78 N85-34265 * #
NAS 1.15:87080 p 52 N85-34176 * #
NAS 1.15:87081 p 58 N85-32148 * #
NAS 1.15:87082 p 136 N85-34406 * #
NAS 1.15:87083 p 178 N85-34631 * #
NAS 1.15:87085 p 59 N85-34223 * #
NAS 1.15:87086 p 52 N85-34177 * #
NAS 1.15:87087 p 52 N85-34178 * #
NAS 1.15:87092 p 92 N85-34284 * #
NAS 1.15:87096 p 136 N85-34407 * #
NAS 1.15:87097 p 137 N85-34408 * #
NAS 1.15:87098 p 52 N85-34179 * #
NAS 1.15:87100 p 78 N85-34266 * #
NAS 1.15:87102 p 152 N85-34427 * #
NAS 1.15:87107 p 137 N85-34409 * #
NAS 1.15:87391 p 12 N85-12887 * #
NAS 1.15:87483 p 134 N85-29295 * #
NAS 1.26:165550 p 71 N85-11225 * #
NAS 1.26:165558 p 23 N85-10998 * #
NAS 1.26:167851 p 23 N85-10999 * #
NAS 1.26:167862 p 167 N85-35534 * #
NAS 1.26:167863 p 167 N85-35535 * #
NAS 1.26:167864 p 167 N85-35536 * #
NAS 1.26:167865 p 167 N85-35537 * #
NAS 1.26:167866 p 168 N85-35538 * #
NAS 1.26:167870 p 22 N85-10993 * #
NAS 1.26:167871 p 23 N85-10997 * #
NAS 1.26:167945 p 18 N85-10950 * #
NAS 1.26:167952 p 175 N85-11791 * #
NAS 1.26:167955 p 23 N85-10995 * #
NAS 1.26:167956 p 22 N85-10994 * #
NAS 1.26:167993 p 23 N85-12059 * #
NAS 1.26:167995 p 25 N85-18058 * #
NAS 1.26:168017 p 31 N85-29957 * #
NAS 1.26:168036 p 23 N85-10996 * #
NAS 1.26:168037 p 34 N85-35199 * #
NAS 1.26:168054 p 9 N85-29916 * #
NAS 1.26:168070 p 33 N85-34141 * #
NAS 1.26:168137 p 31 N85-29956 * #
NAS 1.26:168173 p 132 N85-25848 * #
NAS 1.26:168189 p 30 N85-29955 * #
NAS 1.26:168222 p 159 N85-16300 * #
NAS 1.26:168223 p 160 N85-19511 * #
NAS 1.26:168228 p 32 N85-31057 * #
NAS 1.26:168245 p 33 N85-34138 * #
NAS 1.26:168259 p 48 N85-15806 * #
NAS 1.26:168285 p 130 N85-13235 * #
NAS 1.26:168287 p 124 N85-25792 * #
NAS 1.26:168313 p 103 N85-19328 * #
NAS 1.26:168329 p 116 N85-27164 * #
NAS 1.26:168337 p 18 N85-10948 * #
NAS 1.26:168338 p 164 N85-30483 * #
NAS 1.26:169496 p 22 N85-10989 * #
NAS 1.26:170034 p 22 N85-10990 * #
NAS 1.26:172557 p 168 N85-21990 * #
NAS 1.26:172846 p 31 N85-29958 * #
NAS 1.26:173084 p 22 N85-10992 * #
NAS 1.26:173085 p 22 N85-10991 * #
NAS 1.26:174054 p 97 N85-11265 * #
NAS 1.26:174056 p 183 N85-11862 * #
NAS 1.26:174057 p 158 N85-11457 * #
NAS 1.26:174058 p 62 N85-11149 * #
NAS 1.26:174067 p 35 N85-12071 * #
NAS 1.26:174079 p 92 N85-11252 * #
NAS 1.26:174246 p 24 N85-15724 * #
NAS 1.26:174266 p 159 N85-16293 * #
NAS 1.26:174268 p 98 N85-15944 * #
NAS 1.26:174281 p 98 N85-15943 * #
NAS 1.26:174284 p 86 N85-15916 * #
NAS 1.26:174335 p 159 N85-18451 * #
NAS 1.26:174336 p 98 N85-17258 * #
NAS 1.26:174342 p 114 N85-17324 * #
NAS 1.26:174353 p 114 N85-18291 * #
NAS 1.26:174369 p 114 N85-18292 * #
NAS 1.26:174380 p 103 N85-18259 * #
NAS 1.26:174395 p 93 N85-19185 * #
NAS 1.26:174411 p 74 N85-19078 * #
NAS 1.26:174430 p 185 N85-19894 * #
NAS 1.26:174638 p 157 N85-11456 * #
NAS 1.26:174657 p 48 N85-18084 * #
NAS 1.26:174662 p 99 N85-27092 * #
NAS 1.26:174664 p 176 N85-19791 * #
NAS 1.26:174665 p 176 N85-19792 * #
NAS 1.26:174673 p 46 N85-11131 * #
NAS 1.26:174687 p 89 N85-22758 * #
NAS 1.26:174689 p 185 N85-16698 * #
NAS 1.26:174695 p 85 N85-15892 * #
NAS 1.26:174696 p 177 N85-35728 * #
NAS 1.26:174697-VOL-1 p 98 N85-18239 * #
NAS 1.26:174697-VOL-2 p 99 N85-18240 * #
NAS 1.26:174697 p 98 N85-18238 * #
NAS 1.26:174700 p 145 N85-21686 * #
NAS 1.26:174701 p 18 N85-10947 * #
NAS 1.26:174711 p 34 N85-12901 * #
NAS 1.26:174712 p 178 N85-13594 * #
NAS 1.26:174715 p 91 N85-28109 * #
NAS 1.26:174721 p 157 N85-10445 * #
NAS 1.26:174722 p 157 N85-10447 * #
NAS 1.26:174724 p 165 N85-35471 * #
NAS 1.26:174731 p 126 N85-12341 * #
NAS 1.26:174732 p 158 N85-16291 * #
NAS 1.26:174738 p 28 N85-26709 * #
NAS 1.26:174740 p 72 N85-15877 * #
NAS 1.26:174745 p 47 N85-12937 * #
NAS 1.26:174746 p 184 N85-12808 * #
NAS 1.26:174747 p 133 N85-28372 * #
NAS 1.26:174750 p 35 N85-22400 * #
NAS 1.26:174751 p 12 N85-19978 * #
NAS 1.26:174752 p 93 N85-19176 * #
NAS 1.26:174753 p 157 N85-11455 * #
NAS 1.26:174756 p 70 N85-11221 * #
NAS 1.26:174757 p 144 N85-11380 * #
NAS 1.26:174762 p 70 N85-10166 * #
NAS 1.26:174764 p 7 N85-10919 * #
NAS 1.26:174765 p 147 N85-27261 * #
NAS 1.26:174765 p 33 N85-34140 * #
NAS 1.26:174766-VOL-1 p 33 N85-35197 * #
NAS 1.26:174766-VOL-2 p 33 N85-35198 * #
NAS 1.26:174768 p 46 N85-11132 * #
NAS 1.26:174771 p 163 N85-30481 * #
NAS 1.26:174772 p 48 N85-17023 * #
NAS 1.26:174775 p 157 N85-10444 * #
NAS 1.26:174776 p 172 N85-27584 * #
NAS 1.26:174778 p 92 N85-10209 * #
NAS 1.26:174779 p 71 N85-11223 * #
NAS 1.26:174782 p 9 N85-22368 * #
NAS 1.26:174783 p 185 N85-16699 * #
NAS 1.26:174794 p 159 N85-17421 * #
NAS 1.26:174795 p 102 N85-12300 * #
NAS 1.26:174796 p 84 N85-12162 * #
NAS 1.26:174798 p 31 N85-29961 #
NAS 1.26:174801 p 158 N85-16292 * #
NAS 1.26:174802 p 158 N85-13371 * #
NAS 1.26:174803 p 90 N85-26994 * #
NAS 1.26:174804 p 159 N85-17422 * #
NAS 1.26:174806 p 47 N85-13910 * #
NAS 1.26:174807 p 47 N85-15804 * #
NAS 1.26:174809 p 185 N85-18831 * #
NAS 1.26:174812 p 25 N85-21163 * #
NAS 1.26:174816 p 132 N85-21662 * #
NAS 1.26:174820 p 86 N85-18154 * #
NAS 1.26:174829 p 28 N85-25265 * #
NAS 1.26:174831 p 117 N85-30245 * #
NAS 1.26:174836 p 146 N85-21691 * #
NAS 1.26:174837 p 85 N85-15895 * #
NAS 1.26:174838 p 24 N85-15728 * #
NAS 1.26:174839 p 123 N85-21604 * #
NAS 1.26:174840 p 93 N85-27012 * #
NAS 1.26:174841 p 75 N85-21320 * #
NAS 1.26:174847 p 73 N85-18127 * #
NAS 1.26:174848 p 93 N85-19175 * #
NAS 1.26:174849 p 9 N85-26668 * #
NAS 1.26:174851 p 73 N85-19073 * #
NAS 1.26:174852 p 74 N85-20041 * #
NAS 1.26:174855 p 147 N85-27260 * #
NAS 1.26:174857 p 48 N85-19020 * #
NAS 1.26:174863 p 26 N85-22390 * #
NAS 1.26:174870 p 58 N85-30035 * #
NAS 1.26:174871 p 138 N85-21673 * #
NAS 1.26:174872 p 145 N85-21685 * #
NAS 1.26:174874 p 50 N85-25384 * #
NAS 1.26:174877 p 162 N85-29363 * #
NAS 1.26:174879 p 147 N85-25894 * #
NAS 1.26:174880 p 63 N85-25444 * #
NAS 1.26:174885 p 177 N85-27637 * #
NAS 1.26:174887 p 161 N85-25941 * #
NAS 1.26:174888 p 27 N85-22392 * #
NAS 1.26:174893 p 89 N85-22757 * #
NAS 1.26:174896 p 27 N85-25262 * #
NAS 1.26:174900 p 76 N85-26962 * #
NAS 1.26:174908 p 31 N85-29960 * #
NAS 1.26:174909 p 135 N85-33491 * #
NAS 1.26:174911 p 94 N85-34295 * #
NAS 1.26:174915 p 28 N85-26711 * #
NAS 1.26:174916 p 29 N85-27867 * #
NAS 1.26:174917 p 29 N85-26716 * #
NAS 1.26:174918 p 29 N85-26717 * #
NAS 1.26:174920 p 162 N85-29364 * #
NAS 1.26:174925 p 32 N85-32119 * #
NAS 1.26:174927 p 12 N85-35185 * #
NAS 1.26:174938 p 94 N85-31308 * #
NAS 1.26:174940 p 152 N85-32340 * #
NAS 1.26:174941 p 152 N85-32341 * #
NAS 1.26:174950 p 105 N85-32251 * #
NAS 1.26:174953 p 32 N85-29965 * #
NAS 1.26:174954 p 119 N85-31445 * #
NAS 1.26:174956 p 152 N85-33541 * #
NAS 1.26:174960 p 125 N85-35389 * #
NAS 1.26:174963 p 165 N85-35472 * #
NAS 1.26:174969 p 105 N85-33293 * #
NAS 1.26:174973 p 126 N85-35391 * #
NAS 1.26:174975 p 10 N85-35162 * #
NAS 1.26:175507 p 99 N85-21438 * #
NAS 1.26:175538 p 160 N85-20545 * #
NAS 1.26:175541 p 124 N85-21607 #
NAS 1.26:175551 p 146 N85-23096 * #
NAS 1.26:175552 p 37 N85-21233 * #
NAS 1.26:175573 p 26 N85-21165 * #
NAS 1.26:175574 p 145 N85-21687 * #
NAS 1.26:175585 p 39 N85-21250 * #
NAS 1.26:175586 p 62 N85-21283 * #
NAS 1.26:175605 p 27 N85-22391 * #
NAS 1.26:175609 p 146 N85-21720 * #
NAS 1.26:175619 p 183 N85-23414 * #
NAS 1.26:175625 p 76 N85-22661 * #
NAS 1.26:175627 p 168 N85-27508 * #
NAS 1.26:175743 p 99 N85-25686 * #
NAS 1.26:175747 p 147 N85-25896 * #
NAS 1.26:175795 p 148 N85-27263 * #
NAS 1.26:175811 p 29 N85-26712 * #
NAS 1.26:175831 p 29 N85-26713 * #
NAS 1.26:175832 p 29 N85-26714 * #
NAS 1.26:175833 p 29 N85-26715 * #
NAS 1.26:175835 p 116 N85-27168 * #
NAS 1.26:175839 p 161 N85-27377 * #
NAS 1.26:175856 p 93 N85-28127 * #
NAS 1.26:175885 p 36 N85-27922 * #
NAS 1.26:175901 p 30 N85-27868 * #
NAS 1.26:175998 p 58 N85-30037 * #
NAS 1.26:176003 p 41 N85-29997 * #
NAS 1.26:176070 p 77 N85-32174 * #
NAS 1.26:176071 p 77 N85-32173 * #
NAS 1.26:176072 p 77 N85-32175 * #
NAS 1.26:176077 p 77 N85-32176 * #
NAS 1.26:176104 p 164 N85-33566 * #
NAS 1.26:176154 p 125 N85-33456 * #
NAS 1.26:176162 p 100 N85-34329 * #
NAS 1.26:176163 p 136 N85-34404 * #
NAS 1.26:176186 p 100 N85-35320 * #
NAS 1.26:176189 p 100 N85-35321 * #
NAS 1.26:176190 p 106 N85-35342 * #
NAS 1.26:3836 p 7 N85-12008 * #
NAS 1.26:3845 p 175 N85-13550 * #
NAS 1.26:3846 p 175 N85-13549 * #
NAS 1.26:3847 p 176 N85-17667 * #
NAS 1.26:3851 p 137 N85-16195 * #
NAS 1.26:3866 p 26 N85-21166 * #
NAS 1.26:3869 p 26 N85-21167 * #
NAS 1.26:3877 p 138 N85-20390 * #
NAS 1.26:3878 p 8 N85-21117 * #
NAS 1.26:3904 p 138 N85-29307 * #
NAS 1.26:3925 p 10 N85-35158 * #
NAS 1.26:3926 p 10 N85-35159 * #
NAS 1.55:2338 p 131 N85-14116 * #
NAS 1.55:2347 p 37 N85-16989 * #
NAS 1.55:2352 p 47 N85-13880 * #
NAS 1.55:2359 p 39 N85-22470 * #
NAS 1.55:2369 p 150 N85-31530 * #
NAS 1.55:2381 p 51 N85-27941 * #

NAS 1.55:2386 p 118 N85-31433 * #
NAS 1.60:2359 p 17 N85-10064 * #
NAS 1.60:2372 p 17 N85-10065 * #
NAS 1.60:2378 p 170 N85-17576 * #
NAS 1.60:2388 p 113 N85-12314 * #
NAS 1.60:2390 p 113 N85-14078 * #
NAS 1.60:2398 p 176 N85-22109 * #
NAS 1.60:2403 p 72 N85-13006 * #
NAS 1.60:2404 p 130 N85-13233 * #
NAS 1.60:2405 p 84 N85-13044 * #
NAS 1.60:2406 p 84 N85-13045 * #
NAS 1.60:2407 p 39 N85-14858 * #
NAS 1.60:2408 p 130 N85-13234 * #
NAS 1.60:2419 p 123 N85-16099 * #
NAS 1.60:2421 p 145 N85-20396 * #
NAS 1.60:2422 p 170 N85-28610 * #
NAS 1.60:2424 p 123 N85-16100 * #
NAS 1.60:2426 p 171 N85-17596 * #
NAS 1.60:2435 p 26 N85-21168 * #
NAS 1.60:2437 p 49 N85-21263 * #
NAS 1.60:2443 p 75 N85-21323 * #
NAS 1.60:2449 p 88 N85-21359 * #
NAS 1.60:2453 p 183 N85-24961 * #
NAS 1.60:2460 p 116 N85-27165 * #
NAS 1.60:2461 p 27 N85-25261 * #
NAS 1.60:2463 p 30 N85-28944 * #
NAS 1.60:2473 p 135 N85-32331 * #
NAS 1.60:2477 p 32 N85-31058 * #
NAS 1.60:2488 p 134 N85-32329 * #
NAS 1.60:2495 p 93 N85-31307 * #
NAS 1.60:2496 p 134 N85-31511 * #
NAS 1.60:2498 p 63 N85-31244 * #
NAS 1.60:2500 p 135 N85-32330 * #
NAS 1.61:1094 p 172 N85-19733 * #
NAS 1.71:LEW-13324-2 p 57 N85-21266 * #
NAS 1.71:LEW-13414-1 p 160 N85-20530 * #
NAS 1.71:LEW-13770-3 p 87 N85-21350 * #
NAS 1.71:LEW-13770-4 p 87 N85-21351 * #
NAS 1.71:LEW-13770-5 p 87 N85-21352 * #
NAS 1.71:LEW-13827-1 p 160 N85-21768 * #
NAS 1.71:LEW-13833-1 p 103 N85-21492 * #
NAS 1.71:LEW-13837-2 p 57 N85-21267 * #
NAS 1.71:LEW-13837-3 p 95 N85-20155 * #
NAS 1.71:LEW-13881-1 p 48 N85-21256 * #
NAS 1.71:LEW-13935-1 p 103 N85-20248 * #
NAS 1.71:LEW-14080-1 p 95 N85-20153 * #
NAS 1.71:LEW-14104-1 p 75 N85-21324 * #
NAS 1.71:LEW-14108-1 p 104 N85-29149 * #
NAS 1.71:LEW-14130-1 p 95 N85-20156 * #
NAS 1.71:LEW-14170-1 p 131 N85-20377 * #
NAS 1.71:LEW-14177-1 p 160 N85-20535 * #

NASA-CASE-LEW-12950-2 p 117 N85-29179 * #
NASA-CASE-LEW-13102-1 p 104 N85-29144 * #
NASA-CASE-LEW-13324-2 p 57 N85-21266 * #
NASA-CASE-LEW-13414-1 p 160 N85-20530 * #
NASA-CASE-LEW-13506-1 p 135 N85-33490 * #
NASA-CASE-LEW-13562-2 p 33 N85-35195 * #
NASA-CASE-LEW-13717-1 p 134 N85-30333 * #
NASA-CASE-LEW-13770-2 p 63 N85-28982 * #
NASA-CASE-LEW-13770-3 p 87 N85-21350 * #
NASA-CASE-LEW-13770-4 p 87 N85-21351 * #
NASA-CASE-LEW-13770-5 p 87 N85-21352 * #
NASA-CASE-LEW-13770-6 p 63 N85-30039 * #
NASA-CASE-LEW-13827-1 p 160 N85-21768 * #
NASA-CASE-LEW-13828-1 p 58 N85-30027 * #
NASA-CASE-LEW-13833-1 p 103 N85-21492 * #
NASA-CASE-LEW-13837-2 p 57 N85-21267 * #
NASA-CASE-LEW-13837-3 p 95 N85-20155 * #
NASA-CASE-LEW-13881-1 p 48 N85-21256 * #
NASA-CASE-LEW-13914-1 p 135 N85-33489 * #
NASA-CASE-LEW-13935-1 p 103 N85-20248 * #
NASA-CASE-LEW-14039-1 p 119 N85-33433 * #
NASA-CASE-LEW-14053-1 p 136 N85-34402 * #
NASA-CASE-LEW-14057-1 p 59 N85-35233 * #
NASA-CASE-LEW-14077-1 p 164 N85-34441 * #
NASA-CASE-LEW-14080-1 p 95 N85-20153 * #
NASA-CASE-LEW-14104-1 p 75 N85-21324 * #
NASA-CASE-LEW-14108-1 p 104 N85-29149 * #
NASA-CASE-LEW-14130-1 p 95 N85-20156 * #
NASA-CASE-LEW-14170-1 p 131 N85-20377 * #
NASA-CASE-LEW-14177-1 p 160 N85-20535 * #

NASA-CP-2338 p 131 N85-14116 * #
NASA-CP-2347 p 37 N85-16989 * #
NASA-CP-2352 p 47 N85-13880 * #
NASA-CP-2359 p 39 N85-22470 * #
NASA-CP-2369 p 150 N85-31530 * #
NASA-CP-2381 p 51 N85-27941 * #
NASA-CP-2386 p 118 N85-31433 * #

NASA-CR-165550 p 71 N85-11225 * #
NASA-CR-165558 p 23 N85-10998 * #
NASA-CR-167851 p 23 N85-10999 * #
NASA-CR-167862 p 167 N85-35534 * #
NASA-CR-167863 p 167 N85-35535 * #
NASA-CR-167864 p 167 N85-35536 * #
NASA-CR-167865 p 167 N85-35537 * #
NASA-CR-167866 p 168 N85-35538 * #
NASA-CR-167870 p 22 N85-10993 * #
NASA-CR-167871 p 23 N85-10997 * #
NASA-CR-167945 p 18 N85-10950 * #
NASA-CR-167952 p 175 N85-11791 * #
NASA-CR-167955 p 23 N85-10995 * #
NASA-CR-167956 p 22 N85-10994 * #
NASA-CR-167993 p 23 N85-12059 * #
NASA-CR-167995 p 25 N85-18058 * #
NASA-CR-168017 p 31 N85-29957 * #
NASA-CR-168036 p 23 N85-10996 * #
NASA-CR-168037 p 34 N85-35199 * #
NASA-CR-168054 p 9 N85-29916 * #
NASA-CR-168070 p 33 N85-34141 * #
NASA-CR-168137 p 31 N85-29956 * #
NASA-CR-168173 p 132 N85-25848 * #
NASA-CR-168189 p 30 N85-29955 * #
NASA-CR-168222 p 159 N85-16300 * #
NASA-CR-168223 p 160 N85-19511 * #
NASA-CR-168228 p 32 N85-31057 * #
NASA-CR-168245 p 33 N85-34138 * #
NASA-CR-168259 p 48 N85-15806 * #
NASA-CR-168285 p 130 N85-13235 * #
NASA-CR-168287 p 124 N85-25792 * #
NASA-CR-168313 p 103 N85-19328 * #
NASA-CR-168329 p 116 N85-27164 * #
NASA-CR-168337 p 18 N85-10948 * #
NASA-CR-168338 p 164 N85-30483 * #
NASA-CR-169496 p 22 N85-10989 * #
NASA-CR-170034 p 22 N85-10990 * #
NASA-CR-172557 p 168 N85-21990 * #
NASA-CR-172846 p 31 N85-29958 * #
NASA-CR-173084 p 22 N85-10992 * #
NASA-CR-173085 p 22 N85-10991 * #
NASA-CR-174054 p 97 N85-11265 * #
NASA-CR-174056 p 183 N85-11862 * #
NASA-CR-174057 p 158 N85-11457 * #
NASA-CR-174058 p 62 N85-11149 * #
NASA-CR-174067 p 35 N85-12071 * #
NASA-CR-174079 p 92 N85-11252 * #
NASA-CR-174246 p 24 N85-15724 * #
NASA-CR-174266 p 159 N85-16293 * #
NASA-CR-174268 p 98 N85-15944 * #
NASA-CR-174281 p 98 N85-15943 * #
NASA-CR-174284 p 86 N85-15916 * #
NASA-CR-174335 p 159 N85-18451 * #
NASA-CR-174336 p 98 N85-17258 * #
NASA-CR-174342 p 114 N85-17324 * #
NASA-CR-174353 p 114 N85-18291 * #
NASA-CR-174369 p 114 N85-18292 * #
NASA-CR-174380 p 103 N85-18259 * #
NASA-CR-174395 p 93 N85-19185 * #
NASA-CR-174411 p 74 N85-19078 * #
NASA-CR-174430 p 185 N85-19894 * #
NASA-CR-174638 p 157 N85-11456 * #
NASA-CR-174657 p 48 N85-18084 * #
NASA-CR-174662 p 99 N85-27092 * #
NASA-CR-174664 p 176 N85-19791 * #
NASA-CR-174665 p 176 N85-19792 * #
NASA-CR-174673 p 46 N85-11131 * #
NASA-CR-174687 p 89 N85-22758 * #
NASA-CR-174689 p 185 N85-16698 * #
NASA-CR-174695 p 85 N85-15892 * #
NASA-CR-174696 p 177 N85-35728 * #
NASA-CR-174697-VOL-1 p 98 N85-18239 * #
NASA-CR-174697-VOL-2 p 99 N85-18240 * #
NASA-CR-174697 p 98 N85-18238 * #
NASA-CR-174700 p 145 N85-21686 * #
NASA-CR-174701 p 18 N85-10947 * #
NASA-CR-174711 p 34 N85-12901 * #
NASA-CR-174712 p 178 N85-13594 * #
NASA-CR-174715 p 91 N85-28109 * #
NASA-CR-174721 p 157 N85-10445 * #
NASA-CR-174722 p 157 N85-10447 * #
NASA-CR-174724 p 165 N85-35471 * #
NASA-CR-174731 p 126 N85-12341 * #
NASA-CR-174732 p 158 N85-16291 * #
NASA-CR-174738 p 28 N85-26709 * #
NASA-CR-174740 p 72 N85-15877 * #
NASA-CR-174745 p 47 N85-12937 * #
NASA-CR-174746 p 184 N85-12808 * #
NASA-CR-174747 p 133 N85-28372 * #
NASA-CR-174750 p 35 N85-22400 * #
NASA-CR-174751 p 12 N85-19978 * #
NASA-CR-174752 p 93 N85-19176 * #
NASA-CR-174753 p 157 N85-11455 * #
NASA-CR-174756 p 70 N85-11221 * #
NASA-CR-174757 p 144 N85-11380 * #
NASA-CR-174762 p 70 N85-10166 * #
NASA-CR-174764 p 7 N85-10919 * #
NASA-CR-174765 p 147 N85-27261 * #
NASA-CR-174765 p 33 N85-34140 * #
NASA-CR-174766-VOL-1 p 33 N85-35197 * #
NASA-CR-174766-VOL-2 p 33 N85-35198 * #
NASA-CR-174768 p 46 N85-11132 * #
NASA-CR-174771 p 163 N85-30481 * #
NASA-CR-174772 p 48 N85-17023 * #
NASA-CR-174775 p 157 N85-10444 * #
NASA-CR-174776 p 172 N85-27584 * #
NASA-CR-174778 p 92 N85-10209 * #
NASA-CR-174779 p 71 N85-11223 * #
NASA-CR-174782 p 9 N85-22368 * #
NASA-CR-174783 p 185 N85-16699 * #
NASA-CR-174794 p 159 N85-17421 * #
NASA-CR-174795 p 102 N85-12300 * #
NASA-CR-174796 p 84 N85-12162 * #
NASA-CR-174798 p 31 N85-29961 #
NASA-CR-174801 p 158 N85-16292 * #
NASA-CR-174802 p 158 N85-13371 * #
NASA-CR-174803 p 90 N85-26994 * #
NASA-CR-174804 p 159 N85-17422 * #
NASA-CR-174806 p 47 N85-13910 * #
NASA-CR-174807 p 47 N85-15804 * #
NASA-CR-174809 p 185 N85-18831 * #
NASA-CR-174812 p 25 N85-21163 * #
NASA-CR-174816 p 132 N85-21662 * #
NASA-CR-174820 p 86 N85-18154 * #
NASA-CR-174829 p 28 N85-25265 * #
NASA-CR-174831 p 117 N85-30245 * #
NASA-CR-174836 p 146 N85-21691 * #
NASA-CR-174837 p 85 N85-15895 * #
NASA-CR-174838 p 24 N85-15728 * #
NASA-CR-174839 p 123 N85-21604 * #
NASA-CR-174840 p 93 N85-27012 * #
NASA-CR-174841 p 75 N85-21320 * #
NASA-CR-174847 p 73 N85-18127 * #
NASA-CR-174848 p 93 N85-19175 * #
NASA-CR-174849 p 9 N85-26668 * #
NASA-CR-174851 p 73 N85-19073 * #
NASA-CR-174852 p 74 N85-20041 * #
NASA-CR-174855 p 147 N85-27260 * #
NASA-CR-174857 p 48 N85-19020 * #
NASA-CR-174863 p 26 N85-22390 * #
NASA-CR-174870 p 58 N85-30035 * #
NASA-CR-174871 p 138 N85-21673 * #
NASA-CR-174872 p 145 N85-21685 * #
NASA-CR-174874 p 50 N85-25384 * #
NASA-CR-174877 p 162 N85-29363 * #
NASA-CR-174879 p 147 N85-25894 * #
NASA-CR-174880 p 63 N85-25444 * #
NASA-CR-174885 p 177 N85-27637 * #
NASA-CR-174887 p 161 N85-25941 * #
NASA-CR-174888 p 27 N85-22392 * #
NASA-CR-174893 p 89 N85-22757 * #
NASA-CR-174896 p 27 N85-25262 * #
NASA-CR-174900 p 76 N85-26962 * #
NASA-CR-174908 p 31 N85-29960 * #
NASA-CR-174909 p 135 N85-33491 * #
NASA-CR-174911 p 94 N85-34295 * #
NASA-CR-174915 p 28 N85-26711 * #
NASA-CR-174916 p 29 N85-27867 * #
NASA-CR-174917 p 29 N85-26716 * #
NASA-CR-174918 p 29 N85-26717 * #
NASA-CR-174920 p 162 N85-29364 * #
NASA-CR-174925 p 32 N85-32119 * #
NASA-CR-174927 p 12 N85-35185 * #
NASA-CR-174938 p 94 N85-31308 * #
NASA-CR-174940 p 152 N85-32340 * #
NASA-CR-174941 p 152 N85-32341 * #
NASA-CR-174950 p 105 N85-32251 * #
NASA-CR-174953 p 32 N85-29965 * #
NASA-CR-174954 p 119 N85-31445 * #
NASA-CR-174956 p 152 N85-33541 * #
NASA-CR-174960 p 125 N85-35389 * #
NASA-CR-174963 p 165 N85-35472 * #
NASA-CR-174969 p 105 N85-33293 * #
NASA-CR-174973 p 126 N85-35391 * #
NASA-CR-174975 p 10 N85-35162 * #
NASA-CR-175507 p 99 N85-21438 * #
NASA-CR-175538 p 160 N85-20545 * #
NASA-CR-175541 p 124 N85-21607 #
NASA-CR-175551 p 146 N85-23096 * #
NASA-CR-175552 p 37 N85-21233 * #
NASA-CR-175573 p 26 N85-21165 * #
NASA-CR-175574 p 145 N85-21687 * #
NASA-CR-175585 p 39 N85-21250 * #
NASA-CR-175586 p 62 N85-21283 * #
NASA-CR-175605 p 27 N85-22391 * #
NASA-CR-175609 p 146 N85-21720 * #
NASA-CR-175619 p 183 N85-23414 * #
NASA-CR-175625 p 76 N85-22661 * #
NASA-CR-175627 p 168 N85-27508 * #
NASA-CR-175743 p 99 N85-25686 * #
NASA-CR-175747 p 147 N85-25896 * #
NASA-CR-175795 p 148 N85-27263 * #
NASA-CR-175811 p 29 N85-26712 * #
NASA-CR-175831 p 29 N85-26713 * #
NASA-CR-175832 p 29 N85-26714 * #
NASA-CR-175833 p 29 N85-26715 * #
NASA-CR-175835 p 116 N85-27168 * #

NASA-CR-175839 p 161 N85-27377 * #
NASA-CR-175856 p 93 N85-28127 * #
NASA-CR-175885 p 36 N85-27922 * #
NASA-CR-175901 p 30 N85-27868 * #
NASA-CR-175998 p 58 N85-30037 * #
NASA-CR-176003 p 41 N85-29997 * #
NASA-CR-176070 p 77 N85-32174 * #
NASA-CR-176071 p 77 N85-32173 * #
NASA-CR-176072 p 77 N85-32175 * #
NASA-CR-176077 p 77 N85-32176 * #
NASA-CR-176104 p 164 N85-33566 * #
NASA-CR-176154 p 125 N85-33456 * #
NASA-CR-176162 p 100 N85-34329 * #
NASA-CR-176163 p 136 N85-34404 * #
NASA-CR-176186 p 100 N85-35320 * #
NASA-CR-176189 p 100 N85-35321 * #
NASA-CR-176190 p 106 N85-35342 * #
NASA-CR-3836 p 7 N85-12008 * #
NASA-CR-3845 p 175 N85-13550 * #
NASA-CR-3846 p 175 N85-13549 * #
NASA-CR-3847 p 176 N85-17667 * #
NASA-CR-3851 p 137 N85-16195 * #
NASA-CR-3866 p 26 N85-21166 * #
NASA-CR-3869 p 26 N85-21167 * #
NASA-CR-3877 p 138 N85-20390 * #
NASA-CR-3878 p 8 N85-21117 * #
NASA-CR-3904 p 138 N85-29307 * #
NASA-CR-3925 p 10 N85-35158 * #
NASA-CR-3926 p 10 N85-35159 * #

NASA-RP-1094 p 172 N85-19733 * #

NASA-TM-83022 p 18 N85-10951 * #
NASA-TM-83354 p 57 N85-14882 * #
NASA-TM-83470 p 150 N85-30361 * #
NASA-TM-83471 p 163 N85-30477 * #
NASA-TM-83472 p 162 N85-30476 * #
NASA-TM-83480 p 163 N85-30478 * #
NASA-TM-83517 p 163 N85-30479 * #
NASA-TM-83556 p 11 N85-27839 * #
NASA-TM-83590 p 25 N85-21162 * #
NASA-TM-83621 p 24 N85-14840 * #
NASA-TM-83677 p 158 N85-12465 * #
NASA-TM-83693 p 184 N85-22255 * #
NASA-TM-83698 p 70 N85-10165 * #
NASA-TM-83711 p 85 N85-15896 * #
NASA-TM-83748 p 1 N85-15658 * #
NASA-TM-83750 p 62 N85-10138 * #
NASA-TM-83754 p 57 N85-21273 * #
NASA-TM-83767 p 7 N85-12039 * #
NASA-TM-83771 p 17 N85-10067 * #
NASA-TM-83783 p 170 N85-10683 * #
NASA-TM-83784 p 71 N85-12131 * #
NASA-TM-83790 p 103 N85-13157 * #
NASA-TM-83791 p 70 N85-10168 * #
NASA-TM-83797 p 175 N85-10788 * #
NASA-TM-83798 p 94 N85-11261 * #
NASA-TM-83800 p 184 N85-22204 * #
NASA-TM-83801 p 113 N85-10303 * #
NASA-TM-83803 p 131 N85-15168 * #
NASA-TM-83804 p 83 N85-10186 * #
NASA-TM-83805 p 169 N85-10659 * #
NASA-TM-83806 p 17 N85-10068 * #
NASA-TM-83807 p 92 N85-12183 * #
NASA-TM-86505 p 91 N85-28107 * #
NASA-TM-86858 p 53 N85-10105 * #
NASA-TM-86859 p 84 N85-10187 * #
NASA-TM-86860 p 1 N85-17935 * #
NASA-TM-86863 p 18 N85-10949 * #
NASA-TM-86864 p 84 N85-10191 * #
NASA-TM-86865 p 18 N85-10069 * #
NASA-TM-86866 p 71 N85-12129 * #
NASA-TM-86867 p 158 N85-11458 * #
NASA-TM-86868 p 70 N85-11217 * #
NASA-TM-86869 p 7 N85-12036 * #
NASA-TM-86870 p 183 N85-10844 * #
NASA-TM-86871 p 175 N85-13551 * #
NASA-TM-86872 p 97 N85-10234 * #
NASA-TM-86874 p 92 N85-13066 * #
NASA-TM-86875 p 185 N85-19895 * #
NASA-TM-86876 p 137 N85-10371 * #
NASA-TM-86878 p 56 N85-12095 * #
NASA-TM-86880 p 113 N85-10306 * #
NASA-TM-86881 p 25 N85-18057 * #
NASA-TM-86882 p 71 N85-11224 * #
NASA-TM-86883 p 167 N85-21872 * #
NASA-TM-86884 p 113 N85-11317 * #
NASA-TM-86885 p 184 N85-16663 * #
NASA-TM-86887 p 47 N85-11133 * #
NASA-TM-86888 p 72 N85-13007 * #
NASA-TM-86889 p 72 N85-12132 * #
NASA-TM-86890 p 114 N85-15133 * #
NASA-TM-86891 p 144 N85-15184 * #
NASA-TM-86893 p 23 N85-13798 * #
NASA-TM-86894 p 97 N85-15099 * #
NASA-TM-86895 p 84 N85-14928 * #
NASA-TM-86896 p 24 N85-15725 * #
NASA-TM-86897 p 56 N85-14878 * #
NASA-TM-86898 p 123 N85-16096 * #
NASA-TM-86899 p 186 N85-17928 * #
NASA-TM-86900 p 119 N85-33435 * #
NASA-TM-86901 p 184 N85-13692 * #
NASA-TM-86902 p 85 N85-14929 * #
NASA-TM-86903 p 7 N85-14798 * #
NASA-TM-86904 p 53 N85-14864 * #
NASA-TM-86905 p 72 N85-15878 * #
NASA-TM-86906 p 12 N85-18049 * #
NASA-TM-86907 p 38 N85-15779 * #
NASA-TM-86908 p 144 N85-16205 * #
NASA-TM-86909 p 57 N85-15823 * #
NASA-TM-86911 p 24 N85-15727 * #
NASA-TM-86912 p 8 N85-15688 * #
NASA-TM-86913 p 145 N85-21690 * #
NASA-TM-86914 p 8 N85-15689 * #
NASA-TM-86915 p 85 N85-15893 * #
NASA-TM-86916 p 145 N85-18375 * #
NASA-TM-86918 p 159 N85-16299 * #
NASA-TM-86919 p 35 N85-15757 * #
NASA-TM-86920 p 35 N85-15758 * #
NASA-TM-86921 p 35 N85-18067 * #
NASA-TM-86923 p 24 N85-15726 * #
NASA-TM-86924 p 57 N85-15822 * #
NASA-TM-86925 p 11 N85-15702 * #
NASA-TM-86926 p 86 N85-18153 * #
NASA-TM-86927 p 86 N85-15897 * #
NASA-TM-86928 p 115 N85-21569 * #
NASA-TM-86929 p 72 N85-18124 * #
NASA-TM-86930 p 73 N85-18125 * #
NASA-TM-86931 p 73 N85-18126 * #
NASA-TM-86932 p 86 N85-19136 * #
NASA-TM-86933 p 74 N85-19074 * #
NASA-TM-86934 p 74 N85-19075 * #
NASA-TM-86935 p 176 N85-22108 * #
NASA-TM-86936 p 115 N85-20269 * #
NASA-TM-86937 p 74 N85-19076 * #
NASA-TM-86938 p 73 N85-19072 * #
NASA-TM-86939 p 114 N85-19363 * #
NASA-TM-86940 p 114 N85-19364 * #
NASA-TM-86941 p 74 N85-20042 * #
NASA-TM-86942 p 75 N85-20043 * #
NASA-TM-86943 p 87 N85-20127 * #
NASA-TM-86944 p 115 N85-21570 * #
NASA-TM-86945 p 138 N85-21674 * #
NASA-TM-86946 p 36 N85-21228 * #
NASA-TM-86947 p 48 N85-21258 * #
NASA-TM-86948 p 99 N85-20223 * #
NASA-TM-86949 p 137 N85-20389 * #
NASA-TM-86950 p 161 N85-23242 * #
NASA-TM-86951 p 8 N85-21114 * #
NASA-TM-86952 p 8 N85-21115 * #
NASA-TM-86953 p 186 N85-32043 * #
NASA-TM-86955 p 49 N85-21259 * #
NASA-TM-86956 p 49 N85-21260 * #
NASA-TM-86957 p 103 N85-20246 * #
NASA-TM-86958 p 131 N85-21658 * #
NASA-TM-86959 p 75 N85-21321 * #
NASA-TM-86960 p 49 N85-21261 * #
NASA-TM-86961 p 99 N85-20224 * #
NASA-TM-86962 p 87 N85-21355 * #
NASA-TM-86963 p 26 N85-21164 * #
NASA-TM-86964 p 88 N85-21357 * #
NASA-TM-86965 p 131 N85-21657 * #
NASA-TM-86966 p 62 N85-22644 * #
NASA-TM-86967 p 8 N85-19923 * #
NASA-TM-86968 p 53 N85-21264 * #
NASA-TM-86969 p 37 N85-21231 * #
NASA-TM-86970 p 161 N85-23243 * #
NASA-TM-86973 p 124 N85-21605 * #
NASA-TM-86974 p 88 N85-21356 * #
NASA-TM-86976 p 75 N85-21322 * #
NASA-TM-86977 p 88 N85-21358 * #
NASA-TM-86978 p 132 N85-25847 * #
NASA-TM-86979 p 116 N85-25761 * #
NASA-TM-86980 p 115 N85-21574 * #
NASA-TM-86981 p 89 N85-24000 * #
NASA-TM-86982 p 76 N85-22660 * #
NASA-TM-86983 p 162 N85-29365 * #
NASA-TM-86984 p 9 N85-23711 * #
NASA-TM-86985 p 146 N85-24338 * #
NASA-TM-86986 p 161 N85-27385 * #
NASA-TM-86987 p 76 N85-26963 * #
NASA-TM-86988 p 134 N85-30342 * #
NASA-TM-86989 p 27 N85-25264 * #
NASA-TM-86990 p 146 N85-24339 * #
NASA-TM-86991 p 132 N85-23085 * #
NASA-TM-86992 p 88 N85-22755 * #
NASA-TM-86993 p 89 N85-22756 * #
NASA-TM-86994 p 50 N85-23926 * #
NASA-TM-86995 p 183 N85-26406 * #
NASA-TM-86996 p 28 N85-25266 * #
NASA-TM-86999 p 50 N85-25386 * #
NASA-TM-87000 p 41 N85-23904 * #
NASA-TM-87001 p 9 N85-26670 * #
NASA-TM-87002 p 63 N85-23941 * #
NASA-TM-87003 p 27 N85-25263 * #
NASA-TM-87004 p 146 N85-25893 * #
NASA-TM-87005 p 124 N85-25794 * #
NASA-TM-87006 p 133 N85-27227 * #
NASA-TM-87007 p 90 N85-26991 * #
NASA-TM-87008 p 115 N85-24245 * #
NASA-TM-87010 p 1 N85-23685 * #
NASA-TM-87011 p 115 N85-25760 * #
NASA-TM-87012 p 184 N85-28876 * #
NASA-TM-87013 p 32 N85-31060 * #
NASA-TM-87014 p 133 N85-27228 * #
NASA-TM-87015 p 53 N85-26921 * #
NASA-TM-87016 p 89 N85-25521 * #
NASA-TM-87017 p 132 N85-27226 * #
NASA-TM-87018 p 165 N85-34444 * #
NASA-TM-87019 p 50 N85-25385 * #
NASA-TM-87020 p 77 N85-31284 * #
NASA-TM-87021 p 148 N85-27264 * #
NASA-TM-87022 p 76 N85-26964 * #
NASA-TM-87023 p 51 N85-26912 * #
NASA-TM-87025 p 90 N85-26992 * #
NASA-TM-87026 p 91 N85-28110 * #
NASA-TM-87028 p 185 N85-27769 * #
NASA-TM-87029 p 162 N85-28444 * #
NASA-TM-87032 p 117 N85-30242 * #
NASA-TM-87033 p 30 N85-28945 * #
NASA-TM-87034 p 162 N85-27387 * #
NASA-TM-87035 p 138 N85-32337 * #
NASA-TM-87036 p 90 N85-26993 * #
NASA-TM-87037 p 164 N85-31646 * #
NASA-TM-87038 p 133 N85-28371 * #
NASA-TM-87039 p 28 N85-26710 * #
NASA-TM-87040 p 104 N85-28222 * #
NASA-TM-87041 p 117 N85-30246 * #
NASA-TM-87042 p 63 N85-28983 * #
NASA-TM-87043 p 51 N85-27972 * #
NASA-TM-87044 p 133 N85-28373 * #
NASA-TM-87045 p 58 N85-27978 * #
NASA-TM-87046 p 163 N85-30480 * #
NASA-TM-87047 p 125 N85-30288 * #
NASA-TM-87048 p 38 N85-29987 * #
NASA-TM-87049 p 30 N85-27870 * #
NASA-TM-87051 p 91 N85-30137 * #
NASA-TM-87052 p 91 N85-30135 * #
NASA-TM-87053 p 133 N85-29292 * #
NASA-TM-87054 p 9 N85-29925 * #
NASA-TM-87055 p 95 N85-29085 * #
NASA-TM-87056 p 91 N85-30138 * #
NASA-TM-87058 p 58 N85-30034 * #
NASA-TM-87059 p 52 N85-28971 * #
NASA-TM-87060 p 118 N85-30247 * #
NASA-TM-87061 p 53 N85-30011 * #
NASA-TM-87062 p 77 N85-31283 * #
NASA-TM-87063 p 119 N85-31443 * #
NASA-TM-87064 p 178 N85-28786 * #
NASA-TM-87065 p 177 N85-30770 * #
NASA-TM-87066 p 119 N85-31444 * #
NASA-TM-87067 p 32 N85-29964 * #
NASA-TM-87068 p 64 N85-32156 * #
NASA-TM-87069 p 52 N85-35225 * #
NASA-TM-87070 p 100 N85-31348 * #
NASA-TM-87071 p 125 N85-32302 * #
NASA-TM-87074 p 164 N85-34443 * #
NASA-TM-87075 p 136 N85-34405 * #
NASA-TM-87077 p 38 N85-34150 * #
NASA-TM-87078 p 135 N85-32333 * #
NASA-TM-87079 p 78 N85-34265 * #
NASA-TM-87080 p 52 N85-34176 * #
NASA-TM-87081 p 58 N85-32148 * #
NASA-TM-87082 p 136 N85-34406 * #
NASA-TM-87083 p 178 N85-34631 * #
NASA-TM-87085 p 59 N85-34223 * #
NASA-TM-87086 p 52 N85-34177 * #
NASA-TM-87087 p 52 N85-34178 * #
NASA-TM-87092 p 92 N85-34284 * #
NASA-TM-87096 p 136 N85-34407 * #
NASA-TM-87097 p 137 N85-34408 * #
NASA-TM-87098 p 52 N85-34179 * #
NASA-TM-87100 p 78 N85-34266 * #
NASA-TM-87102 p 152 N85-34427 * #
NASA-TM-87107 p 137 N85-34409 * #
NASA-TM-87391 p 12 N85-12887 * #
NASA-TM-87483 p 134 N85-29295 * #

NASA-TP-2359 p 17 N85-10064 * #
NASA-TP-2372 p 17 N85-10065 * #
NASA-TP-2378 p 170 N85-17576 * #
NASA-TP-2388 p 113 N85-12314 * #
NASA-TP-2390 p 113 N85-14078 * #
NASA-TP-2398 p 176 N85-22109 * #
NASA-TP-2403 p 72 N85-13006 * #
NASA-TP-2404 p 130 N85-13233 * #
NASA-TP-2405 p 84 N85-13044 * #
NASA-TP-2406 p 84 N85-13045 * #

NASA-TP-2407 p 39 N85-14858 * #
NASA-TP-2408 p 130 N85-13234 * #
NASA-TP-2419 p 123 N85-16099 * #
NASA-TP-2421 p 145 N85-20396 * #
NASA-TP-2422 p 170 N85-28610 * #
NASA-TP-2424 p 123 N85-16100 * #
NASA-TP-2426 p 171 N85-17596 * #
NASA-TP-2435 p 26 N85-21168 * #
NASA-TP-2437 p 49 N85-21263 * #
NASA-TP-2443 p 75 N85-21323 * #
NASA-TP-2449 p 88 N85-21359 * #
NASA-TP-2453 p 183 N85-24961 * #
NASA-TP-2460 p 116 N85-27165 * #
NASA-TP-2461 p 27 N85-25261 * #
NASA-TP-2463 p 30 N85-28944 * #
NASA-TP-2473 p 135 N85-32331 * #
NASA-TP-2477 p 32 N85-31058 * #
NASA-TP-2488 p 134 N85-32329 * #
NASA-TP-2495 p 93 N85-31307 * #
NASA-TP-2496 p 134 N85-31511 * #
NASA-TP-2498 p 63 N85-31244 * #
NASA-TP-2500 p 135 N85-32330 * #

NBSIR-84-2949 p 124 N85-21607 #

ORNL/TM-9518 p 89 N85-22758 * #

PB85-127173 p 146 N85-21720 * #
PB85-132322 p 124 N85-21607 #
PB85-187961 p 120 N85-33453 #

PR-715723 p 99 N85-25686 * #

PWA-FR-18323-2 p 32 N85-29965 * #

PWA-5574-149 p 71 N85-11225 * #
PWA-5594-179-VOL-1 p 22 N85-10992 * #
PWA-5594-179-VOL-2-APP-A p 22 N85-10991 * #
PWA-5594-197 p 18 N85-10950 * #
PWA-5594-202 p 31 N85-29958 * #
PWA-5594-231 p 31 N85-29956 * #
PWA-5594-243 p 30 N85-29955 * #
PWA-5594-248 p 18 N85-10947 * #
PWA-5594-251-VOL-2 p 33 N85-35198 * #
PWA-5594-258-VOL-1 p 33 N85-35197 * #
PWA-5698-77 p 25 N85-18058 * #
PWA-5894-17 p 32 N85-31057 * #
PWA-5914-39 p 126 N85-35391 * #
PWA-5928-25 p 172 N85-27584 * #
PWA-5940-19 p 145 N85-21686 * #

QNR-1 p 74 N85-19078 * #

QR-11 p 164 N85-30483 * #

REPT-4-9-T-10-F p 102 N85-12300 * #
REPT-84-SRD-042 p 126 N85-12341 * #
REPT-85-6 p 106 N85-35342 * #
REPT-85-9JDIESL-R1 p 90 N85-26994 * #
REPT-8881-933004 p 32 N85-29965 * #

RFP763340/714952 p 137 N85-16195 * #

RL-1PD-85 p 93 N85-27012 * #

R81-915326-5 p 92 N85-11252 * #
R81AEG284 p 23 N85-10995 * #
R81AEG597 p 22 N85-10994 * #
R81AEG700 p 22 N85-10993 * #
R81AEG709 p 22 N85-10990 * #
R81AEG710 p 23 N85-10998 * #
R81AEG821 p 23 N85-10997 * #
R82AEB285 p 22 N85-10989 * #
R82AEB293 p 34 N85-35199 * #
R82AEB399 p 23 N85-10996 * #
R82AEB400 p 31 N85-29957 * #
R82AEB408 p 33 N85-34141 * #
R82AEB437 p 33 N85-34138 * #
R82AEB492 p 175 N85-13550 * #
R82AEB540-VOL-2 p 23 N85-12059 * #
R83AEB358 p 175 N85-13549 * #
R84-916161-14 p 85 N85-15892 * #
R85AEB014 p 93 N85-19175 * #
R85AEB166 p 12 N85-19978 * #
R85AEB307 p 28 N85-26711 * #

SAE PAPER 841512 p 68 A85-39284 * #
SAE PAPER 841522 p 110 A85-39257 * #
SAE PAPER 841541 p 15 A85-39065 * #
SAE PAPER 841557 p 14 A85-25984 * #
SAE PAPER 841619 p 44 A85-39267 * #
SAE PAPER 850871 p 7 A85-50106 * #

SAPR-8 p 185 N85-18831 * #

SAR-7 p 22 N85-10990 * #
SAR-8 p 22 N85-10989 * #

SASR-7-VOL-1 p 22 N85-10992 * #
SASR-7-VOL-2-APP-A p 22 N85-10991 * #
SASR-8 p 31 N85-29958 * #

SP-06A83 p 9 N85-22368 * #

SRI-06-7963 p 89 N85-22757 * #

SSI-24089 p 31 N85-29960 * #

TACOM-TR-13046 p 134 N85-29295 * #

TIS-R82AEB403-VOL-2 p 23 N85-10999 * #

TR-AAE-85-4 p 125 N85-35389 * #

TR-85-8 p 100 N85-35320 * #

UILU-ENG-85-0502 p 62 N85-21283 * #
UILU-ENG-85-0504 p 125 N85-35389 * #
UILU-ENG-85-2565 p 106 N85-35342 * #

US-PATENT-APPL-SN-202228 p 117 N85-29179 * #
US-PATENT-APPL-SN-282298 p 104 N85-29144 * #
US-PATENT-APPL-SN-375784 p 57 N85-21266 * #
US-PATENT-APPL-SN-375784 p 59 N85-35233 * #
US-PATENT-APPL-SN-404809 p 63 N85-28982 * #
US-PATENT-APPL-SN-463456 p 134 N85-30333 * #
US-PATENT-APPL-SN-465364 p 160 N85-20530 * #
US-PATENT-APPL-SN-473498 p 48 N85-21256 * #
US-PATENT-APPL-SN-486470 p 160 N85-21768 * #
US-PATENT-APPL-SN-486471 p 103 N85-21492 * #
US-PATENT-APPL-SN-495381 p 57 N85-21267 * #
US-PATENT-APPL-SN-500651 p 33 N85-35195 * #
US-PATENT-APPL-SN-507626 p 117 N85-29179 * #
US-PATENT-APPL-SN-516217 p 87 N85-21350 * #
US-PATENT-APPL-SN-516217 p 87 N85-21351 * #
US-PATENT-APPL-SN-516217 p 87 N85-21352 * #
US-PATENT-APPL-SN-516217 p 63 N85-28982 * #
US-PATENT-APPL-SN-516217 p 63 N85-30039 * #
US-PATENT-APPL-SN-523297 p 57 N85-21266 * #
US-PATENT-APPL-SN-523297 p 59 N85-35233 * #
US-PATENT-APPL-SN-537615 p 135 N85-33489 * #
US-PATENT-APPL-SN-560035 p 58 N85-30027 * #
US-PATENT-APPL-SN-561429 p 87 N85-21351 * #
US-PATENT-APPL-SN-561431 p 87 N85-21350 * #
US-PATENT-APPL-SN-561434 p 63 N85-30039 * #
US-PATENT-APPL-SN-561435 p 87 N85-21352 * #
US-PATENT-APPL-SN-580419 p 119 N85-33433 * #
US-PATENT-APPL-SN-580573 p 164 N85-34441 * #
US-PATENT-APPL-SN-591089 p 57 N85-21267 * #
US-PATENT-APPL-SN-596960 p 135 N85-33490 * #
US-PATENT-APPL-SN-602050 p 136 N85-34402 * #
US-PATENT-APPL-SN-628866 p 95 N85-20153 * #
US-PATENT-APPL-SN-636659 p 78 N85-34267 #
US-PATENT-APPL-SN-640712 p 59 N85-35233 * #
US-PATENT-APPL-SN-659475 p 95 N85-20156 * #
US-PATENT-APPL-SN-661481 p 75 N85-21324 * #
US-PATENT-APPL-SN-668433 p 95 N85-20155 * #
US-PATENT-APPL-SN-669140 p 160 N85-20535 * #
US-PATENT-APPL-SN-672224 p 131 N85-20377 * #
US-PATENT-APPL-SN-700255 p 103 N85-20248 * #
US-PATENT-APPL-SN-732321 p 104 N85-29149 * #

US-PATENT-CLASS-136-225 p 160 N85-21768 * #
US-PATENT-CLASS-136-246 p 160 N85-21768 * #
US-PATENT-CLASS-136-253 p 164 N85-34441 * #
US-PATENT-CLASS-136-255 p 103 N85-21492 * #
US-PATENT-CLASS-136-256 p 160 N85-20530 * #
US-PATENT-CLASS-165-104.14 .. p 117 N85-29179 * #
US-PATENT-CLASS-165-32 p 117 N85-29179 * #
US-PATENT-CLASS-204-192C p 95 N85-20153 * #
US-PATENT-CLASS-204-192C p 57 N85-21267 * #
US-PATENT-CLASS-204-192N p 57 N85-21267 * #
US-PATENT-CLASS-204-192R p 95 N85-20153 * #
US-PATENT-CLASS-204-192R p 57 N85-21267 * #
US-PATENT-CLASS-204-192SP .. p 95 N85-20153 * #
US-PATENT-CLASS-219-76.14 p 58 N85-30027 * #
US-PATENT-CLASS-239-402.5 p 33 N85-35195 * #
US-PATENT-CLASS-310-306 p 117 N85-29179 * #
US-PATENT-CLASS-310-77 p 134 N85-30333 * #
US-PATENT-CLASS-310-93 p 134 N85-30333 * #
US-PATENT-CLASS-315-3.5 p 135 N85-33489 * #
US-PATENT-CLASS-315-5.38 p 135 N85-33489 * #
US-PATENT-CLASS-318-611 p 134 N85-30333 * #
US-PATENT-CLASS-335-100 p 134 N85-30333 * #
US-PATENT-CLASS-357-12 p 103 N85-21492 * #
US-PATENT-CLASS-357-30 p 103 N85-21492 * #
US-PATENT-CLASS-357-30 p 160 N85-21768 * #
US-PATENT-CLASS-384-101 p 135 N85-33490 * #
US-PATENT-CLASS-384-99 p 135 N85-33490 * #
US-PATENT-CLASS-415-115 p 119 N85-33433 * #
US-PATENT-CLASS-415-170-R ... p 136 N85-34402 * #
US-PATENT-CLASS-415-174 p 136 N85-34402 * #
US-PATENT-CLASS-415-196 p 136 N85-34402 * #
US-PATENT-CLASS-415-200 p 136 N85-34402 * #
US-PATENT-CLASS-416-174 p 136 N85-34402 * #
US-PATENT-CLASS-416-97A p 119 N85-33433 * #
US-PATENT-CLASS-423-DIG.10 . p 95 N85-20153 * #
US-PATENT-CLASS-423-414 p 95 N85-20153 * #
US-PATENT-CLASS-423-445 p 95 N85-20153 * #
US-PATENT-CLASS-423-445 p 57 N85-21267 * #
US-PATENT-CLASS-423-446 p 95 N85-20153 * #
US-PATENT-CLASS-423-446 p 57 N85-21267 * #
US-PATENT-CLASS-423-449 p 95 N85-20153 * #
US-PATENT-CLASS-423-449 p 57 N85-21267 * #
US-PATENT-CLASS-427-178 p 58 N85-30027 * #
US-PATENT-CLASS-427-37 p 58 N85-30027 * #
US-PATENT-CLASS-427-39 p 57 N85-21267 * #
US-PATENT-CLASS-427-422 p 58 N85-30027 * #
US-PATENT-CLASS-427-85 p 160 N85-20530 * #
US-PATENT-CLASS-428-633 p 57 N85-21266 * #
US-PATENT-CLASS-428-633 p 59 N85-35233 * #
US-PATENT-CLASS-428-656 p 57 N85-21266 * #
US-PATENT-CLASS-428-656 p 59 N85-35233 * #
US-PATENT-CLASS-428-678 p 57 N85-21266 * #
US-PATENT-CLASS-428-678 p 59 N85-35233 * #
US-PATENT-CLASS-428-679 p 57 N85-21266 * #
US-PATENT-CLASS-428-679 p 59 N85-35233 * #
US-PATENT-CLASS-428-680 p 57 N85-21266 * #
US-PATENT-CLASS-428-680 p 59 N85-35233 * #
US-PATENT-CLASS-428-681 p 57 N85-21266 * #
US-PATENT-CLASS-428-681 p 59 N85-35233 * #
US-PATENT-CLASS-428-682 p 57 N85-21266 * #
US-PATENT-CLASS-428-682 p 59 N85-35233 * #
US-PATENT-CLASS-428-683 p 57 N85-21266 * #
US-PATENT-CLASS-428-684 p 57 N85-21266 * #
US-PATENT-CLASS-429-206 p 104 N85-29144 * #
US-PATENT-CLASS-429-249 p 104 N85-29144 * #
US-PATENT-CLASS-445-35 p 135 N85-33489 * #
US-PATENT-CLASS-526-204 p 63 N85-30039 * #
US-PATENT-CLASS-526-217 p 87 N85-21350 * #
US-PATENT-CLASS-526-217 p 63 N85-30039 * #
US-PATENT-CLASS-526-262 p 87 N85-21350 * #
US-PATENT-CLASS-526-262 p 87 N85-21351 * #
US-PATENT-CLASS-526-262 p 87 N85-21352 * #
US-PATENT-CLASS-526-262 p 63 N85-28982 * #
US-PATENT-CLASS-526-262 p 63 N85-30039 * #
US-PATENT-CLASS-528-229 p 87 N85-21350 * #
US-PATENT-CLASS-528-229 p 87 N85-21351 * #
US-PATENT-CLASS-528-229 p 87 N85-21352 * #
US-PATENT-CLASS-528-314 p 63 N85-30039 * #
US-PATENT-CLASS-528-315 p 87 N85-21350 * #
US-PATENT-CLASS-528-322 p 87 N85-21350 * #
US-PATENT-CLASS-528-322 p 87 N85-21351 * #
US-PATENT-CLASS-528-322 p 87 N85-21352 * #
US-PATENT-CLASS-528-322 p 63 N85-28982 * #
US-PATENT-CLASS-528-322 p 63 N85-30039 * #
US-PATENT-CLASS-528-336 p 87 N85-21350 * #
US-PATENT-CLASS-528-342 p 87 N85-21350 * #
US-PATENT-CLASS-528-342 p 87 N85-21351 * #
US-PATENT-CLASS-528-342 p 87 N85-21352 * #
US-PATENT-CLASS-528-342 p 63 N85-28982 * #
US-PATENT-CLASS-60-202 p 48 N85-21256 * #
US-PATENT-CLASS-60-39.23 p 33 N85-35195 * #
US-PATENT-CLASS-60-748 p 33 N85-35195 * #

US-PATENT-4,437,962 p 57 N85-21267 * #
US-PATENT-4,455,418 p 63 N85-28982 * #
US-PATENT-4,466,242 p 48 N85-21256 * #
US-PATENT-4,478,879 p 160 N85-20530 * #
US-PATENT-4,482,778 p 160 N85-21768 * #
US-PATENT-4,482,779 p 103 N85-21492 * #
US-PATENT-4,485,151 p 57 N85-21266 * #
US-PATENT-4,485,151 p 59 N85-35233 * #
US-PATENT-4,490,229 p 95 N85-20153 * #
US-PATENT-4,495,044 p 57 N85-21267 * #
US-PATENT-4,495,339 p 63 N85-30039 * #
US-PATENT-4,497,939 p 87 N85-21351 * #
US-PATENT-4,497,940 p 87 N85-21352 * #
US-PATENT-4,497,948 p 87 N85-21350 * #
US-PATENT-4,505,998 p 104 N85-29144 * #
US-PATENT-4,506,183 p 117 N85-29179 * #
US-PATENT-4,514,557 p 63 N85-28982 * #
US-PATENT-4,517,505 p 134 N85-30333 * #
US-PATENT-4,518,625 p 58 N85-30027 * #
US-PATENT-4,527,092 p 135 N85-33489 * #
US-PATENT-4,527,910 p 135 N85-33490 * #
US-PATENT-4,528,417 p 164 N85-34441 * #
US-PATENT-4,529,358 p 119 N85-33433 * #
US-PATENT-4,534,166 p 33 N85-35195 * #
US-PATENT-4,535,033 p 59 N85-35233 * #
US-PATENT-4,540,336 p 136 N85-34402 * #

USAAVSCOM-TM-84-C-2 p 114 N85-19363 * #

USAAVSCOM-TR-84-C-12 p 1 N85-15658 * #
USAAVSCOM-TR-84-C-18 p 24 N85-15727 * #
USAAVSCOM-TR-84-C-19 p 25 N85-18057 * #
USAAVSCOM-TR-84-C-20 p 85 N85-14929 * #

USAAVSCOM-TR-84-C-21 p 7 N85-14798 * #
USAAVSCOM-TR-84-C-4 p 133 N85-27228 * #
USAAVSCOM-TR-85-C-10 p 30 N85-28945 * #
USAAVSCOM-TR-85-C-11 p 30 N85-27870 * #
USAAVSCOM-TR-85-C-14 p 59 N85-34223 * #
USAAVSCOM-TR-85-C-16 p 136 N85-34406 * #
USAAVSCOM-TR-85-C-1 p 74 N85-19074 * #
USAAVSCOM-TR-85-C-3 p 133 N85-27227 * #
USAAVSCOM-TR-85-C-4 p 89 N85-24000 * #
USAAVSCOM-TR-85-C-5 p 76 N85-26964 * #
USAAVSCOM-TR-85-C-6 p 32 N85-31060 * #
USAAVSCOM-TR-85-C-9 p 136 N85-34405 * #

UTRC-R83-925312-25 p 34 N85-12901 * #
UTRC-R84-915540-34 p 117 N85-30245 * #

VPI-E-84-36 p 146 N85-21720 * #

W-45797 p 105 N85-33293 * #

WGR-85-5 p 100 N85-35321 * #

YU-2115 p 92 N85-10209 * #

☆U. S. GOVERNMENT PRINTING OFFICE:1986/646-116/20430

1. Report No.	2. Government Accession No.	3. Recipient's Catalog No.
NASA TM-87263		

4. Title and Subtitle	5. Report Date
Bibliography of Lewis Research Center Technical Publications Announced in 1985	May 1986
	6. Performing Organization Code: None
7. Author(s)	8. Performing Organization Report No.: E-2960
	10. Work Unit No.
9. Performing Organization Name and Address: National Aeronautics and Space Administration, Lewis Research Center, Cleveland, Ohio 44135	11. Contract or Grant No.
	13. Type of Report and Period Covered: Technical Memorandum
12. Sponsoring Agency Name and Address: National Aeronautics and Space Administration, Washington, D.C. 20546	14. Sponsoring Agency Code

15. Supplementary Notes

Compiled by Technical Information Services Division, Lewis Research Center.

16. Abstract

This compilation of abstracts describes and indexes the technical reporting that resulted from the scientific and engineering work performed and managed by the Lewis Research Center in 1985. All the publications were announced in the 1985 issues of STAR (Scientific and Technical Aerospace Reports) and/or IAA (International Aerospace Abstracts). Included are research reports, journal articles, conference presentations, patents and patent applications, and theses.

17. Key Words (Suggested by Author(s))	18. Distribution Statement
Bibliographies Abstracts Documentation Indexes (Documentation)	Unclassified - unlimited STAR Category 82

19. Security Classif. (of this report)	20. Security Classif. (of this page)	21. No. of pages	22. Price*
Unclassified	Unclassified	306	A14

*For sale by the National Technical Information Service, Springfield, Virginia 22161

National Aeronautics and
Space Administration

Lewis Research Center
Cleveland, Ohio 44135

Official Business
Penalty for Private Use $300

SECOND CLASS MAIL

ADDRESS CORRECTION REQUESTED





Postage and Fees Paid
National Aeronautics and
Space Administration
NASA-451

NASA